

International conference on the respective input of the numerical simulation and the experimental approach in Fatigue design 2005 - 1st edition

November 16, 17 & 18 - Cetim, Senlis - France

cetim www.cetim.fr

AFM MECANICIENS AU CŒUR DU MONDE EN MOUVEMENT

SF2M

DVM

FITNET European Fitness-for-service Network
welded structures • design • fabrication • structural integrity

Fatigue Design 2005

Numerical simulation and/or experimental validation

Dimensioning in fatigue is confronted today with new requirements dealing with the control of the reliability of the products. Indeed, if the methods of numerical simulation and experimental validation of the fatigue strength seem overall satisfactory, when the aim is to assess the behaviour of a component or of a structure, with respect to a given loading condition, another approach is necessary to quantify the failure risk on the whole of a production with respect to the diversity of the situations of life met in service.

To quantify a risk, need to be able to check that the objective of reliability fixed for a component or a system will be well achieved or to bring optimizations necessary in the contrary case. In this context, the question is to design a product subject to fatigue by using an approach of estimated reliability being based on modelling and by applying checks and experimental validations to consolidate the confidence of the design engineer in the objective of reliability.

The duality of this step, prediction by numerical modelling/experimental validation, completely integrated into engineering system, makes it possible to improve the productivity of the development (reduction of the costs and respect of the times of design), the productivity of manufacture by the necessary control of the drifts of manufacture and to guarantee reliability in service.

The purpose of Fatigue Design 2005 is based on this problematic and is to bring concrete answers to the questions that the mechanical engineers and the engineering and design departments are posed confronted at the same time with the following constraints:

- the requirements of improvement of the performances in service,while reducing the power consumptions, thanks to a more precise design, surer (better knowledge of resistance in service of materials implemented and loading conditions of the products) and innovating (reduction of the weights and volumes, integration to the product of new functionalities),
- the difficulty in determining the diversity of the loadings in service,
- the innovation in product design and manufacture processes which does not allow any more the renewal of solutions tested on a preceding product
- the reduction in cost and time, for the marketing of a product.

Therefore, the selected papers aim to answer the following industrial concerns:

- current steps of design of large the industrial sectors (car, aeronautics, naval, energy, public works…) are presented. as well as the difficulties encountered in each case and new waiting of the industrialists,
- the new approach and tools, with respect to fatigue design, either already on the market, or under development are detailed. These approaches relate to the implementation of probabilistic dimensioning, the predictive modelling of the fatigue resistance, as well as the application of recent standards or regulations and the new experimental methods.

The involved topics concern in particular the following fields:

- reliability approaches in fatigue resistance assessment
- evolution of standards and and regulation,
- tools for analysis of the in service loading,
- tools of numerical simulation and post processing,
- new experimental techniques of characterization and validation.

The whole of the approaches and researches presented in the papers constitutes a current state of the design problematic, with respect to fatigue.

Dr. Henri-Paul Lieurade
Conference Chairman

Fatigue Design 2005

Simulation numérique et/ou validation expérimentale

Le dimensionnement en fatigue des structures est aujourd'hui confronté à de nouvelles exigences quant à la maîtrise de la fiabilité des produits

En effet si les méthodes de simulation numérique et de validation expérimentale de la tenue en fatigue apparaissent comme globalement satisfaisante, lorsqu'il s'agit de qualifier le comportement d'une structure vis à vis d'une sollicitation donnée, il n'en va pas de même lorsque l'on veut quantifier un risque de défaillance sur l'ensemble d'une production vis-à-vis de la diversité des situations de vie rencontrées en service.

Quantifier un risque, c'est être en mesure de vérifier que l'objectif de fiabilité fixé pour un composant ou un système sera bien atteint ou d'apporter les optimisations nécessaires dans le cas contraire.

Dans ce contexte, il s'agit bien d'aborder la qualification en fatigue d'un produit par le biais d'une approche de fiabilité prévisionnelle s'appuyant sur la modélisation et de conduire les vérifications et validations expérimentales utiles pour conforter la confiance du concepteur dans l'atteinte de l'objectif de fiabilité.

La dualité de cette démarche, prédiction par la modélisation numerique/validation par l'expérience, complètement intégrée à l'ingénierie système, permet d'améliorer la productivité du développement (réduction des coûts et respect des délais de conception), la productivité de fabrication par la nécessaire maîtrise des dérives de fabrication et de garantir la fiabilité en service.

Fatigue Design 2005 se fonde sur cette problématique et a pour but d'apporter des réponses concrètes aux questions que se posent les ingénieurs mécaniciens et les bureaux d'études confrontés en même temps :

- à des impératifs d'amélioration des performances en service, tout en réduisant les consommations énergétiques, grâce à une conception plus précise, plus sûre (meilleure connaissance à la fois de la résistance en service des matériaux mis en œuvre et des conditions de sollicitation des produits) et innovante (réduction des poids et des volumes, intégration au produit de nouvelles fonctionnalités),
- à la difficulté de cerner la diversité des chargements en service,
- à l'innovation produit ou process qui ne permet plus la reconduction de solutions éprouvées sur un produit précédent,
- à des contraintes de diminution de coût et de délais, pour la mise sur le marché d'un produit.

Pour tenter de répondre à ces questions, Les contributions retenues ont pour objectif de répondre aux préoccupations des industriels concernés :

- les démarches de conception actuelles des grand secteurs industriels (automobile, aéronautique, naval, énergie, travaux publics…) sont présentéesLe premier intérêt de ces contributions est de présenter non seulement les démarches de conception propres à chaque secteur industriel, mais aussi les difficultés rencontrées dans chaque cas et les attentes nouvelles des industriels,
- les nouvelles démarches de conception vis à vis de la fatigue, soit déjà sur le marché, soit en cours de développement sont détaillées. Ces démarches concernent la mise en œuvre du dimensionnement probabiliste, la modélisation prédictive de la tenue en fatigue, ainsi que l'application des codifications et réglementations récentes et les méthodes expérimentales avancées..

Les thèmes abordés concernent en particulier sur les domaines suivants :

- les approches fiabilistes du dimensionnement en fatigue
- l'évolution des codes et des règlements,
- les outils d'analyse des sollicitations en service,
- les outils de simulation et de post-traitement,
- les nouvelles techniques expérimentales de caractérisation et de validation.

L'ensemble des démarches et des travaux présentés constitue ainsi un état actuel de la problématique de conception vis-à-vis de la fatigue.

Henri-Paul Lieurade
Président du comité d'organisation

PROGRAM

1 Methodologies and tools for fatigue life assessment

2 Advanced design tools and approaches

3 Multiaxial loading fatigue assessment

4 Fitness for service approach and applications

5 Experimental validation

6 Design procedures against thermal and thermo mechanical fatigue damage

7 Reliability approaches in fatigue design

8 Improved design and manufacture processes with regard to fatigue

PROGRAM

1 Methodologies and tools for fatigue life assessment

- Automotive components
- Various industrial applications
- Welded structures and assemblies

2 Advanced design tools and approaches

- Fatigue crack initiation assessment
- Contribution to the crack propagation stage
- Modelling of the design behaviour of the welded

3 Multiaxial loading fatigue assessment

4 Fitness for service approach and applications

5 Experimental validation

- Application to automotive parts and structures
- From laboratory testing to field evaluation
- Development of dedicated test devices and procedures

6 Design procedures against thermal and thermo mechanical fatigue damage

7 Reliability approaches in fatigue design

8 Improved design and manufacture processes with regard to fatigue

Integration of the Lifetime Prediction in the Car Development Process – Today and in the Future

Martin Brune [a], Sébastien Chéreau [a], Christina Hackmair [a], Andreas Fischersworring-Bunk [b]

[a] BMW Group, Materials and Durability, Munich, Germany
[b] BMW Group, Power Train, Munich, Germany

Abstract Over the last ten years, the car development process has seen a strong change in relation to time and cost reduction aspects and it is certain, that this demand will continue in the near future. The aim is to create a cost and time optimised process resulting in maximum possible product quality, something that is not feasible without the use of modern methods of calculation and testing. This fact has consequences from many different standpoints, and influences all areas of the component development process. One of these areas is the design and durability process for chassis, body, and power train components. The durability software gives the CAE engineer a tool for applying the fatigue life calculation in the “functional” design of a component. Some procedures used in the functional design will be highlighted using examples from the chassis, body in white and power train design areas.

1 INTRODUCTION

The fatigue life calculation method exhibits considerable potential for improvement with regards to the quality of the results. On the one hand it is dependent on a large number of inputs and functions, such as material characteristic values and load data. On the other hand, the applied algorithms represent empirical functions, because the real fatigue damage mechanisms are ultimately not known. The calculation method is nevertheless established in the present-day development process. The durability software gives the CAE engineer a tool for applying the fatigue life calculation in the "functional" design of a component. It reveals that the CAE engineer consequently plays a key role in the component development process. He acts as intermediary between internal departments such as design and testing departments, and external partners such as software suppliers, system suppliers and research institutes. This paper explains some procedures related to the current situation and tries to find answers and solutions to the questions above regarding the challenges of the future.

2 FUNCTIONAL DURABILITY DESIGN

Vehicle development has undergone considerable change in recent years as both development time and costs have been reduced. The fact is that the process of developing a car is now much more rapid, than was the case ten years ago. There must consequently have been radical changes in all decisive areas of development for these shorter development times to have been made possible. Over and above reducing development time, the measures required in addition have the task of cutting costs. This represents an enormous challenge to the car manufacturer and also to their suppliers, because they ultimately have to deliver a product of an equally high standard of quality to their customers, irrespective of these savings. The following part illustrates how this challenge is nowadays being implemented, with the aid of the design and validation process for vehicle components with regard to cyclic load, in other words the component fatigue life.

2.1 In the past

How did this process look about ten years ago? The Figure 2.1 shows the approach. It is evident here that test components were built very early on in the development process. The design of these components was determined with the aid of quasi-static strength calculations. The material characteristic values that are required for the calculation and information on the load encountered by the component are, as now, very important inputs for the calculation. Where were this information obtained from? Experience of the vehicle loads that occurred played a decisive role, because at that stage of the development process it was not yet possible to measure loads and stresses. These measurements were nevertheless generally available for the predecessor model of the vehicle being developed, so

these then served as the basis for the load data input for the calculations for the new model. On the one hand, the measurement results were rescaled accordingly as a result of the new vehicle dimensions, such as its weight, performance and tyre width, and on the other hand only certain load combinations that were relevant to the strength of the design on the basis of the experience were filtered out of the load time histories. The quasi-static calculations that were then performed, served as the basis of an iterative process of virtual optimisation of component strength, without taking account of the cyclic loads and the resulting effects. These aspects were only taken into account in the subsequent validation process, in which the fatigue test played the most important role.

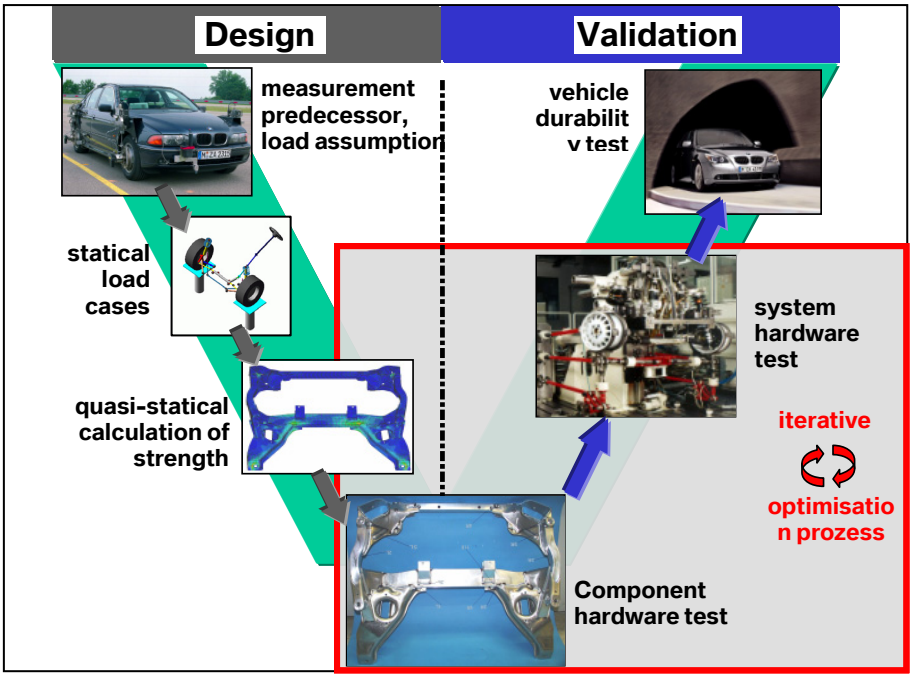


Figure 2.1: Design and validation process for about 10 years ago

The components must satisfy defined fatigue life requirements, which used to be confirmed almost exclusively on the test bench. Design changes resulting from unsatisfactory test results were translated into new test components, which were then tested again. This process was repeated until the required fatigue life of the component or component system was achieved. This process then concluded with a vehicle durability test, intended to confirm the fatigue life of the total vehicle, among other aspects.

This procedure is no longer feasible today in the form described. The reduction in development time and the diversity of vehicle models in recent years have meant that fatigue life validation purely by experimental means is no longer possible because the test bench capacity and time required are simply not available. To handle this diversity in the design process, modern calculation methods provide the solution. Whereas quasi-static strength calculation was used in the design phase of vehicle components in the past, the strength under cyclic load, or fatigue life, is now also calculated.

2.2 Nowadays

The current component design and validation process in terms of fatigue strength is shown in Figure 2.3. It is evident here that the design phase is driven to a very high degree by calculation methods, because no component hardware is available at this point in time. Quasi-static calculations for initial component drafts are still used in the very early phase of the development process. Here too, the underlying component load combinations are based on assumptions and findings relating to the predecessor vehicle. There is no point in conducting a fatigue life calculation at this point, as it necessitates detailed geometric models that are not created until the end of the design phase. As soon as these geometric models are available, fatigue life calculation is commenced in order to boost component quality at an early stage of development and, in particular, simplify the validation process by eliminating several hardware iteration loops.

The entire load time history is used for fatigue life calculation instead of specific load combinations. The cutting force time histories for the components to be investigated are generated by means of dynamic multi body simulation (MBS) and fed into the calculation. The remaining tests are required for continuous matching of the computational methods. At the end of the validation phase there is still the experimental confirmation of fatigue strength of the components and systems, and finally the durability road test of the total vehicle for final confirmation.

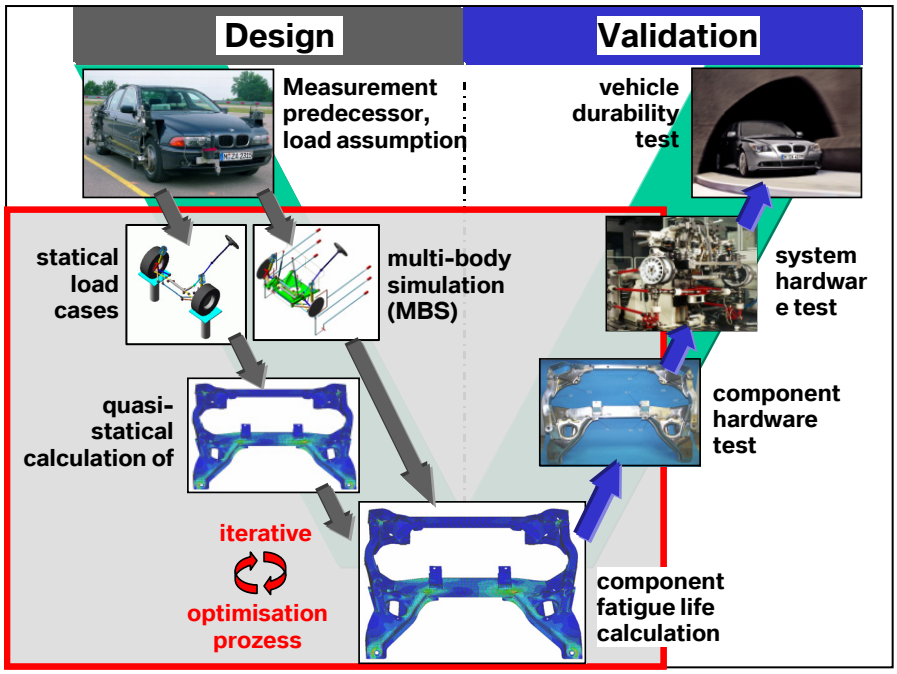


Figure 2.2: Design and validation process nowadays

This design and validation process is still not yet optimal. There are many questions that have currently not or only partially been answered. However, one fact is absolutely clear, and it is very important to emphasize it: the process described here does not envisage replacing fatigue life tests entirely with calculations, neither now nor in the future. Rather, the tests and calculations should complement each other usefully.

The aim is to create a cost and time optimised vehicle development process resulting in maximum possible product quality, something that is not feasible without the use of modern methods of calculation and testing.

The fatigue life calculation method exhibits considerable potential for improvement with regards to the quality of the results. In spite of the fact, that the applied algorithms represent empirical functions (the real fatigue damage mechanisms are ultimately not known) this calculation method is nevertheless already established and indispensable in the present-day development process. However, the users must always be aware that they are working with a method that reacts highly sensitively to errors. In other words, any "blind faith" in calculations is utterly misplaced. As with all calculation methods, they will obtain a coloured picture as the result of fatigue life calculation. What matters is how this picture is interpreted.

2.2 In the immediate future

The load data that are needed for the calculation play hereby an absolutely decisive role. If fundamental mistakes are made at this stage, even the best calculation method will not yield plausible results. Even today, the load assumptions used in the early phase of vehicle development are still essentially based on the findings obtained from the predecessor models. The vision is to obtain more precise load data predictions again with the aid of computational methods. That is why we are working intensively on driving virtual vehicles with virtual drivers along virtual roads in order to deduce the necessary load data from them, as shown in Figure 2.3. Many aspects are already up and running, as a result of which we vehicle developers are very confident, though various hurdles still remain to be taken. The principal elements are the required model quality of the total vehicle as the input for a multi body simulation to reproduce the behaviour of the component and overall system, the dimensioning test tracks in digital form, and an efficient driver model. All these elements must moreover interact optimally in order to deliver a usable picture of

reality. This naturally also includes a functioning tyre model to represent the dynamic systems behaviour between the road surface and the vehicle in a computational way. While we are working on the purely virtual model on the one hand, we have on the other hand already been making use of an experimental method that produces genuine measurement results as early as the constructive design phase, if not in the very early development phase.

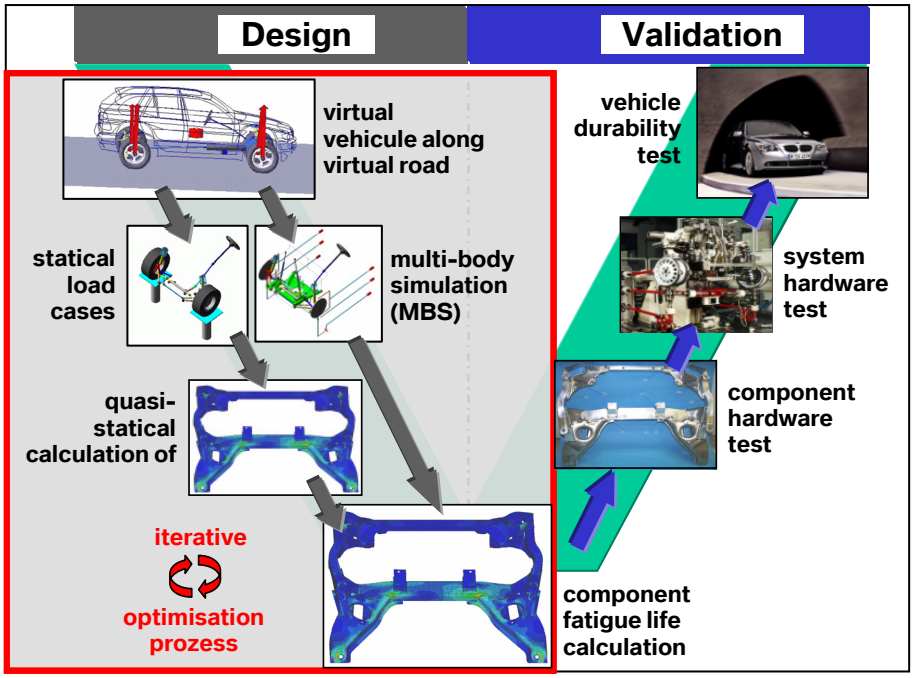


Figure 2.3: Design and validation process in the immediate future

This calculation methodology should be used in the first instance for relative observations, in other words for evaluating component variants. The vision of one day being able to quote a component's fatigue life in kilometres is still many years away, but each step made by improving new calculation methods leads to this aim. With regard to this, there are various possible starting points, for instance the calculation inputs, e.g. involving the use of improved methods of load data determination in order to enhance the quality of the prediction from the early phase on, or the applied algorithms of the fatigue life calculation itself. There is still ample need for research into this area. There are for instance ideas on how to link the macroscopic viewpoint, on which present-day calculations are based, with microcrack growth findings in order to obtain higher-quality results. Conceivable synergies of the micro and macro research domains, which currently operate largely separate from one another, could deliver entirely new findings and thus result in an improved method. Equally, by no means all questions on the subject of multiaxial loads have been answered yet.

3 BODY-IN-WHITE APPLICATIONS

As well as spot and linear welding techniques, structural bonds have found increasing use in body in white manufacturing since the start of the 1970s. Up to 85% of the flanges on a body in white are now spot weldbonded. There are many advantages to this. Bonded or spot weldbonded structures exhibit better crash properties, higher stiffness values and therefore improved riding comfort under conditions including vibration, as well as higher strength under static and cyclic loads. The use of adhesive joints paves the way for implementing new composite design concepts, i.e. the joining of different types of materials together and the joining of ultra-thin parts, both of which are key requirements in innovative lightweight design. It is currently possible to reduce the weight of the body in white by 15-20 kg by means of spot weldbonding.

This part presents a method of fatigue life calculation based on a fracture mechanics approach. It is based on the one hand on a crack propagation model of the adhesive layer to describe the crack propagation speed as a function of the rate of energy release, and on the other hand on calculation of the rate of energy release with the aid of the finite element method. The crack propagation model is determined for a steel-structural adhesive joint for cyclic loads under mode I with R=0.1.

3.1 Principle of fatigue life calculation

As well as the classic view of stress analysis, based on macroscopic failure models such as the equivalent stress hypothesis, fracture mechanics approaches are implemented to describe the failure behaviour of adhesive joints. At the edges of the adhesive layers, adhesive joints exhibit pronounced stress singularities that critically determine the strength behaviour of the adhesive joint under both static and dynamic loads. A stress-based approach to failure description would, however, necessitate detailed, very finely discretised meshes of the adhesive layer. Such an approach is not practicable considering the calculation method is intended for use in vehicle body calculation. Fracture mechanics, on the other hand, describes components with cracks, notches and defects together with their singular areas of distortion. The failure criteria are determined here by means of fracture mechanics parameters, such as the rate of energy release. The rate of energy release as a product of local forces and displacements is largely determined by local stiffness that are well represented in existing vehicle body models.

The method of fatigue life calculation of structural bonds described in this paper is based on a fracture mechanics approach; the principle is shown in Fig. 3.1.

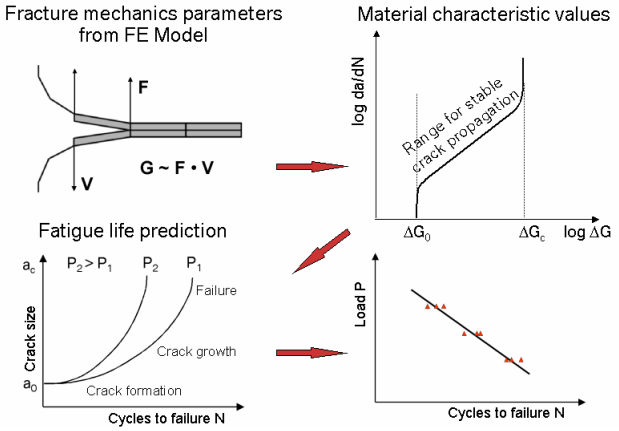


Fig. 3.1: Principle of fatigue life calculation of structural bonds based on a fracture mechanics approach.

The application of linear-elastic fracture mechanics in the fatigue life calculation of structural bonds implies linear-elastic behaviour of the adhesive. Based on the assumption that minor deformation will occur, this approach is justified. The load in the adhesive flange is determined by means of a linear-elastic static calculation; see top left of Fig. 3.1. Modelling of the adhesive flange includes the crack opening in the adhesive layer. Modelling of the crack opening serves merely to represent the local stiffness of the adhesive flange; no modelling of crack propagation is needed. Fracture mechanics parameters, in this instance the rate of energy release G, can be determined with the aid of this FE model. The rate of energy release G is the energy that is made available by the elastic stress field and the external forces for propagating the cracking. Of the boundary conditions governing the local flange modelling, G is the characteristic parameter for the loads on the bond. The G values are calculated from the FE model with the aid of the Virtual Crack Closure Technique (VCCT). For the load, e.g. in mode I, in other words peeling tension in the adhesive flange, G is proportional to the force F at the crack tip and the crack opening V, which are each perpendicular to the crack opening plane.

Material characteristic values are determined with the aid of crack propagation tests. The crack propagation diagram, see Fig. 3.1 at top right, shows the interrelationship between crack propagation speed da/dN and the cyclic rate of energy release ΔG, and describes the strength of the adhesive joint. For this adhesive joint, crack propagation occurs cohesively in the adhesive layer. Under cyclic loads, cracks spread stably if the cyclic rate of energy release lies between the threshold value for stable crack propagation, ΔG_0, and the limit value for unstable crack propagation, ΔG_c. Paris' law, which produces a straight line when plotted on a double logarithmic scale, applies for this range.

$$\frac{da}{dN} = C \cdot \Delta G^m \qquad \text{(Equation 1)}$$

Here, the constants C and m depend on the material and on various influencing factors such as temperature, ambient medium and the stress ratio R. By applying Paris' law, it is a relatively straightforward matter to make a prediction of the life of a component with the aid of fracture mechanics. With the integral in the basic form

$$N = \int_{a_0}^{a_c} \frac{1}{C \cdot G^m} \cdot da \quad \text{(Equation 2),}$$

the life can be calculated by means of an integration process from an initial crack length a_0 to a critical crack length a_c, see Fig. 3.1 below. In this case, the life comprises only the crack propagation phase, not the crack initiation phase. The crack initiation phase is taken into account by determining a hypothetical initial crack length a_0 by calculating back from the experiment. There is no correlation between the hypothetical initial crack length and detectable defects or similar in the adhesive layer.

3.2 FE modelling

The modelling of the adhesive layer in a global FEM mesh of the body structure acquires particular significance in the application of fatigue life calculation within the standard process of vehicle body calculation. The modelling of the adhesive layer must satisfy the requirements and boundary conditions of present-day standard body meshes. An adhesive flange of a total length of e.g. 160 m in the current BMW 7 Series and the calculation of several variants per week in the body design process highlight the challenges that modelling faces. Meshing of the adhesive layer must take place automatically and also be applicable to incompatible FE meshes. A detailed, fine mesh of the adhesive layer would result in impermissibly large models and lengthy computing times in a total body model. As the modelling of the adhesive layer in the stiffness/acoustics and static strength design process has already been defined and has proved effective, this modelling is now to be adopted for fatigue life design.

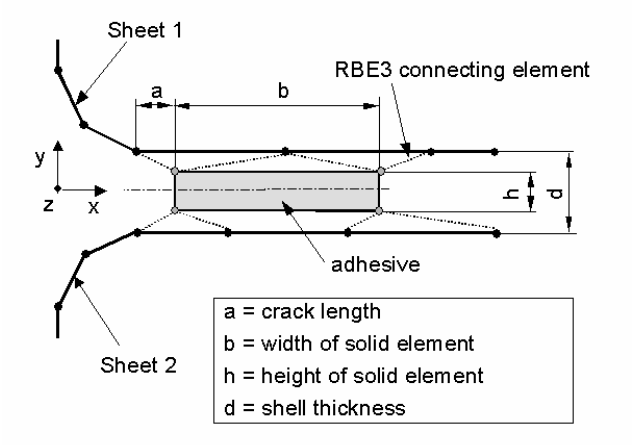


Fig. 3.2: Adhesive flange modelling for vehicle body fatigue life calculation.

Fig. 3.2 is a schematic representation of adhesive flange modelling for vehicle body fatigue life calculation, which in its general form corresponds to the meshing of stiffness models. The joined parts, sheet 1 and sheet 2, are meshed at the sheets' mid-planes by linear shell elements, with compatible meshes of sheets 1 and 2 not being necessary. The adhesive is represented by linear volume elements and connected with the sheets by the linear interpolation elements RBE3.

In view of the special boundary conditions that this method of fatigue life calculation entails, the modelling guideline for adhesive flanges for fatigue life calculations must be correspondingly broadened or clarified. The special boundary conditions include the scope for calculating fracture mechanics parameters such as the rate of energy release from a global FE vehicle body model. To this end, specific geometric ratios for adhesive flange modelling must be defined; these are the crack length, and the width and height of the volume element that the adhesive represents. The "crack length" **a** defines the evaluation nodes for force F and displacement V. The adhesive flanges meshed according to the modelling guideline must represent the local stiffness of correspondingly finely meshed adhesive joints. The scope of validity of the modelling guideline encompasses various flange geometries that are typical for vehicle body models and are subjected to peeling tension loads.

3.3 Numerical fatigue life calculation and experimental verification

Cyclic tests are conducted on a bonded double-hat profile (DHP) specimen in order to validate the calculation method and modelling guideline. Subsequent verification is performed on the cross/shear tension specimen 2 (KS2).

The adhesive joints are subjected to mode I loads, i.e. the adhesive layer of the double-hat profile specimen to peeling tension and the adhesive layer of the KS2 specimen to cross tension as a result of the introduction of the load to both legs of the U-profile. The cyclic tests are conducted with a force ratio of R=0.1. Rupturing of the adhesive layer is defined as the failure criterion.

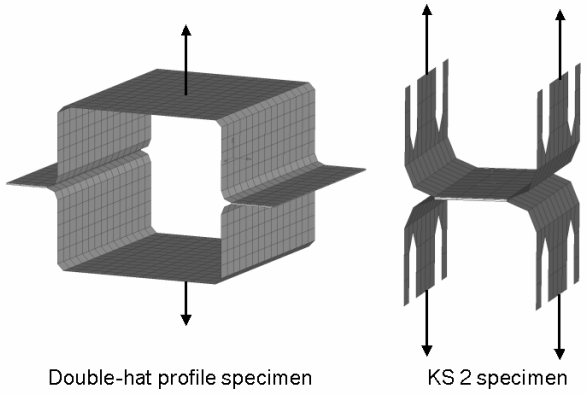


Fig. 3.3.1: FE model of the double-hat profile specimen and the KS2 specimen, subjecting the adhesive joins to mode I loads (peeling tension and cross tension).

Fig. 3.3.1 shows the FEM models of the double-hat profile specimen and the KS2 specimen, and subjecting of the adhesive joints to mode I loads (peeling tension and cross tension). By means of the FEM model of the double-hat profile specimen, a functional interrelationship between the rate of energy release G on the one hand and the crack length **a** and external load P on the other hand is determined. The fatigue life of the specimen can be calculated at a constant-amplitude load with the function G (P, a) and equation 2.

To calibrate the parameters for the modelling guideline and the function G (P,a), numerically and experimentally determined Woehler curves are compared, see Fig. 3.3.2, DHP testing and calculation. The diagrams show the upper force, with the values normalised to the respective maximum tensile strength from the quasi-static tensile tests. The Woehler curve determined experimentally for the double-hat profile specimen (DHP) exhibits a slope of 8.7. The mathematically determined Woehler curve has a slope of 9.4 and lies to the right of the experimentally determined Woehler curve, i.e. the calculation produces a non-conservative result in the range of lower load horizons. Repeated calibration of the function G(P, a) is necessary to achieve a conservative estimate of the fatigue life with the calculations.

With the aid of the function G(P, a), the Woehler curve for force is converted into an Woehler curve for rate of energy release, which is referred to in the following fatigue life calculations for mode I loading as the basic Woehler curve, see Fig. 3.3.2, DHP calculation.

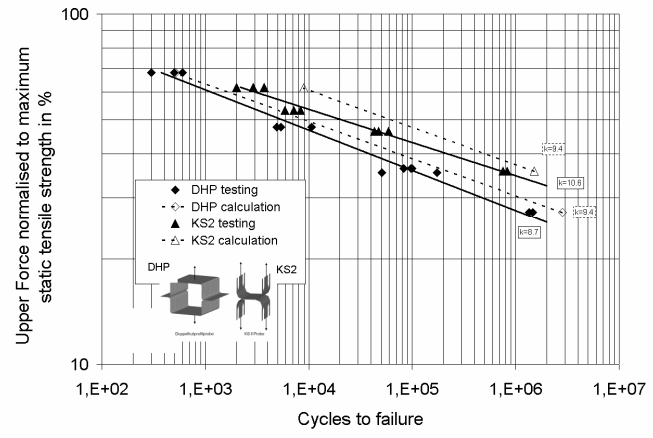


Fig. 3.3.2: Comparison of numerically and experimentally determined Woehler curves for the double-hat profile specimen (DHP) and cross/shear tension specimen (KS2).

Experimental verification of the calculation approach as well as of the general validity of the function G(P, a) and the modelling guideline is obtained with cyclic tests with the KS2 specimen under cross tension. Using the basic Woehler curve, the Woehler curve calculated for the KS2 specimen reveals a high degree of concurrence with the experimental results, see Fig. 3.3.2, KS2 testing and calculation. As expected, the calculated Woehler curve for the KS2 specimen has the same slope as the basic Woehler curve of 9.4. The experimentally determined Woehler curve for the KS2 specimen is somewhat flatter, with a slope of 10.6. With the repeated calibration of the basic Woehler curve as mentioned above, a conservative estimate of fatigue life is likewise to be expected for the KS2 specimen.

It can generally be stated that the calculated results accurately reflect the results of the test. The calculation concept with a basic Woehler curve G-N and the modelling guideline proved to be suitable in an initial verification and are adopted for implementation in the vehicle body calculation standard process.

The vehicle body calculations are initially restricted to identifying critical adhesive flanges. Only when further important factors influencing the fatigue strength of adhesive joints are known, such as temperature and ageing, is it possible to make a computational fatigue life prediction of vehicle body adhesive flanges, with results that are useful both qualitatively and quantitatively.

4 POWER TRAIN APPLICATIONS

Increasing demands on engine efficiency and specific power have resulted in progressively higher loadings on internal combustion engine components. Therefore the durability assessment of such components is increasingly in demand, triggered by both reliability and economic requirements. As power train examples two different engine components have been chosen with different fatigue lifetime requirements. One example is related to the TMF (thermomechanical fatigue) assessment of a modern high power gasoline engine cylinder head designed in the LCF regime with focus in material modelling under TMF conditions. The second example is a crankshaft designed for HCF using a combined MBS (Multi Body System) / FE (Finite Element) analysis allowing the durability assessment for a full engine speed sweep based on modal stress information./DVS 2005/

4.1 Cylinder Head

Thermomechanical fatigue in cylinder heads is often the limiting factor in the conception of new designs. Commonly in diesel and gasoline engines the rapidly increase in power, accompanied by the requirement for reduced consumption levels has led to the demand of increased accuracy in TMF life prediction to ensure field reliability targets, avoiding overdesign and limiting the number of required test runs in order to shorten product development times.

For the cylinder head the main thermomechanical load is caused by the cyclic temperature variation coming from hot/cold cycles induced by the start-stop operation and transient load variation during engine operation. The analysis of thermomechanical fatigue life is a complex task considering the different steps involved in the calculation procedure and is outlined in Figure 4.1.1. The cyclic load is calculated employing a software tool for the analysis of gas exchange, a tool for the three-dimensional simulation of combustion to get local heat transfer information, a tool for the CFD analysis of the water jacket and conjugated heat transfer analysis for the temperature field prediction in the fluid flow and the structure and finally a non-linear structural finite element analysis code.

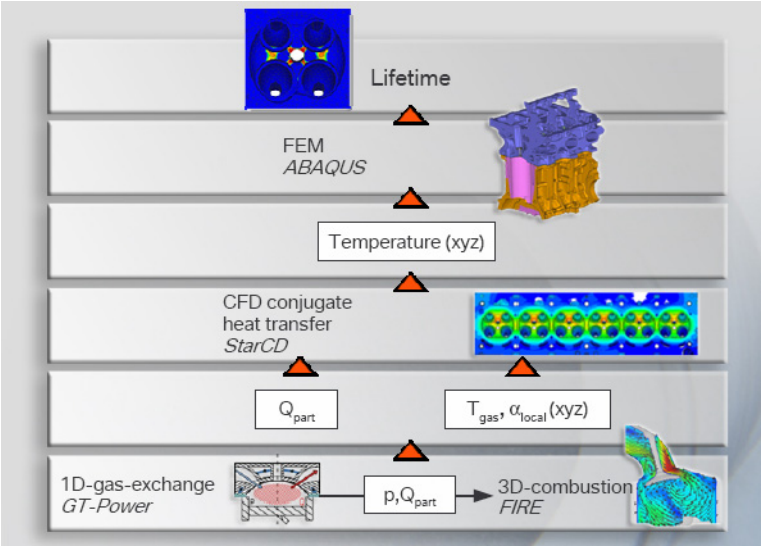


Figure 4.1.1: CAE process for TMF assessment of a cylinder head

The lifing procedure must make use of an integral approach, as the different steps are all strongly interrelated. For application in an industrial context the integration into the product development process has to be possible, i.e. the complexity and resulting computational effort of the constitutive material law have to permit an analysis of a complex structure like a cylinder head with an abundance of degrees of freedom.

The structural FE analysis includes the identification and application of the thermomechanical loading as described before, it requires a constitutive material law for adequate description of the mechanical deformation behaviour, the identification of a parameter for damage accumulation and the lifing criterion itself as outlined in Figure 4.1.2. In addition the mechanical preload condition caused by the assembly loads need to be considered. Critical for success in the prediction is the temperature parameter, hence the correct determination of the temperature field is the crucial step for the life prediction of the cylinder head, as the thermomechanical loading and thus the damage reacts very sensitively on the level and distribution of temperature.

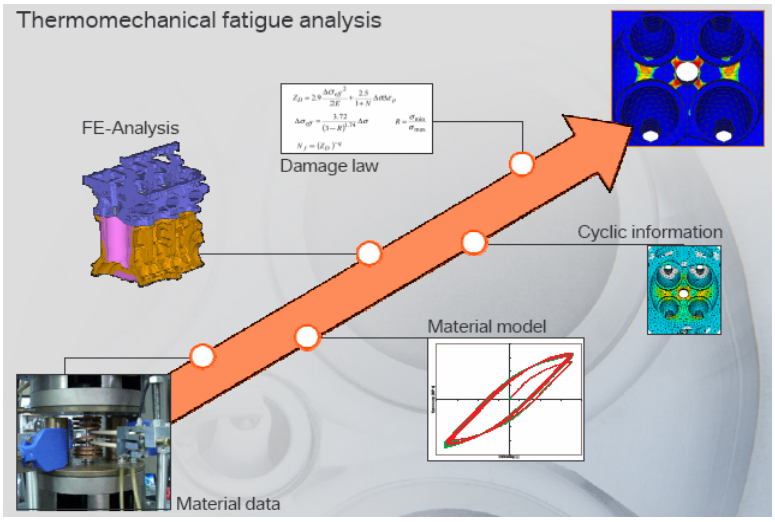


Figure 4.1.2 FE TMF lifetime assessment

The numerical material model is able to account for thermomechanical loading histories, leading to a transient evolution of the material characteristics during the lifetime due to aging in aluminium alloys. Therefore a viscoplastic constitutive model is coupled with an aging model to handle the change in precipitation structure and the effect on the material properties, especially for non heat-treated secondary aluminium alloys. . For the damage description and the life prediction a parameter based on the cyclic J-Integral is used /Fatigue 2002/. In the past BMW has conducted an extensive experimental campaign for the determination of the fatigue characteristics of aluminium-silicon alloys with

different heat treatments and casting processes under thermomechanical loading used in cylinder heads. Cyclic isothermal and anisothermal fatigue tests were conducted in order to calibrate the deformation and lifetime models. Predictions of the ageing model were validated using microstructural investigations and hardness measurements on cylinder heads run under different test conditions. Good agreement was found between measured and calculated lifetimes at the intervalve location for different engines /VPC2005/.

This life prediction for the cylinder head is a good example for a multi-physics and multi-scale problem. On the one side it requires sufficient understanding in the fundamental mechanics of materials, specially the impact of ageing, on the other hand the material modelling needs to be to a level that the analysis of a complex structure is still feasible. Since the accurate prediction of the variable temperature field is crucial for the success, the thermal system understanding is paramount.

4.2 Crankshaft Analysis

The increasing power and torque demands coming from higher engine speeds viz. gas pressure loads result in severely increased loads on the engine crankshaft. Crankshaft have traditionally been designed and assessed for durability in the past using an hybrid approach combining structural analysis, strain gauge measurements and fatigue testing of the crankshaft. The crankshaft loading is estimated from both structural analysis and the use of an instrumented crankshaft tested in an engine. The fatigue endurance test load level in bending viz. torsion give than the margin of safety based on loading equivalence. This factor of safety (FoS) is used to cover the sources on statistical variability, e.g. uncertainties in loading, material/process variability and must be seen in the context of the required level of probability of survival for the crankshaft design. This approach however offers only limited insight into the effects on individual uncertainties. A first improvement in the understanding can be achieved by using a more advanced structural analysis by combining a multi-body analysis (MBS) and FE prior to post processing with a durability software. The variance in input parameters to the numerical model allows to assess the sensitivity and hence robustness of the design.

The current crankshaft design process at BMW is based on a combined MBS/FE analysis combined with a durability analysis of the FE results and is shown in figure 4.2.1 for an inline six spark ignition engine. The crankshaft with its ancillaries (torsional vibration damper TVD, flywheel) is included as flexible body in the crankdrive MBS model. This modelling approach makes the feedback coupling of the component elasticity onto the total system possible. The crankshaft is supported in the mean bearing position with the flexible crankcase using hydro-bearings. The number of degrees of freedom (DoF) of the FE element needs to be reduced ($10^6 \rightarrow 10^2$) to handle the MBS-model which is done using a modal formulation (static-dynamic reduction). With the modal reduction the flexible body is represented in its static deformation modes due to the external loading and its dynamic modes in the relevant frequency range. The static-dynamic reduction is performed within the FE-analysis and provides the modal degrees of freedom (modal shapes) for the MBS analysis. In the case of the crankshaft the element stresses are calculated for each modal shape in addition.

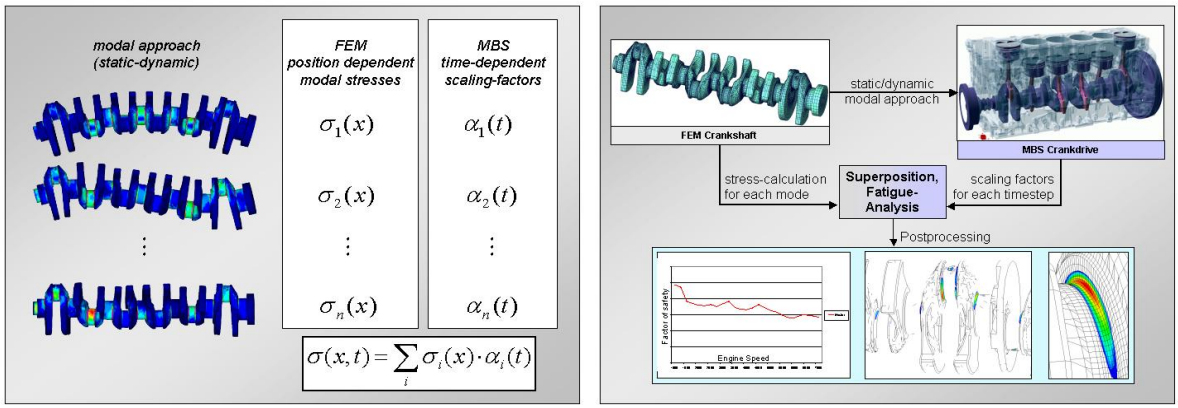


Figure 4.2.1 Combined FE/MBS system

The MBS simulation is currently done or the full engine speed range for the maximum load and the thrust load condition. The post processing is based on the evaluation at discrete engine speeds using the time dependent modal contribution factors of the crankshaft. The deformation and stresses in the crankshaft are calculated for each loading condition of interest using the superposition of the modal shapes with the help of the time dependent modal contribution factors. The multiaxial fatigue assessment of the crankshaft with the commercial tool FEMFAT is based on the superposition of the modal shape stresses, giving Factors of Safety (FoS). With the full engine speed sweep analysis resonances and hence the most critical engine speed/gas load condition can be identified for the full crankshaft.

Using the principle of modal superposition other useful information can be generated. It is possible to calculate modal section forces and moments of the crankshaft. The time dependent section moments can be calculated for the crankshaft webs of interest using the superposition principle. The combination of the maximum allowable bending viz. torsion moment from the experimental fatigue testing with the calculated moment provides the experimental FoS. The strain gauge measurements on the crankshaft during engine testing and calculation of the section moments allows to validate the FE/MBS calculation. In the same context it is also possible to compare stress based FoS from the FE/MBS analysis with the FoS based on loading equivalence using the section forces/moments.

For certain input parameters (e.g. gas pressure loading, gap tolerance variation, lubricant variation) the modal approach provides additional benefits, since it requires only the modification of the MBS model input parameters. The MBS re-analysis will provide the new time dependent scaling factors which then can be re-applied to the position dependent modal stresses. The modal approach can also be extended to calculate the stresses and durability for all other flexible bodies of the MBS model, such as the crankcase, as long as the static-dynamic reduction and the modal stresses are available.

5 TABLES AND FIGURES

5.1 Conference Proceedings

5.1.1 C. Hackmair, S. Mirza, “Fatigue life calculation of structural bonds in body in white manufacturing”, DVS Tagung “Festigkeit gefügter Bauteile”, Juni 2005, Braunschweig.

5.1.2 W.Schmitt, R.Mohrmann, H.Riedel, A.Dietsche, A.Fischersworring-Bunk, ‘Modelling of the Fatigue Life of Automobile Exhaust Components’, Fatigue 2002, Stockholm, Jun. 3-7, A.F.Blom, Ed., EMAS, West Midlands, U.K., 2002, 781-788.

5.1.3 S.Thalmair, H.Mauch, A.Fischersworring-Bunk, T.Brüner, ‘Thermomechanical Cylinder Head Design for the New BMW inline six-cylinder spark ingnition engine’, Virtual Product Conference, Stuttgart, 2005.

5.2 Journal Article

G. Zhang, C.M. Sonsino, „Einfluss der Porosität auf die Schwingfestigkeit von Proben und Bauteilen aus Aluminiumdruckguss“, Materialwissenschaft und Werkstofftechnik, Vol. 35 (2004) Nr.3, S. 125 – 134.

5.3 Dissertation or Thesis

C. Fagschlunger, “Schwingfestigkeit von Aluminium Druckgusslegierungen unter Berücksichtigung von fertigungsprozessbedingten Werkstoffinhomogenitäten“, Dissertation Montanuniversität Leoben (2005).

Lifetime predictions under complex loading for a car application

M. Kaminski[a], P. Kanouté[a], F. Gallerneau[a], J.L. Chaboche[a], S. Kruch[a]

[a]ONERA, DMSE/LCME, Châtillon, France
myriam.kaminski@onera.fr

Abstract Accurate life prediction of metallic components requires to study and take into account spectrum loading nature, multiaxial stress state, anisotropy (initial or induced by damage), dispersion of experimental data… In this paper, the non-linear cumulative fatigue damage model developed by Chaboche is applied on a steel specimen. The purpose of this paper is to demonstrate the ability of the model to predict fatigue life and assess the reliability under spectrum loading. Moreover, a considerable discrepancy in the evaluation of the S-N curve for this material, particularly for high-cycle ranges, can be observed experimentally. This scattering in experimental data is taken into account for the prediction of fatigue life through the concept of the failure probability (P) interconnected with the stress (S) versus number of cycles to failure (N) data. P.S.N (Probabilistic, Stresses, Number of cycles) curves have been generated using the normal distribution function and previous S-N data. Comparisons between the lifetime predictions with the Miner's linear cumulative rule and with the non-linear cumulative fatigue damage model have demonstrated that the non-linear cumulative damage model provides better results than the linear rule but its predictions remain too conservative.

1. INTRODUCTION

The development of safer and reliable designs of mechanical components has led researchers to quantify the fatigue behaviour of materials. Experimental investigations provide frequently a considerable amount of scatter in fatigue data which may be attributed to inhomogeneous material properties, environmental effects ... So, statistic and probability are usually used in the analyse of fatigue data. Weibull [13], first introduced the concept of the weakest link to describe the scatter of the static strength of brittle materials. It was later extented to fatigue behaviour by Freudenthal [8]. More recently, Pascual and Meeker [10] have estimated fatigue curves with a Random fatigue limit model. They have fit the model to fatigue data by maximum likelihood methods and have studied the fits under different distributional assumptions.

The probabilistic fracture mechanics approach results from the combination of fracture mechanics elements and stochastic modeling. Based on the weakest link concept, Delahay and al. [6] have estimated the crack initiation probability in high cycle multiaxial fatigue with a volumetric energy based criterion. Probabilistic models of fatigue crack propagation and their experimental verification have been studied by Wu and Ni [14] and others authors among them, Lin and al [9], Tsurui and Ishikawa [12], Bogdanoff and Kozin [3]. These models include the Markov chain model, the Yang's power law model or polynomial models. Wu has pointed out that the different approaches offered by these models present certain similarities [15].

In this paper a deterministic cumulative fatigue model with a statistical analysis of the experimental data is used. Several types of cumulative fatigue damage models can be found in the literature. Fatemi and Yang [7] provide a review of cumulative fatigue damage theories for metals and their alloys, emphasising the approaches developed between the early 1970s to the early 1990s. They group the theories into six categories: linear damage rules, non-linear damage curve and two-stage linearisation approaches, life curve modification methods, approaches based on crack growth concepts, continuum damage mechanics models and energy-based theories. Among them, models based on strain approaches (Manson-Coffin, Socie, Miller and Brown …) present the advantage of being less sensitive to estimated errors of the non-linearity of the material. Nevertheless, multiaxial complex loading or non-linear damage effects can be more difficult to take into account as well as the effect of the hydrostatic pressure in High Cycle Fatigue. Multiaxial aspects are more easily introduced in stress approaches but need a good knowledge of the stress state in the structure. This paper is concerned with the application of the non-linear fatigue model developed by Chaboche, which will be presented in section 2. In section 3 the determination of the parameters under constant loading is explained. Section 4 illustrates the application of the model to actual fatigue data under complex loading.

2. CUMULATIVE FATIGUE DAMAGE MODEL

The model used in this paper is the non linear cumulative fatigue damage model developed at Onera by Chaboche [4,5] and based on the amplitude and the mean stresses. This stress-based model is revisited in the present study. It allows a correct damage analysis in the whole loading range with, in particular, a correct representation of the mean stress influence on the fatigue life and predicts correctly the remaining life, even below the initial fatigue limit. The model is applied in its uniaxial form :

$$dD = \left[1-(1-D)^{\beta+1}\right]^{\alpha(\sigma_{max},\bar{\sigma})}\left[\frac{\sigma_{max}-\bar{\sigma}}{M(\bar{\sigma})(1-D)}\right]^{\beta} dN \qquad (1)$$

where

$$\alpha = 1 - a\left\langle \frac{\sigma_{max}-\bar{\sigma}-\sigma_l}{\sigma_u-\sigma_{max}} \right\rangle \qquad (2)$$

The symbol $\langle\ \rangle$ is defined as $\langle\ \rangle = 0$ if u<0 and $\langle\ \rangle = u$ if u>0 and $\bar{\sigma}$ corresponds to the mean stress.

$$\sigma_l(\bar{\sigma}) = \sigma_{l_0}(1-b\bar{\sigma}) \qquad (3)$$

$$M(\bar{\sigma}) = M_0(1-b'\bar{\sigma}) \qquad (4)$$

β, M_0, a, b and b' are material dependent coefficients. Their identification is explained in the next section. The function α is a loading dependent function. Its choice is made to obtain a formulation with inseparable variables D and σ which is the necessary and sufficient condition to traduce the non linear damage accumulation.
The number of cycles to failure under constant amplitude loading is obtained by integration of (1) between D=0 and D=1 :

$$N_F = \frac{1}{(\beta+1)(1-\alpha)}\left(\frac{\sigma_{max}-\bar{\sigma}}{M(\bar{\sigma})}\right)^{-\beta} \qquad (5)$$

or

$$N_F = \frac{1}{(\beta+1)aM_0^{-\beta}}\frac{\langle\sigma_u-\sigma_{max}\rangle}{\langle\sigma_{max}-\bar{\sigma}-\sigma_{l_0}(1-b\bar{\sigma})\rangle}\left(\frac{\sigma_{max}-\bar{\sigma}}{1-b'\bar{\sigma}}\right)^{-\beta} \qquad (6)$$

where σ_u and σ_l are respectively the ultime tensile stress and the fatigue limit (expressed in term of amplitude).

For the case of two level tests, the damage D_1 after N_1 cycles at the first level $\Delta\sigma_1$ follows :

$$\left[1-(1-D_1)^{\beta+1}\right]^{1-\alpha_1} = \frac{N_1}{N_{F_1}} \qquad (7)$$

To obtain failure at the second level, the damage law is integrated between D_1 and 1 and leads to :

$$1-\left[1-(1-D_1)^{\beta+1}\right]^{1-\alpha_2} = \frac{N_2}{N_{F_2}} \qquad (8)$$

And finally, $$\frac{N_2}{N_{F_2}} = 1-\left(\frac{N_1}{N_{F_1}}\right)^{p} \qquad (9)$$

with $$p = \frac{1-\alpha_2}{1-\alpha_1} \qquad (10)$$

The exposant p=1 leads to the Miner linear cumulative damage. In this study, according to the expression (2), p≠1 and the cumul is non linear.
Moreover, the model predicts fatigue life even under the fatigue limit. In that case, integrating equation (1) with α=1 leads to

$$N_2 = -N_{F_2}\left(\frac{\sigma_{max_1} - \overline{\sigma}_1}{\sigma_{max_2} - \overline{\sigma}_2}\right)^{\beta} \ln\left(\frac{N_1}{N_{F_1}}\right) \qquad (11)$$

3.IDENTIFICATION OF THE PARAMETERS UNDER CONSTANT LOADING

Constant-amplitude fatigue tests were carried out [11] on a D38MSV5S steel smooth specimen (Kt=1).

3.1 Determination of the coefficients

The model's coefficients β and $aM_0^{-\beta}$ can be easily determined from classical S-N curve (for $\overline{\sigma} = 0$) by plotting $\log\left[N_F \frac{\left(\frac{\Delta\sigma}{2} - \sigma_l\right)}{\left(\sigma_u - \frac{\Delta\sigma}{2}\right)}\right]$ versus $\log\left[\frac{\Delta\sigma}{2}\right]$. The slope of the straight line provides the value of β and the ordinate at $\Delta\sigma/2=0$ provides the value of $(\beta+1)aM_0^{-\beta}$.

The coefficient b reflects the influence of the mean stress on the fatigue limit. Its identification requires two S-N curves with two different stress ratio R.
The coefficient b' is determined from a specific point of another S-N curve (with $\overline{\sigma}\neq 0$, R=0) according to :

$$b' = \frac{1}{\overline{\sigma}}\left[1 - \frac{(\sigma_{max} - \overline{\sigma})\langle\sigma_u - \sigma_{max}\rangle^{\beta}}{\left[(\beta+1)aM_0^{-\beta}\right]^{\beta} N_F^{\beta}\langle\sigma_{max} - \overline{\sigma} - \sigma_{l_0}(1 - b\overline{\sigma})\rangle^{\beta}}\right] \qquad (12)$$

All these coefficients have been determined to fit the best the experimental data. Their values are given in the following tables.

Table 1. Parameters of the raw steel D38MSV5S

B	$aM_0^{-\beta}$	b $(MPa)^{-1}$	b'
3,25	$6{,}23.10^{-14}$	$1{,}5.10^{-3}$	$4{,}5.10^{-4}$

The S-N curve can then be set out (see Figure 1) using Eq. 5 where curves and triangles refer respectively to the analytical results and the experimental data.

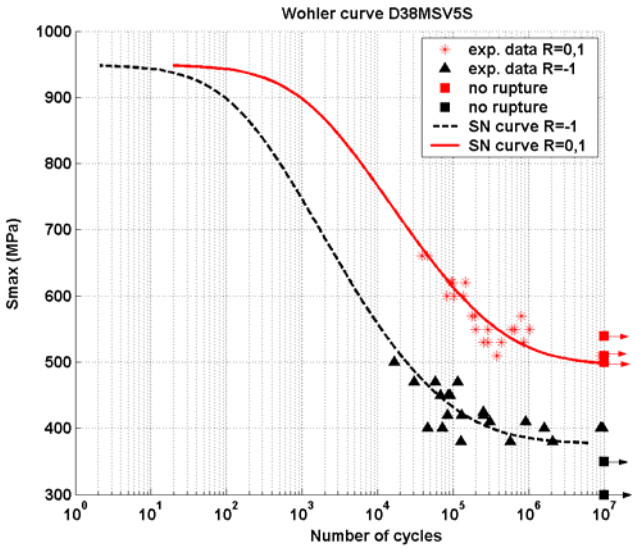


Figure 1. S-N curve for the raw steel D38MSV5S.

The Wöhler curve of the D38MSV5S determined for the stress ratio R=-1 will be henceforth called "reference curve" in the following parts. Nevertheless, the dispersion of experimental data prevents from an accurate evaluation of the parameters.

3.2 Dispersion of the experimental data

An important scatter in the experimental data can be seen under constant amplitude loading as shown in Figure 1. Actually, for a given stress level, the ratio between the maximal and minimal value of the number of failure cycle can exceed 10. This scatter can be due to the heterogeneity of materials, superficial defects, metallurgical factors, etc. In a probabilistic concept, the S-N curve represents the border separating the domain where the failure is unlikely to happen (on the left of the curve) than the one where it is more likely (on the right of the curve). In the following, the dispersion is treated through the concept of the failure probability (P) interconnected with the stress (S) versus number of cycles to failure (N) data.

3.2.1 Stress distribution

This subsection is concerned with the determination of the stress distribution of the available experimental data. For that, the first stage consists in treating the experimental data i.e. determining the amplitude stress level of each experimental data corresponding to a fixed value of N_F (N_F =2.10^5 in that case). It implies to determine the amplitude stress level σ^{ref}_{max} for the reference curve at N_F and to calculate $(\Delta\sigma)_i$ corresponding to the difference between the amplitude stress level of the experimental data i (1<i<n where n is the number of the experimental data) and σ^{ref}_{max}. It amounts to a vertical translation of the reference SN-curve of $(\Delta\sigma)_i$ (see Figure 2). Therefore, each curve passing through each experimental data is built so as :

$$N_F = A' \frac{\left(\sigma_u \pm (\Delta\sigma)_i - \left(\sigma^{ref}_{max} \pm (\Delta\sigma)_i\right)\right)}{\left(\sigma^{ref}_{max} \pm (\Delta\sigma)_i - \left(\sigma_l \pm (\Delta\sigma)_i\right)\right)} \left(\sigma^{ref}_{max} \pm (\Delta\sigma)_i\right)^{-\beta} \qquad (13)$$

with $A' = \frac{1}{(\beta+1)aM_0^{-\beta}}$ determined for each curve by specifying N_F=2.10^5 cycles.

Then, the amplitude stress levels corresponding to N_F are used for the following probabilistic study.

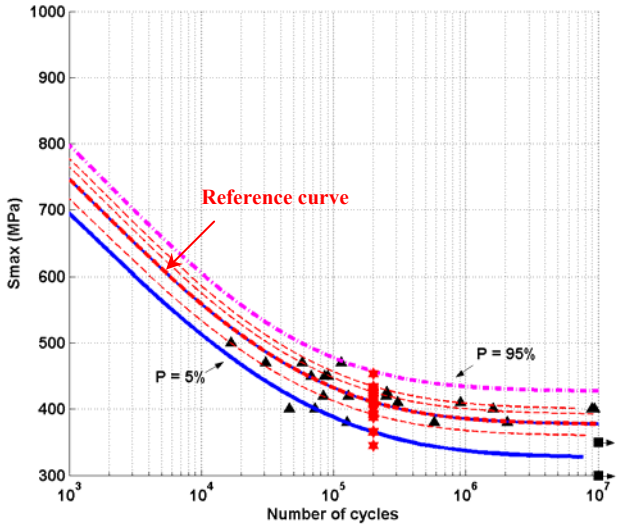


Figure 2. Construction of the different curves passing through the whole experimental data (triangles) and determination of the amplitude stress levels corresponding to N_F (stars).

3.2.2 Failure probability

Once the whole of the experimental data has been treated according to the previous method, it is possible to calculate the mean value μ and the standard deviation s according to the normal law and to determine the failure probability for each curve. This probability results from the application of N cycles at the stress amplitude level σ and is represented as a function F(σ,N).
Assuming this function varies as the integral of the Laplace-Gauss distribution :

$$F(\sigma_{max}, N) = \int_{-\infty}^{+\infty} \frac{1}{s\sqrt{2\pi}} \exp\left[\frac{(\sigma_{max} - \mu)^2}{2s^2}\right] d\sigma_{max} \qquad (14)$$

The assumption of a normal distribution is validated in Figure 3 on which the curves and circles refer respectively to the analytical and the experimental results. The normal distribution function fits well to the experimental data.

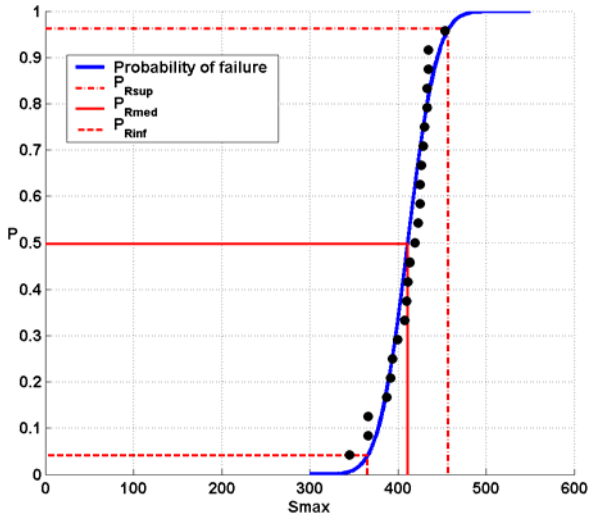


Figure 3. Failure probability P versus S_{max} according to the stress distribution.

The reference S-N curve in solid line on Figure 2 corresponds to a failure probability of about 50%. The PSN curve represented with dash-dot line corresponds to a probability of about 95% and the dashed line to a probability of 5%. The standard deviation s is equal of about 26 MPa which amounts to translating the reference curve of about $\Delta\sigma = \pm 1{,}73s = \pm 46$ MPa.

4. APPLICATION OF THE CARLOS LOADING

This section presents the numerical results obtained under the complex CARLOS loading. The CARLOS (CAR LOading Standard) sequences, filtered or not, are used for car applications and are assumed to be representative of the stress history (vibrations, impacts, ...) supported on the road. This complex sequence needs a Rainflow analysis [1] to extract the characteristic cycles (amplitude, mean stress, ...) related to the closed hysteresis loops in the stress-strain plane. The CARLOS sequence is composed of 95 180 cycles. Figure 4 presents an extract of this loading.

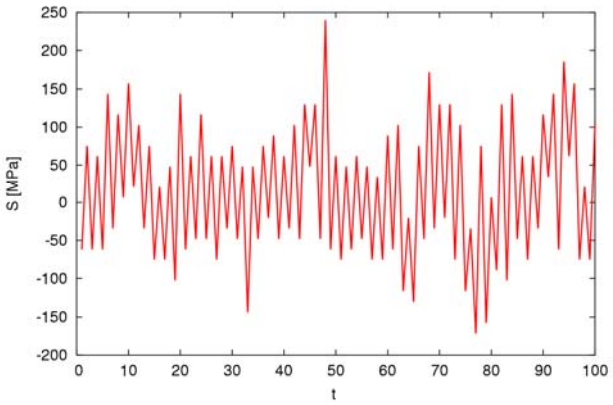


Figure 4. Part of the CARLOS loading.

4.1 Linear cumulative results vs. non linear cumulative results under complex loading

Once the parameters of the model have been determined under constant amplitude levels, predictions of lifetime under complex loading do not require furthermore parameters. Figure 5 presents the experimental data obtained under the CARLOS loading for different stress levels. Tests under this complex loading have been realised by the partners of the Working Group GT1 of the SF2M (French Society for Metallurgy and Materials).

These data are very scattered, particularly in the low-stress domain. The lifetime predictions obtained with the non linear cumulative model are represented in Figure 5. The results considering a linear cumulative damage rule are also reported in this figure.

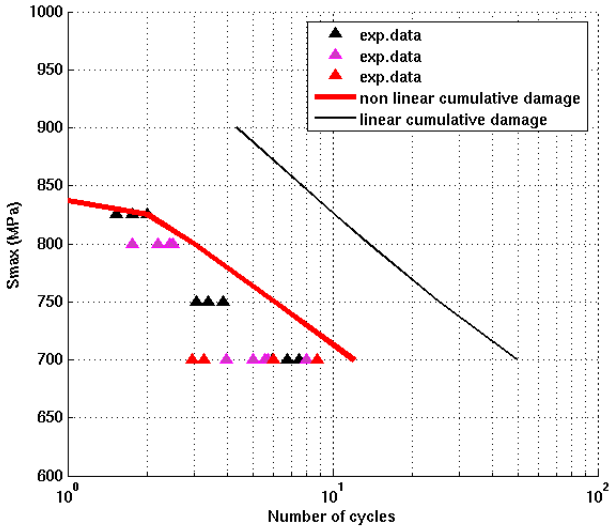


Figure 5. Experimental results (triangles) under CARLOS loading for different stress levels.

It can be observed that the linear cumulative damage rule gives about four times more optimistic predictions (straight thick line) than the non linear one (straight thin line). The introduction of the non linearity in the model improves significantly the results.

On Figure 6 are plotted the curves with the failure probability of 5% et 95% for the two models.

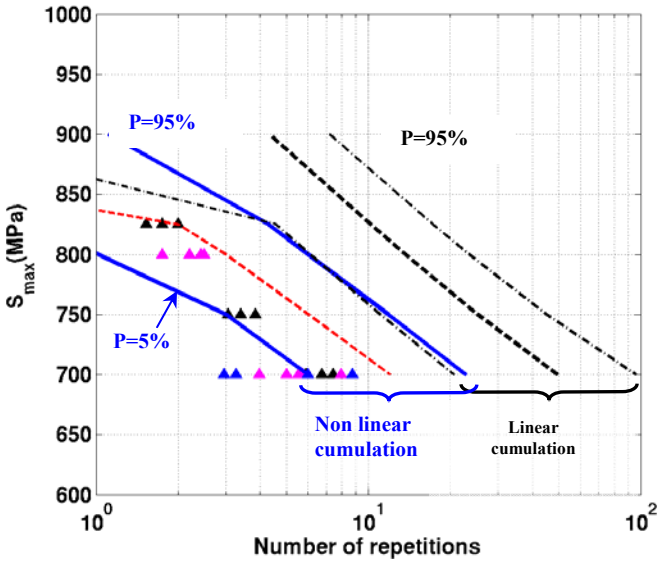


Figure 6. Comparisons between linear and non linear cumulative damage model predictions.

For the lower stress levels the predictions with the non linear model remain too much optimistic. This model could be improved by introducing a new parameter in the expression of the non-linearity α in order to increase its effect. Besides, numerical predictions considering the linear cumulative damage rule but assuming no fatigue limit for the material have been performed (see Figure 7). The lifetime predictions of the linear cumulative damage have been improved with no fatigue limit but not enough to agree with the experimental results.

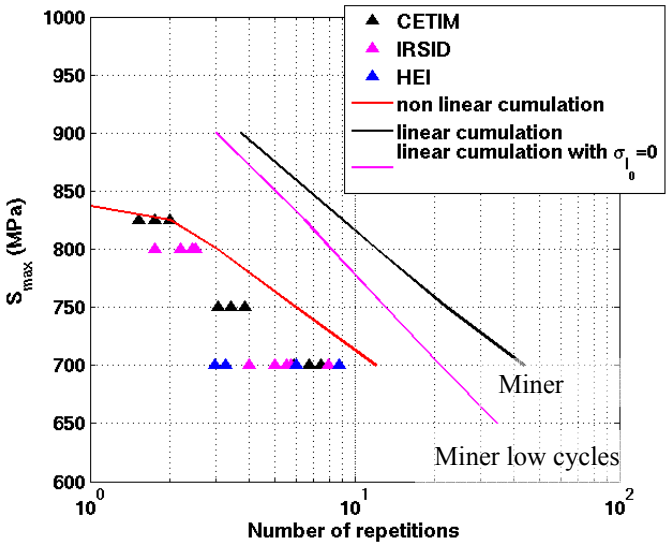


Figure 7. Lifetime predictions of the linear model with no fatigue limit.

CONCLUSIONS

The dispersion of the experimental data has been taken into account by determining the PSN curves (95% and 5% of failure) through a normal distribution function. Numerical results of lifetimes obtained with the non-linear cumulative damage model and the linear damage rule have been compared. It is pointed out that the results obtained under complex loading with the non-linear damage model are better but remain too optimistic (a ratio of 5 between predictions and experimental data for the lowest stress level considered). The non linear cumulative damage model may be modified in order to increase the effect of the non linearity.

An important advantage of this model is that it is not necessary to make a new identification of the parameters for an application under the complex loading once they have been identified and validated under constant loading.

REFERENCES

[1] Amzallag C., Gerey JP, Robert JL, Bahaud J. 1994, June. Standardisation of the Rainflow counting method for fatigue analysis, *Fatigue*, Vol.16, pp.287-293.
[2] Bleuzen C. et al. Validation of life prediction models from representative testing on aluminium alloy specimens, *Proceedings of the seventeenth ICAF (International Committee on Aeronautical Fatigue) Symposium*, Stockholm, Sweden, June 9-11, 1993.
[3] Bogdanoff JL., Kozin F. Probabilistic models of cumulative damage. New-York, Wiley, 1985.
[4] Chaboche. 1974. Une loi différentielle d'endommagement de fatigue avec cumulation non linéaire, *Extrait de la Revue Française de Métallurgie*, n°50-51, pp.71-82
[5] Chaboche. 1986. On the non linear fatigue damage accumulation, *International Conference on Steel Structures,* ONERA TP 1986-121, Budva.
[6] Delahay T and al. Estimation of the crack initiation probability in high cycle multiaxial fatigue with a volumetric energy based criterion, *Seventh International Conference on Biaxial/ Multiaxial Fatigue and Fracture*, June, 26 – July,1 2004, Berlin.
[7] Fatemi A, Yang L. 1998. Cumulative fatigue damage and life prediction theories : a survey of the state of the art for homogeneous materials *Int. J. Fatigue,* Vol.20, No.1, pp.9-14.
[8] Freundenthal AM. Statistical approach to brittle materials, *Fracture*, 2, 1968, pp.591-619.
[9] Lin YK, Wu WF, Yang JN. Stochastic modelling of fatigue crack propagation. Probabilistic methods in mechanics of solids and structure, Berlin : Springer, 1985, p.103-110 .
[10] Pascual FG, Meeker WQ. Estimating fatigue curves with the random fatigue-limit model, *Technometrics,* Vol.41, No.4, p.277-302, Novembre 1999.
[11] SF2M, Fatigue Committee, Working Group GT1 "Fatigue sous chargement d'amplitude variable"
[12] Tsurui A., Ishikawa H. Application of Fokker-Planck equation to a stochastic fatigue crack growth model. *J Struct Safety*, 1986, 4 : 15-29.
[13] Weibull W. A statistical theory of the strength of material, *Royal Swed. Inst. For Eng. Res*., 1939, 151.
[14] Wu WF. 1986. On the Markov approximation of fatigue crack growth. *Proban Engng Mech* 1, 224-233.
[15] Wu WF, Ni CC. 2004. Probabilistics models of fatigue crack propagation and their experimental verification., *Probabilistic Engineering Mechanics* 19 247-257.
[16] Normalisation française, Produits métalliques, Essais de fatigue, *Traitement statistique des données Afnor A03-405* Sept.91

System behavior and fatigue strength under operational conditions of modern fuel injection systems and braking systems

M. Bacher-Höchst, A. Scheffold
Robert Bosch GmbH, Corporate Research and Advance Engineering, Stuttgart (Germany)

Abstract: Due to the wide variety of functions of modern fuel injection systems and braking systems of motor vehicles the complexity degree of these systems is increasing. This has a large effect on the reliable dimensioning of the components, because the particular short periods of development require an early assessment of the component reliability in the system group. By example of components of the diesel direct injection systems as well as components of braking systems the proceeding of the lifetime assessment will be presented.

Keywords: Fuel injection systems, braking systems, fatigue strength under operational conditions, fatigue life assessment, fatigue test

1. INTRODUCTION

Mechatronical systems are characterised by a high degree of complexity based on the networked interaction of various fields of engineering science. This attribute requires the processes of system development and reliability assessment in equal measure. Only a real-time close cooperation of functional development and component realisation – beginning in the virtual (simulated) system up to the “final” release – makes market-oriented and competition-oriented conversion possible. Moreover, the mass-production in automobile technology requires an early specification of production concepts and, consequently, has to take these concepts into account in the early development phases.

An overview of systems in today’s automobiles makes it evident that we are currently in the “Middle Ages of Mechatronics”. The first series launch of ABS systems in 1978 and ASR systems in 1987 by Robert Bosch GmbH can definitely be considered as milestones. Even at that point of time, the fatigue strength of the pressure components led to critical questions related to the pressure spectra strongly influenced by system behaviour, vehicle application, driving route and its state, as well as on the drivers.

The following will give an insight into the problems in today’s mechatronic systems starting from the classical concepts of fatigue strength.

2. THE NOMINAL STRESS CONCEPT FOR FATIGUE STRENGTH DESIGN OF COMPONENTS IN THE DIESEL INJECTION SYSTEM “COMMON RAIL”

The Common Rail (CR) system for diesel fuel injection (see **figure** 1) contains a series of sensors and actuators and can, thus, be called a typical mechatronic system. The sensors are used to collect current data about the engine operating point and environmental conditions. The actuators are, for example, the injectors, the metering unit and the pressure control valve, and are energised or actuated by the Electronic Control Unit (ECU).

The fatigue fracture-proof (service strength) design of highly stressed components of the CR system in Robert Bosch GmbH is carried out according to the nominal stress concept in connection with the relative Miner rule [**1**].

The significant components of the nominal stress concept are:

- Component Woehler-Test rsp. S/N-Curve
- Load spectrum measured in system environement
- Component lifetime assessment by fatigue test under operational conditions rsp. operational load spectrum

2.1 Component S/N-Test

The fatigue strength of highly loaded diesel injection components is generally determined using pulsating tests by internal pressure (stress ratio R = 0). Critical locations for failure typically occur at bore intersections (see **figure 2**) with high stress concentrations.

The component S/N-line (see **figure 2**) can be derived for different failure probabilities (P_A) using statistic evaluation of the test results. Normally, the log-normal distribution is outlined as distribution function.

The execution of S/N-tests on the specimen parts takes place during the development phase. Thus, the definition of samples at tolerance limits is complicated because of the complex geometry and the scatter of material state and production processes.

Common Rail components are manufactured in series in large quantity. The quality control for fatigue strength is supported by fatigue strength tests accompanying series production. This allows, among others, a comparison of the fatigue strength between the specimen parts and series production.

The large number of components in S/N-tests till now provides a good estimation of the scatter by help of the concept of “Normalised Woehler Line” [**1**] or by statistic evaluation of scatter stresses described in [**2**]. The scatter stresses thus determined are a reliable data basis for a good prediction regarding the failure probabilities expected in the field.

2.2 Determination of Representative Load Spectra

A significant characteristic of mechatronic systems is given by the fact that the function and flexibility or differentiation of the product is defined by the software, which can finally have a decisive influence on the load population.

In the case of CR system, the expected load spectrum can change significantly by the engine and car application used. In this context, the simulation of load spectra has an increasing significance, because, with this, the effect of different parameters can be examined in a fast and cost-effective manner [**3**]. With this, the possible influence influence of software changes to fatigue lifetime can be assessed immediately.

Additional functional enhancements in the existing mechatronic injection systems (e.g. multiple injections) may further intensify the load population.

The determination of design-relevant load populations can be carried out only using on-road vehicle measurements at present. The test track defined by Robert Bosch GmbH for load population measurement is divided into city, interurban and highway drive. The ratios, among themselves, correspond to the evaluation shown in [**4**]. The final track structure for the load population measurement is decided in consensus with the customer.

The vehicle is equipped with the common rail system with multiple pressure sensors (see **figure 3**). In addition to the pressure signals, other variables are measured like accelerator pedal position, engine speed, etc. The preparation, execution and evaluation of the measurements require a lot of time and technical effort. The measured data are classified with commercial software packages according to the rain-flow method.

A typical pressure-time signal is shown in **figure 4**. It can be clearly seen that the pressure variations with large stress range are limited in their number, which finally ensures a service strength design. **Figure 5** shows the stress-pair representation of the load population. Here the stress cycles, resulting from injection, and the stress cycles, resulting from change in the load point (e.g. acceleration and braking process) can be differentiated.

A load population measurement is carried out for every new application.

2.3 Fatigue Test at Service Loading

Fatigue strength tests under service load are carried out to determine the tolerable amount of fatigue caused damage. Here the significant aspect is the knowledge of the load-time sequence expected during the lifetime and its frequency distribution. The measures for shortening the test time must be undertaken in order to reach a result within acceptable time. Possibilities for these measures are discussed in [**5-7**].

To shorten our test time we use the “Omission”, i.e. the neglecting of not damaging low stress amplitudes, and in general the increase of amplitudes to shorten the test time until fatigue fracture.

Figure 5 shows a typical spectrum in the stress-pair representation. Small stress cycles are neglected for the fatigue strength test (Omission, see **figure 6**). The effect of the mean load is taken into consideration by amplitude transformation [**1**]. The neglected stress cycles are clearly smaller than half of the fatigue strength (steel components) and need not to be considered as damaging, also taking into account that normally no corrosion is expected in the operation of diesel injection systems loaded with internal pressure [**1**, **8**].

The load amplitudes are increased proportionally over the service level for further shortening of the test time. This can be carried out, as long as no plastic transformations are induced in the component, causing compressive internal stresses resulting in an increase of lifetime. Here the objective is to commit the maximum load value in a way that the mean number of cycles to failure reaches some millions of stress cycles (iterative process).

A subsequence for the test normally includes multiple thousand stress cycles. This spectrum is transformed by rainflow reconstruction in a time sequence with random distribution. This subsequence is run through frequently until fracture at several millions of stress cycles, which leads to a very good mix.

All measures for shortening the test time can be applied only when the fracture location and the damaging process remain unchanged in the experiment and under service conditions.

The fatigue strength tests carried out on the components of injection systems loaded with internal pressure show a quiet small scatter of the tolerable amount of damage. Accompanying fatigue strength tests in the laboratory maerial specimen should expand the database with reference to the scatter of the tolerable amount of damage.

2.4 Relative Miner Rule

The component S/N-tests are carried out under pure pulsating load (R = 0). The load in operation is however $R \neq 0$. Due to this reason all the amplitudes of the rainflow matrix are transformed to R = 0 with the help of Haigh-Diagram [**1**], before carrying out the damage accumulation.

The damage was evaluated with the linear damage accumulation hypothesis according to Palmgren-Miner. Stress cycles below the fatigue strength are evaluated with the suggestion by Haibach [**1**].

In case of relative Miner rule, it is assumed that the fatigue fracture occurs only in very few cases at an amount of damage sum D = 1. Hence, the tolerable amount of damage must be determined in the fatigue strength test under service load spectrum in an experimental manner (see chapter 2.3). This process corresponds to the basic idea of a calibration: The lifetime of the component A is known, the lifetime of the component B should be predicted. Good predictions can be achieved only when both the components have similar prerequisites with reference to the material, local geometry and form of load spectra.

2.5 Statistic Determination of the Failure Probability

The safety proof of the highly stressed injection components requires the specification of an arithmetic possibility of failure by fatigue fracture. Firstly the safety factor j_N is determined based on the procedure described in **figure 7**. Now the failure probability expected in the field can be assessed with the help of the process documented in [**1**] while involving the known safety factor j_N, assumed log normal distribution and the derived lifetime scatter known from fatigue strength tests.

The requirements of Robert Bosch GmbH normally expect a total failure probability against fatigue fracture lesser than 1 ppm (10^{-6})*[1] for the safety-relevant components. Continuous functional operation tests are carried out along with the above-mentioned tests. These in turn round off the design concept.

Positive field experiences confirm the design strategy presented here. Using the process in the hydraulic aggregates for the anti-blocking and traction control system shows good results [**5**].

3. DESIGN AND PROOF OF COMPLEX LOADED COMPONENTS OF DIESEL INJECTION TECHNIQUE

CR-injection systems, currently in series production, are being further developed for further reduction in fuel consumption, emission and noise characteristics in the modern diesel engines providing the same performance, power and dynamics as far as possible.

The valve technology in the injectors takes special importance in the further development. Solenoid valves are replaced by faster switching piezo-driven valves in the new generations of CR systems [**9**]. The piezo actuators responsible for stroke are not fuel-resistant and thus must be sealed. The convoluted bellows shown in the **figure 8** can be deployed as moving sealing elements.

The convoluted bellows are produced by internal high pressure transformation on the drawn pipes and have extremely small wall thickness. There occurs an inhomogeneous strengthening state due to the cold forming process and the related local plastification.

The target development of convoluted bellows can be realised only by using an integrated approach, where the material development, component design and processing technology is taken into consideration. Degree of material purity becomes all the more important with reference to lifetime due to the low wall thickness.

The convoluted bellows deployed in CR injector experience a combined stress from pressure and axial stroke in operation. Here the number of stress cycles, which are considerably larger than 10^8 are to be taken into consideration for design.

The fatigue strength proof can only be fulfilled on experimental basis due to the complex external load; nominal stress concept usage can not be used here. Due to this reason a combined reconstruction test was defined. The safeguarding of the high number of stress cycles from the axial stroke was realised by piezo actors stroking the convoluted bellow, which realized a high load frequency. Here the synchronisation of stroke and pressure collective was specifically important.

4. DERIVATION OF TEST COLLECTIVES FOR ALUMINIUM BRAKE CALIPERS

Increasing trend of light construction in the automobile constructions can also be seen in the brakes division, where aluminium material is increasingly put into use. Especially in case of brake caliper, cast iron materials can be replaced by significantly lighter aluminium alloy.

The service strength design has contributed to the idea of light construction. However, in case of aluminium brake calipers, only the calculated lifetime estimation does not lead to the desired results due to the complex external stress caused by internal pressure and torsion under conditions of temperature and corrosion. The fatigue strength proof test is thus generated in the combined reconstruction test. Specifications for the lifetime proof are compiled [**10**] in the VDA workgroup for brakes (“AK-Bremse”), which consists of representatives from german automotive industry and brake suppliers. Here, two different load spectra with and without traction help (ASR) are recommended.

The derivation of test spectra should be demonstrated in the example of an aluminium brake caliper for electro-hydraulic brake (EHB, [**11**], s. **figure 9**).

*[1] The value 10^{-6} is an arithmetic value and does not mean that one component out of 10^6 will fail. No failure can be expected as long as load capacity and loading correspond to the allocated status of the tests.

Simulation test benches are used in Robert Bosch GmbH for determining near-service pressure-load collectives. These test benches operate all hydraulic brake components in a software environment (Hardware-In-The-Loop (HIL)). Thus near-reality load collectives are obtained with pressure sensors at different points in the braking system. The basis for the HIL-operation are the guidelines of “AK-Bremse” added by data of corresponding vehicle measurements. **Figure 10** shows a comparison of the load collectives according to “AK-Bremse” (supplemented by an internal "pre-drive check" (PDC)) compared with those from the HIL continuous operation for the electro-hydraulic brake. The collectives defined in “AK-Bremse” as brake retardation values were converted into pressure load values. In **fig. 10** the lower collective maximum value of the electro-hydraulic brake and the higher level of fullness can be clearly detected. This has its reasons in ABS and ESP control processes as well as additional functions like the auxiliary brake assistant. The comparison further shows that due to the increasing number of additional functions, the spectra proposed in the “AK-Bremse” are not conservative in all the cases.

The pressure load collective for the reconstruction test as presented in the **figure 11** was derived from the load measurements. Here the omission level recommended in “AK-Bremse” was taken into consideration. A critical observation of different omission levels for the spectra from “AK-Bremse” brake is contained in [**12**]. In addition to the pressure load sequence in the reconstruction test there has to occur a defined temperature cycle as well as the cyclically imposed 5% NaCl solution (see **figure 11**).

5. PROSPECTS

In this paper the demonstrated methods for assessing safety-critical fatigue loaded components are mainly based on experimental data. The deployment of simulation should be further intensified specifically in the design phase. Here material and production process influences on strength are to be considered while predicting fatigue strength or lifetime, in order to improve accuracy of simulation in the future [**13**]. The complete system characteristics induced by mechatronics are to be displayed in the simulation for predicting the load spectra. Here the limits of today’s simulation tools become clear, including the required computer performances.

The design methods for the fatigue strength dimensioning of safety-critical components need further refining. Here it is required to increase the inclusion of scatter influences on the fatigue strength in the design concepts. This allows a target component design without “over design” and safety risk at the market-driven prices. The processes for reliability evaluation of “faulty” material and surface states have a special significance here.

Other increasing requirements in the engine development with reference to consumption, legal and environmental prerequisites require continuous increase in the injection pressures even in the future. Appropriate measures for increasing the fatigue strength of components in the injection technology are currently under development, verification and transformation for a large-scale technical production.

The estimation of the field failure probability with reference to a fatigue fracture of individual components independent of each other can be considered as current technological state - taking into account the severe problem fields outlined in this contribution. However, it is not at all routine to quantify the system reliability of similar high complex mechatronics systems. This should be possible in the future, where even the corresponding scientific background must be improved.



Figure 1: **Common Rail System**

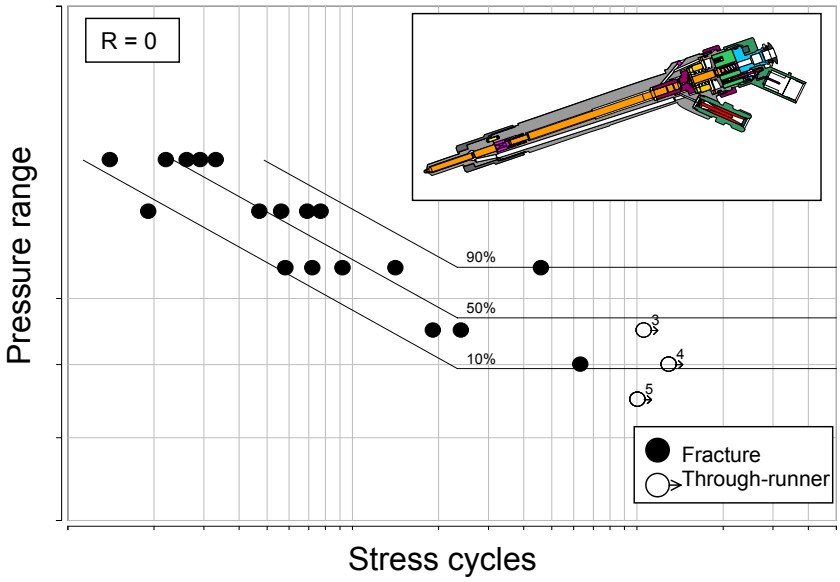


Figure 2:
Woehler Test on Common Rail Components

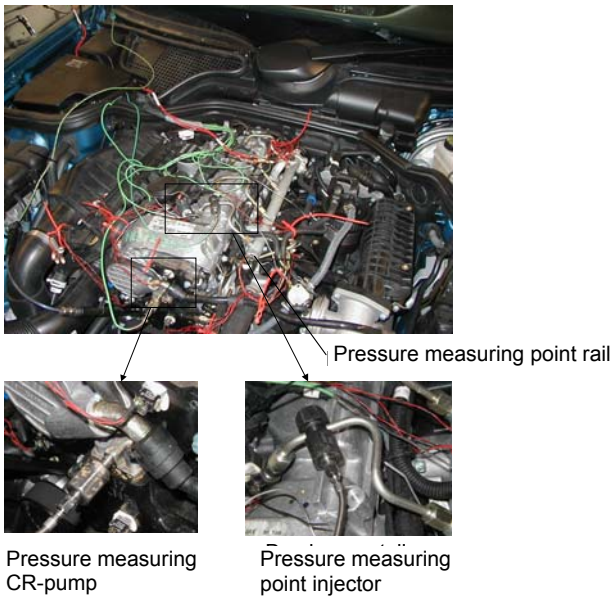


Figure 3:
Instrumented Common Rail System in the Vehicle for Load Spectrum Measurements

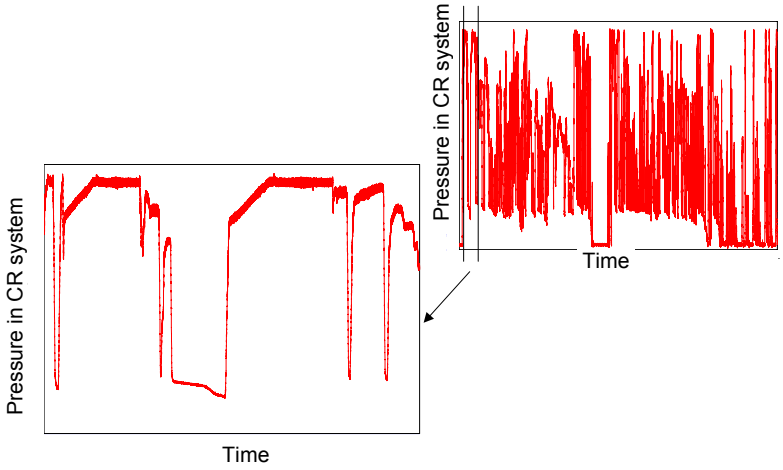


Figure 4: Pressure-Time Sequence Derived From the Load Spectrum Measurement

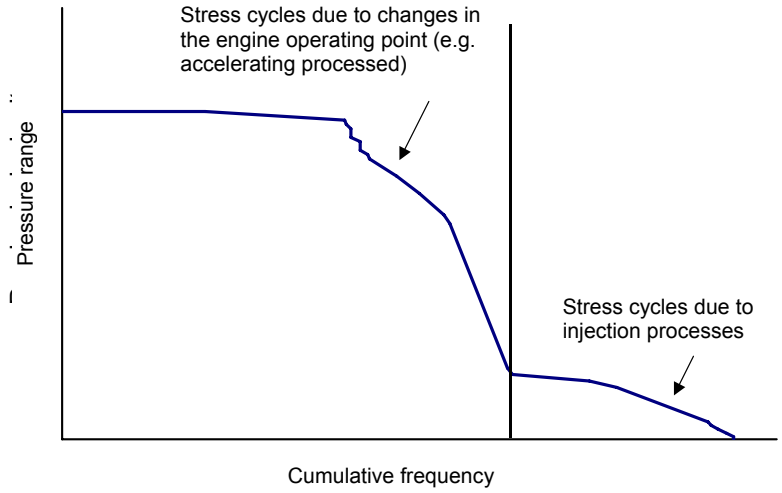


Figure 5: Stress-Range Representation of the Design Spectrum

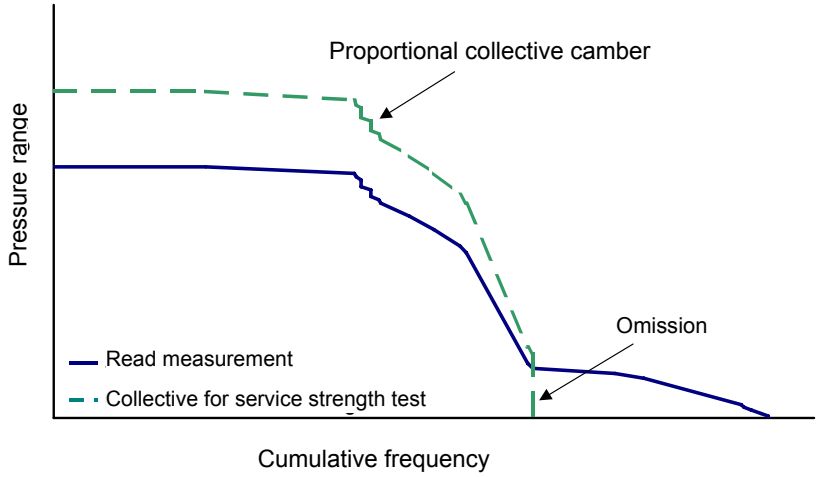


Figure 6: Measures for Shortening the Test Time in the Fatigue Strength Test

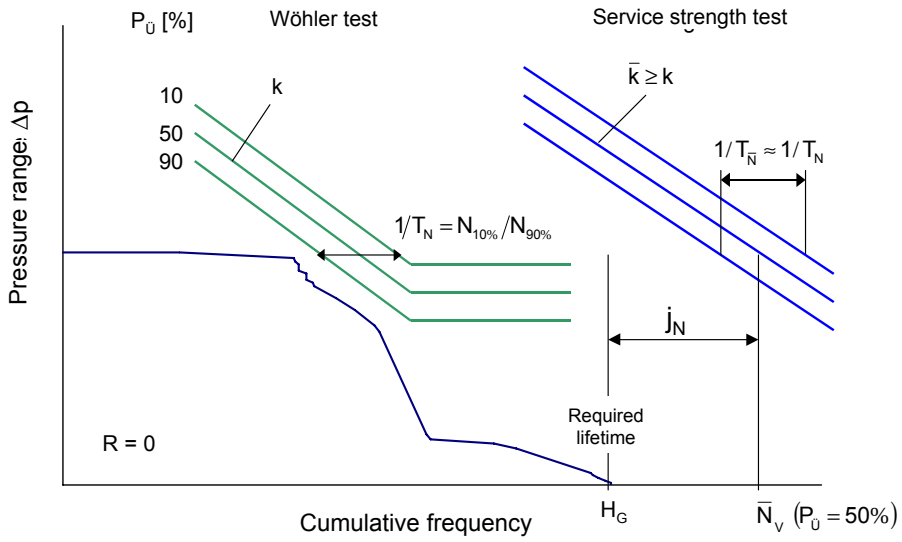


Figure 7: Fatigue Strength Proof for Common Rail Components

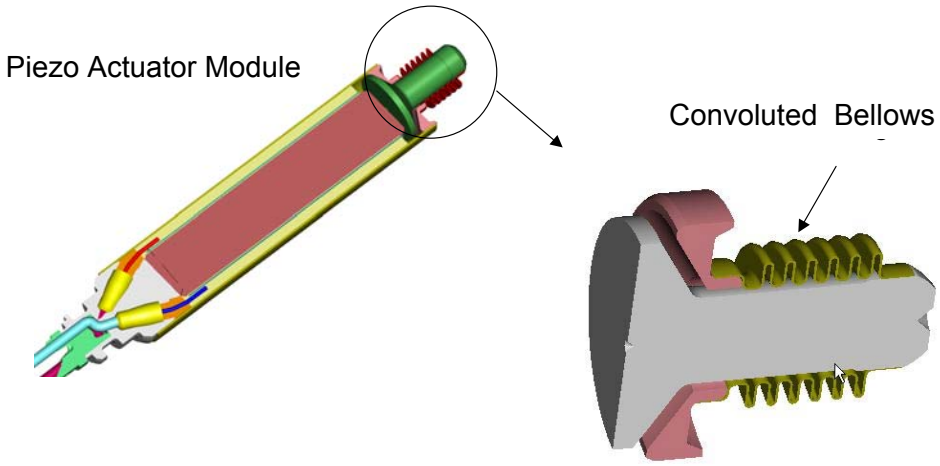


Figure 8: Convoluted Bellows in the Piezo Injectors (comp. [9])

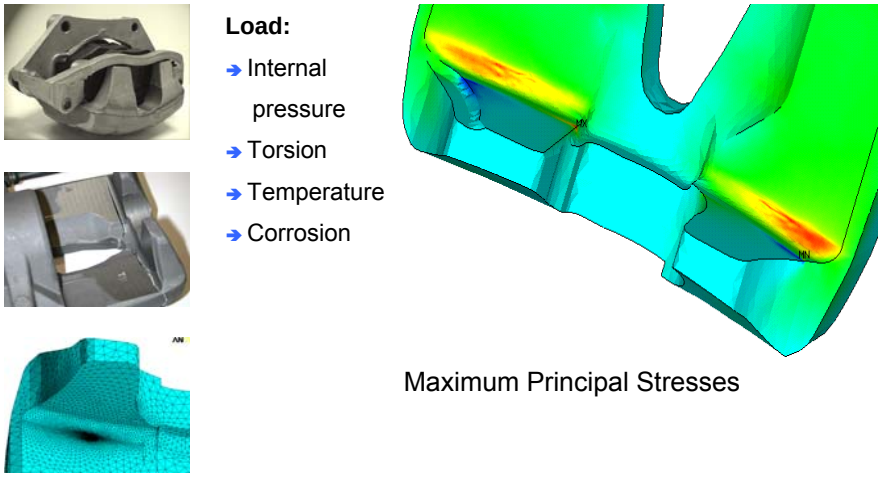


Figure 9: Aluminium-Brake Caliper in Electro-Hydraulic Brake System

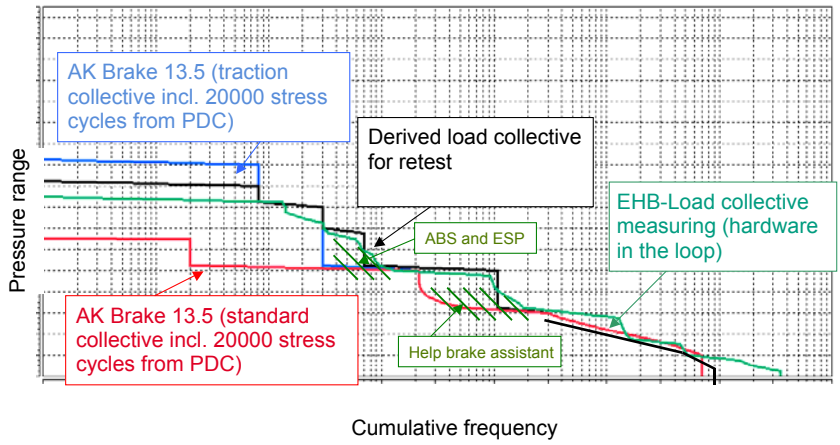


Figure 10: **Comparison of Different Load Spectra According to VDA-Standard "AK-Bremse" and Hardware-In-The-Loop Measurement Data**

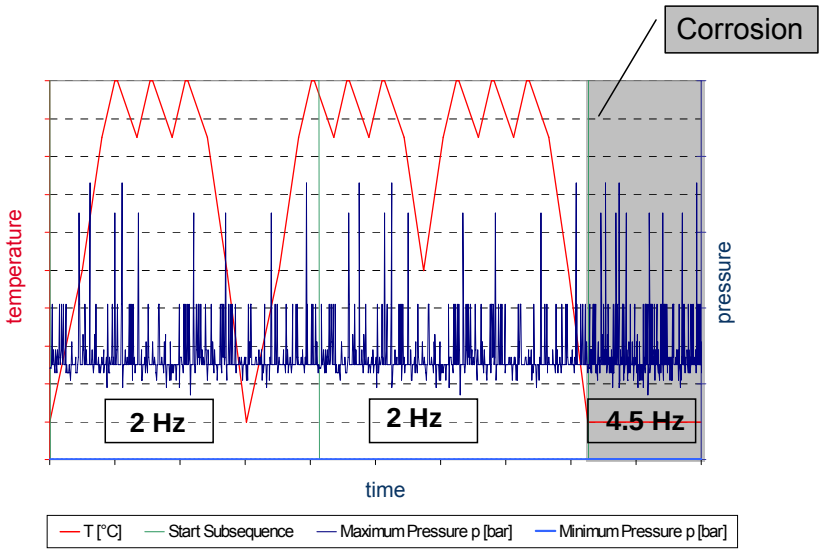


Figure 11: **Load-Time Sequence for Combined fatigue Proof Test for Aluminium Brake Calipers**

6. LITERATURE

[1] E. Haibach
Betriebsfestigkeit – Verfahren und Daten zur Bauteilberechnung, VDI Verlag, Düsseldorf (1989)

[2] R. Adenstedt
Streuung der Schwingfestigkeit, Dissertation, TU Clausthal (2001)

[3] D. Ulrich, B. Bertsche
Simulation von Lastkollektiven für das Diesel Common Rail System,
Berichtsband zur 30. Tagung des DVM-AK Betriebsfestigkeit (2003)

[4] R. Krüger, U. Fahl, A. Voß
Alternative Kraftstoffe und Antriebe – ein Weg zur Minderung der Kohlenwasserstoffemissionen? ATZ Automobiltechnische Zeitschrift 100 (1998)

[5] M. Bacher-Höchst, C.M. Sonsino
Methodik zur sicheren und wirtschaftlichen betriebsfesten Auslegung von Komponenten in ABS/ASR-Bremsystemen, Berichtsband zum DVM-Tag (1997)

[6] H. Oppermann, W. Lipp
Möglichkeiten der Lebensdauerabschätzung im Bereich hoher Lastspielzahlen. In: O. Buxbaum, Vorträge des vierten LBF-Kolloquiums am 31. Januar und 1. Februar 1984 in Darmstadt, Frauenhofer-Institut für Betriebsfestigkeit (LBF), Bericht Nr. TB-171 (1984), S. 57 – 77

[7] H. Oppermann
Zulässige Verkürzung zufallsartiger Lastfolgen für Betriebsfestigkeitsversuche. In: O. Buxbaum, Vorträge des fünften LBF-Kolloquiums am 8. und 9. März 1988 in Darmstadt, Bericht Nr. TB-180 (1988), S. 31 – 49

[8] P. Heuler, T. Seeger
Criterion for Omission of Variable Amplitude Loading Histories. Int. Journal of Fatigue 8 (1986) No. 4, S. 225 – 230

[9] K. Hummel, K. Krieger, N. Hansen
Evolution of the Bosch Common Rail System for passenger cars, Konferenzbericht zum ATA-Symposium ‘The Future of Diesel Engine Technology for Passenger Cars‘ (2000)

[10] VDA-Arbeitskreis Bremse im Strategiekreis Betriebsfestigkeit
ZSB Bremssattel aus Leichtmetall-Werkstoffen AK-LH 13.5, VDA (1998)

[11] U. Stoll
SBC – Die elektrohydraulische Bremse von Mercedes-Benz, Fortschritt-Berichte VDI, Reihe 12: Verkehrstechnik/Fahrzeugtechnik Band 440 (2000)

[12] H.-Chr. Bock, P. Kraemer
Einfluss des Omissionlevels auf die Lebensdauer von Bremsenbauteilen aus Aluminium unter Temperatur- und Korrosionsbelastung, Roell Amsler Symposium (2002)

[13] M. Bacher-Höchst, A. Scheffold
Anwendung des linear-elastischen örtlichen Konzepts auf FE-Rechnungen zur Dauerfestigkeitsvorhersage innendruckbelasteter Bauteile aus Stahl, VDI-Berichte Band 1442 (1998)

Endurance Limit Design of High Pressure Diesel Injection Pipes for Low Failure Probability

Elisabeth Herz[a], Rayk Thumser[b], Michael Vormwald[a] und Joachim Bergmann[b]

[a] Materials Mechanics Group, Technical University Darmstadt,
Petersenstr. 12, D-64287 Darmstadt
[b] Material Research and Testing Institute at Bauhaus University,
Amalienstr. 13, D-99423 Weimar

Abstract The endurance limits of Diesel injection pipes have been investigated both experimentally and analytically. Effective ranges of intensity factor were calculated by FEM with an advanced plasticity model. Endurance is reached when these effective ranges are equal to the corresponding threshold value. The predicted values are valid for a failure probability of 50 %, i.e. half of the parts fail. A statistical method is outlined for the determination of allowable values, typically for 1 ppm failure probability. All predictions are critically discussed on the background of experimental results.

1 INTRODUCTION

In order to meet economic and ecological requirements, maximum internal pressures in Diesel injection systems have been risen to above 2000 bar. This is a big challenge for the fatigue design of injection parts like pumps, common rails, injectors and pipes. The pipes are made from cold drawn tubes. The drawing process causes folds at the inner surface, i. e. surface defects which are detrimental with regard to fatigue. Therefore the inner layer of the tube is usually electro-chemically removed in order to reduce the fold depth to a specific value. Standardized quality grades define allowable defect depths, e. g. quality “Q” with a maximum defect size of 50 µm and “O” with 10 µm. The tubes are usually produced in 2 different material states: Hard drawn (blank) and stress relieved (bk+s) or annealed after drawing (nbk, non blank), respectively. The bk+s-pipes have a higher strength compared to nbk-pipes and are therefore more sensitive against defects. Pipes for high pressure (HP)- Diesel injection systems are mostly autofrettaged, i. e. after bending once an overload of about times higher than the operational pressure level is applied. This high overload introduces a compressive residual stress field in the pipe wall and thus increases the endurance limit and minimizes the influence of the inner wall defects.

Pumps, rails and injectors are usually fatigue critical at bore intersections; and autofrettage enhances the endurance limit by a factor up to three. At this high pressure level, cracks start early in the component life, but stop in the high compressive stress fields introduced by autofrettage. A variety of lucky circumstances allows a relatively robust prediction of the endurance limit of such parts based on material and fracture mechanics [1, 2]. The prediction of the endurance limits of non autofrettaged and autofrettaged pipes, however, is much more difficult: The stress gradient in the wall is low, the stress state at the inner wall is highly hydrostatic compressive, and the crack length is very small. Additionally, the material properties are not isotropic and not measurable in radial direction.

2 TEST PROGRAMME AND EXPERIMENTAL RESULTS

In an experimental and analytical research programme [3], a broad experimental data base has been created on the behaviour of HP-pipes made from S 460 nbk and bk+s. The pipes had an outer diameter of 6 mm, an inner diameter of 2.5 mm and a length of 150 mm. The chemical composition is given in Table 1, the mechanical properties including burst pressures in Table 2. Burst pressures are not depending on defect size.

Table I. Chemical Properties.

C	Si	Mn	P	S	Cr	Ni	Mo	Cu	V	Ti
0.200	0.300	1.550	0.017	0.023	0.060	0.030	0.010	0.050	0.150	0.002

Table II. Mechanical Properties.

Material	State	$R_{p0.2}$	R_m	A_5	Burst pressure
S 460	nbk	490 MPa	655 MPa	25 %	6400 bar
	bk+s	767 MPa	814 MPa	18 %	8300 bar

Two quality grades have been investigated (according to ISO 8535 [4]): "Q" with a maximum defect size of 50 µm and "O" with 10 µm. The autofrettage pressures p_{af} that where applied to the pipes are given in Table 3: For each material stat two autofrettage pressures where applied. Additionally, non autofrettaged pipes where investigated. In total about 340 pipes have been tested in the endurance regime, using the Probit method. The test procedure and the statistical evaluation of the test results is outlined in chapter 3. Mean endurance limit Δp_E, scatter value T, standard deviation s, scatter factor f_s and allowable pressures p(1ppm) are also given in Table 3.

Table III. Test Parameters and Results.

Material	Defect [µm]	p_{af} [bar]	Δp_e [bar]	T	s	f_s	p(1ppm) [bar]
nbk	50	0	1430	≤ 1,107	≤ 0,0182	≤ 1,0429	≥ 1038
		4700	2234	≤ 1,050	≤ 0,0087	≤ 1,0202	≥ 1918
		5900	2313	≤ 1,063	≤ 0,0110	≤ 1,0257	≥ 1906
	10	0	2143	1,190	0,0311	1,0743	1241
		4700	2690	≤ 1,045	≤ 0,0079	≤ 1,0183	≥ 2342
		5900	2772	1,054	0,0094	1,0219	2350
bk+s	50	0	1093	1,234	0,0377	1,0906	565
		6300	2700	≤ 1,063	≤ 0,0109	≤ 1,0254	≥ 2231
		7400	2887	≤ 1,071	≤ 0,0123	≤ 1,0288	≥ 2325
	10	0	2368	1,214	0,0348	1,0834	1287
		6300	3279	1,08*	0,0138	1,0324	2573
		7400	3309	1,08*	0,0138	1,0323	2597

Pipes from S 460 bk+s with quality "O" mostly failed in one of the headed flairs and not in the straight tube. Thus the scatter could not be sufficiently determined. Heading is obviously difficult for this hard material. From some other investigations on tubes from the same material with better flairs, the scatter values are derived and used here. These values are indicated by *. Figure 1 shows besides the mean endurance limit Δp_E, the statistically determined pressure ranges for failure probabilities of 90%, 10% and 1 ppm. The latter is the allowable pressure range for design.

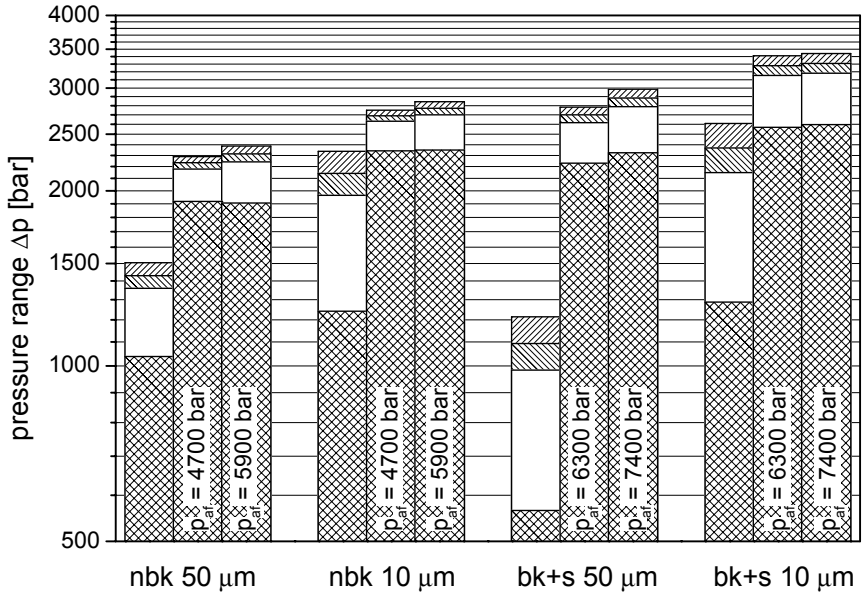


Figure 1.Experimental pressure levels for 90%, 50%, 10% and 1 ppm failure probability

3 TEST PROCEDURE AND STATISTICALLY BASED DESIGN

Comparing the various mean values and the allowable ones, it clearly turns out that the scatter is as important as the mean value. At the end of the design, only the allowable pressures are relevant. Therefore both appropriate test procedures and appropriate statistical methods must be applied.

For endurance limit tests, various procedures are possible [5]. Usually, the Staircase Method or the Probit Method, respectively, is applied. As internal pressure tests can be done on up to 20 parts simultaneously by the aid of a test rail, the Probit Method is appropriate. Only two tests on different pressure levels in the endurance regime are needed. Compared to the Staircase Method, the Probit Method yields, a much higher confidence for the standard deviation with the number of specimens.

The selection of the statistical methods mainly concerns the appropriate random variable, i. e. linear or logarithmic value, and most important, the distribution function. In fatigue problems log-values are preferred. One advantage is negative live or strength values at low probabilities are avoided. The VDA (German automotive industry) and SAE (US automotive industry) recommend the use of the Log-Weibull Distribution, others prefer the Log-Normal Distribution. Based on a 25-years experience in industrial application, we have concluded that the Log-Weibull Distribution appears to be too conservative and the Log-Normal Distribution definitely too unconservative, i. e. unsafe. There are nearly no consolidated data available to the public to decide upon the “right” distribution. E. g. we designed Diesel injection pipes for 1 ppm failure probability using the below explained Log-Logistic Distribution[6, 7], and after 10 years we found about 10 in-service failures among 10 million parts. These pipes were loaded by approximately constant amplitude pressures, a real endurance object. Another example is shown in Figure 2: The loading of the valve rocker arm was also well known with nearly constant amplitudes, and a failure caused by other parts of the engine can be excluded. In this case, Log-Weibull Distribution would be safe and the Normal Distribution unsafe. The Log-arcsin√P Distribution is only introduced for illustration. All distributions are of course based on the same test results. Compared to the divergence of various distributions, the differences caused by the use of linear or logarithmic random values, respectively, are negligible.

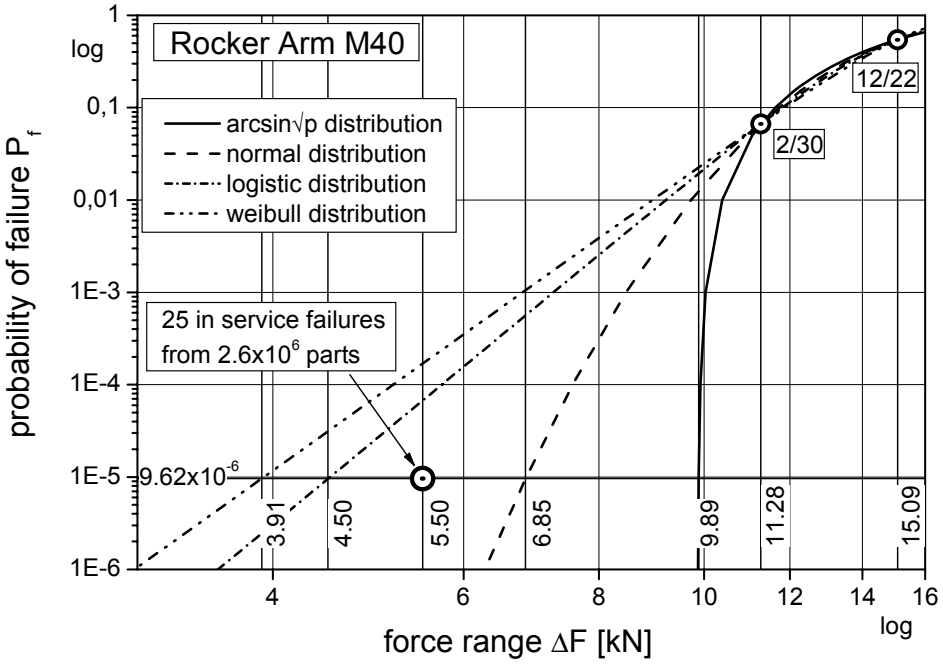


Figure 2. Rocker Arm.

The Probit Method, the proposed Log-Logistic-Distribution, and the statistical evaluation of mean value, scatter, confidence and allowable value are briefly outlined in the following.

3.1 TEST STRATEGY FOR ENDURANCE LIMIT EVALUATION

In general an endurance level is assigned to each specimen. This endurance level x_s can only be determined by running a lot of fatigue tests with different increasing load levels x_i, each of these tests running up to the limit number of $2x10^6$ .. 10^7 cycles. (Very high cycle fatigue has to be taken into account appropriately [8]). A test run at load level x_i can only yield one of two possible results:

Failure if $x_s < x_i$ or Run out if $x_s \geq x_i$

The number of cycles to reach the specimens failure is of no importance in statistics for endurance limit. For the Probit Method fatigue tests with several specimens have to be performed on different load levels x_i (at least 2). The failure probability $P_{f,i}$ at the test level x_i can be evaluated by the Probit Method:

$$P_{f,i}\begin{cases} \geq 0.5^{1/n_i} & \text{for } r_i = n_i \\ = r_i / n_i & \text{for } r_i \neq n_i \text{ and } r_i \neq 0 \\ \leq 1 - 0.5^{1/n_i} & \text{for } r_i = 0 \end{cases} \quad (1)$$

(r_i: number of failed parts at test level x_i, n_i: number of tested parts at test level x_i)

As the number of specimens is limited (e.g. $n_i < 40$), the probability range covered by tests is usually limited to $0.02 \leq P_f \leq 0.98$.

3.2 STATISTICS

There are various reasons using logarithmic values for all fatigue data (load, stress, cycles). Then, instead of x the logarithmic values lg(x) are used. As outlined above, there are some arguments for using the Logistic Distribution with logarithmic random variables (Log-Logistic Distribution). So, the standardized random variable u for log values writes:

$$u = [\lg(x) - \mu]/\sigma \quad \text{and inverse} \quad \lg x = \mu + u\sigma \quad (2)$$

($\lg x$ random variable, μ mean value for $\lg x$, σ standard deviation for $\lg x$)

The probability density function (pdf) is given by:

$$f(x,\mu,\sigma) = \frac{\pi}{\sqrt{3}} \frac{\exp\left(\pi/\sqrt{3}\cdot[\lg(x)-\mu]/\sigma\right)}{\left[1+\exp\left(\pi/\sqrt{3}\cdot[\lg(x)-\mu]/\sigma\right)\right]^2} \quad \text{and} \quad f(u) = \frac{\pi}{\sqrt{3}} \frac{\exp\left(\pi/\sqrt{3}\cdot u\right)}{\left[1+\exp\left(\pi/\sqrt{3}\cdot u\right)\right]^2} \quad (3)$$

The cumulative density function (cdf) is:

$$F(x,\mu,\sigma) = \left[1+\exp\left(-\pi/\sqrt{3}\cdot[\lg(x)-\mu]/\sigma\right)\right]^{-1} \quad \text{and} \quad F(u) = \left[1+\exp\left(-\pi/\sqrt{3}\,u\right)\right]^{-1} \quad (4)$$

The inverse cdf:

$$u = \frac{\sqrt{3}}{\pi}\ln\frac{F}{1-F} \quad \text{and} \quad \lg\frac{x}{\overline{x}} = \sigma\frac{\sqrt{3}}{\pi}\ln\frac{F}{1-F} \quad (5)$$

(Using $\lg\overline{x} = \mu$ as geometric mean value for x)

In S-N diagrams (log-log diagrams), the lines for 10% and 90% failure probability are often printed. The according scatter value T is defined as

$$T = x\left(P_f = 90\%\right) / x\left(P_f = 10\%\right) \tag{6}$$

This is only meaningful for distributions of log values like Log-Normal and Log-Logistic Distribution. The scatter value T is, unlike the standard deviation of the population, dependent upon the distribution. For the Log-Logistic Distribution it is defined as follows:

$$\lg T = \sigma \frac{\sqrt{3}}{\pi}\left[\ln\frac{0.9}{1-0.9} - \ln\frac{0.1}{1-0.1}\right] = 2.42\sigma \quad \text{and inverted} \quad \sigma = \frac{\lg T}{2.42} \tag{7}$$

(For the Log-Normal Distribution: $\lg T = 2.56 \cdot \sigma$)

Using this definition yields for T the following equations for the cdf and inverted cdf:

$$F\left(x, \overline{x}, T\right) = \left[1 + \left(x/\overline{x}\right)^{-1.908/\lg T}\right]^{-1} \quad \text{and} \quad \frac{x}{\overline{x}} = \left[\frac{F}{1-F}\right]^{0.524 \lg T} \tag{8}$$

For this application, the failure probability is equal to the cumulative density function

$$P_f\left(x, \overline{x}, T\right) \equiv F\left(x, \overline{x}, T\right) \tag{9}$$

3.3 Evaluation of statistical parameters from a tested sample

Based on the test results $\left(x_i, P_{f,i}\right)$ for the different test levels x_i (at least 2) the mean value $\overline{x}$ and scatter value T can be determined by a weighted linear fit in a $\left(\lg\left(x_i\right), u_i\left(P_{f,i}\right)\right)$ diagram as follows:

$$w_i = k \cdot \sqrt{n_i} \Big/ \sum_{i=1}^{k} \sqrt{n_i} \qquad \left(k \equiv \sum_{i=1}^{k} w_i\right) \tag{10}$$

k: number of test levels

By substituting $y_i = \lg x_i$ and defining

$$\underline{u} = \sum_{i=1}^{k} w_i u_i \Big/ k \quad \text{and} \quad \underline{y} = \sum_{i=1}^{k} w_i y_i \Big/ k \tag{11}$$

the solution for the standard deviation s and the mean value m for these sample are:

$$s = \left[\sum_{i=1}^{k} w_i \left(u_i - \underline{u}\right)^2\right] \Big/ \left[\sum_{i=1}^{k} w_i^2 \left(u_i - \underline{u}\right)\left(y_i - \underline{y}\right)\right], \qquad \lg T = 2.56 \cdot s \tag{12}$$

$$m = \underline{u} - s \cdot \underline{y}, \quad \text{and} \quad \lg \overline{x} = m \tag{13}$$

The evaluated m and s are random variables themselves. The expected values of m and s are assumed to be μ and σ, respectively, of the population ($\mu = E[m]$ and $\sigma = E[s]$). The confidence level for the evaluated m and s are 50%. For the Log-Logistic Distribution the confidence for m and s can be evaluated by a Monte-Carlo Simulation. It has to be pointed out that these confidences only describe the uncertainty of the sample from one series batch, not of the population of the whole series. In a series consists of a lot of production batches, each with its own mean values and standard deviations. What we are really interested in is thus not covered by the confidence considerations derived from one sample. This might be the reason why the confidence for the standard deviation is usually not taken into

account in design, though it is as important as the standard deviation itself. Confidence for the mean value of one sample is often considered, but the effect for the allowable value is typically around 1 % (20 parts and 90% single side confidence) and thus negligible.

4 STRESS DISTRIBUTION AND MULTIAXIALITY

In order to determine the stress strain behaviour of the material, axial tension-compression tests have been conducted on straight tubes, see Figure 3.

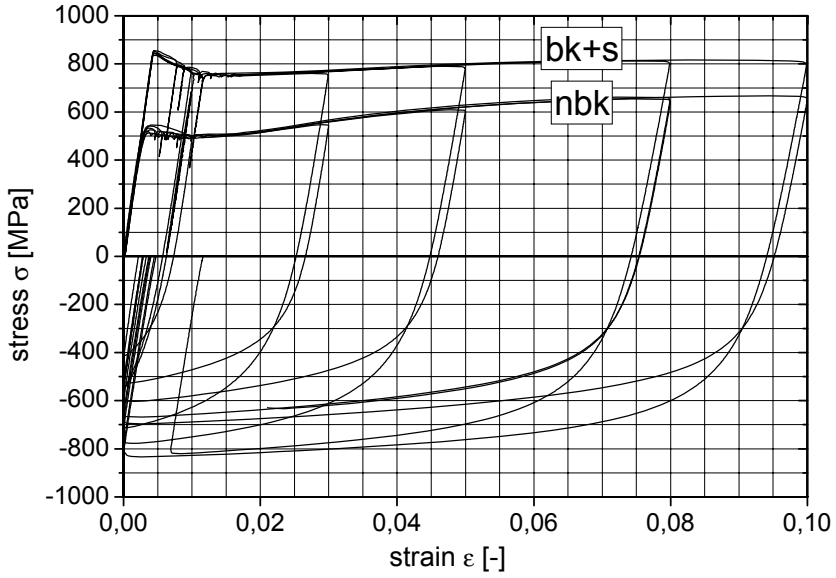


Figure 3 Load and unload material curves.

For lack of better knowledge, it is assumed that the deformation behaviour is isotropic. In a first step, the stress strain behaviour in the tube wall caused by autofrettage and following cycling at the endurance limit has been simulated by FEM. One of the results is shown in the Dang Van-plot [9] in Figure 4. The high hydrostatic stress state in compression due to autofrettage can be clearly seen. The figure also shows that the peaks and troughs of the loops form straight lines, which can probably well describe the fatigue strength of the pipes within the tested parameter field. Extrapolation and interpolation should of course be done with utmost caution, as low autofrettage will probably be detrimental to fatigue strength compared to the non autofrettaged state, and the burst limit is also not yet included in the plot.

5 CRACK PROPAGATION AND ARREST

In the fracture mechanics approach it is assumed that a crack is starting from the defect of 10 or 50 µm, respectively. This crack has to cross the compressive residual stress field built up by autofrettage. The crack is driven by the effective stress ranges between crack opening pressure and maximum pressure. The crack is able to grow only if these effective pressure ranges are larger than the effective threshold pressure range.

The effective pressure ranges have been calculated by extensive finite element calculations, using ABAQUS and a newly developed constitutive model [10] linked by UMAT. With this constitutive model, mean stress and ratchetting can be simulated which especially near the crack tip strongly influences the crack opening and closure behaviour.

The finite element model assumes an axi symmetric pressurized torus with a very large diameter thus reducing the 3D-problem to a 2D-problem. The mesh size at the crack has been determined to 2,5 µm by convergence studies. The simulation was performed in several steps:

- Introducing a crack with the size of the corresponding defect size

- Loading the defect pipe by autofrettage
- Unloading to 50 bar (minimum pressure in cyclic test)
- 250 cycles at Δp_E (near endurance limit) for stress redistribution in the whole tube wall
- Simulating crack propagation in 2,5 µm steps
- In each step stabilizing mean stress ahead of crack tip by 10 cycles
- Determine crack closure and opening level

By this simulation effective pressure ranges have been evaluated. The according effective stress intensity factor has been derived by using weight function proposed by Ma [11]. This ΔK_{eff} (material strain) is compared to the threshold value (material strength) $\Delta K_{th,eff}$ to predict the mean value of the endurance limit.

In a similar way, the endurance limits of the non autofrettaged pipes have also been predicted. Astonishingly, it is the case that be considered the simplest the could not be properly predicted, i.e. the non autofrettaged nbk pipe. Except one, predictions are fairly satisfactory, as can be seen in figure 5. A detailed description of the this fracture mechanics analyses can be found in [3, 12].

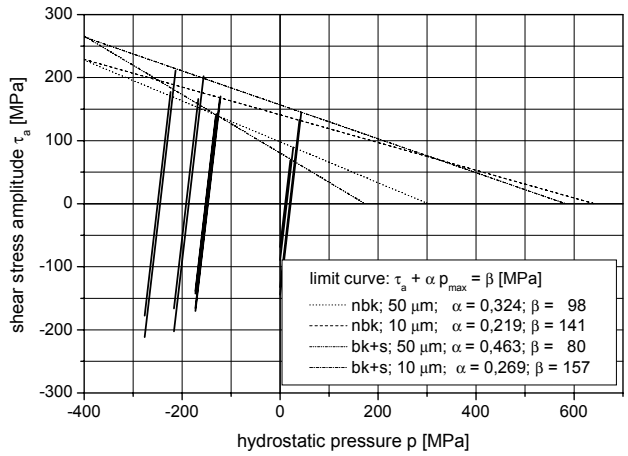


Figure 4 Dang Van-plot

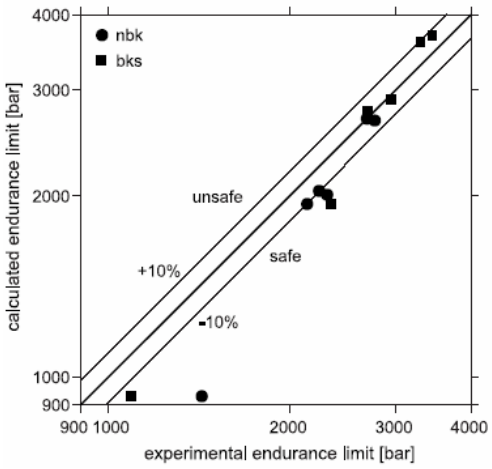


Figure 5 Comparison of calculated and experimental endurance limits [12]

6 CONCLUSIONS

Fatigue design of series parts is always a design for low failure probabilities. For Diesel injection pipes, this means that of a whole series typically 1 ppm is allowed to fail. To achieve this goal, the mean endurance limit for 50% failure probability can be calculated by the means of sophisticated numerical tools with satisfactory accuracy, or it can be experimentally determined. The numerical analyses at least help us to better understand the mechanical behaviour of pipes and thus to progress in the production process. For the low failure probability design, additionally the scatter of the endurance limit must be known. This can only be determined by tests. Fortunately, the scatter of internal pressure parts can be determined at relatively low costs, as simultaneous testing of many parts is possible. The experimental results therefore have a high confidence level. Additionally, the scatter of autofrettaged parts is extremely low, both leading to very small safety factors.

A very important ingredient of the design method is the probability function. The Log-Normal and the Normal-Distribution probably do not yield safe estimates for 1 ppm values. If parts designed with these distributions are nevertheless successfully in service, this does not justify this approach. Pipes of common rail systems, for example, see the maximum pressure range less than 50.000 times, and for 1 ppm failure probability, their fatigue strength for finite life under variable loading is higher than their endurance limit. An insufficient endurance design is then of no relevance, the strength of the part under service condition is then not proven at all by such an endurance design.

In some cases, the fatigue design of autofrettaged Diesel injection parts for variable amplitude loading will help to meet future higher requirements. Because of the extremely high overload due to autofrettage, this will again be a new and challenging object of research.

7 ACKNOWLEDGMENTS

The authors gratefully acknowledge the financial support provided by the Deutsche Forschungsgemeinschaft under contracts Vo729/2-1 and Be2387/2-1. The specimens have been provided by Poppe & Potthof mbH & Co., Werther, Germany, and have been autofrettaged by Maximator GmbH, Nordhausen, Germany. Support of both companies is thankfully appreciated.

8 REFERENCES

1. Thumser, R., J.W. Bergmann, and M. Vormwald, *Residual Stress Fields and Fatigue Analysis of Autofrettaged Parts.* International Journal of Pressure Vessels and Piping, 2001. **79**(2): p. 113-117.
2. Seeger, T., S. Greuling, and J.W. Bergmann, *Autofrettage II: Vorhaben Nr. 671; Dauerfestigkeitssteigerung durch Autofrettage II; Abschlußbericht; Heft 704*. 2001, Frankfurt: Forschungsvereinigung Verbrennungskraftmaschinen e. V. (FVV).
3. Thumser, R., et al., *Bruchmechanische Bewertung der Dauerfestigkeit von autofrettierten Diesel-Einspritzleitungen*, in *Berichtsband 36. Tagung DVM-AK Bruchvorgänge*. 2004: Köln.
4. *Compression-ignition engines -- Steel tubes for high-pressure fuel injection pipes -- Part 1: Requirements for seamless cold-drawn single-wall tubes (ISO 8535-1996)*. 1996.
5. Weibull, W., *Fatigue testing and analysis of results*. 1961, Oxford u.a.: Pergamon Pr.
6. Balakrishnan, N., *Handbook of the logistic distribution*. Statistics; 123. 1992, New York u.a.: Dekker.
7. Johnson, N.L., S. Kotz, and N. Balakrishnan, *Continuous univariate distributions*. 2nd ed. Wiley series in probability and mathematical statistics. 1994, New York: Wiley & Sons.
8. Murakami, Y. *Mechanism of Fatigue Failure in Ultralong Life Regime*. in *Proceedings of the International Conference on Fatigue in the Very High Cycle Regime, 2-4July 2001, Vienna, Austria*. 2001. Vienna: Institute of Meteorology and Physics, Physics Department, University of Agricultural Sciences.
9. Dang Van, K., B. Griveau, and O. Message, *On a new Multiaxial Fatigue Limit Criterion: Theory and Application*, in *Biaxial and Multiaxial Fatigue*, M.W. Brown and K.J. Miller, Editors. 1989, Mechanical Engineering Publications: London. p. 479-496.
10. Döring, R., et al., *A Plasticity Model for Calculating Stress-Strain Sequences under Multiaxial Nonproportional Cyclic Loading.* Computational Materials Science, 2003. **28**(3-4): p. 587-596.
11. Ma, C.C., J.I. Huang, and C.H. Tsai, *Weight Functions and Stress Intensity Factors for Axial Cracks in Hollow Cylinders.* Journal of Pressure Vessel Technology, 1994. **116**(4): p. 423-430.
12. Herz, E., et al., *Endurance limit of autofrettaged Diesel-engine injection tubes with defects.* Engineering Fracture Mechanics, 2005(Article in Press).

Integrated approach to durability analysis

Mohamed Bennebach[a], Peter Heyes[b]

[a] Code International, Maisons-Alfort, France
[b] Code International Ltd., Sheffield, United Kingdom

Abstract Nowadays, manufacturing companies are coming under increasing pressure to reduce the "Time to Market" of new products while assuring a high reliability level of these products. Durability design and analysis is an essential element in achieving these objectives and involves a multi-disciplinary approach. In order to obtain rapid and realistic life predictions, Simulation and Testing should be used in synergy, each field bringing to the other necessary information, making the durability process an integrated one. This paper reviews some modern durability management philosophies and the computer based tools available to meet the needs of design, test and development engineers. Integration of the simulation techniques with laboratory and field testing is discussed and a demonstration example given from the transportation industry.

1 INTRODUCTION

Durability may be defined as the ability of a component or structure to survive its operating environment. In the general case it refers to resistance under several different mechanisms such as: fatigue, wear, corrosion, creep, etc. However from all these deterioration modes, fatigue accounts for the majority of in service failures and the term durability will be used to describe mainly fatigue performance. This performance is dictated by the operating loads, the stresses and strains generated by these loads and the material's behaviour under these conditions. It was traditionally evaluated late in the design cycle when a prototype is available for measurements.

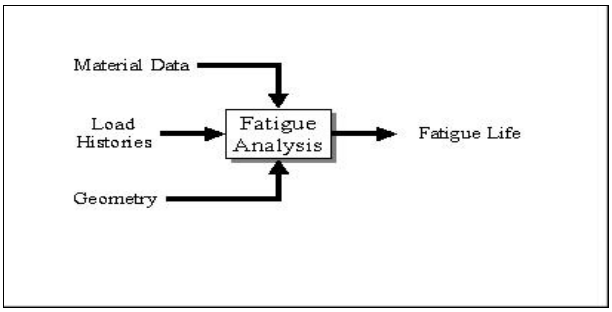


Figure 1. Inputs to fatigue analysis

Nowadays modern computer simulation techniques allow investigating durability assessment and design options before physical testing (what is called Virtual Prototyping). This approach reduces development time and costs, by concentrating on only prevalidated designs. Analytical techniques are available for load generation – Multibody Dynamics -, stress state calculation – Finite Elements – and fatigue analysis. These methods often rely on very complex models and need measured test data as inputs and also for correlation purposes at each stage of the analysis process. The multiple engineering areas and vast amount of data involved require an integrated approach in order to perform accurate durability analysis in a reasonable time scale.

This paper reviews the main components of the durability process and the way they interact between each other. The process is illustrated by an example from an all terrain vehicle project of the Fatigue Design and Evaluation Committee of the SAE.

2 OVERVIEW OF THE DURABILITY PROCESS

The diagram in figure 2 shows how analytical and physical approaches work in synergy in order to successfully analyse product performance.

In this process, it is essential that numerical simulation techniques are employed at the earliest possible stage so that the design can be developed and optimized through analysis. Key elements in making reliable durability calculations, apart from usage of adequate models, is the accuracy of inputs such loads – measured, virtually derived or based on previous design -, stresses induced by these loads on the structure and materials behaviour laws – including manufacturing effects -. Simulation allows conducting sensitivity analysis, until an acceptable durability is obtained. These analysis loops give an insight to the predominant influencing factors and the distribution of fatigue lives.

In parallel to virtual analysis, physical tests are conducted in the field or laboratory. These tests provide necessary information such as loads, material data and also represent final validation of the design. They allow correlation with CAE witch is critical to ensure high confidence in the results.

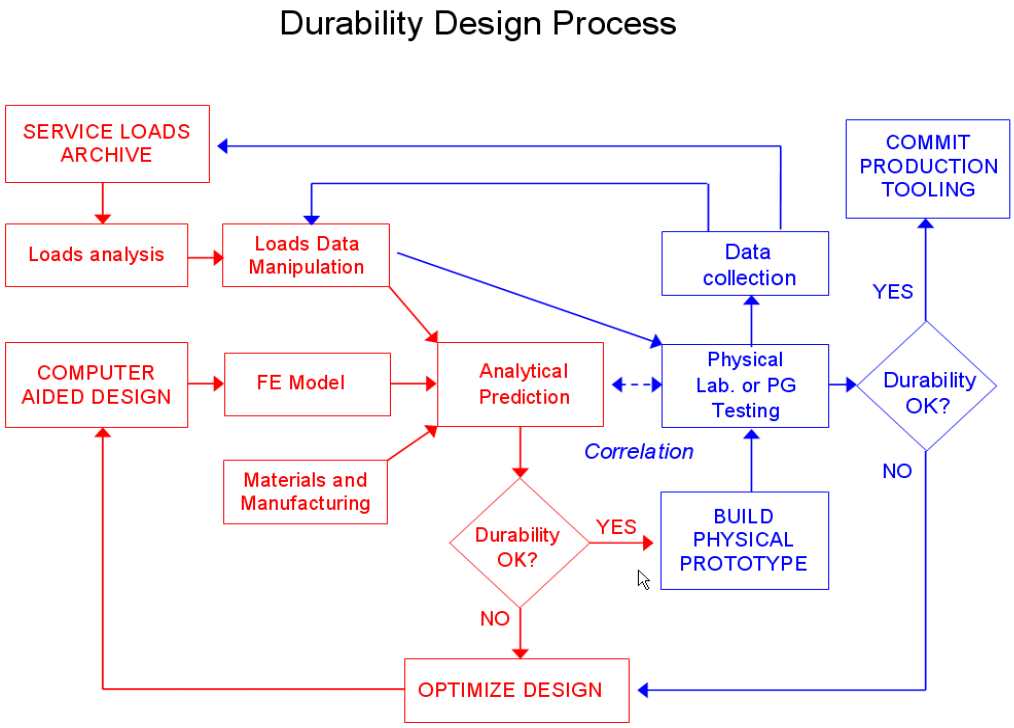


Figure 2. The Durability Design Process

A brief description of the main components of this process is given in the following sections.

2.1 Load Data

Knowing what are the loads that a structure is experiencing in real conditions is not a trivial task and care should be taken when evaluating or measuring these loads so as they are representative of the in service usage.

Physical loads can be obtained from in service measurements using devices such as wheel force transducers, load cells, strain gages, etc. from instrumented prototypes. It is the best source of data possible but it requires long term records and many statistically representative samples.
The process can be accelerated by doing field (proving ground) or test rig measurements, taken over known events, with well established correlation to the real world.
To prevent any errors, it is essential that these measured loads are processed and validated before usage in analytical models.

Virtual loads can be derived using Multibody Dynamics simulation. MBS simulates mechanical systems to describe motion and interaction of assemblies of several parts, especially in a dynamic environment. It is used to determine the loading applied to a component given a system model and inputs. It acts as a transfer function, where external or system loads are the inputs and internal or component loads are the outputs. In order to eliminate prototype measurements, system inputs need to be derived from inputs that are independent of the design (example in the automotive industry could be road profile and driving conditions). System loads can also be actual loads, displacements, accelerations, etc (Ref.1).
This approach is ideal for new breed product where no legacy data is available.

2.2 Finite Elements Analysis

CAE based durability starts with the conception of a CAE model of the component or structure, witch is then used to calculate the stress state due to the loading and boundary conditions.

Most common method consists in applying each load case independently (often as a unit load) and using the principle of linear superposition, combining the loading histories and the Finite Elements analysis results, to obtain the local stress time history at each node or element.
This approach assumes a linear elastic behaviour of the component and material, and is only valid if no dynamic problems occur (no natural frequencies excited by the loadings).

Other methods such as transient, modal or random vibration analysis can also be used in conjunction of the fatigue analysis module.

2.3 Material Information

Another major input to any fatigue life estimation is a description of the material from witch the component or structure has been manufactured. Cyclic material properties are used to calculate stress-strain response and damage accumulation rate. The damage curves usually relate stress or stain amplitudes to life, or crack growth rate to stress intensity factor. The material parameters required depend on the fatigue modelling technique being used. They are usually obtained by testing and may also be available in handbooks or specific literature.
It is worth nothing that due to the statistical nature of the fatigue phenomenon and the associated scatter, each damage curve requires an important number of specimens in order to capture the mean values and also their deviations.

Some empirical models such as those proposed by CETIM (Ref.2), Baumel Seeger (Ref.3), etc. allow deriving cyclic material properties from static ones. These models are approximations and should only be used if no real data is available or for A to B comparisons.

2.4 Fatigue Analysis

Depending on the stress-strain state complexity and operational environment of a component or structure, several fatigue analysis methodologies are available. Classical ones are the stress-life, strain-life, or linear elastic fracture mechanics. The appropriate analysis type depends on the proportion of the total fatigue life that is consumed in initiation and growth of a fatigue crack up to final failure.
For complex situations, involving phenomena such as non-proportional multiaxiality, thermo mechanical conditions, assemblies, etc. more advanced models can be used.
It is mandatory to include in the analysis a variety of influencing factors such as mean stresses, notch effects, residual stresses, surface roughness and treatment, etc.
Details of the methods are beyond the scope of this paper, however more information is available in numerous publications including references 3 and 4.

The final result of an analysis is a fatigue life, number of repeats of the applied load time history until failure or a safety factor.
The failure criterion is somewhat arbitrary and usually means formation of small, easily detectable crack.

Sensitivity analysis can then be carried out on load variability (result of variability in real usage), structure geometry and material properties. These two last inputs are usually more precisely defined than the applied loads.

Figure 3 describes the necessary inputs to the fatigue analysis module and how these inputs are generated.

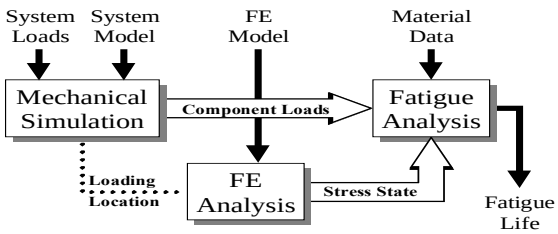


Figure 3. Fatigue analysis process

2.4 Durability Test

Test based durability starts with the development of a prototype from witch physical loads can be measured. A data acquisition is done to acquire these loads and processing and validation of the measurements is required in order to correct for any anomalies.

Durability tests consist of field or laboratory tests, witch should reproduce in an accelerated way the in service or customer usage of the product. They simulate life of systems, sub-systems or components and single point fatigue life calculations can be carried out at a potential critical location.



Figure 4. Sample durability tests

This part of the process is one of the most time consuming and acceleration can be achieved by using fatigue editing techniques that reduce the loading time histories by removing the non damaging events. Any data editing method must reduce the testing time in a technically valid, justifiable and repeatable manner. For the laboratory test to represent the in-service behaviour, it must reproduce the loading environment and the fatigue damage content of the original load data. This should ensure the duplication of the same failure modes and locations in the laboratory. Fatigue analysis can be used to mimic the fatigue life of the test before it is undertaken, to check that the edited drive signals still give a comparable fatigue life (in equivalent repeats of sequence) and to estimate the test duration reduction (Ref.5).

The test results are considered to be the “real” answer and still constitute the final validation of the design.

2.5 Correlation

Correlations for both Test and CAE are critical to ensure high confidence in the results.

Field tests are correlated with the end customer or real usage of the structure. This need some statistical or probabilistic measure of customer variations and patterns of usage, established through a combination of “fleet” measurements and extensive user surveys. Laboratory tests are often correlated with the field.

Numerical simulation results must be correlated with tests or previous results to validate the models:

- Correlate virtual and measured loads
- Correlate calculated and measured responses (comparing for example strain gage measurements with virtual strains)
- Correlate virtual and physical life

It should be noted that correlation is not something that is just done at the end of the process but rather at different stages of this process.

3 DEMONSTRATION EXAMPLE

The following example is an extract from a project on an all terrain vehicle, conducted by the Fatigue Design and Evaluation Committee of the SAE. All data related to this project is available on www.fatigue.org.

The project goal was to study the method of digital prototyping for automotive structural durability, and compare the results between test and simulation.

The ATV durability test is represented in the following figure:

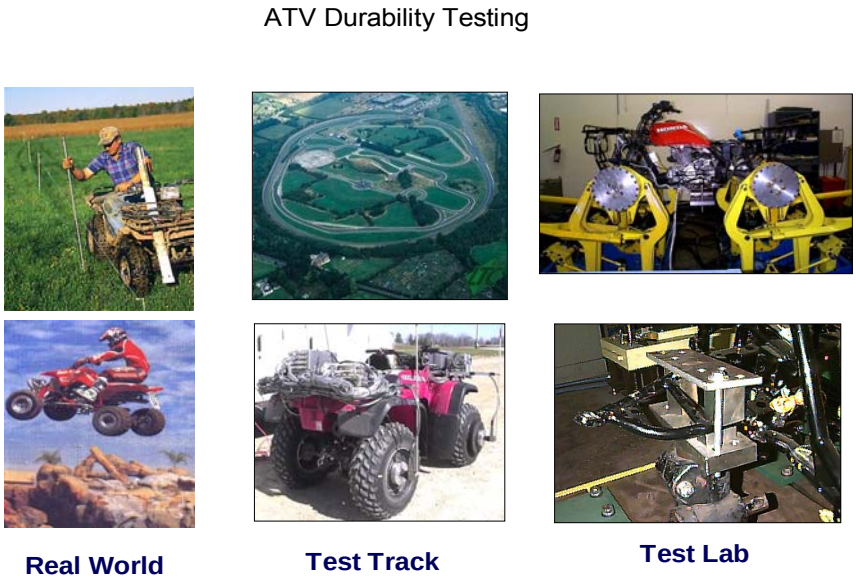


Figure 5. ATV Durability testing

The vehicle has been instrumented, using 58 channels of measurement, including wheel forces and moments transducers, spindle accelerations, strain gages, suspension position, etc.
Proving grounds are used to simulate various events the ATV may experience. These events are then combined to form a duty cycle representing the vehicle's design life.

Table I. Durability schedule

Description	Location	Passes per life
Low speed loop	Tech Center	100
Gravel lot	Sundown	100
Hillwork	Sundown	60
Hillwork with snow	Sundown	60
Aggressive hillwork	Sundown	60
Farm vocation	Sundown	120
Farm vocation 2	Sundown	110
Bump course	Silvis	100
Staggered bumps	Silvis	65
Staggered bumps 2	Silvis	65
Bump course 2 CW	Silvis	70
Bump course 2 CCW	Silvis	70
High speed transport	Silvis	75
ISO track 2	Waterloo	100
Ditch crossing	Waterloo	25
Ditch crossing 2	Waterloo	25
Recreational run	Waterloo	100
Flat offroad CW	Moline	150
Flat offroad CCW	Moline	175
Bump course 3	Moline	90
Jumps	Moline	10

To assess the durability of the ATV in the design phase, simulation is used to calculate system loads, predict the system response and then vehicle life. This allows critical locations in the frame to be identified and design alternatives to be evaluated, during the design phase prior to physical testing.

With measured spindle loads for the 21 events of the durability schedule, multibody dynamics simulation is used to calculate the loads at the attachment points of the frame.
The 24 channels (3 forces and 3 moments per spindle) become 66 channels, 3 forces and 3 moments for each of the 11 attachment points of the frame.

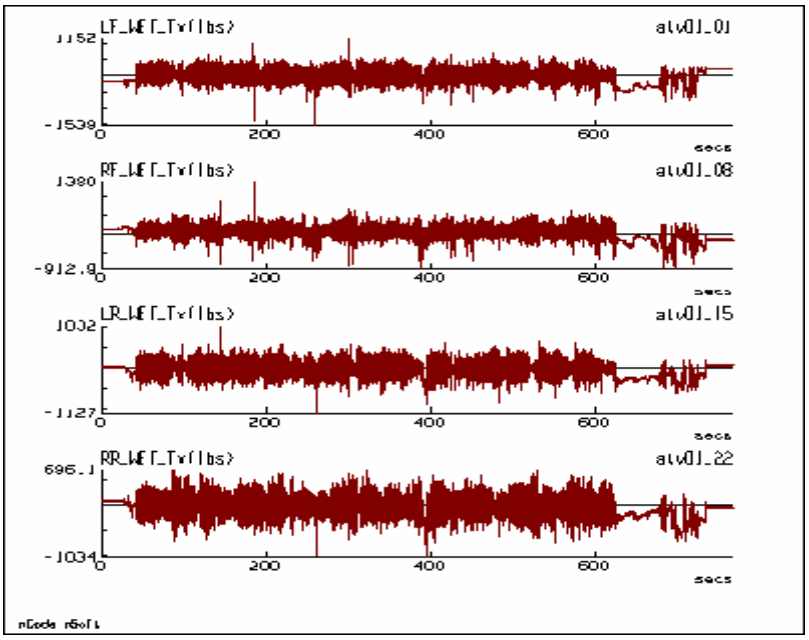


Figure 6. Four channels of wheel forces

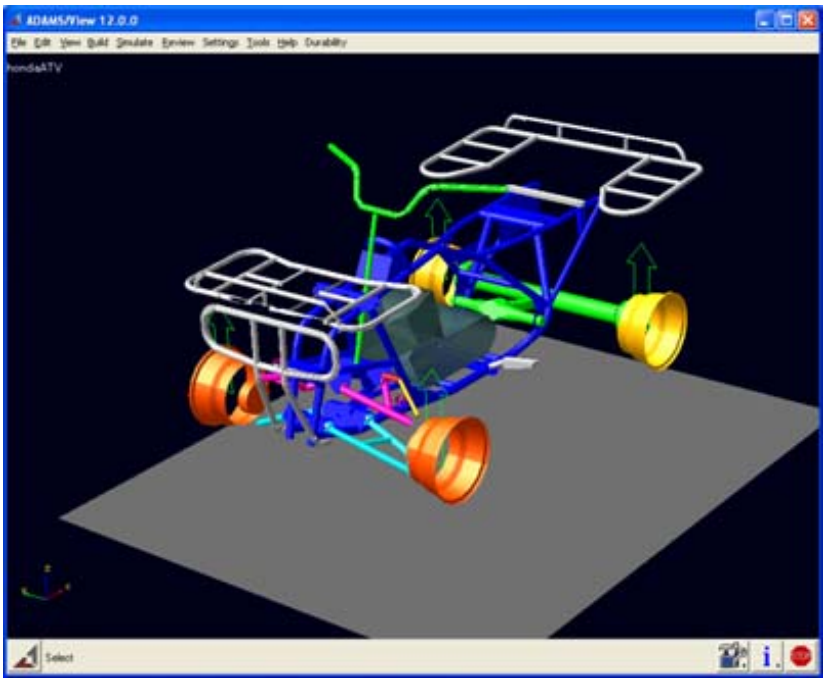


Figure 7. MBD model of the ATV (MSC.ADAMS)

FE analysis is carried out with loads at the attachment points. The frame of the ATV is a welded tubular structure, made from SAE 1015 steel, and modelled with shell elements (28433 elements).
In order to describe the dynamic response of the ATV frame, either linear static stress states are combined with computed time histories of attachment forces, or modal stresses and modal responses are calculated. These are then transferred to the fatigue analysis module for life calculation. The life of the frame will be mainly directed by the resistance of the welds.



Figure 8. Finite elements model

A sample calculation result is given below, showing the life in schedules number and also the contribution of each event to the global damage (calculation made by FE-Fatigue software from nCode).

Duty Cycle Summary - 20 Most Damaged Nodes

Results

Node	808	Top Surface	Rank	1	
Event	Description		Damage		%Contribution
1	Low speed loop		0.00855138		7.76454
2	Gravel lot		0.00093837		0.852028
3	Hillwork		0.00272193		2.47147
4	Hillwork with snow		0.0061602		5.59338
5	Agressive hillwork		0.00201703		1.83144
6	Farm vocation		0.00321725		2.92122
7	Farm vocation 2		0.00165899		1.50634
8	Bump course		0.00131724		1.19603
9	Staggered bumps		0.000793292		0.720298
10	Staggered bumps 2		0.00328961		2.98692
11	Bump course 2		0.00962947		8.74343
12	Bump course 2a		0.00288332		2.61802
13	High speed transport		0.00240097		2.18005
14	ISO track		0.000620635		0.563528
15	Ditch crossing		0.000451998		0.410409
16	Ditch crossing 2		0.000954536		0.866706
17	Recreational run		0.0431515		39.1809
18	Flat offroad		0.00197061		1.78929
19	Flat offroad 2		0.0143897		13.0657
20	Bump course 3		0.000182718		0.165905
21	Jumps		0.00283313		2.57245

Total Damage 0.110134
Life 9.07986 schedules
Equivalent Life 9.07986 Schedules

OK

Figure 9. Sample fatigue results

This life can now be compared to the laboratory test for validation purposes. The test is conducted on a multiple actuators test rig, controlled by wheel forces time histories. As long service life is required high test acceleration factor is needed. This can be achieved by using analytical models to remove the non damaging cycles or events from the duty cycle. Control of the editing process is made by verifying the damage content of the original and reduced excitation files. Strain gages measurements are used for correlation with the CAE analysis.

4 CONCLUSIONS

Modern Durability Management techniques make major contribution to both development time and costs. The ability to derive loads and stresses from MBD and FE simulations, and use those for FE-based damage calculations, greatly enhances the efficiency of early design investigations.

An integrated approach does not eliminate the need for prototype production and testing but, rather, allows concentrating efforts on analytically proven design options. Testing still remains and brings necessary inputs at several steps of the simulation process. It allows correlation and final product validation.

5 REFERENCES

1. M. Pompetzki, Combining Durability with Multibody Dynamics, International ADAMS user conference, Orlando, 2000.

2. A. Brand, J.F. Flavenot, R. Gregoire, C. Tournier, Recueil de données technologiques sur la fatigue, CETIM, 1980.

3. J.A. Bannantine, J.J. Comer, J.L. Handrock, Fundamentals of Metal Fatigue Analysis, Prentice-Hall Inc. 1990 ISBN 0-13-340191-X.

4. P. Heyes, X. Lin, A. Buczynski, M. Brown, Application of biaxial plasticity and damage modeling to the life prediction and testing of automotive components, 5th International Conference on Multiaxial Fatigue and Fracture, 1997, Cracow, Poland.

5. M. Bennebach, W. El Ratal, X. Lin, R. Plaskitt, *Fatigue life modeling and accelerated tests for components under variable amplitude loads*, ASTM STP 1439.

Virtual Fatigue Optimisation of Automotive Structures

Bernhard Unger;[a] Helmut Dannbauer [a] , Wilfried Eichlseder [b]

[a] MAGNA Powertrain Engineering Center Steyr GmbH &CoKG (ECS), Austria
[b] Dept. Mechanical Engineering, Montanistic University of Leoben, Austria

An automated assessment of complex structures with notches, welding seams and spot joints is presented. Based on guidelines and with the help of software-coded procedures, the Finite Element model is conventionally build up including all notches and joints. After having determined the stresses by linear or geometrically non-linear Finite Elemente analysis (FEA), the stresses are postprocessed by a software package which automatic takes the stress gradient in notches and the special properties of welding seams and spot joints as defined in the FE-model into account. The dimension of the notches, the design and the position of the welding, as well as the number and the location of the spot joints have a significant technical and economical impact. An optimum use of the material capabilities is only possible with optimized notch, welding seam or spot joint design of a structure. The paper includes the theoretical background and procedure how the computationally optimisation of these structures is done.

1 INTRODUCTION

The reduction of the vehicle weight is at least since the drastic raise of fuel prices in the seventies a basic requirement for the development of new cars, trucks and busses. Nevertheless there is the general tendency in the opposite direction. The reasons for this contradiction are on the one hand additional features for more comfort and safety as well as increased motor torque. On the other hand the potential for mass savings in the basic structure is not enormous.
Vehicles have to withstand dynamical loads and their components have lots of arc-welds, spot joints and notches. Several technological treatments with positive or negative influence to the lifetime usually are applied.
How can engineers handle all important fatigue influences during the development process? On the one hand, a very good method is to perform fatigue tests with components or total vehicles. Many influences can be considered without any mathematical model, nevertheless the results have absolute accuracy. Unfortunately, experimental tests give only poor information about low stressed areas, so it is very expensive and time consuming to minimize a component's mass based on experiments. Therefore the Engineering Center Steyr, a competence center within MAGNA POWERTRAIN developed a software for the fatigue simulation of dynamically loaded components on the basis of Finite Element examinations. The name of this program is **FEMFAT®** (Finite Element Method + FATigue) . It will be described briefly in the following paragraphs.

2 Fatigue Analysis Concept of FEMFAT®

At each user selected FE-node a component S/N-curve is calculated. The computation of this local S/N curve starts with the well known S/N-curve data of the unnotched specimen and is influenced by the local properties and linear calculated FE-stress tensors for the static and dynamic portions of the loading of the component (Figure 1). The concept of synthetically created S/N-curves was modified (e.g. Kt-free analysis of notch effects and more flexibility of the formula parameters) and extended by influence parameters described in references [9].

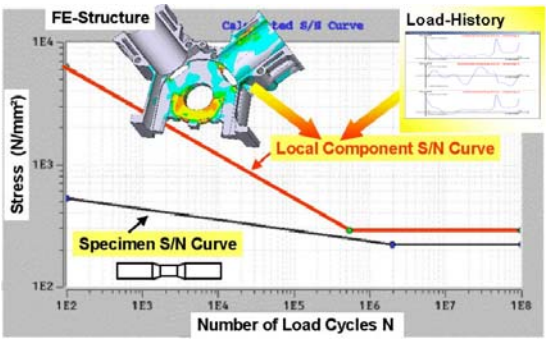


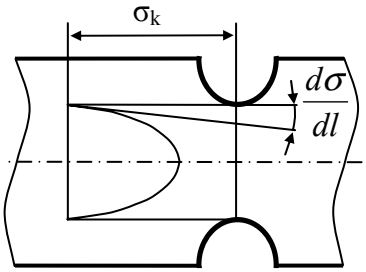
FIGURE 1: Synthetic S/N curve based on specimen material data, load and local fatigue influences for a certain FE-node

3 Arc and Spot Jointed Components

The stiffness and the operating strength of sheet metal parts of bodies is strongly influenced by the properties of their joints. The used joining technology, the design and the position of the welding seams, as well as the number and the location of the spot joints have a significant technical and economical impact. This becomes clear from the fact that in fatigue testing of car bodies more than 90% of the cracks originate from joints [6,7,8], which is mainly due to the considerably lower dynamic loading capability of welding seams and spot joints in comparison to the base material. Therefore, especially for lightweight structures, the joining technology plays a key role. An optimum use of the material capabilities is only possible with optimized weld or spot joint design of a structure. This only becomes practicable by assessing the component in an early phase of the development process. Extensive standards and a large number of publications offer a multitude of assessment methods for evaluating the impact of dynamic loading on the fatigue life of a structure. Most of them are based on nominal stresses. Welding seams and spot joints are classified according to their geometry, their shape and their loading. Meanwhile, the Finite Element Method is a standard analysis tool for structural analysis. When assessing FE-results of such structures with respect to fatigue life, the use of the classical methods yields in numerous difficulties.

4 Kt-Free Estimation of Component Notches

As basic material input data S/N-curves of cylindrical, unnotched and polished specimen are used by FEMFAT. At each node of the FE-mesh a synthetic S/N-curve will be created by modifying the basic specimen S/N-curve in dependence on several influence parameters like stress gradient, surface roughness, etc. This influence parameter method combines the advantages from nominal stress concepts and local concepts. It is named to "local stress concept based on relative stress gradient". Usually for complicated geometries it is not possible to define a nominal stress because the cross-section is not determined uniquely. But the stress concentration factor K_f (and with it some kind of pseudo nominal stress) can be estimated by the relative stress gradient derived from the FE-stress distribution. The relative stress gradient is automatically calculated by FEMFAT and used for the modification of the local S/N-curve by taking into account the important notch effect, quantified by the notch sensitivity factor K_t. A method, how to calculate the ratio K_t/K_f, has been developed by the Engineering Center Steyr [10], but also other methods are provided [3,5].



$$\chi = \frac{d\sigma}{dl} \qquad \left[N/mm^3 \right] \text{ ... Stress Gradient}$$

$$\chi' = \frac{1}{\sigma_k}\frac{d\sigma}{dl} \qquad \left[1/mm \right] \text{ ... Relative Stress Gradient}$$

FIGURE 2: Definition of the Relative Stress Gradient

For the other influence factors mostly methods fixed by the German FKM-guiding rule ("Forschungskuratorium Maschinenbau" = Research Committee Mechanical Engineering) [4] have been implemented into FEMFAT. The list of influence factors include:

- Stress Gradient
- Constant Stress
- Surface Roughness
- Isothermal Temp. Influence
- Technological Size Influence
- Mean Stress
- Statistics Influence
- Surface Treatment Influence Factors
- Thermomechanical Temp. Influence
- Tempering Influence

5 Assessment Concept for Welding Seams

The welding seam assessment concept is integrated as a module in the fatigue life software FEMFAT® [12]. It is based on three key issues (overview see figure 3):

- Finite Element welding seam modelling guidelines
- Databases for welding seam notch factors and S/N curves.
- Recognition and classification of all welding seam areas in the whole structure.
- Automated fatigue assessment.

The Finite Element welding seam modelling guidelines were developed to instruct a FE user how to realize welding seams within a complete structural model so that they can be assessed in an automated manner. The guidelines mainly give rules for setting attributes to nodes and elements representing the local welding seam. Different attributes, like material labels and node colours serve to distinguish the orientation, the geometry and the type of welding seam. An open scheme permits the extension of the guidelines to new, not yet included types of seam shapes or welding seam configurations. The welding seam itself is not modelled. Instead, the seam sheet metals are represented by shell elements. In the following the shell elements which border on the welding seam are called "welding seam elements" or simply "seam elements". The size of these elements may vary widely with the exception of the seam ends, as only the basic stresses ("nominal stresses") will be computed in the seam elements. A possibility to automatically correct the stresses based on the characteristic of the stress curve and the element size is supplied. The contents of the seam elements' material tables as well as their thickness are the same as those of the associated sheet metal.

The additional effort in model preparation is limited to associating certain node and element attributes to the welding seams and to a few manual modifications at the seam ends. Special attention has to be paid to correctly assign the welding seam shell top and bottom. Based on a concept presented by Radaj [2], an approach was developed in [1] which allows to derive the dynamic loading capabilities of welding seams of arbitrary type and geometry from the welding seam notch fatigue strength. In a first step, for structures with almost no residual stresses, the structural S/N curves were determined for different joint geometries, load configurations and plate thickness by 41 test series. In the next step, for every test series, a numerical Boundary Element simulation model was established to compute the linear notch stresses respectively the stress concentration factors at the welding seam locations endangered to crack initiation. A radius of 1mm was used to round the seam roots and the seam transitions to the surrounding basic material. Else, the simulation model was based on the mean value of the properties of the respective test series. Using the notch factors determined by means of simulation and the nominal fatigue strength in the crack-sensitive cross-sections, a fictitious seam notch fatigue strength was calculated.

For the different test series, for a constant stress ratio R a unique value of the seam notch fatigue strength has been found. Therefore, the fictitious seam notch fatigue strength may be used in combination with FE sub-models together with a constant replacement notch radius for the prediction of the fatigue life of complex welding seams. The stress state of the welding seams is determined from FE-results of the stress state in the seam elements using local seam coordinate. The notch factors for a computation of the comparable fictitious seam notch fatigue strength are filed in a welding seam database, covering most widely used seam types. This database has been made for the sake of efficiency, as the costly process of creating and analyzing sub-models with respect to S/N curves and local notch factors is done only once. Depending on the type of welding seam, notch factors for at most 3 load cases at maximally 4 assessment locations per sheet connected to the welding seam are stored. These are, if existing, the heat zone notches (undercuts) at the transition and the root region for the top or bottom side of the sheet panel. The notch factors are associated with the stress normal to the welding seam in the plane of the sheet panel. The S/N curves used for linear damage accumulation are adapted to the actual loading case by interpolation [12]. Applications to a multitude of structures during almost a decade, now,

show that this approach is highly suited to pre-optimize welded structures like car and truck frames or bogies of steel and aluminium.

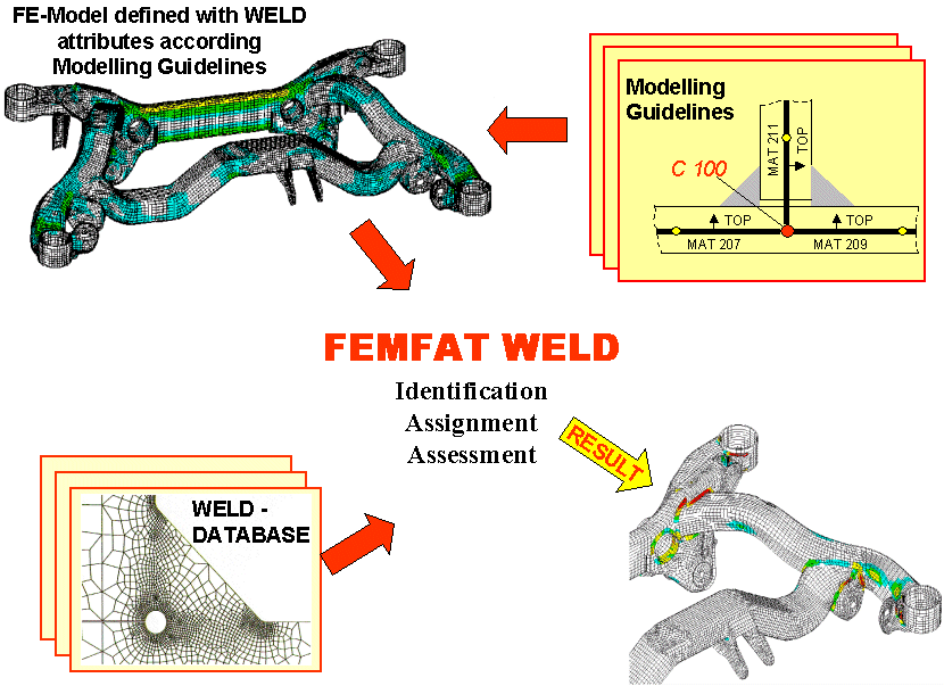


FIGURE 3: Arc-welded vehicle axle, **FEMFAT WELD** concept.

6 Fatigue Analysis of Spot Joints

Second generation FE models of vehicle body structures seduce to the use of the one-dimensional connecting elements (beams or rigid elements) as a basis for the fatigue assessment of the welding spots. The following problems appear using this approach:
Size and quality of the shell elements connected to the one-dimensional beam or rigid elements influence the section forces as well as the local displacement behaviour (see figure 4). The problem to be solved is how to reach a constant element size and quality in a complete structural model.

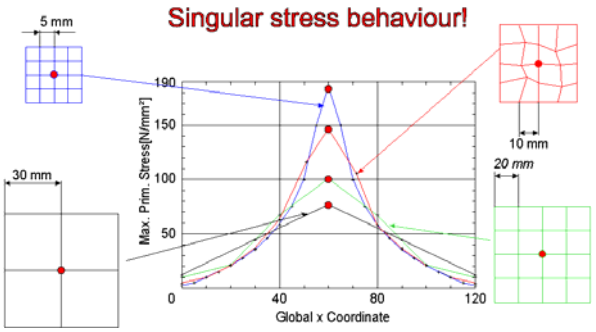


FIGURE 4: Stress results in the joint area **before** preprocessing for different FE-mesh size and quality

The definition and modification of the location of a welding spot requires the respective nodes at the upper and lower sheet-metal panel to be moved. How can be ensured that all one-dimensional connecting elements of a complete structural model are exactly normal to the local panel surfaces? It is a fact that an inclination of a one-dimensional connecting element yields to wrong section forces.

The section forces of the connecting elements only provide information on the force flow in the spot joint itself between both sheets. The section forces however do not give any information on the loading of the welding spot in the sheet-metal panel itself (see figure 5). In case of an in-plane loading without any force flow in the spot joint, such a concept would give zero damage. In reality, however, the welding spot is a potential location of crack initiation due to undercuts.

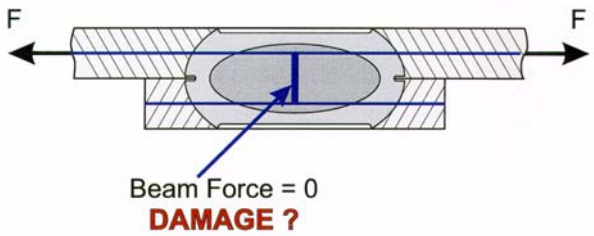


FIGURE 5: Faulty fatigue estimation when using beam forces

6.1 Assessment Concept for Spot Joints

The fatigue assessment concept for spot joints is based on the use of second generation FE-models. The problems described in the previous section are solved by a different assessment approach, which requires a few additional steps. The basic idea is not to use the section forces of the connecting elements but the stresses in a well-defined ring of elements around the spot. The following steps are required:

6.1.1 Modification of the FE-Mesh:

For a raw FE-mesh without any connecting elements, CAD-Data may directly be put in to generate the spot joints at the right location. Otherwise, an on principle arbitrarily meshed second generation FE-mesh, i.e. including connecting elements, is used. A pre-processor has been written which serves to automatically modify the local FE-mesh around the spot welding. The result is a steady circular element arrangement around the spot joint in the magnitude of the diameter of the spot weld (see figure 6 for an example).

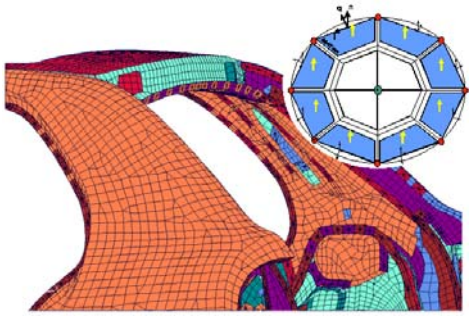


FIGURE 6: Pre-processed local spot joint area of a body in white structure

The new mesh is automatically connected to the rest of the structure. The constant circular FE-mesh around the spot joint is the basis for a standardized assessment quality of the element stresses.

6.1.2 Correction of Stiffness

In the course of automatic generation of the new mesh around the spot joint, the stiffness properties of the elements directly connected to the one-dimensional connecting elements are adapted to correct the singular deformation behavior (see figure 7). In the case of welding spots, Young´s modulus is significantly increased in comparison to regular shell elements.

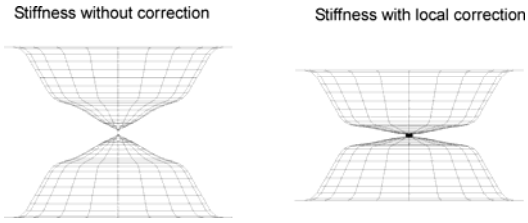


FIGURE 7: Singular deformation behavior of regular DC specimen

6.1.3 Finite Element Analysis

This step generally consists of a linear or geometrically nonlinear FE analysis with commercial software like NASTRAN.

6.1.4 Computation of Fatigue

The prediction of the fatigue behavior is based on the stress distributions in the element rings. The required local specimen S/N curves for different loading types are stored in a data base. They were determined by comparing test and simulation results of specimen (DC-specimen [11], H-specimen [7]). It was found that differences in external loading and boundary conditions have only little influence on the local dynamic strength value in the assessment element ring. The kind of loading is determined by the stress distribution along the ring. Loading conditions can be pure normal tension or pure shear tension or generally a mixture of both. The associated S/N curve is generated by interpolation, considering data from the DC- and H-specimen.

6.1.5 Visualization

For the spot joints, the computed fatigue values in terms of damage or endurance safety factors are stored at the nodes of the element rings. They can be visualized analogously to stress results together with the fatigue results in the base material regions using conventional post-processors. Figure 8 shows an application to a part of a car-body, namely the wheel house panel.

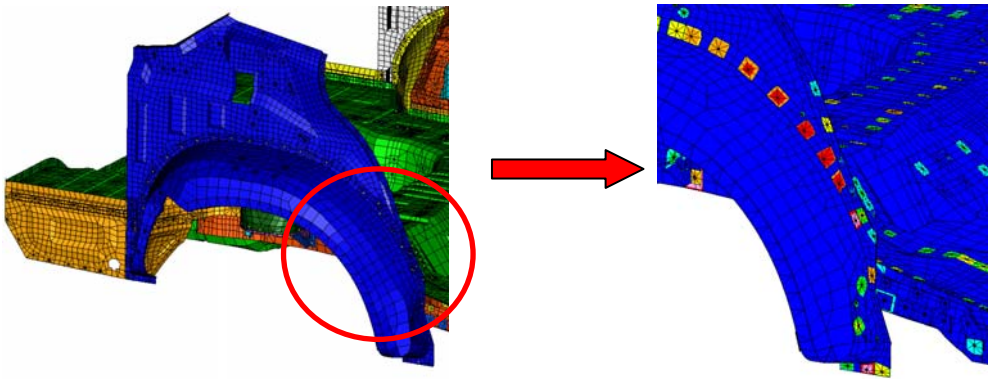


FIGURE 8: Damage distribution of a wheel house panel

7 Conclusion

The presented approach of fatigue assessment proofs to be a highly valuable tool in engineering practice. The main advantages are:

- Improved understanding and assessment of FE results.
- Cost reduction in FE analysis by easier interpretation of results.
- Reduction of experimental fatigue tests due to better initial designs.
- Evaluation of operational performance before existence of prototype.
- Standardisation of fatigue assessment method for suppliers.

8 REFERENCES

8.1 Book

1 Köttgen, V.B.; Olivier, R.; Seeger, T. (1989) "Schwingfestigkeitsnachweise für Schweißverbindungen auf Grundlage örtlicher Beanspruchungen", Research book, book no 143, Forschungskuratorium Maschinenbau, Frankfurt, Germany

2 Radaj, D. (1985): "Gestaltung und Berechnung von Schweißkonstruktionen, Ermüdungsfestigkeit", DVS, Düsseldorf, Germany

3 Hück M., Thrainer L., Schütz W., "Berechnung von Wöhlerlinien für Bauteile aus Stahl, Stahlguß und Grauguß – Synthetische Wöhlerlinien", Verein deutscher Eisenhüttenleute, Bericht Nr. ABF 11, Düsseldorf, Juli 1983

4 German FKM Guiding Rule "Rechnerischer Festigkeitsnachweis für Maschinenbauteile", VDMA Verlag Frankfurt/Main, 3rd edition, 1998

5 DDR-Standard TGL 19340, "Ermüdungsfestigkeit; Dauerfestigkeit der Maschinenbauteile", Verlag für Standardisierung, Berlin, March 1983

8.2 Conference Proceedings

6 Gumpinger, J.; Hahn, O.; Korte, M; Kudrnac, P; Singh, S; Unger, B. (1997) "Computer Simulated Estimation of the Fatigue Behaviour and Stiffness of Spot Joints in Automotive Structures", Proceedings IBEC´97 – International Body Engineering Conference & Exposition, Stuttgart, Germany, September 1997.

7 Singh, S; Schmid, G; Gao, S. (1991) " Leichtbau durch optimierte Fügetechnik", lecture and paper on the occasion of the DVM Meeting "Bauteil 91" at Berlin, Germany. Proceedings page 239-255

8 Singh, S.; Schmid, G. (1993) "Dünnblechkonstruktionen und ihre Eigenschaften – Prüfverfahren und ihre Aussagekraft", Special Meeting of the SLV-Munich "Fügen von Aluminium im Dünnblechbereich", Ingolstadt, Germany, November 1993, lecture and paper, Proceedings page 17-26

9 Eichlseder, W.; Unger, B. (1994): "Prediction of the Fatigue Life with the Finite Element Method", SAE Paper 94 02 45

8.3 Dissertation or Thesis

10 Eichlseder, W., "*Rechnerische Lebensdaueranalyse von Nutzfahrzeugkomponenten mit der FE-Methode*", Dissertation, TU Graz. 1989.

11 Hahn, O.; Kurzok, J.R.; Rohde, A.; Thesing, Th. (1996): "Konzept zur numerischen Auslegung punktförmig gefügter Dünnblechstrukturen auf der Basis experimenteller Versagensanalysen". LWF Paderborn, Germany

8.4 References to Unpublished Sources

12 FEMFAT, Version 4.3 (2002), Users Manual, Engineering Center Steyr, Steyr, Austria, Europe

Fatigue Life Analysis of Geometrically Complex Components

W. Eichlseder[a], A. Leitgeb[b], B. Araujo[a], M. Riedler[b]

[a] Department Product Engineering, Chair Mechanical Engineering, University of Leoben, A-8700 Leoben, AUSTRIA
[b] Christian Doppler Laboratory for Fatigue Analysis, University of Leoben, A-8700 Leoben, AUSTRIA

Abstract Geometrically complex structures are characterised by irregular contours of the stress level, caused by notches, bending loaded sections, or areas with irregular stress flow. This irregularity can be expressed by the derivation of the stress: the stress gradient χ, or, related to the local stress, the relative stress gradient χ'. This gradient is taken to describe the fatigue strength in the case of notches as well as under tension/compression and bending loading. For the description of the slope of the S/N-curve a new method is proposed. It has been applied in aluminium and steel alloys, having shown satisfactory results for the parameters of a S/N curve.

1 INTRODUCTION

The local life approach for fatigue life prediction is nowadays widely accepted by the automotive industry. Nevertheless, the investigation of the local fatigue behaviour only by test is not possible, as the study of parameters influencing the components fatigue behaviour takes too much time and cost. On the many attempts made to simulate the S/N curve and predict the life of a component, the use of the local stress gradient to define the notch sensitivity (see equation 1) in order to be able to calculate the parameters of the S/N curves for notched and unnotched samples has been successfully proved [2, 5, 6]. Furthermore, Hück, Thrainer and Schütz [3] had previously made a proposal based on factors such as the notch sensitivity of the material, the surfaces finish, or a technology factor.

The notch sensitivity has been the starting point for the present work. The mentioned model [2, 5, 6] is based on the relative stress gradient. The stress gradient expresses an irregularity on the contours of the stress level, and it is easily calculated with the help of finite element results. The influence of the different loads and the notch influence are thus studied throughout the following equations for the fatigue limit:

$$\sigma_f = \sigma_{tf} \cdot \left(1 + \left(\frac{\sigma_{bf}}{\sigma_{tf}} - 1 \right) \cdot \left(\frac{\chi'}{2/d} \right)^{K_\chi} \right) \tag{1}$$

This can also be written as:

$$\sigma_D = \sigma_{tf} \cdot n_\chi \tag{2}$$

where n_χ is the proposed notch sensitivity factor that is dependent on the relative stress gradient and the size of the tested sample. Two types of tests are needed as input data for this equation, the axial bending endurance stress (σ_{bf}) which is the basis for the determination of the stress gradient, and the uniaxial tension/compression endurance stress (σ_{tf}) for the notched and unnotched samples.

Besides the fatigue limit, two more equations were proposed to complete the determination of the S/N curve: the slope of the curve, and the number of cycles N_D at which the slope changes:

$$k = k_{\min} + \frac{k_{\max} - k_{\min}}{n_{\chi}^{Kk}} \tag{3}$$

$$\log(N_D) = \log(N_{D\min}) + \frac{\log(N_{D\max}) - \log(N_{D\min})}{n_{\chi}^{Kn}} \tag{4}$$

where the parameters denoted as min or max refer to the values shown by an unnotched and a highly notched sample respectively.

2 PROPOSED MODEL

When HCF tests are carried out, important decisions have to be taken so as to establish the number of samples to be tested and the different testing conditions to obtain a sufficiently wide range of results. In this decision the requested time for each test as well as its costs and required work play an important role. On the researching side, the more number of samples the better, and on the economical side the lesser is the better. These two opposed views have found a solution in the statistical approach to the S/N curves. Nevertheless, the parameters found with the statistical approach usually show a variation range. The goal of the present work is to find a simulation model for the requested parameters of S/N curves of notched samples.

Samples of two different aluminium alloys have been used in the present work, wrought alloy AlCuBiPb and cast alloy AlSi7MgCu0.5.

Since Al alloys, as most face-centred alloys do not have a characteristic fatigue limit, the behaviour has been described with two straight lines with slopes k_1 and k_2. The first stress-life curve with the slope k_1 corresponds, the second stress-life curve slope k_2 is not similar to the well known stress-life curve of ferrous alloys. The fatigue limit is defined as stress amplitude corresponding to the stress-life curve k_2 at N=10^7 load cycles [4, 1].

2.1 Calculation of new S/N curves, in dependence on χ'

To define the S/N curves for any notched geometry (represented by the local stress gradient χ') several data must be available. Since equation (1) is used to determine points on the new S/N curves, the two S/N curves for axial bending and uniaxial tension/compression are needed as well as the curve progression of the exponent K_D against χ'.

2.1.1 Determination of k_1 and k_2

The first step is to compute four points on each of the two basic S/N curves (axial bending and uniaxial tension/compression). Two points must be in the range of HCF (e.g. 10^7 and 10^8 load cycles) and two in the range of LCF (e.g. 10^3 and 10^4 load cycles). To find these points use the well known equation (5):

$$\sigma_{1,b} = \sigma_{bf} \cdot \sqrt[-k_{1,b}]{\frac{N_1}{N_{D,bf}}} \tag{5}$$

Thereby $\sigma_{1,b}$ is the stress-value derived from the axial bending S/N curve for the number of load cycles corresponding to N_1 (e. g. 10^3), $k_{1,b}$ is the slope at N_1.

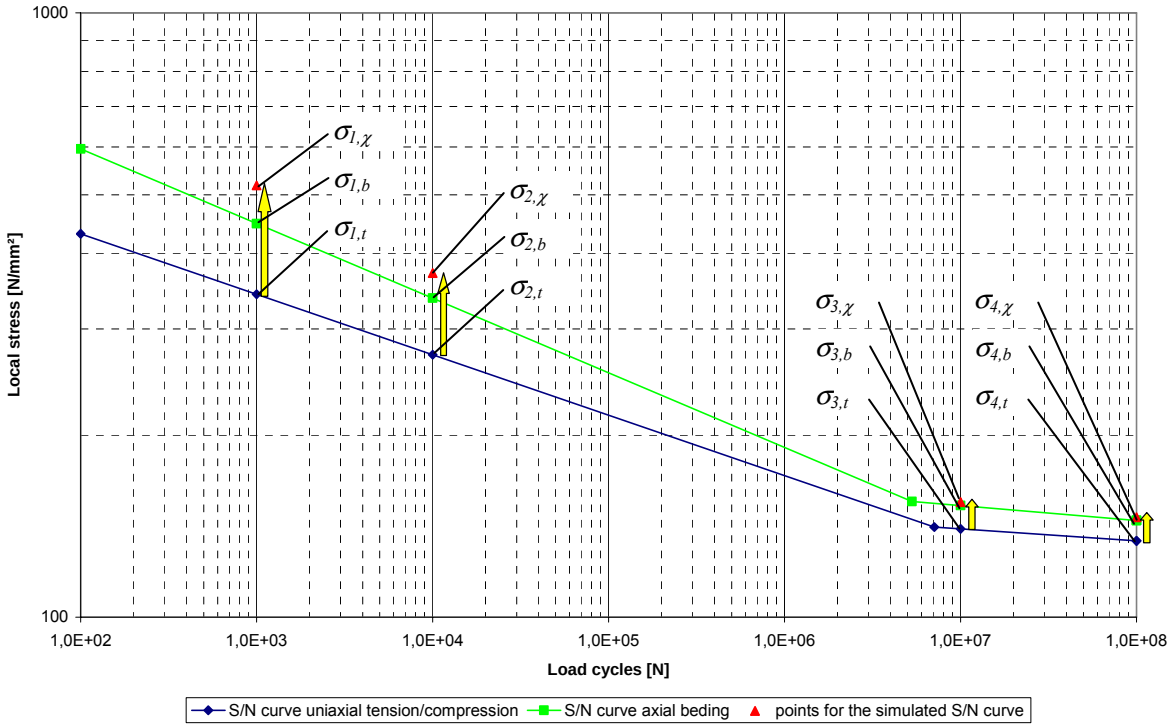


Figure 1. Calculation of the supporting points

Assuming that equation (1) is valid in the range of LCF too, we can calculate four points which define the new S/N curve for a given χ' with these eight points derived from the known S/N curves and the different values of K_χ for the two ranges (see Figure 1):

$$\sigma_{i,\chi} = \sigma_{i,t} \cdot \left(1 + \left(\frac{\sigma_{i,b}}{\sigma_{i,t}} - 1 \right) \cdot \left(\frac{\chi'}{2/d} \right)^{K_\chi} \right), \quad i = 1 \ldots 4 \tag{6}$$

With these four new points it is possible to evaluate the slopes $k_{1,\chi}$ and $k_{2,\chi}$ (Figure 2):

$$k_{1,\chi} = \frac{\log\left(\frac{N_2}{N_1} \right)}{\log\left(\frac{\sigma_{1,new}}{\sigma_{2,new}} \right)}, \qquad k_{2,\chi} = \frac{\log\left(\frac{N_4}{N_3} \right)}{\log\left(\frac{\sigma_{3,new}}{\sigma_{4,new}} \right)} \tag{7}$$

2.1.2 *Determination of N_D*

By knowing the slopes of the two ranges, and one point in each area, it is possible to define two straight lines, which are intersecting each other. This intersection point is $N_{D,\chi}$ (Figure 3).

$$N_{D,\chi} = \frac{k_1 \cdot k_2 \cdot \left(\log\left(\sigma_{2,\chi} \right) - \log\left(\sigma_{4,\chi} \right) \right) + k_2 \cdot \log\left(N_2 \right) - k_1 \cdot \log\left(N_4 \right)}{k_2 - k_1} \tag{8}$$

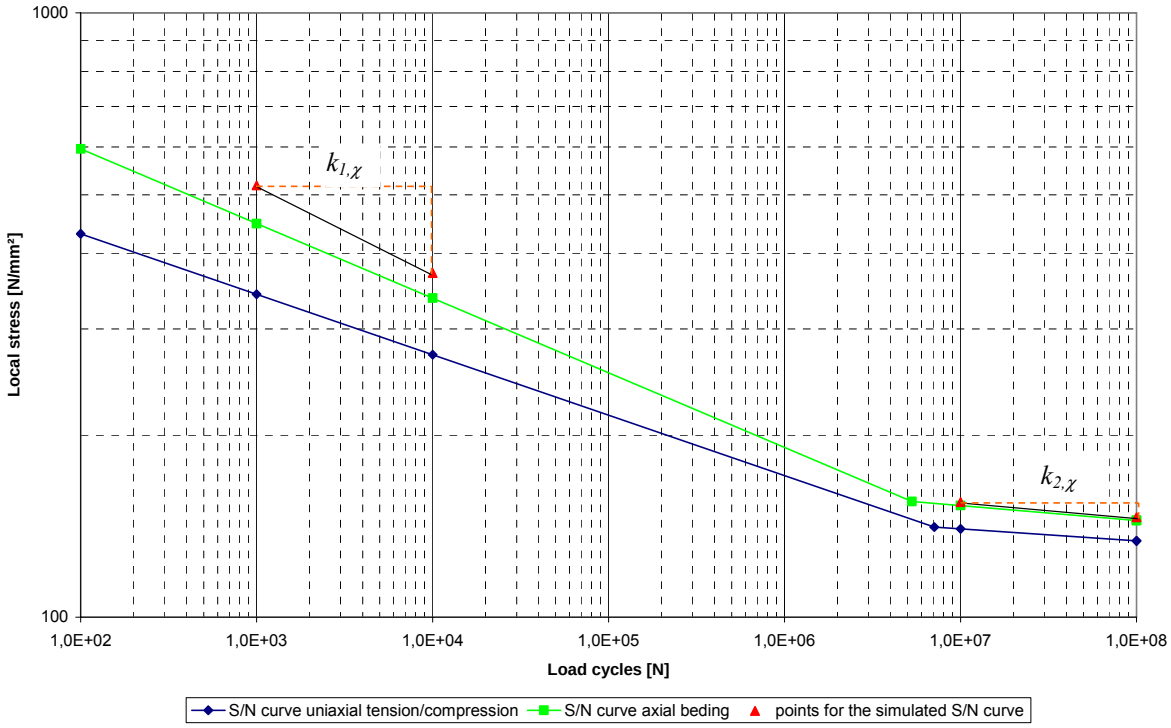


Figure 2. Calculation of $k_{1,\chi}$ and $k_{2,\chi}$

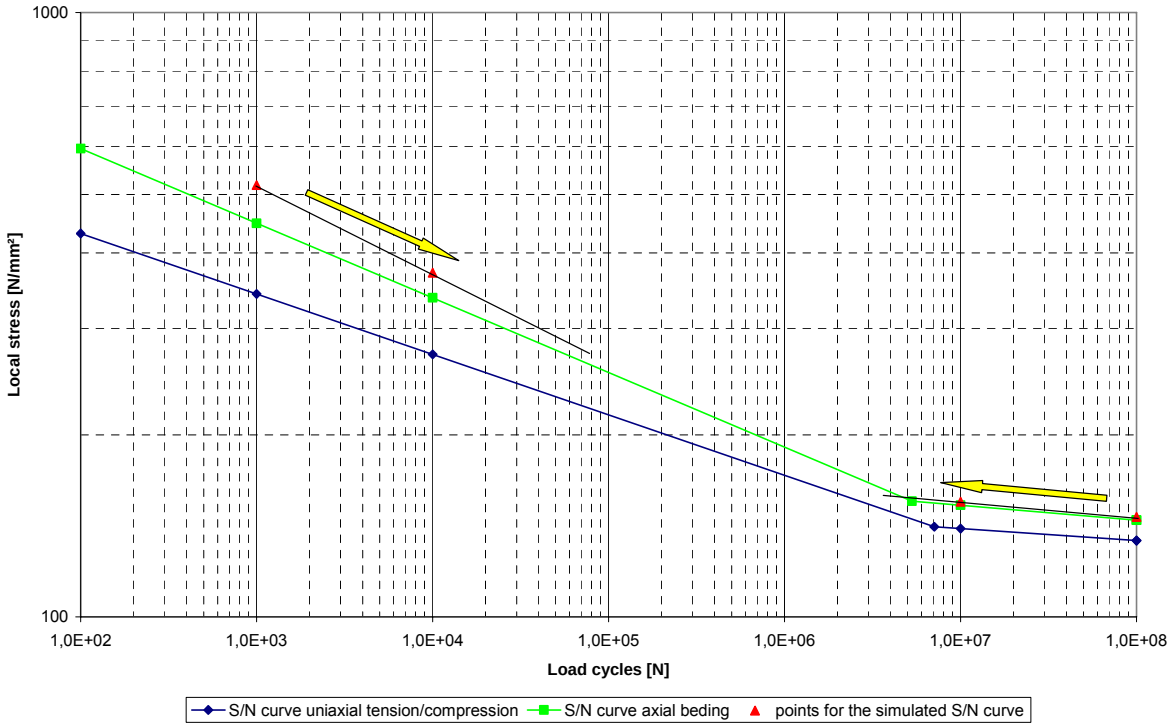


Figure 3. Calculation of $N_{D,\chi}$

2.1.3 *Evolution of K_D against N*

As can be seen in Figure 4 the value for K_χ is dependent on the number of load cycles. To define K_χ for a certain number of load cycles, three stress-values must be known. From the four tested S/N curves, four stress values for uniaxial tension/compression, axial bending, and two notched specimen with a relative stress gradient χ' of 2.23 and 9.6 can be derived (equation (9)). Thus it is possible to calculate the average curve for K_χ against N.

$$K_\chi = \frac{\log\left(\frac{\sigma_{N,\chi} - \sigma_{N,t}}{\sigma_{N,b} - \sigma_{N,t}}\right)}{\log\left(\frac{\chi'}{\chi'_b}\right)} \tag{9}$$

It is possible to approximate this curve by a line in the semi-logarithmic diagram. The region around 10^6 load cycles must be excluded from the calculation. For engineering problems, the physical S/N curve is approximated by two lines in the double-logarithmic diagram. Due to this approximation, the engineering S/N curves are very close together in the region of N_D. So the difference between $\sigma_{N,b}$ and $\sigma_{N,t}$ for certain supporting points in this range is small and because of equation (9) the value for K_χ is overestimated.

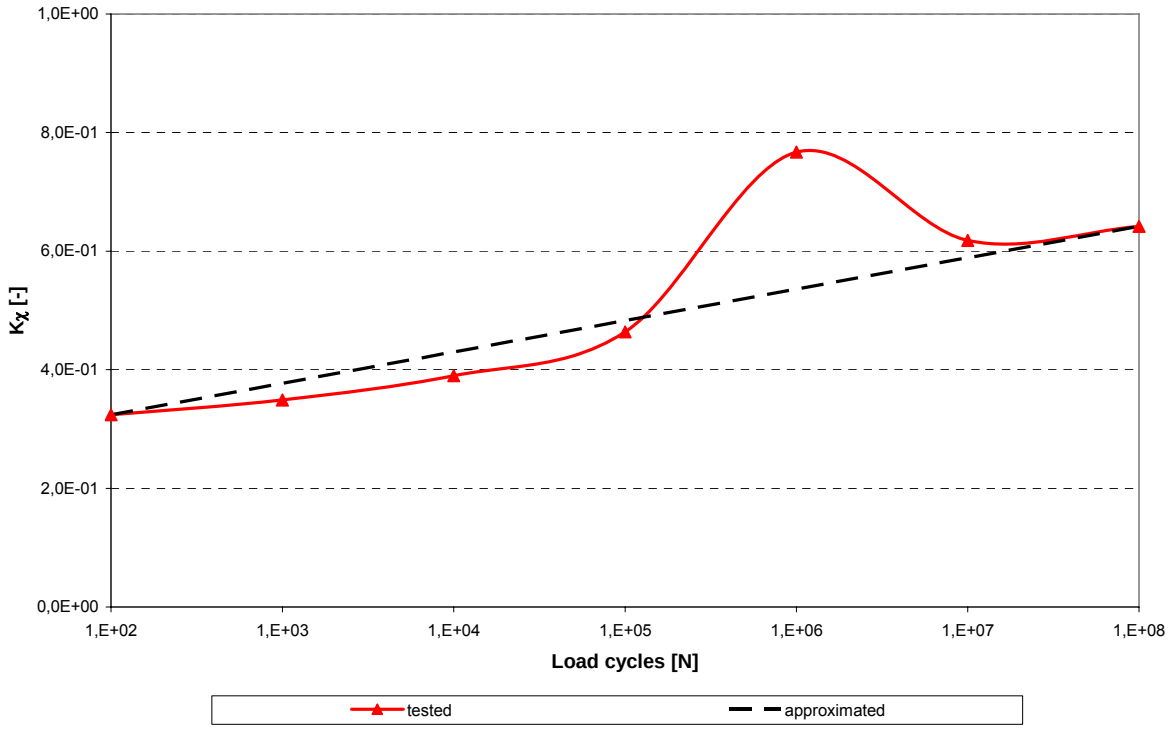


Figure 4. Evolution of K_D against N for material AlSi7MgCu0.5

3 RESULTS

3.1 Comparison of simulated and tested results

In Figure 5 and Figure 6 the tested and simulated results are compared. The S/N curves for axial bending, uniaxial tension/compression and the notched specimen with different values of χ' are displayed by bold lines, whereas the simulated curves are depicted by dashed lines.

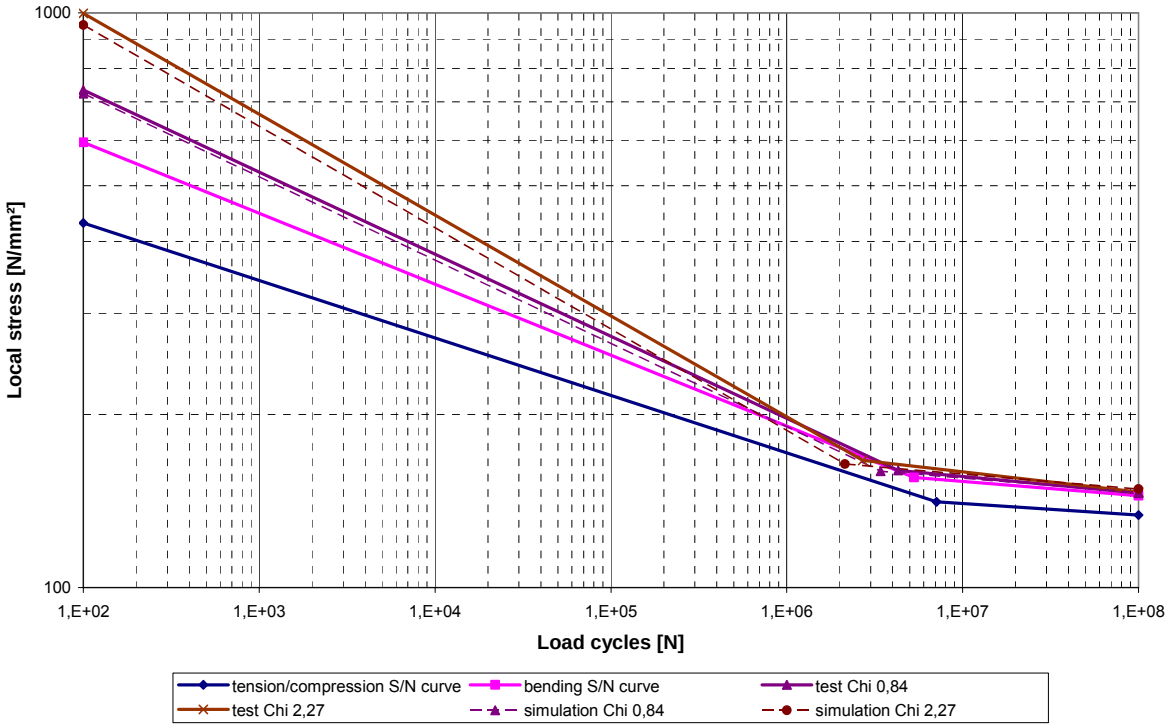


Figure 5. Comparison of material AlCuBiPb for the shape of the S/N curves

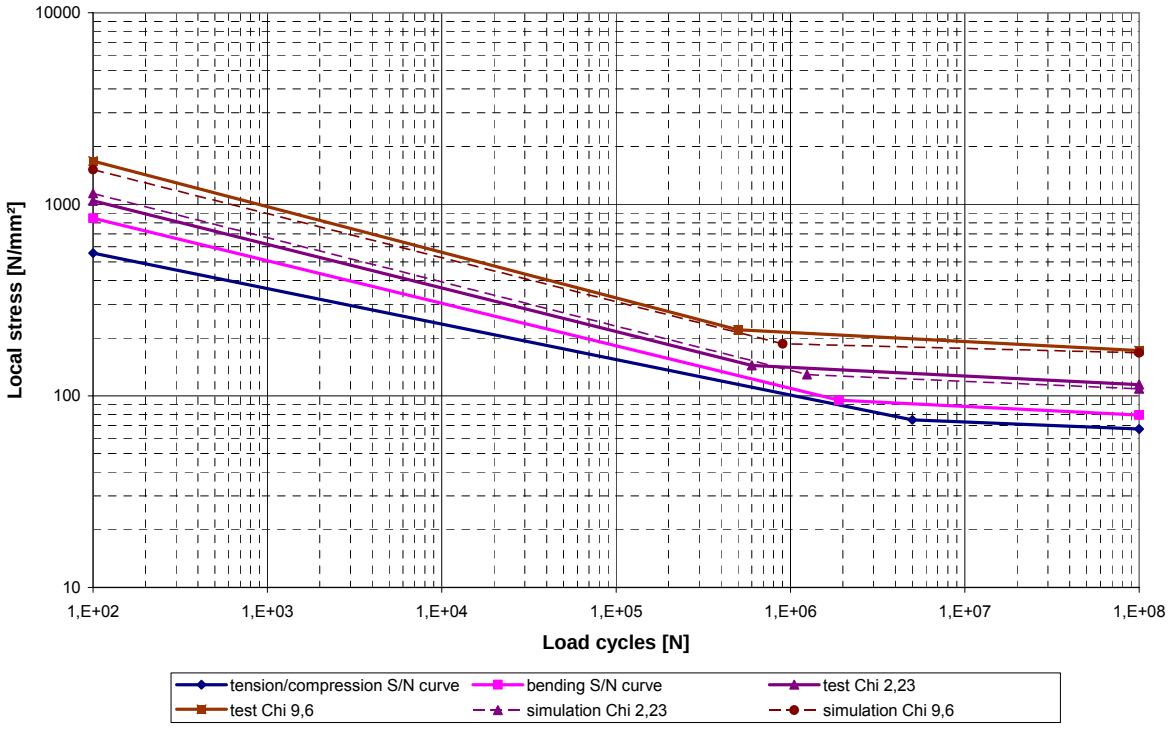


Figure 6. Comparison of material AlSi7MgCu0.5 for the shape of the S/N curve

In Figure 7 simulated S/N curves for various values of χ' are displayed in comparison to their basis curves (axial bending and uniaxial tension/compression). Figure 8 shows the curve progression for N_D against χ', the values for N_D are taken from Figure 7.

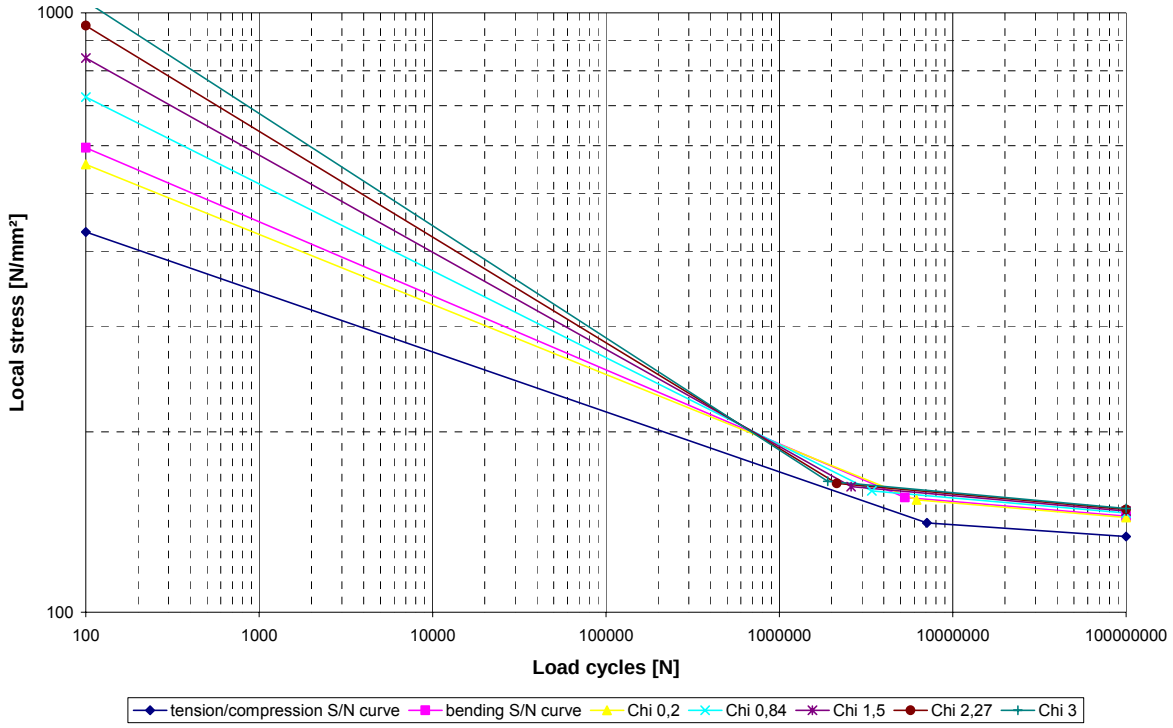


Figure 7. AlCuBiPb: Simulated S/N curves for various values of χ'

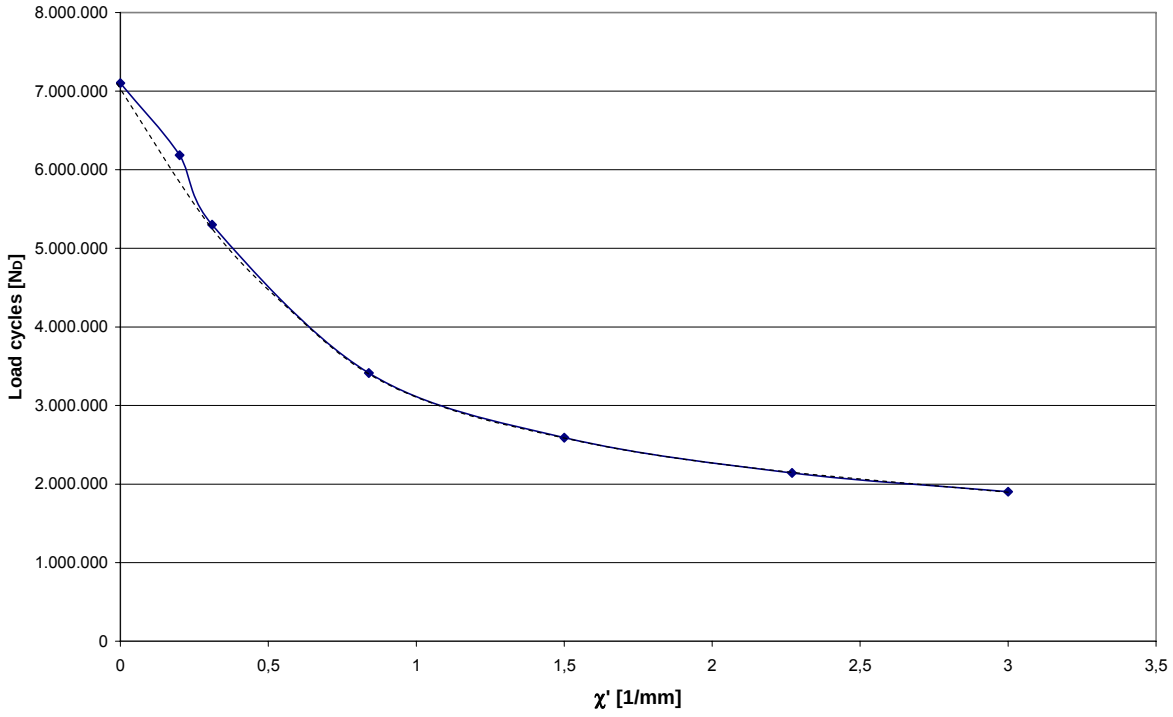


Figure 8. AlCuBiPb: N_D against χ'

4 CONCLUSION

A new method has been proposed for the simulation of the local S/N curve. The two S/N curves for axial bending and uniaxial tension/compression are needed as well as the curve progression of the exponent K_χ against χ' (notch sensitivity curve).This new method has been used at two aluminium alloys, having shown satisfactory results. The method is also usable for alloys with a distinctive fatigue limit, since k_2 can be set to infinite.

This is a step forward to a reduction of the parameters that determine the behaviour of a material or a component, and still takes into account factors as important as the size, the geometry, the surfaces, or the notch influence. Its importance lies on the fact that fewer experiments might be needed in future predictions, with cost reduction and time shortening that is implied.

5 REFERENCES:

5.1 Book

1. E. Haibach, Betriebsfestigkeit, Verfahren und Daten zur Bauteilberechnung, VDI Verlag, 1989, 137-142.

5.2 Conference Proceedings

2. W. Eichlseder and H. Leitner, Fatigue 2002 Conference, Stockholm, 2783-2790.
3. M. Hück, L. Thrainer and W. Schütz, VDEh-Bericht ABF 11, Düsseldorf, 1983.
4. W. Eichlseder, B. Araujo , M. Riedler, H. Leitner and I. Godor, RELMAS 2005 Conference, Juni 14-17, 2005 St. Petersburg.

5.3 Journal Article

5. W. Eichlseder, *Mat.-wiss. u. Werkstofftech.*, 34 (9), 2003, 843-849.

5.4 Dissertation or Thesis

6. H. Leitner, Simulation des Ermüdungsverhaltens von Aluminiumgusslegierungen, PhD thesis, University of Leoben, 2001.

A New Damage Indicator: From Blocks Loading to Random Loading.

A.AID[a,b], J.CHALET[a, c], A.AMROUCHE[a], G.MESMACQUE[a], M.BENGUEDIAB[b]

[a]Lab. de Mécanique de Lille, Université de Lille1, UMR CNRS 8107, Villeneuve d'ASCQ 59650, France. E-mail: abdelwaheb.amrouche@univ-lille1.fr
[b]LPQ3M BP 763, Université de Mascara, ALGERIE.
E-mail: abdelkrim.aid@univ-lille1.fr
[c]ENSAM Lille, Boulevard Louis XIV, Lille.

Abstract One of the largest difficulties in fatigue damage is to find a representative damage indicator which can be easily connected with the Wöhler curve taken as known data of the material. The most used model is the Miner's rule but this one does not take into account the loading history, so for the same loading level the experimental results are higher than the Miner expectations in increasing loading and are lower than the Miner expectations in decreasing loading.
This work presents a new damage indicator which takes into account the loading history, this indicator is connected cycle by cycle to the Wöhler's curve.
Tests were performed in two and four blocks loading under constant amplitude. Four sequences were compared: The increasing and the decreasing magnitude and random block loading were compared. The experimental results were compared to the damage calculated by the Miner's rule and a new damage indicator. This comparison shows that the proposed model, present a good estimation of the experimental results. Moreover, the error is minimized in comparison to the Miner's model.
An experimental investigating is conduced currently for the prediction of the fatigue life under loading by block of Gaussian distribution and under loading to variable amplitude and this to widen the validation of the model of damage proposed.

Keywords:
Damage indicator, Random loading, Block loading, Random block loading.

NOMENCLATURE

D	: damage variable
D_i	: fractional damage
$\sigma_{(i)d}$	: stress of damage.
σ_i	: applied stress at level i,
σ_u	: ultimate tensile strength
N_{Ri}	: number of cycles to crack initiation in the Wöhler curve
n_i	: applied number of cycles at level i

1 INTRODUCTION

The mechanical components generally work under cyclic stresses with varying amplitudes during their lifetime. The fatigue phenomenon is created by these stresses and it is the major cause of failure of the mechanical components during service operation. Assessing fatigue damage is a critical issue. It is one of the most frequently encountered structural engineering problems. In general, fatigue damage cumulative theories can be classified into two categories: (1) linear damage cumulative theories and (2) nonlinear damage cumulative theories.
In order to predict the residual life of these components it is important to formulate a method to evaluate the fatigue damage accumulation. Since many years, design engineers use Palmgreen-Miner law, linear damage rule (LDR), and its modifications to predict fatigue life of components in the case of variable loading [1]:

$$D = \sum_{i=1}^{n} \frac{n_i}{N_{Ri}} = \sum_{i=1}^{n} r_i \qquad (1)$$

where n_i is the number of cycles at a given stress amplitude $\Delta\sigma_i$, N_{Ri} is the number of cycles to failure at the same stress amplitude and D is the damage variable (it is equal to 1 in correspondence of exhausted life). This method is based on assumption of constant work absorption per cycle independent on the loading levels.
Because of the insufficiencies presented with linear damage rule (LDR), the lack of take account of the damage for stress below the limit of fatigue and lack of the interaction between levels of loading applied that can return produce a discrepancy of up an order of magnitude between the predicted and the experimented life and this calculation may be non conservative.
Many researchers tried to modify Miner's rule, but, due to its intrinsic deficiencies, no matter which version is used, life prediction based on this rule is often unsatisfactory [2].
Marco and Starkey firstly proposed a non-linear load dependent damage rule [3], as follows:

$$D = \sum_{i=1}^{n} r_i^{x_i} \tag{2}$$

where x_i is a coefficient depending on ith load. This rule allows to correctly take into account the effects of different loading sequences. Experience showed that only in some case and for some material this law, and the other theories derived from it, have shown good agreement with experimental results; moreover the involved coefficients (x_i) have to be calculated for each different load and load condition limiting their use in engineering applications [4].
Recently, a new approach, based on damage mechanics, has been proposed (the so called continuum damage mechanics). With the original concepts developed by Kachanov [5] and Rabotnov [6]. Chaboche and Lemaitre [7-8] applied these principles to formulate a nonlinear damage evolution equation in the form:

$$\delta D = \left[1-(1-D)^{\beta+1}\right]^{\alpha} . \left[\frac{\sigma_a}{M_0(1-D)}\right]^{\beta} . \delta n \tag{3}$$

where β and M_0 depend on material and $\sigma_a = \sigma_{max} - \sigma_m$ (σ_{max} and σ_m are respectively the maximum and the mean stress of cycle); the exponent α depends on the loading (σ_{max}, σ_m) which results in non-separability between damage and loading. The expression of α proposed by Chaboche is:

$$\alpha = 1 - \frac{1}{H}\left\langle \frac{\sigma_a - \sigma_f}{\sigma_u - \sigma_a} \right\rangle \tag{4}$$

where symbol $\langle\ \rangle$ is defined as $\langle x \rangle = 0$ if $x < 0$ and $\langle x \rangle = x$ if $x > 0$.
Many forms of fatigue damage equation have been derived after Chaboche's work; all of them are similar in form and the main differences lie in the number and the characteristics of parameters used in the model and in the requirement for additional experiments to determine them [9-10].
The model suggested by G. Mesmacque and al. [11] does not require too many properties of material and it takes into account the history of loading. This model is connected cycle by cycle with Wöhler's curve.
The experimental observations highlighted that when a positive average stress, σ_m, is super imposed on the cyclic loading of amplitude its, the life of the specimens decreases. The inverse effect is observed in the presence of a average stress of compression [12].
In order to take into account this phenomenon, the complementary tests can be carried out in order to established Haigh's diagram, for life time fixed at N_R, the alternate stress equivalent σ_{aeq} according to the characteristics (σ_m, σ_a) of the cycle. This returns in fact to modify the curve of Wöhler for each cycle with $\sigma_m \neq 0$.
The real loadings are often more complex. Estimation of fatigue life of a material subjected to random loading needs suitable calculation algorithms. In such algorithms, cycle counting [13] according to a given method (for example, the rain flow method) and damage accumulation according to the assumed hypothesis (for example Palmgren–Miner, Haigh's diagram) are the main operations.

2 DESCRIPTION OF THE MODEL

A detailed description of the damage stress model is given in ref. [11],[14]. We summarise here the concept with an algorithm for the comprehension (see Fig.1).

$$D_i = \frac{\sigma_{(i)d} - \sigma_i}{\sigma_u - \sigma_i} \tag{5}$$

where:

$\sigma_{(i)d}$: stress of damage; σ_i : applied stress, and σ_u: ultimate stress.

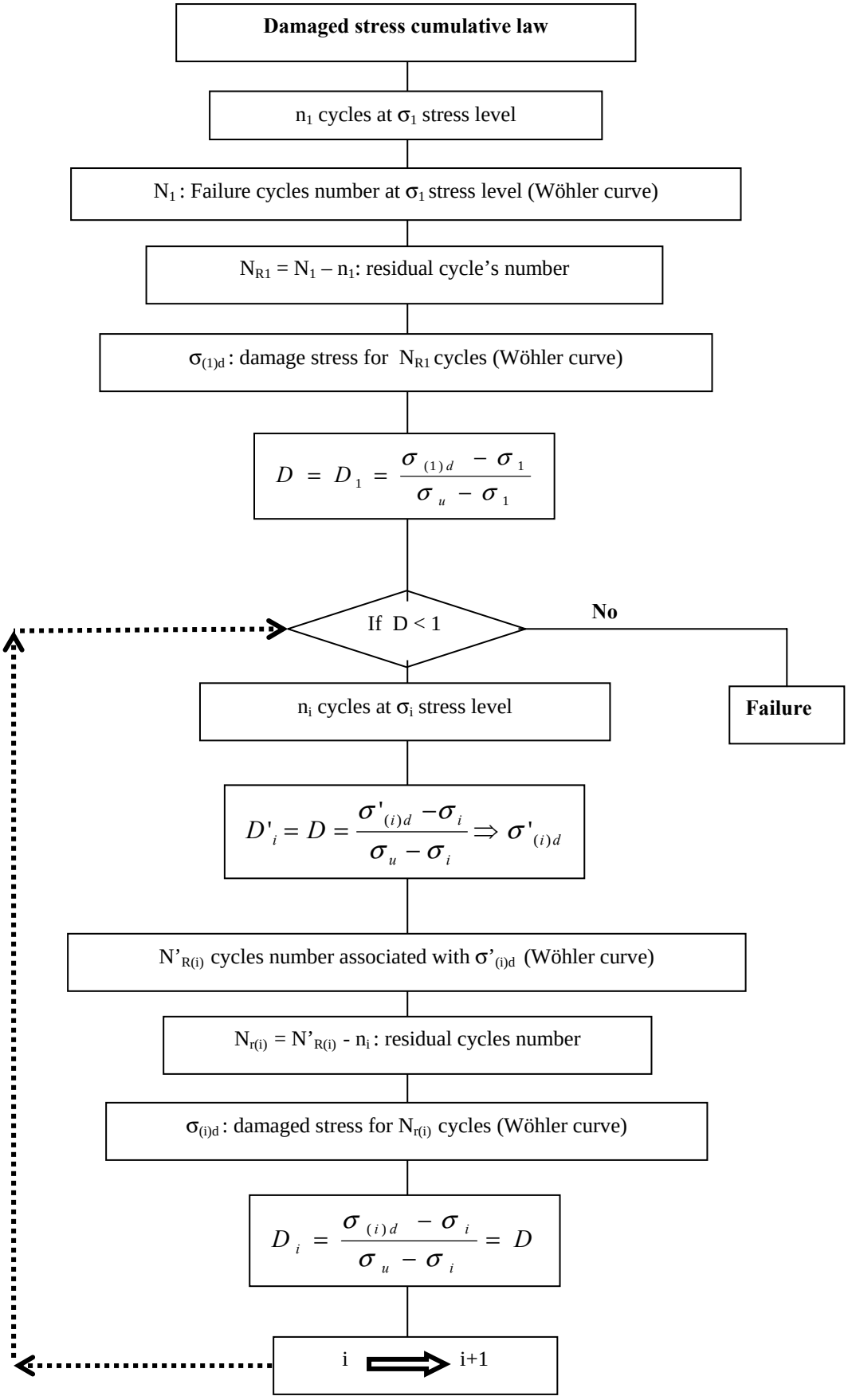


Fig.1. Algorithm of the damaged stress model.

The equivalent stress of damage at the level i+1 is calculated with the relation

$$D_i = \frac{\sigma_{(i)d} - \sigma_i}{\sigma_u - \sigma_i} = \frac{\sigma_{(i+1)d} - \sigma_{i+1}}{\sigma_u - \sigma_{i+1}} \quad (6)$$

where:

$\sigma_{(i+1)d}$: equivalent stress of damage at the level i+1,

σ_{i+1} : stress at the level i+1.

So σ_{ed} is equal to σ_i to the first cycle, it means D = 0 and σ_{ed} is equal at σ_u at the last cycle D = 1.

3 PREDICTION OF THE MODEL WITH BIBLIOGRAPHIC RESULT

Our model is now compared with recent data. They are taken from the Pavlou results [15], and from Krouse and Moore [16]. The loading conditions are illustrated in Fig. 2.

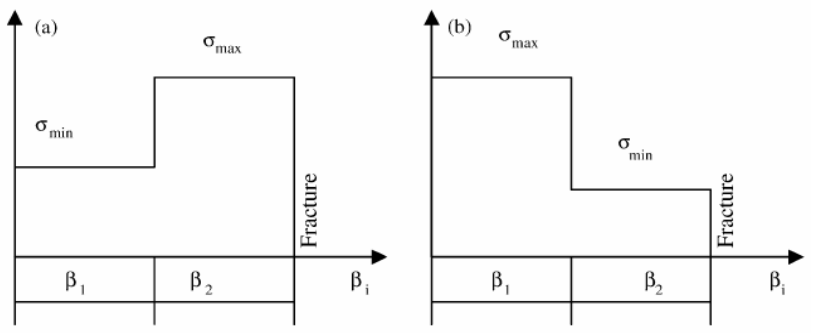


Fig. 2. Loading cycle blocks with (a) increasing amplitude, and (b) decreasing amplitude.

3.1 Results from Pavlou [15]

Life time for σ=150 MPa is N=430.000 cycles and for σ=200 MPa is N=150.000 cycles. Ultimate stress is taken as σ_u=470 MPa.
β_1 fraction of life at level 1,
β_2 fraction of life at level 2 until fracture.
A comparison of experimental results, Miner and damage stress model predicted life is given in Table 1.

Table 1: Experimental results [15], Miner and damage stress model predicted life.

Increasing loading amplitude.								
σ_1=150MPa		σ_2=200Mpa, n_2 residual life						
n_1	β_1	Experimental		Miner		Model		
		result	β_2	result	Dev.	result	Dev.	β_2
86000	0.2	144500	0.963	120000	16.8	123485	14.5	0.82
172000	0.4	133500	0.89	90000	32.5	101187	24.1	0.68
258000	0.6	81700	0.54	60000	26.5	75175	7.7	0.50

Decreasing loading amplitude.								
σ_1=200Mpa		σ_2=150Mpa, n_2 residual life						
n_1	β_1	Experimental		Miner		Model		
		result	β_2	Result	Dev.	result	Dev.	β_2
30000	0.2	228700	0.67	344000	50.5	297550	30.2	0.69
60000	0.4	101050	0.24	258000	155	19106	89.0	0.44
90000	0.6	76050	0.18	172000	126	10402	36.8	0.24

3.2 Results from Krouse and Moore [16]

Krouse and Moore got the following results for maraging 300CVM steel with material properties: yield stress =2098 MPa and ultimate stress 2590 MPa. Number of cycles to failure at different stress amplitudes are given in Table 2.

Table 2: Number of cycles to failure at different stress amplitudes [16].

Stress amplitude	2086	2000	1655	1103	965	900	827
Fatigue life	891	1160	3809	48645	112573	174400	296400

The results, for different fractions of life at the level 1 and the residual part of life at level 2 are illustrated in Fig. 6 with other experimental results [15–16].
As we can see, the deviation is lower with our model and the results are more representative than by using Miner's rule. On the experimental results given by Krouse and Moore, only one test at each loading level was performed.

4 SPECIMEN AND EXPERIMENTS

The material used in this investigation was an aluminium alloy 6082-T6. The chemical composition of the material was (%):
0.6Mg, 0.7Si, 0.24Fe, 0.06Cu, 0.9Mn, 0.02Cr, 0.06Zn, and 0.02Ti. Plane specimens, which were acquired as a plate

with a 8mm thick (see Fig.3).

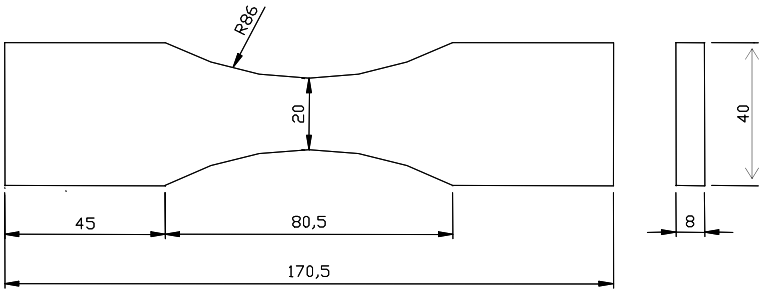


Fig.3. Geometry of a specimen.

The room temperature mechanical properties of aluminium alloy are given in Table 3.

Table 3. Mechanical properties of the aluminium alloy.

Yielding stress (MPa)	Ultimate stress (MPa)	Young's modulus(GPa)	Elongation %
347	370	73	12

The experiments were carried out under uniaxial constant amplitudes for determining the Wöhler curves. An equation for the stress-life curve for the material was determined from a prior investigation according to ASTM standards [16]:

$$\log(\sigma) = A - m.\log(N_R) = 6.8 - 0{,}1024.\log(N_R) \quad (7)$$

where σ_f =220 MPa, $N_G=2\times10^6$; N_R is the number of cycles to fracture, σ is the stress amplitude, m is the exponent of the Wöhler curve, σ_f is the fatigue limit, and N_G is the limit number of cycles corresponding to σ_f.

Four cyclic stress levels were considered and four different sequences were applied. The aim of this set of tests is to determine the influence of increasing or decreasing loading conditions on lifetime and to determinate the life fatigue under random block loading. The experimental conditions are given in table 4.

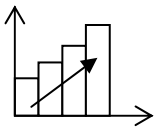
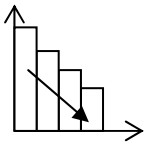
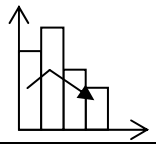
Table 4. Experimental conditions

	Block number			
	1	2	3	4
σ_{max} [MPa]	240	260	280	305
N_{Ri}	412000	105035	77708	43800

5 ANALYSIS OF THE RESULTS

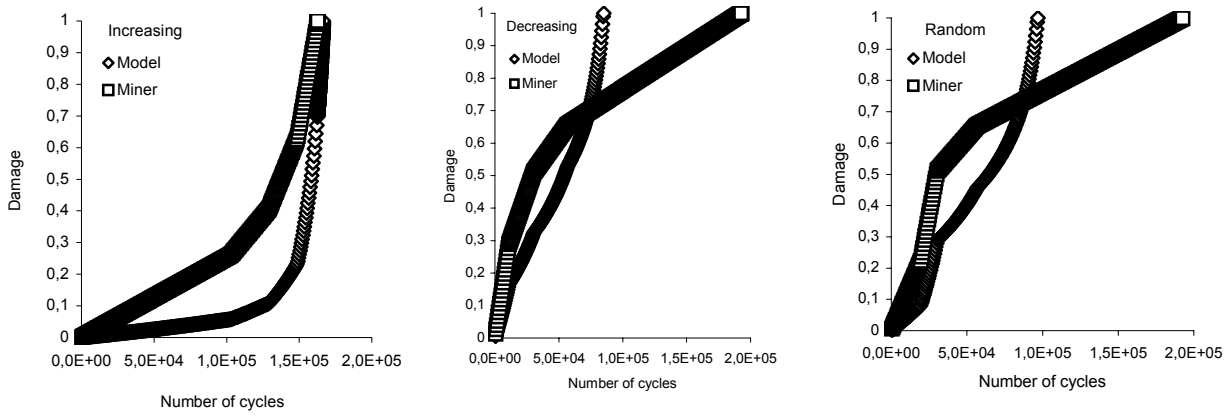
The results of aluminium alloys 6082-T6 for cumulative damage for different blocks loading are given in table 5 and represented in Fig.4.
The figures 4 (a, b, c) represent the fatigue damage evolution for three configurations (increasing, decreasing and random loading), they show the evolution of the damage according of the number of cycles for Damage Stress model and Miner's model.
In the figure 5-a, the damage evolution for Damage Stress's model for all spectres is represented and also the damage evolution for Miner's model in figure 5-b.
- During the totality of the lifetime of the specimens, all the curves of damage cumulative represented the model "Damage Stress" are below the curves of the Miner's rule.
- The curves of the cumulative damage determined by the proposed model have a concave form i.e. the value of the damage remains low during the totality of the loading then believes quickly until the rupture of the specimens.

Table 5. Results carried out, for three configurations (increasing, decreasing and random loading)

01	**Spectre N°01**								**Increasing blocks**
Load	240	260	280	**305***			Variation (%)		
Nbe cycles	103000	26258	19427	Exp.	Miner	Model	Miner	Model	
				16800	**14140**	**19550**	**15,8**	**16,3**	
02	**Spectre N°02**								**Decreasing blocks**
Load	305	280	260	**240***			Variation (%)		
Nbe cycles	10950	19427	26258	Exp.	Miner	Model	Miner	Model	
				52500	**136050**	**51500**	**15,9**	**2**	
03	**Spectre N°03**								**Random blocks**
Load	280	305	260	**240***			Variation (%)		
Nbe cycles	19427	10950	26258	Exp.	Miner	Model	Miner	Model	
				43400	**136050**	**61310**	**213,4**	**41,3**	

*: results of the last block.

- Except the case of the figure 4-a (increasing loading), where the models give the same lifetime (at the end of the lifetime of the specimens). The decreasing and random loading configuration (Fig 4-b,4-c) shown that the model of damaged stress presente a weak variation in comparaison with the Miner's model.
-We notice for the figure 4-b and 4-c, the permutation of the first two blocks does not have an influence of the lifetime especially for the Miner's model.
- In these two last cases, the model "damaged stress" presents a good evaluation of the lifetime (variation = 2% for the decreasing configuration and variation = 41,3% for the random configuration) compared with Miner's model (variation = 159% in the first case and variation = 213,4% for the second case).



(a): increasing blocks. (b): decreasing blocks. (c): random blocks loading.

Fig.4. Fatigue damage evolution with number of cycles for four sequences of loading.

The Fig.6 shown the predicted results from Miner's model who takes the value of 1 and the predicted indicator of the damaged stress in this study with the bibliographic results [15-16] and our results. This results shown that the proposed indicator give a good prediction in comparaison with the Miner's model.

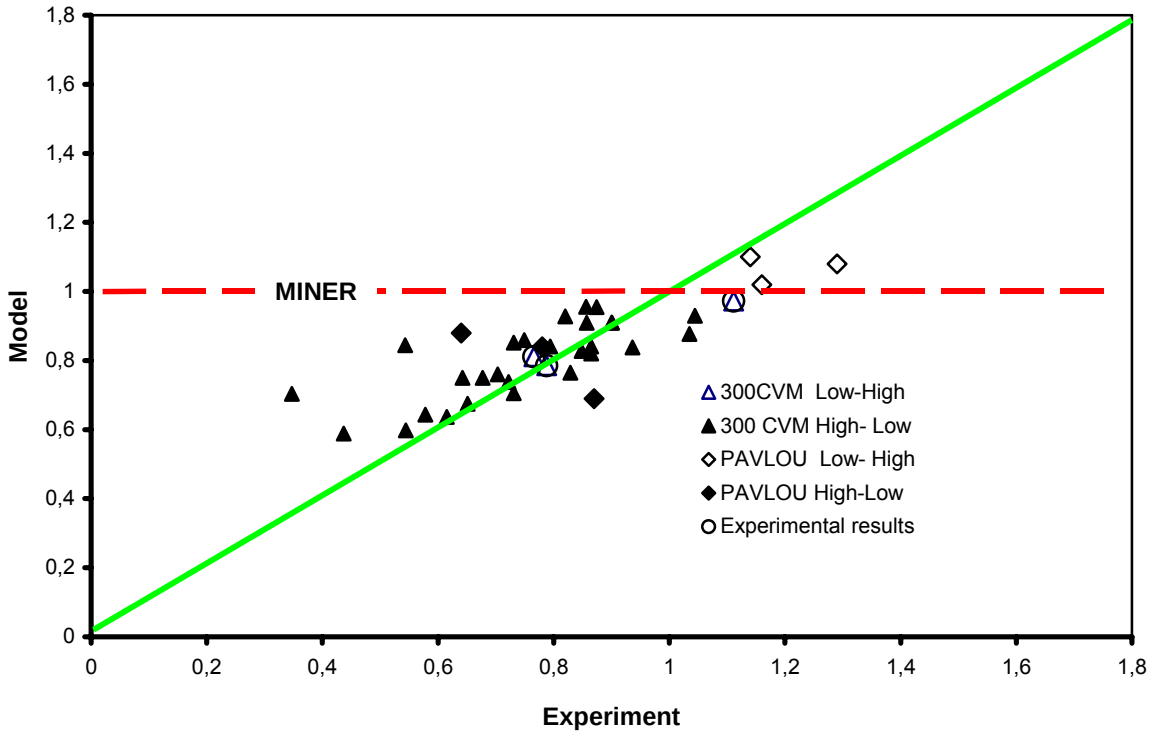


Fig. 6. Comparison of experimental results, experimental results given in [15–16] and prediction by proposed model.

6 CONCLUSIONS

1. A nonlinear fatigue damage cumulative model is proposed, which consider the effects of the ultimate stress, data of lifetime taken by S-N curve of the metal studied and the effect of the loading sequence is also included. The uniaxial fatigue damage evolution equation is derived, which the better descriptive ability is achieved for fatigue damage evolution by experimental verifications.
2. The application of the proposed uniaxial fatigue damage cumulative model is discussed, and the recurrence formula is derived for this model under multilevel loading. The loading case below fatigue limit is also considered.
3. Using the Miner's rule to calculate the cumulative lifetime we found that in all cases, increasing, decreasing and random blocks loading, the experimental results were below prediction.
4. The results obtained by the model of the damage stress are compared with the experimental results and a good agreement has been found.

7 REFERENCES

7.1 Books

5. Kachanov LM. Introduction to continuum damage mechanics. Dordrecht: Martinus Nijhoff; 1986.
6. Rabotnov YN. Creep problems under in structural members. Amsterdam: North Holland; 1969.
7. Chaboche JL. Continuum damage mechanics—a tool to describe phenomena before crack initiation. Nucl Eng Des 1981;64: 233–47.

7.2 Journal Article

1. M.A.Miner, Cumulative damage in fatigue, J Appl Mech **67** (1945), pp. A159–A164.
2. A. Fatemi and L. Yang, Cumulative fatigue damage and life prediction theories: a survey of the state of the art for homogeneous materials, Int J Fatigue **20** (1998) (1), pp. 9–34.
3. Marco SM, Starkey WL. A concept of fatigue damage. Trans ASME 1954;76:627–32.
4.V. Dattoma, S. Giancane, R. Nobile, F.W. Panella, Fatigue life prediction under variable loading based on a new non-linear continuum damage mechanics model, Int J Fatigue xx (2005), pp. 1–7
7. Chaboche JL. Continuum damage mechanics—a tool to describe phenomena before crack initiation. Nucl Eng Des 1981;64: 233–47.
8. Lamaitre J, Chaboche JL. Mechanics of solid materials. Cambridge, UK: Cambridge University Press; 1990.
9. Shang DG, Yao WX. A non-linear damage cumulative model for uniaxial fatigue. Int J Fatigue 1999;21:187–94.
10. Cheng G, Plumtree A. A fatigue damage accumulation model based on continuum damage mechanics and ductility exhaustion. Int J. Fatigue 1998;20(7):495–501.
11. G. Mesmacque, S. Garcia and A. Amrouche. Sequential law in multiaxial fatigue: a new damage indicator. Int.J Fatigue.Vol 27, Issue 4, pp 461-467, 2005.
13. C. Amzallag, J.P. Gerey, J.L. Robert and J. Bahuaud, Standardization of the rainflow counting method for fatigue analysis. Int. J. Fatigue **16** (1994), pp. 287–293.
14. S.Garcia, A.Amrouche, G.Mesmacque, X.Decoopman, C.Rubio. Fatigue damage accumulation of cold expanded hole in aluminum alloys subjected to block loading. Int.J Fatigue. xx (2005) 1–7
15. Pavlou DG. A phenomenological fatigue damage accumulation rule based on hardness increasing, for the 2024-T42 aluminum. Eng Struct. 2002;24:1363–8.
16. Krouse, Moore. Application of a double linear damage rule to cumulative fatigue. ASTM STP 415 1967;384–412.
17. ASTM E 739-91 (1998). Standard practice for: statistical analysis of linearized stress-life (S–N) and strain-life (ε–N) fatigue data. In: Annual book of ASTM standards, vol. 03.01. Philadelphia, 1999. p. 614–20.

7.3 Dissertation or Thesis

12. X. Pitoiset, Méthodes spectrales pour une analyse en fatigue des structures métalliques sous chargements aléatoires multiaxiaux. Thèse de doctorat, Université Libres de Bruxelles (2001).

EN1993-1-9: a code for fatigue design

Alain Nussbaumer[a]

[a] ICOM – Steel structures laboratory
Swiss Federal Institute of Technology, 1015 Lausanne EPFL, Switzerland

Abstract The drafting of a European standard for the fatigue design of steel structures has started during the eighties with, as a basis, the ECCS (*European Convention for Constructional Steelwork, Brussels*) fatigue recommendation. In EN1993-1-9, one can recognize ECCS original work, however, a lot of new knowledge has been included. The code continues to use the nominal stress approach together with the same set of S-N curves as at the beginning. In addition, the concept of the hot spot (geometric) stress approach as well as the combination of fatigue and fracture criteria are also included. This paper describes the fatigue design procedure used in the construction industry with an emphasis on the following issues: the concept of fatigue damage equivalent factor, the rationale behind the classification tables and S-N curves for the different details, the treatment of the size effects on fatigue strength, the steel quality and fabrication requirements and the values of the partial safety factor for strength.

1 INTRODUCTION

1.1 The European standard family system

In Europe, the construction market and its services is regulated through product standards, testing codes and design codes, the whole forming an international standard family. The European standard family prepared by CEN includes so far 10 Eurocodes with design rules, for a total of 58 parts, and many hundreds of EN-standards for products and testing. It also contains so far around 170 European Technical Approvals (ETA's) and European Technical Approval Guidelines (ETAG's), all prepared by EOTA. For steel structures, the relevant parts of the European international standard family are shown on figure 1.

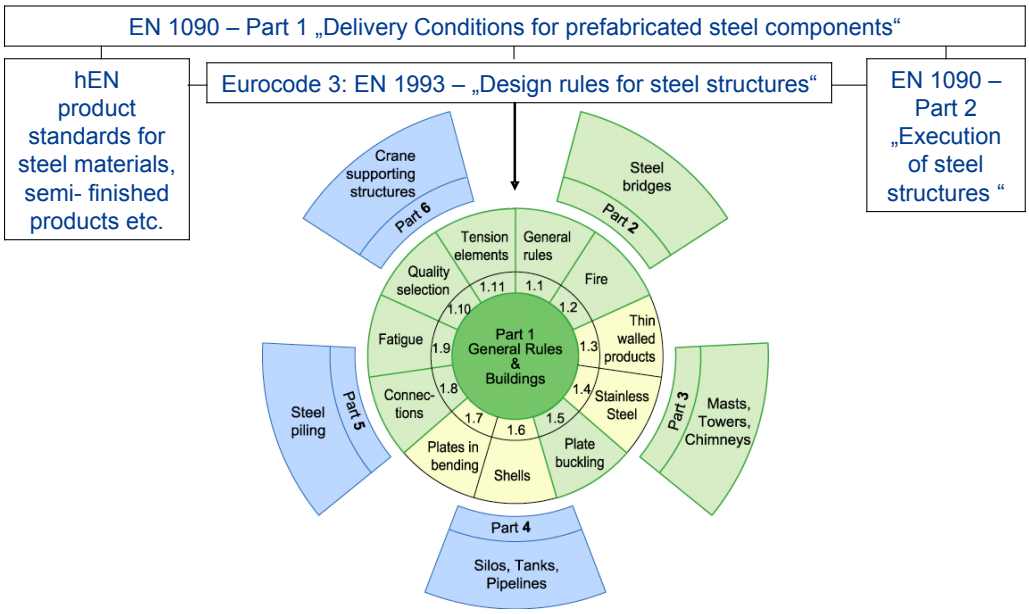


Figure 1. Standard system for steel structures, extract from [Schmackpfeffer, 2005].

In figure 1, the colours indicate the state of advancement of the various design standard parts, the parts indicated in green being the most advanced towards the status of national standards within the CEN members. In the design standards containing the general rules, two parts are related to fatigue. This is part 1-10: material

toughness and through-thickness properties (material quality selection) [prEN1993-1-10:2005], and part 1-9: fatigue [prEN1993-1-9:2005].

1.2 Material quality selection

When a steel structure is built, it shall satisfy the requirements for the execution of steel structures (EN 1090, ISO 5817) but will however contain imperfections that are within the required tolerances. Since it is possible that fatigue cracks develop from these imperfections, or that undetected defects may be present, brittle failure shall be excluded by a proper choice of the material. Part 1-10 of Eurocode 3 provides a method for selecting such a material, for the different possible applications and service conditions (characterized by a minimum reference temperature and stress level). The method in the code is summarized in figure 2. It is based on fracture mechanics calculations and a failure assessment diagram such as the R6 method [PD 7910:1999]. For a given detail, the accidental existence of an initial defect (modelled as an initial crack with size a_0), that should normally have been detected and repaired during welding inspection, is assumed. Under service conditions, the initial crack may grow due to fatigue loading to a size a_d until it is detected during an inspection. Fatigue crack initiation is not considered in the computation because of the severity of the defects in welded structures. With assumptions on the fatigue damage that occurring between two inspections, one can compute the crack size a_d and perform a safety check by comparing stress intensity factors values ($K_{appl,d} \leq K_{mat,d}$). The computations were carried out for various details and loading conditions [RWTH, 2001].

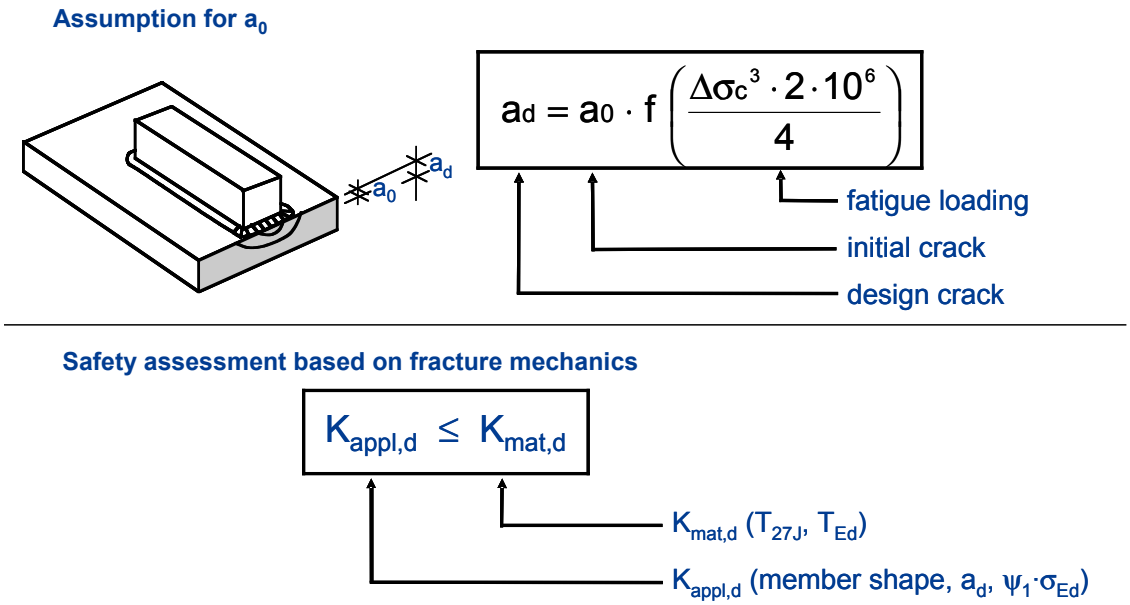


Figure 2. Method used in part 1-10 of Eurocode 3 for avoiding brittle fracture [Schmackpfeffer, 2005].

Since the member thickness influences both fatigue strength and brittle fracture, the material selection is presented in the form of tables with permissible product thicknesses for different steel grades, minimum reference temperatures and stress levels. The stress level considered in this selection is the one corresponding to an accidental load combination, owing to the fact that it occurs with the assumption of having simultaneously the lowest temperature, the presence of a crack, and the lowest admissible material properties. Once the material is properly selected, it can be assumed that fatigue cracking can occur without resulting in a brittle fracture and thus fatigue assessment can be undertaken using either a damage tolerant method or a safe life one.

2 FATIGUE ASSESSMENT

2.1 Verification format

In the mid-eighties, the ECCS (European Convention for Constructional Steelwork, Brussels) published recommendations for the fatigue design of steel structures [ECCS, 1985]. The first European standard for the

fatigue design of steel structures was based on these recommendations and the new code for fatigue design, Part 1-9 of Eurocode 3, also is. The principle of the fatigue verification, which has remained the same, is based on the classification method, or nominal stress method. In this method, a comparison between stress ranges from the loading to the fatigue strength at two million cycles is made. For direct stress range, it can be written as follows:

$$\gamma_{Ff}\Delta\sigma_{E2} \le \Delta\sigma_C / \gamma_{Mf} \quad (1)$$

with

$$\gamma_{Ff} \cdot \Delta\sigma_{E2} = \lambda \cdot \Phi_2 \cdot \Delta\sigma\left(\gamma_{Ff} Q_k\right) \quad (2)$$

where

γ_{Ff}	partial factor on actions (see EN 1991)
γ_{Mf}	partial resistance factor for fatigue, for which the recommended value is 1.00
$\Delta\sigma_{E2}$	equivalent constant amplitude stress range related to 2 million cycles
$\Delta\sigma_C$	reference value of the fatigue strength at 2 million cycles
Φ_2	equivalent impact factor, i.e. dynamic amplification factor
λ	global damage equivalent factor, see section 3
$\Delta\sigma(\gamma_{Ff} Q_k)$	stress range caused by the fatigue loads specified in EN 1991.

In the case of shear stress range, the verification is similar. The concept of the hot spot (geometric) stress approach has also been integrated in the code. The verification format stays the same and the hot spot stress range is computed using FEM analysis or parametric formulas. The fatigue strength for the different types of welds is given in the Annex B of Part 1-9. This method is particularly relevant for the design of tubular structures, in conjunction with the CIDECT publication for fatigue design [CIDECT, 2000]. Moreover, Part 1-9 contains a table (table 8.7) with detail categories for circular and rectangular tubular joints to be used with the classification method, but its application range is limited to small tubes (diameter ≤ 300 mm and thickness ≤ 8 mm).

The damage equivalent factor, called above global, is a combination of several different λ_i factors which allows for taking into account the real traffic, the static system, the service life value and the influence of more than one fatigue load on the structure (train crossings, two cranes on the same supporting beams, etc.). This is explained further in the next section. This verification corresponds to a simplified procedure; it is however always possible to perform a verification using the Miner damage accumulation rule, limiting value being one, when knowing the real loading spectra on the structure (annex A of part 1-9).

2.2 Partial resistance factor

Regarding the partial resistance factor for fatigue, it has no more a unique value as in the previous codes but is function of the fatigue assessment method chosen: damage tolerant or safe life. In the damage tolerant method, an acceptable reliability level is achieved through prescribed inspection and maintenance plans throughout the structure's life. Redundant static systems and structural elements allowing for load redistribution, such as orthotropic deck details, multi-planar tubular trusses, etc., are concerned with this method. With the safe life method, an acceptable reliability level can be achieved with a structure performing satisfactorily for its design life without the need for regular in-service inspection for fatigue damage. Inspections and maintenance for other reasons, corrosion protection system, bridge bearings, expansion joints, etc., will however be carried out. The acceptable reliability level is achieved by specifying different values for the partial factor for fatigue strength γ_{Mf}, see table I. In addition to the fatigue assessment method, the consequences of failure also influence the γ_{Mf} value.

As can be seen in table I, the possibility of detecting cracks or other signs of damage during inspections and thus to be able repair them on time –this is particularly true when there is redundancy in the structure– decreases the uncertainty in structural reliability and is acknowledged for through a reduction of the partial factor for fatigue strength γ_{Mf}.

Assessment method	Consequence of failure	
	Low consequence	High consequence
Damage tolerant	1,00	1,15
Safe life	1,15	1,35

Table I. Recommended values for partial factors for fatigue strength γ_{Mf} (table 3.1 from EN 1993-1-9)

The other parameter considered in table 3 is the consequence of failure. Even though redundancy influences the failure consequences, it is not what is meant by this parameter in the code philosophy. The consequences of failure are related to the perception of the engineer and of the owner regarding: partial or total failure, importance of the structure in the network, probability of human live losses when failure occurs (from people in, on or near the structure), etc.

2.3 Damage equivalent factor concept

The fatigue check of a new structure subjected to a load history is complex and requires the knowledge of the loads the structure will be subjected to during its entire life. Assumption about this loading can be made, still leaving the engineer with the work of doing damage accumulation calculations. The concept of the fatigue damage equivalent factor was proposed to eliminate this tedious work and put the burden of it on the code developers. The computation of the usual cases is made once for all. The concept of the damage equivalent factor is described in figure 3. On the left side of the figure, a fatigue check using real traffic is described. On the right side, a simplified model is used. The damage equivalent factor λ links both calculations in order to have damage equivalence.

The description of the procedure on the left side, procedure that was used by the code developers, is :

1. Modelling of real traffic and displacement over the structure,
2. Deduction of the corresponding stress history (at the detail to be checked),
3. Calculation of the resulting stress range histogram $\Delta\sigma_i$,
4. Calculation of the damage accumulation (using a accumulation rule, usually a linear one : Palmgren-Miner),
5. Either check using total damage must remain inferior to one (in this case, the detail category must be known to make the damage accumulation) or deduction of the resulting equivalent stress range $\Delta\sigma_e$ (or $\Delta\sigma_{E,2}$ for the value brought back at 2 million cycles) and check by comparing it with the detail category curve.

This procedure is relatively complex, notably in comparison with usual static calculations where simplified load models are used. It is however possible to simplify the fatigue check, using a load model specific for the fatigue check, in order to obtain a maximum stress σ_{max} and minimum stress σ_{min}, by placing this load model each time in the most unfavorable position according to the influence line of the static system of the structure. But the resulting stress difference $\Delta\sigma(\gamma_{Ff}\ Q_k)$, due to the load model, does not represent the fatigue effect on the bridge due to real traffic loading! In order to have a value corresponding to the equivalent stress difference $\Delta\sigma_{E,2}$, one must correct the value $\Delta\sigma(\gamma_{Ff}\ Q_k)$ with what is called a damage equivalent factor, λ, computed as :

$$\lambda = \Delta\sigma_{E,2} \Big/ \Phi_2 \cdot \Delta\sigma\left(\gamma_{Ff} Q_k\right) \tag{3}$$

The calculation of the correction factor values are made once for all for the usual cases, and are in function of several parameters such as the real traffic loads (in terms of vehicle geometry, load intensities and quantity) and influence line length, to mention the more important ones.

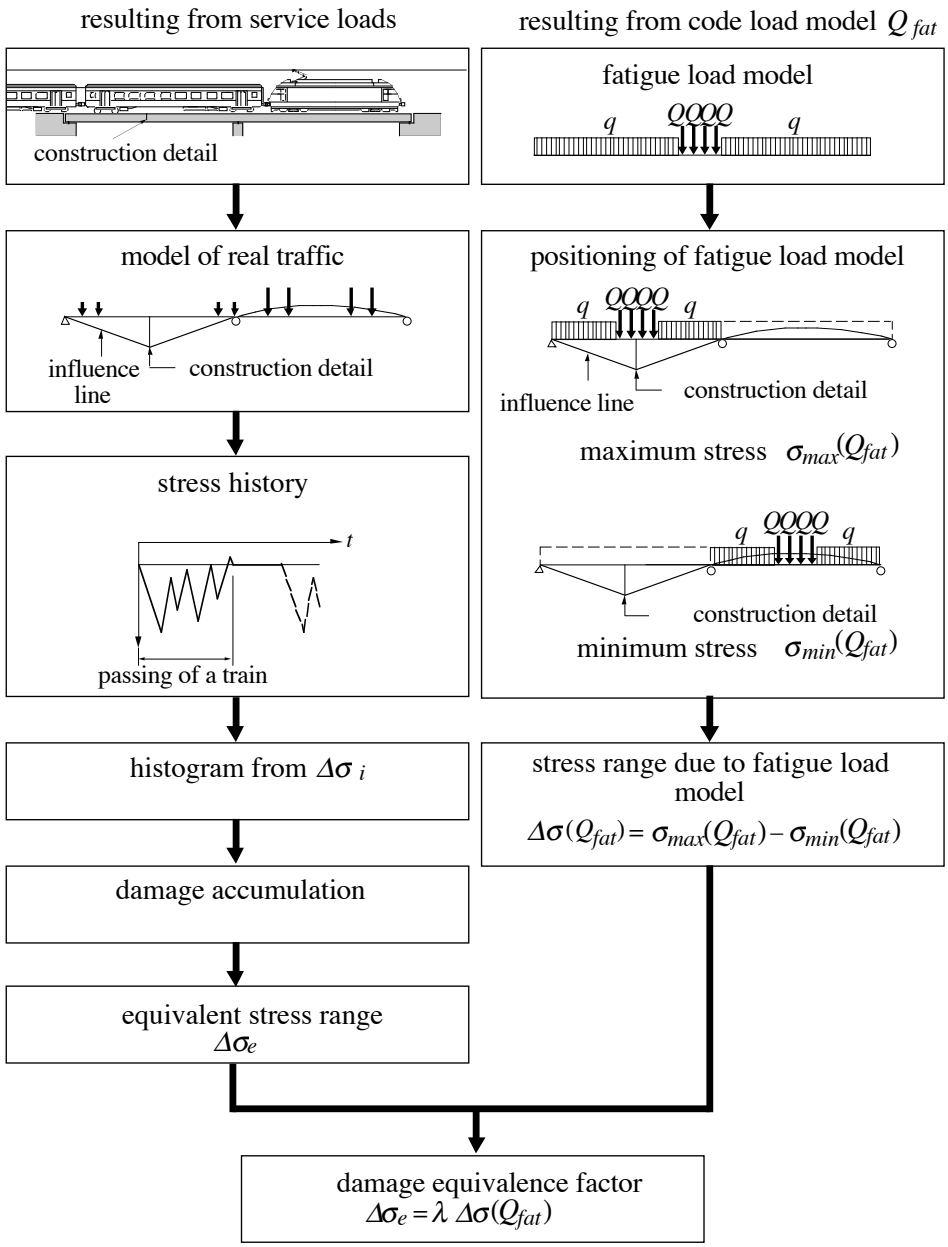


Figure 3. Damage equivalence factor.

The main assumptions are the use of the rainflow counting method and of a linear damage accumulation rule. One can therefore not account for phenomena such as crack retardation, influence of loading sequence, etc. The S-N curves must belong to a set of curves with slope changes at the same number of cycles, but he curves can have more than one slope. This is the case for the set of curves in ECCS or in prEN1993-1-9. The simplified load model has to be not too far from reality (average truck or train). If not, there are some abrupt changes in the damage equivalence factor values when the influence line length value approaches the axle spacing. In the Eurocodes, the fatigue load models for different types of structures can be found in the various parts of Eurocode 1. The damage equivalent factor has been further split into four partial damage equivalence factors in order to allow for more parameters to be accounted for:

$$\lambda = \lambda_1 \cdot \lambda_2 \cdot \lambda_3 \cdot \lambda_4 \quad but \quad \lambda \le \lambda_{\max} \tag{4}$$

where:

λ_1 factor accounting for the span length (in relation with the length of the influence line), see fig. 4 for an example of values for road and rail bridge. Note that since the λ_1 values depends on the closeness of the fatigue load model to real loadings, a direct comparison between the two curves plotted cannot be made

λ_2 factor accounting for the traffic volume

λ_3 factor accounting for the design life of the structure, the reference life for which the factor is one being, for road bridges, equal to 100 years.

λ_4 factor accounting for the influence of more than one load on the structural element

λ_{max} maximum damage equivalent factor value taking into account the fatigue limit.

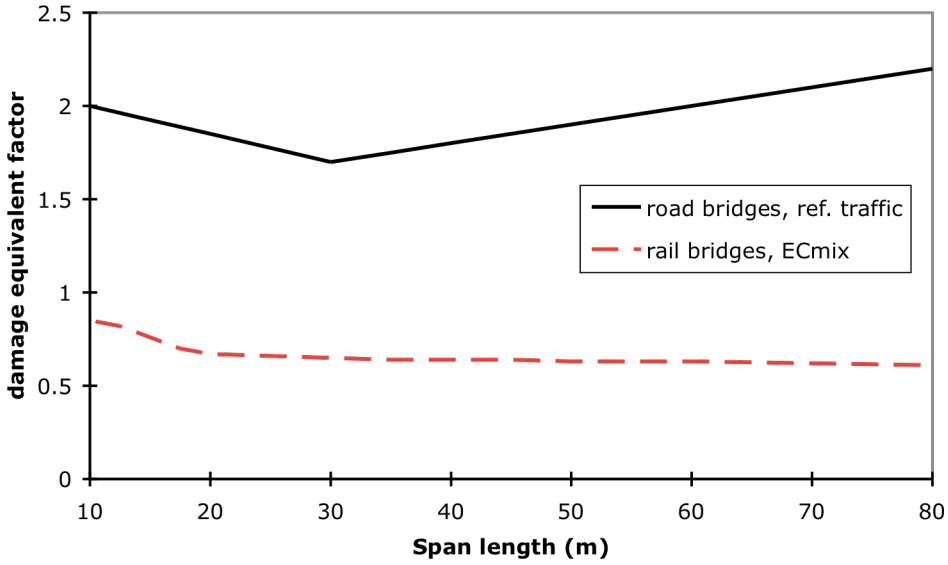


Figure 4. Example of λ_1 values for road and rail bridge.

3 FATIGUE STRENGTH

3.1 Fatigue strength curves

The fatigue strength curves correspond to the original set of 14 curves from ECCS. All curves are parallel and each curve is characterized by the detail category (value of the fatigue strength at 2 million cycles) and a slope change at 5 million cycles. For shorter lives, a slope coefficient m = 3 is used. For longer lives, the slope coefficient m = 5 is used, until 100 million cycles. This later value corresponds to the cut-off limit, which means that all cycles having stress ranges below the stress range value at 100 million can be neglected when performing a damage accumulation because their contribution to the total damage is considered as being negligible. The double slope S-N curve represent better the damaging process due to cycles below the constant amplitude fatigue limit (CAFL) when the spectra follows a distribution close to Rayleigh's, compared to the unique slope curve. The CAFL is fixed at 5 million cycles for all detail categories. The different structural details are classified into different tables (non-welded details, butt welds, weld attachments, …) and detail categories. The detail category attributed to a particular detail comes from statistical analysis of the available worldwide test results on specimen of sufficient size to represent correctly the built-in welding residual stresses. Table II shows some structural details and the results, partial at this time, of the statistical analysis carried out to check their classification. As can be seen, test results from different sources cause a large scatter in the characteristic fatigue strength. The data can however not be pooled together without careful analysis as they may not be from the same population because of significant differences in the welding process or procedure specifications, in the failure criteria, etc. Also, the test database includes tests dating from the 1960's up to today. Therefore, the classification adopted is both quantitative as well as qualitative and includes some engineering judgment. For attachments, one can see that the detail categories at the limits of the validity range for different details are often identical. For example, a very short longitudinal attachment (L < 50mm) is not different from a large transverse stiffener on a plate ($l \leq 50$ mm) or a cruciform full penetration joint ($l \leq 50$ mm), they are all classified as category 80.

The test results considered were all carried out in a laboratory environment and therefore the code requires an adequate corrosion protection system. All the same, the allowable temperature range is limited to -50 ° and +150°C. The range of application extends to structures in weathering steels, but the categories for plain members must be lowered by one category to account for possible rust points. It also extends to steels with yield stress up to 690 N/mm^2 as well as to austenitic steels.

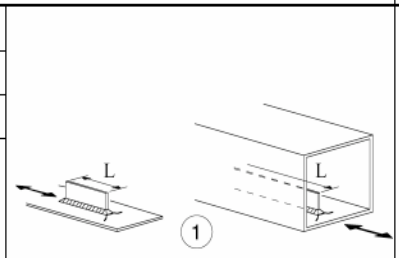
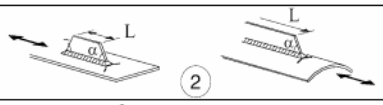
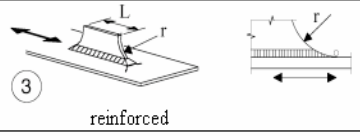
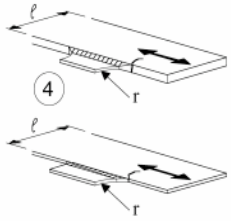
Detail category	Constructional detail		New Evaluation for prEN 1993-1-9 (2002)					
			Detail	# of data	m		$\Delta\sigma_c$	
					variable	constant	m=var.	m=const.
80	L≤ 50mm		1	17	3,26	3	89,10	87,00
71	50<L≤ 80mm							
63	80<L≤ 100mm			109	2,45	3	67,04	77,14
56	L>100mm			62	3,24	3	58,06	55,96
				18	3,32	3	76,08	72,31
				15	3,05	3	94,57	94,73
				17	3,27	3	79,37	76,49
				6	3,81	3	80,59	59,53
				8	3,48	3	84,22	76,73
				12	3,54	3	69,12	60,14
				4	4,59	3	78,39	50,12
				9	2,43	3	53,43	74,94
71	L>100mm α<45°		2	53	2,92	3	69,24	70,58
				27	2,99	3	58,97	59,85
				39	2,73	3	78,95	83,41
80	r>150mm	 reinforced	3	6	3,06	3	100,94	105,20
				4	3,29	3	97,27	96,41
				4	3,31	3	36,16	62,94
				10	3,12	3	59,00	63,76
90	$\frac{r}{L} \geq \frac{1}{3}$ or r>150mm		4					
71	$\frac{1}{6} \leq \frac{r}{L} \leq \frac{1}{3}$			13	1,26	3	18,43	72,84
50	$\frac{r}{L} < \frac{1}{6}$							

Table II. Longitudinal attachment details and results of statistical evaluation [Sedlacek, 2004].

3.2 Size effects

In part 1-9, the influence of the size of the detail on its fatigue strength is recognised in different ways. Firstly, the test results used to fix the fatigue strengths of the details were carried out on specimens with dimensions that are sufficient to represent correctly the built-in welding residual stresses. Secondly, some details in the tables have been separated according to the variation in one or two geometrical dimension; for example a longitudinal attachment can corresponds to four different categories according to the attachment length (see table II). This can be called a non-proportional scaling effect, since only some dimensions are scaled and not the others. Thirdly, for cases that are close to proportional scaling, one can see that the size effect in fatigue is essentially influenced by the element thickness in which the fatigue crack occurs and therefore has been often called a thickness effect. For these cases, the reduction formula fro size effects proposed originally by Gurney is used:

$$\Delta\sigma_{C,red} = k_s \cdot \Delta\sigma_C \qquad with \quad k_s = \left(25/t\right)^n < 1.0 \tag{5}$$

The value of the exponent n in the formula is function of the detail considered. In part 1-9, it is equal to 0.2 for butt joints and 0.25 for bolts in tension.

4 REFERENCES

Schmackpfeffer, H., Hensen, W., Sedlacek, G., and Müller, Chr., advantages of Eurocode 3 for the calculation of steel bridges, 6th Japanese - German Bridge Symposium, Munich, August 29 – September 1, 2005.

prEN1993-1-10:2005, Eurocode 3: Design of steel structures - Part 1.10: Material toughness and through-thickness properties, European committee for Standardization (CEN), Brussels, May 2005, 18 pp.

prEN1993-1-9:2005, Eurocode 3: Design of steel structures - Part 1.9: Fatigue, European committee for Standardization (CEN), Brussels, May 2005, 34 pp.

BS 7910:1999, British Standard Institute. BS 7910 – Guide on methods for accessing the acceptibilty of flaws in metallic structures, UK, with 1st amendment, 2000.

CIDECT, Design guide for circular and rectangular hollow section joints under fatigue loading, Eds. Zhao, X. L., Herion, S., Packer, J. A. and al., CIDECT guide No. 8, TÜV-Verlag Rheinland, Köln, 2000

Sedlacek, G., Hobbacher, A., Nussbaumer, A., and Stötzel, J., Preamble of background document to pr EN1993-1-9, 1st draft, RWTH Aachen, oct 2004, unpublished.

RWTH Aachen, Background document to pr EN1993-1-10, 1st draft, january 2001, RWTH Aachen, unpublished.

Finite Element Assisted Fatigue Analysis of Welded Steel Construction According to AISC Code

Van-Ngan Lê[a], Réjean Foisy[b]

[a] École de Technologie Supérieure, Montréal, Canada
[b] Lafarge Canada Inc., Montréal, Canada

Abstract Finite Element Methods are powerful tools for fatigue design. However, results must be carefully analysed to avoid erroneous interpretations due to a misunderstanding of the said method. The present paper shows the principle of fatigue requirements of American Institute of Steel Construction Code (AISC) for welded structure installations and how to use Finite Element Analysis to comply with this Code. Examples are given for understanding basic principles and for real rotary kilns and mills in the cement industry for which data about fatigue ruptures are available. It is concluded that if Finite Element stress results are properly interpreted, they can be successfully used with AISC fatigue requirements for predicting fatigue life or avoiding crack initiation.

1 INTRODUCTION

Finite Element Aided Fatigue Analysis (FEAFA) needs the knowledge of several aspects including stress categories, related codes and standards, FE result interpretation and operating conditions of the equipments. The lack of knowledge of either one of these aspects could lead to misusing FEAFA. In the following, it will be shown how the FEAFA could be erroneously used and how it is properly used for welded joints according to AISC Code [1] with examples of rotary kilns and mills for cement industry that have experienced cracks.

2 NOMINAL AND REAL STRESSES AROUND WELDED JOINTS

The nominal stresses across a plate thickness "t" are the average plus bending normal stresses given by the following formula, ignoring all stress concentration effects due to local changes of geometry

$$\sigma_{nom} = \frac{N}{t} \pm \frac{6M}{t^2} \qquad (1)$$

where N and M are normal force and bending moment per unit length respectively (line "ab" in figures 1 and 2).

The real stress distribution will be identical to nominal stress "ab" if the thickness "t" is constant and the plate has no internal defects. In the vicinity of welded joints however, the real stress distributions (curves "cd" in figures 1 and 2) are different from the nominal straight line "ab" due to stress concentration effects.

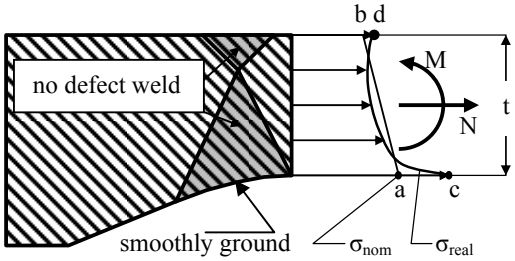


Figure 1. Both nominal and real stresses are known

2.1 Perfect welded joints

The necessary conditions for achieving perfect welded joints, for which real stresses could be determined with certainty, are « full penetration weld, 100% examined by X-ray and repaired accordingly to assure no weld defect and with both sides smoothly ground ». The figure 1 illustrates an example of a perfect welded joint. These conditions imply severe quality control procedure and very high costs. One of the rare codes and standards that implement these requirements is section III of ASME Code [2] for class 1 nuclear pressure vessels. Any approach to calculate real stresses around welded joints, using Finite Element Method for example, is applicable only if the welded joint is a perfect one, such as welded joints that meet the requirements of class 1 nuclear pressure vessel components. It should not be used for analysing stresses in standard welded joints such as explained below.

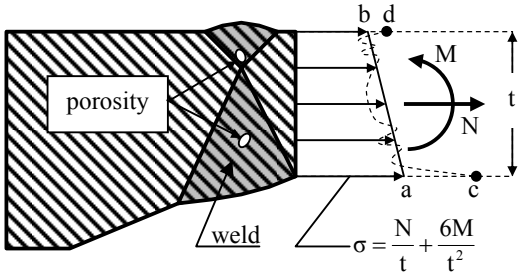


Figure 2. Nominal stress and uncertain real stress

2.2 Uncertainty of real stresses in standard welded joints

Welded joints in standard steel constructions are however far from perfect, mainly due to irregular weld surface, irregular partially penetrated depth and internal (unseen) defects such as porosity. Due to these unknown details, real stress distribution around these joints is not known; see dashed line "cd" in figure 2. Consequently, any attempt to calculate real stresses in standard welded joints, using Finite Element Method for example which wrongly assumes regular geometry, could lead to erroneously interpreted results.

3 AISC FATIGUE CRITERIA FOR STEEL CONSTRUCTION

The American Institute of Steel Construction [1] (AISC) provides code and standards for designing welded steel installations including kilns and mills in the cement industry. Due to the uncertainty of the real stresses around welded joints, the AISC code provides fatigue criteria based on nominal stresses only. The AISC fatigue data are number of cycles of nominal stress ranges without crack initiation for 95% of test specimens with different stress categories. These data are represented by fatigue S-N curves shown in figure 3. The category A fatigue data are for real stress wherever there is no welds while other categories are for nominal stresses adjacent to welded joints. The complete definition of all stress categories for fatigue is provided in the AISC Code.

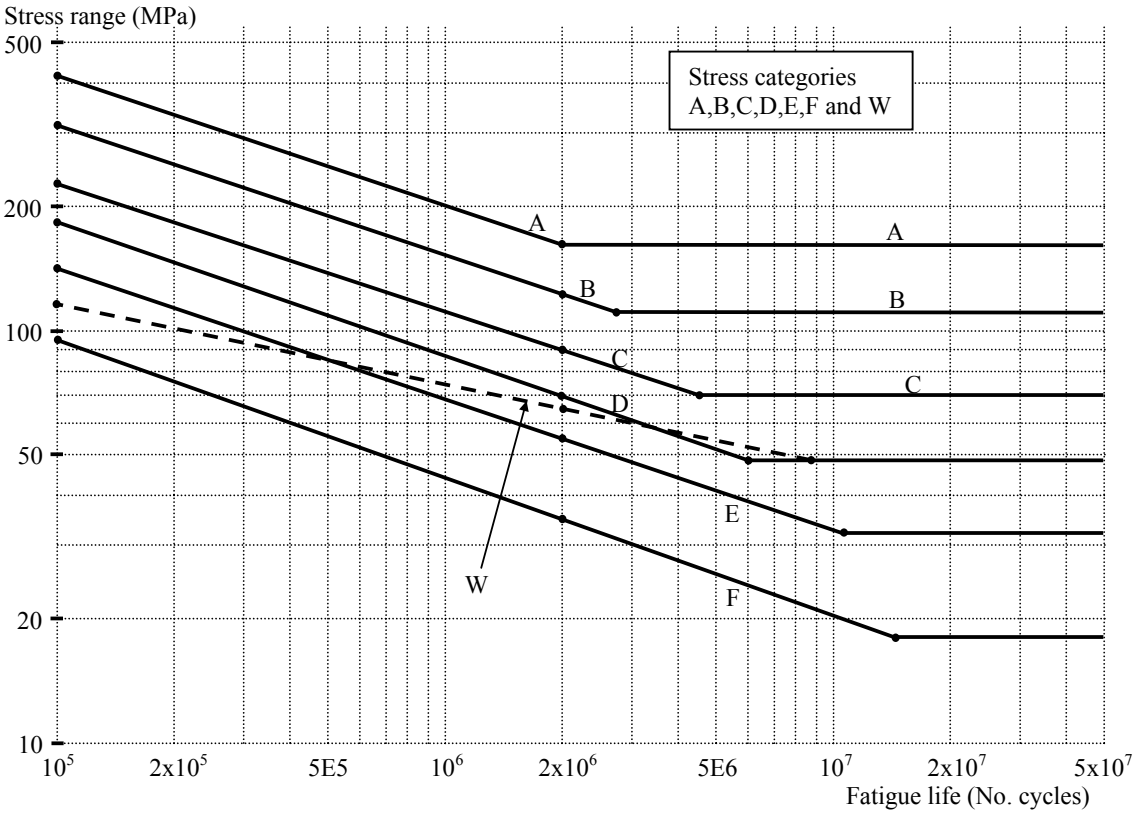


Figure 3. Fatigue curves for welded steel constructions according to AISC[1]

4 METHODOLOGY EXAMPLES

4.1 Example 1

It is asked to estimate the fatigue life of a large 50 mm thick steel plate on which a 400 mm long by 30 mm thick gusset is attached by 15 mm filet welds on both sides. The plate is subject to fluctuations of loads per unit length of ΔN_x = 5000 N/mm and ΔN_z = 2500 N/mm in transversal and longitudinal directions (figure 4).

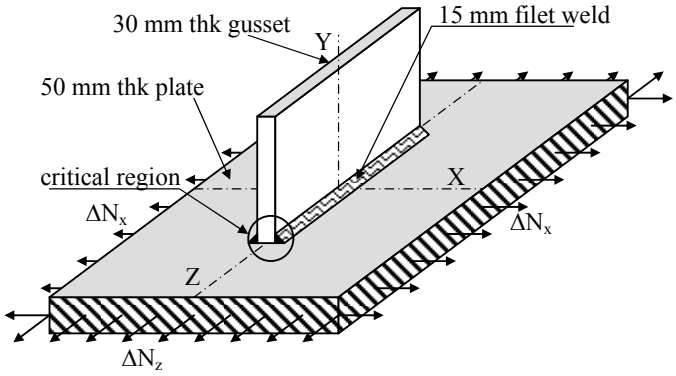


Figure 4 : Plate-gusset-filet-weld assembly.

4.1.1 Proper answer according to AISC

Stress range in the plate in x direction, from formula (1): $\Delta\sigma_{x\ nom} = \frac{\Delta N_x}{t} = \frac{5000\ N/mm}{50\ mm} = 100\ MPa$

This stress is of category C (perpendicular to a thin gusset), for which the allowable number of cycles is about 1.4×10^6 cycles according to figure 3.

Nominal stress range in the plate in z direction: $\Delta\sigma_{Z\ nom} = \frac{\Delta N_Z}{t} = \frac{2500\ N/mm}{50\ mm} = 50\ MPa$

This stress is of category E (parallel to and at end of intermittent weld), for which the allowable number of cycles is about 2.6×10^6 cycles according to figure 3.

4.1.2 Finite Element models and results

Figure 5 shows two Finite Element models of this example using 10-node tetrahedral elements of ANSYS software [3]. The element sizes in welds are 5 mm for model 1 and 3 mm for model 2. Welds are assumed perfectly square triangular prisms. Pressures -100 MPa in x direction and -50 MPa in z direction are applied on edges of the plate.

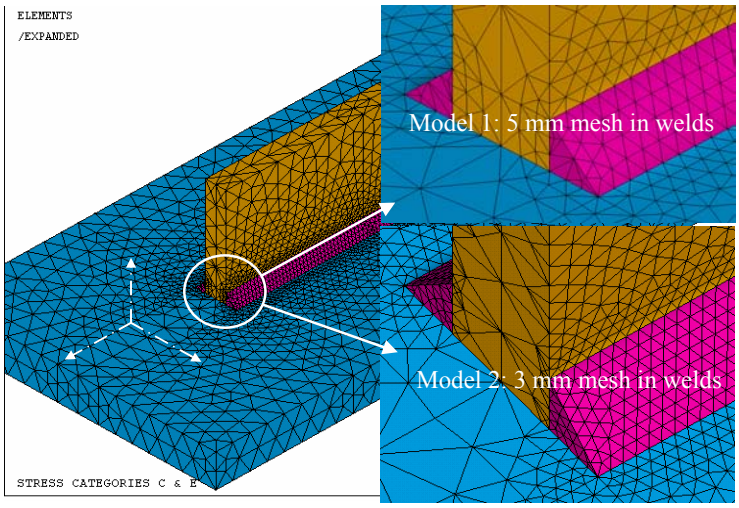


Figure 5. Finite Element models for plate-gusset-filet-weld assembly

The σ_x stresses around welded joint given by the two FE models are shown in figure 6. It is noticed that the average value, $\sigma_{x\ ave}$ = 100 MPa, is the same while the local stress values close to weld toes are very different between models, $\sigma_{x\ max}$ = 173 MPa for the 5 mm mesh model and 215 MPa for the 3 mm mesh model.

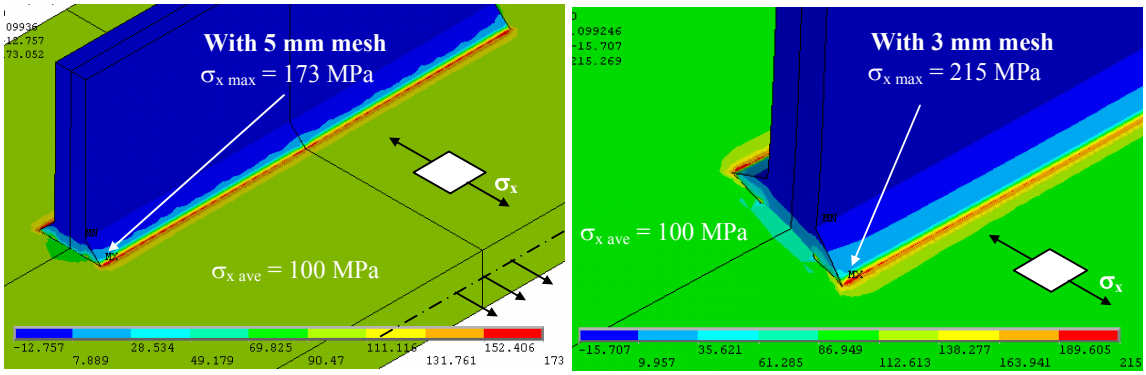


Figure 6. FE σ_x results for two different mesh models

The same phenomena is noticed for the σ_z stresses as shown in figure 7: the average value, $\sigma_{z\ ave}$ = 50 MPa, is the same while the local stress values close to weld toes are significantly different between the two models, $\sigma_{z\ max}$ = 106 MPa for the 5 mm mesh model compared to 133 MPa for the 3 mm mesh model.

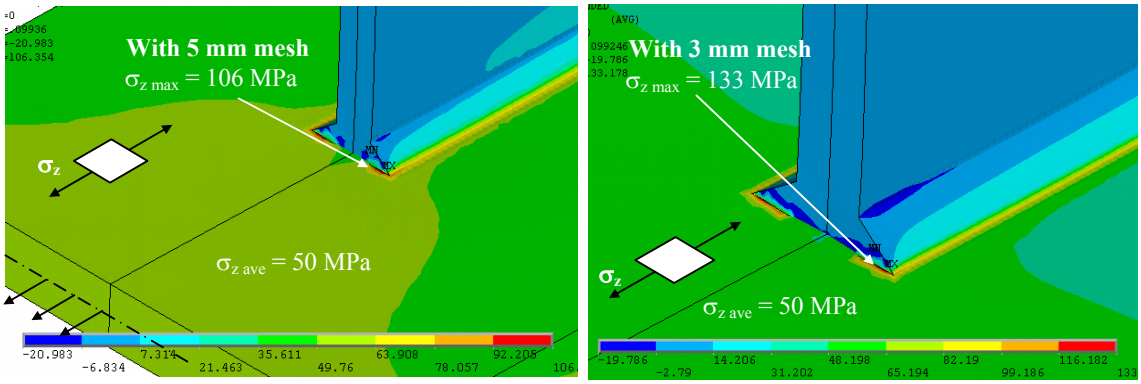


Figure 7. FE σ_z results for two different mesh models

4.1.3 Discussion about FE results

From the theoretical standpoint, Finite Element results close to weld toes are not reliable because they greatly change in function of element size of the model.

From the practical standpoint, these results are not suitable for analysis either because the real geometry at weld toes and internal defects are not taken into account in FE models.

A correct way of using results of these FE models is disregarding local stress values (such as $\sigma_{x\ max}$ = 173 or 215 MPa in figure 6 and $\sigma_{z\ max}$ = 106 or 133 MPa in figure 7) and asking for resultant normal forces and bending moments per unit length on any section of the plate close to welds. With ANSYS [3], this action can be done by selecting elements on one side of a section and appropriately executing the commands SPOINT and NFORCE. The results thus obtained are the same for different element size models. In this example, both models give the same linear forces N_x = 5000 N/mm in x direction and N_z = 2500 N/mm in z direction. Nominal stresses are then calculated by formula (1) and give $\sigma_{x\ ave}$ = 100 MPa in x direction and $\sigma_{z\ ave}$ = 50 MPa in z direction, independently from element size models.

Another way of correctly using Finite Elements for analysing stresses around standard welded joints is modeling the plate as if welded joints were not present; examining stress values at nodes on the plate which is closest to a weld toe and using corresponding stress categories and fatigue curves according to AISC Code. For example, if the FE models contain 50 mm thick plate without gusset and without welds, the values σ_x = 100 MPa and σ_z = 50 MPa will be directly given by FE results and stress category C is directly applied for σ_x and stress category E is directly applied for σ_z as explained above.

4.2 Example 2

Figure 8 shows another methodology example of stress category E (a plate-block-filet-weld joint subject to linear force N_x = 1000 N/mm and bending moment M_z = 2083.33 N.mm/mm): the same remarks as above apply.

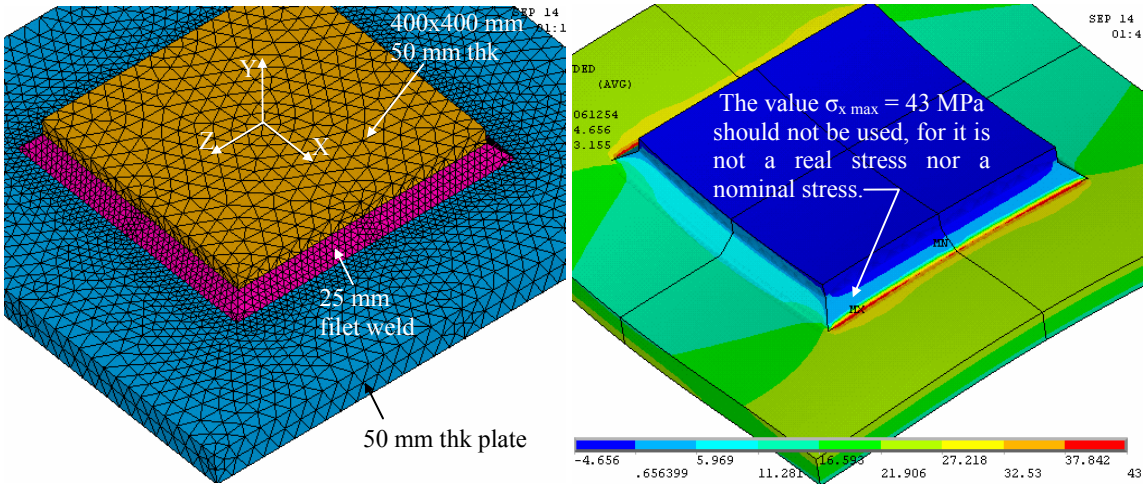


Figure 8. Solid Finite Element model and stress results of a plate-block-filet-weld assembly

5 FATIGUE ANALYSIS OF SOME EQUIPMENT IN THE CEMENT INDUSTRY

5.1 Welded X-block design of Lafarge plant kiln

The following example is a 3D solid Finite Element simulation for calculating stresses in a tire-shell section of a Lafarge cement production kiln [4] subject to 223 t (metric tons) shear force and 1360 t.m bending moment. Fatigue analyses are made for a design with X-blocks welded on the 55 mm shell under tire [5] which experiences cracks in shell around said welded blocks.

The FE model for tire-pad-shell assembly and critical points of welded X-block design are shown in figure 9. It is noticed that the welded joints are not included in the FE model because it would be useless to do so, such as explained in previous examples. The hoop stress in top and bottom regions is also shown in figure 9.

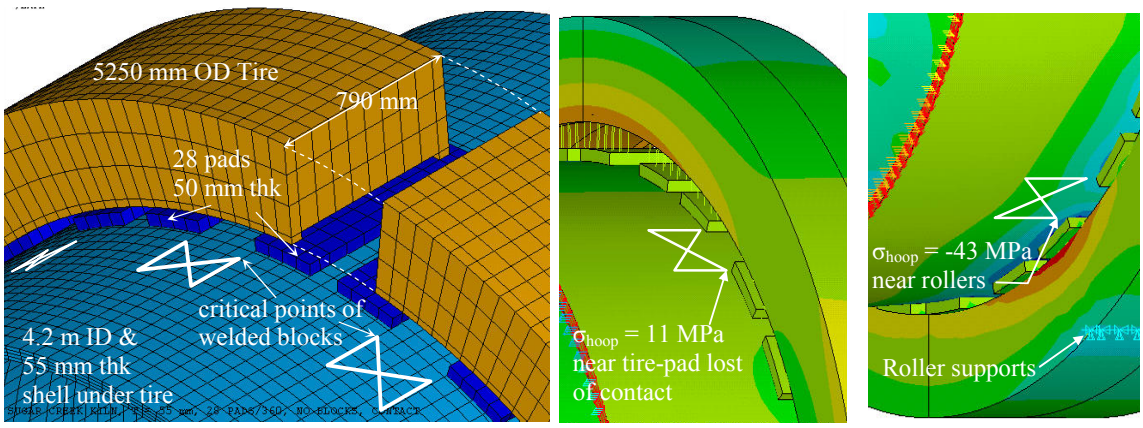


Figure 9. FE model and hoop stresses at top and bottom of tire-shell section with welded X-block design

The variation of nominal hoop stress in shell at the most critical node near a corner of welded X-blocks is shown in figure 10 for one complete revolution of the kiln. The stress range is about $\Delta\sigma_{max}$ = 12 - (-43) = 55 MPa which is classified as stress category E according to AISC Code. By using category E fatigue curve (figure 3), this stress range would last for about 1.75×10^6 cycles, i.e. about 300 operation days for 4.5 RPM rotary kiln.

Comparison with real life of kiln: Lafarge kiln with welded X-Block design has experienced cracks in shell around corners of welded blocks after just a few operating months.

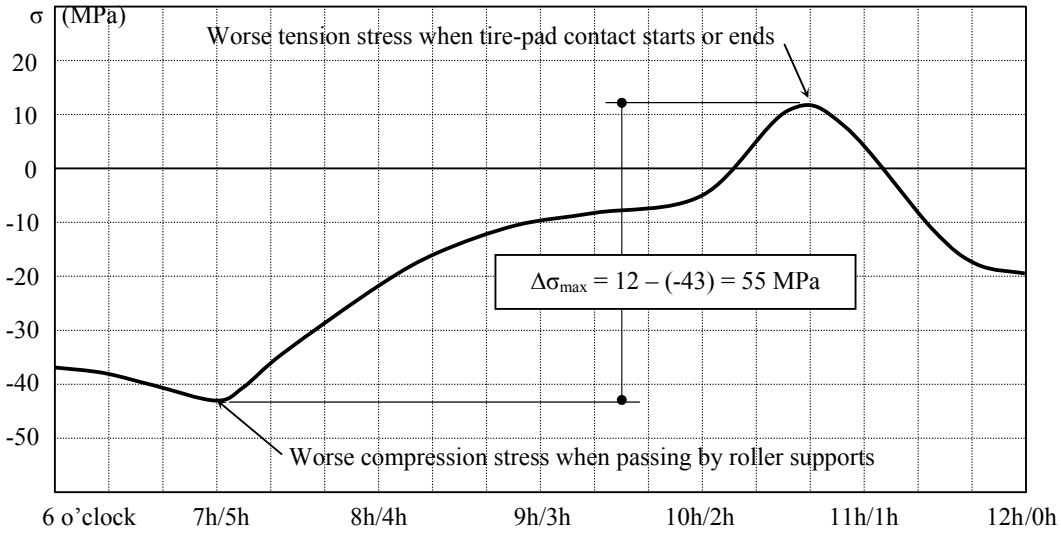


Figure 10 : Typical fluctuation of nominal hoop stress in shell at corners of welded blocks

5.2 Manholes for Raw Mill of a Lafarge plant

A raw mill of a Lafarge plant is a 12,34 m long by 3,96 m inside diameter by 42,86 mm thick rotary steel vessel supported by four lubricated bearing pads at each end, figure 11.a. There are three manholes: one manhole in chamber I and two 180°-apart manholes in chamber II. The old design of the manhole is an opening in shell reinforced by an overlapped plate attached to shell by fillet welds. Fatigue cracks occur and propagate around corners of these manholes, figure 11.b, and they have been replaced by new design manholes with details shown in figure 12. Other technical details concerning the mill are referred to Lafarge CTS of Montreal [6].

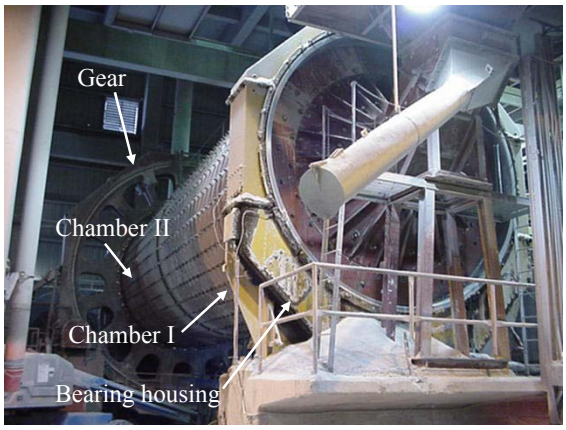
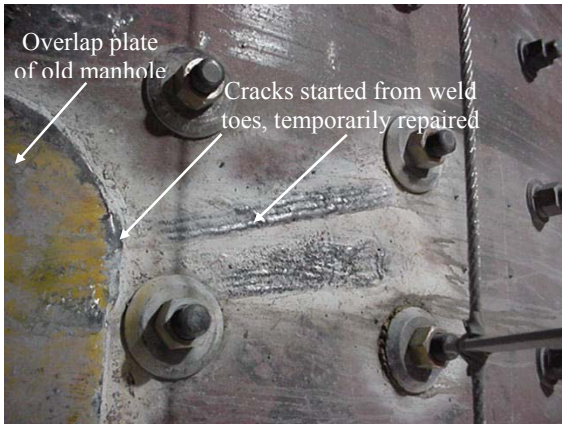


Figure 11.a Overall raw mill from outside view



11.b Zoom around overlap plate of an old manhole

Twelve FE models with ANSYS shell type elements, one for each rotated hour of manholes in one revolution, are used for fatigue analysis of the mill with new manhole design. Figure 13 shows the models for manholes at 12, 3 and 10 o'clock positions. Since shell type element is used, stresses given by FE results are already nominal which are directly used for stress analysis. Figure 14 shows the most critical stress variations at two points, one is at edge of the manhole in chamber I on inside shell radius (point e in figure 14), the other is on the weld seam of manholes in chamber II on the outside surface of shell (point w in figure 14). The maximum and minimum stress values at these points and the corresponding o'clock position of manhole are summarized in the table I.

Table I. Maximum and minimum stress values, ranges and categories at points e and w

Critical points	Maximum stress (σ_{max})	Minimum stress (σ_{min})	Stress range ($\Delta\sigma$)	Endurance limit
e	46 MPa (Manhole at 7 o'clock)	-38 MPa (Manhole at 3 o'clock)	84 MPa category A	165 MPa (from figure 3)
w	37.5 MPa (Manhole at 6 o'clock)	-22.5 MPa (Manhole at 2 o'clock)	60 MPa category B	110 MPa (from figure 3)

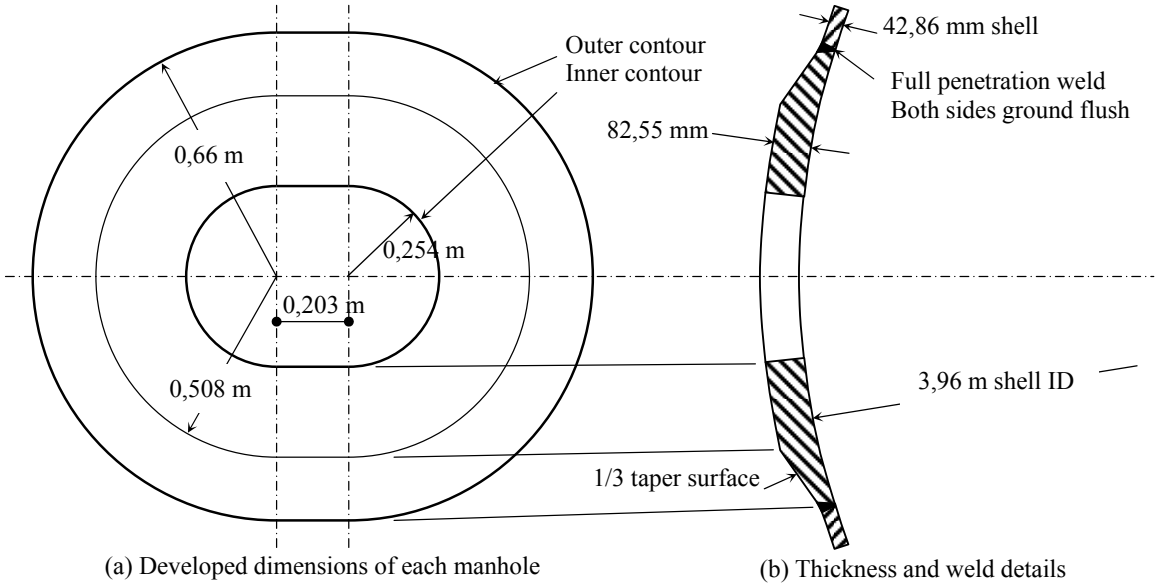


Figure 12. New design details for manholes of Raw Mill

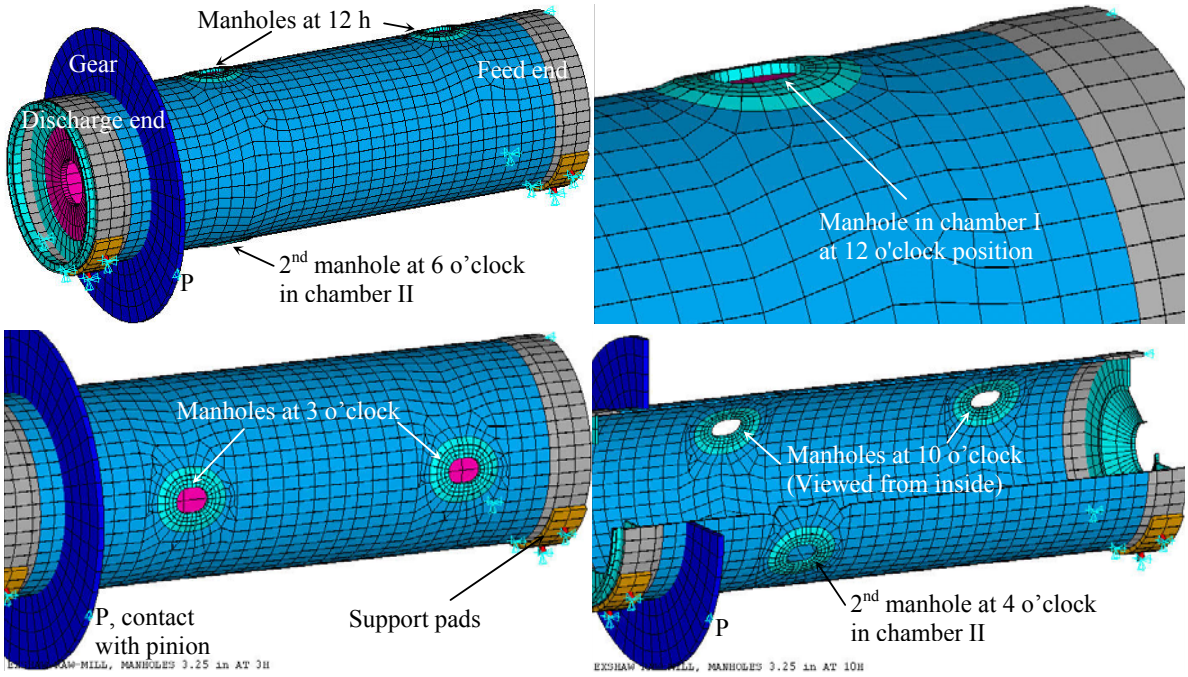


Figure 13 : Finite Element models for different rotated positions of manholes

5.2.1 Discussion

According to FE results shown in table I, the manhole design with details shown in figure 12 will be free from cracks for infinite life with safety factors of about 165/84 = 2.0 at edge of opening (point e in figure 14) and about 110/60 = 1.8 on weld seam of reinforcement plate (point w in figure 14).

If the weld between the reinforcement plate and the shell is not smoothly ground as mentioned in figure 12, the stress at point w ($\Delta\sigma$ = 60 MPa) would be of category C for which the endurance limit is 70 MPa (figure 3) and the safety factor at weld seam would be reduced to about 70/60 = 1.17.

If the transition of the reinforcement plate is not gradual enough (as recommended in figure 12), the stress category at point w may become D for which the stress range $\Delta\sigma$ = 60 MPa would develop cracks after about $3x10^6$ cycles (from figure 3).

With the old manhole design, the reinforcement plate being filet welded onto shell, the stress category becomes E for which the same stress range (60 MPa) would develop cracks after about $1.5x10^6$ cycles.

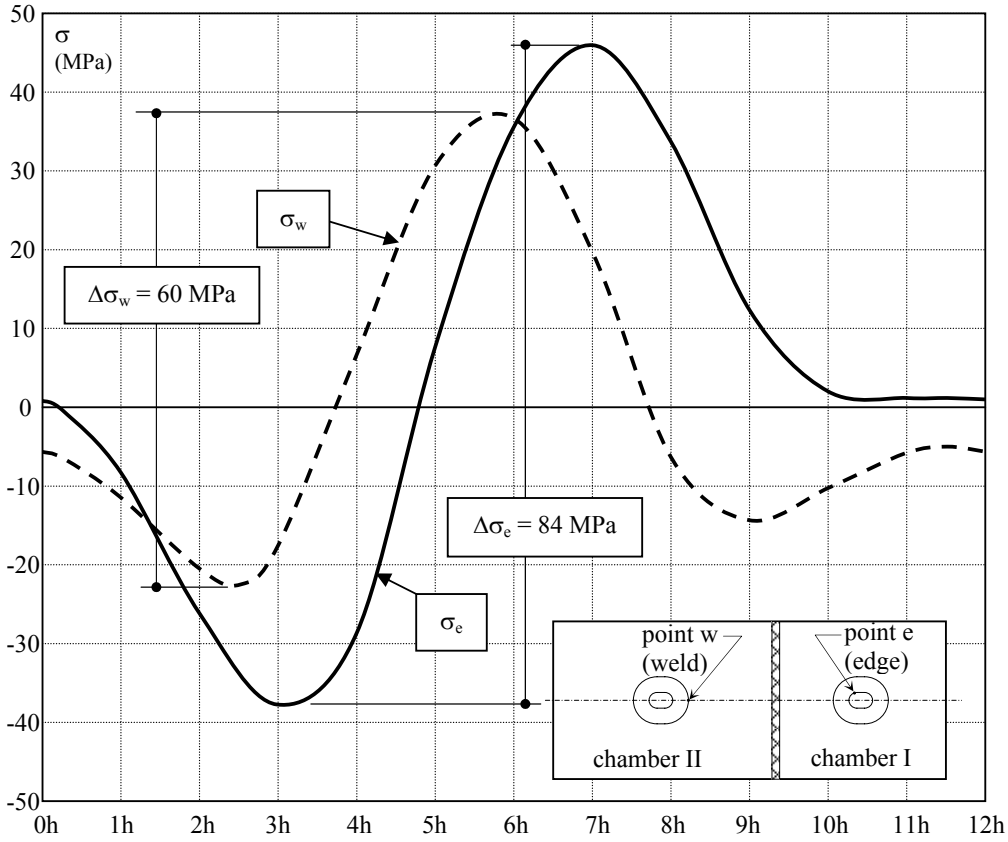


Figure 14. Most critical stress fluctuations at edge and on weld seams of manholes

6 CONCLUSION

It is concluded that cares must be taken when doing Finite Element Assisted Stress Analysis of welded joints for standard steel constructions: If welded joints are included in Finite Element models, the local stress values around welded joints should not be used and if nominal stresses are properly extracted from Finite Element results, they can be successfully used with AISC fatigue requirements for predicting fatigue life of welded constructions.

7 REFERENCES

1. Manual of Steel Construction, American Institute of Steel Construction, Chicago, 2004, www.aisc.org
2. ASME Code, Section III, Subsection NB for Class 1 Components, The American Society of Mechanical Engineers, 2004, www.asme.org
3. ANSYS Multi-physics Finite Element Software, Version 8, 2004, www.ansys.com
4. Lafarge calculation sheets SC NCP 46205, 9/09/1998, Lafarge CTS, Montreal.
5. Polysius drawings No.1107566, 1107564, 1107571 for Lafarge Plant 1999, Lafarge CTS, Montreal.
6. Lafarge Drawings No.A-1035-2033, B-1035-3030, for Exshaw Plant, Lafarge CTS, Montreal.

Experimental and numerical investigation of fatigue life of aluminium alloy welded components

B. Wu, S. Panier*, D. Zakrzewski*, C.Robin[*], G.Mesmacque[**].*

*** Département mécanique et comportement des matériaux, Ecole des Mines de Douai, France**
**** Département mécanique et matériaux de l'IUT A, Université des Sciences et Techniques de Lille, France**

Abstract

The present work is concerned with the fatigue life assessment of welded aluminium components and is aimed to provide useful tools to integrate fatigue behaviour of these components in design.
The fatigue life of welded structures depends on the base material properties, the weld geometry and the stress distribution. To take into account these parameters in fatigue life prediction, the mechanical characteristics (static and cyclic) of the different structures existing in a welded component should be determined. In a first part, experiments were performed on 6000 series aluminium alloy specimen in order to determine the fatigue behavior of the base material, the HAZ structure and welded components under uniaxial and biaxial loading.
In a second part, a numerical fatigue life prediction was carried out. The approach for predicting the crack initiation life by introducing the concept of critical plane was used. The welded joint was considered as deformable with experimental mechanical characteristics of the HAZ. The finite elements software ANSYS was used to model the welded structure. The life prediction was performed using the POSTLIFE software developed at Ecole des Mines de Douai and LML.
A comparison of experimental data and life predictions is made, results are discussed.

1- Introduction

Despite the long history of the research on fatigue(Dang Van, K. [1], F. B. Stulen et al. [2] and Robert, J. L. [3] etc.), we are still far from solving the problem totally. The pieces or components in service, generally jointed together by welding, are often submitted to multiaxial loading, caused by the physical load in service or residual stresses. The fatigue strength of welded joints, is in general much less than that the parts which are welded together. There are a number of reasons for this:
Welding typically introduces geometric features, leading to a stress concentration at the toe of the weld.
The welding process will very often produce defects which can act as crack initiation sites (slag inclusions, incomplete fusion, porosity, etc).
Around the fusion zone, there is a heat affected zone (HAZ) where the parent material has been heated to a high temperature and allowed to cool fairly rapidly. This may cause major changes to the microstructure and properties in this region.
Unless steps are taken to relieve them, welded structures will normally have residual stresses, which may be of the order of the yield stress of the material.

All these factors cause the fatigue behavior of a welded joint to be quite different from that of the parent materials from which it is constructed. For this reason, it is not reasonable to model the behavior of the welded joint based on the parent plate properties, with modifications to take into account the defects, residual stresses, notches, and material property changes, and expect to get accurate predictions.
The main purpose of this paper is to take into account to the HAZ to predict fatigue life of aluminium welded structures. An equivalent structures (simulated HAZ) are tested in fatigue under in-phase, out-of-phase biaxial loads in the High Cycle Fatigue regime. Several existing multiaxial fatigue criteria for this aluminum structures are tested like the criteria of Dang Van [1], F.B. Stulen [2], McDiarmid [4], and Matake [5].

2- Fatigue experiments

Uniaxial tests are performed under 30HZ using a INSTRON 8501 hydraulic machine on both parent metal and the so-called 'Simulated Heat Affected Zone' [6]. The basic characteristics are listed in Table 1. The biaxial tests are carried out on a platform with four horizontal hydraulic jacks.

Simulated HAZ	R_m (MPA)	R_e (MPA)	A%	HV
	274	230	16	80

Table 1: Mechanical characteristics for simulated HAZ

2.1- Uniaxial Experiments and Results

Fatigue tensile tests are carried out to get some basic information on the alloy we are studying. As the residual stresses in a welded structure are important, we carried out three different types of uniaxial fatigue experiments ($R = \frac{\sigma_{\min}}{\sigma_{\max}}$, R = 0.1, 0.3 and 0.5). For each R value, one iterative method [6] is used to carry out the tests and the theoretical curves are presented by using the formula of Bastenaire (figure 1) [7]. Uniaxial results of welded structures show that the nucleation of fatigue cracks often happens in the Heat Affected Zone of the structure, especially at the toe of the weld. To take into account this phenomenon, a specific thermal treatment is proposed to simulate the HAZ structure and applied to the cruciform specimen, after which the control of hardness and other mechanical characteristics are made. The uniaxial test results on 'Simulated HAZ' are shown in figure 1.

2.2- Biaxial Experiments and Results

The biaxial tests on 'Simulated HAZ structures' are carried out on the platform of test figure 2). RS-Console's (INSTRON Software) "Modal Control" is used to make the center of the specimen maintained at the initial position in order to avoid unwanted bending. The cruciform specimen center is much thinner (1mm) than the four ends (8mm). The very similar geometry of cruciform specimen are used already by other authors with success [8]. In-phase load tests and out-of-phase load tests are carried out in different experiments. In the out-of-phase tests, phase differences such as 30°, 45°, 60° and 90° are used. All the biaxial tests results are available in Table 2.

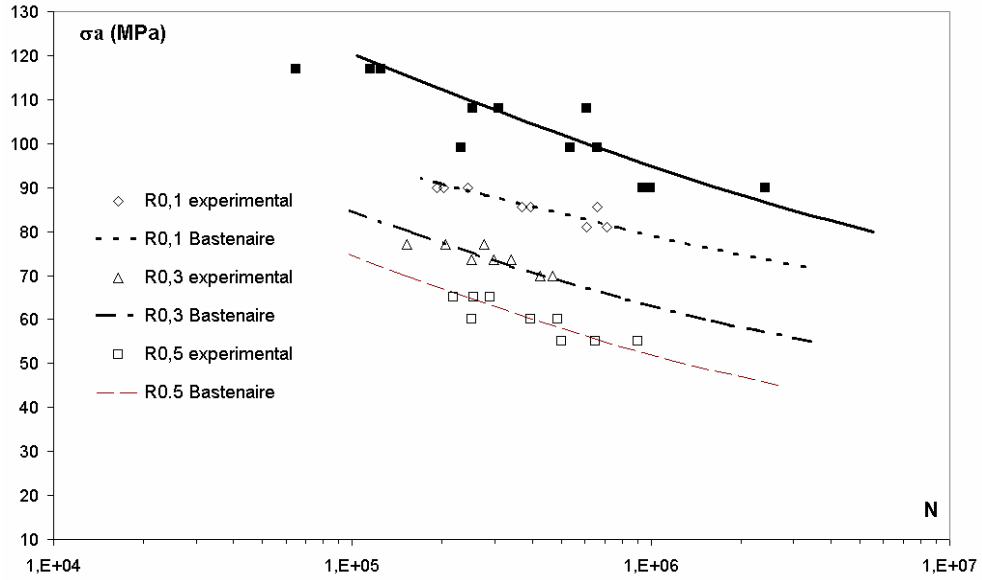


Figure 1: Biaxial Experiments and Results

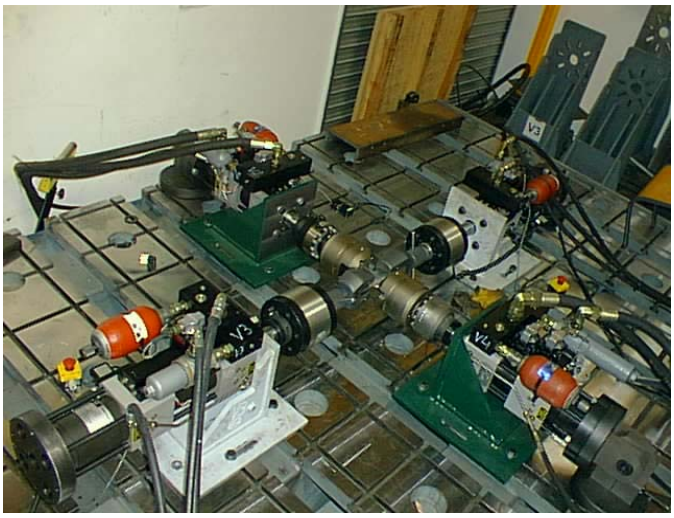


Figure 2: Platform for biaxial cruciform tests with four Jacks

N°	Rx	$\sigma_{x\max}$	Ry	$\sigma_{y\max}$	Φ	Nr	Note
01	0.1	70MPA	0.1	70MPA	0°	154010	R
02	0.1	60MPA	0.1	60MPA	0°	330000	R
03	0.3	60MPA	0.3	60MPA	0°	923782	R
04	0.3	50MPA	0.3	50MPA	0°	1141499	R
05	0.1	50MPA	0.3	50MPA	0°	416500	R
06	0.1	70MPA	0.5	70MPA	45°	348403	R
07	0.3	70MPA	0.3	70MPA	30°	492818	R
08	0.1	60MPA	0.3	60MPA	45°	430867	R
09	0.1	60MPA	0.3	50MPA	90°	446791	R
10	0.3	50MPA	0.3	50MPA	60°	4591712	NR
11	0.3	50MPA	0.3	50MPA	90°	2000000	NR
12	0.4	60MPA	0.6	50MPA	30°	3000000	NR

Table 2: Biaxial Fatigue Test for simulated HAZ

Notes : Axle X is the one where situate the six holes, axle Y is the other one.
Nr is the number of cycles.
R = Rupture, NR = No Rupture.
the stresses are nominal stresses and $R_x = \frac{\sigma_{x\min}}{\sigma_{x\max}}$, $R_y = \frac{\sigma_{y\min}}{\sigma_{y\max}}$
ϕ is the difference in phase : $\sigma_x(t) = Sin(\varpi t)\sigma_{xa} + \sigma_{xm}$; $\sigma_y(t) = Sin(\varpi t)\sigma_{ya} + \sigma_{ym}$

3- Application of the existing criteria

There are several families of fatigue criteria : Critical Plane Criteria or Critical Plane Approach, Global Criteria, Energy Criteria, etc. Only some critical plane criteria are considered in this paper. Global criteria are used in [9]. Such criteria calculate the path of shearing stress in the cyclical load for many planes of different directions, then on each plane the parameters of shear stress amplitude and average values are defined to calculate the damage value, at last find the plane which gives the most high damage value as the critical one. In this way, critical plane criteria give out both the life assessment and the direction of fatigue crack nucleation. The figure 4 shows definition of the amplitude and average values of shear stress on the plane in a general case; σ_{nna} , σ_{nnm} , $\sigma_{nn\max}$ represent the normal stress on the plane in question: Amplitude, Average value, Maximal value respectively. By choosing some of these items, different critical plane criterions gives out different formula to evaluate the damage caused by multiaxial loading in the sense of equivalent stress.

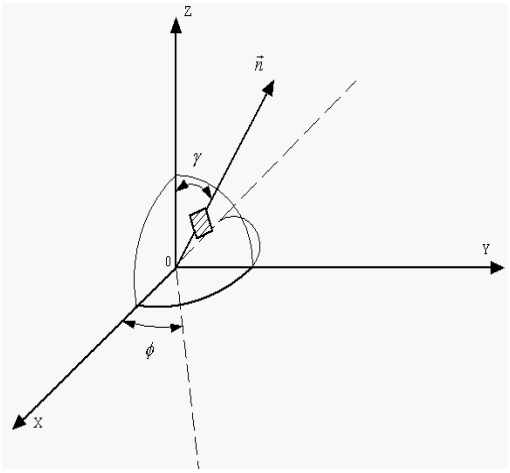


Figure 3: Definition of the planes to search the so-called critical one

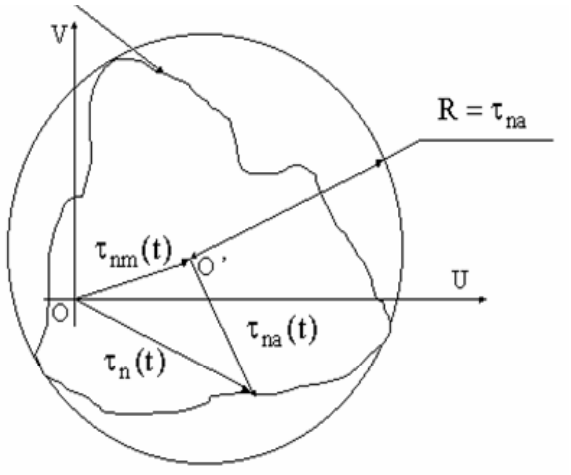


Figure 4: Definition of shear stress on a plane

The following criteria are used: Dang Van, K., F.B. Stulen [2], McDiarmid [4], and Matake [5].

As in our uniaxial test results we don't have the results of alternative torsion fatigue and tensile compression fatigue, so the SN curves of R =0.1, 0.3 and R =0.5 are used to determine the different coefficients of the previous criteria [9].

The Total life approach is used here for life assessment, i.e. the stages of initiation and propagation are not separated here. The life assessment algorithm used is one defined by Weber et al. [10].

Life assessments are normalized using the proportions between the assessments and test results, and the results of comparison are shown in figure 5. Let P to be the ratios between life assessment and test result, i.e. :

$$P_0 = \frac{life \quad assessment}{Nr \quad test} \text{ if } P_0 < 1, P = \frac{1}{P_0},\ P_0 > 1, P = P_0$$

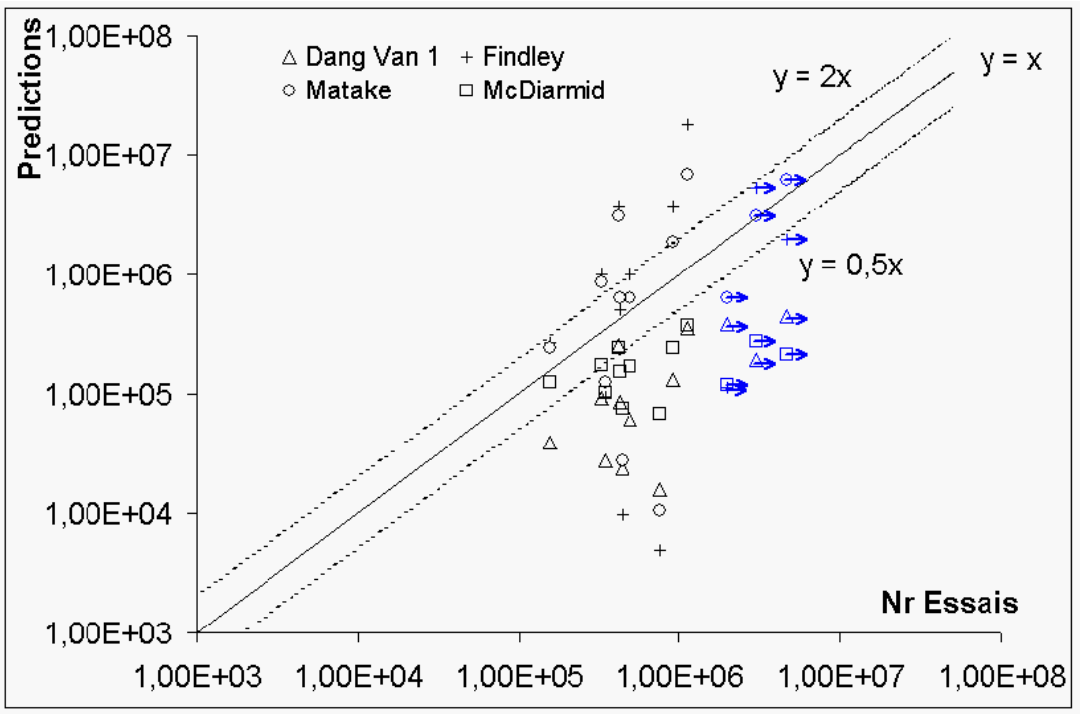


Figure 5: Comparison of life assessments using different criteria

First of all, the range of P for the 9 tests with rupture of each criterion is as follows:

Dang Van: 1.62 ~ 19.0 with always $P_0 < 1$.

Findley: 1.74 ~ 45.6 with $P_0 < 1$ only in the case of test N° 9 where P = 45.6.

Matake: 1.28 ~ 16.2 with $P_0 < 1$ only in tests N° 6 and N° 9.

McDiarmid: 1.22 ~ 5.87 with $P_0 < 1$ in all nine cases.

So, the criterion of McDiarmid works the best among them and its predictions of biaxial fatigue life is conservative, the worst will be 17% of the real life. The other three criteria have no significant difference in the precision of life assessment. In fact, they do not agree so well with the test results. Secondly, looking at the band of P = 2 ~ P =6, we found six cases for Findley, six also for Matake, but only four for Dang Van. In the two criteria, Findley and Matake, only the term of maximal normal stress $\sigma_{nn\max}$ is used. But the effects of σ_{nnm} and σ_{nna} are different from each other on fatigue crack propagation. That is probably the reason that they do not work well for the life assessment. In the criterion of McDiarmid, which works the best in our cases, the average value and amplitude of normal stress are treated respectively. No

significant influence of phase difference on the assessment precision is observed. Only in the case test N° 9, where the phase difference is 90°, the three criteria (Findley, Matake, Dang Van.) show more difficulty to make the predictions close to test results.

Conclusions and perspectives :

This study has made it possible to compare the four criteria on the prediction of fatigue life and critical directions of fatigue crack on the aluminum alloy based on the biaxial test results.

- Among the four criteria studied, the two criteria of Dang Van and McDiarmid work well for our aluminum alloy as life assessment is concerned.
- Regarding the critical directions fatigue crack, no preference among them is found.
- Tests on welded cruciform structures will be carried out to verify the criteria with residual stress taken into account.

Acknowledgements:
The paper realised in co-operation with IUT A LILLE 1, within the project proposed by ALSTOM Transport and BENALU, partly financed by Ecole des Mines de Douai.

References

[1] Dang Van, K., Sur la résistance à la fatigue des métaux. Sciences et techniques de l'Armement, 1973, N° 47, 3ème fascicule
[2] F. B. Stulen & H. N. Cummings, A Failure Criterion For Multi-axial Fatigue Stresses, Proceedings of American Society of Testing and Materials, 1954, Vol. 54, pp. 822-835
[3] Robert, J. L., Contribution à l'étude de la fatigue multiaxiale sous sollicitation périodiques ou aléatoires, PhD Thesis I.N.S.A., 1992
[4] D.L. McDiarmid , A general criterion of fatigue failure under multi-axial stress, 1973 ,2nd International Conferecne on Pressure Vessel Technology, pp.851-861
[5] Tomokazu MATAKE, An Explanation on Fatigue Limit under Combined Stress, Bulletin of the JSME, Vol. 20, No. 141, March 1977, pp. 257-263.
[6] L. Ferraton, Fatigue Damage of Aluminium Alloy Welded Components, Proceedings of the Eighth International Fatigue Congress, Vol. 1, PP.379-386
[7] Lieurade, H.P., *La pratique des essais de fatigue*. Edited by PYC édition, Paris, 1981.
[8] Tadeusz £agoda, Ewald Macha , Wodzimierz Be¸dkowski, A critical plane approach based on energy concepts: application to biaxial random tension-compression high-cycle fatigue regime. International Journal of Fatigue, 1999 Vol. 21, pp. 431–443
[9] Bo Wu, Contribution à l'étude des critères de fatigue multiaxiaux pour les assemblages soudés en alliage d'aluminium, PhD Thesis Lille 1, 2003
[10] Weber B., Kenmeugne B., J.C. Robert, Improvement of multiaxial fatigue criteria for a strong reduction of calculation duration. Computational Material Science, 1999, Vol. 15, pp. 381-399

PROGRAM

1 Methodologies and tools for fatigue life assessment

- Automotive components
- Various industrial applications
- Welded structures and assemblies

2 Advanced design tools and approaches

- Fatigue crack initiation assessment
- Contribution to the crack propagation stage
- Modelling of the design behaviour of the welded

3 Multiaxial loading fatigue assessment

4 Fitness for service approach and applications

5 Experimental validation

- Application to automotive parts and structures
- From laboratory testing to field evaluation
- Development of dedicated test devices and procedures

6 Design procedures against thermal and thermo mechanical fatigue damage

7 Reliability approaches in fatigue design

8 Improved design and manufacture processes with regard to fatigue

Fatigue of Drillstring: a Multiscale Approach

Mohamed Ferjani[a], Daniel Averbuch[a], Andrei Constantinescu[b], Habibou Maitournam[b], Ky Dang Van[b], Olivier Vincké[a]

[a] Institut Français du Pétrole, 1 & 4 avenue de Bois-Préau, 92852 Rueil-Malmaison, France
[b] Laboratoire de Mécanique des Solides- CNRS UMR 7649, Ecole Polytechnique, 91191 Palaiseau, France

Abstract: The aim of this paper is to elaborate a methodology (based on a multiscale approach) to calculate the life duration of the drillstring. The components of the drillstring are subjected to cyclic loading such as alternate flexure or vibrations occurring during a drilling operation. The proposed methodology is based on a multiscale approach passing from a large scale to the grain scale. The loading history is determined at the scale of the drillstring with the use of a quasi static model called Torque & Drag. This modeling does not take into account the geometrical details, the plasticity and the contact at the scale of the threaded connection. Therefore a numerical model developed with the Finite Element code Abaqus is employed to obtain a more realistic macroscopic stress field at the scale of the connection. Finally the fatigue life of the threaded assembly is calculated with the use of a modified Dang Van criterion, which is based at the scale of the grain of metal. Examples of the use of the methodology are given for representative industrial cases.

1. INTRODUCTION

The drillstring is compound of different tubular elements connected by a threaded assembly called tool-joint. The schematic view and the details of a tool-joint are displayed in Figure 1.

The failure of drillstrings is one of the most expensive accidents encountered in the oil and gas industry. These events appear in average in 14% of wells and the losses are estimated at 100 000 $ per event as detailed in [VAI 02]. Hill [HIL 92] has inventoried the causes of 76 failures taken place during 1987 and 1990 as:

- *fatigue* is the main cause in 65%,
- 13% are due to exceeding loadings in tension and torsion,
- low mechanical characteristics are involved in 8%.

The failures induced by fatigue are often due to two dynamical phenomena [SPA 03]. The first cause is due to the fact that the contact between the drillstring and the borehole and the contact between the bit and the rock can generate vibrations which will induce cyclic loadings in tension (bit-bouncing), torsion (stick-slip) and bending (whirling) along the drillstring. The second cause is the curvature of the well (dog-leg), which associated with the rotation of the drillstring, will generate alternated flexion.

Fatigue inducing cracks appear generally at the level of the tool-joint. Due to their particular geometry (threads, shoulders, …), the tool-joint is subjected to high stress concentrations (up to ten times the applied load) [TAF 93], which can lead to failure. Moreover, dies of gripping system mark the pipes surface creating stress concentrations also [RAH 99]. These marks are shown in Figure 1.

The present paper proposes to analyze the fatigue of the drillstring using a global computational approach based on a mechanical and a fatigue analysis using the Dang Van criterion. This type of methods has been successfully applied to predict the lifetime for other problems [DAN 02]. The novelty of the present study lies on the application of the method to a new domain adjoining a further scale in the mechanical analysis and a full discussion of stress concentrations in this context.

In the next sections, we will describe first the details of the methodology at each scale: the use of a Torque & Drag model at the scale of the drillstring, the presentation of the Abaqus FEM model at the scale of the tool-joint and the modified Dang Van criterion at the scale of the grain of metal. Then, different results on the stress concentrations as well as on the application of the Dang Van criterion will be presented. Finally concluding remarks will be given in the last section.

2. A GLOBAL MULTISCALE APPROACH FOR FATIGUE DESIGN

In a first stage of the analysis of the structure, we assume that we have an a priori knowledge of the loading cycles representing the in service functioning of the structure. A series of previous works have shown that even extreme phenomena like bit-bouncing or whirling conduct after a short number of cycles to a limit cycle [RIC 01]. In a second stage, an extension of the analysis to cycles of random amplitude can be envisaged, but this will not be presented in this paper.

The design method proposed next is based on two distinct steps:

- a complete mechanical analysis of the system providing the limit shakedown cycle of the mechanical fields in the connection,
- a fatigue analysis based on the fields computed before which provides the fatigue life and the critical points of the structure.

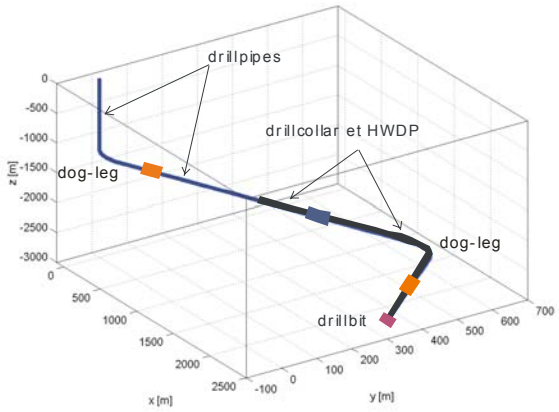




Figure 1. Schema of a drillstring (left) and marks done by the gripping system on a tool-joint (right).

We recall that the drillstring is a complex structure with a length of the order of magnitude of kilometers and radius of some tenth of centimeters. If the global dynamic evolution of the system can be well represented with a rod model, we can however not expect to understand local strains and stresses in the connection without a full three dimensional model.

Therefore the method presented here is based on three different scales, each associated to different parameters and models which are relevant for the resolution of the associated problems (see Figure 2). These scales are the following:

- *the scale of the drillstring* associated with a rod model in order to represent the complete dynamics of the drillstring considering the control and cutting problems. The main variables are here the generalized stresses in the rod: the tension *T*, the torsion *C* and the flexion *M*, which are functions of the curvilinear coordinate along the drillstring.
- *the scale of the tool-joint* associated to a FEM model with which the contact and the plasticity occurring in the connection are taken into consideration. The macroscopic stress field $\underline{\underline{\Sigma}}$ is the main parameter at this scale.
- *the scale of the grain of metal* associated to the mesoscopic stress field $\underline{\underline{\sigma}}$, where the macro-meso passage is actually provided by the Dang Van fatigue criterion [DAN 93]. We recall that this criterion is only applicable if the structure presents an elastic shakedown under the applied loading.

Scale of drillstring: Torque & Drag model

The dynamical problem can be solved with the help of a numerical code developed at Institut Français du Pétrole: DeepLines [FER 05]. The main idea is to introduce different laws as boundary values that will model the different vibrations occurring during the drilling operation, and compare the results with experimental data such as the database TRAFOR collected by IFP. This method will allow us to model the coupling between all the vibrations as well as the buckling occurring at the compressive zone of the drillstring. Once this work done, we will be able to obtain the cyclic loading in tension *T*, torsion *C* and flexion *M*.

In the present study, the loads are estimated with the help of a Torque & Drag model developed originally by [JOH 83]. Although the modeling is quasi-static, it gives information about the neutral point (locus where the drillstring goes from traction to compression state), the flexural moment *M* taking place in the dog-leg, and estimations of the generalized stresses *T* and *C*.

Scale of the connection: FEM model

The second step of this work consists in determining the macroscopic stress field $\underline{\underline{\Sigma}}$ induced by the cyclic loadings on the components of the drillstring. For components presenting simple geometries such as notches, the computations can be dealt with analytical tools [FIL 04]. Nevertheless, the difficulty arises when the component is a threaded assembly. Indeed, one has to take into account the contact between the two pieces pin and box, respectively male and female, and the plasticity induced by stress concentrations. Therefore a Finite Element Model has been realized with the commercial code Abaqus.

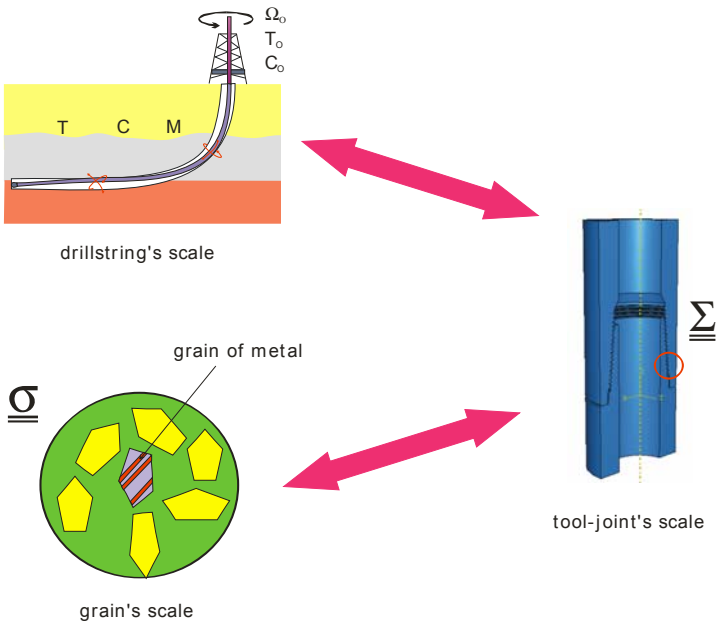


Figure 2. Description of the three scales.

The mechanical cyclic behavior of the steel 4145H constituting the tool-joint has been modeled with an elastoplastic law with a linear kinematic hardening. This type of behavior has shown good agreement with respect to uniaxial cyclic test [VAI 03].

For the time being, two kinds of models have been elaborated: an axisymmetric one for the case of traction and compression loading and a complete 3D model for the case of bending loading. For both models the helix angle of the threads is neglected. The axisymmetric model is composed of about 42000 elements which 1900 are devoted for the contact. The minimum size of the contact element is 0.1mm and the minimum size of the element in the root of the thread is 0.01mm. These values are a good compromise between the precision of the results and the computation time. All computations done with this model has been performed on a SUN computer 2 GHz with 2 Go RAM. The computation time on this machine is about 3 hours to perform five loading cycles.

The 3D model devoted for bending loading has 58000 elements which 6100 are devoted for the contact, the minimum size element is 0.5mm for the contact element and 0.02mm for the element at the root of the thread. These computation has been carrying out on a cluster IBM p655 with 2 processors 1.7 GHz and 6 Go RAM. The computation time is about 13 hours when performing 5 loading cycles.

All the calculations take into account the influence of the Make-Up torque C_{up}. The Make-Up torque represents simply the tightening angular moment of the screw and actually ensures a good fit between the male and female pieces in order to avoid leakages of the drilling mud. The Make-Up torque has been simulated by penetrating the female into the male at the level of the shoulder and the contact algorithm provided by Abaqus will compute the resulting contact pressures in order to obtain a zero clearance between the two pieces. Finally the Make-Up torque is deducted from the contact pressures and the friction coefficient.

For all the results presented in this paper, the friction coefficient is equal to 0.2, which is a good approximation for lubricated tool-joints.

Scale of the metallic grain: Dang Van Fatigue model

Once the stabilized cycle of the macroscopic strain and stress field is determined, a post-treatment will provide the critical points and the fatigue life N, i.e. number of cycles to failure, of the components of the drillstring. The used fatigue criteria are based on the critical plane concept as for example the Dang Van criterion [DAN 93].

The criterion of Dang Van, in its initial formulation, allows to define the limit of the imposed external loads under which the structure will have an infinite life. A passage between the macroscopic scale of the components and the mesoscopic scale of the grain allows to state that the lifetime is infinite if the mesoscopic shear stress $\tau(t)$ and the hydrostatic pressure $P(t)$ satisfy the following inequality:

$$\max\left[\tau(t)+a_\infty P(t)\right]\le b_\infty \qquad (1)$$

where the coefficient a_∞ and b_∞ are defined as:

$$a_\infty=\frac{t_\infty-f_\infty/2}{t_\infty/3} \qquad b_\infty=t_\infty \qquad (2)$$

Those coefficients are deduced from two Wöhler curves giving the fatigue limit t_∞ in alternate torsion and f_∞ in alternate flexion.

We recall that the inequality Eq. (1) has to be verified for all points of the component. This dependence is considered as obvious and will not appear explicitly in the next description.

In order to obtain a criterion suitable for the High Cycle Fatigue regime, some modifications must be done. Let us assume that we have a complete series of torsion and bending Wöhler curves for the material under discussion. For each finite number of cycles N we can define from the preceding Wöhler curves the limit amplitude in torsion and bending, denoted t_N and respectively f_N, which will conduct to a lifetime of exactly N cycles. Each of these pairs (t_N, f_N) defines a corresponding pair of coefficients:

$$a_N = \frac{t_N - f_N/2}{t_N/3} \qquad b_N = t_N \tag{3}$$

of a new line in the Dang Van plot representing the stress path in the mesoscopic shear-pressure coordinates.

Thus the structure will have a lifetime of at least N cycles if:

$$\max\left[\tau(t) + a_N P(t)\right] \le b_N \tag{4}$$

The different lines obtained form then a bundle in the Dang Van plot, which will be cut by the stress path in this space (see Figure 3). The number of cycles to failure is given by the line tangent to the shear-pressure path.

From a physical point of view, the fatigue life defined before by the number of cycles to failure N corresponds to the nucleation of a small macroscopic crack. This is consistent with experimental observations since the propagation phase of the macroscopic crack can be neglected when compared to the initiation phase [LEV 84].

From a practical point of view, one can consider as a first approximation that the Dang Van lines are all parallel. Therefore the direction of the Dang Van line can be approximated with a constant, in other words one can assume that:

$$a_N \approx a_\infty \tag{5}$$

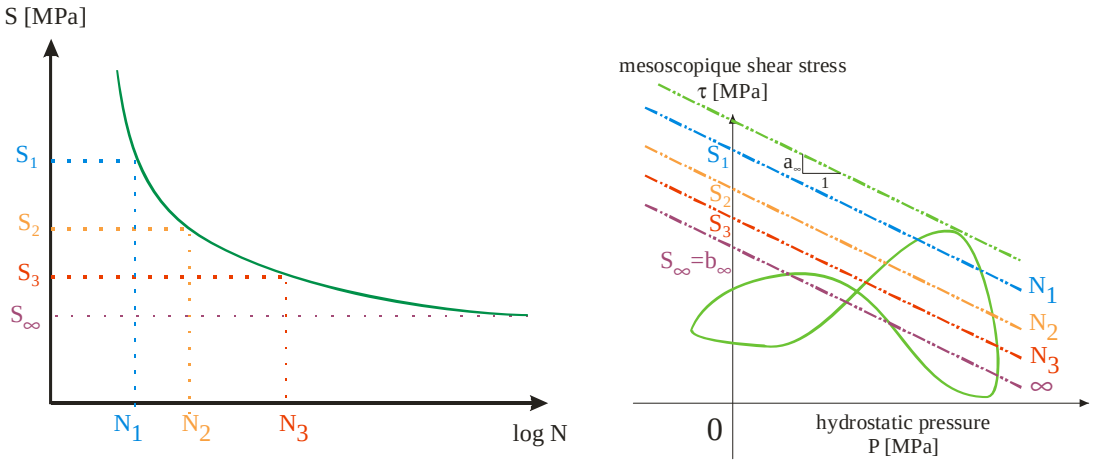


Figure 3. The adaptation of the Dang Van criterion for finite lifetime.

Recently Papadopoulos [PAP 01] proposed a similar extension of the Dang Van criterion for finite lifetime, based on a finer analysis of the stress invariants determining the lifetime. His proposal is based on a split of the hydrostatic pressure into a mean part and the amplitude part denoted respectively P_m and P_a. When applied to the Dang Van criterion defined before, he states that the structure lasts N cycles if:

$$\max\left[\tau(t) + a_\infty \frac{b_N}{b_\infty} P_m(t) + a_\infty P_a(t)\right] \le b_N \tag{6}$$

where the coefficient a_∞, b_∞ and b_N are defined by Eqs. (2) and (3). A schematic view of this criterion is shown in Figure 4.

The two criterions represented by Eqs. (4) and (6) can now be used to estimate the fatigue life of the tool-joints. When those predictions will be compared to experimental data, one will have to choose the more suitable.

3. RESULTS AND DISCUSSIONS

In the sequel we present the application of previous methodology to the lifetime computation of a classical tool-joint.

The global stresses of the drillstring have been computed using the Torque & Drag model. As mentioned earlier, this model can mainly be used to determine the flexural moment encountered by the drillstring in the dog-leg regions. Nonetheless, order of magnitude of tension and torsion are similar to the magnitudes obtained from a complete dynamical computation including the vibration phenomena (stick-slip, bit-bouncing and whirling). It can therefore be used as an input for the FEM model of the threaded connection.

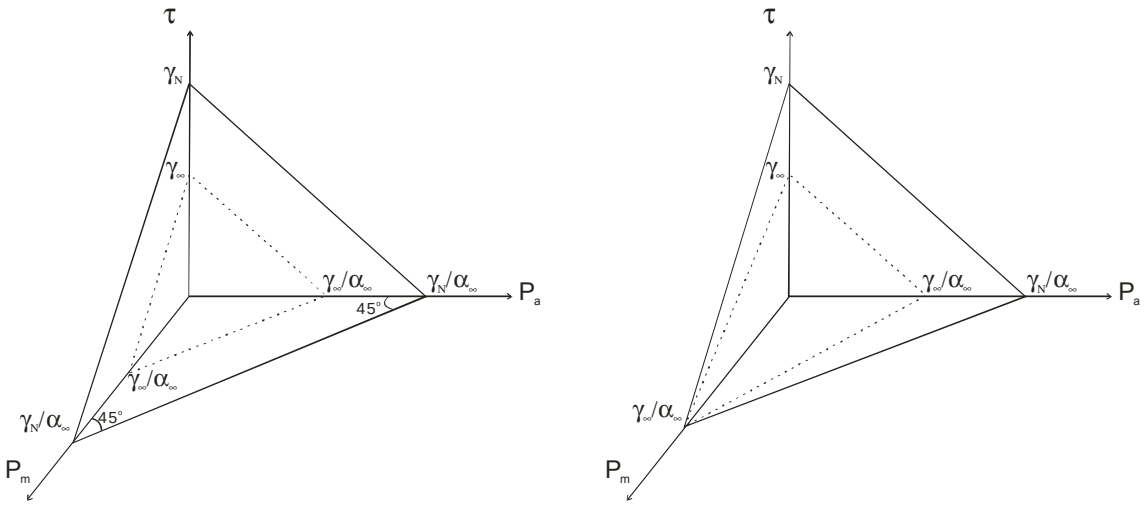


Figure 4. Representation of the Dang Van criterion (left) and Papadopoulos criterion (right) in the $\{\tau, P_m, P_a\}$ coordinates.

A complete tool-joint NC46 has been analyzed using a FEM model in the Abaqus program [ABA]. The model has already been presented in section 2. The loading cases of tension (traction and compression) and pure bending have been performed for a tool-joint and for different values of Make-Up torque C_{up}. For loading case in tension, the tension T applied ranges from –250MPa to 300MPa, and for bending case the moment M applied range from 0 to 60kNm. We can notice that the maximum applied bending moment corresponds to a curvature in the dog-leg region equal to 83 m and the minimum curvature admissible in drilling well is about 50 m.

The first remark concerns the distribution of stresses, which depends on the loading case. For traction and bending loading, the maximum stresses are located at the last engaged thread of the pin as shown in Figure 5c. And for compression loading, the maximum is reached at the shoulder (see Figure 5d) and at the first engaged thread of the box (see Figure 5b). These results match with the results reported in [TAF 93].

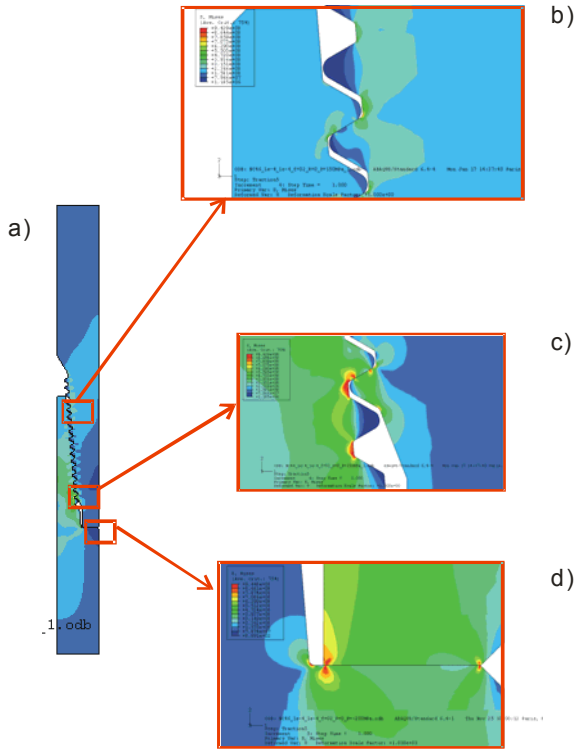


Figure 5. Highly stressed zones in the tool-joint: a) tool-joint NC46; b) first engaged threads; c) last engaged threads; d) shoulder.

Concerning the strains, only localized plasticity has been observed in the computations. Generally plasticity occurs at the roots of the last engaged thread of the pin for bending and traction cases and at the shoulder for

compression case. This remark permits us to model the thread zone with an elastoplastic behavior and the remaining zones with an elastic behavior in order to reduce the computation time.

Under cyclic loading, the structure will reach different shakedown states depending on the loading value and the Make-Up torque C_{up}. We recall that the cyclic loading is constituted of five cycles and stabilized state has been reached at the end of the third cycle. The Figure 6 shows different shakedown regimes and also the zones where the contact at the shoulder is lost. The zones where elastic shakedown behavior prevails are the ones where the DangVan criterion is applicable. Moreover, this type of plots can help the drilling operator to act on the control parameters such as the Weight On Hook in order to remain in a "safety" regimes with respect to fatigue.

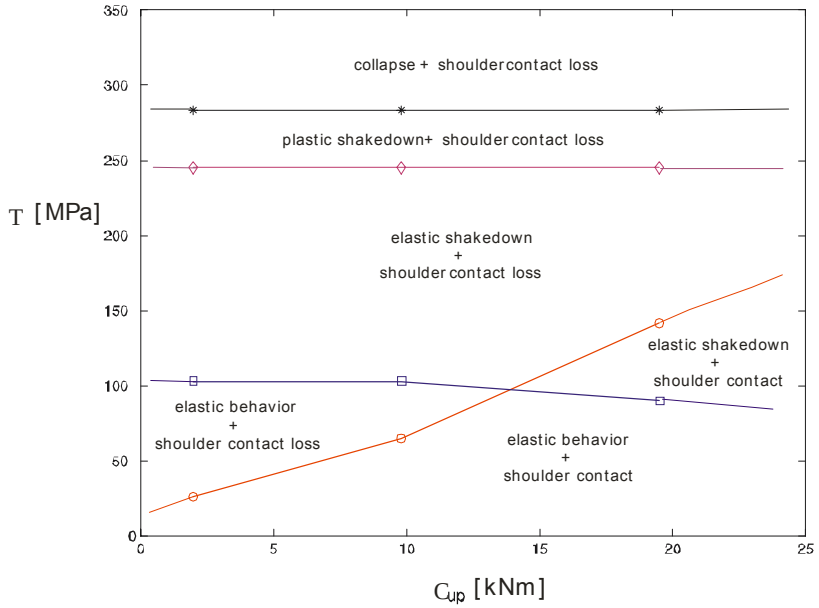


Figure 6. Functioning zones of a tool-joint NC46 under traction loading.

The use of the Dang Van criterion allows to determine the critical points of the threaded assembly. Material parameters, fatigue limits in flexion and torsion and a complete Wöhler curve in alternated flexion have been found in [BOL 87]. As expected, the critical points are at the root of the last engaged thread of the pin for traction loading as well as for flexion loading. This means that the stress concentrations at the root of the thread are the main cause of fatigue phenomena occurring in the tool-joint.

The stress paths in the Dang Van diagram for traction and bending loadings are shown in Figure 7. The plots illustrate the benefit of the Make-Up torque C_{up} on the fatigue life of the tool-joint. Basic intuition implies that the higher the torque make up, the longer the lifetime should be. A close inspection of the Dang Van plot shows that the interpretation is not straightforward. We can observe that a higher torque implies a smaller amplitude of the path which is a beneficial effect for the lifetime. However at the same time, the higher the torque, the larger will be the translation towards high traction pressure, which has a detrimental effect on the lifetime. The balance between these two phenomena defines the optimal torque from the point of view of fatigue. In our case the optimal Make-Up torque is close, but smaller than, the recommended API torque of 22.2 kNm.

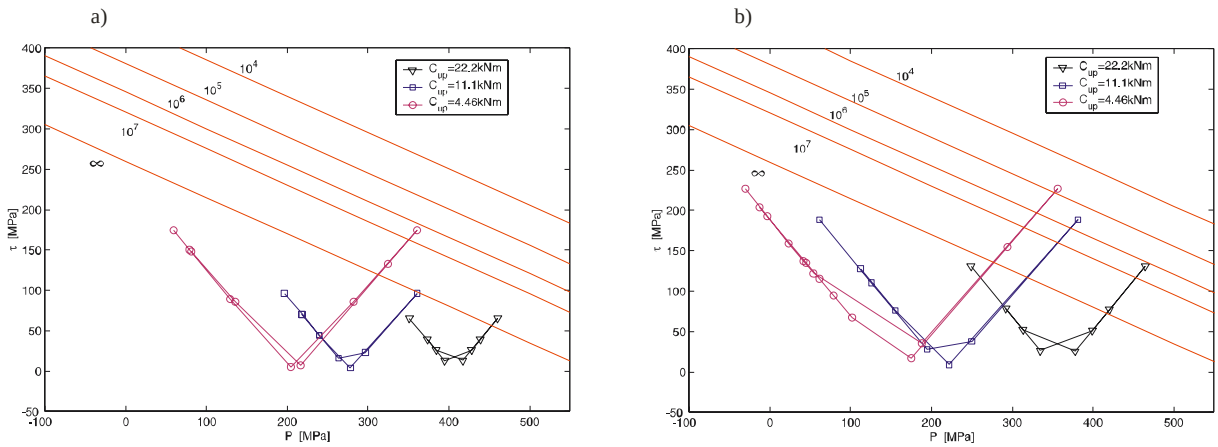


Figure 7. Stress path in the Dang Van plot: a) traction loading T=70MPa; b) flexion loading M=30kNm.

Figure 8 shows the comparison between the fatigue lives obtained by Eqs. (4) and (6). The middle line represents the case where the prediction are equal and the two lines surrounding this middle line represent a discrepancy of 50% in the fatigue life predictions. Clearly, we can see that the predictions of the fatigue life done with the Papadopoulos criterion Eq. (6) are less conservative than the ones done with the Dang Van criterion Eq. (7) except for the case where the Make-Up torque C_{up} is equal to zero.

A final comparison should be obtained soon between the predictions and experimental data on small scale tool-joint.

4. CONCLUSIONS

A fatigue life prediction methodology devoted to the components of the drillstring has been presented in this paper. The proposed model lies on a multiscale approach in order to take into account all the phenomena taking place at the scale of the drillstring to the scale of the grain of metal. The dynamical problem of the drilling process can be solved with a rod model leading to the loading history. For the time being, only a quasi-static formulation called Torque & Drag model has been used and estimation of the loading in tension and torsion can be obtained. Nonetheless the model is adapted for the computation of the alternated flexion occurring in the dog-leg.

Once the loading history has been obtained, a more accurate study has been performed at the scale of the tool-joint. Indeed at the scale of the drillstring, phenomena such as plasticity and contact are not taken into account in the calculations. Therefore a FEM model has been developed to obtain a more realistic stress field. Also the model incorporates the influence of the Make-Up torque.

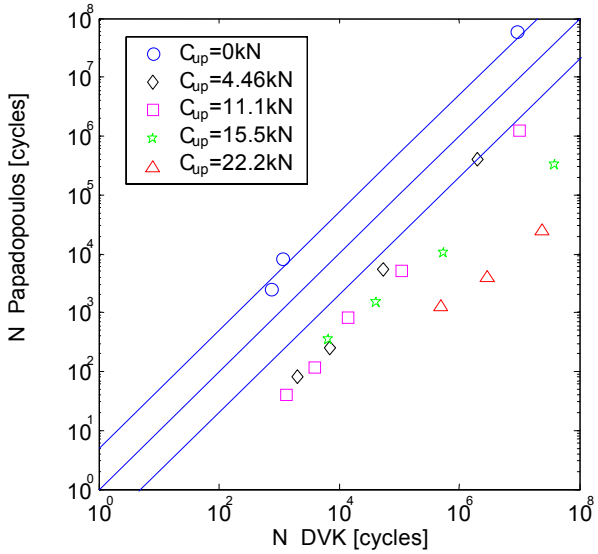


Figure 8. Comparison between Dang Van and Papadopoulos criterions.

Finally, a multiaxial criterion has been used to predict the fatigue life of the connexion. The criterion is based on the Dang Van model but it has been adapted in order to be applicable in the High Cycle Fatigue regime.

The different results obtained on this work are the following:

- the maximum stresses are obtained at the root of the last engaged thread in the case of traction and bending loading, and at the shoulder for compression loading;
- in terms of fatigue life, the critical points are at the same location as the maximum stresses explained before;
- the fatigue life of the connexion increases with the Make-Up torque up to an optimal value and then decreases.

An extension of the present work using an analytical calculation of the stress concentrations at the root of the thread is already under development.

The present methodology and results are easily extendable for all thread assemblies.

5. REFERENCES

[VAI 02] VAISBERG O., VINCKE O., PERRIN G., SARDA J. P. and FAY J. B. (2002). Fatigue of Drillstring: State of the Art. Oil & Gas Sci. and Tech - Rev. IFP, 57(1):7—37.

[HIL 92] HILL T. H. (1992). A Unified Approach to Drill Stem Failure Prevention. SPE Drilling Engineering.

[SPA 03] SPANOS P. D., CHEVALLIER A. M., POLITIS N. P. and Payne M. L. (2003). Oil Well Drilling: A Vibrations Perspective. The Shock and Vibration Digest., 35(2):81—99.

[TAF 93] TAFRESHI A. and DOVER W. (1993). Stress analysis of drillstring threaded connections using the finite element method. Int. J. Fatigue, 15(5):429—438.

[RAH 99] RAHMAN M. K., HOSSAIN M. and RAHMAN S. S. (1999). Survival assessment of die marked drill-pipes: Integrated static and fatigue analysis. Engineering Failure Analysis, 6:227—299.

[DAN 02] DANG VAN K., MAITOURNAM M.H. (2002). On some recent trends in modeling of contact fatigue and wear in rail. Wear, 253:219-227.

[RIC 01] RICHARD T. (2001). Self Excited Stick-Slip of Drag Bits. PhD thesis, Minnesota University, Minneapolis, USA.

[DAN 93] DANG VAN K. (1993). Macro-Micro Approach in High-Cycle Multiaxial Fatigue, *Advance in multiaxial fatigue*, ASTM STP 1991, D.L. McDowell and R. Ellis Eds, American Society for Testing and Materials, Philadelphia, 120-130.

[FER 05] FERJANI M. (2005). Rapport de mi-thèse : Intégration des phénomènes dynamiques dans l'analyse en fatigue des garnitures de forage. Internal report, Institut Français du Pétrole.

[JOH 83] JOHANSCIK C. A., FRIESEN D. B. and DAWSON R. (1983). Torque and Drag in Directional Wells - Prediction and Measurement. New Orleans, Louisiana. SPE/IADC Drilling Conference.

[FIL 04] FILIPPI S., LAZZARIN P. (2004). Distribution of the elastic stress due to notch in finite size plates and rounded bars uniaxially loaded, Int J Fatigue, 26:377-391.

[VAI 03] VAISBERG O., AVERBUCH D., PERRIN G. (2003). Projet "Fatigue des garnitures de forage": Calcul d'une connexion vissée par éléments finis et estimation de la durée de vie. Internal report, Institut Français du Pétrole.

[LEV 84] LEVAILLANT C.(1984). Approche métallographique de l'endommagement d'aciers inoxydables austénitiques sollicités en fatigue plastique ou en fluage. PhD thesis, Université Technologique de Compiègne.

[ABA] Documentation *ABAQUS*. http://www.abaqus.com.

[PAP 01] PAPADOPOULOS I. V. (2001). Long life fatigue under multiaxial loading, Int J Fatigue, 23:839-849.

[BOL 87] BOLLER C., SEEGER T. (1987). Material Data for Cyclic Loading Part B: Low-Alloy Steels. Elsevier.

A numerical tool for optimization of grain flow orientation in forged parts submitted to multiaxial loading

N. Caillet, P.O. Bouchard, Y. Chastel

CEMEF – Centre de Mise en Forme des Matériaux
Ecole Nationale Supérieure des Mines de Paris
B.P. 207
06904 Sophia-Antipolis Cedex

Abstract Forging of metal components induces grain flow orientation, which gives rise to anisotropic mechanical properties. The scope of this paper is to insert this grain flow anisotropy into fatigue life calculation. We have focused on high cycle fatigue, and we deal with steels containing malleable inclusions above a critical size. A new multiaxial criterion has been developed on the basis of the Murakami equation. This criterion has been implemented in the finite element code Forge 3®. This computational tool uses a new variable to represent the grain flow orientation provided by forging simulation to account for subsequent fatigue anisotropic behaviour. Moreover, residual stresses resulting from forging are also taken into account to perform the fatigue calculation. Finally, a global optimization loop including Forging and Fatigue calculation is carried out. The final goal is to improve fatigue properties by modifying forging conditions.

1 INTRODUCTION

Structural analysis is an important stage in the global conception and design of industrial parts. Numerical software are now able to provide a good estimation of the mechanical strength of a part for different loading conditions: static, dynamic, fatigue and so on. Once a design has been validated by the structural analysis department, the forming processes department is usually asked to find an adequate forming sequence to manufacture the required geometry without getting any significant damage in the final part. In this strategy, it is assumed that the thermo-mechanical state of a component after forming does not modify its mechanical strength and consequently its design. In some cases, this assumption can lead to a premature fracture of these parts during their life-cycle.

Many efforts are now being carried out in order to connect the forming process simulations with the conception stage. This requires:

- accurate numerical simulations of various forming stages leading to the final geometry including an accurate final thermomecanical state in the part;
- transfer of the final mechanical (or even microstructural) fields which can modify the mechanical strength of the part;
- ability of the structural mechanical models to integrate these input data;
- ability of the numerical software to integrate these input mechanical (or microstructural) fields.

Forging processes of metal parts induce grain flow orientation, which leads to anisotropic mechanical properties. Numerical models for forming processes such as forging can provide output not only in terms of geometrical features or simple stress fields, but also in terms of microstructure evolution throughout the part (grain flow, residual stress, inclusions distribution and shape). It is indeed the microstructure which makes a forged component better than a cast or a machined part. In practice, design departments try to use efficiently these specific properties, but the quantitative link between grain flow orientation and mechanical properties is not yet established.

Fatigue calculations are often performed on parts without considering mechanical history. The well-known Dang Van criterion [1], devoted to high-cycle fatigue, is often used to predict the limit stress before the collapse of a part, for a high number of cycles. Murakami equation [2] can also be used in high-cycle fatigue when defects size becomes significant. Some authors are now using some mechanical data such as plastic strain or residual stresses in their structural analysis simulations. However, a lot of work still needs to be done to improve the design stage.

The aim of this paper is to show how fatigue calculations can be performed for a forged part, taking into account residual stresses and anisotropy induced by the process. The choice of a specific criterion will be explained as well as the way to use it for anisotropic materials submitted to multiaxial loadings. Finally, some numerical results will show the impact of grain flow orientation.

2 FORGING AND GRAIN FLOW ORIENTATION

Forging is one of the key industrial production technologies. It allows producing parts more resistant than those manufactured by casting of machining for instance. This partly comes from the fact that forged components develop a specific microstructure and mechanical state during the forming process itself.

Today, all forging operations can be modelled with numerical simulation tools and commercial software. Over the last decade, efficient algorithms have been developed and implemented in commercial codes to deal with complex thermo-mechanical boundary value problems in large strain. Automatic 3D remeshing techniques are available and used in these software products. Emphasis has been placed recently in integrating microstructure models to simulate the metallurgical evolutions of the metal during forging that is to say for such thermo-mechanical treatments.

In our study, we have used Forge3®, which is a process simulation tool based on the finite element method. Based on a mixed velocity-pressure formulation, FORGE3® provides the material flow in 3D hot, cold and warm metal forming processes. The available constitutive laws include elastic, viscoplastic and elastic-viscoplastic models, which give access to residual stresses at the end of the process.

In order to study the grain flow orientation induced by forging, a specific fiber vector has been defined. First, we have focused on malleable inclusions, and so, stress concentrations induced by inclusions alignment do not need to be dealt with. Despite the complexity of the evolution of inclusions during forging, malleable inclusions can be assumed to undergo nearly the same strain as the matrix surrounding. Moreover, these inclusions are assumed to become ellipsoids of revolution, as the metal is deformed. The goal is then to calculate the orientation and the shape factor of ellipsoids which model inclusions, at the end of the forging process. This calculation is performed by using the left Cauchy-Green tensor V. Using the polar decomposition, the strain tensor F can be split in a spherical (R) and an orthogonal (U or V) part:

$$F = R.U = V.R \tag{1}$$

$$V^2 = F.F^T \text{ where } F_{i,j} = \delta_{i,j} + \frac{\partial u_i}{\partial x_j^0} \text{ and } u \text{ is the displacement vector} \tag{2}$$

Indeed, an initial material segment colinear to an eigenvector of U is colinear to an eigenvector of V in its final position. So, if we consider an initial spherical inclusion (Figure 1), it becomes an ellipsoid with the axes directions given by the eigenvectors of V.

For ellipsoids of revolution, one vector is able to contain the information (direction and length of the axis which is also axis of symmetry). It is possible to model an ellipsoidal inclusion if the initial volume of the inclusions and this vector are known. This vector is called the «**fiber vector**».

Figure 1 shows the z component of the fiber vector at the end of a compressive test and its comparison with a micrography:

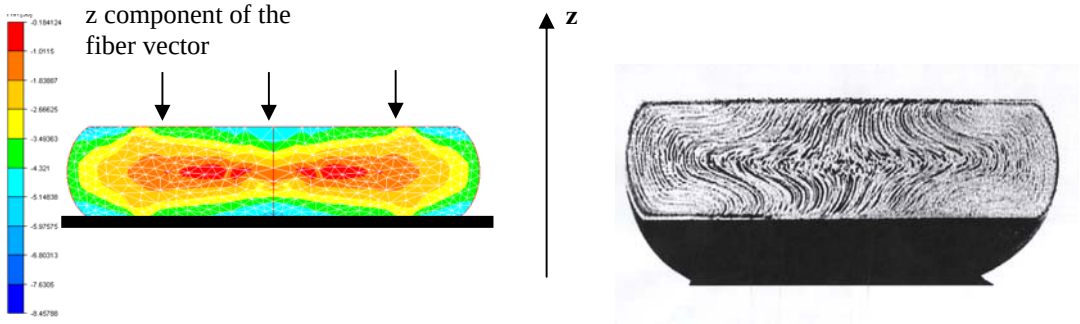


Figure 1. Qualitative comparison between numerical and experimental grain flow orientation

3 ANISOTROPY AND FATIGUE CRITERIA

«Grain flow orientation» of forged parts is a common term which combines several phenomena. Indeed, during forging, deformation leads to grain flow orientation, and also to the stretch of ductile inclusions and to alignment of hard inclusions. Experiments have shown that fatigue strength is different as a function of the orientation of fibering in the sample. Therefore, fatigue criteria must be able to take into account these phenomena. This can be achieved by improvements made on the basis of large experimental campaigns to obtain laws, or on the basis of theoretical considerations.

Dang Van criterion, previously mentioned, is based on the existence of a limit stress for crack nucleation, in a defect free material. Practically, the Kitagawa diagram shows the existence of a critical size of inclusions, delimiting two fatigue behaviours. Figure 2 shows an example of a Kitagawa diagram [3]. Below a critical inclusion size, fatigue strength is independent of the inclusion size. This is the domain in which the Dang Van criterion is valid. On the other hand, above the critical size, the fatigue limit stress is a power function of the inclusion size. In this second domain, Murakami equation [2] gives fatigue limit stress as a function of the inclusion size, for uniaxial loading.

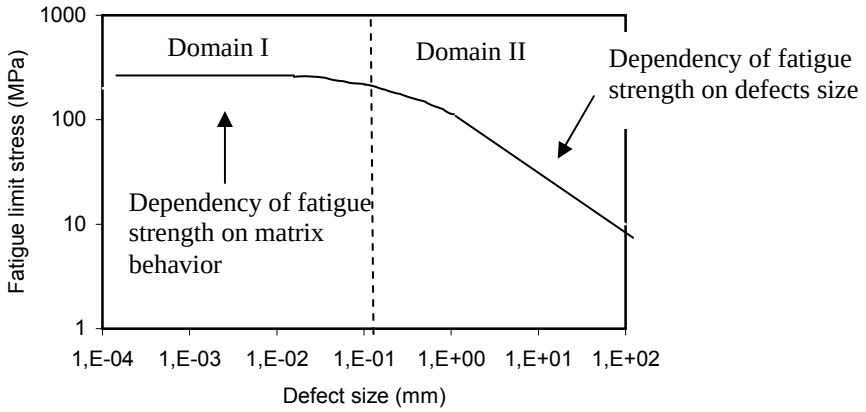


Figure 2. Example of the relationship between defect size and fatigue limit stress

We can also notice that fatigue anisotropy is more important in the case of large inclusions.

Moreover, the Murakami equation introduces the anisotropy through the shape of inclusions. In fact, the important parameter is related to the projected area of the inclusion in the direction of normal stress. However, another major phenomenon may occur and induce fatigue anisotropy. During cyclic loading, the alignment of inclusions may induce stress concentrations, depending on the relative directions of stresses and alignments.

Results about previous criteria are summarized in table I.

Table I. Characteristics of fatigue criteria

	Dang Van criterion	**Murakami equation**
Validity	Below critical size	Above critical size
Anisotropy in each field	Weak in this field	Important in this field
Criteria and anisotropy	Can be introduced by phenomenology	Linked to inclusions shapes
Residual stresses	YES	YES
Multiaxiality	YES	NO

Both domains are of interest when it comes to forged parts. First, Dang Van criterion was implemented in the finite element code Forge3®. This makes it possible to take into account the residual stresses of forging process. Nevertheless, the criterion has not yet been extended, to take into account the weak anisotropy in this domain. More emphasis was placed on the development of Murakami equation which is able to take into account the anisotropy in the domain where it is the most significant. This equation was indeed extended to a multiaxial criterion.

4 DEVELOPMENT BASED ON MURAKAMI MODEL

4.1 Murakami equation

Defects (and also inclusions) are considered such as cracks. The stress intensity factor (SIF) range, at the tip of these defects, can be calculated using the Murakami relationship (3):

$$\Delta K = 0{,}65 \times \Delta\sigma \sqrt{\pi \sqrt{area}} \tag{3}$$

where *area* is the defect area projected onto a plane perpendicular to the applied stress, and $\Delta\sigma$ is the stress amplitude. This geometrical parameter is efficient for both two-dimensional and three-dimensional defects. To achieve fatigue strength prediction Murakami and Endo [2] have introduced a model which describes the relationship between ΔK_{th} and the defect size, for axial loading and a given stress ratio $R = \sigma_{\min} / \sigma_{\max}$ (for surface defects):

$$\Delta K_{th} = 3 \times 10^{-3} (Hv + 120) (\sqrt{area})^{1/3} * (0.5 - R/2)^{0.226 + Hv \times 10^{-4}} \tag{4}$$

where Hv (kgf mm^{-2}) is the Vickers hardness of the metal matrix. Combination of equations (3) and (4) leads to the fatigue limit stress amplitude, σ_w:

$$\sigma_w = 1.43 \times \frac{Hv + 120}{\sqrt{area}^{1/6}} \left(0.5 - \frac{R}{2} \right)^{0.226 + Hv.10^{-4}} \tag{5}$$

No fatigue test is necessary to use this equation, and it is sufficient to measure the values of $\sqrt{area}$ and Hv, and to estimate the stress ratio R.

4.2 Extension to multiaxial stresses

When dealing with multiaxial stresses, Murakami equation must be modified. Attention has to be paid to two points: the expression of the stress intensity factor (equation (3)), and the term concerning the stress ratio in equation (4).

4.2.1 New expression of the Stress Intensity Factor

Beretta and Murakami [4] have proposed to use the weight function method to calculate the ratio between stress intensity factors in tension and in a biaxial loading. Equation (6) shows their results, which are in good agreement for in-phase torsion and tension at R=-1.

$$\frac{K_{I,tension}}{K_{I,biaxial}} = 1 + 0.1804 \frac{\sigma_{II}}{\sigma_I} + 0.0329 \left(\frac{\sigma_{II}}{\sigma_I} \right)^2 \tag{6}$$

where σ_I and σ_{II} are the two principal stresses at the defect location.

We use this method to calculate the stress intensity factor for any loading and as a first approximation we assume that the effect of the third principal stress can be neglected.

4.2.2 Stress ratio in multiaxial loading

For uniaxial loading, the stress ratio is clearly defined, while for biaxial loading it can be different for the two principal stresses.

Murakami takes into account the influence of stress ratio on fatigue strength, on the basis of experimental results. In order to extend his equation to multiaxial loading, we tried to give a meaning to the term $(0.5 - R/2)^{0.226 + Hv.10^{-4}}$ in equation (5). This term is meant to include the change of effective stress, with the displacement of the loading path center from the origin (at R=-1). So, it may be largely linked to a kinematic hardening occurring during cyclic loading. Our method [5] consists in calculating an equivalent kinematic hardening. The extended Murakami criterion uses modified stresses (σ') taking into account this equivalent kinematic hardening.

4.3 Extended Murakami criterion

By using the weight function method and our method to introduce the effects of kinematic hardening, a new form for a Murakami equation extended to multiaxial loading (7) can be written:

$$\underset{cycle}{Max}\left(\frac{\sigma'_I}{1+0.1804\frac{\sigma'_{II}}{\sigma'_I}+0.0329\left(\frac{\sigma'_{II}}{\sigma'_I}\right)^2}\right)=1.43\times\frac{Hv+120}{\sqrt{area}^{1/6}} \quad (7)$$

It must be noted that the directions of principal stresses change during the cycle.

Now, this equation can be used to predict the fracture of a part submitted to multiaxial stresses. Our final work consists in calculating the appropriate values for the variable called area, as a function of the deformation history of a material volume.

5 FROM FORGING TO HIGH CYCLE FATIGUE

It was shown that links between fibering and fatigue can be naturally done with the shape of inclusions in Murakami criterion.

These ellipsoids can then be used to calculate the *area* parameter in Murakami criterion. Figure 3 shows the value of the big axis of the ellipse resulting from the projection of the ellipsoid onto the plane perpendicular to the normal stress direction $\vec{n}$.

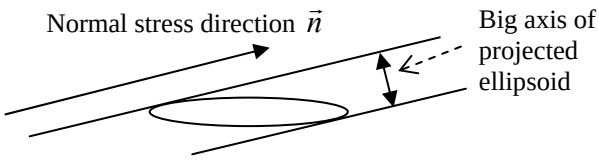


Figure 3. Calculation of area parameter for inclusions with ellipsoidal shape

Equation (8) shows the anisotropic criterion.

$$\underset{cycle}{Max}\left(\frac{\sigma'_I\cdot\sqrt{area(\vec{n})}^{1/6}}{1+0.1804\frac{\sigma'_{II}}{\sigma'_I}+0.0329\left(\frac{\sigma'_{II}}{\sigma'_I}\right)^2}\right)=1.43\times(Hv+120) \quad (8)$$

where $\vec{n}$ is the direction of the principal stress σ'_I .

This criterion has been implemented in the finite element code Forge3®.

5.1 Tensile-Compression tests and Torsion

Experimental and numerical results have been compared for a steel grade containing elongated inclusions. Experiments showed important anisotropy on tensile-compression tests (about 40% between longitudinal direction and 90°). A homogeneous fibering in samples was initialized in Forge3® and fatigue calculations were performed. Results are satisfactory, as shows table II. Nevertheless, anisotropy was found to be smaller than in simulations.

Table II. Fatigue strength in traction-compression

Sample direction	**Traction-compression**		
	Experimental	Simulation	Error
Long	516 MPa	475 MPa	-8%
45°	427 MPa	415 MPa	-3%
90°	329 MPa	355 MPa	9%

Alternate torsion was then studied; such results should be linked to traction-compression. Indeed, locally, stresses are similar to tensile stresses. The results are in good agreement for the longitudinal direction and 45°. Figure 4 shows cross-sections at the centre of samples. In the first case, the sample is in the longitudinal direction and decreasing values of Murakami criterion are observed from the surface to the centre. The second case shows the results for a sample at 90°. The effect of anisotropy is noticeable, with maximum values localised on the right and left sides in the figure.

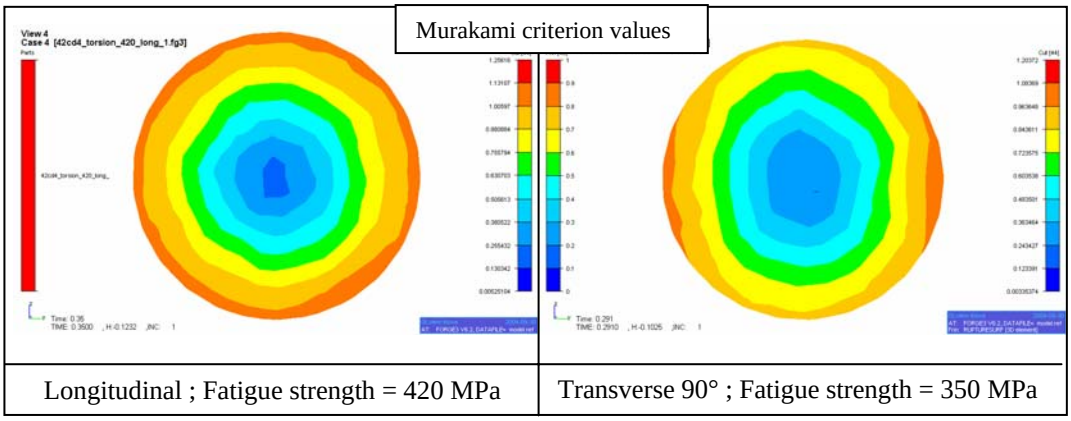


Figure 4. Cross-sections of samples submitted to alternate torsion

5.2 Application to a valve cap

The following example deals with a valve cap submitted to a simplified cyclic loading, as shown in figure 5.

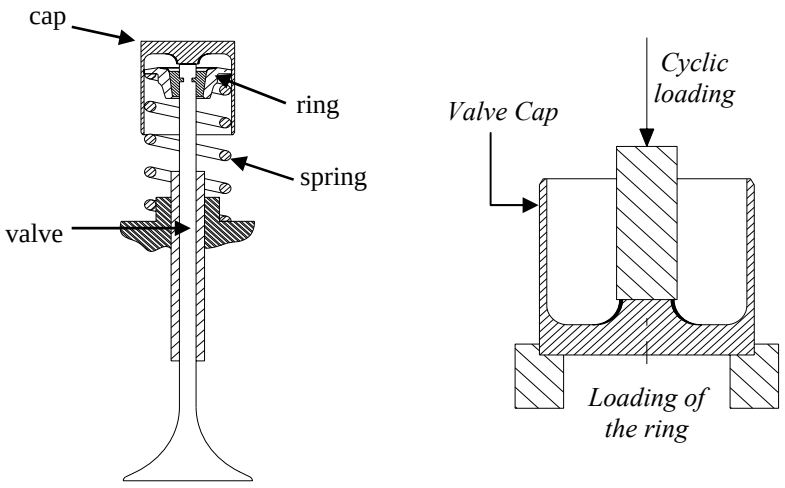


Figure 5. Valve cap submitted to a simplified cyclic loading

Forging of this valve cap is achieved in four stages using FORGE3®. As the initial billet is obtained by a hot rolling process, an initial fiber vector (perpendicular to the forging direction) is used. During each stage, the fiber vector is computed and transferred from one simulation to the other (just as stresses, plastic deformation and so on).

A simplified cyclic loading, depicted in figure 5, is then applied to the valve cap. Figure 6 shows the mesh of the final geometry for the valve cap and the Murakami criterion field after cyclic loading.

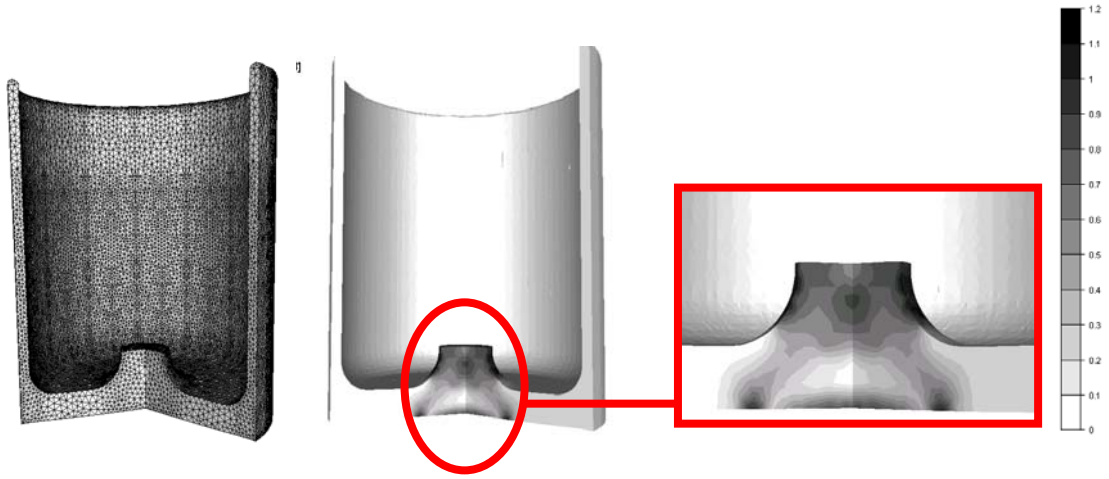


Figure 6. Mesh of the final geometry of the valve cap and Murakami criterion field

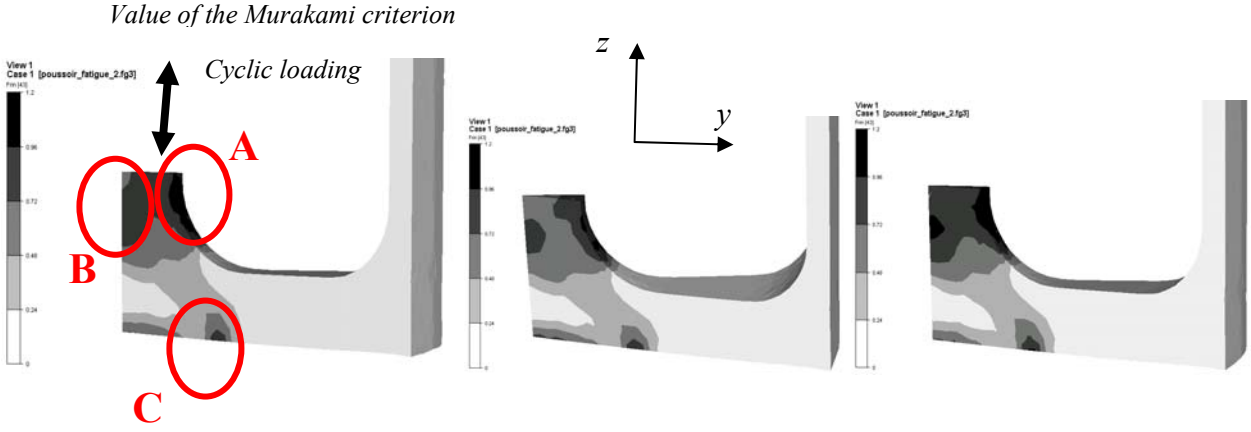
5.3 Towards Optimization

We are now developing optimization tools in order to improve the final mechanical strength of components submitted to cyclic loadings. The optimization parameters can either be the initial fiber orientation or the geometry of the valve cap. Evolution strategies are being developed within the scope of another PhD study [6]. We plan to use this optimization tool soon to build a global optimization loop including forming processes simulations and fatigue analysis. Up to now, we have studied the influence of two parameters on the Murakami equation results:

- the height of the centre part of the valve cap: no significant results were found on the Murakami values by modifying this height up to 10%.

- The initial grain flow orientation: Figure 7 shows Murakami criterion fields in three different configurations : a) without any initial grain flow; b) with an initial grain flow oriented in the z direction; c) with an initial grain flow oriented in the y direction.

As shown in figure 7, there is a significant difference between computed Murakami values whether initial grain flow is considered or not. Three different areas (A, B and C) give relatively high values but the maximum is reached in area A. Murakami criterion clearly gives lower values when an initial grain flow in the z direction is used in our model. Inversely, if the initial grain flow is oriented in the y direction, Murakami values are higher. This means that grain flow induced by forging can improve or decrease the final fatigue strength of the valve cap.



a) Without any initial grain flow orientation

b) With an initial grain flow orientation in the **z direction**

c) With an initial grain flow orientation in the **y direction**

Figure 7. Values of the Murakami criterion with and without considering grain flow orientation

6 CONCLUSIONS

By considering the elongation of inclusions as governing anisotropic fatigue behaviour of forged parts, it seems possible to use a fatigue criterion giving anisotropic results. This criterion is the Murakami equation, which has been extended to multiaxial loadings. The link between a «fiber vector» computed during forging simulation, and this criterion, provides a new way to calculate fatigue strength of forged parts, taking into account some specificities of this process. Optimization strategies can now be used to improve fatigue strengths of forged components by modifying several parameters such as geometry, grain flow orientation, forging conditions and so on. We are now developing different optimization strategies in order to include Forging and High Cycle Fatigue computation in a global optimization loop.

In the longer term, multiaxial high cycle fatigue models should be able to integrate other microstructural parameters such as grain size or texture. Such microstructural parameters, now available at the end of forging simulations, could then be used as new optimization parameters to improve components fatigue strength.

ACKNOWLEDGEMENTS

This work is supported by the French Ministry of Industry through the OPTIMAT-RNTL project. The authors also want to thank ASCOMETAL CREAS (LUCCHINI GROUP) for helpful discussions.

7 REFERENCES

1. K. Dang Van, B. Griveau and O. Message, Biaxial and Multiaxial Fatigue, EGF 3, Mechanical Engineering Publications, London, 1989, 479-496.
2. Y. Murakami and M. Endo, *Fatigue*, Vol 16, 1994, 163-182.
3. H. Kitagawa and S. Takahashi, Proceedings 2nd Int. Conference Mech. Behaviour Mater. ICM2 , Boston, 1976, 627-631.
4. S. Beretta and Y. Murakami, *Fatigue Fract. Engng. Mater. Struct*. 23, 2000, 97-104.
5. N. Caillet, P.-O. Bouchard and Y. Chastel, CD-ROM of WCCM VI in conjunction with APCOM'04, 2004 Beijing.
6. L. Fourment, T.T. Do, A. Habbal, M. Bouzaiane, 8th International ESAFORM Conference on Material Forming, Cluj-Napoca, Romania, 2005.

Design Against Fatigue Emanating From Stress Concentrators

H ADIB and G PLUVINAGE

Laboratoire de Fiabilité Mécanique
ENIM
Ile du Saulcy
Metz 57045

ABSTRACT

Design against fatigue emanating from stress concentrators uses generally the concept of *« hot spot"* i.e. the value of maximum stress range through elastic stress concentration factor k_t or fatigue strength reduction factor k_f.
Modern methods use possibility of computing cyclic stress distribution at stress concentrator tip. They are base on the assumption that fatigue process needs a process volume describe by a distance (point or line methods), an area or a volume.
The paper is mainly devoted to "Volumetric method ". It is focused on the following points :

- Numerical determination of effective distance and stress,
- The choice of the weight function,

Examples will be given for uniaxial or multiaxal loading, for simple or complex notches as keyways and different kind of welded joints including spot welds.

Key words: Fatigue, stress concentrators, volumetric method.

INTRODUCTION

Design against fatigue of notched component such as riveted, bolted or welded joints is generally done by considering the presence of stress concentrations. Behind such a use is the idea that the peak stress plays the essential role in fatigue. However the fact that the use of the maximum stress leads to conservatism for fatigue life prediction, this approach is kept by reducing the stress concentration factor into the fatigue strength reduction factor arguing that cyclic plasticity produces stress relaxation. To solve this problem, Neuber [1] has proposed to take the effective stress at a given distance to notch tip defining a line method. The concept was extend to an area [2] and later to a volume [2]. Averaging stress distribution into a process volume is a method which is used in the so called "local approach" in fatigue and fracture. The difficulty is to define the size of the process volume, grain, plastic zone volume short crack length or other. In the "volumetric method" which is described in the following, the fatigue process zone is defined physically as the "high stress " region and limited by an inflexion point visible on the notch tip stress distribution. Determination is made by graphical or numerical procedure. This volume was found intuitively and check on numerous case of fatigue of notched components where 4 are presented in the next. The accuracy of the method is checked by the fact that each assessment point (number of cycles, effective stress) is located on the fatigue reference curve which is generally the smooth specimen Wöhler curve. Similar concept of high stressed regions was introduced using σ_{90} or $\sigma_{95\%}$ stresses as effective stress (90 or 95% of maximum stress value).. However these values are closed to the volumetric method effective stress, they are arbitrary defined and cannot be used for transferability of results to another loading mode or geometry because fatigue is a phenomenon sensitive to hydrostatic pressure and stress gradient. This problem is solve in volumetric method by coupling the fatigue process volume definition with a "weighted "stress

distribution like in the stress field intensity concept [3]. The stress distribution is corrected by a weight function taking into account the position of the acting stress close or far to the notch tip and influence of stress gradient.
This paper explains how to found the size of the fatigue process volume and to compute the effective stress. To illustrate the accuracy of the method 4 examples are used
Example 1 Fatigue life prediction of shafts with keyseats,
Example 2 of fatigue life prediction of T welded joints,
Example 3 Influence of loading mode on fatigue of cylindrical notched specimens,
Example 4 Fatigue life of welded joints.

2 PRINCIPLE OF VOLUMETRIC METHOD

The volumetric methods calculates average stress in stress field near notches via area and volume integration. This average stress is called "effective stress σ_{ef}" The last investigations about 2D and 3D methods reveal that the area and volume integration cannot notably manipulate effective stress average stress by numerical integration techniques. In simple cases of geometry and loading mode a line methods which calculates average stress by numerical integration techniques for specific distance is preferable for simplicity and rapidity.
It has been mentioned that the fatigue process zone is defined physically as the "high stress " region and limited by an inflexion point visible on the notch tip stress distribution.
A typical example of opening stress at notch tip is given in Fig 1.

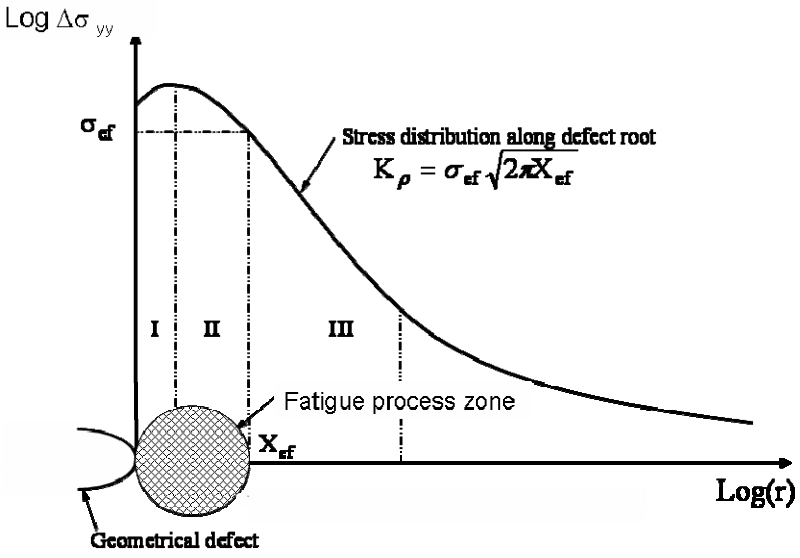


Figure 1 : Typical stress distribution in a bilogarithmic graph ahead of a defect tip.

This stress distribution can be fitted as polynomial terms and Taylor's expansion.

$$\sigma_{yy}(x) = \sum_{i=0}^{n} a_i x^i \qquad (1)$$

wherein $\sigma_{yy}(x)$, a_i and x are opening stress, polynomial coefficients and distance along crack opening direction, respectively.
The position of the above mentioned "inflexion point on the stress distribution can be found by the way of the relative stress gradient written as:

$$\chi(x) = \frac{1}{\sigma_{yy}(x)} \frac{\partial \sigma_{yy}(x)}{\partial x} \qquad (1)$$

The relative stress gradient can be derived by equation (3)

$$\chi(x) = \frac{1}{\sigma_{yy}(x)} \frac{\partial \sigma_{yy}(x)}{\partial x} = \frac{\sum_{i=0}^{n} i a_i x^{i-1}}{\sum_{i=0}^{n} a_i x^i} \qquad (3)$$

According to the polynomial formulation, effective distance which is corresponding to minimum point of relative stress gradient can be obtained as below:

$$\left.\frac{\partial \chi(x)}{\partial x}\right|_{x=X_{eff}} = -\frac{1}{\sigma_{yy}^2(x)}\left(\frac{\partial \sigma_{yy}(x)}{\partial x}\right)^2 + \frac{1}{\sigma_{yy}(x)}\frac{\partial^2 \sigma_{yy}(x)}{\partial x^2} = 0 \qquad (4)$$

The equation (4) is named to "volumetric method effective distance characteristics equation" as:

$$\left(\sum_{i=0}^{n} a_i i\, X_{ef}^{i-1}\right)^2 = \left(\sum_{i=0}^{n} a_i i(i-1)\, X_{ef}^{i-2}\right) \times \left(\sum_{i=0}^{n} a_i\, X_{ef}^{i}\right) \qquad (5)$$

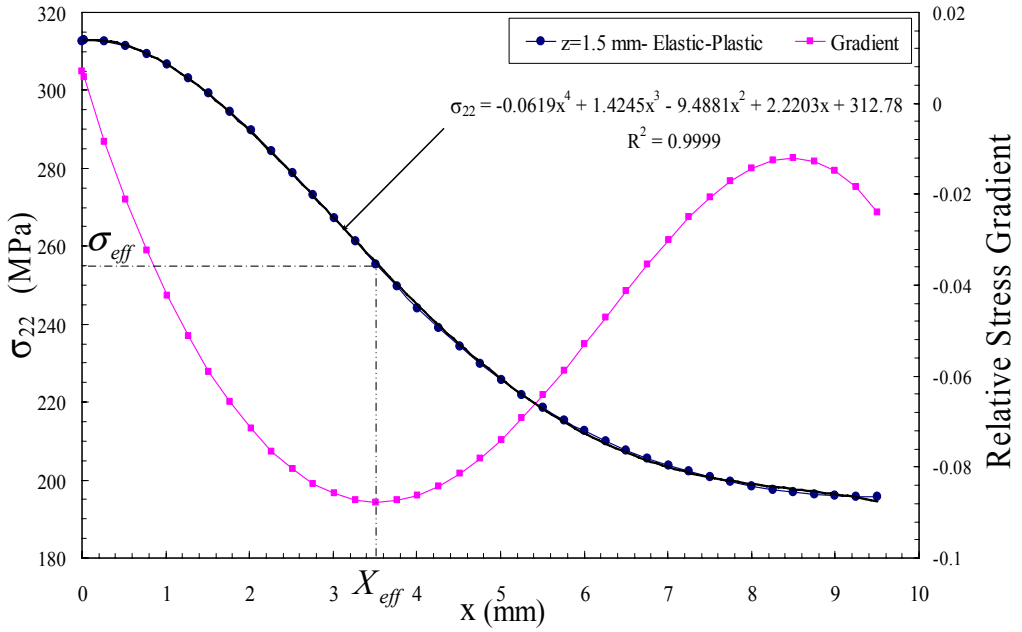


Figure 2: Graphical determination of the effective distance.

Effective stress is defined as the average value of the "weighted stress distribution" can be rewritten including unknown weight function ϕ n as following:

$$\sigma_{ef} = \frac{1}{X_{ef}} \int_0^{X_{eff}} \left(\sum_{i=0}^{n} a_i x^i\right) \times \phi(x, \chi)\, dx \qquad (6)$$

Weight function deals with stress contribution in process zone. Thee weight function explicitly depends on stress, stress gradient and distance from notch root in process zone and

it implicitly depends on notch geometry, loading type, boundary conditions and material properties. The main objective of weight function is to emphasize integrant quantity in special range for predicting equivalent or so called effective stress.
In the following section, volumetric method is exhibited as simplified configuration (line integration). The complete form of volumetric method can be elucidated as below:

$$\sigma_{ef} = \frac{1}{V_{ef}} \int_{\Omega} \sigma_{yy}(x,y,z) \times \phi(x,y,z,\chi)\ dv \qquad (7)$$

The weight function can be chosen as unity. It leads to equal stress contribution for each point in process zone and it can be denoted as general form:

$$\phi(x,y,z,\chi) = 1 \qquad (2)$$

where in, x, y, z and χ are coordinates and relative stress gradient, respectively. The mentioned weight function is the simplest weight function. The methods which use unit weight function must be deemed as AVERAGE MODEL or LINE METHOD and was introduced first by Peterson .

The weight function was first proposed at specified point around notch root and it can be generally written as:

$$\phi(x,y,z,\chi) = \delta(x-x_0)\delta(y-y_0)\delta(z-z_0) \qquad (9)$$

where, $x_0, y_0, z_0, \delta(x-x_0), \delta(y-y_0)$ and $\delta(z-z_0)$ are coordinates of specified point and delta functions, respectively. The delta function in weight function definition describes the so called " POINT METHOD ". Indeed, the mathematical integration is omitted and integrant value at specific point is calculated due to the delta function feature. Consequently, the relation (7) reduces to:

$$\sigma_{eff} = \sigma_{yy}(x_0, y_0, z_0) \qquad (10)$$

The definition of this particular point around notch roots is one controversial debate. It was introduced by Neuber [1] as a material constant but grain size, plastic zone, short crack distance have been used by other authors..

For STRESS FIELD CONCEPT, Yao [4] suggested weight function including stress gradient at notch root in polar form **Erreur ! Source du renvoi introuvable.**:

$$\phi(r,\theta,\chi) = 1 - |\overline{\chi}| \times r \times (1+\sin\theta) \qquad (11)$$

Yao et *al.* have modified their proposed weight function as **Erreur ! Source du renvoi introuvable.**:

$$\phi(r,\theta,\chi) = 1 - c^* \times r \times (1+\sin\theta) \qquad (12)$$

where, c^* depends on stress gradient $\overline{\chi}$ $(c^* = c^*(\overline{\chi}) \geq 0)$.

The VOLUMETRIC METHOD[5] uses weight function incorporating relative stress gradient χ (Equation 2) and it is enable to consider not only relative stress gradient at notch ahead but also whole effective zone around notch root. The general first order volumetric method weight function involves following form:

$$\phi(r,\theta,\chi) = 1 - c_s \times |\chi| \times r \times f(\theta) \quad (13)$$

where, c_s and $f(\theta)$ are weight function skew factor and polar function for area integration purposes, respectively.
For reducing volumetric method to line method integration, polar function $f(\theta)$ is withdrawn and skew factor is equal to 1. Consequently, Equation (17) is simplified as:

$$\phi(x,\chi) = 1 - |\chi| \times x \quad (14)$$

Recently Kadi and al [6] have proposed to used the following weight function :

$$\phi(x,\chi) = e^{r\chi/2} \quad (15)$$

We can note that all the used method to obtain the effective stress in fatigue (line, point, area or volumetric methods can described similarly using appropriate weight function. However, the use of a weight function incorporating the relative stress gradient allows transferability when the fatigue reference curve is produce with a different mode of loading or with specimens with different geometry.
For multiaxial loading, the reducing line method cannot be applied and equation (6) needs to be used. The fatigue process zone is similarly by the value of the minimum of by the relative stress gradient but in 3D. In this case, computing time significantly increases. An example of such application can be found in [7] but not described in this paper. The method can be extended for non proportional by averaging the fatigue process zone using another weight function. Application of this idea on non proportional loading of railway wheel is under progress but not yet publish.

Application of the Volumetric Method is simple and follows this steps:

i) By using finite Element method the stress distribution at notch tip is computed.
ii) Solving equation (5) the effective distance is extracted.
iii) Integrating the weighted stress distribution over he effective distance we get the effective stress.
iv) Reporting the effective stress on fatigue reference curve, we get the corresponding fatigue life duration.

The following 4 examples demonstrate the application of the method.

3. EXAMPLE 1 FATIGUE LIFE PREDICTION OF SHAFT WITH KEYWAYUNDER BENDING AND TORSION

Fatigue tests on shafts with two types of key sat (semi circular and sled runner) and under two loading modes, rotating bending and alternating torsion were carried out. A 42CD4 steel (French standard) was used to manufacture the specimens. The specimen geometry is given in figure 3as well the experimental results. These results are presented according to Basquin's law according to the following relation ship :

$$\Delta\sigma = \sigma'_f \left(N_r\right)^b \quad (16)$$

$\Delta\sigma$ is the applied stress rang, σ'_f the fatigue resistance and b coefficient of Basquin's law.
We can notice on figure 3 that a strong notch effect is introduced by the presence of key seats. This effect is close for the different types of key seats. Fatigue strength reduction k_f at $N_r = 10^6$ cycles varies from 1.5 to 1.7.
Effective stress range was computed by finite element method using equ (7) and reported versus number of cycles to failure. Results are closed to the fatigue reference curve obtained

on same material but with smooth specimen and confirm the validity of the volumetric method.
In the case of key ways, it is important to note that we cannot use the traditional Neuber and Peterson model which used the notch radius value instead to define an equivalent bidimensional notch radius.
The prediction of fatigue life by volumetric method is based on the stress distribution at notch tip. This needs the geometry of the components and the applied load. Computing is made using the cyclic stress strain curve of the material generally described by the following relation ship:

$$\Delta\sigma = K'\Delta\varepsilon^{n'} \qquad (17)$$

Where n' is the cyclic strain hardening exponent and K' cyclic hardening coefficient. These coefficients and the one of the Basquin's law are the only material coefficients needed for the method. Any other empirical constant are required. Like in Neuber and Peterson's methods for example. In addition Finite element methods extends the possibility for 3D case where these constants doesn't exists.

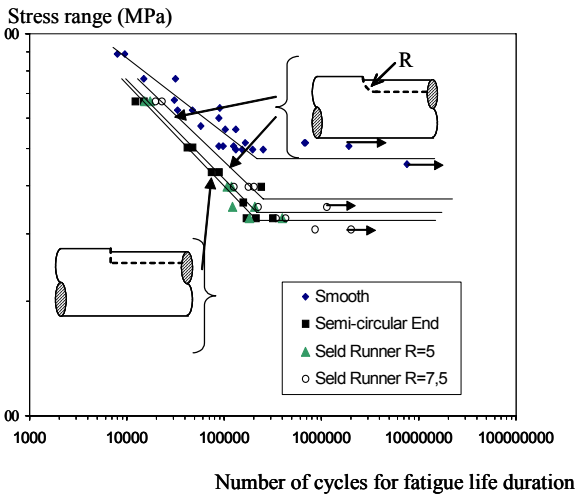


Fig 3 : Wöhler's curve for smooth and key seats specimens. Bending tests. 42CD4 Steel.

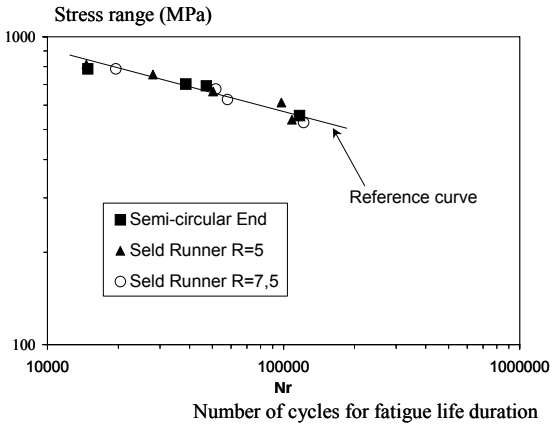


Fig 4 :Application of the Volumetric method to fatigue of key seats specimens. The reference curve is obtained on smooth specimens. Bending tests. 42CD4 Steel.

4) EXAMPLE 2 FATIGUE LIFE PREDICTION OF WELDED JOINTS

An experimental verification of the application of the Volumetric Method for the prediction of the fatigue life duration of symmetric T welded joint in HLE steel (Thickness 8mm has been made and results can be seen in figure 6. T The geometry of the specimen is described in Fig 5. Predictions given by this method are relatively good if we overcomes the problem of residual stresses introduced by the welding process. For that, the cyclic stress strain curve and the fatigue reference curve are made on the same welded specimen where the seal has been erased. In our case the weld toe radius has been taken as 0.22mm. This value is the mean value of 20 measurements on different specimens. Results suffer of large scatter but this value is generally admitted for a welded toe radius. This scatter introduces consequently, scatter fatigue life prediction.
To overcome this difficulty, it is often assumed that the notch radius at the welded toe is zero. Atzori et Al [8] and Verreman et Al [9] have used this assumption. This approach is justify by

these authors by the fact that generally the weld toe radius is very small compared to other geometrical parameters. Consequently, the stress distribution at welded toe assumed to be singular. In this case the fatigue parameter is the notch stress intensity factor which has unit as $MPam^{\alpha}$ where α is the singularity exponent with $\alpha < 0.5$ ($\alpha = 0.31$) if weld toe angle is 135°). The question of units of the fatigue governing parameter is an obstacle to application of this method and leads to over conservatism.

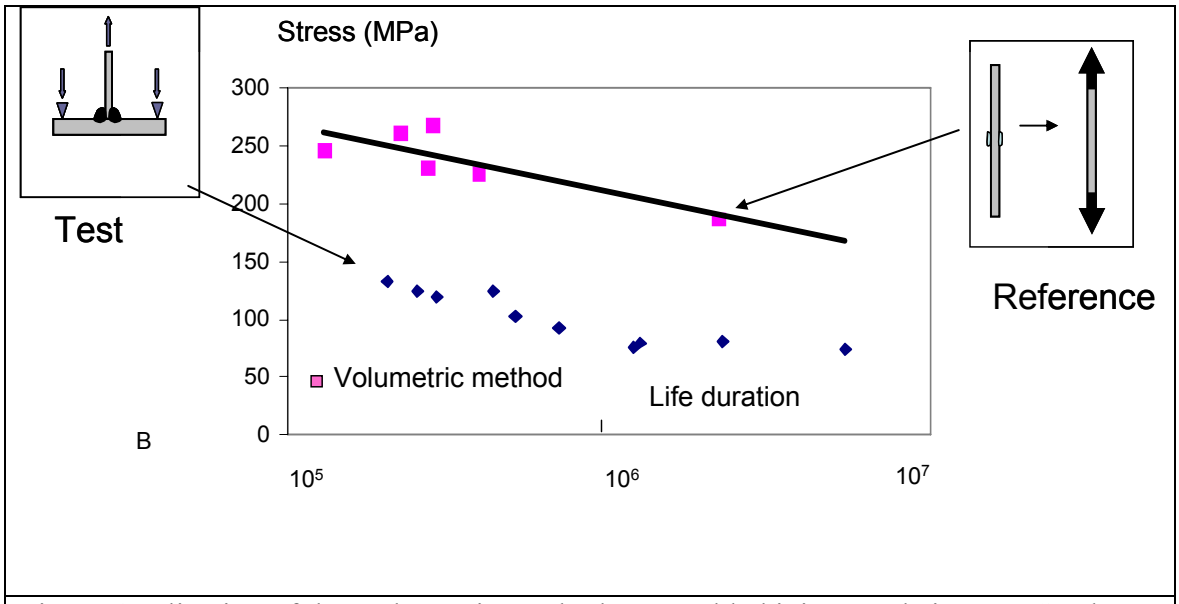


Fig 5 : Application of the Volumetric Method to T welded joints made in HLE Steel.

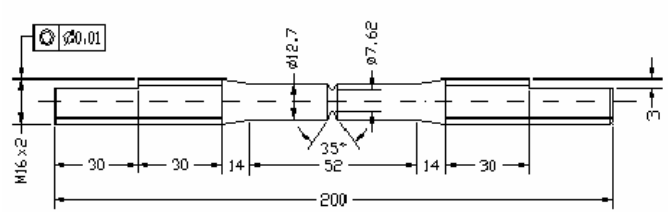
5) EXAMPLE 3 INFLUENCE OF THE LOADING MODE ON THE FATIGUE STRENGTH REDUCTION FACTOR

The effect of different loading modes on the fatigue behvoiur of notched components can be seen from both the S-N curves and the Basquin's law parameters. In order to show this influence, it is convenient to examine evolution of fatigue strength reduction factor versus the number of cycles to failure.
The fatigue strength reduction factor is defined as the ratio of the stress ranges on smooth and notched specimens leading to the same fatigue life duration :

$$k_f = \frac{\Delta\sigma(N_R)_{smooth}}{\Delta\sigma(N_R)_{notched}} \qquad (18)$$

From fig 6.b, we can see that the fatigue strength reduction factor for notched cylindrical (see geometry on figure 6.a increases linearly with the logarithm of the number of cycles for life duration. Values vary nearly 1for low cycle fatigue for each type of loading and increases more rapidly in bending than in tension. A small increase also occurs in torsion ($k_f = 1.16$ for 10000 cycles and $k_f = 1.47$ for 10 millions of cycles).
The fatigue strength reduction factor is more important in bending and increase more rapidly with the number of cycles than for torsion. The influence of the loading mode is attributed to the joint influence of the stress gradient an the hydrostatic pressure. For that the effective maximum shear stress and effective hydrostatic pressure are computed. These quantities are defined as the average values of maximum shear stress and hydrostatic pressure over the effective distance. A non linear but elliptical relationship has been found between these two parameters [7]

The volumetric method allows using a fatigue reference curve in a reference mode of loading (tension for example) to predict fatigue life duration of tests performed in another type of loading (bending for example). However, the level of confidence is always better if the results and the fatigue reference curve are made with he same type of loading. Improvement of the method for solving this problem has been made by introducing the effective hydrostatic pressure $\overline{\sigma}_h$ in the weight function $\phi(r, \chi, \overline{\sigma}_h)$.



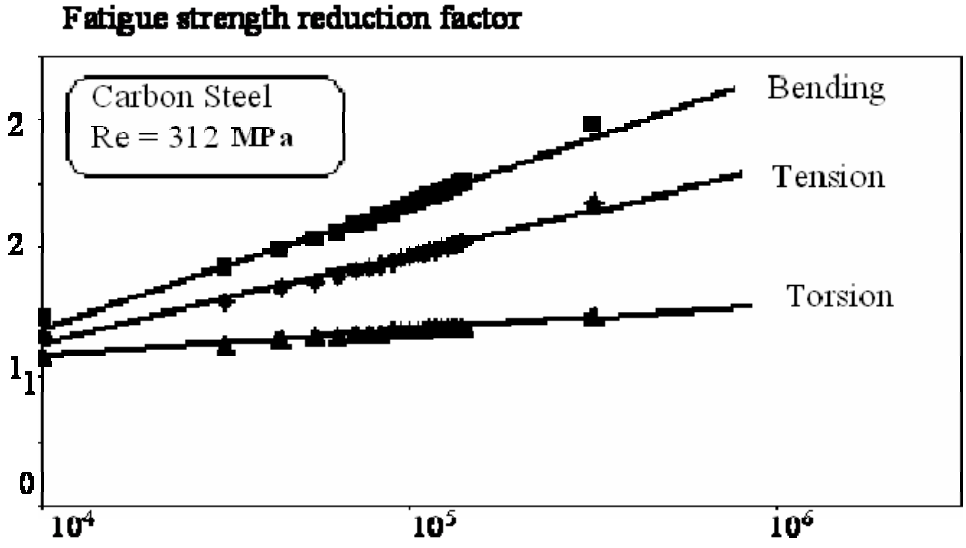


Fig 6 a) Geometry of notched cylindrical specimen for tension, torsion and bending tests. Carbon steel, Yield stress312MPa.
b) Evolution of the fatigue strength reduction factor with the number of cycles. Influence of the loading made.

6) EXAMPLE 4 FATIGUE LIFE PREDICTION OF WELDED SPOTS

Mono point , triple points and multiple points hot spot welded joints have been tested in fatigue with a load ratio o r= 0.1 and load frequency 30Hz [10]. The specimen geometries are presented in figure 10. The material is a mild steel with a yield stress σ_y = 299 MPa and ultimate strength Rm= 431 MPa. The experimental results for mono point, triple points and multiple points are shown in figure 7 as load range versus number of cycles curves. Comparison of triple points and multiple points (in fact 5 spot welds) indicate that the two additional and longitudinal spots welds have no effect on the fatigue resistance curve. In the previous section the Volumetric Method uses a fatigue reference curve obtains from smooth specimen. In this particular case, taking into account the size of the spot, it is not possible to determine the fatigue resistance of weld metal. To overcome, this difficulty, one of the fatigue curve is regarded as source of reference and the other as test curve. The aforementioned procedure is utilized in figure 8. The curve relative to experimental result with mono point is

considered as the fatigue reference curve. Experimental results and prediction are in good agreement in this case

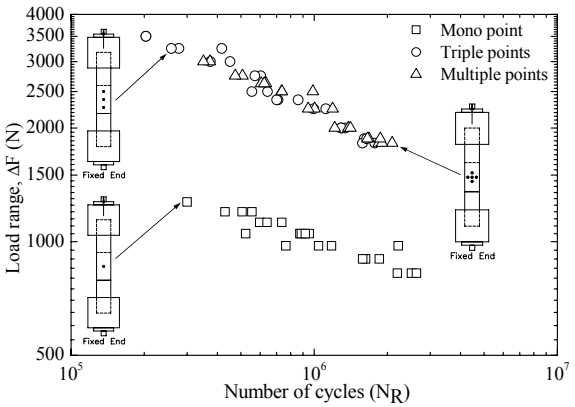


Fig 7 : Fatigue curves (load versus life duration) for three types of welded spots: mono points, three points and multipoints.

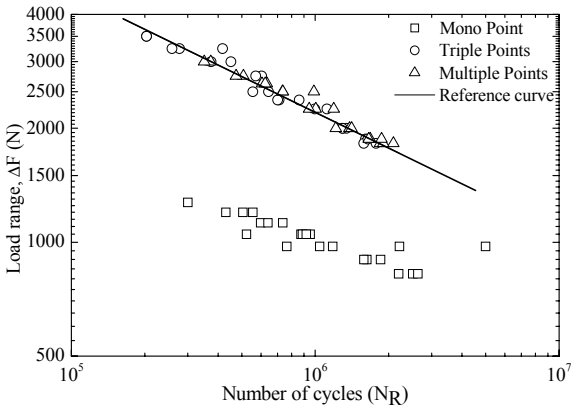


Fig 8 : Application of the volumetric Method to the three points and multi points specimens; the fatigue reference curve is made with results of fatigue tests on mono points welded spots.

CONCLUSION

Prediction of live duration with the classical "Hot spot" approach leads to non conservative life duration and not applicable in case of non availability of elastic stress concentration. The use of the fatigue strength reduction factor is of few interest because this parameter depends on loading mode and number of cycles to failure.

Volumetric method is based on the presence of a physical fatigue process volume where damage and energy for the process is stored. The difficulty to determine the size of this volume is overcome by the procedure of the minimum of the relative stress gradient. This method uses widely possibility of FEM method and requires two sets of data : cyclic stress strain curve and a fatigue reference curve built in with smooth specimens. The four examples provides in this paper illustrate the accuracy of the method. However the transferability problem of loading mode needs to be improved mainly by incorporating in the weight function, the influence of hydrostatic pressure.

REFERENCES

[1] Neuber .H., Theory of stress concentration for shear strained prismatic bodies with arbitrary nonlinear stress-strain law, Journal of Applied Mechanics, 28;(1961),p254.
[2] Peterson.R.E, "Notch sensitivity" In G.Sines and J.L Waissman Editors, (1959).
[3] De –Guang Shang, Da-Kang Wang, Ming Liand Wei-Xing Yao „Local stress-strain field intensity approach to fatigue life prediction under random cyclic loading" International Journal of Fatigue,23 (10) , (2001), pp 903-910.
[4] YAO
[5] Pluvinage.G, "Fracture and Faigue emanating from notches", Kluwer , (2004).

[6]Kadi N., Azari Z., Qylafku, G. Gilgert J et Pluvinage. G, » Modélisation par l'approche volumétrique en fatigue des arbres clavetés », Revue Francaise de Mécanique Vol 4, pp. 243-246, (2000)
[7] G. Qylafku,N. Kadi, J. Dobranski, Z. Azari, M. Gjonaj, G. Pluvinage, Fatigue of specimens subjected to combined loading role of hydrostatics pressure, International Journal of Fatigue, 23(8), (2001), pp689-701.
[8] Atzori.B, Blasi.G. and Pappalettere. C ”Evaluation of fatigue strength of welded structures by local strain measurements. Experimental Mechanics,N°25-2, (1985), pp 129-139.
9) Verreman.Y.E and Nie.B.3 Early development of fatigue cracking at manual fillet welds”. Fatigue and Fracture of Engineering Materials and Structures,vol19, (1996),pp 669-681.
[10] H. Adib, G. Pluvinage, theoretical and numerical aspects of volumetric approach for fatigue life prediction in notched components, International Journal of Fatigue, 2003; 25(1): 67-76.

.

New presentation method to evaluate the stress concentration in offshore welded tubular joints (based on finite element analysis)

M. F. Ghanameh [a], D. Thevenet [b], A. Zeghloul [a]

[a] University of Metz, LPMM- U.M.R. CNRS N° 7554, Metz, France
[b] ENSIETA, LMSN, Brest, France

Abstract In building offshore platforms, tubular members are used because of their good structural and mechanical properties. Tubular members are connected by special welded joints which represent structural discontinuities causing significant stress concentrations in the vicinity of the weld. Under repeated loading, fatigue failures always initiate at the area which referred to as "hot-spot" where there are high-level stress concentrations which called "Hot-Spot Stress (HSS)". For this reason, accurate computation of stress concentration is very important in tubular joints design. In this paper, we present a new representation method of the stress distribution curves around the chord/brace intersection, to evaluate the stress concentration zones and values. We used the previous work results obtained by finite element method in the cases of the twelve tubular joints form subjected to axial loading (AX) "tension or compression", in-plane bending (IPB), and out-of-plane bending (OPB) or combined loading (Com).

Keywords Finite element method; ABAQUS; Welded tubular joints; Stress concentration; Stress distribution, Stress concentration factor, geometric stress; Nominal stress; Offshore platform.

1 INTRODUCTION

Offshore structures consist of a large number of tubular members connected to one another by special joints. Tubular members are jointed together at their intersections in a variety of geometrical forms. These joints represent structural discontinuities, which incur a large amount of stress concentration. The stress concentration can produce a maximum stress at the intersection as high as thirty times the nominal stress acting in the members. The combination of high stress concentration with dynamic loads makes fatigue damage almost unavoidable. Because of these facts, a large number of investigations have been devoted to study the offshore tubular.

The bibliographical review gives a lot of offshore tubular joints topics, such as: 2D and 3D linear and nonlinear stress and deflection analysis; static and dynamic studies; stress concentration factors; force-displacement characteristics; hot spot stresses; influence of loading on the joint performance; fracture mechanics problems; strength and failure analysis; ultimate strength analysis; stress intensity factors; cracked tubular joints; damage; fatigue; multi-axial fatigue; residual stresses; NDT detection of cracks; effect of imperfection on the strength. Moreover, the joints can be at different types and forms, such as: simple or multi-planar tubular joints; square-to-round, square-to-square or round-to-round tubular joints; stiffened, cast or composite joints , T-, Y-, X-, K-, DT-, DY-, DX-, TY-, TK-, DTX-, DTDY-, and DTDK-tubular joints.

To investigate these different topics and forms, the researchers follow several numerical analysis and experimental analysis. In the numerical analysis, firstly shell elements were used widely for modeling tubular joints. B. E. Healy and N. Zettlemoyer [1] have studied the case of a number of T and Y-joints. J. K. Ward and C. J. Billington [2] have performed a very complicated nine brace multi-planar joint. Additional shell elements might be arranged around the chord/brace intersection of a joint to model the weld for the joint (S.R. Wilmshurst and M. M. K. Lee [3]), but shell element are not suitable to construct a model including welds with or without cracks; so, J. Cao et al [4] developed a new method to generate meshes for different types of welded circular joints with or without cracks by using 3D solid element. On the other hand, S. P. Chiew and C. K. Soh [6] have used large-scale steel multi-planar DX-joint subjected to three different cases of brace axial loading for an experimental investigation, and P. Gandhi et al. [7] have tested stiffened and unstiffened T- and Y-joint.

One of the most important purposes of the offshore structures researchers is to maintain the structural integrity of these structures, which means to make an initial prediction about the safety of the structure over its life and to plan inspections. So, it's very useful to know previously the stress distribution around the weld toe and the stress concentration values and zones. This paper concerns a new method to present the stress concentration results of finite element analysis of the offshore welded tubular joints. This method can show easily and rapidly the stress distribution and the stress concentration zones around the brace/ chord intersection for different form of planer tubular joints.

2 MAXIMUM AND MINIMUM STRESS DISTRIBUTION CURVES

In practice, tubular joints are always subjected to a combination of axial loading (AX) "tension or compression", in-plane bending (IPB), and out-of-plane bending (OPB). To date, limited research work has been performed and published on studying the different joint forms subjected to different loading conditions specially the combined loading, and the effects of joint configuration and those loadings conditions on the location and values of HSS. E. Chang and W. D. Dover developed a parametric equation to predict the stress distributions around the intersection of: X and DT-joints subjected to single and balanced Ax, IPB and OPB loading [8]; and Y and T-joints subjected to simple Ax, IPB and OPB loading [9]. On the other hand, M. R. Morgan and M. M. K. Lee [10] carried out a study distribution of stress concentration factor in K-joints under OPB loading. S. T. Lie et al. [11] proposed a systematic finite element modeling of Y-joints with any surface crack and located at any position along the brace–chord intersection. This modeling method is used to analyze three tubular T-joint specimens which were tested to failure earlier, and they were subjected to IPB only, combination of IPB and OPB, and a combination of AX, IPB, and OPB, respectively. An experimental fatigue tests were carried out by S. P. Chiew et al. [12], on these three tubular T-joints.

In previous work [5, 13], twelve forms of planer joints: T, Y, X, K, DT, DY, DX, TY, TK, DTX, DTDY, and DTDK (Fig.1) were numerically analyzed to study the effect of loading and joint forms, on the stress concentration zone and values. The braces of these joints subjected to different loading conditions: Ax, IPB, OPB and combined (Com) loading (Table I). This combined loading is composed of an axial loading with a continuation of rotational bending loading obtained while making the centre of the brace rotate around a circle in 36 steps.

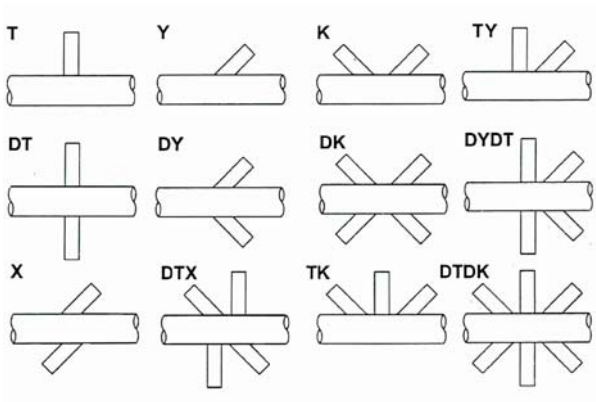
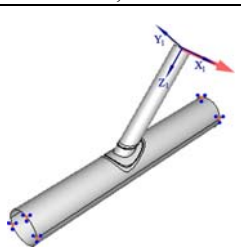
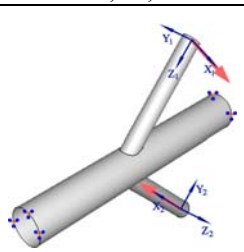
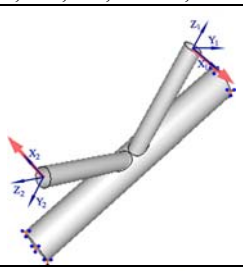
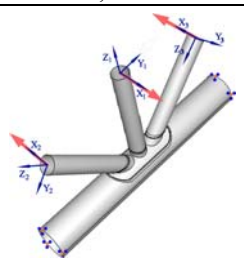
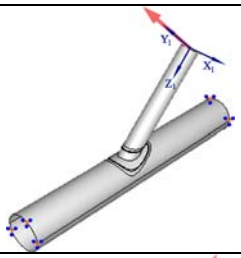
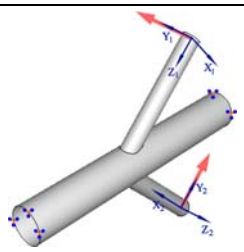
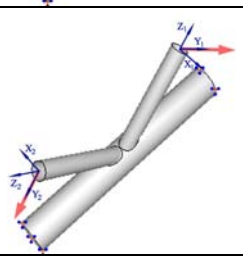
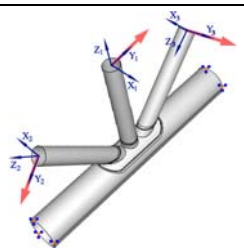
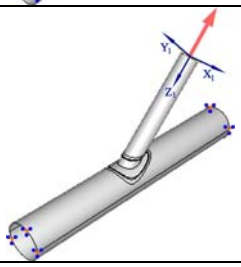
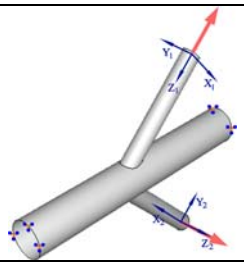
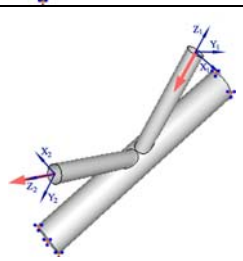
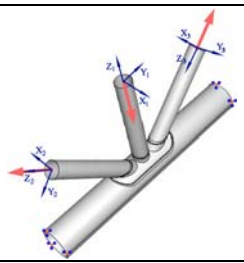
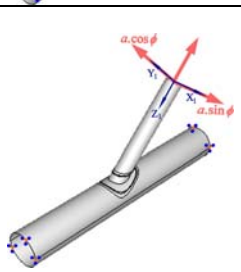
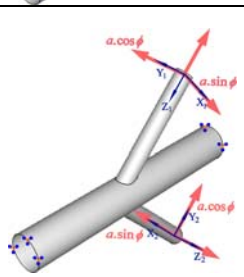
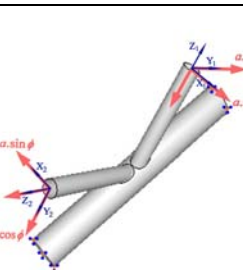
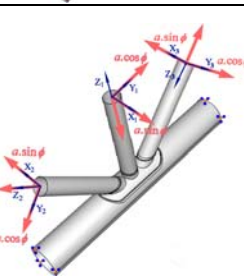


Fig.1 Studied joints.

Distributions of the local stress along the intersecting lines (of T-joints for example) are showed on Fig.3 for the three simple load cases and for the 36 combined loading steps in Fig.4. From the stress distribution curves of the 36 steps of combined loading, two curves (Fig.5) were plotted representing the maximum and minimum values of the curves group. These curves are called respectively maximum Stress Distribution Curves (SDC_{max}) and minimum Stress Distribution Curves (SDC_{min}). The advantage of using these two curves is the ability to replace the curves resulting from 36 steps of combined loading with only one or two similar curves corresponding to different simple loading cases. This allows simple evaluation of the effect of the combined loading on the stress concentration around the intersection chord/brace. Using these two curves makes it possible to determine the stress amplitude needed to calculate the fatigue life.

Table I. Various loading cases

	T,Y	DY,DT,X	K, DK, TY, DTDY, DTX	TK, DTDK
OPB				
IPB				
Ax				
Com				

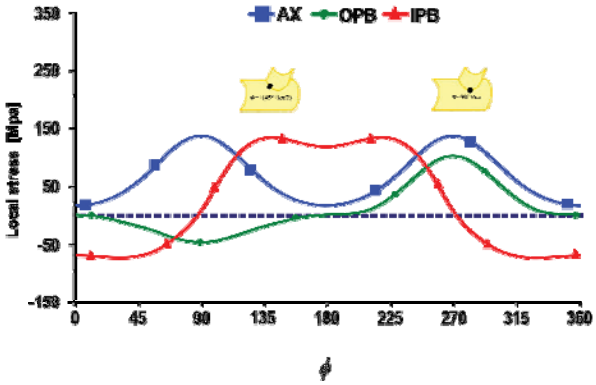


Fig.3. Stress distribution for T-joint in the simple loading cases.

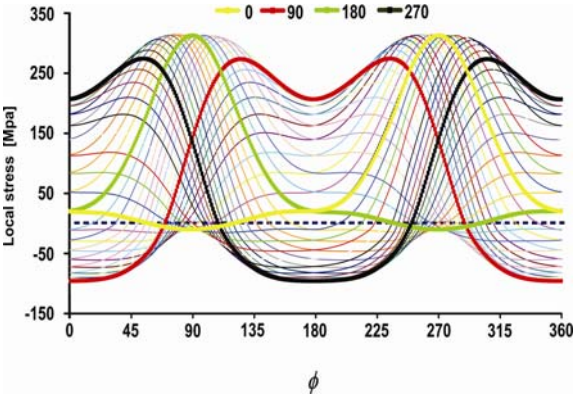


Fig.4. Stress distribution for T-joint in the combined loading case.

3 POLAR STRESS DISTRIBUTION CURVES:

The mean objective of this study is to formulate a simple method to evaluate the stress concentration around the intersection chord/brace. So, the stress distribution curves of the three simple loading cases and the two curves SDC_{max} and SDC_{min} were traced in the polar coordinates as it shown in Fig. 6. This method of tracing gives a very clear and rabid image of the stress concentration state and the effect of each type of loading on the place and the value of this concentration around the chord/brace intersection.

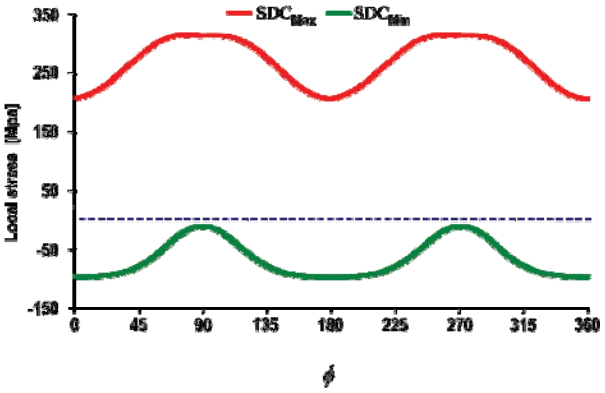


Fig.5. Maximum and minimum Stress Distribution Curves (SDC_{max} , SDC_{min})

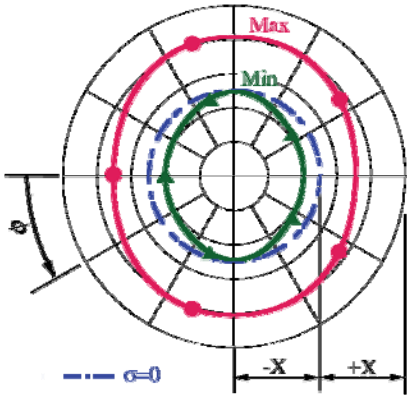
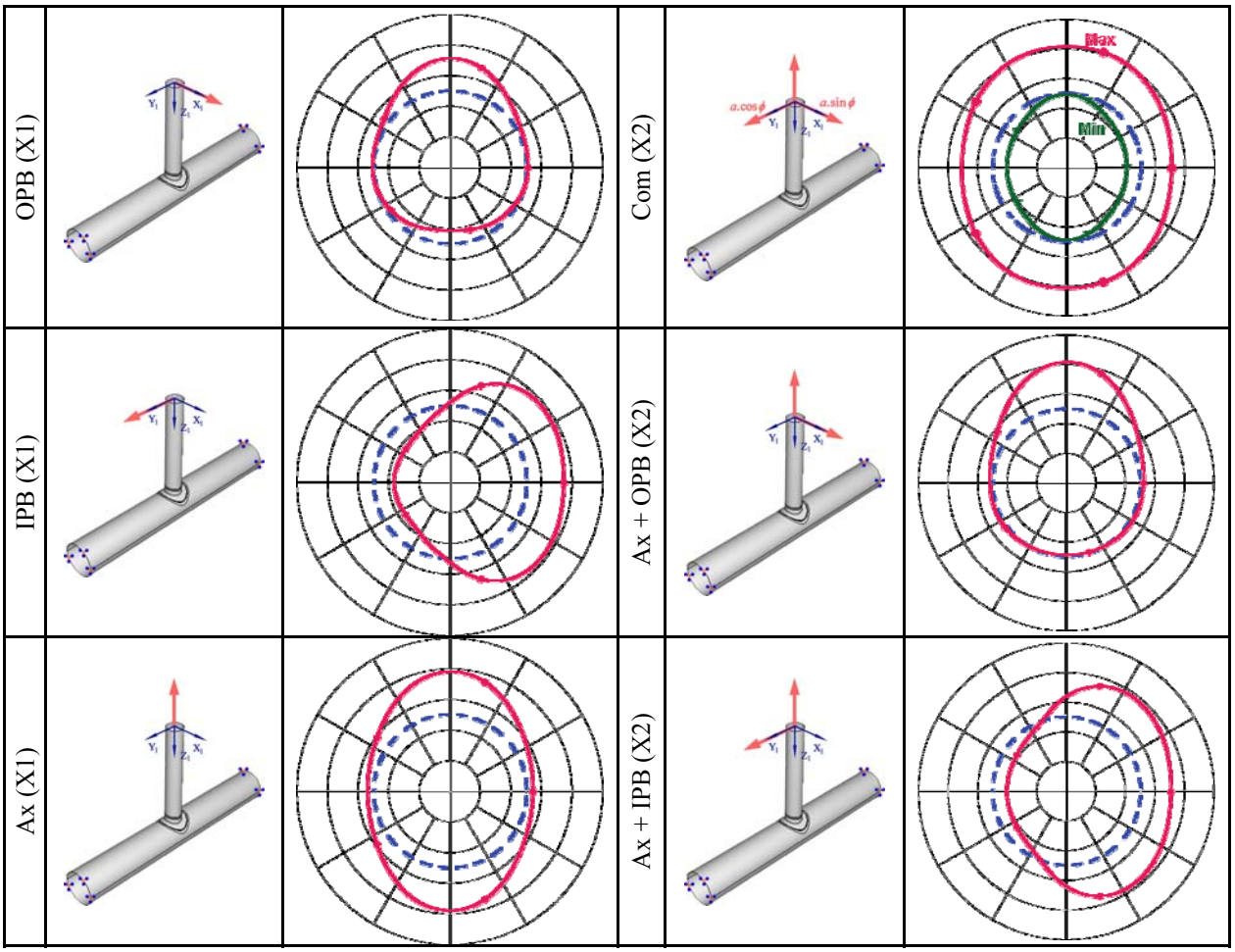


Fig.6. Polar stress distribution curves for T-joint in the combined loading case.

Table II. Polar stress distribution curves of the T-joint.



Scale : X1=250 MPa, X2=2*250 MPa, X3= 3*250 MPa.

The Table II show the polar stress distribution curves of the different loading types applied to the T-joint, by using these curves it's possible to determine quickly and easily the positions of the hot spot points corresponding to each type of loading. This table indicate that the "hot spot" stress for the chord was found to occur at the saddle location for Ax and OPB loading and it was found between of the saddle and crown locations for IPB loading, or at $\phi = 45°$ with respect to the crown locations. This result is in a good agreement with the results of H. L. J. Pang and C. W. Lee [14]. The Table can show also that the combination of loadings will raise the "hot spot" stress values to two times that in the case of the simple loadings; This stress was found to occur at the saddle location for Com loading and the case of the combination of Ax and OPB loading, and it was found at $\phi = 45°$ with respect to the crown locations for the case of the combination of Ax and IPB loading. The "hot

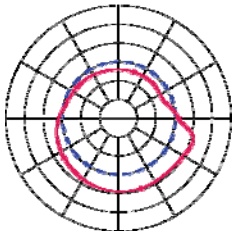
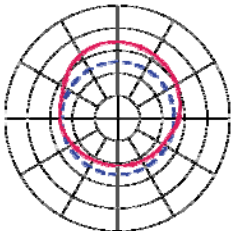
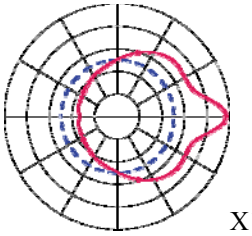
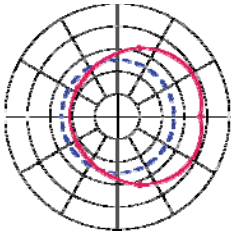
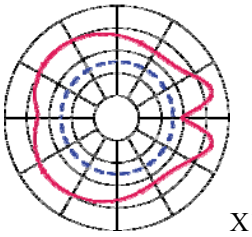
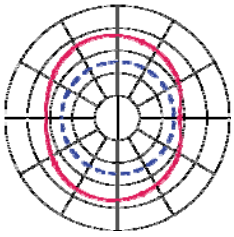
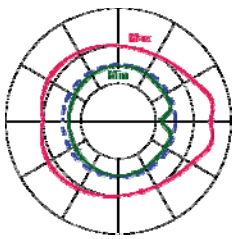
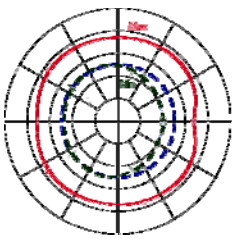
spot" stress locations in the Y-joints (Table III) move toward the crown heel point of ($\phi = \pi$) with decreasing brace inclination from 90° (case of T-joint) to 60° then 45° and 30°. if the brace subjected to Ax or OPB loading, regardless of the loading direction, whereas the "hot spot" stress locations move in the inverse direction of the loading direction if the brace subjected to IPB loading.

The comparison of the polar stress distribution curves relating to the various joints reveals two models of stress distributions (Table III):

Model 1: Corresponding to the stress distribution of the T-, Y-, DT-, DY- and X-joints where there is only one brace on each side of chord.

Model 2: Corresponding to the stress distribution of the K-, TK-, DX-, TY-, DTDY-, DTDK- and DTX-joints where there are at least two brace located on the same side of chord. In this case of joints, we obtain several shapes of curves according to the brace and its position and the direction of the axial loading applied.

Table III Comparison of the various types of the stress distribution of TK- and Y-joints

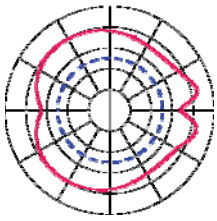
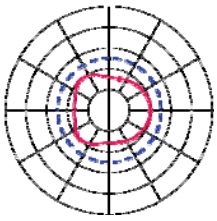
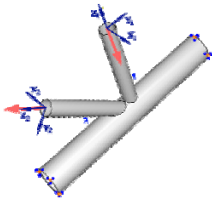
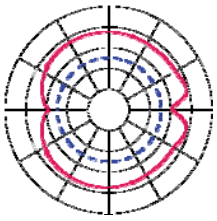
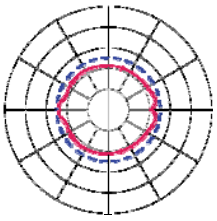
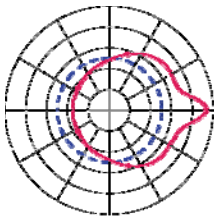
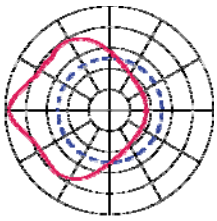
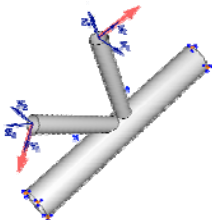
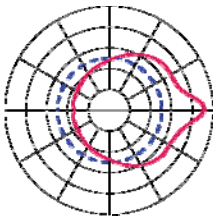
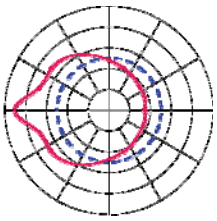
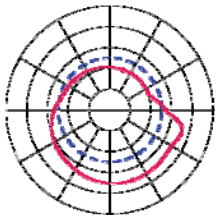
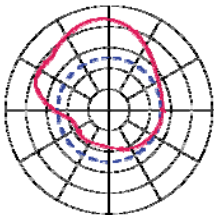
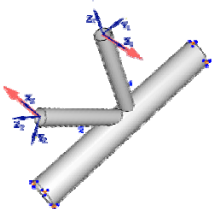
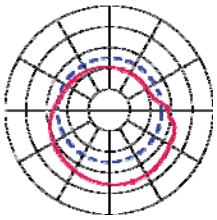
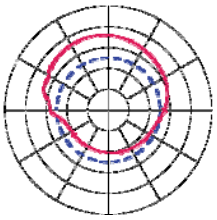
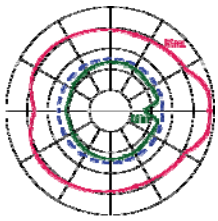
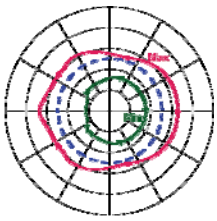
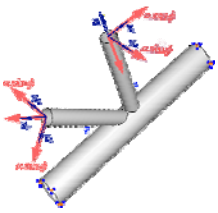
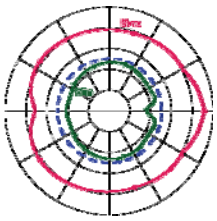
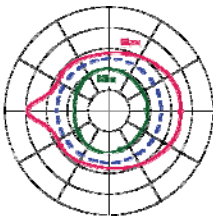
	TK	Y
OPB	 X1	 X1
IPB	 X1	 X1
Ax	 X1	 X1
Com	 X3	 X2

Scale : X1=250 MPa, X2=2*250 MPa, X3= 3*250 MPa.

The Table III illustrates these two models, since it give the polar stress distribution curves of Y-joints for an example of model 1 and TK-joints for an example of model 2. In this Table, because of the geometric symmetry in the multi-brace joints, only the polar stress distribution curves corresponding to the braces of one side of chord were considered; and in the cases DTDK, DTDY, DTX, DTX, DX, TK, TY and K –joints, the polar stress distribution curves corresponding to the braces where the strongest stress concentration appears.

In the cases of TY-, DTDY-, TK-, DTDK- and DTX-joints, containing at least two braces (one in straight position and the other is inclined) in the same side of chord and subjected to a loading balanced FDP or FHP, the maximum values of constraint are obtained around the straight brace. On the other hand, in the case of balanced axial loading or Com loading, the maximum values of constraint appear around the inclined brace (Table IV). Moreover, the levels of constraint relating to this group of junctions are higher than those observed in the junctions K and DK, where the two brace located in the same side of chord, are inclined.

Table IV Two examples of junctions having several braces located on the same chord side.
K-joints: two inclined brace, TY-joints: one straight brace and one inclined brace.

	TY-Joints			K-Joints	
Ax(X1)					
IPB (X1)					
OPB (X1)					
Com (X2)					

Scale : X1=250 MPa, X2=2*250 MPa.

4 CONCLUSIONS

Tubular elements used to design offshore platforms are subjected to combined loading conditions. These loading conditions generate, in the vicinity of the joints, hot-spot points or zones of strong stress concentration which often constitute sites for fatigue crack initiation and propagation. The determination of stresses at these hot-spot points by finite element analysis gives results in good agreement with literature for simple loading, which validates the modeling approach employed.

The proposed method for evaluating the stress concentration is useful for quick estimation of the "hot spot" areas (where the stress concentration occur) for different types of joints subjected to different loading cases. Specifically, the case of combined loading simulating true loading of tubular elements of offshore structures has been studied which is very important for manufacturing and testing operations.

Drawing the SDC_{max} and SDC_{min} curves helps to easily read the effect of this combined loading on the stress concentration around the chord/brace intersection, and moreover to determine the stress amplitude $\Delta\sigma$ needed to calculate fatigue life.

5 REFERENCES:

5.1 Conference Proceedings

1. B. E. Healy and N. Zettlemoyer, "In-Plane Bending Strength of Circular Tubular Joints", Proceeding of the 5th International Symposium on Tubular Structures, Nottingham , UK, 1993, PP.325-344.
2. J. K. Ward and C. J. Billington, "Strength Assessment of a Multi-planar Joint in a North Sea Jacket Structure", The Proceeding of the second International Offshore and Polar Engineering Conference, San Francisco, USA, vol. IV, 1992, PP.369–376.
3. S.R. Wilmshurst and M. M. K. Lee, "Ultimate Capacity of Axially Loaded Multi-planer Double K-joints in Circular Hollow Section", Proceeding of the 5th International Symposium on Tubular Structures, Nottingham , UK, 1993, PP.712-719.
4. J. Cao, G. Yang and J.A. Packer. "FE mesh generation for circular joints with or without cracks", The Proceeding of the 7th International Offshore and Polar Engineering Conference, USA, vol. IV, 1997, PP.98–105.
5. M. F. GHANAMEH, D. THEVNET and A. ZEGHLOUL, "Effects of joint configuration and loading type on stress concentration in offshore welded tubular joints", The Proceeding of the International Summer School-Conference Advanced Problems in Mechanics , St. Petersburg , Russia, 2005.

5.2 Journal Article

6. S. P. Chiew and C. K. Soh, "Strain concentrations at intersection regions of a multiplanar tubular DX-joint", Journal of Constructional Steel Research, Volume 53, Issue 2, February 2000, Pages 225-244.
7. P. Gandhi, D. S. Ramachandra Murthy, G. Raghava and A. G. Madhava Rao, "Fatigue crack growth in stiffened steel tubular joints in seawater environment", Engineering Structures, Volume 22, Issue 10, October 2000, Pages 1390-1401.
8. E. Chang and W. D. Dover, "Parametric equations to predict stress distributions along the intersection of tubular X and DT-joints", International Journal of Fatigue, Vol. 21, Issue 6, 1999, pp.619-635.
9. E. Chang and W. D. Dover, "Prediction of stress distributions along the intersection of tubular Y and T-joints", International Journal of Fatigue, Vol. 21, Issue 4, 1999, pp.361-381.
10. M. R. Morgan and M. M. K. Lee, "Parametric equations for distributions of stress concentration factors in tubular K-joints under out-of-plane moment loading", International Journal of Fatigue, Vol. 20, Issue 6, 1998, pp.449-461.
11. S. T. Lie, S. P. Chiew, C. K. Lee, and Z. W. Huang, "Fatigue Performance of Cracked Tubular T Joints under Combined Loads. II: Numerical", J. Struct. Engrg., Volume 130, Issue 4, 2004, pp. 572-581.
12. S. P. Chiew, S. T. Lie, C. K. Lee, and Z. W. Huang, "Fatigue Performance of Cracked Tubular T Joints under Combined Loads. I: Experimental", J. Struct. Engrg., Volume 130, Issue 4, 2004, pp. 562-571.
13. M. F. GHANAMEH, D. THEVENET and A. ZEGHLOUL, "Stress concentration in offshore welded tubular joints subjected to combined loading", Journal of Materials Science & Technology, Vol.20 Suppl.1, 2004, La Chine.
14. H. L. J. Pang and C. W. Lee, " Three-dimensional finite element analysis of a tubular T-joint under combined axial and bending loading", International Journal of Fatigue, Vol.17, Issue 5, 1995 , pp 313-320.

Effect of Porosity on Fatigue Crack Propagation Behaviour of a Laser Beam Welded Aluminium Alloy

W. V. Vaidya[a], M. Koçak[a], M. Horstmann[a], V. Ventzke[a], M. Pakdil[a] and J. Hackius[b]

[a] GKSS Research Center, D-21502 Geesthacht, Germany
[b] AIRBUS Germany, D-28183 Bremen, Germany

Abstract CO_2-laser beam welded butt joints of a weldable airframe alloy AA6056-T6 exhibited bimodal pore distribution when the sheet thickness was increased to 6 mm. In addition to almost uniformly distributed micropores (≤ 100 µm) occasional large pores (≤ 1 mm) formed randomly in the weld. When tested for fatigue crack propagation using C(T) specimens, the crack in the weld exhibited occasional retardation even at a high load ratio R (≤ 0.7). Such retardation is attributed from fractographic examination to the interaction between the crack front and a large pore.

1 INTRODUCTION

Fusion welding has been a well-established process over decades and conventional techniques such as arc welding known from welding of ferrous materials have been applied also to Al-alloys [1]. Al-alloys can be welded, although with difficulties. When compared with the ferrous material, one of the inherent peculiarities of the aluminium alloys is the excessive amenability to form pores. Molten aluminium has a very high solubility for gaseous impurities, in particular for hydrogen, however, the solid solubility of the latter is nearly zero. This has the consequence that the porosity increases with the increase in temperature reached before welding [2]. Moreover, compared to tungsten inert gas (TIG), processes such as metal inert gas (MIG) become more susceptible to pore formation since the thin filler wire offers increased surface area for moisture adsorption [2]. The latter becomes the source for hydrogen during welding. A very early investigation has shown that pores reduce load bearing area and hence contribute to the decrease in tensile and fatigue strength, whereby the total area occupied by pores in the fracture plane is more deciding rather than the size distribution of pores [3]. As regards elongation after fracture, porosity has apparently no effect, so also the effect of porosity on fatigue strength of an age hardenable cast Al-alloy is found to be negligible in the presence of external notches [4]. Thus, it seems that fatigue rather than fatigue crack propagation (FCP) behaviour is affected more by porosity. In butt welds of AA5083 produced by gas metal arc welding (GMAW) and by using the filler wire AA5183 the base metal and the weld are found to exhibit a comparable FCP behaviour for a given load ratio R [5]. In fact, irregularities in the FCP behaviour resulting from pores or other defects are not reported for Al-alloy welds [5-7] or for a nearly defect-free cast A356 (Al-7 % Si-0.4 % Mg) [8]. How and whether the FCP behaviour of *fusion* welded 6XXX alloys is affected has rarely been investigated in the literature.

In addition to the hydrogen pick-up, the good thermal conductivity of Al-alloys makes it difficult to control property changes since the heat affected zone (HAZ) tends to be wide with MIG or TIG. The progress in the laser beam welding (LBW) technology offers, however, new perspectives. It has been demonstrated that very narrow welds with narrow HAZ can be produced in an airframe alloy by LBW [9]. In turn, LBW technology has found its place in the civil aerospace industry for replacing riveted structure by welded integral structure [10]. LBW skin-stringers (T-joints) have already been used for civil aeroplanes A318 and A380. Skin-skin (butt joints) can be the next step for further weight reduction. The alloy AA6056 [11] is basically an AlMgSiCu precipitation hardenable and weldable wrought alloy, and is being considered as an airframe candidate. In a series of investigations initiated by AIRBUS we observed that thin sheets (≤ 4.5 mm) can be CO_2-LBW to a nearly pore-free quality. With thick sheets (6 mm), however, porosity increased, which may have an effect on the damage tolerance behaviour. Therefore, the present study was undertaken to find out the effect of pores on FCP. In the present investigation, focus is placed on the performance of the weld and not on the LBW technique.

2 EXPERIMENTAL PROCEDURE

Coupons (500 X 500 mm^2) of 6 mm thick AA6056 in butt-weld configuration were welded in the peak-aged condition T6 using the filler wire Al-12 % Si and CO_2-laser. For FCP testing, C(T) specimens having the dimensions, width W = 100 mm and pre-notch length a_n = 20 mm, were extracted using electric discharge

machining. For LBW specimens the notch was placed in the mid-fusion zone. A typical appearance of the weld in cross section is shown in Figure 1. The excess material at the top and the root was flushed off by milling to facilitate crack length measurements on the specimen surface. For comparison with the weld, the base metal specimens were extracted in the T-L orientation. So as to study the effect of crack orientation on FCP, also the L-T orientation for the base metal was investigated.

FCP tests were carried out on a servo-hydraulic machine operated at 10 Hz under ambient laboratory conditions. The data were acquired using a computer interface with the maximum crack mouth opening displacement ($CMOD_{max}$) as the correlating parameter which was calibrated initially against optical crack length. Additionally, in-house developed AC potential drop technique was used for indirect crack length measurement [12]. Specimens were tested over a range of R ratio ($0.1 \leq R \leq 0.7$). At high R ratio crack generation at the notch becomes difficult; either K_{max} needs to be increased or the time must be extended. To save time and avoid K_{max} as an additional parameter, a method developed earlier [13] was employed. All specimens were first pre-cracked at R = 0.1 and then while keeping K_{max} nearly constant ($\approx P_{max}$ for short crack extension), R ratio was increased to the desired level by increasing K_{min} ($\approx P_{min}$ for short crack extension). The test was then continued as a constant amplitude test. Extensive fractographic investigations were undertaken to understand the role of porosity on FCP.

3 RESULTS

3.1 Porosity

The LBW coupons were investigated by X-ray radiography for identification of defects (resolution better than 0.1 mm). The major defect was the occurrence of the large pores [corresponding to classification P = 4 ($Ø \leq 0.6$ mm) and 8 ($Ø \leq 1$ mm) according to ASTM E155]. A typical example is shown in Figure 2. The pores were randomly distributed and the frequency of occurrence was more within the center than at the edge of the weld. At the given resolution, micropores could not be detected. These became visible on the fracture plane as shown in Figure 3. It must be pointed out here that in contrast to investigations, in which pores were purposely introduced or concentration of pores was high [3], the pores in the present investigation needed to be *sought* and their concentration was *low*. Tensile data are given in Table I. The decrease in tensile properties of the weld shows strength undermatching which causes plastic strain concentration within the weld and, hence, reduction in the elongation capacity of the weld.

Table I. Tensile data of the base metal (T6) and the LBW butt joint of AA6056-T6/6 mm.

Material State	Yield Strength, $R_{p0.2}$ (MPa)	Tensile Strength, R_m (MPa)	Elongation after Fracture, A** (%)
Base Metal*	347	374	13.2
Weld (transverse)	226	275	0.94

* Loaded transverse to the rolling direction; ** $L_0 = 50$ mm

3.2 FCP Behaviour

The initial tests were carried out at R = 0.1. The crack path was nearly straight, and deviation or deflection was insignificant, as shown in Figure 4. FCP data are shown in Figure 5. It was found that for the base metal, FCP depends on the specimen orientation, whereby the T-L orientation was found to be more susceptible to FCP in high ΔK regime (≥ 20 MPa$\sqrt{m}$) than the L-T orientation. There was a transition in FCP such that the FCP curve flattened [13] which became more pronounced in the L-T than in the T-L orientation. In LBW such a transition was not observed. Instead, FCP retardation (denoted by arrows) was observed intermittently and at low as well as high ΔK values. The retardation occurred over a very short crack length and nearly at a constant ΔK value. Thereafter, FCP rate picked-up again at a nearly the same slope, as if there was a continuation (see also Figure 8 to follow). The specimen surface was checked for possible changes (Figure 4), however, there were none (such as overload), which could be correlated to the retardation. The ranking of FCP response in the specimens tested was more clear above 15 MPa$\sqrt{m}$, and was in terms of better performance: L-T, T-L followed by LBW (Figure 5).

3.3 Effect of Load Ratio

The retardation in FCP in the weld was rather unexpected and was also unknown from the literature [5-8]. Since the slope of the FCP curve did not change and changes on the surface such as excessive increase in the plastic zone size and extensive crack deflection were not observed, the retardation was certainly not an effect

resulting from overloading or crack closure changes. Moreover, retardation in FCP was not observed in the base metal, so that the effect was related only to LBW. Hence, in the following only results from LBW are reported for the sake of clarity, although the base metal specimens were also tested at high R. It is sufficient to mention that in the base metal with the increase in the load ratio the difference in FCP between the T-L and the L-T orientation tended to be negligible and the ΔK range over which the transition in FCP occurred [13] became also smaller. Moreover, the weld exhibited a nearly comparable FCP behaviour as that of the base metal at high R (≥ 0.5).

A majority of effects which occur at a low R value disappear when load ratio is increased, since crack closure decreases. So as to verify whether retardation was an effect or an artefact, R ratio was increased to 0.3, 0.5 and 0.7. These results are shown in Figure 6. The FCP data of LBW from Figure 5 are also included for comparison. That the retardation in FCP occurs turns out to be a fact, and in this sense it is an effect which does *not* depend for a given R. The results obtained at R = 0.1 are thus confirmed. Duplicated tests yielded similar results, with the difference that the ΔK value at which crack retardation occurred, was random.

4 DISCUSSION

FCP behaviour can successfully be explained in terms of crack closure. This also includes microstructural effects which are taken into consideration via crack closure; usually by roughness-induced closure which is caused by crack path deviation and deflection. In high ΔK regime plasticity-induced closure may operate, which should be dependent in the first instance on K_{max}. For welds an additional parameter is traditionally discussed: residual stresses. The latter are also supposed to induced crack closure [7]. How application of crack closure for explanation of results can be complex is demonstrated by considering some recent results. In SENT specimens of 5083 crack closure is found to be higher in arc welded and weld-repaired specimens than that in the base metal [7], but, only initially ($0.1 \leq a/W \leq 0.25$). Thereafter, crack closure is found to decrease nearly to zero in all specimens after a very short crack extension ($a/W < 0.3$) which remained so for the rest of the test even as ΔK (hence, K_{max}) increased. A systematic correlation between crack closure and FCP is, however, not evident here. In cast A356 (Al-7 % Si-0.4 % Mg) dendritic microstructure was substantially modified by varying the casting procedure [8]. Porosity was either already low or was otherwise decreased by hot isostatic pressing (HIP). Although fracture path varied and should have caused roughness-induced closure, the effect of microstructure on FCP was not evident in this case.

Returning to the present results, the crack path in LBW was relatively straight (Figure 4) and since retardation in FCP occurred even at high R and even with increasing K_{max} (Figure 6), roughness-induced or plasticity-induced crack closure should not have been the major cause. Residual stresses are always present in the weld. On cutting the LBW coupons, however, their nature should change systematically and exhibit a geometrical dependence such that if the nature of stresses is compressive at the notch, it should be compensated by tensile residual stresses over the rest of the ligament. In such a case, FCP should be initially low and shift systematically to high FCP rates as the crack propagates into the tensile residual field. A retardation followed by a pick-up in FCP without change in the slope is, however, not explained by the first order residual stresses resulting from the welding.

Since retardation in FCP occurred at random and persisted for a very short crack extension, it was thought to be resulting from local defects such as large pores (see Figure 2). Figure 7 shows the macrofractographs of the specimens tested at various R. From the comparison with FCP curves it was found that to the first approximation, retardation was associated with large pores. Such a correlation is shown in Figure 8. Micropores ($Ø \leq 100$ µm) or small pores ($Ø \leq 500$ µm) had, on the other hand, a less influence on retardation in FCP. To understand such a difference, extensive fractographic investigation was undertaken on LBW.

The major fracture feature in the mid-FCP regime was found to be striations, which agrees well with that in the hypoeutectic cast Al-Si-Mg alloy [8]. Thus, whether it is the base metal or the weld (essentially cast Al-Si), the fracture process in both is comparable. This should partly explain relatively low difference in FCP at low ΔK in these cases (Figure 5). Initially, striation spacing was very small at low ΔK values (≤ 15 MPa$\sqrt{m}$, R = 0.1)), and could be resolved only at a high magnification (X10000). Later, with the increase in ΔK, striations became broader and secondary cracks formed (see Figure 9 later). This fracture sequence persisted essentially also in specimens tested at different R values.

It was mentioned that the major defect was two types of pores: micropores which were distributed more or less uniformly, and large pores which were isolated and distributed randomly (Figures 2 and 3). Out of these

the former were ineffective for retardation in FCP. The probable reason is deducted from Figure 9. This is an isolated micropore and has been apparently cut in its equatorial plane. The dendritic structure is visible and does not show any deformation traces. The structure just before the crack front cuts the pore and just thereafter as the crack front re-enters into the defect-free weld is shown at a higher magnification. Practically, there is no difference in the fracture features before and after the micropore is cut-through. In other words, the interface weld metal-micropore or the interior of the latter does not offer any resistance against FCP. This was confirmed for various locations and on different specimens, also when clusters of micropores occurred. The case of the large pore was, however, different.

Large pores of different shapes are shown in Figure 10. That such pores occurred so closely was observed seldom. The interesting point here is the difference in appearance. Whereas the micropores were near to perfectly spherical (Figure 3), the larger once had irregular shape and were to some extent cylindrical. Like micropores, interior of large pores also exhibited dendritic structure. Formation of large pores appears to be a gas-absorbing process, since micropores were absent in their immediate surrounding. Contrary to the interface of a micropore (Figure 9), a sudden change in the appearance at the interface before the large pore is cut-through was found, however, not afterwards, Figure 11. Namely, the markings (striations or deformation traces or both) left behind by the crack front were fine, particularly at R = 0.7. This indicates that a large pore acts as a barrier (see Figure 8 also). Once the pore is cut-through, the progress of FCP continues again without obstruction in the weld, which explains why the slope remains unchanged. Thus, the retardation in FCP turns out to be a result of an interaction between the large pore and the crack front. Such an interaction certainly indicates stress relaxation which may result due to crack tip blunting or adoption of a new crack path or both. When the cyclic plastic zone is smaller than the size of a large pore, the crack front shall be obstructed and the crack tip shall be blunted. This should lead to retardation in FCP, also because a new crack path should be adopted. Then afterwards, as the large pore is cut-through and when the crack tip re-sharpens again, the FCP process should continue as before the interaction with the large pore. Whether such an interaction is dependent on the loading condition, that is, in turn on the specimen geometry such as M(T), needs further consideration. It can be concluded for the time being that large pores investigated presently do not appear to be detrimental for FCP.

5 SUMMARY

CO_2 Laser beam butt welds of the airframe alloy AA6056-T6 with 6 mm thickness contained micropores (≤ 100 µm) and occasionally distributed large pores (≤ 1 mm). The effect of porosity on the fatigue crack propagation behaviour was investigated on C(T) specimens with the notch in the fusion zone. Compared to the base metal, the weld exhibited an inferior resistance to fatigue crack propagation at low load ratio and particularly in the upper ΔK regime (≥ 15 MPa√m; R = 0.1). Interestingly, the weld exhibited retardation in crack propagation, which occurred at random and even with increasing K_{max}, and also at different R values. As regards retardation, micropores were not found to be influential. In contrast, from fractographic investigations large pores were found to hinder the crack front and contribute to the retardation. Once cut-through, however, also large pores become non-influential.

Acknowledgement M. Pakdil, now at Dokuz Eylül University, Bornova-Izmir, Turkey, gratefully acknowledges the opportunity provided to work on the present topic.

6 REFERENCES:

1. American Welding Society, Welding Aluminium, (Welding Handbook, 6th edition), Miami, Florida, USA, 1972.
2. M. Mazur, *Welding International*, 6, 1992, 929-931.
3. J. F. Rudy and E. J. Rupert, *Welding Journal (Welding Research Supplement)*, July 1970, 322-s-336-s.
4. C. M. Sonsino and J. Ziese, *Int. J. Fatigue*, 15, 1993, 75-84.
5. U. Brandt, F. V. Lawrence and C. M. Sonsino, *Fatigue Fract. Engng. Mater. Struct.*, 24, 2001, 117-126.
6. R. Galatolo and A. Lanciotti, *Int. J. Fatigue*, 19, 1997, 43-49.
7. K. Shankar and W. Wu, *Materials & Design*, 23, 2002, 201-208.
8. S.-W. Han, S. Kumai, A. Sato, *Mater. Sci. Engng.*, A308, 2001, 225-232.
9. G. Neye and P. Heider, 5th European Conference on Laser Treatment of Materials: ECLAT'94, (DVS-Report N°. 163), Sept. 26-27, 1994, Bremen (Germany), DVS-Verlag, Düsseldorf, 108-117.
10. W. Zink, 19th European Conference on Materials for Aerospace Applications, (DGLR Report 2001-02), Dec. 6-8, 2000, Munich (Germany), 25-32.

11. R. Dif, T. Warner, B. Bes, P. Lequeu, H. Ribes and P. Lassince, P., Advances in the Metallurgy of Aluminium Alloys, M. Tiryakioglu, Ed., ASM International, 2001, 390-398.
12. M. Horstmann, G. K. Gregory and K.-H. Schwalbe, *Materials Testing*, 35, 1993, 212-217.
13. W. V. Vaidya, K. Angamuthu and M. Kocak, FATIGUE'2002, A. F. Blom, Ed., EMAS, West Midland, UK, 2002, 1467-1474.

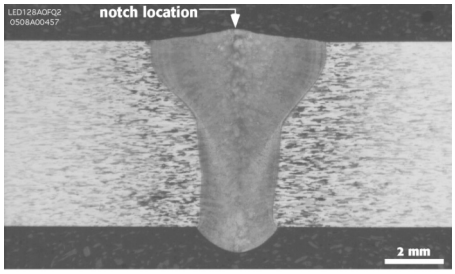


Figure 1. Butt joint of AA6056/6 mm laser beam welded in T6. The notch was placed in the center of the fusion zone. Colour changes on both sides of the weld have resulted from heat affected zone which etches differently.

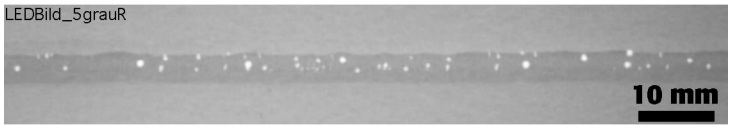


Figure 2. X-ray radiograph of the laser beam weld showing macro-porosity. Note that the pores are distributed randomly and are isolated (positive contrast print).

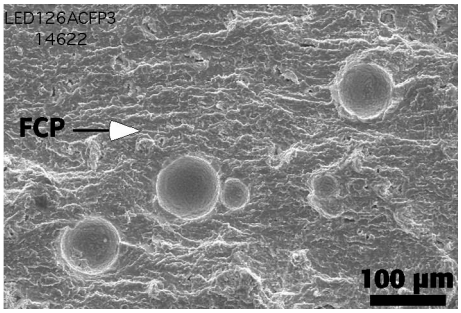


Figure 3. Micropores in butt joint of AA6056-T6/6 mm as observed on a fracture surface of fatigue crack propagated specimen. These pores have formed isolated, are not internally connected, and are cut by the crack front nearly in the equatorial plane (crack propagation direction is from left to right).

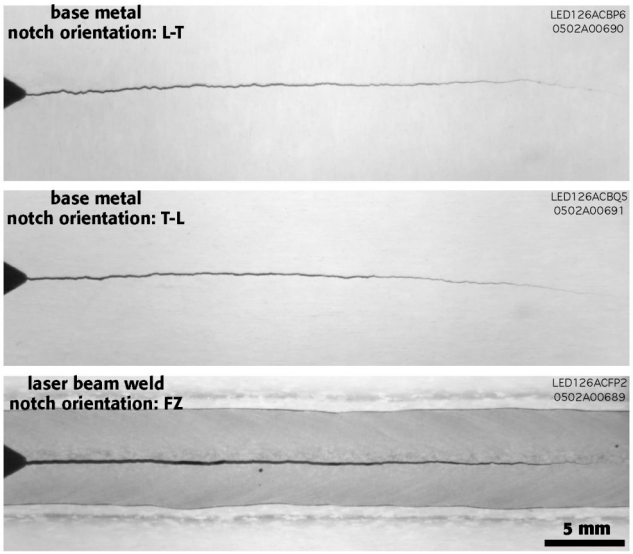


Figure 4. Crack path in the base metal and the laser beam weld AA6056-T6/6 mm after fatigue crack propagation at R = 0.1 (the LBW specimen was etched so as to reveal the weld area).

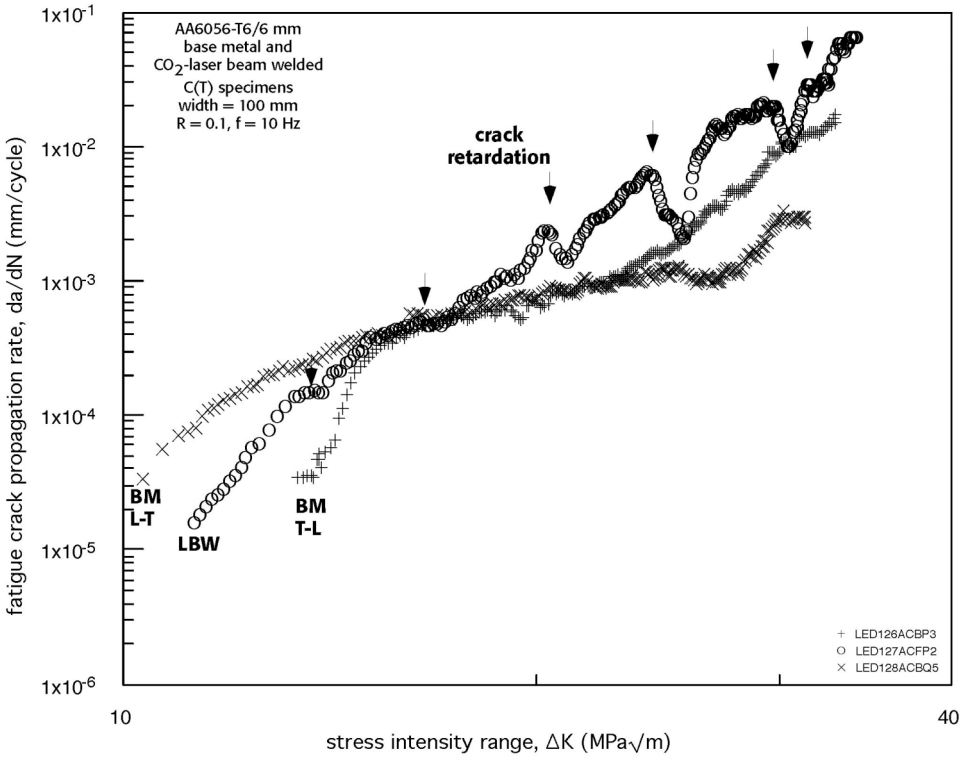


Figure 5. Fatigue crack propagation behaviour of the base metal and the laser beam weld at R = 0.1. Crack retardation event in the laser beam weld is denoted by the arrow.

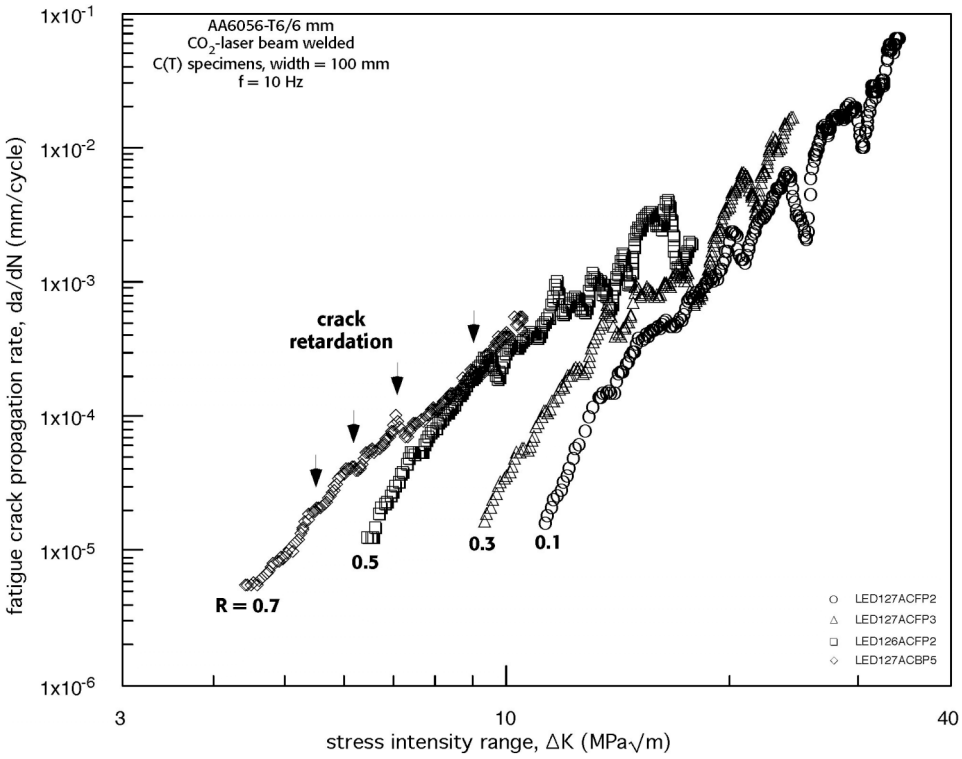


Figure 6. Occurrence of crack retardation in the laser beam weld at different R values (for the sake of clarity only for R = 0.7 the crack retardation event is denoted by the arrow).

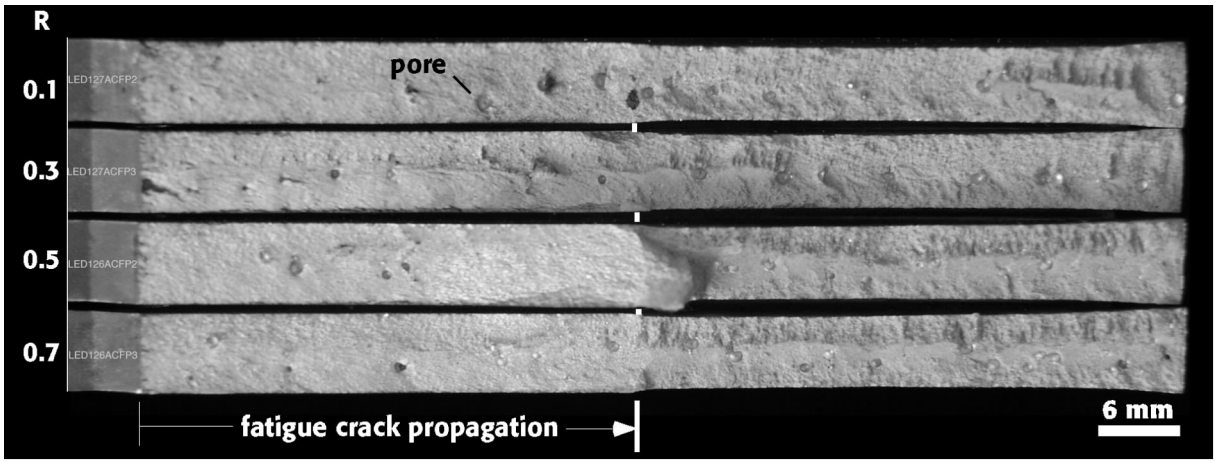


Figure 7. Fracture surface of the specimens tested at various R values. Large pores are clearly seen on the fracture surface (specimens were tested nearly to the same final crack length).

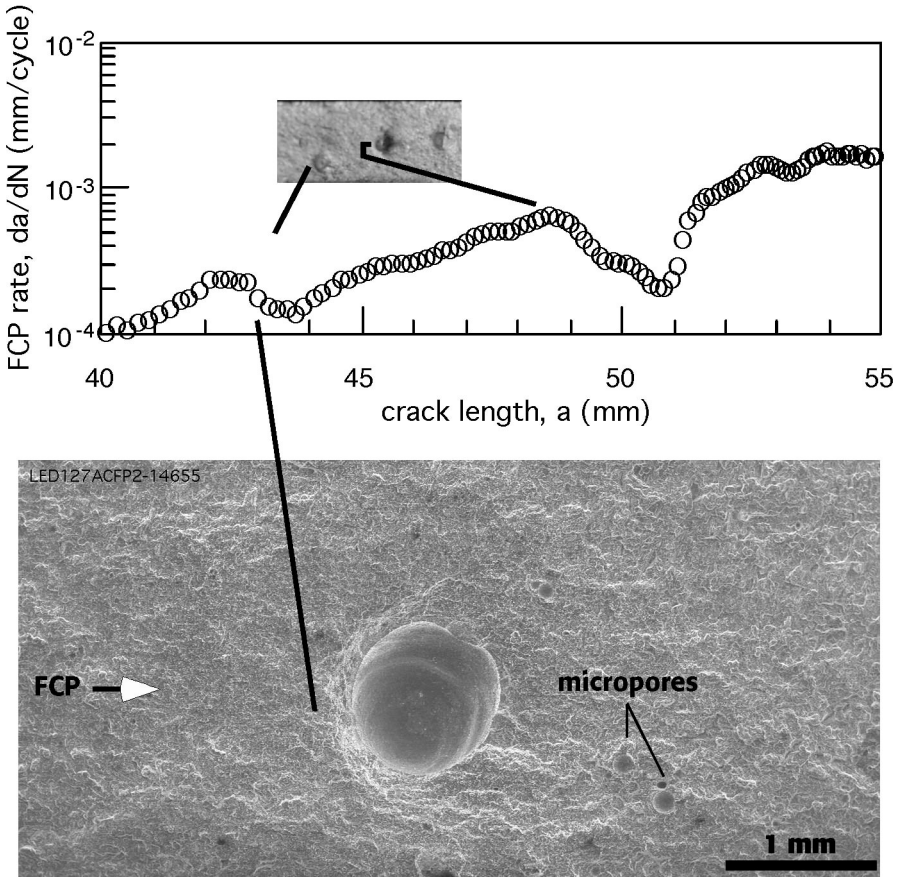


Figure 8. Correlation between fatigue crack propagation and macrofractographic features in the laser beam welded specimen tested at R = 0.1 (such a correlation is found to be good within approximately ±1 mm). The inset in the diagram is extracted from the top fractograph in Figure 7. The bottom fractograph is taken at low magnification in SEM. The direction of fatigue crack propagation is from left to right. Note that even at this magnification the rough surface pattern (due to deformation) on the left hand side of the large pore (which acts as a barrier) is evident, however, not after the pore is cut-through.

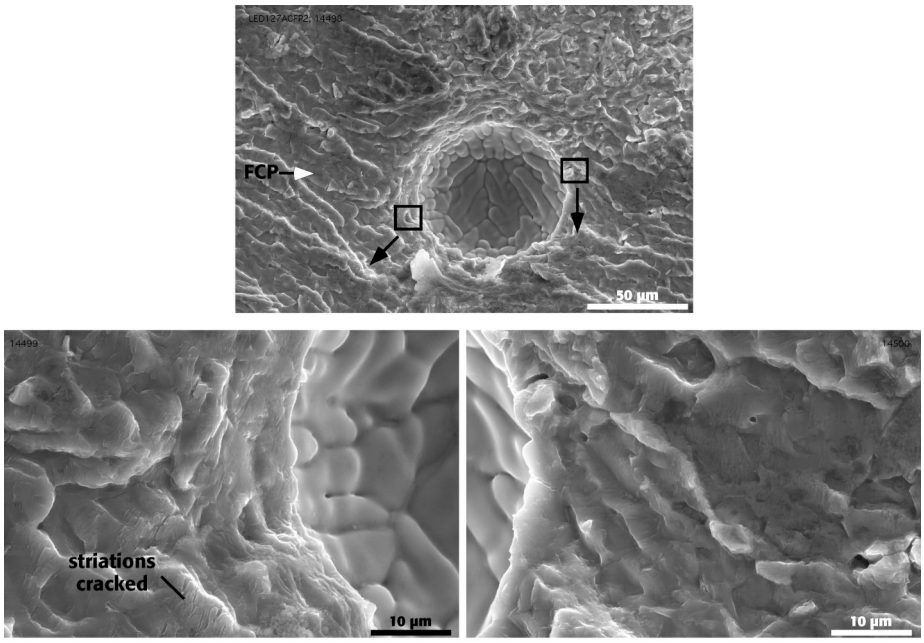


Figure 9. Similarity of microfractographic features at the interface of a micropore (fatigue crack propagation direction is from left to right; R = 0.1). The insets denote the approximate area viewed at a higher magnification.

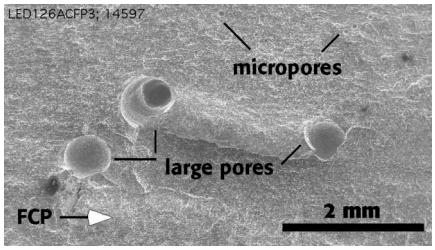


Figure 10. Difference in the appearance of large pores. (That such large pores became visible on the fatigue fracture surface over such a narrow distance was seldom; fatigue crack propagation direction is from left to right).

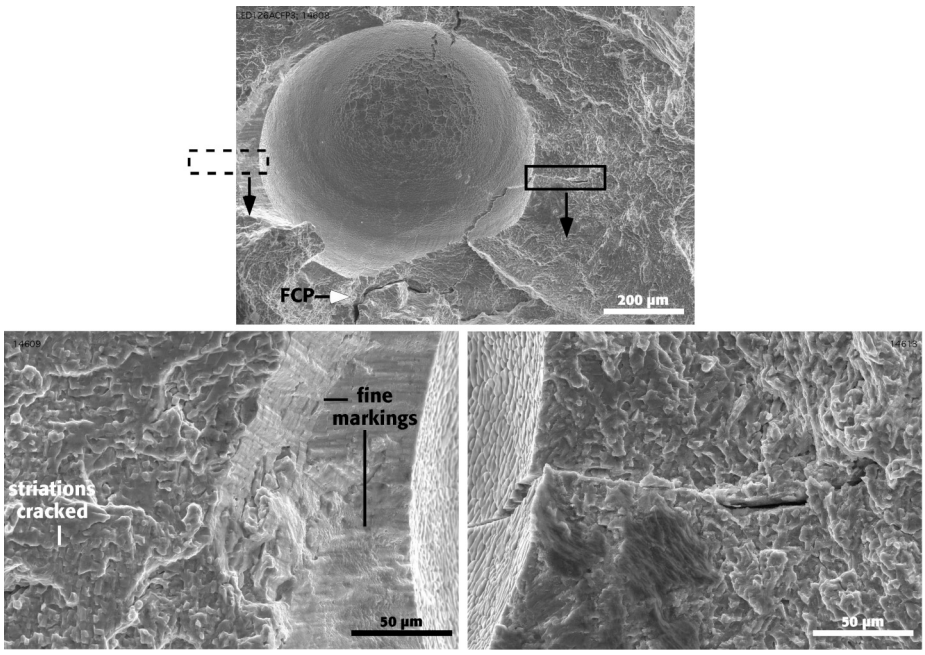


Figure 11. Dissimilarities of microfractographic features at the interface of a large pore (fatigue crack propagation direction is from left to right; R = 0.7). The insets denote the approximate area viewed at a higher magnification.

Prediction Method for Crack Growth Life of MSD Structure

Zhang Jiangyu, Bao Rui, Fei Binjun

School of Aeronautic Science and Technology,
Beijing University of Astronautics and Aeronautics, Beijing, 100083, PR China

Abstract The problem of multiple-site damage (MSD) has got more attention in ageing structures. Cumulative effects of interacting cracks may significantly degrade the damage tolerance capacity of the structure. Cracks caused by MSD are extremely difficult to detect and greatly reduce the residual strength, fatigue life and overall structural integrity of aircraft panels. Methods for predicting crack growth life of MSD structure have been developed. But most of the presented numerical methods must calculate the fatigue life cycle by cycle. These methods spend much time to calculate the stress distribution. This paper presents a simple numerical method, which use the principles of fracture mechanics and the computation results, to predict the fatigue crack growth life of MSD structure. Comparing with calculating crack growth life cycle by cycle, this method will save much time. Representative MSD structures are given in numerical examples. Using this method, MSD structures with different initial length cracks were adopted in the numerical examples. Crack interaction effect was found obviously, but it occurred mainly in the last part of the crack growth lives. The relative size of MSD cracks depends significantly on scatter of the initial cracks.

1 INTRODUCTION

The phenomenon of aging structures has focused attention on the problems of multiple-site damage (MSD). MSD refers to multiple cracks of arbitrary length, commonly occurring along rows of fastener holes in the fuselages and wings of commercial and military aircrafts. In isolation each flaw or crack may be safe. However, the cumulative effect of multiple, interacting cracks may significantly degrades the damage tolerance of the structure. Cracks caused by MSD are extremely difficult to detect and greatly reduce the residual strength, fatigue life and overall structural integrity of aircraft panels. It has become increasingly important to develop methodologies to predict the fatigue crack growth life in damaged fuselage structures in the presence of widespread fatigue damage. Developments of these methodologies for complex loading are essential to ensure the continued safe operation of the aging commercial transport fleet and aircraft for the next generation.

Over the years, stable crack growth in metallic materials has been studied extensively using elastic–plastic finite-element methods. Methods for predicting crack growth life of MSD structure have been developed. But most of the presented numerical methods must calculate the fatigue life cycle by cycle. These methods spend much time to calculate the stress distribution. It's unnecessary. This paper presents a simple numerical method to predict the fatigue crack growth life of MSD structure. Representative MSD structures are given in numerical examples. And some significative conclusions are given at the end of the paper.

2 CRACK GROWTH LAW

For MSD structures, fatigue crack growth can be represented by the Paris equation, which is a power law relation between the crack growth rate da/dN and the stress intensity factor range ΔK. Then fatigue crack growth rate of the *i*th crack can be written as:

$$\frac{da_i}{dN} = C_i \Delta K_i^{m_i} \tag{1}$$

Where da_i/dN is the crack growth rate of the *i*th crack; ΔK_i is the stress intensity factor range of the *i*th crack; C_i, m_i are constants of the Paris equation. Mostly, cracks in the MSD structure follow the same crack growth law. As a result, C_i, m_i are same for each crack. This equation can be changed to:

$$\frac{da_i}{dN} = C\Delta K_i^{\ m} \tag{2}$$

Here, ΔK_i can be written as:

$$\Delta K_i = F_i(a_1, a_2, \cdots, a_n)\Delta\sigma\sqrt{\pi a_i} \tag{3}$$

Where $F_i(a_1, a_2, \cdots, a_n)$ is the influence factor controlled by all of the cracks geometry characteristic; $\Delta\sigma$ is the stress range of MSD structure; a_i is the crack length of the *i*th crack.

Eq.(2) can be rewritten as:

$$\frac{da_i}{dN} = C(F_i(a_1, a_2, \cdots, a_n)\Delta\sigma\sqrt{\pi a_i})^m \tag{4}$$

This is the crack growth rate of the *i*th crack. In one cycle, the length of crack growth is:

$$\Delta a_i = C(F_i(a_1, a_2, \cdots, a_n)\Delta\sigma\sqrt{\pi a_i})^m \tag{5}$$

If we calculate crack growth rate of each crack cycle by cycle from the initial crack lengths to the crack lengths that bring on structure failure, we can get the crack growth life of MSD structure. Unfortunately, it is a hard work for FEM software to calculate the crack growth rate of each crack cycle by cycle. Most of the calculating time is wasted to get the stress intensity factor range.

3 FAST PREDICTION OF MSD CRACK GROWTH LIFE

As we known, there are statistical errors in determining constants of the Paris equation by experiment. At the same time, there are errors in calculating the stress intensity factor range by FEM program. Therefore, calculating the crack growth rate cycle-by-cycle is insignificant.

For predicting the crack growth life fleetly, we can calculate the crack growth length by multi-cycle. At the same time, errors must be controlled. Equation to calculate the crack growth length is:

$$(\Delta a_{ij})_N = C(F_i(a_{1j}, a_{2j}, \cdots, a_{nj})\Delta\sigma\sqrt{\pi a_{ij}})^m \Delta N_j \tag{6}$$

Where, *j* means the *j*th step.

The crack growth length calculate cycle by cycle is:

$$(\Delta a_{ij})_R = \sum_{l=1}^{\Delta N_j} C(F_i(a_{1l}, a_{2l}, \cdots, a_{nl})\Delta\sigma\sqrt{\pi a_{il}})^m \tag{7}$$

The maximal crack growth length can be estimated:

$$(\Delta a_{ij})_M = C(F_i(a_{1j+1}, a_{2j+1}, \cdots, a_{nj+1})\Delta\sigma\sqrt{\pi a_{ij+1}})^m \Delta N_j \tag{8}$$

Error of Eq.(6) is:

$$err = \left|(\Delta a_{ij})_N - (\Delta a_{ij})_R\right| \le \left|(\Delta a_{ij})_N - (\Delta a_{ij})_M\right| \tag{9}$$

Relative error is:

$$e = \left|\frac{(\Delta a_{ij})_N}{(\Delta a_{ij})_R} - 1\right| \le \left|\frac{(\Delta a_{ij})_N}{(\Delta a_{ij})_M} - 1\right| \tag{10}$$

For controlling the error of Eq.(6), error tolerance is used:

$$e = \left|\frac{(\Delta a_{ij})_N}{(\Delta a_{ij})_R} - 1\right| \le \left|\frac{(\Delta a_{ij})_N}{(\Delta a_{ij})_M} - 1\right| \le et \tag{11}$$

We can get:

$$\left|\frac{C(F_i(a_{1j}, a_{2j}, \cdots, a_{nj})\Delta\sigma\sqrt{\pi a_{ij}})^m \Delta N_j}{C(F_i(a_{1j+1}, a_{2j+1}, \cdots, a_{nj+1})\Delta\sigma\sqrt{\pi a_{ij+1}})^m \Delta N_j} - 1\right| \le et \tag{12}$$

Then:

$$\left|\left(\frac{F_i(a_{1j}, a_{2j}, \cdots, a_{nj})}{F_i(a_{1j+1}, a_{2j+1}, \cdots, a_{nj+1})}\right)^m \left(\frac{\sqrt{a_{ij}}}{\sqrt{a_{ij+1}}}\right)^m - 1\right| \le et \tag{13}$$

Where:

$$\sqrt{a_{ij+1}} = \sqrt{a_{ij} + \Delta a_{ij}} \approx \sqrt{a_{ij}} + \frac{\Delta a_{ij}}{2\sqrt{a_{ij}}} \tag{14}$$

As we known, the variety of influence factor is small than that of crack length when crack growth. It means:

$$\frac{F_i(a_{1j}, a_{2j}, \cdots, a_{nj})}{F_i(a_{1j+1}, a_{2j+1}, \cdots, a_{nj+1})} \le \frac{\sqrt{a_{ij}}}{\sqrt{a_{ij+1}}} \tag{15}$$

The final equation is:

$$(\Delta a_{ij})_N \le 2a_{ij}\left[(1 - et)^{-\frac{1}{2m}} - 1\right] \tag{16}$$

In calculating process, *et* is a small number, such as 0.01~0.001. If the length of crack growth is small than Eq.(16), the relative error is small than *et*.

4 NUMERICAL EXAMPLES AND ANALYSIS

In this section, results from numerical analyses of MSD structure are discussed in detail. The stable crack growth analyses of 200 mm wide panels with initial MSD cracks are calculated. The specimen configuration and a typical finite-element model for the wide panel with MSD are shown in Fig.1 and Fig.2 respectively.

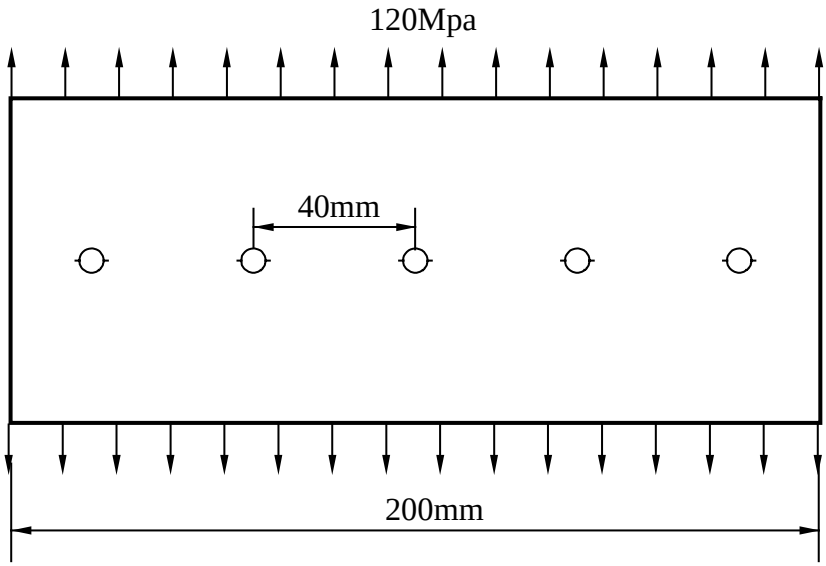


Fig.1. specimen configuration

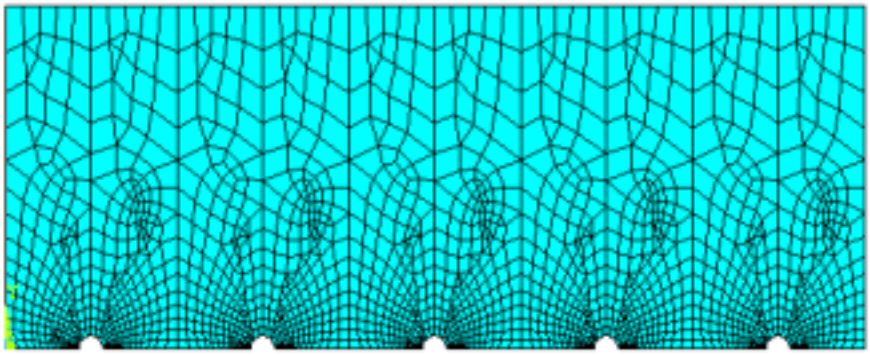


Fig.2. Typical finite-element model of 200 mm wide panel

The following examples discuss three different models, and the corresponding calculation results are summarized in tables. In all the examples, crack length refers to the distance from the centre of the hole to the corresponding crack tip.

Firstly, considering that the initial cracks present on each side of the central hole, and the other four holes on the panel have no flaws. The crack growth lives were calculated as the initial crack length various from 5.0mm to 7.0mm. The result is shown in table I.

Table I. Calculating results of model one.

No.	Initial length of cracks	Crack growth life	Calculating steps
1a	5.0mm	7721	227
1b	6.0mm	5691	173
1c	7.0mm	4081	128

Secondly, the circumstance that the iso-length initial cracks distribute on both sides of the holes is considered. When the initial crack length changes, we get different crack growth lives as shown in table II.

Table II. Calculating results of model two.

No.	Initial length of cracks	Crack growth life	Calculating steps
2a	4.0mm	8168	245
2b	5.0mm	5564	179
2c	6.0mm	3658	125

Finally, the model of wide panel with leading crack and multiple small cracks is studied. The leading cracks lie on the sides of the central hole, the length of which is much lager than that of the other cracks. Table III lists the calculation results of this model.

Table III. Calculating results of model three.

No.	Initial length of leading cracks	Initial length of other cracks	Crack growth life	Calculating steps
3a	5.0mm	4.0mm	6628	202
3b	6.0mm	4.0mm	5023	157
3c	7.0mm	4.0mm	3649	117

The calculating results of model 1 and model 2 show that the crack growth lives are greatly reduced when MSD cracks are presented.

Compared the results of model 1 and model 3, an obvious crack interaction effect is found. The crack growth lives reduced by 14.15%, 13.30% and 10.59% as a result of the existing of MSD.

Table IV shows the distribution of crack length after about 4,000 cycles of model 2a and model 3a.

Table IV. Crack length distribution for different initial crack.

No.		1	2	3	4	5	6	7	8	9	10
2a	Initial length (mm)	4.00	4.00	4.00	4.00	4.00	4.00	4.00	4.00	4.00	4.00
	Final length (mm)	5.73	5.72	5.69	5.68	5.68	5.67	5.68	5.68	5.72	5.72
3a	Initial length (mm)	4.00	4.00	4.00	4.00	5.00	5.00	4.00	4.00	4.00	4.00
	Final length (mm)	5.72	5.71	5.71	5.71	7.33	7.33	5.72	5.70	5.71	5.71

It is obviously seen from table IV that the growth lengths of leading cracks are much large than that of other cracks. The relative size of MSD cracks depends significantly on scatter of the initial crack.

5 CONCLUSIONS

A simple numerical method was developed for predicting the fatigue crack growth life of MSD structure rapidly. Comparing with calculating crack growth life cycle by cycle, the method will save much time. Using this method, MSD structures with different initial length cracks were adopted in the numerical examples. An obvious crack interaction effect was found in the last part of the fatigue crack growth lives. The relative size of MSD cracks depends significantly on scatter of the initial length of cracks.

6 REFERENCES:

1. L. Ma, P. W. Lam, M. T. Kokaly, A. S. Kobayashi, CTOA of a stable crack in a thin aluminum fracture specimen. Eng. Frac. Mech., 70, 2003, 427-442.
2. R. M. V. Pidaparti, M. J. Palakal, Z. A. Rahman, Simulation of structural integrity predictions for panels with multiple site damage, Advances in Eng. Software, 31, 2000, 127-135.
3. G. S. Wang, Analysing the onset of multiple site damage at mechanical joints, Int. J. Fracture, 105, 2000, 209-241.
4. R. M. V. Pidaparti, M. J. Palakal, Fatigue crack growth predictions in aging aircraft panels using optimization neural network, AIAA Journal, 36, 1998, 1300-1304.
5. L. Wang, F. W. Brust, S. N. Atluri, The elastic-plastic finite element alternating method (EPFEAM) and the prediction of fracture under WFD conditions in aircraft structures. Computational Mechanics, 19, 1997, 356-379.

X-FEM method for elastic-plastic fatigue crack growth simulation

Thomas Elguedj[a], Anthony Gravouil[a], Alain Combescure[a]

[a] Laboratoire de Mécanique des Contacts et des Solides UMR5514
INSA de Lyon, Bât. Jean d'Alembert
18-20 rue des Sciences
69621 Villeurbanne, France

Abstract This paper presents a bidimensionnal elastic-plastic (with unilateral contact) fatigue crack growth analysis using the eXtended Finite Element Method (X-FEM) which has the main advantage to avoid remeshing when the crack propagates. An augmented Lagrangian formulation is used with an appropriate elastic-plastic enrichment basis and X-FEM interface elements to treat unilateral contact on the crack lips. This algorithm is applied to mode I crack propagation.

1 INTRODUCTION

The eXtended Finite Element Method (X-FEM) has been used with success in the past few years to simulate linear elastic fatigue crack growth. This paper presents a bidimensionnal elastic-plastic (with unilateral contact) fatigue crack growth analysis using the X-FEM method which has the main advantage to avoid remeshing when the crack propagates. A new enrichment strategy, which captures the Hutchinson Rice Rosengren plastic singularities, is used in conjunction with an augmented lagrangian algorithm for the treatment of contact and a Newton-like iteration scheme to compute equilibrium.

2 DISCRETIZATION

2.1 The eXtended Finite Element Method

In the eXtended Finite Element Method, first presented in Reference 1, an enrichment basis is added to the classical finite element basis approximation. The enriched basis shape functions are associated to new degrees of freedom and the displacement field can be written:

$$U = \sum_{i \in N} N_i(x) U_i + \sum_{i \in Ncut} N_i(x) H(x) a_i + \sum_{J} \sum_{i \in Nfront} N_i(x) B_\alpha(x) b_{i,\alpha} \qquad (1)$$

Where N is the set of standard finite element (FE) nodes, *Ncut* the set of nodes which belongs to elements totally cut by the crack, and *Nfront* the set of nodes which belongs to an element containing a crack front. N_i are the standard FE shape functions; H is a jump function and B_α is derived from the asymptotic fields.

2.2 Elastic-plastic case

A new enrichment basis, composed of six functions, admissible for elastic-plastic solids that follow a Ramberg-Osgood power law with various power coefficients was developed:

$$[B_\alpha] = \left[r^{\frac{1}{n+1}} \sin\frac{\theta}{2}, r^{\frac{1}{n+1}} \cos\frac{\theta}{2}, r^{\frac{1}{n+1}} \sin\frac{\theta}{2}\sin\theta, r^{\frac{1}{n+1}} \cos\frac{\theta}{2}\sin\theta, r^{\frac{1}{n+1}} \sin\frac{\theta}{2}\sin 3\theta, r^{\frac{1}{n+1}} \cos\frac{\theta}{2}\sin 3\theta \right] \qquad (2)$$

This basis captures well the Hutchinson Rice Rosengren (see References 2-3) plastic singularity and is equivalent to the basis proposed in Reference 4 in the framework of the Meshless Method. An appropriate numerical integration scheme is developed in order to avoid the projection of stress and internal variables when the crack propagates. The subtriangle partitioning technique previously used for linear elastic X-FEM calculations (see Reference 1) is replaced by a subquadrangle technique which is independent of the crack position within an element. Numerical comparisons, without propagation, were done with classical finite element method and show good agreement for the J integral as well as the local displacement solution.

3 CONTACT TREATMENT

As the crack lips are not modelled by the mesh in the X-FEM, one has to create interface elements to treat unilateral contact if the crack closes itself due to compressive loading. These interface elements are created by intersecting the crack faces and the subelements edges in an equivalent way to the one presented in Reference 5. Following the work done in References 6-7, an X-FEM augmented lagrangian formulation is used to treat at the same time the material plastic non-linearity and the unilateral contact problem. The treatment of the local contact equations is done using the method presented in Reference 8. This formulation is able to treat residual crack opening (due to plasticity around the crack tip) as one can see on Figure 1 (the deformed mesh of the specimen is presented).

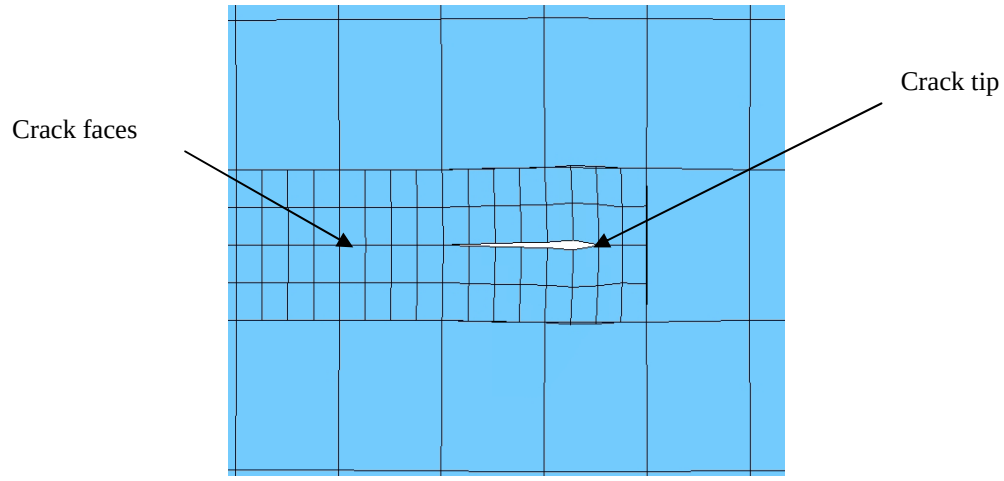


Figure1: *Zoom on the residual crack opening (due to plasticity) on a mode I specimen submitted to tension-compression cyclic loading.*

4 CRACK GROWTH SIMULATION

The former algorithm is extended to crack propagation and tested in mode I. Problems inherent to crack propagation in plastic materials, such as the conservation of the plastic variables, are addressed. The method is compared to finite element controlled mode I crack growth simulation and experimental results.

5 CONCLUSION

An X-FEM augmented Lagrangian method that can treat fatigue crack growth in elastic-plastic materials with treatment of unilateral contact was presented. The results present good accuracy for the evaluation of standard fracture parameters in static case. The first solutions are obtained in mode I crack growth situation and show promising results. This method will be extended to mixed mode fatigue crack growth and compared to experimental results.

6 REFERENCES:

6.1 Journal Article

1. N. Moës, J. Dolbow and T. Belytschko, A Finite Element method for crack growth without remeshing, *International Journal for Numerical Methods in Engineering*, 46, 1999, 131-150.
2. J. Hutchinson, Singular behaviour at the end of a tensile crack in a hardening material, *Journal of the Mechanics and Physics of Solids*, 16, 1968, 13-31.
3. J. Rice and G. Rosengren, Plane strain deformation near a crack tip in a power-law hardening material, *Journal of the Mechanics and Physics of Solids*, 16, 1968, 1-12.
4. B. Rao and S. Rahman, An enriched meshless method for non-linear fracture mechanics, *International Journal for Numerical Methods in Engineering*, 59, 2004, 197-223.
5. J. Dolbow, N. Moës and T. Belytschko, An eXtended Finite Element Method for modelling crack growth with frictional contact, *Computer Methods in Applied Mechanics and Engineering*, 190, 2001, 6825-6846.
6. L. Simo and T. Laursen, An augmented lagrangian treatment of contact problems involving friction, *Computers and Structures*, 42(1), 1992, 97-116.

6.2 Book

7. T. Belytschko, W. Liu and B. Moran, Nonlinear finite element for continua and structures, 1st edition, Wiley, Chichester, 2002.

6.3 References to Unpublished Sources

8. R. Ribeaucourt, M. Baietto-Dubourg and A. Gravouil, A mixed mode fatigue crack model for a steady state non monotonous formulation, submitted to *International Journal for Numerical Methods in Engineering*, 2005.

Fatigue design of armourd vehicle

Eric PETITPAS, Ludovic DUPONT, David LEBAILLIF, Robert PERINET

GIAT Industries, 11 allée des marronniers 78023 Versailles – France

ABSTRACT

The military vehicles are subjected to high dynamic loadings coming from driving on chaotic grounds and crossing over obstacles. These loadings induce a dynamic behaviour of the vehicle on its shock absorber. They are transmitted to the chassis which can present at its turn a dynamic behaviour, according to its rigidity and type of loading. This dynamic behaviour can involve an amplification of the stresses in certain parts of the chassis. Consequently, the various parts are subjected to a stress spectrum mixing low and high amplitude cycles. These stress cycles can induce a fatigue damage located on structural details like welded joints. To take into account the driving loadings in fatigue design, a multi-scale approach has been developed. This approach is based on a sequence of simulation at various levels of representation; from the generation of grounds until the calculation of fatigue life of structural details, the dynamics of driving, the dynamic of structures, the localization of the weak points and the fatigue calculation of structural details corresponding to each weak points are connected. This multi-scale approach is presented and illustrated with the example of design of a cross-country vehicle.

1. CONTEXT

Military vehicles are subjected to high dynamic loadings coming from driving on chaotic grounds and crossing over obstacles. These loadings induce a dynamic behaviour of the vehicle. They are transmitted to the chassis through the suspension components. The chassis can present at its turn a dynamic behaviour, according to its rigidity and types of loadings, which can induce an amplification of the stresses in certain parts of the chassis. Consequently, the various parts are subjected to a stress random spectrum with low and high amplitude cycles. These stress cycles can induce a fatigue damage localized on structural details like welded joints.

To master the design of the vehicles a fatigue design process of the structures submitted to several random loadings has been developed since 1997 and has been applied for the conception of military vehicles. In other hand the process has been completed since 2001 to assess crack propagation in vehicles to extend the life of old vehicles.

The approach developed to design in fatigue the vehicles is presented and illustrated with an example.

2. MULTI-SCALE APPROACH

Since the fatigue phenomenon is very local, whereas the phenomenon generating it is vehicle-wide, the design approach must necessarily be multi-scale. The developed approach is composed of 3 steps [1].

2.1. Loadings calculation

The approach start from the use spectrum of the vehicle, defining the grounds on which it must move on, as well as the speeds and the kilometers per year. The first step consists in simulating the driving of the vehicle on each ground at various speeds. For that, a rigid body model of the vehicle is achieve, with precise modeling of suspensions components, wheels and grounds. Simulation are used to determine the internal loadings induced by the suspension components on the chassis due to the driving off road at different speeds.

2.2. Stresses calculation

The second step consists in simulating the behaviour of the chassis submitted to various loadings coming from the vehicles. Driving process induces no-proportional multi-axial random loadings on the structure. Those loadings give either a quasi-static or dynamic behaviour of the chassis. So a complete calculation method has been developed allowing to take into account the real behaviour of the structure; the equation below gives the expression of stress various time [2]:

$$\{\sigma(t)\} = \left[Q_{qs}^{\sigma}\right]\{f(t)\} + \left[Q_{dyn}^{\sigma}\right]\{q(t) - q(t; statique)\} \qquad (1)$$

$$\text{with : } m.\ddot{q}(t) + 2.\xi.\sqrt{k.m}.\dot{q}(t) + k.q(t) = \Phi_{dyn}^{U}.f(t)$$

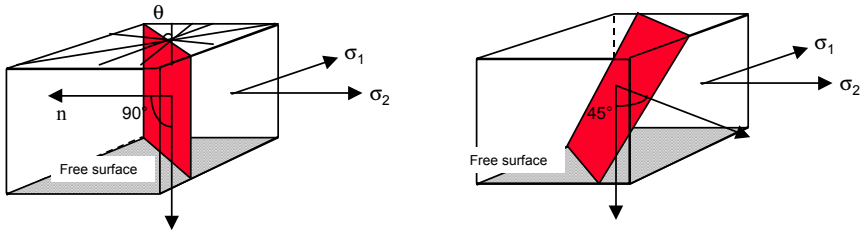
The first term $\left[Q_{qs}^{\sigma}\right]\{f(t)\}$ represents the quasi static part of the stress; $\left[Q_{qs}^{\sigma}\right]$ is the matrix of quasi-static modes of the structure; it is calculated from the finite element model of the structure with a series of calculation with unit loads; the vector $\{f(t)\}$ represents the history of the various components of the loading, coming from dynamic simulation of the vehicle on a ground at one speed.
The second term $\left[Q_{dyn}^{\sigma}\right]\{q(t) - q(t; statique)\}$ represents the dynamic part of the stress; $\left[Q_{dyn}^{\sigma}\right]$ represents the matrix of dynamics mode of the structure; it is calculated from the finite element model of the structure wit a modal analysis; the term $q(t)$ represents the response of each mode; the term q(t, static) represents the quasi static part of the response of each mode; it is essential to correct the dynamic response from the quasi-static part to avoid taking it into account two times. It is calculated by numerical integration of the modal dynamic equation $m.\ddot{q}(t) + 2.\xi.\sqrt{k.m}.\dot{q}(t) + k.q(t) = \Phi_{dyn}^{U}.f(t)$.

In a first time, the quasi-static $\left[Q_{qs}^{\sigma}\right]$ and the dynamic $\left[Q_{dyn}^{\sigma}\right]$ modes are calculated and stored in a file. Then the dynamic response of the dynamic mode $\{q(t) - q(t; \text{statique})\}$ are calculated and stored in a other file. Then the combination $\{\sigma(t)\} = \left[Q_{qs}^{\sigma}\right]\{f(t)\} + \left[Q_{dyn}^{\sigma}\right]\{q(t) - q(t; \text{statique}\}$ is calculated at each node, and send to the fatigue program to calculate the damage at this node.

2.3. Damage calculation for crack initiation

The third step of the multiscale approach is split into two stages; the first one consists to locate the critical areas where there is a risk of fatigue crack; the second stage consists of calculating the lifetime of each weak point by a local approach [1].

The location of critical areas consists in calculating a multiaxial fatigue criterion; it is only made at the nodes for which the maximum stress during the loading history is over a threshold. The fatigue criterion is a facet criterion. On each facet liable to be damaged [3], a Rainflow count carried out on the shear stress, makes it possible to extract the cycles ; for each cycle extracted, the criterion is constructed by combining the shear's



amplitude and the maximum hydrostatic stress encountered during the cycle.

$$\sigma_{fat}^{\vec{n}} = \underset{cycle}{MAX}\left[\tau_a(t) + \beta.\sigma_H(t)\right] \qquad (2)$$

The damage associated with each cycle is calculated by using Miner's linear rule and the material fatigue strength curve expressed in the form of Basquin's law.

$$d_{\vec{n}} = \sum_i \frac{1}{N_f} = \sum_i \frac{1}{\left(\sigma_{fat}^{\vec{n}} / \sigma'_f\right)^{\frac{1}{b}}} \qquad (3)$$

$$d = \underset{\vec{n}}{MAX}\left[d_{\vec{n}}\right] \qquad N = \frac{1}{d}$$

The lifetime at this node is calculated by maximizing the damage on all of the facets.
This procedure allows to locate the weak points of the structure.

The lifetime at each weak point is calculated with a more precise fatigue damage procedure. It consists to take into account the real geometry of the structural detail to calculate the local stresses at its hot spots.
Welding joints represent the most frequent structural details; in the precise fatigue damage procedure, the geometry of the joint must bee considered. For that, it is necessary to proceed previously to statistical measures of the geometry of welds [6,7]. Figure 1 shows the statistical distribution of transition radius measured on aluminum fillet welds.

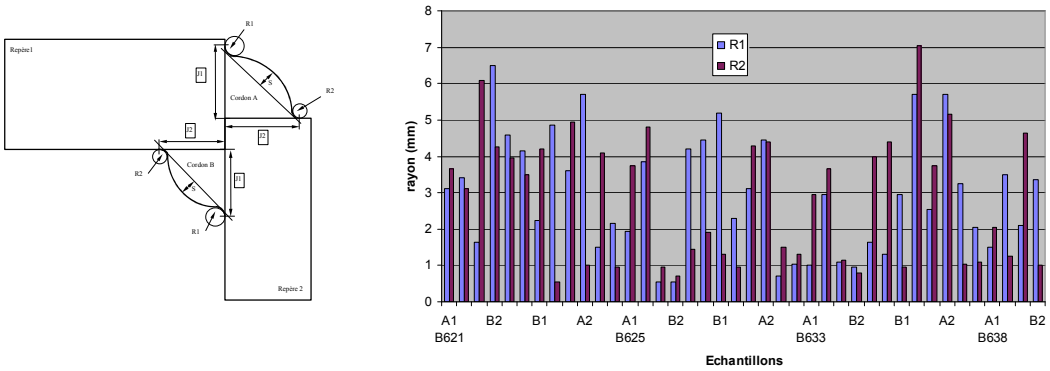


Figure 1 : Distribution of the transition radius of aluminium fillet welds

To take into account the real geometry of structural details in the calculations, two methods could be used.
The sub-modelling consists to describe precisely the real geometry of structural detail with a volumic model of which the displacement of boundary nodes are driven with the corresponding nodes of the global model. So for each quasi-static or dynamic mode of the global model, the corresponding displacement of the boundary nodes are used to drive the sub-model in order to calculate the stresses at each nodes. Then the stress history at each nodes of the sub-model is calculated combining the response of all modes. Figure 2 shows an example of sub-model in a complex welding area.

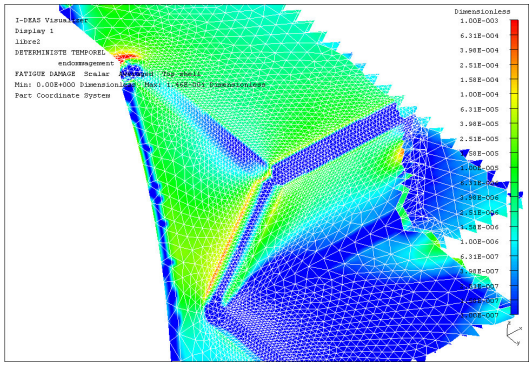


Figure 2 : sub-modelling of a complex welding area

The second method consists to calculate a **Stress concentration matrix**, comparing the stresses, at the hot spot of the structural detail (weld toe for the welding joints), between its global modelling (coarse shell elements) and its local modelling (volumic elements). Figure 3 shows an example of the method.

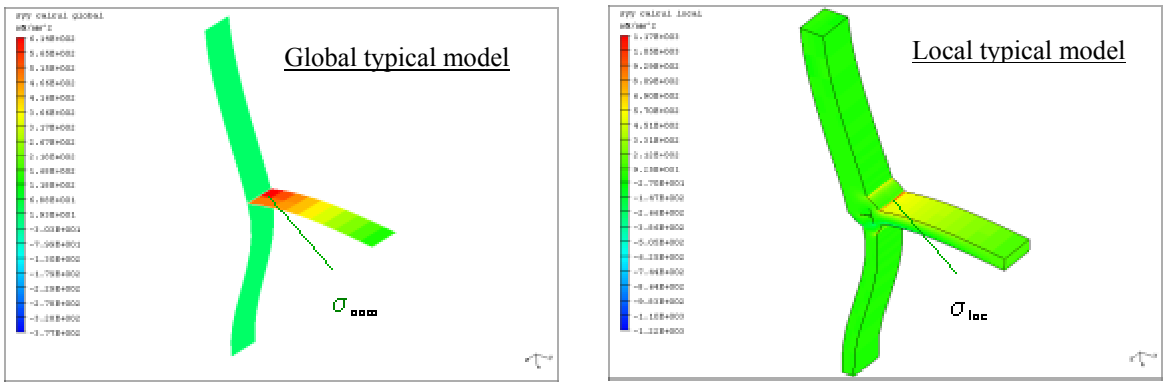


Figure 3 : Calculation of the stress concentration matrix associated with a fillet weld for a given loading [K] defined as $[\sigma]_{local} = [K].[\sigma]_{nom}$

If necessary, residual stresses coming from the welding are added to the local stresses as initial stresses :

$$[\sigma]_{total} = [\sigma]_{residual} + [\sigma]_{local}$$

Stress history may present peaks overshooting the yield stress of the material. In that case, a plastic correction is made. The elastic-plastic model corresponds to the Chaboche non-linear isotropic and kinematic hardening law [4].
The multi-axial fatigue criterion presented before is then used to calculate the damage on the critical plane and the lifetime of the structural detail.

3. APPLICATION TO DESIGN A NEW VEHICLE

This approach has been applied to design vehicles since 2000. Let's see the case of a 8*8 wheels vehicle.

We start from driving specifications, for example 60% roads, 30% all tracks, 10% cross country. Then rugosity profiles are associated to each ground, and some driving simulations on the grounds at different speeds are carried out. Figure 4 give some rugosity profiles and shows the dynamic model of the vehicle.

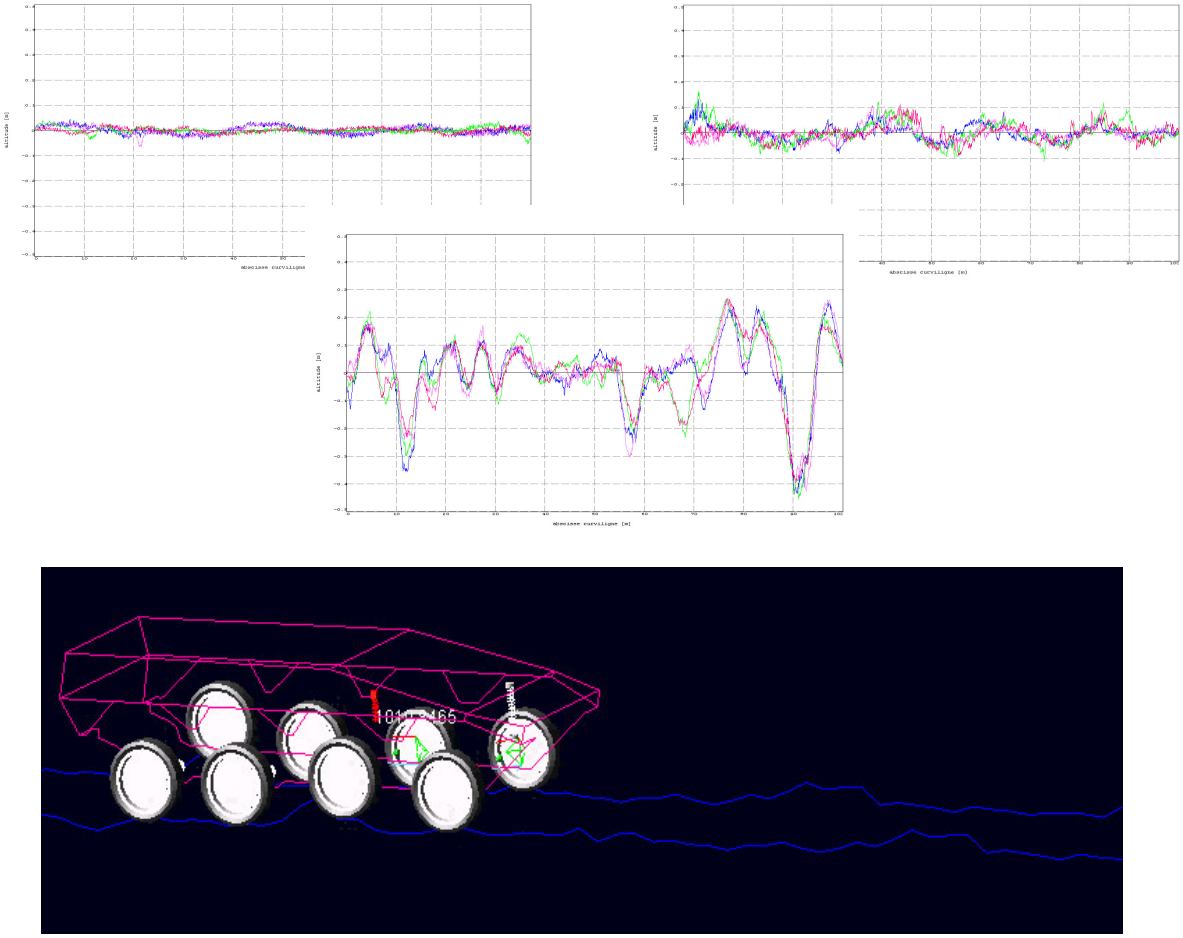


Figure 4 : rugosity of various tracks [5] and driving simulation of a 8*8 vehicle

From driving simulations, we get multi-axial loadings at the interface between suspension components and the chassis.

Figure 5 shows the multi-axial loading for the 8*8 vehicle and an example of loading component in a suspension due to driving on tout terrain at 9 km/h.

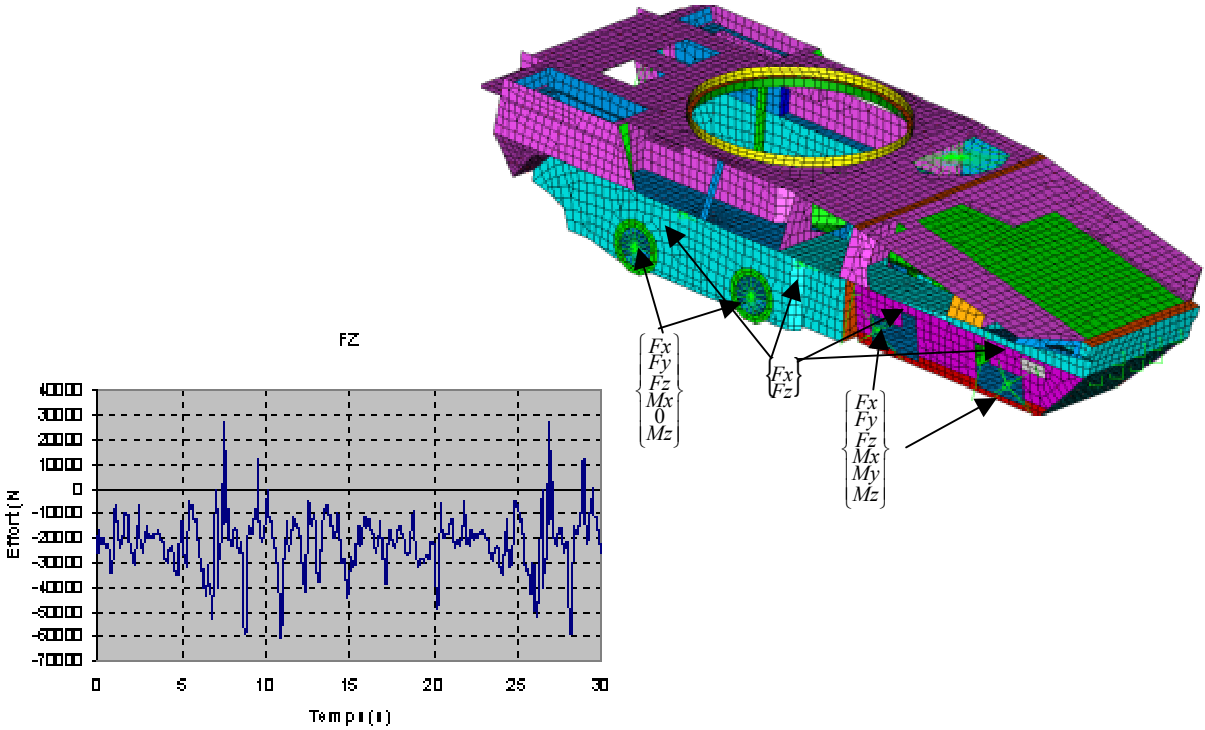


Figure 5 : multi-axial random loadings applied on chassis model and axial loading in front suspension due to driving on cross country at 9 km/h

The stress history computation is made in three steps.

- First the structural modes are calculated; the quasi-static modes $\left[Q_{qs}^{\sigma}\right]$ are calculated with successive static finite element calculations at unit loading; the dynamics modes $\left[Q_{dyn}^{\sigma}\right]$ are calculated with modal analysis.
- In a second time, the dynamic response of all the dynamic modes $\{q(t)-q(t;\text{statique})\}$ are calculated using finite element calculation code (ABAQUS).
- At last, the stresses are calculated at each nodes combining the responses of all quasi-statics and dynamics modes :

$$\{\sigma(t)\}=\left[Q_{qs}^{\sigma}\right]\{f(t)\}+\left[Q_{dyn}^{\sigma}\right]\{q(t)-q(t;\text{statique})\}$$

Figure **6** shows the maximum of the Mises stresses versus time on the chassis of the vehicle driving on cross country at 9 km/h.

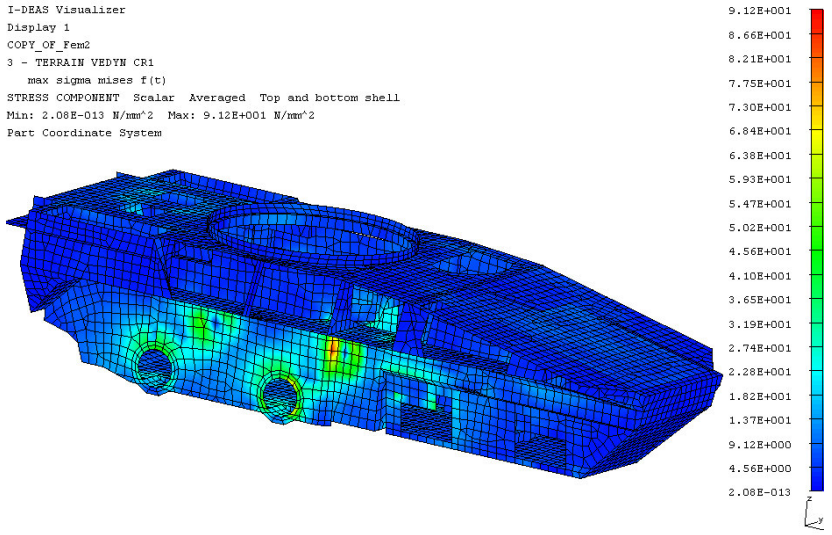


Figure 6 : maximum Mises stresses versus time during the driving on tout terrain at 9 km/h

Then damage calculation is achieve on each node where the maximum of each stress component exceeds a threshold during the driving process. Figure 7 shows the distribution of damage on chassis due to driving on tout terrain at 9 km/h. It allows to locate the weak points of the structure.

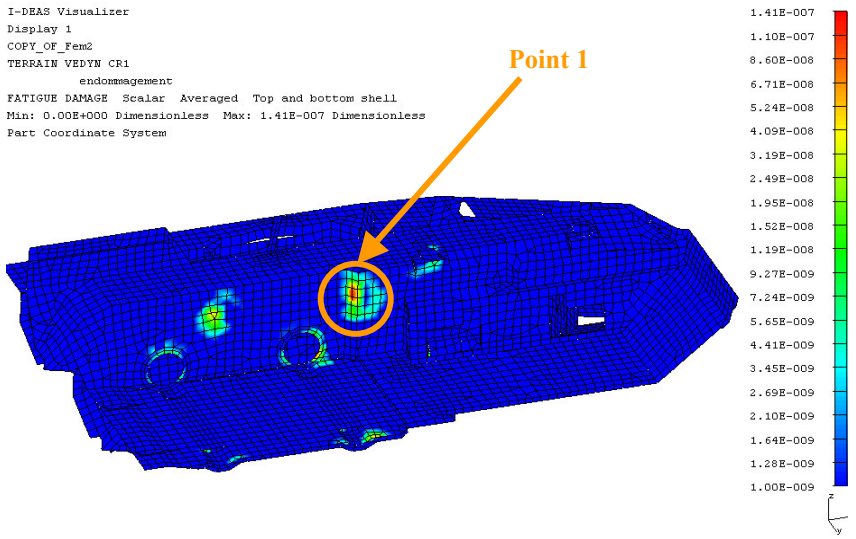


Figure 7 : damage distribution due to driving on cross country at 9 km/h

The last part of the fatigue assessment consists to calculate precisely the fatigue life on each structural detail associated with the checked weak points. Those correspond to welding joints. The stress concentration matrix method has been used; this matrix allows the calculation of local stresses at the weld toe. An example of matrix corresponding to one welding joint is given below :

$$[\sigma]_{local} = [K].[\sigma]_{nom}$$

$$[K] = \begin{bmatrix} 2.5 & 0 & 0 \\ 0 & 1 & 0 \\ 0 & 0 & 1 \end{bmatrix}$$

Residual stresses coming from the welding have been took into account as initial stresses of the local stresses:

$$[\sigma]_{total} = [\sigma]_{residual} + [\sigma]_{local}$$

$$\begin{Bmatrix} 75 \\ 75 \\ 0 \end{Bmatrix} MPa$$

The local stresses calculated at the weld toe of one of the weak points of the vehicle driving on cross country at 9 km/h is given at Figure 8.

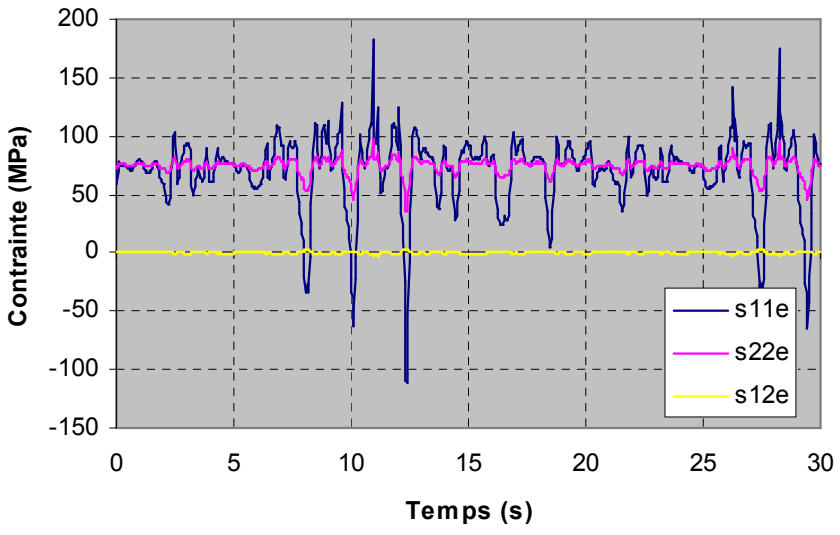


Figure 8 : evolution of the local stress at the weld toe of a weak point due to driving on cross country at 9 km/h

No need of plastic correction in that case, while the stresses do not exceed the yield stress.
The multi-axial fatigue criterion is then calculated on each facet liable to be damaged, using the expression (2) The extraction of the fatigue cycles is made on the history of shear component on the facet, thanks to the Rainflow method. Figure 9 shows the value of the fatigue criterion of each cycle on the facet which maximises the damage; the stress history corresponds to the one of the Figure 8.

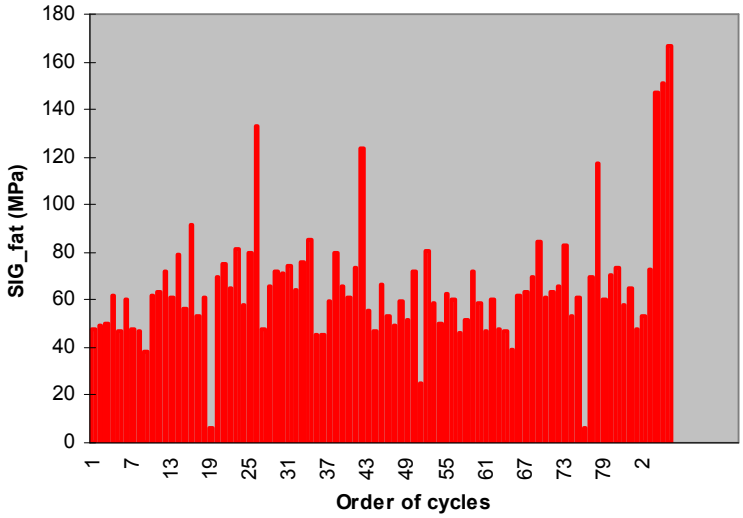


Figure 9 : multi-axial fatigue criterion values calculated on each extracted cycle at the weld toe of a weak point

At last, the damage at each weak point, corresponding to the process of driving of the vehicle on one track at one speed is calculated using the expression (3). This process is made for each speed and each track. In general all the combination are not took into account while many situations induced very few stresses. For each weak point, the damage par second is calculated for each driving situation. Figure 10 shows the damage per second calculated on a weak point due to the driving on various tracks at maximum speed.

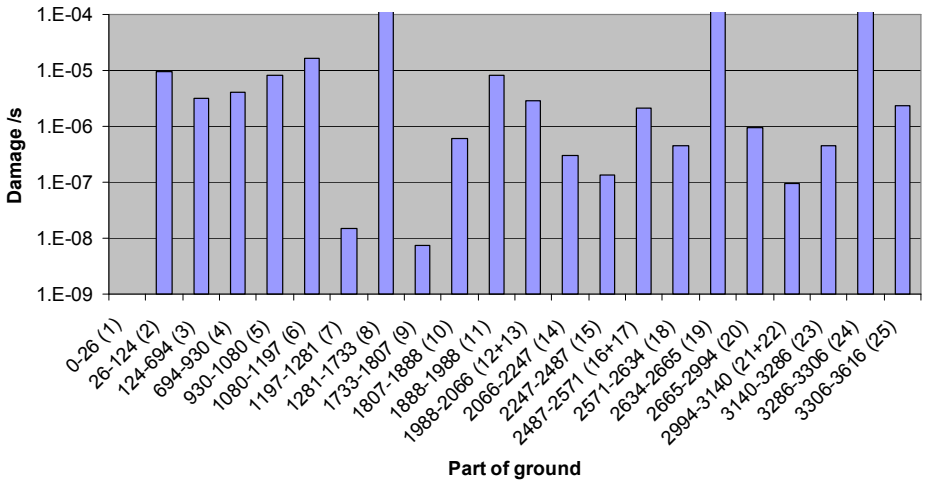


Figure 10 : damage per second on a weak point due to driving on various tracks at maximum speed

The total damage is obtained combining the damage per unit time coming from each situation and the expected time for each situation.

4. CONCLUSION

This fatigue design method has been developed since 1997 and has taken 3 years to develop it. In 2000 validation process started, using experimental results on trials or real case of crack in structural parts. Two of the validation campaign have been made with SNCF company on 2 welded structures in steel and in aluminium alloy submitted to dynamic loadings. An other big validation campaign is under way with the French Ministry of Defense. It consists to validate the calculation at each step of the process; the loading in the suspension equipments of the vehicle driving on various tracks, the stresses induced in various parts of the vehicle during the driving. And a total of 7 structures are under test with different kind of loading to validate the location and the lifetime to initiate cracks.
The method has been used or is underway to design various vehicles like the CAESAR and the new Infantry Fighting Vehicle.

More recently the method has been extended to increase the life of old vehicles beyond their normal lifetime. It is the case of the old Infantry Combat Vehicle AMX10P showing some cracks in the chassis. This extension of method has been occurred in a national collaboration between Giat-Industries, Bureau Veritas, CETIM and LERMES. The principle used to assess the crack propagation is to calculate the Stress Intensity Factor for each quasi-static and dynamic modes in order to calculate a SIF versus time as the superposition of the SIF of all the modes :

$$K_I(t;a) = \sum_{k \text{ modes QS}} K_{I,k}^{QS}(a) \,.\, f_k(t) + \sum_{l \text{ modes dyn}} K_{I,l}^{dyn}(a) \,.\, (q_l(t) - q_l(t; \text{statique}))$$

This method is explained in detail in the paper presented by David Lebaillif [8] .

REFERENCES

[1] E.Petitpas, B.Lebrun, S.De Meerleer, P.Fournier, A.Charrier, F.Pollet; Use of the local approach for the calculation of the fatigue strength of welds; IIW Florence, 9-14 July 2000

[2] M. Gérardin et D. Rixen . "Théorie des vibrations - Application à la dynamique des structures" Edition Masson - Physique fondamentale et appliquée

[3] Bannantine, J.A. and Socie, D.F. "Advances in Fatigue Lifetime Predictive Techniques". ASTM STP 1122, ASTM, Philadelphia. 1992 pp. 249-275.

[4] Lemaitre, J. and Chaboche, J.L. *Mécanique des matériaux solides*. 1988 Dunod, Paris. 188 p.

[5] P.Lelan. Traitement des données terrain IGN de Fontevraud et Canjuers. Note ETAS, Angers 2004

[6] F. Labesse-Jied , B. Lebrun , E. Petitpas, J.L. Robert : Local approach for multiaxial fatigue assessment of welded structures 6th International Conference on Biaxial/Multiaxial Fatigue and Fracture; Lisbon, 25-28 June 2001

[7] H.P. Lieurade, I. Huther, D. Lebaillif. Evaluation de la qualité des soudrues vis-à-vis de la résistance à la fatigue. Mécanique et Industries. Vol 6. No. 2. 2005

[8] D.Lebaillif, I.Huther, M.Serror, N.Recho. Fatigue Crack Initiation and Propagation : a complete industrial process compared with experiments on industriel welded structure. Fatigue Design 2005. Senlis, 16-18 Nov 2005.

Fatigue Life Prediction For Arc Welded Sheet Structural Parts

Yuichi Yoshida[a], Atsushi Seto[a], André Galtier[b]

[a] Steel Research Laboratories, Nippon Steel Corp. 20-1 Shintomi, Futtsu
Chiba, 293-8511, Japan
[b] Automotive Research Centre, Arcelor Research SA, Voie Romaine BP 30320
57283, Maizieres-les-Metz, France

Abstract Automobile components such as chassis parts are generally made of sheet structures connected by arc welding. In this paper the fatigue life of arc-welded steel sheet structures is predicted using FE-Fatigue, which is a fatigue analysis software tool, and these predicted results are evaluated by reference to corresponding experimental results. The arc weld fatigue life predictions were in good agreement with corresponding experimental results in the case where the SN curve database was modified in accordance with the experimental fatigue data for arc welded lap joints with weld start and end points. In addition, we attempted to predict the fatigue life of the automobile component by applying the above method, and a good correlation was observed. Furthermore, we propose changing the shape of the bracket, which is joined to the component by arc welds in order to enhance the fatigue strength using the above method.

1 INTRODUCTION

Steel sheet structures connected by spot welds and arc welds have generally been used for automobile components, especially the body and chassis. Welded parts typically tend to cause fatigue failure owing to the local stress concentrations around the welded parts. Therefore, design tools have been required to predict the fatigue life of welded components simply and accurately. Various methods for predicting the fatigue life of arc welded parts have been proposed by various organizations and researchers. In recent years several fatigue analysis software tools have been released, and are being adopted gradually in the field of CAE-based durability simulation, but the applicability of these tools to thin steel sheet structures has not been sufficiently validated. In this paper the fatigue life prediction accuracy of the fatigue analysis software FE-Fatigue supplied by nCode International was evaluated by reference to corresponding experimental results concerning arc welded specimens and several types of arc welded structures. Also we attempted to calculate the fatigue lives of arc welded joint specimens using the prediction method developed by the JSAE fatigue and reliability committee to compare the corresponding results as calculated by FE-Fatigue. The JSAE prediction method is one that is based on determining the size of the cyclic small scale yield area at the weld toe.

2 OUTLINE OF PREDICTION SYSTEM

The prediction method implemented in FE-Fatigue is based on that proposed by the Volvo Car Corporation and Chalmers University of Technology [1]. For the FE analysis, arc welds are modelled as shell elements, and the structural stresses used in this method are derived from the principal stresses of these shell elements. The structural stress at the weld toe is effective in correlating the fatigue strength of arc-welded sheet structures. This method determines the contribution of bending to the total stress and determines whether the welded parts are essentially “flexible” or “stiff.” There are two distinct S-N curves in this software. Equations (1) and (2) are used to distinguish between the “flexible” and “stiff” cases, by setting a threshold value with the flex ratio r. The default value for this threshold in the software is 0.5.

$$r = \frac{|\sigma_b|}{|\sigma_b| + |\sigma_n|} \qquad (1)$$

$$\sigma_b = (\sigma_{top} - \sigma_{btm})/2 \qquad \sigma_n = (\sigma_{top} + \sigma_{btm})/2 \qquad (2)$$

σ_{top}, σ_{btm} : Maximum principal stresses from the top and bottom surface of the weld toe elements

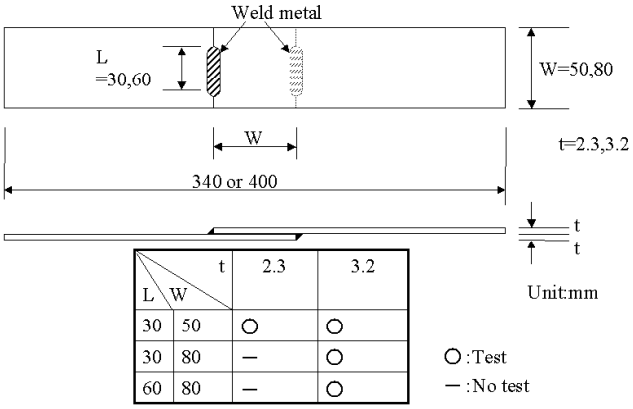
In this paper, by using the ω* method [2,3] based on determining the size of the cyclic small scale yield area at the weld toe, the fatigue lives of arc welded joint specimens were estimated and compared with FE-Fatigue. This method assumes that the toe of an arc-weld is a sharp notch and uses the stress singularity that occurs at the notch tip. ω* value can be calculated by Equations (3), see Figure 6.

$$\omega^* = \frac{1}{1-\lambda}\sqrt[\lambda]{\frac{K}{2\sigma_y}} \qquad \sigma = \frac{K}{r^{\lambda}} \qquad (3)$$

K : local stress parameter
λ : local stress singularity index
r : distance from the toe on the flank angle bisecting line
σ_y : static yield stress

3 EXPERIMENTAL FATIGUE DATA

The arc welded lap joint specimens with weld start and end points were prepared and fatigue tests on these specimens were conducted to verify the validity of FE-Fatigue. There are two types of specimens as shown in Figure 1 and Figure 2. One is the two-sheet arc welded lap joint, and the other is the three-sheet arc welded lap joint. In terms of the two-sheet arc welded lap joint specimens, four types of configurations were prepared as shown in Figure 1. These specimens were made from a 440MPa grade hot rolled steel sheet. Table Ⅰ shows the chemical compositions and mechanical properties of steel. The tension load was controlled with a load ratio of 0.1. Strain gauges with a gauge length of 1mm were placed at four points in the vicinity of the weld toe to monitor the changes in dynamic strain during fatigue tests. In this investigation the time point when the strain range is reduced by 20% was defined as the crack initiation life Nc. A small piece of sheet with the same thickness as the specimen was placed on the clamped area to avoid out of plane deformation. Figure 3 shows photographs of typical examples of tested specimens. At the start point of the weld bead the crack propagated along the curve of the weld toe. It is possible for the stress concentration to affect the crack propagation path. It was also confirmed that the strain range reduction of the gauge near the start point was comparatively earlier than that of the other gauge. Therefore, the crack might initiate at the start point of the bead. Moreover, the fatigue lives of several types of arc-welded structures were calculated using FE-Fatigue and the prediction accuracy was evaluated based on the experimental results presented by the JSAE fatigue and reliability committee [4,5]. Configurations and loading directions of arc welded structures are shown in Figure 4.



L	W	t = 2.3	t = 3.2
30	50	○	○
30	80	—	○
60	80	—	○

Figure 1. Schematic representation of two-sheet arc welded lap joints with weld start and end points.

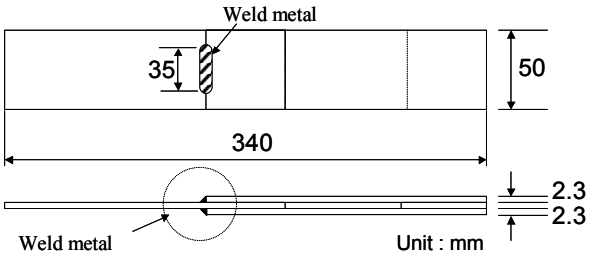


Figure 2. Schematic of three-sheet arc welded lap joints with weld start and end points.

Table Ⅰ. Chemical compositions and mechanical properties of base metals

Steel	Thickness (mm)	Chemical compositions (wt%)					Mechanical Properties*		
		C	Si	Mn	P	S	Yield stress	Tensile strength	Elongation
440MPa Class	2.3	0.14	0.01	0.42	0.011	0.0054	306	430	36.5
	3.2	0.13	0.09	0.76	0.018	0.0035	323	474	34.7



Figure 3. Photograph of typical tested specimens

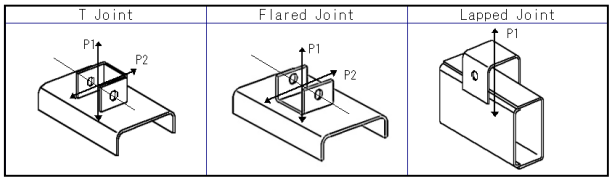


Figure 4. Schematic of arc welded structures studied by JSAE

4 FE MODEL

When using FE-Fatigue, arc welded structures are modelled by shell elements as described in the previous subsection. The FE models of arc welded parts are shown in Figure 5. MSC.Nastran was applied for calculation. Contact was not taken into account and 3 dimensional elastic FE analysis was performed. When using the ω* method based on determining the size of the cyclic small scale yield area at the weld toe, the FE model of the steel sheet parts and welding parts consisted of solid elements. The FE solid models of arc-welded lap joints are shown in Figure 6. In the same manner, contact was not taken into account and 3 dimensional elastic FE analysis was conducted. The flank angle of the weld bead was defined as 135°. The cross section which suffered maximum stress at the weld bead was modelled by a element with mesh size of around 0.001mm in order to calculate the ω* value at the weld toe. Displacement data calculated by 3D analysis was used for the boundary conditions of the 2D plane stress models and the stress distribution in the vicinity of the weld toe was calculated. The ω*-N diagram obtained by Koibuchi et al. [2] was used for calculating the fatigue lives of these joints. Since the load ratio R is 0.1 in the lap joints' fatigue test, the load range was adopted for the loading condition of 3D elastic analysis [6]. As shown in Figure 6, the maximum stress points occur at the weld start and end points in every case.

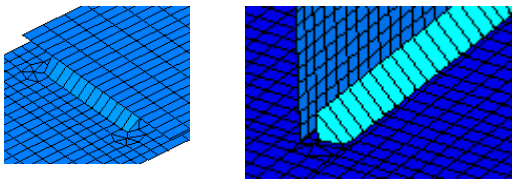


Figure 5. Schematic representation of FE models of arc-welds for FE-Fatigue

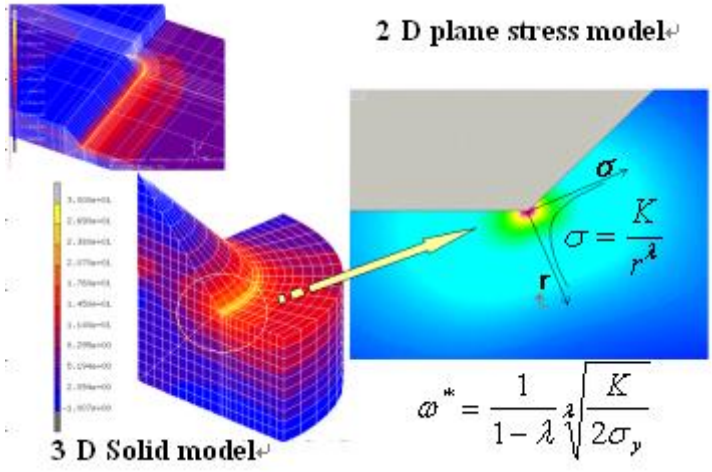


Figure 6. Schematic representation of FE models for arc-welded lap joints with weld start and end points for the ω* method

5 RESULTS OF PREDICTIONS

The L-N diagrams for each two-sheet arc welded lap joint with weld start and end points show the comparison between the predicted and experimental results in Figure 7～9. Fatigue lives predicted by FE-Fatigue were higher than the experimental results and predicted values did not agree with the experimental results. On the other hand, the fatigue lives predicted by the ω* method were in good agreement with the experimental results. In every case the flexibility ratio values r used in FE-Fatigue were above 0.9. Since the lap joints' fatigue tests were determined to be flexibile cases, which were subjected mainly to bending stress, the fatigue lives were calculated based on the "flexible curve" in FE-Fatigue. All the experimental results for the two-sheet arc welded lap joints are summarized in the SN diagram in Figure 10, where the vertical axis $\Delta\sigma$ denotes the structural stress range calculated by FE-Fatigue. It was revealed that the experimental results were lower than the fatigue strength of the flexible curve.

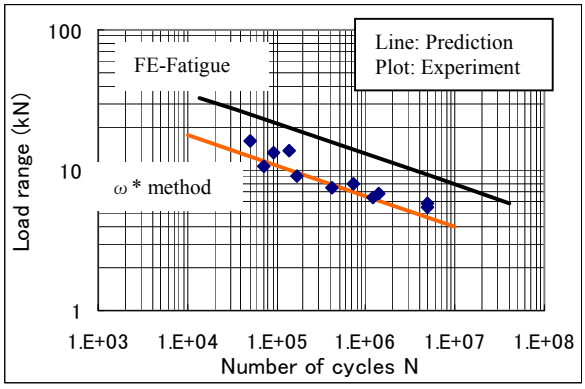


Figure 7. Comparison between predicted and experimental results for two-sheet lap joints (L=30mm, W=50mm, t=2.3mm)

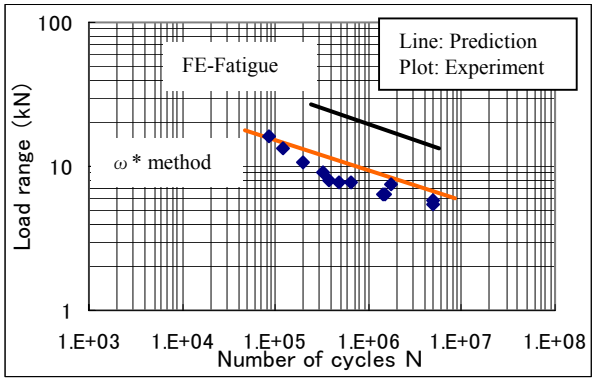


Figure 8. Comparison between predicted and experimental results for two-sheet lap joints (L=30mm, W=50mm, t=2.3mm)

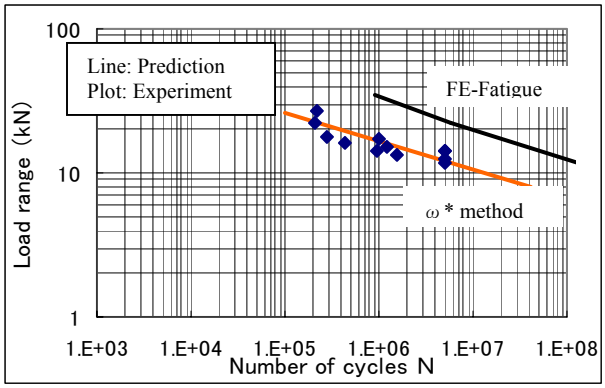


Figure 9. Comparison between predicted and experimental results for two-sheet lap joints (L=30mm, W=50mm, t=3.2mm)

Also the fatigue lives of arc welded structures studied by JSAE, such as T-joint, flared joint, and overlapped joint, were predicted using FE-Fatigue. All the experimental results for several arc-welded structures studied by JSAE are summarized in the SN diagram in Figure 11. The experimental results studied by JSAE and the regression line of the arc welded lap joints' fatigue data were correlated. It was revealed that the all the plotted points fell within a certain band if one used the structural stress range $\Delta\sigma$. Moreover, the experimental data for the three-sheet arc welded lap joints are summarized in the SN diagram in Figure 12. In this case the flexibility ratio values r were less than 0.1. Since the three-sheet lap joints' fatigue tests were determined to be stiff cases, which are not subjected to bending stress, the fatigue lives were calculated based on the "stiff curve" in FE-Fatigue. It was revealed that the experimental results were lower than the fatigue strength of the stiff curve as with the two-sheet lap joints discussed above. Consequently, the experimental fatigue data did not agree with the flexible curve and stiff curve implemented in FE-Fatigue regarding arc welded lap joints and arc-welded structures. A full explanation of this is beyond the scope of this paper, but the discrepancy might be due to the fact that both lap joints and JSAE arc welded structures have start and end points at the weld bead. According to the previous study [1], it seemed that the arc welded structures which did not have the weld start and end points are mainly used for taking S-N curves, such as the flexible curve and the stiff curve. Therefore, we proposed that the regression curves ($\Delta\sigma = 6372.7N^{-0.2088}$, $\Delta\sigma = 5564.1N^{-0.2544}$) of the lap joints' fatigue data were used instead of the flexible curve and stiff curve implemented in FE-Fatigue in cases where the fatigue lives are calculated for arc welded structures with the weld start and end points. In FE-Fatigue the S-N database can be edited and created easily. The L-N diagram in Figure 13 is one such example of the prediction results for arc welded structures studied by JSAE. These experimental results show the influence of steel sheet thickness on the fatigue strength. The broken lines indicate prediction results based on the implemented default of the flexible curve, and the solid lines are based on the modified flexible curve. The predicted results agreed qualitatively with the experimental results when one modified the flexible curve. Since the vertical axis denotes the load amplitude, the fatigue strength is proportional to the steel sheet thickness and the predicted results show this behavior.

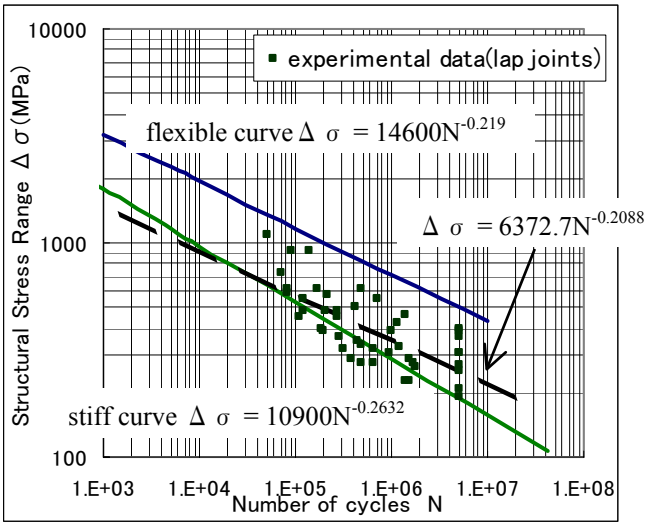


Figure 10. $\Delta\sigma$-N curve with experimental data of two-sheet arc welded lap joints

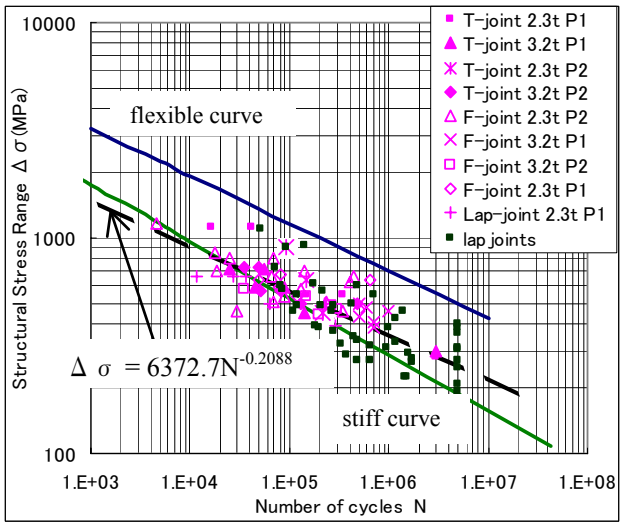


Figure 11. $\Delta\sigma$-N curve with experimental data of arc welded structures studied by JSAE

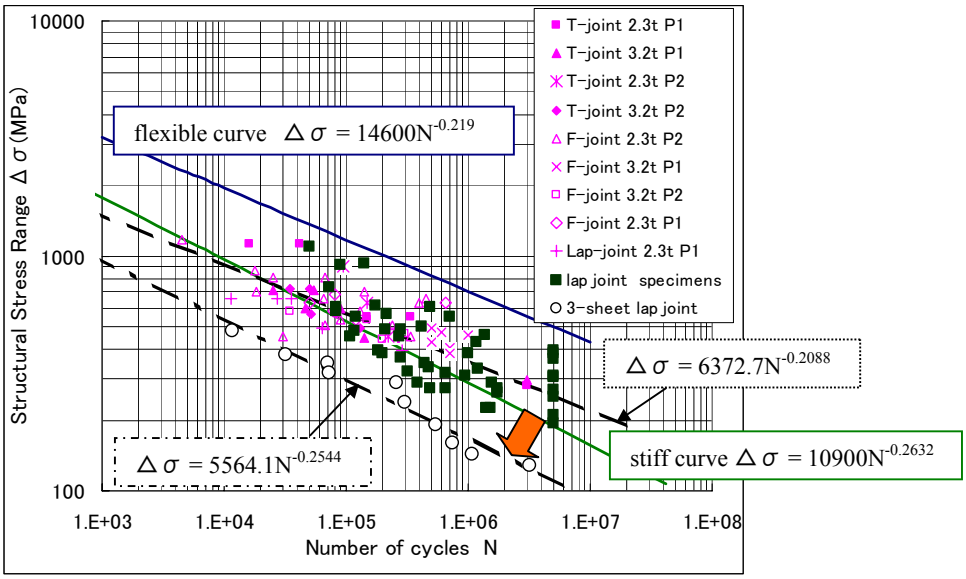


Figure 12. Δ σ -N curve with experimental data of three-sheet arc welded lap joints

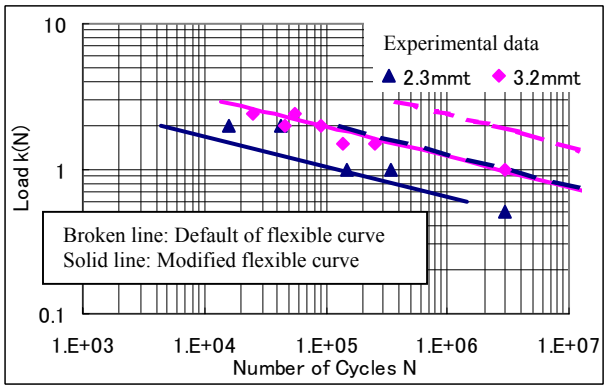


Figure 13. Comparison between predicted and experimental results for T-joint with P1 Load

6 APPLICATION FOR THE COMPONENT

Using FE-Fatigue we attempted to calculate the fatigue life of the automobile chassis component with some brackets. The cyclic load ±6kN in the front-back direction was applied to the chassis component through the lower arm. The maximum stress range occurred at the toe of the welds of the lower arm bracket and the arc weld bead of the lower arm bracket has the weld start and end points. Since the flexibility ratio r was around 0.3 in terms of the arc weld bead of the lower arm bracket, stiff curves were used for fatigue life predictions in FE-Fatigue. Calculations indicated that the fatigue failure would occur after 20,500 cycles on the edge of the arc weld of the bracket using the stiff curve which had been modified in accordance with the experimental fatigue data for the three-sheet arc welded joint specimens. Using the default stiff curve implemented in FE-Fatigue, calculations showed the fatigue failure would occur after 189,000 cycles. In parallel the laboratory fatigue test was performed to examine the durability and the fatigue failure in the vicinity of the welds of the lower arm bracket was observed after 15,000 ~20,000 cycles under the load range of ±6kN. It was revealed that the calculated result was in good agreement with the test result using our proposed method.

Furthermore, we attempted to investigate the influence on improving the shape of the lower arm bracket in order to enhance the fatigue strength of this chassis component using our proposed method above. The improved bracket shape which has the removed part in the center of the bracket is shown in Figure 14 . It was revealed that the maximum stress region shifted from the edge of the arc weld to the removed part of the bracket owing to the change in the bracket shape. The calculation predicted that the fatigue failure would occur after 85,900 cycles on the edge of the arc weld of the bracket and the fatigue life of the chassis component with the improved bracket would be around four times greater than that with the original bracket. This should be compared with the laboratory test. According to the test result, the fatigue failure near the removed part of the bracket was observed after 99,500 cycles under the load range of ±6kN. The calculated fatigue life was in good agreement with the test result, but it was different between the calculation and the test result in terms of the fatigue failure position. Consequently, the improved bracket was both numerically and experimentally revealed to be a good replacement for the original bracket thanks to increasing the fatigue strength.

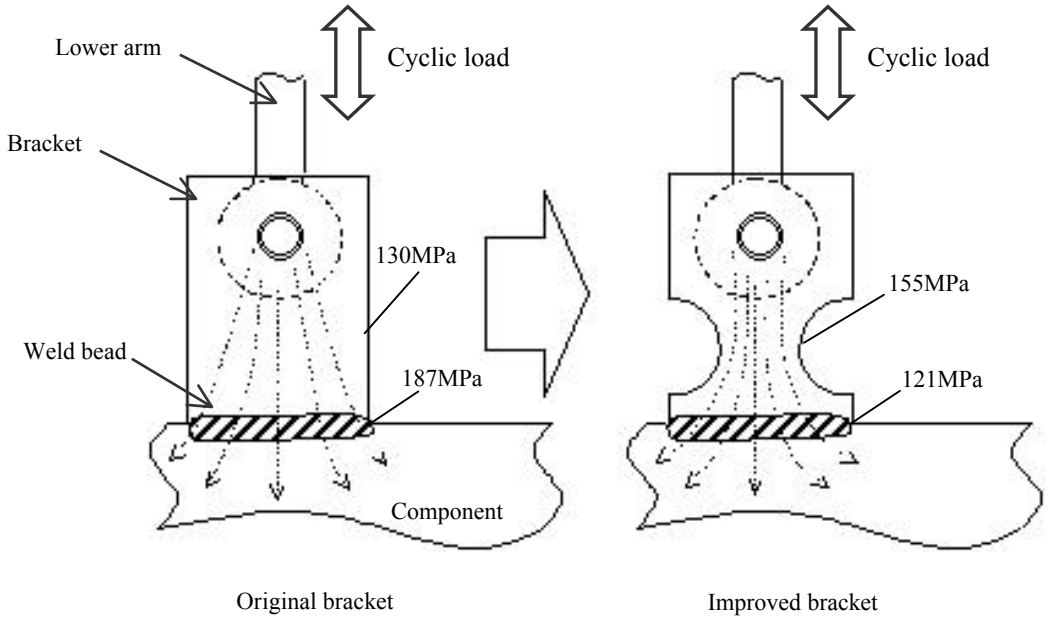


Figure 14. Schematic of the improved bracket shape

7 CONCLUSION

The fatigue lives of arc welded joints and structures were predicted using FE-Fatigue and these predicted results were validated by comparing them with corresponding experimental data. In terms of arc welded lap joints with weld start and end points, the predicted results do not agree with the experimental results using the default of the SN data of "flexible curve and stiff curve" implemented in FE-Fatigue. On the other hand, results predicted using the ω* method are in good agreement with the experimental results. With the arc welded automobile component , the predicted results are in good agreement with experimental results provided that the SN data of "flexible curve and stiff curve" has been modified in accordance with the experimental fatigue data for arc welded lap joints with weld start and end points. Also using our proposed method above, it is possible to enhance the durability of the chassis component by improving the bracket shape.

8 REFERENCES:

1. Fermér, M., Andréasson, M., Frodin B. "Fatigue Life Prediction of MAG-Welded Thin-Sheet Structures," IBEC '98., 1998, SAE Technical Paper 982311
2. Koibuchi, K., To, K., Iida, M., Hosomi, T. "Fatigue Strength Assessment at Weld Toes and Defects of Structures Based on Cyclic Plastic Zone Size," Engineering Against Fatigue, 1997, CHAPTER 40: 377-379 references over these paragraphs.
3. Hirata, T., Nakamaru, T., Magara, S., Akasaki, T., Toyama, K et al., "A Study on the Cyclic Plastic Zone Size Method, ω^*, for Digital Fatigue Life Prediction of Arc-Welded Joints," IBEC '03 Conf., Oct. 27-29, Chiba, Japan, 2003, SAE 2003-01-2835, 343-348.
4. Kasahara, T., Maruo, Y., Nakamaru, T., Magara, S., Koibuchi, K., "Method of Fatigue Life Estimation for Arc-Welded Structures," SAE 2000 World Congress, Mar.6-9, Detroit, Michigan, 2000, 2001-01-0781.
5. Shinmura, R., Werkhausen, A., Urakawa, K., "Fatigue Life Prediction of Arc-Welded Structures of Automobiles by CAE," Proceedings of the 2001 Annual Congress of JSAE, 2001, 20015188 (in Japanese).
6. Usami, S., Shida, S., "Elastic-Plastic Analysis of The Fatigue limit For A Material with Small Flaws," Fatigue of Engineering Materials and Structures Vol.1, pp. 471-481,1979.

Strain Analysis on an Al-Foam Structure with ESPI

Eberhard Moser[a], Hermann Buschermöhle[b] ,Andreas Ettemeyer[a]
[a]Dantec Ettemeyer GmbH, Kässbohrerstr. 18, 89077 Ulm, Germany
[b]Wilhelm Karmann GmbH, Karmannstraße 1, 49084 Osnabrück, Germany

1. ABSTRACT

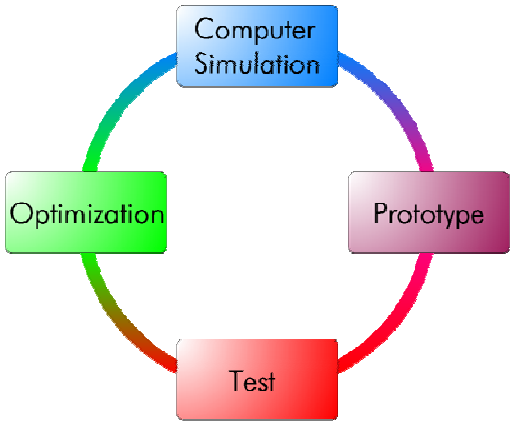
The motivation of the study was the demand for light weight designs in automotive techniques, as well as the enhancement of the stiffness of convertible bodies and an improvement of the FEA elements and methods. Hence follow a acceleration of component design.



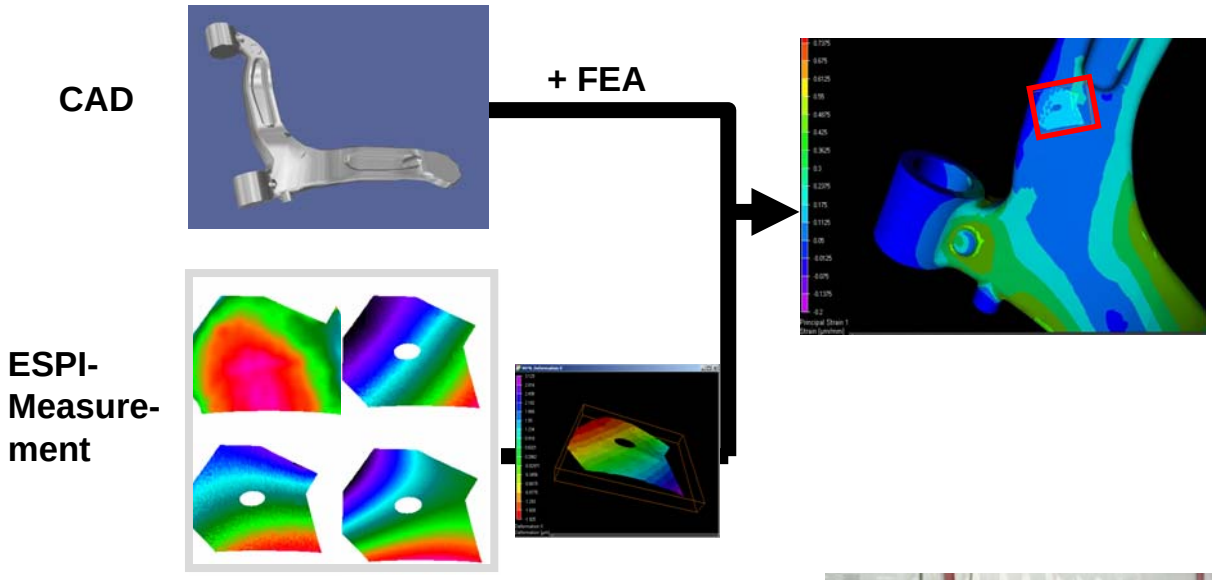
Fig. 1 Development time of the new crossfire: 18 months!

2. INTRODUCTION

By the use of **Dantec Ettemeyer Products** the development cycle can be improved. The proven validity of ESPI technique allows the validation of simulation. It shows the applicability of this concept in the design phase in the generation of a new prototype. The closure and abbreviation of the development cycle is provided by a correlation of simulation and experiment and allows a acceleration of the development cycles.



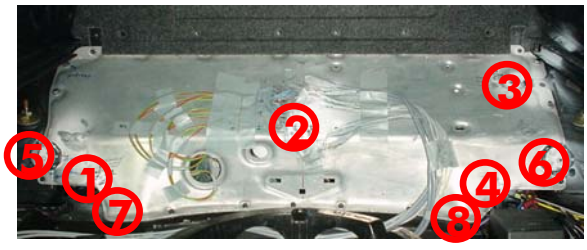
By means of the **ESPI Technique** and the included VRML Module the graphic information, given by the measurement results of **ESPI** measurement, can be mapped on CAD and FEA Data. This allows a comparision between **ESPI** and FEA data.



Measurement Procedure:
The rear plate of a Mercedes- Benz CLK Model was identified as a critical area. As main goals of the measurement were determined the validation of critical areas and the resulting improvement of FEA Models. The required data of the critical areas were delivered by the Dantec Ettemeyer Q-100 strain/ stress measuring device.

Contact points of the foamed aluminium structure and the car body were determined as measuring areas.





Foamed aluminium structure of a rear plate of a Mercedes-Benz CLK model with indicated measuring areas

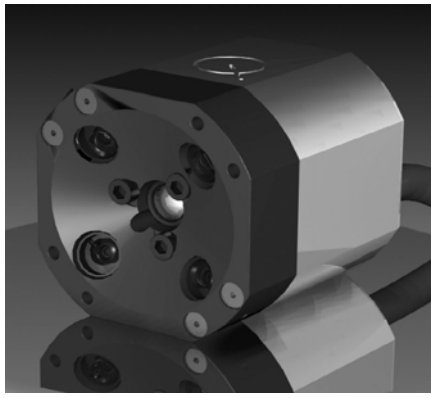
Torsion load was applied by the test bench. 8 measuring Positions were determined.



1 2

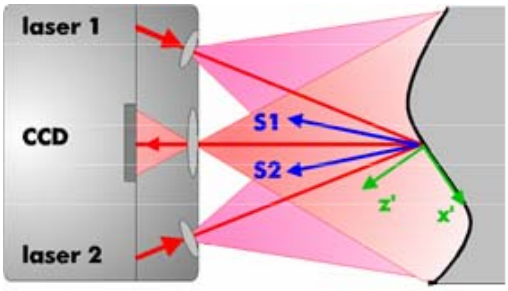
Scheme of torsion load; Numbers indicate the applied torsion load condition

The measurement device: **Dantec Ettemeyers Q-100**



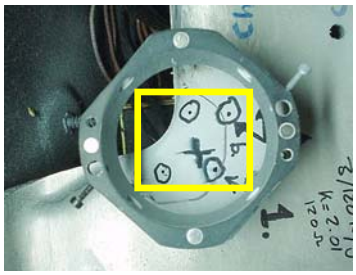
The measuring sensor provides a full field laser illumination of 4 directions which delivers a 3D information of the specimens surface. With the redundant 4 th illumination 3D information is extractable on even difficult shapes. The reflected beams of the surface are observed by the CCD camera.

This features allow that the complete 3D Contour and 3D Deformations can be recorded while loading the specimen. With the measured results of displacement the strain information can be extracted by mathematical transformation. In addition the e.g. “van Mises” stress information can be displayed by entering the material parameters (E-Modul and poissons ratio).

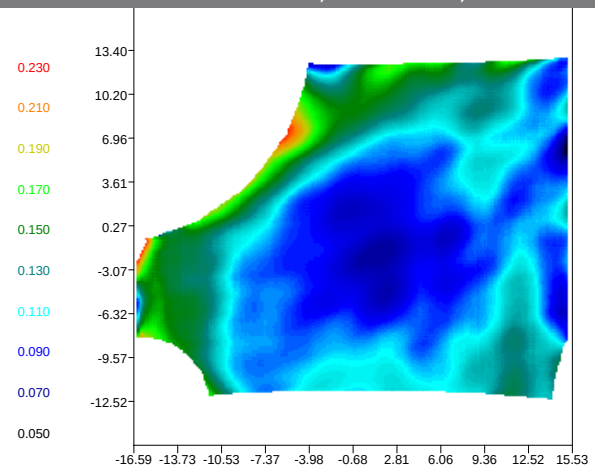


Measurement Results:

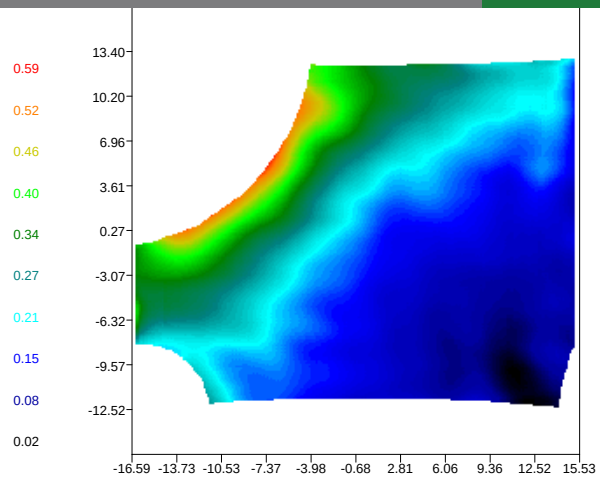
The image on the right shows the corner of position 1. The Measurement results indicate the principle strain 1 under 2 torsion load conditions.



L:\BERICHTE\BEITRÄGE\2005\Cetim Fatigue Nov.05\Manuscript Strain Analysis.doc 30.06.05 EMR

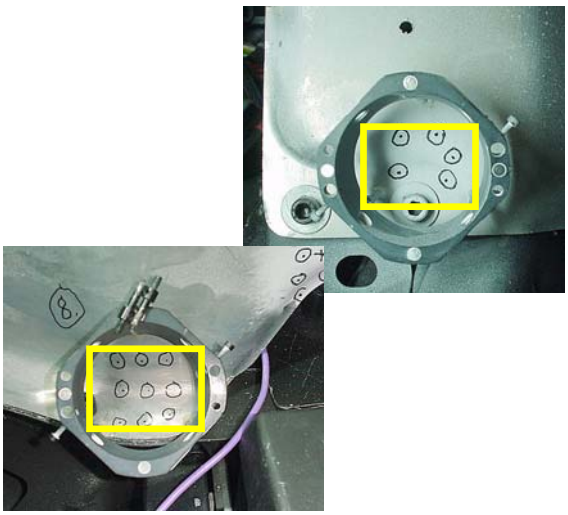


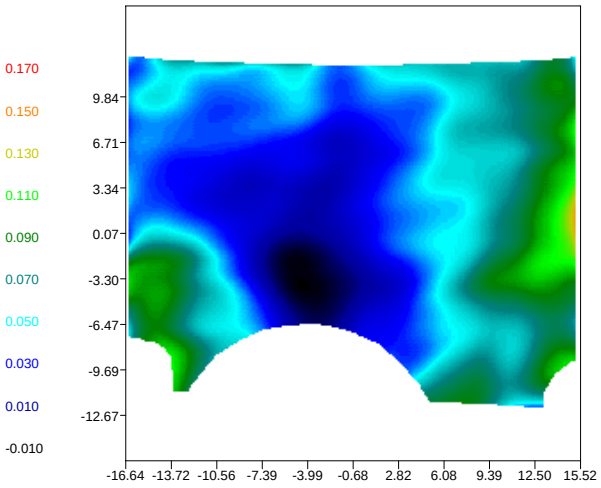
Loading Condition 1



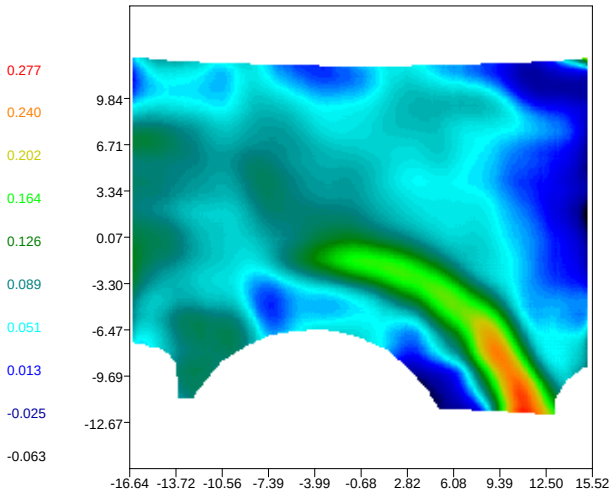
Loading Condition 2

The image on the right shows the measuring field of position 6 of the right side on the stucture. The Measurement results indicate the principle strain 1 under 2 torsion load conditions.



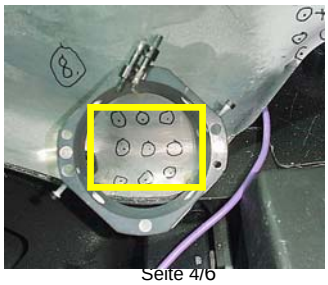


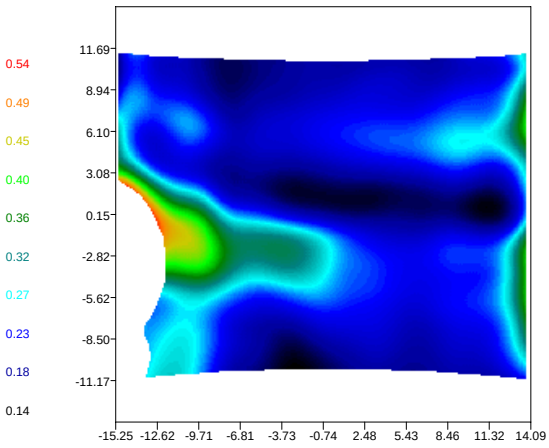
Loading Condition 1



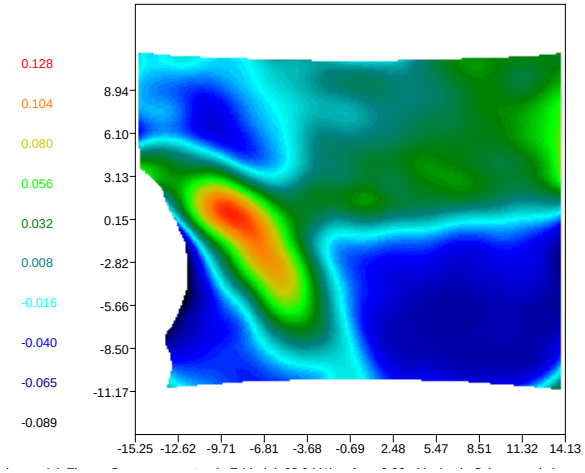
Loading Condition 2

The image on the right shows the measuring field of position 6 of the lower right side on the stucture. The Measurement results indicate the maximum principle strain under 2 torsion load conditions.





Loading Condition 1

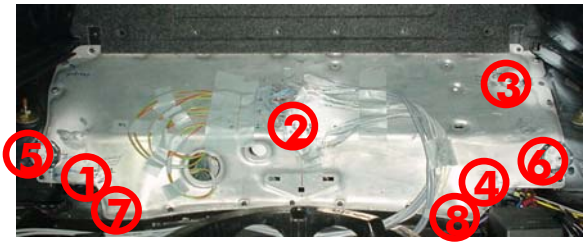


Loading Condition 2

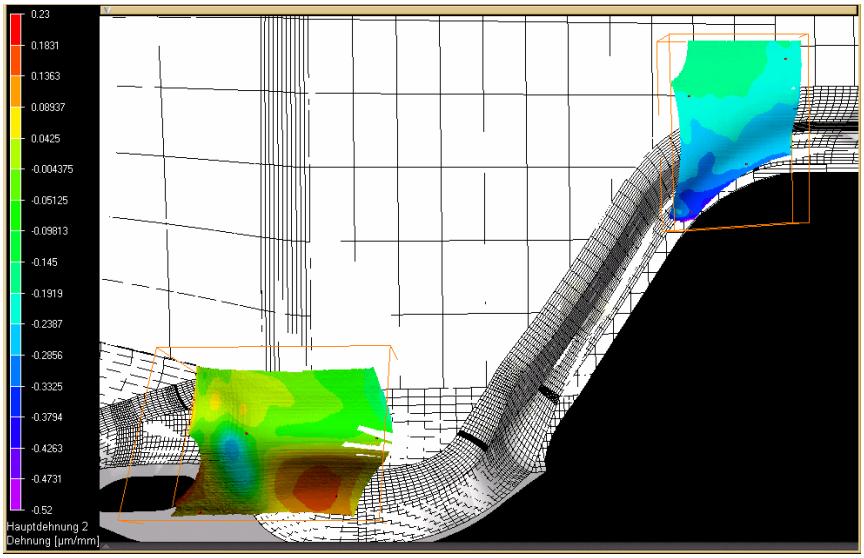
Introduction of all measuring areas in one VRML-File:

As above mentioned the ISTRA Software, based on all ESPI Systems, is able to map the measured results with the CAD and FEA data as an overlay view.





The image indicates the different measuring fields from position 1 to 8 introduced into the VRML Player



The image shows an overlay of the maximum strain fields onto the CAD information in position 4 and 8

3. SUMMARY AND RESULTS:

- Critical areas of a new aluminium foam structure were analysed, where conventional measuring techniques could not be applied
- Comparison between ESPI measurement and FEA was successfully done
- The idea to combine simulation and ESPI measurement in fatigue testing proved to be a positive concept for future applications

An Experimental Study on Corrosion-Fatigue-Crack-Propagation Behaviour of 2024-T3 Aluminium Alloy

Bao Rui, Zhang Jiangyu, Zheng Xiaoling, Fei Binjun

School of Aeronautic Science and Technology, Beihang University, Beijing, 100083, PR China

Abstract Corrosion-fatigue-crack-propagation behaviour of 2024-T3 aluminium alloy was studied in this paper. Some typical experiments of fatigue-crack-propagation in both laboratory air and two kinds of aggressive environments with CC(T) specimens are conducted and reported, and the results show the significantly increasing of fatigue-crack-growth rate by the environment. A description way based on modified form of Paris law is presented to describe the corrosion-fatigue-crack-growth rate in both mono-medium and aggressive environments. Moreover, the methodology to predict corrosion-fatigue-crack-propagation life with certain reliability in composite environments is established.

1 INTRODUCTION

Corrosion is one of the important structural integrity concerns of aircrafts. Failure under fluctuating loads of aircraft structural components subjected to an aggressive environment, which is caused by the initiation and propagation of corrosion fatigue cracks, is more dangerous than that in benign environment for the crack initiation and propagation behaviour is changed under corrosive environments and crack initiation and propagation life is greatly reduced. Corrosion-fatigue damage occurs more rapidly than would be expected from the individual effects or from the algebraic sum of the individual effects of fatigue, corrosion, or stress-corrosion cracking. Despite the significant progress that has been achieved to establish the effects of various mechanical parameters on the corrosion-fatigue behaviour, the description method of crack growth laws as well as the prediction of corrosion-fatigue-crack-propagation life and its reliability are still persecuting aircraft designers.

2024-T3 Aluminium alloy is widely used as structural materials in aerospace industry due to its low weight, high strength and good corrosion resistance. However, in the presence of aggressive environments, it is subjected to localized corrosion, which often induces crack initiation and accelerates crack propagation of corrosion fatigue (CF) so as to shorten the service life and even result in catastrophic accidents. Significant developments in understanding the corrosion-fatigue-crack-propagation behaviour of 2024 aluminium alloy in gaseous and aqueous saline environments have been made by using linear-elastic-fracture-mechanics methodology. Most of the previous research conducted in the area of corrosion-fatigue involved the study of fatigue crack growth behaviour in mono-medium environment and the study of the influence of loading frequency on crack growth rate. Little attention has been paid to understanding the influence of composite aggressive environments and the crack growth life prediction method as well as its reliability estimation in this condition.

In this paper, some typical experiments of corrosion-fatigue-crack-growth in both laboratory air (i.e. reference environment) and two kinds of aggressive environments (wet air and 3.5% NaCl solution) are conducted and reported. The work was carried out on centre-crack-tension (CC(T)) specimens made from 2024-T3 aluminium alloy. Based on these test results, attempts have been made to describe the crack growth rate in mono-medium and composite environments properly, and the corrosion-fatigue-crack-growth life prediction methodology with certain reliability is discussed.

2 EXPERIMENTAL WORK

2.1 Specimen

The test material 2024-T3 aluminium alloy had the following analysis values: Si(0.5%), Fe(0.5%), Cu(3.8%-4.9%), Mn(0.3%-0.9%), Mg(1.2%-1.8%), Cr(0.1%), Zn(0.25%), Ti(0.15%), other(0.15%), Al(balance). It had yield strength of about 335MPa, tensile strength of about 470MPa.

Centre-crack-tension specimens were used. The shape and dimensions of the specimen are given in Figure1.

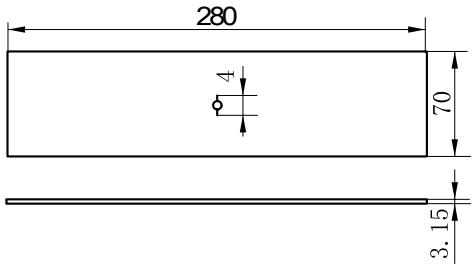


Figure 1. CC(T) specimen configuration used in the experiments; all dimensions in mm.

2.2 Test procedure

All fatigue tests were conducted at constant stress amplitudes and a frequency of 2 Hz, and the load ratio was 0.2. Crack growth procedures were observed with reading microscope, and fracture morphologies of the specimens in different media were observed and analyzed by a scanning electron microscope.

Corrosion-fatigue tests were conducted in laboratory air, which is the reference environment, and in wet air and saline frog, these two kinds of aggressive environments were made by spraying pure water and 3.5% NaCl solution. The solution was aerated and circulated from and to reservoirs via a corrosion cell fitted on to the specimen. The sketch map of the equipments was shown in Figure 2.

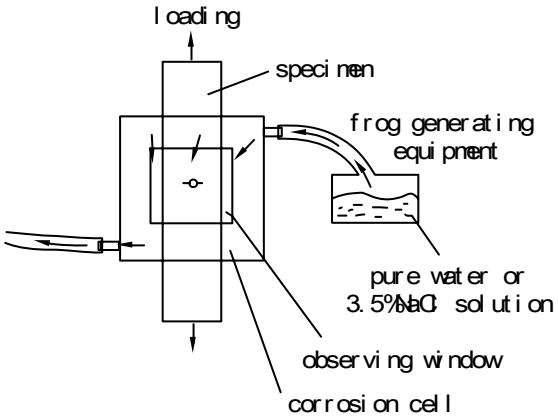


Figure 2. Sketch map of environment equipments.

The test was stopped at pre-selected intervals and the observing window was opened for registering the position of crack tip. A typical test procedure is shown in Figure 3. The procedure satisfies the requirements of GB/T6398-2000.

3 RESULTS

3.1 Crack growth rate

Crack growth behaviour was studied by examining a series of displacements of crack tip on the surface of the specimen and the corresponding loading cycles. Then the crack growth rates of 2024-T3 aluminium alloy in environments of laboratory air, wet air and saline frog can be got. Figure 4 shows the relationship between da/dN and ΔK. When the stress intensity factor range (ΔK) is between 8 and 20 MPa$\sqrt{\text{m}}$, the relationship of the crack growth rate and ΔK is almost a linear function in double logarithm coordinate. It is easily seen that the crack growth rate increased gradually with the aggravating of environment causticity.

3.2 Fracture morphology

The fracture morphologies in different environments are shown in Figure 5 and 6. The figures show that the fracture morphology in aggressive environment has significantly different characteristics comparing with that in benign environment. At the stages of crack initiation and early crack propagation, there were many corrosion pits and some corrosion deposits on the fracture surface. At the medium propagation stage, a few of corrosion deposits and fatigue striation were found at the same time. At the late propagation stage, it tends to put up brittle fracture characteristics in corrosive environment other than toughness characteristics in laboratory air environment.

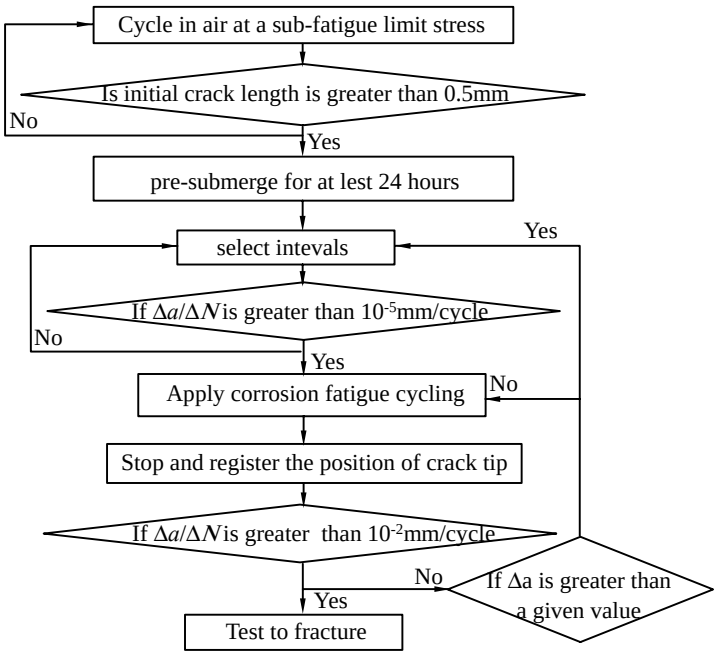


Figure 3. Test procedure.

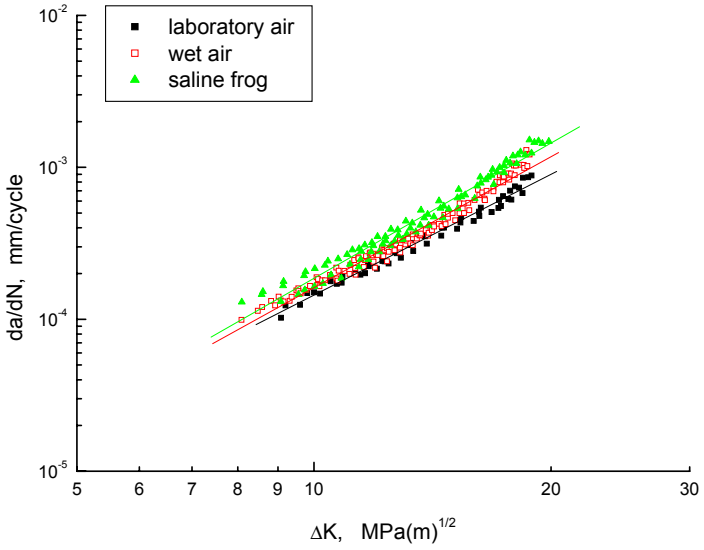
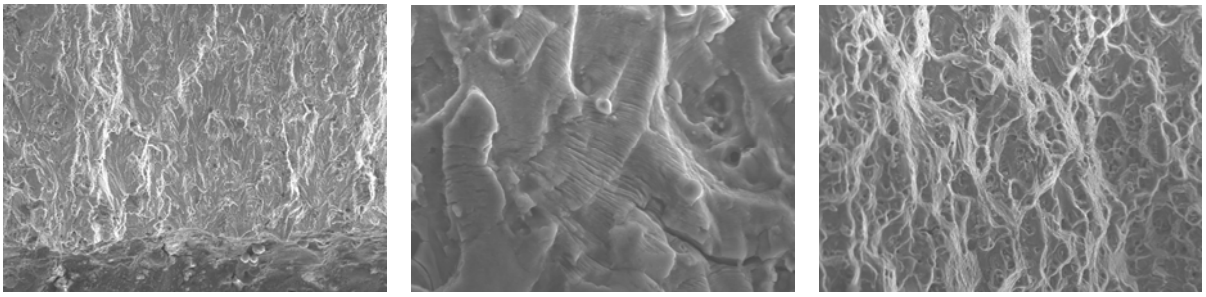


Figure 4. The relationship between da/dN and ΔK for 2024-T3 aluminium alloy in three different environments.

4 DISCUSSION

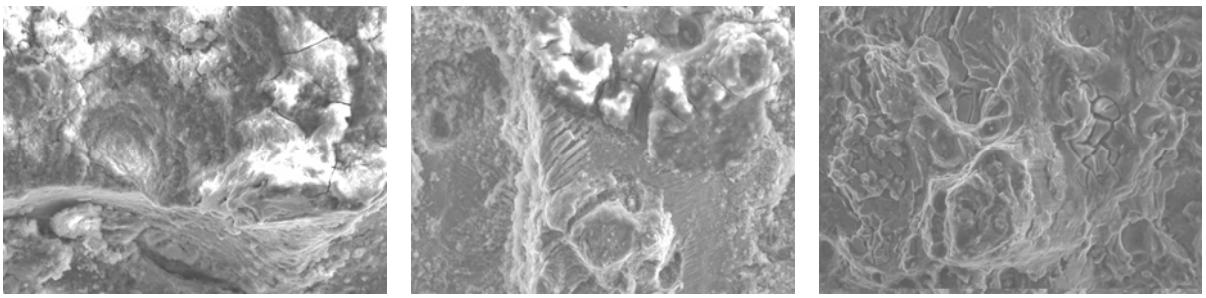
4.1 Description of crack growth rate in single medium environment

The generalized fatigue-crack-growth behaviour in a benign environment is a special case of the corrosion-fatigue-crack-propagation behaviour for metals. It represents the "corrosion-fatigue" behaviour of metals subjected to load fluctuations in the presence of any environment that does not affect the fatigue-crack-growth behaviour for the metal. Thus the corrosion-fatigue for a given environment-material system could be investigated by establishing the base-line fatigue behaviour and then by determining the effect of the environment on the fatigue behaviour.



a) fountains of crack | b) crack growth | c) fracture

Figure.5 Fracture morphologies of different propagation stages for 2024-T3 in laboratory air



a) fountains of crack | b) crack growth | c) fracture

Figure.6 Fracture morphologies of different propagation stages for 2024-T3 in saline frog

The crack growth rate of the propagation stage in benign environment can be expressed by Paris law as shown in Equation 1.

$$\frac{\mathrm{d}a}{\mathrm{d}N} = C\left(\Delta K\right)^n \tag{1}$$

It is easily seen from Figure 4 that the crack growth rate in aggressive environments is faster than that in reference environment when ΔK is the same. So the form shown in Equation 2 is acceptable to describe the accelerated crack growth rate.

$$\frac{\mathrm{d}a}{\mathrm{d}N} = \gamma C\left(\Delta K\right)^n \tag{2}$$

Further more, it is observed in the tests, and also mentioned in some achievements, that the corrosive environments affect the corrosion-fatigue crack initiation, small crack growth and threshold value of stress

intensity factor K_C. Thus, the modified Paris law to describe the corrosion-fatigue crack growth rate can be written as Equation 3.

$$\frac{\mathrm{d}a}{\mathrm{d}N} = \gamma C\left(\Delta K + B\right)^n \tag{3}$$

where, C and n have the same value with that in reference environment, γ and B are corrosion correction parameters.

There are also some other existing forms of functions to express the relationship of crack growth rate da/dN and ΔK in corrosive environment, such as:

$$\frac{da}{dN} = C_e\left(\Delta K - \Delta K_{the}\right)^2 \tag{4}$$

Based on the test results, the value of all the parameters in Equation 1-4 in the above-mentioned three environments are given in Table I. Where R is the correlation ratio.

Table I. Results of parameters fitting.

	Equ.1	Equ.2	Equ.3	Equ.4
Laboratory air	C=3.3008×10^{-7} n=2.64044 R=0.99179	γ=1 R=0.99179	γ=1 B=0 R=0.99179	C_e=2.99176×10^{-6} K_{the}=3.09195 R=0.97971
Wet air		γ=1.18945 R=0.95685	γ=1.41451 B=-0.81193 R=0.97025	C_e =3.8935×10^{-6} K_{the} =3.50037 R=0.95805
Saline frog		γ=1.4158 R=0.95874	γ=1.82597 B=-1.194 R=0.97859	C_e =4.95745×10^{-6} K_{the} =3.8074 R=0.96690

From the results shown in Table I, it can be concluded that Equation 3 is more efficient to describe the corrosion-fatigue-crack-growth rates for its high correlation ratios in both wet air and saline frog environment.

That γ is grater than 1 shows that the crack growth is accelerated by the causticity of the environments, and B is negative illustrates the lowering action by the environments on the threshold value of stress intensity factor. The effect of γ is more significant than that of B on crack growth rates.

4.2 Crack growth rate in composite environment

The composite environment is too complex to be studied. For engineering simplification, a composite environment can be considered to be made up of several kinds of single medium, and each of them has its molar percentage y_i.

$$\sum y_i = 1 \tag{5}$$

And the crack growth rate in composite environment can be written as

$$\frac{\mathrm{d}a}{\mathrm{d}N} = \gamma C\left(\Delta K + B\right)^n$$
$$\gamma = \sum y_i \gamma_i \qquad (6)$$
$$B = \sum y_i B_i$$

Where γ_i and B_i are the corrosion correction parameters of *i*th kind of single medium environment.

For example, a kind of environment of aircraft structures is considered to be made up of 35% laboratory air, 60% wet air and 5% saline frog, and then the crack growth rate of the specimen in this environment can be considered reasonably to be:

$$\frac{\mathrm{d}a}{\mathrm{d}N} = 1.2900 \times 3.3008 \times 10^{-7} \times \left(\Delta K - 0.53609\right)^{2.64044} \qquad (7)$$

4.3 Prediction of crack growth life

By integration of Equation 3, the crack growth life can be predicted.

$$N = \int_{a_0}^{a_c} \frac{\mathrm{d}a}{\gamma C\left(\Delta K + B\right)^n} \qquad (8)$$

For this kind of CC(T) specimen,

$$\Delta K\left(a\right) = \frac{\Delta P}{B}\sqrt{\frac{\pi\alpha}{2W}\sec\frac{\pi\alpha}{2}} \qquad (9)$$

Where, a_0 and a_c are initial and critical crack lengths respectively. a_0 is determined by the means of NDI and a_c is respected to fracture criterion.

The value of a_0 is often selected to be 0.8 mm and the value a_c of different fracture criterion for the specimen in this experiment is shown in Table II.

Table II Values of a_c gained by different fracture criterion

	Fracture criterion		
	Net-section-stress criterion ($\sigma_{max} = \sigma_b$)	Critical-stress-intensity-factor criterion ($K_{max} = K_c$)	Crack growth rate criterion ($\mathrm{d}a/\mathrm{d}N < 10^{-2}$ mm/cycle)
a_c / mm	23	>35	18

Crack growth lives gained by prediction method and test are given in Table III. It shows that for this kind of specimen crack growth rate fracture criterion seems more efficient.

Table III Predicting crack growth life and testing values

	Laboratory air	Wet air	Saline frog
Testing life N_{50}	57368	49102	42465
Predicting life N_{c1} (a_c=23 mm)	61446	52726	45057
Predicting life N_{c2} (a_c =18 mm)	56235	48626	41712
$err1=(N_{50}-N_{c1})/N_{50}$	7.11%	7.38%	6.10%
$err2=(N_{50}-N_{c2})/N_{50}$	-2.0%	-0.97%	-1.77%

If randomicity of crack growth is considered, the fatigue-corrosion crack growth rate function can be written as

$$\frac{\mathrm{d}a}{\mathrm{d}N}=X\gamma C\left(\Delta K+B\right)^{n} \tag{10}$$

Where X is a lognormal random variable, the mean value of which is 1 and the log-standard-deviation is σ_z obtained from experiments.

The integration form of Equation (10) is

$$XN=\int_{a_0}^{a_c}\frac{\mathrm{d}a}{\gamma C\left(\Delta K+B\right)^{n}} \tag{11}$$

And

$$\lg N=\lg\left(\int_{a_0}^{a_c}\frac{\mathrm{d}a}{\gamma C\left(\Delta K+B\right)^{n}}\right)-\lg X \tag{12}$$

Then, the logarithm of prediction-crack-growth-life follows the normal distribution

$$\lg N\sim N\left(\lg\left(\int_{a_0}^{a_c}\frac{\mathrm{d}a}{\gamma C\left(\Delta K+B\right)^{n}}\right),\sigma_z\right) \tag{13}$$

5 CONCLUSIONS

The following conclusions may be drawn from the present study of corrosion-fatigue crack growth behaviour of 2024-T3 aluminium alloy under both laboratory air and aggressive environments (wet air and frog of 3.5%NaCl solution):

1. The crack growth rate of 2024-T3 aluminium alloy was accelerated significantly with the aggravating of the causticity of the environments, and the fracture morphologies in aggressive environments disappear clear corrosion characteristics.

2. The relationship of crack growth rate and stress intensity factor of stable crack growth stage in both benign and aggressive environments appears good linearity in double logarithm coordinate. The relationship can be expressed by a modified Paris law presented in this paper.

3. The crack growth life prediction method based on the modified Paris law is also presented in the paper, and the reliability estimation way is also discussed in a nutshell. Comparing with the test results, crack-growth-rate-fracture-criterion is more reasonable for this specimen-environment system.

6 REFERENCES:

1. R. Bao, A Study of DFR Method and Crack Growth Law under Corrosion Environments for Civil Aircraft Structures, PhD thesis, Beijing University of Aeronautics and Astronautics, 2005. (in Chinese)
2. J. M. Barsom, S. T. Rolfe, Fracture and Fatigue Control in Structures: Applications of Fracture Mechanics, ASTM 100 Barr Harbor Drive West Conshohocken, PA 19428-2959 U.S.A., 1999.
3. R. Wang, Corrosion Fatigue of Metals, Northwest Poly University Press, 2001. (in Chinese)
4. G. Murtaza and R.Akid, Corrosion fatigue short crack growth behaviour in a hogh strength steel, *Int. J. Fatigue*, 18(8), 1996, 557-566.
5. X. F. Liu, S. J. Hang, H. C. Gu, Crack growth behaviour of high strength aluminum alloy in 3.4% NaCl solution with corrosion inhibiting pigments, *Int. J. Fatigue*, 24(7), 2002, 803-809.

Fatigue Analysis and Experimental Verification of Aircraft Structural Joint

ZHAO Libin[1], BAO Rui[2], ZHANG Jianyu[2], FEI Binjun[2]

[1] School of Astronautics, Beihang University, Beijing, 100083, P.R.China
[2] School of Aeronautic Science and Technology, Beihang University, Beijing, 100083, P.R.China

Abstract Fatigue analysis and optimal structural design of the fatigue-prone parts in the whole aircraft structures are significant for safety life and economy of aircrafts. In this paper, to get the fatigue life of an aircraft structural joint, the numerical simulation based on the large-scale general software ANSYS is processed to find the maximum local stress concentration and the related fatigue theory to estimate the fatigue life is discussed. Then, a series of fatigue experiments of the aircraft joint structure were executed adopting the same fatigue cycle loads and environments with the computational case. The receivable relative error between the experimental result and the result of numerical analysis verifies the computational efficiency. The work in this paper lays a foundation for the further optimal structural design and the fatigue performance prediction of the aircraft structural joint.

1 INTRODUCTION

Fatigue analysis of aircraft structures is an important aspect taking into account the safety life and economy of aircrafts. The optimization design for the fatigue-prone parts of the structure can elongate the fatigue life of the aircraft obviously with only less increasing of the weight. The fatigue behaviors analysis of the aircraft structural joint, which belongs to fatigue-prone parts, is of greater importance for its criticality for flight safety of the whole aircraft structure. Now, fatigue failures in aircrafts are, in principle, prevented by design, testing, loads monitoring, inspection and the retirement of known fatigue-prone parts at scheduled intervals. With the development of the computers and the technique of the finite element method (FEM), the numerical analysis using FEM software has already been the primary means to predict the fatigue behaviors of structure and perform the structural optimization design, while the experiment analysis becomes an instrument to verify the computational validity.

In this paper, the fatigue life of an aircraft structural joint is discussed by numerical simulation and experimental method. To begin with this paper created the finite element (FE) analytical model of the aircraft structural joint based on the large-scale general software ANSYS and processed a non-linear static contact analysis. Then, the middle value of structural fatigue life based on the *S-N* curve with stress concentrate factor 1 was estimated according to the fatigue theory and the stress results of pre-mentioned analysis. At last, the experiments of the aircraft joint structure were executed adopting the same fatigue cycle loads and environments with the computational case. The receivable relative error between the experiment and the numerical analysis verifies the computational efficiency. The work in this paper lays a foundation for the further study on the local stress concentration and optimal design of fatigue-prone structural details.

2 THEORETICAL METHOD

2.1 Finite element method

All engineering structures will exist sharply break section inevitably for its self-structural characters, such as the step, hole, etc. Local stress concentration will occur near these regions due to applied loads. Lots of fatigue accidents and experimental researches show that the fatigue phenomenon always appears at the situation with high local stress concentration. Since the FEM can compute the stress or strain at surface or inside of structure exactly [1]. It is always used to do fatigue damage analysis and estimate safety life of arbitrary complicated structures with complex geometries. Generally, for these structures with sharply break section, a fine mesh division near the local stress concentration is necessary to ensure the accuracy and rather a coarse mesh division off the local stress concentration may economize vast computational cost. In this paper, the large-scale general software ANSYS, which is based on the FEM, is used to perform the static analysis of the aircraft structural joint.

2.2 Estimation of fatigue life

The middle value of structure fatigue life at stress concentration situation under the 1st principal stress (In this paper, the stress along y direction is mainly, thus we select the SY stress) cycle is estimated by the middle value *S-N* curve with stress concentration factor K_t = 1. That is, the effect of local stress concentration is reflected through computing the detail stress at stress concentration location rather than the middle value *S-N* curve of related theoretical stress concentration. This method is adopted because it is hard to confirm the exact stress concentration factor of the joint structure for the complexity of load form. Moreover, looking for a related middle value *S-N* curve is also difficult even that the exact stress concentration factor can be obtained by computation.

3 THE NUMERICAL ANALYSIS OF AIRCRAFT STRUCTURAL JOINT

3.1 ANSYS Parametric Design Language (APDL)

Analytical models in the software ANSYS fall into two basic categories: Graphical User Interface (GUI) mode and APDL command flow mode. The former is a menu system that lets beginners and experienced ANSYS users perform virtually all ANSYS operations interactively. It is an easy and intuitive way to communicate with ANSYS. For a simple analysis model, this mode seems quick and effective. However, the shortcoming is obvious for a complex analysis, since accomplishment of a complex analysis needs many amendments; and the result files will tie up enormous HD capacity, which is very inconvenience for preservation and intercommunion, etc. These problems can be easily overcome by the APDL command flow mode. The APDL is a scripting language that you can use to automate common tasks or even build your model in terms of parameters (variables). It also encompasses a wide range of other features such as macros; branching, looping, and repeating; array parameters; and scalar, vector and matrix operations. While APDL is the foundation for sophisticated features such as design optimization and adaptive meshing, it also offers many conveniences that you can use in your day-to-day analyses[2].

In this paper, the finite element analytical models adopt the APDL command flow mode. Besides the aforementioned convenience of this mode, this program can provide a convenient platform for the further study on the local stress concentration and optimal design of fatigue-prone structural details.

3.2 Finite element analysis of aircraft structural joint

The structural joint comprises three parts: single-piece, double-piece and bolt, as shown in Fig.1 and Fig.2. The structural material properties are Young's modulus E_1=210Gpa, and Poisson ratio v_1=0.3 for bolt structure, Young's modulus E_2=116Gpa, and Poisson ratio v_2=0.32 for others. Since the maximum stress occurs at location near the holes. A fine mesh division is adopted near the holes with 3-D hexahedral SOLID95 elements after considering the practical fillet of the hole. Moreover, a coarse mesh division is adopted off the holes. This is a non-linear static contact analysis process. The applied surface force on the right end surface is 87.6Mpa. The left end surface of this analytical model is fixed and the right end surface is free only along y-direction (longitudinal direction). Fig.3 gives the finite element analytical model, which has 9157 elements and 32411 nodes.

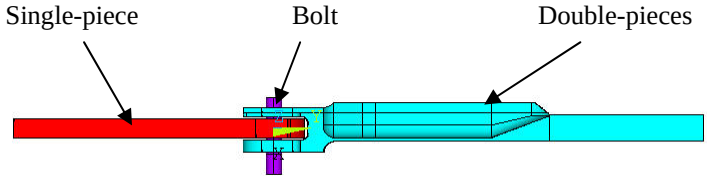


Fig.1 The front view of the structural joint

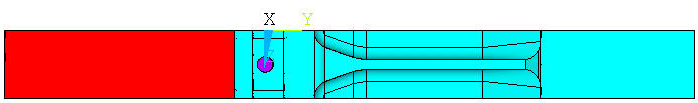


Fig.2 The top view of the structural joint

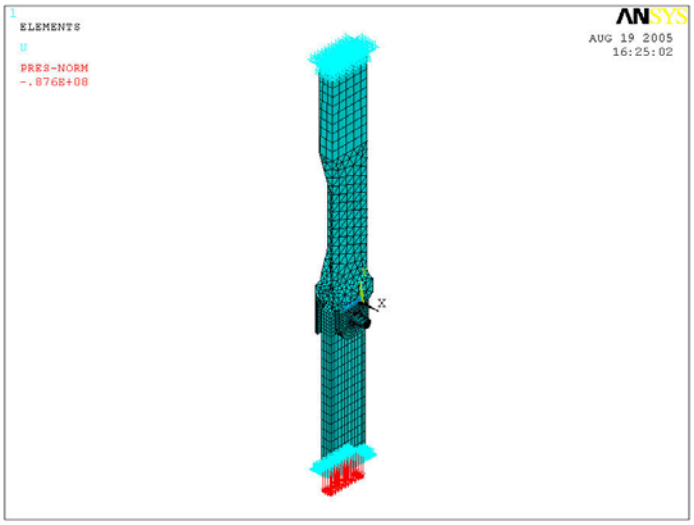


Fig.3 The finite element model

Considering the fatigue performance of structures, we pay attention to the maximum extensive stress of the structural joint. Fig.4 to Fig.6 show that the double-piece endures the maximum extensive stress along y-direction. Furthermore, the maximum stress occurs at the stress concentration location of the hole, which located the thin piece of the double-piece, as shown in Fig.4. The maximum extensive stress is 702Mpa.

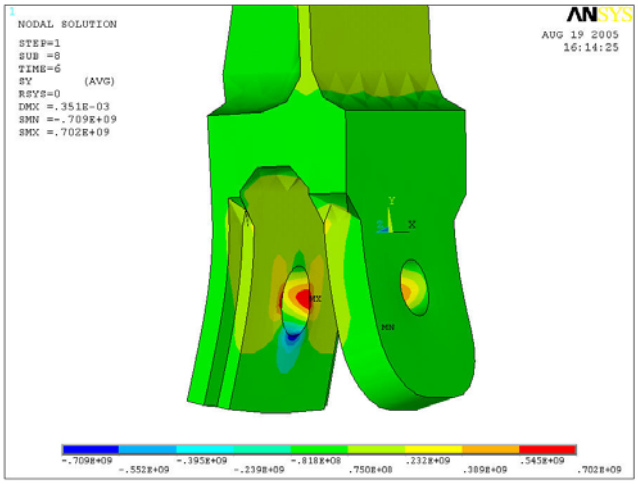


Fig. 4 The stress contour along y-direction of double-piece

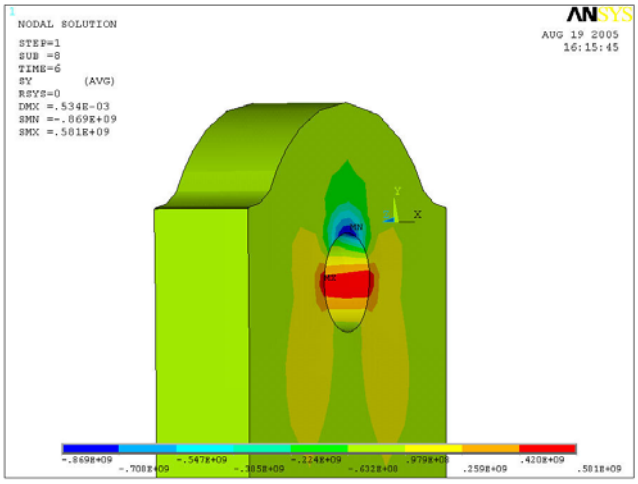


Fig.5 The stress contour along y-direction of single-piece

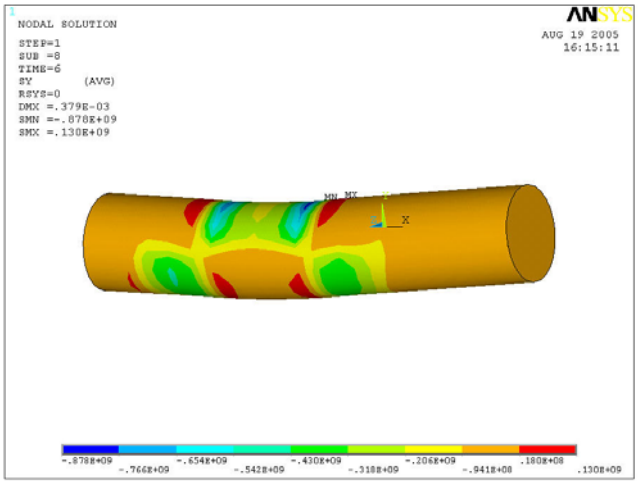


Fig. 6 The stress contour along y-direction of bolt

3.3 Estimation of fatigue life

When the applied surface force varies from zero to max 87.6Mpa, the aircraft structural joint endures the most serious fatigue load cycle. Thus, we adopt the pulse cycle as the fatigue load to estimate fatigue safety life of joint, i.e. the cycle stress is 702Mpa. The middle value *S-N* curve under condition of R=0 can be described as Eq.(1). The equation of middle value *S-N* curve of smooth pieces under condition of theoretical stress concentration factor K_t=1 is:

$$\lg N = 9.3783 - 1.912 \times \lg(S - 536.84) \tag{1}$$

From Eq. (1), the middle value fatigue life of joint structure can be obtained: $N_{c\,50}$=137,298cycles.

4 EXPERIMENTAL VERIFICATION OF AIRCRAFT STRUCTURAL JOINT

A series of 'three detail' specimen of aircraft structural joint are used to determine the fatigue life. Each detail of the specimen is just same as the finite element method model. The specimen in test is illustrated in Fig.7. All fatigue tests were conducted at constant stress amplitudes and a frequency of 5Hz, and the load ratio was R=0. The maximum surface force is 87.6Mpa, which is same as the force in calculation.



Fig.7 The specimen in test

A typical failure specimen is illustrated in Fig.8. A long fatigue crack is in the middle part of the specimen, and there are no cracks in the other details. Fatigue crack initial lives of each detail of specimen list in table 1. The middle value of fatigue life can be estimated using these data: $N_{t\,50}$=151,000cycles.

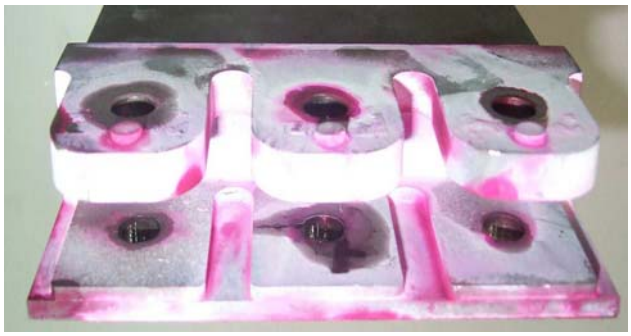


Fig.8 The long crack in specimen

Table.1 Fatigue crack initial life of details

	Specimen 1	Specimen 2	Specimen 3	Specimen 4	Specimen 5
Detail 1	85,000	>150,000	>151,000	>159,000	>197,000
Detail 2	>101,000	115,000	>151,000	126,000	141,000
Detail 3	>101,000	>150,000	136,000	>159,000	>197,000

Comparing the numerical life $N_{c\,50}$ with fatigue test life $N_{t\,50}$, the relative error is only –9%. The numerical result is receivable for structure fatigue life prediction.

5 CONCLUSION

In this paper, an effective FE analytical model of the aircraft structural joint is established and a non-linear static analysis under maximum fatigue load is processed. Based on the numerical result of the local stress concentration and the fatigue theory of the *S-N* curve with stress concentration factor 1, the middle value of structural fatigue life of the joint is estimated. Then, a series of experimental results verify the efficiency of the numerical analysis. The work in this paper lays a foundation for the further optimal structural design and fatigue performance prediction.

6 REFERENCES:

1. O. C. Zienkiewicz. The finite element method(third edition), McGraw-Hill, 1977.
2. ANSYS, Inc. ANSYS APDL Programmer's Guide Release 8.0
3. GAO Zhentong, Statistics in Fatigue, National Defense Industry Press,1986.
4. Wu Xueren. Handbook of mechanical properties of aircraft structural metals. Vol.1. Aviation Industry Press, 1996.

Modélisation numérique de la croissance des fissures courtes en fatigue

R. YAHIAOUI et B. AIT SAADI

Laboratoire de microscopie électronique et des sciences des matériaux – USTO
BP : 1505 El Ménaouer Oran – Algérie.

Résumé :

L'étude de l'endommagement en fatigue des matériaux est fortement liée au développement des fissures courtes en surface. En effet, leur évolution occupe près de 90% de la durée de vie du matériau. Cependant, le mode de croissance de ces microfissures est fortement influencé par la microstructure du matériau, et leur coalescence peut donner naissance à des fissures fatales causant la rupture finale.
Ainsi, il paraît très utile de prendre ces microfissures comme critère de l'endommagement, d'autant plus que leur densité et leur longueur sont des quantités mesurables.
Cette étude décrit ainsi l'endommagement du matériau en se basant sur la description de la croissance d'une population de microfissures. Ainsi, un modèle numérique est proposé, simulant la surface du matériau à un ensemble d'hexagones représentant les grains du matériau, alors que l'amorçage des microfissures et leur croissance sont basés sur des principes probabilistiques. Le modèle tient aussi en compte l'interaction mutuelle des microfissures entre elles et la possibilité de leur coalescence. Il est ensuite appliqué dans le cas du 316L à température ambiante et pour des déformations plastiques $\Delta\varepsilon p$ égales à 4.10^{-3} et 8.10^{-3}.

Mots clés : fatigue, amorçage, types de fissures, coalescence, durée de vie, 316L.

1. INTRODUCTION :

L'endommagement en fatigue est considéré par beaucoup d'auteurs comme étant un phénomène surfacique. Certains le lient à la formation des extrusions et des intrusions des BGPs, ainsi que leur interaction avec les joints de grains [1]. Cependant, d'autres auteurs caractérisent cet endommagement par la densité de dislocations et les contraintes résiduelles qui prennent naissance.
D'autres, par contre, associent le dommage par fatigue à la formation et à la croissance des microfissures en surface [2,3,4]. Car il apparaît que la notion de résistance à la fatigue des matériaux cristallins est intimement liée à la présence des microfissures dont la croissance entraîne la rupture. L'avantage de considérer une population de fissures comme facteur physique de l'endommagement est que les longueurs de fissures et leur nombre sont des données quantifiables avec précision. Les modèles numériques d'endommagement qui en résultent sont parmi les plus efficaces en terme de prédiction de la résistance à la rupture.
Cette nouvelle approche permet de traiter le problème de la multifissuration. Ainsi , il est possible de prendre en compte l'influence mutuelle des fissures entre elles et la possibilité de leur coalescence. D'autre part, il est possible de caractériser, aussi, l'influence des joints de grains sur la croissance des fissures. En effet, tout au long du processus de l'endommagement du matériau, les fissures sont, en grande partie, bloquées au niveau de ces barrières microstructurales.

2. CLASSIFICATION DES FISSURES :

La plus grande partie de la durée de vie du matériau N_i (où N_i marque le début de la propagation des fissures en volume et qui correspond à 90 % N_{rup}) est caractérisée par le développement et la croissance des microfissures. En effet, le développement des bandes de glissement au seins des grains est la cause principale de la formation de ces microfissures. Cette évolution commence dès les premiers 10% de N_i. Une fois ces microfissures se sont formées, elles vont se propager suivant ces bandes de glissement en premier lieu , ou bien à travers un joint de grains, puis continuent leur croissance ensuite jusqu'à ce qu'elle devient à la fois en surface et en volume.

Cependant, il apparaît que pour différents matériaux, des fissures de longueurs équivalentes se forment pour certaines proportions de la durée de vie réduite N/N_i. Par conséquent, les fissures sont classées selon leur longueur en quatre types, où dans le cas du 316L [2,3] :

- Fissure type I : $l \leq 50$ µm
- Fissure type II : 50 µm $< l \leq 150$ µm
- Fissure type III : 150 µm $< l \leq 500$ µm
- Fissure type IV : $l > 500$ µm

3. PRESENTATION DU MODELE :

3.1 Principe du maillage

La surface du matériau, constituée d'un ensemble de grains de formes et de tailles différentes, est assimilée à un réseau d'hexagones. L'orientation de ces grains est prise de telle sorte que chaque grain a une orientation différente de celle de ces premiers voisins, afin de mieux représenter le caractère aléatoire de la distribution de ces orientations dans le matériau.

3.2 Calcul du nombre de grains déformés

Le calcul de la proportion des grains déformés plastiquement est basé sur les travaux réalisés par Kitagawa [5] qui montrent bien que pour des amplitudes de déformations inférieures à une certaine limite, dépendant de la nature du matériau, la contrainte de cission développée dans certains grains n'est pas suffisante pour activer le système de glissement au sein de ces derniers. Par conséquent, la proportion des grains déformés est donnée par la relation suivante :

$$P(\%) = C\,\Delta\varepsilon_p / 2 \qquad (1)$$

Où, dans le cas du 316L, C vaut 15.10^4 [4].

3.3 Génération des fissures

La formation des fissures se fait au sein de la proportion des grains déformés plastiquement, mais au fur et à mesure que le cyclage continu, la déformation se voit localiser surtout autour des grandes fissures. Cependant, le taux de formation de ces fissures varie en fonction du nombre de cycles. Par conséquent, on va considérer dans notre modèle que l'amorçage des fissures suit une loi de distribution de type Weibull à deux paramètres :

$$F(N) = 1 - \exp[-(N\beta)^{\alpha}] \qquad (2)$$

où, F(N) est la somme des fissures formées, N le nombre de cycles, α et β sont respectivement les paramètres de forme et d'échelle. Ces paramètres (fig.1) sont choisis de telle sorte à reproduire les densités expérimentales.

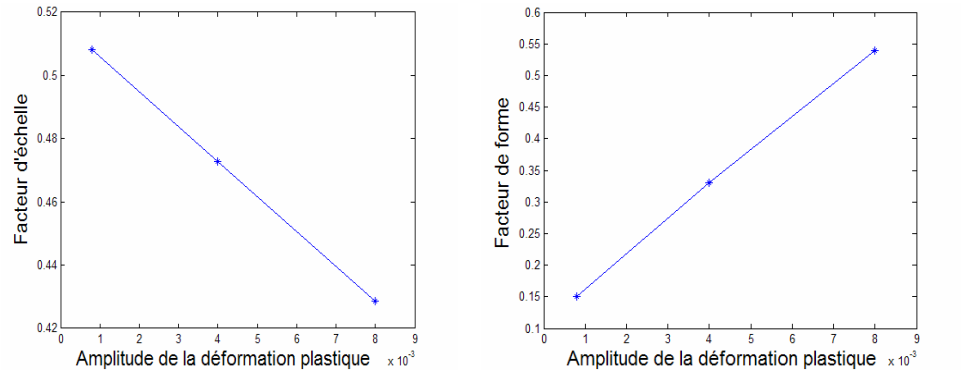


Figure 1. Variation du facteur de forme et d'échelle en fonction de déformation plastique

3.4 Propagation des fissures

La croissance des microfissures est fortement influencée par la microstructure du matériau. En effet, les joints de grains présentent un grand obstacle pour l'avancement des microfissures où ces dernières présentent souvent des temps d'arrêt à l'approche de ces barrières microstructurales. Pour cela, une variable aléatoire est générée et qui sera, par la suite, comparée à la valeur du seuil de propagation. La valeur de ce dernier va dépendre de l'amplitude de la déformation plastique et du type de la fissure concernée. Aussi, elle diffère selon que la fissure se propage au sein du grain ou bien au sein du grain voisin, traversant ainsi le joint du grain. Ce seuil de propagation caractérise dans ce cas l'énergie de cette barrière, qui est d'autant plus grande que la différence d'orientation des grains est importante.
Au cours de la croissance de la fissure cette dernière évolue au sein d'une population de fissures. Ainsi, il peut y avoir coalescence selon la longueur et la densité des fissures. Un phénomène qui peut réduire considérablement la durée de vie du matériau [6].
Pour cela, avant chaque avancement de la fissure, un test de coalescence est effectué et qui suggère que deux fissures coalescent si la distance entre leurs deux pointes est inférieure à 11 % de la somme de leur longueur [7].

3.5 Vitesse de fissuration

La fissure, durant son premier stade de développement, montre souvent une discontinuité de croissance due à la présence des joints de grains. Cependant, certaines auteurs suggèrent une vitesse moyenne constante. Ainsi, pour les fissures de type I et II [2,4]:

Type I : $$\frac{da}{dN}=6.67(\Delta\varepsilon_p)^{1.14} \qquad (3)$$

Type II : $$\frac{da}{dN}=757.83(\Delta\varepsilon_p)^{1.96} \qquad (4)$$

tandis que pour les fissures de type III, leur vitesse est proportionnelle à leur longueur :

Type III : $$\frac{da}{dN}=0.33(\Delta\varepsilon_p)^{1.33}L \qquad (5)$$

4. RESULTATS :

Le modèle décrit précédemment est appliqué dans le cas des déformations plastiques 8.10^{-3}, 4.10^{-3} et 8.10^{-4}. Les résultats de la simulation montrent une bonne cohérence avec les résultats expérimentaux [2] (fig.2), montrant de ce fait qu'un amorçage des fissures selon une loi de distribution de type Weibull permet de bien décrire l'évolution de l'endommagement en surface. On peut remarquer qu'une grande partie de fissures reste bloquée au niveau des joints de grains (fig.3). Ces fissures sont, principalement, de faible taille ne dépassant pas la taille du grain.

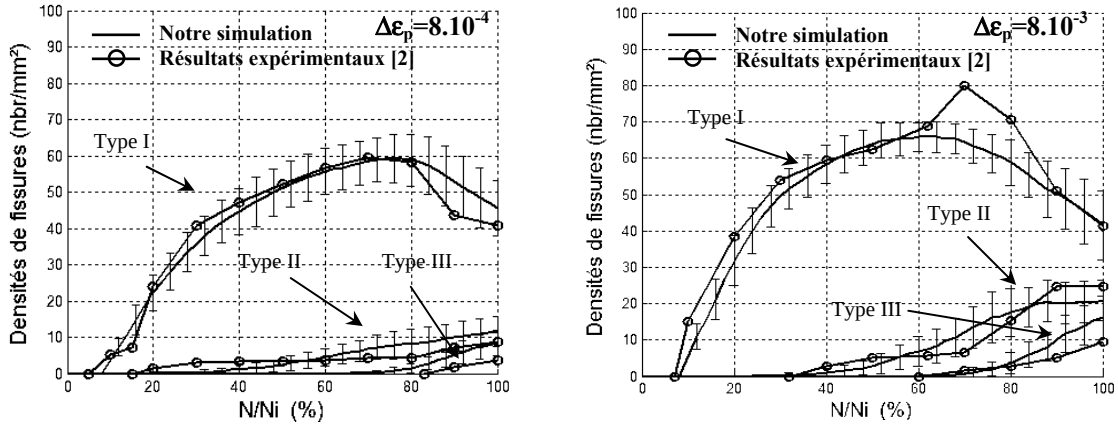


Figure 2. Densité des différents types de fissure en fonction de la durée de vie réduite.

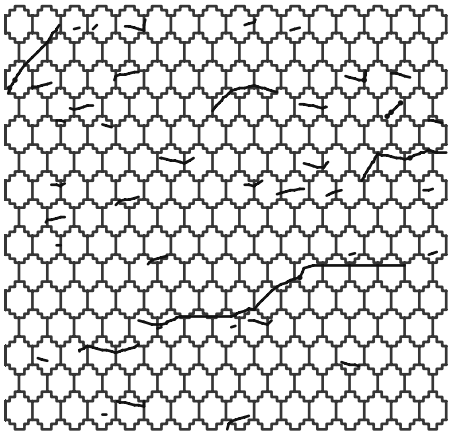


Figure 3. Représentation de la surface après simulation pour $\Delta\varepsilon_p = 8.10^{-4}$

On relève, également, le développement d'une fissure de type IV marquant le début de la fissuration en volume et qui se propage perpendiculairement à l'axe de sollicitation, pris dans notre cas, comme étant l'axe vertical.

5. CONCLUSION :

Le modèle proposé, basé sur une approche probabilistique concernant l'amorçage et la propagation des fissures, permet de bien décrire l'évolution de l'endommagement du matériau. En effet, il montre une bonne cohérence avec les résultats expérimentaux. Il permet, ainsi, de vérifier l'hypothèse d'une initiation de fissures selon une loi de distribution de type Weibull à deux paramètres et montre le rôle que joue la coalescence, du fait qu'elle permet d'avoir des fissures d'une longueur importante (de type III ou IV) à partir seulement de fissures de type I ou II, diminuant ainsi considérablement la durée de vie du matériau.

6. RÉFÉRENCES :

[1] Viggo Tvergaard, Y. Wei, J.W.Hutchinson (2001), Edge cracks in plastically deforming surface grains, Eur. J. Mech. A/Solids 20, 731–738

[2] A. Bataille, T. Magnin and K.J. Miller (1992) Numerical simulation of surface fatigue microcracking processes, Mechanical Engineering Publications, London, 407-419

[3] T. Magnin, C. Ramade (1989) Low-cycle fatigue mechanism of B.C.C. polycristals : homologous behaviour ?, Materials Science and Engineering A118, 41-51.

[4] V. C. Jesper (1998) Structural evolution and mechanisms of fatigue in polycristalline brass, Thèse de Doctorat, Technical University of Denmark.

[5] H. Kitagawa, S. Takahashi, C. M. Suh & S Miyahita (1978) Quantitative analysis of fatigue process-microcracks and slip lines under cyclic strains, ASTM-STP 675, 420-439.

[6] S.-H. Song & B.-H. Choi (2001), Effect of Plastic Zone on the Fatigue Crack Propagation Behavior Between Two Fatigue Cracks, Experimental Mechanics, Vol. 41, No. 3, 225-231.

[7] Y. Ochi, A. Ishii, K. Sasaki (1985) An experimental and statistical investigation of surface fatigue crack initiation and growth, Fatigue Fract. Engng. Mater. Struct., vol 4, n° 4, 327-339.

Angelika B., Xinyue H., Yasuko M. (2004), Mesoscopic Simulations of Damage Accumulation Under Fatigue Loading, ECF15.

PROGRAM

1 Methodologies and tools for fatigue life assessment

- Automotive components
- Various industrial applications
- Welded structures and assemblies

2 Advanced design tools and approaches

- Fatigue crack initiation assessment
- Contribution to the crack propagation stage
- Modelling of the design behaviour of the welded

3 Multiaxial loading fatigue assessment

4 Fitness for service approach and applications

5 Experimental validation

- Application to automotive parts and structures
- From laboratory testing to field evaluation
- Development of dedicated test devices and procedures

6 Design procedures against thermal and thermo mechanical fatigue damage

7 Reliability approaches in fatigue design

8 Improved design and manufacture processes with regard to fatigue

Multiaxial fatigue behaviour of metallic materials with controlled defects – Effects of mean stress.

Hicham Gadouini, Yves Nadot, Gerard Bezine

LMPM/ENSMA Téléport 2, 1 Avenue Clément Ader BP 40109 86961 FUTUROSCOPE CHASSENEUIL Cedex, Tel 05 49 49 82 15, Mail gadouini@ensma.fr

Abstract Fatigue behaviour of flawed materials is mainly governed by the presence of defects that modify considerably the stress distribution in the material. The complexity of the stress field can also be increased by the presence of cyclic loading effects, especially when a non symmetric loading is applied.
In order to improve the prediction capability of a multiaxial fatigue criterion for defect containing materials, the Chaboche combined isotropic-kinematic hardening elastic-plastic model is used in the present study to calculate local stress distribution around the defect. The introduction of this model in finite element simulation leads to a more realistic description of the effects of cyclic loading.
To study the influence of mean stress on the fatigue limit, experiments have been conducted under non symmetric loading on a steel containing artificial defects and FE simulation have been performed using a cyclic plasticity model in the aim to compare fatigue criterion prediction and experimental results.

1 INTRODUCTION

Fatigue behaviour for nodular cast iron or generally flawed materials are mainly governed by defects. Critical defects are located either at the surface or within the bulk. It has been shown that the near surface defects are much more dangerous with regard to the fatigue limit than internal defects [1]. Different approaches considering the defect as a crack or a notch exist. However the approaches are often based on 2D description which are limited to uniaxial loading and do not allow to predict fatigue limit evolution under multiaxial conditions.
To describe the influence of surface defect geometry on fatigue behaviour, a stress based multiaxial fatigue limit criterion has been proposed by Nadot and al [2]. This model uses Crossland criterion formulation; it considers the amplitude of the second invariant of the deviatoric stress tensor and the maximum hydrostatic stress as governing variables in the crack initiation process, even for flawed materials.
The influence of the defect is taken into account through Murakami's parameter $\sqrt{area}$, and the gradient of the maximum hydrostatic stress. This criterion gives accurate results for symmetrical tension and torsion loading. Nevertheless, the prediction of this criterion for non symmetrical torsion and tension loading shows some differences with experiments probably due to the use of the isotropic hardening to describe local plasticity around defect.
In order to improve the prediction capability of the criterion, the plasticity model of Chaboche is used in the present study to calculate local stress field around the defect.
The multiaxial fatigue criterion used in this study does not consider explicitly the mean torsion stress effect on fatigue limit for metallic materials with defects. In order to verify this point, experiments have been conducted under non symmetric torsion loading on a C36 steel containing artificial defects in order to compare the results obtained to those predicted by the criterion.

2 THE FATIGUE BEHAVIOUR OF DEFECT CONTAINING MATERIALS

2.1 Fatigue initiation mechanisms

It has been shown on the fatigue process of defect free metal that slip bands are first induced by shear component of cyclic stress, and then with sufficient advance of cumulated slip bands microscopic cracks initiate along these slip bands or along the grain boundaries where the slip bands are blocked. These cracks have been called stage-one cracks. Usually some of these cracks propagate out of the plane of slip bands perpendicularly to the direction of the maximum principal stress.
To study crack initiation mechanisms in defect materials, Billaudeau and al [1] introduced artificial defects at the surface of fatigue samples and observe cracks on these samples after fatigue tests under tension and torsion loading close to the fatigue limit.
As shown in Figure 1, the first stage of crack nucleation at the tip of the defect occurs in the maximum shear plane and in the maximum loaded part of the defect under both tension and torsion loading. The stress distribution around defects given by FE simulation gives rise to a high stressed volume generally located in the plane perpendicularly to the direction of the maximum principal stress. Consequently, the macroscopic crack that leads to failure of the sample propagates in that plane in mode I (governed by the opening stress).

After these observations, the authors conclude that it seems appropriate to use a multiaxial fatigue criterion based on both normal and shear stress to describe the fatigue limit of a defect material.

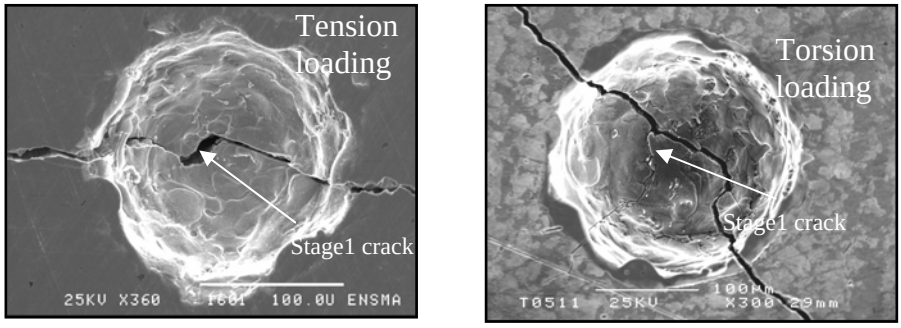


Figure1. Crack path around defect under tension and torsion loading close to the fatigue limit [1].

2.2 Multiaxial fatigue criterion for defective materials

Based on the previous experimental observations, a second paper by Nadot and Billaudeau [2] propose a multiaxial fatigue criterion for defective materials.

$$\sigma^*_{cr} = \sqrt{J_{2,a}} + \alpha J^*_{1\max} \le \gamma \qquad \text{with} \qquad J^*_{1\max} = J_{1\max}\left(1 - a\frac{G}{J_{1\max}}\right) \qquad G = \frac{J_{1\max}(point\,A) - J_{1\max}(\sqrt{area})}{\sqrt{area}} \qquad (1)$$

$J_{2,a}$: Amplitude during the load cycle of the second invariant of the deviatoric stress tensor (MPa^2)

$J_{1\max}$: Maximum value, during a load cycle, of the hydrostatic stress $J_{1\max} = \frac{1}{3} tr(\underline{\underline{\sigma}})$ (MPa)

α and γ are material parameters in Crosland's criterion [5]

a is a material parameter describing defect influence (μm^{-1})

G is the gradient [2] of hydrostatic stress $J_{1\max}$ based on Papdopoulos work [3]

To calculate this gradient a method based on observations of stress distribution is proposed (see Equation (1) and Figure2)

$\sqrt{area}$ is the equivalent defect size measured perpendicularly to the direction of the maximum principal stress in Murakami's equation [4]

The stress distribution around defects is influenced over a distance comparable to the defect size. Therefore the gradient is calculated over a size of the defect on the plotting line.

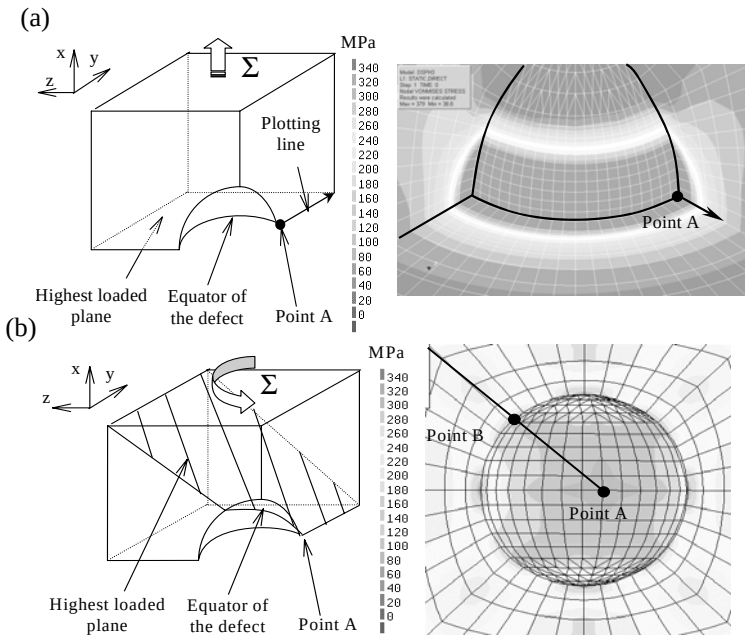


Figure2. Details of the geometry and mesh for (a) tension simulations (b) and torsion simulations.

2.3 Criterion identification

The criterion is limited to surface defects and can be identified by different ways depending on the type of material concerned:

2.3.1 Defect free materials

It is the case for impacted materials, for in service defect creation (corrosion, damage...) and generally for materials where it is possible to test samples with or without defects (machining surfaces of cast materials). In this case the identification of α and γ needs alternating fatigue limit under tension and torsion for the defect free material. The identification of a needs one alternating fatigue limit under tension for a given defect size.

2.3.2 Surface defects containing materials

It is the case of most of industrial casting materials, the identification of α and γ needs alternating fatigue limit under tension and torsion for one given size. The identification of a needs one alternating fatigue limit under tension for another given defect size.
The other material data needed is the elastic-plastic stabilised cyclic stress strain curve in order to calculate stress level at point A and stress gradient.

2.4 Validation

2.4.1 Review of experimental results

The criterion proposed (1) has been validated on a three different steels in ref [2]. Major results for C36 steel are presented below.
The identification for this material is based on three experiments:
The fatigue limit under tension (defect free material) σ_D=240MPa**,** the fatigue limit under torsion (defect free material) τ_D=169MPa and the fatigue limit under tension (170 µm spherical defect) σ_D=190MPa
The parameters of the criterion are therefore**:** α=0.3804**,** γ=169 MPa and a=377 μm^{-1}
All the simulations were conducted with an elastic-plastic Prandtl-Reuss type model based on Von Mises energetic criterion and with a linear isotropic hardening law. Identification of the hardening law is done using cyclic stabilised experimental stress-strain curve and all simulations are done for one load cycle.
Table1 presents the experimental results for all the set of cases studied and Figure3 the prediction of the criterion.

Case number	Loading type	Defect type	Defect size (μm)	σ_{max} MPa	σ_{moy} MPa	τ_{max} MPa	τ_{moy} MPa
Case 1	Tension	No defect		240	0		
Case 2	Tension	Elliptical H	170	200	0		
Case 3	Tension	Elliptical H	400	157	0		
Case 4	Tension	Elliptical V	170	235	0		
Case 5	Tension	Spherical	95	230	0		
Case 6	Tension	Spherical	170	195	0		
Case 7	Tension	Spherical	400	150	0		
Case 8	Tension	Spherical	880	135	0		
Case 9	Torsion	No defect				169	0
Case 10	Torsion	Spherical	170			160	0
Case 11	Torsion	Spherical	380			145	0
Case 12	Torsion	Spherical	950			125	0
Case 13	Tension	Spherical	370	280	154		
Case 14	Tension	Spherical	850	246	135		

Table1. Description of the different experimental cases for the C 36 steel.

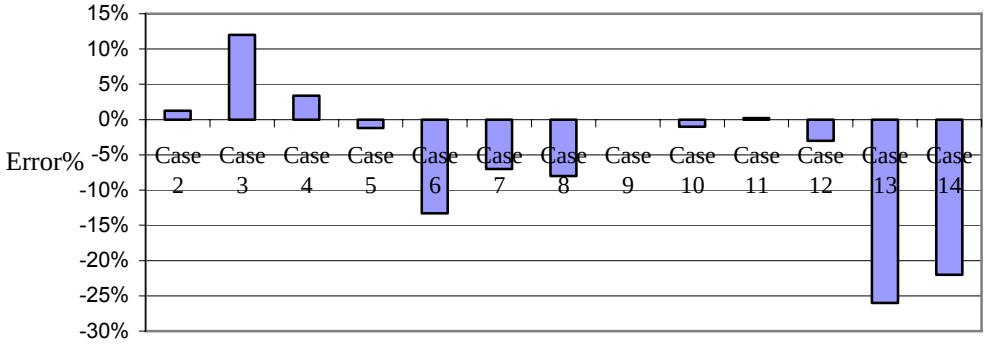


Figure3 .Prediction of the criterion (1) for C 36 steel using an isotropic elastic-plastic law.

Under tension for load ratio R = 0.1 (cases 13 and 14), results are not good: the error is up to 26 %. The plasticity model used is poor because it does not consider kinematics hardening. This is the reason why the local stress state at the tip of the defect has to be described in a better way**.**

In order to improve the prediction capability of the criterion, the Chaboche combined isotropic-kinematic hardening elastic-plastic model is used in the next section to calculate local stress distribution around the defect. The introduction of this model in finite element simulation leads to a more realistic description of the effects of cyclic loading to determine local stress state.

2.4.2 Validation of the criterion with the elastic-plastic Chaboche model

The employed material model uses an elastic-plastic non linear hardening law. The model used here was originally proposed by Chaboche and Lemaitre [6] and is included in the commercial FE-package ABAQUS used for the present calculation.

The evolution law of this model contains two components: a non linear kinematic hardening component, which describes the translation of the yield surface in the stress space through the backstress, $\overline{\overline{\alpha}}$; and an isotropic hardening component, describes the change of equivalent stress defining the size of the yield surface, σ^0, as a function of plastic deformation.

When temperature and field variable dependencies are omitted, the hardening law is

$$\dot{\overline{\overline{\alpha}}} = C\frac{1}{\sigma^0}(\overline{\overline{\sigma}} - \overline{\overline{\alpha}})\dot{\varepsilon}^{pl} - \beta\overline{\overline{\alpha}}\dot{\varepsilon}^{pl}, \qquad (2)$$

Where C and β are material parameters that must be calibrated from cyclic test data.

The isotropic hardening is defined by the exponential law:

$$\sigma^0 = \sigma|_0 + Q_\infty\left(1 - e^{-b\bar{\varepsilon}^{pl}}\right), \qquad (3)$$

Where $\sigma|_0$ is the yield stress at zero plastic strain and Q_∞ and b are material parameters.

The materials parameters are, in the present study, taken as C =75000MPa, β =500, b =10 and Q_∞=30MPa.

With the cyclic elastic-plastic law, we calculate the stress state around defect for six cases: 7, 11, 13, 14, 15, and 16. Results of validation of the used criterion with the Chaboche are presented Figure 4

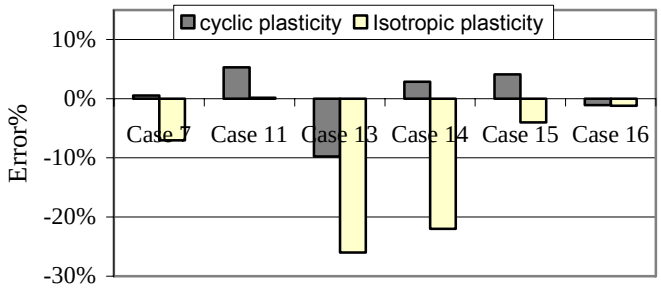


Figure4. Prediction of the criterion (1) for C 36 steel using the two elastic-plastic models (isotropic and cyclic).

We can observe that for cases 13 and 14 (tension for load ratio R=0.1), the used criterion gives good predictions with the combined isotropic and kinematic hardening law. The introduction of Chaboche model in finite element simulation leads to a more realistic description of the effects of cyclic loading to determine stress field.
For non symmetric loading, the description for local stress around defect shows stress relaxation phenomena. This effect cannot be described with the simple isotropic law as shown on Figure 5**.**

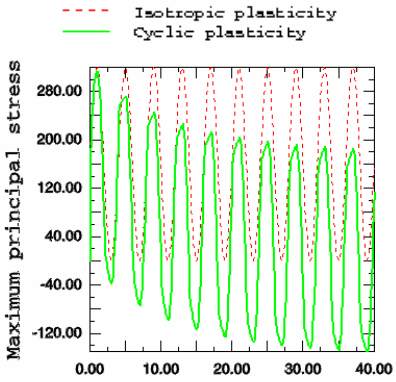


Figure5. Evolution of the maximum principal stress at the tip of defect (point A) for non symmetric tension loading. Comparison between cyclic and isotropic plasticity.

3 MEAN STRESS EFFECT

The influence of a superimposed mean stress on the high cycle fatigue behaviour is a question that has been discussed for a long time. In the high cycle fatigue literature, the mean shear stress effect has frequently been neglected. In support of this opinion, the classical paper of Sines [7] is recurrently cited. In this paper Sines reached the conclusion that a superimposed mean static torsion has no effect on the fatigue limit of metal subjected to cyclic torsion.
The same conclusion can be drawn from the analysis of Smith's data [8].The results, in Smith's words, are thus summarised." The magnitude of any endurance of stress is constant and equal to the magnitude of the endurance range of stress for completely reversed cycles of stress, provided that the maximum stress in the range does not exceed the torsional static yield strength of the steel".
For a ductile cast iron, it was found that the shear endurance strength was reduced by about 30% by the applied shear mean stress in R=0 tests, where the maximum shear stress of 365MPa exceeded the shear yield stress of 340MPa for this material [9].
When a tensile stress is applied to a fully reversing torsion loaded specimen, such as under cyclic torsion of a shaft subjected to a mean bending stress, a decrease in fatigue life is often reported [10].
In presence of defects, stress distribution is different than defect free material, therefore the influence of mean stress on high cycle fatigue behaviour may be considered differently.
In order to verify this point, experiments have been conducted under non symmetric torsion loading on a C36 steel containing artificial defects of different sizes and shapes.

3.1 Experimental results

The material tested is a low carbon steel C36, it is the same material as presented in section 2.4(see [1,2] for more details).
Artificial spherical defects with controlled size ($\sqrt{area}$=400µm) have been introduced by electric discharge machining (EDM) at the surface of fatigue samples. Fatigue limit tests have been conducted under tension and torsion loading. Every tested sample has been tempered (1 hour, 500°C, vacuum). The material's Young modulus is 212 GPa, the cyclic yield stress is 273MPa, fatigue limits of defect free material under symmetric tension and torsion loading are respectively 236MPa and 169 MPa. Tension and torsion experiments have been conducted at respectively 125Hz and 45 Hz. The size of the defect is characterised by the $\sqrt{area}$ parameter [4].
Fatigue tests have been performed under tension and torsion loading in order to determine the fatigue limit
Every fatigue limit is defined using at least two specimens , the uncertainty of measurement is less than $\pm$ 5 MPa .
All results are presented in Table2.

Case number	Loading	σ_{max} MPa	σ_a MPa	σ_{moy} MPa	τ_{max} MPa	τ_a MPa	τ_{moy} MPa
Case7	Tension R=-1	150	150	0	0	0	0
Case13	Tension R=0,1	280	126	154	0	0	0
Case11	Torsion R=-1	0	0	0	145	145	0
Case15	Torsion R=-0,5	0	0	0	173	130	43
Case16	tension-torsion R=-1	128	128	0	72	72	0
Case17	Torsion R=0	0	0	0	280	140	140
Case18	Torsion R=0,5	0	0	0	320	80	240
Case19	Tension R= -5	77	230	-153	0	0	0
Case20	Torsion R=-0,7	0	0	0	175	150	25

Table2. Experimental fatigue limit for spherical artificial defect of 400µm containing material

Results under torsion

To represent mean shear influence Figure 7 represents the evolution of shear stress amplitude as a function of the normalized maximum stress. τ_a is the fatigue limit under torsion, $\tau_{R=-1}$ the fully reversed fatigue limit under torsion, τ_{moy} the mean shear stress and τ_y the yield torsional stress.

As shown in Figure6, fatigue limit under torsion is constant and equal to the fully reversed torsional fatigue limit for mean stresses between 0 MPa and 140MPa. For the last point where the mean shear stress is equal to 240 MPa the fatigue limit decrease by 44% compared to the fully reversed torsional fatigue limit.

In general, the majority of authors make the same conclusion than Smith [8] (The magnitude of any endurance of stress is constant and equal to the magnitude of the endurance range of stress for completely reversed cycles of stress, provided that the maximum stress in the range does not exceed the torsional static yield strength of the steel).

In the case of C36 steel with defects this conclusion is not verified, we don't observe evolution of the torsional fatigue limit while the mean shear stress does not exceed the torsional static yield stress of the studied material.

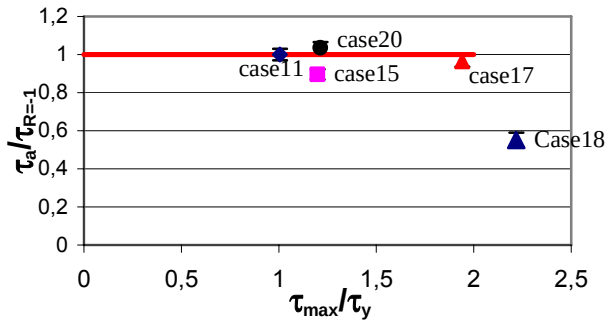


Figure6. Evolution of torsional fatigue limit depending on maximum shear stress.

Results under tension

In order to define the influence of mean tensile stress, three fatigue tests have been performed under tension loading with three different mean tensile stresses (see Table3).

Figure 8 presents the evolution of the tensile stress amplitude as a function of mean stress.

σ_a is the fatigue limit under tension, $\sigma_{R=-1}$ the fully reversed fatigue limit under tension, σ_{moy} the mean tensile stress and σ_y the yield tensile stress.

In the studied domain of mean tensile stress, we can observe that the fatigue limit of this containing defect material decrease linearly with the mean tensile stress.

A number of researchers proposed different empirical relationships capable of accounting for the mean stress effect on the material fatigue strength under uniaxial fatigue loading. These formulations can be summarised by formulation Marin's cited in the paper of Susmel [10] general relationship:

$$\left(\frac{\sigma_a}{\sigma_{R=-1}}\right)^n + \left(f\frac{\sigma_{moy}}{\sigma_Y}\right)^m = 1 \qquad (4)$$

Where *f*, *m* and *n* are constants to be defined. In particular we can obtain the linear Soderberg's relationship when n=1, m=1, f=1:

This relation can be easily plotted in the non dimensional diagram.Figure7.

The fatigue limit predicted by Soderberg's relationship for the case13 (tension loading R=0.1) is 57MPa. The fatigue limit obtained by experience is 126MPa.

For the case19 the fatigue limit predicted by the used relationship is 241MPa and the experimental fatigue limit is 230 MPa.

For the studied material, the Soderberg's model gives good prediction for describing the crack closure effect due to the presence of the mean stress of compression. However, the opening effect is not predicted correctly by this model.
In presence of defects, stress distribution is different than stress applied far from the defect during fatigue tests, Thus the mean stress effect should be studied locally around defect and we should also consider cyclic plasticity stress state during fatigue tests.

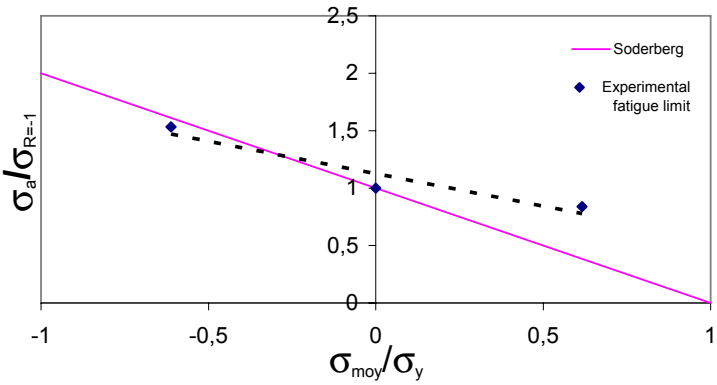


Figure7. Evolution of fatigue limit under tension loading depending on mean tensile stress.

3.2 Stress distribution around defects

In order to characterise the 3D stress distribution around the defect, finite element simulations have been conducted for each type of defect and each type of loading. Symmetry and boundary conditions are directly representative of the fatigue samples used: the applied load corresponding to the experimental fatigue limit.
For most of our defects, plasticity occurs around the defect so that we need to perform elastic-plastic simulations. Consequently, all the simulations are conducted with the elastic-plastic Chaboche [4] type model based on Von Mises energetic criterion and with combined isotropic and kinematic hardening law.

The criterion presented in section 2-2 is used here to analyse the results.
We calculate the local stress state around defect using cyclic plasticity model of Chaboche[6] and determine $\sqrt{J_{2,a}}$ and $J^*_{1\max}$. Error values of the used criterion's prediction are defined using equation (5) and summarised in Figure8.

$$error\ (\%) = \frac{\left(\sqrt{J_{2,a}} + \alpha\, J^*_{1\max}\right) - \gamma}{\gamma} 100 \qquad (5)$$

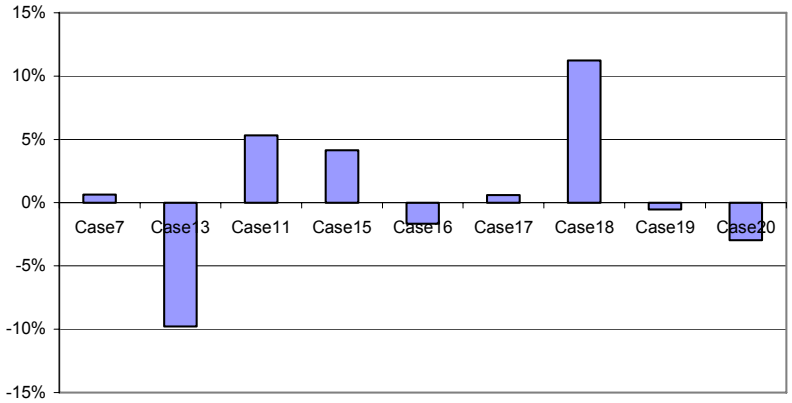


Figure8. Errors prediction of criterion (1).

We can observe that the maximum error obtained by the criterion [2] is 11%, the criterion gives good results in all the range of loading studied including torsion with high mean shear stress (R=0.5) where this one exceeds the yield torsional stress.
Contrary to criteria that use relations between macroscopic stresses to describe the influence of the mean stress on the fatigue limit, the multiaxial fatigue criterion presented in section 2-2 ,based on the local stresses calculated with a

cyclic plasticity model, gives good predictions of fatigue limit even if the maximum stress exceed the yield stress of the steel.

4 CONCLUSION

Fatigue tests have been conducted on a C36 steel containing 400µm spherical artificial defect. Fatigue limit have been determined for different mean stresses under both torsion and tension loading. For this study, the following conclusions can be drawn:

1) The fatigue limit under torsion is not influenced by the presence of a mean stress when this one is lower than the torsional yield stress of this material. This defect containing material seems to be less sensitive to the mean shear stress compared to a classical defect free material.
2) Classical macroscopic approaches using uniaxial expressions to account for the effect of normal mean stress on fatigue can not be extended up to those cases of defect containing materials. The stress state should be studied locally around defects using plasticity models able to describe cyclic effects.
3) The use of an adapted cyclic plasticity model to determine local stress state around defect permit to take into account some of cyclic loading effect due to the presence of a mean stress and then improve the prediction capability of multiaxial fatigue criterion tested.

5 REFERENCES

1. T.Billaudeau, Y.Nadot, G Bezine: *Multiaxial fatigue limit for defective materials: mechanisms and experiments,* Acta Materialia, Vol 52(13), 2004, 3911-3920
2. Y. Nadot and T. Billaudeau: *Multiaxial fatigue limit criterion for defective materials,* Engng Fract. Mech in press 2005, available online
3. Papadopoulos IV: *Critical plane approach in high-cycle fatigue on the definition of the amplitude and mean value of the shear stress acting*. Fat Fract Engng Mater Struct, 21, 1998, 269-285
4. Murakami Y: Metal fatigue: Effect of small defects and non metallic inclusion, Amsterdam, Elsevier, 2002
5. Crossland B: *Effect of large hydrostatic pressures on the torsional fatigue strength of an alloy steel.* Proc. Int. Conf. Fatigue of metals. London J. Mech. Eng; 1956, 138-49
6. J L Chaboche: *Constitutive equations for cyclic plasticity and cyclic viscoplasticity.* Int. Journal of Plasticity, l5(3), 1989, 247-302
7. Sines G, Ohgi G: *Fatigue criteria under combined stresses and strain*, Transactions of ASME, Journal of Engineering Materials and Technology, 103, 1981
8. Smith JO: *The effect of range of stress on the torsional fatigue strength of steels.* Bulletin Series No. 316. Engineering experiment Station, University of Illinois, 1939.
9. Marquis G; Socie D: *Long-Life torsion fatigue with normal mean stress.* Fatigue Fract Engng Mater Struct 23, 2000, 293-300.
10. Susmel L, Tovo R, Lazzarin P: *the mean stress effect on the high cycle fatigue strength from a multiaxial point of view.* International Journal of Fatigue 27, 2005, 928-943

Assessment of components under multiaxial service loading - calaculations ands experiments

C.M. Sonsino[1], H. Zenner[2], F. Yousefi-Hashtyani[3], M. Küppers[1]

[1] Fraunhofer-Institute for Structural Durability (LBF), Bartningstr. 47, D-64289 Darmstadt, Germany
[2] Institute for Plant Engineering and Fatigue Analysis (IMAB), Technical University of Clausthal, Leibnizstr. 32, D-38678 Clausthal-Zellerfeld, Germany
[3] Adam Opel AG, International Technical Development Center (ITDC), IPC S1-01, D-65428 Rüsselsheim, Germany

Abstract: This paper is focused on a research project supported by the German automotive industry and international software producers. Six multiaxially loaded components were tested under random multiaxial service loading conditions and evaluated by different algorithms. The results reveal a large scatter of calculated fatigue lives which are, in most cases, on the unsafe side. The contradictory unsatisfactory results are determined by the complex interaction of the multiaxial stress state with cumulative damage. Therefore, in case of safety critical components, experimental structural durability tests must be carried out.

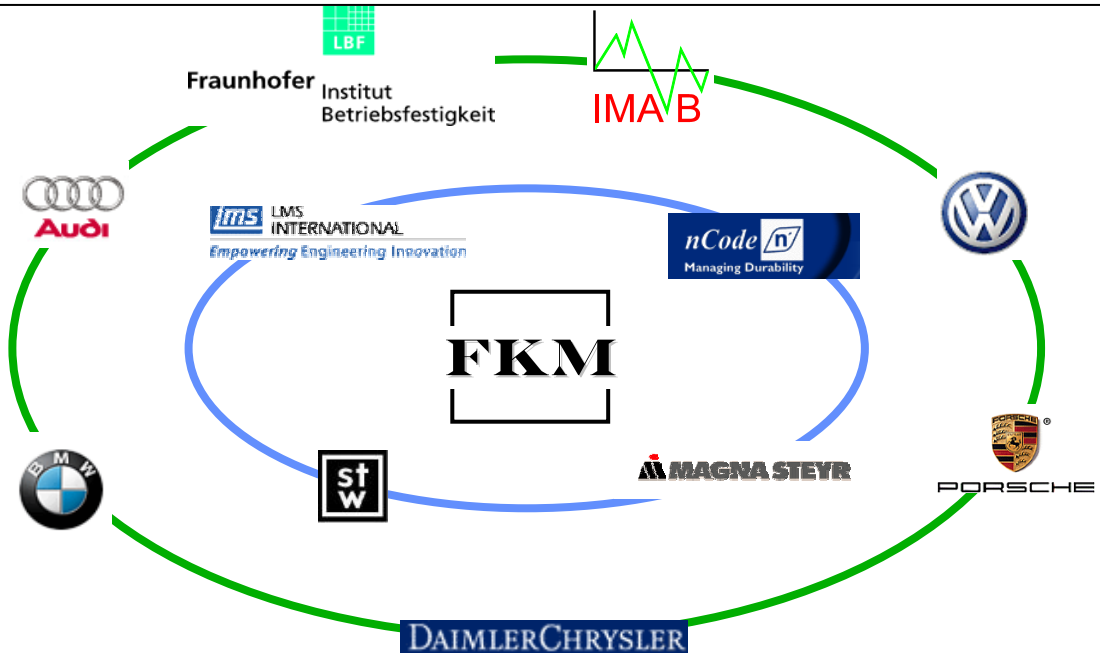
Keywords: Multiaxial lifetime assessment, multiaxial fatigue software, multiaxial stress state algorithms, nonproportional service loading, multiaxial loaded components, test results

1 INTRODUCTION

For an economic and rapid development of components a reliable fatigue simulation is required. In the past years different commercial fatigue software tools for multiaxial loading have been developed and they are used by industry.

However, lifetime assessments are still unsatisfactory. There is a large scatter between assessment and test, particularly, for multiaxial loaded components. For multiaxial lifetime evaluation various hypotheses have been developed and applied in software. Most of the calculation algorithms are seen by the user as a “black box”, although the user still has to choose the method.

From this background a research project [1] was carried out to identify and characterize a number of currently applied hypotheses. For different components subjected to multiaxial loading, lifetime calculations were performed with different software. The project has been a mutual cooperation between the research centres IMAB and LBF and the following industrial organisations, Fig. 1.



Software used: FALANCS, FATIMAS, FEMFAT, FEMSITE, WINLIFE, *maxi* ^{pro} (IMAB), LBF-Software

Figure 1: Project participants

Fig. 2 gives an overview of the investigated components and their materials. All the spectrum loads were derived from service measurements [1]. As an example Fig. 3 shows the stresses at the critical area for the wheel hub and Fig. 4 the change of principal stress directions. Further components are discussed in [2] and [3].

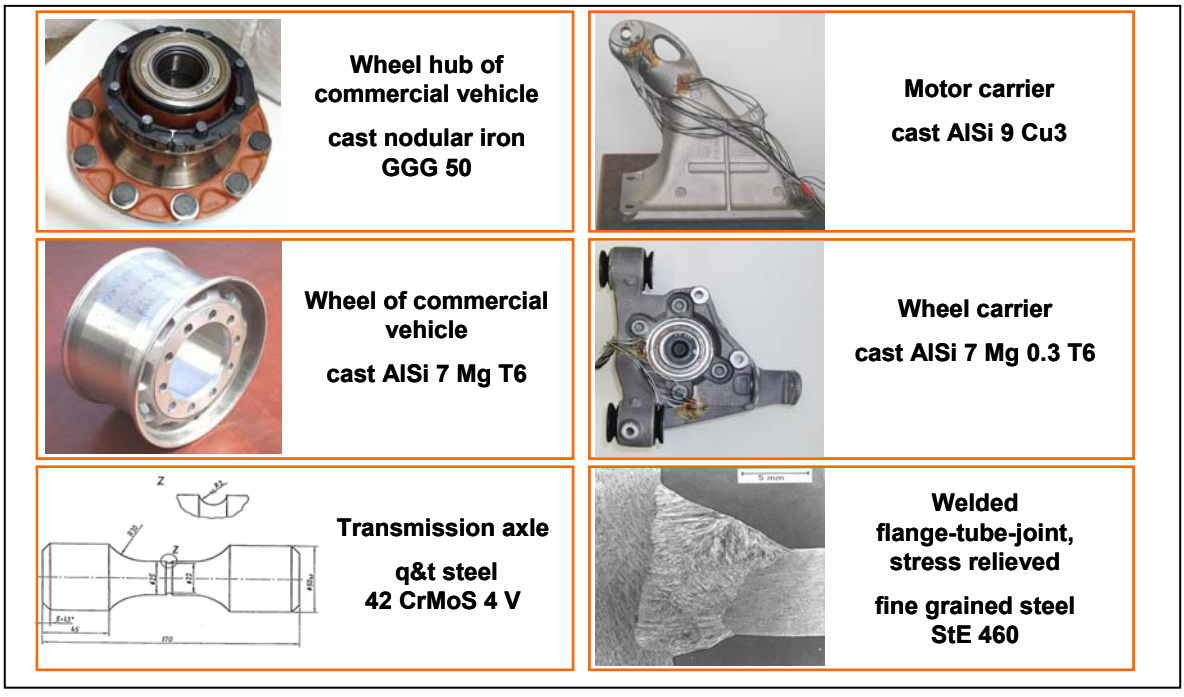


Figure 2: Investigated components

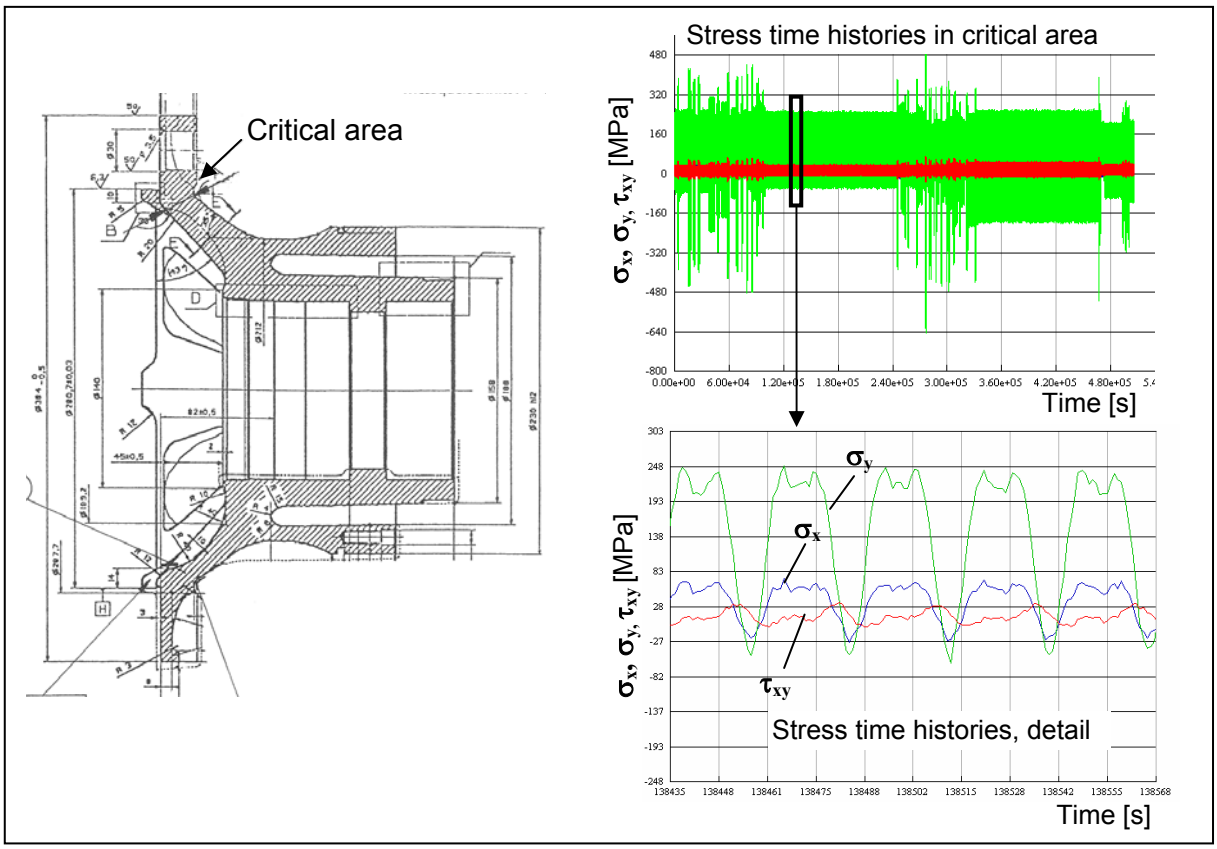


Figure 3: Local stress time histories in critical area of the wheel hub

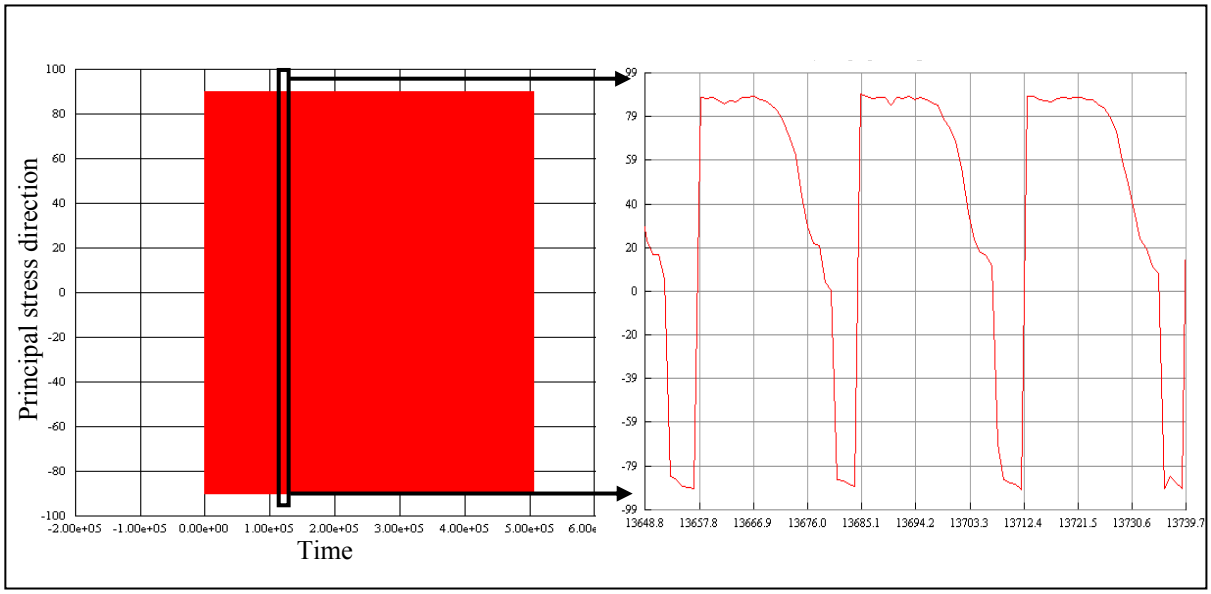


Figure 4: Change of principal stress direction in critical area of the wheel hub

The cyclic properties for all components were determined by strain controlled tests using specimens removed from the components. In all component testing the failure criterion used was the technical crack with a depth of 1 mm.

All investigated hypotheses were local plane based hypotheses as illustrated in Fig. 5. All the commercial software use the Critical Plane approach with the possibility to choose between several different hypotheses and modifications, the Integral approach is only embedded in IMAB and LBF-software. Most of the software permits calculations with several hypotheses.

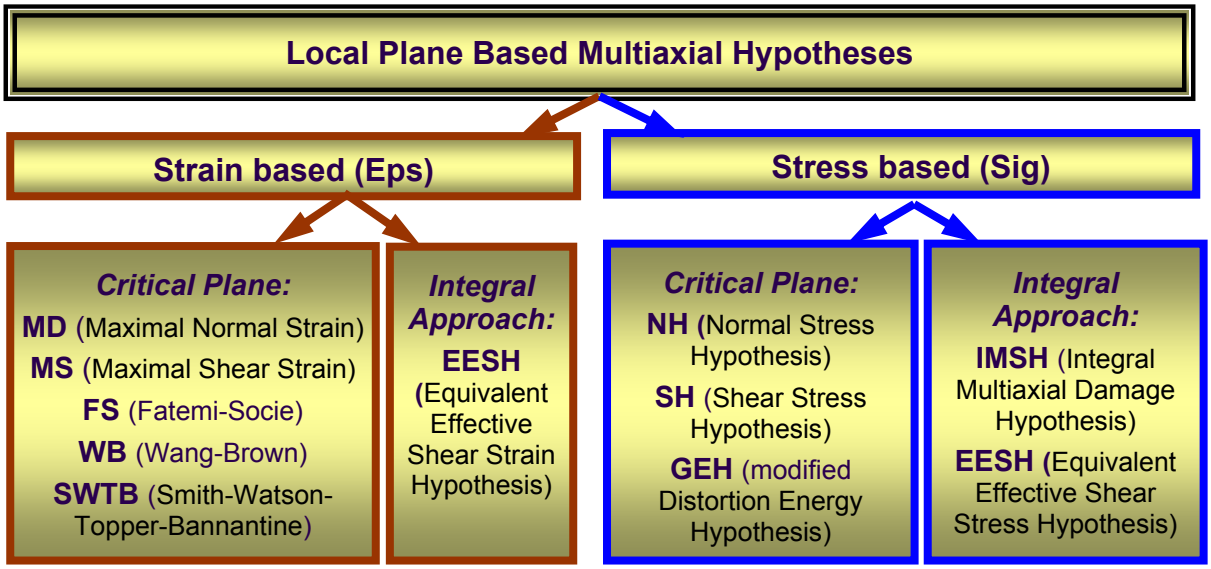


Figure 5: Overview of the investigated hypotheses (the abbreviations are used in the following figures to identify the hypotheses, for example: Sig_NH = Stress based Normal Stress Hypothesis)

For all components lifetime assessments were carried out by all the software providers in the project themselves. The input data were the parameter material properties and the measured strains/stresses in the failure critical location of the component. All components are designed for high cycle variable amplitude fatigue.

2 RESULTS AND DISCUSSION

The applied hypotheses (methods) produced a large scatter of the calculated fatigue lives, which were, in most cases, on the unsafe side [1]. Some software results in a large overestimation of lifetime, whereas others lead to a large underestimation, neither of which lead to a sufficiently strong yet lightweight construction. Fig. 6 shows the comparison of the calculated lives with the test results for the example of the in Fig. 3 and Fig. 4 shown "wheel hub" where most of the calculations show a large overestimation of lifetime.

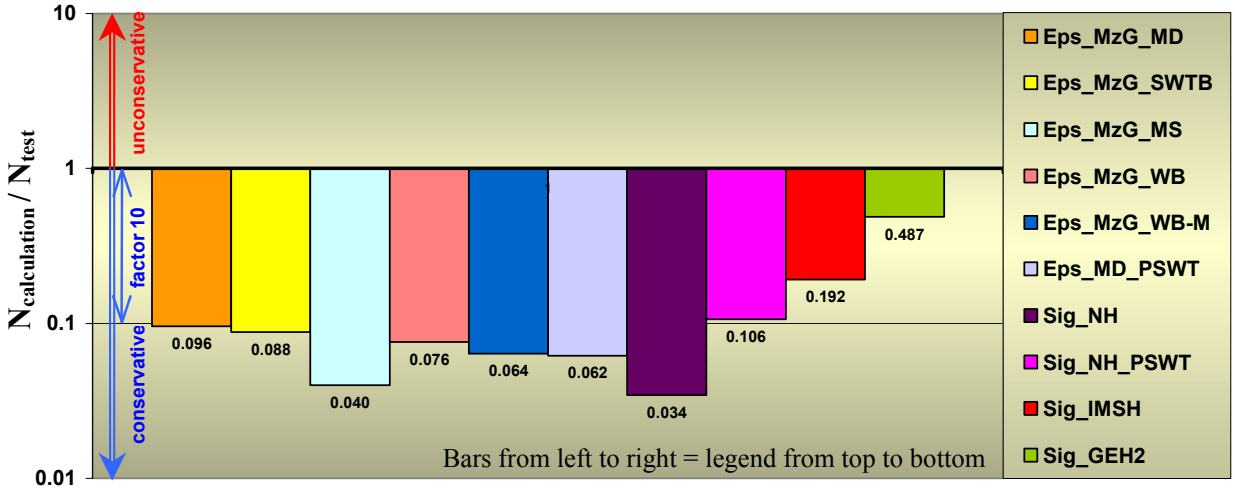


Figure 6: Comparison of the calculated lifetimes with the test results of the wheel hub (for the legend see Fig. 5; MzG: plasticity model Mroz-Garud)

Fig. 7 displays the calculation flow chart with the parameters that influence the calculation results. For assessing the complex fatigue behaviour of the components under service loading in the simulation a lot of information is required as input. The data of the loading conditions are required as load time histories. The geometry is built as a FE-model based on CAD data to analyse the stress situation in the structure. Also required are static and cyclic material data. Cyclic plasticity models are used to take into account the elastic-plastic behaviour of the material under cyclic loading. For the fatigue analysis, different models are necessary to consider the effects on fatigue life. The consideration of multiaxial stress state with the hypotheses is one of

them. The damage accumulation with a modification of the Palmgren Miner´s rule is the last step in the fatigue calculation.

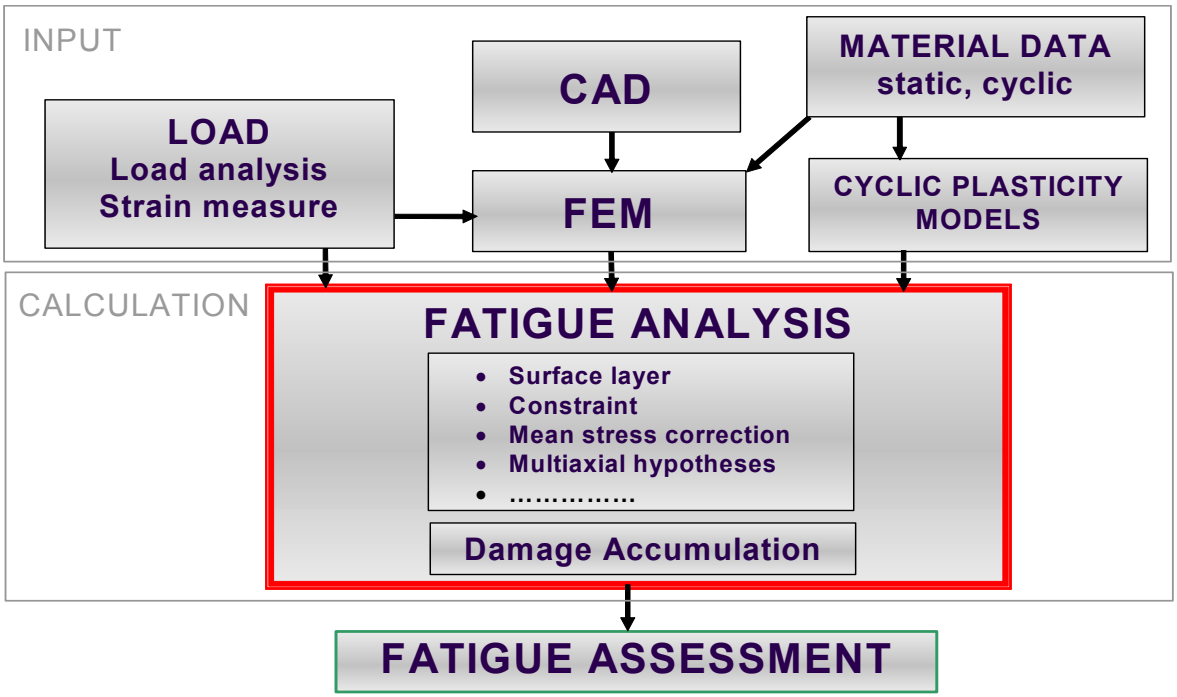


Figure 7: Lifetime calculation flow chart

The reasons for deviations in lifetime assessment can be divided into two main groups:

1. Input data (Load, FE-model, material data)
2. Fatigue calculation

In each group it is possible to have more than one source of error and these may even interact.

2.1 Input data

- FE-model

In the simulation the FE-model provides the first possible geometrical information to analyse the stress situation of the component. It is also necessary to make a fatigue assessment in this phase of development before prototypes exist. For three of the investigated components, FE-models were available and used for calculation. For the motor carrier strain gauge measurements in the critical area were also available. The investigations showed that, beside the general FE-specific problems of boundary and loading conditions as well as contact definitions, the fineness of the meshing at the critical area can have a significant influence on the final result. Fine meshing at the hot spot is necessary for a local stress analysis and to take into account the constraint. On the other hand, over-fine meshing increases the calculation time and the size of output files. How fine a mesh should be depends on the user. Further, due to mesh refinement there can be a large difference between the strain gauge measurement and the FE-analysis. This can cause a factor of difference of up to 70 in the calculated lifetime. General guidelines and instructions for suitability of a FE-model from the viewpoint of fatigue do not exist.

- Load

A detailed analysis of service load conditions is the basis of an efficient lifetime calculation. Data reductions of the load time histories are required for the handling of data and for an acceptable calculation time. Strain gauge measurements are used for the determination of loading conditions. So a component must exist for analysis. The measurements can be used to determine the load signals acting on the component. Although a strain gauge measurement on the hot spot can be used to calculate the lifetime, it is not always possible to make a strain gauge application on the critical area for geometrical or functional reasons. Further, the knowledge of the location of the crack initiation is necessary. Information about the stress gradient is also in most cases not measurable and must be estimated. However, it is possible to make acceptable lifetime calculations under service loading based on strain gauge measurements and derived local stresses with all of the software considered. For

example, lifetime calculations are carried out for three components in this study using strain gauge measurements and the associated local stresses on the hot spots known from previous tests.

- Material data

For all components cyclic material data were determined by strain controlled tests using specimens removed from the components. The determined material properties differ from the data, which are embedded in the software, and from the Uniform Material Law [4] (in some cases strongly). It is not always possible to remove specimens from the critical area. For brittle materials like cast aluminium, a specimen can be removed on solid sections. Due to unsteady cooling conditions in these sections it is possible that porosity will considerably affect the fatigue behaviour. The comparability of the specimen and the critical location should be considered.

Furthermore, the transferability of material data to component behaviour is important. For example, with the provided material data the constant amplitude bending SN-curve of the notched shaft could not be estimated from most software. The 42 CrMo 4 is a widely used material and the geometry a simple one. The building and usage of a general fatigue database for materials and notch shapes can help for an efficient assessment.

2.2 Fatigue calculation

The fatigue calculation includes a series of modules to take into account the influences of different factors on the fatigue behaviour. The number of the modules depends on the selected method. Essentially the mean stress correction, the micro-constraint and the multiaxiality are considered. Further factors such as macro-constraint, surface effect, size effect, manufacturing, surface layer and the environment are considered by modifying the material properties, e.g. by modifying the S-N curve. The last module in the calculation is the damage accumulation. In this example, to check the capability of the multiaxiality modules in the case of nonproportional stress state, further calculations were carried out in advance. This investigation was based on a series of sinusoidal tests of notched shafts of a ductile material (Ck 45), Fig. 8, and a brittle material (cast aluminium G-AlSi 12 CuMgNi), Fig. 9.

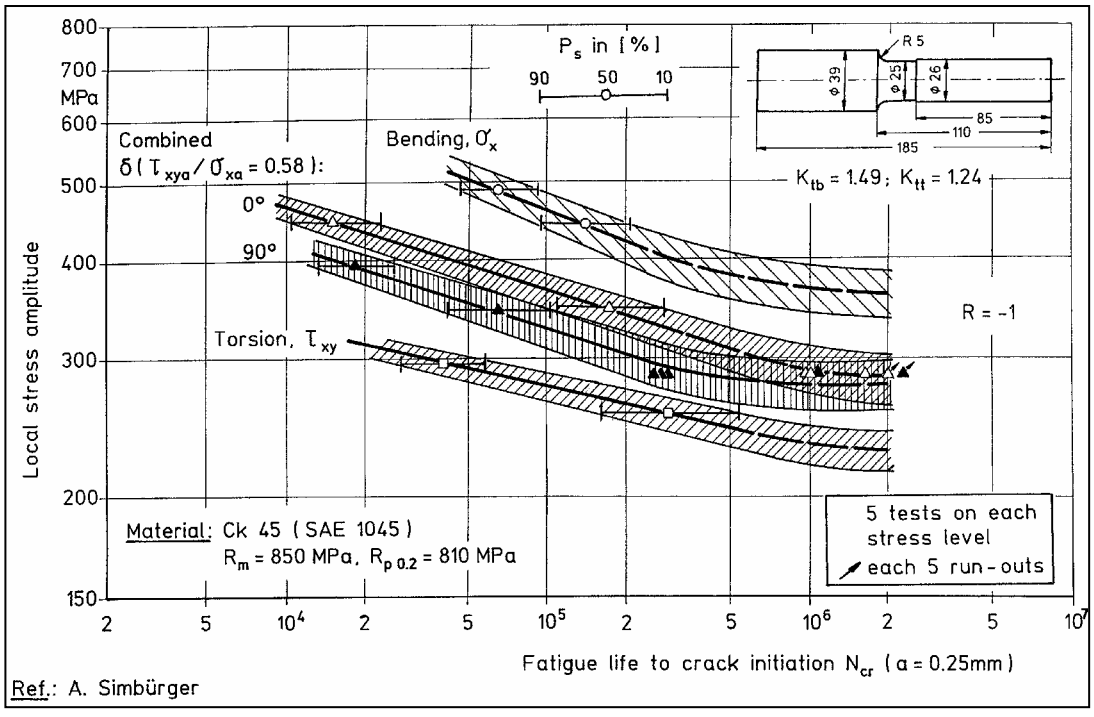


Figure 8: SN-Curve of forged steel Ck45 (SAE1045) under uni- and multiaxial loading

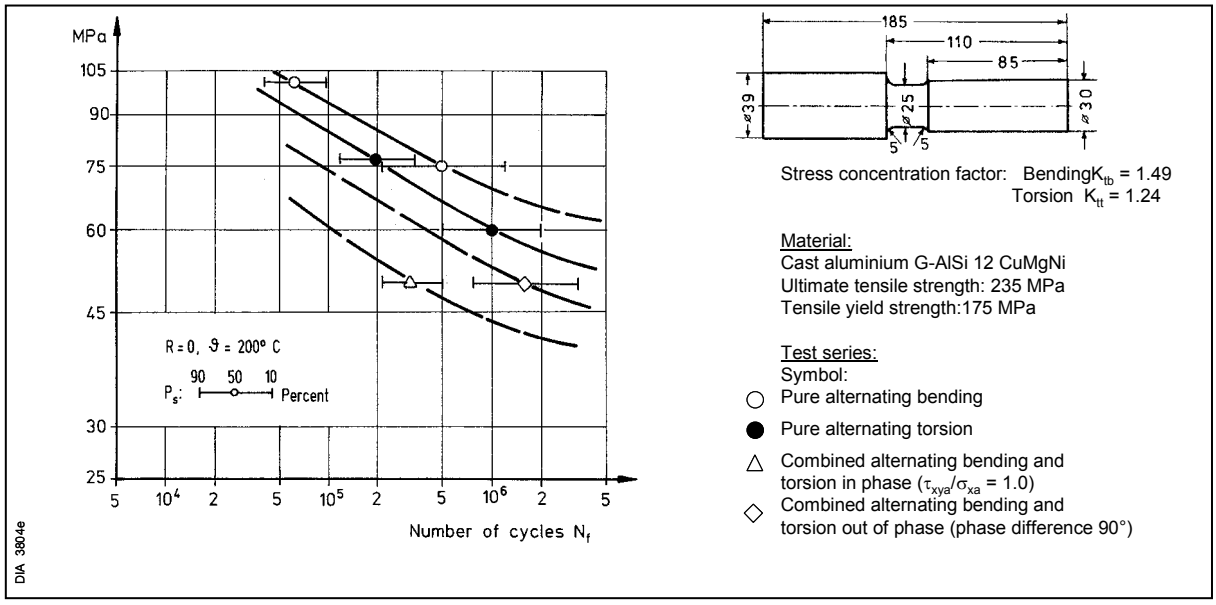


Figure 9: SN-Curve of the cast aluminium alloy G-AlSi 12 CuMgNi under uni- and multiaxial loading

In this way the damage accumulation factor could be precluded. The test series was pure bending, pure torsion, combined bending and torsion, both proportional and 90° phase shifted. Compared with proportional loading cases the two materials show different fatigue behaviour under 90° phase shifted loading, where the direction of the principal stress changes: the ductile sample shows a decrease and the brittle one an increase of durability. All the test results were known and uniform material data was used. The results showed a big scatter of the calculated lifetimes. None of the hypotheses in the commercial software could build the effect of the lifetime reduction for the ductile steel due to 90° phase shifted loading, as illustrated in Fig. 10. Only the EESH [5] shows here a lifetime reduction.

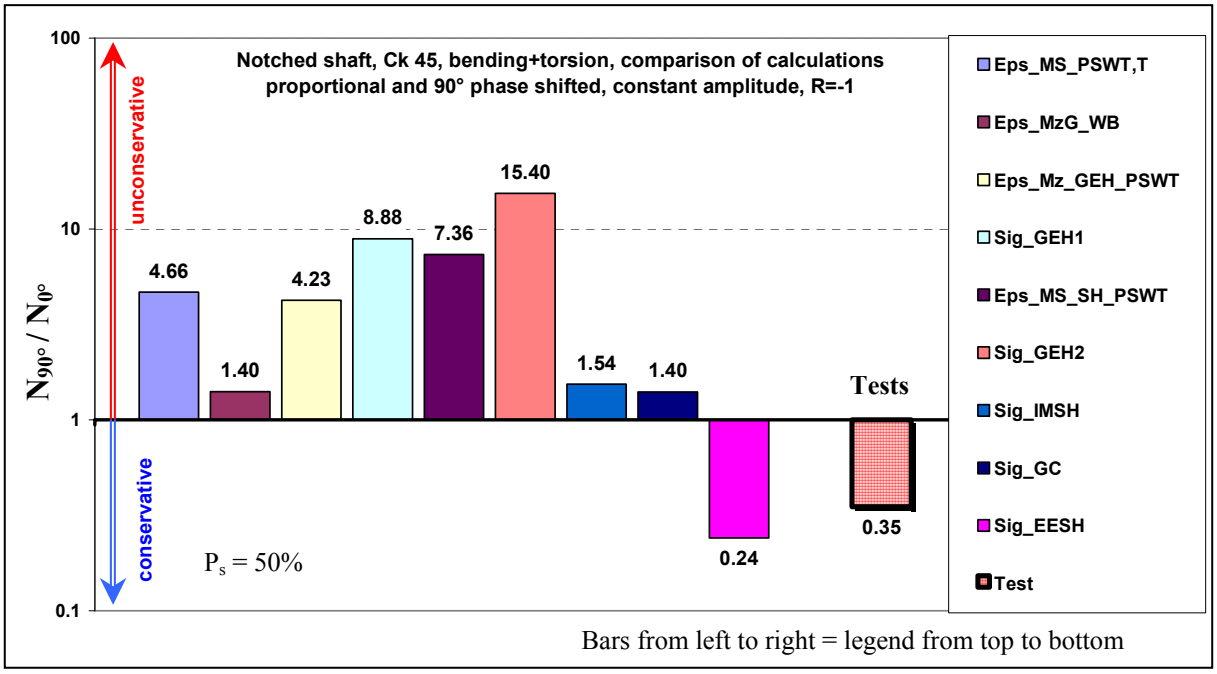


Figure 10: Comparison of calculations and test results for combined bending and torsion, Ck45, (for the legend see Fig. 5; MzG: plasticity model Mroz-Garud, GC: Gaier-Chu)

In case of the brittle material G-AlSi 12 CuMgNi the increase of fatigue life due to out of phase loading is considered principally by all applied hypotheses, Fig. 11, but the best approach is rendered by MS_PSWT;T, MzG_SWTB, MS_SH_PSWT and EESH.

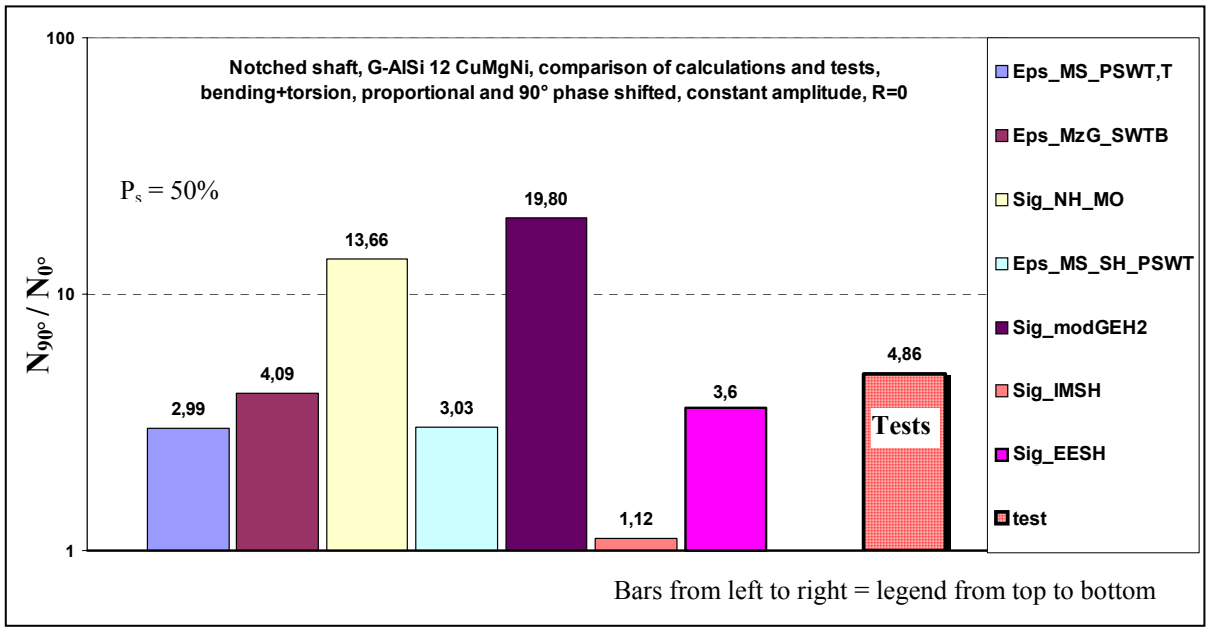


Figure 11: Comparison of calculations and test results for combined bending and torsion, G-AlSi 12 CuMgNi, (for the legend see Fig. 5; MzG: plasticity model Mroz-Garud)

In evaluation of the investigations with the welded flange-tube connection the results were compared by the hypotheses EESH and Dang Van [6]. This comparison reveals that the Dang Van Hypothesis underestimates the fatigue life reducing effect of out-of-phase loading, Fig. 12.

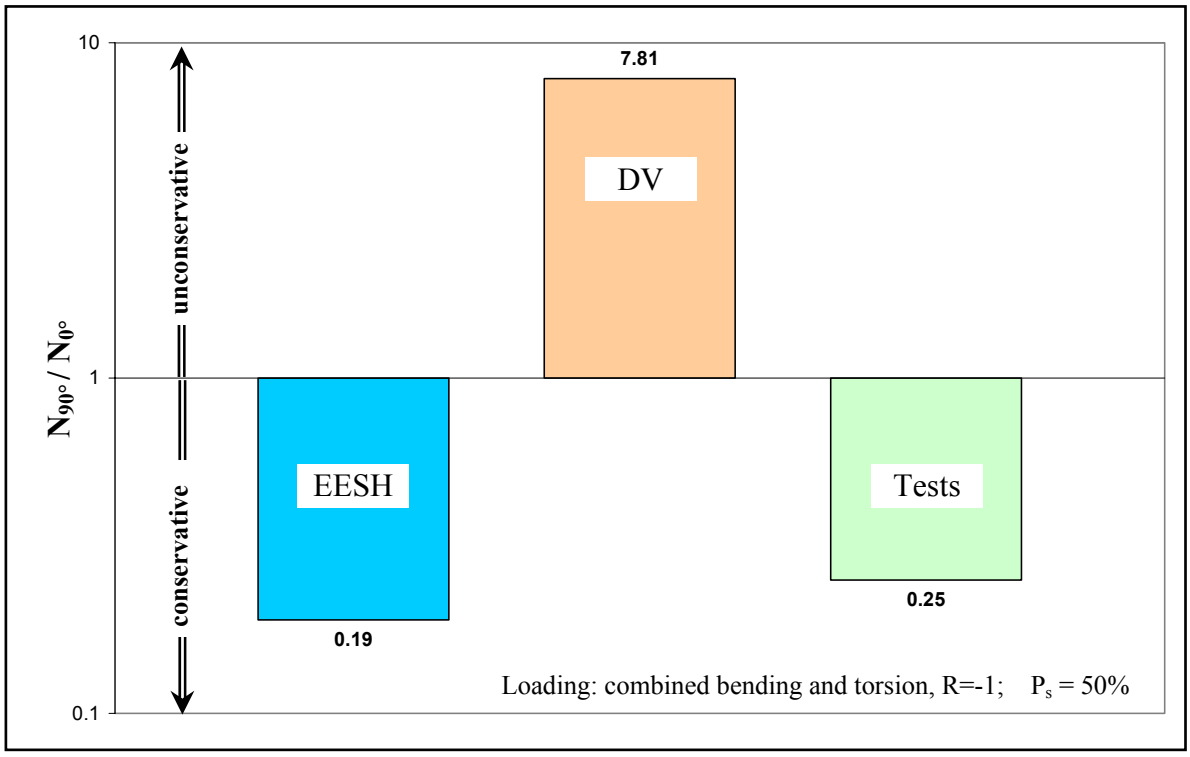


Figure 12: Welded flange-tube connections evaluated by the hypotheses EESH and Dang-Van

It is important to consider ductility dependent damage mechanism and appropriate algorithms, Fig. 13 [7].

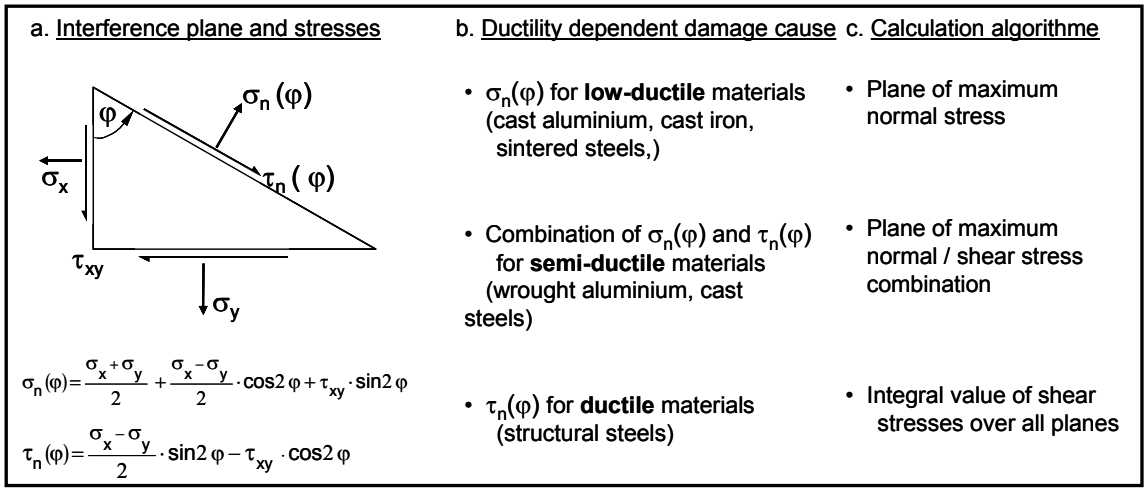


Figure 13: Interference plane stresses and damage models

The investigations show that the mean stress has a high influence on the fatigue assessment results. Knowledge of the mean stress sensitivity of the material used can simplify the selection of a suitable method for the lifetime assessment, Fig. 14. It should be noted that the widely used P_{SWT} parameter presumes a mean stress sensitivity of M=0.41. Depending on the mean stress sensitivity of the material, the P_{SWT} can cause an over- or under-estimation of the lifetime. This is discussed in the example of the truck wheel in [2].

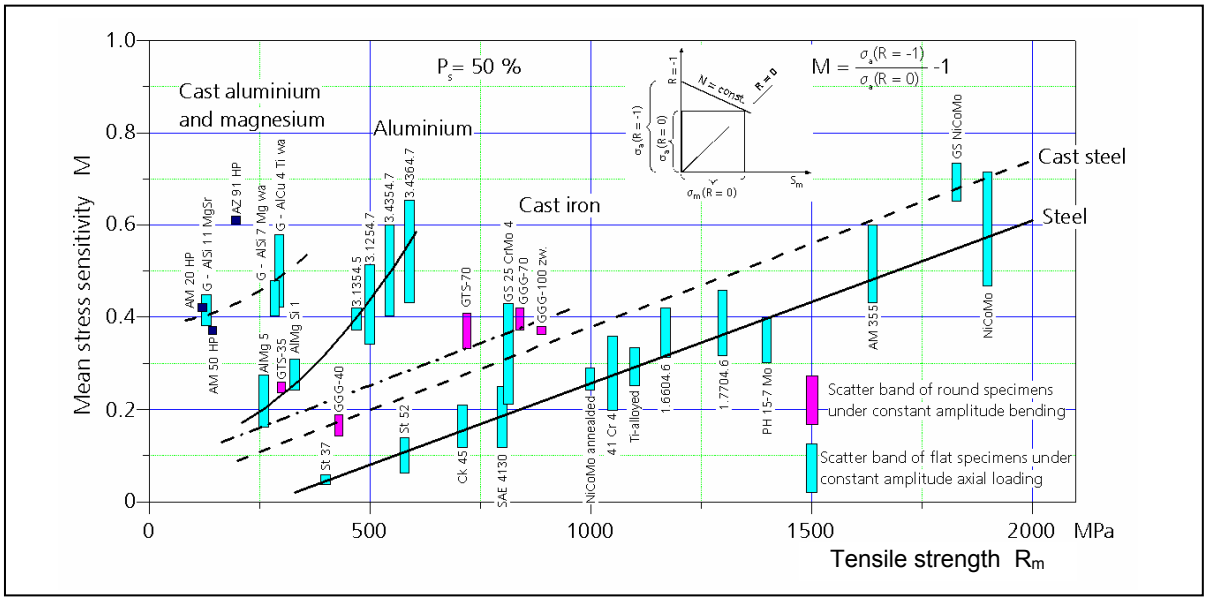


Figure 14: Mean stress sensitivity for different materials

Furthermore, the consideration of the micro constraint can result in a difference of a factor of 3 in the lifetime calculation.

Significantly, the damage accumulation has a big influence on the accuracy of the fatigue assessment. Calculations with different Palmgren Miner modifications confirm this. It is worth mentioning that the damage accumulation with Palmgren Miner´s rule is still unsteady and shows a large scatter in the damage sums, which is the quotient of calculation and test, [8], depicted in Fig. 15. Therefore, in many cases lifetime calculations are carried out with damage sums not equal to one. For comparability all the calculations in this project were carried out with the damage sum of one.

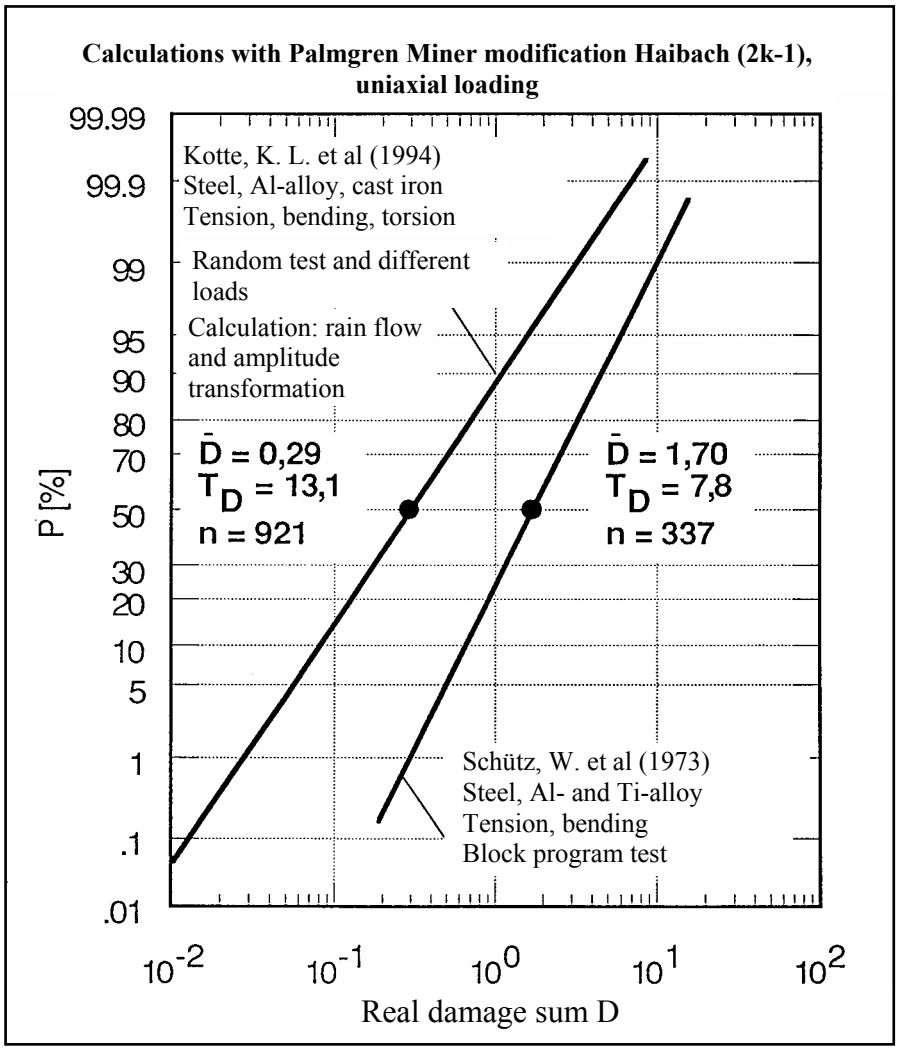


Figure 15: Distribution of damage sums with nominal stress concept, uniaxial loading (block program and random loading are considered separately due to the lifetime difference of factor 6 in tests)

For random loading, as it occurs in practice, 90% of determined real damage sums are below the conventional value D=1.0, i.e. a calculation with D=1.0 results in most cases unsafe estimate. Therefore, for a preliminary assessment the value D=0.3 should be used for non-welded material parts and D=0.5 for welded joints [9], as far as mean load fluctuations do not occur. Otherwise, the allowable damage sum must be reduced to D=0.1 and D=0.2, respectively.

Besides, for the damage accumulation in the case of complex nonproportional stress state, emphasis has to be put for the definition of a cycle and the cycle counting.

The comparison of the tests and calculations for the investigated components showed that for local nonproportional multiaxial stress states with a **small change of principal stress directions** acceptable lifetime calculations with suitable methods are possible. For this, an accurate analysis of the local stress condition, knowledge of the material behaviour for the given stress state and knowledge of the available methods are necessary. For local nonproportional multiaxial stress states with a **large change of principal stress directions** there is unsteadiness and wide scatter in the calculated lifetimes with big deviations from experimental test results. This is the case for the half of the investigated components. The most important point is to define large and small change of principal stress direction. This subject is discussed in [3]. No available method considers the changing direction of the principal stress due to nonproportional service loading conditions.

A general statement about the comparative accuracy of the strain based or the stress based methods within the scope of this investigation is not possible.

The study showed that the Integral Approach methods are suitable for lifetime calculations of components under multiaxial service loading, especially in the case of nonproportional stress state.

CONCLUSIONS

In general, the investigations showed that a lifetime assessment for a complex component under multiaxial service loading can not proceed with a mouse click on some software. An automation of the lifetime calculation steps should be based on well-founded expert knowledge. Furthermore, to stabilize the calculation, an adjustment of the included modules is required for each method.

The study showed that, for nonproportional multiaxial stress state, the magnitude of the direction change of the principal stress in interaction with the ductility of the material has a decisive influence on the accuracy of the lifetime calculation. Therefore, the consideration of changing principle stress directions and of ductility in the hypotheses and methods is necessary.

Due to the large scatter and the unsteadiness of the calculated lives, in case of safety critical components, experimental structural durability tests must be carried out.

Acknowledgments

The authors would like to thank the FKM/AiF, BMWi and the above-mentioned automotive industry for their financial support and the software houses for their participation.

3 REFERENCES

[1] F. Yousefi-H., H. Zenner, M. Küppers, C.M. Sonsino
Lebensdauerberechnung von Bauteilen bei mehrachsiger Betriebsbeanspruchung
FKM-Vorhaben Nr. 235, BMWi /AiF-Nr. 12043 N, Heft Nr. 271, FKM, Frankfurt/M., 2002

[2] C.M. Sonsino, M. Küppers, G. Fischer, K. Stoerzel
Structural durability of a cast aluminium truck wheel under complex service loading
7th International Conference on Biaxial\Multiaxial Fatigue & Fracture, Berlin, 2004, pp. 589-594

[3] F. Yousefi-H.
Lifetime assessment under multiaxial random loading - calculations and tests
7th International Conference on Biaxial\Multiaxial Fatigue & Fracture, Berlin, 2004, pp 343-348

[4] T. Seeger
Stahbau Handbuch, Band I, Teil B
Stahlbau-Verlagsgesellschaft mbH, Köln, 1996

[5] C.M. Sonsino
Overview of the state of the art on multiaxial fatigue of welds
In: Macha E., Bedkowski W., editors. Multiaxial fatigue and fracture. 2000. pp. 195-217
(ESIS Publ. No. 25)

[6] C.M. Sonsino, T. Lagoda
Assessment of multiaxial fatigue behaviour of welded joints under combined bending and torsion by application of a fictitious notch radius
International Journal of Fatigue 26 (2004), pp. 265-279

[7] C.M. Sonsino,
Einfluß der Werkstoffzähigkeit auf das Festigkeitsverhalten unter mehrachsiger Beanspruchung am Beispiel von Schweißverbindungen aus Stahl und Aluminium,
Mat.-wiss. und Werkstofftechnik 34 (2003), pp. 1-9

[8] H. Zenner, J. Liu,
Vorschlag zur Verbesserung der Lebensdauerabschätzung nach dem Nennspannungskonzept
Konstruktion 44, pp. 9-17, 1992

[9] FKM-Guideline, Analytical Strength Assessment of Components in Mechanical Engineering
VDMA Verlag, 5th edition, 2003

The shakedown theory and the fatigue damage: Industrial application.

Ky Dang Van[a], André Bignonnet[b]

[a] LMS, Ecole Polytechnique, 91128 Palaiseau, France
[b] ab consulting, 49750 Beaulieu, France

Abstract The application of the shakedown theory to the analysis of the fatigue problems is presented. This point of view on the fatigue strength and the fatigue damage allows to interpret in an efficient manner all types of industrial fatigue problems. The description of the stabilised mechanical state after shakedown at all scales, gives access to the engineering values which will drive the fatigue damage of the structure. The evolution of stress and strain tensors thus obtained for a cycle of fatigue, allows to predict the fatigue strength of structures. At High Cycle Fatigue when elastic shakedown occurs, the fatigue strength can be described by a simple combination of shear amplitude and hydrostatic pressure at any point of the calculated structure, whatever the complexity of the structure and of the loading. At Low Cycle Fatigue, from the stabilised state of the stress and strain, the fatigue strength is derived from a combination of the plastic, or the inelastic, strain energy and the hydrostatic pressure Numerous examples of fatigue analysis for different industrial areas are presented.

1 INTRODUCTION: PRESENTATION OF THE NEW FATIGUE MODELLING

Current industrial design is highly concerned by fatigue, which is the main failure mode of mechanical structures. Depending on the main interest of the scientist, the scale of studies range from microscopic (and even sub microscopic or atomistic) levels to dimensions of meters or tenth of meters (see for instance offshore structures) of structural components. Of course, these approaches are very different from each other and it is difficult for a non specialist to see any relation between them. For the engineer, the great number of points of view and consequently of methods and criteria may be an obstacle to have a clear idea of the computational tools that he has to use for the design of structures that have to resist to fatigue.
Main existing proposals for fatigue design can be classified in a simplified way as follows:
-stress approaches, generalizing the S-N curves which are mainly used in the high cycle fatigue regime;
-strain approaches, particularly plastic strain which are widely used in low cycle fatigue; some damage mechanic approaches can be ranged in this category since damage is often related to plastic strains;
-approaches based on fracture mechanic; fatigue is then considered as a pure propagation phenomenon.
Generally, these different approaches work well when the geometry of the structure and the loadings are simple, situations which are rarely encountered on industrial structures.
It is possible to use an other new approach, in which the material is considered as a structure (microstructure) submitted to cyclic loadings. The use of shakedown theorems and multiscale modelling permits to propose alternative original methods. These methods are robust and have been validated on a great number of industrial applications, particularly in the automotive industry. By that way, it is possible with a unique formulation, to calculate fatigue resistance of different types of structures undergoing different types of loadings (like plain specimens, assemblies,…, contact fatigue, fretting fatigue…). Moreover, using this theoretical basis, it is possible to propose an approach which unifies the thermomechanical fatigue in the low and high cycle regime.
In what follows, we shall distinguish three scales for the material description:
-the microscopic scale of dislocations;
-the mesoscopic scale of grains; σ, ε, ε_p, ρ are respectively the stress strain, plastic strain and residual stress tensors at the mesoscopic scale;
-the macroscopic scale representing phenomena at the scale of engineers; Σ, E, E_p, R are the macroscopic stress, strain, plastic strain, residual stress tensors which are supposed to be uniform in a representative volume element surrounding a point x where these quantities are evaluated.

The factors which favour the manifestation of fatigue phenomena are numerous. In a simplified analysis, one can say that it starts with the appearance of persistent slip bands in grains which broaden progressively during the first cycles. The proportion of grains in which slip bands develop increases with the applied load.
In the high cycle fatigue regime, the material at the macroscopic scale is apparently elastic (there are exceptions like in contact problems which will be studied hereafter). However at the mesoscopic level, plasticity occurs in certain grains and after a period which represents a large part of fatigue life, microcracks appear in these locus. Due to these local plastic strains, mesoscopic quantities will differ from the macroscopic quantities evaluated by engineers: for instance dissipated energy is zero at the macroscopic level (since the behaviour is elastic) and different from zero in some grains. In order to derive the mesoscopic parameters from the macroscopic ones, it is necessary to solve a localisation problem which cannot be achieve without some assumptions.
On the other hand, in the low cycle regime, plastic strain occurs at both levels so that there are few difference between macroscopic and mesoscopic quantities.
The general relation valid at any time t of the loading between macroscopic and mesoscopic stresses is:

$$\sigma = A.\Sigma + \rho \quad (1)$$

A is the elastic localisation tensor and ρ local residual stress tensor which depends on plastic strains. This additive term thus depends closely from the loading path. To illustrate this relation, one can consider the Lin Taylor model which supposes that total macroscopic and mesoscopic strain are equal, E=ε. Thus, $\varepsilon_e+\varepsilon p = Ee + Ep$; if l and L are the mesoscopic and macroscopic compliance of the material, one obtains:

$$\sigma = lL^{-1}.\Sigma + l.(E_p-\varepsilon_p) \quad (2)$$

which is similar to equation (1). lL^{-1} corresponds to localization tensor A and $l.(E_p-\varepsilon_p)$ corresponds to ρ. Most of the time A is taken equal to Identity. One can see that if there is few difference between ε_p and E_p as it is expected in the low cycle fatigue regime, ρ becomes negligible. Then $\sigma \approx A.\Sigma$, which is the Sachs model. Thus at low cycle regime mesoscopic and macroscopic parameters are not very different. In cyclic loading, all the mechanical parameters of equation (1) depend of time except when elastic shakedown occurs. In that case ρ (as well as E_p and ε_p) becomes independent of time t after a certain number of loading cycles.
In the proposed fatigue modeling, the concept of shakedown is essential. It is why it is necessary to recall some mathematical results, particularly the famous Melan-Koiter theorem which give a sufficient condition for elastic shakedown for a structure made of elastic perfectly plastic material ($J_2(\Sigma)<K^2$). It can be stated as follows:
"If there exist a time θ and a fixed self equilibrated stress field R(x) and a safety coefficient m>1 such that for any point x of the structure and $\forall t>\theta$, $J_2[m(\Sigma_{el}(x,t)+R(x)]<k^2$, *the structure will shakedown elastically*."
Σ_{el} is the stress response of the structure under the same external loading, but under the assumption that the constitutive material has a pure elastic behavior. In this paper, Koiter [1] draw our attention on the fact that the original formulation and demonstration of the theorem by Melan [2] is not correct since this author does not say anything about the magnitude of plastic deformation (and as a consequence on dissipated energy) which may occur before the structure reaches the shakedown state. It is clear that too large plastic strain has no physical meaning, so that Koiter added that *"if the total amount of plastic work performed in the loading is accepted as suitable criterion for assessing the overall deformation, boundedness of the overall deformation may be proved if the structure has a safety factor m>1 with respect to shakedown*. Thus, boundedness of dissipated energy, bounded plastic strain and existence of stabilized residual stress distribution are different aspects of elastic shakedown.
Melan's theorem is extended recently by Q.S. Nguyen [3] to generalized strain hardening materials. In these cases, the (intensive and extensive) strain hardening parameters must be bounded too and independent of time for t>θ.
Melan theorem is difficult to apply, since, the residual stress field must be self equilibrated, which is difficult to fulfill. An other proposal due to Mandel et al. [4] makes possible to overcome this difficulty in the case of strain hardening materials; the plasticity criterion can be written $J_2[(\Sigma-\alpha)]<k^2(P_{eq})$; α the kinematic strain hardening parameter is the center and $k(P_{eq})$ the isotropic parameter is the radius of the actual convex of plasticity. Generally, k increases with equivalent plastic strain P_{eq} until some maximum value k* and then decreases. Since $\Sigma=\Sigma_{el}+R$, one obtains:

$$J_2[(\Sigma_{el}-Z)]<k^2(P_{eq}) \quad (3)$$

Where Z= α-R. *Z is not necessarily self equilibrated* since α has not to fulfill this condition.
For cyclic loadings, Σ_{el} and R are functions of time t; however, Z(t) must be inside or on the convex (hypersphere) the center of which is $\Sigma_{el}(t)$. The trajectory of $\Sigma_{el}(t)$ is known at any point x of the structure because it is the solution of an elastic problem. *Shakedown may occur only if for* $t>\theta$*the intersection of these convex is not empty. The limit of possibility of elastic shakedown occurs when the intersection domain is reduced to a point, for a value corresponding to the maximum of* $k^2(P_{eq})=k^*$. *The dissipated energy density required for reaching this limit state corresponds to the local bound for possible shakedown. Beyond this bound failure will occur*.

In the following, we shall use these different results at different scales in order to propose a new fatigue modelling. We shall make the following fundamental assumption: *fatigue corresponds to the limit of elastic shakedown possibility of the material of the structure at the mesoscopic and macroscopic scale*. We then examine the consequences of this hypothesis in order to derive a unified fatigue modelling and the associate computational methods for high cycle and low cycle fatigue.

High Cycle Fatigue:

Characteristics of this fatigue regime are: the loadings are not very important, the structure is globally elastic and fatigue failure initiates only in some grains. It is difficult to evaluate directly the plastic strains and the dissipated energy in the grains which will fail. It is more judicious to proceed indirectly by an inverse way: since the fatigue limit corresponds to the shakedown limit, one can evaluate the local stress at the stabilized state if these grains are at (or near) the fatigue limit. Starting from the knowledge of $\Sigma(x,t)$ at a point x of the structure, we derive the local stress σ by constructing the smallest hypersphere containing $\Sigma(x,t)$ the center of which corresponds to $\Sigma^*=\alpha^*-\rho^*\approx \rho^*$, because it can be shown that $|\alpha^*|/|\rho^*|<<1$.
Thus we have an estimation of the local stress tensor $\sigma(t)=\Sigma(t)+\rho^*$ in grains which may fail by fatigue. Different fatigue criteria can be formulated based on the stabilized stress tensor:
-for instance a linear combination of shear ι and concomitant hydrostatic tension p (Dang Van): $\iota+ap<b$
-Papadopoulos criterion, $k^*+ap_{max}<b$, can be interpreted in the same way. The radius of the elastic domain at the limit state of possible shakedown depends of the maximum hydrostatic tension in the loading cycle.
The different computation steps for the application of these criteria can be found for instance in ref [5].

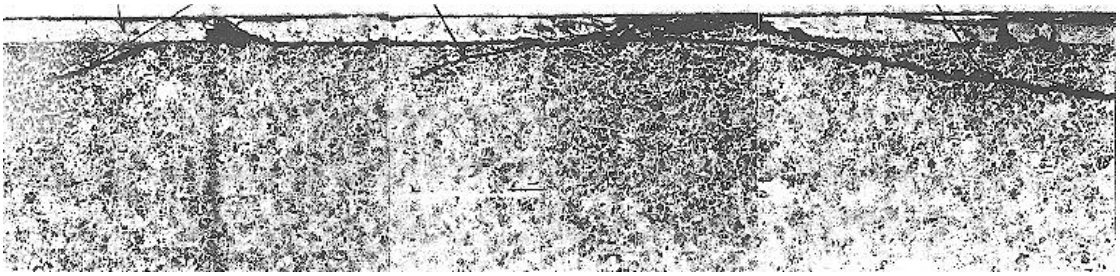
Low Cycle Fatigue:

In this regime macroscopic plastic strain is important and then difference between Ep and εp decreases so that there is few difference between macroscopic and mesoscopic parameters. However we propose to chose the dissipated energy because it is a scalar parameter easy to compute (particularly in presence of thermomechanical loadings) and which leads to good predictions on structures.

The following chapters are devoted to three applications which proved the efficiency of the proposed theory.
In the high cycle regime, many automotives structures (connecting rods, crankshafts, wheels…) have been designed using the proposed criteria. Prediction of damage induced by contact fatigue which is very difficult using existing approaches, (these type of problems involves multiaxial stress situations), can be studied using criteria derived from the proposed theory. An other example is devoted evaluation of the fatigue life of a structure undergoing thermomechanical loading in the low cycle fatigue regime. Finally we shall present an adaptation of the theory to predict fatigue resistance of welded structures.

2 CONTACT FATIGUE

Fatigue induced by contact is a very important topic, but very difficult to simulate and to predict, because it occurs most of the time under complex multiaxial loading and can sometime be at the origin of catastrophic failures. This type of fatigue.(fretting fatigue [6|, rolling or rolling-sliding [7]) can be studied using the proposed high cycle fatigue approach. Cracks fatigue initiation X induced by the traffic in the rail head like tache ovale, squat, head checks… interests all railways administrations and rail manufacturers. Quantitative modelling of these defects in relation with traffic parameters, require to use a multiaxial fatigue criterion because the stress and the strain fields are multiaxial and vary in a complex way. Moreover, due the type of loading (which is mainly compressive so that application of propagation laws is questionable) , plastic deformation may occurs under the repeated rolling contact which induce a macroscopic residual stress. Depending on the load level, three types of asymptotic responses may occur: elastic shakedown, plastic shakedown or ratchet. The two last asymptotic states lead to shelling or severe wear. Dangerous fatigue crack initiation like tache ovale or squat occurs in the elastic shakedown regime. To evaluate of the risk of crack initiation in relation with the traffic parameters and the plastic and fatigue properties of the rail, we first calculate the stabilized macroscopic residual stress distribution induced by the traffic, second we use the Dang Van's multiaxial criterion.
The first task necessitates to develop special original computational elastoplastic algorithms (stationary algorithm, direct cyclic method…) in order to evaluate the asymptotic state under repeated rolling , see [7].
We then apply the Dang Van criterion. The parameters a and b are derived from classical fatigue tests in tension , bending or torsion test.
An example of prediction of initiation of squat defect is represented on figure 1. Many other applications of this approach were done for the prediction of different types of contact fatigue. For more details, see for instance ref [6,7].



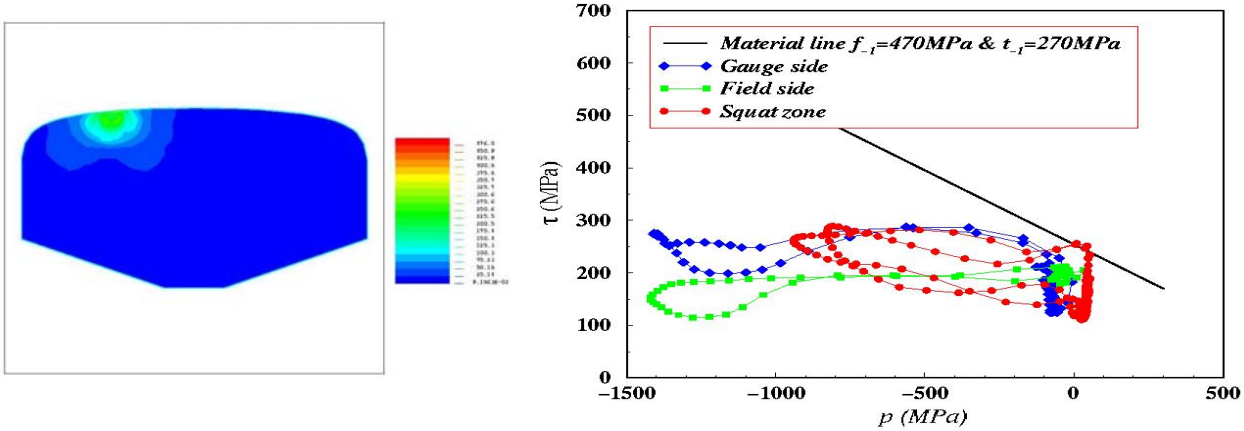


Figure 1. Prediction of squat type damage induced by wheel-rail interaction

3 THERMO MECHANICAL FATIGUE APPLICATION

The difficulty of the thermo mechanical damage simulation comes from the complex steps of the analysis. The success of such simulations is conditioned by the modelling of the limit conditions, the choice of the constitutive equations of the material, the numerical strategy, the damage driving force identification and finally the fatigue criterion.
Based on these observations, to be appropriate to the industrial context, thermo mechanical modelling should respect several constraints :

- the necessity to represent the behaviour of the material in the structure by simple constitutive equations. Thus, one should favour the representation of the mechanical behaviour without coupling with damage.
  From experience most of the time this coupling is not necessary and does not improve the accuracy of the on prediction on structure. Usually it is not necessary to describe the evolution of the structure cycle by cycle and particularly the early stage of the life of the structure. Therefore the identification of the parameters of the constitutive equations can be done on the steady state cycles obtained from material testing.
- the implementation in a finite element code using a numerical integration algorithm for the constitutive law stable and robust enough to authorise large integration steps.

Reasonable hypothesis should be introduced in the analysis: the thermal analysis is independent of the mechanical behaviour, the mechanical analysis is not coupled with damage, the fatigue analysis is based on a stabilised cyclic behaviour of the structure. Thus the objective of the thermo mechanical calculations is to obtain this stabilised fatigue cycle.
A cast iron exhaust manifold of a diesel engine, computed by PSA Peugeot Citroën, illustrates our proposal.

4.1 Loading conditions and numerical method for thermal computation

The fatigue assessment and the validation are made on a standard prototype durability cycle with a classical motor testing device. The equivalent damage history consists in a succession of full load at 4000 rpm and light load at the same regime. The transient period from full to light load and light to full load takes 30 s and the total cycle takes approximately 700 s. The external surface of manifold is monitored by regular visual inspection to detect crack apparition.
The aim of the thermal computations is the prediction of the temperature field distribution on the manifold from engine data, exhaust gas temperature and mass flow rate, which can already be estimated in the early phases of the project. The thermal computation is performed in two steps. A steady state temperature field distribution is first determined and afterwards the transient response is computed under some assumptions concerning the evolution of the boundary conditions and the evolution of thermal exchange coefficients.

4.2 Mechanical analysis

The constitutive law has to characterise the material from ambient to 800°C. At 20°C it presents an elastoplastic behaviour, above 700 °C an almost purely viscous one. The fact that one has to deal with a simple unifying law over the whole temperature range is dictated both by the F.E. transient analysis and the short development time constraint. This conducts to the choice of an elasto viscoplastic (EVP) material model. A reasonably representative model of the high temperature EVP behaviour of the material is achieved with a visco elastoplastic constitutive law with six temperature depending coefficients. An important point is to take care of the representativity of the characterisation tests in the sense of aging and stabilisation of the behaviour corresponding to long term service conditions

. The FE analysis has been performed in two steps: first the manifold has been screwed on the cylinder head and second a series of thermal cycles have been computed. The imposed temperature distribution was a result of the previous transient thermal calculations.
The number of cycles is chosen in order to obtain a stable cycle for the mechanical fields. The results has been analysed in term of dissipated energy per cycle, as indicated in Figure 2.

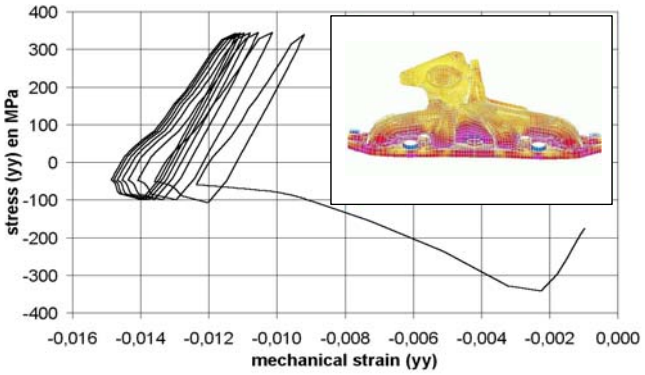


Figure 2 : Thermo mechanical calculation and stabilisation.

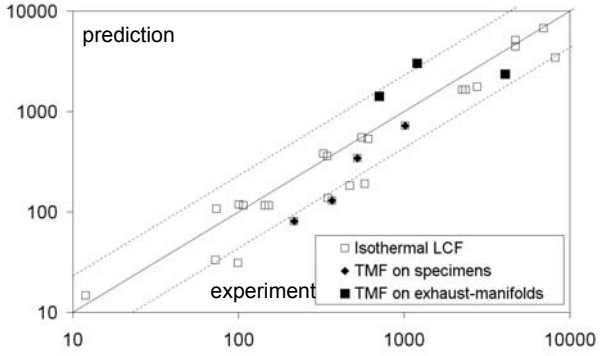


Figure 3 : Predicted versus experimental fatigue life

4.3 Fatigue life estimation

The final objective is to evaluate the fatigue strength, or the life time of the structure, from the stabilised response of this structure. Charkaluk and Constantinescu [8] observe that the dissipated energy per cycle at steady state

$$Ws = \int_{cycle} \sigma : \dot{\varepsilon}^{p} \, dt$$

can be representative of the fatigue behaviour of a material.
The interest of the dissipated energy per cycle comes from three main points :

- this energetic quantity can be easily generalised to multiaxial situation
- its determination is dependant of the temperature because it integrates the whole loading path and therefore allows calculations with anisothermal loading.
- W_S is representative of the cyclic behaviour of materials.

The fatigue criterion can be simply expressed by a relationship :

$$W = c \, N^{\beta}$$

The predictivity of the calculation is satisfactory as indicated by numerous comparative results between experiments and calculation on figure 3.
Take into account the fact that the dissipated energy is based only on the deviatoric part of the stress tensor, Amiable and Constantinescu [9] introduce the instantaneous hydrostatic pressure in the criterion in order to improve the predictivity of the previous relation when high triaxiality is present, $(W + \alpha \, p_{max}) = c \, N^{\beta}$.

4 FATIGUE ASSESSMENT OF WELDED STRUCTURES

4.1 A structural approach

Current practice in welded structure design is based on the use S-N curves, hot spot principal stress or structural principal stress limited to specific geometries. However, they are difficult to handle on complex shape components and for multiaxial loadings which is the case in most of industrial structures. To overcome this difficulty, we come

back to the structural approach with a clear definition of the design stress which can be transposed to multiaxial structural problems.

The classical introduction of the design stress is based on the extrapolation of far field stresses with unclear rules. In order to clarify the description of this design stress we propose an approach deriving from an analogy with the concepts which are at the origin of the Fracture Mechanics. Actually, it is known that the mechanical state in the highly damaged crack tip zone, called by H.D. Bui [10,11] the process zone, is inaccessible by the usual continuum solid mechanics. In this zone, the material is neither really continuous nor homogeneous and the local strains are not small. Nevertheless, the stress solution obtained from linear homogeneous and isotropic elasticity in small strains allows the correct description of the mechanical state *outside of the process zone*. Although it is erroneous at the vicinity of the crack tip, it makes sense in terms of *an asymptotic solution* which allows the correct control and the interpretation of the phenomena produced in the process zone. Likewise, we will look for a way to build the asymptotic solution which allows the correct control and interpretation of the phenomena produced in the critical zone of the weld. For that purpose we adopt an approach with meshing rules taking into account the local rigidity due to the weld instead of the local geometry of the weld itself (as it is the case in Fracture Mechanics, where the actual geometry of the crack tip is not taken into account) which is a very hazardous data. Therefore, the fatigue design can be based on a structural stress calculation from a finite element shell analysis. On this basis we can establish design rules for welded structures [12] with a structural stress, the asymptotic solution, which gives access to the fatigue strength through a unique S-N line where S is a local equivalent stress defined from τ and p at the Hot Spot $\tau_0=\tau+\alpha p$, as described in the next paragraph.

This implies the notion of elastic shake down at all scales, the shake down at the mesoscopic scale, in the sense of the Dang Van criterion, can exist only if the elastic shake down occurs at the structural scale.

4.2 Computing procedure and applications

J.L. Fayard et al. [13] developed an efficient numerical tool to evaluate the asymptotic mechanical field which defines precisely the design stress.

On the basis of a shell model, a meshing rule was established [13] with simple ideas: reproduce as precisely as possible the local rigidity induced by the weld, simulate the stress flow from one sheet to another through the weld. For that purpose, rigid body elements were used to link the two shells. Thus, the size of the elements at the intersection area has been particularly defined such that the geometrical stress is calculated without interpolation at nodes at the weld toe and the weld root, as shown in Figure 4, precisely where cracks commonly appear.

The stress tensor is kept from the center of gravity of the elements, which should be positioned in front of the critical areas, weld toe and weld root The same methodology can also be applied to any welded joint.

From a large data base the Dang Van criterion for welded steel structure is: $\tau_a = \alpha\, p + B$ as shown in Figure 5

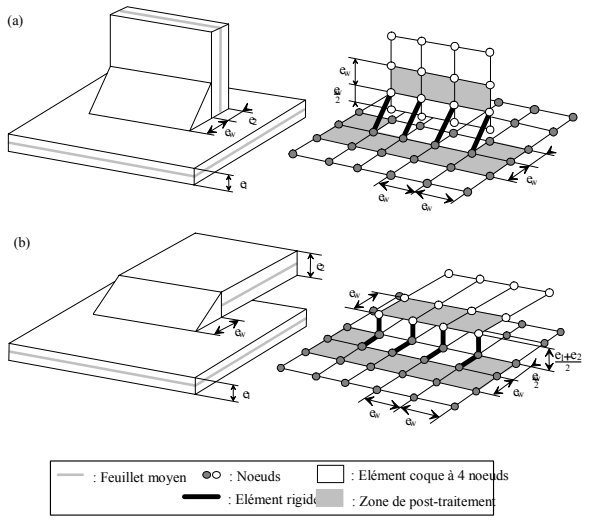


Figure 4. Meshing rules for continuous arc-welded joints. The geometry on the left hand side is associated to the thin shell modelling on the right hand side : (a) for fillet weld; (b) for overlap welded joint.

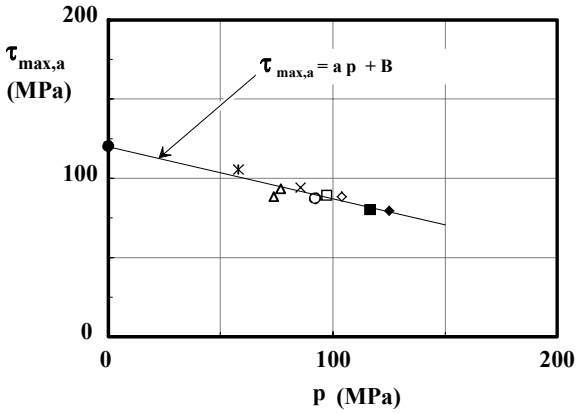


Figure 5. Mean fatigue strength at 10^6 cycles obtained on elementary arc-welded structures.

An application to industrial structures was carried out to predict fatigue resistance. For instance, Figure 6 summarizes the application of the local approach to predict the fatigue resistance of an engine sub-frame made of a metal sheets joined by continuous welds submitted to out of phase multiaxial loading. For an easier interpretation by the design office, the calculated value of the criterion displayed graphically is the quantity $\tau_a = \alpha\, p + B$. The failure happens at the predicted locus and fatigue limit can be evaluated.

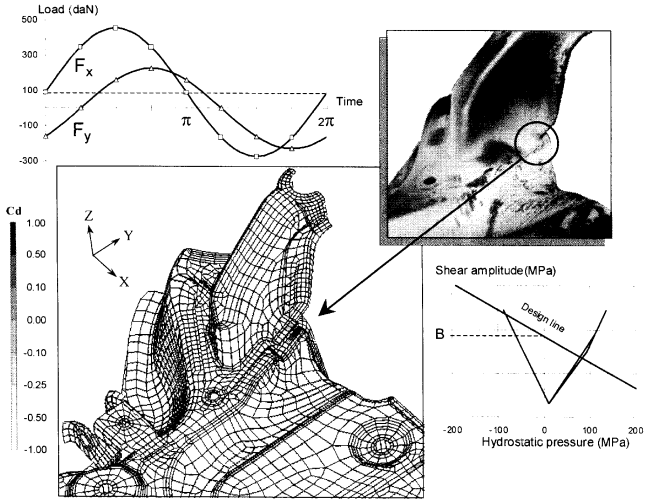


Figure 6. Application of the structural approach to assess fatigue resistance of an engine sub-frame undergoing multiaxial out of phase loading

5 REFERENCES:

1. Koiter,W.T. (1960), General Theorems for Elastic-Plastic Solids, In Progress in Solid Mechanics, eds. Sneddon, J.N. and Hill, R., 1, North-Holland, Amsterdam, pp. 165-
2. Melan, E. (1938), Zur Plastizität des räumlichen Kontinuums, Ing. Arch., 9, 116.
3. Nguyen, Q. S., (2000), Stability and Nonlinear Solid Mechanics, J. Wiley & Sons
4. Mandel, J., Halphen, B., Zarka, J. (1977), Adaptation d'une structure Elastoplastique à Ecrouissage Cinematique, Mech. Res. Comm.
5. Dang Van, K., Fatigue Analysis by the Multiscale Approach, High Cycle Metal Fatigue, From Theory to Applications, C.I.S.M. Courses and Lectures N° 392, Ed. Ky Dang Van &Ioannis V. Papadopoulos, Springer 1999 pp.57,
6. Dang Van, K., Maitournam, H.M., On a New Methodology for Quantitative Modelling of Fretting Fatigue, Fretting Fatigue: Current Technologies and Practices, ASTM. STP 1367, D.W. Hoeppner, V. Chandrasekaran and C.B. Elliot, Eds., American Society of Testing Materials, West Conshohocken, PA, 19428-2959
7. Dang Van, K., Maitournam, H.M., Rolling contact in railways: modelling, simulation and damage prediction, Fatigue Fract. Engng. Mater. Struct., Vol. 26, 2003, 939-948.
8. E. Charkaluk and A. Constantinescu. Energetic approach in thermomechanical fatigue for silicon molybdenum cast-iron. Materials at High Temperatures, 17, (3), pp. 373-380, 2000.
9. S. Amiable, A. Constantinescu, S. Chapuliot, A. Fissolo. Prédiction de durée de vie des structures sous chargement de fatigue thermique. 17ème congrès de Mécanique, Troyes sept. 2005,
10. Bui, H.D. Problèmes généraux de croissance de fissure. Partie I, approche de l'endommagement. Revue française de Mécanique, Vol. 4, (1983), pp. 3.
11. Bui, H.D., Dang Van, K. Some recently developed aspects of Fracture Mechanics. Nuclear Engineering and Design, Vol. 105, (1987), pp. 3.
12. Dang Van, K., Bignonnet, A., Fayard Assessment of Welded Structure by a Structural Multiaxial Fatigue Approach , Biaxial/Multiaxial Fatigue and Fracture, A Carpinteri, M de Freitas, A. Spagnoli Ed., ESIS/STP 31, Elsevier 2003, pp3-22.
13. Fayard, J.L., Bignonnet, A., Dang Van, K., Fatigue Design Criterion for Welded Structures, Fatigue Fract. Engng. Mater. Struct., Vol. 19, 1996, 723-229,.

14. Dang Van, K., Bignonnet, A., Fayard Assessment of Welded Structure by a Structural Multiaxial Fatigue Approach , Biaxial/Multiaxial Fatigue and Fracture, A Carpinteri, M de Freitas, A. Spagnoli Ed., ESIS/STP 31, Elsevier 2003, pp3-22

15. .

16. Fayard, J.L., Bignonnet, A., Dang Van,K., Fatigue Design Criterion for Welded Structures, Fatigue Fract. Engng. Mater. Struct., Vol. 19, 1996, 723-229,.

A volumetric energy based multiaxial fatigue life calculation method

J. Bénabès[a,b], T. Palin-Luc[a], N. Saintier[a], J-L. Charles[a], F. Cocheteux[b]

[a] ENSAM CER de Bordeaux
Laboratoire Matériaux Endommagement Fiabilité et Ingénierie des Procédés (EA 2727)
Esplanade des Arts et Métiers, F-33405, Talence Cedex, France
[b] Agence d'Essai Ferroviaire – SNCF
21 avenue du Président Allende, 94407 Vitry-Sur-Seine, France

Abstract A reliable design of industrial components against high-cycle multiaxial fatigue requires a fatigue criterion capable of predicting both the load-type and the stress-strain gradient effects. Gradient effects are of prior importance for the applicability of fatigue models to real structures. An extension of the existing volumetric energy based criterion, proposed by Lasserre, Palin-Luc [1] and Banvillet [2], is presented. Based on the volumetric strain-work density given to the material per load cycle, this proposal was validated for constant amplitude loadings (in or out-of-phase, with or without mean stresses). An extension of the criterion to fatigue life prediction for $N>5.10^4$ cycles based on the expression of a single fatigue crack initiation curve (master curve) is presented. The predictions of the method, available for constant amplitude loadings or loadings with small amplitude variations, with different frequencies or block sequences, are compared with results from literature. An application to a signal recorded in service (on a railway wheel) is presented.

1 INTRODUCTION

Designing metallic components against fatigue is still a difficult problem to handle for engineers since the transfer of fatigue data from specimen to real component is an arduous task. Two major phenomena are responsible for that: the stress gradient effect and the so called "size effect". In literature, many experiments show the influence of notches on the fatigue strength but components have seldom a well defined notch factor. Consequently, the use of data from laboratory tests has to be done very carefully (Sonsino et al. [3], Palin-Luc et al. [4]). Furthermore, in high cycle fatigue, the influence of the load type on the fatigue strength is well known (endurance limits in tension and in bending are different). A precise design against fatigue requires a method able to consider both the volumetric distribution of stresses-strains and the load type. Several authors proposed different methods to take into account the stress gradient effect: Flavenot and Skalli [5], Papadopoulos [6], Sonsino et al. [7], Lasserre and Palin-Luc [1] and Banvillet. et al [2]. Between these approaches the last one is, according to the authors, the only one able to predict experimental differences between endurance limits in tension and in bending. The criterion presented here is based on this volumetric energy based approach.

2 ENERGY BASED VOLUMETRIC FATIGUE CRITERION

Any criteria expressed only as a function of local variables (such as stress, strain tensors) at a point can not distinguish load types and predict stress-strain gradient effect because they do not take into account the distribution of stresses around this point. They can not take into account a non-local effect. To avoid this default Palin-Luc and Lasserre [1] proposed an energy based multiaxial fatigue criterion for fully reversed sinusoidal loads. This proposal uses the concept of volume influencing fatigue crack initiation around the critical point (with regard to fatigue), but this method has the main drawback to be load shape dependent for uniaxial loading (sinus, triangle, square). This is not in agreement with the fatigue data of Mielke [8] and Dietmann et al. [9]. Moreover such proposal can not be used for loadings with non-null mean value.

To avoid these lacks, Banvillet et al. [2] proposed to consider the strain work density given to each elementary volume of material per loading cycle, *Wg*, as the driving force for damage initiation and growth (1).

$$Wg(M) = \sum_{i,j} \int_T < \sigma_{ij}(M,t)\, \dot{\varepsilon}_{ij}(M,t) > dt = \sum_{i,j} \int_{\varepsilon ij,\max - \Delta\varepsilon ij}^{\varepsilon ij,\max} < \sigma_{ij}(\varepsilon_{ij}(M,t))\, d\varepsilon_{ij}^{e} > \qquad (1)$$

where <a> = a if a > 0 and <a> = 0 if a ≤ 0; $\dot{\varepsilon}_{ij} = \frac{d\varepsilon_{ij}}{dt}$.

The principal drawback of this energy based formulation is that it does not differentiate a mean tension state and a mean compression state. This is in disagreement with the experimental results which show that a normal mean stress in compression increases the fatigue strength [10, 11]. To avoid this insufficiency, we propose to separate *Wg(M)* in two parts: $Wg^{Sph}(M)$ due to the spherical part of the stress tensor and $Wg^{Dev}(M)$ due to the deviatoric part of this tensor (2).

$$\sigma_{ij} = \sigma_{ij}^{Sph} + \sigma_{ij}^{Dev} \text{ with } \sigma_{ij}^{Sph} = \sigma_{kk}\delta_{ij} \Rightarrow Wg(M) = Wg^{Sph}(M) + Wg^{Dev}(M) \quad (2)$$

$$W_g^{Sph}(M) = \sum_{i,j} \int_T < \sigma_{ij}^{Sph}(M,t)\ \dot{\varepsilon}_{ij}^{Sph}(M,t) > dt \quad (3)$$

$$W_g^{Dev}(M) = \sum_{i,j} \int_T < \sigma_{ij}^{Dev}(M,t)\ \dot{\varepsilon}_{ij}^{Dev}(M,t) > dt \quad (4)$$

It is assumed that only the strain work given by the spherical part is damaging when the hydrostatic stress is positive, the deviatoric part being all the time taken into account. The latter is always supposed to take part in the damage whereas the spherical part does not participate if the hydrostatic stress is negative. With the Banvillet definition of the strain work given, this decomposition is not possible in certain configurations. The formulation of *Wg* is consequently modified and called *Wf* according to equation (5) to allow this decomposition..

$$Wf(M) = \sum_{i,j} \int_T \sigma_{ij}(M,t)\,\dot{\varepsilon}_{ij}(M,t) < sign(\sigma_{ij}(M,t)\,\dot{\sigma}_{ij}(M,t)) > dt \quad (5)$$

This parameter is equal to the integral over a loading cycle of the positive part of the strain power density, this is also equal to the positive variation of the potential strain energy density over a loading period [2]. *Wf* is calculated from elastic strains after elastic shakedown of the material since usually the endurance limit is low enough to consider that the material remains elastic at the macroscopic scale [12]. It has to be noticed that for a uniaxial stress state *Wf* is not shape dependent (sinus, triangle, square, etc...).

2.1 Volume influencing fatigue crack initiation V*

As proposed by Palin-Luc and Lasserre [1], to predict the effect on the fatigue limit of the stress-strain distribution inside the component, we consider a volume influencing fatigue crack initiation, V* is considered. For a fully reversed uniaxial stress state, this volume is defined by the set of points loaded by a stress amplitude higher than a material dependent threshold stress σ*. From fully reversed fatigue experiments on a spheroidal graphite cast iron, these authors show that a threshold stress, σ*, can be defined below the conventional endurance limit σ^D (Palin-Luc and Lasserre [13]). At a considered point, a stress amplitude lower than this threshold does not initiate observable damage at the microscale (no micro-crack). A stress amplitude between σ* and σ^D contributes to micro-damage initiation only, which could develop if, either near this point or in the course of time there is a stress amplitude higher than σ*. The stress limit σ* is considered as a threshold stress of no damage initiation at the microscale, whereas the usual endurance limit σ^D corresponds to a macrocrack initiation.

By reference to an homogenous fully reversed uniaxial stress state (tension on smooth specimen) the threshold value corresponding to σ* is $Wf^* = (\sigma^*)^2/E$, where E is the Young modulus of the material. The volume influencing fatigue crack initiation is then defined by (6) around each critical point Ci (where *Wf* has a local maximum). Over this volume, the damaging parameter is the strain work density, exceeding the threshold *Wf**, given to the material (7). This damaging strain work density is supposed to be constant for a given material loaded at its endurance limit in a uniaxial stress state.

$$V^*(Ci) = \{\text{points } M(x,y,z) \text{ around } Ci \text{ such that } Wf(M) \geq Wf^*(Ci)\} \quad (6)$$

$$\varpi f(C_i) = \frac{1}{V^*(C_i)} \iiint_{V^*(Ci)} [Wf(C_i) - Wf^*]dv \quad (7)$$

2.2 Uniaxial Stress State

The condition for no fatigue crack initiation is thus $\varpi_f(C_i) \leq \varpi_f^D$, where ϖ_f^D is the value of ϖ_f at the endurance limit for an uniaxial stress state. By applying this hypothesis with the fatigue limits under fully reversed tension $\sigma_{-1,tens}^D$ and rotating bending $\sigma_{-1,rotbend}^D$ on smooth specimens, the threshold stress σ* can be identified (8); this equation is the same as proposed by Palin-Luc et al. [1].

$$\sigma^* = \sqrt{2\left(\sigma_{-1,tens}^D\right)^2 - \left(\sigma_{-1,rotbend}^D\right)^2} \quad (8)$$

It is assumed that for any loading and stress state at the endurance limit the value of ϖ_f, noted $\varpi_f^D(uniax)$, is constant (9, 10).

$$\varpi_f^D(uniax) = \varpi_f^D(tens) = \varpi_f^D(plane\ bend.) = \varpi_f^D(rot.bend.) \qquad (9)$$

$$\varpi_f^D(uniax) = \frac{\left(\sigma_{-1}^D(rot.bend.)\right)^2 - \left(\sigma_{-1}^D(tens)\right)^2}{E} \qquad (10)$$

2.3 Multiaxial Stress State

For a multiaxial stress state at the fatigue critical point a "multiaxial correction" is used as proposed in [1, 2, 17, 18] and previously introduced by Froustey et al. [15]. The triaxiality degree of stresses $dT(M)$ is defined by the ratio between the strain work density Wf^{Sph} due to the spherical part of the stress tensor and Wf (11). This ratio varies between 0 (pure distorsion) and 1 (pure equitriaxial stress state).

$$dT(M) = \frac{W_f^{Sph}(M)}{W_f(M)} \qquad (11)$$

In order to take into account the influence of the stress triaxiality, the strain work given at critical point C_i which is equivalent to a uniaxial stress state, $Wf_{eq}(C_i)$, is introduced:

$$Wf_{eq}(C_i) = Wf(C_i).\frac{F(dTuniax,\beta)}{F(dT(Ci),\beta)} \qquad (12)$$

At the endurance limit, whatever the loading and the stress state at the critical point, $Wf^D(C_i)$ is assumed to be related to the value of Wf in torsion $Wf^D(tors)$ by the F function (13). This function depends on both the triaxiality degree at the C_i point, $dT(C_i)$, and a material dependent parameter β (see Palin-Luc [1] and Banvillet [2] for details) . This parameter is representative of the material sensitivity to the stress triaxiality; its identification has to be done by applying equation (13) with the fully reversed endurance limits in rotating bending and in torsion.

$$F(dT(Ci),\beta) = \frac{Wf(Ci)}{Wf(tors)} = \frac{1}{1-dT(Ci)}\cdot\left\{1-\frac{1}{\beta}\cdot\ln\left[1+dT(Ci)\cdot\left(e^{\beta}-1\right)\right]\right\} \qquad (13)$$

The stress triaxiality influence is also taken into account in the definition of $\varpi f(C_i)$ which becomes $\varpi f_{eq}(C_i)$:

$$\varpi f_{eq}(C_i) = \frac{1}{V^*(C_i)}\iiint_{V^*(C_i)}\left[Wf_{eq}(C_i) - Wf^*\right]dv \qquad (14)$$

This quantity depends on the stress state at C_i and on the volumetric distribution of stresses inside $V^*(C_i)$.

To prevent fatigue crack initiation at the critical point, the volumetric energy based multiaxial fatigue criterion is $\varpi f_{eq}(C_i) \le \varpi_f^D(uniax)$. The criterion can then be applied for any multiaxial loadings.

2.4 Use of the proposal

To apply this volumetric energy based proposal the following parameters have to be identified: σ^*, β, ϖf^D_{uniax}, the Young modulus, E, and the Poisson ratio, ν, of the material. Only three experimental endurance limits on smooth specimen under fully reversed loadings are needed: in tension, $\sigma_{-1,tens}^D$, in rotating bending $\sigma_{-1,rotbend}^D$, and in torsion, τ_{-1}^D.

From the stress-strain evolution on a loading period, $Wf(M)$ is computed at all the points M of the component. The critical points C_i are localized by looking for the local maxima of Wf. At each critical point, $dT(C_i)$, $Wf_{eq}(C_i)$ and $\varpi f_{eq}(C_i)$ are computed. No fatigue crack initiates if the inequality $\varpi f_{eq}(C_i) < \varpi_f^D(uniax)$ is verified.

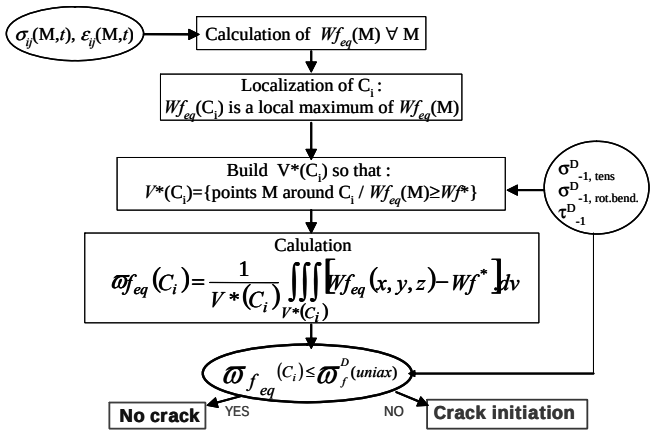
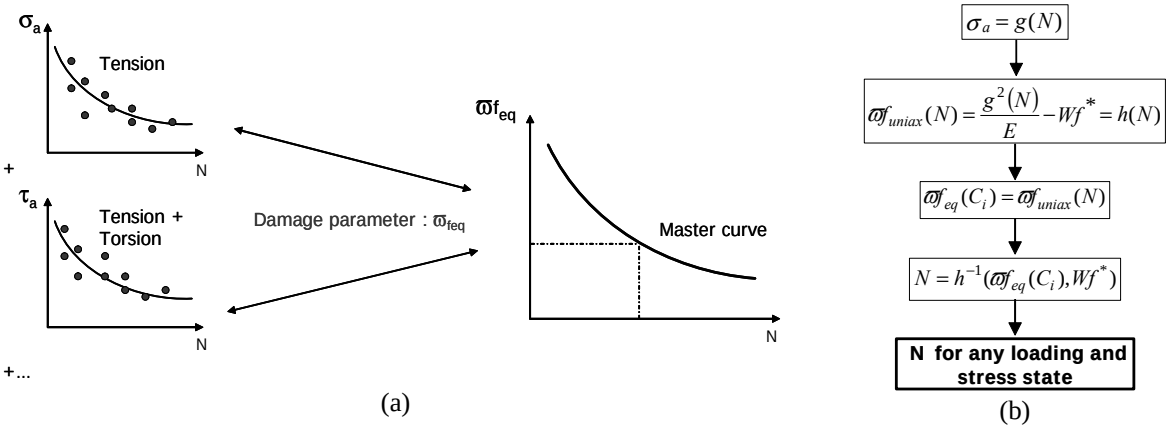


Figure 2. Synoptic of the proposal

3 FATIGUE LIFE PREDICTION

3.1 A master curve to fatigue crack initiation

The proposed energy based volumetric criterion distinguishes simple and combined loadings. We show that it can also be applied in limited endurance to predict the S-N curves corresponding to any load type for fatigue life higher than approximatively 5.10^4 cycles. These predictions are possible, from a reference experimental median S-N curve (crack probability 50%). From a median experimental S-N curve on smooth specimens, $\sigma_a = f(N)$, it is possible to link ϖf_{eq} and the median fatigue life N (Figure 3a). Indeed, as the proposed criterion distinguishes loadings, it is possible, by using the relations developed in paragraph 2 and with the assumption that ϖf_{eq} is constant for a fixed number of cycles whatever the load type and the stress state, to identify a master curve $\varpi f_{eq} = G(N)$. The synoptic of the proposal is described in Figure 3b.



(a) (b)

Figure 3. a) Relation between any S-N curve and $\varpi f_{eq}(N)$ as damage parameter, b) Synoptic of the fatigue life calculation

3.2 Comparison predictions / experiments from literature

3.2.1 Material

The fatigue data used to test the accuracy of the fatigue life calculation method are extracted from Bennebach [16], Palin-Luc [17] and Banvillet [18] who carried out tests on the SG cast iron EN-GJS800-2. The mechanical characteristics of this cast iron are given Tables I and II.

Table I. Static mechanical characteristics of the SG cast iron EN-GJS800-2.

E (MPa)	ν	$Re_{0.02}$ (MPa)	$Re_{0.2}$ (MPa)	Rm (MPa)	A (%)
164900	0,275	320	462	795	9

Table II. Experimental endurance limit at 10^6 cycles on cylindrical smooth specimens of the SG cast iron EN-GJS800-2.

$\sigma^D_{tens,-1}$ (MPa)	$\sigma^D_{pla.bend,-1}$ (MPa)	$\sigma^D_{rot.bend,-1}$ (MPa)	τ^D_{-1} (MPa)
245	294	280	220

3.2.2 Specimen geometry and test conditions

All the fatigue tests on the SG cast iron EN-GJS800-2 presented in this part were carried out on the same smooth specimens, with a diameter of 12 mm and a median torus of radius 24.5 mm [23]. The theoretical

stress concentration factors are: Kt (bending)=1.07 and Kt (torsion)=1.05. All the experiments were carried out until fatigue macrocrack initiation was detected by monitoring, in real time, the specimen stiffness decreasing. The size of the detected macrocrak is around 1 mm in depth. Three different variable amplitude fatigue tests were carried out.

a). Combined plane bending and torsion ($R\sigma$ = - 1) with different frequencies [17, 18]

Fully reversed combined plane bending and torsion with different frequencies are illustrated in Figure 4a. The duration of the loading sequence T is the longest period of the 2 stresses (torsion in Figure 4a). The loading conditions are indicated in Table III, where f_σ/f_τ indicates the frequency ratio between the bending and torsion stresses; the bending stress frequency, f_σ is 50 Hz. The tests were carried out under load control. Ten specimens were tested for each tests series.

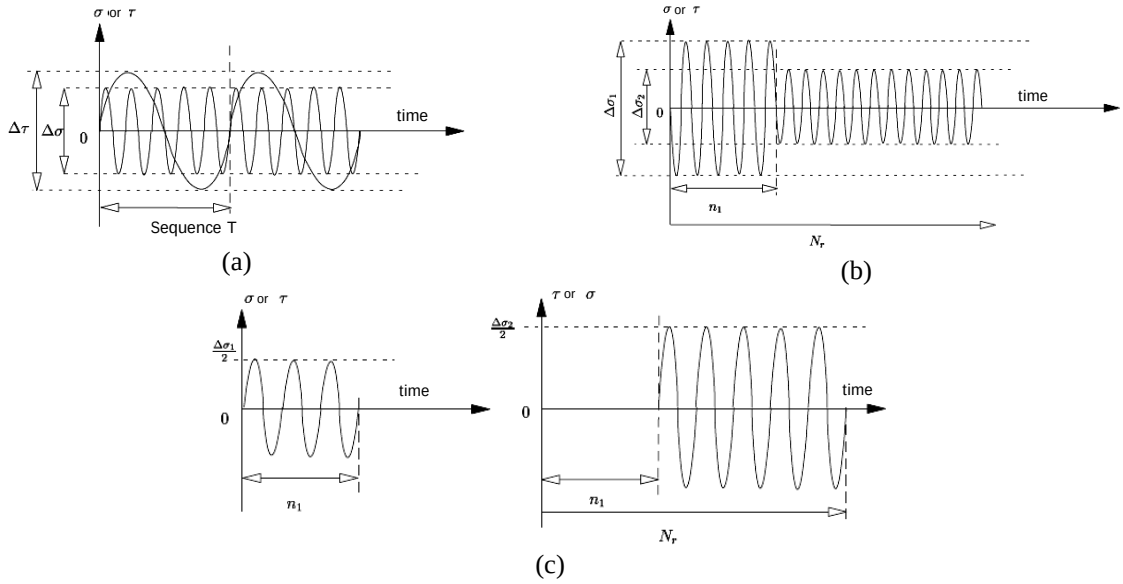


Figure 4. Different variable amplitude fatigue tests: a) Fully reversed plane bending and torsion combined loadings with different frequencies, b) Loadings with two successive blocks under simple loading (R_σ = - 1) until crack initiation, c) Loadings with 2 blocks of different stresses, applied successively until crack initiation.

Table III. Conditions and results of the combined plane bending and torsion tests (R_σ = - 1) with the same frequency and different frequencies on cast iron EN-GJS800-2.

σ_a (MPa)	τ_a (MPa)	f_σ/f_τ	N_{exp} (cycles)	$N_{predicted}$ (cycles)
225	167	1	122 191	235 000
225	167	5	49 645	37 565
155	204	1	119 911	106 000
155	204	5	86 785	65 237

b). Loadings with two blocks under simple loading (R_σ = - 1) [16]

During these tests illustrated in Figure 4b, the stress is the same for the two successive blocks (plane bending or torsion), only the stress level varies. ½ $\Delta\sigma_1$ and ½ $\Delta\sigma_2$ indicate the amplitudes of the local stresses (computed by finite element analysis) of the first and second block, n_1 represents the number of cycles imposed during the first block and N_{exp} the total number of cycles for a probability of crack of 50 %. The loading conditions are in Table IV. The first block is the " high " or " low " block.

Table IV. Fatigue tests with two blocks: conditions and experimental data [16]

Loading	½ $\Delta\sigma_1$ (MPa)	½ $\Delta\sigma_2$ (MPa)	n_1 (cycles)	N_{exp} (cycles)	$N_{predicted}$ (cycles)
Plane bending	320	352	110 000	194 070	189 021
Plane bending	352	320	50 000	181 550	241 898
Plane bending	352	303	50 000	258 040	398 067
Plane bending	303	352	160 000	278 420	246 741
Torsion	249	233	50 000	204 970	551 925
Torsion	233	249	160 000	210 300	286 297

c). Loading with two blocks of different loadings [16]

These tests are similar to the previous ones but the loadings change from one block to another (bending then torsion or conversely). Four tests of this type were carried out by Bennebach [16] on smooth specimens

made of cast iron EN-GJS800-2. The load path is proportional for each block but non proportional on the whole of the loading (Figure 4c). The loading conditions are in Table V.

Table V. Fatigue tests with two blocks of different loadings: conditions and experimental data [16]

Loading	½ $\Delta\sigma_1$ (MPa)	½ $\Delta\sigma_2$ (MPa)	n_1 (cycles)	N_{exp} (cycles)	$N_{predicted}$ (cycles)
Torsion/Plane bending	233	352	110 000	239 180	251 994
Torsion/Plane bending	249	303	50 000	265 580	467 580
Plane bending/Torsion	352	233	50 000	296 330	468 373
Plane bending/Torsion	303	249	160 000	265 740	279 086

3.2.3 Results and discussion

Figure 5 shows that the predictions of the proposed fatigue life calculation method remains in an interval of more or less 2 times the experimental fatigue life. These predictions are reasonably good for both proportional or non proportional loadings. The method gives good predictions even for tests known as discriminating (combined loadings with different frequencies, two blocks of different loadings).

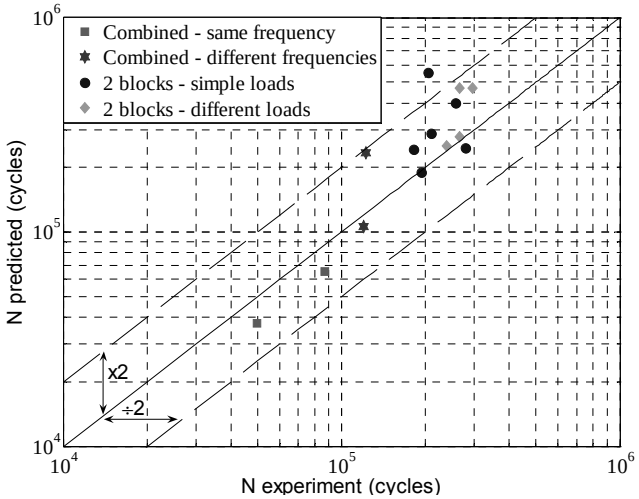


Figure 5. Comparison of the predicted and experimental fatigue life for the combined plane bending and torsion tests, and tests by blocks on the SG cast iron EN-GJS800-2.

3.3 Comparison predictions / experiments on a railway application

3.3.1 Material

The fatigue data used to test the predictions of the fatigue life calculation method are extracted from ERRI [19] work carried out on the R7 steel (close to Ck45 or SAE1045 steel). The various characteristics of this steel are given in tables VI and VII.

Table VI. Static mechanical characteristics of the R7 steel.

E (MPa)	ν	$Re_{0.2}$ (MPa)	Rm (MPa)	A (%)
195000	0,29	440	795	19

Table VII. Experimental endurance limit at 2.10^6 cycles on cylindrical smooth specimens of the R7 steel.

$\sigma^D_{tens,-1}$ (MPa)	$\sigma^D_{pla.bend,-1}$ (MPa)	$\sigma^D_{rot.bend,-1}$ (MPa)	τ^D_{-1} (MPa)
272	296	283	198

3.3.2 Specimen geometry and test conditions

All the fatigue tests on the R7 steel presented in this part were carried out on the same smooth specimens, with a diameter of 8 mm and a median torus of radius 50 mm [19].

With regard to the test conditions, a multiaxial loading is applied on a wheel by a biaxial test bench. Strain gauges stucked on this wheel allow, after post treatment, to plot the evolution of stresses at a given point. This load path is then restored on smooth specimen with a combined tension-torsion loading. The variable amplitude loading is illustrated Figure 6. In order to obtain various fatigue life, this loading is magnified by a factor k (Figure 6). Different magnification factors were applied on the specimens, experimental and predicted number of cycles to fatigue crack initiation are given in Table VIII.

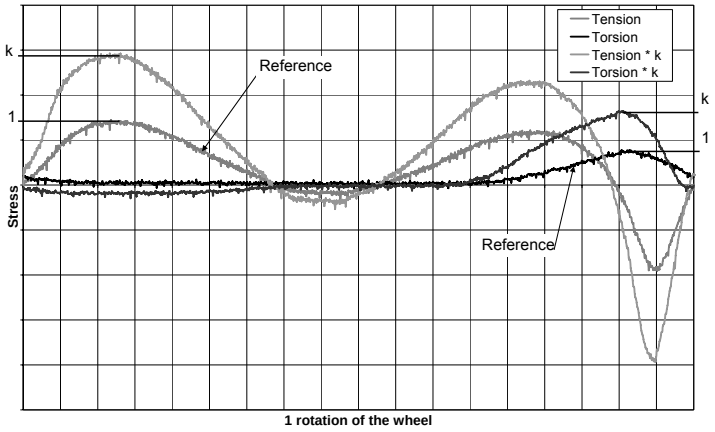


Figure 6. Variable amplitude combined tension-torsion load history and illustration of the magnification factor k.

Table VIII. Predictions and experimental data of the variable amplitude combined tension-torsion tests.

k	N_{exp} (cycles)	$N_{predicted}$ (cycles)	Comments
2.5	> 1 000 000	2 384 258	No crack during test
4	894 766	715 276	
5	57 843	52 935	
5	67 731	52 935	

3.3.3 Results and discussion

Figure 7 illustrates that the predictions of the proposed fatigue life calculation method remains in an interval of more or less 2 times the experimental fatigue life. These predictions are reasonably good for variable amplitude loading. The method gives good predictions even for tests giving low number of cycles to fatigue crack initiation.

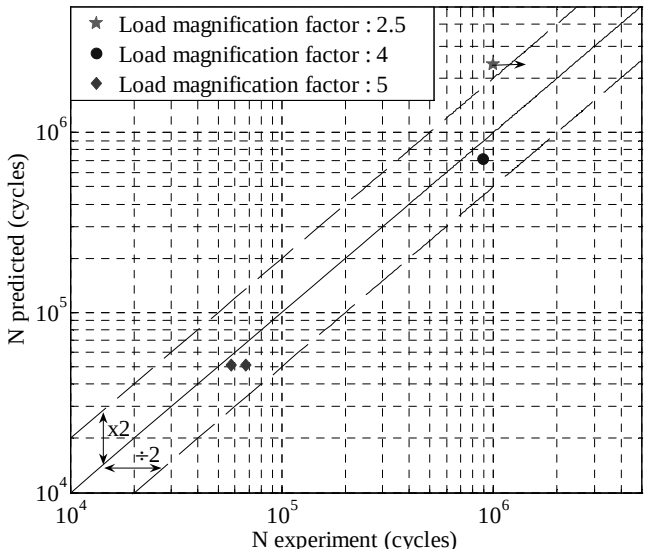


Figure 7. Comparison of the predicted and experimental fatigue life for the variable amplitude combined tension-torsion tests on R7 steel.

4 CONCLUSION AND PROSPECTS

This paper presents a high cycle multiaxial fatigue criterion depending on the stress-strain volumetric distribution. Its predictions distinguish load type. A fatigue life calculation method leading to good predictions for various types of loading is presented. To apply the proposal on a component with a complex geometry, a post-processor for finite element calculation software is needed.

The next goal is to widen the method with random loadings in order to take into account service loadings. Tests under service loadings on specimens and components will finally be carried out to validate the proposal.

5 REFERENCES:

1. PALIN-LUC T., LASSERRE S., An energy based criterion for high cycle multiaxial*., A/Solids*, 17, 1998, pp. 237-251. fatigue, *Eur. J. Mech*
2. BANVILLET A., PALIN-LUC T., LASSERRE S., A volumetric energy based high cycle multiaxial fatigue criterion, *International Journal of Fatigue,* Volume 25, Issue 8, August 2003, Pages 755-769
3. SONSINO C.M., KUEPPERS M., Fatigue behaviour of welded aluminium under multiaxial loading, In: *Proc. 6th ICB/MF&F*, M.M. de Freitas Ed., Lisboa, Portugal, 2001, pp. 57-64.
4. PALIN-LUC T., KAUFMANN H., LASSERRE S., SONSINO C.M., Prise en compte de l'influence de la distribution des contraintes et des effets d'échelle pour une utilisation pratique en fatigue, In: SF2M, 18èmes Journées de Printemps de la Fatigue, Paris, France, pp. 30(1)-30(10), 1999.
5. FLAVENOT J-F., SKALLY W., L'épaisseur de couche critique ou une nouvelle approche du calcul en fatigue à long terme des structures soumises à des sollicitations multiaxiales en présence de gradient de contrainte. *Rev. Mécanique Matériaux et Electricité*, 397, 1983, pp.15-25.
6. PAPADOPOULOS I.V., PANOSKALTSIS V.P., Invariant formulation of a gradient dependent multiaxial high-cycle fatigue criterion, *Engng. Fract. Mech.,* 55, 4, 1996, pp. 513-528.
7. SONSINO C.M., KAUFMANN H. , GRUBISIC V., Transferability of material data for the example of a randomly loaded truck stub axle, *SAE Tech. paper series*, 970708, 1997, pp. 1-22.
8. MIELKE S., Festigkeitsverhalten metallischer werkstoffe unter zweiachsig-schwingender beanspruchung mit verschiedenen spannungszeitverlaufen, PhD thesis, Aachen, Germany, 1980.
9. DIETMANN H., BONGHIBHAT T., SCHMIDT A., Multiaxial fatigue behavior of steels under in-phase and out-of-phase loading including different wave forms and frequencies, In: *Proc. 3rd ICB/MF*, Stuttgart, FRG, 1989, pp. (61)1-17.
10. SINES G., Behavior of metals under complex static and alternating stresses, In: *Metal Fatigue*, G. Sines, J.L. Waisman and T.J. Dolan Ed., Mc. Graw-Hill, 1959, pp.145-169.
11. SMITH J.O., The effect of range of stress on fatigue strength of metals, *Eng. Experiment Station*, bulletin 334, University of Illinois, 1942, 52 p.
12. LEMAITRE J., CHABOCHE J-L., Mécanique des matériaux solides, Bordas, Paris, 1988.
13. PALIN-LUC T., LASSERRE S., Experimental investigation on the significance of the conventional endurance limit of a spheroidal graphite cast iron, *Fat. Fract. Eng. Mater. Struct.*, 21, 1998, pp. 191-200.
14. FROUSTEY C., Fatigue multiaxiale en endurance de l'acier 30NCD16, PhD Thesis, E.N.S.A.M., Bordeaux, France, 1987.
15. FROUSTEY C., LASSERRE S., DUBAR L. Essais de fatigue multiaxiaux et par blocs. Validité d'un critère pour les matériaux métalliques', In: *Proc. Mat-Tech 92*, L. Castex, G. Pluvinage and L. Vincent Ed., IITT-International, France, 1992, pp. 79-85.
16. BENNEBACH M., Fatigue d'une fonte GS. Influence de l'entaille et d'un traitement de surface, PhD thesis, ENSAM CER de Bordeaux, France, 1993. (157 p.).
17. PALIN-LUC T., Fatigue multiaxiale d'une fonte GS sous sollicitations combinées d'amplitude variable, PhD Thesis, ENSAM CER de Bordeaux, France, 1996. (261 p.).
18. BANVILLET A., Prevision de durée de vie en fatigue multiaxiale sous chargements réels : vers des essais accélérés, PhD thesis, ENSAM, CER Bordeaux, 2001.
19. ERRI, Dimensionnement des roues - Critère de fatigue multiaxiale, Rapport final, ERRI B 169/RP 19, 2004.

Duration life prediction on real rubber parts with road load data

Pierre Charrier[a], Elisabeth Ostoja-Kuczynski[a], Ida Raoult[b], Laurent Gornet[c]

[a] Trelleborg Automotive AVS Europe, Advanced Engineering Department, Carquefou, France
[b] PSA Peugeot Citroen, DRIA/SARA/MATE, Vélizy Villacoublay, France
[c] Ecole Centrale de Nantes, GeM UMR CNRS 6183, Institut de Recherche en Génie Civil et Mécanique, Nantes, France

Abstract The key point of the present work is the application of new scientific results regarding cyclic behaviour of filled natural rubber to the analysis of stochastic signals, so-called Road Load Data. After briefly recalling the theoretical background of elastomer durability properties, we will propose a generalised mean stress correction efficient to predict the specific reinforcement phenomenon under tensile-tensile condition. Finally, we will face our model to real endurance test results.

1 INTRODUCTION

Durability is an essential key point for automotive industry and its suppliers. To increase the reliability of the endurance specifications, most carmakers have chosen to measure the loads applied on the parts directly on vehicle driven on reference tracks (bad pavements, normal road, highway…). The whole endurance is then defined by a list of tracks and, for each track, an associated number of repetitions. This is the so-called Road Load Data (RLD), and the complete sequence is associated with a known severity. The obvious gain of reliability is balanced by the increase of entanglements for the design of the part:

- ✓ Finite Element calculations are more complex and test duration is increased.
- ✓ Moreover, an extensive knowledge about durability theory is needed to analyse these stochastic and multiaxial signals.
- ✓ Finally, expensive multiaxial test rigs are used to validate the parts (see Figure 1).



Figure 1. MTS three-axis test rig used for engine mounts endurance validations based on RLD

For elastomeric parts, e.g. engine mount, torque rod, bushing or exhaust hanger (see Figure 2), fatigue design is in an increasing degree of complexity due to the critical lack of theoretical background about rubber durability. Only a few rare and recent published scientific papers deal with this problematic. To face this situation, Trelleborg Automotive Europe decided, five years ago, to start a vast research program focused on rubber durability. Three main deliveries were defined: increase of Finite Element simulation reliability, increase of the time reduction factor of RLD and material enhancement. A large part of this work includes a scientific collaboration with the French Carmaker PSA Peugeot Citroen.

The aim of the present paper is the duration life prediction of rubber parts submitted to monoaxial RLD. The procedure is based on the establishment of a simple mean stress correction and the validation of the applicability of the Rainflow counting method. In the first paragraph, we will present the experimental test rig, the test specimens and the chosen material. The second paragraph deals briefly with FEA simulation and highlights the need of adapted behaviour law to capture the local stress or strain state of rubber materials loaded cyclically. Then, we will focus on the analysis of test specimens loaded with uniaxial sinusoidal signals. Results will be used to establish the RLD analysis procedure. In particular, the Haigh diagram of filled natural rubber will be compared to classical metallic mean stress correction (e.g. Goodman and Gerber). In the fourth part of the study, we will present test results based on two different stochastic signals including compression-tension and tension-tension cycles. The measured duration lives will be compared to the predicted ones using Rainflow counting method and various mean stress corrections.

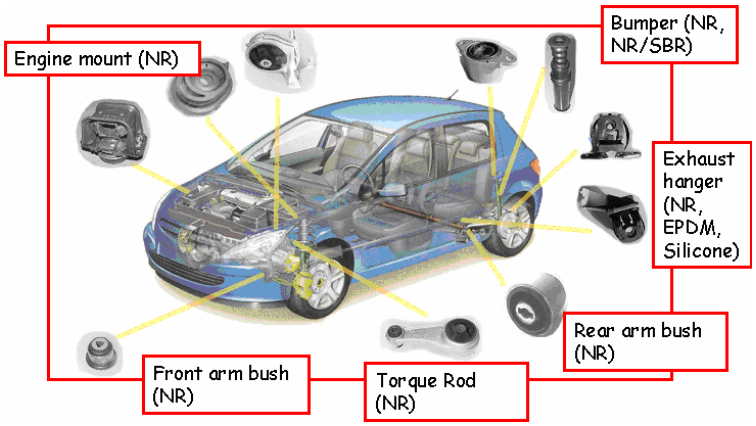


Figure 2. Some rubber parts used on vehicle to reduce the level of vibration and increase the passenger comfort

2 EXPERIMENTAL CONTEXT

Previous works propose two different approaches to characterise elastomer durability. The first one, called crack initiation prediction, assumes that the test specimen does not initially contain cracks (Ref. 5). The result of this approach is a Wöhler curve (durability versus local load amplitude) where the durability Ni represents the number of cycles before occurrence of a predefined critical size crack. This leads to the general equation:

$$N_i = A \cdot criterion^{\alpha} \qquad (1)$$

where A and α are two parameters depending on the tested material, and criterion represents a measure of the applied mechanical load. Maximal principal strain or stress or elastic energy density are frequently used and discussed in most scientific papers.

The second one, called crack propagation prediction, is introduced by Thomas (Ref. 6) and resumes the initial work of Rivlin and Thomas on crack propagation under monotonic loads (Ref. 7). Using a notched test specimen, the crack growth rate dc/dN is measured as a function of dynamic applied tearing energy ΔT. The crack growth curve obtained is modelled by the following equation:

$$\frac{dc}{dn} = B \cdot \Delta T^{\beta} \qquad (2)$$

Where B and β are two parameters depending on the tested material, and ΔT is the effective tearing energy range (Ref. 11):

$$\Delta T = T_{max} - max(T_{min}, 0) \qquad (3)$$

Automotive industry gives priority to the prevention of crack initiation. As a consequence, the first strategy is preferred when it comes to analyse the endurance properties of an elastomer, even though it has been demonstrated that these two approaches have a lot of similarities (Ref. 1 and 8).

Two test samples were designed for the present experimental campaign and are presented in Figure 4 and 5. The first sample is called AE42 and the second one AE2 (both are axi-symmetric notched samples, with a radius of the notch being equal to 42 or 2 mm). It allows tensile-compression and tensile-tensile test to be performed with a range of biaxiality ratio of the local stress state. Furthermore, two different linear actuators are used for the experiments. The maximum loading displacements are 50 and 100 mm, and maximum loading rates are 0.6 m.s-1 and 0.3 m.s-1, respectively. They can bear a loading of 3 kN. Good performances by this test equipment enables to study simple sinus, multi-blocs sinus and also RLD (in that case, the main restriction is due to the maximum test velocity). Finally, fatigue tests are performed in a climatic chamber, and the temperature is set to 23°C. The test conditions (amplitude and frequency), are chosen to limit the rubber heat build up. All tests are performed with a controlled skin temperature of the elastomer allowing the assumption of constant temperature (Ref. 2).

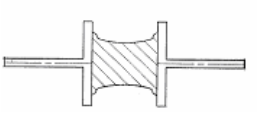


Figure 4. AE42 test specimen

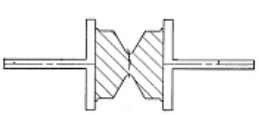


Figure 5. AE2 test specimen

Post-treatment of crack initiation tests requires a clear and generalised definition of the “end of life” (also called number of cycles until crack initiation Ni). It should be physically motivated, applicable to different loading conditions, and suitable for real component design. Such a definition was already proposed previously for test specimens and we will adopt it in the present work (Ref. 2). We can briefly recall the chosen theoretical and physical background. From a classical point of view, fatigue failure should be dissociated in two phases: crack nucleation and crack propagation. For natural rubbers, the existence of these two separated steps is not yet proved. Only some recent publications propose experimental procedures to quantify the respective duration of each theoretical stage (Ref. 12 and 9). The main conclusion is that after less than 20 % of an endurance test realised with test specimens similar to the AE42 one, internal micro cracks are detectable. Moreover, most of the scientific community assume that pre-existing flaws can be found in vulcanised rubber and that there is no nucleation stage. Having in mind this statement, “end of life” has to be linked to a defined critical size of the growing crack. However, this natural approach is not suitable for component design (final acceptance is frequently based on the part stiffness evolution after endurance test). A second strategy based on the apparent stiffness K is preferred. Two physical phenomena are responsible for the sample loss of stiffness during cyclic load: the viscoelasticity and the growth of a macroscopic defect in the sample. As long as no defect is observed, the stiffness decrease is driven by viscoelasticity and the sample stiffness is simply related to the number of cycles by:

$$K(N) = K_0 \, log(N) + B \tag{3}$$

Where K_0 and B are material parameters. The differentiation of Equation 3 with respect to N yields:

$$\frac{dK}{dN} = \frac{K_0}{N} \tag{4}$$

Thus, as long as the loss of stiffness is mainly due to viscoelasticity, the following simple equation should be verified:

$$N \cdot \frac{dK}{dN} = \text{cte} \tag{5}$$

The experimental sample end of life corresponds to the cycle number for which Equation 5 is no longer satisfied. A simple example is presented in Figure 6 where the flaw growth is outlined next to the stiffness and criterion (equation 5) evolutions versus the number of cycles (test realised with sinusoidal enforced displacement and an AE42 test specimen). The end of life is associated here with the forth step of the crack growth described in figure 5. This criterion has the advantage of being applicable to both enforced displacement and enforced force experiments and various types of cycles (tensile-compression, tensile-tensile, torsion…). It predicts the apparition of a crack big enough to affect the global stiffness of simple components.

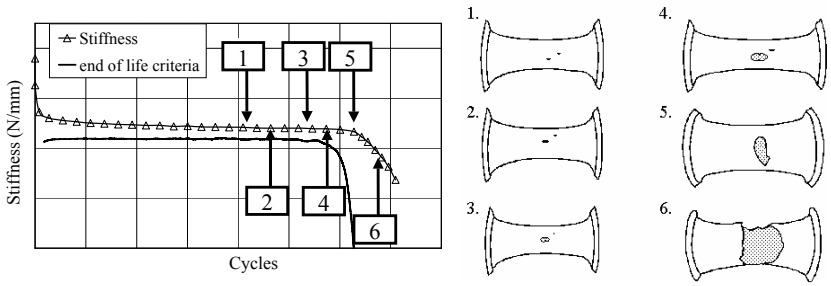


Figure 6. Example of application of the end of life detection procedure

The material studied is a carbon black-filled natural rubber. Its recipe and mechanical characteristics are given in Table I.

Table I: Recipe and mechanical characteristics of the reference material

Formulation	
NR	100.00
Zinc Oxide	9.85
Plastificant	3.00
Carbon black	34.0
Stearic acid	3.00
Antioxidant	2.00
Accelerators	4.00
Mechanical characteristics	
Density	1.13
Shore hardness A	58
Failure stress (Mpa)	22.9
Failure stretch (%)	635

3 FINITE ELEMENT SIMULATION

Using the experimental tools presented in the previous paragraph, one can obtain a macroscopic Wöhler curve that links the global load (e.g. the maximum displacement applied during the cycle) to the number of cycles until initiation (see Figure 7). Next step, i.e. prediction for a new test specimen or real part requires a local approach. Finite Element Simulation can help us to get a good representation of the local stress state and, as a result, to transform the applied global displacement into a local criterion estimated in the critical zone where the crack initiates. In the present paper, we will restrict our study to a nearly monoaxial stress state (local tension). In this case (small variations of the biaxiality ratio), it has been demonstrated that all classical criteria (maximum principal strain, maximum principal stress or strain energy density) are equivalent (Ref. 13). Having choosing one of these criteria, one has to focus on the modelisation of the rubber behaviour under large strain. The importance of the chosen behaviour law to predict the duration life with high level of accuracy has already been demonstrated. For more details, the reader can consult the work of Raoult (Ref. 3). An example of the resulting local (and intrinsic) Wöhler curve is outlined in figure 7.

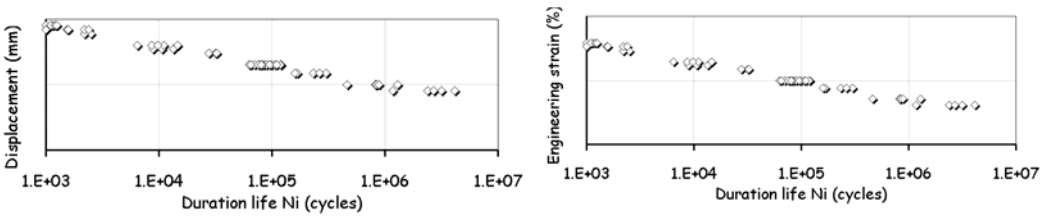


Figure 7. Wöhler curve measured on AE42 test specimen (on the left: global analysis, on the right, local approach)

4 MATERIAL CHARACTERISATION UNDER SINUSOIDAL UNIAXIAL LOAD

Full characterisation of fatigue properties under uniaxial loading condition classically requires two essential tools: a criterion that allows to superpose Wöhler curves measured with different local multiaxial stress or strain states and a diagram that highlights the influence of the effect of the pre-load. Because of the chosen test specimen geometry, local stress state is not really varying. Therefore, the choice of a local fatigue criterion is of little importance. In the present work, we will concentrate our effort on the second aspect, namely the mean stress correction.

Classically, for filled natural rubbers, three types of monoaxial loads are considered: tension-compression, relaxing and tension-tension. When tests are performed with enforced displacement, the cycle can be defined with two values: Lmax and Lmin that represent the minimum and the maximum of the cycle, or Lmean and Lamp that represent the mean load and the load amplitude (half of the global range). Relaxing conditions are associated to a value of Lmin equal to zero. In this case, strain induced crystallisation that appears during the tensile part of the cycle totally disappears when the load crosses the stress free state. This phenomenon does not affect the duration life. An important consequence is that compression-tensile and relaxing test should show a similar behaviour. On the other hand, when the cycle never comes back to zero (tensile-tensile load), permanent strain induced crystallisation appears leaving the crack propagation behaviour greatly affected. Some authors have observed macroscopic branching, crack turning from a direction perpendicular to the load to a new direction parallel to the load (Ref. 10). Returning to the crack initiation, it is observed that the duration life dramatically increases under tensile-tensile test (Ref. 5 and 12). This phenomenon is called reinforcement and is typical for filled natural rubbers. The Wöhler curve presented in the previous paragraph was measured with relaxing loading conditions and enforced displacements. Extension of this curve to any type of monoaxial cycle consequently requires a specific study of compression-tensile and tensile-tensile tests.

A first test campaign dedicated to the study of mean stress effect for compression-tensile cycles was performed. Keeping the maximum enforced displacement constant, the minimum of the cycle was decreased from 0 to nearly -Lmax. Results are presented in Figure 8. The compression part of the cycle does not affect the duration life, it depends only on the maximum enforced displacement. A first mean stress correction law is then obtained for compression-tensile cycles.

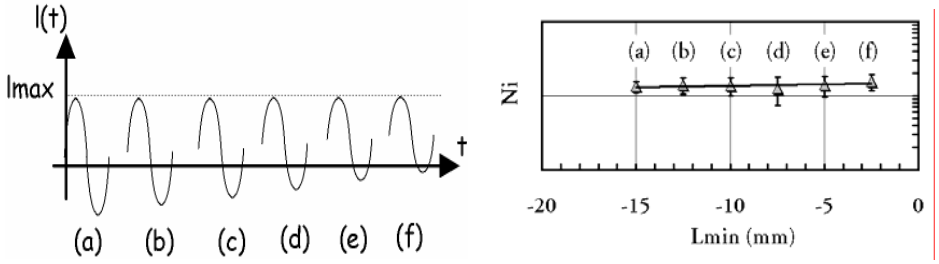


Figure 8. Mean stress correction for compression-tensile cycles (on the left: detail of the test campaign, on the right: experimental results)

The second test campaign is focused on tensile-tensile cycles. In the same way, maximum enforced displacement was maintained constant and minimum displacement was increased above 0 step by step. For that specific test condition, duration life depends both on minimum and maximum displacement (see Figure 9.). The result highlights the reinforcement behaviour of filled natural rubber: the increase of Lmin (when it is positive) induces a huge increase of the duration life due to permanent strain induced crystallisation. A generalised mean stress correction has to be built for tensile-tensile cycles.

Therefore, new test campaigns were realised with four different maximum enforcement displacements. Duration life for tensile-tensile cycles (Lmin >0 → Lmax) divided by duration life for the corresponding relaxing condition (0 → Lmax > 0) is plotted versus displacement ratio (Lmin / Lmax) on figure 10. In that way, all the results can be superposed and a correction law for reinforcement can be identified:

$$N_{i_R>0} = N_{i_R=0} \times 10^{f(R)} \qquad (7)$$

Where $N_{i_R=0}$ is the duration life for the relaxing test condition (0 → Lmax).

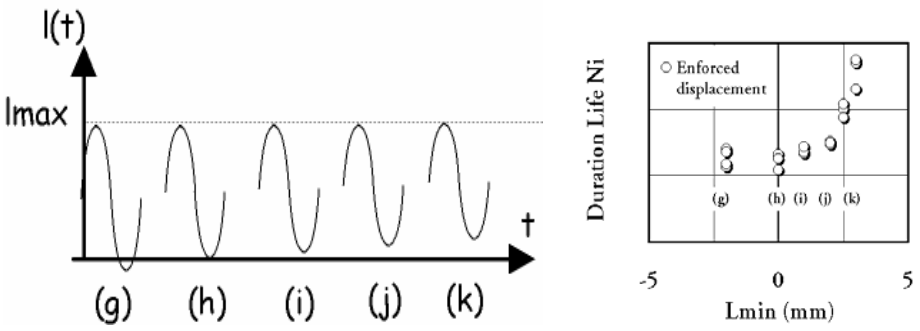


Figure 9. Mean stress correction for tensile-tensile cycles (on the left: detail of the test campaign, on the right: experimental results)

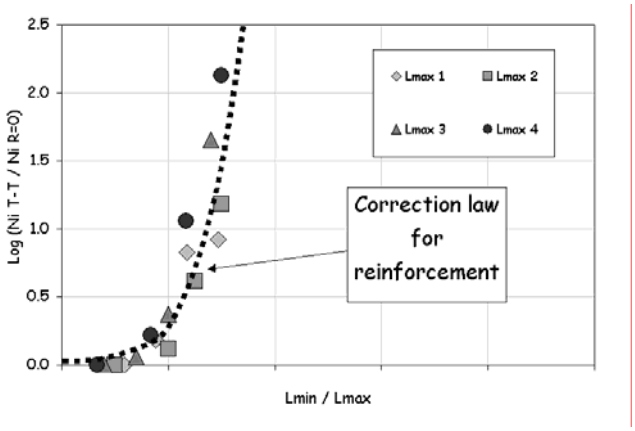


Figure 10. General mean stress correction for tensile-tensile cycles

The generalised mean stress correction is then:

$$\begin{aligned} N_{i_R=0} &= A \cdot criterion_{\max}{}^{\alpha} \\ N_{i_R<0} &= A \cdot criterion_{\max}{}^{\alpha} \\ N_{i_R>0} &= A \cdot criterion_{\max}{}^{\alpha} \times 10^{f(R)} \end{aligned} \qquad (8)$$

An example of an Haigh diagram is outlined in Figure 11, based on a local (intrinsic) approach. Dashed lines represent iso-Lmax conditions. Non-expected result compare to steel behaviour is that the iso-duration life curves are not continuously decreasing when the mean load grows. This is the so-called cyclic reinforcement phenomenon, a characteristic of filled natural rubber.

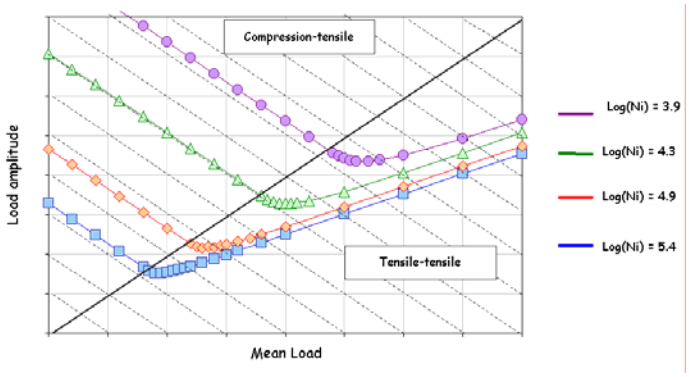


Figure 11. Example of Haigh diagram for filled natural rubber

Trelleborg uses the standard software package GlyphWorks (édité par nCode) to analyse RLD. Three mean stress corrections are classically available (for metallic components): Goodman, Gerber and "without mean stress correction". Using the static failure value of the criterion of filled natural rubber and the Wöhler curve measured for a load ratio equal to zero (relaxing condition), we have rebuilt the Haigh diagrams of these three corrections. They are presented on Figure 12. This picture highlights that both for compression-tensile cycles and tensile-tensile cycles, the three "metallic" mean stress corrections will underestimate the duration life of filled natural rubber.

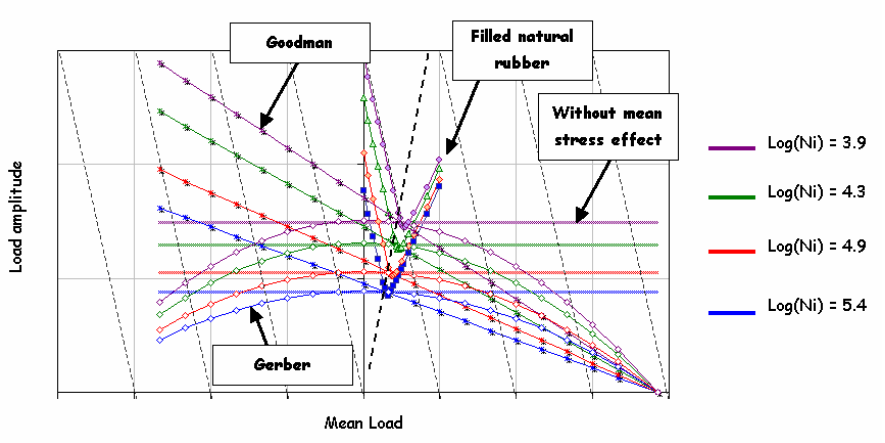


Figure 12. Four superposed mean stress corrections: Goodman, Gerber, without mean stress effect and filled natural rubber

5 ROAD LOAD DATA

To quantify the deviation between "metallic" mean stress corrections and the specific one of filled natural rubber, two different RLD tracks were chosen (see Figure 13). The first one is characterised by compression-tensile cycles and the second one is more focused on tensile-tensile cycle effect. The test specimen used for these tests is the AE2. For each signal, 5 tests were conducted at 23°C. Duration life is defined in a similar way to the one presented in Figure 6.

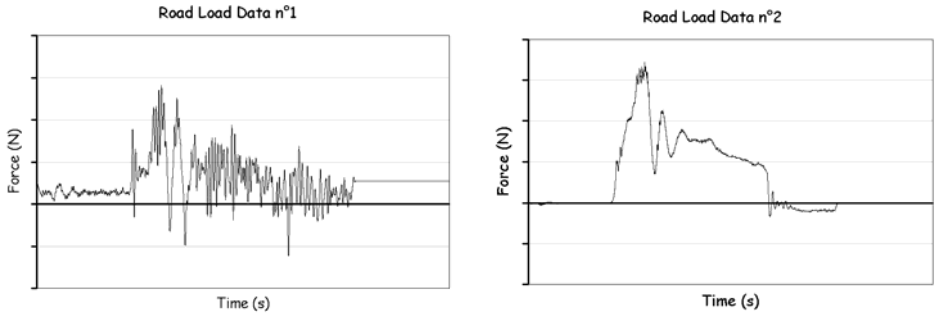


Figure 13. Two stochastic signals used for mean stress correction analysis

To increase the reliability of the study, we have chosen to work with the measured sequences (force measured with the sensor versus time) not the desired one programmed on the test rig. Small deviations could appear and perturb the comparison of the experimental and calculated duration lives.

Each signal is analysed using GlyphWorks (Rainflow counting method and Miner rule for damage cumulating are supposed to be valid for filled natural rubber – see Ref. 4). A specific option of this software package allows to implement user's mean stress corrections (see option Interpolate). The filled natural rubber one was easily added to the material database of the software. So, for each test, 4 duration lives were calculated and one was measured with the test rig.

Results of the RLD study are presented in Figure 14. First of all, we can conclude from the results that there are only small variations from one test to another and the test rig capacity for RLD is validated. Second, in both cases (RLD number 1 and 2), using suitable mean stress correction, Rainflow counting method and Miner rule, one can estimate precisely the duration life of a stochastic test conducted on filled natural rubber test specimen. Finally, the three "metallic" mean stress corrections adapted to the characterised filled natural rubber largely underestimate the duration life. This phenomenon is more pronounced when the stochastic signal includes compression-tensile cycles. It is however clear when the study focuses on tensile-tensile cycles effect.

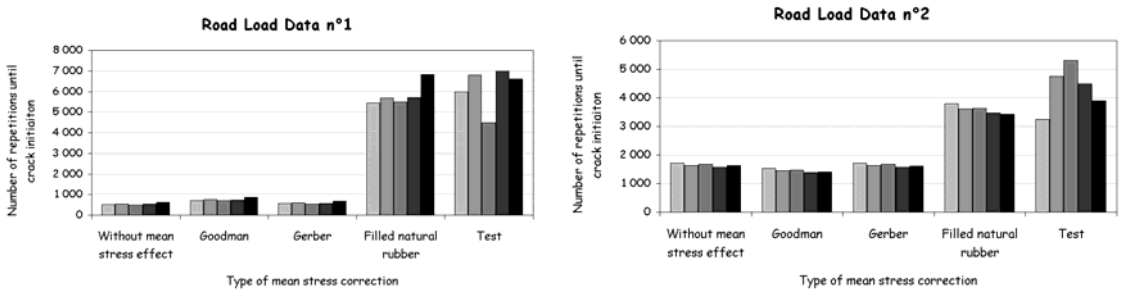


Figure 14. Comparison of predicted and measured duration lives for the two RLD

6 CONCLUSIONS

In a first part, we have proposed a generalised mean stress correction for filled natural rubbers. In a second part, we have compare this correction to experimental test results. The correlation is excellent and the easy implementation in commercial software allows the correction to be used in the analysis of Road Load Data during the design stage of the project (duration life prediction, serenity comparison and test duration reduction). Finally, the comparison of filled natural rubber mean stress correction to the classical Goodman or Gerber correction demonstrate definitively that elastomer have a specific behaviour that can't be captured with such approximation.

Authors would like to thank PSA Peugeot Citroen and Trelleborg Automotive allowing to publish this paper and Mohamed Bennebach form nCode for his support in understanding GlyphWorks.

7 REFERENCES:

1. E. Ostoja-Kuczynski, P. Charrier, E. Verron, L. Gornet and G. Marckmann, Constitutive Models For Rubber IV, 4th ECCMR, Stockholm, June 2005.
2. E. Ostoja-Kuczynski, P. Charrier, E. Verron, G. Marckmann, L. Gornet and G. Chagnon, Constitutive Models For Rubber III, 3rd ECCMR, London, September 2003.
3. I. Raoult, C. Stolz, M. Bourgeois, T. Nguyen and J.J. Thomas, Constitutive Models For Rubber IV, 4th ECCMR, Stockholm, June 2005.
4. T. Steiweger, M. Flamm and U. Weltin, Constitutive Models For Rubber III, 3rd ECCMR, London, September 2003.
5. S.M. Cadwell, R.A. Merril, C.M. Sloman and F.L Yost, *Ind. Eng. Chem*., 12 (1), 1940, 19-23.
6. A. Thomas, *J. Polym. Sc*., XXXI, 1958, 467-480.
7. R.S. Rivlin and A.G. Thomas, *J. Polym. Sc.*, X (3), 1953, 291-318.
8. W.V. Mars and A. Fatemi, *Rubber Chem. And Tech*, 76, 2003, 1241-1258.
9. J.B. Le Cam, B. Huneau, E. Verron and L. Gornet, *Macromolecules*, 37 (13), 2004, 5011-5017.
10. W.F. Busse, *Ind. and Eng. Chem*., 26 (11), 1936.
11. P. Charrier, Dimensionnement d'un joint élastomère. Application aux baies vitrées de navires à passagers, PhD thesis, Ecole Centrale de Nantes, 1999.
12. N. Saintier, Prévisions de la durée de vie en fatigue du NR sous chargement multiaxial, PhD thesis, Ecole des Mines de Paris, 2000.
13. W. Mars, Multiaxial Fatigue of Rubber, PhD. Thesis, University of Toledo, 2001.

Fatigue of elastomers : physical mechanisms and multiaxial damage prediction

J-B. Le Cam [a,b], E. Verron [a], B. Huneau [a], F. Pérocheau [b]

[a] Institut de recherche en Génie Civil et Mécanique, UMR CNRS 6183, Ecole Centrale de Nantes, BP 92101, 44321 NANTES cedex 3
[b] Allevard-Rejna Autosuspensions, 201, rue Sin Le Noble, 59500 DOUAI

Abstract In order to improve fatigue life prediction in elastomeric materials, physical phenomena involved in fatigue crack nucleation have to be identified. In the present work, we propose to investigate fatigue crack nucleation using scanning electron microscopy and X-rays micro-tomography. Then, the determination of physical phenomena at the microscopic scale leads to propose an original mechanical quantity based on configurational mechanics theory to predict fatigue crack nucleation. Taking into account the maximum value of this quantity during a fatigue cycle, damaged zones of parts can be identified.

1 INTRODUCTION

Most of the studies that focus on fatigue of elastomers are based on purely mechanical approaches. They are often inspired by results established for metallic materials. Because of the complexity of the mechanical properties of rubber, the determination of physical mechanisms that drive fatigue damage is an essential prerequisite to improve phenomenological theories. As an example, crack nucleation is always defined as the occurrence of a visible to the naked eye crack on the sample surface and is rarely considered from a microscopic point of view. The aim of the first part of the present paper is to examine crack nucleation at the microscopic scale in order to establish its origin and kinetics. For this purpose, scanning electron microscopy (SEM) and X-rays micro-tomography techniques were employed to analyze samples previously stretched under cyclic loading conditions. The second part of the paper deals with a multiaxial damage quantity; its derivation is based on the previous observations and it is used to determine the most damaged zones in parts.

In the next section, the experimental procedure is described and the corresponding results are detailed. Then, the multiaxial damage quantity is briefly presented and concluding remarks close the paper.

2 EXPERIMENTS

In order to localize nucleation zones on fracture surfaces and determine its chronology, several fatigue tests are needed. This section details the material and samples used, the fatigue tests loading conditions and the original observation methods carried out.

2.1 Material and sample

The material considered here is a 34 phr carbon black filled natural rubber. Table I summarizes its chemical composition and some mechanical characteristics. The recipe was cured during 7 min and the mold temperature was set to 160°C. In order to overcome ageing problems, samples were frozen at -18°C 48 h after their moulding. They are thawed out 24h before testing. The sample considered for fatigue testing is axisymmetric and is usually called the “diabolo” sample.

Table I. Material Formulation and Mechanical Properties.

Material formulation (pce)		Mechanical properties	
Natural rubber	100	Density	1.13
Zinc oxide	9.85	Shore A hardness	58
Oil	3	Stress at break (Mpa)	22.9
Carbon black	34	Elongation at break (%)	635
Stearic acid	3		

Antioxidant	2		
Accelerators	4		

2.2 Fatigue loading conditions

Two fatigue tests were performed. The first one was carried out until fracture under enforced displacement in order to identify the features of the fracture surface, i.e. the crack growth zone, the final rupture zone and especially the initiation zone, and to highlight the influence of the maximum stretch level on these zones. Sinusoidal cyclic strain waves were used in the fatigue cycle. Table II summarizes the loading conditions.

Table II. Loading conditions for each fatigue test.

Samples	Minimum stretch ratio	Maximum stretch ratio
A	1	1.33
B	1	1.5
C	1	1.67
D	1	2
E	1	2
F	1	2.17
G	1	2.33
H	1	3

The second fatigue test was performed to answer the following questions: when occurs fatigue damage ? Does it appear suddenly or is it a progressive phenomenon ? In order to answer these questions, experiments consist in stopping the test at different numbers of cycles (N_s) before a macroscopic crack takes place on the sample surface. Fatigue loading conditions are those of sample D of the previous test (see Table II). As shown in Figure 1, several stopping numbers of cycles were chosen from one cycle to number of cycles necessary for crack nucleation, denoted N_i. Generally, N_i is a macroscopic criterion which corresponds to the number of cycles needed to create a few millimeters self-initiated crack at the sample surface (2 mm here). It is followed by the propagation of the crack in the depth of the sample, then by the final fracture.

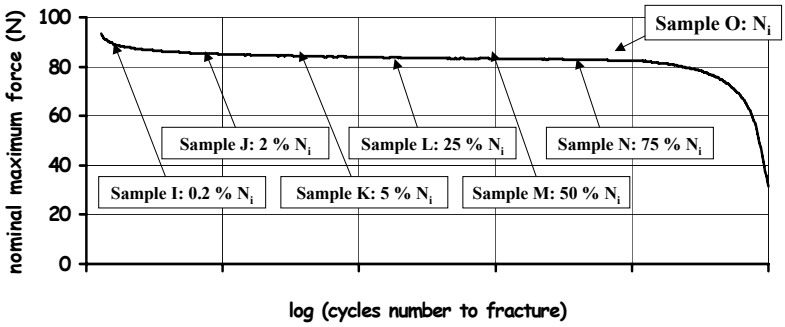


Figure 1.Stiffness decrease in sample D as a function of N.

2.3 Observation methods

First, fracture surfaces were examined by scanning electron microscopy (SEM) to localize initiation zones and to highlight their origin. Photomicrographs were performed using a HITACHI S-3200N model SEM. An Energy Dispersive Spectrometer of X-rays (EDSX) coupled with the SEM is used to determine the chemical elements located onto observed surfaces. In order to overcome ageing problems, broken samples were frozen at -18°C 48 h after the end of the fatigue test. They are thawed out 24h before SEM observation.

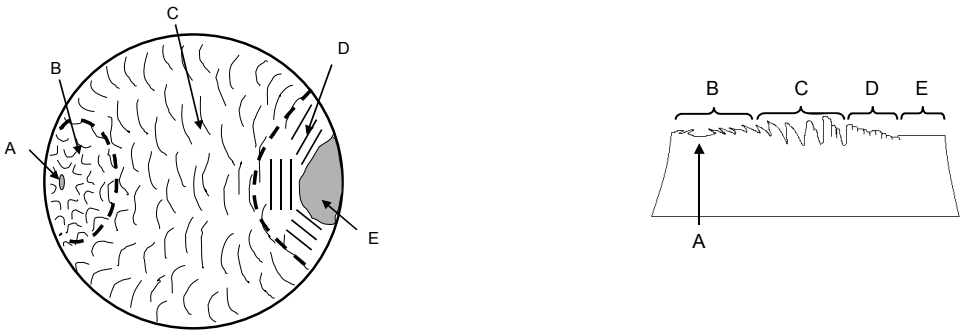
Second, X-rays micro-tomography was used to observe fatigue damage before that a macroscopic crack occurs on the surface. Nondestructive observation methods such as X-rays micro-tomography consist in visualizing density variation in the sample bulk before that a crack appears on its surface.

2.4 Results

2.4.1 Localization and origin of initiation zones

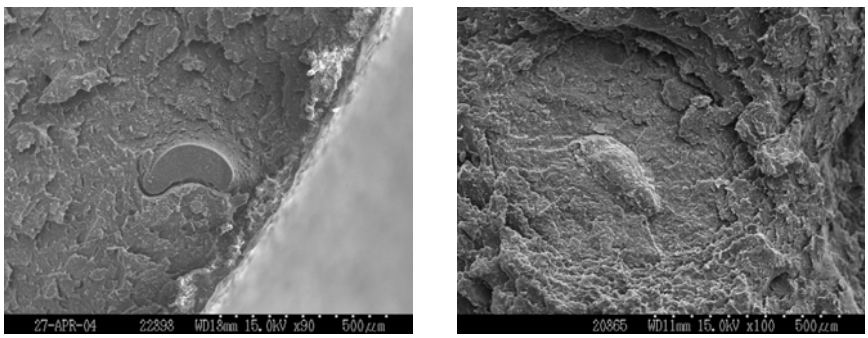
Here, samples tested until fracture were observed. Crack always propagates in the plane of the middle section of the sample. Even if the maximum stretch level slightly modifies fracture surfaces, their fracture morphology can be sketched as in Figure 2. Figure 2(a) is the top view and Figure 2(b) is the side view of the fracture surface. Five zones can be defined to describe it:

- zone A is the initiation zone. It is always located closed to the sample surface, between 200 and 500 µm far from it. Figure 3 shows photomicrographs of different initiation zones and illustrates the major reason of crack nucleation. Figure 3(a) presents a broken agglomerate which generates a micro-crack. Figure 3(b) corresponds to a micro-crack issued from a cavity appearing closed to the carbon black agglomerate in rubber matrix. It is also possible that initiation occurs from decohesion between matrix and oxides. It is to note that the average size of carbon black agglomerates from which initiation occurs is about 300 µm diameter,
- zone B contains zone A and corresponds to the zone where the fatigue crack begins to grow, forming an elliptical crack tip (due to the surface vicinity) which propagated to both the surface and to the sample depth,
- zone C is the major crack growth zone which contain wrenchings[1],
- zone D is composed by smooth striations,
- zone E corresponds to the final fracture surface. It is smooth.



(a) (b)

Figure 2. (a) Top and (b) side views of a fracture surface.



(a) (b)

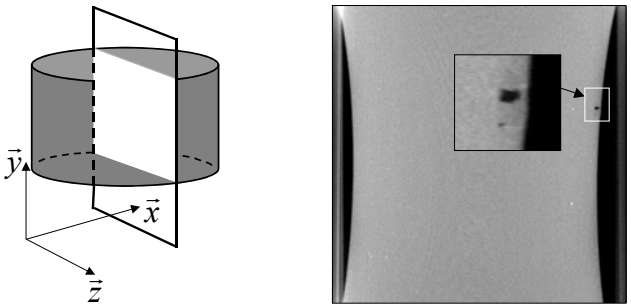
Figure 3. (a) Failure of a carbon black agglomerate. (b) Cavitation in the neighborhood of a carbon black agglomerate.

As a summary, fatigue crack initiation occurs most of the time from carbon black agglomerates and the initiation zone is located between 200 and 500 µm far from the sample surface. It is now necessary to define when occurs the fatigue crack nucleation at the macroscopic scale.

2.4.2 Chronology of fatigue damage

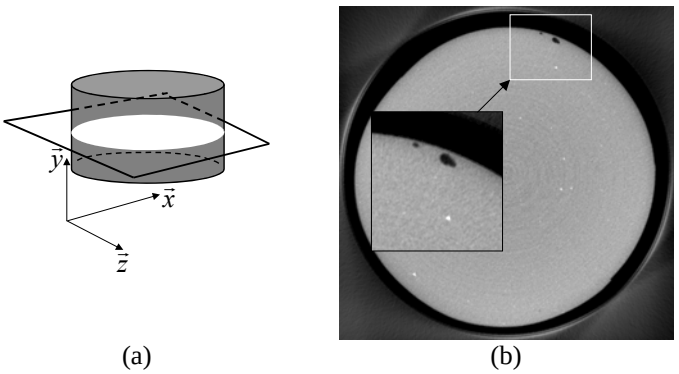
The previous fatigue test has demonstrated that crack initiation occurs in sub-surface and consequently that cracks detected in surface correspond to the propagation of microscopic cracks. Significant questions arise: Is the number of cycles of initiation (at the microscopic scale) large or not and is the damage a continuum phenomenon or not, i.e. is there any cycles between initiation and propagation ? As an answer, X-rays tomography is an "non-destructive" observation method of the samples microstructure which allows to visualize microscopic cracks inside the sample. As initiation occurs in the middle of the sample, scanned areas are restricted to this zone. In order to visualize micro-cracks, samples were stretched to an elongation inferior to the ones enforced during fatigue test. Here, the problem is to determine if micro-cracks appear nearly N_i or earlier during fatigue test. Samples used here are those of the second fatigue test stopped at different number of cycles.

Figures 4 and 5 present some pictures resulting from the scanning process of sample L ($25\%N_i$). Figure 4(a) and Figure 5(a) are schematic views which show the middle section and the plane in which pictures were obtained. As shown in Figure 4(b) and Figure 5(b) low density areas like cavities (in black) and high density areas like talc particles or natural rubber impurities (in white) can be easily visualized. Moreover, these figures show that cavities are detected in subsurface: their size (superior the one of carbon black agglomerates) indicates that they correspond to fatigue crack in the propagation step. It means that fatigue crack initiation occurs before $25\%N_i$.



(a) (b)

Figure 4. X-rays tomography pictures of sample L (N_s = 25% N_i).



(a) (b)

Figure 5. X-rays tomography pictures of sample L (N_s = 25% N_i).

As a summary, the analysis of fracture surfaces and X-rays microtomography observations exhibit that under uniaxial tensile fatigue loading conditions, initiation occurs in sub-surface for a number of cycles which corresponds to at least 25% of the number of cycles necessary to produce a 2 mm length macroscopic crack on sample surface.

3 MULTIAXIAL DAMAGE QUANTITY

As mentioned above, crack nucleation in elastomers involve small intrinsic flaws (cracks) which grow under mechanical loading. Nevertheless, crack nucleation criteria should be defined in terms of continuum mechanics parameters in order to be combined with finite element computations in engineering applications. In fact, the influence of microstructural defects on damage distribution has to be estimated considering continuum mechanical fields. In order to study a real part which contain defects with a homogeneous model, the Eshelbian mechanics[2,3,4] (or the mechanics in material space) is revealed to be an appropriate tool. Here, only basic results are given. For a more complete presentation of this theory, the reader can refer to Verron et al.[5] and Verron[6].

In the material space, rubber can be considered as a material with a uniform distribution of defects. From a microscopic point of view, these defects can be voids (porosities, cavities), micro-cracks or rigid inclusions (filler agglomerates). As demonstrated above and also proposed recently by Mars[7], crack nucleation in elastomers is assumed to be the consequence of the growth of pre-existing small flaws. Depending on the geometry of the considered part and loading conditions, not all of the stored elastic energy is available for the growth of defects (see for example the experiments conducted by Roberts and Benzies[8] under fatigue loading conditions). Thus, for a given rubber part the energy release rate of small flaws has to be determined in each particle (material point) in order to exhibit the most propitious zones for crack occurrence.

Consider a rubber body and a current particle M in the reference configuration as shown in Figure 6(a).

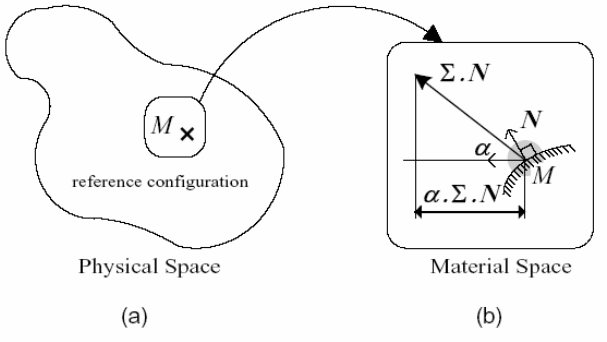


Figure 6. (a) A rubber body in its undeformed configuration. (b) Zoom in near the particle M in the material space.

In the Material Space, the point defect in M can be modelled by a small circular void (see the right-hand side of Figure 6(b)). In this point, energetic properties of defects behaviour are completely defined by the configurational stress:

$$\boldsymbol{\Sigma} = W\mathbf{I} - \mathbf{CS}$$

where W is the strain energy density, $\mathbf{I}$ the 3x3 identity tensor, $\mathbf{C}$ the right Cauchy-Green strain tensor and $\mathbf{S}$ the second Piola-Kirchhoff stress tensor. More precisely, for a given oriented unit surface of outward normal vector $\boldsymbol{N}$ in M, the vector $\boldsymbol{\Sigma N}$ represents the configurational traction across the surface. Considering the definition of Σ_{ij}, for a given unit direction $\boldsymbol{\alpha}$, the scalar $\boldsymbol{\alpha}.\boldsymbol{\Sigma N}$ is the change of the total energy at the point M due to a material unit translation in direction $\boldsymbol{\alpha}$ of the unit surface with normal $\boldsymbol{N}$. The configurational stress tensor being symmetric, it admits three real eigenvalues, denoted Σ_i, (i=1,3) in the following, and three eigenvectors $\boldsymbol{V}_i$ (i=1,3).

These three vectors correspond to the directions in which the energy release rates tend to open or close the void by material normal traction without material shear traction. Moreover, as the force on a defect is defined as the negative gradient of the total energy with respect to the change in position of the defect[2], the morphology of the defect evolves with respect to the direction opposite to the material force. So, as the body will ever tend to reduce its total energy, the minimum eigenvalue of $\boldsymbol{\Sigma}$ should be considered in order to predict the evolution of the defect: if it is negative the defect grows to form a plane crack which normal is defined by the corresponding eigenvector and if it is positive the three eigenvalues are positive and the defect tends to shrink. The later case can be seen as the theoretical counterpart of the well-known physical "crack-closure effect". Finally, the new multiaxial damage quantity for rubber is denoted Σ^* and can be summarized as follows:

$$\Sigma^* = |\min[(\Sigma_i)_{i=1,3}\ ,\ 0]|$$

Moreover, if $\Sigma^* > 0$ the eigenvector associated with the minimum eigenvalue of $\boldsymbol{\Sigma}$ is normal to the plane of crack growth. The complete formulation is available in [5,6].

4 ACKNOWLEGMENT

We thank for Allevard Rejna Autosuspensions for its support in this study.

5 REFERENCES:

1. J.-B. Le Cam, B. Huneau, E. Verron and L. Gornet, *Macromolecules,* 37(13), 2004, 5011 – 5017.
2. J. D. Eshelby , *J. Elast*. 5, 1975, 321–335.
3. G. A. Maugin, Material Inhomogeneities in Elasticity, Chapman and Hall, London, 1993.
4. R. Kienzler and G. Herrmann, Mechanics in Material Space, Springer, Berlin, 2000.
5. E. Verron, J.-B. Le Cam and L. Gornet, *Mech. Res. Commun.*, 2005, in press.
6. E. Verron, *Constitutive Models for Rubber IV*, P.-E. Austrell and L. Kari editors, 3-8, 2005.
7. W. V. Mars, Multiaxial fatigue of rubber. Ph.D. thesis, University of Toledo, 2001.
8. B. J. Roberts and J. B. Benzies, 1977. Proceedings of Rubbercon'77, vol. 2, 2.1–2.13.

Fracture mechanics evaluation of a cast sleeve by 3D finite element modelling

Anders Björkblad
Department of Aeronautical and Vehicle Engineering, KTH
Teknikringen 8, 100 44 STOCKHOLM
anbj@kth.se

Abstract The object of this paper was fracture mechanic modelling of solids using finite element (FEM) and linear elastic fracture mechanics (LEFM). The main tool that has been utilized was the software Mcrack which is a group of macros intended for use jointly with ANSYS finite element software. One major advantage of the Mcrack software is that it supports solid modelling with a crack located at an arbitrary location. This implies that it is possible to calculate also torsion and mixed mode cases within a most reasonable work effort. However, Mcrack was originally developed to cover complex weld geometries. Utilizing Mcrack for general solid modelling requires an analysis of the calculation capability for arbitrary crack paths, i.e. when the global geometry is not exactly covered by the crack front sub model. Such analysis is included in this paper. As test object to apply the method a sleeve made of nodular cast iron has been used. Previous to this investigation the component was submitted to a fatigue test at ABB, Sweden. This paper is thus a continuation of the ABB work, and at the same time an extension of the field of application for the Mcrack software. For initiation and validation purposes the software AF-Grow as well as elementary cases has been used in parallel. The investigation was a part of the Nordic project "Cast Design 2005".

1 INTRODUCTION

Linear elastic fracture mechanics (LEFM) is a most powerful tool for analysis of fatigue processes. As the applicability range is from initiated cracks to failure the initiation period is not covered. However, due to the problem at issue it can be a considerable amount of the life time left for the crack propagation phase. For practical use, nowadays it is more or less compulsory to utilize finite element method (FEM) for structural analysis. Yet, the application of LEFM within FEM is a very demanding task. In fact, it is probably one of the main reasons why LEFM is not utilized in a larger extent. This is a pity considering that the LEFM is capable of analysing intricate geometries and complex load cases. The present paper proposes a method for solid modelling of LEFM. It is based on a group of macros that onwards will be called Mcrack, Martinsson, J, [1], and which are supposed to be used in conjunction with ANSYS [2]. Mcrack was originally developed for weld analysis and is well suited to exact follow a weld geometry. When considering an arbitrary solid body this is however not possible, but one will have to accept a certain degree of misalignment between global model and crack front sub model. The theme in this paper was thus to show that it is possible to apply Mcrack to arbitrary solid models despite the modelling issue. In order to cover the matter of validation, the software AF-Grow [3] as well as elementary cases and ordinary solid modelling where used in parallel. It should also be known that the applicability was intended to serve practical industrial purposes.

The component that was used for the application of Mcrack was a sleeve made of nodular cast iron. The nodular iron is a material that is widely used in load carrying components as axle's housings, transmission housings, hubs, linkage, brackets and attachments in both trucks and heavy construction equipment. It is also used in the main structure in robotics and in hubs in wind mills. The material has a number of attractive properties that makes it convenient for instance in the automotive industry. Both the strength and the toughness can be varied in wide ranges depending on current demands. This makes the material suitable for all the same applications as grey iron but also for application that requires resistance against shock- and fatigue loadings. It is also relatively easy to found and machine, important matters with respect to productivity. As being used for moving structural parts, it will be exposed for fatigue. The issue of fatigue strength for cast materials is mainly governed by the presence of cast defects, Nadot *et al.* [17], Björkblad, A, [9], Mörtsell *et al.* [11]. Cast materials always contain (relatively) large amounts of contaminations. The size of the defects emanating from those

impurities comprises the whole range from micrometer up to several millimetres. On top of this there are also more pronounced defects emanating from the cast process. Those are most often different kinds of porosity, e.g. shrinkage pours. The common property for all of the impurities and defects are that they generally form an irregular, sharp interior geometry that will give rise to sharp stress concentrations. The stress concentrations in its turn facilitates crack establishment and this mechanism is often so severe that the fatigue crack initiation phase can be more or less disregarded, thus leaving the fatigue life for the crack propagating phase. Commonly (for a continuum like material) the initiation phase constitutes a main part of the fatigue life, so by omitting it one will miss a substantial part of the service life for a component. Under such conditions, it became extra important to manage fracture mechanic calculations in order to perform reliable forecasts for service life.

The preliminary work which preceded this investigation was performed by ABB in Västerås, Sweden. ABB did also design the component and made all the testing, see ABB report [4]. Originally the intention was to investigate mixed mode behaviour of the GJS500 [7] material under alternating load (load ratio R=-1), and the evaluation was planned to be made by a classic fatigue approach, i.e. S/N-curves.

One of the main themes of the present work was to make a fracture mechanic evaluation of the component life by aid of FEM and LEFM. The other main theme was the application of the fracture mechanic macro collection Mcrack which was developed at the department of aeronautical and vehicle engineering, KTH. This line of action will not only produce a solution for this specific component, but also point out a user friendly way of utilizing FEM for fracture problems. It is a well-known fact that the fracture mechanics in FEM is not a very simple manoeuvrable technique, yet it constitutes a powerful tool. The Mcrack software offers, along with other aids as AF-Grow, a great extent of simplifying in the analyse work. In order to verify the correctness of the Mcrack calculation capability comparisons where made between calculated results and elementary cases.

2 COMPONENT

The component was a cast iron sleeve designed by ABB solely for fatigue testing. The dimensions are given in Fig. 1 and the appearance of the component is given in Fig. 5. Total material thickness at the critical area was 6 mm. The material was GJS 500-7 (European standard SS-EN 1563) [7], a medium strength nodular iron. The chemical composition of the material is given in Tab. 1. and mechanical properties are given in Tab. 2.

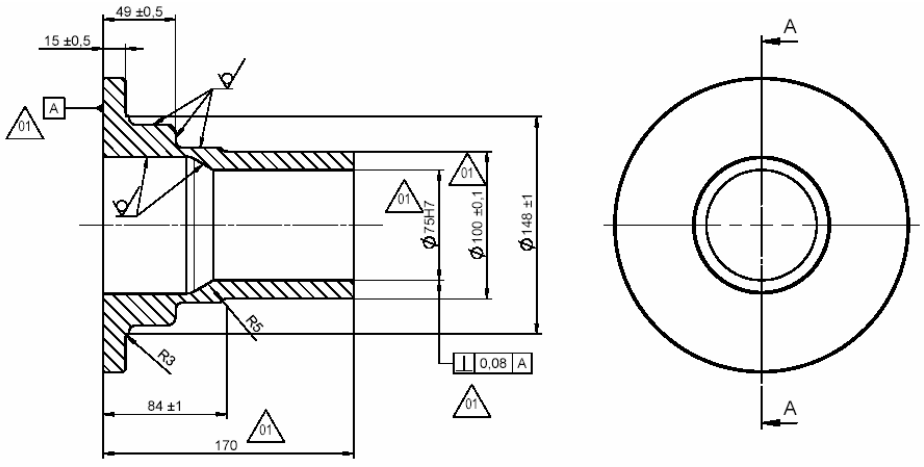


Figure 1. The nodular cast iron sleeve.

The components where all around shot blasted with cut steel wires and most of the components were tested in that condition. In order to determine the influence of the residual stresses a minor number of sleeves where annealed or machined (just at the very surface) before testing.

Measurement of the residual stress field were performed by x-ray diffraction technique, see Fig. 8 for stress profile.

Table 1. Chemical composition of GJS 500-7.

	C	Si	Mn	P	S	Cu	Sn	$C_{equivalent}$
Content [weight %]	3.59	2.35	0.37	0.09	0.08	0.27	0.05	4.18

Table 2. Mechanical data.

σ_y [MPa]	σ_B [MPa]	A_5 [%]	Hardness [HB]
340	510	7	200

2.1 Component testing

All testing of the component was done by ABB in Västerås. The following description is an outline of the test procedure.



Figure 2. Experimental setup.

The component was mounted with the flange attached against an angle shelf. The shelf in its turn was bolted to the test machine base. In order to apply torque there was an arm attached at the outer diameter at the cylindrical outer end of the sleeve. This arm was designed so it would not give any bending moment with respect to the most highly stressed areas at the sleeve, i.e. only torque and shear force where applied at the critical location. A bending arm was inserted inside the inner diameter of the outer end in order to apply bending moment. The torsion and the moment arms where connected to the sleeve by a friction attachment. Two servo hydraulic cylinders where then connected to respectively torque arm and bending arm by push-pull rods. The complete appearance of the test set up is shown in Fig. 2. The testing was accomplished by stress ratio R= -1 for both bending and torsion. Also mixed mode tests were conducted, then with phase relations between bending and torsion of 0 and 90 degrees respectively. Load frequency during the tests was 5 Hz.

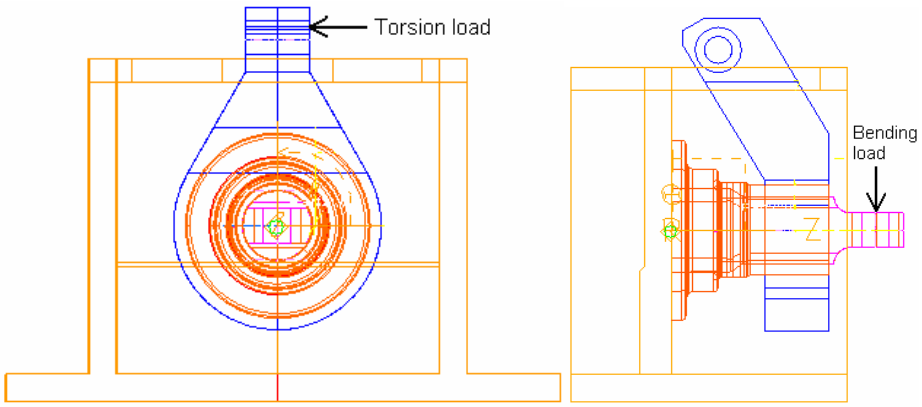


Figure 3. Front view and side view of model. Load introduction for torsion respectively bending.

2.2 Test results

The original evaluation was made at ABB in connection with the tests. A classical fatigue approach with S/N-curves was planned. It was expected that the measured life should be in accordance with results extruded from testing of smooth, straight cast specimens. However test results showed something quite different. Although the local stress was over the yield limit at the stress concentration, the measured life was longer than expected from the S/N approach, see report from ABB [4].

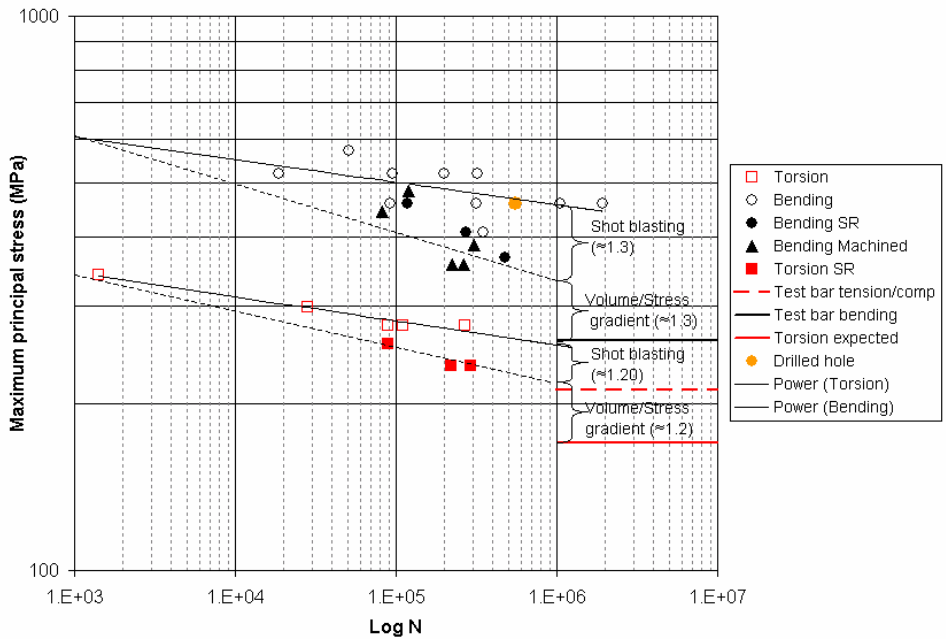


Figure 4. S/N-curves from tests for bending and torsion (ABB).

It turned out that the stress gradient seriously affects the crack initiation and the crack growth. In Fig. 4 it can be seen one example of the outcome from the tests. Extruded data from Fig. 4 shows that the difference between expected fatigue level and true fatigue level in bending is about 80 MPa or ~33% at 1e6 cycles, which corresponds to a factor of about three for the total life. It can also be seen that the shot blasting affects the fatigue limit about 30% at the same number of cycles. In Fig. 6 the typical bending respectively torsion crack faces is shown.



Figure 5. Critical area at the component.

Both the bending and the torsion case exhibit evident multi crack initiation with ridges and x-crack formations respectively. Using the stress ratio R= -1 the load will also act in two directions, and consequently there will form line cracks at both upper and lower side for the bending case and multiple x-formed cracks for the torsion case.

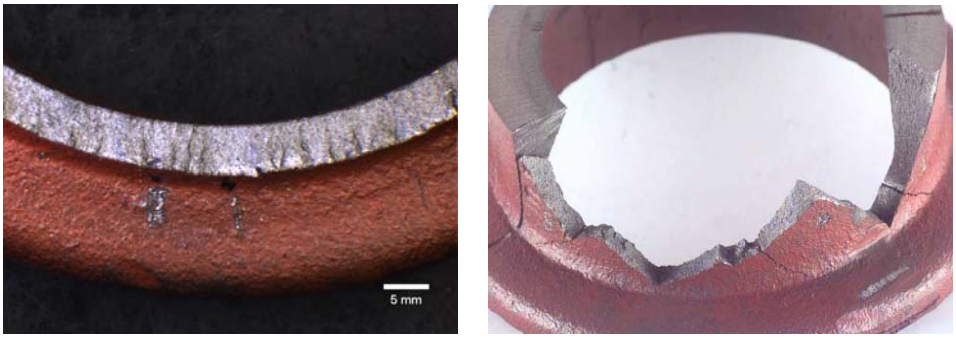


Figure 6. Typical crack faces from bending (left) and torsion (right).

It can however be questioned how to evaluate the outlook from the testing since the maximal stress was to be considered more or less as overload. In all cases the bending will behave different from the usual defect initiated semi elliptical crack development, instead forming a line crack. The torsion case still shows a normal appearance despite the high load level.

3 SIMULATION

The analyses in this investigation are based on LEFM for determination of stress intensities and Paris law, Eq. 1, for life calculations.

$$\frac{da}{dN} = C * (\Delta K)^m \qquad (1)$$

$$\Delta K = K_{\max} \;;\; K<0 \qquad (2)$$

$$(a,c,w,t) > 2.5 * \left(\frac{K_1}{\sigma_y} \right)^2 \qquad (3)$$

$$m = 5 \qquad C = 2.5e-11\,[\text{mm/cycle}] \qquad [15]$$

The Paris parameters m=5 and c=2.5e-11 (valid for R=0) was chosen as medium range values representing a broad variety of cast components from various foundries. The variation range of published data is

relatively large and, just to cite one source, m-values of 4.08-5.65 and c-values between 9.6e-12 and 4e-10 [mm/cycle] are reported for R=0 [16]. This is presumably a major part of the explanation to the discrepancies between individual test components, and underlines the importance of using valid material parameters.

The present form of Paris law uses nominal K-range and assumes the crack closure to be included in parameter c. Further, in consistence with the unity of parameter c, $\Delta K=K_{max}$ was used according to Eq. 2. Because of the non-symmetric boundaries there was a slight difference in between the upwards- and the downwards bending solution in the model. For stress ratio R= -1 the test object will experience both those stress levels, and it was presumed that the higher level ($S1_{max}$) was constituting upper bound and therefore used for calculations.

For the rest the regular conditions for LEFM where presumed, i.e. small scale yielding according to ASTM [14] directions, see Eq. 3, which is considered as a general limit for LEFM validity. The value 2.5 is however in practice not a sharp limit, Ljustell, P, [13], has shown that the LEFM can remain applicable for loads as high as 15 times the criterion limit for certain materials. The implication is that LEFM is likely to be valid also for the highest loads in the present investigation, especially as the fracture toughness is quite low for nodular iron.

The presumed crack front evolution was perpendicular to the first principal stress, S1, due to the maximum principal stress criterion [12]. The cracks were thus modeled consequently which means that there where neither mode II nor mode III stable crack growth for any of the cracks. The initiation position directly in an angle corresponding to first principal stress is most plausible in cast materials since there are small internal defects everywhere and in any direction. The shear stress where also small in comparison to the stresses from the bending and torsion and therefore neglected.

In the bending analysis the local stress at the stress concentration (radius) was between 1.2 and 1.68 times the yield limit for the material. In Fig. 7 the normalized stress gradient through the thickness can be seen. Stresses at such levels will quickly relax residual stresses for what reason they where neglected in analyses. This substantial overload will also seriously affect the behavior of the material so that the fatigue initiation mechanism will be switched away from being ruled by defects.

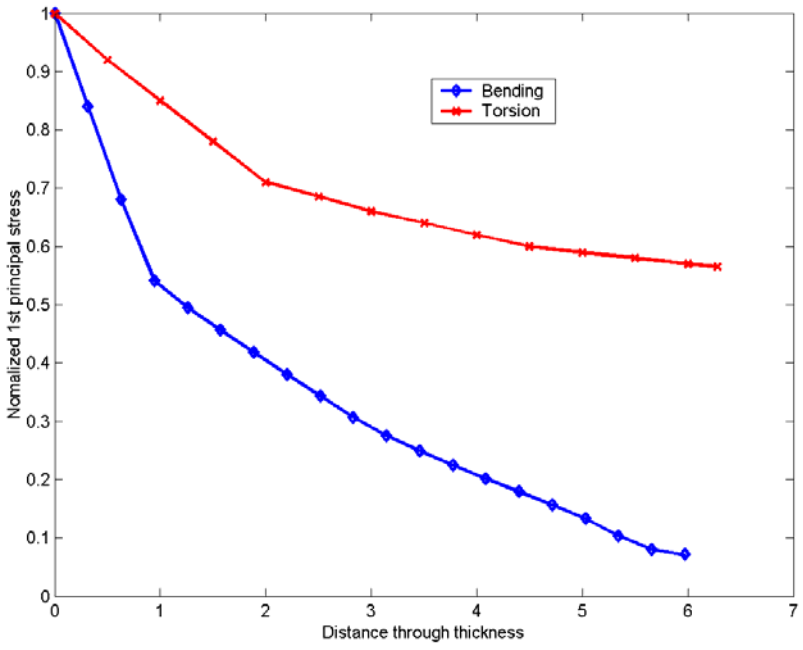


Figure 7. The stress gradient thru thickness in bending respectively torsion.

The strain will be in such level that the Coffin-Manson [8] relationship is valid, see Eq. 4, which will rule the initiation at the most highly stressed areas of the sleeve. First thereafter, with an established crack as deep and long as the overstrained material, the LEFM will determine the process.

$$\frac{\Delta\varepsilon_p}{2} = \varepsilon_f^{'}(2N_f)^C \qquad (5)$$

$$\varepsilon_f^{'} = 0.540648 \qquad c = -0.675431 \qquad [5]$$

The material parameters for Coffin-Manson, Eq. 5, are retrieved from Samuelsson, J, [5]. In Tab. 3 it can be seen the catastrophic low number of cycles to crack initiation as a result of the high strain level. Mörtsell *et al*. [11] have showed that for nodular cast iron this severe strain state cause immediate crack initiation in the matrix around nodules and at micro pores even at the first load cycle. This implies that the damage is made at a very early stage and the crack establishment will continue fast in the affected volume, circumstances that where confirmed by the test results.

Table 3. Crack initiation phases due to Coffin-Manson for present load levels.

Stress level [MPa]	*408*	*459*	*520*	*571*
Number of cycles	*26,000*	*14,200*	*8,000*	*5,400*

The dept of the initiated crack is hard to predict as the behavior is unclear at the transition point between strain govern fatigue and the following crack propagation, but it is probable that the dept will be about the same size as the extent of the overstrained material. With respect to the present stress gradient it means an initiation crack dept between 0.5 and 1.1 mm depending on the load. It could be worth noting that normally the low-cycle regime is not applicable for mechanical design because of the resulting low service life. Herein it is utilized only by necessity for initiation at high stress levels.

In most of the numerical models no concern has been taken to multiple initiations. At current load levels this is not relevant for the bending load seeing that a line crack quickly will establish, but for lower load levels an multiple initiation approach certainly would be much appropriate.

3.1 Numerical model

The FE model of the component was modelled with solid 20-node brick elements. It was a full model and also the surrounding fixing shelf and load introduction devices where solid modelled. There where no contact elements in the model between the different parts since it was supposed that the areas of interest for analysis where located sufficiently far away from the boundaries. The evaluation was supposed to be valid for general components in heavy vehicles and within heavy industry. In such applications the final portion of life, where non-linear conditions prevails, is of no interest because of the short life remaining. By that reason only linear solutions where performed.

3.2 Residual stresses

Residual stresses descend from almost every kind of processes that engineering materials is exposed to. Cast components are very often shot-blasted in order to remove sand and oxides after the cast process. This treatment induces very high magnitudes of negative residual stresses and sharp stress gradients in a thin layer at the surface [8]. The shot-blasting are also smoothing the surface so that small defects at or near the surface can disappear. The effect of the shot-blasting and the surface smoothing is thus normally beneficial. The residual stresses origin in the shoot blasting is considered in this evaluation but the stresses origin in the cast process, which normally is of a lower level, is not. For the components that where stress annealed or machined the contribution from the residual stresses where neglected.

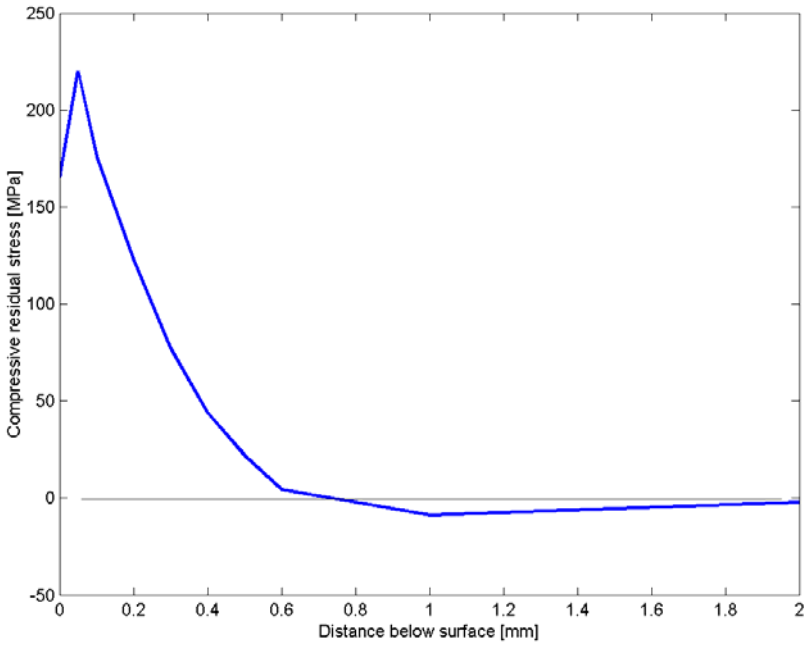


Figure 8. Residual stress profile.

The characteristic appearance of the stress gradient curve was obtained from an investigation on cast steel [9]. Nadot and Denier [17] report the residual stress magnitude 300 MPa for the current material and state. This is a value for flat easily accessible surfaces, but as the critical area at the present component are a little bit more difficult to access, the residual stress magnitude for this investigation was set to 75% of 300 or 225 MPa.

The residual stress profile was used as input load in AF-Grow using a semi-infinite plate with the same thickness as the critical section at the cast sleeve. The output SIF's from AF-Grow, origin in the residual stress and valid for respectively crack size, was then subtracted from the SIF of the applied load calculated in ANSYS. For the calculation of the residual K-distribution the weight functions available in AF-Grow were utilized.

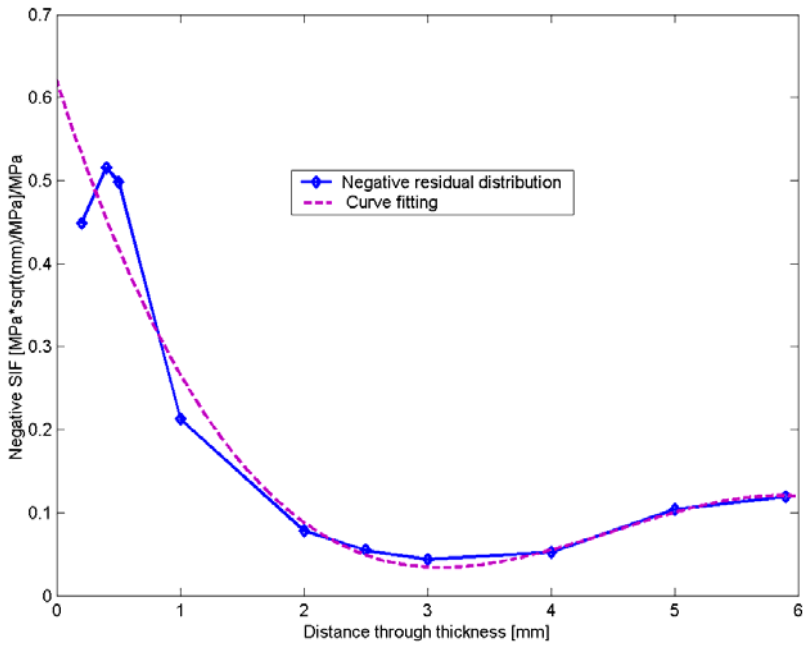


Figure 9. Distribution of (specific) residual stress induced negative K-contribution through the thickness.

Because of the high strain magnitude at the present test conditions a quick relaxation of residual stresses was expected. The difference in life between included residual stresses or not was only a few thousand of cycles.

The residual stresses where therefore considered only for academic interest, for practical use they should be disregarded in the evaluation of a highly (over) stressed component like the current sleeve.

3.3 Software tools

The finite element program used was ANSYS 8.1. As a supplementing tool Mcrack was utilized. Mcrack is a collection of macros intended for use in conjunction with ANSYS. Mcrack enables immediate sub-modelling of complex fracture mechanic weld problems. In this paper it was showed that it might be utilized also for arbitrary solid modelling. For validation purpose and for handling small cracks (i.e. closely after initiation phase) the software AF-Grow was used.

The Mcrack macro collection is founded on a sub modelling technique. Schematically it replaces a part of the finite element structure with a crack front sub model. All original elements located within the sub model boundaries will be deleted and the resulting boundary is joined with the sub model by constraint equations. Then the global problem is solved, thus involving the current crack size in the stiffness calculation. This line of action implies that the correct stiffness, including redistribution of stresses, is taken into consideration. After the displacement solution is available there will be another sub model consisting of singular quarter point crack elements laid out along the crack front. From this second sub model the K-solutions are then derived. When used for weld geometries Mcrack also include the option of automatically move the crack front forward. In such case both crack front deviation (because of mode II load) and individual crack growth increment is considered. By geometrical reasons it is not possible to utilize the automatic crack growth option for solid modelling carrying semi elliptical cracks. In case of semi elliptical cracks one has to perform separate, discreet K-solutions with increasing crack sizes.

3.4 Verification

Mcrack was developed especially for complex weld geometries. In that application the sub models that the program creates encompass the geometry of the weld. When using Mcrack for solid modelling it is not always possible to exactly follow the geometry of the global model. Instead, the beginning and/or the ending of the sub model is situated with some angle against the surface or slightly below/above the surface. This raises the question of the correctness of the K-solution under such circum stances.

In order to verify the correctness of the SIF calculations a number of comparisons where made between elementary cases, Mcrack and solid crack modelled solutions. The specimen model for this purpose was a centre semi elliptic surface crack specimen with dimensions 10x20x200 mm, see Fig. 10. The dimension of the crack was a=3mm and c=3mm. The crack was located perpendicular to the longitudinal direction except for one model where an angle (bias) of 10 degrees was applied. The load was set to 100 MPa and the SIF was evaluated at specimen surface and at middle bottom of the crack. The alignment between global model and sub model, which in parallel with the overall SIF solution was the object of the convergence study, was supposed to range from -0.5 mm below up to +1.5 mm above the surface, see Fig. 11-14.

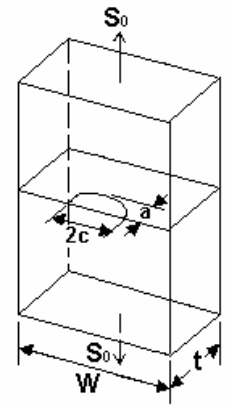


Figure 10. Centre semi elliptic crack specimen used for the verification study.

Also, one simulation was made with a sub model bias of 10 degrees from the perpendicular position. As seen in Fig. 15, if one holds within ±0.25mm, there is a consensus within 5-15 percent between the SIF from the different models even at surface of the specimen, a figure that must be considered fairly good keeping in mind all other sources that may contribute to the discrepancy. Also note that the SIF solution is almost unaffected some small distance below the surface and towards the interior.

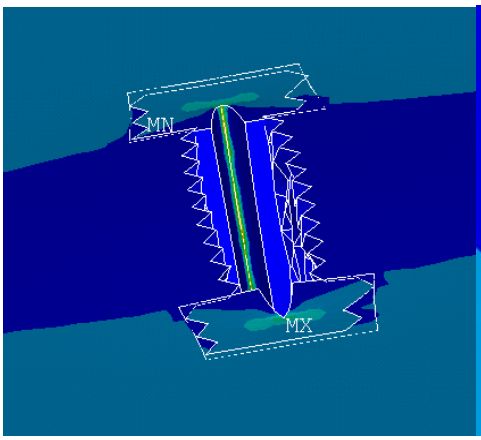


Figure 11. Exactly aligned with surface.

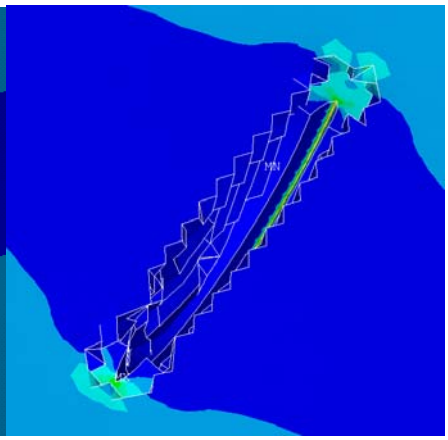


Figure 12. Below surface.

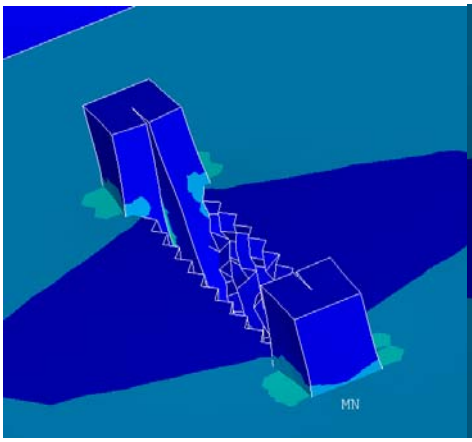


Figure 13. Above surface.

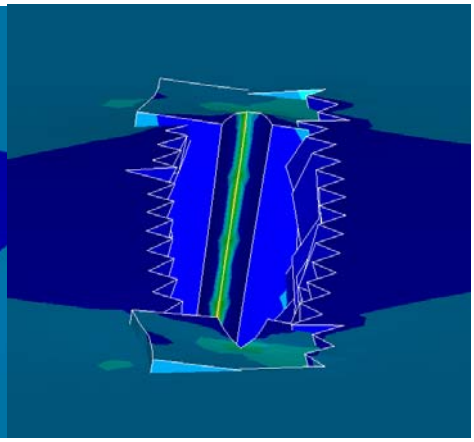


Figure 14. Non perpendicular to surface.

In Tab. 4 it can be seen that the Mcrack sub modelling technique, as well as homogeneous solid modelling, is in excellent agreement with analytical solutions. This implies that the type of fracture mechanics evaluation where the growth at crack centre is at issue, which is a most common case for crack propagation, is practically unaffected of the sub model alignment. Disregarded the mode II and mode III SIF that appears, even the biased model shows the same accuracy. The conclusion is that the accuracy is most sufficient for practical use even though the alignment is inexact within some tenth of a millimetre.

Table 4. Verification of SIF solutions for perfectly aligned sub model. Units in MPa(mm)$^{1/2}$.

	ANSYS/Mcrack	ANSYS pure solid modelling	AF-Grow	Analytical [6]
K (at surface)	230	225.5	238	235
K (at middle bottom of crack)	203	202.8	210	208

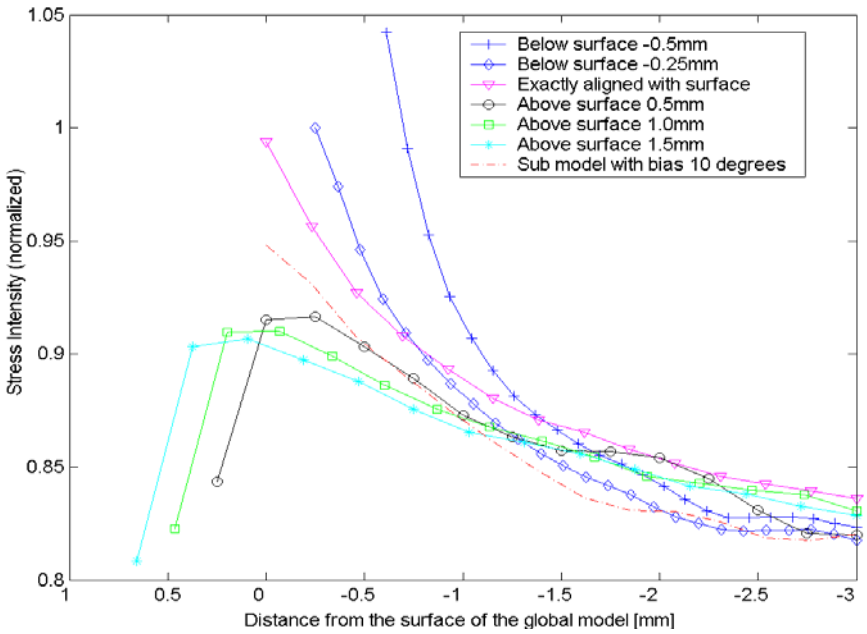


Figure 15. SIF solutions for varying misaligned sub models compared to exactly aligned sub model.

4 RESULTS

4.1 Bending

The bending solution is somewhat cumbersome at present load levels. As the maximum principal stress clearly exceeds the yield stress for all load cases tested, the resulting fatigue damage will obey the Coffin–Manson relationship. This means an overload situation and a short initiation phase.

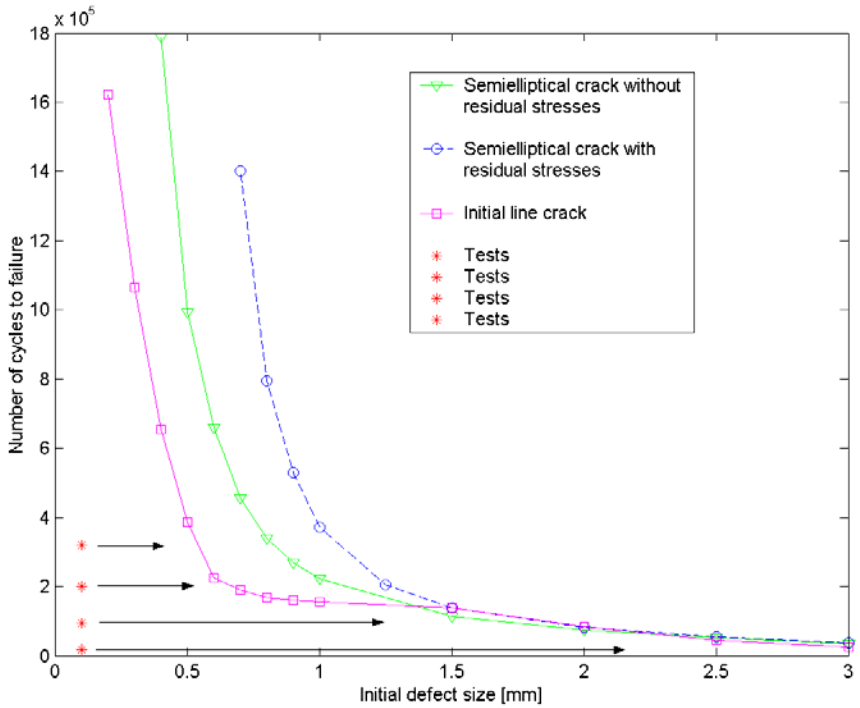


Figure 16. Predicted life for bending load corresponding to max S1=520MPa.

In this specific case the stress level is caused by a stress concentration and therefore it is not as severe as it should be without the stress gradient through the thickness, but in general such circum stances is not applicable in engineering design. The consequence of the local overload is a line crack covering roughly a 45 degree arc at top and bottom of the critical section. The initial crack dept is depending on several causes and is hard to predict exactly (see reasoning in section 3), but it should be between 0.5 and 1.1 for the tested load levels.

Table 5. Tested vs. simulated life in bending without residual stresses

No of cycle's vs. Load level	Test 1	Test 2	Test 3	Test 4	Simulation by FEM/Paris law
460 MPa	91879	317614	1052580	1935913	351300
520 MPa	18722	95077	200907	319691	188000

In Fig. 16 it can be seen that the test results for an initial line crack are quite well arranged around a crack size of about 1 mm, the expected size for the current load level. Further it can be noted that the difference between the line crack and the semi elliptical approach is vanishing at an initial crack size of roughly 1.5 mm. This is a most natural effect as the stress concentration rapidly will force the semi elliptic crack to spread out along the surface and approach the line solution. It deserves once again to point out that the prediction for the elliptical solution is not valid at those stress levels. Assuming a significantly higher yield stress for the material, the predictions would be true also for the elliptical solution.

4.2 Torsion and mixed mode

The torsion case tests shows pronounced multiple crack initiation in line with knowledge of cast material behaviour, i.e. initiation at several defects as the stress was about uniform along the highly stressed area. In a cast material no geometrically determined crack path exists, so for the pure torsion cases it will immediate form a factory-roof appearance from the 1st principal stress pattern. In this work an initiative was taken to model the torsion crack propagation by a single crack, see Fig. 17.

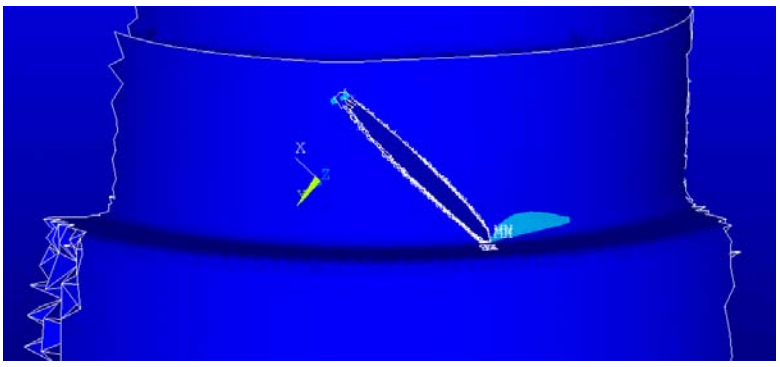


Figure 17. Single crack in torsion load, perpendicular to 1st principal stress.

The simulation result for this approach indicated an initial defect as large as 2.5-4 mm, see fig. 18. This was probably not the situation in question. The largest material defects found in the components were 0.5-1.5 mm.

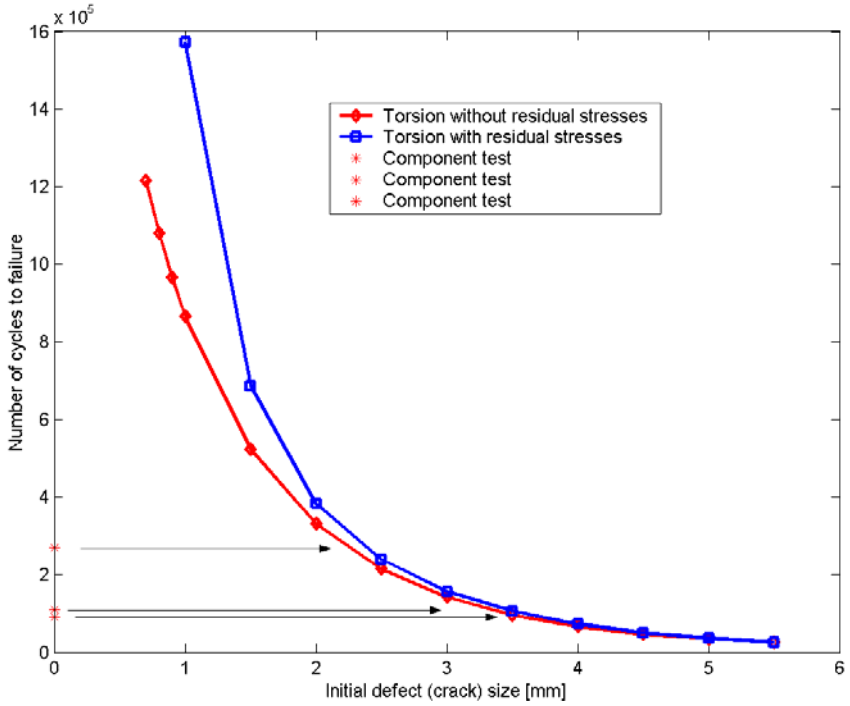


Figure 18. Predicted life for the torsion case compared with test results.

It must further be kept in mind that also the applied torsion loads where at equal or over the yield stress level for the material, which implies that the initiation maybe was govern by another mechanism. Yet, if one assume Coffin-Manson initiation and locally defect free material the initial crack depth should be up to 2 mm but hardly more. This must be interpreted as that the stiffness is too high with only one crack modelled.

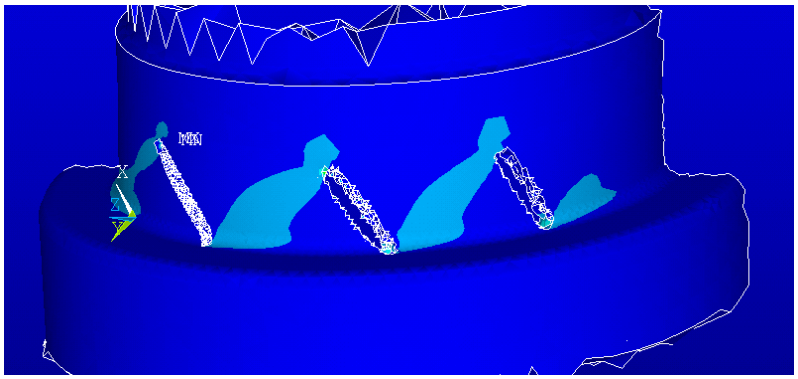


Figure 19. One real crack modelled and two additional openings simulating lowered stiffness because of multiple cracks under torque load

One possible way of handling the situation is to introduce cut-outs where the tension loaded multiple cracks are supposed to occur, compare fig. 6. The influences from the cracks loaded in compression where then supposed to be insignificant. This way of modelling multiple cracks resulted in roughly 8-10% higher SIF´s and also a good accordance with tests. Even though the technique seems to be suitable for some special cases it was still not evident that the crack pattern could be known a priori for what reason the evaluation was not continued. However, the path indicated by the 1st principal stress criteria agree very well with test results.

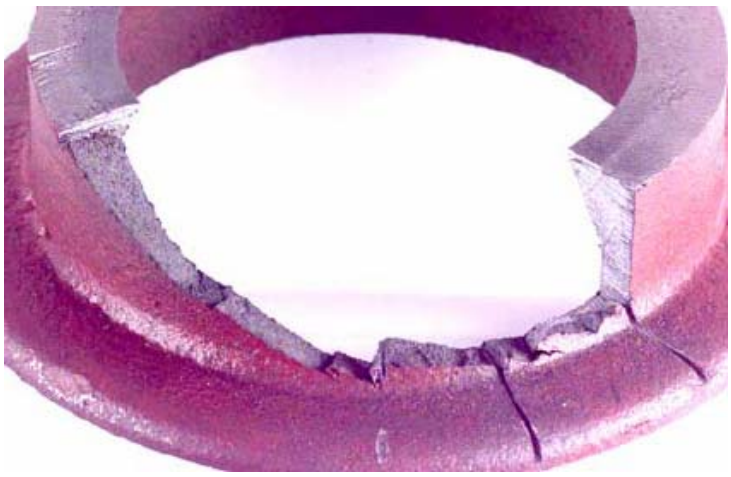


Figure 20. Crack path from bi-axial in phase load (bending and torsion)

When it comes to bi-axial load, i.e. bending and torsion at the same time, the conditions are a bit different. The out-of-phase case contains sequence effects and was not treated herein. The in-phase case, which holds no sequence effects, was modelled. With load ratio R=-1, the loads interact and closes the crack in pressure for half the load cycle. As a result, only one major crack will be established, see fig. 20. With this it was suited for modelling with Mcrack and according to 1st principal stress criteria.

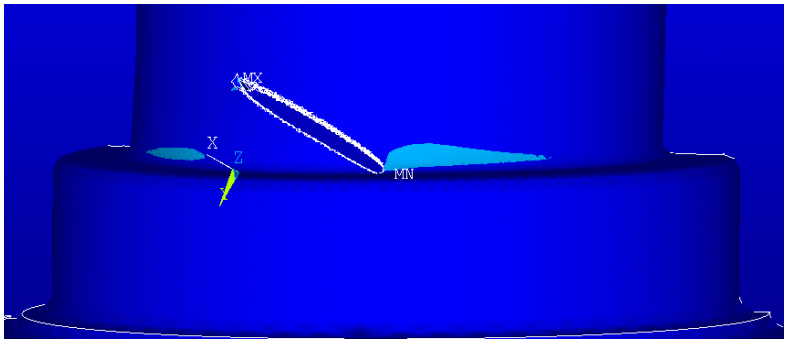


Figure 21. Single crack model for in-phase mixed mode

The result from the mixed-mode evaluation was showing excellent agreement with tests. As can be seen in tab. 6 there is a substantial scatter in test results, but on the other hand it's a rather small basis. However, the simulated life is in the middle of the range indicating a fair estimation but perhaps not covering aspects of individual deviations.

Table 6. Tested vs. simulated life in mixed mode without residual stresses

No of cycle's vs. Load level (von M.)	Test 1	Test 2	Test 3	Simulated by FEM/Paris law
516	127912	127934	228400	153300

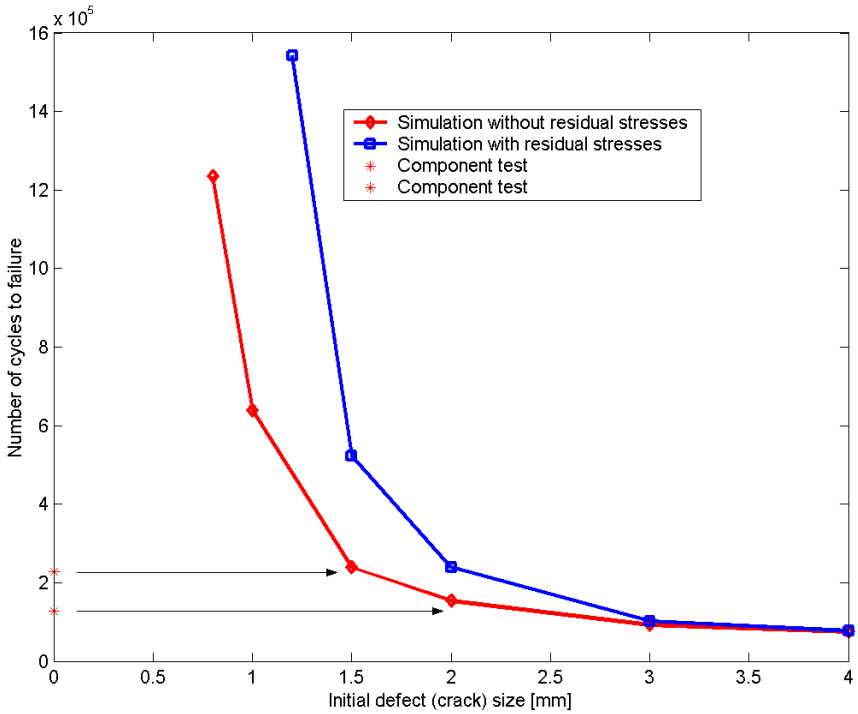


Figure 22. Predicted life for in-phase mixed mode load compared to test results

Fig. 22 shows the predicted life for mixed mode with and without residual stresses. The initial defect (crack) size follows the same reasoning as for the bending case but with another stress gradient. The initial crack depth, regarded the current stress gradient, can be estimated to 1.5-2 mm. It is noted that the prediction curve for the case without residual stresses then is located at the expected level. As earlier stated, the case with residual stresses is not treated because of the high stress level from the load which is supposed to relax more or less all residual stresses.

5 CONCLUSIONS

In this paper a fracture mechanics evaluation of a nodular cast iron sleeve was made. During the course of action it has been showed that the software Mcrack in conjunction with ANSYS is a powerful and versatile tool for crack modelling in arbitrary solids.

The most significant conclusions of the work (not classified):

- It is of greatest importance to take a local approach for evaluations. All calculations should be made as local analysis with local stresses, local R-values, local material behaviour etc, etc.

- The field of application for the Mcrack software has been extended. The relative error in SIF caused by non exact sub modelling was relatively small, within 5-10% for about 0.25 mm misalignment.

- The timesaving utilization of AF-Grow for implementing residual stresses was very successful. It contributes greatly to the improvement of prediction capability without consuming non proportional amounts of resources, yet it was not crucial for this particular evaluation.

- Fracture mechanics has once more showed to be well suited for analysing troublesome, complexly loaded components. The results shows, still, that methods must be developed to cover individual circum stances in a better way.

- The maximum principal stress criterion has shown to be in good agreement to test results for cast components exposed to various multiaxial loads. This fact is especially valid in cast materials as there is no intrinsic crack path.

- The Mcrack/ANSYS software combination has been proven to give satisfactory results also for complex loading, although no phase effects are yet investigated. Multiple crack situations are possible to handle, but this requires explicit knowledge about the crack pattern.

ACKNOWLEDGEMENTS

The author would like to thank Jack Samuelsson, Volvo CE, and Kenneth Hamberg, Chalmers Lindholmen, for being sources of inspiration and for supervision. Johan Martinsson for fruitful discussions and for support with Mcrack. Further, Tommy Thors and Magnus Hellberg, ABB, for underlying test results, tested components and general support. Gunnar Åkerström, Volvo Truck, for material investigations. Last, but not least, Nordic Industrial Found (NI), Vehicle Research Program (PFF) and Volvo for funding.

REFERENCES

1. Martinsson, J, *Fatigue Assessment of Complex Welded Steel Structures*, doctoral thesis, Department of Aeronautical and Vehicle Engineering, KTH, Sweden 2005, ISBN 91-2783-968-6.

2. ANSYS official web page, *http://www.ansys.com/*

3. AF-Grow official web page, *http://afgrow.wpafb.af.mil/index.php*

4. Dahle, T, et al., *Multi-axial fatigue tests of a component in nodular iron*, In Proceedings of Cast Design 2005-Final seminar, VTT, Finland, 2005, 331-350.

5. Samuelsson, J, *Fatigue Design of Vehicle Components: Methodology and applications*, PhD Thesis, Dept. of Aeronautical Structures and Materials, Report 88-23. The Royal Institute of Technology, Stockholm, 1988.

6. Anderson, T. L, *Fracture Mechanics, fundamentals and applications, 2nd ed*, CRC Press LCC, Florida, USA, 1995, ISBN 0-8493-4260-0.

7. Swedish standard Institute, SIS, *SS-EN 1563 spheriodal graphite cast iron 1st ed*, Stockholm, Sweden, 1997.

8. Suresh, S, *Fatigue of materials, 2nd ed*, Camebridge university press, Camebridge, UK, 1998, ISBN 0-521-57847-7.

9. Björkblad, A, *On the Prediction of crack propagation in Cast Steel Specimens*, In Proceedings of the 9th Portuguese Conference of Fracture, edited by C.M. Branco, IST, Lisbon, Portugal, 2004, pp. 167-175.

10. Björkblad, A, *Conventional vs. Closure Free crack growth in Ductile iron*, In Proceedings of the 15th European Conference of Fracture, KTH, Sweden, 2004.

11. Mörtsell, M, et al., *Fatigue crack initiation in ductile cast irons,* International Journey of Cast Metal Research, vol.16, no. 1-3, pp. 245-250, 2003.

12. Keesecker, A.L, et al., *Crack path bifurcation at a tear strap in a pressurized shell*, Computers and structures, pp. 1633-1642, 2003.

13. Ljustell, P, *On Predictions of Fatigue Crack Growth Rate*, licentiate thesis, Solid mechanics, KTH, Sweden, 2005.

14. ASTM E-647, Measurement of fatigue crack growth rate, American Society for Testing and Materials, Philadelphia.

15. Lindeborg, B and Nilsson, J, *Fracture mechanical data for ductile iron, malleable iron and cast steel*, Sveriges mekanförbund, Stockholm, Sweden, 1985, ISBN 91-524-0791-8.

16. Nadot, Y, Mendez, J, Ranganathan, N, *Influence of casting defects on the fatigue limit of nodular cast iron*, Int. J. of Fatigue, vol. 26, pp. 311-319, 2004.

17. Nadot, Y and Denier, V, *Fatigue failure of suspension arm: experimental analysis and multiaxial criterion*, Engineering Failure Analysis No 11, pp. 485-499, 2004.

PROGRAM

1 Methodologies and tools for fatigue life assessment

- Automotive components
- Various industrial applications
- Welded structures and assemblies

2 Advanced design tools and approaches

- Fatigue crack initiation assessment
- Contribution to the crack propagation stage
- Modelling of the design behaviour of the welded

3 Multiaxial loading fatigue assessment

4 Fitness for service approach and applications

5 Experimental validation

- Application to automotive parts and structures
- From laboratory testing to field evaluation
- Development of dedicated test devices and procedures

6 Design procedures against thermal and thermo mechanical fatigue damage

7 Reliability approaches in fatigue design

8 Improved design and manufacture processes with regard to fatigue

EUROPEAN FITNESS-FOR-SERVICE NETWORK (FITNET)

"Fatigue Module Development"

Jean-Jacques. Janosch, Caterpillar France, Grenoble, France
Michel Huther (Bureau Veritas), France
Henri Paul Lieurade, CETIM, France
Nigel Taylor, (Joint Research Centre, Petten), The Netherlands
Steve Maddox (TWI), UK
Mustafa. Kocak, GKSS Research Center, Geesthacht, Germany

Summary: FITNET is a four-year European thematic network with the objective of developing and extending the use of fitness-for-service (FFS) procedures for welded and non-welded metallic structures throughout Europe. It is partly funded by the European Commission within the fifth framework programme and it was launched in February 2002. The network currently consists of about 50 organisations from 17 European countries and supported by institutions from USA, Japan and Korea. Further information can be found in the FITNET TN website: **http://www.eurofitnet.org**. The FITNET FFS Procedure is built up in four major analysis modules namely fracture, fatigue, creep and corrosion. The first official draft is available in early 2006 in the form of an official CEN document. Industrial components are as a rule exposed to fluctuating loads and hence consideration of fatigue damage accumulation or of fatigue crack growth is a critical issue. The aim of this paper is to present the features and the main analysis routes of the FITNET FFE Fatigue Module of the FITNET FFS Procedure to assess the fatigue life of the load carrying metallic components manufactured with and without welds. The paper includes an industrial case from ship structure for the application of two fatigue assessment routes.

Keywords: Fitness-for-Service, Fatigue, Cyclic Loading, Defect Assessment, Welds, Engineering Structures

1 INTRODUCTION

FITNET is a European networking project designed to promote the development of a Fitness-for-Service (FFS) Procedure for assessing the structural integrity of metallic welded or non-welded structures transmitting loads. In particular it embodies techniques for dealing with defects known or postulated to be present in a structure together with the possible growth of such defects by a range of mechanisms and the assessment techniques required to evaluate failure risk. It is intended to provide an umbrella scheme into which results from EC-funded projects, national programmes and in-kind funded contributions from industry and academia are harnessed to the common goal of a fitness-for-service procedure based on European advanced technology. The FITNET FSS procedure aims to provide methodologies for the assessment of fatigue damage in components, which may affect its fitness for service.

It is aimed to develop FFS Procedure to satisfy following basic requirements:

- Be an advanced, fully validated method for determining the fitness for service of various structures or components manufactured from metallic materials with and without welding.
- To cover four major failure modes of engineering structures, namely; fracture, fatigue, creep and corrosion damage and all aspects essential for advanced design in all industrial sectors.
- To be readily usable by general industry and make a major contribution to cost saving, particularly for small and less technically advanced companies, whilst still improving structural safety.

To support these objectives, **FITNET Thematic Network** with its wide range of expertise and activities of its member organisations embraces results obtained in numbers of completed EU projects such as SINTAP, ASPOW, HIDA, DISMEW, INTEGRITY, PLAN, WAFS and JOTSUP etc. It also covers the recent developments in other on-going EC funded projects, networks and advances in national and industrial codes such as BS7910, R5&R6 and AP1 579.

Although several fitness-for-service procedures already exist (e.g. BS7910, API579, R6 and SINTAP) (1,4-8), they tend to be aimed at a particular industrial sector, or a single failure mode (e.g. SINTAP covers only fracture), or are national documents. There is therefore a need for a single and agreed European FFS Procedure, which could ultimately become a European (CEN) standard for assessing the flaws (such as cracks, welding defects and corrosion damage) in welded and non-welded metallic load carrying structures operating under various loading conditions.

A European-wide **FITNET-FFS** procedure is essential to regulators, especially as they are now faced with an increase in multi-national owners and operators of industrial systems. By the same token industries will benefit from having at their disposal a tool for cross regional benchmarking and to provide increased flexibility in choosing their suppliers as all can work to the same basis and calculations/solutions can be re-used for similar components. FITNET FFS Procedure is currently under development is structured in four major assessment modules, to assess the postulated flaw (at the design and fabrication stages of a new component) or real flaw(s) detected during in-service inspection. The present work aims to present the current state of the FITNET FFS Fatigue Module and describe its major features and assessment routes.

II - FITNET FSS PROCEDURE - FATIGUE MODULE

New FITNET-FFS procedure with its easy-to-use feature and similarly structured four assessment modules is developed in a coherent fashion to the currently used FFS procedures. Special effort is made to develop welding sections for each module (similar to the SINTAP procedure) to treat the conventional and advanced (e.g laser beam, friction stir etc.) structural welds.
In order to develop four assessment modules, FITNET Thematic Network operates during last three years on four respective working groups (WG);
WG1: Fracture (Leader: S. Webster, CORUS),
WG2: Fatigue (Leader: JJ. Janosch, CATERPILLAR)
WG3: Creep (Leader: RA. Ainsworth, BRITISH ENERGY)
WG4: Corrosion (Leader: R. Koers, SHELL)

Each WG is working on the implementation of currently available and technically sound international procedures as well as technical items need to be improved, added or validated for the **European Fitness for Service (FFS)** procedure with the overall structure as given in Fig. 1.

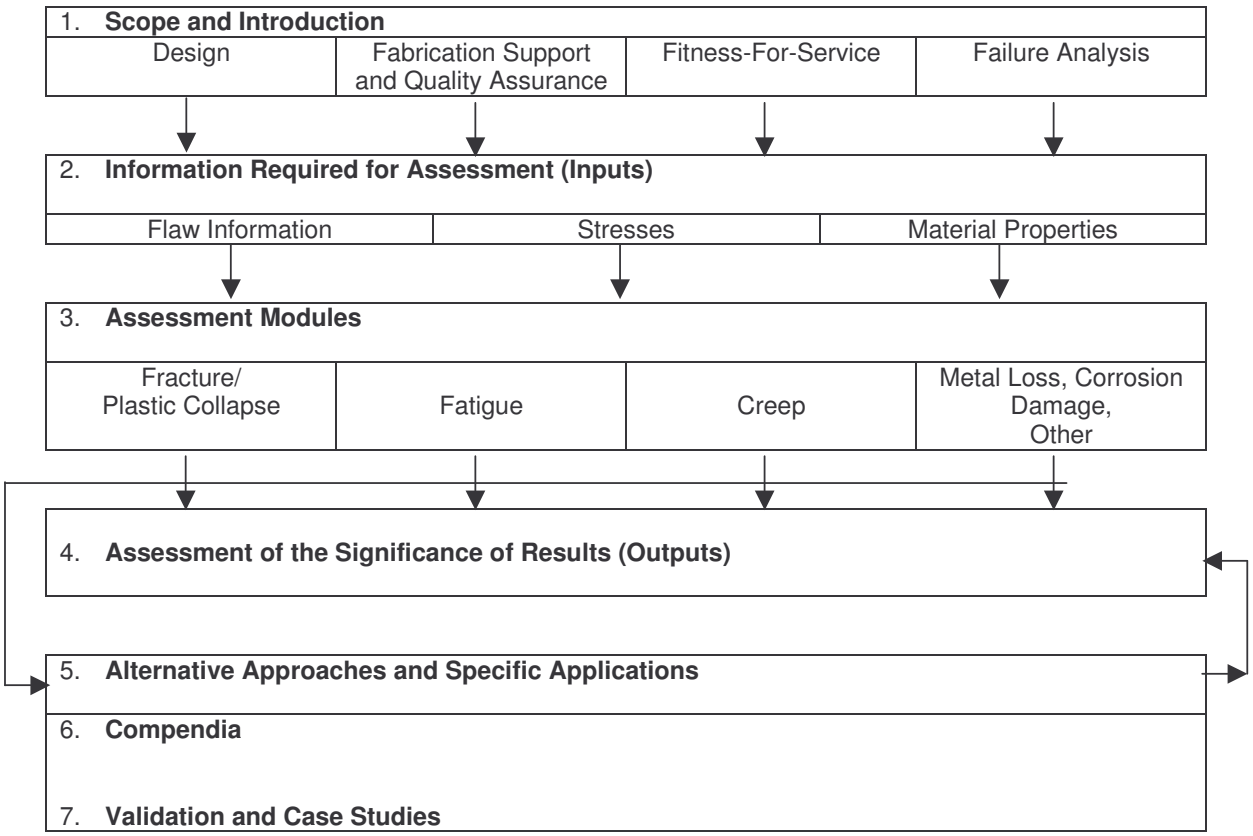


Fig. 1 Overall flowchart of the FITNET FSS procedure

III - BACKGROUND INFORMATION ON FATIGUE MODULE DEVELOPMENT

The FITNET fatigue module will draw on existing procedures, notably fatigue design rules and recommendations (e.g. IIW, Eurocode) and flaw assessment procedures (e.g. BS 7910, API 579, R6). Noting that many of these were developed for a specific manufacturing technology, a single industrial sector, or as a national document, the aim will be to extract relevant information for presentation as a general procedure that addresses the needs of a wide range of industries. In this respect, the industries represented by the WG memberhip is suitably diverse, including offshore, shipbuilding, bridges, pressure vessels, chemical, earth moving, automotive, railway, nuclear, mechanical industry & SMEs. It is anticipated that the procedures embody the following:

+ The development of a coherent, multidisciplinary and “easy to use” fatigue assessment routes based on representative and significant existing documents,
+ The implementation of advanced fatigue databases (covering various materials); and new manufacturing or assembly processes (laser, laser-hybrid, friction stir welding,…),

+ The development of a "multi-scale mechanical approach" by providing conventional and multiaxial fatigue criteria (semi-local and local mechanical approach) for either constant or variable amplitude loading conditions.
+ The development of a specific guideline on conventional and advanced fatigue design methods for welded assemblies (S-N curves, structural stress) and non-welded assemblies
+ The establishment of a practical "Non Destructive Technology" recommendation (capability, accuracy; reliability…) for defect size assessment,
+ The implementation of dedicated databases which will be the input for other WG Modules (Such as a "Compendium of Residual Stresses") in order to have a rational link with the global FFS procedure.

IV - THE FATIGUE MODULE AND ASSESSMETN ROUTES

The FITNET fatigue module draws on existing procedures, notably fatigue design rules and recommendations (e.g. IIW, Eurocode) and flaw assessment procedures (e.g. BS 7910, API 579, R6). Noting that many of these were developed for a specific manufacturing technology, a single industrial sector, or as a national document, the aim will be to extract relevant information for presentation as a general procedure that addresses the needs of a wide range of industries. In this respect, the industries represented by the WG2 membership is suitably diverse, including offshore, shipbuilding, bridges, pressure vessels, chemical plant, earth moving equipment, automotive, railway, nuclear, mechanical industry & SMEs. It is anticipated that the procedures embody the following:
+ The development of a coherent, multidisciplinary and "easy to use" fatigue assessment routes based on best practices in existing documents,
+ The implementation of an advanced fatigue properties database (covering various materials) and new manufacturing or assembly processes (laser, laser-hybrid, friction stir welding, etc.),
+ The development of a "multi-scale mechanical approach" by providing the possibility to use semi-local and local mechanical approaches for either constant or variable amplitude loading conditions.
+ The development of specific guidelines for welded assemblies (S-N curves, structural stress) and non-welded assemblies
+ The establishment of a practical recommendations for using "non-Destructive inspection technology" (capability, accuracy; reliability…) for defect size assessment,
+ Contribution to dedicated databases which support the use of all the modules (such as the "compendium of residual stresses") to ensure commonality in the overall procedure document.

Route 1 – Fatigue damage assessment using nominal stresses

This route considers nominal elastic stress values for the location of interest and the fatigue life N_f is determined from a set of S-N curves classified according to different classes or levels of fatigue resistance i.e. the effects of local geometric, weld or microstructural details and, if relevant, residual stress are accounted for in the S-N curve itself. It is based on currently used procedures (e.g. IIW (ref (1)) for welded joints). The linear cumulative damage law is used to deal with variable load spectra.

$$\frac{N_1}{N_{f1}} + \frac{N_2}{N_{f2}} + \frac{N_3}{N_{f3}} + \ldots\ldots \leq 1$$

where D is a scalar measure of the allowable damage at the end of the required life (commonly D=1, but it can also be set to a value less than one)

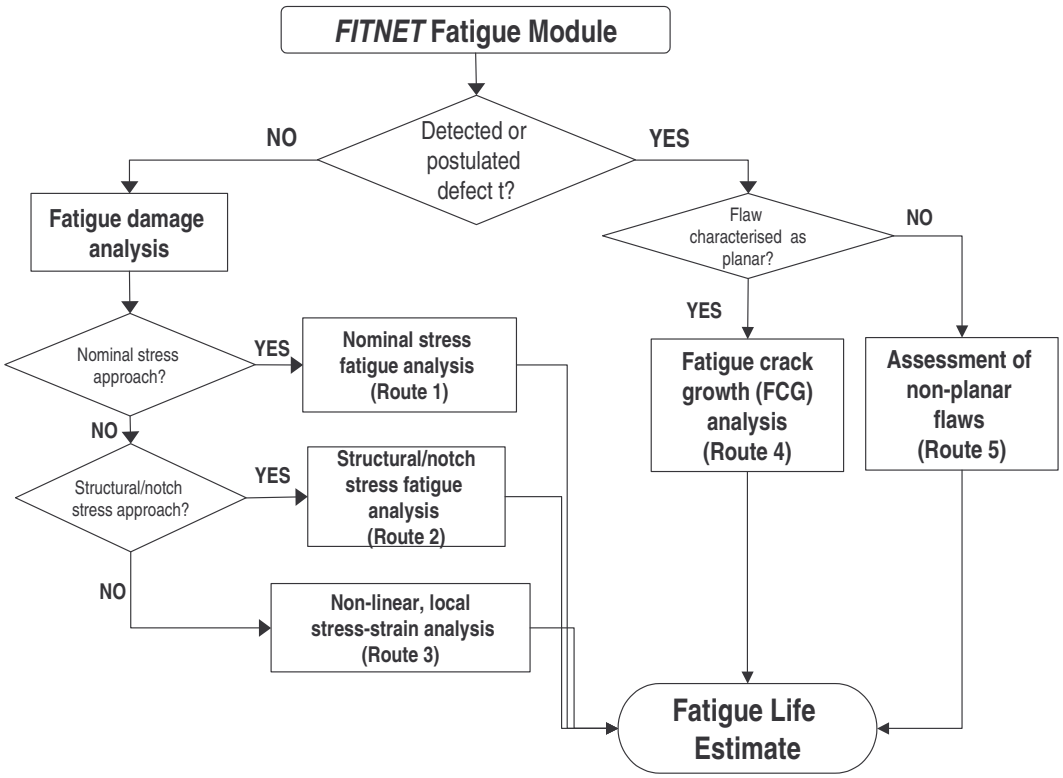


Fig. 2 Overall flow chart of the FITNET FFS Procedure and its five routes.

Route 2 – Fatigue damage assessment using either structural stress or notch stress, coupled with appropriate S-N curves

This route considers that the appropriate structural stress in a critical area of a component could be calculated by FEA or by formula. In some case it could also be measured by following specific methods. Two approaches are possible:

a) calculate the structural stress and apply with appropriate class S-N curves,
b) calculate a notch stress via stress concentration factors such as K_t or K_f, and apply with appropriate S-N curves, ref (2,3)

Route 3 - Fatigue damage assessment considering elastic-plastic material behaviour at critical features and strain-range based fatigue life curves

This route is mainly directed at non-welded applications and foresees direct calculation of strains at a critical location using an appropriate elastic or elasto-plastic description of the material behaviour. The fatigue life is then determined from a strain range vs. cycles relation such as the Manson-Coffin law, for which the implicit failure criterion is related to crack initiation. It is also noted that the analysis can be taken further by considering subsequent crack growth using fracture mechanics (route 4).
These analyses can be performed cycle-by-cycle, allowing for non-linear damage accumulation effects if necessary.

Route 4 – fatigue crack propagation

This route addresses the assessment of detected or postulated planar flaws that can be considered as macro-cracks (i.e. with dimensions typically greater than millimeters). The initial flaw position, size and orientation can be determined in two ways:

a) based on the reported or detected size from non-destructive inspection results
b) postulated defect, based on consideration of service experience, the manufacturing process, resolution limits of a NDE technique, from the threshold stress intensity factor etc.

Recommendations are given for assessing flaws in plain, unwelded material and for those associated with welds.

a. Flaws in unwelded material:

The selected baseline fatigue crack growth equation is that originally proposed by Forman and Mettu and subsequently used in the NASGRO software for non-welded application. It accounts for the stress intensity factor range, the mean stress level and other important parameters, and is considered a suitable universal formula for fatigue crack growth (FCG) analysis. It has the form:

$$\frac{da}{dN} = C\left[\left(\frac{1-f}{1-R}\right)\Delta K\right]^n \frac{\left(1-\frac{\Delta K_{th}}{\Delta K}\right)^p}{\left(1-\frac{K_{\max}}{K_c}\right)^q}$$

where C, n, p, and q are material constants, f is the ratio of opening and maximum, K_{max}, stress intensity factors, R is stress ratio, K_c is the critical stress intensity factor, and ΔK_{th} is the threshold stress intensity factor range.

b. Flaws in either welded or unwelded material

For the assessment of flaws associated with welds or for assessing flaws in unwelded material for cases where the NASGRO parameters are not available, use is made of the NASGRO expression is reduced to the standard Paris Law form:

$$\frac{da}{dN} = A.\Delta K^m$$

where A and m are constants that depend on the material, environment and the applied conditions, including any that are specifically relevant to flaws in welds, notably the presence of residual stress.

If it can be shown that ΔK is below an appropriately determined threshold value, the crack growth rate may be deemed negligible. These expressions can be integrated to provide estimates of crack growth over a fixed number of cycles or for the number of cycles required to reach a critical crack size, determined using the FITNET fracture assessment module. The acceptability of the real or postulated flaw can then be determined in relation to the required cyclic life.

For the K solutions themselves, the user will have access to a special compendium common to all the FITNET modules.

Route 5 – Non-planar flaw assessment

Non-planar flaws can be assessed in the same way as planar flaws using route 4. Since they are not crack-like, this will be conservative. However, it may be the only option if it is necessary to quantify the growth of the flaw under fatigue loading and to ensure the margin against unstable fracture at a specific crack size. Otherwise, Route 1 using S-N curves for welded joints can be applied directly, in cases for which the equivalent fatigue strength are established for the non-planar flaw under consideration.. At present, this approach is only available for assessing slag inclusions or porosity in steel or aluminium alloy butt welds

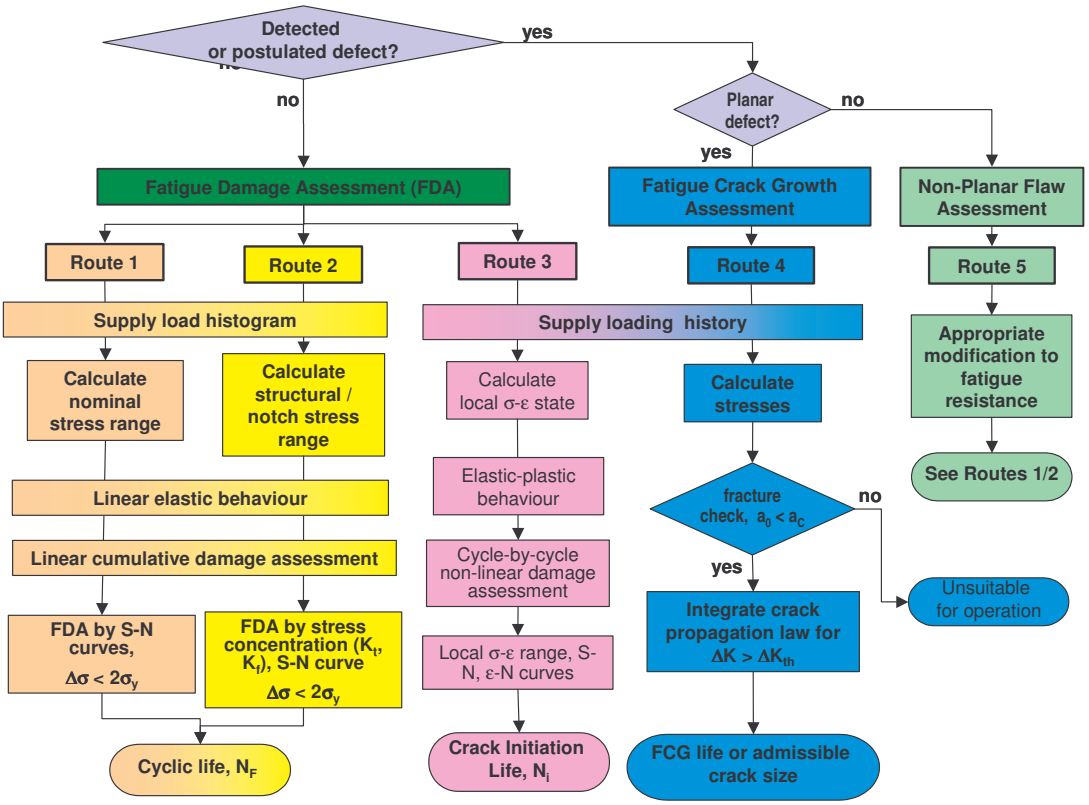


Fig. 3 Detailed flow chart of the five FITNET fatigue assessment routes

V ALTERNATIVE AND SPECIFIC ASSESSMENTS

Alternative approaches and specific assessments in fatigue are also included in the FITNET procedure. The objective is to identify "bridges" between the modules in the overall FITNET procedure for complex service conditions, and also to consider "emergent" industrial approaches to assess fatigue life under specific conditions. The areas covered by this part are focussed on:

+ Equivalent constant amplitude stress
+ Stress intensity approach
+ Multi-axial fatigue assessment
+ Contact and fretting fatigue
+ Fatigue - creep interactions
+ Fatigue - corrosion interactions

VI - APPLICATION EXAMPLES (ROUTES 1 & 2)

1 - Presentation of the Shipbuilding Industry Case study:

This example illustrates the fatigue assessment routes used by the shipbuilding industry during the design phase. In particular, a scallop in a longitudinal stiffener of the deck of a tanker is considered.
The ship has the following dimensions:

Length	L = 300 m
Breadth	B = 57 m
Depth	D = 30 m
Draught	d = 21 m

Block coefficient $C_b = 0.85$ (ratio of the loaded ship mass to 1.025 LBT)

Figure 4 presents the cross section of the overall design of the ship structure. Figure 5 presents the structural class of weld detail under study.

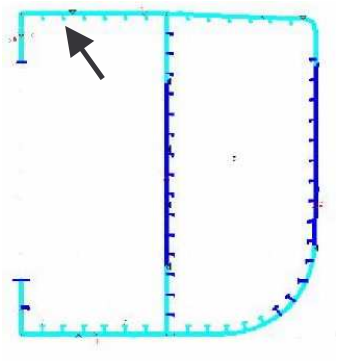


Figure 4

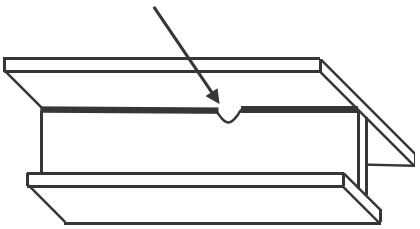


figure 5

The structure scantling (dimensions) fulfil the classification rules which means that the midship modulus is equal to:

$$W_m = F\, L^2\, B\, (C_b + 0.7)\, 10^{-6} \qquad \text{in } m^3$$

Loading conditions

The maximum midship wave bending moments are:

hogging: $M_{wH} = 190\, F\, L^2\, B\, C_b\, 10^{-3}$ in kN.m

sagging: $M_{wS} = 110\, F\, L^2\, B\, (C_b + 0.7)\, 10^{-3}$ in kN.m

From the rules, the long-term wave bending moment distribution for 25 years life can be represented in terms of stresses and number of associated cycles by Table 1

$\Delta S_i/S_{max}$	n_i
1	5
0.88	68
0.74	342
0.63	1 895
0.51	8 160
0.44	13 160
0.40	47 370
0.35	47 370
0.32	92 105
0.30	131 580
0.28	265 260
0.22	568 420
0.16	1 684 210
0.13	2 736 840
0.09	26 315 790
0.05	68 421 055
Σ	100 333 630

Table 1 Long-term wave bending moment distribution for a 25 year period

2 - Analysis

This industrial example directly involve routes 1 and route 2 of the FITNET fatigue module, ref (4. The objective is to evaluate the accuracy of the results which could be provided by each route.

a- Fatigue damage Analysis according to Route 1 (Nominal stress approach)

Inputs parameters
Route 1 uses the nominal stress, i.e., the longitudinal stress range in deck induced by the wave bending moment.
In that case the bending moment range is:

$$\Delta M = M_{wS} + M_{wH}$$
$$\Delta M = F\, L^2\, B\, 10^{-3}\, [190\, C_b + 110\, (C_b + 0.7)] \qquad \text{in kN.m}$$

Then the associated maximum stress range is:

$$\Delta S = \frac{\Delta M}{W_m}$$
$$\Delta S = \frac{190\, C_b + 110\, (C_b + 0.7)}{C_b + 0.7}\, 10^3 = 214 \text{ MPa}$$

The S-N curve can be found in the extract from the FITNET classification scheme in Table 2.

Welded Joint Classification (cont'd)

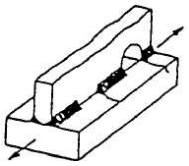
Joint Classification	Description	Examples
Category 6 E F	2) Intermittent fillet welds 3) As (2) but adjacent to cutouts.	

Table 2

Therefore the S-N curve is the F curve which characteristics are:

$m = 3$ $K_{50} = 1.726\ 10^{12}$ Stdv = 0.2183

The design curve is considering 2 slopes curve without cut-off at minus 2 standard deviation. The change of m=3 slope fixed at 10^7 cycles:

$$K_{D1} = 6.316\ 10^{11}$$

The slope change stress range is:

$$\Delta S_1 = (K_1 / 10^7)^{1/3} = 39.8 \text{ MPa}$$

then the second part of the S-N curve is:

$m = 5$ $K_{D2} = \Delta S_1^5 \times 10^7 = 9.987\ 10^{14}$

Results of the calculation (route 1)

Based on the stress distribution in Table 1 and the above S-N reference curve, the cumulative fatigue damage based on Miner's rule can be calculated (Table 3). The resulting total damage calculation for this structure was D = 0.61, which is < 1. Thus, according to Miner's rule the structure is safe.

b- Fatigue damage analysis according Route 2 (notch stress approach)

Input parameters

The second possibility is to assess the fatigue damage using FITNET Route 2, by introducing the "notch stress range approach". The appropriate equation is given to calculate the notch stress using the nominal stress, the local hot-spot stress concentration factor and the notch effect factor. In the present example, the local hot-spot stress concentration factor K_g was determined by finite element analysis of the detail in tension to be 1.1

The FITNET procedure provides the following notch factor: $K_f = \lambda\ (\theta / 30)^{1/2}$ and the following values:

fillet weld $\theta = 45$

well contoured end, perpendicular $\lambda = 2.15$

Then

$K_f = 2.15\ (45 / 30)^{1/2} = 2.63$

$K_f\ K_g = 2.90$

The rules book S-N curve to be associated to the notch stress is the following curve:

$m = 3$ $K_{D1} = 1.692\ 10^{13}$

The slope change stress range is:

$$\Delta S_1 = (K_1 / 10^7)^{1/3} = 119 \text{ MPa}$$

and the second part of the S-N curve is:

$m = 5$ $K_{D2} = 2.386\ 10^{17}$

Results of the calculation (route 2)

Working as before, the Miner's rule sums and total summation are included in Table 3. The total damage calculation using this route is D = 0.52, which is again < 1, indicating that the structure is safe.

Table 3

$\Delta S_i/S_{max}$	ΔS nom	ΔS notch	n_i	n_i / N_i nom	n_i / N_i notch
1	214	611	5	0	0
0.88	188	537	68	0	0
0.74	158	451	342	0.002	0.002
0.63	135	386	1 895	0.007	0.006
0.51	109	311	8 160	0.017	0.015
0.44	94	268	13 160	0.017	0.015
0.40	86	246	47 370	0.048	0.042
0.35	75	214	47 370	0.032	0.027
0.32	69	197	92 105	0.048	0.042
0.30	64	183	131 580	0.054	0.048
0.28	60	171	265 260	0.091	0.079
0.22	47	134	568 420	0.093	0.081
0.16	34	97	1 684 210	*0.077*	*0.061*
0.13	28	80	2 736 840	*0.047*	*0.037*
0.09	19	54	26 315 790	*0.063*	*0.052*
0.05	11	31	68 421 055	*0.011*	*0.008*
Σ			100 333 630	0.61	0.52

italic ==> m = 5

where:

$N_i = K_{D1} / \Delta S^3$ or $N_i = K_{D2} / \Delta S^5$, K_{D1} and K_{D2} being the constants of the design S-N curves for the two stages with slopes of 3 and 5 respectively; $D = \Sigma\ n_i / N_i$

C -Synthesis

This example illustrates the fatigue assessment routes used by the shipbuilding industry during the design phase by considering the example of a scallop in a longitudinal stiffener of a tanker ship deck.
Route 1 and 2 of FITNET Fatigue module were used to calculate fatigue damage of this structural detail. By using both of these applications, the results of this analysis evidenced safe service condition. The fatigue damage calculated by using Route 2, which incorporates more accurate input parameters (FEA), provides a damage factor D = 0.52, which is 17% less than that from route 1

VI CONCLUSION

FITNET is a four-year European thematic network with the objective of developing and extending the use of fitness-for-service procedures for welded and non-welded metallic structures throughout Europe.
New FITNET-FFS procedure, currently under development and validation, has four major modules namely; Fracture, Fatigue, Creep and Corrosion. It is aimed to have a similarly structured modules and overall coherent to currently used procedures with the feature of easy to use procedure. Special effort is made to develop welding sections for each module (similar to the SINTAP procedure) to treat the conventional and advanced (e.g laser beam, friction stir etc.) structural welds.
This paper presented the overall FITNET FSS Fatigue Module and to provide an overview of the main routes which are currently under development to assess the fatigue life of the welded and non-welded metallic structures. . Special effort has been made to include approaches for welded sections and to treat the conventional and advanced (e.g laser beam, friction stir etc.) structural welds.
By providing a range of assessment routes, the module aims to cover the needs of analysts which can vary according to the basic fatigue resistance data available (S-N curves or fatigue crack growth laws) and the level of knowledge of local stress distributions (nominal, structural or notch stresses). Further it exploits the global framework of the FITNET procedure to provide access to K solutions, basic materials properties, residual stress distributions, guidance on NDE etc.

An industrial example illustrated the fatigue assessment routes, with an example from the shipbuilding industry . Routes 1 (nominal stress) and 2 (local notch stress) of the FITNET fatigue module were used to calculate fatigue damage . Both indicated that the design was safe, but route 2, with the local notch stress derived by FEA, proved to be the less conservative of the two, indicating 17% less damage.

Acknowledgements
The authors wish to express their sincere thanks to the European Commission for the support provided to the FITNET Thematic Network, and a to all the members of FITNET and the WG2 fatigue working group for their contributions.

References

1- A. Hobbacher, Recommendations for fatigue design of welded joints and components, IIW document XIII-1965-03/XV-1127-03, February 2004
2- IIW Recommendation for fatigue design of welded joints and components –doc XIII-1965-03 / XV-1127-03 (revision of doc XIII-1539-96 / XV-845-96)
3- IIW Structural Hot-Spot stress approach to fatigue analysis of welded components –doc XIII-1819-00
4- Bureau Veritas rules for steel ships classification – Fatigue check of structural details –
5- R6: 'Assessment of the Integrity of Structures Containing Defects', British Energy Generation Report R/H/R6, Revision 4, 2001.
6 - British Standard BS 7910: 'Guide on Methods for Assessing the Acceptability of Flaws in Metallic Structures', 2000.
7 -'SINTAP: Structural Integrity Assessment Procedures for European Industry', Brite-Euram Project No. BE95-1426, Contract No. BRPR-CT95-0024, Final Report, September 1999.
8- API 579, 'Recommended Practice for Fitness-For-Service', 1st Edition March 2000, American Petroleum Institute

New fatigue analysis approach
Application to the welded assemblies of railway rolling stock

Emigliano CAMPUS[a]: ALSTOM structure expert – emigliano.campus@transport.alstom.com
Franck DEFFARGES[b]: SNCF structure specialist– franck.deffarges@sncf.fr

[a] ASLTOM La Rochelle - avenue Commandant LYSIACK F- 17440 AYTRE
[b] SNCF Centre d'ingénierie du Matériel – 4, allée des gémeaux F- 72100 Le Mans

The railway equipment constructor ALSTOM and the French state railway operator SNCF have joined up with partners in the industry (MECAMIX, LMS X and the Institut de Soudure (French Welding Institute) to develop a new approach in fatigue design of welded railway car body structures.

As things stand today, the structures of car bodies are dimensioned with no precise references as regards the methods of calculation by finite elements. In order to harmonise and improve these methods, work has been accomplished to define the meshing rules and combine them with a fatigue criterion using thin shell elements, preferably without modelling the welding beads, so as to approach the present finite element models as closely as possible.

In the end, the results of the development work have lead to defining a new approach to dimensioning fatigue stresses, determining a relation between the manufacturing process, the finite element meshing and the Dang Van multi-axial fatigue criterion set up in the MXFAT software.

1 INTRODUCTION

Today, the fatigue strength of boiler plate for railway car bodies is based on a static test to measure the stresses using uni-axial gauges 10 millimetres long located perpendicular to and at the foot of the welding bead. These stresses are associated to the fatigue limit of the ERRI B12/RP60 recommendations (1) valid for the geometry corresponding to the design categories A, B, C, D and E. The other geometries for which the form is specific are examined with the interpretation of the engineer and along one direction only of the stresses of the foot of the bead. In actual fact, railway boilerplate weld fabrications are often locally under multi-axial stress conditions with angular variations of the main stresses. Alone, the uni-axial fatigue tests carried out are not suitable for evaluating all the stress statuses as well as are digital simulation tools. Accordingly, without special requirements to make a correct assessment of the fatigue behaviour, a new approach for calculating the fatigue strength of the welding seams based on the method of finite elements had to be developed. In the remainder of this paper, the former and the new dimensioning approach are explained.

Just as what is practised in the automobile industry (5, 8), the same approaches were adopted, though allowing for the specific nature of railway equipment and a restriction -the simplicity of use of the mesh.

2 ALSTOM: DESIGNER AND BUILDER

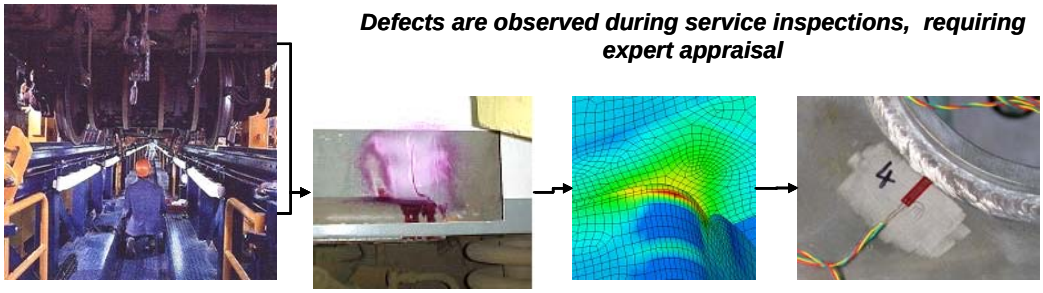
The constructor ALSTOM, the designer of the rolling stock, must master their dimensions in order to optimise the structures whilst guaranteeing the service life with time constraints for implementation of finite element models with a predicted quality deduced from the results of analyses. To optimise the choice of the welds in accordance with the computing principles and standard PR EN 15085 (3), a numerical tool had to be developed. With the time constraints, and "industrial" methodology had to be developed to allow for the recommendations of the design code so as to be able to predict a guaranteed level of safety. In the long term, the reduction and eradication of static and fatigue tests on mock-ups or boilerplate is the objective.

Overall, the need of the constructor can be summed up by the reduction in costs combined with better design, a shorter development time and optimisation of production with fewer checks during manufacture.

3 SNCF: OPERATOR AND INDUSTRIAL MAINTENANCE SERVICE PROVIDER

The SNCF railway operator that stipulates its technical requirements and maintains its rolling stock must naturally develop references so as to define more precisely in its contract requirements and develop the appropriate tools so as to keep constantly abreast with new computing technologies. The first and foremost mission of the operator is to achieve safety. Accordingly, the specifications indicating the strength of the equipment with time must ensure that no fatigue stress appears on the structures throughout the lifetime of the rolling stock.

When certain equipment no longer meet the expectations of the customers or the needs of the service, its mission is to adapt and increase performance levels. This may result in the appearance of fatigue stresses on the structures and generate considerable costs to monitor these during maintenance. The second mission is hence to modify and validate repairs throughout the life cycle of the rolling stock.



Defects are observed during service inspections, requiring expert appraisal

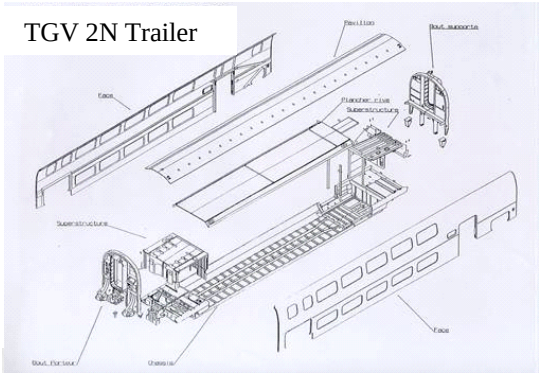
4 THE ROLLING STOCK

4.1 Structure of the rolling stock: The carbody

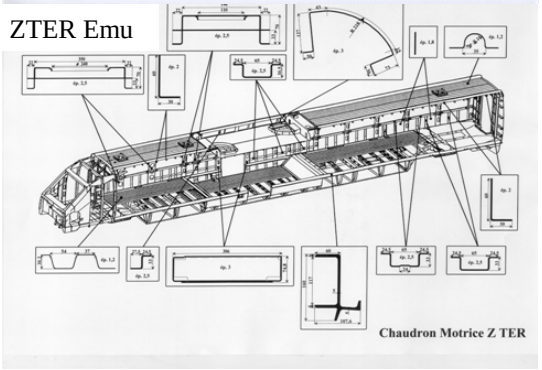
The carbody (i.e. the body structure) is a zone principally dimensioned to protect the passengers in the event of accidents. With the increasing number of derailing incidents and collisions since the beginning of rail trasportation, the natural development train went towards design with a network of beams. It became clear that superimposition of a strong frame on which the non-structural body resided did not offer optimum safety in the event of collision. The fact is that after an accident, the frame displayed only scanty damage, whereas the body was completely destroyed. The status of the assembly techniques with the builders improved, and since safety remained of first order importance, the body structures were considerably overdimensioned as time went by. The progress as a whole achieved since this period has enabled structures to be lightened as the design computation methods developed, particularly those based on finite elements. Each kilogramme of weight gained on the structure whas been used to offer additional equipment to enhance the comfort of the passengers in the train. Today, body structures are lighter despite the fact that they can withstand identical loads, or even greater loads resulting from the increase speeds.

- *Make-up: steel and aluminium structures assembled by welding, bolting and riveting.*
- *Welding processes are continuously changing (FSW welding)*
- *Thickness of assembled metal sheets may vary from 1.5 mm to 12 mm on the same coach body*
- *Length of coach bodies varies from 14 m to 25 m*
- *Assembly of cut, bent or punched metal sheets, profiles and cast parts*
- *Steel grades: S235, S355, S500*
- *Stainless steel grades: 304, 316*
- *Aluminium grades: 6082, 6005, 5754, AS7G*

TGV 2N Trailer



ZTER Emu



4.2 Assemblies

The assemblies present on a carbody shell are generally made by welding metal plates about 1.5 to 12 millimetres thick by the MAG process for steel or MIG process for aluminium. Through their thermal effects, these welding processes spread out residual stresses along the seam. The carbody structures are not given any treatment for relieving the residual stresses, which is highly important to the fatigue behaviour.

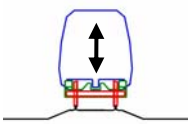
The carbody shell steel structure consists of stamped or folded sheeting pieces assembled together by welding. For aluminium, the body sections consist of extruded profiles arranged in the longitudinal direction and connected together by welding. Choice of the alloy is the outcome of the search for extrudability, weldability, corrosion strength, the mechanical properties of the base metal and the welded seams.

In the design of the assemblies, the welded components may turn out to be particularly complicated in shape. Accordingly, distribution of the local stresses inside these components is made up of the residual stresses and the multi-axial stress conditions originating from the dynamic stresses when in service. For these most critical zones, comparison with the fatigue strength determined on welded test pieces of simple shape, which are subjected to bending, is not suitable. Consequently, the recommendations of ERRI B12 RP60 for dimensioning railway rolling stock carbody shells, just like the other Eurocode or British Standard dimensioning codes, are not applicable to the fine analysis of the multi-axial stresses of the welding beads resulting from calculation by finite elements.

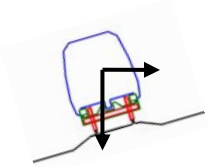
On a carbody structure, the weld-fabricated assemblies are generally supplemented by bolted assemblies at the ends of the carbody to secure the mechanically connected parts and assemble the carbody shell structures, for example the frame with the faces or faces with the roof.

4.3 Stresses in service

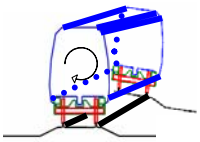
In general, railway rolling stock is subjected to loads that can be broken down into two groups – the first is that of great many cycles of small amplitude and the second only few cycles of great amplitude. In the first group, we find the main loads generated by running on tracks: vertical bounce, cross-acceleration, twist of the body, traction and braking. The levels of the forces involved in these normal and commonplace operating events are known and defined in standard EN 12663 (2). There are also the aerodynamic stresses resulting from crossing of trains and pressure waves encountered in tunnels. The details of aerodynamic phenomena are defined by another standard: EN 14067 (4). The values of the pressure gradients increase in amplitude and variation speed as the speed of the train increases. The associated number of cycles is difficult to foresee throughout the entire life cycle of the rolling stock, that is from thirty to forty years. In the second group, we find the cases termed “exceptional” though with a number of cycles sufficiently high to allow for their influence by superimposition on the damage resulting from the first group. The present practice to define the number of cycles is adapted to the fatigue endurance limit of the material used and the two types of events concerned, from 2.10^6 to 10^7 cycles. The design methods may be based on the limit of endurance or the accumulated damage. It is assumed that one can combine the loads in phase in order to obtain the maximum values at a common time.



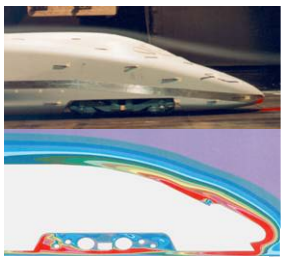
Bounce: Vertical forces



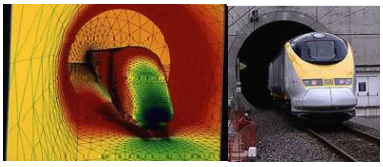
Running through curves: transversal forces



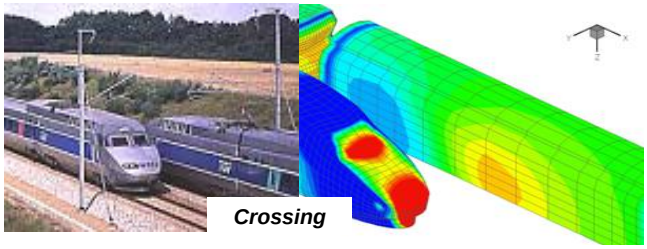
Track twist: torsion



Air penetration



Pressure waves



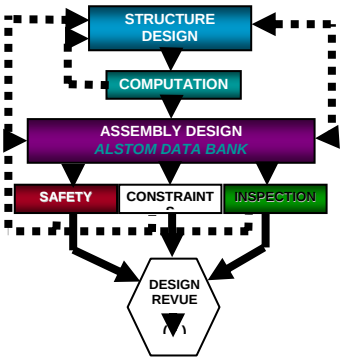
Crossing

5 DESIGN UNDER FATIGUE STRESSES

Design of assemblies with regard to fatigue stresses is in important phase, just as is that for the exceptional and dynamic events enabling the thicknesses of the sheeting to be defined and the dimensions of the constituent parts of the carbody shell. Through the dimensioning timing, ALSTOM must arrive at the most accurate results through modern finite element methods in order to define the most suitable welded joint. With regard to the various stresses, a weld-fabrication must withstand all of them whilst remaining in compliance with standard EN 15085 (3), i.e. it must guarantee safety and depending on the need, define the application of quality verifications after the production process has been completed.

5.1 Chronology of dimensioning

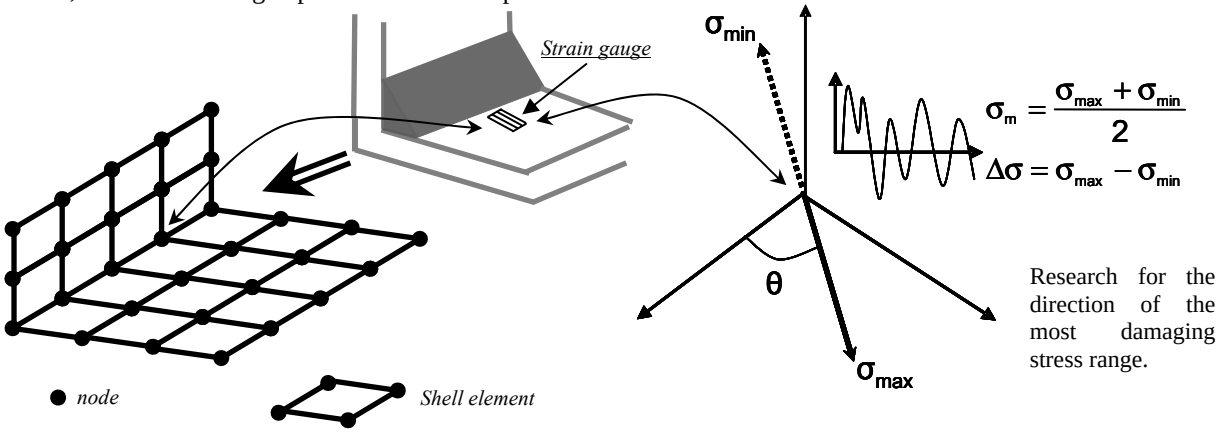
The performance of a design is based on the quantity and quality of the databank of the assemblies one can offer to the engineers and technicians of the design office. The fact is that choice of the welded seam is predominantly directed towards the ability to withstand the different loads. In this context, ALSTOM has developed a welded assemblies design assistance tool. This tool enables the welding operating modes to be defined in terms of the fatigue limit resulting from finite elements analysis and if necessary combine them with quality checks. To do so, the fatigue limits must be defined and the correct stress levels computed.



5.2 Current analysis method of fatigue stresses in railway structures

5.2.1 Fatigue stress analysis procedure

The meshes of the carbody shell structures consist mainly of thin shell elements without integrating the rigidity resulting from the welding beads, and the fatigue strength of the foot of the bead is analysed with the results of calculations of cases of fatigue loads. However, for thin shell modelling at the welding bead, the elements representing the average surface at the intersection of two plates and the junction between plates is defined by common nodes situated inside the core of the material. This position is not appropriate to experimental measurement of stresses obtained by strain gauges. Furthermore, to analyse the results, it is considered that the stress perpendicular to the bead is a significant value responsible for cracking. Whereas in calculating the analysis, it is a maximum main stress and not one averaged out that is extracted from the shell elements of minimum size, the sides of which are about 20 mm in length. Accordingly, the dimensioning constraint is defined as the maximum principal amplitude and is obtained by static calculation by finite elements in the elastic limit and extracted to a position corresponding to the core of the material, whereas the fatigue phenomenon takes place on the surface.



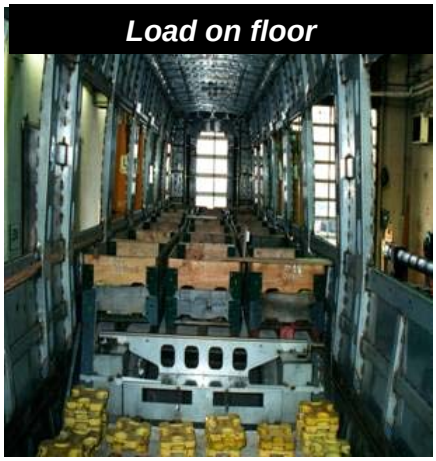
Research for the direction of the most damaging stress range.

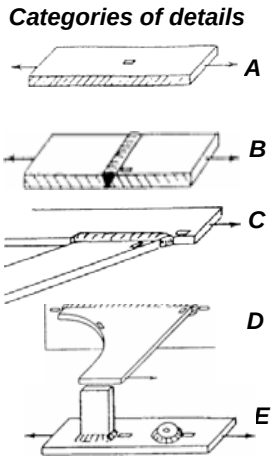
At the intersection of thin shell elements where the hot points generally occur, the stress gradient is highly sensitive to the meshing rules, i.e. the size of the element. Unfortunately, the size and the type of the finite elements are not defined in document ERRI B12/RP60 (1) since this is a document to check the compliance by testing. The position of extraction of the stresses by calculation with measurement by strain gauges, which is the dimensioning criterion, is not adequate.

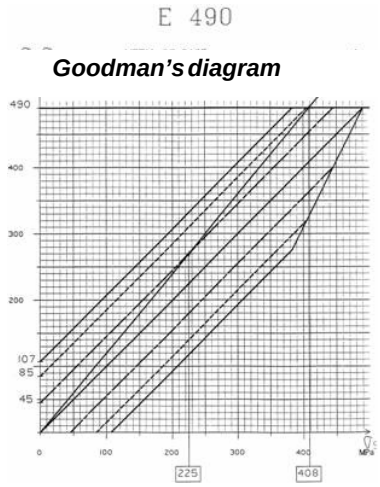
5.2.2 Verification of compliance: Measurements of distortions under static loads

Verification of the level of stress under vertical static loads and twisting of the car body are the only testing conditions that can be conducted to check the fatigue behaviour. It is impossible to assess the stresses caused through transverse, longitudinal and aerodynamic stressing on a complete body structure owing to the cramped space available. To counter this, mock-ups representing certain parts of the structure are sometimes used.

With regard to the vertical stresses and twisting of the body, verification of conformance is brought about through a static test with distribution of loads equivalent to the service loads in the body structure. Experimental measurements of the stresses on over two hundred gauges are the compared against the fatigue limit of Goodman's diagram. The concepts of mean stress and residual stresses are taken into consideration by plotting the limits of the diagram. The acceptable stresses used for tests on body structures are identified for steels with three classes of minimum elastic strength for five classes of slots defined generally as follows: case A: full metal; case B: butt-welding; case C: butt-welding with change of inertia; case D: corner welding; case E: boss welding.







Note: The angle positioning the stress gauge must be perpendicular to the welding bead to measure the maximum stress in accordance with the recommendations of ERRI B12/RP60. (1)

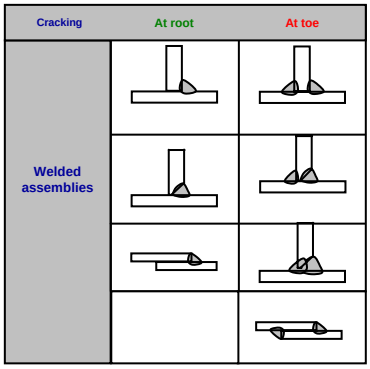
5.3 New procedure for fatigue analysis of body structures

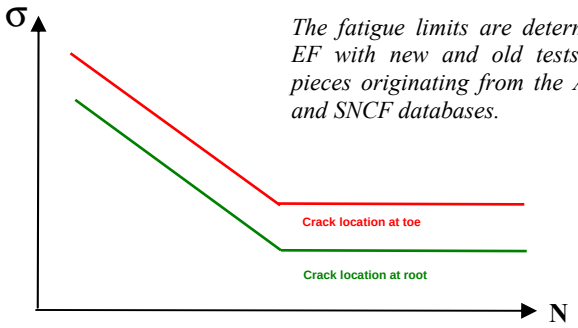
With experience and the new approach to fatigue analysis, we have defined new rules for meshing and new fatigue criteria for the finite element models of the body structures. To allow for the requirements of the maker, the initial meshing rules have not been changed, that is to say without modelling the rigidity brought about by the welding beads. However, a stress corresponding to the position of the foot of the welding bead is extracted, corresponding to a manufacturing quality (6), and the fatigue limit is now defined by a Dang Van multi-axial fatigue criterion (7), whilst the direction of the main stress no longer has to be analysed. Unfortunately, to obtain an accurate response at the welding beads, one has to pass through a meshing phase integrating the rigidity of the bead. To validate the fatigue predictions, the computing models must be validated. To do so, the limit conditions of the movements and loads applied to the finite elements model are checked by comparison against the finite element results and the experiment results of static tests for measuring the stresses and strains – in other words, the computations/tests phase must be reset.

Time sequence of new method:

1. *Modelling with meshing rules without including the welding beads*
2. *Static calculations and analysis of the Dang Van detection criteria (cracking criteria at root or foot)*
3. *Selection of the critical points for improvement of the strength for the case of at notch, choosing a more expensive process)*
4. *Re-meshing of the critical points, modelling the rigidity of the welding bead in accordance with precise rules*
5. *Static calculations and analysis of the Dang Van detection criteria (cracking criteria at root or foot)*
6. *Verification of conformance after resetting the calculations/tests.*

The fatigue criterion brings together two groups of weld-fabrications with classification of the positions of the cracks.





The fatigue limits are determined by EF with new and old tests on test pieces originating from the ALSTOM and SNCF databases.

6 RESULTS OF THE WORK

The results of the work have enabled meshing rules to be defined and fatigue criteria associated to them, adapted to finite element analysis of the welded joints. On completion, a new approach has been set up linked to manufacture of rolling stock and a new MXFAT software for fatigue analysis. The methodology for calculation of welded joints on the body structure uses a fatigue criterion adapted to finite element calculations and multi-axial stress states at the foot of the welding bead and certain roots. However, development of the meshing rules and criteria for designing railway carbody structures does not establish the conformance of the vehicle under fatigue stresses, since the finite elements model must be usable. To validate the fatigue predictions, in other words the limit conditions and loads on the finite elements model, the behaviour of the model must be validated.

In the end, it was difficult to obtain a method with precise results that are both simple and rapid at the same time. One has to pass through a welding bead meshing phase. The objective of the development program has hence been partly achieved.

The railway references with relation to the procedures for compliance with fatigue stresses now have to be evaluated allowing for systematic recourse to the finite elements method.

7 REFERENCES:

7.1 Code and Standards

1. European Rail Research Institute - ERRI B12 /RP60 – Test of resistance of railway coach body and bogie-June 1995
2. Standard EN 12663 Railway applications — Structural requirements of railway vehicle bodies- Juliet 2001
3. Draft Standard PR EN 15085-Welding requirements
4. Standard EN 14067: Railway applications — Aerodynamics — Part 2: Aerodynamics on open track and Aerodynamics in tunnels – February 2004

7.2 Conference Proceedings

5. K. Dang Van, A. Bignonnet, J.L Fayard, multiaxial fatigue of welded structures, assessment of welded structures by a structural multiaxial fatigue approach, Biaxial/Multiaxial Fatigue and Fracture, ESIS STP Vol 31, Editeurs Andrea Carpinteri, Manuel de Freitas, Andreas Spagnoli, ELSEVIER, International Series on Structural Integrity 31 (2003).
6. Local approach for defining an aid for the design department for optimising the geometry of fatigue loaded fillet welds“, J.J Janosch, S. Debiez; Institut de Soudure, K. Dang Van, LMS Ecole Polytechnique, Palaiseau, Doc: IIW-XIII-1550-94, International Institute of Welding, Beijing, Chine, July 1994.

7.3 Journal Article

7. K. Dang Van (1999) Introduction to fatigue analysis in mechanical design by the multiscale approach, Metal fatigue in the context of mechanical Design, K. Dang Van and I. Papadoupoulos, Eds., CISM Courses and Lectures N°392,Springer-Verlag,169-187.

7.4 Thesis

8. J-L Fayard, High cycle fatigue design of welded structures, PhD thesis, Polytechnic-school, 1996.

.

EDF experience in fatigue of pressure equipments

C. Faidy

EDF SEPTEN
12-14 Avenue Dutrievoz
69628 Villeurbanne CEDEX, France

Abstract In electrical plants a lot of pressure equipments are subjected to fatigue cyclic loading and different analysis are done to manage the damage all along the life of the plant. This paper present some operating field experience, the consequences and the needs in methodologies to perform life evaluation of components. To do that EDF has developed a very large experimental and analytical work on structures submitted to low and high cycle fatigue with crack initiation and crack growth. From all that work different rules or improvement of existing rules have been done in France with FRAMATOME and CEA, in Europe in the Euratom Framework programs. These rules and complementary needs are discussed in the last part of the paper.

1 INTRODUCTION

Thermal fatigue is widely recognised as important potential damage mechanism in cooling piping systems of electrical plants, and in particular the Nuclear Power plants [1, 2, 3]. The significance increases as plants get older, requiring safety justifications the initial design life or over.
The field experience confirms different types of fatigue damage : mechanical fatigue under pressure cycling, thermal fatigue damage at low and high cycle, crack like defects , stress concentration factors, vibration fatigue… The consequences is a set of rules derived for Fatigue Design of components more based on crack initiation and an other set of rules for plant operation more based on a limited crack growth rate. The practical consequences are : surveillance and monitoring, in particular the frequencies and the performance of ISI that clearly very costly tasks.

2 FIELD EXPERIENCE

EDF operate 58 similar PWR plants since 1977, and different degradations or leaks have been encountered along the years.
The fist event appears in 1978 when a thermal sleeve attached to a nozzle has been discovered with a large break in the attached welds. The root cause has been attributed to vibration fatigue connected to crack like situation in the attached weld. In the same the question of thermal shock cycling of thermal sleeve attached weld has been largely studied.
All the other crack like situation has been re-evaluated, like socket weld or tube penetration in vessels…
Different leaks and deep cracks has been encountered on different plants : Reactor Heat Removal System dead-leg (1981), RHR small bore connected piping under vibration (1983), stratification in Safety Injection System (1983), leak at a pressurized valve and dead leg vortex in Safety Injection pipe (1984, 1992, 1996), thermal stripping around the Reactor Coolant Pump (1989), RCP thermal barrier cracking (1990) by high cycle and low frequency thermal fatigue loads load, bolt mechanical fatigue in Control Rod Mechanism (1995) and some other cases of vibration fatigue of small bore piping.
In 1998, a major fatigue event has been encountered in all the 58 plants with local degradation, few deep cracks and one through wall crack in CIVAUX RHR system. The root cause was attributed to high cycle thermal fatigue in mixing tee under large temperature differences.
This quick review of field experience confirms different difficulties :

- At the design level : local thermal or vibration loads are not known at the design level, and many degradation are connected to this fact
- Some design rules don't clearly request detailed fatigue analysis of some piping systems
- Monitoring of some locations are needed, but are not sufficient for high cycle thermal fatigue
- Reasonably conservative methods have to be included in the design codes, and periodic review of all the hypotheses of these design analysis have to be up-dated, in accordance with field experience and in-service inspection results
- Due to excessive conservatism, the design rules requirements have to be slightly reduced in order to make reliable residual evaluation and ISI performance and frequencies optimisation.

3 EXPERIMENTAL AND ANALYSIS PROJECTS

The EDF fatigue program has started in the beginning of the 1980s, in collaboration with FRAMATOME and CEA.

The major projects were:

- fatigue rules on crack like defects under tension and share cyclic mechanical loads
- thermal fatigue in nozzles with thermal sleeves [4-5] and figures 1-2-3
- thermal fatigue of piping butt-welds and socket-welds [6] and figures 6 and 7
- thermal fatigue in valves (in the inner surface small radius) [7] and figures 4 and 5
- thermal fatigue on a stratified pipe [8]
- high cycle thermal fatigue in piping with and without welds INTHERPOL (figures 8 and 9)
- thermal fatigue in mixing tees under large ΔT

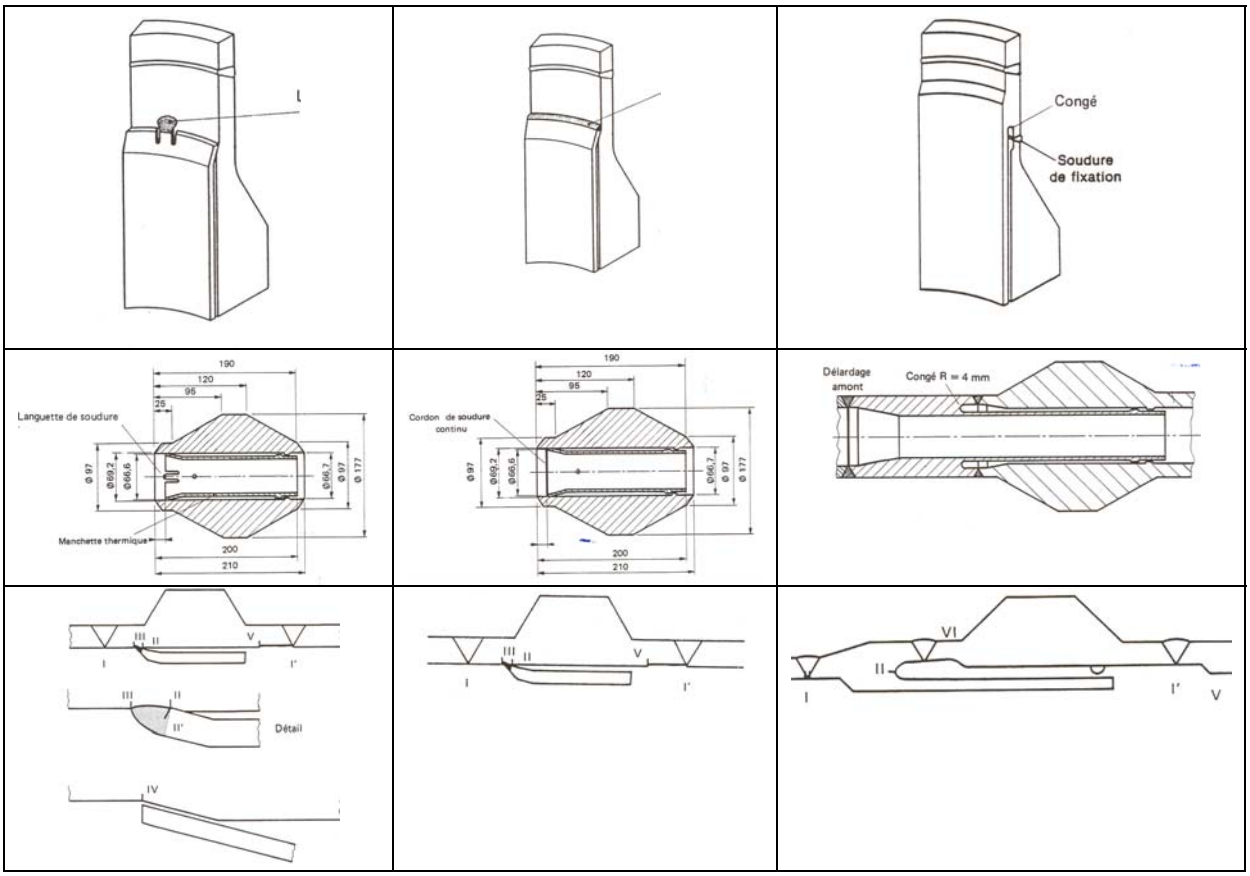


Figure 1 : Different tested thermal sleeves

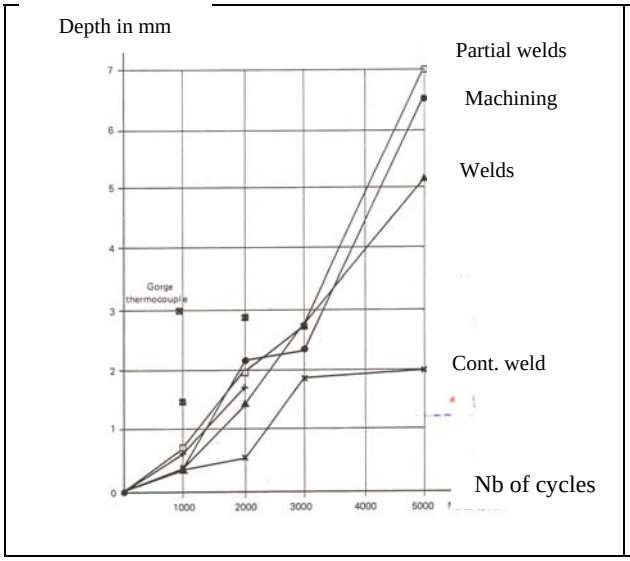


Figure 2 : Experimental results

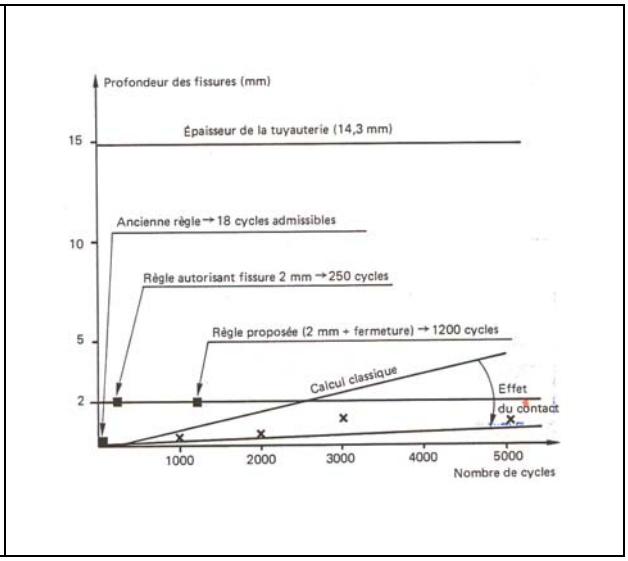


Figure 3 : Analysis results

Some other test programs ar looking in fatigue of inner surface of valves (stress concentration) and butt and socket welds.

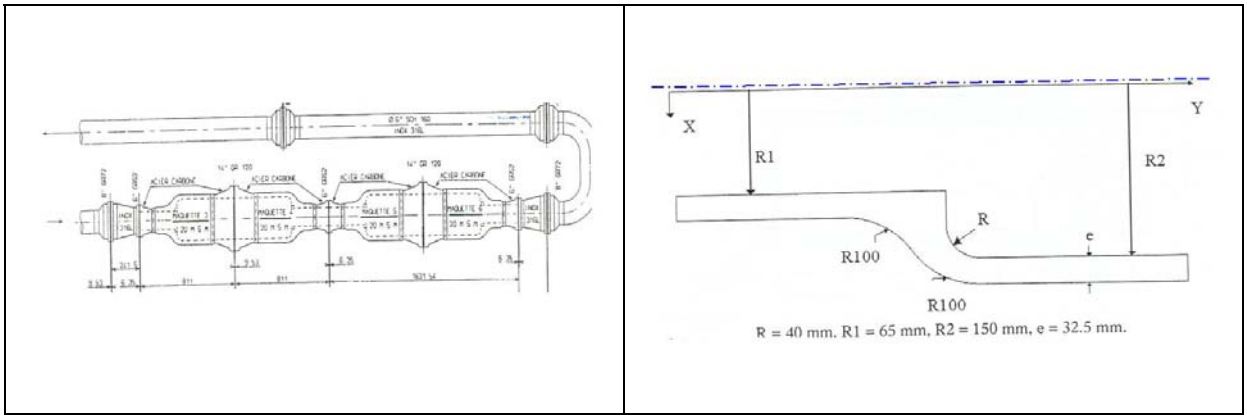


Figure 4 : Valve body testing loop

Figure 5 : Valve body mock-up

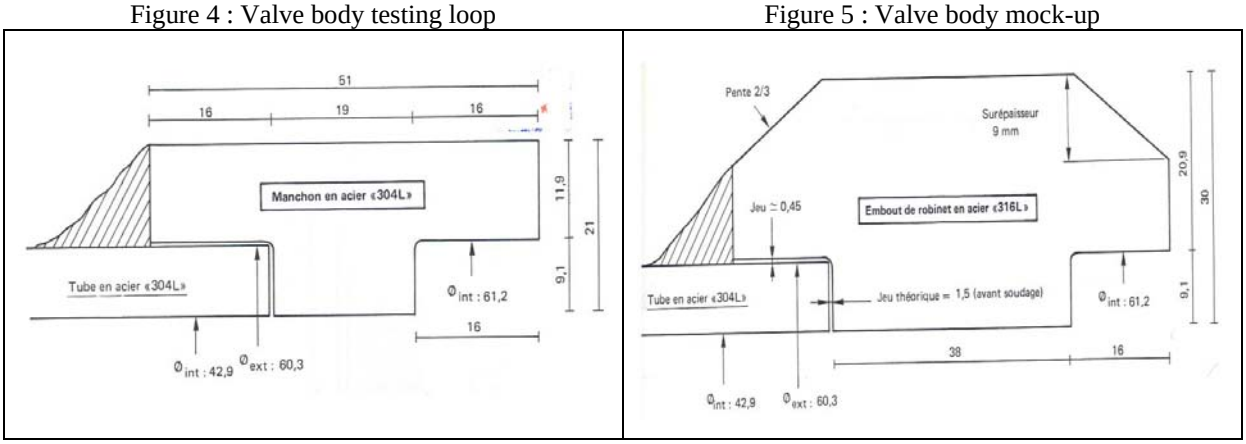


Figure 6 : Piping socket weld

Figure 7 : Pipe to valve socket weld

Other programs:

- SPLASH : high cycle thermal shocks on rectangular bars [9-14] and figure 10.
- FAT-3D : thermal fatigue of cylinder under non-axi-symetrical thermal load and figure 11.
- THERFAT : thermal fatigue with test on base metal small piping, welds in large pipe and nozzle corner. [15]

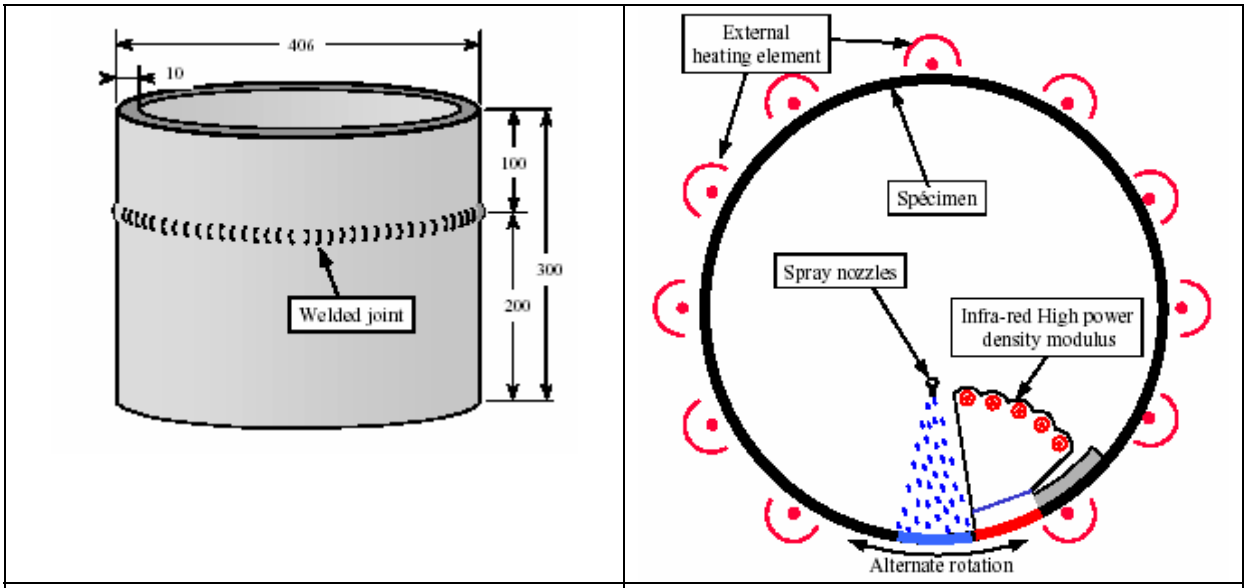


Figure 8 : INTHERPOL cylinder test

Figure 9 : INTHERPOL test principle

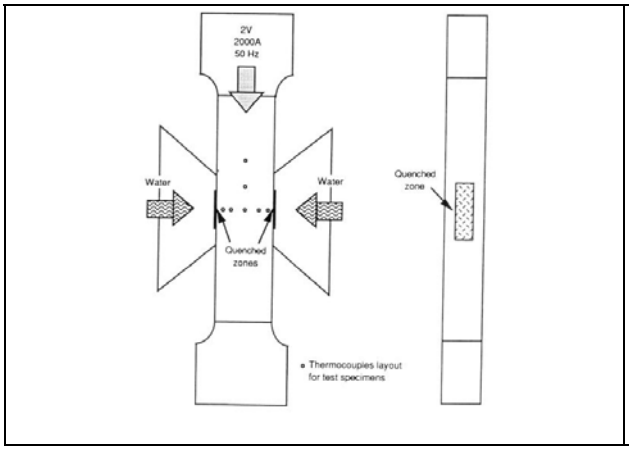


Figure 10 : SPLASH mock-up

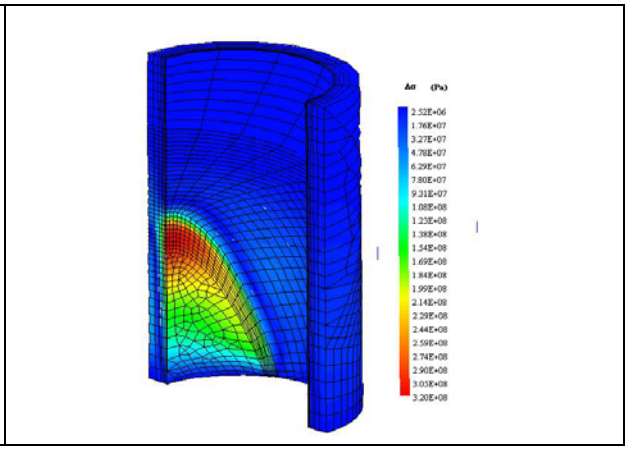


Figure 11 : FAT 3D modelisation

4 EXISTING METHODES

Crack initiation

Generally based on the (S,N) curve of the material and different transfert function and fatigue strength reduction factors for different part of a piping system (ASME III [17], RCCM [18], RCC-MR [19], KTA). All the rules lead to a cumulative usage factor (CUF) that confirm no risk of leaks if CUF is less than 1.
An important difference is based on the Ke formulae that are less conservative in RCCM than in ASMEIII for thermal loads through the wall (figure xx); and with a different procedure in RCCMR.
Different ways are proposed for crack like defects (like thermal sleeve or non fully penetrated weld) :

- ASME III : a stress concentration factor not less than 4
- RCC-M : ($\Delta\sigma_{\theta\theta}^{d}$, Na) with specific d value for different type of materials and specific material curves
- RCC-MR : $\Delta\sigma_{\theta\theta}^{d}$ with d=50µm, using the Neuber rules to evaluate the strain amplitude, fatigue curves with a fatigue strength reduction factors of 4

Some of the previous tests have been used for validation and a specific program has developped tests on CT type specimen and share load type of specimen. The d distance is the distance that reduce the scatter band of the different test results.
The 3 different Code have also slightly different methods to evaluate fatigue cumulative usage factor, mainly for plasticity corrections (K_e, Kv); all of them use the same (S,N) fatigue curve up to 10^6 cycles.
In the same time, French methodology and EC contribution are working on the specific problem of high cycle thermal fatigue. A specific conservative methode has been developped and checked with field experience and laboratory data, similar to EDF proposal [20]. Figure 12 presents a typical degradation area from an elbow inner surface. Figure 13 presents the results of the EDF methodology for high cycle fatigue.
Some complementary work is done in Japan on environmental effects and spectrum load effects [20- 23].
Some other contribution to high cycle thermal fatigue are presented in [24, 25].

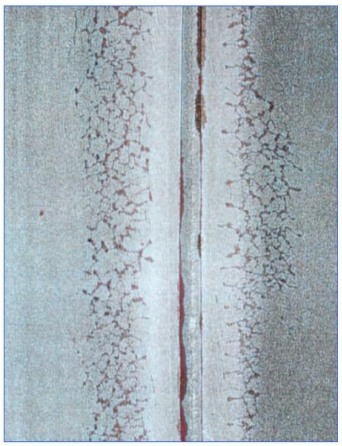


Figure 12 : Example of high thermal fatigue degradation

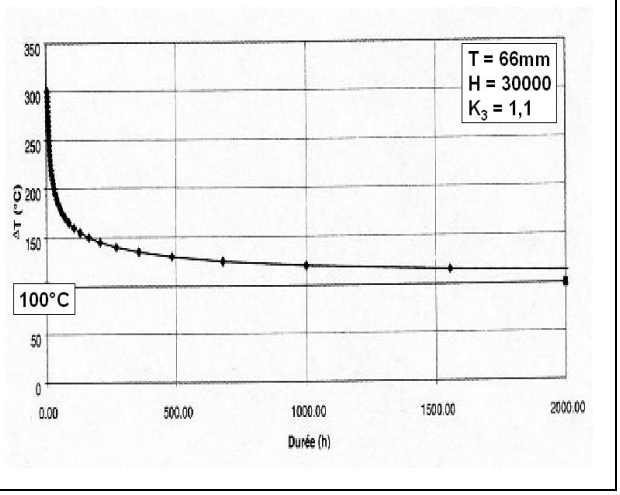


Figure 13. An example of a damage reference curve (ΔT vs. minimum admissible fatigue duration) used in the sinusoidal method

Crack propagation

Generally based on (da/dN, ΔK) Paris law, with different effects like environment or mean stress effects.
Specific developments have been tested on cyclic thermal shocks on a small piping : crack closure and short crack effects [16].

5 RESULTS AND COMPLEMENTARY NEEDS

Results

All these tests have been analysed by different ways :

- elastic strain evaluation and (S,N) curves
- cyclic plastic strain evaluation and (S,N) curves
- crack initiation + crack growth analysis
- crack like defect specific method and material resistance curves.

All the results are consistent with the Design objectives : for a usage factor less than 1, no crack through the wall with margins.
Few cases have to be analysed with a maximum of precautions : small wall thickness or small ligament cases (less than 5mm)

Complementary needs

Different open questions are extracted from all these studies in order to better understand and improved the existing methodologies:

- reference fatigue (S,N) curves and fatigue strength reduction factors (welds, surface finish, mean stress, environmental effects...)
- endurance limit value, constant amplitude versus spectrum loads
- plasticity effects and K_e or K_v
- bi-axiality effects
- crack like defect material properties
- transferability of small specimen test to large structures : crack initiation / crack growth
- short crack and crack closure effects
- mechanical versus thermal loads crack growth
- multi crack initiation and propagation
- damage evaluation : counting methode and linear cumulation of fatigue design

6 CONCLUSIONS

In front of all these data, different conclusions can be drawn :

- a design methode is available for low and high cycle fatigue of components,
- no realistic quantified method is available and validated for residual life evaluation, taking into account independently all the major contibutors to fatigue resistance of components.

Consequently, R&D efforts have to be pursued actively to better understand and reduce uncertainties.

ACKNOWLEDGEMENTS

The authors gratefully acknowledge the contributions from all the THERFAT EC-project partners and EC sponsorship, as well as the contribution from OCDE-NEA-IAGE partners, E. Paffumi and KF Nilsson from JRC-IE, S. Chapuliot and A. Fissolo from CEA, JC Masson, D. Moinereau and JM Stephan from EDF-R&D.

REFERENCES

1. IAEA, “Assessment and management of ageing of major nuclear power plant components important to safety. Primary piping in *PWRs”,* TECDOC-1361, July 2003
2. OECD, “Thermal cycling in LWR components in OECD-NEA member countries”, NEA/CSNI/R(2005)8, July 2005
3. C. Faidy et al, Thermal Fatigue of Reactor Components in OECD-NEA countries: a Three-fold Program to Enhance cooperation, Proc. SMiRT-18, Beijing, China, August 2005
4. J.C. Masson, "Use of local approach for predicting fatigue cracks in sleeves subjected to repeat thermal shocks", Nuclear Ingeneering and Design 105 (1987) pp 139-145
5. J.C. Masson, D. Moinereau, C. Arnaud, "New experiments of welded thermal sleeves under thermal shocks and their interpretation by calculation", SMIRT 8, Bruxelles, 19-23 august 1985
6. D. Moinereau, L. Scliffet, J.C. Capion, P. Genette, "Thermal fatigue behaviour of valves - Validation of a new rule to estimate fatigue damage resulting from thermal shocks", ASME-PVP 1991, SAN DIEGO
7. J.C. Masson, D. Moinereau, M. Rioland, "Fatigue behaviour of welded junctions submitted to thermal shocks", SMIRT 10, Anaheim, august 1989
8. J.C. Masson, J.M. Stephan, "Fatigue by thermal stratification. Results of Tests and Calculations of COUFAST model", Specialist Meeting Proceedings. Paris 8-10 JUIN 1998 - IPSN/OECD - NEA/WANU
9. A. Fissolo, V. Maillot, G. Degallaix, B. Marini, "Prediction of cracking under thermal fatigue", Eighth International Fatigue Congress ‘‘FATIGUE 2002’’, proceedings p. 1673, Stockholm, 3 - 7 Juin 2002
10. V. Maillot, A. Fissolo, G. Degallaix, S. Degallaix, B. Marini , J. C. Le Roux, "Initiation and Growth of Thermal Fatigue Crack Networks in a 304 L type steel", European Congress of Fracture 14 th Fracture mechanics beyond 2000, proceedings p. 425, Cracovie, 8 – 12 Septembre 2002
11. A. Fissolo, V. Maillot, G. Degallaix, S. Degallaix, C. Robertson, J. C. Le Roux, B. Marini, F. Bouchet, "Fissuration par fatigue thermique des aciers austénitiques", Matériaux Tours 2002 : Colloque Matériaux pour l’industrie nucléaire, Tours, Octobre 2002
12. A. Fissolo, V. Maillot, J.C. Le Roux, G. Degallaix, S. Degallaix, C. Robertson , F. Bouchet, "Initiation, growth and stability of thermal fatigue crack networks in austenitic steels", International Conference on the Mechanical Behaviour of Materials 9 th - ICM 9, Genève 25, 29 Mai 2003
13. A. Fissolo, C. Robertson, V. Maillot, "Thermo-Mechanical Fatigue and Fracture Advances in Fracture Mechanics", Chapter 3 pp. 67- 105, Wit press, editor Professor M. H. Aliabadi, ISBN 1-85312-549-0, 2000, 2002.
14. A. Fissolo, "Advanced in thermal fatigue investigations performed by CEA for French PWR piping", OCDE-NEA Proc. 3rd Int. Conf. on Fatigue of Reactor Components, Seville, Spain, October 2004, OCDE-NEA/CSNI/R(2004)21.
15. K.-J. Metzner & U. Wilke, European THERFAT project—thermal fatigue evaluation of piping system “Tee”-connections, Nuclear Engineering and Design, Volume 235, Issues 2-4 , February 2005, Pages 473-484
16. E. Paffumi, KF Nilsson and N. Taylor, “On thermal fatigue crack initiation, propagation and arrest in 316L model pipe components ”, ASTM STP, ASTM International, West Conshohocken, PA, 2002.
17. ASME – Nuclear Boiler and Pressure vessel Code – Section III – ASME 2004
18. RCC-M – Design and Construction rules for PWR Nuclear Island – AFCEN – Paris – RCC-M 2000+addendas
19. RCC-MR - Design and Construction rules for FBR Nuclear Island – AFCEN – Paris – RCC-MR 2000+addendas
20. C. Faidy, "Thermal fatigue in mixing areas : status and justification of French Assessment Method", OCDE-NEA Proc. 3rd Int. Conf. on Fatigue of Reactor Components, Seville, Spain, October 2004, OCDE-NEA/CSNI/R(2004)21.
21. N. Kasahara et al, Thermal Fatigue Evaluation Method based on power spectrum density functions against fluid temperature fluctuation, Proc. ASME PVP2005, Denver, Colorado, USA, July 2005.
22. JSME, Guideline for Evaluation of High-cycle Thermal Fatigue of a Pipe, S017-2003, 2003
23. M. Higuchi at al, “Development and Evaluation Method of Fatigue Damage on Operating Plant Components Considering Environmental Effects”, OCDE-NEA Proc. 3rd Int. Conf. on Fatigue of Reactor Components, Seville, Spain, October 2004, OCDE-NEA/CSNI/R(2004)21.
24. J.D. Keller et al, “Thermal Cycling Screening Criteria and Evaluation Methodology and Application to Pressurized Water Reactor Branch Line Piping”, OCDE-NEA Proc. 3rd Int. Conf. on Fatigue of Reactor Components, Seville, Spain, October 2004, OCDE-NEA/CSNI/R(2004)21.
25. J.D. Keller et al, “Thermal Fatigue Management Guideline for Normally Stagnant Non-Isolable RCS Branch Lines”, Proc. 3rd Int. Conf. on Fatigue of Reactor Components, Seville, Spain, October 2004.

A data bank to size validation tests in the automotive for the fatigue failure mode

PONCET Anthony (1), SCHIMMERLING Paul (1), DUMAS Christian (2)

(1) RENAULT
67, rue des bons raisins
92508 – Rueil Malmaison –
Tel: 01 76 87 27 67 –
anthony.poncet@renault.com

(1) RENAULT
67, rue des bons raisins
92508 – Rueil Malmaison –
Tel: 01 76 87 20 09 –
paul.schimmerling@renault.com

(2) RENAULT
1, avenue du Golf
78288 – Guyancourt –
Tel: 01 76 85.94.56 –
christian.dumas@renault.com

Abstract:

In the automotive industry, numerous actions are realized to prevent and avoid failings in field. Validation tests, which are one of these, are necessary to make sure that the part has been correctly sized.

Validation tests are as well realized on component test bench as on engine test bed.
They consist in:

· detect as soon as possible weaknesses of the part not envisaged previously
· verifying that the system will resist to the stresses applied by the customer.

Each test is realized to put in evidence a failure mode identified by studies during the design phase.

To size these tests correctly, two data are required:

- Firstly, the stresses that the system have to support: These are known from customer profile in use
- Secondly, the strength of the part: The strength is known from the calculations of the Design Office for an innovative system or tests realized on a similar system with a similar failure mode.

Today stresses due to customer use are generally well known, through the various studies done with the vehicle's instrumentation. On the contrary, the strength of the parts to these same stresses is not always well known for a given failure mode representative for real solicitations.

Numerous reliability databases exist in aerospace industry, the nuclear and the armament industries. However, they do not fit with the requirements of mechanical part in automotive industry. Indeed, in these databases we usually find constant failure rates, and conditions of use which are very different.

A work has been defined to establish a data bank for the fatigue failure mode. We will explain:

- the structure of the data bank on pessimistic value of strength and pessimistic value of the law parameters.
- the classification of parameters function of characteristics : material, temperature, solicitation, …etc.
- the way to obtain pessimistic parameters from the knowledge on the part design.
- the interest of the data bank to design a part and a validation test with stress strength method

1. What is the aim of a validation test?

The aim of a validation test is to:
- detect unknown weaknesses of the component
- verify that the component will support the stresses applied by the customer
- check the component reliability in service

One difficulty of validation test is to demonstrate the achievement of reliability objectives in service.

2. General methodology main steps to size validation tests

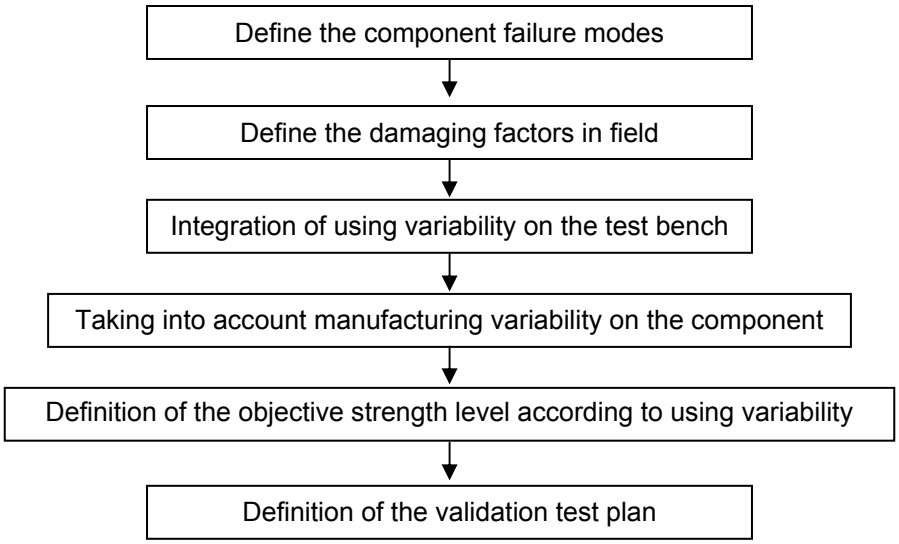


Figure: Methodology to size a validation test

2.1. Define the component materials failure modes

Before sizing a validation test, it is necessary to identify the potential component material failure modes. The failure mode depends on the stresses applied to the component, its environment... The failure modes analysis leads to identify basic failure modes. The ruin of component materials as polymers or metal can be described by basic elementary failure modes. Examples of elementary failure modes are: fatigue, fracture, wear, corrosion.

2.2. Define damaging factors

A damaging factor is a parameter that degrades the component or accelerates the component degradation. For example, a damaging factor can be: a number of cycles, a load intensity, a temperature...
In the automotive industry, mission profiles describe the damaging factor statistical distribution related to the customer use.

2.3. Validation test plan sizing

A well known method to demonstrate reliability objectives achievement is the Stress Strength method [1], [2], [3].

2.3.1. Integration of using variability on the test bench

In order to integrate the variability of the component in field on the test bench, the damaging factor is represented by a mission profile

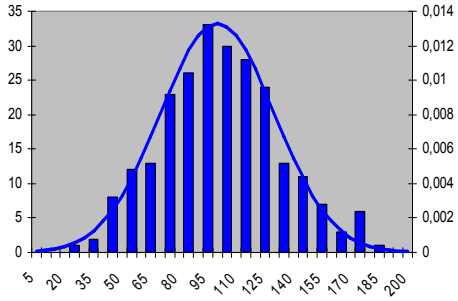


Figure: Mission profile representation for a damaging factor

2.3.2. Taking into account manufacturing variability on the component

The manufacturing variability on the component may be represented by the shape parameter of the statistical distribution: β for the Weibull distribution, coefficient variation for a normal distribution…

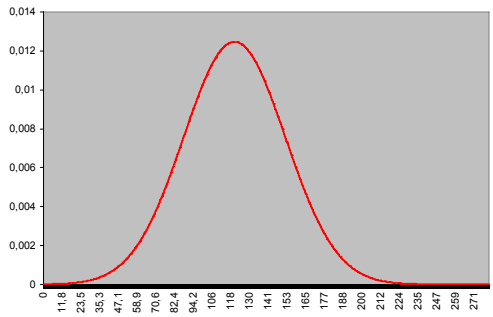


Figure: Strength distribution representation

2.3.3. Definition of the objective strength level according to using variability

If the mission profile, the shape parameter and the objective failure proportion are known, we calculate the objective strength by iteration of the following formula:

$$P_{failure} = 1 - \int_0^1 F_{Stress}(r)\, dF_{Strength}(r)$$

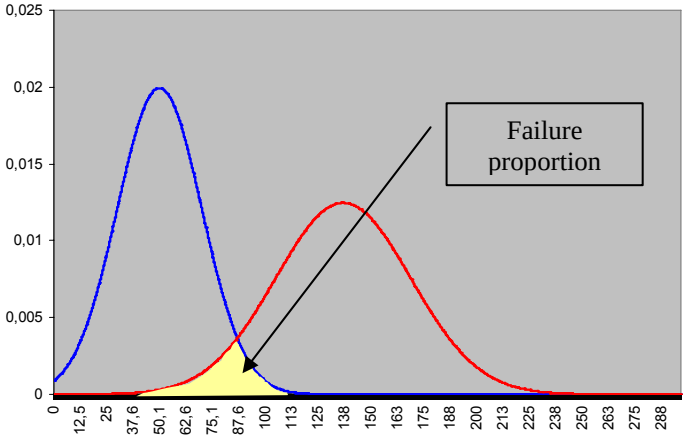


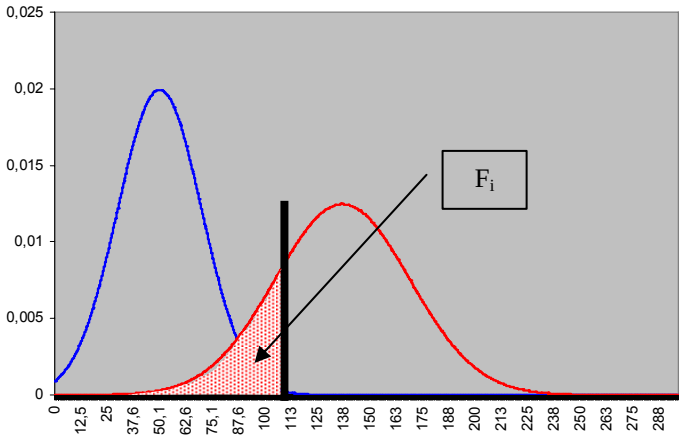
Figure: Representation of the Stress / Strength method

2.3.4. Validation test plan definition

We determine the damaging factor value to apply in test and the part number to test in order to have a high confidence in the detection of an objective reliability level during the test.

$$1-\beta=\gamma=1-(1-F_i)^n$$

with F_i: the probability to have a fail of the component if the component have an objective reliability level.



2.4. Parameters just necessary to size a fatigue validation test

The failure condition determines the parameters just necessary to size validation test. If we focus on fatigue failure mode, two failure conditions are developed:

- 1st case: a fracture in high cycle fatigue: coefficient variation of the endurance limit
- 2nd case: a fracture in low cycle fatigue with a damage accumulation: coefficient variation of the endurance limit and the slope of the fatigue model

Explanations on calculation method for fatigue fracture are detailed on [4], [5].

3. Knowledge data bank description

3.1. Objective

The objective of databank is to:

- Familiarize to the several failure modes
- Notify on probabilistic models and acceleration laws
- Capitalize the shape parameter of the probabilistic models

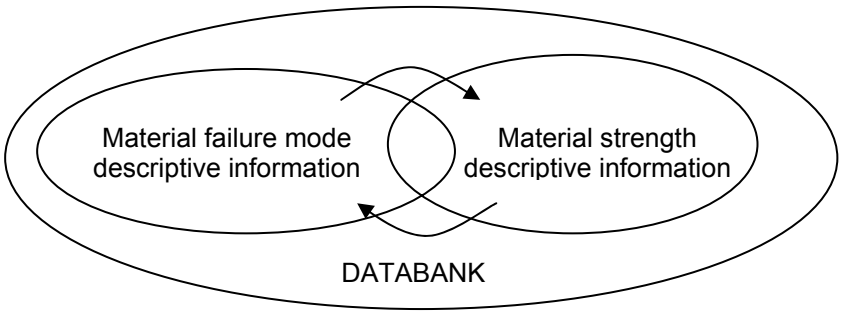


Figure: Databank structure

3.2. Parameters capitalized in the databank

Several parameters are capitalized in the databank:

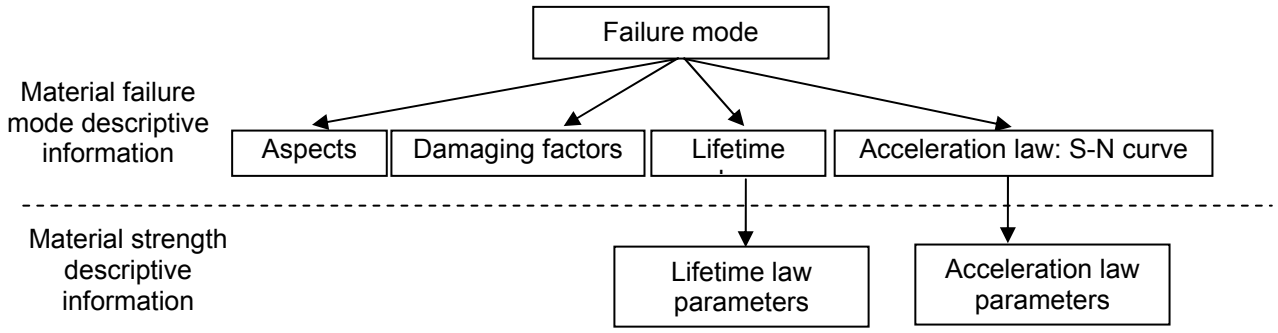
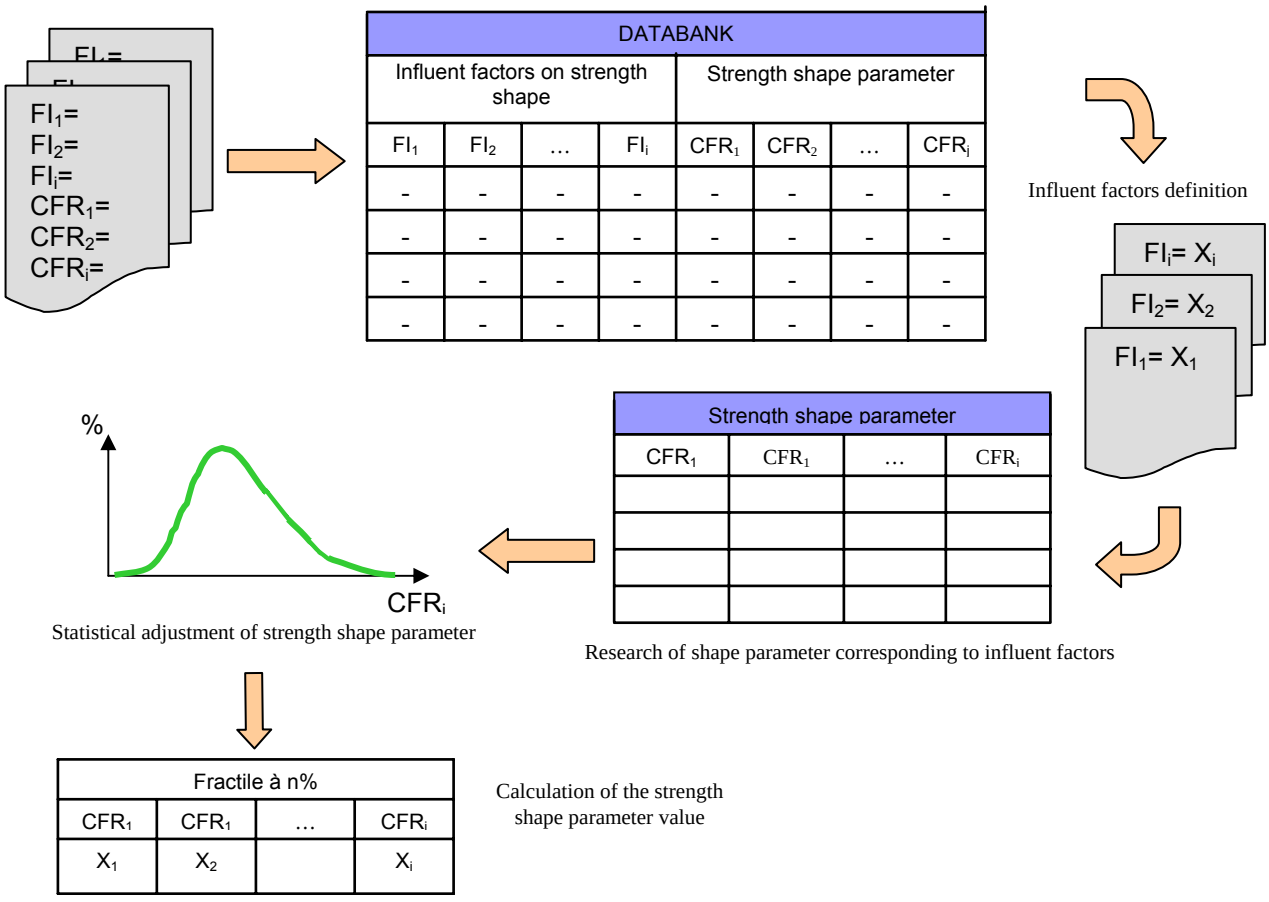


Figure: Parameters capitalized in the databank

3.3. Description of the databank implementation and extraction



4. Conclusion

Parameters just necessary to size a validation test are identified in this article. A tool to capitalize the strength parameters values is presented for the fatigue failure mode. This article advances the data bank interest to size validation test.

5. References

[1] PERROUD G., « Accéder au juste nécessaire par une expérimentation adaptée »conférence S.I.A., 16 mai 2000
[2] TRIBOULET François, « Fiabilité prévisionnelle des composants de châssis automobile : calcul probabiliste du dommage en fatigue », ASTEFORUM 2002, 2002
[3] PRINCE O., SCHIMMERLING P., « Prévoir la fiabilité en clientèle à partir de données du réseau, de résultats d'essai ou de calculs. Quatre méthodes de base illustrées par des exemples », conférence S.I.A., 12 mars 2003.
[4] A. PONCET, P. SCHIMMERLING, P. LYONNET, « A knowledge bank on material failure modes to size mechanical component validation test », ESREDA 2003
[5] A. PONCET, P. SCHIMMERLING, P. LYONNET, C. JOUZEAU, C. TALVASSON "Le dimensionnement des essais de validation par la méthode « contrainte - résistance »" λμ14 Bourges 2004
[6] O. PRINCE, G. MORIN, C. JOUZEAU, "Validation test optimization based on statistical approach fo diesel engine cylinder heads reliability", SAE 2004

PROGRAM

1 Methodologies and tools for fatigue life assessment

- Automotive components
- Various industrial applications
- Welded structures and assemblies

2 Advanced design tools and approaches

- Fatigue crack initiation assessment
- Contribution to the crack propagation stage
- Modelling of the design behaviour of the welded

3 Multiaxial loading fatigue assessment

4 Fitness for service approach and applications

5 Experimental validation

- Application to automotive parts and structures
- From laboratory testing to field evaluation
- Development of dedicated test devices and procedures

6 Design procedures against thermal and thermo mechanical fatigue damage

7 Reliability approaches in fatigue design

8 Improved design and manufacture processes with regard to fatigue

Investigating the Fatique Strength of Commercial Vehicle Clutches

Klaus Steinel
ZF Sachs AG

ABSTRACT

The torsional damper of a vehicle's clutch is, as part of the drive train, subjected to various dynamic loads. Increasing torques and spatial limitations call for lightweight construction. The design of these components is now increasingly being influenced by the need to consider them from an fatigue strength standpoint. A new testing concept which aims at providing evidence of fatigue strength is introduced here, taking commercial vehicle clutch disks as an example, and touching upon the areas of analysis and evaluation of the load collective characteristic and of control systems for servo-hydraulic test rigs.

INTRODUCTION

Increasing torques and growing rotational irregularity are characteristic of current and future vehicle engine development. Quite often gearboxes are used which were not originally designed to withstand the loads in question. This in turn causes the manufacturers to increase their specifications in terms of reducing dynamic torque loads and minimizing noise. These requirements have a direct effect on the design of the clutch`s torsional damper. Alongside factors such as correct function and cost optimised design, these devices must also be highly reliable. The enforced move towards lightweight construction, and also spatial limitations, effectively rule out the provision of generous safety factors to withstand breakage. For development engineers, this entails matching component design as precisely as possible to the anticipated operating stresses. Proof of fatigue strength is, therefore, increasingly taking over in significance from the current standard test procedures.

On the following pages an attempt is made to illustrate how the new test concept is integrated into the development process, using commercial-vehicle clutch disks as an example. At this point it has to be mentioned that it is not possible to produce proof of service life with regard to the wear characteristic of the clutch facings in accordance with the fatigue strength concept described here, owing to the fact that these are subject to entirely different wear and damage mechanisms.

CURRENT AND FUTURE PROOF OF SERVICE LIFE FOR TORSIONAL DAMPERS

The usual method of proving fatigue strength for clutch disk torsional dampers until now was by means of single-stage tests (Fig. 1). The amplitudes for the traction and coasting flanks of the torsion characteristic were almost identical, and their total sum was coupled by way of a factor to the nominal engine torque with which the clutch disk was intended to be used. Any remaining influences on the drive train were generally disregarded. Targets stating the number of stress cycles to be withstood were deduced empirically or resulted from the vehicle manufacturer's requirements. These service-life test methods tended to be confirmed by field operation in the majority of cases. Unfortunately, as a result of the above mentioned limitations, it is probable that these tests will no longer be adequate in future as a reliable check on fatigue strength, due to the extreme simplification of the stress cycles.

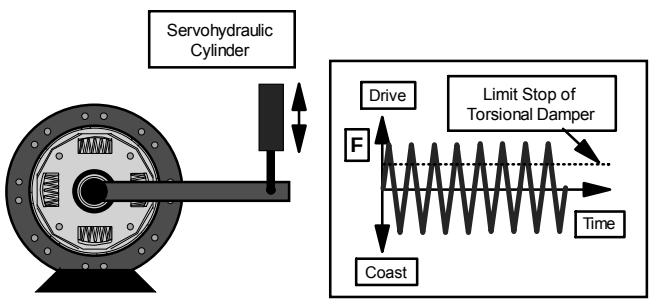


Figure 1: Previous single-stage test to determine lifetime of torsional dampers

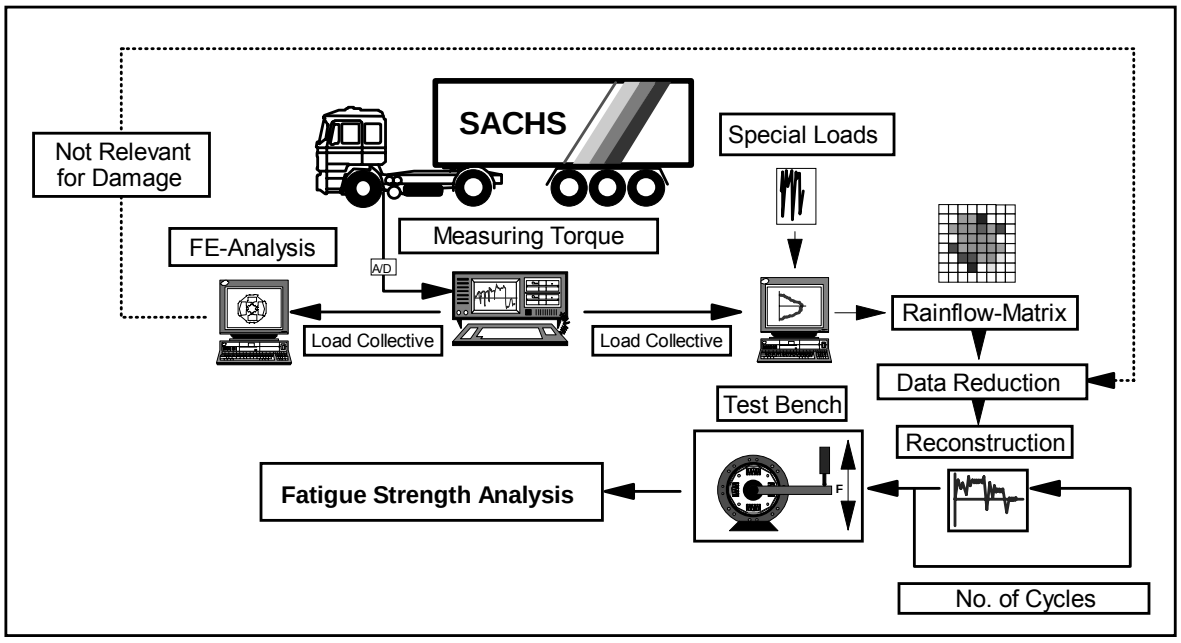


Figure 2: Procedure for fatique strength analysis on torsional dampers

For this reason, Fichtel & Sachs will switch all their torsional damper test rigs over to a new method within the next few years. Fig. 2 provides an overview of the procedures.

VEHICLE MEASUREMENTS TO DETERMINE REPRESENTATIVE LOAD COLLECTIVES

Although several tests have already been carried out on drive train loads, there have until now only been very few comprehensive tests on passenger-car clutch torsional damper loads. Fichtel & Sachs ,therefore, equipped several passenger cars and commercial vehicles in the last few years with measuring equipment, in order to determine the necessary representative load cycles for torsional damper tests.

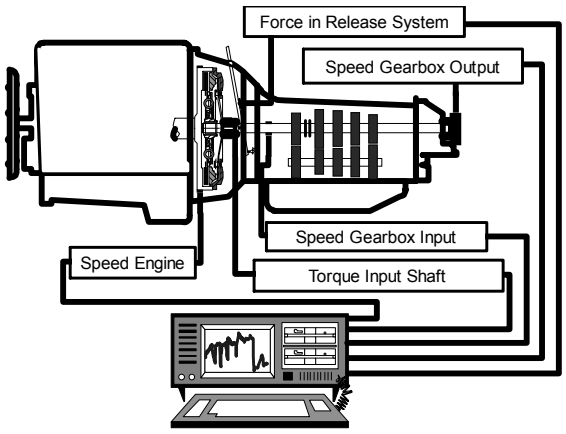


Figure 3: Test setup to record load collectives for torsional dampers

The gearbox input`s torque signal, which is required when determining the dimensions of the clutch disk, is augmented by various speeds of rotation and actuator sensors in order to arrive that not only the actual load signal but also detailed information on the operating context and, as a result, to obtain a means of explaining the occurrence of the resulting individual load cycles. These data are particularly significant in order to facilitate subsequent computer simulation of the procedures. One of the targets should be the ability to forecast collectives for new vehicle configurations within certain limits. Fig. 3 shows the selected measuring points.

Torque measurements are not taken from the propeller shaft or half-shafts, as is usually the case, but from the gearbox input shaft, in order to pick up loads on the torsional damper in as direct a manner as possible. This is especially important for detecting pulse-type torque peaks, such as may occur when the torsional damper reaches its limit stop. These higher-frequency signals cannot always be detected adequately at the propeller shaft or half-shaft sides, due to the filtering effect of gearbox inertia.
Fig. 4 is an example of local telemetry for measuring torque.

Data are collected by a mobile measuring system on a PC basis, with integrated A/D converter. The sample rate for the long-life collectives was 150 Hz;
when recording single procedures the frequency was set at 800 Hz. Fig. 5 shows, for example, the starting-off procedure on a level stretch of road with a fully-loaded vehicle (40 t), including subsequent gearshifts.

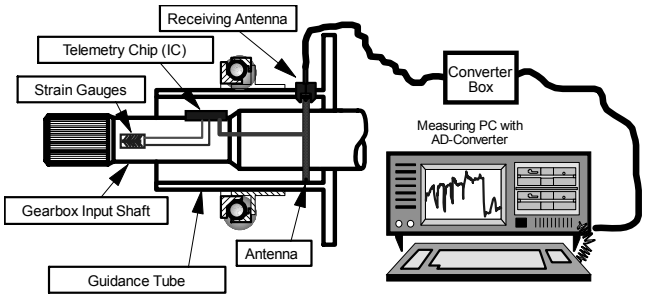


Figure 4: Telemetry system to measure torque at gearbox input shaft

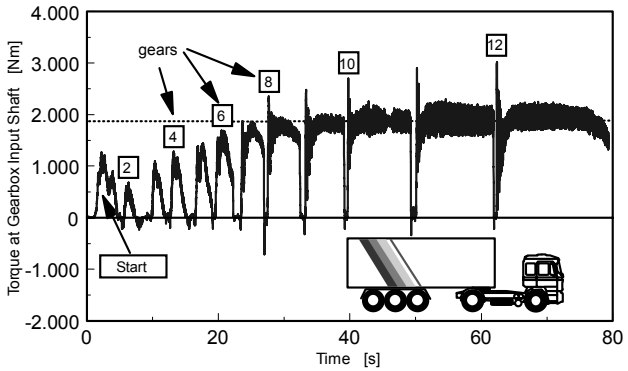


Figure 5: Starting-off procedure including subsequent gearshifts with a heavy truck

Particularly worthy of note is the fact that maximum engine torque is only built up in the higher gears, despite the attempt to use full-load acceleration.

There are two main reasons for this: on the one hand, the engine gathers speed so quickly in the lower gears that the increased torque obtained from the turbocharger cannot develop fully, and, on the other hand, the rapid increase in speed of rotation causes a major part of the engine`s torque to be consumed in the form of acceleration torque by the engine`s inertial masses and as a result is no longer available at the gearbox.

MEASURING PROGRAM AND ANALYSIS OF LOAD COLLECTIVES

Measurements were mainly carried out on public roads, which are classified as follows:

- city
- level country roads
- hilly country roads
- highway (level and hilly)

In order to create particularly critical operating conditions, the test drivers were instructed to drive briskly and to change gear frequently. As well as the topography of the route, the load was also varied and, in particular, the clutch system was modified in order to illustrate the influence exerted on the load collectives. As the torsional damper is to a large extent exposed only to torque loads and not additional rolling-contact movements, as in the gearbox which follows, the speed-of rotation-information can initially be disregarded. The additional load on the clutch components resulting from centrifugal force must be tested separately.

CLASSIFICATION OF LOAD COLLECTIVES FOR COMPARATIVE EXAMINATION

By means of suitable classification methods, the load-time function patterns, some of which take several hours to complete, can be displayed on a single diagram. For this purpose, the level-crossing method was selected /1/ and the results displayed on a semi-logarithmic scale. The measuring range is divided up into torque classes (usually 64 or 128). The count yields the level-crossing frequency: these are cumulative values. This method does indeed display the absolute torque values, but the information relating to amplitude and mean value of the individual oscillations is lost.

LOAD-COLLECTIVE STANDARDIZATION

In order to be able to make a comparison between routes of varying length and vehicles with differing engine torques, the diagrams have to be standardized. With regard to the route, it is practical to relate the level-crossing cases to the distance in kilometres actually driven. For the torque signal, engine torque has proved suitable /2/. Careful standardization is of great importance for the intended load-collective standardization process. By varying a few parameters, it should be possible in the future to synthesize the load collectives for new vehicle configurations. Fig. 6 shows the comparison between the collectives evaluated for a small delivery truck and a heavy long-distance truck according to the methods described in the standardization proposal above. Although the vehicles' engine torques vary by a factor of roughly eight, the standardized diagram display illustrates an astonishing similarity in terms of classification results.

INFLUENCE OF THE ROUTE ON THE LOAD COLLECTIVE

As was the case in Figure 5, the loads at the gearbox input and, by inference, also at the clutch`s torsional damper during load-cycle shocks and shifts to higher gears are greater than in the lower gears. If one looks at the drive train`s behaviour from the clutch standpoint,

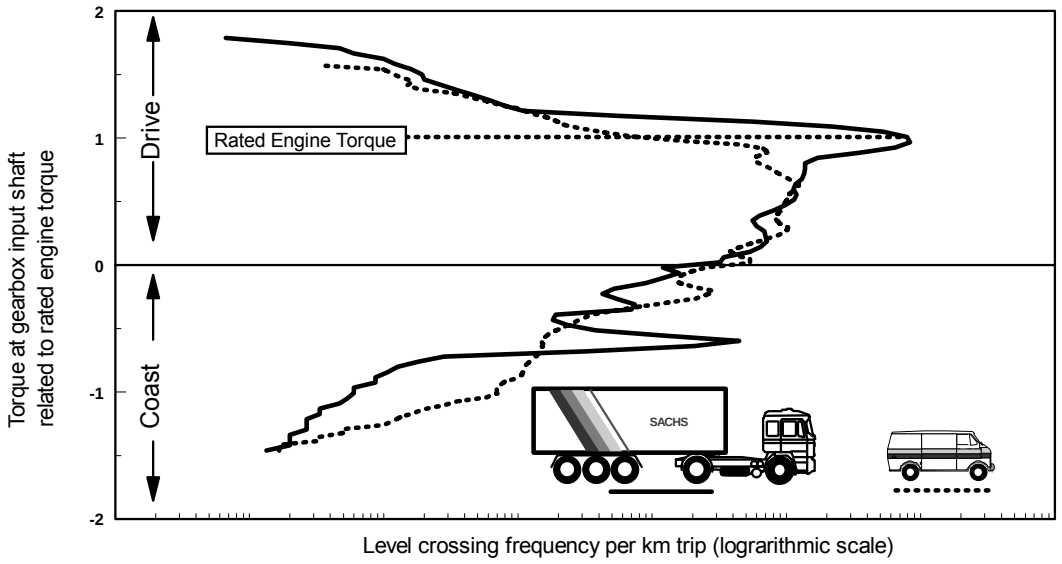


Figure 6: Normalization of a truck-collective and a van-collective in comparison

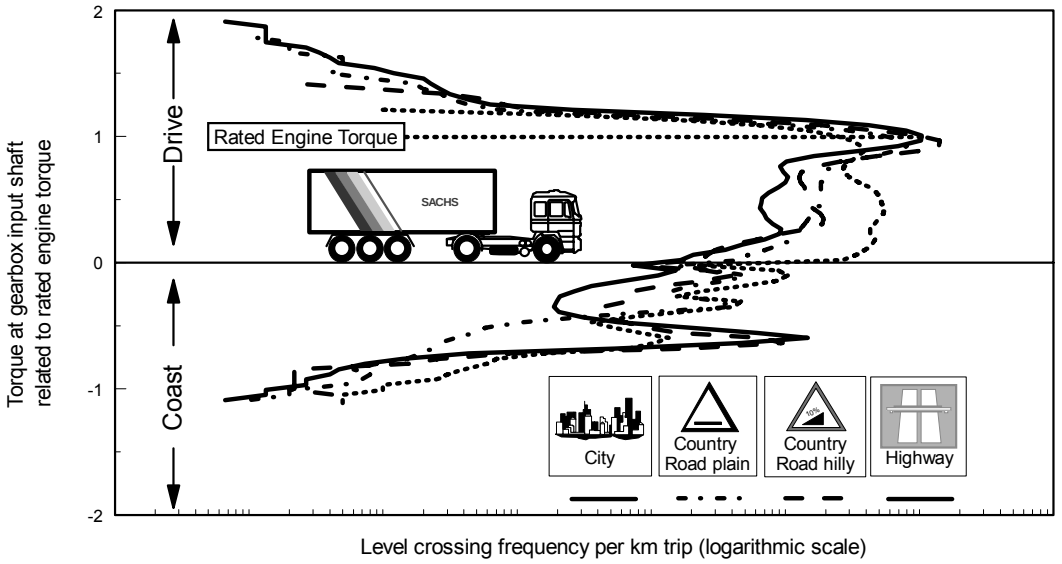


Figure 7: Influence of road type on load collective

the system becomes increasingly more rigid with each higher gear selected. At the same time, the effective moments of inertia greatly increase, with the result that if there are any sudden pedal movements or rapid shift operations, the drive-train is no longer as weak as it was in the lower gear ranges. This causes higher peak torques to occur at the gearbox input. If one compares the various routes, it becomes clear that maximum torque on the traction side mainly occurs when driving on highways and country roads (Fig. 7). Of lesser importance is the situation in city traffic where, especially in the case of commercial vehicles, only the lower and mid-range gears are ever used in practice.

INFLUENCE OF THE CLUTCH ON THE COLLECTIVE

The clutch, which in this case is regarded as the component undergoing test, can also exert an influence on its own load collective as a result of its maximum transmission capacity. It is well known that starting and gear-shift clutches have to be designed in such a way as to ensure reliable transmission of engine torque even in the most negative of conditions.

The friction coefficients of the facing materials used for brakes and clutches may be subject to a certain amount of fading at excessive temperatures. In order to ensure that adequate clutch functions can still be guaranteed within certain limits, even in operating conditions effectively resulting from misuse, their clamping loads must be chosen to include the corresponding safety factor. If this is set too high, it may have a negative effect on the torque load throughout the drive train. One of the additional and most important tasks of the clutch, is often one of the most frequently disregarded, is its ability to afford overload protection.

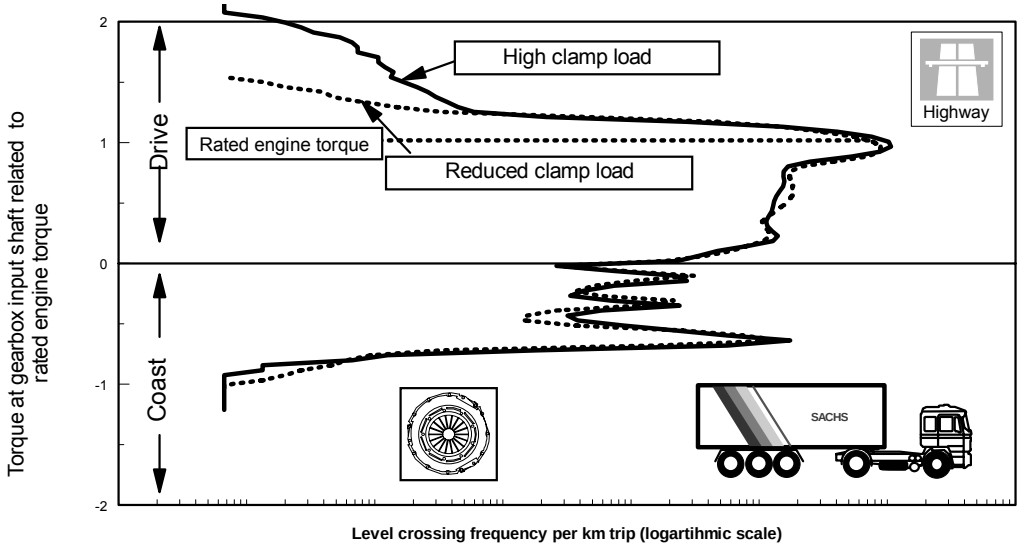


Figure 8: Influence of clamp-load on load collective

Reducing clutch cover clamping load - Facings which are more stable in terms of fading, and controlled engine-management intervention when impermissible slip occurs, will in the near future permit a reduction in clamping loads. Fig. 8 displays the influence of various transmission safety factors on the clutch`s load collective.

It is clearly seen that a lower safety factor contributes more significantly towards effective limiting of the torque peaks. The clutch only slips by up to half a revolution under full clamping load in extreme cases. The resulting facing wear is insignificant. Calculation of the frictional work shows that it takes approximately 500 such slipping torque limiting procedures to cause wear equivalent to a single starting-off procedure.

SPECIAL OCCURRENCES

In general, a special occurrence in the operating fatigue strength area is regarded as a procedure which under normal operating conditions occurs very rarely and only then as a result of an operator`s error /3/. Further special occurrences may for example relate to special approval trials by vehicle manufacturers. (e.g. jump-starting) /4/.

Special loads which are of significance for conventional clutch torsional dampers result mainly from shifting errors in the higher gears. During the comprehensive range of measurements for evaluating the drive train`s collective for heavy-duty commercial vehicles, only a limited number of such events are recorded.
In general, it can be said that in this case the clutch`s slip limit is also reached at high degrees of transmission safety. This serves at the same time as a statement about the physical limits of special loads.

DEFINING THE DIMENSIONING COLLECTIVE FOR THE FATIQUE STRENGTH CERTIFICATE

Taking the existing load collective measurements as a basis, it is necessary to define as general as possible a measurement collective for evidence of the fatigue strength of clutch disks in the relevant vehicle class.

On all the vehicles investigated it was found that the loads relevant to the torsional damper occurred when driving on highways and long-distance roads. Only such routes were therefore used when determining the test-rig collective for heavy-duty commercial vehicles, in view of the fact that the proportion of driving on highways and overland routes is approximately 90 % /5/.

SUPPLEMENT FOR SPECIAL LOADS; EXTRAPOLATION

In addition to the highway collectives, the gear-shift errors declared as special occurrences were also taken into consideration, whereby over a distance of 300 kilometres one such procedures was incorporated.

With regard to the demand for extrapolation of collectives, it is generally accepted that the loads registered are insufficient and in the case of data collected over longer periods, additional events may occur which otherwise would have remained unconsidered.

Experience has however shown that the test routes selected here, at approximately 250 km per installation, and the special loads incorporated can be regarded as sufficient for determination of the load collective`s stationary parameters /6/. This means that the collective values will no longer alter in the course of the test, or if at all, only insignificantly.

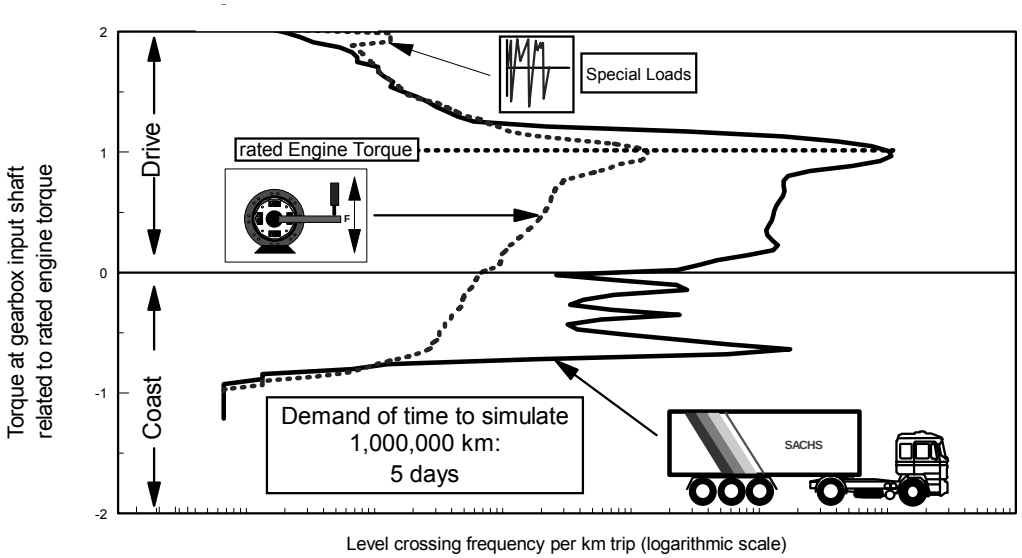


Figure 9: Comparison of dimensioning collective and driving collective

PREPARATION OF LOAD COLLECTIVES FOR CONTROL OF SERVO-HYDRAULIC TEST RIGS

The level-crossing method represents only one possible way of conducting a comparative evaluation of the load collectives. However, it contains insufficient information regarding the extent of damage. In particular, collectives exhibiting a strong displacement towards medium load require another method of further processing. Displacement towards medium loads is in fact always present in drive train systems, due to the fact that engine torque is overlaid with dynamic processes such as load-reversal or gear-shift oscillation (see Fig. 5).

A recommended counting method for the almost zero-loss further processing of the load-time function is the „Rainflow method“ /1/. Here, both the load`s amplitude and its starting and finishing points are recorded. The result of the count is filled in the so called Rainflow matrix. Only the information concerning the sequence of results is discarded. This matrix, however, has the disadvantage that it is difficult to display and therefore individual load cycles are extremely difficult to compare.

REDUCING TEST TIMES BY REMOVING ELEMENTS WHICH DO NOT CAUSE DAMAGE

Contemporary expectations regarding the service life of clutches lie between 700,000 and 1,000,000 km for heavy-duty commercial vehicles operating on long-distance journeys. This distance will also contain, however, several steady-state driving periods, where few shifting and load-cycle procedures occur. Due to the fact that these particular driving conditions do not exert any significant influence on the clutch disk`s operating fatigue strength, they are to a large extent (90 %) removed from the overall calculation.

Fig. 9 shows the measurement collective for the test rig control system in comparison to a stringent highway collective. The reduction in small and medium torques as well as the additions caused by the special loads can be clearly seen.

Integration of FE (Finite Element) analysis - FE analysis is an essential aid when removing non-damaging elements (see Fig. 2). The components which the designer has designated as critical are subjected to stress analysis. The loads introduced into the FE structure are taken from the dimensioning collectives. Since the relationship between load and strain on clutch disk components is only linear for part of its course, various load cases have to be examined. If the torsional damper limit stops are passed, additional load introduction points result, and coasting operation cannot merely be obtained by reversing the sign for the traction mode, since the contact made by the torsional damper springs on the traction and coasting sides also causes different load introduction points to take effect. From the load situations mentioned above and the partially linear response, transmission functions are defined for selected zones, and with their aid the stress collectives derived from the load collectives. The most difficult task at the moment is still determining the stress limits at which no damaging influence needs to be anticipated. For this to be possible, Woehler curves must be available for the component. However, access to these is currently incomplete in view of the very considerable experimental complexity involved. The different versions and the need to take different manufacturing processes into account have the effect of enlarging the matrix to be checked. The limit stress for the omission of non-damaging elements therefore has to be estimated empirically at the moment.

RECONSTRUCTION OF REDUCED LOAD SEQUENCES FOR TEST-RIG CONTROL

As already mentioned, the rainflow matrix contains the principal damage-relevant information from the load collective, assuming that sequential influences are disregarded. This can be assumed to be the case if the clutch is operating in the field.

With the aid of the procedures described in /8/, /9/ and /10/ it is possible to convert a Rainflow matrix back to the load-time function, the individual load-cycle sequence then being generated in a random manner by the computer. The resulting data file initially consists of a series of reversal points with no direct time relationship. The latter takes place only at a later stage, and depends on the situation at the test rig which is to be controlled.

REDUCING TEST TIMES BY OPTIMIZING THE TEST FREQUENCY

In view of the demand, for cost and deadline reasons, that the time taken to prove operating fatigue strength should be minimized, the dimensioning collective reconstructed from the Rainflow matrix must be processed further. In its initial form it cannot yet be used practicably for test rig control, since no time-optimized allocation of the extreme-value sequence has yet taken place.

The servo-hydraulic tests rigs which are in use need a time-allocated test torque pattern in the form of an analog electric desired-value signal. A regulating amplifier compares this signal with the actual-value signal supplied by the torque measuring device and, if any deviation is detected, transmits a control signal to an electro-hydraulic servo valve. This valve regulates the high-pressure oil flow from the pump to the cylinder chambers until the difference between the desired and actual test torque values is compensated for. However, this is only possible as far as an upper limit frequency which is system-specific and strongly dependent on amplitude /10/.

Since torques are recorded during collective measurements, it initially seemed appropriate to adopt torque-governed control. However, since the torsional damper characteristics, as already mentioned, may be severely non-linear and are also subject to virtual play as a result of the soft pre-damper, it was not possible to arrive at a practicable test time despite attempts at optimization. When passing through the pre-damper zone in particular the test rig repeatedly exhibited a tendency to overshoot at the desired frequencies. As a consequence of this, torque control was rejected in favour of angle control. For this, however, a number of intermediate steps first had to be taken.

The existing form of test rig could not be retained, since satisfactory angular control was only possible up to the point at which the torsional vibration damper reached its limit stop. However, the dimensioning-collective torques are frequently higher and must exhibit good reproducibility in this range in articular. The problem was solved by introducing additional stiffness in the form of a torsionally yielding shaft placed in series with the test specimen. This reduced the overall stiffness of test specimen and test rig, so that adequate control was still possible using the angular signal after passing over the torsional damper's limit stop (Fig. 10).

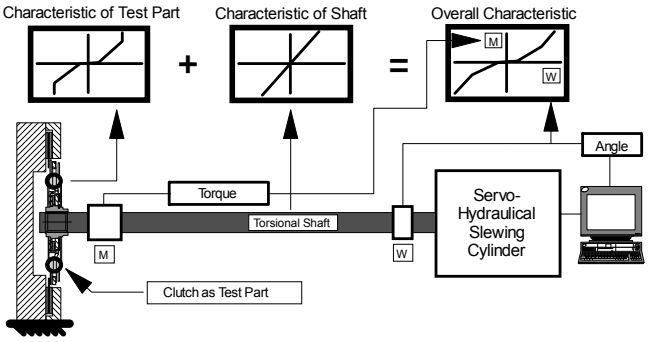


Figure 10: Testing rig with additional shaft for angle-control

Fig. 11 summarizes the current test rig control procedure. The sequence is explained below:

1. After installing the test specimen the test set-up's overall torsional characteristic is recorded by measuring instruments and memorized digitally.

2.The relevant dimensioning collective is then reconstructed from the edited Rainflow matrix.

3.The stochastically distributed sequence of extreme torque values is calculated with the test set-up's characteristic data file and converted into an angular signal.

4. After this,the test rig characteristic map is taken into account by a computing program in order to optimize the angular signal's extreme-value sequence in such a way that the test rig can always be operated as close as possible to its upper limit frequency. This ensures that the smaller amplitudes which occur frequently are run very quickly. Although the medium-value and large amplitudes run more slowly, each load reversal is allocated a specific time.

5.The number of test cycles depends on the distance for which proof of operating fatigue strength is needed. In the case of clutch disks for heavy commercial vehicles, for instance, this is 1,000,000 kilometres.

The test rig currently needs about 5 days to test a commercial-vehicle torsional damper; this represents a considerable saving in time and cost compared with field testing.

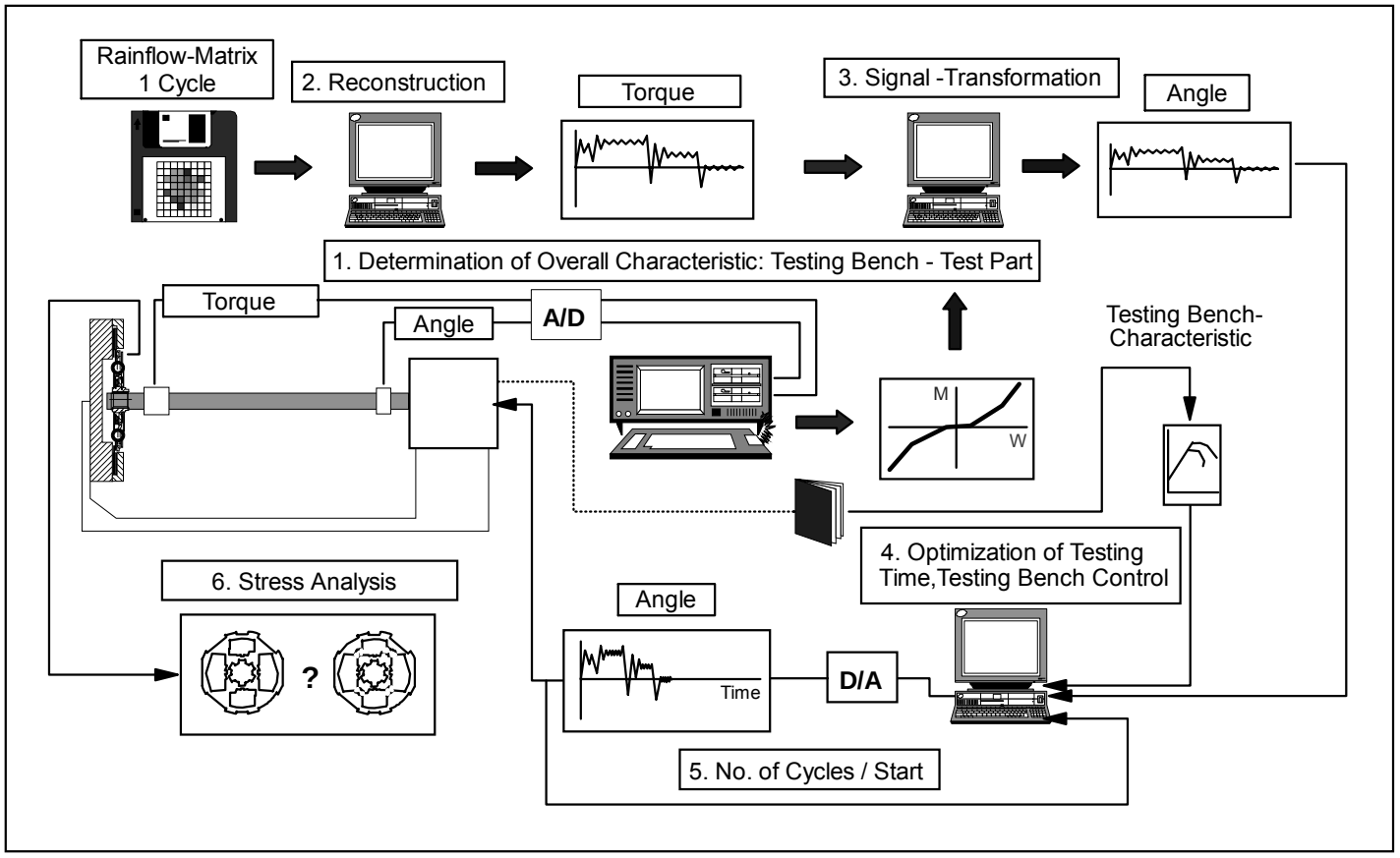


Figure 11: Testing rig control for fatique strength analysis

Proof of operating fatigue strength is normally obtained on two parts of identical construction. The torsional dampers' characteristics are measured before and after the test, so that in this way information can also be obtained about possible settling of the springs and the stability of the integrated friction device. After this the parts are stripped down and subjected to crack testing and a wear assessment under laboratory conditions. If these tests prove satisfactory, the clutch disk can be approved.

CONCLUSIONS

1. Increasing torques and spatial limitations call for lightweight design
2. Single-stage tests will no longer be adequate in the future as a reliable check on fatique strength
3. Maximum torque in the clutch mainly occurs when driving on highways and country roads
4. Limited clamp load of the clutch helps to reduce torque peaks in the whole powertrain
5. Rated engine torque has proved suitable to standardize collectives
6. Reducing test times by using angle control at the test rigs

OUTLOOK

In the future, load sequences generated from simulation computing will be used for test rig control as well as standardized load collectives. Individual load sequences can already be represented to a satisfactory standard of accuracy, but work is still needed on a practicable link between them and the overall collective.

A further priority in coming years will be the plotting of Woehler curves for the principal torsional damper components. In addition to experimental proof of operating fatigue strength, it will then be possible to make increasing use of computer fatique strength estimating tools. These procedures have particular advantages when assessing the relative damaging effects of various collectives.

Adaptive regulating concepts will also be used in future as test rig control methods. A continuous automatic actual-desired value comparison will be undertaken, and any deviations corrected by altering the desired value. In addition, this method enables the test rig to reach its own maximum limit frequency, which promises a further reductions in experimental time.

REFERENCES

/1/ Westermann-Friedrich, A.; Zenner, H.:
Zählverfahren zur Bildung von Kollektiven aus Zeitfunktionen - Vergleich der verschiedenen Verfahren und Beispiele
FVA-Merkblatt 0/14, Feb. 1988
Forschungsvereinigung Antriebstechnik e.V.
Frankfurt, 1988

/2/ Kötzle, H.; Oelmann, B.:
Herleitung repräsentativer Lastabläufe für den Betriebsfestigkeitsnachweis von Pkw-Antriebssträngen
Mitarbeiterveröffentlichung-Daimler-Benz, Nr: ..(1990) S: 82 - 95

/3/ Zenner, H.; Jung, L.:
Auswirkungen von Sonderereignissen auf die Lebensdauer
FVA-Forschungsreport 1990

/4/ Kücükay, F.; Pfau, W.:
Extrembelastungen in Personenwagen-Antriebssträngen
ATZ Automobiltechnische Zeitschrift 91 (1989) 7/8

/5/ Vöhringer, K.-D.; Geißler, H.; Müller, W.:
Zukünftige Anforderungen an Nutzfahrzeug-Getriebe aus der Sicht des Fahrzeugherstellers
VDI-Berichte Nr. 1175, 1995
VDI-Verlag GmbH, Düsseldorf, 1995

/6/ Wolf, J.-U.:
Ausarbeitung und Erprobung einer Methodik zur Bestimmung gesicherter Gesamtnutzungsdauerkollektive
Diplomarbeit, TU Dresden, 1988

/7/ Best, R.; Klätschke, H.:
Belastungsanalyse manuell geschalteter Fahrzeuggetriebe - Voraussetzung zur beanspruchungsgerechten Dimensionierung
VDI-Berichte Nr. 1230, 1996, VDI-Verlag Düsseldorf, 1996

/8/ Krüger, W.; Scheutzow, M.; Beste, A.; Petersen, J.:
Markov- und Rainflow-Rekonstruktionen stochastischer Beanspruchungs-Zeitfunktionen
Fortschr.-Ber. VDI Reihe 18 Nr. 22
VDI-Verlag GmbH, Düsseldorf, 1985

/9/ Petersen, J.; Krüger, W.:
Experimenteller Lebensdauernachweis für Kfz-Komponenten auf Basis von rekonstruierten stochastischen Beanspruchungen
VDI-Berichte Nr. 613, 1986
VDI-Verlag GmbH, Düsseldorf, 1986

/10/ Haibach, E.:
Betriebsfestigkeit, Verfahren und Daten zur Bauteilberechnung
VDI-Verlag GmbH, Düsseldorf, 1989

/11/ Buxbaum, O.:
Betriebsfestigkeit - sichere und wirtschaftliche Bemessung schwingbruchgefährdeter Bauteile
Verlag Stahleisen mbh, Düsseldorf, 1992
(2.Auflage)

/12/ Labes, K.; Miehe, B.-O.; Stolze, F.-J.; Jacoby, G.:
Die Gesamtfahrzeug-Betriebsfestigkeitsprüfung im Entwicklungsprozeß von Automobilen
ATZ Automobiltechnische Zeitschrift 97 (1995) 5

/13/ Müller, A; Grubisic, V.; Buxbaum, O.:
Betriebsfestigkeitsbewertung von Torsionsdämpfernabenscheiben
LBF-Bericht Nr. 7026/2
Fraunhofer-Institut für Betriebsfestigkeit Darmstadt, 1993

Fatigue Crack Initiation and Propagation : a complete industrial process compared with experiments on industrial welded structure

D. Lebaillif [a], I. Huther [b], M. Serror [c], N. Recho [d]

[a] GIAT INDUSTRIES, CBO,7 route de Guerry 18000 BOURGES
[b] CETIM, 52 avenue Félix LOUAT, 60300 SENLIS
[c] BUREAU VERITAS, 17bis pl Reflets, La Défense 2, 92400 COURBEVOIE
[d] LaMI, Université de Clermont-Ferrand, Avenue Aristide Briand, 03100 MONTLUCON
[d] LMM, Université Pierre et Marie Curie, Paris VI, 4 place Jussieu. 75252 PARIS Cedex 5

Abstract : This work is part of a global study performed, among a research partnership between three industries and a research laboratory, on the development of a method which allows to better estimate the fatigue life of welded structures (armoured vehicles, ships, Floating Production Storage Off-loading units, wrecking cranes, cars …) submitted to variable loading conditions. The complexity of these structures has lead to adopt a multi-scale approach, based on the use of finite element codes associated to various levels of modelling, going from the global cartography of damaged zones to the local calculation with cracks inserted in the models. The aim of this project is to develop an industrial process, avoiding successive re-meshing, being an efficient and easy tool to apply. It is also open enough to provide tools allowing the engineer to assess crack initiation, propagation until failure. The crack initiation is calculated by the use of a multi-axial fatigue damage criterion based on the local approach. Coupled with an extension of the Line Spring Method, multi-initiation of fatigue cracks in welds and through crack growth are then considered, in order to calculate the stress intensity factors for various loads and geometries. Furthermore, sets of tools were developed to predict crack bifurcation and take into account the influence of the loading history on fatigue crack growth, such as crack growth retardation effect, as a result of overloads. This approach is then applied to an overall aluminium welded structure experiment, which was designed to allow several cracks to initiate and propagate. Local micro-geometries and residual stresses were measured at weld toe, as needed for local stress calculations. Furthermore, a complete instrumentation and test of this welded structure allowed to determine precisely crack initiations and to follow crack propagation. The results are in good agreement with calculations and point out the industrial necessity to measure the local characteristics of welds and to control the quality for fatigue design.

1 INTRODUCTION

The aim of a fatigue analysis on welded complex structures is to evaluate the lifetime to initiate a crack and to propagate it, until the failure of the structure occurs. Those structures as ships, FPSO, armoured vehicles, cars, are submitted to variable amplitude loads, sometimes random, as the wave loads or the haulage on any grounds. The results of such a calculation is to help operators to take decisions for inspection, repair and maintenance process.

In this study, we present a multi-scale approach, based on the use of finite elements from the global cartography of the damaged zones to the local calculation with cracks inserted in the models. The originality of this study is to treat first the crack initiation which expends on a lot of time of the lifetime of those structures and then the crack propagation, avoiding successive re-meshing, until the failure.

Crack initiation can be calculated by several ways. The possibility to define the crack initiation period using S-N curves is available. The other way to take into account the initiation phase of a crack is to perform a calculation using the local approach, taking into account the residual stress fields, notch and plastic corrections. This methodology is then used to take into account multi-initiation of fatigue cracks as damage is accumulated during simulation (where cracks are not initiated). The crack propagation through the thickness of the plate is performed using Fracture Mechanic Theory and those of Line Spring model introduced by Rice and Levy to estimate stress intensity factors for various loads.

All these developments were performed in the software VERICRACK which is efficient and easy to carry out and sufficiently open to provide the engineer tools in order to assess the three phases of initiation, propagation of a crack and failure.

2 MODELLING METHODOLOGY

2.1 Aim of the methodology

The failure of a structural component may be explained by the presence of a crack initiation and propagation under complex and random repeated loads. These loads due to the environment induce fatigue phenomenon which depends on the joint geometry, the material microstructure, and the type and the size of the defects. The aim of the proposed methodology is to forecast crack initiation and crack growth in industrial components until failure. We shall note that, in industrial area, loads are particularly complex. These loads, which can be static or dynamic, can be represented by a combination of unitary loads or modes if the response of the component is linear elastic. But a crack represents a non-linearity and if we want to take into account the effect of the crack on the stiffness of the global structure, the crack must be introduced in a finite element model and propagated, that implies re-meshing. Re-meshing is very time consuming and can be easily used in industry only with 2D models [1]. For part-through crack, the problem is more difficult, because modelling the crack tip requires three-dimensional refined elements. Furthermore, as the crack propagates in complex geometries, under multi-axial loads, analytical solutions can not be used. Considering the component response linear elastic, the use of Line Spring method allows to take into account the stiffness variation during crack propagation without re-meshing.

2.2 Global flow chart

The global flow chart of the method to study the crack from its initiation until the failure occurs is given in Figure 1. Different subroutines using either damage determination or crack growth calculation were combined to define a software called VERICRACK.

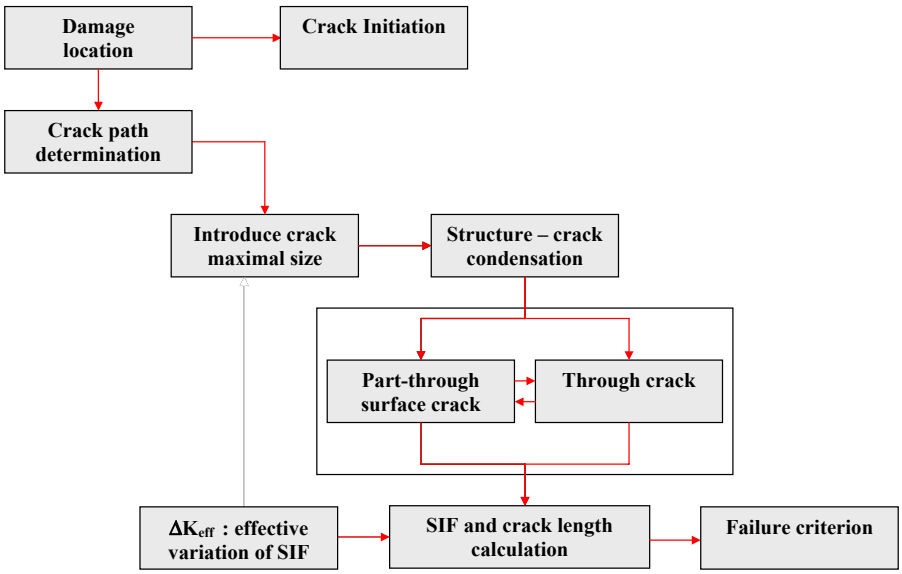


Figure 1 : Flow chart of VERICRACK

The first step is to determine the stress field of the component. From the knowledge of the stress field, we are able to forecast where the most damaged zones are located, and to estimate the crack path. A more precise estimation of the crack initiation duration is made. The crack of the maximum length is introduced in the global meshing and all loads are firstly applied on the fully open crack. Structure is then condensed on the crack. From the crack stiffness, we can compute the displacements of the crack nodes for a part-through (Figure 2b) or a through crack (Figure 2c), determining the loads on the crack nodes necessary to close the crack.

During the simulation, after that a crack initiates from the nodes with critical damage (Figure 2a), the Stress Intensity Factors (SIF) are calculated for the crack. Moreover, as the stiffness of the structure evolves when the crack propagates (Figure 2b), stress field is updated (stresses are redistributed) and damage is accumulated for the crack nodes that have not already initiated. This allows to take into account multi-initiation crack phenomenon for welded structures. The various steps of the above flow chart are described in the following.

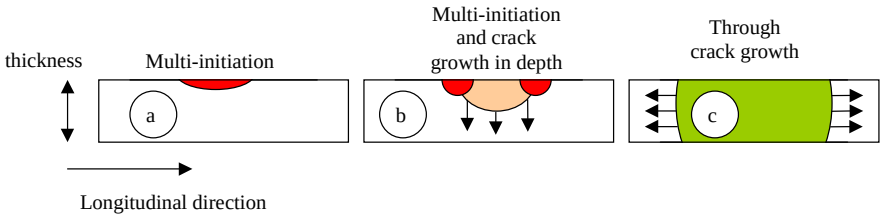


Figure 2 : Different crack front shapes

2.3 Crack initiation by the local approach

The software CALEND [2] is used to evaluate the damage. It is based on a local approach, i.e. the local stresses have to be calculated. For designing welded components, it allows to take into account stress concentration factor K_t to evaluate the stress tensor at the weld toe. Residual stresses can be included too. As the local stresses are often greater than the yield stress, a plastic correction has to be done (using the hardening law of Chaboche [3]). Then a fatigue stress criterion is calculated on different planes of the stress tensor (using Dang Van criterion) and damage is accumulated (using Miner's rule and Basquin's law) on extracted cycles (using Rainflow counting). Finally, damage is taken as the maximum damage obtained on all planes of the stress tensor and the crack initiation occurs when damage is over a critical value (for example equal to 1).

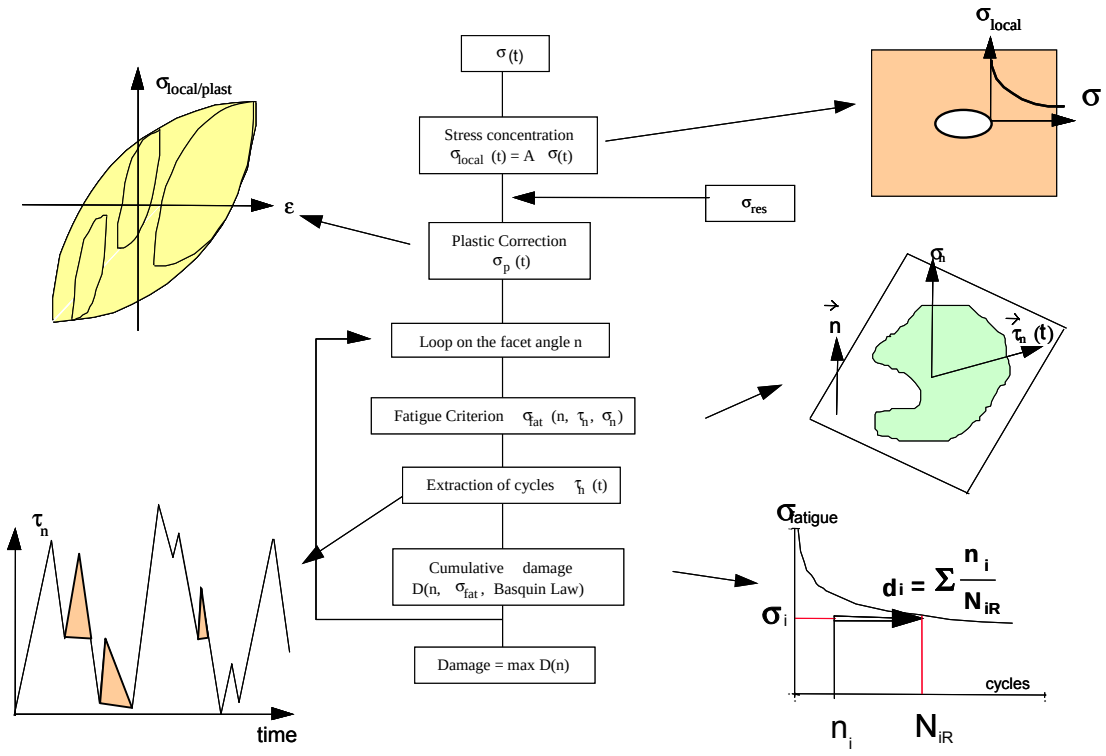


Figure 3 : Damage calculation

For crack location, a light version of CALEND is used without considering Kt and plastic correction. It allows to quickly evaluate the damaged zones on the whole structure. Fine calculations are only carried out in the most damaged zones.

CALEND is fully integrated in VERICRACK and performs damage calculations to determine when a crack could initiate and on which nodes. When the crack propagates, damage is accumulated for all non-initiated nodes.

2.4 Crack path determination

A strong assumption has to be made on the crack path : it must be determined *a-priori*. Indeed the crack of maximum length has to be introduced in the global model and the SIF are calculated when the crack path is already chosen. To check this hypothesis, SIF in mode I are compared, at each increment, with SIF in mode II and in mode III in VERICRACK. So how is the crack path chosen ? Considering that the crack propagates in the direction orthogonal to the maximum principal stresses [3]. This direction is obviously chosen for one load case

and we have to check that for all load cases, the crack path is approximately the same. Moreover, automatic crack box re-meshing can be used for bi-dimensional elements but, for industrial application, it is avoided.

2.5 Crack propagation : part-through surface crack

The Line Spring model was introduced in 1972 by Rice and Levy [4, 5] to estimate stress intensity factors due to tension and bending in large plates containing part-through surface cracks. The line-spring model is based on the fact that there is a relationship between local displacements and loads at each point along the crack, noted compliance coefficients. Then, from the point of view of the plate, the surface crack is modelled as a through-crack with a continuous distribution of generalised springs connected across the line of discontinuity: the line springs. It must be noted that the opening displacements of the crack lips are function of the crack depth thanks to Tada coefficients [6].

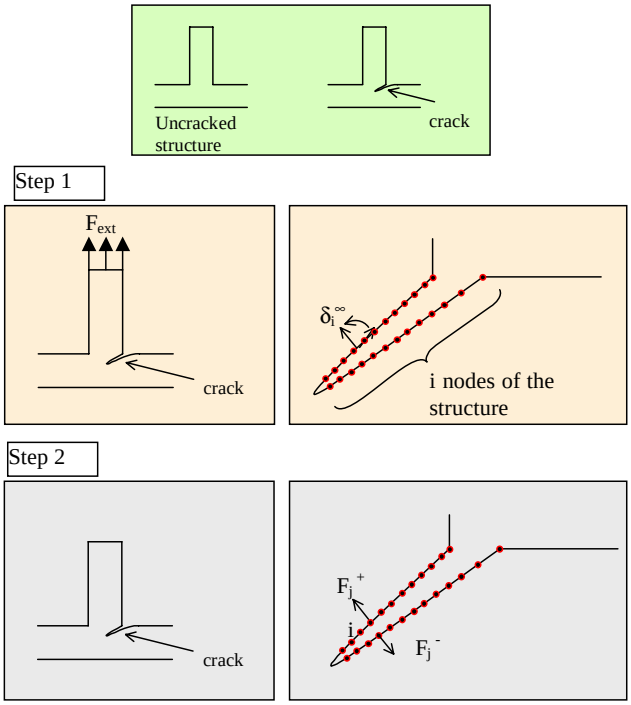


Figure 4 : Step 1 and step 2 to prepare for VERICRACK simulation

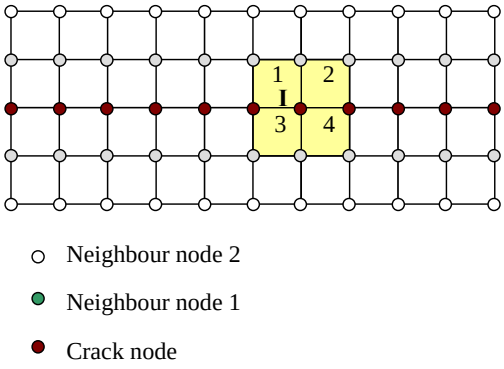


Figure 5 : Definition of neighbour nodes

Two finite element calculations are needed to proceed a VERICRACK simulation (Figure 4). Firstly, the external loads F_{ext} are applied (Step 1) on the fully-cracked component and we can obtain all displacements of the crack lips δ_i^{∞}, $i \in N$ (all Nodes). Then, the stiffness S_{ij} of the cracked component is obtained (Step 2) applying unitary loads on each node j, in all directions, and calculating the displacement at the node i : $S_{ij}.F_j = \delta_i$.

Then for the desired crack shape, the aim is to find loads {F} and displacements {δ} to solve :

$$-S_{ij}.F_j = \delta_i - \delta_i^{\infty} \qquad (1)$$

One condition has to be added for part-through crack, with Tada coefficients A_{ij} , depending on a/h (a : crack depth and h : plate thickness) :

$$-A_{ij}.F_j = \delta_i \qquad (2)$$

Displacements are calculated not only on the crack nodes but also on the neighbour nodes (Figure 5) which close the crack. Indeed obtaining these displacements allow to precisely determine the stresses at each nodes for damage calculation. So, for node ***I***, stresses are calculated from displacements at neighbour node ***1*** and tip crack node, using interpolation functions of elements ***1*** to ***4***.

2.6 Through crack growth : the crack box technique

It is important to emphasize that SIF calculated with Tada coefficients are available for cracks propagating in the depth of a plate. When the crack front is straight in the depth of the plate, the Line Spring assumption can no longer be used as the crack propagates now in the longitudinal direction (see Figure 2c).

So the idea is to use the technique of sub-modelling : the displacements of nodes at the neighbourhood of the crack are used to drive a 3D sub-model of the structure, including the crack tip which is meshed using fracture mechanic elements. In order to avoid finite element calculations during VERICRACK simulation, the SIF at all the crack tip nodes of the sub-model are previously calculated with unitary displacements applied at its border. Then during VERICRACK simulation, unitary SIF in the crack box are easily combined with the displacements of the neighbour nodes to obtain SIF at each increment. The Figure 6 represents the sub-model with an unitary displacement applied, all the other nodes of the border being clamped.

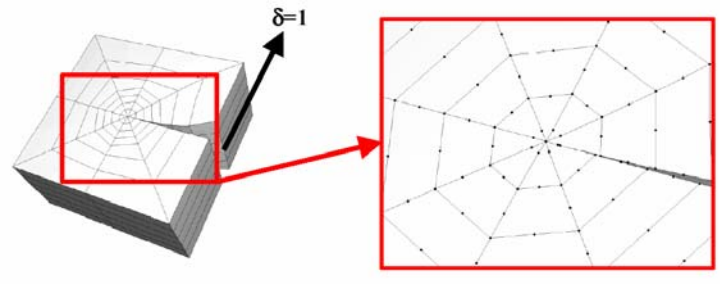


Figure 6 : Sub-model of the structure : 3D crack box (left), zoom on crack tip (right)

The precision of this method depends on the distance between the crack line and the neighbour nodes used to drive the crack box. If we use the first line of neighbour nodes, errors on SIF are between 7 to 13 %, depending of the crack length. But when we use the second line of neighbour nodes, errors on SIF are between 1 to 5 %. Errors can also depend on the sub-model refinement and on the type of elements chosen for the global model (linear or quadratic). In the future, the aim of this technique is to include in the sub-model geometry details (like welds).

2.7 Crack propagation rate

The crack growth is controlled by the Paris law, using the SIF range calculated either from Tada equations or from J-integral calculations in the crack box. It can be corrected using the SIF necessary to open the crack (K_{op}) to determine the effective range of stress intensity factor ΔK_{eff}. The value of K_{op} can be fixed, or determined by using Elber's equation or calculated with a Dugdale-Barenblatt model [7].

3 EXPERIMENTAL TESTS

3.1 Description

This approach is applied to an overall aluminium welded component (Figure 7). The plate thickness is equal to 10 mm. A complete set of strain gauges was used to determine precisely the stress field in the component and the time when a crack initiates. The gauges were placed at 10 mm from the weld toes. Furthermore, dye penetrant was used to detect crack initiation. The back floor of the component was bolted on the ground. An hydraulic jack was placed on the sides of the component to load 4 weld beads, allowing so 8 possible cracks at weld toes. The stress ratio of the applied load is R=0.1 and the maximum load is 15000 N.

3.2 Results

Three cracks have initiated : weld toes ***3*** and ***2*** on the right side (Figure 8) and weld toe ***3*** on the left side. The first crack is initiated on weld toe ***3*** at the left side (between 50000 and 280000 cycles) and then on the right side (between 300000 and 400000 cycles). Later, a crack is initiated on the weld toe ***2*** at the right side (between 400000 and 550000 cycles). The crack was difficult to observe when its length was less than 100 mm because a multi-initiation phenomenon seems to be the origin of the crack initiation. The case of the left side was different ; when the crack was observed at 280000 cycles, its length was about 250 mm, whereas the evolution of gauges seems to give 50000 cycles. This crack did not propagate through the plate thickness at the weld toe, in contrary to other cracks, but it has followed the HAZ. So all calculations on crack growth will be carried out on cracks on the right side.

3.3 Weld toe geometry

The difference between the left side and the right side may be explained considering local parameters (residual stresses and weld toe radius). Residual stresses were measured at the surface and at 100 µm depth by X-ray diffraction. Measurements at 100 µm depth were performed to avoid the superficial residual stresses introduced by wire brushing after welding. Local geometry of the weld toe was measured using CAGEP [7].

Profile recordings were performed thanks to a laser and a CCD camera and were used to obtain the radius distribution along the weld toes (Figure 9). Results for all weld toes are presented in Table 1. The value of transverse stress at 10 mm from the weld toe and the mean radius value can explain why only 3 cracks have initiated. More precise calculations are done in the following.

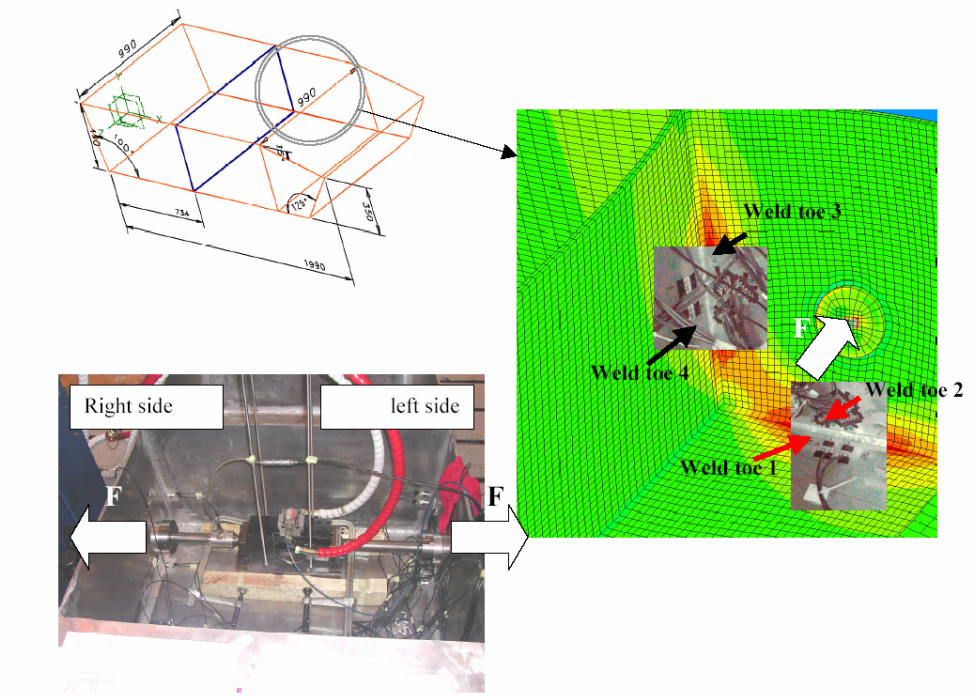


Figure 7 : Description of the component and experimental boundary conditions (dimensions in mm)

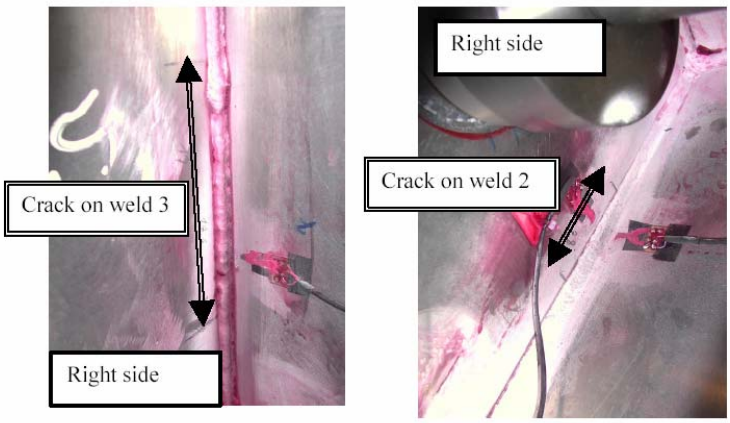


Figure 8 : Picture of crack on weld toes 2 and 3 (right side)

4 NUMERICAL CALCULATIONS

4.1 Crack initiation

In order to determine the crack initiation, it is necessary to calculate the local stress at the weld toe, which depends on the residual stresses and the local radius. The global model used is a shell modelling of the structure, with linear displacement field elements. 3D calculations were performed using either a 3D sub-model or a 2D sub-model in plane strain, driven by the global model displacements (Figure 10). The plane strain assumption can be done so that the crack initiates in the middle of the weld. The 2D modelling was used because it is enough simple to perform calculations for mean radius varying between 0.2 and 1.2 mm. Results are shown in Figure 11 and compared with experimental results. It shows that a good prediction is given considering the residual stresses at 100 µm depth and the mean radius of the weld toe.

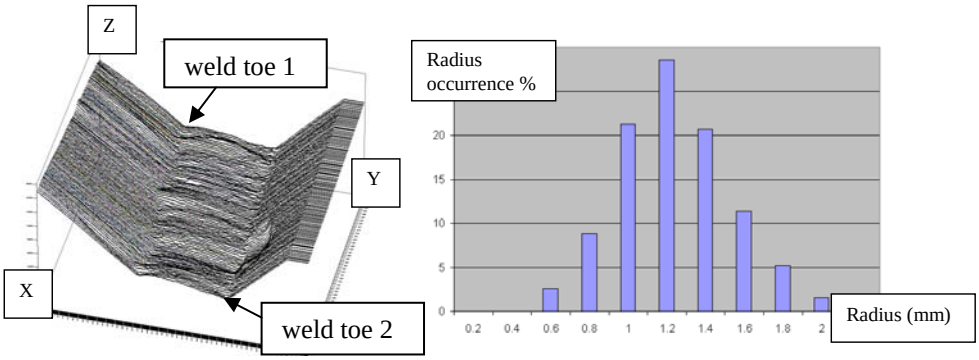


Figure 9 : weld profile measurement (left) and radius distribution for weld toe 1 on the right side (right)

Table 1 : Transverse stress at 10 mm from the weld toe and weld toe mean radius

side	Weld toe	Transverse stress at 10 mm (MPa) (FEM)	mean radius (mm)
left side	weld toe 1	82	1.31
	weld toe 2	78	0.97
	weld toe 3	95	**0.59**
	weld toe 4	50	1.23
right side	weld toe 1	82	1.26
	weld toe 2	78	**0.42**
	weld toe 3	95	**1.05**
	weld toe 4	50	0.9

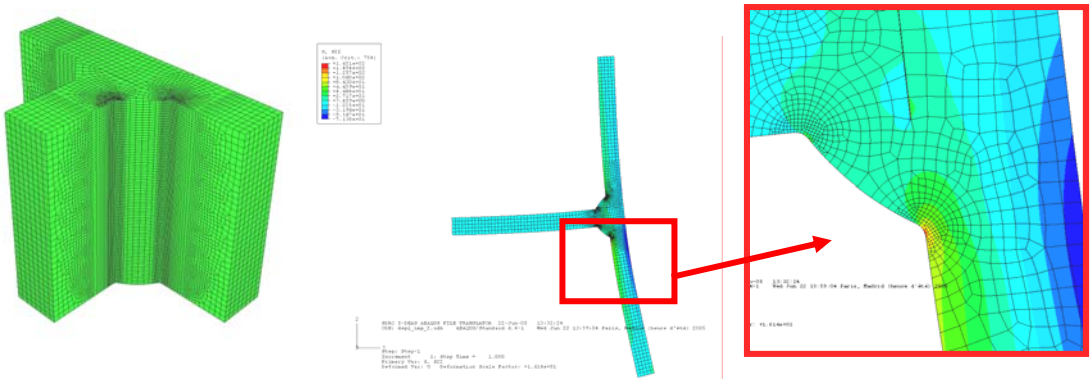


Figure 10 : Zoom of the weld toe in 3D and in 2D modelling

4.2 Crack growth

Crack initiation and growth are then simulated in VERICRACK, for the right side of the component. For crack initiation, the calculations are based on experimental material data and local approach with mean radius. For crack growth, experimental crack growth of MIG welded joints is used.

Different hypothesis were done for the simulation with VERICRACK :

- a crack initiates when the damage accumulation is equal to 1 ;
- when the damage accumulation is equal to 1 at a node, a crack of 1 mm depth is introduced ;
- when the stress in the ligament is greater that the Yield Stress at a node : the crack is supposed to have fully grown in the thickness of the plate ;
- when the crack front is almost straight, the crack can propagate thanks to the crack box ;
- there is a competition between crack growth using fracture mechanics and using damage accumulation at nodes ;
- the radius of the weld toe ***2*** is the minimum value of radii instead of mean radius.

Results are shown in Figure 12 where the crack shape is presented during simulation. Simulations are compared with experimental results for crack ***3*** (weld toe ***3***) and crack ***2*** (weld toe ***2***). With the assumption made, the agreement seems to be good but many sensitivity tests have to be carried out.

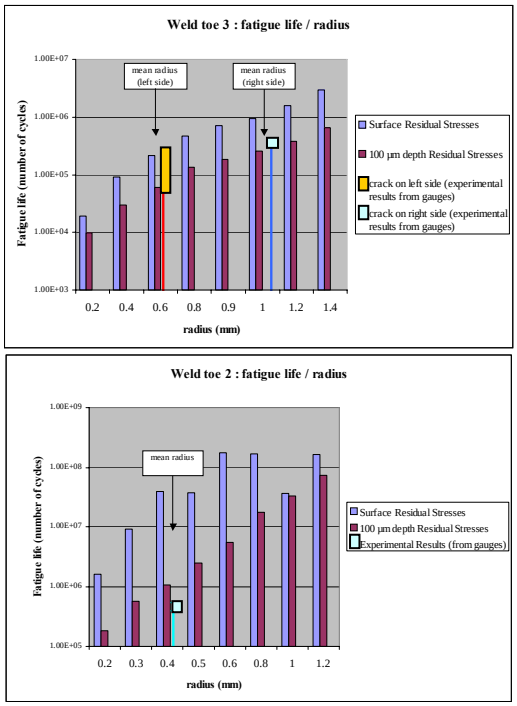


Figure 11 : Crack initiation determination for weld toe 2 and weld toe 3 for both sides

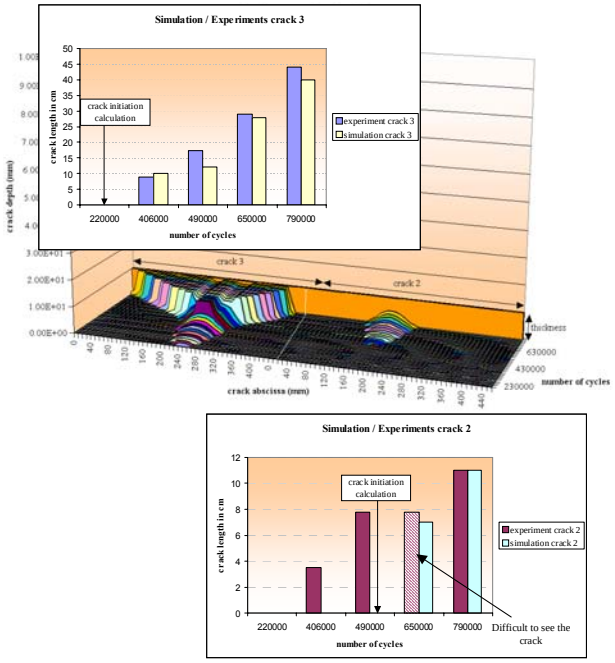


Figure 12 : Crack growth simulation with Vericrack for weld toe 2 and 3 on the right side of the component

5 CONCLUSION

In this paper, a global methodology was introduced to forecast crack initiation and propagation without re-meshing. As the behaviour is globally linear, the principle of superposition has been used. So all calculations are made using unitary loads (for static response) or modes (for dynamic response) that are combined in the VERICRACK code. Furthermore, this principle is also used to drive a three-dimensional sub-model of the component including the crack tip in order to determine the SIF for through crack, as the Line Spring method can only be used for part-through surface cracks. So this program can determine crack initiation in welds and make part-through and through crack grow in a 3D shell structure. This method was applied on an aluminium welded structure designed to make various crack initiate. Results of crack initiation life are in good agreement with experiments if we consider the local geometry of the weld toes (radius) and the residual stress at 100 µm depth. Results of crack growth simulation are close to experiments, considering different hypothesis, knowing that it is very sensitive to parameters like the size of the initial flaw and the Paris law parameters. The aim of such experiments is to determine the appropriate parameters to predict the lifetime of a component until it fails.

6 ACKNOWLEDGMENTS

The authors would like to thank all those who have taken part in the project to create the global flow chart, to program the VERICRACK code, and to carry out the experiments and simulations.

7 REFERENCES

[1] D.Lebaillif, N. Recho. Automatic Crack Box Technique for Brittle and Ductile Crack Propagation and Bifurcation Criteria. 11th International Conference on Fracture (ICF 11) , 2005, Turin (Italy)

[2] E.Petitpas , B. Lebrun, S. de Meerleer, P. Fournier, A.Charrier, F. Pollet Use of the local approach for the calculation of fatigue strength of welds. IIW, Florence, 9-14/07/2000

[3] D. Lebaillif, S. Ma, M. Huther, H.P. Lieurade, E. Petitpas, N. Recho Fatigue Crack Propagation and Path Assessment in Industrial Structures "International Conference on Fatigue Crack Paths / FCP 200318-20 Sept. 2003, Parma (Italy), 18-21 September 2003. ESIS, European Structural Integrity Society

[4] Rice J.R. and Levy N., The Part-Through Surface Crack in an Elastic Plate, *Journal of Applied Mechanics*, March 1972,185-194

[5] Parks D.M., The Inelastic Line-Spring: Estimates of Elastic-Plastic Fracture Mechanics Parameters for Surface-cracked Plates and Shells. *Journal of Pressure Vessel Technology* **103**, August 1981, 246-254.

[6] Tada H., Paris P.C. & Irwin G.R., The stress analysis of cracks handbook- DEL Research Corporation

[7] H.P. Lieurade, I. Huther, D. Lebaillif. Evaluation de la qualité des soudures vis-à-vis de la résistance à la fatigue. Mécanique et Industries. Vol 6. No. 2. 2005

Fatigue design with engineering steels

Applications and relevant criteria

Pascal DAGUIER, Gilles BAUDRY

ASCOMETAL CREAS, BP 70045, 57301 HAGONDANGE Cedex, France

Abstract As fatigue life is governed by many factors like metallurgical phases, non-metallic inclusions, residual stresses, surface roughness, leading to different damage mechanisms, the fatigue criteria must take into account the damage mechanisms to predict suitably the endurance limit and thus, to propose the best material solution.

At the same time, each component is submitted to a specific in-service type of loading, in a specific environment. Thus, laboratory fatigue tests must be also representative of this type of loading, to get the same type of damage.

This paper has for aim to discuss these two points, by using concrete examples chosen among mechanical parts used in mechanical engineering and transportation (forged parts, machined parts, pinions, bearing, springs, …)

1 INTRODUCTION

The general trend in automotive and truck industry is cost reduction, downsizing, reliability and fulfilling the new pollution standards. As a consequence, new motorizations lead to a severe increase of stresses on main critical components. Facing this situation, the steel maker has to adapt his material solutions for each type of component. In close collaboration with his customer, he identifies the major damage mechanisms, and thus is able to design the best material (grade, cleanliness, heat / surface treatments) by using representative laboratory tests. The KITAGAWA diagram constitutes a good tool to reach this target [1] (figure 1).

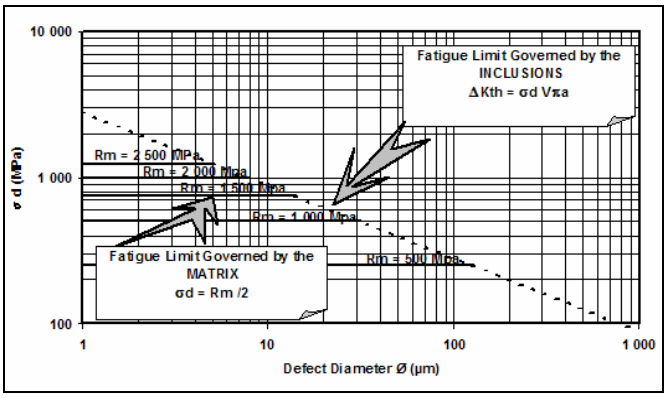


Figure 1 –KITAGAWA diagram [1]: Relation between the fatigue limit and the defect size for a wide range of materials)

This diagram presents the evolution of the endurance limit vs. defects size. It was established for a wide range of steel and defects (inclusions, shrinkages, surface defects, welding defects…). It highlights 2 domains:

- a domain where the endurance limit is governed by the matrix (the steel fatigue limit is mainly determined by the matrix structure -hardness, stability, homogeneity – and by the residual stresses),
- a domain where the endurance limit is governed by defects (defects such as surface or internal defects - inclusions, porosities - play a major contribution in the parts' reliability).

As these two domains exhibit different fatigue damage mechanisms, different ways are needed to improve fatigue resistance. This paper will present examples of applications for which the fatigue limit is governed either by the matrix, either by the distribution of defects.

2 STEELS FOR MODERATELY STRESSED MACHINED COMPONENTS (INJECTION, CRANKSHAFT...)

To reduce the manufacturing costs, an optimised microstructure for machinability adapted to the customer's means of production should be obtained after air-cooling in the forging heat. This is achieved by controlling the inclusion population and/or the microstructure of the steel. The steelmaker's know-how consists in finding the best compromise between machinability and fatigue. According to the Kitagawa-Takahashi diagram, such compromise will be mainly related to the strength level of the steel. For moderate hardness steel, with a population of defect lower than a critical size, fatigue criterion based on the matrix behaviour (DANG VAN like criterion) allows an efficient and realistic component design.

2.1 Example 1: Diesel direct injection systems

The two main systems present on the market are the common rail and the unit injector system. The increasing of the injection pressure with each generation of injection system leads to the development of adapted metallurgies. Moreover, the need of a very precise geometry of the components requires a high level of machinability and this, in materials sometimes presenting high mechanical characteristics. Table 1 presents the different metallurgical solutions adapted to the successive generations of rail present on the market or in development.

Table 1 different steel grades for the forged rail application

range of pressure (bars)	Ultimate tensile strength (Mpa)	grade	microstructure	comments
1350	800	38MnSiV5	FP	limited in UTS
1400 - 1600	1000	42CrMo4	QT	-expensive -distorsion
		44MnV6	FP	compromise between fatigue and machinability
1600-2000	1200	30MnSiCrV6 METASCO D1200	bainitic	for high efficient machining
		15MnCrMoV6 METASCO R1200	tempered bainite	for standard machining

As can be seen in figure 2, application with higher strength level need to be optimised between machinability (level of "good inclusion") and fatigue resistance. Indeed, above 1000 MPa, fatigue limit could be lowered by defects larger than 30µm (order of magnitude in tensile/compression test at R ratio of minus 1) so a better understanding of the mechanisms which control machinability is a key point for the development of higher stressed mechanical parts.

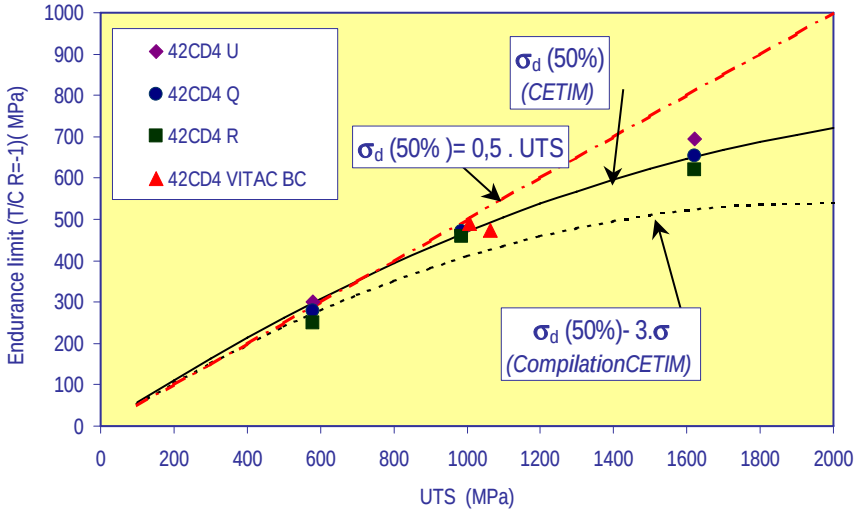


figure 2

Evolution of fatigue limit with tensile strength (tensile / compression test R=-1)

2.2 Example 2: The crankshafts

In this case, the two critical places, regarding the fatigue limit, are the oil hole and the crankpin fillet. The problem of the fatigue limit of the oil hole can be handled by using the multiaxial DANG VAN criteria, because it deals with a machined part. For the case of the crankpin fillet, this zone has to be reinforced, because the stress level is very high. The crankshaft working essentially in bending, we performed bending tests on representative samples (figure 3) with the same conditions as for crankshafts.

The most classical method of local reinforcement is the deep rolling process. Compressive residual stresses are developed at the bottom of the fillet. The fatigue loading (bending) in this zone leads to important local surface stresses due to the stress concentration brought by the crankpin fillet. These loading could overpass the yield strength, leading to a stress relaxation of the residual stresses at the surface. Because of the high stress gradient, the material remains in an elastic domain under the surface.

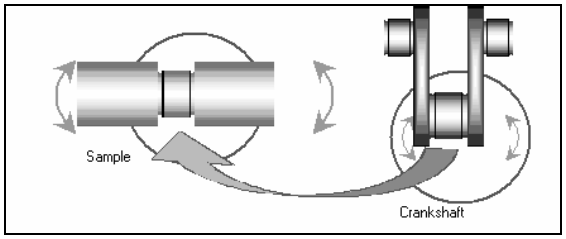


Figure 3: Fatigue sample used to estimate the fatigue limit of crankshafts

It was shown that with these conditions, a surface crack could quickly initiate at the surface and propagate inside the sample till it is blocked by the compressive residual stresses. Thus two endurance limits are obtained:

- an endurance limit for crack initiation, for which no crack is allowed,
- an endurance limit for crack arrest, below which one a no propagating crack is admitted (true fatigue limit).

The most used grades for this application are the micro-alloyed ferrite-pearlite grade, 38MnSiV5S, and the bainitic grade, 35MnV7 (METASCO® BA). But with these grades the crankshafts will not be able to cope with the high stress level of the next generation of engines. This brought to the development of a new bainitic grade: 25MnCrSiVB6 (METASCO® MC), which allows a performance increase of 40%, thanks to a fine microstructure composed mainly of bainite and retained austenite (10-15%).

Table 2 compares the endurance limit of grades for this application. It shows that by keeping constant the deep rolling process, the new bainitic grade allows an increase of crack initiation and fatigue limit more than 40%.

Table 2: mechanical properties of main grades for deep rolled crankshafts
(*base 100: Endurance limit of 38MnSiVS5 deep rolled at 900 daN)

grade	Ultimate tensile strength MPa	Endurance limit (*)			
		deep rolling (900 DaN)		deep rolling (1200 DaN)	
		crack initiation	specimen fracture	crack initiation	specimen fracture
38MnSiV5	807	53%	100%	50%	124%
35MnV7 METASCO BA ®	830	54%	112%	-	-
25MnCrSiVB6 METASCO MC®	1040	76%	149%	-	-
42CrMo4	998	56%	112%	-	-

Moreover, this solution preserves good formability (necessary for the straightening of the crankshaft during the deep rolling process).

3 STEELS FOR MODERATELY STRESSED AS FORGED PARTS (CONNECTING RODS…)

The main characteristic of such parts is that the fatigue stressed zone is used in as-forged conditions without machining the whole surface. So, the surface defects related to the forging process control the fatigue limit of the part. The fatigue strength can be improved by increasing the mechanical properties of the steel but is lowered by the surface quality of the component.

3.1 Example: the connecting rod

The evolutions of manufacturing process and the increase of the in-service loading induced these last years an important change of steel grades for con-rods. To meet these requirements, high strength and/or "splitable" grades have been developed, maintaining a goof hot-forming capability .Tables 3 and 4 give examples of mechanical properties and formability of such grades.

Table 3: Mechanical properties and endurance limits of split ability grades obtained on con-rods (Indicative results). The loading ratio is R-1.

steel grade	yield strength (Mpa)	Ultimate tensile strength (MPa)	YS/UTS	KCV (J/cm2)	σ_D (MPa)	σ_D/UTS
45Mn5 (reference)	470	805	0.58	not splitable	284	0.35
C70S6	545	950	0.58	5.5	310	0.33
50MnP6 SPLITASCO 50 ®	575	954	0.60	4.0	330	0.35
38MnSiV5 SPLITASCO 38 ®	670	933	0.72	5.4	350	0.38
38MnSiV4 SPLITASCO HC ®	750	1010	0.74	7.0	429	0.42

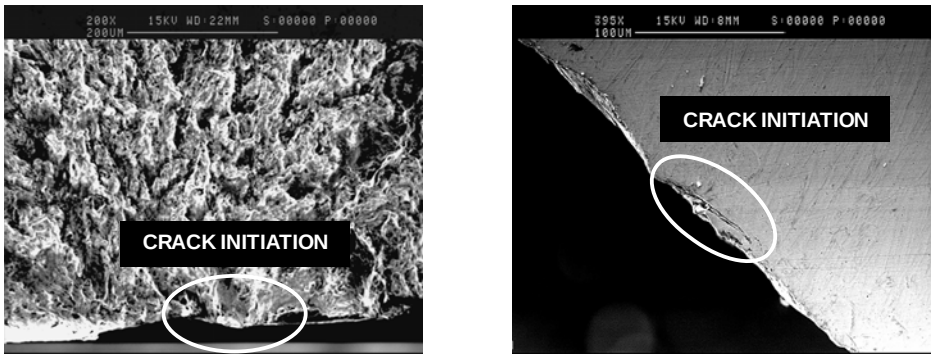
Table 4: Summary of the advantages and disadvantages of each solution

grade	mechanical properties	splitability	forgeability	machinability
45Mn5				
C70S6	-	+	++	-
SPLITASCO 50 ®	-	+	-	+++
SPLITASCO 38 ®	+	++	+	-
SPLITASCO HC ®	+++	++	++	+

To estimate their in service properties, these grades have been tested in fatigue (traction/compression) with different loading ratios R = P_{min}/P_{max}, representative of the in service conditions. R = -1 corresponds to "standard" conditions. Figure 4 presents the surface fracture generally observed at the initiation area on con-rod after rupture in fatigue test. It clearly shows that a surface defect made by the forging process is at the origin of this failure. Thus it appears that the surface quality is one of the main parameter of the con-rod fatigue limit.

MURAKAMI [2] method appears as a suitable approach able to describe these experimental results. In this approach, a surface defect S in a material with a Vickers hardness (Hv) leads to a fatigue limit σ_d given by:

$$\sigma_D = \frac{1.43\left(H_V + 120\right)}{\left(\sqrt{S}\right)^{1/6}} \qquad (1)$$



SEM View of the broken surface sub-surface after a slight polishing

Figure 4: fracture surface observed on con-rod after rupture in fatigue test

Table 5 from [3] shows a good agreement between the experimental fatigue limit and those estimated by the MURAKAMI method applied to defect size distribution at the origin of the failure. These results are also in very good agreement with those obtained by Beretta & Al. [4] on cast iron and forged con-rods. Its highlight that the mechanical properties of the material gives a potential fatigue limit which may be lowered by the presence of defects(cf. formula (1)).

Table 5: Comparison of the endurance limits measured

and estimated by the Murakami approach on con-rods

batch of con-rod	fatigue limit (Mpa)		
	experimental results	estimated with the murakami method	
		with the area of defect measured on the fracture surface	with the area of defect measure on subsurface after ligth polishing
batch 1	223	195	
batch 2	270	226	225

4 STEEL GRADES FOR HIGH LOADED MACHINED PARTS (GEARS, BEARINGS…)

In this case, loads are extremely high, and the maximal steel performance is required. This one is obtained by using extremely hardened steel grades. KITAGAWA diagram shows that the sensitivity to defects is maximum for this kind of application.

4.1 gears

Beyond the in-service properties, it is important, in the field of gears steel grades, to consider the phenomenon of distortion of the components during the heat treatment which has two major dramatic consequences:

- the shaft's straightness,
- the inhomogeneous tooth distortion, leading to in service local over stresses.

At the beginning, the main concern was the control of the hardenability band in order to limit the distortions. Criteria have been defined on the JOMINY curves, mainly on the scattering of the experimental data. This approach has evolved during the past decade and has been today even more improved by the "JOMASCO® concept". This concept based on:

- straigtheness of the JOMINY curves,
- adapted hardenability,

allowed to define an "optimised" family of steel grade for automotive gear components: the MnCrMo5 grade. This concept is also transposable to classical gear steel grades. Its typical hardenability curve is described in the figure 5.

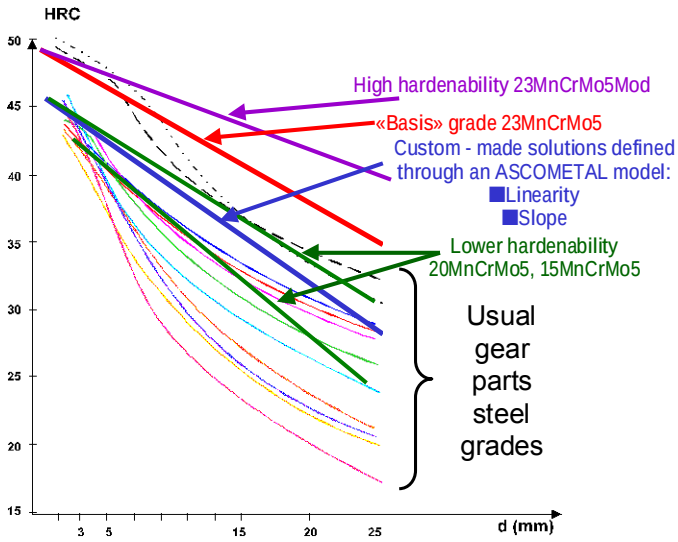


Figure 5 - JOMINY curve of usual gear parts steel grades (schematic).

These customised steel grades are defined within the chemical composition range of the specification from an appropriate calculation pattern devised by ASCOMETAL.
Steels produced from this "JOMASCO® concept" allow for a wider range of thermochemical surface treatments, such as case hardening, carbonitriding or nitriding, layers all achieving required depth, surface and core hardness for better use by gear components.

The expected gains on such metallurgies depend, among others, on the component's geometry and its massivity. As an example, using 23MnCrMo5 JOMASCO® for a gas quenched shaft allowed to reduce from 33 to 50 % the value of the distortion in bending, and decrease rupture or appearance of crack during straightening from 0.95 % to below 0.1 % (Source: PSA Borny).

Concerning in service properties of gears steel, 3 kinds of damage could be encountered :

- bending fatigue at the root of teeth
- rolling contact fatigue at the surface of teeth
- teeth breaking by impact loading

So the development of new metallurgies for such application should take into account these 3 points. As the manufacturing of components is cost and time consuming in the development of new steel grades, representative tests have been developed [5]. So the bending fatigue at the root of teeth is modelised by a four point bending test on sample with a representative notch; A twin-disc machine is used to simulate micro-pitting and spalling of the raceways; charpy type test is used to quantify the resistance to impact loading. For example, figure 6 presents the distribution of micropits observed on the surface after rolling contact fatigue test on a twin-disc machine for different case hardened gear steel grades.

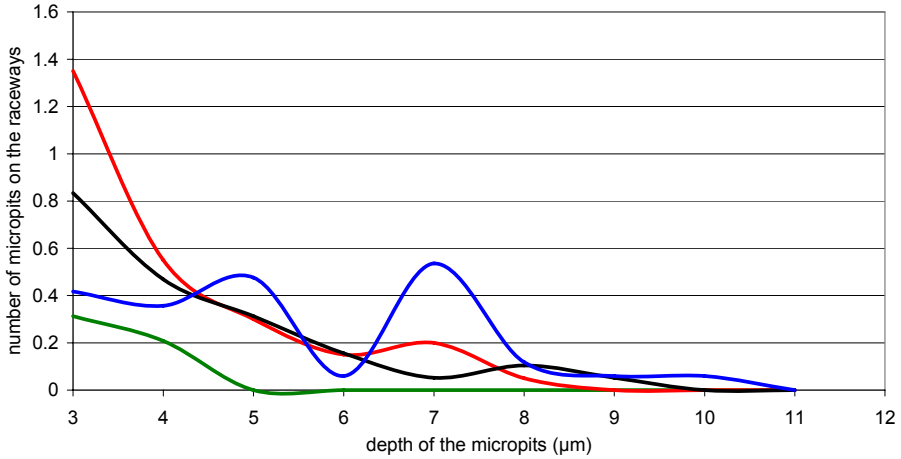


figure 6

Evolution of the distribution size of micropits for different gear steels

4.2 Bearings

In this case, the hardness is extreme, and the steel cleanliness is thus dramatically critical. These components are essentially submitted to contact fatigue, with crack initiation on inclusions in Hertzian zone. It is well known that these inclusions induce an over damaged zone (butterfly) at the crack origin. We thus developed a physical fatigue model, in association with INSA and SNR [6] modelizing the initiation and propagation steps. In this model, the inclusions are randomly distributed within the material. The size and inclusion distribution nature depend on the steel making and rolling process (endogenous and exogenous inclusions). This distribution must be measured in a sufficient volume to have a sufficient probability to detect the biggest (but the rarest) ones, that constitutes the inclusions harmful in fatigue (diameter > 15-20 microns) [7]. As in modern steelmaking process the density of these last inclusions is too low to be detected by classic methods like optical quantitative metallography on large area, we have developed high frequency ultrasonic testing methods (50 and 80 MHz), allowing the examinations within sufficient volumes (Some cm^3).

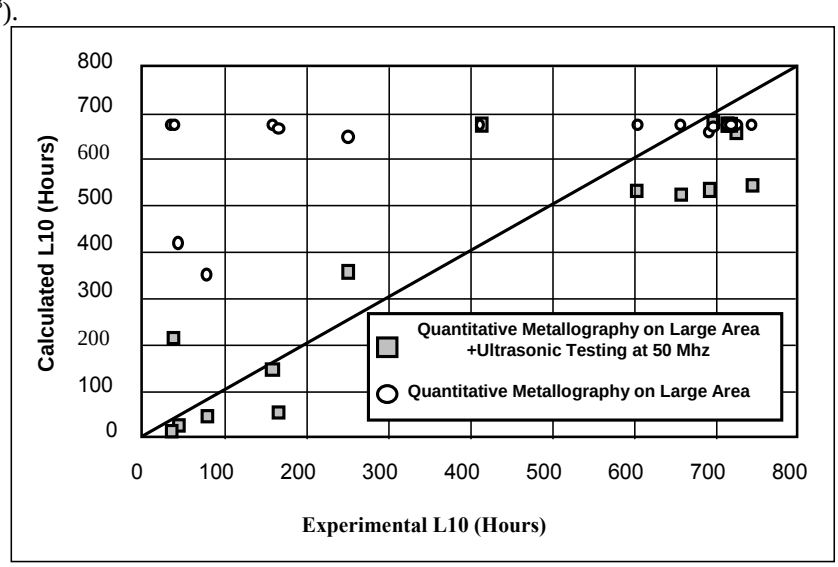


Figure 7 – Flat Washer test (FB)– Comparison of L_{10} fatigue lives measured and calculated from inclusion distributions

This model was validated on fatigue Flat Washer test for a wide range of cleanliness. Figure 7 shows, as an example, that L_{10} fatigue lives (10 % damage of the whole population) calculated from the inclusion distribution with this model are in good agreement with those experimentally measured for a wide range of durations (L_{10} ranging from 20 up to 800 hours).
Thus, this tool appears as an efficient tool for the steelmaker, because it allows to master its steel production, and to guarantee its in service properties, and not only as an empirical cleanliness index.

5 STEELS FOR COMPONENTS WORKING IN THE VERY HIGH CYCLE DOMAIN (10^{10} CYCLES)

Finally, we would like to briefly present first results obtained in the gigacyclique fatigue domain (10^{10} cycles = order of magnitude of the number of cycles applied to engine components during their total life). The table 6 shows that, in numerous cases, the fatigue limit classically determined at 10^7 cycles is not conservative, and that all the materials are not equivalent. These first results were also compared by using the ASHBY [8] approach, estimating the possible performance for a given weight (higher indexes give the best solutions). To summarize, table 6 shows that the steel constitutes a very good compromise.

Table 6 - Order of magnitude of the compared performances of various materials in gigacyclic fatigue, with indices proposed by ASHBY [7] (100 base : martensitic steel UTS ≅ 1 000 MPa)

Material	UTS (MPa)	σ_d / UTS 10^{10} cycles	σ_d decreasing betw. 10^7 and 10^{10} cycles	ASHBY Index Tensile (relative)	ASHBY Index Torsion (relative)
Cast Aluminium	220	≅ 0,3	≅ 25 %	≅ 50	≅ 80 - 110
Cast iron	800	≅ 0,35	≅ 10 %	≅ 60	≅ 80 - 110
Martensitic Steel	**1 000**	**≅ 0,5**	**≅ 2 %**	**100 (base)**	**100 (base)**
Spring Steel	1 700	≅ 0,45	≅ 5 %	≅ 130	≅ 120
Bearing Steel	≅ 2 500	≅ 0,4	≅ 10 %	≅ 240	≅ 160

6 CONCLUSION

This brief overview on engineering steels has pointed out all their potentialities, and their capacity of adaptation to severe and different conditions encountered in the main critical parts of an engine. It was also shown how, through a good knowledge of the damage mechanisms of each component, the (steel grade + cleanliness + heat treatments or surface treatments) can be optimised, by using the support provided by simple and representative fatigue tests. Obviously, all these developments can only be achieved through a close collaboration with customers, who are the only one able to well know the in-service conditions of the different components.

7 REFERENCE

1. H. Kitagawa, S. Takahashi – Proc. 2nd Int. Conf. on behaviour of materials – Boston – pp. 627-631 (1976)
2. Y. Murakami, H. Usuki, "Quantitative evaluation of effect of non-metallic inclusions on fatigue strength of high strength steels – A fatigue limit evaluation based on statistic of extreme values of inclusion size", *Int. Journal. of Fatigue*, vol 5 , pp. 299-307 (1989)
3. J.M. Jachmich, G. Baudry, D. Forest, "Tenue en service des bielles. Influence de la peau de forge", *Revue Traitement Thermique*, N° 341, pp. 38-43 (Aout-Sept 2002)
4. S. Beretta, A. Blarazin, M. Endo, T. Guinti, Y. Murakami, "Defect tolerant design of automotive components", *International Journal of Fatigue*, Vol 19, N°4, p.319-333 (1997)
5. P. Daguier, "Analyse quantitative des états de surface après fatigue de contact des aciers de pignonnerie", Journée de printemps 2005,
6. R. Fougères, G. Lormand, A. Vincent, G. Dudragne, D. Girodin, G. Baudry, P. Daguier, "A new physically based model for predicting the fatigue life distribution of bearing", ASTM STP 1419, pp.197-212 (2002)
7. G. Auclair, F. Ruby-Meyer, R. Meilland, P. Rocabois, "Cleanliness assessment : a critical review and a real need to predict rolling contact fatigue behaviour", ASTM STP 1327, pp 39-54 (1998)
8. M.F. Ashby – Choix des matériaux en conception mécanique – DUNOD (2000)

Fatigue Design of Web Stiffened Cruciform Connections

Inge Lotsberg, Trond Arve Rundhaug, Harald Thorkildsen and Åge Bøe

Det Norske Veritas
Oslo
Norway

Abstract Fatigue design of dynamic loaded ship structures is normally based on finite element analysis using shell elements where the welds are not included in the analysis models. FE-analyses of a fatigue tested hopper knuckle type specimen were performed for calibration of analysis methodology in a joint industry project. The test specimen was analysed using 20-node solid elements, 4-node and 8-noded shell elements. The solid element model included the weld leg. In the present work the FE-analyses were extended to that of other geometries at web stiffened cruciform joints such as typical found at hopper connections, at stringer heels and at joints connecting deck structures to vertical members in ship structures. Based on the result from these analyses a methodology for derivation of hot spot stress at welded connections using shell finite element models was developed. The basis for this procedure is presented in this paper.

1 INTRODUCTION

Fatigue design of dynamic loaded ship structures is normally based on finite element analysis using shell elements where the welds are not included in the model, ref./1/. A joint industry project on fatigue capacity of floating production vessels (FPSO Fatigue Capacity JIP) was carried out in two phases from 1998 to 2003, refs. /2-9/. Fatigue analysis of fatigue tested side longitudinals using FE models with shell elements showed in general good agreement with measured stress where the hot spot is a result of global force flow through the structural details. It was found to be less good for details where the hot spot stress is a result of local behaviour such as at bracket connections between transverse frames and bulb longitudinals. In this project also a number of fatigue tests of hopper corner connections were performed. FE-analyses were performed for calibration of analysis methodology. The test specimen was analysed using 20-node solid elements, 4-node and 8-noded shell elements. The solid element model included the weld leg.

The current method for hot spot stress derivation of stiffened cruciform joints given in DNV Classification Note 30.7 “Fatigue Assessment of Ship Structures” is considered to be conservative. Results from the FPSO Fatigue Capacity project showed that an effective stress can be obtained by reducing the plate bending stress, see section 2. In the present work the FE-analyses were extended to that of other connections at stiffened cruciform joints such as typical found at hopper connections, at stringer heels and at joints connecting deck structures to vertical supports in ship structures, ref. Figure 1. The present project is performed in order to document a procedure for derivation of hot spot stress at such joints using shell elements.

2 PROCEDURE FOR DERIVATION OF EFFECTIVE HOT SPOT STRESS

At hot spots with significant plate bending one might derive an effective hot spot stress for fatigue assessment based on the following equation:

$$\Delta\sigma_{e,spot} = \Delta\sigma_{a,spot} + 0.60\,\Delta\sigma_{b,spot} \qquad (1)$$

where

$\Delta\sigma_{a,spot}$ = membrane stress

$\Delta\sigma_{b,spot}$ = bending stress

The reason for a reduction factor on the bending stress is load shedding effect during crack growth. The effect is limited to areas with a localised stress concentration, which occurs for example at a hopper corner. However, in a case where the stress variation along the weld is small, the difference in fatigue life between axial loading and pure

bending is much smaller. Therefore it should be noted that it is not correct to generally reduce the bending part of the stress to 60 percent. This has to be restricted to cases with a pronounced stress concentration.
This procedure is based on crack growth analysis using fracture mechanics as shown in Figure 2 and Figure 3, ref. /9/. Figure 2 shows crack growth curves through the thickness of the flange for different stress gradients having the same hot spot stress. Semi-elliptic crack growth is assumed as indicated in Figure 2. The procedure is also supported by fatigue tests subjected to bending in ref. /10/. The S-N curve for specimens subjected to pure membrane stress is at a level of 60 % of that of specimens subjected to bending load. Thus equation (1) represents physical behaviour and applies to members where the stress can be divided into membrane and bending based on finite element analyses using either three-dimensional elements or shell elements.

3 FINITE ELEMENT ANALYSIS

2.1 Models

The present study has covered hot spot stress related to a 135 degrees, 120 degrees and 90 degrees stiffened cruciform connection. The FE model included 20-nodes solid elements and 8-nodes shell elements. The solid model included also a weld created by 15-nodes solid elements. The analyses cover variation of weld leg size (without weld leg, weld leg equal to half plate thickness, t/2, and weld leg equal to plate thickness, t, and extrapolation of calculated stresses to the weld toe. The weld was modelled with a radius and a smooth weld toe. The shell element model was made without any weld.

A hopper knuckle model that was tested by HHI in Korea and in the laboratories of DNV was selected for structural analysis. The critical weld toe is located at the transition from the beam consisting of 10 mm thick flange (simulating the tankers inner bottom plate) and plates simulating the sloped hopper plate, Figure 2. The DNV Sesam programs were used for these analyses, refs./11/. The test specimen from the FPSO Fatigue Capacity project contained eccentricity and the target hot spot stress values used for calibration are derived for this geometry. Therefore also one of the finite element models included the same eccentricity. Thus the finite element models for the 135 degree connection were created with and without eccentricity. The main emphasis of a finite element analysis is to make a model giving stresses with sufficient accuracy at the hot spot region, ref. Figure 4. The finite element model consist of two types 3D solid elements, isoparametric triangular prisms, used for modelling of welds, and isoparametric hexagons for the remaining structure. Fillet welds below the upper flange (below innerbottom/tanktop) has been included in the model. The welded connection is typically modelled by use of two separate superelements in order to connect the plates through the fillet weld only.

2.2 Derivation of stress

Element stresses in the solid FE models are derived at the gaussian integration points (result points). The Gaussian stresses are manually extrapolated to the surface and further interpolated within the element for derivation of stress at the read out points. The 8 node shell element has 4 surface result points in the upper (top) surface (at the Gaussian points). These stresses are extrapolated to nodes in the upper top surface from the result points. The element stresses in the middle top surface point for the two closest elements to the system line corresponding to a distance t/2 and 3t/2 from the system line are used directly as extrapolation points to calculate the hot spot stress. Results for 135 degrees hopper knuckle based on 20-nodes solid model without weld leg and with weld leg = t/2 and t, is compared with results based on 8-nodes shell elements. The stresses at positions 10 mm and 20 mm away from weld toes/intersection line is derived by fitting a second order function through the values derived at 5, 15 and 25 mm. The hot spot stresses from the solid models were derived from linear extrapolation of stresses at t/2 and 3t/2 from the weld toe. These hot spot stresses are used as basis for derivation of target hot spot stress that is used for calibration of analysis methodology.

2.3 Analyses results

2.3.1 Cruciform connection 135 deg. with eccentricity (- 7 mm)

Calculated results for cruciform connection 135 deg. with eccentricity are shown in Figure 5. From this figure it seen that approximately the same stresses at the hot spot region is derived using solid element model (20 node elements) as from shell element model (8-node elements). From this figure it is also seen that addition of weld material increases slightly the stress distribution in front of the weld as compared to calculated stress using a FE model where the weld is not included. Thus, if some additional weld is added, and if the stresses are read out at the relevant weld toe position, they should be increased by a factor corresponding to this stress increase. The target hot spot surface stress value from fatigue tests is 1.64 when linked to a design hot spot stress fatigue S-N curve that corresponds to 90 MPa at 2 mill cycles (Denoted FAT 90 by IIW, ref. /12/ and curve D in DNV-RP-C203, ref. /9/). From FE analyses

the target hot spot surface stress is somewhat larger, in the range 1.84-1.96. The calculated stress from the present three-dimensional analysis is 2.08. Then the stress is reduced by the factor 1.96/2.08 = 0.942 to get a target factor equal 1.96. The same factor is used for all the three-dimensional analyses for derivation of target values. Based on an assessment of this together with the performed analyses the target values in Table 1 are derived. It is assumed that there is a relative difference in the target values as derived from the three-dimensional models where the actual weld geometry is included.

2.3.2 *Cruciform connection 135 deg. without eccentricity*

Calculated stresses for cruciform connection 135 deg. without eccentricity are shown in Figure 6. From this figure it is seen that approximately the same stresses at the hot spot region is derived using solid element model (20 node elements) as from shell element model (8-node elements). From this figure it is also seen that addition of weld material increases slightly the stress distribution in front of the weld as compared to calculated stress using a FE model where the weld is not included. The stress distribution at the hot spot area for the geometry without additional weld is shown in Figure 7. The stress distribution at the hot spot area for the geometry with additional weld equal t is shown in Figure 8. From these figures it is seen that it is the local bending that is the main contribution to the stress increase at the hot spot. This bending stress is located within an area of 1.5 t from the weld toe. By adding weld it is seen that the bending stress is moved to the right in Figure 8 as compared with that of bending stress in Figure 7. However, the absolute value of the bending stress is also slightly reduced by addition of a fillet weld at the hot spot. The target hot spot stresses from the three-dimensional analyses are presented Table 1.

2.3.3 *Cruciform connection 120 deg. without eccentricity*

Calculated results for cruciform connection 120 deg. without eccentricity are shown in Figure 9. It seen that approximately the same stresses at the hot spot region is derived using solid element model (20 node elements) as from shell element model (8-node elements). The result for the solid model with weld leg t, shows slightly higher stress than for the other.

2.3.4 *Cruciform connection 90 deg. without eccentricity*

Finite element model for 90 degree web stiffened cruciform connection with weld leg length equal the thickness is shown in Figure 10. The calculated results for this model are shown in Figure 11. From this figure it is seen that approximately the same stresses at the hot spot region is derived using solid element model (20 node elements) as from shell element model (8-node elements). The stress distribution at the hot spot area for the geometry without additional weld is shown in Figure 12. The stress distribution at the hot spot area for the geometry with additional weld equal t is shown in Figure 13. From these figures it is seen that it is the local bending that is the main contribution to the stress increase at the hot spot. This bending stress is located within an area of one thickness from the weld toe. By adding weld it is seen that the bending stress is moved to the right in Figure 13 as compared with that of bending stress in Figure 12. However, the absolute value of the bending stress is also slightly reduced by addition of a fillet weld at the hot spot. Target values for different weld length are assessed as shown in Table 1. Here we do not have target values from fatigue tests or other FE analysis. However, it is assumed that the same conservatism is included for this detail without any weld present as for the 135^o hopper connection. Thus the same procedure is used to derive target values. This gives target values for weld size t/2 and t as shown in Table 1.

Table I. Target hot spot stresses for different geometries

Geometry	Weld leg length x_{wt}		
	0	t/2	t
135 (with eccentricity)	1.96	1.62	1.42
135 (without eccentricity)	2.15	1.66	1.47
120 (without eccentricity)	2.37	1.85	1.72
90 (with eccentricity)	2.42	2.05	1.87
90 (without eccentricity)	2.56	2.07	1.88

2.3.5 *Discussion of numerical results*

The methodology and target hot spot stress values in this investigation were derived from FE analysis and fatigue testing of a hopper corner connection (in this study denoted cruciform joint with 135^o with no weld, but with eccentricity. There is a weld, but no significant fillet weld from the hopper plate into the bottom plate). Then target

values were derived for geometries without eccentricities as listed in Table 1. FE-analysis without fillet weld and with fillet welds equal t/2 and t were performed (t = thickness of bottom plate). Based on this an assessment of read out points from shell FE models, where the weld is not included, has been made. It is suggested to read out stresses from a shell finite element model at read out points shifted away from the intersection line for derivation of surface hot spot stress by the following value

$$x_{shift} = \frac{t_1}{2} + x_{wt} \tag{2}$$

where t_1 = plate thickness of plate welded to the plate number 1 in Figure 10 and x_{wt} = additional fillet weld leg length. ($t_1 = t_2 = 10$ mm is used for the calibration).
The stress at the shift position is denoted $\sigma(x_{shift})$. Then the surface hot spot stress is increased by a factor to account for the local bending due to presence of a weld by the following equation

$$\sigma_{hot\ spot} = \sigma(x_{shift}) * \beta \tag{3}$$

where

$$\beta = \gamma + \alpha_1 \frac{x_{wt}}{t_1} + \alpha_2 \left(\frac{x_{wt}}{t_1} \right)^2 \tag{4}$$

where t_1 is plate thickness at considered hot spot region.

The factor β is shown in Figure 14. This figure is derived for the different cruciform connections without eccentricity.

The ratio of bending stress to the total stress in the shell finite element model relative to that of the three-dimensional model where the weld toe is included at different positions is assessed. It is found that this ratio is similar in the shell finite element model as in the three-dimensional model. Thus, it is also considered acceptable to reduce the local bending stress derived from a FE analysis using shell elements at hot spots of this type by a factor 0.6 before an equivalent stress is entered into the S-N curve as explained in section 2. It is observed that some negative eccentricity is beneficial for the fatigue life as calculated hot spot stress is less with eccentricity included as compared without eccentricity for the 135 degree joint. The difference was found to be less for the 90 degree joint.

4 PROCEDURE FOR FE ANALYSIS USING SHELL ELEMENT MODELS AND HOT SPOT S-N CURVE D (FAT 90)

Based on an assessment of the derived numerical results it is found acceptable to use results from finite element analysis where the weld is not included in the model also for read out of hot spot stress at a position of the actual weld toe when a fillet weld is added. From the analyses with three-dimensional solid elements it is seen that the fillet weld increase the local bending stress at the weld toe area. It is observed that the local bending stress is moved to be in front of the new weld toe. However, its absolute value is reduced by addition of a fillet. The net result is a slight increase of stress in front of the new weld toe. This increase in stress should be accounted for by a correction factor as expressed by equation (4).

Based on the performed work it is suggested to read out stress from a shell finite element model at read out points shifted away from the intersection line for derivation of surface hot spot as expressed by equation (2). This stress is derived directly from the analysis (without any extrapolation of stresses). The surface stress (including membrane and bending stress) is denoted $\sigma_{surface}(x_{shift})$. The membrane stress is denoted $\sigma_{membrane}(x_{shift})$ and $\sigma_{bending}(x_{shift})$. Then the hot spot stress is then derived as

$$\sigma_{hot\ spot} = \left(\sigma_{membrane}(x_{shift}) + \sigma_{bending}(x_{shift}) * 0.60 \right) * \beta \tag{5}$$

where

$$\sigma_{bending}(x_{shift}) = \sigma_{surface}(x_{shift}) - \sigma_{membrane}(x_{shift}) \quad (6)$$

For 135 ° connections a correction factor is derived as

$$\beta = 1.07 - 0.15\frac{x_{wt}}{t_1} + 0.22\left(\frac{x_{wt}}{t_1}\right)^2 \quad (7)$$

For 120 ° connections a correction factor is derived as

$$\beta = 1.09 - 0.16\frac{x_{wt}}{t_1} + 0.36\left(\frac{x_{wt}}{t_1}\right)^2 \quad (8)$$

For 90 ° connections a correction factor is derived as

$$\beta = 1.08 + 0.03\frac{x_{wt}}{t_1} + 0.26\left(\frac{x_{wt}}{t_1}\right)^2 \quad (9)$$

The β-factors are shown in Figure 14. The procedure is calibrated for $0 \leq x_{wt}/t_1 \leq 1.0$. The derived hot spot stress to be entered the D-curve (DNV-RP-C203) or FAT90 curve (IIW (2004)). The analysis procedure is illustrated in Figure 15.

5 CLOSURE

Fatigue design of dynamic loaded ship structures is normally based on finite element analysis using shell elements where the welds are not included in the analysis models. FE-analyses of a fatigue tested hopper knuckle type specimen were performed for calibration of analysis methodology in a joint industry project. The test specimen was analysed using 20-node solid elements, 4-node and 8-noded shell elements. The solid element model included the weld leg. In the present work the FE-analyses were extended to that of other geometries at web stiffened cruciform joints such as typical found at hopper connections, at stringer heels and at joints connecting deck structures to vertical members in ship structures. Based on the result from these analyses a methodology for derivation of hot spot stress at welded connections using shell finite element models has been developed as presented in section 4. The basis for this procedure is presented in this paper.

6 REFERENCES

1. CN 30.7 (2003) “Fatigue Assessment of Ship Structures”. DNV, Oslo.
2. Lotsberg, I. (2001). Overview of the FPSO Fatigue Capacity JIP. OMAE, Rio deJaneiro.
3. Fricke, W. (2001). “Recommended Hot Spot Analysis Procedure for Structural Details of FPSO’s and Ships Based on Round-Robin FE Analyses”. Proc. 11th ISOPE, Stavanger. Also International Journal of Offshore and Polar Engineering. Vol. 12, No. 1, March 2002.
4. Maddox, S. (2001). “Recommended Design S-N Curves for Fatigue Assessment of FPSOs”. Proc. 11th ISOPE, Stavanger.
5. Bergan, P. G., Lotsberg, I. (2004): “Advances in Fatigue Assessment of FPSOs”. OMAE-FPSO'04-0012, Int. Conf. Houston.
6. Lotsberg, I. (2004) “Recommended Methodology for Analysis of Structural Stress for Fatigue Assessment of Plated Structures”. OMAE-FPSO'04-0013, Int. Conf. Houston.
7. Storsul, R., Landet, E. and Lotsberg, I. (2004) “Calculated and Measured Stress at Welded Connections between Side Longitudinals and Transverse Frames in Ship Shaped Structures”. OMAE-FPSO'04-0017, Int. Conf. Houston.
8. Kim, W.S. and Lotsberg, I.(2004) “Fatigue Test Data for Welded Connections in Ship Shaped Structures” OMAE-FPSO'04-0018, Int. Conf. Houston.

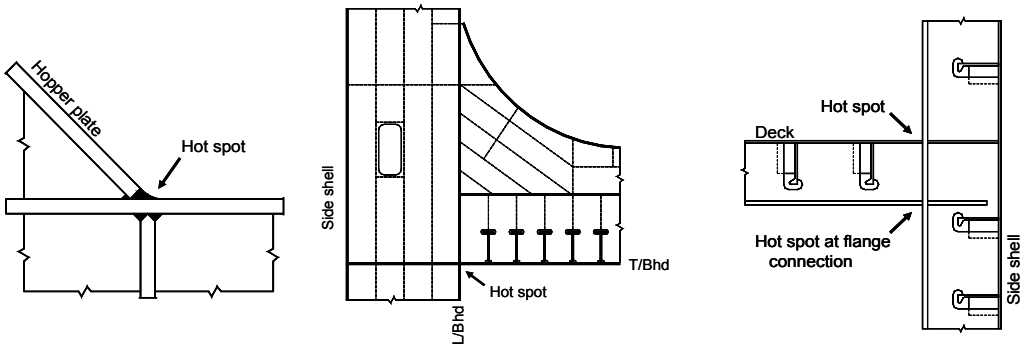
9. Lotsberg, I. and Sigurdsson, G. (2004) "Hot Spot S-N Curve for Fatigue Analysis of Plated Structures". OMAE-FPSO'04-0014, Int. Conf. Houston.

10. Kang, S. W., Kim, W. S. and Paik, Y. M. (2002), "Fatigue Strength of Fillet Welded Steel Structure under Out-of-Plane Bending", International Welding / Joining Conference – Korea.

11. Sesam User Manuals, DNV, Oslo. 2004.

12. Hobbacher, A. 2004. IIW document XII-1965-03/XV-1127-03 "Recommendations for Fatigue Design of Welded joints and Components".

13. DNV- RP- C203 (2005) "Fatigue Analysis of Offshore Steel Structures".



a) Hopper knuckle in tanker, 135°

b) Heel of stringer in tanker, 90°

c) Connection between deck web frame and side web frame in vehicle carrier, 90°

Figure 1. Examples of web stiffened cruciform connections

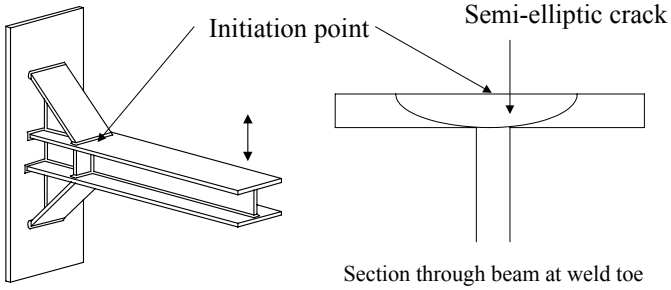


Figure 2. Crack growth analysis of hopper corner

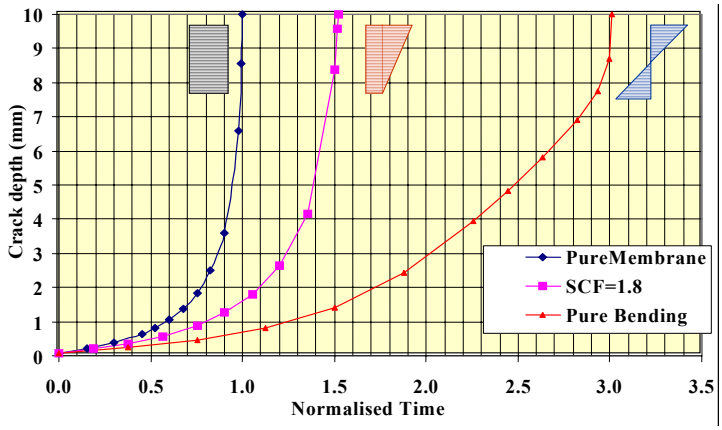
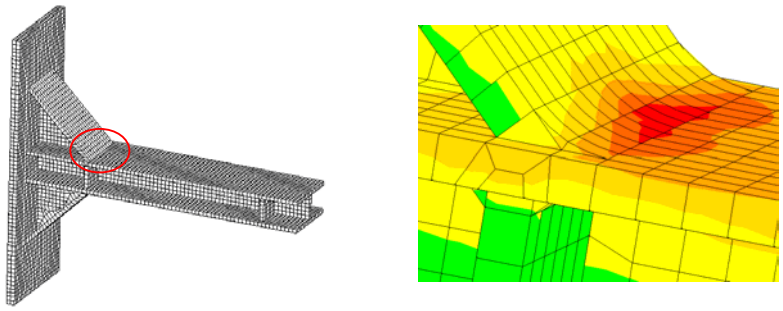


Figure 3. Crack growth curves for same hot spot stress with different stress gradients through flange



Hot spot region Solid model with t-size weld leg

Figure 4. Solid model of tested specimen

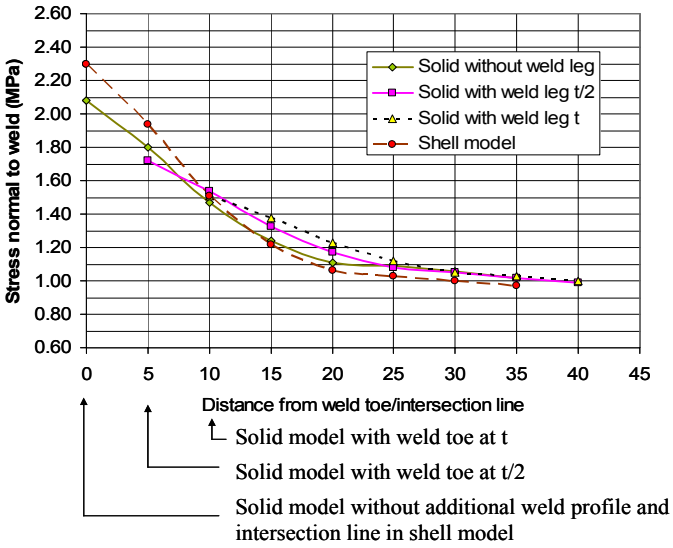


Figure 5. Surface stress at hot spot region of 135° model with eccentricity

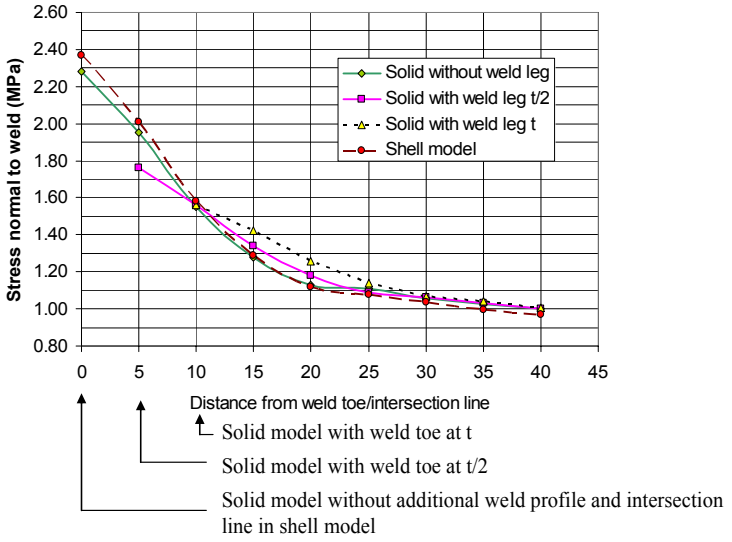


Figure 6. Surface stress at hot spot region of 135° model without eccentricity

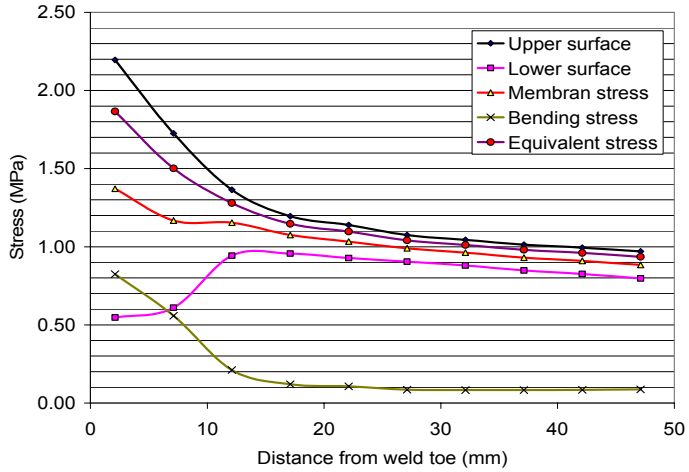


Figure 7. Stress at hot spot region of 135° model without eccentricity and additional weld

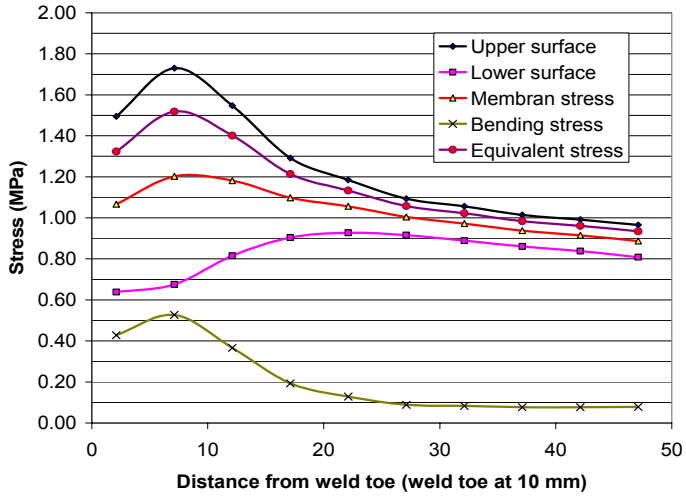


Figure 8. Stress at hot spot region of 135° model without eccentricity and with weld leg t

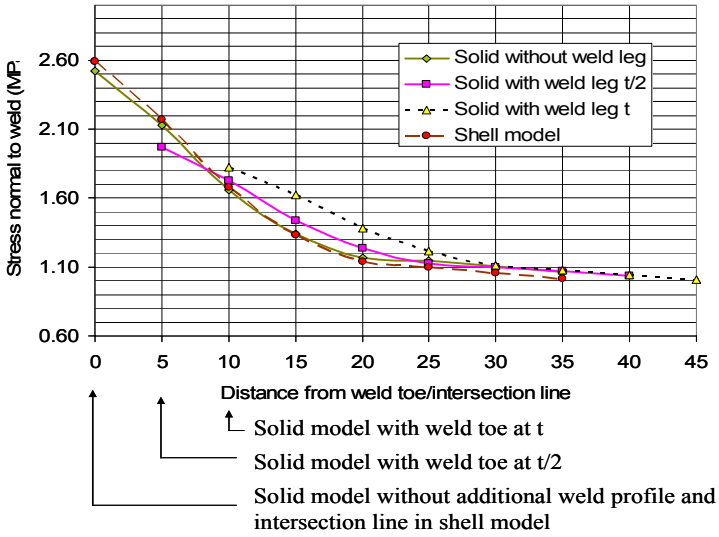


Figure 9. Surface stress at hot spot region of 120° model without eccentricity

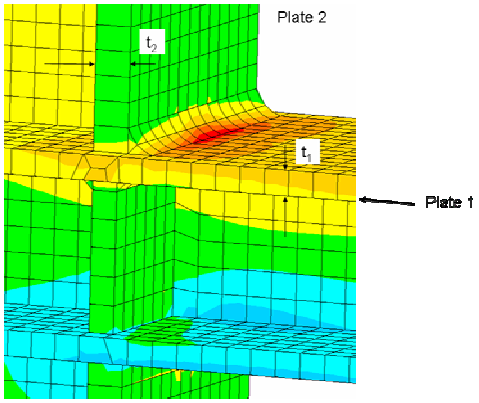


Figure 10. Finite element model of 90 degree connection with weld leg equal t

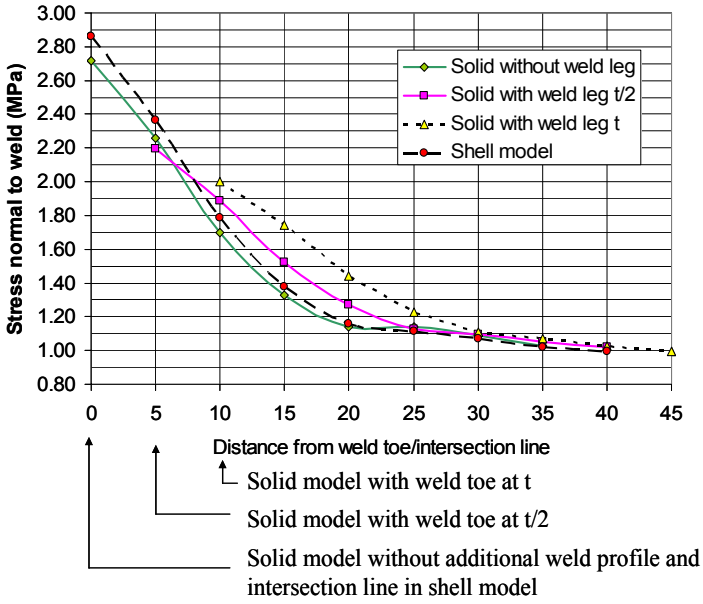


Figure 11. Surface stress at hot spot region of 90° model without eccentricity

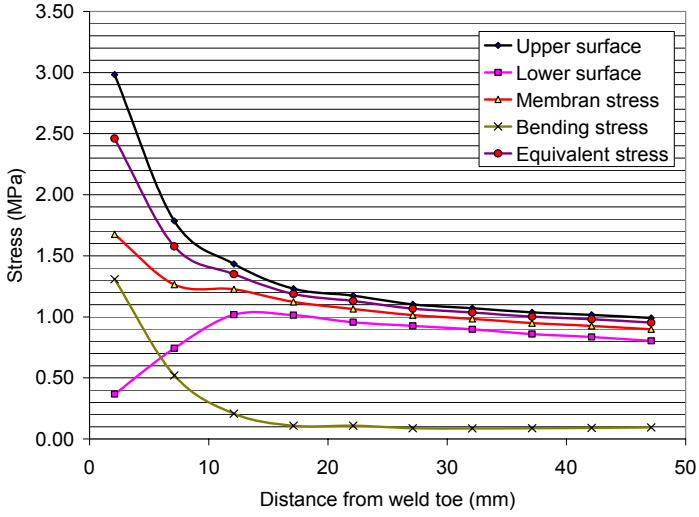


Figure 12. Stress at hot spot region of 90° model without eccentricity and additional weld

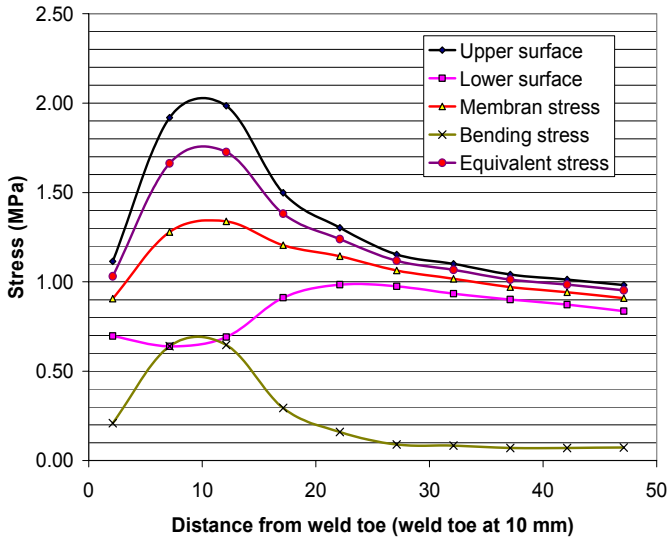


Figure 13. Stress at hot spot region of 90° model without eccentricity and with weld leg t

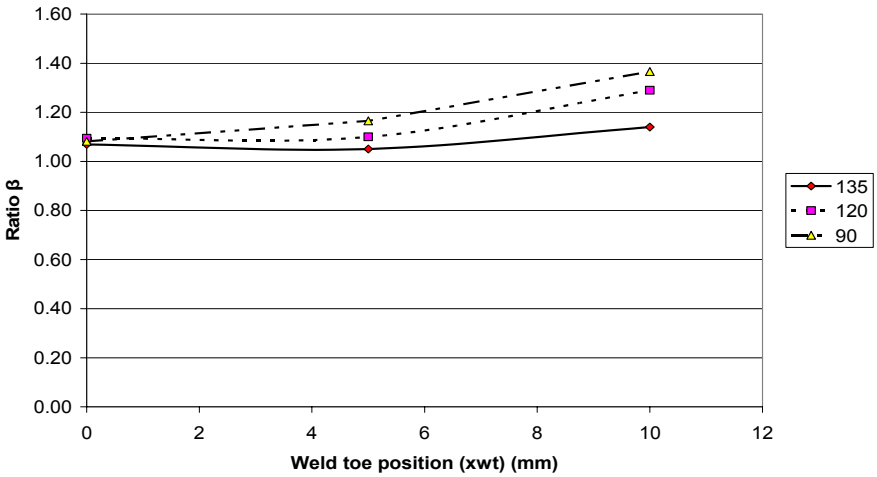


Figure 14. Ratio β as function of weld toe position

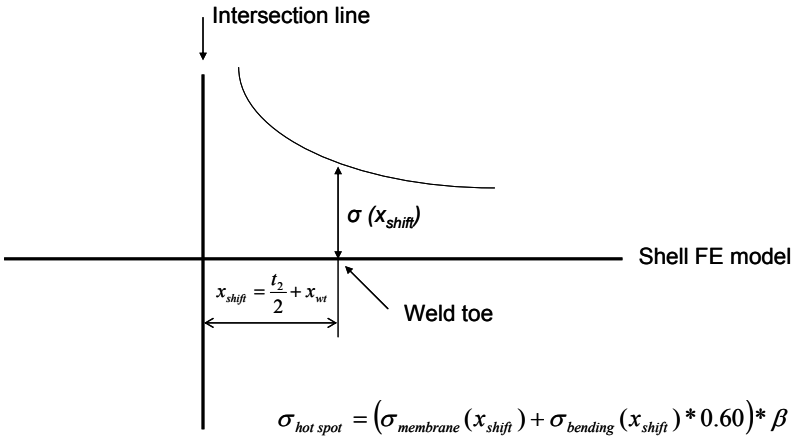


Figure 15. Illustration of procedure for derivation of hot spot stress using shell finite element model

Determination of the limit of endurance of a composite with infra-red thermography

Lotfi Toubal, Bernard Lorrain, Moussa Karama

LGP, CMAO, Ecole Nationale d'Ingénieurs de Tarbes
47, Avenue d'Azereix
BP 1629, 65016 Tarbes, France, moussa@enit.fr

Abstract : A new method of determination of the limit of endurance of a composite by an infrared camera measurement is proposed. Fatigue tests performed on one specimen with load level gradually increased, alloy to make the analogy between the local heating and the damage. The results are compared with the Wöhler's curves obtained with a great number of specimens.

1 INTRODUCTION

The dimensioning of the mechanical structures depends on nature of the stresses to which they are subjected. The loading can be constant or, and it is the most general case, variable versus time. We can quote for example the automobile parts of suspension or the wings of a plane whose strains in service vary. The phenomenon of fatigue affects in fact all the objects which surround us and which a repeated use ends up deteriorating. The number of repetitions and the level of the loading are determining parameters as for the fatigue life of these elements, i.e. the period during which they provide their function correctly. The essential reason for which mechanical engineers hesitate to carry out fatigue tests is their important cost. This is due to the particularly dispersive character of the phenomenon of fatigue which forces to perform more tests and the duration itself of the tests. This great dispersion imposes, for each type of experimental checking in fatigue, of many tests in order to obtain representative results. In the aim of quantify the fatigue life of material, an infra-red camera has been used to follow-up the variation in the temperature during the fatigue test and then evaluate the sample damage according to the number of cycle. An approach of the fatigue damage mechanisms based on the treatment of images of dissipation is proposed. The limit of endurance obtained by energy methods is presented [1].

The material of our study is realized by the Turbomeca company (Bordes, 64), and is employed for its high mechanical properties in the design of turbomotors air intake. It is a laminate obtained by stacking carbon/epoxy woven layers of satin 5 type. The composite plates are woven with ± 45°, they are 250 mm length and 25 mm width with a 5 mm hole in the center of the sample, in accordance with standard NF T57-301.

2 EXPERIMENTAL STUDY

2.1 Experimental device

The fatigue tests are carried out on a servo-hydraulic machine (figure 1) equipped with a force sensor of 30 kN. The longitudinal strains are measured using a 25 mm gauge length extensometer. The power station of acquisition ensures the data processing of the sensor of force, the extensometer and the encoder position. The data are recorded on the PC via the driving software. The fatigue tests are carried out in stress control with 0.1 load ratio. All the samples are submitted to fatigue stresses at a 10 Hz frequency. The total number of cycles is limited to 10^6 cycles. An infra-red camera is used to measure the variation and the change of the temperature during the fatigue tests. In effect, this measurement technique of temperature uses the infra-red radiation emitted naturally by the objects since their temperature is higher than the absolute zero (0 K). The analysis is consequently done without contact what is one of the requirements to measure without disturbance of so weak variations in temperature. The other decisive advantage is the access to a surface cartography. Thus all the points on the surface of an object can be measured simultaneously. The thermal resolution of our camera (difference in temperature equivalent to the noise) is about 20 mK with 30°C.

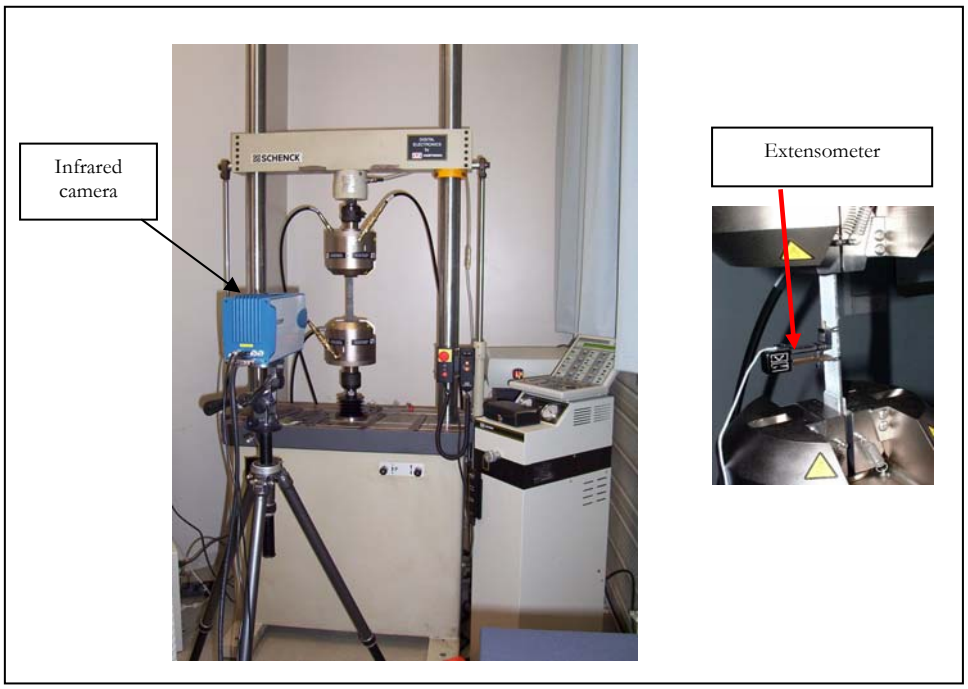


Figure 1. Testing device

The fatigue behaviour of materials is determined by cyclic tests. These tests are classified in function of stress applied (traction, bending, compression, torsion, and combination of several types) and signal (square, sinusoidal, triangular). When the stress type and the signal are chosen, the concepts of constraints ratio R ($R = \sigma_{min}/\sigma_{max}$) and of median constraint (σ_{moy}) are introduced in order to differentiate the various tests. In the mechanical characterization of the structures, the fatigue tests allow to obtain several characteristics (limit stress, limit of endurance, fatigue life, endurance ratio). In this study our interest is the determination of the limit of endurance. This is the constrain for which it is noted 50% of rupture after a finished number of cycles (usually 10^7 cycles).

2.2 Analysis of damaging with infrared thermography

2.2.1 Infrared Thermography

Infrared thermography is a measurement technique which allows obtaining the temperature distribution on the surface of the examined object. Thermography proceeds by decoding, using an adapted detector, "temperature" information resulting from the infra-red radiation emitted by any object. The principal advantage of infra-red thermography is its non intrusive character. The deformation of solid materials is always accompanied by heat appearance. When the material is submitted to strains or when it is damaged and fissured, a part of energy necessary to the starting and the propagation of the damage is transformed into heat [2]. This technique is used for its speed and its simplicity of setting in process. The principal applications concern several sectors like engineering automotive, or aeronautical and more recently the rapid determination of stress limit and the localization of zone of damage [3].

2.2.2 Measure of thermal dissipation

This method of thermographic analysis is rather based on the measure of the energy dissipated because of degradation of material than on the measure of the quantity of released total heat. The dissipated energy becomes from the irreversible structural modifications of the sample during a fatigue test (plasticity, rupture of the inter atomic connections) [4]. Thus released heat due to the thermo elastic coupling is filtered and measurement becomes more exact [1]. The evolution of thermal dissipation is schematized on figure 2. This test is performed at σ_{max} = 60 % of the limit stress.

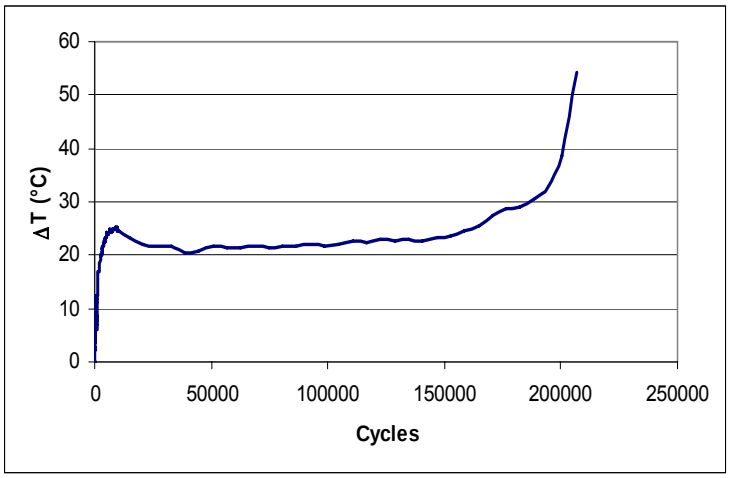


Figure 2. Infrared measurement of temperature evolution during fatigue test

Three different phases can be distinguished [1], a first phase no more than 20 % of the fatigue life and which shows the behaviour of the matrix and the appearance of transverse cracks. A second phase after 5000 cycles where the temperature seems stabilized. In this part of the test the damage evolves little but continuously. This related the multiplication and the propagation of the transverse cracks in the matrix until reaching the critical density of cracks. And then a third phase where the damage grows quickly is visible. That corresponds to the rupture of fibres and the complete delamination of the composite.

3 DETERMINATION OF LIMIT OF ENDURANCE USING INFRA RED PROCESSING

To determine the limit of endurance of material, we performed tests for several load levels. For each test, we measured the stabilized temperature. that corresponds to the average temperature in the neighbourhoods of the hole, i.e. in the most stressed zone at the end of 10000 cycles. Thus we are located in the 2nd phase of damage of our material. For the tests not exceeding 10^4 cycles, the phase of stabilization is no-existent so we consider as reference the point which corresponds to the appearance of the third phase of material damaging. We take for that the inflection of the temperature curve.

We have let all the tests continue until the rupture of the test-tube or until the limit of 10^6 cycles to be able to plot a Wohler's curve. The different temperature curves for all the performed tests are presented on figure 3.

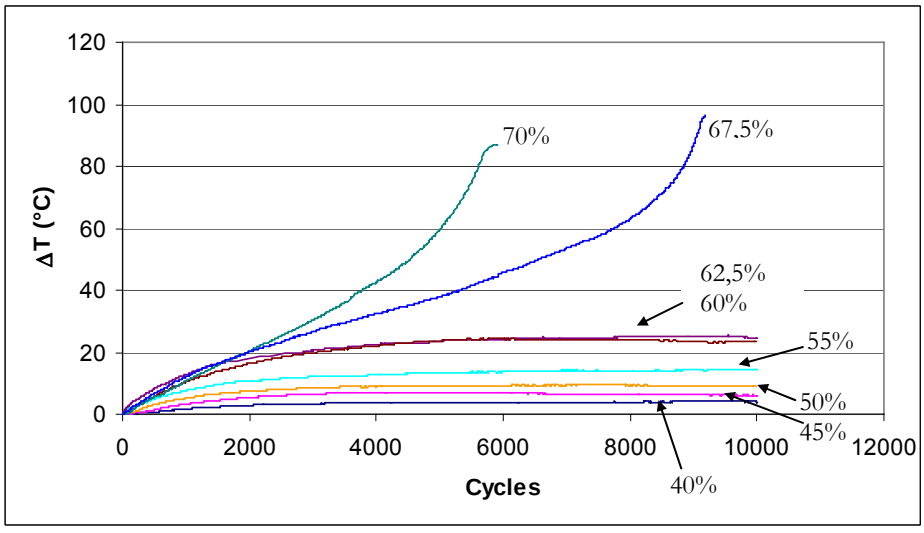


Figure 3. Determination of stabilized temperature for different loadings

By raising for each test the ΔT representative of the first damage, we can plot another curve. With this curve we can obtain an estimated value of the limit of endurance (figure 4).

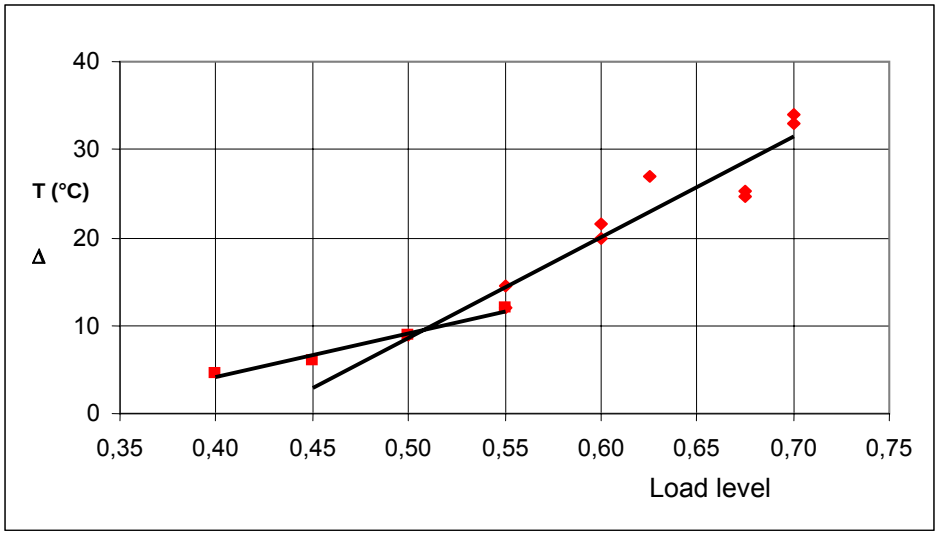


Figure 4. Limit of endurance determination by infrared thermography

The data of stabilized temperature for each load level can be approximated with several method. It is possible to approximate the data distribution by a polynomial function of which we can extract the asymptotes. The intersection of these asymptotes gives an outline of the limit of endurance.

In our case we have chosen to approximate the curve by two lines and the limit of endurance is defined by the intersection of the two segments. The result of this approach gives for our material a limit of endurance around 50 % of the load to rupture.

If we plot now a S-N curve (figure 5) for our material we can determine the limit of endurance we will call the mechanical limit.

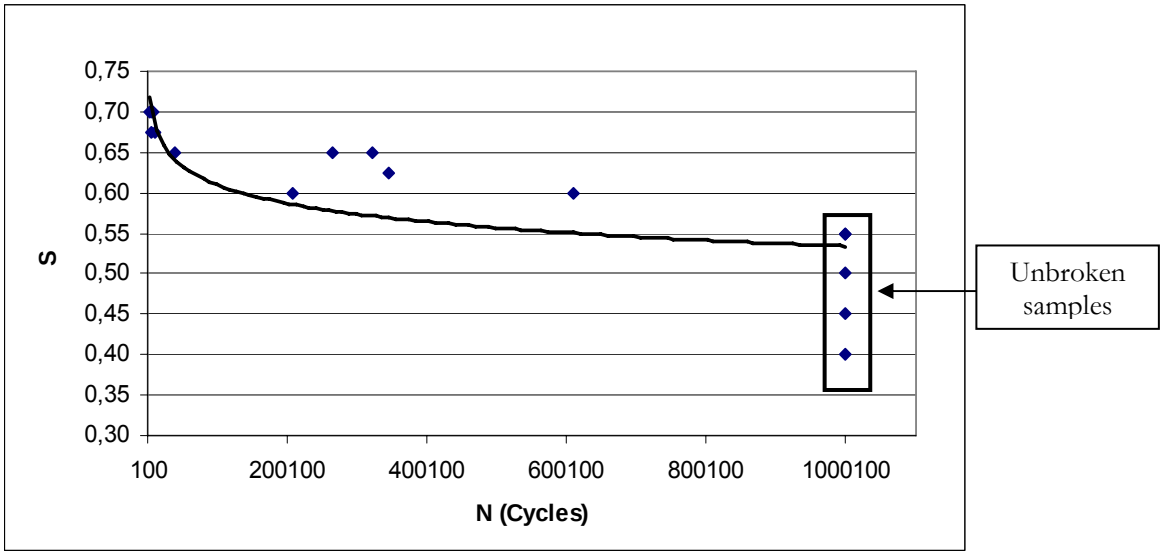


Figure 5. Limit of endurance determination by S-N curve

With the S-N curve reveals we obtain a limit of endurance around 53 % of the load with rupture. This "mechanical" limit of 53 % is very close to the "thermal" limit of 50 %.

We can say that the two methods of determination are very similar. It thus appears interesting to look further into the thermal approach which, contrary to the mechanical one, requires only the determination of the stages of stabilization and not the number of cycles with rupture. This approach must thus be faster.

4 INFRA RED DETERMINATION OF LIMIT OF ENDURANCE BY USING ONLY ONE SAMPLE

In a preoccupation with a saving of time and in order to minimize the number of samples, we planned to determine the limit of endurance of a test-tube by carrying out only one test. For that we decided to load our sample by stage successive of 10000 cycles. We estimate that with this number of cycles the sample temperature is stabilized. Then the load is increased at each stage (figure 6).

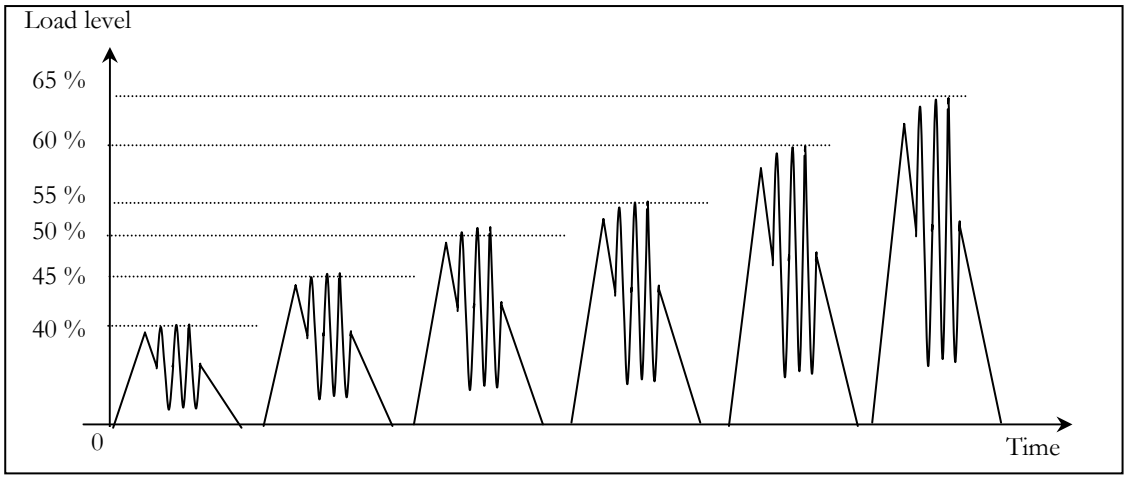


Figure 6. Testing process for one sample.

During the test, we measured the temperature of stabilization which corresponded to the temperature measured at the end of 10000 cycles. The tests not exceeding 10000 cycles, the temperature of stabilization is considered on the level of the inflection point of the temperature curve. The tests were carried out at a frequency of 10 Hz between 40 % and 65 % of the load to rupture.

For the change of load level the test is paused and the sample not dismounted. The statements of the temperature evolution for various loading level are presented on figure 7.

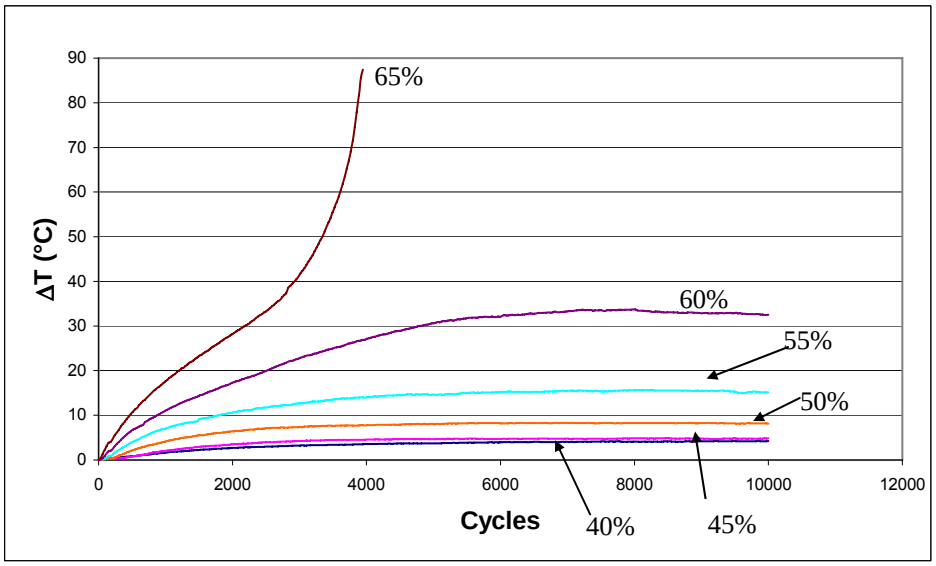


Figure 7. Determination of stabilized temperature for different loadings of the sample

We can already note that the curves obtained with only one sample are very similar to those obtained with seven samples (figure 3). So we can, from these statements, to take again the preceding step and to plot the curve which will enable us to obtain an estimate of the limit of endurance (figure 8).

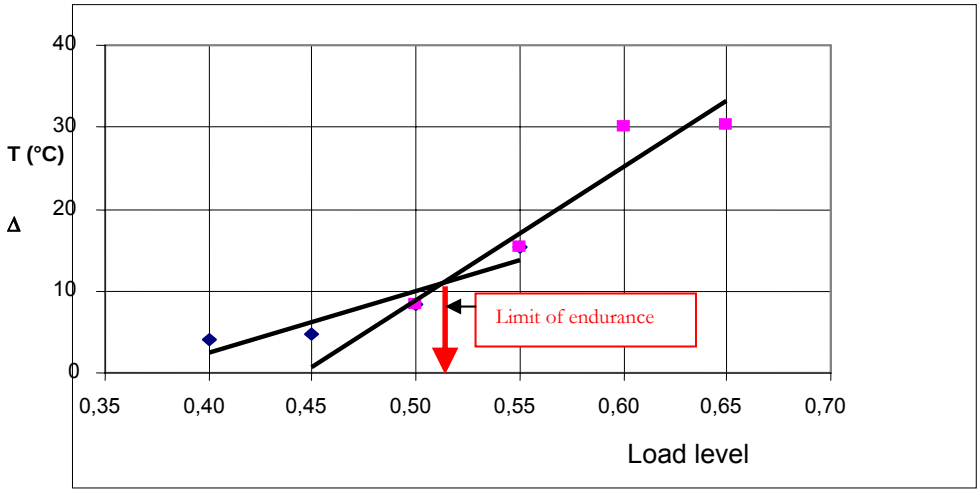


Figure 8. Limit of endurance determination with one sample

The results we obtain are very interesting. They show that starting from only one sample and using an infra-red camera a first estimate of the limit of endurance of a material can be given. The limit of endurance obtained by this method (51 %) is very close to the first two values; 53 % starting from the curve (SN) and 50 % with a sample for each load level. The use of this method allows a considerable profit in the time of the fatigue tests and the cost decreases in a considerable way

5 CONCLUSION

This study is intended to highlight the relation between the dissipation of heat and the damage of the composites. The various comparisons of the results show that infra-red thermography is a good means of measurement without contact to follow the damage of a composite. The changes of the temperatures correspond well to the evolutions of the damage of material, and this tool can now allow a rapid determination of the limit of endurance of material, by using only one small number of sample.

It could be now interesting to test our method with other materials, with other types of loading and with other frequencies of solicitation.

6 REFERENCES

[1] Lotfi Toubal, Approches analytique et expérimentale de l'endommagement par fatigue d'un composite carbone/époxy. *Thèse de doctorat*, Université Paul Sabatier, Toulouse 2004.

[2] A Chrysochoos, Infrared thermography, a potential tool for analysing the material behaviour. Mécanique & Industries 2002 - 3 – pp. 3-14.

[3] P Brémond, P Potet, Lock-In Thermography : A tool to analyse and locate thermo-mechanical mechanisms in materials and structures. Thermosense XXIII, April 2001.

[4] M.P Luong, Fatigue limit evaluation of metals using an infrared thermographic technique. Mechanics of Materials 1997 - 28 - pp. 155-163.

Fatigue tests on thin sheet materials

André GALTIER, Bastien WEBER

ARCELOR Research, Voie Romaine, BP 30320, 57283 Maizières les Metz, France

Abstract Fatigue modelling through the use of computer software requires a deeper and deeper knowledge of material behaviour. Some tests are well known and standardised since a long time but others need to be improved or even developed. In this paper, focus is done on the fatigue testing of thin sheet materials. Some problems encountered for strain controlled fatigue testing are presented and proposals are made to increase the reliability of the results. Furthermore, a new test for characterising sheet material under shear stress is presented. This test can be use to better fit multiaxial criteria for design of structural parts.

1 INTRODUCTION

Arcelor is one of the main steel producers of the world. Arcelor objective is to develop new grades in order to fulfil customer needs in terms of strength, weldability and formability. It is thus important to perform the better characterisation than possible in order to have all material properties needed by all customers.

Some of the characterisation tests are well known and standardised long time ago, but, due to software and modelling development more and more material properties are requested. That is why some of our activities consist in adapting mechanical testing procedures or apparatus to new steel grades or new demands.

This paper presents some recent progress in the fatigue behaviour field: the adaptation of the ISO standard to perform strain-life curves and the design of a fatigue test under shear loading.

2 PLASTIC FATIGUE

The main fatigue properties needed to asses the fatigue strength of structural parts are the Wöhler curve (or SN curve) and the Manson-Coffin curve (EN curve). While the first one is used for high cycle fatigue (over 100 000 cycles for steels), the second one is usually determined for low number of cycles. The table I contains the main differences between the 2 tests as recommended by ISO 12106 standard.

Table I- Differences between EN and SN curves

	SN curve	EN curve
Controlled parameter	Load	Strain
Cycles range	100 000 → ∞	100 → 100 000
Cycle shape	Sinus	Triangle
Speed	Frequency ≈ 30 Hz	Strain rate ≈ 5.10^{-3} s^{-1}

In order to simplify the testing procedure and to avoid the determination of two different curves, more and more designs are conducted with an EN approach whatever the number of cycles to failure. This approach simplifies damage accumulation calculation, and also databases.
To do so, two mains problems have then to be solved:

- Does the design of the specimen is suitable for both plastic and elastic field?
- What are the best testing conditions (frequency, shape of signal) that leads to a good compromise between cost and reliability.

2.1 Uniaxial fatigue specimen design

In the ISO 12106, dealing with fatigue testing under strain controlled condition, the recommended specimen geometry is given in figure 1.

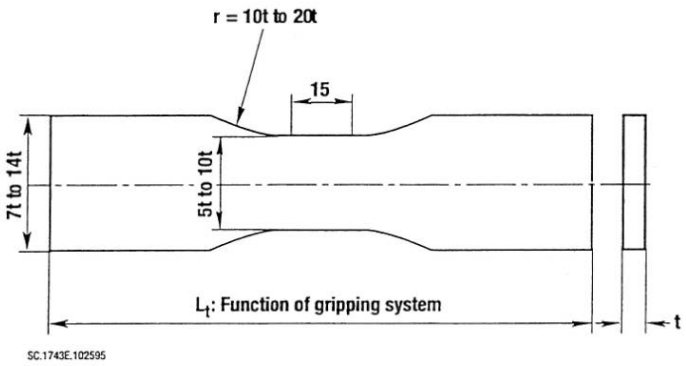


Figure 1. Strain controlled specimen given in ISO standard for flat products

This geometry has to be a compromise between the possible bucking (in compression phase) and the strain measurement. For sheet thickness below 3mm, an anti-buckling system is always needed.
Because this geometry is just a recommendation, many other geometries can be found in the literature and are strongly dependant of the testing laboratory. The main parameters are the radius (R), the testing length (l), and the calibrated width (w). It also has to be noted that the extensometer gage has also an influence on the measured strain. The figure 2, gives an example of the influence of the specimen geometry on the total EN curve of a mild steel.

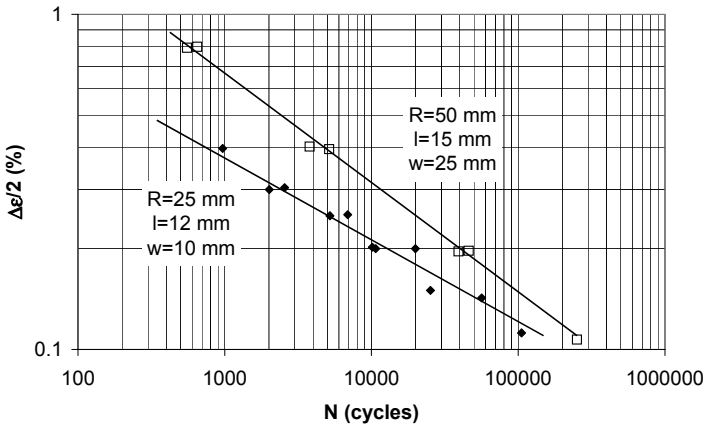


Figure 2. EN curve obtained on 2 different geometries

The origin of the specimen geometry influence can be easily illustrated by finite element calculations. The figure 3, corresponds to the longitudinal plastic strain in a specimen for a high load value.

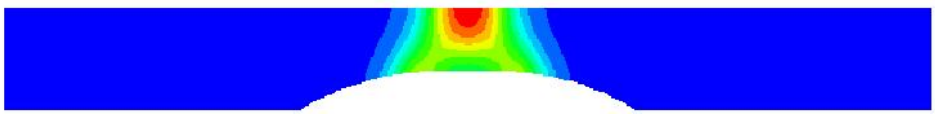


Figure 2. Plastic strain pattern (specimen geometry : R=50mm, l=15mm, w=25mm)

The measurement of the controlled strain is usually done with an extensometer placed on the specimen edge, and in the case presented in figure 2, the measured value is much more lower than the one in the center on the specimen. This strain concentration in the center of specimen is induced by the low ratio l/w and can be experimentally checked with strain gages. Always in the case of a mild steel, a difference of 65% exists between the value given by the extensometer and the center where the strain gage is glued (Figure 3).

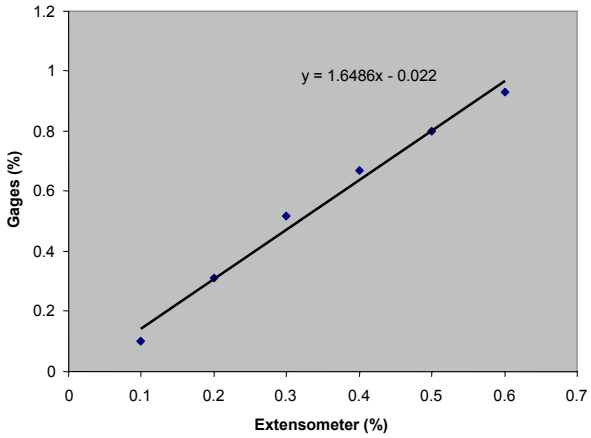


Figure 3. Relationship between the extensometer measurement and the strain gage value

A numerical study has been performed in order to obtain some guidelines regarding the specimen geometry. More than 100 calculations with different geometry parameters and material properties show that in order to not exceed 10% error of strain measurement, the following conditions have to be respected:

$l/w > -0.18\ r/w + 2.33$ and $r/w > 3$

with l the calibrated length, w the calibrated width and r the radius

The maximum errors are obtained on mild steels. For example, while this error is about 10% for deep drawing quality, it reaches 6% for Dualphase 600 grade steel.

The final aspect that has to be checked as regard as specimen geometry is the crack initiation location. What is important is to measure the strain that will lead to failure. This location, is very different according the load level:

- for low levels, close to the endurance limit, the maximum strain is observed at the radius toe,
- for higher levels (large plasticity), it has been seen in figure 2, that the maximum strain is at the center of the specimen.

This means that the tested material and the critical area is not the same all along the EN curve (plain or edge). Fortunately, in most cases the extensometer edges indent the specimen edge and lead to a localisation of the crack initiation site. So, despite all differences observed according the specimen geometry, the real question is what strain value really has to be considered to plot the EN curve. Laser or optical extensometer will probably help to answer this question in a near future.

2.2 Testing conditions

In order to avoid viscoplastic behaviour influence (high plastic range or high temperature test); the strain rate has to be constant for all tests of the same batch and its value must be from 5.10^{-4} s^{-1} up to 5.10^{-2} s^{-1} (ISO 12106). To respect this condition, the input signal must be triangular. The main drawback with this recommendation is that testing time becomes very long for long fatigue lives. As example, to reach 2 million cycles at the maximum strain rate of the standard, it takes for a medium steel (Rm=500 Mpa) about 45 hours. In this case the frequency is equal to 12 Hz, and even if the input signal is triangular, the real signal is more likely a sine.

In order to plot EN curves from 100 up to 2 or 10 million cycles, no economically reliable solution can be found keeping the frequency constant for all strain levels. This was one of the reasons why a new procedure has been proposed by the 'Verein Deucher Eisenhüttenleute' (VDEh). It is recommended to consider a sine signal with a frequency dependant of the number of cycles to failure, such as:

- below 1000 cycles : 0.1 to 1 Hz
- from 10000 to 50000 cycles : 1 à 3 Hz
- from 100000 to 500000 cycles : maxi 5 Hz
- from 500000 to 1000000 cycles : maxi 10 Hz

From these values, several remarks can be done:

- for very long lives (some million cycles), the frequency is limited to 10Hz, while the SN curve is usually 30-50Hz
- for short lives, the recommendation allows a wide range (0.1 to 1 Hz)
- and finally, one must know the number of cycles to failure appreciatively before testing.

From our point of view the main parameter is the strain rate on one side but also the temperature increase of the specimen due to plastic energy. That is why we propose to define the frequency in order to keep constant the plastic energy whatever the strain range applied. This methodology requires a first test on a specimen with different strain levels in order to measure the plastic energy. In order to avoid this preliminary test, we have measured the plastic energy for different grades (22 in total); from mild steel to Dual phase or ferrito-bainic and multiphase steel. The ultimate tensile strength of these materials go from 400 Mpa up to 1500 Mpa.

On each specimen, strain levels of 0.1%, 0.2%, 0.3%, 0.4%, 0.5%, 0.6%, 0.7% and 0.8%, have been applied with the following bloc cycling:

- 20 cycles with a triangular input signal and a strain rate equal to 4.10^{-3} s^{-1} (set up 1),
- 10 cycles with a triangular input signal and a strain rate equal to 5.10^{-2} s^{-1} (maximum of Iso standard) called set 2,
- 10 cycles with a triangular input signal and a frequency identical to the set up 2 signal (set up 3).

The energy, calculated by the formula E = loop area * frequency is set to correspond at a frequency of 0.125 Hz for 0.8% of applied total strain. Then, for each level, the frequency corresponding to the same energy can be calculated. An example of the results is given in figure 4. It can be seen that both the strain rate and the signal shape have no influence on the plastic energy. Furthermore, the frequency obtained for the endurance limit is about 20-30 Hz, which fit with conventional SN frequency testing.

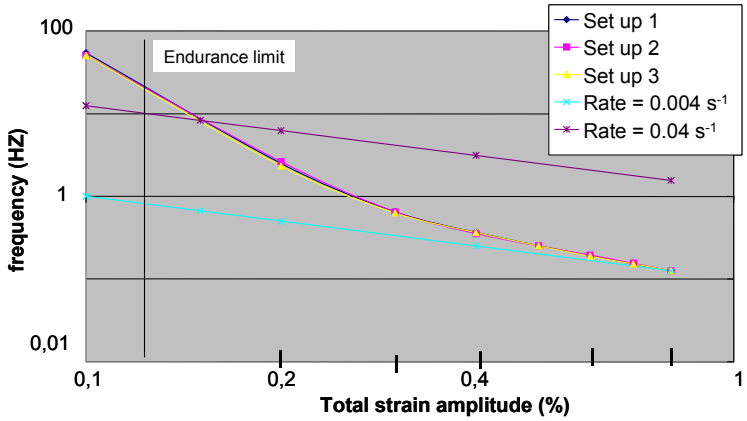


Figure 4. Example of frequency evaluation

Then, from the experiments performed on all the steel grades, it has been possible to obtain an evaluation of the testing frequency in relation to the yield stress of the material. The fitting relations are :

For 0.2% ≤ εt < 0.7%: $$\boxed{f(\varepsilon, Rp02) = A(\varepsilon)Rp02 + B(\varepsilon)}$$

with $$A(\varepsilon) = \frac{0{,}01983}{50{,}422 * \varepsilon - 9{,}0134} - 0{,}00084 \quad \text{and} \quad B(\varepsilon) = \frac{-0{,}5212}{9{,}778 * \varepsilon - 1{,}827} + 0{,}2877$$

For εt ≥ 0.7%: $$\boxed{f = \frac{0.1}{\frac{\Delta\varepsilon}{2}}}$$

An example of comparison between the frequencies obtained with the experiment and those calculated by the previous equations is presented in the figure 5.

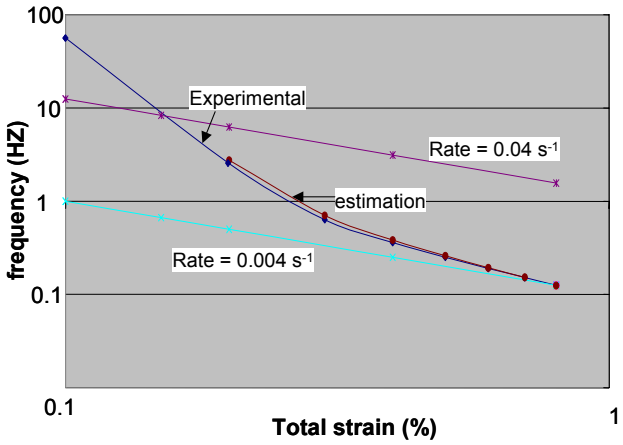


Figure 5. Comparison between estimated and experimentally determined frequencies.

3 HIGH CYCLE FATIGUE SHEARING TEST

French carmakers, but also a great part of fatigue investigations, use a multiaxial criterion to assess fatigue life of structures submitted to multiaxial loadings. Most of multiaxial criteria based on stress consider a component related to a shear stress as Dang Van [1], Robert [2], Papadopoulos [3], Sines [4] and Crossland [5]. One main difficulty remains for obtaining fatigue data on shearing mode when the base metal is a flat product. In our case, it concerns all the steel grades for automotive applications requesting fatigue strength.

For a long time one way to evaluate the multiaxial criteria coefficients consists of only use tensile fatigue data with different loading ratio. Most of time, the fatigue limits given for 2 loading ratio in a tensile mode are sufficient to define the criteria coefficients. Usually, the two load ratio are -1 (symmetrical tension-compression) and 0,1 (tension-tension).

The confidence of such fatigue criteria is never ensured because a fitting with 2 fatigue limits in tension very closed one to each other induces important statistical uncertainty. As major error is not permitted for fatigue design, such uncertainty has to be avoided. The figure 6 below gives an illustration of our statement. The sensitivity in a tensile mode of a criterion is represented on the x abscissa whereas the y abscissa gives the sensitivity considering shearing mode (such as Dang Van criterion for instance). As it can be seen, each uncertainty implies great error on the assessment of the fatigue strength for a given multiaxial cycle. If you take into account the uncertainty by their minimal or maximal values (fig. x. a), it seems difficult to know whether there is a risk of failure occurrence for both loading paths (blue line and red dotted line). If you mixed now the minimal and maximal uncertainties (fig x. b), you will obtain either an unrealistic slope or quite the same situation than in case a.

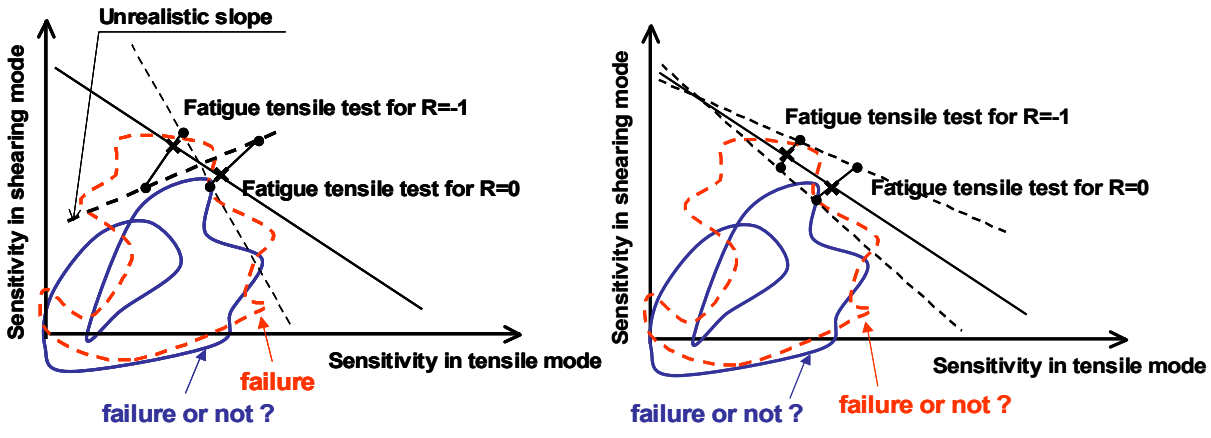


Figure 6. Illustration of the fatigue strength given by a multiaxial criterion. Evaluation of 2 loading paths taking into account the uncertainties of fatigue limits in tension used to fit the criterion.

The purpose of this section is to present a new device allowing High Cycle Fatigue tests in shearing. Managing a shear stress test in fatigue on a steel sheet appears much more complex than a tensile test. Some proposals have been studied such as applying a torsion on a tube obtained by sheet rolling and welding. This kind of solution is difficult to achieve because of cracks occurrence most of time in welding, the cost of the specimen and the effect of the forming (hardening induced by the rolling).

A new device easily adaptable to a standard fatigue machine (vertical load frame) and allowing to perform pure shearing on a flat specimen has been imagined in Arcelor. Several evolutions were necessary to reach a reliable solution (fig. 7.).

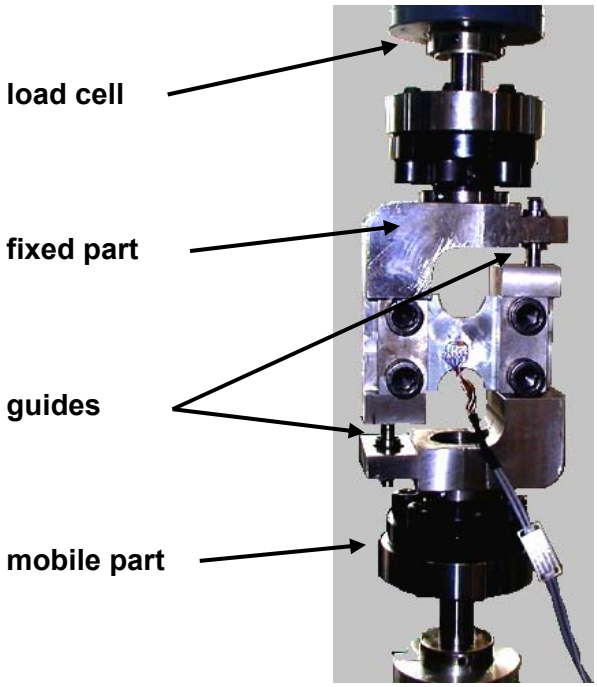


Figure 7. Device allowing shearing test on flat steel.

2 parts compose the device: a lower one fixed to the load cell and the mobile one fixed to the actuator of the fatigue machine. 2 guides insure a perfect vertical move and alignment between the 2 parts. The specimen is clamped at its both sides which undergo each one an opposite vertical load.

As shown on the figure 8, there are 2 section reductions: one in the width (tooling of 2 radius), the other one in the thickness (spherical electro-erosion with 50% thinning or less).

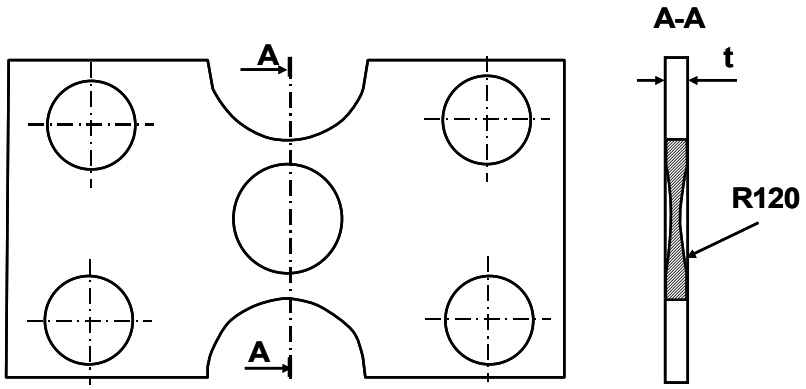


Figure 8. Definition of the shear specimen.

The central thinning and the shape of the specimen has been design to concentrate in the center the maximal stress (maximal equivalent Von Mises stress as well as a shear stress-state). This definition of the specimen required numerous numerical studies (FEA) in order to obtain a pure and maximal shear stress state at the center of the sample. Measurements thanks to strain gauges validate the numerical results within a range lower than 5% error: a pure stress state is obtained at the center of the specimen (figure 9).

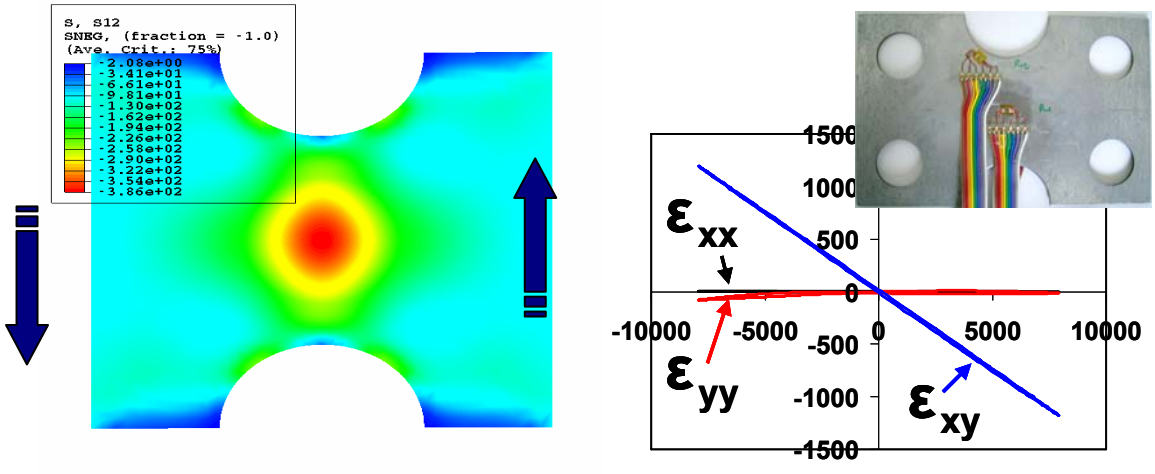


Figure 9. Shear stress-state in the plane of the specimen obtained by FEA and validation of the stress-state using strain gauges.

High cycle fatigue tests have been carried out. For a given shear stress, the corresponding load is deduced from the FEA (validated before by strain gauges measurements). The failure criterion is defined either by a loss of stiffness (i.e. an increase of the displacement for a given load) or by an electric detection (potential drop). The graph after shows the SN curves obtained on mild steel in tension and shearing with a loading ratio -1.

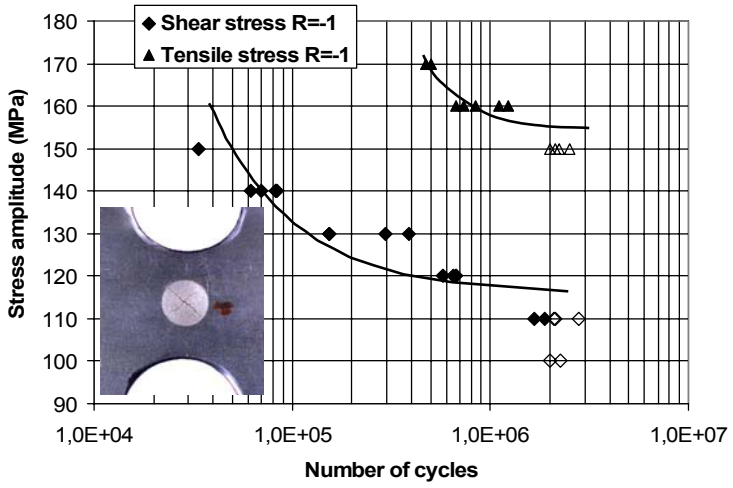


Figure10. SN curves obtained on a mild steel in tension and shearing.

Both fatigue limits τ_{-1} and σ_{-1} at 2.10^6 cycles, respectively 111 MPa and 155 MPa, are suitable to fit parameters of multiaxial criteria accounting the influence of torsion (i.e. influence of a shear stress). The figure x gives the corresponding Dang Van diagram with an uncertainty of 10% on each fatigue limit. The diagram appears reliable and coherent. So, know the shear stress fatigue limit ensures better prediction using such multiaxial criteria.

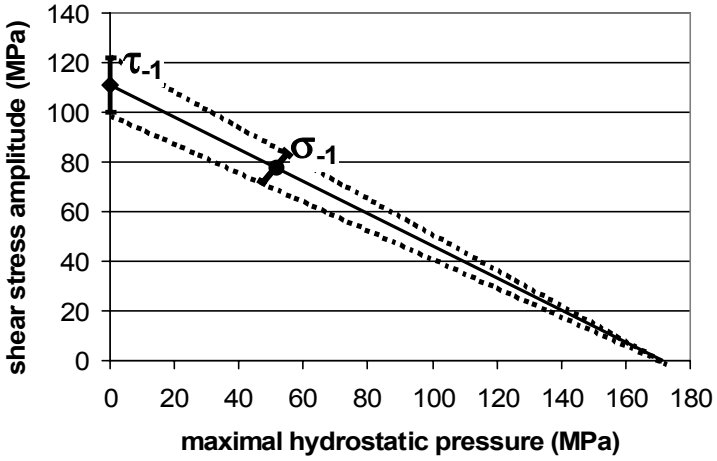


Figure 11. Example of Dang Van diagram including the shear fatigue limit

Fatigue shear tests allowing characterization on flat steel products are now available in Arcelor even if some problems remain as non-valid failure and still require some evolution. In future, Arcelor expects supply to its customers the shear stress fatigue limit of its products.

4 CONCLUSIONS:

A better assessment of fatigue behaviour of structures requires accurate modelling but also reliable and suitable material properties.

For fatigue testing thin materials under strain controlled, a new experimental testing procedure is proposed with the definition of specimen geometry specification and testing conditions suitable to the economical and technical environment.

For high cycle fatigue, material characterisation under tension or plane bending loading is completed with the design of a shear fatigue test for a better fitting of multiaxial criteria.

5 REFERENCES:

1. Dang Van K., Griveau B., Message O. On a new multiaxial fatigue criterion: theory and application. Biaxial and Multiaxial Fatigue. EGF 3 (Edited by M.W. Brown and K.J. Miller), London: Mechanical Engineering Publications, 1989, pp. 479-496.
2. Robert J.L., Contribution to the study of multiaxial fatigue under periodic or random solicitations (in French). PhD from National Institute of Applied Sciences (INSA) of Lyon. Order n° 92 ISAL 0004, January 1992, 229p.
3. Papadopoulos I.V., Polycyclic fatigue of metals: a new approach (in French). PhD from Ecole Nationale des Ponts et Chaussées, December 18th, 1987, 443p.
4. Sines G., Behavior of metals under complex static and alternating stresses. Metal Fatigue - New-York: Mac Graw-Hill, Book Company, 1959, pp. 82-90.
5. Crossland B., The effect of large hydrostatic pressures on the torsional fatigue strength of an alloy steel. Institution of Mechanical Engineers, International Conference on Fatigue on Metals, London, 1956, pp.138-149.

PROGRAM

1 Methodologies and tools for fatigue life assessment

- Automotive components
- Various industrial applications
- Welded structures and assemblies

2 Advanced design tools and approaches

- Fatigue crack initiation assessment
- Contribution to the crack propagation stage
- Modelling of the design behaviour of the welded

3 Multiaxial loading fatigue assessment

4 Fitness for service approach and applications

5 Experimental validation

- Application to automotive parts and structures
- From laboratory testing to field evaluation
- Development of dedicated test devices and procedures

6 Design procedures against thermal and thermo mechanical fatigue damage

7 Reliability approaches in fatigue design

8 Improved design and manufacture processes with regard to fatigue

FATIGUE LIFE PREDICTIONS OF ALUMINIUM CYLINDER HEADS

R. Salapete[a,b], B. Barlas[c], E. Nicouleau[b], D. Massinon[c], G. Cailletaud[a], A. Pineau[a]

[a] Centre des materiaux , Ecole Nationale Supérieure des Mines de Paris UMR CNRS 7633, BP 87, 91003 Evry Cedex, France
[b] RENAULT, 67 rue des bons raisins , 92508 Rueil Malmaison, France
[c] Fonderie Montupet, 67 rue J. de la Fontaine, 60181 Nogent-sur-Oise, France

Abstract Thermal fatigue induces in-service damage in industrial components, such as cast aluminum cylinder heads. The alternative heating and cooling of the operative engine generates fatigue cracks, initiating from the flame face which can lead ultimately to engine failure. A propagation fatigue life model derived from fracture mechanics concepts and based on Skelton approach is assessed. This model is used in order to estimate initiation and propagation fatigue lifetime in cylinder heads. A crack arrest phenomenon in the intervalve bridge is numerically reproduced using this approach.

1. INTRODUCTION·

Thermal fatigue induces in-service damage in industrial components, such as cast aluminium cylinder heads. The temperature history applied to operative engines generates fatigue cracks, initiating from the flame face and propagating under pure mode I in extreme case. These cracks can lead to engine failure . It is therefore easily understood that engineers and material scientists in the automotive industry pay very much attention to this mode of failure, see eg [1-7].

The aluminum alloy studied here is an 319 Type (Al-Si(7%)Cu(3%)-Mg(<1%), weight percent) used in the T5 temper condition. In this alloy, the foundry process may produce 3D pores which can be as large as an equivalent 500 µm diameter sphere [5-6]. A low cycle fatigue specimen was specially designed to investigate the behaviour of short cracks initiated from these porosities. Artificial short cracks, with a 500 µm surface length, were machined by Electro-Discharge-Machining (EDM) in order to follow crack propagation from a well-known defect geometry. CT specimens were also tested at various loading ratios to determine long fatigue crack propagation rates.

A special methodology was developed in order to study crack propagation growth rates : the main particularity of the study is that the material has been directly extracted from diesel cylinder heads. This has the advantage to guarantee the same microstructural configuration in the specimens and in the cylinder head (Composition, secondary Dendrite arm spacing , porosity, …). Figure 1a presents the extraction scheme of the LCF specimens. Of course, the LCF specimens have a small size due to the reduced place available in the cylinder head.

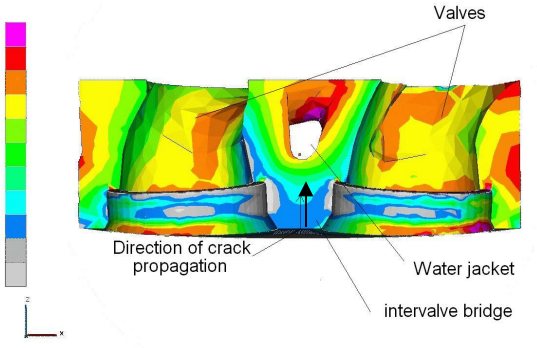


Fig. 1.a) Localisation of specimens extracted from cylinder heads ; b) 3D stress field in intervalve bridge.

· Corresponding author : raphael.salapete@gmail.com

The global methodology followed in the present study is described in figure 2 . The definition of the constitutive equations and a model predicting crack initiation were previously developed for this material [1,2]. They are now in use for the design of new car engines. As a example, the contour of the von Mises stress obtained by finite element (FE) method is shown in figure 1b . The main concern of car manufacturer is now to assess and control the crack propagation rate. To complete the fatigue lifetime evaluation in the cylinder head, the present study has been focused in crack propagation on laboratory specimens and on the comparison with real structural tests performed on cylinder heads. This paper describes the general methodology and the models adopted.

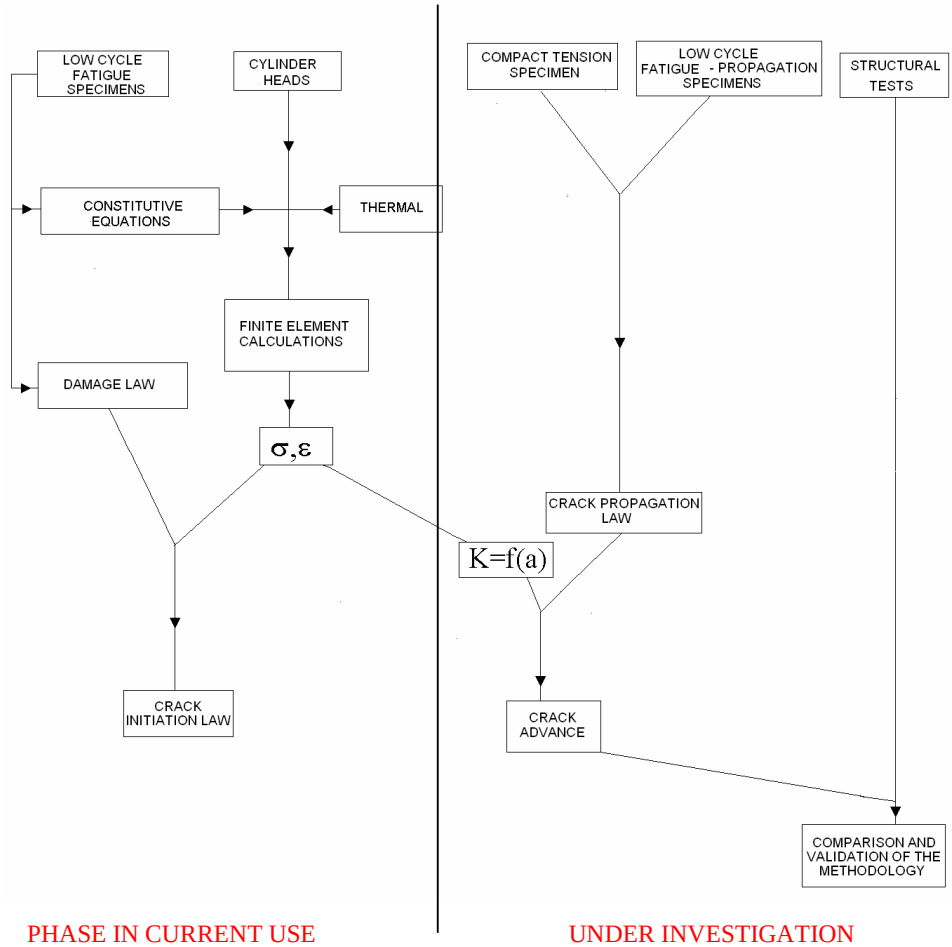


Fig. 2. General scheme of fatigue lifetime determination in cylinder heads

The main objective of the study is to provide a large data base for da/dN evaluation under elastic and elastoplastic loading conditions. A methodology is also derived to evaluate the relevant loading parameter . Finally this model is used to show how we can evaluate the cylinder head fatigue lifetime and an eventual crack arrest.

2. MATERIALS AND EXPERIMENTAL PROCEDURES

The material used in this study is an 319 T5 alloy . The composition of this aluminium alloy is given in table I. Car manufacturers usually request a range of acceptable composition values shown in this table.

Compact tension (CT) specimens were directly machined from an heat-treated cylinder head. These specimens which were used to investigate long (> 1 mm) fatigue crack growth rate behavior had an in-plane dimension W=24 mm and a thickness of 10 mm (Fig. 3d). Tests were performed at 20°C using an electro-mechanical machine with a loading frequency of 20 Hz . Load ratios ranging from 0.1 to 0.7 were applied in order to measure crack closure effect.

Small fatigue crack growth tests were conducted on specimens whose dimensions are shown in figure 3c. These specimens were tested under load and strain control conditions on an MTS servohydraulic fatigue testing system. The test apparatus is shown in figure 3a and 3b. A load ratio of -1 with a maximum total strain ranging from 0.4 to 0.6% and a load ratio of 0.1 with a maximum stress of 220 MPa were applied. Tests were performed at 20°C with a loading frequency of 0.1 Hz. Semi-circular notches of 150 to 250 µm depths (figure 3a) were machined in short crack growth specimens using a electro discharge machined technique. The accuracy of the semi circular shape was controlled after failure using SEM microscope.

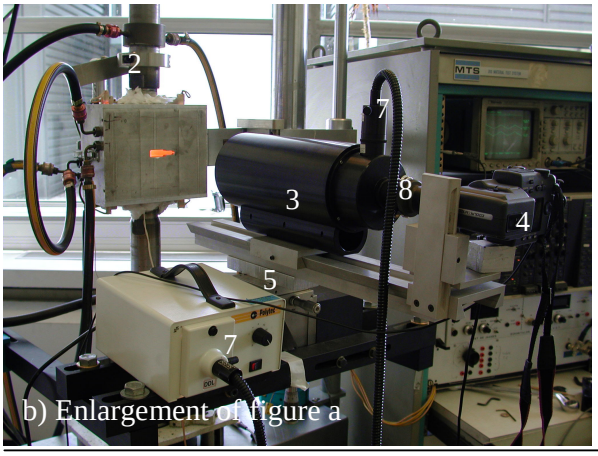
Table I : Chemical analysis of the investigated A319 T5 aluminum alloy

Element	Range (wt%)
Si	**7. - 8.5**
Cu	**2.8 – 3.5**
Mg	**0.25 – 0.4**
Fe	**0 – 0.7**
Ti	**0.15 – 0.20**
Zn	**0 – 0.8**
Mn	**0 – 0.6**
Ni	**0 – 0.3**

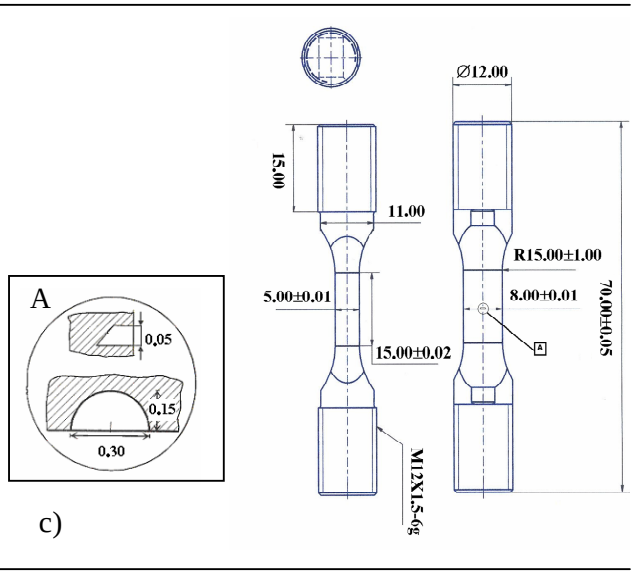


1: *MTS controller;* **2:** *Fatigue test machine;* **3:** *Questar, optics with a large focal distance;* **4:** *digital camera;* **5:** *micrometric platine X,Y,Z ;* **6:** *Observing and recording system;* **7:** *Specimen lighting crossing the optical system ;* **8:** ***Lens and adapter ring***

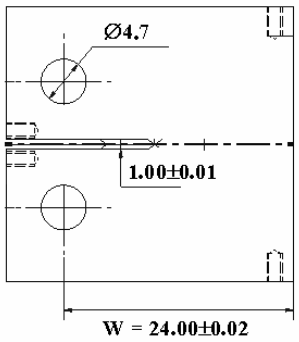
a)



b) Enlargement of figure a



c)



d)

Figure 3.a) and b)Testing machine devices ; c) Low cycle fatigue specimen and notch dimensions ; d) CT specimen dimensions

Cracks initiating from this notch were observed using a QUESTAR telescope set up on the testing frame. Crack length was measured by acquiring the image at periodic time ranging from 5 minutes to more than 3

hours for long time tests. The crack length was projected in the pure – mode I plane for analysis and the resolution of the measurement was close to 1 µm.

3. NUMERICAL CALCULATIONS

3.1 The macroscopic model

The model used to calculate the local stresses and strains from the knowledge of the thermal loading is an extension of a classical unified elastoviscoplastic model for cyclic loadings [8], with additional terms to take into account alloy's ageing. Full details are given elsewhere [3,8].

The ageing part is represented by a scalar as an internal variable a , starting from zero , and tending to an asymptotic value a_∞ (when the maximum ageing state is reached, $a_\infty = 1$), depending on temperature and describing the precipitate growth. Its evolution is exponential, with a temperature dependent time constant τ :

$$\dot{a} = \left\langle \frac{a_\infty - a}{\tau} \right\rangle \qquad (1)$$

This model can thus describe softening effect related to over-ageing. It has been identified on isothermal LCF tests and validated on anisothermal thermomechanical fatigue tests [1].

3.2 ΔK_{eff} Calculation on low cycle fatigue specimens

The stress intensity factor calculation corresponding to measurements realized on small crack growth tests consists of 2 steps. First, in order to take into account cyclic plasticity, an equivalent stress amplitude is derived, as shown in a previous study [9] Haigh and Skelton [10] expression to define this equivalent stress was used :

$$\sigma_{eq} = U\Delta\sigma + E\Delta\varepsilon_p \qquad (2)$$

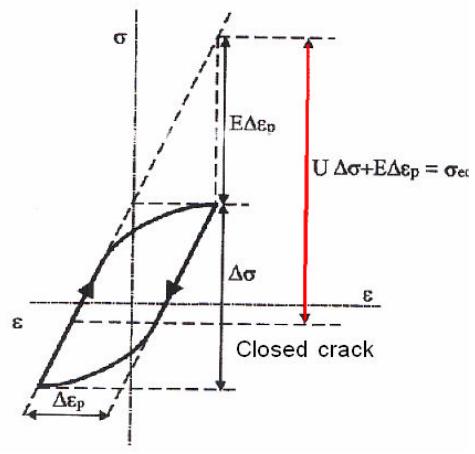


Fig. 4. Skelton's equivalent stress amplitude

It corresponds to the sum of the effective stress amplitude (with the crack closure stress $U\Delta\sigma$) and a pseudo elastic stress (elasticity modulus and plastic deformation amplitude product). Figure 4 shows the rule used to compute the equivalent stress amplitude calculation on a fatigue loop.

The stress intensity factor is then calculated with the expression proposed by J.C.Newman and S.R.Raju [11]. This calculation is applied to the case of a surface semi-elliptical crack under an uniform load. The stress intensity factor is calculated at the free surface point.

3.3 ΔK_{eff} Calculations on CT specimens

CT type specimens are loaded in the elastic regime. The corresponding stress intensity factor has a well known expression which depends on crack length a, the applied load P and geometrical parameters such as specimen width W and thickness B.

$$K_{CT} = \frac{P}{B\sqrt{W}} Y \text{ with,}$$

$$Y = 29.6\left(\frac{a}{W}\right)^{1/2} - 185.5\left(\frac{a}{W}\right)^{3/2} + 655.7\left(\frac{a}{W}\right)^{5/2} - 1017\left(\frac{a}{W}\right)^{7/2} + 638.9\left(\frac{a}{W}\right)^{9/2} \quad (3)$$

In order to take into account the crack closure effect, we introduce the parameter q which is a function of loading ratio R:

$$q = \frac{\Delta K_{eff}}{\Delta K} = f\left(R = \frac{\sigma_{\min}}{\sigma_{\max}}\right) \quad (4)$$

3.4 da/dN calculations.

The crack length projected in pure-mode I plane is used for the analysis. The crack growth rate is obtained from the crack length versus number of cycles curve, using a standard secant method.

One can then relate this crack propagation rate to the equivalent loading parameter using a Paris law type :

$$\frac{da}{dN} = C\Delta K_{eff}{}^{m} \quad (5)$$

3.5 Crack growth simulation in cylinder heads.

The cylinder head is subjected to 3D thermomechanical loadings. The weight function method developed by Bueckner [12] and primarly used for nuclear reactor applications in the 70's was used in order to calculate the stress intensity factor amplitude in the cylinder heads.

The weight functions relevant to cracks in cylinder head were determined using Parks method [13] for the evaluation of stress intensity factor for a given crack length. The interest of this method is that it allows to quickly determine the stress intensity factor for any given geometry and for any given crack length. In these calculations it is assumed that the crack front remains straight during propagation (see figure 5).

When these weight functions have been derived, the stress intensity factor can be calculated for any given stress distributions. In our case, the thermomechanical fields in the depth of the intervalve bridge are known from 3D finite element calculations. Fig 5 shows a typical stress-temperature curve obtained at a point located near the flame face. This point is in compression when the maximum temperature is reached and in tension during cooling, so that crack opening may be present at this stage.

A curve relating the stress intensity factor and the crack length **a** can then be obtained in the form :

$$\Delta K_{eff} = f(a) \quad (6)$$

Combining (5) and (6), we obtain :

$$\frac{da}{dN} = C(f(a))^{m} \text{ and, after integration, } a = g(N, a_0) \quad (7)$$

Where a_0 is an initial crack length representative of the microstructure and N is the number of fatigue cycles.

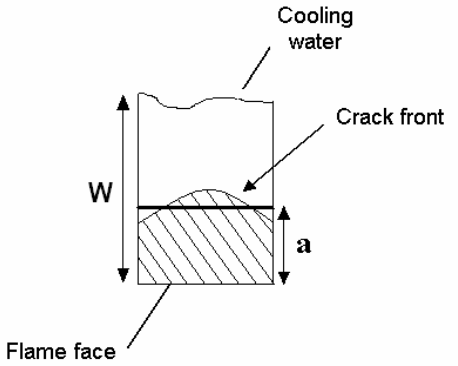


Fig. 5. Schematical view of crack modelisation in the intervalve bridge

4 RESULTS AND DISCUSSION

4.1 Crack propagation results

A picture of two cracks originating from the initial defect is shown in figure 6. It can be seen that the cracks have the same length on both sides of the defect. The semi-circular crack front shape was verified after failure. The tortuous aspect of the crack path is related to the large grain size encountered in this type of cast alloy

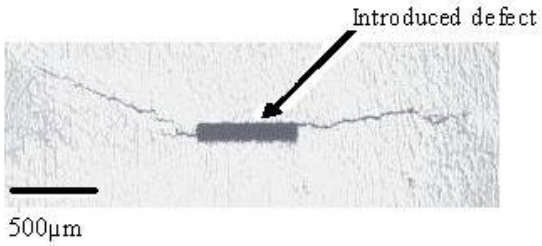


Fig. 6. Crack propagation from a known defect size

Figure 7 is a fatigue crack propagation master curve that summarizes the different tests performed both on CT and LCF specimens at 20°C. Further tests were also performed at elevated temperature in order to account for the temperature dependence of fatigue crack with crack growth rates. For simplicity's sake the results are not included here. For long crack growth , an appropriate value of **q** is chosen. For LCF tests, the Skelton approach allows to create a master curve. For this set of parameters, crack growth rates in the cast aluminium correlate with the equivalent stress intensity factor amplitude. Cyclic plasticity and crack closure effect can therefore be accounted for using this approach. Small fatigue crack growth curves at 20°C (from [7]) for an 319 type T7 heat-treated cast aluminium alloy have been added to this figure. These results are in good agreement with those found by these authors.

As a result , it can be concluded that growth behaviour can be described by a power-law dependence of growth rates with the calculated equivalent stress intensity factor.

4.2 Crack propagation lifetime in cylinder heads

The variation of the equivalent stress intensity factor with crack length calculated for a part-through crack in a cylinder head is shown in figure 8a. In these calculations , the crack length is normalized by the distance between the fire deck and the cooling water chamber. A maximum value of the stress intensity factor is obtained at one third of the depth. The stress intensity factor is then decreasing to reach a minimum value when the ratio of crack length over full-length reaches 0.7. This value of the stress intensity factor is very close to the value producing crack opening. This result is interesting since it suggests that crack arrest can take place at intervalves bridges.

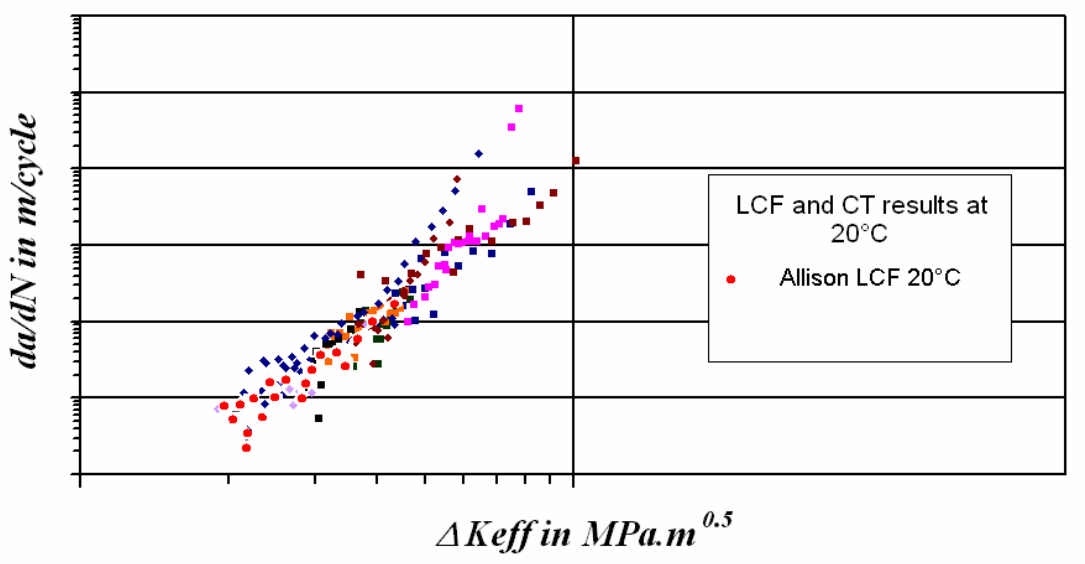


Figure 7. Crack propagation rate in AS7U3G master curve

Different structural tests were realized by Renault and Montupet to simulate the damage occuring in cylinder heads during road rolling. One of them consists in applying thermal cycles to the cylinder heads from a minimum temperature T_1 to a maximum temperature T_2. It allows to reproduce in-service failure as a crack is propagating from the fire deck. The tests are stopped from time to time, and the corresponding crack length is measured. Curves representing crack length vs Number of cycles are then plotted; they depend on maximum temperature and on the cylinder head parameters. To evaluate the reliability of the fatigue life model, we compare the Crack length vs Number of cycles for experimental and calculated results. The results are given in figure 8b.

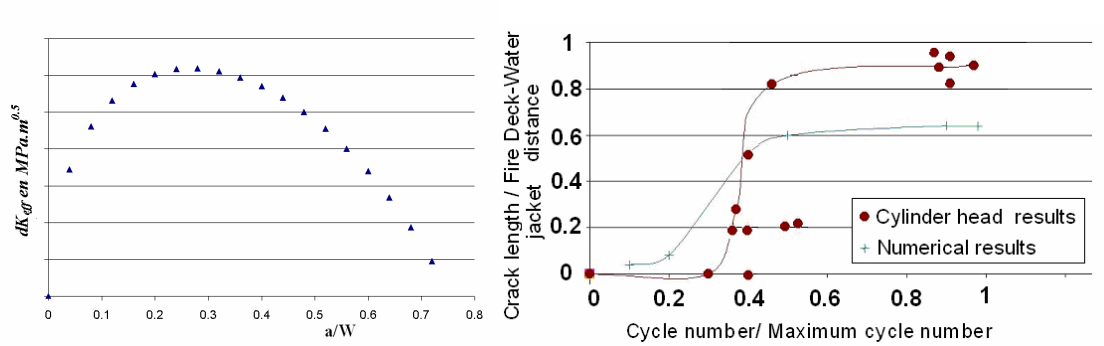


Figure 8a) Stress intensity factor evaluation in intervalve bridge depth 8b) Comparison between experimental and numerical results from engine failure test.

These curves show that three zones can be defined in the fatigue lifetime of this specific cylinder head. The first part represents fatigue crack initiation, which corresponds to a crack that is smaller than 0.1 times the final crack length. The second phase corresponds to a fast propagating region where the crack rapidly deepens in the intervalve bridge. The final zone represents a slow down and a crack arrest phenomenon where the crack is no longer propagating. The comparison between experimental and numerical results clearly shows that numerical results qualitatively reproduce the observed crack arrest phenomenon and the general three zone configuration. However the crack seems to initiate too early in the calculations and to stop at crack length smaller than the experimental one.

These preliminary results are nevertheless quite encouraging, since we are able to reproduce, with a relatively good approximation the crack propagation behaviour for the intervalve geometry considered in the study. Other calculations were also made on different geometries which did not lead to crack arrest. The calculated crack propagation rates were also found to be in good agreement with the experiments . Therefore this method seems to be predictive and simple enough to be used for design purposes. This is probably a good starting point to develop improved design rules.

5 CONCLUSION

1. A master curve giving the fatigue growth rate as a function of equivalent stress intensity factor has been obtained on an A319 aluminium alloy. The definition of this equivalent stress intensity factor involves both elastic and elasto-plastic calculations
2. A method based on weight functions has been proposed to calculate the variation of the equivalent stress intensity factor corresponding to a part-trough crack in a cylinder head.
3. Comparison between calculated and observed crack length in a tested cylinder head shows a reasonable agreement.

ACKNOWLEDGMENTS : Support from ANRT for one of the authors (R.Salapete) is greatly acknowledged.

6 REFERENCES

1. E. Nicouleau-Bourles, Etude expérimentale et numérique du vieillissement d'un alliage d'aluminium. Application aux culasses automobiles, PhD thesis, Ecole Nationale Supérieure des Mines de Paris, 1999.
2. B. Barlas, Etude du comportement et de l'endommagement en fatigue d'alliages d'aluminium de fonderie, PhD thesis, Ecole Nationale Supérieure des Mines de Paris, 2003.
3. B.Barlas, D.Ovono-Ovono,I.Guillot, G.Cailletaud, *Mat. Sci. Forum* , 2002 ,396-402
4. J.J.Thomas,L.Verger,A.Bignonnet,E.Charkaluk, *Fatigue and Fracture of Engineering Materials and Structures*, 27(10), 2004, 887-895.
5. Y.X.Gao,J.Z.Yi,P.D.Lee,T.C.Lindley, *Fatigue and Fracture of Engineering Materials and Structures*, 27(7), 2004, 559-570.
6. J.Fan,D.L.McDowell,M.F.Horstemeyer,K.Gall, *Engineering Fracture Mechanics*, 70(10),2003,1281-1302.
7. A.Shyam,J.E.Allison,J.W.Jones, *Acta materialia*, 53(5),2005,1499-1509.
8. J.Lemaitre, J.L Chaboche : Mécanique des matériaux solides , Dunod , Paris ,1988
9. H.Burlet,S.Vasseur,J.Besson,A.Pineau, *Fatigue and Fracture of Engineering Materials and Structures*, 12, 1989,123-133.
10. J.R. Haigh R.P. Skelton , *Materials Science and Engineering* , 36,1978,133-137
11. J.C. Newman and S.R. Raju, *Engineering fracture mechanics*, 15(1-2),1981,185-192.
12. H.F Bueckner, *Z. Agew. Math. Mech*, 50, 1970, 129-146
13. D.M. Parks , *International Journal of fracture*, 10(4),1974,487-502

A probabilistic approach for the thermomechanical fatigue design of engine hot components : Application to a diesel cylinder head

T.Mac-Lan Nguyen-Tajan[a], Jean-Jacques Thomas[a]

[a] PSA Peugeot Citroën
Automotive Research and Innovation Division, DRIA/SARA/STEO/MAST
Bat.62, Route de Gisy, 78943 Vélizy-Villacoulay Cedex, France
e-mail : maclan.nguyen@mpsa.com, jeanjacques.thomas@mpsa.com
tel. : 01 57 59 85 09, 01 57 59 84 02 ; fax : 01 57 59 90 70

Abstract The probabilistic approach developed by PSA Peugeot Citroën for the fatigue design of engine components is described. The method is applied to a diesel cylinder head, made of aluminum alloy, which major risk of failure is a thermomechanical fatigue crack initiation and propagation in the intervalve bridge area. The proposed approach is an extension to the thermomechanical fatigue context of the Stress-Strength Interference Method, now widely used in the automotive industry for the design of components under mechanical loads. The paper will focus on the different steps of the thermomechanical fatigue equivalence method, which enable to transform random signals of engine speed and torque into a scalar measuring the fatigue severity of the load applied to the cylinder head. From customer inquiries, the distribution of the customer severity can then be built and relevant specifications for the calculations and the experiments can be defined. With a predictive and robust numerical modeling, the engine component reliability can be guarantied, consistent with a predefined failure risk.

1 INTRODUCTION

In the automotive industry, the challenges for tomorrow concern fuel consumption, low exhaust gas emissions, acceleration of design process delays, control of the reliability… They lead to technological solutions (diesel engines, new material solutions, downsizing, new combustion strategies, active engine controls, after-treatment systems such as Nox trap or particle filters…) which globally increase the severity of the loads applied to automotive components, especially engine components (cylinder head, exhaust manifold, piston, cylinder block…). In order to anticipate the impact of such architectural and technological evolutions on the engine durability, it is imperative to have an overall design method which enables to guaranty the reliability of the components, as soon as possible in the design process. To reach this objective, it is firstly necessary to know how to model and assess the fatigue limit of a component under a given thermomechanical load, and secondly to know what loads the automotive part must be designed for. To answer this latter question, one must acquire a good knowledge of the loading induced by a real usage of a vehicle in order to link the specifications to the customers usage.

In this article, a brief description of the thermomechanical fatigue damage which can occur in an aluminum cylinder head and the modelling approach developed by PSA Peugeot Citroën to calculate the local damage is given. This overall approach [6,8] lies on four main points : a good representation of the thermal and mechanical loads which the structure is submitted to, the material modelling consistent with the functioning conditions of the structure, a numerical strategy enabling relatively fast and robust cyclic calculations of the cylinder head and a thermomechanical multiaxial and non-isothermal crack initiation law. After these reminders, the new methodology developed at the Direction of Research and Innovation of PSA Peugeot Citroën is explained. This approach permits to make a relevant statistical analysis of the customers loads in order to measure their severity from a fatigue point of view and to have a better estimation of their scattering. From the understanding and the modelling of the damage mechanisms, a macroscopic parameter driving the local damage and a global damage law can be identified, from which a counting cycles method and a fatigue-equivalence definition can derive. Once one knows how to analyze a customer, one can build the Stress distribution of the Stress-Strength Interference Analysis, as long as one has data from a customers population, representative of the market. Specifications can then be defined, linked to the customers severity. A probabilistic acceptance criterion for the thermomechanical fatigue design of cylinder head can at last be defined, consistent with a desired probability of failure

2 THERMOMECHANICAL FATIGUE AND MODELING APPROACH

2.1 Failure description

For the diesel cylinder head, the most often encountered failure is the initiation and propagation of a fatigue crack in the intervalve bridge area on the fire desk (Fig. 1). It is well known that this kind of failure occurs under cyclic thermal loads (heating and cooling of the engine) and is linked to a thermomechanical fatigue phenomenon : because of the heat flow, the intervalve bridge area undergoes expansion but is clamped by the surrounding areas where the temperatures are lower. Compressive stresses are generated and transform into tensile stresses when the engine cools down, with plastic and viscous strains at each cycle. This kind of fatigue crack can also occur on exhaust manifolds or on pistons on the bowl edges.



Figure 1. Fatigue cracks in the intervalve bridge area of a diesel cylinder head

2.2 Modelling approach

In order de model this physical phenomenon and to prevent the failure, the Research and Innovation Division of PSA Peugeot Citroën has developed an overall design methodology [6,8]. This approach is based on four main steps : the material behaviour modelling, the load identification and modelling, the predictive and robust numerical thermomechanical simulation of the component and a relevant criterion of crack initiation in the non-isothermal low-cycle fatigue domain. The good understanding of these four items enables the assessment of the durability of automotive components subjected to thermomechanical loads. In this part, the main ideas and choices of the modelling and the numerical strategies are briefly described.

2.2.1. The thermomechanical load

Because of the combustion of the gas in the combustion chamber, the cylinder head is subjected to cyclic thermal heating and cooling, corresponding to a starting and stopping of the engine. This thermal load can be modelled by a heat flow concentrated in the fire desk of the structure, and calculated with results from a 3D gas combustion simulation. A classical assumption of weak-coupling between the thermal and the mechanical histories is made. First, a transient thermal analysis with relevant boundary conditions gives the temperature evolution of the cylinder head. At the most critical points, the temperature can rise from 20°C up to more than 250°C. Finally, a mechanical calculation with the known temperature evolution gives the stress-strain response of the structure.

2.2.2. The material behaviour

The PSA approach is based on the assumption that the material behaviour can be dissociated from the damage evolution and the ageing occurring at high temperatures (higher than 150°C for the studied aluminium alloy). This hypothesis is partly motivated by the statement that, once the ageing being stabilized, under a cyclic thermomechanical load representative of what occurs in an engine, the structure response stabilizes after a few cycles (about ten cycles). The fatigue crack initiation is a phenomenon which appears after thousands of cycles. We can then assume that the material behaviour and the damage can be calculated separately and that the fatigue limit only depends on the cyclic response of the structure.

All PSA diesel cylinder heads are now made of aluminium alloy. At the very high temperatures reached, the yield limit of the alloy collapses and the material behaviour becomes plastic, viscous and strongly non-linear. To model the material, PSA has chosen a Chaboche elastic-viscous-plastic law with a non-linear kinematic Norton Hoff hardening. The constitutive law has 6 parameters which reveals to be enough to represent the structural response with a sufficient precision. This model has the advantage to be simple enough to guaranty a robust parameter identification and calculation times that are compatible with the design process. The parameters of the law are identified on cyclic isothermal and non-isothermal tests made on pre-aged specimens which undergo the same manufacturing process as the cylinder head. They vary with the temperature.

The material behaviour model can be represented by the scheme drawn in Figure 2. The constitutive equations are also given underneath, with the classical notations. The material law has been implemented in Abaqus/Standard via a user routine.

$$
\begin{cases}
\underline{\underline{\sigma}} = \underline{\underline{\underline{\underline{C}}}} : (\underline{\underline{\varepsilon}} - \underline{\underline{\varepsilon}}^{vp}) \\
\underline{\underline{X}} = \frac{2}{3} H \underline{\underline{\alpha}} \\
J_2(\underline{\underline{\sigma}}, \underline{\underline{X}}) = \sqrt{\frac{3}{2} \underline{\underline{dev}}(\underline{\underline{\sigma}} - \underline{\underline{X}}) : \underline{\underline{dev}}(\underline{\underline{\sigma}} - \underline{\underline{X}})} \\
\dot{\underline{\underline{\varepsilon}}}^{vp} = \frac{3}{2} \left\langle \frac{J_2(\underline{\underline{\sigma}}, \underline{\underline{X}}) - \sigma_y}{\eta} \right\rangle^m \frac{\underline{\underline{dev}}(\underline{\underline{\sigma}} - \underline{\underline{X}})}{J_2(\underline{\underline{\sigma}}, \underline{\underline{X}})} \\
\dot{\underline{\underline{\alpha}}} = \dot{\underline{\underline{\varepsilon}}}^{vp} - \frac{2}{3} \sqrt{\frac{2}{3} \dot{\underline{\underline{\varepsilon}}}^{vp} : \dot{\underline{\underline{\varepsilon}}}^{vp}} \frac{\xi}{H} \underline{\underline{X}}
\end{cases}
$$

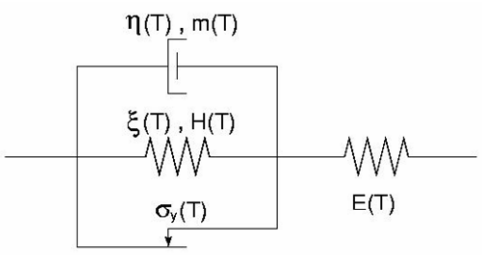


Figure 2. Elasto-visco-plastic material constitutive model for aluminium alloy

2.2.3. The thermomechanical simulation of a cylinder head

Because of the complexity of the geometry of the structure, the finite element model has a great number of degrees of freedom (around 1 million DOF). Moreover, under the severe thermal load, the structure response is viscous plastic and strongly non-linear. Hence, the generated calculation times are quite long. Still, in order to estimate the lifetime of the cylinder head, it is necessary to calculate its stabilized cyclic response. Indeed, as pointed out before, the cylinder head mechanical response stabilizes with a plastic shakedown after about ten cycles. It is obvious that to fit in the design process, one has to find an original solution not to calculate these ten cycles.

In order to reduce the calculation times, PSA has developed an efficient numerical algorithm which enables to directly calculate the stabilized response of a structure submitted to a cyclic thermomechanical load, without simulating the first transient cycles. This method, called the Direct Cyclic Algorithm, has been developed in collaboration with the Ecole Polytechnique and implemented in Abaqus [1,7]. The calculation time reduction is very appreciable (from a factor 3 to 20, depending on the severity of the load, the material behaviour and the finite element model size).

2.2.4. The low-cycle fatigue criterion

Once an efficient structural simulation is achieved with a proper material law, the lifetime of the cylinder head can be evaluated. It is based on a thermomechanical fatigue criterion which connects the number of cycles before failure to the local plastic energy dissipated during the stabilized cycle at the most critical point [8]. The expression of the criterion is given in (Eq.1). This criterion has been preferred to traditional low-cycle fatigue criteria because it is consistent with the non-isothermal and multiaxial properties of the loads, which is required for the automotive context.

$$\max_x(\Delta W(x)).N^{\beta} = C \qquad \text{Eq.1}$$

In Figure 3, the estimated lifetime calculated with the dissipated energy densities is compared to the experimental results for specimens and a cylinder head. The crack initiation is well localized and the lifetime of the cylinder head is correctly estimated. At PSA, this overall approach has been many times confronted to experimental data and has given satisfaction. All cylinder heads and exhaust manifolds are now numerically validated with this overall approach.

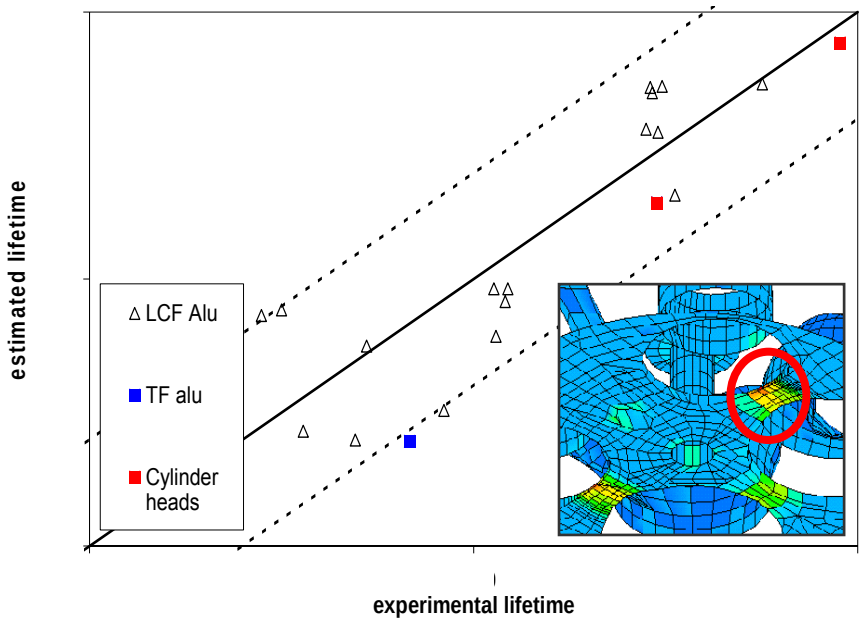


Figure 3. Lifetime assessment for a cylinder head

3 THERMAL MECHANICAL FATIGUE EQUIVALENCE METHOD

The next step to the handling of the reliability of engine hot components is the definition of relevant specifications for an optimal design. How can one estimate the customers severity in order to take into account their scattering and make a probabilistic design ?

The objective of this work is to propose an extension to the thermomechanical fatigue context of the Stress-Strength Interference Method which permits to analyze random load signals measured on a vehicle and transform them into a scalar measuring their fatigue severity. The data analysis techniques used are based on the knowledge of the physical damage mechanisms.

3.1 Stress Strength Interference Analysis for high-cycle fatigue

Because all drivers are different and the roads are different, the loads applied to automotive components are variable. Likewise the strength of automotive parts are scattered because of the scattering of the material and the manufacturing processes. To guaranty the probabilistic design of automotive components which can fail by high-cycle fatigue, the Stress Strength Interference Method is widely used [2,3]. The main idea of the approach is to estimate the severity and the scattering of the loads and the scattered strength of the components in order to compare them and guaranty a predefined probability of failure (Fig. 4).

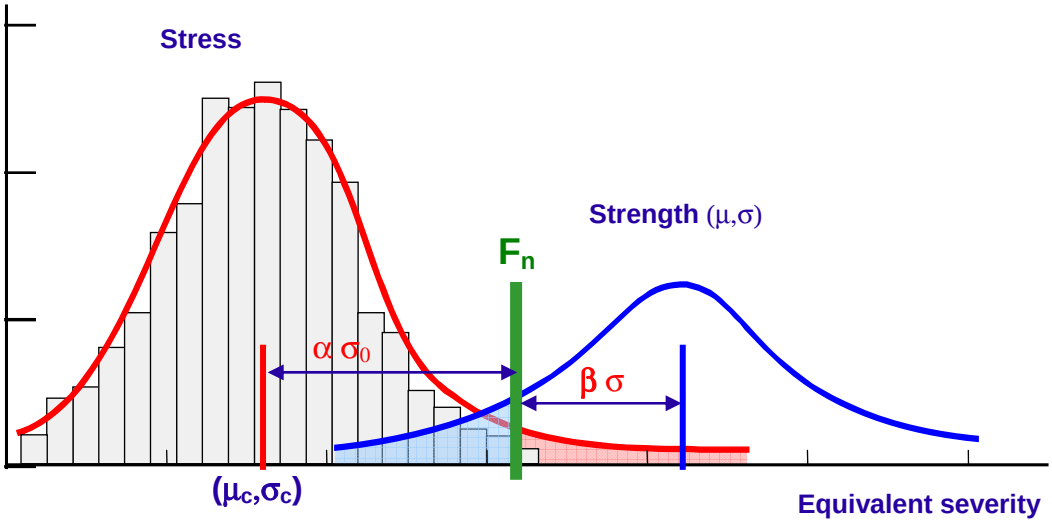


Figure 4. Stress Strength Interference Analysis

To do so, a relevant severity parameter must be identified. This parameter must be global enough to be measured on a vehicle but must also be linked to the local damage that can occur in the structure. In mechanical high-cycle fatigue, it is well known that damage is driven by the local stresses reached at the most critical point. In this range of fatigue, under cyclic loads, the mechanical response of a structure is an elastic shakedown. So the stabilized stresses are always elastic. One can then assume that the forces and the stresses are proportional and choose the forces as the severity parameter.

In order to have data on the loads applied by the customers on vehicles, tests are made on PSA tracks and inquiries are organized among customers. These inquiries consist in lending a car to a voluntary customer during a period of one month or in mixing results from a usage survey (customers estimate their proportions of usage in different types of road - mountain, city, highway, road – and different weight of load) and behaviour tests giving access to the different driving styles of the customers. Sensors are implemented in the vehicles and measure random signals of accelerations and forces at different points of the car. Essentially for cost reasons, sometimes only the accelerations are measured while in fatigue, the severity parameter analyzed is the force. To estimate it from the accelerations, neurone network methods can be used [5].

The different steps in the mechanical load analysis are described in Figure 5. The high-cycle fatigue limit of a structure depends on the amplitude and the mean value of the stresses cycles. This observation leads to make a Rainflow counting of the random force signals to extract a Rainflow matrix giving the number of cycles in terms of the amplitude and the mean value of all elementary cycles included in the initial signal. Each cycle is then transformed into a new cycle with zero mean value, which induces the same damage. This transformation is done by using the iso-damage parabola of Gerber. The initial force signal is finally condensed into a histogram “force amplitude-number of cycles”. For metals, the damage law can be modelled by a Basquin curve, whose equation is :

$$N_i * \Delta\sigma_i^{\alpha} = \beta \qquad \text{Eq.2}$$

where $\Delta\sigma_i$ is the stress amplitude, N_i is the number of cycles before failure and α, β are material parameters. Knowing this damage law and using a linear cumulative damage Miner law, the damage induced by the cycles in the histogram can be calculated. To measure the severity of the initial signal with a scalar, one can calculate the amplitude of the cycle (with zero mean value) which, if it is repeated N_{ref} times, will produce the same damage than the random signal. This amplitude is called the fatigue equivalence F_{eq} and is calculated for each customer.

With this load analysis method, the distribution of the customer severity can be built and specifications (F_n in Fig.4) can be defined in terms of the mean value and the scatter of this distribution. The acceptance criterion is then defined to guaranty the desired failure probability.

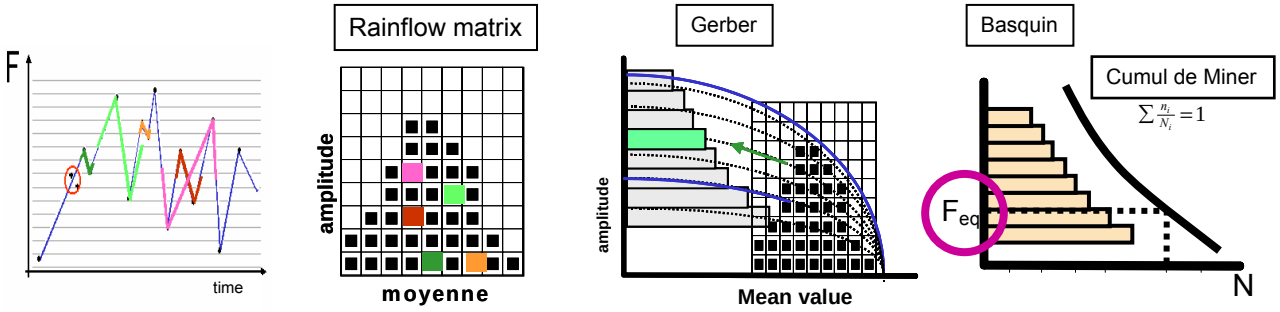


Figure 5. Fatigue equivalence under a mechanical load

This one-dimensional fatigue equivalence methodology is being used for mechanical components at PSA. The extension to multi-dimensional loads is being developed by Genet [4].

3.2 Thermomechanical loads analysis for low-cycle fatigue

As explained in the first paragraph, the cylinder head is subjected to a thermomechanical fatigue damage. An extension of the Stress Strength Interference Method to the thermomechanical fatigue domain is proposed.

The very first difficulty is the identification of an appropriate severity parameter which must be directly linked to the local damage and in the meantime, be accessible. On a vehicle, the measurable parameters are the engine speed and torque. Sometimes, the torque is not recorded. In spite of it, to take benefit of all the enquiries that have been done in PSA for years, a method of rebuilding non-measured quantities from other measured signal has been developed for the engine torque, based on neuronal network analysis. It gives quite satisfactory results. The difficulty is that the engine speed and torque are not directly linked to the fatigue damage, which is assumed to be locally measured by the dissipated plastic energy density at the most critical point of the component, as described in the first paragraph. And the relation between the speed and the torque and the dissipated energy is not linear !

To circumvent this difficulty, an intermediary parameter has been searched for. This parameter must be sufficiently global so that finite element calculations are not to be made, but it must drive the damage at the first order.

As explained below, the cylinder head is submitted to a cyclic thermal load, generating a cyclic temperature evolution in the intervalve bridge area. Let's consider such a temperature cycle. It can be defined by several parameters (Fig. 6) : the initial temperature T_{min}, the maximum temperature reached T_{max}, the amplitude of temperature ΔT, the temperature rise speed $\dot{T}$, the maintenance duration $t_{maintenance}$, the spatial temperature gradients $\nabla_{x/y/z} T$, etc. Finite Element calculations of a cylinder head have been completed by varying the different parameters within ranges that are representative of an operating engine, in order to identify the most damaging parameters. It led to the definition of a global thermal load parameter, called CT_{max}.

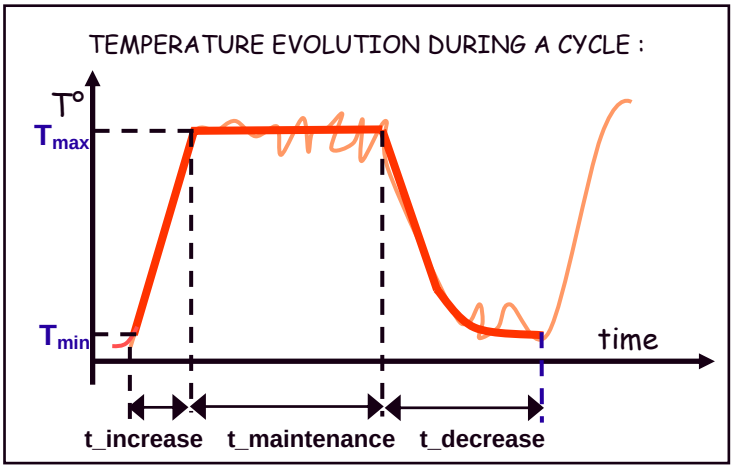


Figure 6. Temperature cycle

Simulations with different cylinder heads and different solid structures under similar thermomechanical loads showed that a global damage law can be identified, giving the number of cycles before crack initiation in terms of the global parameter CT_{max}. Its equation is given by (Eq. 3) :

$$CT_{\max} = \alpha \ln N_f + \beta \qquad \text{Eq.3}$$

where α is a material parameter but β is associated to the structure.

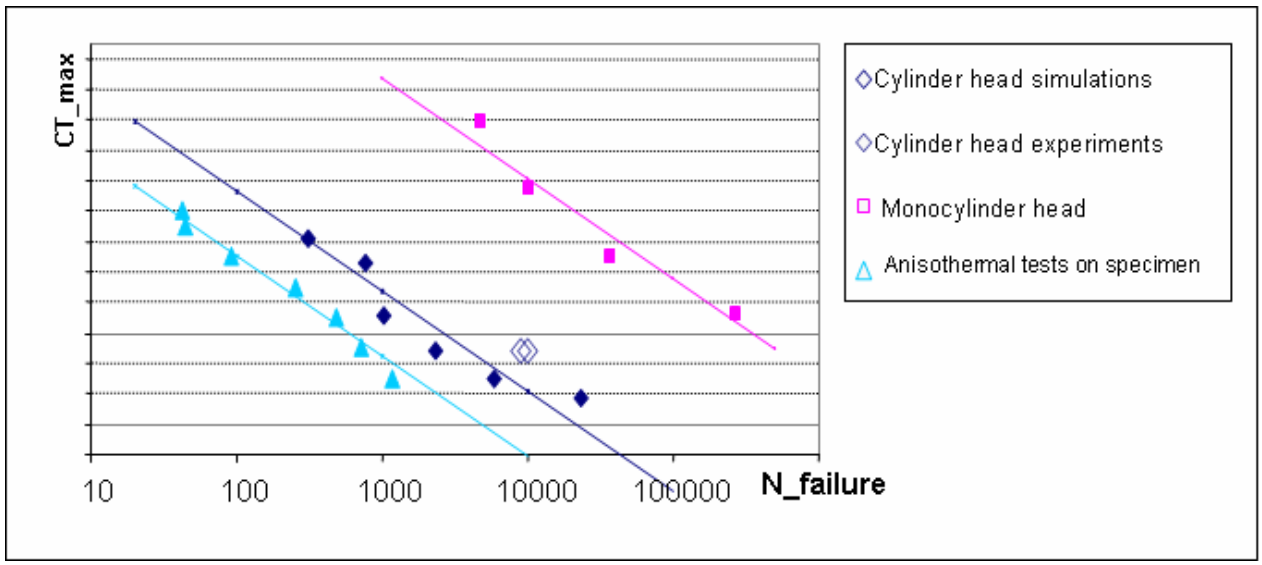
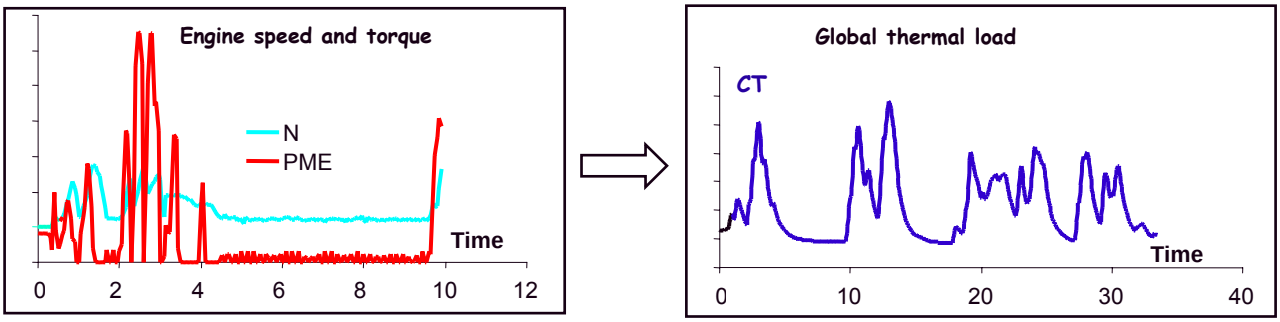


Figure 7. Global damage law

The second step is the transformation of random signals of engine speed and torque into a global thermal load parameter *CT*. A 2D simplified engine thermal model has been used for this purpose. For a one month measurement of speed and torque, the global thermal load parameter *CT* is calculated within one hour. Its evolution in time is given in Figure 8.



The third step is to extract from this temporal signal the elementary cycles. The rainflow couting method is not appropriate here. Indeed, the damage analysis shows that the important values are the maximum values reached by the global thermal load parameter. Another result from the fatigue analysis is the statement that all variations of CT under a given value $CT_{threshold}$ do not generate any damage. Hence, each cycle will be defined by a sequence $CT_{threshold}$-CT_{max}-$CT_{threshold}$. A cycle counting method has been developed in order to identify in any random signal the damaging events.

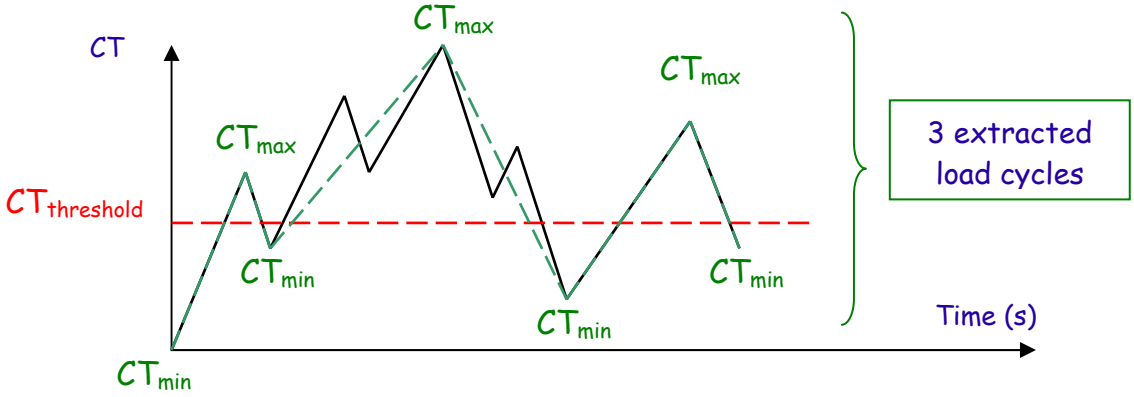


Figure 9. Cycles counting

For each customer, a histogram of ($CT_{max(i)}$, n_i) can be calculated with the described method. Knowing the global damage law (Eq. 3), the partial damage induced by each cycle can be calculated. A miner cumulative damage calculation gives the total damage induced by the sum of all elementary cycles. A new cycle is then defined, which generates the same damage than the total elementary cycles if repeated N_{eq} times. The value of this equivalent global thermal load parameter $CT_{\max}^{eq}$ is the measurement of the customer severity.

3.3 Application to a small customers enquiry

The thermomechanical load analysis methodology has been applied to a diesel cylinder head for which a small customer inquiry has been carried out. For 9 customers, the engine speed and torque have been recorded. From these random signals, the time evolution of the global thermal load parameter CT is calculated and a relevant cycle counting method gives a histogram of ($CT_{max(i)}$, n_i), from which a thermomechanical fatigue equivalence $CT_{\max}^{eq}$ is calculated. An example of histogram is given in Figure 10. The fatigue equivalences of the 9 customers are given in Figure 11.

The experimental tests made at PSA can also be analyzed with this methodology and be put in the same graphics, in order to evaluate their severity compared to the customers. The results obtained (they can not be showed in this paper for confidentiality reasons) showed that the benches are pretty well defined for the current engines (with a traditional architecture and traditional combustion strategies).

4. CONCLUSION

A new methodology (which is still under development at PSA) has been described. Its objective is to improve the reliability of automotive engine hot components and to anticipate the impact on the severity of the applied loads of the introduction of new architectures, new engine technologies or new after-treatment systems.

This methodology enables a reliable thermomechanical fatigue design of engine components, within the Stress Strength Interferece Approach. A new thermomechanical load analysis method is proposed, consistent with the physical damage mechanisms, and a thermomechanical fatigue equivalence is defined.

The approach can be applied to any component submitted to thermomechanical fatigue, such as exhaust manifolds, pistons…, but needs a preliminary work of identification of a global load parameter and a global damage law.

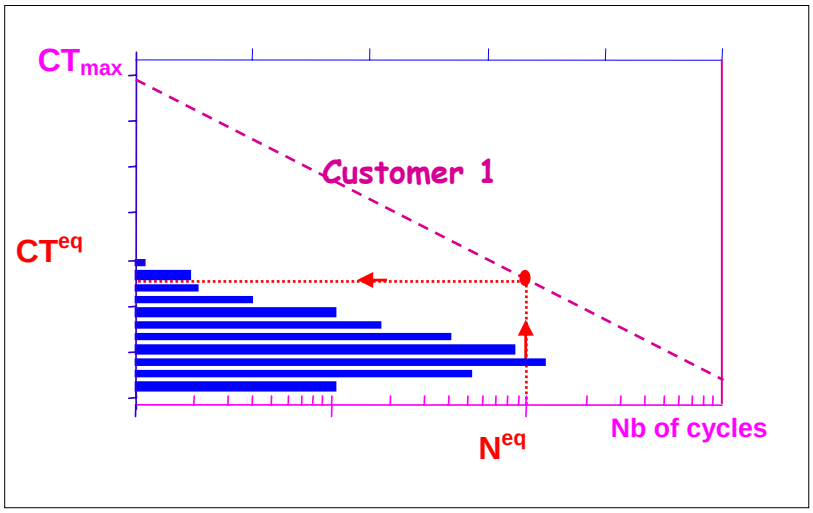


Figure 10. Customer analysis and fatigue equivalence definition

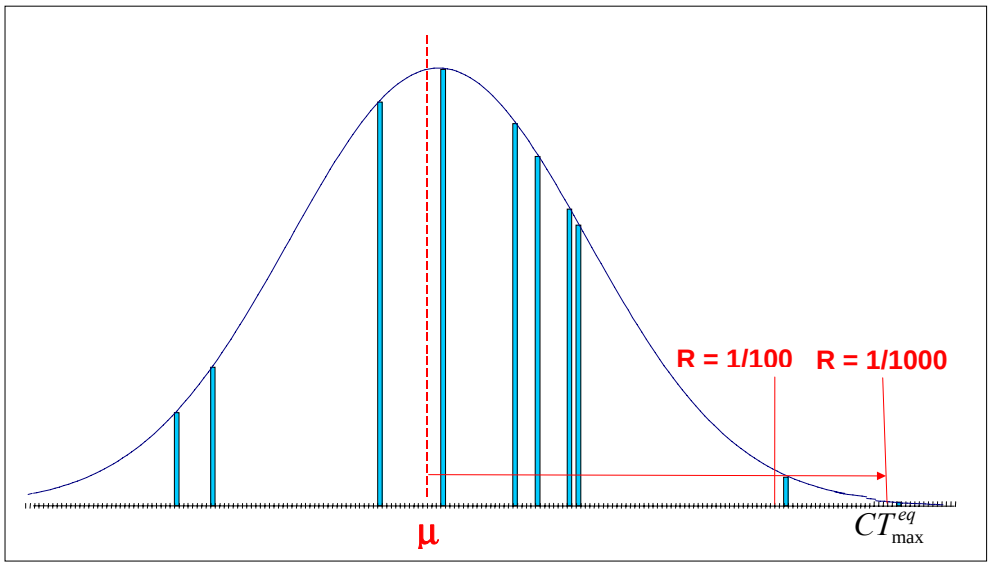


Figure 11. Customers severity distribution

5. REFERENCES

Conference Proceedings

1. Nguyen-Tajan T.M.L., B. Pommier, H. Maitournam, M. Houari, L. Verger, Z.Z. Du, M. Snyman. Determination of the stabilized response of a structure undergoing cyclic thermal-mechanical loads by a direct cyclic method, Abaqus Users Conference, 2003.
2. Thomas J.J., A. Bignonnet, 2001, Equivalence fatigue – état de l'art, Journées de printemps SF2M, Paris, Publ. Société Drançaise de Métallurgie et de Matériaux, 2001.
3. Thomas J.J. : Approche fiabiliste du dimensionnement dans l'industrie Automobile. Phoebus Tome 1, n°.23, pp. 45-58, 2003.
4. Genet G., Johannesson P., Gualandris D., De Maré J., Nguyen-Tajan T.M.L. : « An approach to multi-dimensional equivalent fatigue loadings", Proceeding of IMECE 2005, ASME International Mechanical Engineering Congress and Exposition, Orlando, Florida, USA, November 2005.

Journal Article

5. R. Le Riche, D. Gualandris, J.J. Thomas, F. Hemez : Neural identification of nonlinear dynamic structures. Journal of Sound and Vibration, 2001, 248(2), pp.247-265.
6. Charkaluk E., Bignonnet A., Thomas J.J. : Dimensionnement à la fatigue thermomécanique dans l'industrie automobile. Mécanique et Industrie 5, 27-40, AFM EDP Science, 2004.

Dissertation or Thesis

7. Pommier B., Dimensionnement thermomécanique des culasses par la méthode cyclique directe , Thèse de Doctorat de l'Ecole Polytechnique, 2003.
8. Charkaluk E., Dimensionnement des structures à la fatigue thermomécaniques, Thèse de doctorat de l'Ecole Polytechnique, 1999.

Thermal Fatigue Design of Stainless Steel Exhaust Manifolds

Pierre-Olivier Santacreu[a], Laurent Bucher[b], Alain Koster[b], Luc Remy[b]

[a] UGINE&ALZ Research Center, Isbergues, France
[b] ENSMP-Centre des Matériaux, Evry, France

Abstract The paper will deal with the thermal-mechanical fatigue of stainless steels at high temperature, specially used for exhaust gas manifold fixed to the engine. A dedicated thermal fatigue test on V-shape specimen was early developed in order to simulate such thermal and mechanical conditions. The examination of failed specimens tested in different thermal cycles indicates that cracks could be generally attributed to out-of-phase thermomechanical fatigue. On the other hand, when an important coupling with oxidation damage occurs especially with austenitic grades or when temperature is critical for the grade, In-phase thermomechanical fatigue has to be considered and it may be preponderant. In parallel an effort was achieved for the identification of the elastoviscoplastic behaviour of stainless steel from the room temperature to 950°C. Based on finite element calculation of the thermal fatigue test, a damage criterion is proposed for Out-of Phase TMF which correlates very well the amplitude of the viscoplastic strain, the maximal temperature, dwell time during the cycle and the number of cycles to failure.

1 INTRODUCTION ON THE APPLICATION AND MATERIALS

In an effort to decrease the polluant emission of vehicle by catalytic conversion, the temperature of the exhaust gas tends to increase. Consecutively the durability of the exhaust line, especially both corrosion and thermomechanical fatigue (TMF) resistances, need to be improved significantly by the use of stainless steel rather than cast iron. The manifold is the hottest part of the exhaust system, bolted on the motor block to collect the hot burned gas and to remit them to the catalytic converter. The exhaust manifolds are now widely made of stainless steel bent tubes or stamped shells (Fig. 1). The ferritic F12T (AISI 409-EN 1.4512) is the most common grade for exhaust line application but can be use only up to 850°C, so for temperature up to 950°C the ferritic grades F17TNb (AISI 441 EN1.4509) or F14Nb (SUS429 EN1.4595) need to be used because these grades exhibit better high temperature (HT) properties [10,14]. Well known austenic grades as AISI 304 EN1.4301 or AISI321-EN1.4541 are rarely used because of their very poor cyclic oxidation resistance due to important oxide layer spallation and their higher thermal expansion coefficient. So, only more costly autenitic refractory grades can be considered at such HT, like R20-12 (AISI 308Lsi – EN 1.4828), but they exhibit also poor cyclic oxidation properties for maximal temperature higher than 900°C.

Focusing on the TMF, the in-vehicle loading history for the exhaust manifold is not well known and no failed parts were returned from customer vehicles because of a quite new application of stainless steel exhaust manifold market. On the other hand, the motor bench test which is the validation test for acceptance performed by exhaust makers, is more accessible. A typical motor bench cycle has duration of around 1000 seconds including a full load period of 400 seconds leading to the highest temperature an idling period where the temperature decreases below 600°C. The maximal and minimal temperature depends on the power and stroke of the engine, but they are generally in the range from 100°C to 950°C. An exhaust manifold has to pass approximately 1500 cycles to be considered validated for production. When fractures are observed, they are characterized by orange peel or striction around the cracks due to a plastic deformation, and further by a multiple cracking [12]. Oxidation is often observed, especially in case of austenitic grades.

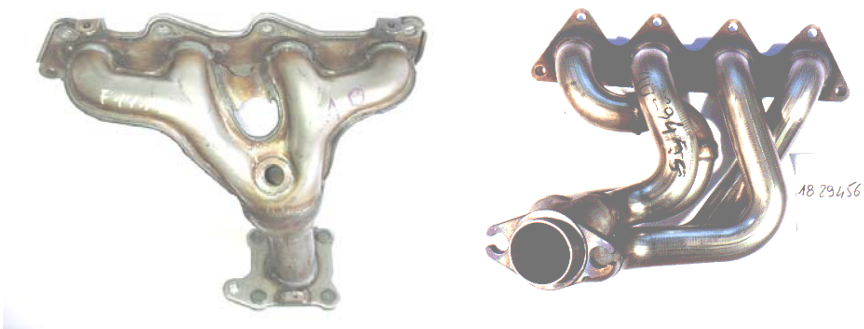


Figure 1. Exhaust manifolds, clamshell (left) and tubular (right).

2 STUDY OF THE THERMAL FATIGUE

2.1 Simulation test of the thermal fatigue

A constricted part submitted to a thermal cycle evidences a typical thermal fatigue process. Due to the drop of the mechanical properties of the metal with the increasing temperature, a plastic accommodation is observed during the first half cycle - first heating - leading to a state of low stresses at the highest temperature. Further, the first cooling and the following cycles lead to stabilized loops characterized by a maximal tensile state of stress at the minimal temperature. Such cycle is designated as out-of-phase thermo-mechanical fatigue cycle. The experimental adaptation of this principle is quite impossible on thin sheet sample because of buckling of the geometry due to the compressive stress during the first heating. Consecutively, a dedicated thermal fatigue test has been early developed which permits to impose thermal cycle on a clamped V-shaped specimen by alternate resistance heating and air-cooling. The thermal fatigue life of a specimen is expressed as the number of cycles to failure and is determined for a 50%-drop of the constrained force. For a given grade, the fatigue life depends on the maximal and minimal temperature of the cycle, dwell time at the maximal temperature and specimen thickness. The advantage of this test is that it is both simple for classing the stainless steel grades and representative of the thermal fatigue process occurring in an exhaust manifold, and so aiming a study of the damage mechanisms. It has been already described in detail in references [4,5,6] and figure 2 recalls its main features.

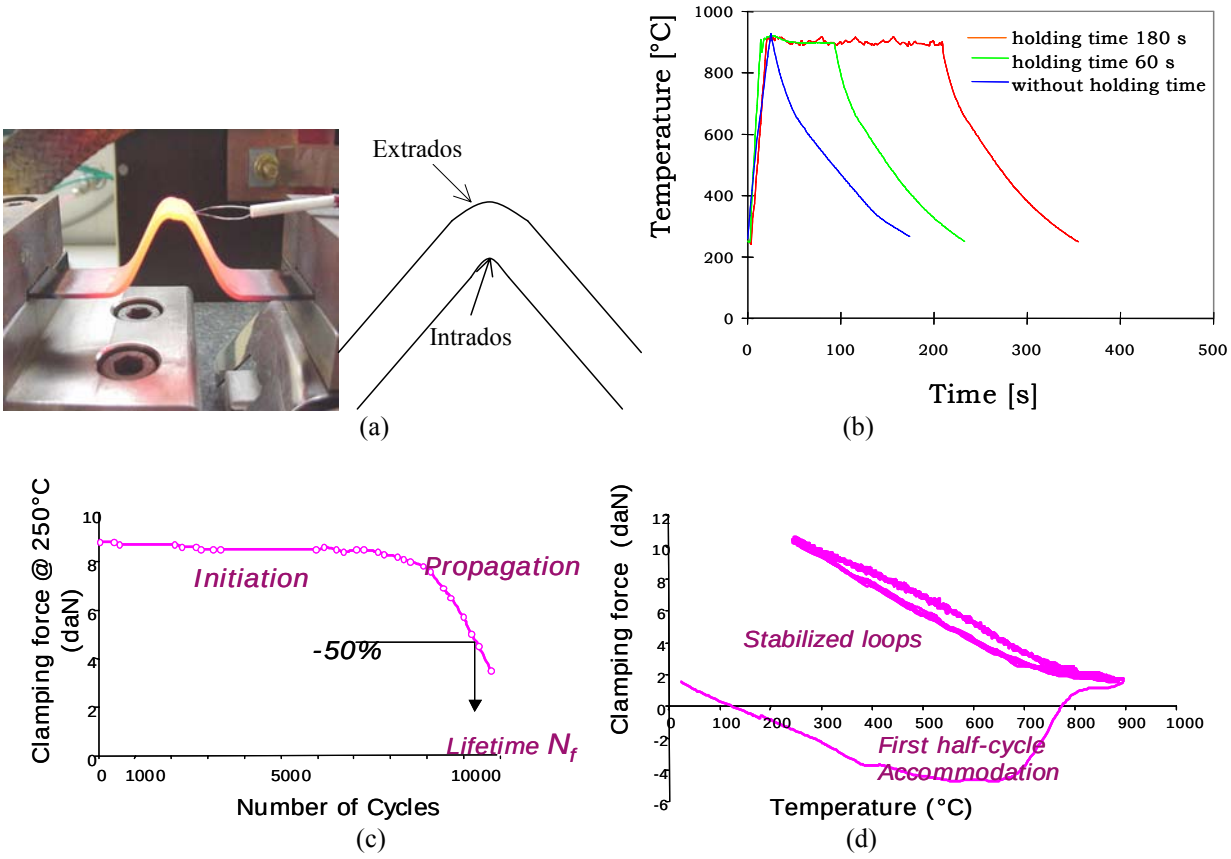


Figure 2. Thermal Fatigue test developed (a) V-specimen and definition of intrados and extrados, (b) example of thermal cycles, (c) curve of the clamping force as function of number of cycles and (c) curve of the clamping force as function of temperature.

2.2 Thermal fatigue damage

Many results were obtained on the different stainless steel grades, for peak temperature from 650°C to 1000°C and for dwell time up to 180 seconds. In fact, metallographic observations performed on cut specimens at the end-of life or for a given intermediate number of cycles have revealed two types of cracks (Fig.3):

- At intrados, multi crack initiation, generally follow by the propagation of one of the cracks. This damage process occurs in all cases, the crack exhibits blunted tip.

- At extrados, a multi crack initiation coupled with an important oxidation. Voids probably due to creep cavitation can be also observed. This damage process occurs when the stainless steel is an austenitic one and becomes predominant when the peak temperature is higher than a given critical temperature.

A progressive plastic deformation as shown by the profile evolution of the specimen is evidenced in case of austenitic grade (Fig.4).

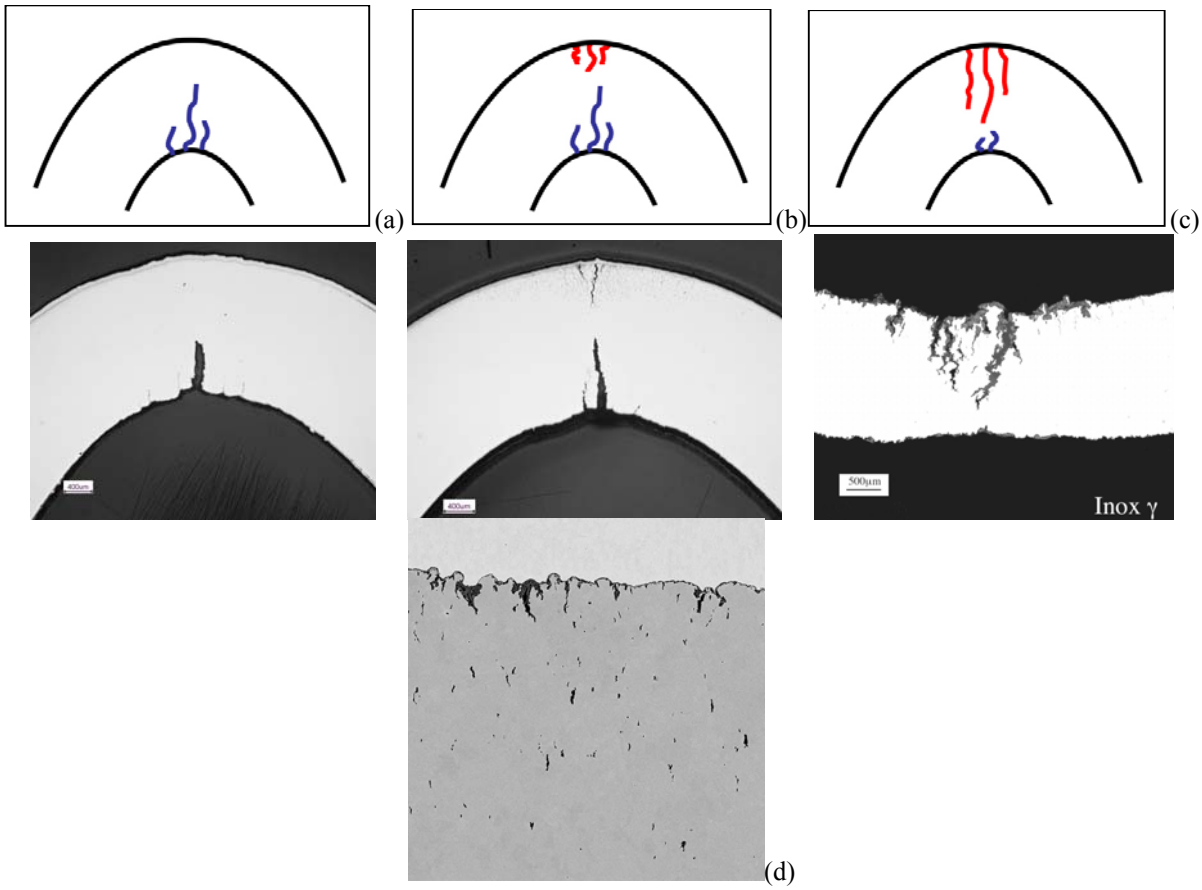


Figure 3. Schematic representation of the damage process at intrados (blue) and at extrados (red) on the V–shaped specimen and metallographic examination of specimen made of ferritic AISI 441 (a), of austenitic AISI308LSi (b) both under thermal fatigue between 250°C and 850°C, (c) of austenitic AISI308LSi submitted to a cycle 250-950°C and (d) shows creep voids.

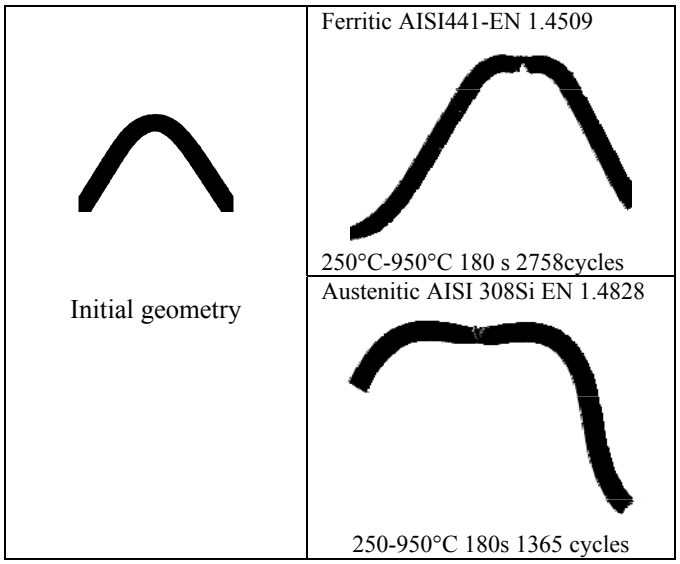


Figure 4. Profile of the V-shape specimen after thermal fatigue testing.

2.3 Thermal fatigue life

Figure 5 shows thermal fatigue life for different stainless grades and the effect of dwell time at the maximal temperature, especially its more detrimental effect on austenitic grades

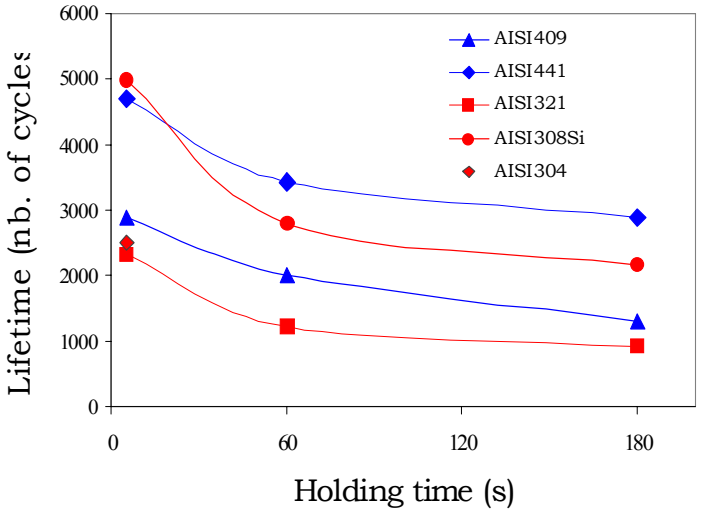


Figure 5. TF results for 250°C-900°C cycles with different dwell times

3 DAMAGE MODEL AND THERMAL FATIGUE DESIGN

3.1 Behaviour model and FE modelling of the TF test

In order to simulate numerically the stress and strain in the V-shape specimen, an accurate behaviour model is necessary. Because of the involved temperatures, an elasto-viscoplastic (EVP) behaviour description has to be preferred to a solely elastoplastic one. In fact, the EVP behaviour of a metal subjected to cyclic loading at high temperature is well-described using a non linear kinematic hardening model coupled with a Norton law; like the model proposed by J.L.Chaboche [1]. Identification of such model was already described in detail in different references [7,8,13, 15]. ABAQUS Finite Element software [2] was used as solver for both thermal and mechanical analysis of the different experiments where thickness, maximal and minimal temperatures, holding time and grade were varied. First, the thermal analysis was done to fit precisely the experimental measurements by thermocouples. A User Material procedure was necessary to perform the thermomechanical analysis [3]. Different experimental conditions were simulated but, considering the rapid stabilization loop, only the four first cycles are simulated. The FE modelling of the TF test permits to compute the state of strain and stress in the specimen along the duration of the cycle and will help for the identification of a dedicated damage criterion. Thus, finite element simulation evidenced 2 types of TMF cycles: an out-of-phase TMF cycle at intrados of the specimen and an in-phase TMF cycle at extrados (Fig.6).

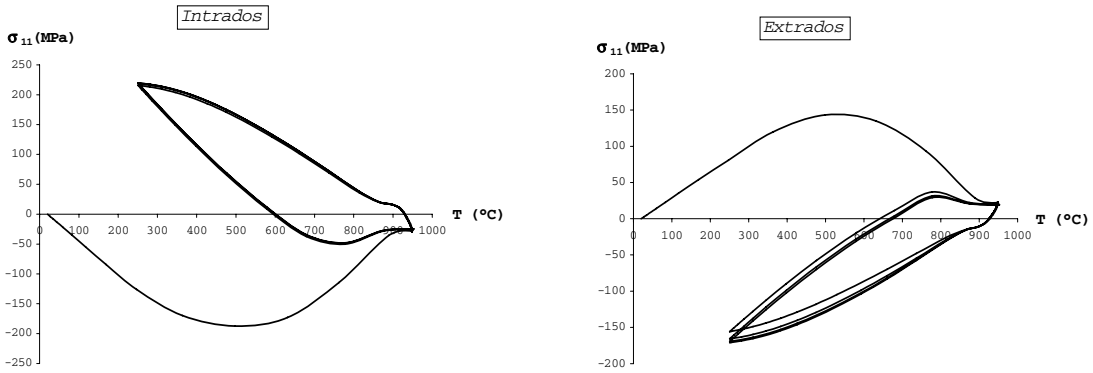


Figure 6. Out-of-phase TMF at intrados of the specimen & in-phase TMF at extrados.

3.2 Modified Taira damage model

Correlation between the number of cycles to failure obtained from the TF test and the amplitude of cumulated plastic strain ($\Delta\varepsilon_p$) at intrados obtained after a FE analysis of the same test allows to build a predictive model. Indeed, Taira in reference [11] proposed a relation between thermal fatigue and low-cycle fatigue durability:

$$N = \lambda(T)\Delta\varepsilon_p^{\ t}$$

T represents the maximum temperature or the mean temperature of the thermal cycle. Moreover, according to Taira, t is expected to be around –1. In our case, we assumed the exponent t independent of temperature and λ is a function of the maximal temperature and the dwell time. Given that mechanisms of oxidation and creep are temperature activated in the form of $e^{-Q/RT}$, the Taira model was modified in the following form :

$$N = \lambda\,(T_{eq})\,\Delta\varepsilon_p^{\ t} \quad \text{where} \quad T_{eq} = \frac{T_{max}}{1 - aT_{max}\ln(1+b\tau)}$$

With τ is the dwell time, a and b are parameters evaluated from tests. This predictive model has been evaluated from experimental points at different maximal temperatures between 650°C and 1000°C and for three dwell times up to 180 seconds. Exponent t was found around to –0.9. Indeed, this model is so far limited to "out-of-phase" mode which is the main mode occurring in ferritic exhaust manifold (Fig. 7).

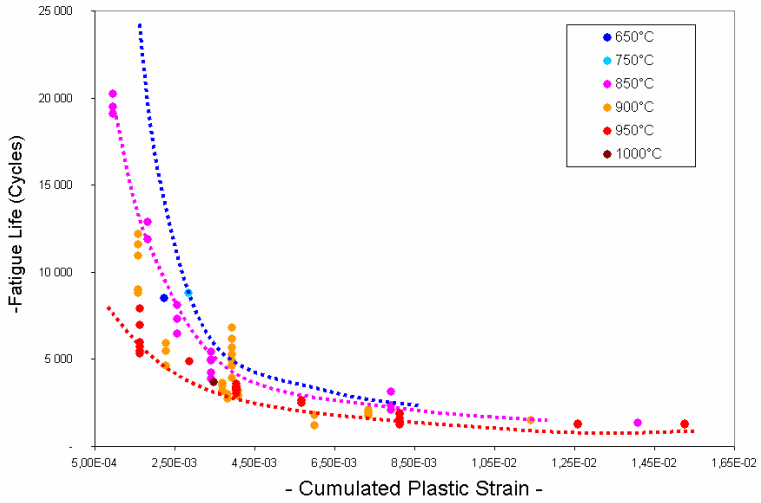


Figure 7. Fatigue life as function of the plastic strain amplitude

3.3 Crack propagation model

At time, studies are performed on the crack propagation under thermal fatigue (Fig.8) using Tomkins propagation law [15].

$$\frac{da}{dN} = f(\Delta\varepsilon_p, \Delta\sigma).a$$

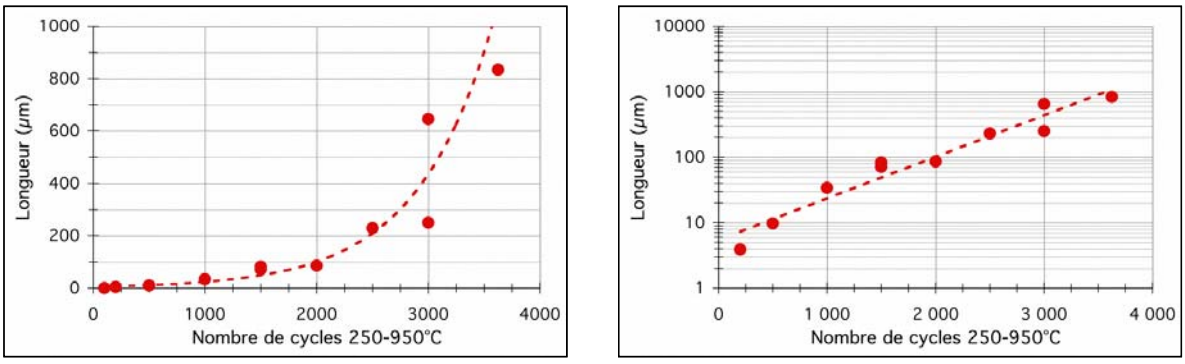


Figure 8. Crack propagation curves : crack length as function of number of cycles

4 DESIGN TOOL OF STAINLESS STEEL EXHAUST MANIFOLD

A dedicated tool, called Xhaust-LIFE, has been developed to apply the predictive model after an ABAQUS simulation [9]. It consists of reading the data recorded in the "output data base" (ODB) file created by ABAQUS, then computed the lifetime, and finally writes the results in the (ODB) file so the visualization can be done with ABAQUS Viewer. The figure 9 shows the links between Xhaust-LIFE and ABAQUS. The calculation can use material parameters defined by the user or material in a library. The library includes data for the ferritic grade F17TNb (EN 1.4509), for the austenitic R20-12 (EN 1.4828) and for the new developed grade F14Nb. Because of the identification procedure, models for ferritic grades are valid only for Out of Phase mode (cracks start at intrados) and must be completed by other tests. In opposite, model for austenitic grade features both Out of Phase and In Phase parameters.

Xhaust-life is today applied for the design of exhaust manifold, so for prediction of possible crack location and assumption of life time of the part (fig.10).

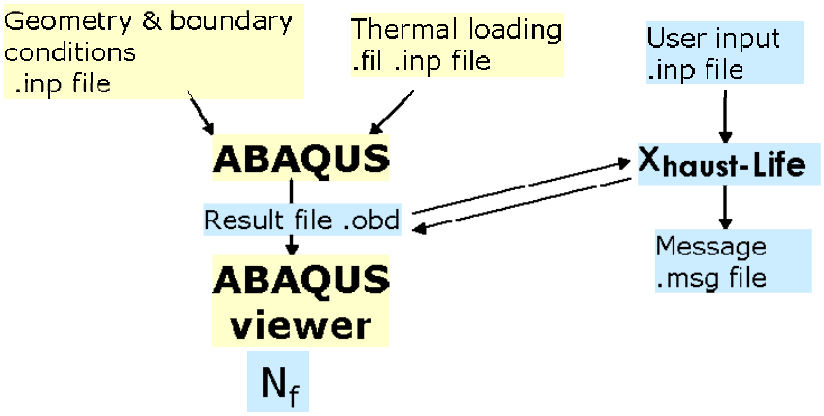


Figure 9. Links between Xhaust-LIFE and ABAQUS

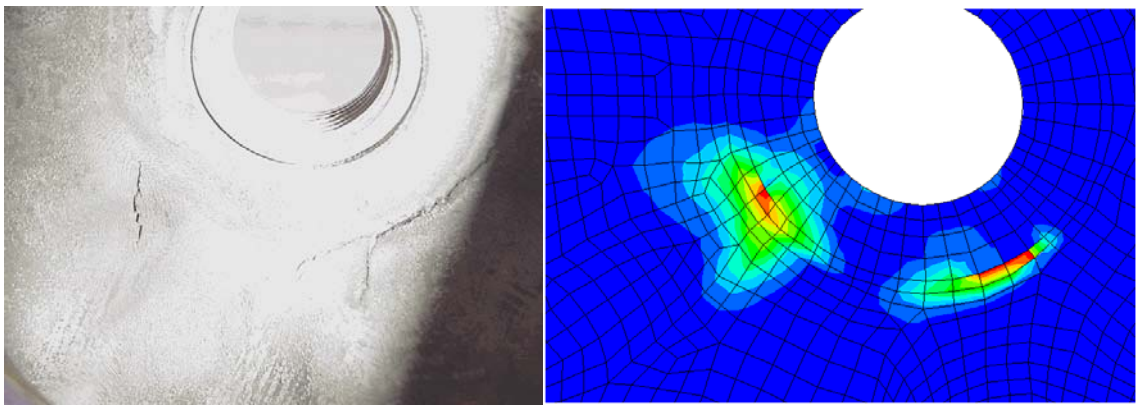


Figure 10. TF damage prediction on Exhaust manifolds

5 CONCLUSIONS

The V-shape thermal fatigue test developed and its thermal-mechanical analysis evidences two main damage mechanisms of stainless steel grades:

- A plastic crack propagation in an out-of-phase process when the maximal temperature is below a critical temperature which is a function of the grade. This is the main damage mechanisms for stainless ferritic grades like AISI 441 and up to 950°C.
- A creep-oxidation damage in in-phase process when the peak temperature is higher than a critical temperature. This mechanism could become predominant when cyclic oxidation resistance is weak, and appears to be very detrimental in case of austenitic grades, like AISI308S, when T>850°C.

Accurate elastoviscoplastic behavior model has been identified and is now available to simulate the stresses and strains in a part submitted to thermal fatigue. The modified-Taira predictive model is now available through a post-processor developed by UGINE&ALZ and named Xhaust-Life. Results of the TMF analysis can be visualized using the ABAQUS viewer. The database of Xhaust-life includes parameters for Ugine & ALZ grades used in exhaust manifold application. First trials on real manifolds provided satisfactory results. The use of a virtual thermomechanical fatigue design approach permits to optimize the design of the manifold and limits both the number of prototype and motor bench tests and, finally, reduces the risk of failure.

6 REFERENCES:

6.1 Book

1. J.Lemaitre, J.L.Chaboche, Mécanique des matériaux solides, Dunod Eds, Paris, 1985.
2. Abaqus, Hibitt, Karlsson and Sorensen, Inc, 1998.
3. Northwest Numerics and Modeling Inc. And Ecole des Mines de Paris, Z-Set /Z-Aba, version 8 manuel,1999.

6.2 Conference Proceedings

4. P.-O. Santacreu et al., Third International Congress on Thermal Stresses,Thermal Stress'99, Cracow, Poland, Skrzypek and R.B.Hetnarski Eds., 1999, pp.245
5. H.Sassoulas, P.-O.Santacreu, 18ème Journée de Printemps, Commission de Fatigue des Matériaux-Dimensionnement en Fatigue des Structures: Démarches et Outils, Société Française de Métallurgie et de Matériaux SF2M, Paris, 2-3 Juin 1999, p. 161.
6. P.-O.Santacreu, Lifetime Prediction on Stainless Steel Components under Thermal Fatigue Load. 9th International Spring Meeting , Temperature-Fatigue interaction, 2001, pp.393-402.
7. C. Simon and P.-O.Santacreu, (2002) Lifetime prediction of exhaust manifold in TMF, Proc. CAMP2002, High temperature Fatigue, Eds. G.Ballias et al., pp.257-267.
8. L.Bucher et al., Thermomechanical fatigue behavior of stainless steels for automotive components, 5th International Conference on Low Cycle Fatigue (LCF5) 9-11 September 2003, Berlin, Germany.
9. C.Simon and P.-O.Santacreu, Technological Innovation for land transportation, TILT2003, 2-4 Décembre 2003 Lille, France.
10. J.-H.Schmitt et al., Stainless Steels for exhaust line , Int. seminar on Modern developments in metallurgy and technologiesof steels for automotive industry, Moscou, 17-18 Feb, 2004, p281.

6.3 Journal Article

11. S. Taira, Relationship Between Thermal Fatigue and Low-Cycle Fatigue at Elevated Temperature, Fatigue at Elevated Temperatures, ASTM STP 520, ASTM, 1973, pp.80-101
12. Y. WATANABE et Al. *"Thermal Fatigue Life Prediction for Stainless Steel Exhaust Manifold"*, SAE Technical paper series 980841, ASTM STP 520, 1998, pp. 147-152.
13. P.-O. Santacreu, C.Simon, A. Coleman, (2002) Thermomechanical Fatigue Behavior of Stainless Steel Grades for Automotive Exhaust Manifold Applications, Thermomechanical Fatigue Behavior of Materials: 4th Volume, ASTM STP 1428, M.A. McGaw, S. Kalluri, J.Bressers, and S.D.Peteves, Eds, ASTM Int.
14. P.-O.Santacreu et al, Design of stainless steel automotive exhaust manifold, La revue de Metallurgie, CIT, Juillet Août 2004, p.615.

6.4 Dissertation or Thesis

15. L.Bucher , Fatigue thermique des aciers inoxydables F17TNb et R20-12 pour application automobile, PhD thesis, Ecole des Mines de Paris, 2005.

Development of a cohesive model for the crack propagation in single crystal superalloys for turbine blade applications

J.L. Bouvard, J.L. Chaboche, F. Feyel, F. Gallerneau

ONERA, DMSE / LCME,
29 avenue de la Division Leclerc, BP 72, F-92322 Châtillon
Jean-Luc.Bouvard@onera.fr

Abstract A numerical coupled analysis using a cohesive zone modelling under cyclic loading is proposed in order to develop a coupled predictive approach of the crack growth in single crystal. The process of material separation during fatigue crack growth is described by the use of an irreversible cohesive zone model which governs the separation of the crack flanks and eventually leading to the formation of free surfaces.The cohesize zone element is modeled to accumulate fatigue damage during loadings and no damage during unloadings. The paper presents the damage model and its application in the study of the crack growth in a precracked specimen.

1 INTRODUCTION

In blading components, a large amount of service life time is taken up in initiating and growing surface or near surface short cracks through the Stage I regime in fatigue, that is when the crack length is small compared to the scale of the crack tip plasticity. Such fatigue cracks driven by mechanical and thermal stresses can lead to catastrophic failures of components. This is why the short cracks behaviour in Ni-base superalloys has received considerable attention.

Following the pioneering work of Paris et al. [1], phenomenological laws, relating the crack growth rate, da/dN and the amplitude of the applied stress intensity factor, ΔK, have provided a valuable engineering analysis tool. Paris's law successfully describes the experimental data under 'ideal' conditions: small-scale yielding, constant amplitude loading and long cracks. This has encouraged a number of modifications of Paris's law like taking into account R-effects, threshold limits, closure effects and others. The case of short cracks can also significantly underestimate the growth rate [2]. The proliferation of fatigue laws seems to suggest that the essential physics of fatigue crack growth is not completely described by the theory.

Another approach, which is explored in this paper, is the use of cohesive theories of fracture. Cohesive zone models consider fracture as a gradual process in which the separation between material surfaces is resisted by cohesive tractions. A number of cohesive zone models has been proposed and successfully applied to describe monotonic fracture processes [3-5]. But the use of such damage models in the case of fatigue regime shows that the crack arrests due to redistribution of stresses at crack tip. Thus specific cohesive zone models have to be developed to simulate the crack propagation under cyclic loadings[6-8].

In this work a cohesive zone model is developed to simulate the fatigue crack growth. In the first part a fatigue damage model is developed. Then the geometry of the test problem is presented and constitutive equations of the single crystal material used are defined. In the last section we validates the using of cohesive zone approaches with convergence study and then different numerical results are presented to simulate the crack propagation in a tensile fatigue specimen.

2 COHESIVE ZONE MODELS: A THERMODYNAMIC CYCLIC DAMAGE MODEL

The virtual power principle including cohesive zone models reads :

$$\int_V \sigma : \delta\varepsilon dV + \int_{S_{int}} T_{cz} \cdot \delta\Delta U dS = \int_{S_{ext}} T_e \cdot \delta u dS \tag{1}$$

Where, V is the specimen volume and S_{ext}, the external specimen surface. $x_i = (x, y, z)$ are the coordinates, U_i and T_e^e are the components of displacement and traction vector, respectively; σ is the Cauchy stress while $\delta\varepsilon$ is the symmetric gradient of the test field δu. Traction vectors and stresses are related by $T = n\sigma$, with n being the surface normal.

The second term in the left hand side of Eq. 1 is the contribution of the cohesive surface, representing the crack and the process zone in front of the crack tip.

The separation process is defined through the relationship between the cohesive traction, T_{CZ}, and the material separation, ΔU. The cohesive law, developed to describe material separation under fatigue loading, is built using a potential function, Φ:

$$\Phi = \frac{1}{2} \cdot (1 - D_f) \cdot k_N \cdot \left[\frac{\langle U_N \rangle^2}{\delta_c} + \alpha \frac{U_T^2}{\delta_c} \right] \tag{2}$$

Cohesive tractions in normal and shear, T_N and T_T, are obtained by deriving Φ. In the present paper, we choose a constitutive equation set in which the traction is a linear function of the separation, while the energy dissipation is taken into account through a nonlinear damage variable.

$$T_T = \frac{\partial \Phi}{\partial U_T} = \alpha \cdot k_N \cdot (1 - D_f) \cdot \frac{U_T}{\delta_c} \tag{3}$$

$$T_N = \frac{\partial \Phi}{\partial U_N} = k_N \cdot (1 - D_f) \cdot \frac{U_N}{\delta_c} \tag{4}$$

The material parameters in Eq. 3 and 4 are the initial stiffness of the cohesive zone k_N, a constant α, the critical displacement δ_c and D, the damage variable, ranging from zero to one.

The associated thermodynamic force reads:

$$Y = -\frac{\partial \Phi}{\partial D_f} = \frac{1}{2} \cdot k_N \cdot \left[\frac{\langle U_N \rangle^2}{\delta_c} + \alpha \frac{U_T^2}{\delta_c} \right] \tag{5}$$

Following Roe and Siegmund [10], we choose an incremental evolution of damage $\dot{D} = \dot{D}(D, Y, \dot{U})$. A positive part function is used so that damage occurs only under loading conditions.

$$\dot{D}_f = A \cdot \delta_c \cdot (1 - D)^m \cdot \left\langle \sqrt{Y} - \sqrt{Y_0} \right\rangle^n \cdot \frac{\|\dot{U}\|}{\delta_c} \quad \textbf{if } \dot{Y} \geq 0 \tag{6}$$

$$\dot{D}_f = 0 \quad \textbf{else} \tag{7}$$

where A is a parameter controlling the damage accumulation, ||.|| is a norm of the displacement equal to $\sqrt{(\frac{U_N}{\delta_c})^2 + \alpha(\frac{U_T}{\delta_c})^2}$, $\dot{U}$ is the opening displacement rate, m and n are parameters which control the damage rate and Y_0 is the cohesive zone endurance limit .

Figure 1 shows the response of the analytical model under cyclic loading. During the first loading, characterized by a large intensity, the "damage locus" is reached (cohesive law for monotonic loading). Then, for a cyclic loading with a non-zero stress ratio (R), the locus of traction/separation ranges between a maximum and a minimum load level. The damage increases during loading and remains constant during unloading. Moreover, we consider that all the energy dissipated by the crack growth is transformed into elastic energy.

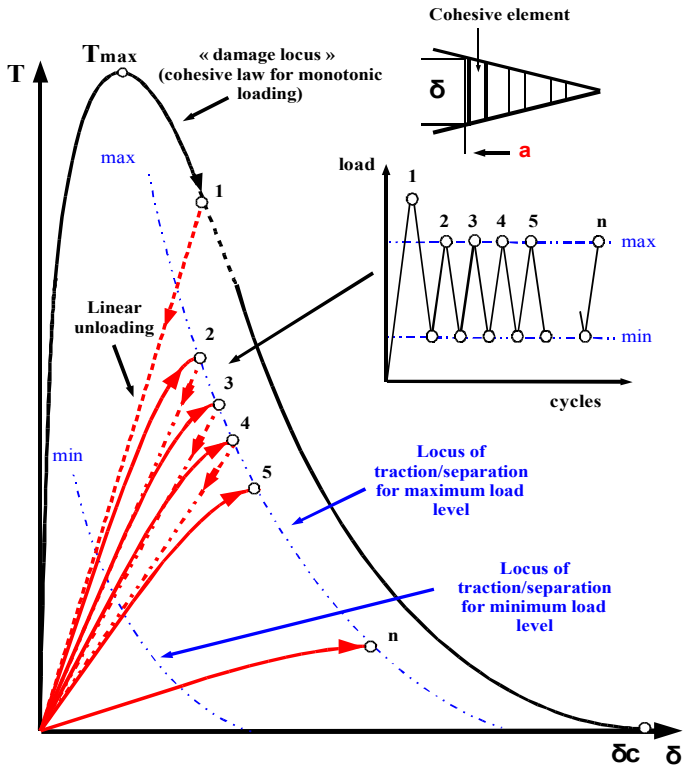


Figure 1. Cohesive law with damage accumulation during cyclic loading

3 PROBLEM DEFINITION

3.1 Problem geometries

For the purpose of analyzing the crack growth problem, we consider a single edge notch (SEN) specimen as shown in figure 2 with an initial crack length a_0. The finite element discretization takes into account the symmetry of the loading and the geometry. Some details of the mesh near the crack tip are shown in figure 3.

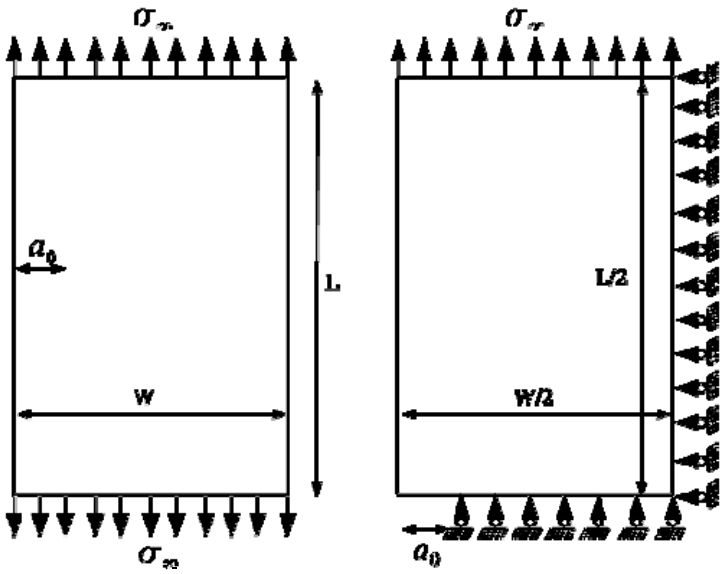


Figure 2. Dimension of the single edge notch specimen, geometry and boundary conditions used in FE model.

The mesh contains quadratic triangular elements (with a reduced integration rule) under the plain stress assumption. A zoom in the refined mesh zone shows up a regularly meshed box where cohesive elements are. The crack propagation is assumed to occur along the line of symmetry (as observed experimentally) and modelled with cohesive zone elements having zero thickness in the direction normal to the crack growth. Several mesh sizes are considered. The precracking is modelled with a node release method in the order to get a good estimation of the wake plastic zone and to decrease the strain localisation due to crack initiation.

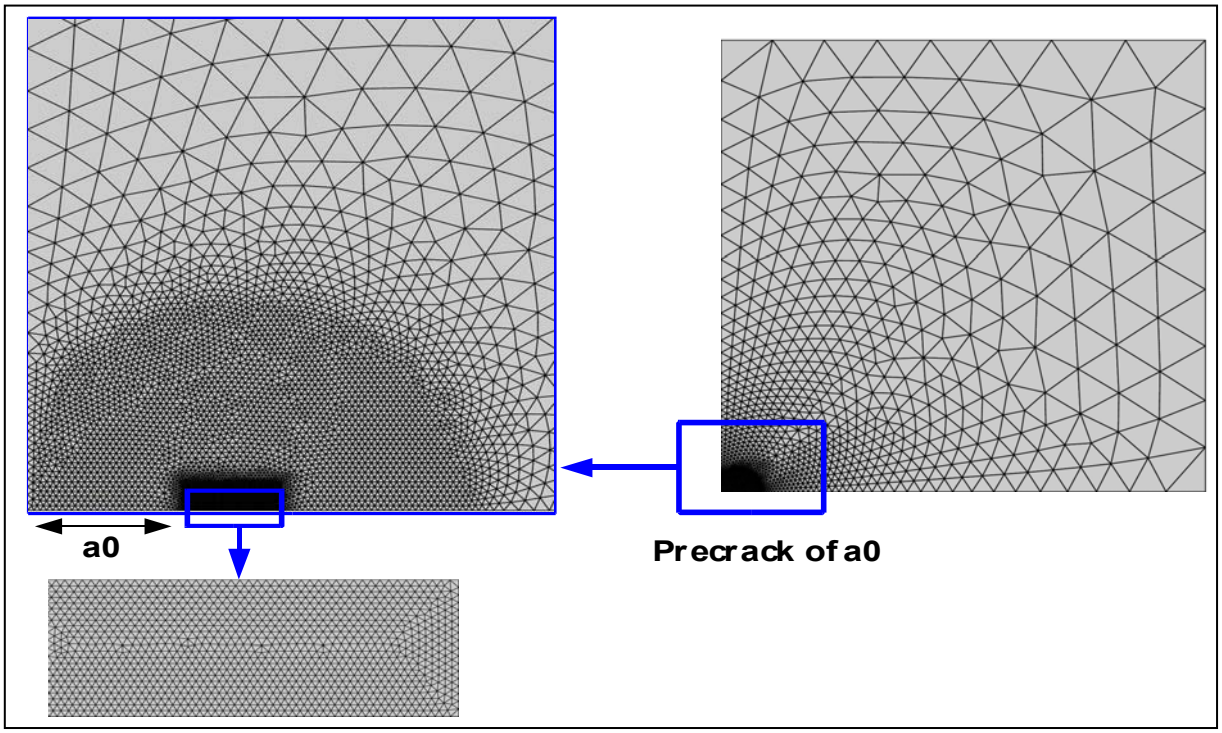


Figure 3. The mesh used for the FE analysis.

3.2 Material properties

Single crystal superalloys are widely used in high pressure turbine blades. In this work, a model is used that describes the elasto(visco)plastic behavior of f.c.c single crystals ([11]). It is based on crystal plasticity theory. The total strain is split into an elastic and a plastic part :

$$\tilde{\varepsilon} = \tilde{\varepsilon}^e + \tilde{\varepsilon}^p, \tilde{\sigma} = \tilde{\tilde{C}} : \tilde{\varepsilon} \tag{8}$$

where $\tilde{\tilde{C}}$ is the elastic modulus. Plastic deformation is the result of slip processes according to 12 octahedral slip systems :

$$\dot{\tilde{\varepsilon}}^p = \sum_{s=1}^{12} \tilde{m}^s \dot{\gamma}^s \qquad \tilde{m}^s = \frac{1}{2}\left(\bar{l}^s \otimes \bar{n}^s + \bar{n}^s \otimes \bar{l}^s\right) \tag{6}$$

where $\bar{l}^s$ is the glide direction and $\bar{n}^s$ the normal to the slip plane, for each slip system s.

The amount of slip rate $\dot{\gamma}_s$ is given by an unidimensionnal viscoplastic model:

$$\dot{\gamma}_s = \left\langle \frac{\tau^s - x^s - r^s}{k} \right\rangle^n sign\left(\tau^s - x^s\right) \tag{10}$$

where $\tau^s = \sigma : m^s$ is the resolved shear stress. For each slip system, internal variables are used to describe the hardening of the material using an isotropic hardening variable r^s and a kinematic hardening variable x^s. The flow rule is used in this work near its rate–independent limit, that is for large values of n and $\frac{1}{k}$. The nonlinear evolution rule for isotropic hardening involves an interaction matrix H^{sr} that is set to the identity matrix (Meric et al.[11]) :

$$r^s = r_0 + Q\sum_r H^{sr}\left(1 - e^{bv^r}\right) \quad with \quad \dot{v}^r = \left|\dot{\gamma}^r\right| \tag{11}$$

Finally a nonlinear kinematic hardening is used:

$$\dot{x}^s = c\dot{\gamma}^s - \dot{v}^s d\left(x^s - \bar{x}\right) \tag{12}$$

The second term in the right–hand side of this equation is the nonlinear part associated with the irreversibility of the to and fro dislocation motion (especially possible change of plane during reverse motion). The additional constant term $\bar{x}$ introduces a tension–compression asymmetry observed in nickel based superalloys at specific temperatures.

4 APPLICATIONS

In this section in order to validate the use of cohesive zone approaches, the independence of the solution with respect to the mesh used is checked. Then some results are presented concerning the use of this cohesive zone model for a precracked tensile fatigue specimen made of single crystal superalloy. Mode I loading under generalized plane strain hypothesis are simulated.

Figure 4 shows, for a given crack length, the evolution of the crack growth rate versus the choosen element size. Below 4 microns the convergence is reached and the cohesive zone approach become mesh independant. This element size has been choosen for the other computations shown in this paper.

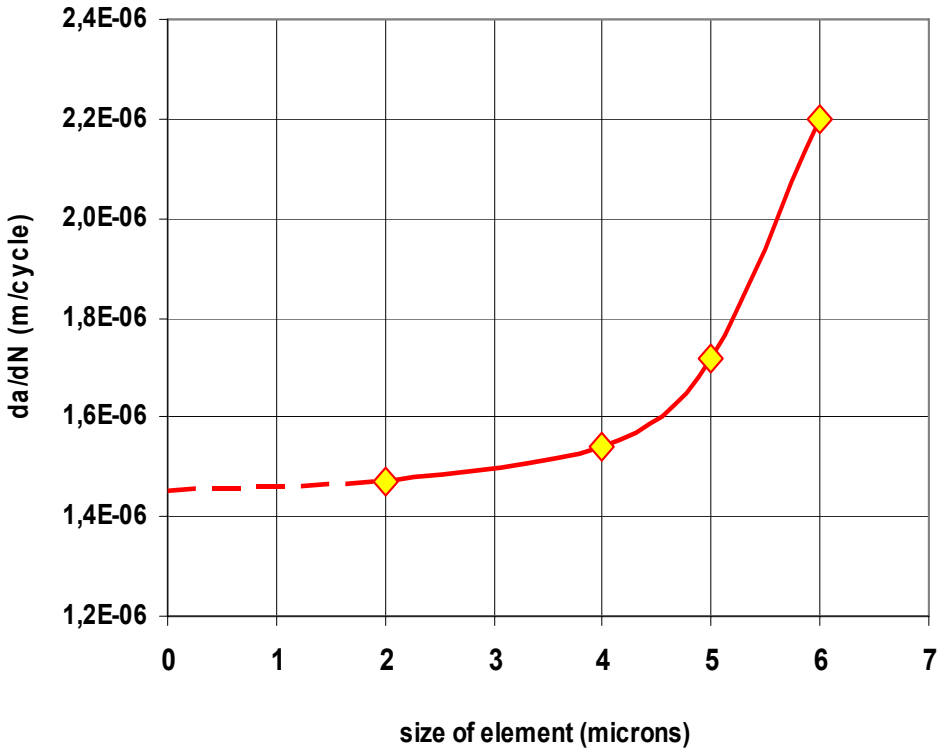


Figure 4. Convergence study.

Figure 5 shows the stress and the plastic strain fields at crack tip for a crack length of about 1mm. The plastic history due to the crack growth under cyclic loadings is described through the plastic wake zone. Figure 6 shows a plot of the cyclic damage and the stress field versus the X-coordiante along the crack path: the damage evolution is continuous across different cohesive zone elements. The analytical elastic solution near the crack tip has also been drawn and shows that the finite element discretization is fine enough.

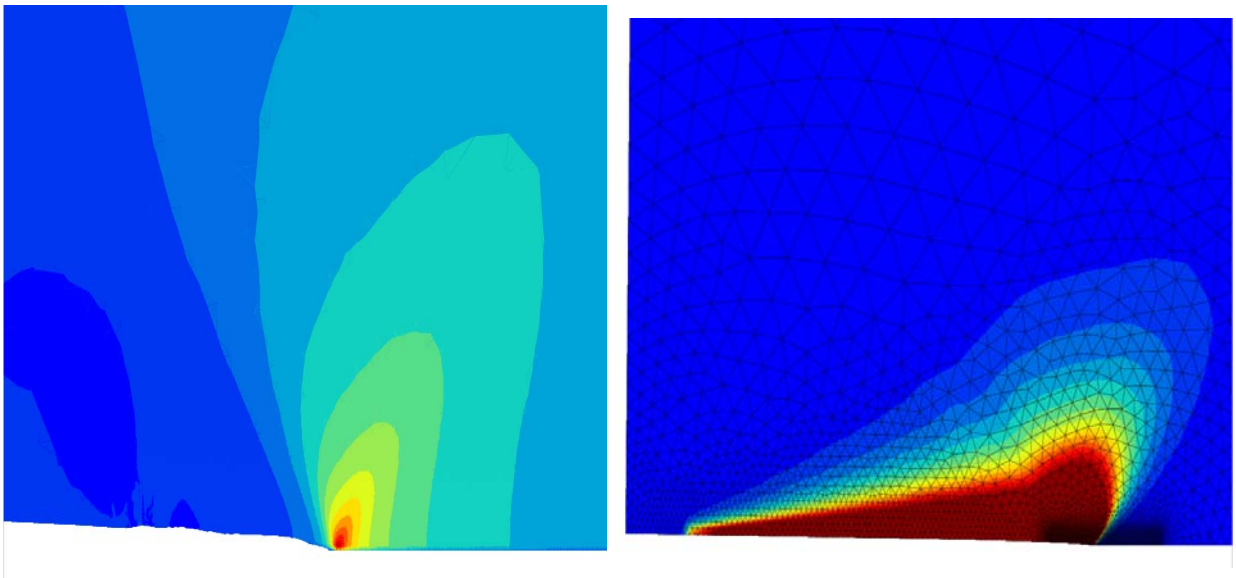


Figure 5. Stress and plastic strain field at crack tip.

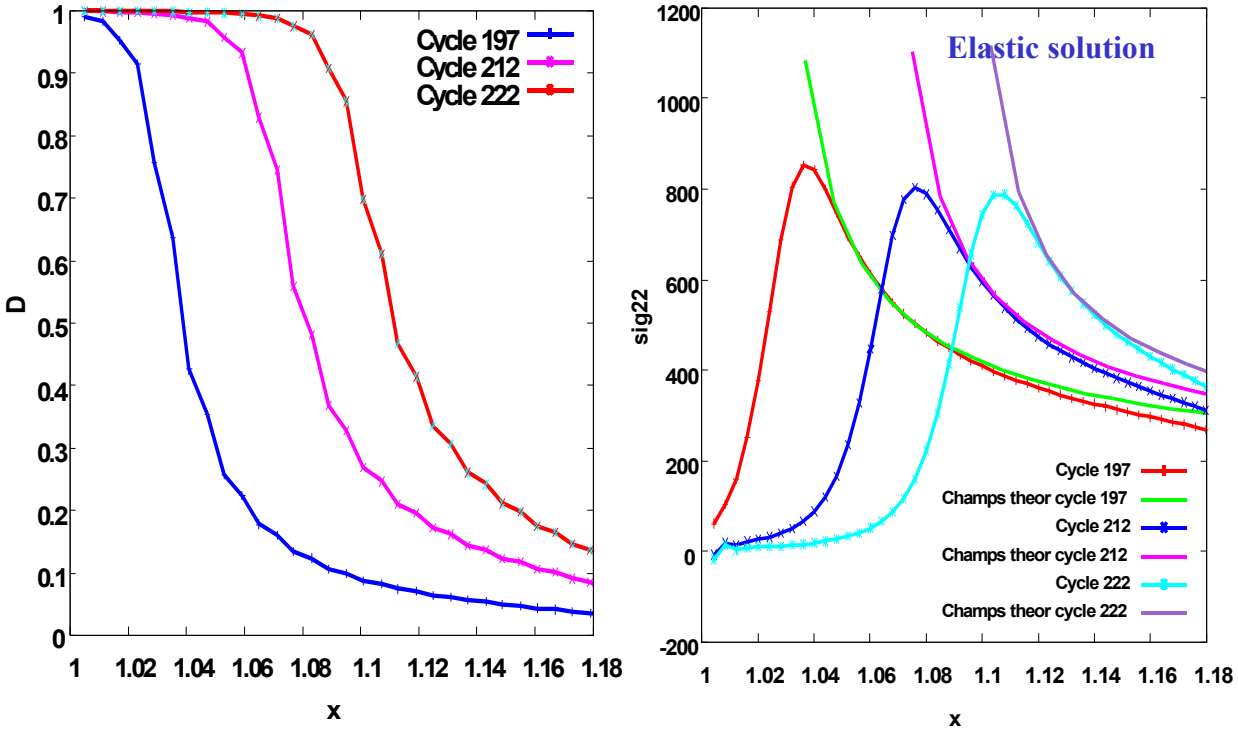


Figure 6. Evolution of the fatigue damage and the stress field as a function of X-coordinate along the crack path.

Several computations have been run for several model parameters sets and for two loading levels (200MPa and 400MPa) in order to calibrate the cohesive zone model with the experimental crack growth datas. Figure 7 shows the different numerical Paris plots taken out these computations. The A and n parameters have a strong influence in the calibration of the cohesive zone model. A allows to translate the Paris plot and n to change the Paris plot slope.

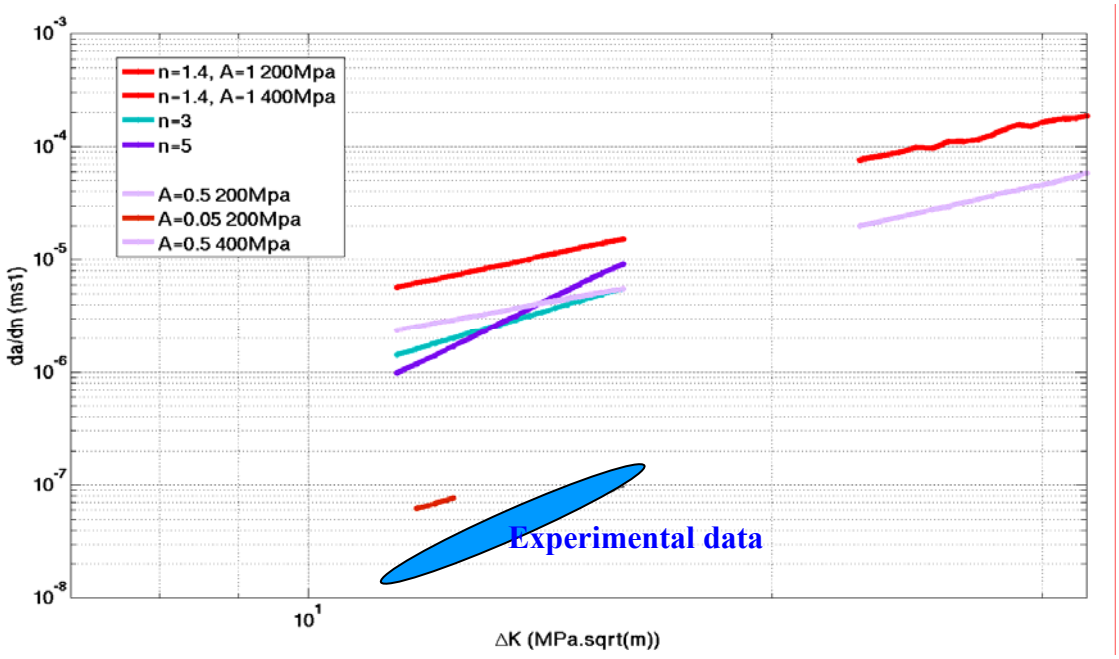


Figure 7. Role of differents parameters in the identification of the Paris plot.

5 CONCLUSION

The numerical modelling of the crack growth in single crystal superalloys with the use of coupled approaches have not been widely studied. We developed a cohesive zone model suited to fatigue regime. This model has still to be calibrated on experimental datas in pure fatigue regime. It has also to be improved by introducing the coupling of cyclic damage with the creep damage and the oxidation effect, in order to extend the use of this model to other complex loading.

6 ACKNOWLEDGMENTS

This research is sponsored by the European Commission within Project SOCRAX.

7 REFERENCES

1. Paris P., Gomez M., Anderson W., "A rational analytic theory of fatigue", The trend in engineering, 13, 9-14, 1961.
2. Tvergaard V. And Hutchinson J.W., Effect of strain dependent cohesive zone model on predictions of interface crack growth,"Journal de Physique iV", 6, 165-172, 1996.
3. Dugdale D. S. Yielding of steel sheets containing slits. J. Mech. Phys. Solids, 8, 100-104, 1960.
4. Barenblatt G. I. The mathematical theory of equilibrium cracks in brittle fracture. Adv. Appl. Mech., 7, 55-129, 1962.
5. Needleman A. A continuum model for void nucleation by inclusion debonding. Journal of Applied Mechanics, 54 , 525-531, 1987.
6. De-Andres and al., "Elastoplastic finite element analysis of three-dimensional fatigue crack growth in aluminium shaft subjected to axial loading", Int. J. Of Solids And Struct., pp. 2231-2258,1999.
7. Nguyen and al., "A cohesive model of fatigue crack growth", Int. J. Of Fract., pp. 351-369, 2001.
8. Yang and al., "A cohesive zone model for fatigue crack growth in quasibrittle materials", Int. J. Of Solids And Struct., pp. 3927-3944, 2001.
9. Roe and Siegmund T. An irreversible cohesive zone model for interface fatigue crack growth simulation. Eng. Fract. Mech., 70, 209-232, 2003.
10. Lemaitre J., « A course on damage mechanics ». Berlin, Springer-Verlag, 1996.
11. Meric L., Poubanne P., Cailletaud G., "Single crystal modeling for structural calculations : Part 1-Model presentation", J. Eng. Mat. Techn., vol. 113, pp 162-170.

A procedure for thermal fatigue damage assessment due to turbulent mixing in nuclear piping systems

N. Taylor[a], K.-F. Nilsson[a], M. Dahlberg[b], C. Faidy[c]

[a] European Commission Joint Research Centre, Institute for Energy, Petten, The Netherlands
[b] DNV Technology Sweden, Stockholm, Sweden
[c] EDF SEPTEN, Lyon, France

Abstract In nuclear plant piping systems thermal fatigue damage can arise at locations where there is turbulent mixing of different temperature flows. Furthermore, the severity of this phenomenon can be difficult to assess via plant instrumentation due to the high frequencies involved. Several recent R&D programmes have been devoted to better understanding the induced thermal loads and associated damage mechanisms. To exploit this work, the Network for Evaluation of Structural Components (NESC) set up a project involving both utilities and R&D organisations and aimed at developing a consensus methodology for assessing thermal fatigue in piping components, with special attention at mixing tees in light water reactor systems.. The paper describes the proposed procedure and the on-going verification work.

1 INTRODUCTION

Thermal fatigue is widely recognised as important potential damage mechanism in cooling piping systems of light water reactors [1, 2] and its significance increases as plants get older, requiring safety justifications for up to 60 years of operation. Three loading scenarios are typically identified:
Thermal stratification: this occurs when a horizontal pipe experiences a layer colder water which flows under the upper, hotter stream; it results in axial and circumferential bending stresses, with maximum axial stresses near the mixing layer. A periodic rising and falling of the mixing layer induces through wall cyclic stresses that may contribute to both crack initiation and growth.
Vortex penetration in tees, dead leg; valve leaks: Turbulent flow in a main coolant pipe can cause penetration of hot water into a connecting pipe with water of a lower temperature.
Turbulent mixing at Tee-connections: turbulent mixing of hot and cold fluids can induce local cyclic stresses on the piping wall, as shown schematically in Fig. 1. The stress is greatest on the inside surface and, in the absence of other significant loads, the orientation of any resulting cracks is random. The damage process is also referred to as thermal striping, which is defined as a random temperature fluctuation produced by the incomplete mixing of fluid streams at different temperatures N.B. thermal striping can also occur in junction with stratification due to instabilities at the interface of the hot and cold flows

While most common thermal fatigue issues are well understood and can be monitored by plant instrumentation systems, mixing tees present several distinct challenges for structural integrity assessment: the inherent difficult in determining the local thermal loads since these cannot be adequately monitored by common thermocouple instrumentation, the availability of appropriate high cycle fatigue data and the fatigue damage assessment process for variable loading histories. The components potentially affected by turbulent mixing include the surge and spray lines and several branch lines and nozzles (charging line, safety injection lines etc.).

A number of recent R&D programmes have considered thermal fatigue /turbulent mixing phenomenon. In Japan, extensive work has been performed both regarding the assessment process [3] and environmental effect on the fatigue curves [4] (although this aspect is less relevant in the high cycle regime for $N > 10^6$ cycles. The JSME has issued a code in 2003 on dealing with high-cycle thermal fatigue in 2003 [5]. In the US thermal fatigue has been addressed as part of EPRI's Materials Reliability Project [6, 7] with the aim to provide guidelines for evaluation, mitigation, monitoring and non-destructive examination. In parallel work is also underway concerning proposals to revise the ASME fatigue curves [8], which would have direct consequences for thermal fatigue evaluation procedures. In Europe several national programmes are under way or have been completed in this area, notably the French studies [9] which followed the leak at the Civaux plant in 1998. The European Commission has also sought to promote collaborative work in this area. The THERFAT project [10] ran from December 2001 to November 2004. Its objectives were to advance the accuracy and reliability of thermal fatigue load determination in both engineering tools and research oriented approaches and to outline a science-based practical methodology for managing safety risks due to thermal fatigue. Fluid dynamics tests were performed on steel and Plexiglas models with varying mass flows in main and branch pipe in order to quantify the thermal spectrum loads. The feasibility of using CFD models to simulate such tests was demonstrated, although a huge

computational effort is necessary to capture real time turbulence effects. Thermal cycling tests on small and medium scale specimen with high temperature differences showed that crack initiation and propagation could be predicted. A further action concerned the implementation of fuzzy logic monitoring systems to avoid unnecessary repairs and reduce operator dose. THERFAT has also produced a road-map for development of a European fatigue evaluation methodology and this challenge has been taken up in the NESC Thermal Fatigue project, which is the subject of this paper.

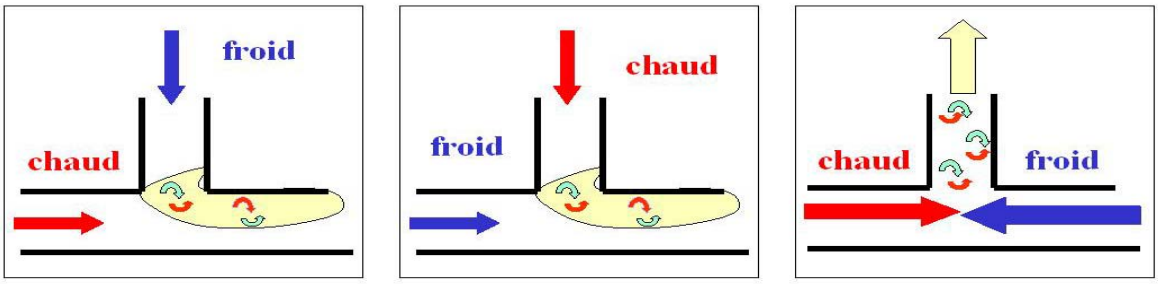


Figure 1. Turbulent mixing scenarios at tee junctions.

2 NESC NETWORK THERMAL FATIGUE PROJECT (NESC-TF)

The Network for Evaluating Structural Components (NESC) was set up over 10 years ago to address the verification of advanced structural integrity assessment techniques for safety-critical reactor components [11]. Through its self-funded activities and associated projects, partly funded by the European Commission's DG-RTD, it has developed a significant body of benchmark R&D data, in particular for large-scale tests performed under closely monitored conditions. The added value of combining the efforts of utilities, manufacturers and R&D organisations is stressed.

Based on the positive experience in THERFAT (which had been initiated largely by NESC members) and a survey of European utilities which identified strong interest for a further work, a group of utilities and R&D organisations have come together under the NESC umbrella to form the NESC-Thermal Fatigue project. The objective of the NESC Thermal Fatigue project is the development of a European Methodology for assessing thermal fatigue in LWR components. The procedure should reflect the multi-disciplinarity of the thermal fatigue problem. It should be verified or validated by a database of suitable experimental and service data. Participation is subject to a commitment to contribute to the work of the project i.e in-kind contribution, whereby its funding is up to the participant. To promote exchange of data and open discussions between the participants, it was decided that the project group should be autonomous within NESC, although there is an obligation to report progress to the NESC Steering Committee. However the group's working documents are reserved to the participants of the project itself.

NESC-TF kicked-off in 2003 and now involves 10 organisations. Phase 1 has produced a draft assessment procedure and a verification database with over 40 component damage cases and 7 laboratory mock-up cases. The draft "European Thermal Fatigue Procedure" foresees a preliminary screening criterion in terms of the ΔT between the two mixing fluids, followed by three assessment levels: a) fatigue damage derived from a simplified sinusoidal wave model of the thermal load; b) fatigue damage derived from the local load spectrum itself and c) determination of crack growth rate for a planar flaw. In parallel, a set of validation documentation is being assembled to provide the technical background for the various elements of the procedure. Currently the participants are applying the procedure to the verification database, which will then be revised to reflect consensus. No large benchmark tests (a hallmark of previous NESC projects) are planned, although this aspect may be considered in the final recommendations arising from the analysis of the available verification data.

3 VERIFICATION DATA

A major goal of the NESC-TF project was to exploit existing experience of thermal fatigue, in particular to identify and compare the most influential parameters and to enable their ranking. To meet this need a database work package was set up with three distinct sub-tasks:

- collation, classification and analysis of data from service data on components,
- collation and analysis of data from features tests
- collation of materials properties testing.

It is stressed that the data collected are intended to serve the needs of the project and is not intended to duplicate existing national or international pipe failure databases such as OPDE [12]. The following sections describe the

so-called verification data collected to date for both operational components and from features tests; evaluation of fatigue life curves together with available test and cyclic stress-strain data is on-going. No large benchmark tests (a hallmark of all previous NESC projects) are planned, although this may be considered in the recommendations arising from the analysis of available data.

3.1 LWR Cases of Thermal Fatigue

The project has built up a database of 45 cases of identified thermal fatigue damage, drawn largely from Swedish BWR and French PWR sources. Although a standard reporting format was developed specifically for this task, the extent of documentation for the individual cases is of variable quality and this has hampered detailed comparisons. It is noted that, the term “damage” means evidence of cracking, but not necessarily a leak i.e. penetration of the wall. It is also stressed that no case of pipe rupture was found. As shown in Fig. 2, the majority of the cases concern mixing tees (without internal mixers). In comparison the results of an 1997 analysis [12] found that only about 33% of the thermal fatigue failures were linked to tees, which may indicate a bias in the present collation. This can, however, be justified by the focus of NESC-TF on turbulent mixing/thermal striping phenomena, which are typically linked to tees.

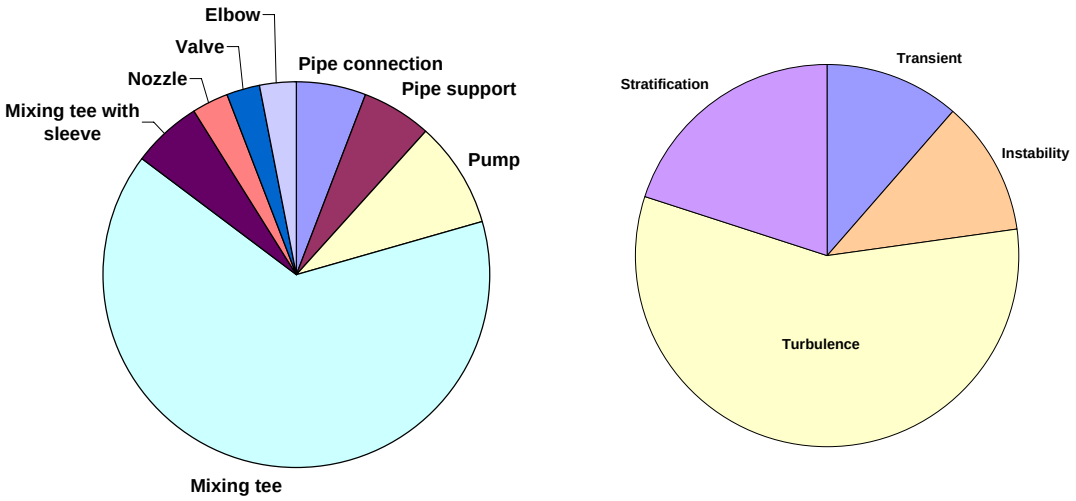


Figure 2. Distribution thermal fatigue cases according to a) component type and b) loading type.

One difficulty has been to isolate the cause of the observed damage and the associated loading regime. The evolution of damage is frequently influenced by several parameters relating to the loading, the environment and to the local material condition. Also, a chain of events may be involved, e.g. when a valve leakage leads to stratification and then turbulence, finally producing surface damage. The available records rarely provided a full picture of such factors. Notwithstanding this, Fig. 2 shows the categorisation of the cases in terms of the predominant load type, identified here as: transients, turbulence, stratification and other types of instable flows. The distribution in Fig. 2 is in line with other studies. While turbulence dominates as a loading regime and leads to penetration depths of more than 50% wall thickness in a few cases, it is noted that none of the through wall cracking cases could be attributed to this alone. Hence consideration of stratification phenomena remains an important aspect of any overall thermal fatigue assessment procedure.

The location of damage has also been analysed. A natural feature of thermal fatigue is that the region affected by the load extends over larger areas and is not necessarily confined to notches or other stress concentrations as in mechanical fatigue. In fact, as shown in Fig. 3, for the whole set of cases the majority of damage appears at the base material. However if just the main sub-set of mixing tees is considered, out of a total of 28 crack sites, about 58% of the observed cracks are confined to welds. This has implications also for in-service inspection, which generally focuses on welds. A possible explanation is that the potential sites for thermal fatigue are primarily influenced by thermohydraulic factors.

Finally, the question of the relation between the nominal temperature difference and the presence of damage has been addressed to establish if there is a threshold below significant fatigue damage can be excluded. At least two of the collected cases indicate that fatigue damage may occur at as low local temperature difference as 20^{o}C. However the nominal difference may be much higher.

.

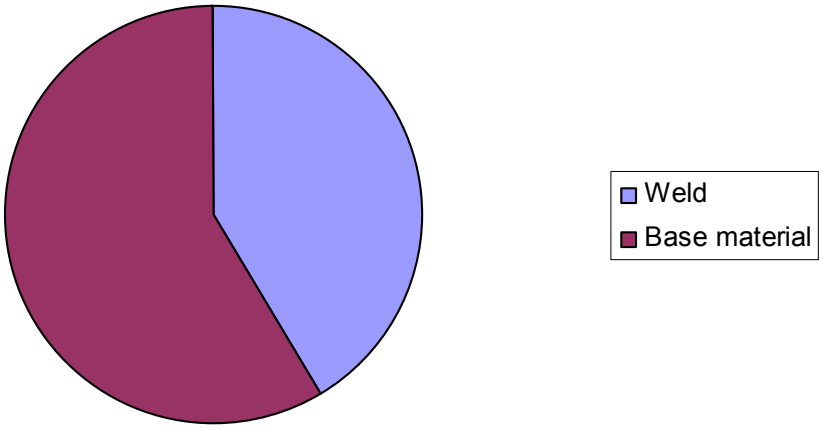


Figure 3. Distribution of thermal fatigue damage cases according damage location.

3.2 Feature Test Database

Feature tests i.e. tests involving simulated thermal fatigue performed under laboratory conditions, have an important role to play for verification of assessment procedures and for establishing transferability of standard fatigue curves to component-life situations. For NESC-TF five cases have been brought together, including digital records of the induced temperature distributions, as well as calculated thermal stresses from reference finite element calculations, where available.

- The CEA FAT3D test [14] was designed produce a 3-D thermal loading field for the OECD/IAGE thermal fatigue benchmark exercise to. The heated pipe test piece was cyclically quenched at one point on its inner surface.
- The EDF Interpol Test [15] was a high cycle thermal fatigue experiment on a large cylindrical pipe component in 304L steel with a circumferential weld. The thermal loading is applied by alternating infrared heating and cold spraying. The size of the defects that formed at the surface is measured with a dye penetrant technique.
- The JRC down-shock experiments [16] are a series of down-shock tests was performed on relatively small cylindrical 316L pipe specimens. The pipes are induction heated from the outer surface and cyclically cooled from the inside by room temperature water. The surface cracking is monitored by the replica technique and the evolution of crack length and depth is measured with a special ultrasound technique.
- The CEA SPLASH [17] test reproduced temperature gradients on two opposite sides of a bar specimen, which is continuously heated by electrical DC current and cyclically submitted to cold shocks by water-air mixture sprayed on the opposite faces. The test allows for relatively high frequencies.
- The Fatherino series of thermo-hydraulic tests on a ½ scale T-junction mock-up were performed by CEA as part of the THERFAT project [10]. The registered thermal loading data provide a unique benchmark for CFD analyses.

4 THERMAL FATIGUE ASSESSMENT PROCEDURE

A key feature of the NESC-TF project is the commitment to produce a procedure document that can be used by the industry. This should contain three parts:

a) the procedure itself, including: definition of the component and type of operation, determination of the thermal loads, assessment of stresses and strains and assessment of crack initiation and crack propagation
b) a full listing of underpinning supporting data and analysis, to allow full understanding of the logic adopted and to ensure future transparency
c) identification of open issues where additional R&D activities are needed.

A draft procedure has been written and is currently being analysed and verified by the project group. Its scope is restricted to the assessment of fatigue life of mixing tees subjected to turbulent mixing of two fluid flows. The components concerned are mixing tees of nuclear power plant Class 1-2-3 piping systems, which should have been designed using an appropriate code such as ASME Section III, RCC-M or similar. The procedure is intended for application to mixing tees without any internal devices. However, it be useful for other components, but this has not been investigated in the NESC-TF project so far.

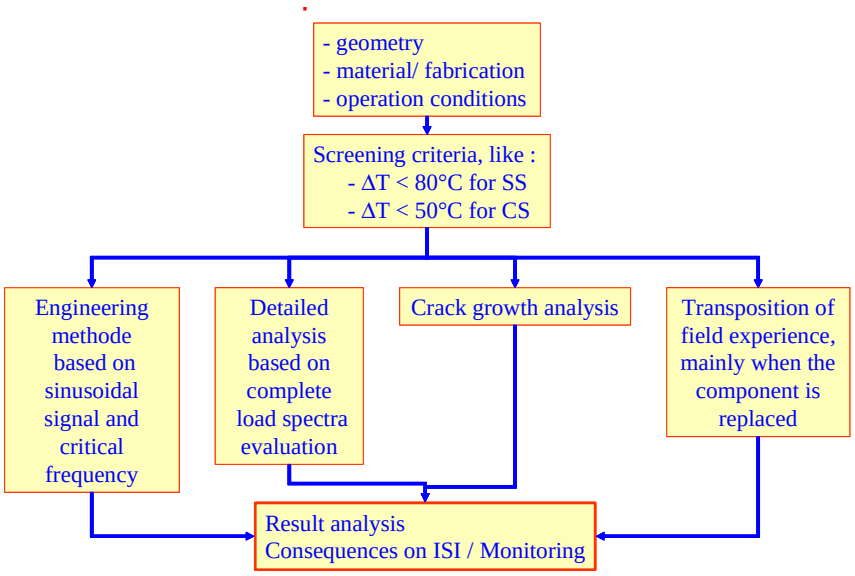


Figure 4. Overall scheme for the proposed thermal fatigue assessment procedure.

The overall scheme (Fig. 4) provides for 4 assessment methods differing in approach and sophistication:
- simple screening criteria in terms of the (nominal) ΔT between the two mixing fluids
- fatigue usage factor determined by the so-called sinusoidal method, whereby the thermal loading is treated as an idealised sinusoidal wave
- fatigue usage factor determined by analysis of the complete local load spectra
- calculation of the growth of a detected or postulated crack-like flaw and comparison with local critical crack size (based on fracture mechanics principles)

The required input data (which vary according to the method adopted) include:
- load: a set of temperature differences ΔT_i with corresponding flow velocities and durations (N_i)
- geometry: diameter and thickness of the run and branch of the tee, nozzle corner geometry
- installation: down and up-stream piping layout, including relevant discontinuities (diaphragm, pump, valve, elbow, other tees etc.)
- material type and material properties: basic mechanical and thermal properties, cyclic stress-strain curves, SN-curves, da/dN.vs. K curves and fracture toughness (with associated temperature dependence effects in the appropriate range). For S-N curves and da/dN vs. K data, reduction factors due to weld, mean stresses or environment may also be necessary.
- fabrication: location and type of welds, surface finishing parameters, residual stresses

In the following sections more details are provided of the analysis routes, in particular for the screening criteria and the sinusoidal method. The load spectrum and fatigue crack methods are still under development.

a) Screening criteria

The following screening criteria are defined:
i) For stainless steel, no specific fatigue analysis or fabrication improvements are necessary if $\Delta T_{nom} \leq 80°C$.
ii) For ferritic steel, no specific fatigue analysis or fabrication improvements are necessary if $\Delta T_{nom} \leq 100°C$
In the case of a variable ΔT_{nom}, the screening is to be applied to the maximum value in the loading spectrum.

b) Fatigue Usage Factor from the Sinusoidal Method

This method uses a first-order approximation of the loading conditions in turbulent mixing. The basic assumptions are:
- 1-D model of the component wall
- Sinusoidal temperature variation on the inner surface, $T(t) = \Delta T_o/2 * \sin(2\pi f.t)$, where ΔT_o is 80% of the temperature difference between the flows, f is frequency and t is time.
- Adiabatic conditions on the outside of the component
- Homogeneous load, i.e. the load is time-dependent only
- Heat transfer by convection
- Linear model with linear material parameters

The model predicts a quasi-static sinusoidal stress/strain response on the surface, the magnitude of which is proportional to the applied ΔT and varies also with the frequency. As shown in Fig. 5, the stress range will be maximum at a certain critical frequency. The fatigue usage evaluation for given ΔT reduces to an optimisation problem involving the sinusoidal surface temperature i.e. stress response, function, and the fatigue resistance S-N curve. No knowledge or assumptions about the actual loading spectrum are required. The procedure all the material properties are evaluated at mean temperature of the fluctuations. It can be assumed that ΔT, is 80% of ΔT_{nom} if no specific data are available. Note that the fatigue evaluation is based on a rather traditional approach as suggested for example by ASME or RCCM-R.

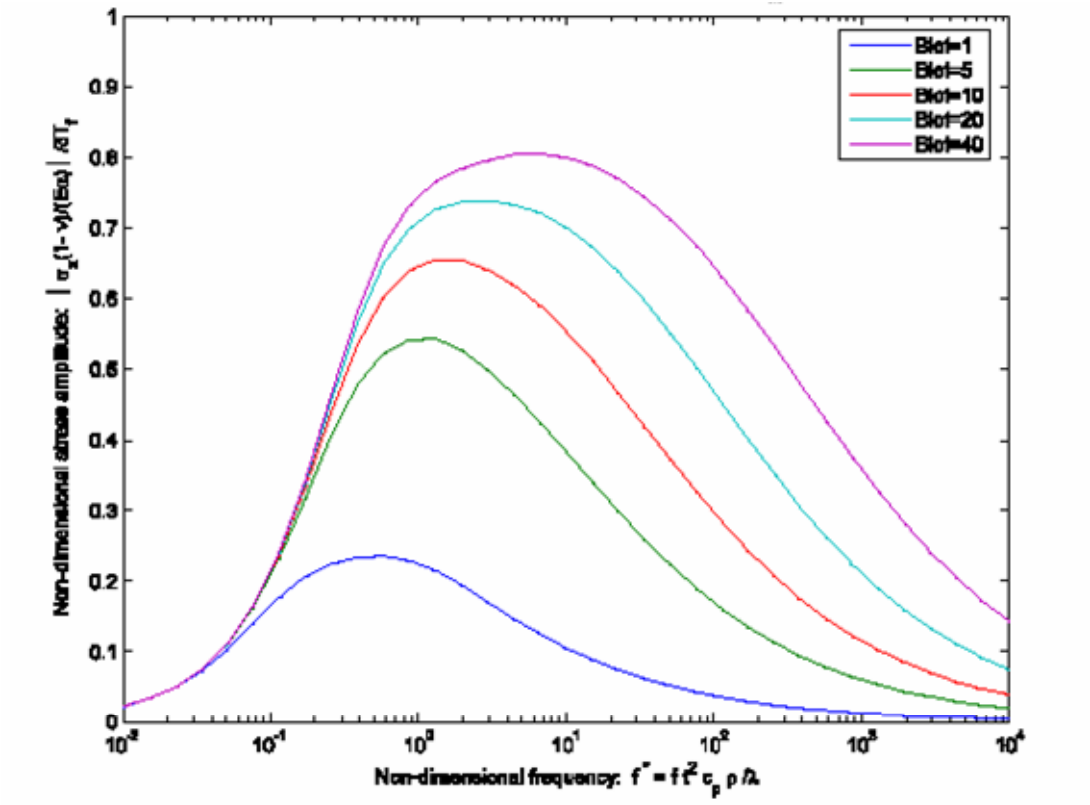


Figure 5. Normalized stress response as a function of normalised frequency for different levels of heat transfer (specified in terms of the Biot number)

For practical application the loading is assumed to be made up of series of $\Delta T_{nom,i}$ values, associated with a heat exchange coefficient h_i and of duration D_i (in hours). For each combination of $\Delta T_{nom,i}$. and h_i, a critical frequency can be evaluated that leads to a minimum acceptable life $D_{i,adm}$, To do this the stabilized peak to peak thermal stress amplitude $S_{p,i,j}$ is calculated over a range of j different frequencies (normally between 0.1 and 10 Hz). These values are then related to the stress amplitude parameter S_{alt} used in the S-N curve via the formula:

$$S_{alt,i,j} = K_r\left(E/E_C\right).K_v.\left(S_{p,i,j}/2\right)$$

where E_c is the reference Young's modulus of the S-N curve, E is the Young modulus at the reference temperature used for the analysis, K_v is a plastic strain amplification factor due to biaxial thermal stresses and K_r is a fatigue strength reduction factor for weld, surface finish, environmental effects etc. Using the chosen S-N curve, each value of $S_{alt,i,j}$ will yield a cyclic life, $N_{f,i,j}$ and corresponding duration $D_{i,j}$. The minimum value of $D_{i,j}$ provides the minimum admissible life value for the frequency range considered. Performing this analysis for a set of $\Delta T_{nom,I}$ values therefore produces a corresponding set of $D_{adm,i}$ data, which then constitutes the damage evaluation curve (an example is shown in Fig. 6). A total usage factor F_u can be obtained from the damage evaluation curve:

$$F_u = \sum D_i / D_{adm,i}$$

This method was applied to an appropriate subset of the Tee junction cases from the verification case database, in combination with the fatigue curve due to Jaske [18] for austenitic steels (together with the usual reduction factors of 2 on stress amplitude and 20 on cyclic life). The results confirmed the overall conservatism of the approach; with usage factors well above 1 (in fact the lowest value obtained was 2.0 and the average was 13.7).

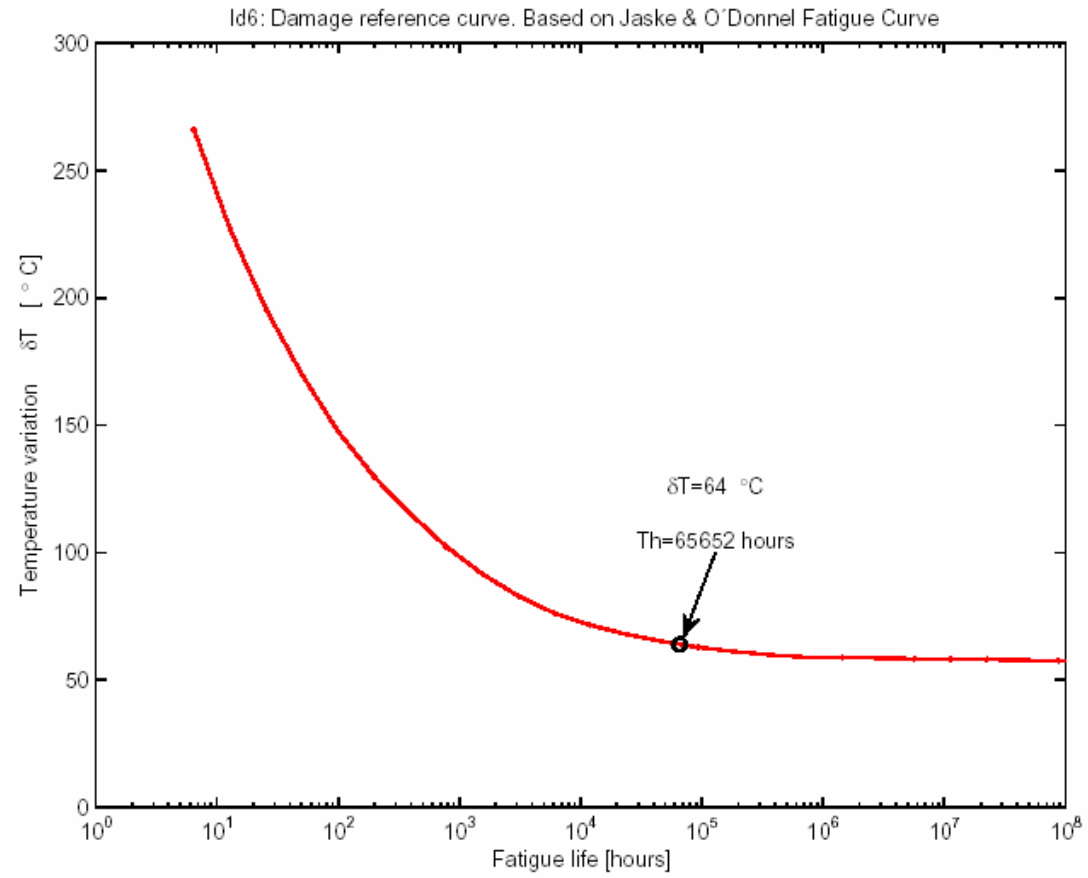


Figure 6. An example of a damage reference curve (ΔT vs. minimum admissible fatigue duration) used in the sinsuidal method

c) Fatigue Usage Factor from Load Spectrum Analysis

This method is intended to allow consideration of the actual thermal loading spectrum (or at least a typical envelope). All the other aspect will be similar to conventional fatigue analysis for piping as set out in codes such as ASME section III, RCCM-R or similar. Two main results will be obtained: the potential extent of degradation for a given set of hypotheses and the most critical location (in terms of maximum usage factor). Evaluation of the loads is a critical aspect and several approaches are possible:

- direct measurements of temperature fluctuations from plant instrumentation, if these can be shown to be feasible and reliable
- measurements of temperature fluctuations and heat exchange coefficients from mock-ups, if adequately representative of the plant and component conditions
- computational fluid dynamics analyses

d) Fatigue Crack Growth Analysis

This approach is based on the presence of a real or postulated crack –like flaw, the behaviour which can be analysed using fracture mechanics and fatigue crack growth methods, such as those described ASME Section 11, RSEM code and several fitness-for-service procedures. For the evaluation of the loads acting on the flaw, the thermal stress distributions need to be calculated. This is in itself a complex task, as outlined for the load spectrum analysis method described above. Furthermore factors such as biaxial stressing, crack closure and variable amplitude loading history may need consideration to ensure an adequate degree of conservatism in the in the fatigue growth assessment.

5 CONCLUSIONS

- A group of utilities and R&D organizations have formed a project group (NESC-TF) with the aim of developing a European procedure for thermal fatigue analysis, considered specifically thermal striping due to turbulent mixing at tee connections. Wherever possible, advantage is taken of recent R&D work at national, European and international levels.
- NESC-TF has collected databases of instances of thermal fatigue damage on nuclear power plant components (45 verification cases) and of features simulation tests conducted under laboratory conditions (5 datasets). These provide a basis for understanding of the physical damage mechanism and for verification of assessment procedures.
- The present revision of the thermal fatigue assessment procedure details two methods: basic screening criteria and a fatigue usage factor calculation based on the assumption of a sinusoidal thermal loading. Both provide conservative results with respect the relevant verification cases.
- The project group is continuing to work on the verification of procedure and its extension to include guidance on methods for consideration of full thermal loading spectra and for treatment of detected or postulated crack-life flaws.

ACKNOWLEDGEMENTS

The authors gratefully acknowledge the contributions from all the NESC-TF project partners and sponsor organisations, as well as the support from the Joint Research Centre of the European Commission,

REFERENCES

1. IAEA, “Assessment and management of ageing of major nuclear power plant components important to safety. Primary piping in *PWRs”,* TECDOC-1361, July 2003
2. C. Faidy et al, Thermal Fatigue of Reactor Components in OECD-NEA countries: a Three-fold Program to Enhance cooperation, Proc. SMiRT-18, Beijing, China, August 2005
3. N. Kasahara et al, Thermal Fatigue Evaluation Method based on power spectrum density functions against fluid temperature fluctuation, Proc. ASME PVP2005, Denver, Colorado, USA, July 2005.
4. M. Higuchi at al, “Development and Evaluation Method of Fatigue Damage on Operating Plant Components Considering Environmental Effects”, NEA/CSNI/R(2004)21 , Proc. 3rd Int. Conf. on Fatigue of Reactor Components, Seville, Spain, October 2004
5. JSME, Guideline for Evaluation of High-cycle Thermal Fatigue of a Pipe, S017-2003, 2003
6. J.D. Keller et al, “Thermal Cycling Screening Criteria and Evaluation Methodology and Application to Pressurized Water Reactor Branch Line Piping”, NEA/CSNI/R(2004)21, Proc. 3rd Int. Conf. on Fatigue of Reactor Components, Seville, Spain, October 2004
7. J.D. Keller et al, “Thermal Fatigue Management Guideline for Normally Stagnant Non-Isolable RCS Branch Lines”, NEA/CSNI/R(2004)21, Proc. 3rd Int. Conf. on Fatigue of Reactor Components, Seville, Spain, October 2004
8. W. J. O’Donnell et al, Proposed new fatigue design curves for carbon and low alloy steels in high temperature water, Proc. ASME PVP2005, July 2005, Denver, Colorado, USA
9. S. Chapuliot et al, Hydro-thermal-mechanical analysis of thermal fatigue in a mixing tee, Nuclear Engineering & Design, 235 (2005) 575-596
10. K.-J. Metzner & U. Wilke, European THERFAT project—thermal fatigue evaluation of piping system “Tee”-connections, Nuclear Engineering & Design, Vol.. 235, Issues 2-4 , 2005, 473-484
11. N. Taylor & D.P.G. Lidbury, “Improving Structural Integrity Assessment Techniques”, 1st Symposium - Nuclear Pressure Equipment Expertise and Regulation, International Conference, Dijon, June 2005
12. OECD pipe failure data exchange project (OPDE) – 2003 status report, Proc. ICONE-12, April 2005, Arlington, Virginia, USA
13. C.L. Atwood et al, Analysis of pressurized water reactor coolant leak events caused by thermal loads, Proc. ESREL ’99, European Safety and Reliability Conference, 1999
14. NEA/CSNI/R(2005)2, FAD3D – An OECD/NEA benchmark on thermal fatigue in fluid mixing areas.
15. F. Curtit et al, INTHERPOL thermal fatigue test, NEA/CSNI/R(2004)21, Proc. 3rd Int. Conf. on Fatigue of Reactor Components, Seville, Spain, October 2004,
16. E. Paffumi et al, , On thermal fatigue crack initiation, propagation and arrest in 316L model pipe components, ASTM STP 1461, ASTM International, West Conshocken, PA, USA, 2004
17. V. Maillot, PhD Thesis in French, Ecole Centrale de Lille, Univ des Sc de Tech de Lille. CEA report R – 6041 (2003)
18. Jaske, C.E. et al., Fatigue Design Criteria for Pressure Vessel Alloys, Transactions of ASME, 1977

Crossed contribution of testings and numerical simulations in the assessment of the risk of damage in piping mixing zones

J.M. STEPHAN[a], F. CURTIT[a], C. PENIGUEL[b], T. PASUTTO[b]

[a] EDF R&D / Material and Mechanics of Components,
Les Renardières, Ecuelles, F-77818 Moret-sur-Loing, France
[b] EDF R&D / Fluid Mechanics and Heat Transfert
6, Quai Watier, F-78401 Chatou, France

Abstract : On May 1998, a crack was discovered on the principal mixing zone of the residual heat removal system (RHR) at EDF CIVAUX nuclear plant. In consequence, EDF initiated a R&D programme to understand the incident and assess the risks of damage on other nuclear plant mixing zones. The programme includes different sectors of developments: assessment of temperature fluctuations in mixing zones, study of high-cycle thermal fatigue behaviour of austenitic steel and development of mechanical methodologies for damage assessment and propagation of crazing zones (thermal striping). The paper develops the conjoined use of tests and their numerical simulations in the development of a methodology to evaluate the risk of damage. Thermal loadings in mixing zones are characterized by a fluctuating spatial and temporal distribution, not fully accessible by sensors on a full-scale mock-up. Numerical simulations complete the knowledge of the loading and give the type of resulting stress distribution. In complement, analytical thermomechanical tests were performed on a pipe and simulated to assess a new methodology.

PRESENTATION OUTLINE

INTRODUCTION

THERMAL SOLICITATIONS

MATERIALS

MECHANICS

INTHERPOL tests

Description of INTHERPOL tests

Numerical simulation of INTHERPOL tests

Fatigue analysis

Discussion

FATHER tests

Description of the FATHER experimental tests

Numerical evaluation of thermal fluctuations

Evaluation of mechanical stresses

Discussion

CONCLUSION

Propagation of multiple cracking under thermal fatigue

A. Fissolo [a] , Li Zheng [a] , N. Haddar [a], L. Taleb [b]

[a] Commissariat à l'Energie Atomique Saclay
SEMT/ LISN CEA Saclay Bâtiment 607
91191 Gif sur Yvette Cédex, France
[b] Institut National des Sciences Appliquées de Rouen Avenue de l'Université - BP 08
F - 76801 Saint-Étienne-du-Rouvray Cedex, France

Abstract Thermal fatigue cracking has been clearly detected in some components of Pressurised Water Reactors (PWRs) and Liquid Metal Fast Breeder Reactors (LMFRs). The present study focuses only on the crack network development. To simulate multiple crack growth, an efficient automatic remeshing algorithm has been developed. This algorithm, together with elastic-plastic calculation using the cyclic stress-strain relationship and crack growth relations, has been implemented in an automatic two-dimensional crack propagation program. The program enables to simulate the continuum initiation (using linear stored damage model) and the propagation (under elastic-plastic loading) of a crack network. Simulation is in good agreement with experimental results obtained with a thermal fatigue device (SPLASH) where temperature drop is obtained in 0.25 second (f = 4 Hz).

1 INTRODUCTION

Thermal fatigue damage sometimes occurs in different types of nuclear reactor components. In LMFBRs, strong thermal fatigue fluctuations are generated by the mixing of sodium flows at different temperatures or by a cyclical movement of sodium stratification interface [1]. In PWRs, crack networks may appear in auxiliary loop zones, close to a cold water injection site [2], [3]. Two types of fatigue damage were observed: single deep cracks at geometrical singularities (root of welds) and thermal fatigue crack networks in straight zones. The present study focuses only on the crack network development.

2. EXPERIMENTAL PROCEDURES

The steels studied here are 304 L and 316 L(N) type austenitic stainless steels. Grain sizes are about 50 µm. Chemical compositions are given in Table I.

Table I. Chemical compositions (wt %) of 304 L and 316 L(N) stainless steels

	C	Mn	Si	Cr	Ni	Mo	S	P	N	Fe
304 L	0.031	1.48	0.55	19.4	8.6	0.23	0.003	0.028	0.058	Bal.
316 L(N)	0.024	1.82	0.46	17.44	12.33	2.3	0.001	0.003	0.06	Bal.

These materials have been used for nuclear reactor structures, since they have a good corrosion resistance. Therefore, they are very sensitive to thermal fatigue, because a very weak thermal specific conductivity is combined with a strong thermal expansion coefficient.

On components, thermo-mechanical loading usually comes from temperature gradients in specimen thickness. Experimental device called SPLASH was developed in order to reproduce such gradients on two opposite sides of a specimen (240x30x20 mm^3). It is continuously heated by an electrical DC current, and cyclically submitted to thermal down-shocks (corresponding to a cooling rate of about 500 to 1000°C/s) when water is sprayed on opposite faces (Figures 1 and 2). In the present case, quenching corresponds to a frequency of 4 Hz (1/0.25 s). Two types of specimens were used: calibration and test specimens. Both were instrumented with K-type thermocouples brazed at the surface and different depths for calibration specimens, in depth only for test specimens.

The number of cycles to initiation N_i is determined by optical microscopic observation of the quenched specimen surfaces. It is considered that initiation occurs when at least one 50 to 150 µm long crack is observed at the surface [4], [5].

Crack networks were analysed by image analysis on quenched specimen surface during the test, at regular time intervals, and in depth after successive surface layer removing after decided stop of the test [4].

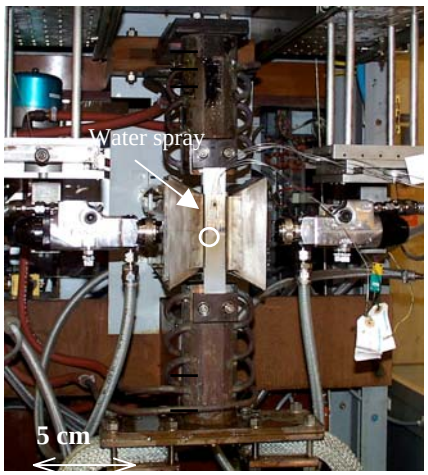


Figure 1. *SPLASH facility*

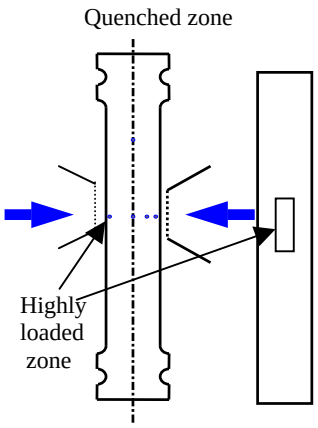


Figure 2. *SPLASH specimen*

3 EXPERIMENTAL RESULTS

For the temperature range of 150 °C, a continuous cracking is observed at the surface with a low density (Figure 3). To calculate crack density, a reference surface is chosen: it should correspond roughly to the uniform temperature region obtained on the SPLASH specimen during the thermal shock. Density is calculated dividing the total cracks length with this reference surface. Such surface is defined as 200,000 cycles crack network surface [6]. Although a relative scattering, one can consider that a stabilisation of the crack network is obtained on surface as shown in Figure 4.

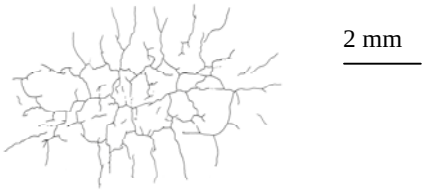


Figure. 3. 300,000 cycles, ΔT = 150 °C.

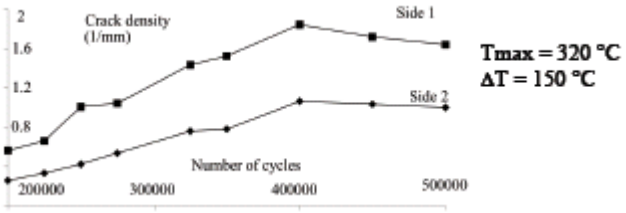
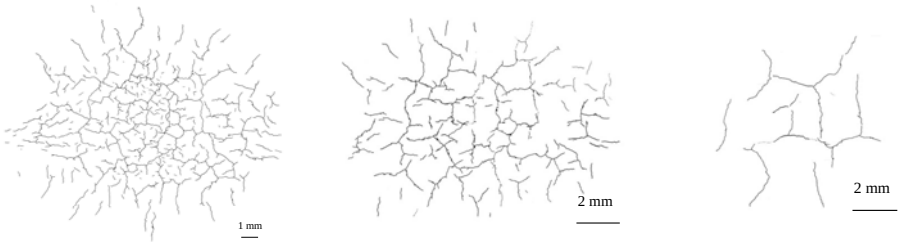


Figure 4. Evolution of the crack density as a function of number of cycles.

- *:* In Figure 5, one crack network is presented, respectively at the surface, at 360 µm and at 1 mm in depth beneath the surface. The network is less dense in depth and only few cracks reach a 1 mm in depth.



Surface 450 µm 1 mm

Figure 5. Crack network observed at the surface, 450 µm and 1 mm in depth.

4. SIMULATION

Simulation deals with the cracking in the depth direction. First we perform thermal computations. Temperature field is then projected on the cracked structure, assuming that the presence of the cracks do not influence the distribution of the temperature in the specimen.

These thermal-mechanical computations will enable us to carry out an analysis of initiation (evaluation of the damage by grain) as well as an analysis of propagation (estimation of an effective stress intensity factor [14] and application of a Paris' law).

Thermal computations: The computations are carried out using the Finite Element code CAST3M developed by CEA. The FE-mesh and thermal conditions are presented on Figures 6 and 7 [7]. Main characteristics of AISI 304 L steel are: ρ : volumic mass: 7800 kg/m^3 , C : specific heat: 500 J.kg^{-1}.K^{-1}, K : thermal conductivity: 19 W.m^{-1}.K^{-1} , α : linear thermal expansion: 18.10^{-6} K^{-1}.

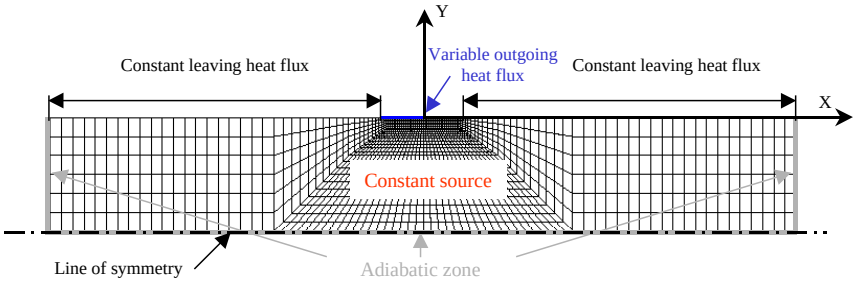


Figure 6. Thermal conditions of the model

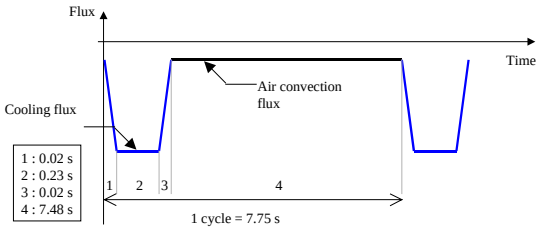


Figure 7. Evolution of thermal conditions in the quenched zone.

Mechanical calculations: calculation was performed using a Ramberg-Osgood cyclic hardening curve (Equation 2). The Young's modulus, material coefficients K, n are given in Table II in comparison with the coefficients of the cyclic curve of consolidation of the 316L at 350°C given by the French code RCC_MR [14].

$$\Delta\varepsilon_t(\%) = \left(\frac{\Delta\sigma}{E}.100\right) + \left(\frac{\Delta\sigma}{K}\right)^{1/n} \quad \text{Eq. 2}$$

Table II. Material parameters of the Ramberg-Osgood law (Equation 2)

Steel	E (GPa)	K	n
304L_320°C	173.250	525	0.224
316_RCC_MR _350°C	174.000	592	0.266

Figure 8 presents the distribution of the thermal variation imposed on the surface for three conditions (ΔT = 125°C, 150°C and 200°C). It shows that for the three conditions tested, the variation of the temperature on the surface remains constant on a zone of size 8 mm. On the peripherals of the quenched zone, we observe a decrease of the ΔT during a thermal cycle.

In-depth, the evolution of the temperature variation in the middle of the thermal strain is given by Figure 9. for the three studied conditions. The in-depth gradient decreases, and at 2.5 mm depth the thermal effect is cancelled.

Figure 10 shows the distribution of the total strain variation on the surface as function of the position with respect to the centre of the quenched zone. It is noted that, on a zone of 3 mm, the variation of $\Delta\varepsilon_t$ is very small and that it decreases while moving away from the centre of the thermal shock. The level of total strain reached in the specimen centre varies between 0.32% (for ΔT = 125°C) and 0.54% (for ΔT = 200°C). In-depth, and as for the temperature, we notice that the variation of the total strain decreases (Figure 11). To 4 mm depth, the reached levels become negligible and quasi-constant for more important depths.

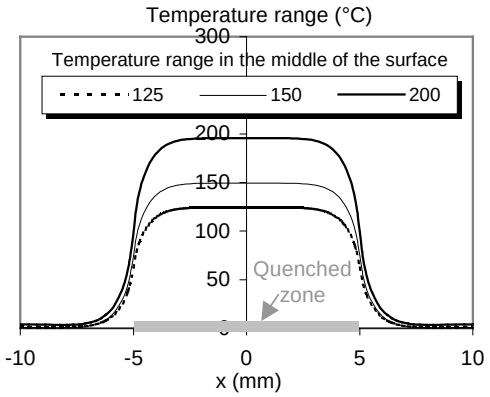


Figure 8. Distribution of the temperature range on the surface

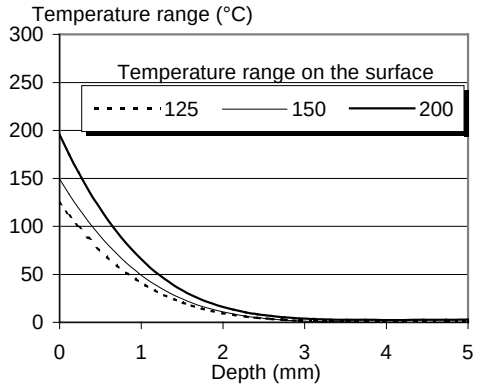


Figure 9. Evolution of the temperature range with respect to the depth of the specimen

Main stages of the model: This 2D model is designed to take into account the initiation and the in-depth propagation of multiple cracks under thermal loading conditions. It is composed of two stages as shown in Diagram 1:

*The first stage simulates the first initiation of the thermal fatigue cracks. For that a distribution of sizes of grains is created on the surface according to the Monte-Carlo method. The first thermal-mechanical calculation will allow simulating thus the first cracked grains and consequently the initial configuration of the crack network. The sizes of the cracks correspond to those of the grain depth.

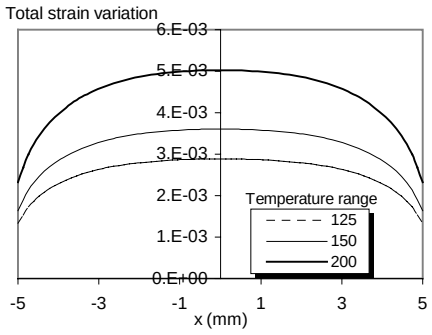


Figure. 10. Distribution of the total strain variation on the quenched zone.

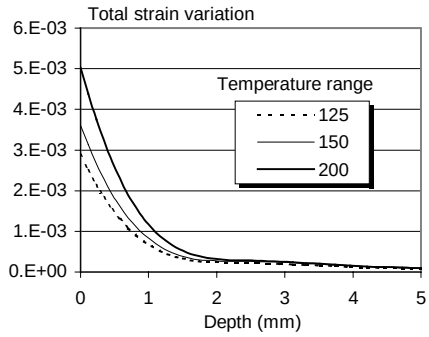


Figure. 11. Evolution of the total strain variation with respect to the depth T_{max} = 320°C.

* The second stage deals with the propagation of cracks under elastic-plastic loading and the continuum initiation of other cracks. The program is divided into five steps:

- Specimen is meshed including the actual crack network.
- The stabilised temperature field is projected on the meshed structure.
- Elastic-plastic computations are performed.
- The propagation analysis of the crack network is performed.
- A linear stored damage model is used to determine the number of cycle of initiation for each not cracked grain.

Initiation stage: It is performed in two steps. In the first step, a Monte Carlo randomisation method is used to determine the size of the surface grains, according to a distribution law of the experimentally measured grain sizes. Grains are square-shaped. Another Monte Carlo randomisation assigns to each grain a position relatively to the surface [4].

In the second step, and for each program iteration (Diagram 1) a linear stored damage model (Equation 8) is used to determine the damage of each grain on the surface. Indeed, at each program iteration, the damage of the uncracked grains is calculated. A crack will appear in the medium of a grain when its damage reaches 1. Coupled elastic-plastic calculation makes possible to take into account the effect of the mechanical unloading that decrease due to the cracks in the structure.

The corresponding number of cycles to initiation Ni_k^j (for the grain 'k' at the iteration 'j') is calculated from the lifetime model (Equation 7). This equation is deduced from the experimental initiation results of the thermal tests [17]. Figure 12 shows a comparison between the isothermal fatigue tests (T = 300°C) and the thermal fatigue tests as well as the dimensioning curves of French code RCC-MR [14]. The corresponding total strain (in ordinate) is the one reached in the middle of the quenched zone on the surface (See Figure 10).

The lifetime model integrates a dependence of the grain size (Equation 8). Several work highlighted the effect of the grain size on fatigue behaviour of metallic materials [8]. Equation 8 describes a simple model that takes into account this dependence by multiplying the fatigue curve in thermal fatigue by the ratio between the average grains size $\overline{\Phi}$ and the size of each grain k Φ_k.

$$D_k^j = D_k^{j-1} + dD_k^j \quad \text{Where: } dD_k^j = \frac{dN^j}{Ni_k^j} \qquad Ni_k^j = \left(\frac{\Delta\varepsilon_t}{C_1}\right)^{-1/\gamma_1} \cdot \frac{\overline{\Phi}}{\Phi_k} \qquad \text{Eq.7 and 8}$$

Where $\Phi_k = (x_k + y_k)/2$: size of the grain k and $\overline{\Phi}$ is the average value of the grain sizes. C_1 = 0.366 and γ_1 = 0.395 are the coefficients of the thermal fatigue curve (Figure 12).

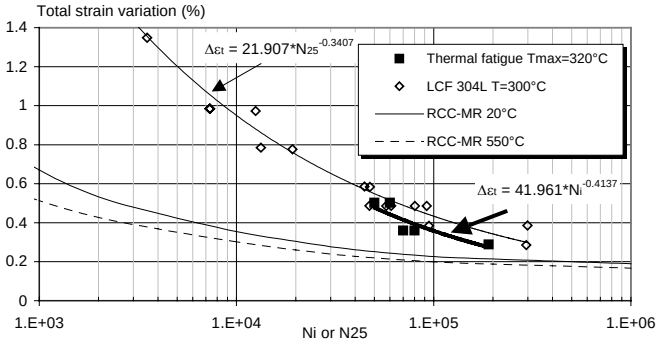


Figure 12. Fatigue lifetime curve of the austenitic stainless steel: mechanical loading and thermal loading

Elastic-plastic crack propagation: The use of the cyclic stress-strain relationship in the analysis comes from the fact that the material at the crack tip exhibits a stabilised cyclic behaviour. [9] showed that notch root strain measurements indicated that more than 90 percent of the plastic strain accumulation was achieved within a small number of applied cycles.

Since the value of the J-integral is strongly dependent on the strain and much less on the stress, the crack closure effect due to residual stresses is expected to have a limited influence on this parameter. Furthermore, it has been shown by [10] and by [11] that in plane stress large-scale yielding conditions, the J-integral could be used for characterising the crack tip field. Thus, in the present case involving high cyclic stress levels (especially near the surface), where large flow zones occur in the critical section; it is expected that the J-integral values would be an appropriate parameter for describing the crack propagation rate. For each crack the rate of energy release G is calculated via CAST3M by G_THETA method. It consists in calculating the derivative of the quantities with respect to the crack extension. Since we impose a thermal variation, we actually compute the variation of J-integral (ΔJ).

The French dimensioning code of the nuclear structures [15] recommends to deduce from the computed values of ΔJ a variation of an effective Stress Intensity Factor ΔK_{eff} (Equation 9).

$$\Delta K_{eff\,i}^{\,j} = q.\sqrt{E^* \Delta J_i^j} \quad \text{Where: } E^* = \frac{E}{1-\nu^2} \text{ for plane strain and } E^* = E \text{ for plane stress, q: closure coefficient whose value is equal to 1 in our case} \qquad \text{Eq.9}$$

The growth of each crack then follows a generalised Paris' law, as presented in Eq.10 (Maillot 2003), for a given increment of cycles (dN^j).

Erreur! Signet non défini. Where: $C = 2.0510^{-10} \frac{mm}{cycle}(MPa\sqrt{m})^{-m}$ and $m = 4.2$

Erreur! Signet non défini.: effective stress intensity factor of the crack 'i' at the iteration 'j'
Erreur! Signet non défini. : number of cycles corresponding to 30 µm propagation of the dominant crack.

The calculated growths of the four lengthier cracks are presented in Figure 13 for three thermal conditions. Initiation of the various cracks takes place for a ΔT=125°C more later than for a ΔT=150°C. However, in the three cases, the cracks are initiated in the same order: n°83, n°50, n°18 then n°118.

Figure 13-left also shows that the propagation rate of the dominant crack (crack n°83) is gradually slowed down before reaching the chosen limit of 2.5 mm. We think that such deceleration of the longest crack (up to 2.5 mm length) is rather allotted to the thermal loading attenuation. For the highest temperature variation (Figure 13 -b), the crack n°83 has a much more important propagation velocity than in the cases with lower ΔT. The kinetics of propagation of crack n°50 (initiated in a second position) is characterised by a first stage where the

propagation velocity is increasing. After reaching 0.2 mm depth, the crack growth rate starts decreasing and the crack growth stops at 1.1 mm of depth (for a ΔT=150°C). The same kinetics behaviour is observed under the two other thermal conditions. The two peripheral cracks (n°18 and n°118) are later initiated as compared with the two first cracks (n°83 and n°50). The low shielding effect existing at their initiation time allows them to have a constant increasing crack growth rate.

Figure 14 shows an example of a crack network configuration. Evolution of the six most propagated cracks is presented on Figure. 15. We plotted also the evolution of the single crack by adding the number of cycles to initiation.

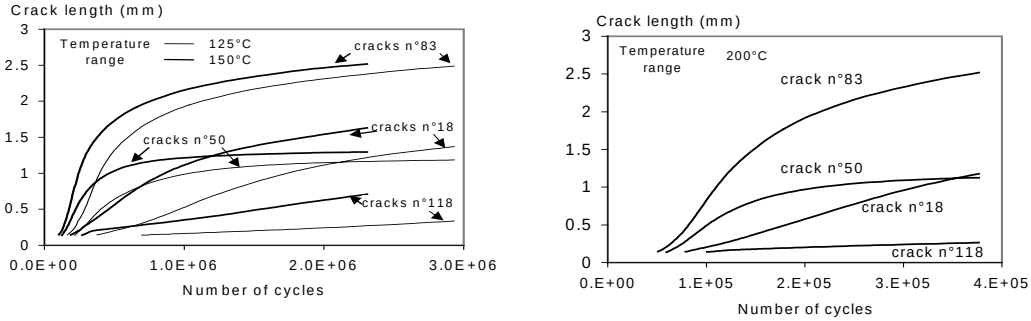


Figure 13. Temperature effect on the crack network growth.

All the curves are compared with the measured maximum depths. We note that:

- The crack growth of the dominant crack decreases towards a 2.5 mm depth.
- The shielding effect of the dominant crack on the other cracks is less and less important that the distance between cracks is important. For this reason, the peripheral cracks (numbers 18 and 118) are the most propagated.

Evolution of the size of the dominant crack is in good agreement with measurements on transversal sections (empty symbols). The maximum depths measured by removal layers accords with the propagation of the single crack.

- However, some points still must be improved:

Actually, we applied Paris's law starting from the initial size of the cracks. But, it was established that such short cracks propagate with a higher speed than the predicted by Paris's law. In this context, we could take as a starting point the work of [12], [13], [16]. by expressing the propagation rate in terms of loading parameters (inelastic strain…) and as a function of the size of the crack.

Some improvements are to be brought on the initiation law used. A law based on experimental observations and taking into account the effect of the grain orientation would better reproduce the spacing between cracks of the network. This last parameter will be also influenced by the propagation law.

5 . CONCLUSIONS

We have developed an efficient automatic remeshing algorithm. This algorithm, together with elastic-plastic calculation using the cyclic stress-strain relationship and a modified Paris relation, has been implemented in an automatic two-dimensional crack propagation program. The program enables to simulate the continuum initiation (using linear stored damage model) and the propagation (under elastic-plastic loading) of a crack network.

Simulation is in good agreement with the experimental results obtained for SPLASH conditions where temperature drop is obtained in 0.25 second (f = 4 Hz).

Such program thus gives an estimation of the continuum initiation, the effect of cracks in the initiation of other cracks and the shielding effects.

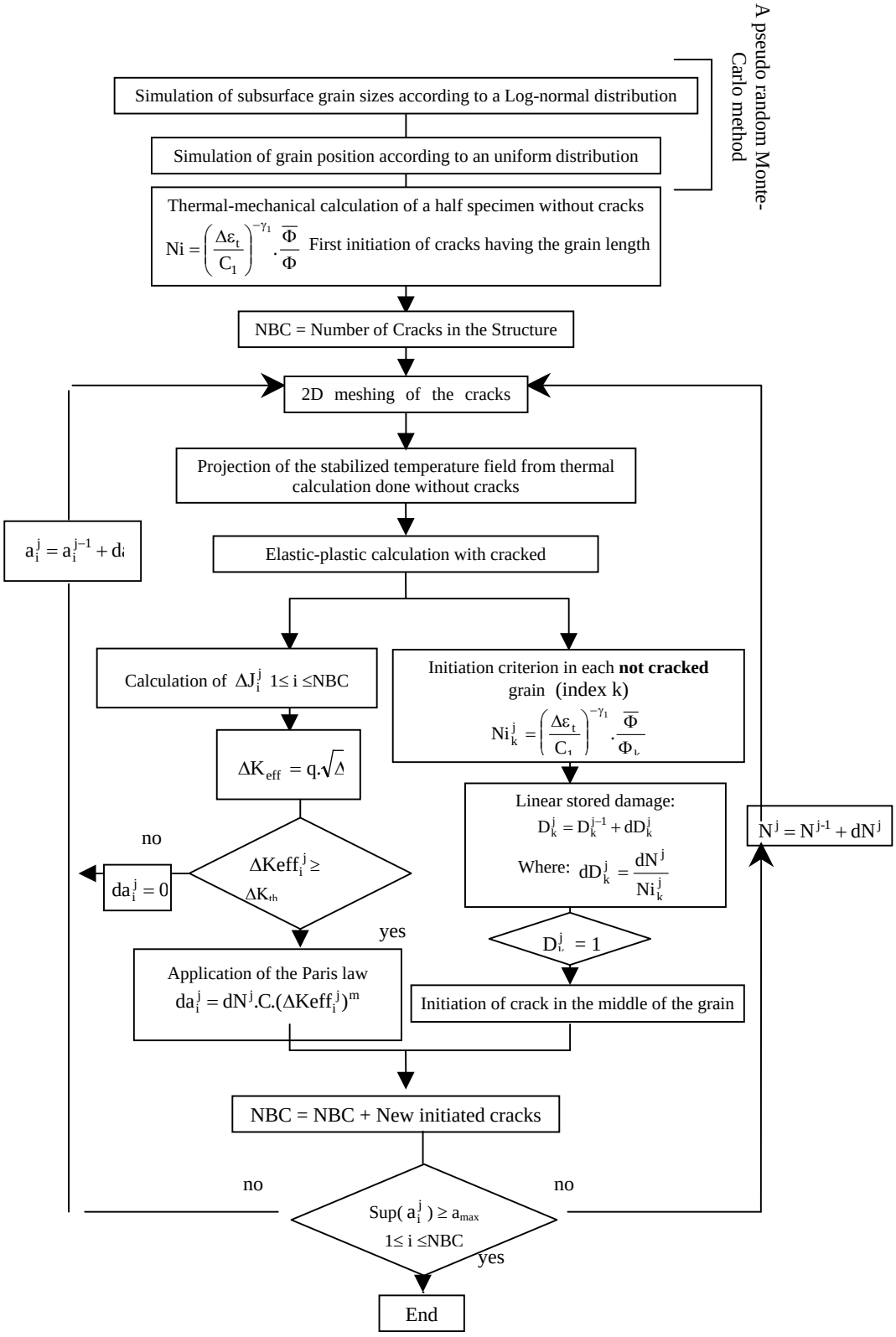


Diagram 1

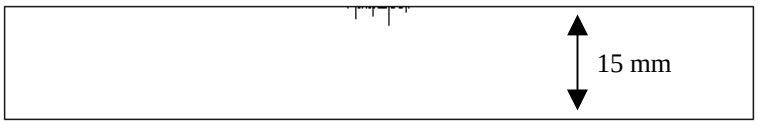


Figure 14. Crack network N = 2 309 240 cycles (T_{max} = 320°C, ΔT = 150°C).

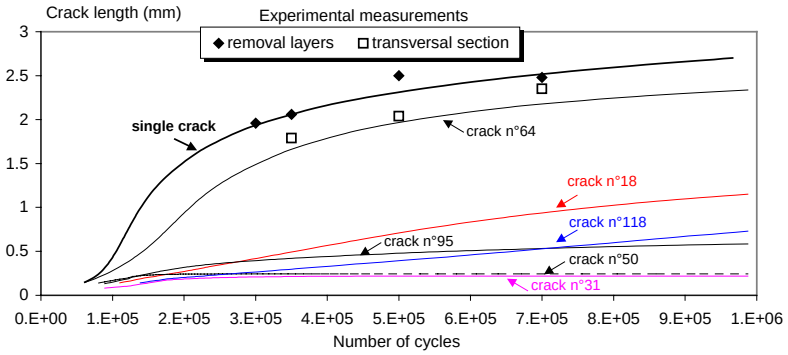


Figure 15. Crack network propagation (T_{max} = 320°C, ΔT = 150°C).

Acknowledgements
The authors whish to thank The French Institute of Radioprotection and Nuclear Safety (IRSN) and particularly Mr. François Mermaz to have supporting this action.

6. REFERENCES

6. 1 Conference Proceedings

1 Gelineau O., Speriando M., Martin P., Ricard J. B., Bougault A., 1994. Thermal fluctuation problems encountared in LMFRs., Aix en Provence.

2 Crutzen S., Birac C., Champigny F., Dugué C., Benoist P., Fontevraud 3, Vol.1, 12 – 16, 1994.

3 Cipière, M.F., Le Duff, J.A., 2001. Thermal fatigue experience in French piping. International Institute of Welding. Document n° XIII-1891-01 Lubjana 2001.

4 Fissolo, A., Robertson, C., Maillot, V., Marini, B. *Prediction of cracking under thermal fatigue. Proceedings of ECF 13*, San Sebastian, Spain, 6-9 September 2000.

6. 2 Journal Articles

5 Fissolo, A., Marini, B., Nais, G., Widen, P., 1996. *Journal of Nuclear Materials* 233-237, pp.156-161.

6 Maillot V., Degallaix G., Degallaix S., Fissolo A., 2004. *Thermal fatigue crack networks: an experimental Study. International Journal of Solids and Structures.*

7 Haddar N., Fissolo A., Maillot V., 2004. *Thermal fatigue crack networks: an computational Study. International Journal of Solids and Structures.*

8 Polak, J., Obrtlik, K., Liskutin, P., 1988. *Mechanisms of fatigue crack initiation. Materials Science Monographs 46*, pp.101-109.

9 Merah, N., Bui-Quoc, T., Bernard, 1999. *Trans of the ASME* Vol. 121, February pp. 42-48.

10 Liu, H. W., and Zheng, T., 1985. *A Dual Parameter Elastic-Plastic Fracture Criterion. Int Journal of Fracture. Vol 27*, pp. R87-R91

11 Lambert, Y., Saillard, P., and Bathias, C., 1988. *Application of the J-Concept to Fatigue Crack Growth in Large-scale Yielding. ASTM STP 969*, T.A. Cruse, ed., pp. 318-329.

12 Tomkins, B., 1974. *Fatigue crack propagation – An analysis. Philosophical magazine* 18, pp.1041-1066.

13 Skelton, R.P, 1988. *Low cycle fatigue*, ed. Salomon, H.D., Halford, G.R., ASTM STP 942, pp. 209-235.

6. 3 Book

14 RCC-MR 2002, French Code, *"Règles de conception et de construction des centrales electro-nucléaires", AFCEN*, édition 2002 TOME I – Vol. Z : Annexe Technique A3.

15 Chapuliot, S., Marie, S., Lacire M-H., Kayser Y., 2002. *RCC-MR, Volume Z, Annexe A16: Méthodes d'Ingénieurs en Mécanique de la Rupture*, P595_03_v2 pp. 6_12.

16 Murakami, Y., 1988. *Correlation between strain singularity at crack tip under overall plastic deformation and the exponent of the Coffin-Manson law. Low cycle fatigue*, ed. Salomon.

6. 4 Dissertation or Thesis

17 Maillot V. 2003. PhD Thesis in French, Ecole Centrale de Lille, Univ des Sc de Tech de Lille.

PROGRAM

1 Methodologies and tools for fatigue life assessment

- Automotive components
- Various industrial applications
- Welded structures and assemblies

2 Advanced design tools and approaches

- Fatigue crack initiation assessment
- Contribution to the crack propagation stage
- Modelling of the design behaviour of the welded

3 Multiaxial loading fatigue assessment

4 Fitness for service approach and applications

5 Experimental validation

- Application to automotive parts and structures
- From laboratory testing to field evaluation
- Development of dedicated test devices and procedures

6 Design procedures against thermal and thermo mechanical fatigue damage

7 Reliability approaches in fatigue design

8 Improved design and manufacture processes with regard to fatigue

Estimation of Random Load Histories by Spline Density Estimation and Bootstrap Method

Olli Alkkiomäki[a], Juha Kilkki[b] and Gary Marquis[b]

[a] Department of Information Technology
[b] Department of Mechanical Engineering
Lappeenranta University of Technology
P.O.Box 20, FIN-53851, Finland

Abstract

Keywords: bootstrap, rainflow histogram, service life, spline density estimation

For many industrial applications, the accumulation of fatigue load cycles is a stochastic process. In order to predict future service loading, the load cycle histogram should be extrapolated over a longer period of time. In order to obtain an estimate of the reliable service life, the variance of the damage produced by the random service loading process should be estimated. Variable amplitude load histories are often transformed into two-dimensional histograms of load cycle amplitudes and means. The service life of a component or a structure can be calculated from the histogram with fatigue analysis techniques. This paper describes a method for estimating the fatigue life from a short period of measured variable amplitude load history. The method transforms the two-dimensional load cycle histogram by means of a spline density estimation technique. Confidence intervals are then calculated for the density estimation using the bootstrap sampling method. The service loading over a longer period is predicted from the density estimation and the variance of the service loading is calculated from the confidence intervals. The proposed method is considered to be most suitable for the fatigue assessment of structures and components subject to random service loadings, such as ground vehicles or off-road machinery. The method can also be used to model non-random load histories. Spline density estimation is fully automatic and represents a good compromise between low computational cost and good accuracy. The bootstrap method was successfully used to calculate the confidence intervals for the spline density estimation. The variance of the predicted service loading, caused by the short time period of strain gauge measurements, can be determined with the developed method.

1 INTRODUCTION

Fatigue is the main cause of breakdowns in structures. 50 to 90 percent of mechanical failures in structures are caused by fatigue [1]. Fatigue damage occurs when a cyclic load is applied to a material. The fatigue is a result of cyclic fluctuation of stresses and strains, when the damaging load is not large enough to cause immediate failure. After a sufficient number of load cycles, the material will fail. The number of cycles before a failure, or fatigue strength, can be predicted using different fatigue analysis techniques. Due to uncertainties and the variability of material properties, loads and geometric tolerances, there is variance in fatigue strength distribution.

The load history can be measured by attaching strain gauges to the critical locations of a component or a structure. The variable amplitude load history is converted into a histogram of load cycle amplitudes and means by using cycle counting methods. It is possible to estimate how much fatigue damage the material has been subjected to from this histogram. Service loading for the whole lifetime is then predicted from the measured fatigue damage.

Load cycle accumulation is a stochastic process where the load cycles obey an unknown distribution. The measured load history represents only a fraction of the whole lifetime of a component or a structure. During the short measurement period, rare high amplitude load cycles causing the most damage may not exist. This is why the service loading is underestimated and the fatigue life is approximated to be higher than it actually is. Determining the variance of the service loading is also problematic. As the load cycle accumulation is a random process, the service loading for each identical component or structure is different. A method for estimating the variance from a single measurement has not been previously studied.

Estimating the load cycle accumulation of a region with no measured data is possible by using continuous density estimation methods. The noisy histogram of load cycle amplitudes and means is converted into a smooth, continuous surface. Smoothing spreads the high peaks locally, giving nonzero density estimation on the regions with no measured data. Once the density estimation of the load cycle accumulation is obtained, the fatigue life of a component or a structure can be estimated. In this paper a spline density estimation method is used and further developed by automatic smoothing parameter selection using generalized cross validation (GCV).

The service loading is a probabilistic rather than a deterministic value. Thus confidence intervals for the density estimation are calculated. Confidence intervals for rainflow distributions have not been previously studied. Bootstrap confidence intervals based on the resampling of the original data are used in this paper. Two-dimensional confidence intervals, or confidence planes are derived from the one-dimensional bootstrap confidence intervals. A new method for generating bootstrap samples is also introduced in this paper. This method is independent of the unknown variance, unlike other bootstrap sampling methods. Analysis of variance is used in fatigue analysis calculations to combine the variance of density estimation and the values used in the fatigue analysis equations.

The scope of this paper was restricted to the study of the fatigue life of components and structures under variable amplitude loadings. Load cycle accumulation was assumed to remain unchanged over time. Wear and damage may alter the behaviour of the component or the structure, which could have an effect on load cycle accumulation. The amount of load cycles is assumed to have random variance. For example mobile and marine vehicles and aircrafts have random loadings. If only the mean and amplitude of the load cycles vary, but the number of cycles can be estimated, the confidence intervals do not apply. Extending the bootstrap method for such cases is discussed in conclusions.

2 DENSITY ESTIMATION METHODS

Load cycle amplitudes and means can be extracted from the load signal with Rainflow counting [2]. Rainflow matrices can be used to represent the load cycle accumulation. The probability density function (PDF) is divided to a number of bins, each storing a number of rainflow cycles within a specific range of mean and amplitude. Figure 1 shows a Rainflow counted histogram of normally distributed load cycles. The fatigue damage can be calculated from the matrix using fatigue analysis techniques for the constant amplitude loadings.

As for all the histograms, the bin-size must be chosen manually and it controls the trade-off between presenting too much detail or too little detail. Methods for estimating the optimal bin width have been developed [3], but as there is usually no knowledge of the data beforehand, one should choose a small enough bin-size.

Often a data sample does not contain enough information to fully resolve the distribution. It is possible to restore a continuous probability density function from a discrete data sample by smoothing. In a Rainflow histogram, there may be peaks and valleys that would not exist in a larger sample. By smoothing, also the noise can be eliminated. There are several smoothing methods that present the probability density function as a continuous smooth surface. Most of the methods use kernel functions to represent the density, but also splines can be used.

The kernel functions are probability density functions that are usually of symmetric shape. Gaussian densities can be used to approximate any bounded continuous PDF, if the number of the Gaussian kernels is large enough [4]. The kernel method has a similar smoothing parameter as the histogram bin-size. If the kernel is much narrower than the distance between the data points, the density estimate will become bumpy. On the other hand, if the kernel is too wide, it will wipe out any details in the density estimate. Some methods use either variable kernel widths or non symmetric kernels. When the distribution of the load cycles is known, the fatigue life can be calculated.

Splines are continuous and derivative piecewise polynomials. The joining points of the polynomial pieces are called internal knots, which do not have to be evenly spaced. The shape of the spline is defined by control points. The degree of polynomial in each piece is constant and determines the degree of the spline. The spline of degree n has continuous derivatives up to order n-1 in each knot. Splines can be used for both interpolating and smoothing of multidimensional data. The cubic smoothing splines are piecewise polynomials of second degree. They can be used to smooth noisy gridded data, such as the rainflow histograms. The knots are evenly spaced and when smoothing the rainflow histograms, the knots can be inserted at bin borders. Due to the evenly spaced knots, the precision of the fit is not affected by the amount of data points in a certain region. Therefore the rainflow matrices have the same amount of control points in every region of the matrix, regardless of the amount of the load cycles in that region.

Cubic smoothing spline minimizes:

$$\lambda \sum_{i} (y_i - s(x_i))^2 + (1-\lambda) \int \left(\frac{d^2 s}{dx^2} \right)^2 dx \qquad (1)$$

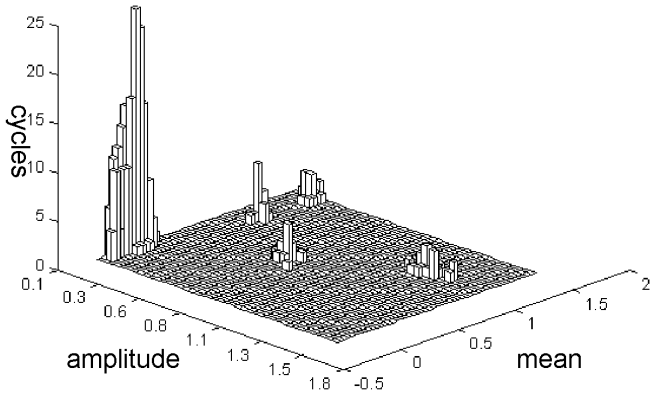
where x is the data point location and y the value, λ is the smoothing parameter and s is the smoothing spline. [5]

The cubic smoothing splines are computationally light for density estimation, as the time complexity is only $O(n^3)$, where n is the number of bins in rainflow matrix. The optimal smoothing parameter λ can therefore be found by using leave-one-out methods.

The smoothing parameter λ controls the trade-off between the roughness and goodness of the fit. Generalized cross validation (GCV) [6] can be used to find the optimal smoothing parameter. GCV is a leave one out -method, where one data point is omitted and the data is modelled using the rest of the data. The error between the true value of the omitted data point and the approximation is calculated. This procedure is repeated for each data point and the sum of the error values is calculated. For example the golden section search [7] can be used to minimize the sum of the error by modifying the parameter of the model.

The optimal smoothing parameter was chosen with GCV. GCV is feasible, since the amount of data points is small. If the rainflow matrix is very large, the optimal smoothing parameter can be approximated by selecting only a fraction of the data points for GCV.

a)



b)

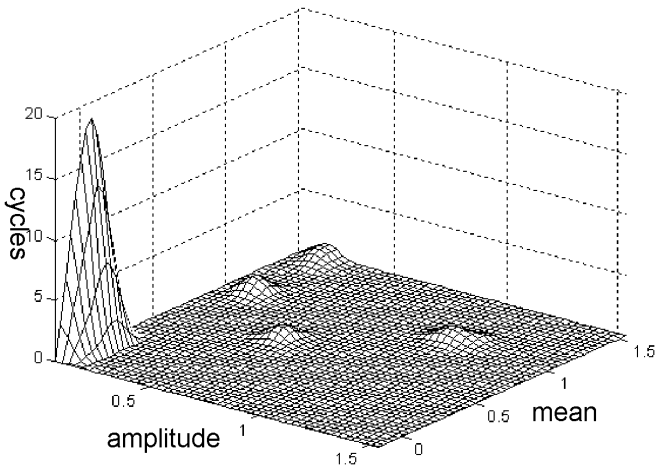


Figure 1. a) Example of a discrete two-dimensional rainflow histogram and

b) the same histogram represented by probabilistic spline density estimation

2.1 Calculating confidence intervals

Calculating confidence intervals for the probability density function of the load cycles is essential when approximating the fatigue life. Two dimensional confidence intervals have not been widely studied and only a few methods were found in literature.

The bootstrap confidence interval method is based on the assumption, that the distribution of the data points can be used as an estimate of the true distribution. In the bootstrap method, the data is resampled by generating simulated samples obeying the smoothed distribution obtained earlier. Usually the bootstrap samples are generated by adding Gaussian noise to the smoothed distribution. This process is repeated B times, resulting in B bootstrap samples. The variance of the bootstrap samples is then calculated and the confidence intervals can be created.

Wang and Wahba [9] compare several bootstrap methods and the Bayesian confidence intervals. The bootstrap method is computationally more intensive compared to the Bayesian method. However, the bootstrap method can be used for any distribution and not just for the splines. It also appears to work better with small sample sizes than the Bayesian intervals [9]. The bootstrap method is easy to transform to a multivariate case unlike the Bayesian.

Normal bootstrap intervals were chosen for this paper and they are calculated as follows:

$$\hat{f}_{\hat{\lambda}}(t_i) \pm n_{1-\frac{\alpha}{2}} \sqrt{T_i^*} \tag{2}$$

where T_i* is the bootstrap estimate of the squared error T_i, $\hat{f}_{\hat{\lambda}}(t_i)$ is the spline smoothed distribution and $n_{1-\alpha/2}$ is the $\alpha/2$ percentile of the standard normal distribution. T_i* can be calculated from the variance of the bootstrap samples. [9]

Individual squared errors are used instead of the MSE. The confidence interval methods based on the average MSE cannot reliable predict the error for the whole surface. Areas with high number of load cycles lower the MSE and such methods generate too narrow confidence intervals on the areas with low number of load cycles. However, the areas with few load cycles are the most important, because they usually are the areas with the highest fatigue damage.

A modified version of generating a bootstrap sample was developed. In the original bootstrap method, an estimate of the variance is required. However, in case of the simulated rainflow cycles, where the number of cycles is known, the bootstrap samples can be generated without a knowledge of the variance. The method is also used to simulate rainflow matrices obeying known distributions and is described in chapter: generating simulated rainflow matrices. Either the original rainflow matrix, or the spline fitted smoothed distribution can be used.

When using the spline fitted smoothed distribution with a large amount of bootstrap samples, the smoothing of the bootstrap samples is not necessary. The variance can be calculated directly from the simulated rainflow matrices and smoothed afterwards.

In Wang's and Wahba's [9] experiments the bootstrap samples were smoothed and the smoothing parameter was recalculated with GCV for each bootstrap sample independently. However, in a bivariate case the computational cost would have been too high. The smoothing parameter obtained earlier using GCV for the original rainflow matrix, could be used for each bootstrap sample as well. When the amount of data points remains the same, and all the bootstrap samples obey the same original distribution, this assumption should be reasonable.

The error in rainflow histograms is assumed to be Gaussian. The number of load cycles in each bin is a discrete value. When observing bootstrap rainflow matrices generated from known distributions, the amount of load cycles in each bin seem to be normally distributed.

3 CONCLUSIONS

The objective of this paper was to find a method for estimating the fatigue life from short period strain gauge measurements. The variance of fatigue life is also important, when determining the failure probability of a component or a structure. The spline density estimation method is a good compromise between low computational cost and good accuracy. This method is fully automatic as the smoothing parameter can be selected using a leave-one-out method.

The confidence intervals can be used to model the uncertainty of the density estimation. Such methods have not been previously studied in the field of fatigue analysis. The bootstrap method was successfully used to calculate the confidence intervals for the spline density estimation. The variance of the predicted service loading, caused by the short time period of strain gauge measurements, can be determined with the developed method.

The methods presented in this paper are best applicable to structures and components under random service loadings, such as mobile vehicles. When the amount of measured load cycles is large enough and the distribution of the load cycles does not change over time, the service loading and its variance can be predicted reliably.

A sufficient number of load cycles is required for accurate density estimation. Strain gauge measurements usually have a low number of high amplitude load cycles which cause the most damage. When using the bootstrap method for determining the confidence intervals for the density estimation, the distribution of the predicted service loading may become too wide. The only way to overcome this problem is to conduct more measurements.

The methods require that the service loading remains unchanged over time. The methods cannot predict the changes that are caused by for example wear and damage. Further research could include adding the time scale into the density estimation. The time varying regions of the rainflow matrix could be detected and the future service loading could be extrapolated. Piecewise defined splines are not applicable for this problem, because extrapolating over the piece borders is not possible. The kernel methods using non-Gaussian functions such as the joint Weibull-normal mixtures could be used instead. However, adding the time scale increases the computational complexity, and it might become too high for the kernel methods.

The next step in integrating the methods as a part of the product process, is to test the methods in real world industrial cases. As the measurement devices using rainflow matrices are commonly used in industrial applications, applying the methods to existing systems should be straight forward.

4 REFERENCES:

1 Al-Sugair, Hamad, F. A. Semi-Markovian Model for Low-cycle Elastic-plastic Fatigue Crack Growth, Ph.D. dissertation, Stanford University, 1989.

2 Matsuishi, M., Endo, T. Fatigue of Metals Subjected to Varying Stress, paper presented to Japan Soc. Mech. Engrs., Jukvoka, Japan, 1968. Reprinted in “The Rainflow method of fatigue” Ed. by Y. Murakami, Butterworth & Heinemann, London, 1991.

3 Scott, D., W. Multivariate Density Estimation, John Wiley & Sons, New York, 1992. ISBN: 0-471-54770-0

4 Feller, W. An Introduction to Probability Theory and its Applications, volume II. John Wiley & Sons Inc., New York, 1971. ISBN: 0471257095

5 M. Unser, Splines: A Perfect Fit for Signal and Image Processing, IEEE Signal Processing Magazine, 16(6), 22-38, 1999.

6 Wahba, G., Spline Models for Observational Data, SIAM, Philadelphia. CBMS-NSF Regional Conference Series in Applied Mathematics, 59, 1990. ISBN 0-89871-244-0

7 Press, W., H., Teukolsky, S., A., Vetterling, W., T., Flannery, B., P., Numerical Recipes in C: The Art of Scientific Computing, Cambridge University Press, 1988-1992. ISBN 0-521-43108-5

8 Wahba, G. Bayesian confidence intervals for the cross-validated smoothing spline. Journal of the Royal Statistical Society B, 45, 133-150, 1983.

9 Wang, Y. and Wahba, G. Bootstrap confidence intervals for smoothing splines and their comparison to Bayesian confidence intervals, Journal of Statistical Computation and Simulation, 51, 263-279, 1995.

Comparison of two statistical treatments of fatigue test data

Frédéric Perrin[a,c], Bruno Sudret[b], Maurice Pendola[a] , Maurice Lemaire[c]

[a] PHIMECA Engineering S.A., 1 allée Alan Turing 63170 Aubière, France
[b] EDF R&D, Department of Materials and Mechanics of Components, Site des Renardières, 77818 Moret-sur-Loing Cedex, France
[c] Institut Français de Mécanique Avancée – LaMI, Campus de Clermont-Ferrand – Les Cézeaux, BP265, 63175 Aubière, France

Abstract: Fatigue behavior is affected by numerous uncertainties, making the number-of-cycles-to-failure $N(S)$ for a given strain level S a random variable. The purpose of the present paper is to introduce and to compare two methods that allow a statistical treatment of fatigue laboratory data. Both approaches are described and discussed in order to characterize the random variable $N(S,\omega)$. The first method considers that the fatigue life time $N(S,\omega)$ at each strain level S is a lognormally distributed random variable. The second approach is based on the ESOPE method (AFNOR standard) which gives an iso-probability S-N curve. The experimental data used to develop both methods come from a private database and allow to compare and to validate the probabilistic assumptions made in each case by applying appropriate statistical tests.

1 INTRODUCTION

A number of components in nuclear power plants are submitted to thermal and mechanical loading cycles. The choice of the methodology of statistical treatment is of importance to establish a probabilistic framework for fatigue analysis [1]. Usually, the results of fatigue endurance tests are plotted on graphs relating applied loading (*e.g.* force, stress, strain...) and the number of cycles to failure. Two different methods that allow a statistical treatment of fatigue laboratory data are developed in this paper. The aim of each approach is to characterize the random number of cycles to failure $N(S,\omega)$ for a given strain level S.

The first method considers that the fatigue life time $N(S, \omega)$ at each strain level S is a lognormally distributed random variable [1]. The scatter of experimental values at each strain level is thus directly taken into account. The second method is based on the statistical treatment of fatigue data investigated in the 60's by Bastenaire [3] and put in French Standards [2]. A chapter in the Standard deals with the probabilistic characterization of the S-N curve. The so-called ESOPE method does not provide a closed-form expression of the probability density function of the number of cycles to failure but an iso-probability S-N curve. From these elements, a complete framework that allows the determination of the distribution of the random variable $N(S, \omega)$ for a given strain level S is developed.

The experimental data used to develop the statistical methods described in the sequel is based on a private database consisting of 153 austenitic stainless steel specimens. These tests are carried out in air under zero-mean tension-compression condition in the strain control mode. Among those tests, 8 did not reach failure. We compare both approaches as follows:

- The median fatigue curve is obtained by maximization of the likelihood given by the experimental observations.
- Statistical tests such as the Kolmogorov-Smirnov test are applied to validate the assumptions made in the formulation of each approach.
- Iso-probability S-N curve are derived from each approach and compared.

2 STATISTICAL TREATMENT BY THE FIRST METHOD (GUÉDÉ *ET AL.)*

This part takes back the main elements developed in [1], [4] and [6].

2.1 Principles of the probabilistic characterization of specimen fatigue life

Let $N(S,\omega)$ denote the random variable "number-of-cycles-to-failure" observed at stress level S. The notation ω recalls the randomness of this quantity. At each strain level, $N(S,\omega)$ is supposed to be a lognormally distributed random variable. This can be written:

$$\ln N(S,\omega) = \lambda(S) + \sigma(S,\omega) \tag{1}$$

where $\lambda(S)$ is the mean value of the logarithm of N at stress level S and $\sigma(S,\omega)$ is zero-mean Gaussian random variable. We also suppose that these variables (representing the scatter of ln N around its mean-value) are perfectly correlated: this means that a given sample (which is a "realization" of the material in the probabilistic vocabulary) is good or bad with respect to fatigue life whatever the stress level applied. Under this assumption, Eq.(1) may be simplified as:

$$\ln N(S,\omega) = \lambda(S) + \sigma(S)\xi(\omega) \tag{2}$$

where $\xi(\omega)$ is a standard normal random variable. The mean value $\lambda(S)$ and standard deviation $\sigma(S)$ of ln N have to be given a particular form of S.

In this paper, the form of the curve used for the mean $\lambda(S)$ is inspired by the Langer model [8] based on the early work by Stromeyer (1914):

$$\lambda(S) = a - b\ln(S-E) \tag{3}$$

where E is the endurance limit, and a and b are unknown parameters that allow the best fit for the median curve.

As far as $\sigma(S)$ is concerned, three assumptions have been investigated in [1, 6]. According to these results, the best representation consists in assuming that the standard deviation of ln N, $\sigma(S)$, is proportional to the mean value:

$$\sigma(S) = \delta.\lambda(S) \tag{4}$$

According to Eq.(2),(3), the scatter of the fatigue specimen data may be represented by a single standard normal random variable $\xi(\omega)$, whose expression is given by:

$$\xi(\omega) = \frac{\left(\dfrac{\ln(N(S,\omega))}{a\ln(S-E)+b} - 1\right)}{\delta} \tag{5}$$

Under the above assumptions, the median number-of-cycle-to-failure $N_{50\%}(S)$ can be written as:

$$N_{50\%} = e^{\lambda(S)} = e^{a-b\ln(S-E)} = e^{a}(S-E)^{-b} \tag{6}$$

or, equivalently:

$$S = E + e^{\frac{a}{b}}(N_{50\%})^{-\frac{1}{b}} \tag{7}$$

The postulated model requires determining four unknown parameters: E (endurance limit), a and b (form of the median curve), and δ (scatter of the data). These parameters are determined simultaneously using the method of Maximum Likelihood (ML) described below.

2.2 Maximum likelihood estimation

The ML method is used here to estimate the unknown parameters of the random fatigue model. Assuming that the Q experimental points $\ln(N_j)$ are independent and follow a Gaussian distribution with mean value and standard deviation given by (3) and (4) respectively, the likelihood of the observations reads [5]:

$$L_Q(a,b,E,\delta) = \prod_{j=1}^{Q}\left\{\left[f(N_j,S_j,a,b,E,\delta)\right]^{\alpha_j}\left[1-F(N_j,S_j,a,b,E,\delta)\right]^{1-\alpha_j}\right\} \tag{8}$$

where:

$$\alpha_j = \begin{cases} 1 \text{ if } N_j \text{ is a failure} \\ 0 \text{ if } N_j \text{ is a censored observation} \end{cases}$$

In Eq.(8), the expressions for a failure (resp. a censored) point are given by:

$$f(N_j,S_j,a,b,E,\delta) = \frac{1}{\delta\left(a\ln(S_j-E)+b\right)}\varphi\left(\frac{\ln N_j - a\ln(S_j-E)-b}{\delta\left(a\ln(S_j-E)+b\right)}\right) \tag{9}$$

and:

$$F(N_j,S_j,a,b,E,\delta)=\int_{-\infty}^{\ln N_j}\frac{1}{\delta\left(a\ln(S_j-E)+b\right)}\varphi\left(\frac{t-a\ln(S_j-E)-b}{\delta\left(a\ln(S_j-E)+b\right)}\right)dt \tag{10}$$

where φ is the standard normal probability density function (PDF).

The determination of parameters *E*, *a*, *b* and δ is performed by requiring that they maximize the likelihood defined in (8), or equivalently minimize the following quantity:

$$-2\ln(L_Q)=-2\sum_{j=1}^{Q}\left\{\alpha_j\ln\left[f(N_j,S_j,a,b,E,\delta)\right]+(1-\alpha_j)\ln\left[1-F(N_j,S_j,a,b,E,\delta)\right]\right\} \tag{11}$$

The minimization problem described above is solved using classical routines implemented in MathCad [9].

3 STATISTICAL TREATMENT BY THE NORMALIZED METHOD

The statistical treatment of fatigue data has been investigated since the 60's and normalized in French Standard A 03-405 [2]. This standard proposes several recommendations. The present method is related to §8 of this document, which is entitled "Iso-probability *S-N* curve modelling by the ESOPE method". In this section, a method is proposed, which takes into account and clarifies all the remarks proposed in the Standard in order to be applicable from low-cycle to high-cycle domain.

3.1 Principles

3.1.1 Mathematical model

Let $F(S,N)$ be the fraction of samples which fail before *N* cycles at stress amplitude *S*. this fraction is comprised between 0 and 1. In the ESOPE method, following the work by Bastenaire [3], it is supposed that this quantity $F(S,N)$ varies as a normal cumulative distribution function (CDF) as follow:

$$p=F(S,N)=\Phi\left(\frac{S-\mu(N)}{\sigma}\right) \tag{12}$$

In this expression, σ is supposed to be constant, whereas $\mu(N)$ has to be given an analytical form. Note that σ is sometimes referred to the constant standard deviation of *S* at a given *N*. This is incorrect since *S* is never considered as a random variable, in contrary to $N(S)$ which is the (random) number of cycles to failure.

If a large number of tests were carried out at the same amplitude *S*, the quantity $F(S,N)$ would converge to the probability of failure before *N* cycles at *S*, i.e. the cumulative distribution function (CDF) of $N(S,\omega)$.Thus, the probability distribution function (PDF) of $N(S)$, denoted by $f(S,N)$ may be written as the derivative of $F(S,N)$ with respect to *N*:

$$f(S,N)=\frac{\partial F(S,N)}{\partial N} \tag{13}$$

It is easy to show that the form of *F*(*S*,*N*) in Eq.(12) allows to plot iso-probability curves of failure. Each curve represents a constant probability of failure $p=F(S,N)=\Phi\left(\frac{S-\mu(N)}{\sigma}\right)$. For a given *p*, this leads to:

$$S=\mu(N)+\sigma\,\Phi^{-1}(p) \tag{14}$$

The iso-probability median curve defined by $p=0.5$ satisfies:

$$S=\mu(N) \tag{15}$$

Thus $\mu(N)$ exactly represents the median *S-N* curve, also called Wölher curve.

Fatigue data on stainless specimens indicate that experimental samples tested below a particular stress level are unlikely to fail. The limiting stress level is called the *fatigue limit* or *endurance limit E*. Thus $\mu(N)$ exhibits an asymptotic behavior near the fatigue limit, so that:

$$E=\mu(\infty) \tag{16}$$

Taking this notation into account, Eq.(12) is written:

$$F(S,N)=\Phi\left(\frac{S-\gamma(N)-E}{\sigma}\right) \tag{17}$$

where $\gamma(N)=\mu(N)-E$ .Thus, Eq.(14) rewrites:

$$S=\gamma(N)+E+\sigma\,\Phi^{-1}(p) \tag{18}$$

Suppose now that $S=S_0$ .When N tends to infinity, $\gamma(N)$ tends to 0. Thus:

$$\Phi\left(\frac{S_0-E}{\sigma}\right)\neq 1 \tag{19}$$

This remark implies that there is always a probability of no-failure at any stress amplitude S_0 whatever N. The French Standard concludes from this remark that $\psi=S-E-\gamma(N)$ is a right censored Gaussian random variable, with zero mean and standard deviation σ:

$$\psi\equiv N(0,\sigma) \tag{20}$$

3.1.2 Fatigue model

To define the whole ESOPE model, we have to select a form for the median *S*-*N* curve. In order to be consistent with the first method developed in Section 1, a closed form expression as in Eq.(3) is chosen:

$$S=E+e^{\frac{a}{b}}N_{50\%}{}^{-\frac{1}{b}} \tag{21}$$

Defining $c=\frac{1}{b}$ and $A=\exp\left(\frac{a}{b}\right)$, Eq.(21) rewrites:

$$S=E+AN_{50\%}{}^{-c}=\mu(N) \tag{22}$$

The ESOPE model requires to determine four unknown parameters: E (endurance limit), A and c (form of the median curve), and δ (usually referred to as the scatter in the S direction).

Using Eq.(22), Eq.(12) is now rewritten as:

$$F(S,N,A,c,E,\sigma)=\Phi\left(\frac{S-E-AN^{-c}}{\sigma}\right) \tag{23}$$

By taking into account the truncation of the random variable N and by using Eqs.(13),(23) , the distribution of the number-of-cycle-to-failure reads:

$$f_N(S,N,A,c,E,\sigma)=\frac{1}{\Phi\left(\frac{S-E}{\sigma}\right)}\frac{\partial}{\partial N}\left[\Phi\left(\frac{S-E-AN^{-c}}{\sigma}\right)\right] \tag{24}$$

One finally gets:

$$f_N(S,N,A,c,E,\sigma)=\frac{1}{\Phi\left(\frac{S-E}{\sigma}\right)}\varphi\left(\frac{S-E-AN^{-c}}{\sigma}\right)\frac{c}{\sigma}AN^{-c-1} \tag{25}$$

where φ is the standard normal PDF.

3.2 Estimation of model parameters

Based on the experimental fatigue database, the four unknown parameters of the ESOPE model have to be determined by using the ML method as expressed in Eq.(11) by replacing f and F with $f_N(S,N,A,c,E,\sigma)$ and $F_N(S,N,A,c,E,\sigma)$, defined in Eqs.(24),(25), respectively.

As a conclusion, we present the ESOPE method in the tradition of Bastenaire's work. We complete the original method in order to have an iso-probability *S*-*N* curve whose unknown parameters can be estimated by the maximum likelihood method.

4 APPLICATION TO AUSTENITIC STAINLESS STEEL FATIGUE DATA

In this section, the two models described in Sections 2 and 3 have been fitted to fatigue data provided by EDF R&D. The data comprise from a 153 specimens of austenitic stainless steel. Experimentally speaking, fatigue life N is defined as the number of applied cycles at which the stress amplitude in tension side decreases to 75% of the maximum stress amplitude. See [7] for more details.

The dataset also includes 8 censored observations. Figure 1 shows the data and random fatigue models on a log-log scale with number of cycles in the horizontal axis, as is traditional in the plot of *S-N* curves. In this figure, "O" and "□" represent failure and censored observations, respectively.

Remark: it is to be noted that no experimental values appear on the two obtained curves since the database is private. Only the methodology of statistical treatment is of importance.

4.1 Maximum likelihood estimates of the random fatigue models

The Levenberg-Marquardt algorithm (see [9] for more details) is used to fit the models. The quality of the fit is estimated by calculating two coefficients:

- The determination coefficient R^2 $\left(0 < R^2 \leq 1\right)$ which is useful because it represents the ratio of the explained variance to the total fluctuation. In other words, it is a measure of how well the regression model represents the data.

- The Akaike Information Criterion (*AIC*) statistic [11] for each model allows identifying which best approximates the true underlying model. The *AIC* statistic is given by:

$$AIC = -2\ln(L_Q) + 2k \tag{26}$$

where k is the number of model parameters. Higher values of R^2 and smaller values of *AIC* indicate better fits, see [11] and [12] for further details.

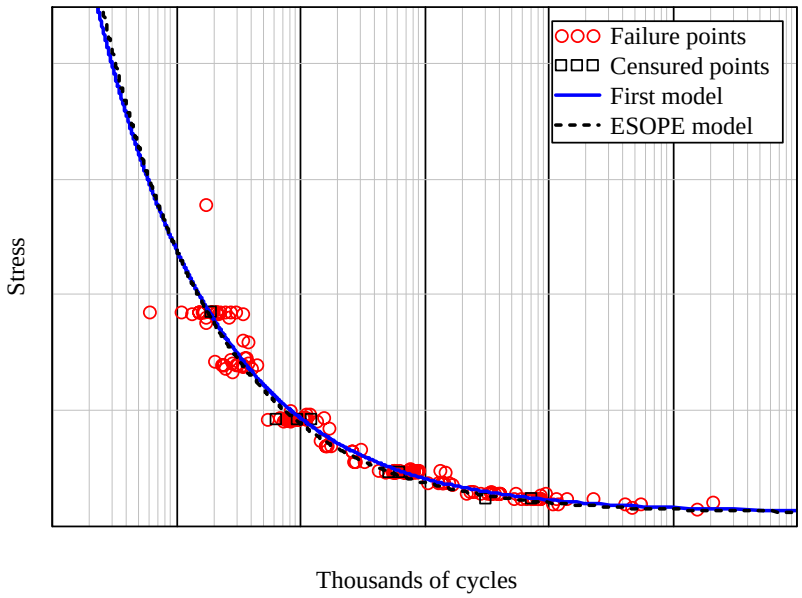


Figure 1. *S-N* plot of the data points and the models' fits

Table I. Fitting results for the austenitic stainless steel database

	First model	ESOPE model
R^2	0.96	0.81
AIC Statistic	158	2075

According to Figure 1, the two approaches give almost the same *S-N* median curve. Nevertheless, based on the values of Table I, the first method provides the best fit to the data among the two models.

4.2 Evaluation of statistical assumptions

The application of each model defined above involves validating by statistical tests the assumptions made by using these random fatigue models.

4.2.1 Goodness-of-fit tests

It is important to have a tool for assessing the distribution fit. The statistical significance of departures from each random fatigue model is assessed by performing empirical distribution function goodness-of-fit tests. Table II shows the Gaussian assumptions that have to be rejected or not by statistical tests.

Table II. Statistical assumptions for each method

Method	Probabilistic assumption
First method	$H0 : \xi \equiv N(0,1)$ Eq.(5)
ESOPE method	$H0 : \psi \equiv N(0,\sigma)$ Eq.(20)

Several common statistics are used to perform these tests [10]: Kolmogorov-Smirnov test (KS), Cramer-Von Mises test (CVM), Watson test (W) and Anderson Darling test (AD).

Table III. Results of the goodness-of-fit tests for each random fatigue model

	Test	Upper percentage point	Statistic limit value	Statistic test value	Reject *H*0
First model	KS	5%	1.358	1.071	no
	CVM	5%	0.187	0.260	yes
	W	5%	0.461	0.272	no
	AD	5%	2.492	1.875	no
ESOPE model	KS	5%	1.358	2.918	yes
	CVM	5%	0.187	2.112	yes
	W	5%	0.461	2.791	yes
	AD	5%	2.492	9.183	yes

Table III gives the different statistics values for each model. The hypothesis of normality of the random variable ξ defined in (5) is only rejected by the Cramer Von Mises test at 5 % however it cannot be rejected at $\alpha = 1\%$. On the other hand, the normal hypothesis made on the random variable ψ is not satisfied here: all the tests allow to reject with a 95 % confidence level. According to these goodness-of-fit tests and to the fitting curves evaluation made above, the first probabilistic model provides better results than the second one.

4.2.2 Quantiles of the number of cycles to failure

To assess the validity of both models, we also study plots of quantiles of the number of cycles to failure. The quantile estimates under each model are plotted in Figure 2. The following curves are representative of the relationship between the variables *S* and *N* at constant probability failure *p*.

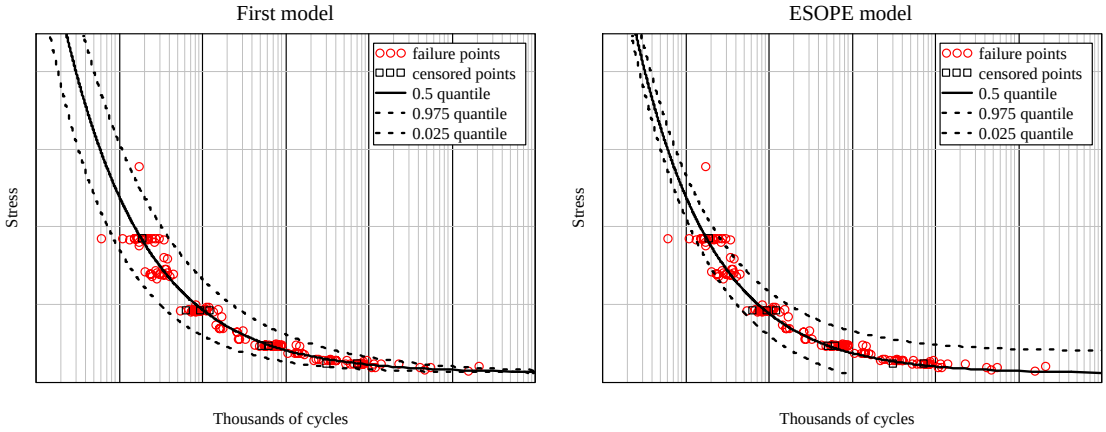


Figure 2. *S-N* plot for the data base with 0.025, 0.50 and 0.975 fractile curves

By considering a 95 % confidence interval around each median model *S-N* curve, we can see that each probabilistic model give different fractile curves. On the one hand, at greatest values of *S*, the scatter of the random variable seems to be better represented by the first model since all data points except 2 are included in the interval. On the other hand, near the endurance limit *E*, the ESOPE model does not provide a good representation of the scatter of the data.

4.2.3 Probability density function for a given stress level S

The aim of the proposed methods is to give, by applying a maximum likelihood method, the distribution of the number-of-cycle-to-failure *N* for a given stress level *S*. The PDF of *N* is of importance when a complete probabilistic framework is been set up to assess the fatigue life of components of nuclear plants, see for example [1]. The following plots are only given as a rough guide.

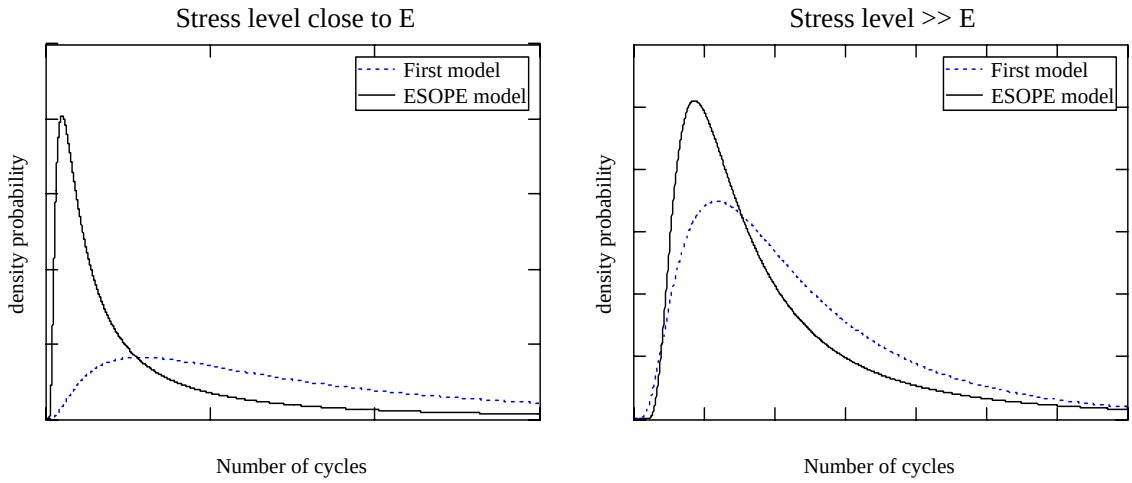


Figure 3. Schematic plot PDF at selected stress level

Figure 3 shows that both methods give almost the same probability density functions at high stress level. In contrary, at lower stress level (*e.g.* near the endurance limit), the first approach and the ESOPE method give significantly different PDFs. In order to validate precisely one method to the other, a large number of experiments at one single amplitude *S* should be carried out. This is yet to be done.

However, the experimental evidence of large scatter at low stress amplitude is obviously better represented by the first method.

5 CONCLUSION

To investigate the fatigue behavior and variability under tensile fatigue loading, we develop and compare two methods that predict the fatigue life *N* under alternative stress loading *S*. In the first model, specimen fatigue life at stress amplitude *S* is represented by a lognormal random variable whose mean and standard deviation depend on *S*.

Moreover, the correlation between fatigue life levels is supposed to be perfect. In the second part, another approach based on the ESOPE model defined in a French Standard is developped which gives an iso-probability *S-N* curve. Each method allows the determination of the Wölher curve and the distribution function of the random lifetime at a given stress level *S*.

Based on an experimental database comprising 153 austenitic stainless steel, we show that the first methodology gives better results. Indeed, the statistical tests show that the ESOPE hypotheses are not satisfied when applied to our samples.

The application of the statistical treatment in a complete probabilistic fatigue framework including the characterization all other sources of uncertainties is currently in progress.

6 REFERENCES

1. Guédé, Z., Approche probabiliste de la durée de vie de structures sollicitées en fatigue thermique, PhD Thesis, Université Blaise Pascal, Clermont-Ferrand, 2005.
2. AFNOR, Produits métalliques: essais de fatigue: traitement statistiques des données, norme A 03-405, 1991.
3. Bastenaire, F., Etude statistique et physique de la dispersion des résistances et des endurances à la fatigue, PhD Thesis, Faculté des Sciences de l'université de Paris, 1960.
4. Guédé, Z., Sudret, B. and Lemaire M., Analyse fiabiliste en fatigue thermique, Proc. 23èmes journées de Printemps – Commission fatigue, « Méthodes fiabilistes en fatigue pour conception et essais », Paris, 2004.
5. F. G. Pascual and W. Q. Meeker, Analysis of Fatigue data with Runouts based on a model with non constant standard deviation and a fatigue limit parameter, Journal of Testing and Evaluation, 1997, 25, 292-301.
6. Sudret, B. and Guédé, Z., Probabilistic assessment of thermal fatigue in nuclear components, 2005, Nuc. Eng. Des., 235, 1819-1835.
7. AFNOR, Pratique des essais oligocycliques, norme A 03-403, 1990.
8. Langer, B. F., Design of pressure vessels for low-cycle fatigue, Journal of Basic Engineering (Trans. ASME), 1962, 389-402.
9. Mathsoft Inc., Mathcad user's manual, 2001.
10. Pearson E.S. and Hartley H.O., Biometrika tables for statisticians volume II, Editions Biometrika Trustees,1972.
11. Akaike H., Information theory and an extension of the maximum likelihood Principle, Second International Symposium on Information, Budapest, 1973, 297-281.
12. Saporta G., Probabilités, analyse de données et statistique, Editions Technip, 1991.

Probabilistic Approach to Crack Propagation based on XFEM and FORM

Lukas Nespurek[a], Jean-Marc Bourinet[a], Anthony Gravouil[b], Maurice Lemaire[a]

[a] Laboratoire de Mécanique et Ingénieries, EA 3867-FR TIMS/CNRS 2856
Université Blaise Pascal – Clermont II & Institut Français de Mécanique Avancée
Campus de Clermont-Ferrand – Les Cézeaux
[b] Laboratoire de Mécanique des Contacts et des Solides, INSA de Lyon

Abstract An approach to perform reliability analysis of problems of linear-elastic, quasi-static, constant-amplitude, in-plane, mixed-mode propagation of multiple cracks is presented. The novelty of the approach consists in using the Extended Finite Element Method (XFEM) to calculate the stress intensity factors within a reliability analysis. In addition, a procedure is developed to integrate the crack growth law accurately, using a local polynomial fit to discrete points of the stress intensity factor curve obtained by post-processing of the XFEM solution. The reliability analysis itself is carried out using the First Order Reliability Method (FORM) with gradients obtained by the finite difference method. The approach is illustrated by means of a representative numerical example.

1 INTRODUCTION

Due to its importance for lifetime assessment, safety requirements and maintenance scheduling, applied to various components subject to fatigue loading, an efficient modelling of crack propagation is of a continued interest in nuclear, aeronautical, automotive and other industries. In the above context, probabilistic modelling and reliability assessment provide tools to capture the effects of the inherent uncertainties and give a deeper insight to the problem studied than the classical deterministic analysis does.

The approaches to model stochastic crack propagation described in the literature are usually based on the following concepts: a) a random variable approach, whereby the parameters of the crack growth law, such as the Paris law, are treated as random variables [3]; and b) the random process approach, which includes the cumulative jump models [9], representing the crack growth increment by a random variable and summing the increments within a stochastic counting process, as well as the Markov-chain models [1] using a matrix of probabilities of transition from one damage state to another, and the Markov diffusion process models, in which the crack growth law is multiplied by a random process [6],[4].

The random process approaches generally seek to establish the statistical moments of the time to failure or of the damage size after a certain number of cycles. To make this possible, it is assumed that an analytical expression exists that explicitly relates the stress intensity factor to the crack length. On the other hand, this paper focuses on reliability analysis applied to crack propagation problems where the geometry and the related interaction of multiple cracks cannot be neglected. For such problems, the analytical prediction of the crack driving forces is generally not available and a numerical model needs to be used. The objective of this paper is to show the advantages of the Extended Finite Element Method (XFEM) [7],[8] as the numerical model to provide the structural response for the purposes of the reliability analysis of complex-geometry crack propagation problems. Although the random variable approach mentioned above takes into account only the inter-specimen randomness while neglecting the randomness during crack growth, we adopt this approach for the purposes of this paper, as this does not compromise the instructiveness of the example in terms of the contribution of XFEM modelling.

2 RELIABILITY ANALYSIS

The use of reliability analysis is motivated by its two major contributions. First, it allows for including in the analysis the available statistical information on the input variables involved. And second, it provides information on the actual level of probability of failure of the component analysed and besides it also the sensitivity to uncertain variables and their parameters.

The reliability analysis provides an overall framework for the developments of this paper. It involves the reliability method used, as discussed in this Section 2, the failure model (Section 3), the statistical model of the random variables (Section 5), and the mechanical model (Section 4) to obtain the structural response.

The probability of failure p_f is defined by:

$$p_f = \int_{g(\mathbf{x})\le 0} f_X(\mathbf{x})dx \ , \tag{1}$$

where $f_X(\mathbf{x})$ is the joint probability density of the problem random variables $\mathbf{x}$ and $g(\mathbf{x})$ is the performance function. $g(\mathbf{x}) = 0$ may not be known explicitly. In the case of complex-geometry crack propagation problems, its evaluation involves a full numerical simulation of crack growth until failure.

In this paper, we use the First Order Reliability Method (FORM) [5], in which g(x) = 0 is approximated by a linear function passing through the design point $\mathbf{x}^*$, which is a point on $g(\mathbf{x}) = 0$ which has the highest probability density in the standard normal space. When the variables $\mathbf{x}$ are transformed to a set of uncorrelated standard normal variables $\mathbf{u}$, then $\mathbf{u}^*$ is the point on $g(\mathbf{x}(\mathbf{u})) = 0$ which is the closest to the origin of the $\mathbf{x}$-space. The analysis then consists in solving the minimisation problem:

$$\text{minimise } \sqrt{\mathbf{u}^T\mathbf{u}} \quad \text{under the constraint } \mathbf{u} \in \mathbf{x}(\mathbf{u}) = 0 \,. \tag{2}$$

Note that minimisation algorithms require the gradients of $g(\mathbf{x}(\mathbf{u}))$, which are obtained by the finite difference method. The distance from $g(\mathbf{x}(\mathbf{u})) = 0$ to the origin is called the Hasofer-Lind index β_{HL} and the FORM-based failure probability is $p_f = \Phi(-\beta_{HL})$, where Φ is the standard normal distribution function.

3 FAILURE MODEL

The state of failure $g(\mathbf{x}) \le 0$ is defined as the event that the calculated lifetime at failure N_R under crack propagation due to fatigue loading is less than the target service life N_S , so that the performance function reads:

$$g(\mathbf{x}) = N_R - N_S \,. \tag{3}$$

For numerical reasons, the natural logarithm of (3) is used in the calculations, i.e. $g(\mathbf{x}) = \ln(N_R/N_S)$. The lifetime N is counted in load cycles.

4 MECHANICAL MODEL

The lifetime N_R entering the performance function (3) is obtained by numerical simulation of crack propagation involving XFEM analyses to compute the stress intensity factors (SIF). This procedure is developed taking the following assumptions: linear-elastic, quasi-static, mixed-mode, in-plane curvilinear propagation of multiple cracks in a homogeneous, isotropic material and under constant amplitude high-cycle fatigue loading with no crack closure considered. N_R is obtained using the Paris crack growth law:

$$N_R = \int_{a_i}^{a_f} \frac{1}{C\left(\Delta K_{eq}\right)^m} \mathrm{d}a \tag{4}$$

The term $1/C\left(\Delta K_{eq}\right)^m$ will be denoted dN/da in the following. a_i is the initial crack size. The final crack length a_f is defined as the length at which the equivalent Mode I stress intensity factor K_{eq} [2] attains the fracture toughness K_{Ic}:

$$K_{Ic} = K_{eq} \equiv K_I \cos^3\frac{\theta}{2} - 3K_{II}\cos^2\frac{\theta}{2}\sin\frac{\theta}{2}, \tag{5}$$

where K_I and K_{II} are the Mode I and Mode II stress intensity factors, respectively, and θ is the crack propagation angle determined based on the maximal circumferential stress criterion:

$$\theta = 2\arctan\left[\frac{1}{4}\left(\frac{K_I}{K_{II}} \pm \sqrt{\left(\frac{K_I}{K_{II}}\right)^2 + 8}\right)\right], \tag{6}$$

As there is a ± sign in (6), the equation yields two different values of θ. The value for which the circumferential stress $\sigma_{\theta\theta}$ is maximum, is taken as the crack propagation angle. If multiple cracks are present, N_R corresponds to the lifetime when the criterion (5) is first fulfilled at any of the cracks.

4.1 Crack Growth Integration Procedure

As there may be multiple mutually interfering cracks, each of which propagates with a different rate governed by the stress intensity at its tip, it is not a priori known at which crack the critical stress intensity K_{Ic} will be attained first and at which crack length a_f this will happen. The latter fact precludes a prior discretisation of the integration domain between a_i and a_f and requires that the actual evolution of the cracks and the stress intensity factors at their tips be followed along the loading history.

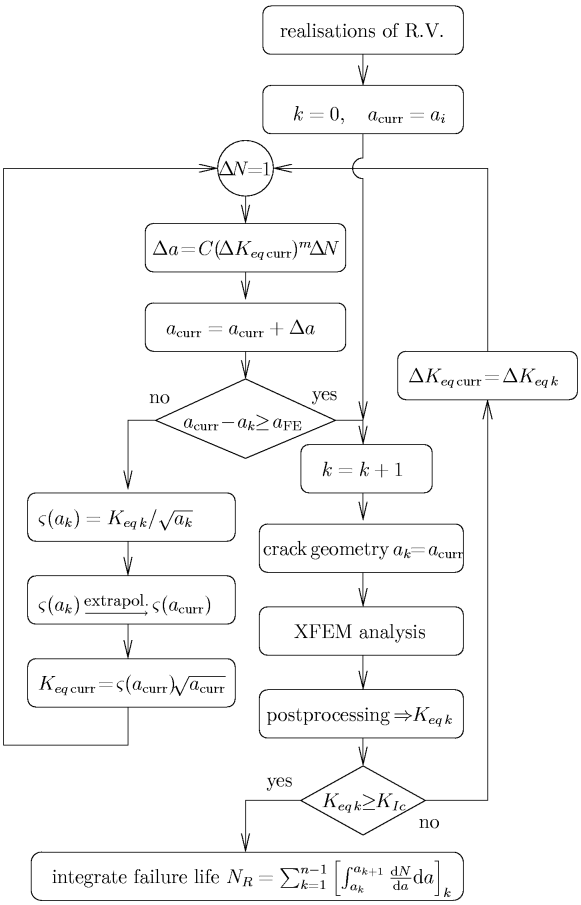


Figure 1. Fatigue crack growth simulation procedure

The cracks are assumed to propagate obeying to the Paris law:

$$\Delta a = C\left(\Delta K_{eq}\right)^m \Delta N\,. \tag{7}$$

where the load cycle increment is taken equal to a single cycle: $\Delta N = 1$. The propagation simulation approach, illustrated in Figure 1, consists in updating the stress intensity factors K_{eq} by values obtained from an XFEM solution at the beginning of the propagation and every time that the increment of any crack's length since the last update exceeds a predetermined value a_{FE}. Between the XFEM update points, the crack is assumed to grow by straight-line increments and K_{eq} is extrapolated to the current crack length a_{curr} from the previously obtained XFEM values, whereby it is assumed that K_{eq} is proportional to $\sqrt{a}$ as $K_{eq} = \varsigma\sqrt{a}$, see Figure 1. At the XFEM update point, the

crack direction may change, being determined using Eq. (6). It is important to note that the latter inaccurate method to calculate K_{eq} is used only to determine the discretisation of the domain between a_i and a_f for each of the cracks, and K_{eq} entering into Eq. (4) is obtained from the XFEM analysis.

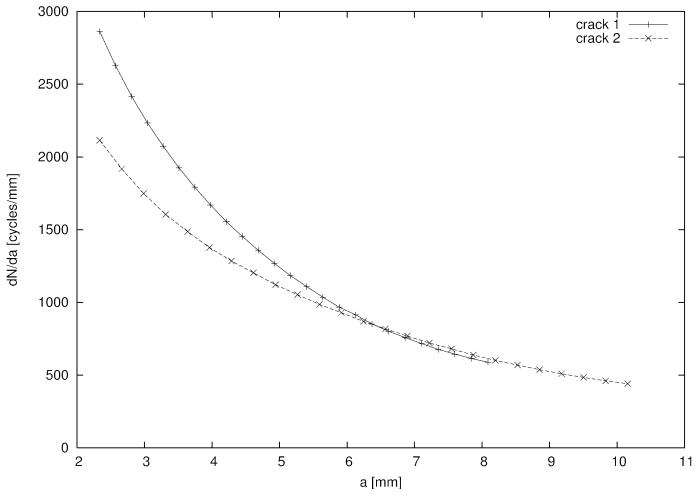


Figure 2. An example of the $[a;\ \mathrm{d}N/\mathrm{d}a\ ]$ history for 2 cracks. The discrete points of the curve, obtained from the XFEM analysis, are used to integrate the number of cycles at failure N_R

When the criterion (5) is fulfilled, we are left with a set of n couples $[a; K_{eq}]$ for each crack at n points of the crack length discretisation. The discretisation intervals are in general not equidistant. Using Eq. (7), these n couples $[a; K_{eq}]$ for each crack are easily converted to a set of n couples $[a;\ \mathrm{d}N/\mathrm{d}a\ ]$ – see Figure 2, which is what we need for the numerical integration of Eq. (4). The integration is carried out interval by interval, i.e.:

$$N_R = \sum_{k=1}^{n-1} \left[\int_{a_k}^{a_{k+1}} \frac{\mathrm{d}N}{\mathrm{d}a}\,\mathrm{d}a \right]_k , \tag{8}$$

where a_k and a_{k+1} are the lower and upper limit of the k-th interval, respectively. In the last interval, the upper limit $a_n = a_f$, where the actual a_f is determined for the leading crack (at which the failure actually occurred) by interpolating between the last two $[a; K_{eq}]$ couples for the crack, and for any other crack, say the j-th crack, by constructing a quadratic least-square fit of the curve $a_j(a_{cr})$, where a_{cr} is the length of the leading crack. The integrand of (8) is an expression of the form:

$$\frac{\mathrm{d}N}{\mathrm{d}a} = \alpha_1 a^{-2/m} + \alpha_2 a^2 + \alpha_3 a + \alpha_4 , \tag{9}$$

where the coefficients α_1 to α_4 are fit using four points of the discrete $\frac{\mathrm{d}N}{\mathrm{d}a}(a)$ history that lie the closest to the k-th interval. The values N_{Rj} obtained from (8) for each crack are averaged arithmetically to provide the final value N_R passed to the reliability analysis.

4.2 Stress Intensity Factors Calculation by XFEM

The structural response is calculated using the extended finite element method. The main advantage of XFEM from the crack growth modelling point of view is that the crack geometry does not need to coincide with the element edges. This liberates the engineer from the tedious remeshing work to follow the path of the growing curvilinear crack.

In XFEM, the finite element approximation is locally enriched with additional base functions associated with additional nodal parameters at the enriched nodes. The approximation on the elements containing the crack tip is enriched with base functions spanning the near-tip displacement field, whereas a heaviside function enrichment is added to the remaining elements along the crack to capture the displacement discontinuity. By virtue of the principle of minimum energy, the correct nodal displacements associated with the classical shape functions and nodal

parameters associated with the enrichment are obtained when the total system is solved. For further details on XFEM, see e.g. [7].

The stress intensity factors KI and KII are obtained from finite element post-processing using the domain form interaction integral method [11].

5 INPUT VARIABLES STATISTICAL MODEL

The variables considered as random in this study are the initial crack length a_i and the point of departure of each crack, and the factor C and exponent m of the Paris crack growth law. It is noteworthy to discuss the statistical modelling of C and m.

Recalling the form of the Paris law: $\mathrm{d}a/\mathrm{d}N = C(\Delta K_{eq})^m$, where the units of d$a$/d$N$ are millimeters per cycle and the units of ΔK are MPa√mm, we note that by changing the value of m, we change the units of C, and vice-versa. Therefore, next to a possible statistical correlation of C and m, there is also a dimensional interdependence of these two variables. We model the scatter and dependence of C and m by considering normally distributed correlated random variables log C and m, the statistical parameters of which were established from the Virkler data [10]. Taking the exact values of the estimated statistical parameters, we were able to reproduce Virkler's results with sufficient accuracy. The statistical models of all random variables are given in the example, see Section 6.

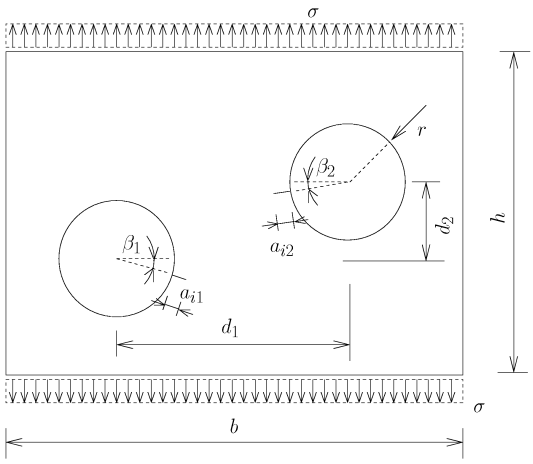


Figure 3. Example problem geometry

6 EXAMPLE

The above described stochastic crack propagation approach is applied to an example of a plate with two holes, from each of which a crack emanates. With reference to the notation introduced above and in Figure 3, the values of the problem random variables are given in Table I. In total, there are six random variables.

variable	unit	model	mean	std. dev.	correlation
β_1, β_2	°	normal	0.0	5.0	–
a_{i1}, a_{i2}	mm	exponential	2.0	2.0	–
ln C	–	normal	-26.056	0.972	-0.99795
m	–	normal	2.855	0.167	

Table I. Example problem random variables.

The remaining problem parameters are as follows: b = 90 mm, h = 60 mm, d_1 = 40 mm, d_2 = 10 mm. The radius of both of the holes is 10 mm. The applied stress σ has a constant-amplitude with σ_{max} = 100 MPa and the minimal to maximal stress ratio is R = 0.2. The toughness K_{IC} is 1000 MPa√mm.

Figure 4 shows a typical crack path, the generally curvilinear crack line consisting of straight-line segments. The elements intersected by the crack are seen to be partitioned to sub-triangles to ensure a correct integration of the

finite element equations, see e.g. [7], [8]. Note that no new elements are created in the partitioning, the displacements are still interpolated over the parent elements, with no degrees of freedom being added. The partitioning is taken care of by the FE code itself, with no requirements on the user.

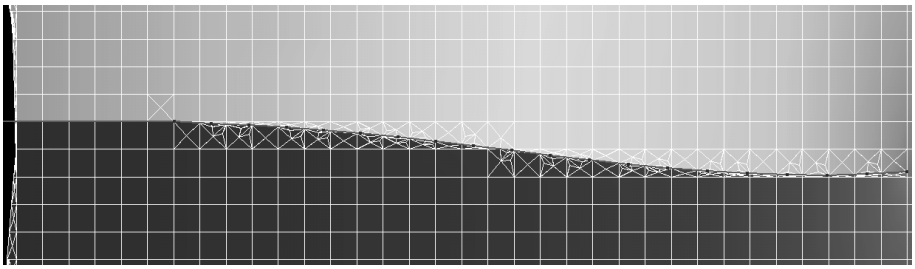


Figure 4. Crack path with partitioning of elements to sub-triangles for integration purposes

Figure 5 shows the history of the iterations to find **u*** for the target service life $N_S = 8000$ cycles. The convergence to the correct **u*** is the key issue of the FORM based reliability analysis. In fact, it is necessary to ensure a good accuracy and a high stability of the calculated cycles at failure N_R. Any numerical noise in the values obtained may effectively impede the convergence process. Note that the accuracy and numerical stability has to be ensured at all stages of the calculation: in the numerical simulation of crack propagation, in the calculation of the stress intensity factors and in the integration of the crack propagation law – Eq. (8).

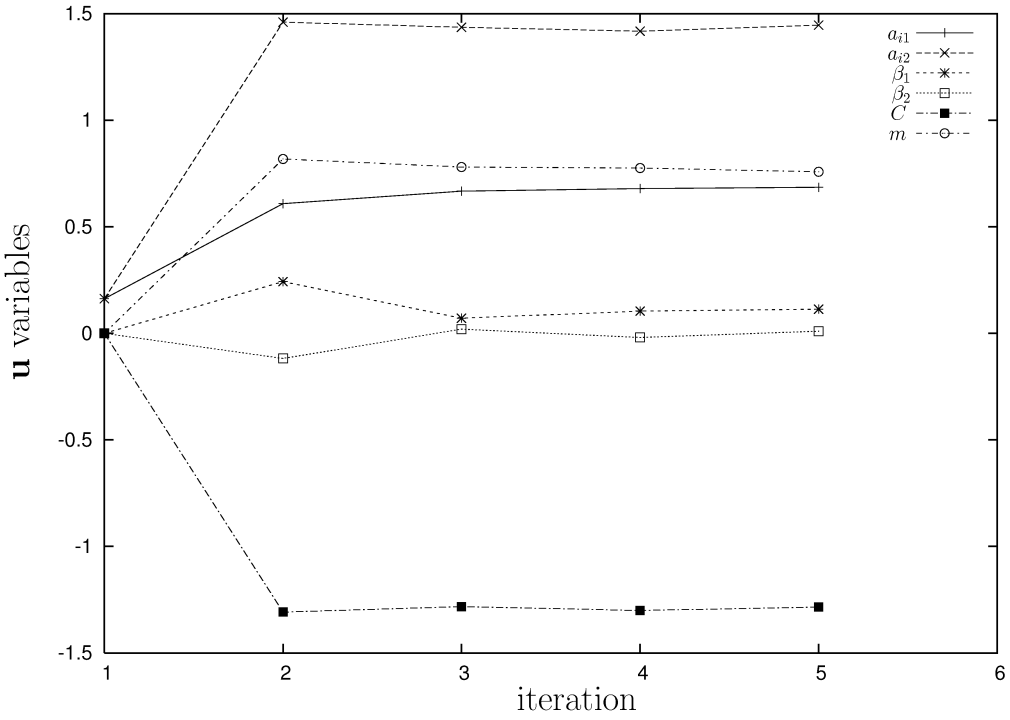


Figure 5. Design point search history.

The location of **u*** in the standard normal space corresponds to a Hasofer-Lind reliability index of β_{HL}=2.19. In a first-order (FORM) approximation, this corresponds to a probability of failure of 0.014.

Figure 6 shows the sensitivities of the individual variables at the design point, which are a measure of the respective variable's contribution to failure. It can be seen that the crack initiation angles bring only little contribution to failure. This is because the distance of two holes is large enough to suppress any mutual influence of the holes and the cracks at the onset of the propagation. Thus, the crack growth direction quickly reverts to the direction determined by Eq. 6. As expected, the Paris law factor C and the initial crack lengths a_{i1} and a_{i2} are the most significant variables in terms of reliability.

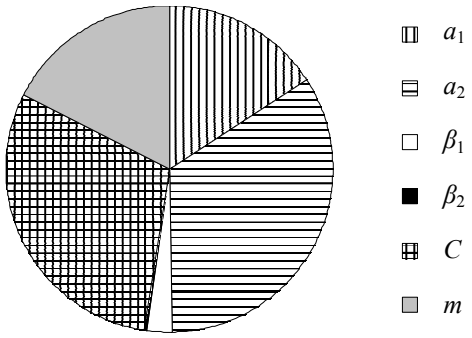


Figure 6. Sensitivities at the design point.

7 CONCLUSIONS

This paper presents an approach to model stochastic in-plane crack propagation under constant-amplitude high-cycle fatigue loading. The use of the Extended Finite Element Method (XFEM) to obtain the stress intensity factors allows for considering of complex crack and structural geometries in a very easy way. In particular, no remeshing is necessary as the crack propagates. In addition, the stress intensity factors calculated from the XFEM post-processing results show a better stability as compared to the classical finite elements, where the stability of the stress and strain field calculated is perturbed by successive remeshing. Note that the stability of the stress intensity factors is essential for the overall stability of the calculated number of cycles at failure N_R, which in turn a key issue to achieving convergence of the reliability algorithm. The other factors include the numerical simulation of crack propagation and the integration of the crack propagation law. In the approach presented, care has been taken to integrate the crack growth law correctly – an aspect which is rarely discussed in the literature.

In the future work, the authors wish to enhance the computational efficiency in the reliability analysis as compared to the present approach, namely with regard to the necessity to obtain the gradients of the performance function by the finite difference method.

8 REFERENCES

8.1 Book

1. J.L. Bogdanoff and F. Kozin. Probabilistic Models of Cumulative Damage. John Wiley & Sons, 1985.
2. D. Broek. Elementary Engineering Fracture Mechanics. Martinus Nijhoff Publishers, Dordrecht, The Netherlands, fourth edition, 1986.
3. H.O. Madsen. Probabilistic Methods for Structural Design, chapter Stochastic Modelling of Fatigue Crack Growth and Inspection, pages 59–83. Kluwer Academic Publishers, The Netherlands, 1997.

8.2 Journal Article

4. O. Ditlevsen, *Engineering Fracture Mechanics*, 23(2):467–477, 1986.
5. A.M. Hasofer and N.C. Lind, *Journal of Engineering Mechanics Division, ASCE*, 100(1):111–121, 1974.
6. Y.K. Lin and J.N. Yang, *Engineering Fracture Mechanics*, 18(2):243–256, 1983.
7. N. Moës, J. Dolbow and T. Belytschko, *International Journal for Numerical Methods in Engineering*, 46(1):131–150, 1999.
8. N. Moës, A. Gravouil and T. Belytschko, *International Journal for Numerical Methods in Engineering*, 65(11):2549–2568, 2002.
9. K. Sobczyk and J. Trebicki, *Engineering Fracture Mechanics*, 34(2):477–493, 1989.
10. D.A. Virkler, B.M. Hillbery and P.K. Goel, *Journal of Engineering Materials and Technology, ASME*, 101:148–153, 1979.
11. J. Yau, S. Wang and H. Corten, *Journal of Applied Mechanics*, 47:335–341, 1980.

Probabilistic Approach to Crack Propagation based on XFEM and FORM

Lukas Nespurek[a], Jean-Marc Bourinet[a], Anthony Gravouil[b], Maurice Lemaire[a]

[a] Laboratoire de Mécanique et Ingénieries, EA 3867-FR TIMS/CNRS 2856
Université Blaise Pascal – Clermont II & Institut Français de Mécanique Avancée
Campus de Clermont-Ferrand – Les Cézeaux
[b] Laboratoire de Mécanique des Contacts et des Solides, INSA de Lyon

Abstract An approach to perform reliability analysis of problems of linear-elastic, quasi-static, constant-amplitude, in-plane, mixed-mode propagation of multiple cracks is presented. The novelty of the approach consists in using the Extended Finite Element Method (XFEM) to calculate the stress intensity factors within a reliability analysis. In addition, a procedure is developed to integrate the crack growth law accurately, using a local polynomial fit to discrete points of the stress intensity factor curve obtained by post-processing of the XFEM solution. The reliability analysis itself is carried out using the First Order Reliability Method (FORM) with gradients obtained by the finite difference method. The approach is illustrated by means of a representative numerical example.

1 INTRODUCTION

Due to its importance for lifetime assessment, safety requirements and maintenance scheduling, applied to various components subject to fatigue loading, an efficient modelling of crack propagation is of a continued interest in nuclear, aeronautical, automotive and other industries. In the above context, probabilistic modelling and reliability assessment provide tools to capture the effects of the inherent uncertainties and give a deeper insight to the problem studied than the classical deterministic analysis does.

The approaches to model stochastic crack propagation described in the literature are usually based on the following concepts: a) a random variable approach, whereby the parameters of the crack growth law, such as the Paris law, are treated as random variables [3]; and b) the random process approach, which includes the cumulative jump models [9], representing the crack growth increment by a random variable and summing the increments within a stochastic counting process, as well as the Markov-chain models [1] using a matrix of probabilities of transition from one damage state to another, and the Markov diffusion process models, in which the crack growth law is multiplied by a random process [6],[4].

The random process approaches generally seek to establish the statistical moments of the time to failure or of the damage size after a certain number of cycles. To make this possible, it is assumed that an analytical expression exists that explicitly relates the stress intensity factor to the crack length. On the other hand, this paper focuses on reliability analysis applied to crack propagation problems where the geometry and the related interaction of multiple cracks cannot be neglected. For such problems, the analytical prediction of the crack driving forces is generally not available and a numerical model needs to be used. The objective of this paper is to show the advantages of the Extended Finite Element Method (XFEM) [7],[8] as the numerical model to provide the structural response for the purposes of the reliability analysis of complex-geometry crack propagation problems. Although the random variable approach mentioned above takes into account only the inter-specimen randomness while neglecting the randomness during crack growth, we adopt this approach for the purposes of this paper, as this does not compromise the instructiveness of the example in terms of the contribution of XFEM modelling.

2 RELIABILITY ANALYSIS

The use of reliability analysis is motivated by its two major contributions. First, it allows for including in the analysis the available statistical information on the input variables involved. And second, it provides information on the actual level of probability of failure of the component analysed and besides it also the sensitivity to uncertain variables and their parameters.

The reliability analysis provides an overall framework for the developments of this paper. It involves the reliability method used, as discussed in this Section 2, the failure model (Section 3), the statistical model of the random variables (Section 5), and the mechanical model (Section 4) to obtain the structural response.

The probability of failure p_f is defined by:

$$p_f = \int_{g(\mathbf{x})\le 0} f_X(\mathbf{x})dx \ , \tag{1}$$

where $f_X(\mathbf{x})$ is the joint probability density of the problem random variables $\mathbf{x}$ and $g(\mathbf{x})$ is the performance function. $g(\mathbf{x}) = 0$ may not be known explicitly. In the case of complex-geometry crack propagation problems, its evaluation involves a full numerical simulation of crack growth until failure.

In this paper, we use the First Order Reliability Method (FORM) [5], in which g(x) = 0 is approximated by a linear function passing through the design point $\mathbf{x}^*$, which is a point on $g(\mathbf{x}) = 0$ which has the highest probability density in the standard normal space. When the variables $\mathbf{x}$ are transformed to a set of uncorrelated standard normal variables $\mathbf{u}$, then $\mathbf{u}^*$ is the point on $g(\mathbf{x}(\mathbf{u})) = 0$ which is the closest to the origin of the $\mathbf{x}$-space. The analysis then consists in solving the minimisation problem:

$$\text{minimise } \sqrt{\mathbf{u}^T\mathbf{u}} \quad \text{under the constraint } \mathbf{u} \in \mathbf{x}(\mathbf{u}) = 0 \,. \tag{2}$$

Note that minimisation algorithms require the gradients of $g(\mathbf{x}(\mathbf{u}))$, which are obtained by the finite difference method. The distance from $g(\mathbf{x}(\mathbf{u})) = 0$ to the origin is called the Hasofer-Lind index β_{HL} and the FORM-based failure probability is $p_f = \Phi(-\beta_{HL})$, where Φ is the standard normal distribution function.

3 FAILURE MODEL

The state of failure $g(\mathbf{x}) \le 0$ is defined as the event that the calculated lifetime at failure N_R under crack propagation due to fatigue loading is less than the target service life N_S , so that the performance function reads:

$$g(\mathbf{x}) = N_R - N_S \,. \tag{3}$$

For numerical reasons, the natural logarithm of (3) is used in the calculations, i.e. $g(\mathbf{x}) = \ln(N_R/N_S)$. The lifetime N is counted in load cycles.

4 MECHANICAL MODEL

The lifetime N_R entering the performance function (3) is obtained by numerical simulation of crack propagation involving XFEM analyses to compute the stress intensity factors (SIF). This procedure is developed taking the following assumptions: linear-elastic, quasi-static, mixed-mode, in-plane curvilinear propagation of multiple cracks in a homogeneous, isotropic material and under constant amplitude high-cycle fatigue loading with no crack closure considered. N_R is obtained using the Paris crack growth law:

$$N_R = \int_{a_i}^{a_f} \frac{1}{C\left(\Delta K_{eq}\right)^m} \mathrm{d}a \tag{4}$$

The term $1/C\left(\Delta K_{eq}\right)^m$ will be denoted dN/da in the following. a_i is the initial crack size. The final crack length a_f is defined as the length at which the equivalent Mode I stress intensity factor K_{eq} [2] attains the fracture toughness K_{Ic}:

$$K_{Ic} = K_{eq} \equiv K_I \cos^3\frac{\theta}{2} - 3K_{II}\cos^2\frac{\theta}{2}\sin\frac{\theta}{2}, \tag{5}$$

where K_I and K_{II} are the Mode I and Mode II stress intensity factors, respectively, and θ is the crack propagation angle determined based on the maximal circumferential stress criterion:

$$\theta = 2\arctan\left[\frac{1}{4}\left(\frac{K_I}{K_{II}} \pm \sqrt{\left(\frac{K_I}{K_{II}}\right)^2 + 8}\right)\right], \tag{6}$$

As there is a ± sign in (6), the equation yields two different values of θ. The value for which the circumferential stress $\sigma_{\theta\theta}$ is maximum, is taken as the crack propagation angle. If multiple cracks are present, N_R corresponds to the lifetime when the criterion (5) is first fulfilled at any of the cracks.

4.1 Crack Growth Integration Procedure

As there may be multiple mutually interfering cracks, each of which propagates with a different rate governed by the stress intensity at its tip, it is not a priori known at which crack the critical stress intensity K_{Ic} will be attained first and at which crack length a_f this will happen. The latter fact precludes a prior discretisation of the integration domain between a_i and a_f and requires that the actual evolution of the cracks and the stress intensity factors at their tips be followed along the loading history.

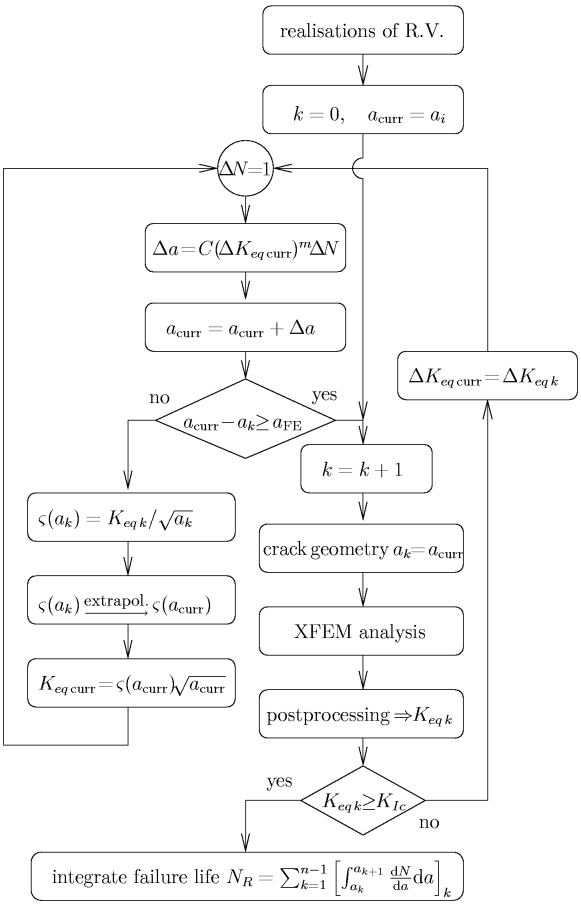


Figure 1. Fatigue crack growth simulation procedure

The cracks are assumed to propagate obeying to the Paris law:

$$\Delta a = C\left(\Delta K_{eq}\right)^m \Delta N\,. \tag{7}$$

where the load cycle increment is taken equal to a single cycle: $\Delta N = 1$. The propagation simulation approach, illustrated in Figure 1, consists in updating the stress intensity factors K_{eq} by values obtained from an XFEM solution at the beginning of the propagation and every time that the increment of any crack's length since the last update exceeds a predetermined value a_{FE}. Between the XFEM update points, the crack is assumed to grow by straight-line increments and K_{eq} is extrapolated to the current crack length a_{curr} from the previously obtained XFEM values, whereby it is assumed that K_{eq} is proportional to $\sqrt{a}$ as $K_{eq} = \varsigma\sqrt{a}$, see Figure 1. At the XFEM update point, the

crack direction may change, being determined using Eq. (6). It is important to note that the latter inaccurate method to calculate K_{eq} is used only to determine the discretisation of the domain between a_i and a_f for each of the cracks, and K_{eq} entering into Eq. (4) is obtained from the XFEM analysis.

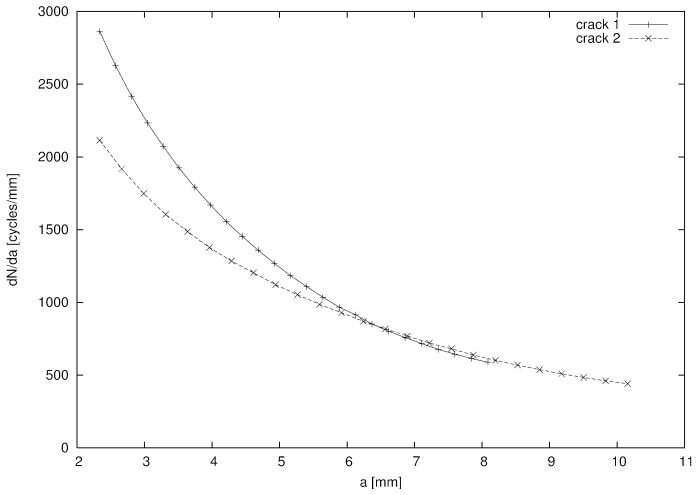


Figure 2. An example of the $[a;\ \mathrm{d}N/\mathrm{d}a\ ]$ history for 2 cracks. The discrete points of the curve, obtained from the XFEM analysis, are used to integrate the number of cycles at failure N_R

When the criterion (5) is fulfilled, we are left with a set of n couples $[a; K_{eq}]$ for each crack at n points of the crack length discretisation. The discretisation intervals are in general not equidistant. Using Eq. (7), these n couples $[a; K_{eq}]$ for each crack are easily converted to a set of n couples $[a;\ \mathrm{d}N/\mathrm{d}a\ ]$ – see Figure 2, which is what we need for the numerical integration of Eq. (4). The integration is carried out interval by interval, i.e.:

$$N_R = \sum_{k=1}^{n-1} \left[\int_{a_k}^{a_{k+1}} \frac{\mathrm{d}N}{\mathrm{d}a}\,\mathrm{d}a \right]_k , \tag{8}$$

where a_k and a_{k+1} are the lower and upper limit of the k-th interval, respectively. In the last interval, the upper limit $a_n = a_f$, where the actual a_f is determined for the leading crack (at which the failure actually occurred) by interpolating between the last two $[a; K_{eq}]$ couples for the crack, and for any other crack, say the j-th crack, by constructing a quadratic least-square fit of the curve $a_j(a_{cr})$, where a_{cr} is the length of the leading crack. The integrand of (8) is an expression of the form:

$$\frac{\mathrm{d}N}{\mathrm{d}a} = \alpha_1 a^{-2/m} + \alpha_2 a^2 + \alpha_3 a + \alpha_4 , \tag{9}$$

where the coefficients α_1 to α_4 are fit using four points of the discrete $\frac{\mathrm{d}N}{\mathrm{d}a}(a)$ history that lie the closest to the k-th interval. The values N_{Rj} obtained from (8) for each crack are averaged arithmetically to provide the final value N_R passed to the reliability analysis.

4.2 Stress Intensity Factors Calculation by XFEM

The structural response is calculated using the extended finite element method. The main advantage of XFEM from the crack growth modelling point of view is that the crack geometry does not need to coincide with the element edges. This liberates the engineer from the tedious remeshing work to follow the path of the growing curvilinear crack.

In XFEM, the finite element approximation is locally enriched with additional base functions associated with additional nodal parameters at the enriched nodes. The approximation on the elements containing the crack tip is enriched with base functions spanning the near-tip displacement field, whereas a heaviside function enrichment is added to the remaining elements along the crack to capture the displacement discontinuity. By virtue of the principle of minimum energy, the correct nodal displacements associated with the classical shape functions and nodal

parameters associated with the enrichment are obtained when the total system is solved. For further details on XFEM, see e.g. [7].

The stress intensity factors KI and KII are obtained from finite element post-processing using the domain form interaction integral method [11].

5 INPUT VARIABLES STATISTICAL MODEL

The variables considered as random in this study are the initial crack length a_i and the point of departure of each crack, and the factor C and exponent m of the Paris crack growth law. It is noteworthy to discuss the statistical modelling of C and m.

Recalling the form of the Paris law: $\mathrm{d}a/\mathrm{d}N = C(\Delta K_{eq})^m$, where the units of d$a$/d$N$ are millimeters per cycle and the units of ΔK are MPa√mm, we note that by changing the value of m, we change the units of C, and vice-versa. Therefore, next to a possible statistical correlation of C and m, there is also a dimensional interdependence of these two variables. We model the scatter and dependence of C and m by considering normally distributed correlated random variables log C and m, the statistical parameters of which were established from the Virkler data [10]. Taking the exact values of the estimated statistical parameters, we were able to reproduce Virkler's results with sufficient accuracy. The statistical models of all random variables are given in the example, see Section 6.

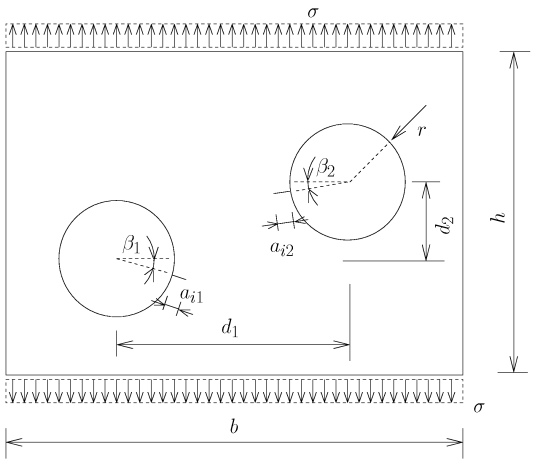


Figure 3. Example problem geometry

6 EXAMPLE

The above described stochastic crack propagation approach is applied to an example of a plate with two holes, from each of which a crack emanates. With reference to the notation introduced above and in Figure 3, the values of the problem random variables are given in Table I. In total, there are six random variables.

variable	unit	model	mean	std. dev.	correlation
β_1, β_2	°	normal	0.0	5.0	–
a_{i1}, a_{i2}	mm	exponential	2.0	2.0	–
ln C	–	normal	-26.056	0.972	-0.99795
m	–	normal	2.855	0.167	

Table I. Example problem random variables.

The remaining problem parameters are as follows: b = 90 mm, h = 60 mm, d_1 = 40 mm, d_2 = 10 mm. The radius of both of the holes is 10 mm. The applied stress σ has a constant-amplitude with σ_{max} = 100 MPa and the minimal to maximal stress ratio is R = 0.2. The toughness K_{IC} is 1000 MPa√mm.

Figure 4 shows a typical crack path, the generally curvilinear crack line consisting of straight-line segments. The elements intersected by the crack are seen to be partitioned to sub-triangles to ensure a correct integration of the

finite element equations, see e.g. [7], [8]. Note that no new elements are created in the partitioning, the displacements are still interpolated over the parent elements, with no degrees of freedom being added. The partitioning is taken care of by the FE code itself, with no requirements on the user.

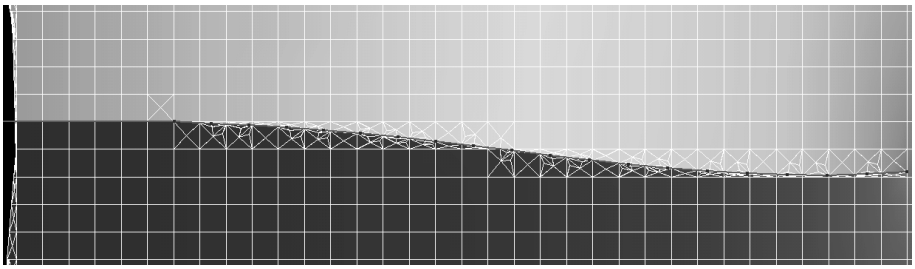


Figure 4. Crack path with partitioning of elements to sub-triangles for integration purposes

Figure 5 shows the history of the iterations to find **u*** for the target service life $N_S = 8000$ cycles. The convergence to the correct **u*** is the key issue of the FORM based reliability analysis. In fact, it is necessary to ensure a good accuracy and a high stability of the calculated cycles at failure N_R. Any numerical noise in the values obtained may effectively impede the convergence process. Note that the accuracy and numerical stability has to be ensured at all stages of the calculation: in the numerical simulation of crack propagation, in the calculation of the stress intensity factors and in the integration of the crack propagation law – Eq. (8).

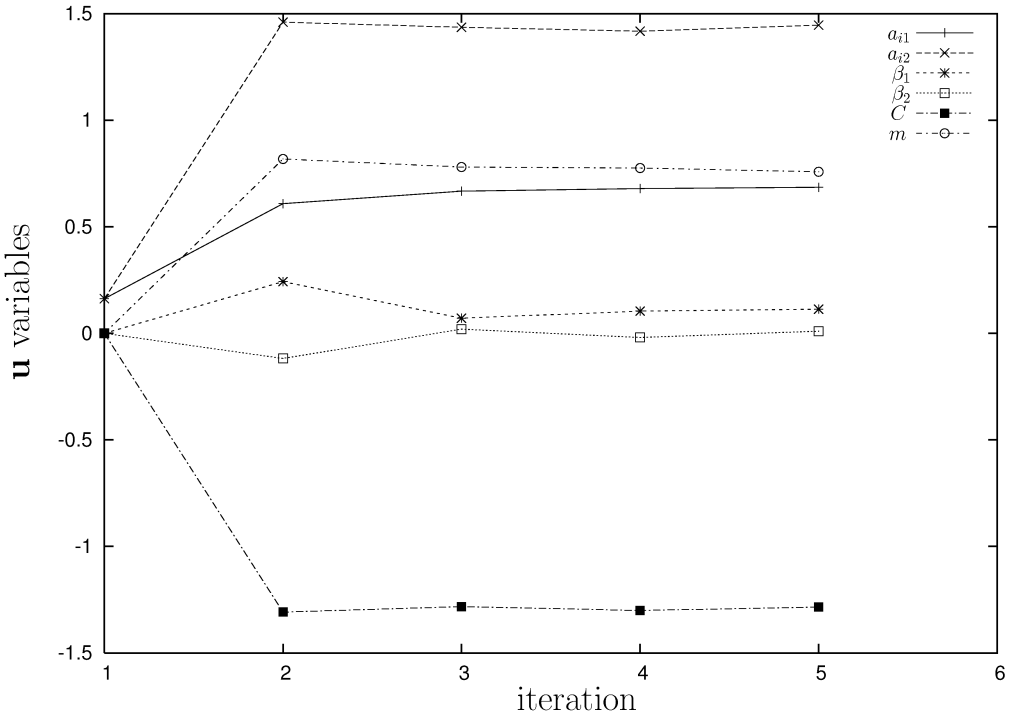


Figure 5. Design point search history.

The location of **u*** in the standard normal space corresponds to a Hasofer-Lind reliability index of β_{HL}=2.19. In a first-order (FORM) approximation, this corresponds to a probability of failure of 0.014.

Figure 6 shows the sensitivities of the individual variables at the design point, which are a measure of the respective variable's contribution to failure. It can be seen that the crack initiation angles bring only little contribution to failure. This is because the distance of two holes is large enough to suppress any mutual influence of the holes and the cracks at the onset of the propagation. Thus, the crack growth direction quickly reverts to the direction determined by Eq. 6. As expected, the Paris law factor C and the initial crack lengths a_{i1} and a_{i2} are the most significant variables in terms of reliability.

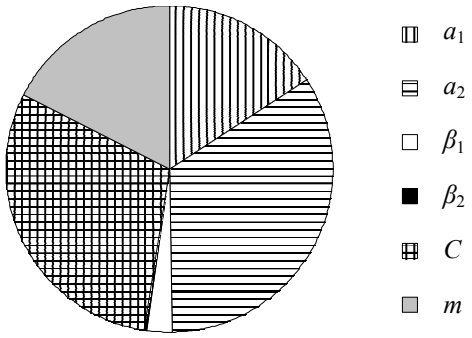


Figure 6. Sensitivities at the design point.

7 CONCLUSIONS

This paper presents an approach to model stochastic in-plane crack propagation under constant-amplitude high-cycle fatigue loading. The use of the Extended Finite Element Method (XFEM) to obtain the stress intensity factors allows for considering of complex crack and structural geometries in a very easy way. In particular, no remeshing is necessary as the crack propagates. In addition, the stress intensity factors calculated from the XFEM post-processing results show a better stability as compared to the classical finite elements, where the stability of the stress and strain field calculated is perturbed by successive remeshing. Note that the stability of the stress intensity factors is essential for the overall stability of the calculated number of cycles at failure N_R, which in turn a key issue to achieving convergence of the reliability algorithm. The other factors include the numerical simulation of crack propagation and the integration of the crack propagation law. In the approach presented, care has been taken to integrate the crack growth law correctly – an aspect which is rarely discussed in the literature.

In the future work, the authors wish to enhance the computational efficiency in the reliability analysis as compared to the present approach, namely with regard to the necessity to obtain the gradients of the performance function by the finite difference method.

8 REFERENCES

8.1 Book

1. J.L. Bogdanoff and F. Kozin. Probabilistic Models of Cumulative Damage. John Wiley & Sons, 1985.
2. D. Broek. Elementary Engineering Fracture Mechanics. Martinus Nijhoff Publishers, Dordrecht, The Netherlands, fourth edition, 1986.
3. H.O. Madsen. Probabilistic Methods for Structural Design, chapter Stochastic Modelling of Fatigue Crack Growth and Inspection, pages 59–83. Kluwer Academic Publishers, The Netherlands, 1997.

8.2 Journal Article

4. O. Ditlevsen, *Engineering Fracture Mechanics*, 23(2):467–477, 1986.
5. A.M. Hasofer and N.C. Lind, *Journal of Engineering Mechanics Division, ASCE*, 100(1):111–121, 1974.
6. Y.K. Lin and J.N. Yang, *Engineering Fracture Mechanics*, 18(2):243–256, 1983.
7. N. Moës, J. Dolbow and T. Belytschko, *International Journal for Numerical Methods in Engineering*, 46(1):131–150, 1999.
8. N. Moës, A. Gravouil and T. Belytschko, *International Journal for Numerical Methods in Engineering*, 65(11):2549–2568, 2002.
9. K. Sobczyk and J. Trebicki, *Engineering Fracture Mechanics*, 34(2):477–493, 1989.
10. D.A. Virkler, B.M. Hillbery and P.K. Goel, *Journal of Engineering Materials and Technology, ASME*, 101:148–153, 1979.
11. J. Yau, S. Wang and H. Corten, *Journal of Applied Mechanics*, 47:335–341, 1980.

Probabilistic modelling of fatigue crack growth parameters for standard development

Wangwen Zhao

ABS Consulting, Warrington, UK

Abstract This paper demonstrated a probabilistic method to model the fatigue crack growth parameters in Paris Law. This paper firstly examines uncertainties in fatigue crack growth process and choose to model the uncertainty of Paris Law parameters for variations between testing specimen only, as for high cycle fatigue prediction the within specimen variation will not affect the final crack growth. Based on the fatigue crack growth test data base collated in the UK HSE, statistical regression was conducted to obtain C and m values in each test. The results from the regression show strong correlation between m and ln(C), to almost linear correlation, which compared well with other studies. Recommendation was therefore given in appropriate probabilistic models of fatigue parameters. The final fatigue prediction should have reduced the uncertainties from previous recommendations. This can be used as a base for future standard development.

1 INTRODUCTION

Paris Law has been used extensively to predict fatigue crack size. However, there exist great uncertainties in fatigue prediction. Conservative estimates have to be made in standard recommendations. For example, in BS 7910 [1] the design lines of Paris Law are set to be the mean lines plus 2 standard deviations of the random variable ln(C). This uncertainty has been further separated into the inter-specimen and within-specimen variations. Similar approach has been adopted in ABS [2] and DNV [3] standards.

Some notable research works have been carried out to model fatigue crack growth process as stochastic processes [4] [5]. The stochastic models can be best used for modelling within-specimen spatial variation. They are seldom applied in practical engineering design and assessment for offshore or marine structures, as this approach requires large data input and reasonably degrees of statistical analysis technique. In contract, little work has been carried out specifically for modelling the between specimen variations.

Based on a fatigue crack growth database available from the UK HSE, this paper presented the analysis of the fatigue uncertainties in particular from the view of inter-specimen variations. From these analysis new insight into fatigue uncertainties has gained with the following questions in mind:

1. What probabilistic models should we use for the fatigue crack growth parameters?
2. How the margin of safety in crack growth prediction related to these models?
3. How well this models to be used for practical application?

It should be noted that uncertainties of fatigue crack growth parameters could result from loading, geometry and material. This study addresses only the material uncertainty from available data.

This paper is also a continuation of work on the probabilistic framework for fatigue and fracture problems published in previous occasions [6][7].

2 OVERVIEW OF FATIGUE CRACK GROWTH PROBABILICTIC PREDICTION

2.1 Model uncertainties of the Paris Law – do more complicated models lead to better results?

Although Paris Law has been used to fit with experimental results, its application to predict fatigue crack growth often gives rise to model uncertainties as the conditions are rarely the same between different specimens. A benchmark study was carried out by the NEA committee [8] on the Safety of Nuclear Installation for the test of fatigue subjected to constant cyclic bending from 14 participants to the study using various prediction techniques. It was concluded that on the crack propagation of a semi-elliptical defect under a constant number of cycles, the simplified

methodologies of Paris Law together with the Raju and Newman SIF formula gives the best results. A number of reasons are discussed, among which are:

1. Low magnitude loading gives less plasticity hence elastic studies gives good results

2. FE analysis is rather complex in defining the parameters hence increase the uncertainties

A later benchmark study [9] compared crack initiation prediction and crack instability prediction in addition to crack propagations for the same test conditions. It showed that there were more agreements in predicting crack initiation than predicting crack growth. Again, this may be attributed to the rigorous definition required, hence more uncertainty, for the parameters in fatigue crack growth definitions.

These benchmark studies showed that for fatigue analysis, complicated analysis does not necessarily leads to reduction of modelling uncertainties if the parameters are not defined to the same level of details and it is very important to correlate material properties from experiments with the fatigue prediction. These benchmark studies showed the pitfalls of using more complicated fatigue prediction models when relevant data are not available.

2.2 The stochastic models – the time dimension

Fatigue crack growth within a specimen is a stochastic process, with time being a factor, as the material properties vary when the crack advances. The conventional Paris Law based approach can predict the mean crack growth but may not be able to predict the dispersion caused by the time factor. An early model was developed by Yang et al [4] by randomizing the crack growth equation. The shortcomings of the Yang's models are:

- the correlation distance, ξ^{-1}, needs to be computed from test data
- it models the stochastic variation within a specimen, hence it is mostly suitable for detailed calculation with known test results
- it restricts the m value to be deterministic and fixed

Lately, Proppe and Schuller [5] compared fatigue prediction results by using the test data of Virkler [10] in randomised Paris and Forman's laws. The parameters in the crack growth equations were obtained directly from the full dataset. They found that the relative errors in the mean values are relatively small but the errors in variances are quite large. They then suggested methods based on stochastic analysis. The stochastic models typically use the Markov chain theory to model the stochastic crack growth. This however requires substantial tests data in terms of crack size at different stages and for mathematical tools for utilising those data, which are not available for most cases.

The stochastic model has two extremes with one being the white noise process and the other being the fully correlated process, e.g. by the Lognormal random variable model. The realistic behaviour of crack propagation lies between these two extremes.

2.3 Models with fixed m and random C

Based on the assumption that statistical analysis is conducted by fitting Normal distributions with ln(C) with fixed m. Regression analysis gives

$$\left(\frac{da}{dN}\right) = e^{-\varepsilon} C_1 \Delta K^m \quad \text{from original Paris Law} \quad \left(\frac{da}{dN}\right) = C_1 \Delta K^m$$

with constant m and C_1 and the Lognormal random variable C modelled through variable ε.

The random variable model for the random process is always conservative in predicting the crack growth, as the statistical dispersion based on the model is the largest among the class of random processes. With the additional

benefit of simplicity, the Lognormal variable model has gained wide range applications in engineering practice. Implicitly, this approach fixes the value of m. These approaches are commonly found in BS 7910 or other codes.

3 STATISTICAL ANALYSIS OF FATIGUE CRACK GROWTH DATA

3.1 HSE fatigue crack growth (FCG) data

The UK HSE has collated fatigue crack growth database from major national programmes and joint industry projects such as UKOSRP II. The number of investigations assessed in each category is shown in Table 1. The data is obtained by digitising values of da/dN and ΔK in graphical form from the published literature by using as a computer graphic file (TIFF) from an image scanner. The data selected displayed a consistent experimental technique, supplemented by other investigations that evaluated a wider range of materials. Most of the investigations have been performed in air rather than in other environments, usually due to the simpler experimental techniques and the ability to accelerate the tests by using a high cyclic frequency.

Steel Type	Environment	R ratio	Number of data sets	Data group ID
Ferritic (Fy <=45O Mpa)	Air	0.0-0.1	16	1
		>=0.5	13	2
High strength (Fy >450 Mpa)		0.0-0.1	6	3
		>=0.5	4	4
Fenitic (Fy <=45O Mpa)	Seawater (free corrosion)	0.0-0.1	8	5
		>=0.5	8	6
High strength (Fy >450 Mpa)		0.0-0.1	4	7
		>=0.5	3	8
Ferritic (Fy <=45O Mpa)	Seawater + CP (-850mv)	0.0-0.1	8	9
		>=0.5	6	10
High strength (Fy >450 Mpa)		0.0-0.1	4	11
		>=0.5	2	12
Ferritic (Fy <=45O Mpa)	Seawater + CP (-1100mv)	0.0-0.1	7	13
		>=0.5	6	14
High strength (Fy >450 Mpa)		0.0-0.1	2	15
		>=0.5	7	16
Austenitic	Air	0.0-0.1	10	17
		>=0.5	9	18

Table 1 HSE Fatigue crack growth database

3.2 Crude statistical analysis

Figure 1 shows the FCG data from the HSE database for air in logarithmic paper of Δk and da/dN. The data points appear to scatter within a certain band, from which the Paris Law relation can be fit on. Figure 1 also shows that the fatigue threshold changes not only to the stress intensity range but also to R ratios. The minimum crack growth rate, below which the crack growth tend to be in the threshold region. is about 5e-7 mm/cycle. It seems that this minimum crack growth range is unaffected by the R ratios.

Environment	R ratio	ln(C) for Stage A			ln(C) for Stage B		
		m	Mean	Standard Deviation	m	Mean	Standard Deviation
air	0.0 – 0.1	8.16	-59.6	0.70	2.88	-28.6	0.35
	>=0.5	5.1	-39.7	0.67	2.88	-28.2	0.39
Free corrosion	0.0 – 0.1	3.42	-31.1	0.53	1.3	-15.9	0.24
	>=0.5	3.42	-31.1	0.53	1.11	-14.5	0.28
Corrosion with CP -850	0.0 – 0.1	8.16	-59.5	0.96	2.67	-26.2	0.57
	>=0.5	5.1	-40.3	1.09	2.67	-25.8	0.62
Corrosion with CP -1050	0.0 – 0.1	8.16	-58.7	0.89	1.4	-16.8	0.33
	>=0.5	5.1	-39.0	1.03	1.4	-16.9	0.47

Table 2 Summary of crude statistical analysis results assuming normal distribution of Ln(C) and fixed m

Statistical analysis of these data points has been conducted with no distinction of test groups or tests. Table 2 shows the summary of statistical analysis of the Paris Law parameters by assuming a lognormal distribution of C with fixed m values. The analysis also follows the bi-linear definition of fatigue crack growth as in BS 7910 and treated stage A and stage B separately for statistical analysis. The analysis is called “crude” statistical analysis as each of the

data point of crack growth collected is accounted as one data point. This would bias in favour of those experiments with more data points collected.

Table 3 shows comparisons of some typical statistical models of Paris parameters for fatigue crack growth in Air in literature with fixed m values.

Investigator		m (fixed)	*ln(C)* (N,mm)	
			Mean	Standard deviation
DNV (1984) [3]		3.1	-29.84	0.55
Johnston [12] (1983)		3.0	-29.31	0.24
Snijder *et al* (1987) [13]		2.8	-27.66	0.23
BS 7910 Air stage B	R= 0.0 – 0.1	2.88	-28.55	0.35
	R >=0.5	2.88	-28.17	0.56

Table 3 Statistical models for fatigue crack growth parameters

Johnston based his analysis upon data from Guerney 14. Snijder based his analysis upon data from Maddox 15. Figure 2 demonstrate the mean line and dispersion from the above models, together with data points from test results. Three lines are plotted for each model: the mean line and the lines for + - 2 standard deviations. It can be seen that these models provide the general trend lines of data but may be over-conservative or too optimistic at some points.

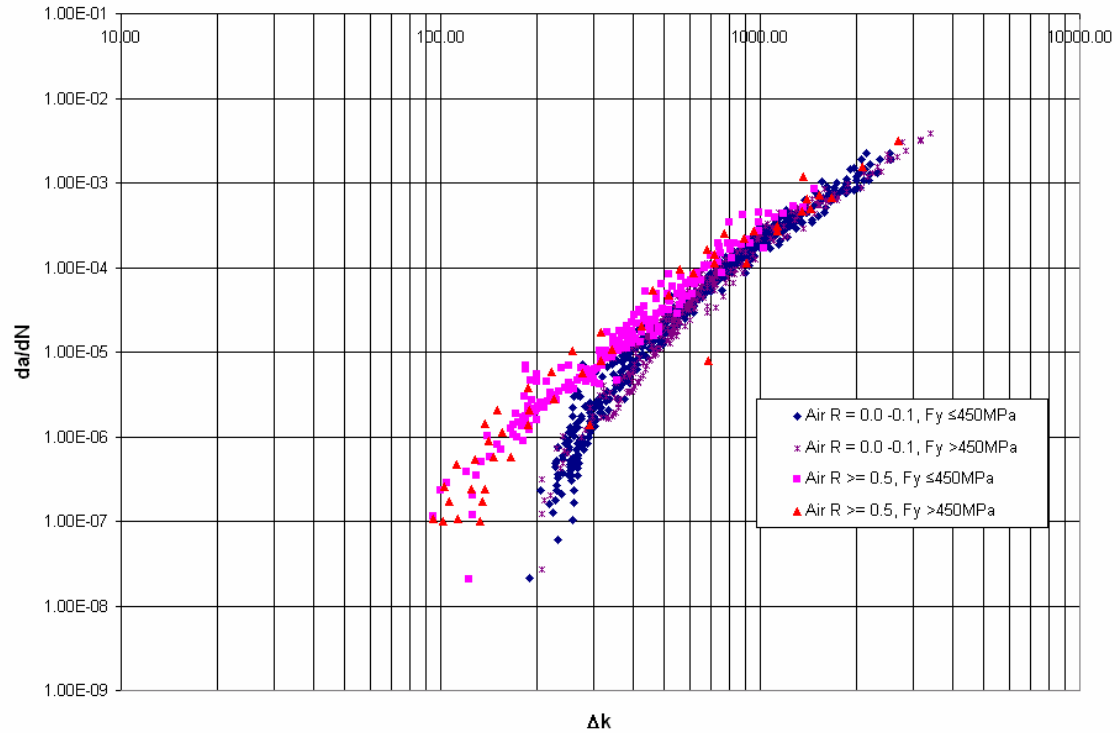


Figure 1 Fatigue crack growth data for air

3.3 Statistical Analysis of fatigue crack growth data for each test

The fatigue uncertainty U from material variation could be represented is the sum of within-specimen uncertainty and inter-specimen uncertainty. The variation of C and m in different tests can be viewed as from the uncertainty of inter-specimen. This uncertainty is often mixed up with the within-specimen variation in various statistical analyses. The uncertainties of within-specimen give the stochastic variations of fatigue crack growth. However, the determination of the Paris parameters C and m for the whole range of fatigue test do not need to consider the individual stochastic process, i.e. only the inter-specimen variation need to be studied. The regression for is described in more detail as follow. It should be noted that:

1) The dependence of ΔK on a leads to ambiguously defined independent variable.
2) The regression is conducted not for the entire database but for each test in turn

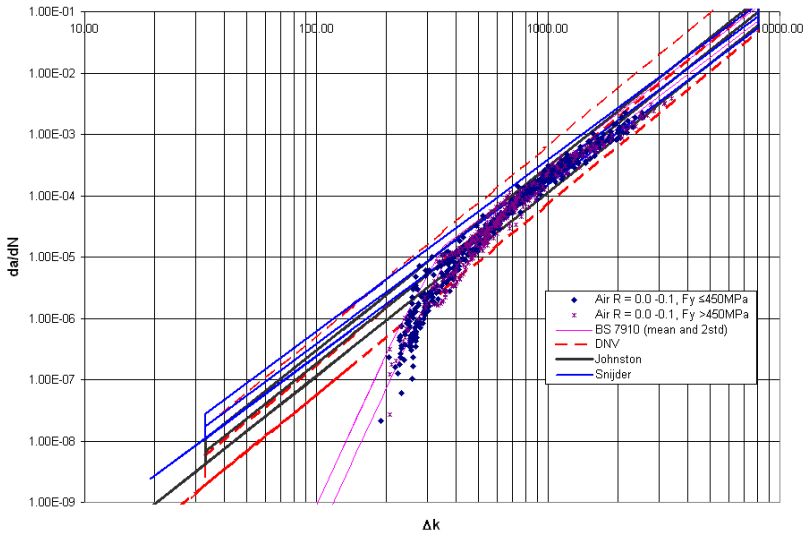
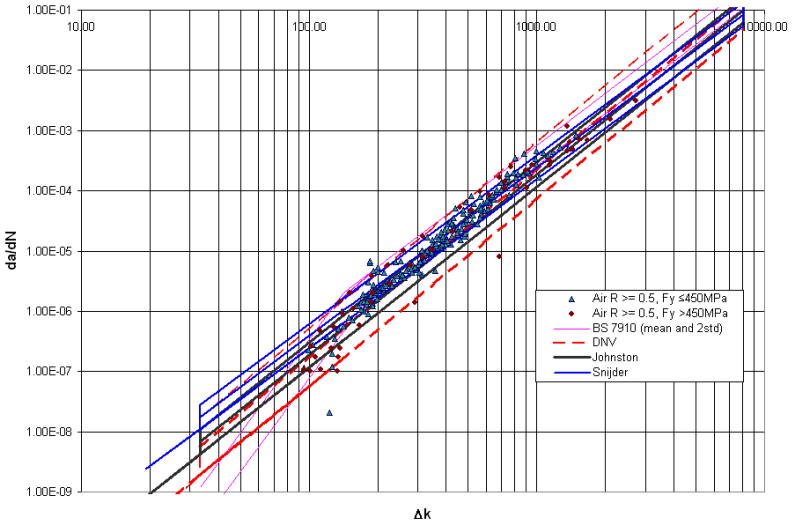
R = 0.0 – 0.1	
R>0.5	

Figure 2 Comparison of uncertainty models against FCG data points

Take

$x = (1, \ln\Delta K)^T$ as the vector of independent variables,
$b = (\ln(C), m)^T$ as the parameter vector,
$y = \ln(da/dN)$ as the dependent variable,

Then $y = x^T b + \varepsilon_1$

The standard least square method requires

$\text{Mean}(\varepsilon_1) = 0$ and $\text{Var}(\varepsilon_1)$=minimum

Applying transformations, we could end up with

$$\left(\frac{da}{dN}\right) = e^{\varepsilon_1} C\Delta K^m$$

which fulfils the physically obvious demand of da/dN being non-negative.

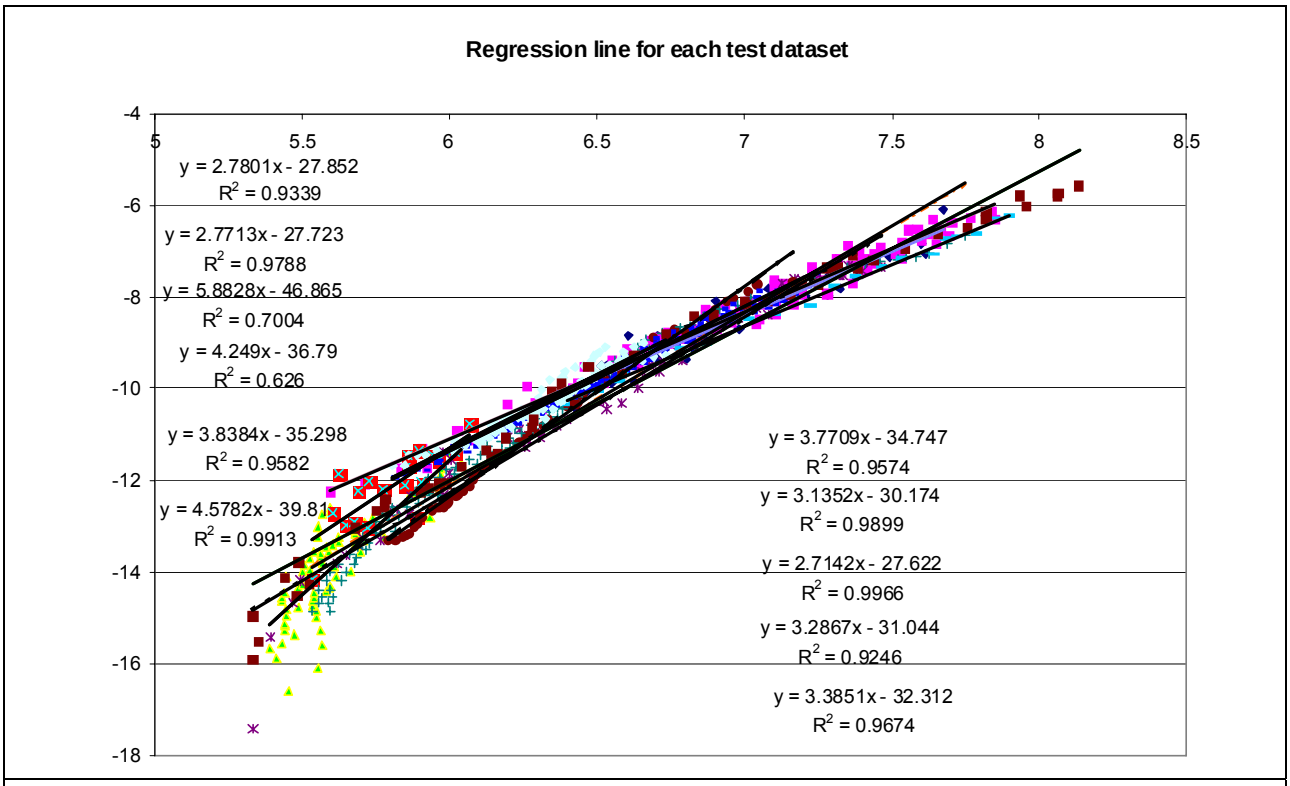


Figure 3 Linear regressions with individual test data groups of FCG in air

The relationship of m and ΔK appears to be non-constant and non-linear, as the result of non-linear relationship of the ln(da/dN) vs. ln(ΔK). Indeed Toth (17) found that m can be linearly related to the specific absorbed energy, equal to the area under the true stress/strain curve by

$$m = 5.065 - 0.00168\ w$$

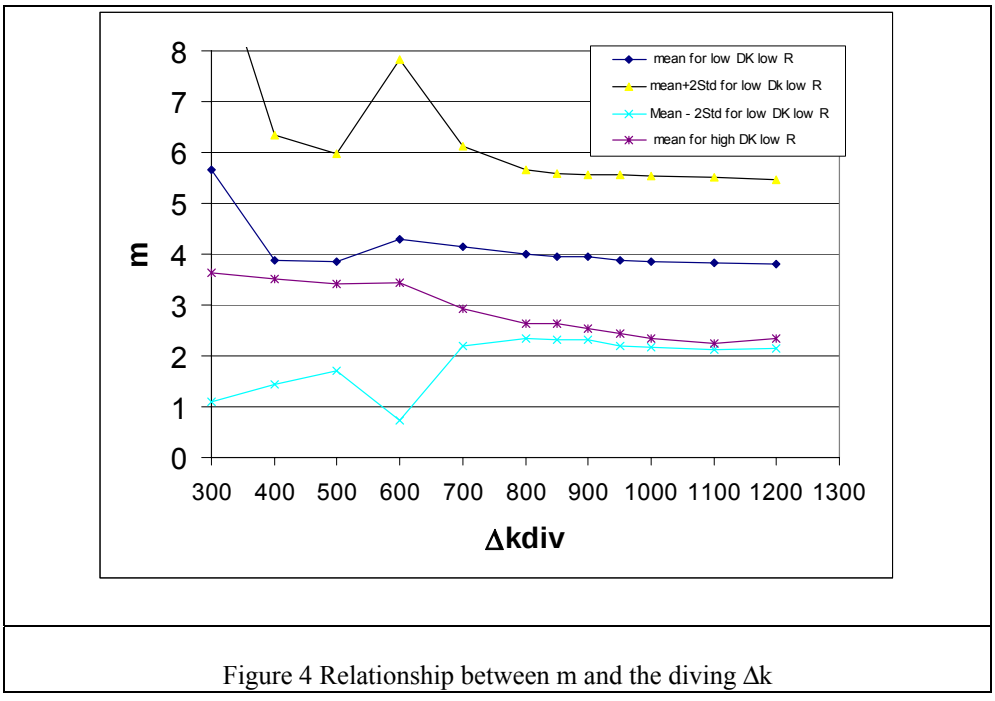


Figure 4 Relationship between m and the diving Δk

3.4 Bi-linear Divisions ΔKdiv

For practical reasons, the Paris Law needs to maintain a logarithmic linear relationship. It becomes useful to adopt a bilinear approach, as a compromise to a more complicated non-linear relation between m and ΔK.

For regression analysis based on bilinear Paris Law relationship, the data groups are divided into two groups, those above the dividing value of ΔKdiv and those below ΔKdiv. Different values of m and C can be achieved. ΔKdiv is determined from having the least residue errors. It is highly arguable to have the most optimal ΔKdiv as m, the slope from the regression, would change gradually with changing ΔK shown in Figure 4. It is observed in Figure 4 that a more stable m values can be achieved with ΔK > 800. By further trial and error, the following values are chosen:

ΔKdiv = 820 Nmm

3.5 Correlation of ln(C) and m

As early as in the 1970s', it has been recognised that there is a relationship between C and m for tests carried out independently. This is typically in the form of

$\ln(C) = A + B\ m$ or $C = A1/\ B1^{\ m}$

for $\frac{da}{dN} = C\Delta K^{m}$

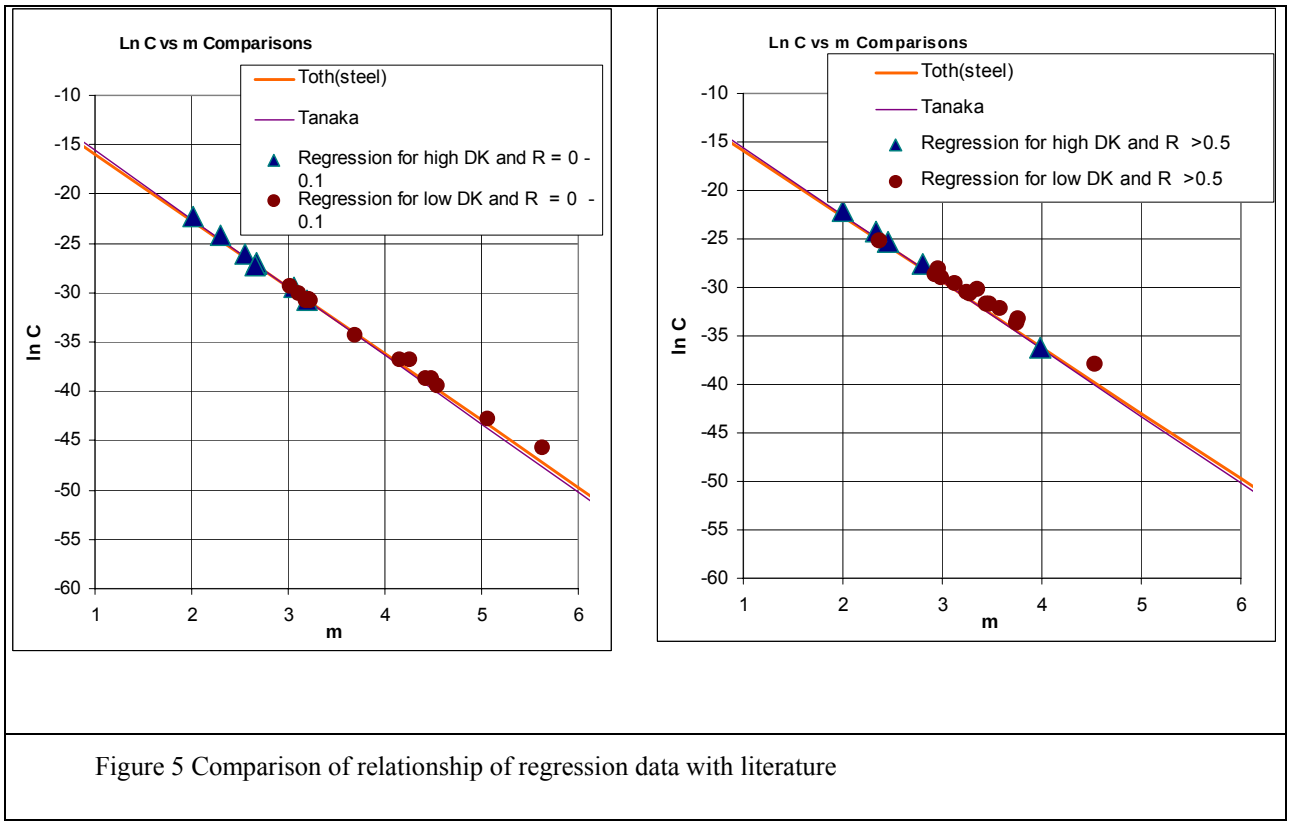


Figure 5 Comparison of relationship of regression data with literature

Toth (17) carried out a survey of fatigue crack growth tests for more than 500 steel with the same general loading condition (frequency, waveform and the environmental circumstances - i.e. room temperature, medium). Toth found that the correlation between C and m, characterized by $C = A1/\ B1^{\ m}$, is of rather stable nature with A1=1.03e-4 and B1=27.2 for ΔK based on Mpa .sqrt(m). A1 and B1 can be converted in unit of Nmm as

A = -9.18, B = 6.76

Tanaka18 has conducted similar works earlier albeit in a smaller scale with A' = -15.59 and B' = – 3.47 in terms of NM, this is converted to Nmm as

A= -8.68, B = -6.92.

C and m values from regression analysis of fatigue crack growth data for each of the test specimen in the HSE database are plotted in together with lines from Toth and Tanaka.

The following points are observed:

1. There is a strong correlation between m and ln(C), close to a linear relationship
2. The data point fit well with both lines from Toth and Tanaka
3. In general m for low Δk is higher than m value for high Δk

4 RECOMMENDATION OF PROBABILISTIC MODELS

4.1 Probabilistic distribution of m

Given that C and m are closely correlated, only one of the variables may be used to model the combined variations. Therefore, the determination of the distribution of m is of critical importance in predicting the variation of fatigue crack growth. However, to fit statistical distribution functions requires a reasonably large database. As one test set can only make one data point in the histogram of m, the data points available to make a statistical population are generally small which makes it difficult to determine their statistical distribution with great confidence.

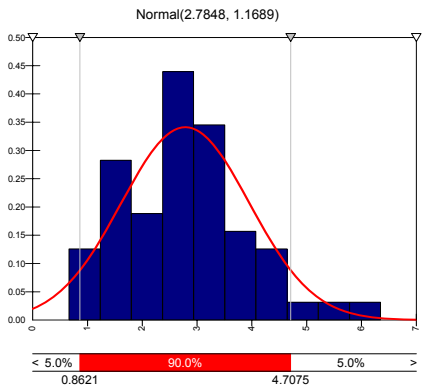


Figure 6 Fit of Normal distribution with histograms of m for all FCG data with high ΔK

Figure 6 shows the histogram of the population of m for all the FCG data for high ΔK fit with a Normal distribution. However, this does not distinguish environmental condition and stress ratios so that it is limited to only give a general overview. Normal distribution can be used for m.

4.2 New Probabilistic models

From further regression analysis of the relationship between ln(C) and m, a linear approximation can thus be made for the correlation between ln(C) and m.

$$\ln(C) = A + B\,m + \varepsilon_2$$

where ε_2 is the error term.

Paris Law can be re-written as $$\left(\frac{da}{dN}\right) = e^{\varepsilon_2+\varepsilon_1} e^{A} \left(\frac{\Delta K}{e^{-B}}\right)^{m}$$

where
A and B are constants

m is a random variable
ε_1 represents errors introduced from within specimen uncertainty (regression to determine m the each test)
ε_2 represents errors introduced from linearization of ln(C) and m relation.

ε_1 is related only to variation of FCG data within specimen. The effect on crack growth would be cancelled out for high cycle fatigue problems from variations of data from both sides of the mean line. Also ε1 is significantly smaller than the errors in the case of fixed m for all tests, as different m is calculated for each test to achieve a least square. It is proposed therefore to ignore the effect from ε1.

ε_2 is the result of approximation of linear relation of Ln C and m. However, this is very small with the smallest RSQ – the parsons product of coefficient product to be 0.993. The RSQ is a measure of correlation between m and Ln C. This RSQ figure is so large that the relationship between Ln C and m may be treated as a direct linear relationship.

Assuming m has a normal distribution, the following values of probabilistic model parameters has been obtained from statistical analysis of these data with m normally distributed:

R ratio	ΔK Nmm	m		standard error to obtain m	ln C		ln C = a+ bm		Standard error to determine a and b	Correlation
		Mean	Standard deviation	Max ε_1	Mean	Standard deviation	a	b	ε_2	
0.0 -- 0.1	<820	**3.907**	**0.702**	0.5678	-35.772	4.792	**-9.808**	**-6.509**	0.332	-0.998
	>820	**2.665**	**0.402**	0.2509	-26.939	5.813	**-8.144**	**-7.052**	0.204	-0.998
>= 0.5	<820	**3.279**	**0.486**	0.4093	-30.652	2.773	**-11.311**	**-5.894**	0.270	-0.996
	>820	**2.642**	**0.486**	0.4586	-26.546	5.813	**-7.707**	**-7.129**	0.134	-1.000

Figure 7 presents the comparison of individual test data points and the dispersion lines of the probabilistic models using mean m +- 2 standard deviation and C is linearly related to m.

4.3 Discussions

Analysis based on the FCG data in this study showed consistent correlations between ln(C) and m. It is possible to establish a strongly correlated or linear relationship between ln(C) and m as shown in the demonstrations.

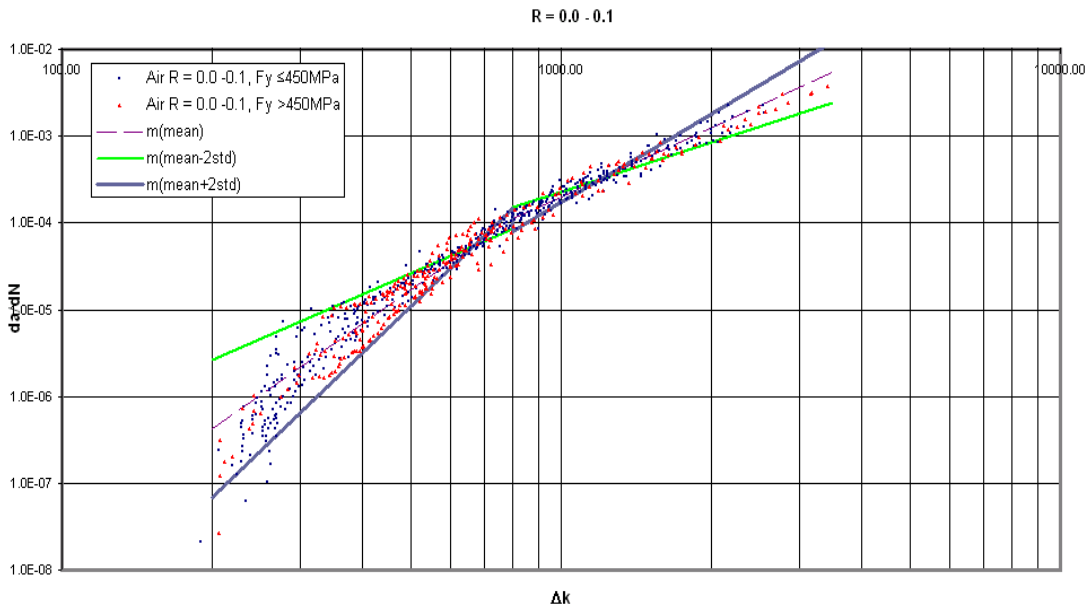
The simple statistical regression analysis of all fatigue data points include variations from both within specimen as well as from between specimen. The new model only includes variation between specimen. This would substantially reduce conservatism of fatigue prediction.

The critical aspect for fatigue prediction is not the prediction of fatigue crack growth rate but the final crack size. In this aspect, the new probabilistic approach would give smaller errors for high cycle fatigue prediction.

However, future study may look into the possibility of treating ln (C) and m as two variables with joint probabilistic distributions. However, problems in finding the mean points for both Ln(C) and m for such joint probabilistic distributions and lack of better-defined data prohibit this route to be further explored.

5 CONCLUSION

A probabilistic method to model the variation of fatigue crack growth has been investigated by treating the within-specimen and inter-specimen variation independently and by relating m and C values. Two different regression analyses have been carried out. The first regression analysis obtains the bilinear mean Paris Law parameters m and ln(C) for each test, thus separates the within specimen variation and excludes the complex stochastic analysis. The second analysis determines the relation between the mean Paris Law parameters i.e. m and ln(C) for groups of data from the first regression analysis. The distribution of m in such groups represents the major part of the inter-specimen variations. Paris Law lines with dispersion defined by standard deviation of m from the second regression analysis have been compared with FCG data.



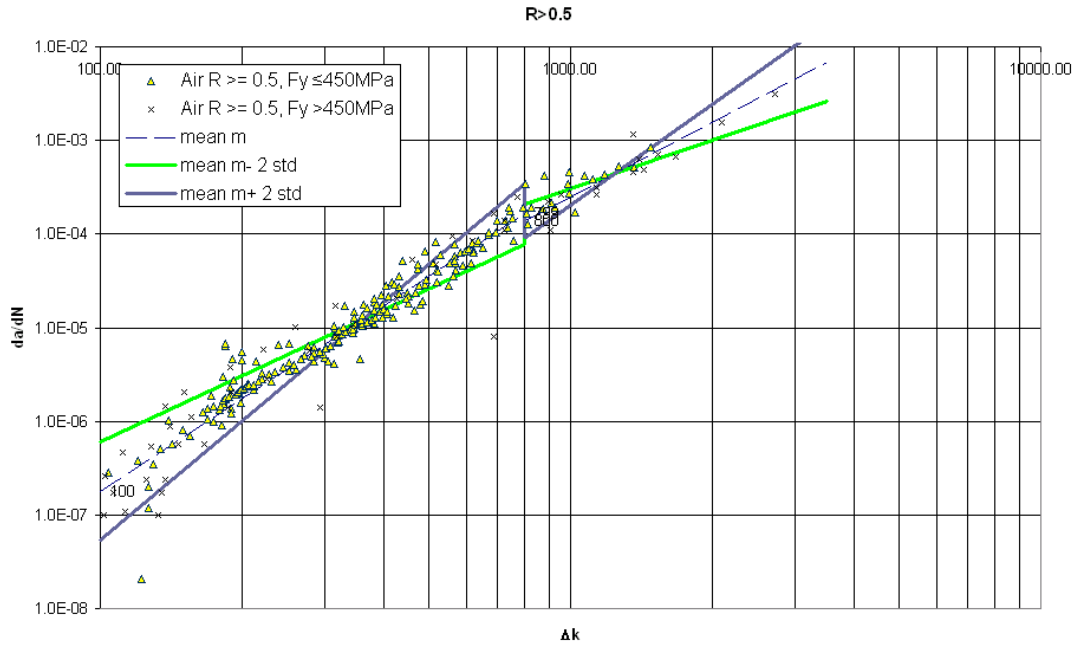


Figure 7 Comparison of probabilistic model to test data points

The following conclusions can be made:

- There is a strong correlation between Ln C and m from real test data
- m can be modeled by a Normal distribution and ln(C) can be related to m by a linear relation.
- The new probabilistic models give more realistic prediction of final fatigue crack size
- This model has the potential to reduce the conservatism from recommendations in previous standards substantially

- Future study may be required 1) to enable easy presentation of fatigue parameters, 2) to have more data comparisons and 3) to make use of joint probability functions.

6 ACKNOWLEDGEMENT

The author wishes to thank the Health and Safety Executive (HSE) for permission to use their data for analysis in this paper.

7 REFERENCES

1. BSI, BS 7910 "Guide on methods for assessing the acceptability of flaws in metallic structures", 1999
2. ABS, "GUIDE FOR THE FATIGUE ASSESSMENT OF OFFSHORE STRUCTURES",2003
3. DNV, DNV Classification Notes No. 30.6, "Structural Reliability Analysis of Marine Structures", July 1992
4. Yang, J. N., Manning, S. D., His, W. H., and Rudd, J. L., Stochastic crack growth models for applications to aircraft structures, in Probabilistic Fracture Mechanics and Reliability, edited by J. W. Provan, Martinus Nijhoff publishers, Dordrecht/Boston/Lancaster, 1987
5. Proppe, C. and and Schu¨eller G. I, "STATISTICAL PROCESSING OF FATIGUE CRACK GROWTH DATA", 8th ASCE Specialty Conference on Probabilistic Mechanics and Structural Reliability PMC2000-307, 2000
6. W. Zhao, A. Stacey, "Review of Defect Distributions for Probabilistic Structural Integrity Assessment", by, Norway, OMAE 2002
7. W. Zhao, A. Stacey and P. Prakash, "Probabilistic Models of Uncertainties in Fatigue and Fracture Reliability Analysis", OMAE 2002
8. NEA committee on the Safety of Nuclear Installation, "Report on the benchmark on fatigue propagation of a semi-elliptical crack in a plate subjected to constant cyclic bending", OECD, NEA/CSNI/R(97)8, 1998
9. NEA committee on the Safety of Nuclear Installation, "Technical Report on the Fatigue Crack Growth Benchmark Based on CEA Pipe Bending Tests", OECD, NEA/CSNI/R(2001)14, 2001
10. Virkler D. A., Hillberry B. M., Goel P. K., "The statistical nature of fatigue crack propagation", Transactions of the ASME - Journal of Engineering Materials and Technology, vol.101, pp. 148-153, 1979.
11. Paris P. C., Gomez R. E., Anderson W. E. (1961) "A Rational theory of Fatigue. The Trend in Engineering", 13 No.1. 9-14.
12. Johnston, G. O. "A Review of Probabilistic Fracture Mechanics Literature," Reliability Engineering, Vol. 3, 1982, pp. 423-448.
13. Snijder et al "Probabilistic fracture mechanics approach of fatigue and brittle fracture in tubular joints", Steel in Marine structures, editted by Noordhoek and de Back, 1987
14. Gurney, T. R., "Fatigue tests under variable amplitude loading", Report No. 220/83, TWI, UK, July 1983
15. Maddox, S.J., "An analysis of fatigue cracks in fillet welded joints", Welding Institute Report E/49/72, January 1973
16. Benson, J. P. and Edmonds, D.V. "The relatioship between the parameters C and m of Paris Law for fatigue crack growth in a low-alloy steel", Scripta Metall, Vol 12, 645-647, 1978
17. TÓTH, László "FATIGUE CRACK GROWTH LAWS AND THEIR MATERIAL PARAMETERS" VII Summer School of Fracture Mechanic – Current Research on Fatigue and Fracture Pokrzywna (Poland) 18-22.06.2001
18. Tanaka, K. and Matsuoka, "A tentative explanation for two parameters,C and m, in Paris equation of fatigue crack growth", Int. J. Fatigue, Vol. 13, 563-583, 1977
19. Guerney, T. R., "Fatigue of welded structures", 2nd edition, Cambridge University Press, Cambridge, 1979

Life-time reliability based assessment of structures submitted to random thermal loading

Z. Guédé[a], B. Sudret[b], M. Lemaire[a]

[a] Institut Français de Mécanique Avancée – LaMI – Campus des Cézeaux – 63175 Aubière Cedex, France
[b] EDF R&D, Site des Renardières, 77818 Moret-sur-Loing Cedex, France

Abstract The paper presents a probabilistic approach of the current thermal fatigue design of nuclear components, including all kinds of uncertainties that affect the thermal fatigue behaviour. Two kinds of reliability analysis are defined, respectively, in the time domain and the frequency domain. They are based on the theory of structural reliability and provide the failure probability and the sensitivity of the reliability index to each random variable. The proposed method is applied on a pipe submitted to thermal loading due to water flow. Both high cycles fatigue (HCF) and low cycles fatigue (LCF) regimes are investigated. The results show that it is possible to perform a complete reliability analysis to assess the failure probability. It is observed that the scatter of fatigue data and the heat transfer coefficient are the most important variables in the thermal fatigue reliability.

1 INTRODUCTION

The behaviour of structures submitted to thermal fatigue is affected by numerous uncertainties due to the random nature of the variables and the lack of knowledge on the physical phenomenon. This feature concerns in particular the nuclear industry, where structural components, such as pipes or turbine blades, are subject to thermal loading. The current nuclear design code [1] takes into account the uncertainties through empirical margin factors in order to make the design conservative. They do not allow for a quantification of the associated risk yet.

In this context, the aim of the present paper is to propose a probabilistic approach of the current thermal fatigue design of nuclear component including all kinds of uncertainties that affect the thermal fatigue behaviour. In this way, it is possible to compute the risk associated to the retained design and the effects of each uncertainty onto the reliability of the structure.

First of all, we recall the main steps of the actual thermal fatigue design. Then, the method for the thermal fatigue reliability analysis is presented. Finally, an application example of a pipe subject to variable thermal loading is given.

2 CLASSICAL THERMAL FATIGUE DESIGN

The current thermal fatigue design of nuclear components [1] contains the following main items as shown in Figure 1:

- The definition of a *deterministic thermal loading history* $\theta(t)$ as a periodic temperature sequence, which may be either representative of the real loading (best-estimate calculation) or penalized (conservative design).
- The calculation of the evolution in time of the *stress tensor* $S_{ij}(t)$ at the point where the crack initiation is likely to occur, assuming a linear elastic material behaviour.
- The use of the Tresca criterion to reduce the stress tensor $S_{ij}(t)$ to an *equivalent scalar stress* $S(t)$.
- The extraction of *stress cycles* from the equivalent stress $S(t)$ using the Rainflow counting method [2].
- The choice of a *fatigue design curve* known as *S-N* curve, which represents the fatigue strength of the material. This curve is obtained from the best-fit curve to strain-controlled fatigue data, and from margin factors applied to this best-fit-curve (*e. g.* 2 on stress amplitude S or 20 on cycles number N, whichever was more conservative). These factors are intended to account for the differences and uncertainties in relating the fatigue lifetime of laboratory test specimens to those of the actual reactor components. The best-fit curve is expressed in terms of the Langer's equation of the form [3]:

$$\ln N = A \ln(S - S_D) + B \tag{1}$$

where A, B and S_D are parameters of the model. In particular, S_D is the material endurance limit.

- The correction of the applied stress amplitude S to account for the maximum *mean stress effect* using the following formula derived from the Goodman diagram:

$$S' = \frac{S_u - S_y}{S_u - S} S \quad \text{for } S < S_y \tag{2}$$

where S is the applied stress amplitude, S' is the corrected value, S_u is the ultimate tensile strength and S_y is the yield strength.

- The computation of the *cumulative fatigue damage D* (also known as the usage factor) in a given period using the Miner's rule [4].

The nuclear design code requires that the usage factor D remains less than 1. In practice, the thermal load history is supposed to be periodical in time and the usage factor D_{seq} is computed on a single period. Then, the fatigue life-time of the component, expressed in terms of number of sequences, is given by $T_d = 1/D_{seq}$.

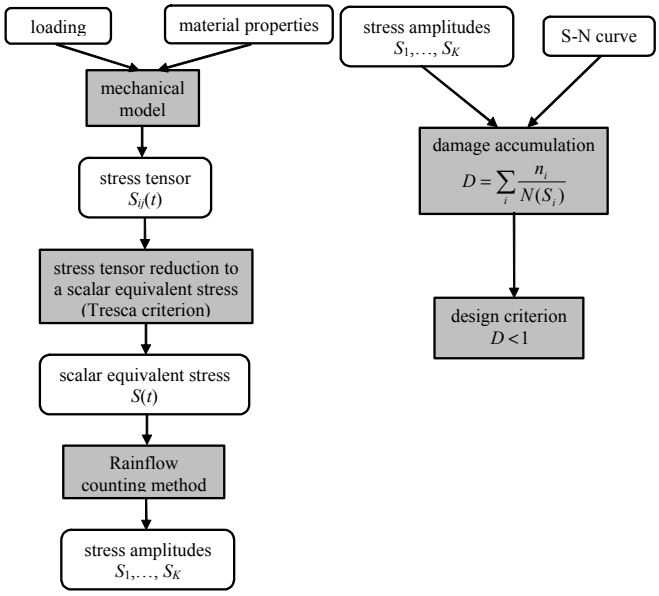


Fig. 1. Overview of the classical thermal fatigue design of nuclear component.

3 REVIEW OF STRUCTURAL RELIABILITY METHODS

Structural reliability analysis is based on [5]:

- The choice of a stochastic model for the set $\mathbf{X}$ of input random variables (*i.e.* marginal density and correlation matrix or better, the joint density function $f_{\mathbf{X}}(\mathbf{x})$);
- The definition of a failure scenario through the determination of a limit state function $G(\mathbf{X})$ which splits the safe domain (defined by $G(\mathbf{X}) > 0$) from the failure domain (defined by $G(\mathbf{X}) \leq 0$). The boundary defined by $\{\mathbf{X}$ such that $G(\mathbf{X}) = 0\}$ is called the limit state surface.

The failure probability reads:

$$P_f = \int_{G(\mathbf{X}) \leq 0} f_{\mathbf{X}}(\mathbf{x})\, d\mathbf{x} \tag{3}$$

This probability may be evaluated using the *FORM* and *SORM* (First and Second Order Reliability Method). *FORM* requires initially a transformation $\mathbf{U} = T(\mathbf{X})$, where $\mathbf{U}$ is a set of uncorrelated standard normal variables. The transformed limit state function is denoted by $H(\mathbf{U})$. Then, the design point $\mathbf{u}^*$, which belongs to the limit state surface and lies closest to the origin, is obtain solving an optimization problem (*e.g.* $\|\mathbf{u}^*\| = \min \|\mathbf{u}\|$ under the constraint $H(\mathbf{U}) \leq 0$). The distance from the origin to the design point is the reliability index denoted by β. Finally, using a linearization of the limit state function at the design point and the circular property of the standard normal space, an analytic approximation of the failure probability is derived by: $P_f = \Phi(-\beta)$, where Φ is the standard normal integral. *FORM* gives also the sensitivity of the reliability index to changes in any input variable (*e. g.* the direction cosines of the unit normal vector at the design point to the limit state surface). *SORM*

approximation additionally uses the curvatures κ_i of the limit state function at the design point and the failure probability is estimated by [6]:

$$P_f = \Phi(-\beta)\prod_{i=1}^{n-1}\left(1-\beta\kappa_i\right)^{-1/2} \tag{4}$$

where n is the number of random input variables.

To check *FORM* and *SORM* approximations, one can use simulation methods such as importance sampling, which is a Monte-Carlo simulation targeted at the design point. In this case, the failure probability is estimated by:

$$P_f = \frac{1}{K}\sum_{i=1}^{K} I\left[H(u^{(i)}) \le 0\right]\frac{\varphi_n(u^{(i)})}{\psi(u^{(i)})} \tag{5}$$

where K is the number of samples, ψ is termed "importance sampling" distribution and φ_n is the multinormal distribution. This method allows to obtain accurate values of the failure probability for a relatively low number of samples (*e. g.* 1000 samples). These three methods are illustrated in Figure 2.

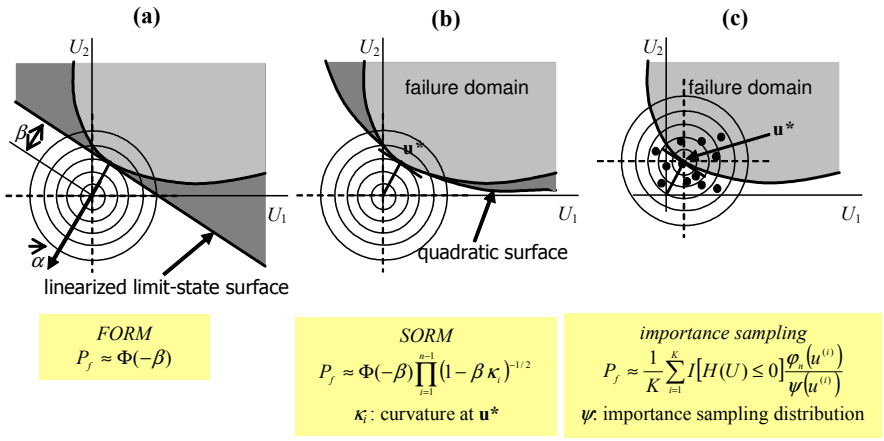


Fig. 2. Failure probability approximation: (a) by *FORM* ; (b) by *SORM* ; (c) by importance sampling.

In practice, the computation of the failure probability using the above methods is carried out by coupling the stochastic model (*e. g.* the probabilistic characterization of the input random variables) and a mechanical model (*e. g.* the procedure to compute the limit state function) [7]. The structural reliability methods are implemented in the software *PHIMECA Soft* ® [8] which is used in the present analysis.

4 THERMAL FATIGUE RELIABILITY ASSESSMENT

The proposed probabilistic approach of thermal fatigue design is based on the theory and methods of structural reliability which are briefly recalled in section 3. The objective is to compute the failure probability for a given service life-time.

Let us denote **x** a sample of **X,** the vector of the random input variables. Given N_0, the target number-of-cycles in service of the structure under consideration, the failure occurs when the random number-of-cycles-to-failure $N(\mathbf{x})$ is less than N_0. Therefore, the limit state function associated with this problem reads: $G(\mathbf{x}) = N(\mathbf{x}) - N_0$. An alternative and equivalent expression is given by: $G(\mathbf{x}) = 1 - D(T_0, \mathbf{x})$, where $D(T_0, \mathbf{x})$ is the total fatigue damage produced during the target life-time T_0. Two dual approaches of the reliability analysis are defined, respectively in the time domain and in the frequency domain.

4.1 Reliability analysis in the time domain

Given **x**, a sample of the input random variables of the problem under consideration, the total fatigue damage is computed using the deterministic design procedure (see Fig. 1):

$$D(T_0, \mathbf{x}) = \sum_{k=1}^{N_c} \frac{1}{N^{\text{struct}}\left(S_k(\mathbf{x}), \mathbf{x}\right)} \tag{6}$$

where $N^{\text{struct}}\left(S_k(\mathbf{x}), \mathbf{x}\right)$ is the number-of-cycles-to-failure at the stress amplitude $S_k(\mathbf{x})$, and N_c the total number of extracted Rainflow stress cycles.

In particular, a sample of thermal loading process is given by a time history on the target service life-time T_0. If the thermal load was considered as a Gaussian random process, it is noted that it shall be *discretized*, *i.e.* represented by a finite set of random variables (see for example Shinozuka and G. Deodatis [9] or Zhang and Der Kiureghian [10]). Then, these random variables can be considered as input data of the problem. Each realization of these variables produces a trajectory of the temperature process that is included in the whole procedure.
In conclusion, when the probability distributions of all random variables are defined, it is possible to compute the limit state function from a sample of the random input variable, using the currently codified design procedure (*e.g.* RCC-M, [1]). It is therefore possible to link the stochastic model to the mechanical model, then to assess reliability of the structure submitted to thermal fatigue.

4.2 Reliability analysis in the frequency domain

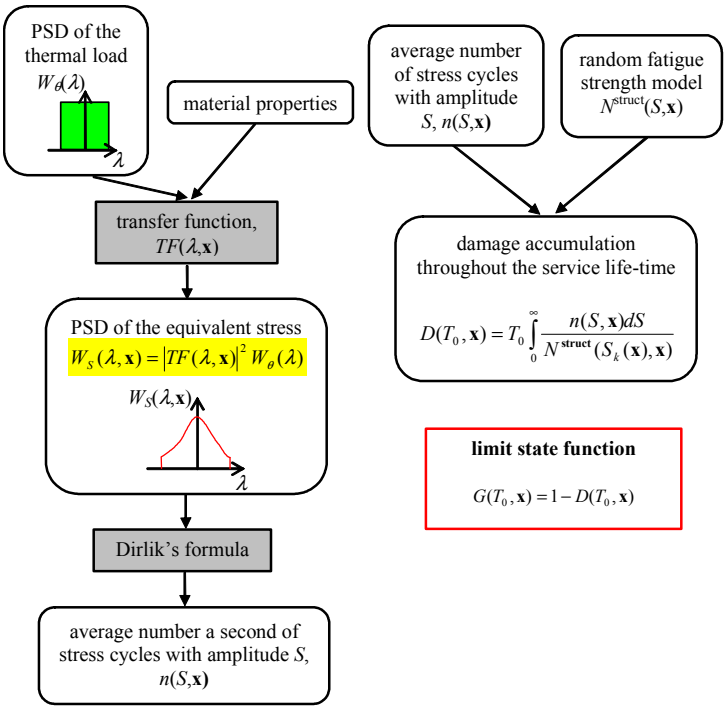


Fig. 3. Mechanical model for the reliability analysis in the frequency domain.

Given **x**, a sample of the input random variables of the problem under consideration, the total fatigue damage is computed using the spectral methods of fatigue life-time prediction for mechanical components submitted to a stationary load random process (see Fig. 3):

$$D_T(\mathbf{x}) = T_0 \int_0^\infty \frac{\mathbf{E}[M_T]\, f_S(S,\mathbf{x})\, d\,S}{N^{\text{struct}}(S,\mathbf{x})} \tag{7}$$

In this equation, E[M_T] is the mean number of peaks per unit time and $f_S(S,\mathbf{x})$ is the PDF of the stress amplitudes. These quantities are obtained directly from the spectral properties of the stress random process using the empirical Dirlik's formula [11].

The power spectral density function (PSD) $W_S(\lambda)$ (λ is the frequency in radius per second) of the stress process is obtained, under the assumption of a linear material behaviour (as is common practice in the nuclear design code) and a stationary load process, by [12]: $W_S(\lambda) = |TF(\lambda)|^2 W_\theta(\lambda)$, where $W_\theta(\lambda)$ is the PSD of the thermal load process and $TF(\lambda)$ denotes the transfer function of the system.

Note that, in the particular case of a multi-axial state of stress, the transfer function becomes a matrix and the multi-axial fatigue criteria formulated in the frequency domain can be used to compute the PSD of the scalar equivalent stress [13].

5 APPLICATION

5.1 Problem statement

We want to perform a complete reliability analysis a free end pipe subject to variable temperature due to water flow (Figure 4). All the input variables are considered as random variables and the failure reliability and the associated reliability index for a given service life-time are computed. Moreover, the sensitivity of the result to each random variable is estimated. Both high cycle fatigue (HCF) and low cycle fatigue (LCF) regimes are investigated.

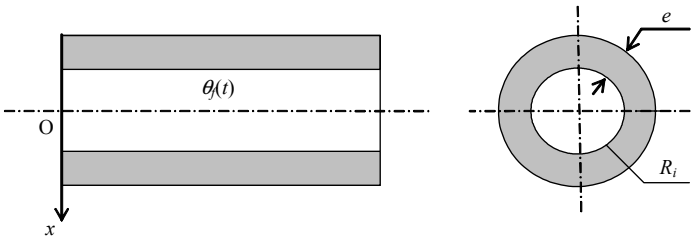


Fig. 4. Straight free end pipe.

5.2 Probabilistic modelling of the input variables

5.2.1 *Thermal loading model*

The thermal load is assumed to be a random Gaussian stationary pseudo-white noise random processes with zero central frequency and a cut-off frequency equal to f = 20 Hz. Its mean value is 130°C and standard deviation is equal to 20°C (Figures 5).

In the frequency domain, the random loading is represented by its PSD, denoted by $W(\lambda)$. However, in the time domain, the thermal load can be supposed deterministic, since it has been shown that, under the assumption of stationarity and for large number of stress cycles, the fatigue damage is not affected by the load variability [14]. The thermal load is therefore given by a deterministic temperature sequence in the time domain analysis. In order to compare both approaches, the temperature sequences is simulated from its PSD. For cost reduction issues, it is considered periodical with periodicity equal to 360 s. Thus, we implicitly assume that the time-history of the thermal loading calculated on that period is representative of the real thermal load. Practically, the temperatures trajectory is discretized into 2^{14} = 16384 points.

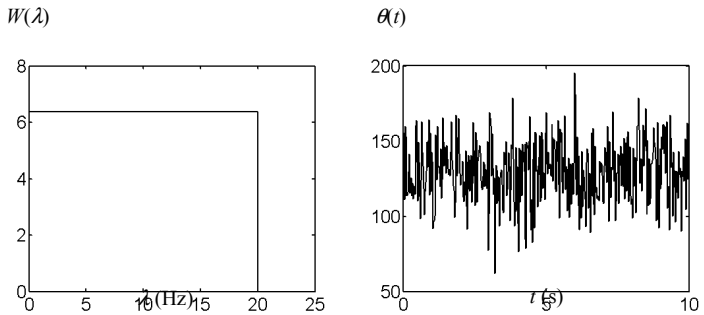


Fig. 5. Thermal loading model.

Under the considered thermal load, the pipe operates in the HCF regime. In order to investigate the LCF regime, the stress amplitudes are raised by a factor k which may be interpreted as a stress concentration factor to account for the presence a welded joint or a geometrical irregularity. In this numerical application, the factor k is artificially given a value of 4, intentionally exaggerated to emphasize the required phenomenon (*i.e.* being in the LCF domain).

5.2.2 *Thermo-mechanical parameters*

These parameters include geometrical dimensions, material properties and fluid/structure boundary conditions. The geometrical dimensions are not fixed but vary within the allowed manufacturing limits. For this reason, they are assumed to be random and lognormally distributed so that they remain strictly positive. The material properties (*e.g.* Young's modulus, Poisson's ratio and thermal expansion coefficients) are also random in nature

due to the material heterogeneity at the microscopic scale. However, the spatial variability of these properties is neglected in this study and they are consequently treated here as random variables with a lognormal distribution (which is common practice in literature [15]). The fluid/structure boundary condition is characterised by the heat transfer coefficient. This coefficient, which depends on the fluid temperature and the flowing rate, is not well known. It is therefore treated as a random variable whose probabilistic distribution is assumed to be lognormal with a large coefficient of variation of 30% to take into account the big scatter on this parameter usually observed in model testing.

5.2.3 *Fatigue strength of the material*

Because of the large scatter observed in fatigue data, the number-of-cycles-to-failure at a given stress level is considered as a random variable. The probabilistic distribution of the number-of-cycles-to-failure at any stress level can be regarded as lognormal, whose parameters depend on the stress level [16]. The characteristics of this distribution are estimated by a statistical analysis carried out on a database provided by Electricité de France [17]. This database consists on strain-controlled fatigue tests of small polished 304 and 316 austenitic steel specimens at room temperature in air. Only those tests under alternating stress (*i.e.* mean stress equal to zero), which lead to failure are considered, leading to a set of $Q = 99$ values.
The lognormally distributed number of cycles to failure $N(S,\omega)$ at any stress level S may be written as:

$$\ln N(S,\omega) = \eta(S) + \sigma(S)\xi(\omega) \tag{8}$$

where $\eta(S)$ and $\sigma(S)$ are respectively the mean value the standard deviation of $\ln N$ and $\xi(\omega)$ is a standard normal variable. In Eq. (8), it is assumed that the variables representing the scatter of $\ln N$ around its mean-value are *perfectly correlated*. This assumption means that a given sample is good or bad with respect to fatigue life whatever the stress level applied. This assumption appears reasonable, although it is practically impossible to check, since each fatigue test are conducted up to the failure of the specimen.

It is further assumed that $\eta(S)$ is expressed in terms of Langer's equation (Eq. (1)) and $\sigma(S)$ is proportional to $\eta(S)$ (*i.e.* the coefficient of variation δ of $\ln N(S,\omega)$ is constant).

$$\sigma(S) = \delta\eta(S) \tag{9}$$

Then the four parameters A, B, S_D and δ are determined in a single shot using the method of maximum likelihood.

5.2.4 *Specimen-to-structure passage factors*

In the existing nuclear design code, the factors $\gamma^N = 20$ and $\gamma^S = 2$, which are introduced to relate the number-of-cycles-to-failure of laboratory test specimens to those of actual reactor components, can be interpreted as the product of two sub-factors: $\gamma^j = \gamma^j_{scatter} \cdot \gamma^j_{passage}$; $j = N,S$, where the subfactors $\gamma^j_{scatter}$ cover the scatter of the experimental data and the sub-factors $\gamma^j_{passage}$ account for the effects of the size, the surface finish and the industrial environment of the actual structure (*e. g.* Chopra and Shack [18]). Noting that the scatter of the experimental data is already included in the probabilistic characterization of the number-of-cycles-to-failure, the subfactors $\gamma^j_{passage}$ appear as conversion factors that must be applied to the fatigue lives of specimens to estimate the lives of actual reactor structures. However, the literature shows that these subfactors, which are more or less empirical, are still not well known (e.g. Framatome [19]). For this reason, they are regarded in this application as random variables. Since it is possible to bound these factors, they are supposed to follow a Bêta distribution. The parameters of this Bêta distribution are yet to be determined from experiments carried out both on laboratory test specimen and operating structures and comparison thereof.

The statistical properties of the input random variables are given in the Table 1.

5.3 Mechanical model

The pipe is assumed to be thin ($e << R_i$) and uniformly loaded onto its inner surface. Under these assumptions, the temperature field in the thickness is solution of a one dimension unsteady heat conduction equation:

$$\frac{\partial\theta(t,x)}{\partial t} = C\frac{\partial^2\theta(t,x)}{\partial x^2} \tag{10}$$

where $C = L/\rho C_p$ is the thermal diffusivity of the material, L is the conductivity and ρC_p is the heat capacity. The boundary conditions, which account for a perfectly insulate outer surface and a standard heat transfer model with the fluid, read respectively:

$$\left.\frac{\partial \theta(t,x)}{\partial x}\right|_{x=R_i+e} = 0 \quad \text{and} \quad -L\left.\frac{\partial \theta(t,x)}{\partial x}\right|_{x=R_i} = h\left[\theta(t,x=R_i)-\theta_f\right] \tag{11}$$

where h is the heat transfer coefficient and θ_f is the fluid temperature.
Once the temperature profile in the thickness is obtained, the stress tensor is given by the equilibrium equation: $div(S_{ij}) = 0$, under the following boundary conditions:

$$\begin{cases} S_{rr}(x=R_i) = 0 & \textbf{(zero inner pressure)} \\ S_{rr}(x=R_i+e) = 0 & \textbf{(free outer border)} \\ \int_{R_i}^{R_i+e} x\, S_{rr}(x)\, dx = 0 & \textbf{(free ends)} \end{cases} \tag{12}$$

Due to the assumption of a free end thin pipe, the generalized plane strain conditions are applied (*i.e.* strain component ε_{zz} is regarded as a constant throughout the pipe thickness and is an unknown parameter of the problem).
When time domain analysis is considered, the stress field in the thickness of the pipe is computed numerically using the finite difference code *OSTAND* developed by EDF R&D, while it is obtained by an analytical transfer function in the frequency domain analysis (*e. g.* Musi and Beaud [20]). In both analyses, the two stress components $\sigma_{\theta\theta}$ and σ_{zz} are equal at the inner wall, all other components being zero. Thus, the equivalent scalar stress (based on Tresca criterion), from which the stress cycles amplitudes are obtained, is $\sigma_{\theta\theta} = \sigma_{ZZ}$.

Variable name	Distribution	Mean	Coef. of variation
Inner radius, R_i	log-normal	0.12827 m	5%
Thickness, e	log-normal	9.27 10^{-3} m	5%
Young's modulus, E	log-normal	1.8908 10^{5} MPa	10%
Poisson ratio, ν	Bêta [0.2, 0.4]	0.3	10%
Thermal expansion, α	log-normal	1.695 10^{-5}	10%
Thermal conductivity, L	log-normal	16.645 W.K^{-1}.m^{-1}	10%
Specific heat capacity, ρC_p	log-normal	4.024 10^{6} W.K^{-1}.m^{-3}	10%
Heat transfer coef., h	log-normal	20,000 W.K^{-1}.m^{-2}	30%
Yield strength, S_y	log-normal	188 MPa	10%
Ultimate tensile strength, S_u	log-normal	496 MPa	10%
$\gamma^S_{passage}$	Bêta [1,2]	1.68	10%
$\gamma^N_{passage}$	Bêta [7,11]	9.39	10%
Fatigue strength scatter, ξ	normal	0	std. dev. = 1

Table 1. Statistical properties of the input random variables.

5.4 Results

The reliability analysis is carried out for 4 case studies. Indeed, HCF and LCF (using the stress factor k) regimes are investigated, each of them being treated in the time and the frequency domain. Note that in the HCF domain the reliability in computed on a target service-life-time N_0 = 10000 temperature sequences of 360 s (*i.e.* 10^7 stress cycles), while in the LCF domain it is performed on a target service-life-time N_0 = 10 temperature sequences (*i.e.* 10^4 stress cycles).
For each case study, the failure reliability was calculated using *FORM*, *SORM* and importance sampling methods. Since the generalized reliability indice $\beta = -\Phi^{-1}(P_f)$ given by these three methods are very close, only the *FORM* results are presented (Table 2). Concerning the importance factors, their values in both the time and the frequency domain, which are very closed, are shown in Figure 6. The complete results of this analysis are reported in Guédé [21].

From the reliability index values shown in Table 3, one can see that the frequency domain approach is always more conservative than time domain one (*i.e.* β is always smaller). This is due to the fact that the frequency domain approach, which, unlike the time domain approach, incorporates the loading randomness and this includes more uncertainties. A larger difference between the respective reliability indices of both approaches (*i.e.* approximately 20%) is observed. This large difference does not question the equivalence of both approaches

yet. It comes from the fact that the assumption of large number of damaging stress cycles is no longer satisfied Indeed, 2 – 4 damaging stress cycles are obtained for a number of 4000 extracted cycles extracted from the loading time history $\theta_1(t)$ throughout the chosen time duration of the temperatures sequence (*i.e.* 360 s). The observed difference should decrease for a higher period, which was not checked is the present work for CPU reasons.

Reliability analysis	HCF	LCF
Time domain	2.28	2.48
Frequency domain	1.88	2.07
Discrepancy (%)	21.3%	19.8%

Table 2. Reliability index obtained by *FORM* analysis.

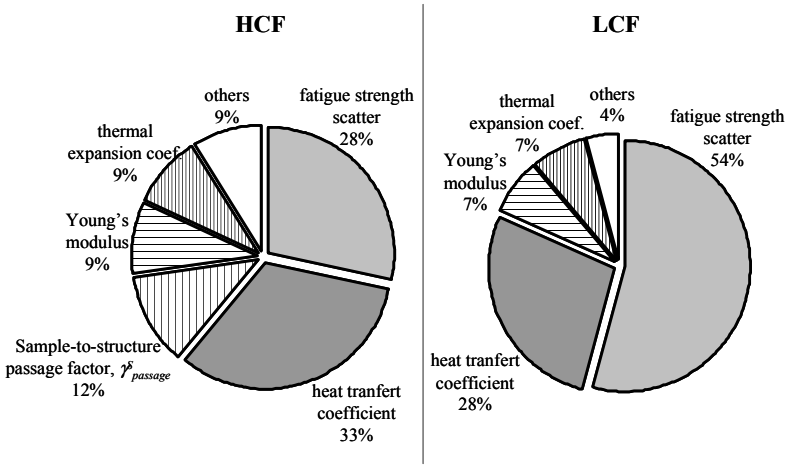


Fig. 6. Sensitivity factors both in HCF and LCF regimes.

The importance factors shown in Figures 6 reveal that the scatter in fatigue strength and the heat transfer coefficient are the most significant variables in the thermal fatigue reliability. On the other hand, the effect of the heat transfer coefficient decreases in the LCF regime, since it acts directly on the variations of the stress cycles number, which are not that significant for the fatigue damage in the LCF domain.

The stress amplitude assessment via the passage factor $\gamma^{S}_{passage}$ is significant for the reliability only in the HCF domain where it is applied. On the other hand, the effect of the life-time reduction factor $\gamma^{N}_{passage}$ remains negligible in the LCF where it is applied. Indeed, even with the majoration of the stress amplitude by a high k factor, the pipe does not operate exclusively in the LCF regime, but there are still many stress amplitudes in the HCF domain. The effect of $\gamma^{N}_{passage}$ should raise if only LCF regime is considered.

The Young's modulus and the thermal expansion coefficient are the most important thermal parameters for the fatigue reliability, due to the assumption of material linear elastic behaviour. Moreover, because of their symmetrical role in the mechanical model, their respective weights are equal. They may therefore be grouped into a single random variable, namely the product $E\alpha$.

6 CONCLUSION

In the present work, a probabilistic approach for the assessment of nuclear components submitted to thermal fatigue is set up, making it possible to take account for all the uncertainties that affect the thermal fatigue behaviour. The procedure is applied to a pipe subjected to a random thermal loading. It is shown that it is possible to perform a complete reliability analysis against thermal fatigue, and to compute the reliability indices and the sensitivity factors with respect to any variation in each input variable. It is important to note that the proposed approach does not depend on the models used to describe thermal fatigue behaviour of the structure, and it could be adjusted for any other more accurate modelling.

It is also shown that the assessment of thermal fatigue reliability can be carried out equivalently in the time and frequency domain under the assumption of stationary Gaussian loading and large number of damaging stress cycles. However, it should be noted that the frequency domain approach can be used only for stationary random

loading with an elastic material behaviour. On the other hand, the application of the time domain approach may be extended to non-stationary random loading, provided the non-stationary process is correctly discretized.

7 REFERENCES

1. Collectif. *Règles de Conception et de Construction des Matériels des Ilots Nucléaires* (RCCM). AFCEN, Paris La Défense, 2000.
2. C. Amzallag, J. P. Gerey, J. L. Robert and J. Bahuaud. *Standardization of the rainflow counting method for fatigue analysis*. Int. Jnl of Fatigue 1994;16:287-293.
3. B. F. Langer. *Design of pressure vessels for low-cycle fatigue*. ASME Jnl of Basic Eng. 1962;84:389-402.
4. M. A. Miner. *Cumulative damage in fatigue.* J. Appl. Mech. 1945;12:A-159.
5. O. Ditlevsen and H. O. Madsen. *Structural reliability methods*, Wiley, 1996.
6. K. Breitung. *Asymptotic approximations for multinormal integrals*. Jnl Eng. Mech. ASCE 1984 ;110(3):357-466.
7. M. Lemaire. *Fiabilité des structures – couplage mécano-fiabiliste statique*. Hermes Science Publication 2005.
8. PHI-MECA Engineering S.A. *Manuel d'utilisation*, PHIMECA Soft. 2003.
9. M. Shinozuka and G. Deodatis. *Simulation of stochastic process by spectral representation*. Appl. Mech. Review 1991 ;44 :191-204.
10. Y. Zhang and A. Der Kiureghian. *Dynamic response sensitivity of inelastic structures*, Comp. Methods Appl. Mech. Eng. 1993 ;108(1) :23-36.
11. T. Dirlik. *Application of computers in Fatigue Analysis*. PhD thesis, University of Warwick, 1985.
12. A. Preumont. *Random vibration and spectral analysis*. Kluwer Academic Publishers 1994.
13. X. Pitoiset and A. Preumont. *Spectral methods for multiaxial random fatigue analysis of metallic structures*. Int. Jnl. of Fatigue 2000 ;22 :541-550.
14. B. Sudret, Z. Guédé and M. Lemaire. Probabilistic framework for fatigue analysis. In Proc. 11th IFIP WG7.5 Working Conf. on Reliability and Optimization of Structural Systems 2-5 November 2003, Banff, Canada, pp. 251-257.
15. JCSS. *Probabilistic model code*. The Joint Committee on Structural Safety, 2001.
16. C. Bathias and J. P. Baïlon. *La fatigue des matériaux et des structures*. Hermes, 1997.
17. B. Sudret and Z. Guédé. *Probabilistic assessment of thermal in nuclear component*. Nucl. Eng. Des. 2005;235:1819-1835.
18. O. K. Chopra and W. J. Shack. *Low-cycle fatigue of piping and pressure vessel steels in LWR environments*, Nuc. Eng. Des. 1998;184:49-76.
19. Framatome. *Re-evaluation of fatigue analysis criteria*. Technical report EE/S 98.317, 1998.
20. S. Musi and F. Beaud. *An analytical model for thermal fatigue crack initiation and propagation in mixing zones of piping systems*. PVP – Fatigue, Fracture and Damage Analysis, 2003 ;461 :111-118.
21. Z. Guédé. *Approche probabiliste de la durée de vie des structures sollicitées en fatigue thermique*. PhD thesis. Université Blaise Pascal de Clermont-Ferrand – France, 2005.

RELIABILITY APPROACH IN FATIGUE DESIGN: A MULTIPARTNERS PROJECT

André Bignonnet[a], Henri-Paul. Lieurade[b]

[a] a b consulting, 49750 Beaulieu, France
[b] CETIM, 60300 Senlis, France

Abstract. In our society the consequences of a failure of a system invented by men are no longer accepted. This natural exigency, the concurrency between companies, the risk on the company image, push the industry towards new processes and towards the development of strategy to quantify and to anticipate the risk of failure of the products they design and fabricate. The projects are, or will be, managed by the risk.
Within this context, CETIM opened a multipartners project: Reliability Approach in Fatigue Design. This two-year project has the ambition to develop methods and tools to analyse the fatigue failure risk for structures and mechanical components. CETIM want to help its partners to integrate and to handle the reliability approach in fatigue design with the objective to quantify the risk, to analyse the variety of loading, to qualify the fabrication scatter in fatigue strength, to define the reliability criterion of acceptance. This project will provide:

- a generic methodology of reliable fatigue design for structures and mechanical components, which can be adapted to any industrial context.
- a software platform with a modular form to accept the necessary modules and the extension to future modules coming from the evolution of skills in the domain.
- experimental practice adapted to the characterisation of fatigue parameters of material/process couples and its statistical content with regard to the modelling needs.
- experimental practice adapted to the validation of the predicted reliability of new products.
- Capitalisation methods of characterisation data and of validation data, guidance notes and recommendations.

1 INTRODUCTION

With regards to the reliability questions in fatigue design, CETIM launches a Great Project on the Approach of Reliable Design in Fatigue. On the scientific and technical aspects the topic is indeed at a hinge period. The methods and tools for fatigue design are existing and used in a deterministic way although progress remains to be made in the dissemination of the new methods in the industrial world. On the other hand the evolution of the Western countries society claims the zero failure which the current approaches appreciate badly, only the reliability methods of design will be able to quantify risks and therefore helps to answer this requirement.

The awakening in industry by the need for guaranteeing the reliability of the products manufactured and for qualifying the reliability with regard to a definite objective is clear. It opens the way for new scientific and technical developments in particular concerning the problems of durability or resistance to fatigue of the mechanical structures and components. The concurrency, the transfer of competences and responsibilities from big companies towards their subcontractors, the international dimension of the exchanges between industrial groups and their suppliers make that it is necessary to cover all the industrial chain.

2 STAKES OF THE PROJECT

It becomes obvious that this project must bring a vision, breakdown methods with the practices currently met in the majority of the mechanical engineering. The stake requires crossing a decisive step. Indeed the industrial reasons set that the methods and recommendations resulting from such a project prevail during a score of years.
We will specify the major orientations, which the project must take to reach this ambition according to two axes:

- the numerical simulation in industry
- the culture aspect of reliability

2.1 Evolution of the methods of design and validation

2.1.1 The numerical simulation extended to all industry

The first ingredient which will allow a significant step compared to the current situation is to take into account the fact that in the decade which comes CAD tools and the numerical simulation of the mechanical structures behaviour will have conquered the whole of the mechanical engineering industry, including the SME, and the transfer of know-how of the large companies in the field of the structural analysis towards companies of more modest size is already, or will be, a reality. CETIM, partner of all, registers his action in this topicality.

2.1.2 The difficulty of the transfer of know-how in this new context

In a concrete way the difficulties of transmission of know-how are as follows:

- the computer codes in mechanics are accessible to all and the engineering and design departments are able, or will be, to precisely calculate the mechanical fields in any point of the structure. The engineer who was calculated his structure with the usual rules of Resistance Of Materials, and used coefficients of correction resulting from the experiment, and specific to the types of products manufactured by his company, does not have any more a reference frame when the detailed numerical simulation gives him precise information on a local scale. He can no longer interpret this information to decide on the acceptance of the structural design. The gained experience is not transmissible any more just as it is; it is necessary to build new reference frames of acceptance of the design adapted to the methods of numerical simulation.

- in the experimental field, the modern test facilities make it possible to reproduce loadings really measured in service or reconstituted using mathematical and statistical methods. Again, with regards to a severised experimental practice and a reference frame of acceptance of the test results builds on experience, the use of loads simulating the reality of the in service loadings requires new strategies of experimentation and of probabilistic interpretation of the results to take into account the diversity of service loadings and the scatter fabrication. The observation of a failure, or not, in a fatigue test does not authorize to validate the level of reliability of the production. The coupling with modelling on the one hand, the characterization of the quality of manufacture on the other hand, are necessary to validate the required level of reliability.

- the difficulty of transmission of the know-how; For much of industry people that will correspond to a real difficulty of transmission of know-how, the richness of the information thus obtained being in complete shift compared to the usual interpretations based on classical engineering calculation approaches and experiments which are supposed severe. It is a significant stake which must make it possible to draw one of the major objectives: take into account the full stress and strain tensor in any point of the structure, interpret these mechanical fields with respect to the fatigue strength and validate the provisional reliability by tightening the footbridges between design and validation.

It is thus a question of vulgarisation of the experimental methods of validation coherent with the methods of calculation of provisional reliability used in design.

2.2 The engineering culture of the reliability

Nevertheless the strongest rupture will be on another plan. We will find the stake paramount of this project in new perception that the producer has of his product. The evolutions of the Western society result in rejecting any fate and people does not accept any more that the systems invented by the man can be failing.

2.2.1 The evolution of the society

Compared to this evolution, the risks on the public image, the play of competition or quite simply the durability of the company push the industry towards:

- a rigour in the working methods: deployment of the engineering system,
- a rigour in the processes of control of the activity: CMMI qualifications (Capability Maturity Model Integration), for example

·a strategy of anticipation of the default risks: development of the operating safety. It is in the heart of this strategy that our project is.

2.2.2 A project to implement the fatigue design reliability method

The stake for the project is to precede or to support industry and to propose fatigue damage risk analysis approaches corresponding to this new vision. It is thus necessary, in the field of fatigue design of the structures, to leave or enrich the deterministic register by climbing the step of the reliability analysis. It is a difficult change to take because it corresponds to a major change of thinking or intellectual approach in industry. Which are the delicate points:

reliability approach is synonymous with:

- to quantify the risks, it is necessary to evacuate the coefficients known as safety factor, which too often hide in fact the shades in the knowledge of the product and of its loading,

- to analyse without ambiguity the variety of the loading which will be met in service,
- to calibrate and control the scatter of fabrication to quantify the statistical distribution of the strength which results from this,
- to define the level of risk which one tolerates or the objective of reliability which one sets.

The project will define objectives and deliverables corresponding to these problems, and will integrate professional specificities or regulation aspects when necessary

3 TARGET OF THE PROJECT

Taking into account the context and the stakes described previously the "mission" of the project, in other words the direction of the action and its framework, is synthesized in a sentence:
To introduces into the mechanical engineering industry the methods of reliability in fatigue design and validation for reliable structures and mechanical components. The topic being relatively vast, the perimeter of the project and its limits were defined in the following way**,**

Included fields:

- tools of identification and capitalization of the loadings and their handling for a probabilistic use.
- development of a coherent experimental strategy in the global approach (loading analyses, structural calculation, probabilistic approach).
-·quantitative evaluation of the parameters allowing to validate the hypothesis on which is based the probabilistic approach**.**

Excluded fields:

- new developments in static and dynamic structural analysis.
-·development of new laws on the behaviour and the damage of materials.

4 RISKS OF THE PROJECT

The risks identified in this project are several natures:
-·risk of dispersion in the aims with regard to the extent of the field, from the knowledge of the in service loadings to the control of the quality of fabrication.
Clearly identified general objectives and priority targets have been established to drive the action.
-·risk to provide usable deliverable but not used.
This pitfall is avoided by strongly implying industrial people in the project so that the deliverable take into account the industrial constraints, thus guaranteeing their real integration in the engineering and design departments.

5 WAITED RESULTS OF THE PROJECT

5.1 New products and new services

The project gives an answer to the new request that is rising around the topic of reliability in fatigue of structures and mechanical. Waited results are new products and methods answering the problems reliability engineer based on:

- a modular software engineering made up of generic modules adaptable to the questions of each one
- adapted methods and experimental means

5.2 New methods and new tools

The technical and scientific contents of the program will end in:
-·the creation of a generic approach of fatigue design reliability of structures and mechanical components adaptable to the various industrial needs
-·a platform software exploited by CETIM allowing the reception of the whole of the modules necessary and the extension to new modules resulting from the evolution of knowledge
-·experimental practices adapted to the characterization of the fatigue parameters of the material/process couples and to its statistical contents with regard to the needs for modelling
-·new experimental practices of validation of the provisional reliability of the industrial products
-·methods of capitalization of the characterisation and the validation data

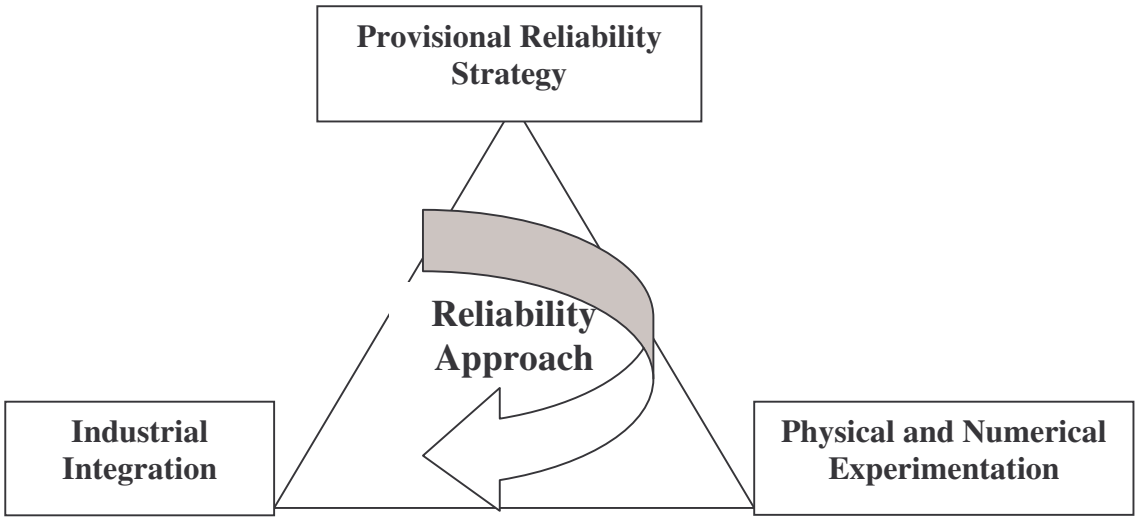
6 PRINCIPAL OBJECTIVES

6.1 Position of the problem

We identified a significant risk of dispersion of the objectives taking into account the extent of the set of themes treated by the project. Initially and to simplify architecture, we will consider the project in the form of a triptych whose elements can be detailed separately but must remain coherent between them to make a whole. The elements of this triptych are:

-·modelling strategy or general approach of the reliability question
-·experimental methods of characterization and validation
-·integration in the industrial constraint

Let us examine each one of these three elements to get the broad outline of coherent objectives.



6.2 Modelling strategy

The choice of a modelling strategy set the coherence of the all the tasks. It should take into account the constraints that will rise from the requirements of the other elements of the triptych. It deals with:

- the type of reliability approach to be implemented
- the analysis of the service loadings and their expression in probabilistic terms.
- the criteria of acceptance or the objective of reliability
- the stress and strength interference reliability method

As a basis one should set that the parameters of modelling must be measurable by the experiment. The main competences necessary for this part of the project are: probabilities and statistics, methods of measurement and analysis of the severity of the loadings,

6.3 The physical and the numerical experimentation: the characterization and validation.

The aim of these activities is to quantify and validate the provisional reliability by modelling and limited amount of testing. The waited results are:

·the characterization:

- the implementation of tests allowing to reach the parameters of modelling chosen,
- the description of dispersions of manufacture parameterised according to the needs for the probabilistic approach,
- methods of capitalization and establishment of databases proceeded materials.

·the validation:

- the implementation of coherent tests with the modelling of the behaviour of the structure and the validation of the assumptions selected,
- tests representative of the conditions of use of the structure and the damage to be simulated,
- methods of analysis of the test results allowing validating estimated reliability.

To reach this objective one should be sure that each test aiming at generating a damage get sense only if:

- it is representative of the damage to avoid in service,

- if this damage can be modelled and thus if the test result is interpretable in a different context by modelling.

The main competences necessary for this part of the project are: experimental methods in fatigue it, interactivity between testing and modelling, probabilistic analyses.

6.4 Industrial integration.

The project should make sure that the totality of the industrial constraints are well taken into account with respect to the applicability of the methods suggested and their appropriation by each industry. The project will have to take care of:

- the ways and means used in industry more than in research laboratories
- the regulation contexts if necessary
- the most adapted way for the dissemination of know-how on a European scale.

7 CONCLUSION

This project as the ambition to introduce into the mechanical engineering industry the reliability approach for the fatigue design and validation of structures and mechanical components.

The objectives are: to build the necessary evolution to manage industrial projects by the technical risk control, to create the team spirit and the engineering reliability culture, to develop adapted tools for industrial application.

The mastery of the design and validation reliability approach it is:

- the true driving force to the **structural optimisation**. With efficient methods and tools for provisional reliability analysis, the optimisation of structures and components make sense in term of weight saving and technico-economics performance. An optimisation based on the right and bare essentials will guarantee the cost control of the product when limiting inadapted safety margin.
- to be in a position to analyse in pragmatic way its product with regard to **the reliability performance waited by the customer**. Indeed the reliability approach asks for setting clearly the cycle of development cycle key points, the variety of in-service loading, the scatter in strength of the manufactured products, the definition of the acceptance criteria.
- to afford a strong element of decision taking for the acceptation of a design and a fabrication through the risk quantification and control.

Determining the variance of the loading of a work cycle

Olli Alkkiomäki[a], Juha Kilkki[b] and Gary Marquis[b]

[a] Department of Information Technology
[b] Department of Mechanical Engineering
Lappeenranta University of Technology
P.O.Box 20, FIN-53851, Finland

Abstract Strain gauge measurements from the prototype and production models provide relevant information about the loadings of a structure or a component during its service life. However, the measured variable amplitude loading history represents only a fraction of the whole service life. Methods for extrapolating the service loading for a longer period of time exist in literature, but the variance of the service loading distribution is often neglected. Variance between individual work cycles is considered in this paper. By estimating the variance of the work cycles, it is possible to predict the service loading and for a larger population of work cycles than there is measured data. This would allow, for example, determining the loadings for a larger population of users from a small group of users and determining the most damaging user from the population.

1 INTRODUCTION

To determine the probability whether a certain component or a structure will have a failure during its service life, both the fatigue strength and service loading distributions must be known. The fatigue strength distribution for a certain material and geometry can be determined by fatigue tests. Probabilistic methods for determining the service loading distribution from a measured load history have only recently being studied. In this paper methods for determining the fatigue strength and service loading distributions are discussed. The methods presented in this paper require several measurements of the same work cycle. If there is only one measurement available, bootstrapping methods [1] can be used to approximate the service loading distribution. In Figure 1, the fatigue damage of each individual measured work cycle is calculated and a service loading distribution is approximated based on the few measured samples.

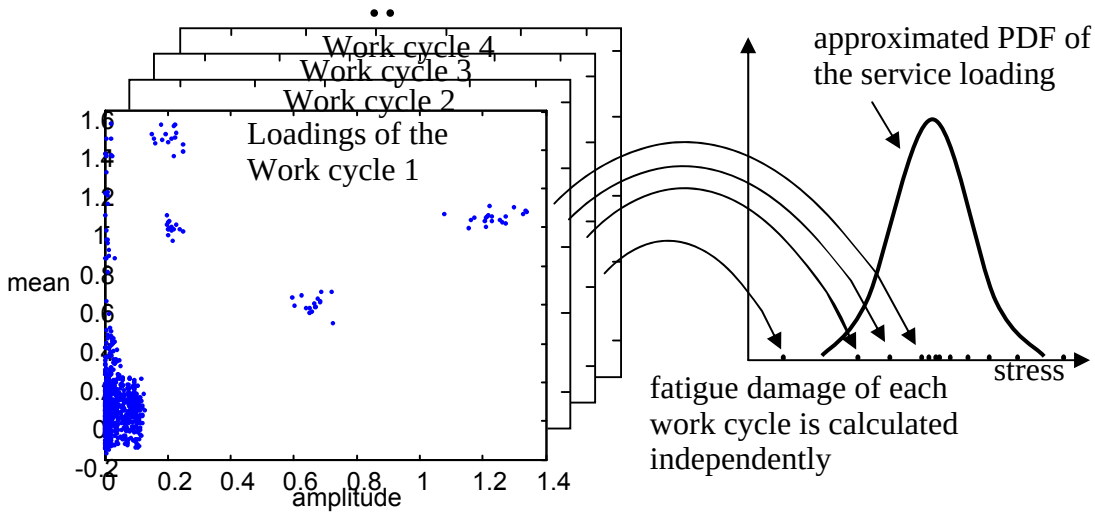


Figure 1. Transforming loadings of an individual work cycles into a service loading distribution

Strain gauges can be used to measure strains of a component or a structure during a work cycle. By using fatigue analysis techniques the damage caused by the measured load cycles can be calculated. It is possible to determine the service loading distribution by calculating the fatigue damage of several work cycles independently. In this example the work cycle loadings are presented as a distribution of individual rainflow counted load cycles, but also rainflow matrixes or Miner's sum calculated directly from the measurement could be used. Any fatigue assessment technique can be used to determine the fatigue damage from the loadings. The probability density function (PDF) of the service loading can be modelled for example with a Gaussian distribution. Other methods for determining the PDF are also presented in this paper.

2 FATIGUE STRENGTH DISTRIBUTION

To determine the probability whether a certain component or a structure will have a failure during its service life, both the fatigue strength and service loading distributions must be known. Failure probabilities for each detail can be determined separately and the failure probability for the whole structure can be calculated using analysis of variance. Fatigue strength distributions for different materials and details can be determined by fatigue tests.

Data from experimental fatigue tests is scattered. Identical test specimens have different fatigue lives due to imperfections in material and randomness of the fatigue process. Characteristic design curves for each material and joint type can be found from literature. IIW standards define characteristic design curves with at least 95% survival probability with 75% confidence level of the mean. In order to model the fatigue strength distribution, the mean value and scatter of the original fatigue test must be estimated. Characteristics design curve, mean curve and scatter are presented in Figure 2. Usually only a few test specimens are used in fatigue tests. Mean value can be determined by using linear regression, but calculating the standard deviation from as few as 2-6 test specimens is not reasonable. IIW defines conventional values for standard deviation. For simple structures with a low number of cycles between 10^4 and 10^5, a standard deviation of 0.178 is used. For more complex structures with cycles up to 10^6, a standard deviation of 0.25 is used.

With these values it is possible to give a rough estimate of the mean value and scatter of the original fatigue test. However, some of the IIW design curves actually meet 97.5% survival probability with 95% confidence level. The mean and scatter can still be predicted using standard 95% survival probability and 75% confidence level values. The prediction is only more conservative as the mean is predicted too low and the scatter too high. More accurate mean value and standard deviation can be calculated, if the original test data is available.

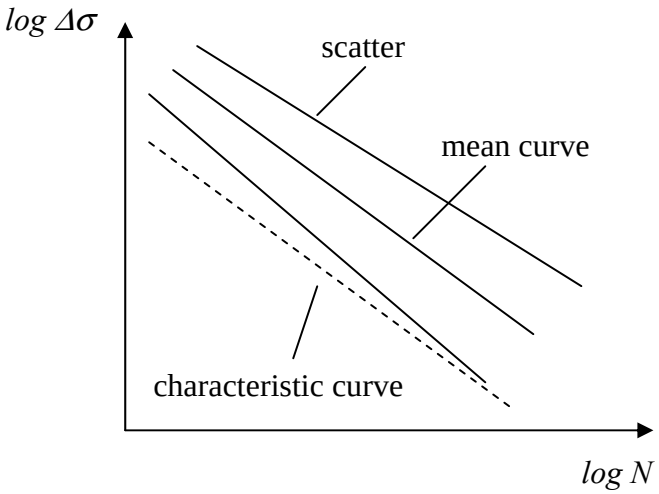


Figure 2. S-N curve

3 SERVICE LOADING DISTRIBUTION

Service loading spectrums for certain operating situations exist in literature. The spectrums can be used to predict periodic loadings in nature such as sea motion, wind loads and snow loads. These spectrums account only for the amplitude of the load cycles and not the mean value. For more random loadings, the service loading must be measured from a prototype. Random loadings such as those for land or off-road vehicles can be measured using strain gauge measurements.

To determine the service loading distribution for a work phase, the fatigue damage for each individual work cycle is calculated separately. Miner's law or other fatigue analysis technique can be used to calculate the fatigue damage during one work cycle. Rainflow matrix can be used to store the loadings of a single work cycle or each load cycle can also be stored individually. The fatigue damage of each work cycle is reduced into a single value and a probabilistic distribution is used to model the values. Deriving fatigue damage from a measurement is not straight forward. Better fatigue assessment techniques are developed and therefore the original measured data should be stored as accurately as possible. Measurement devices usually only store the rainflow matrix and preserving all the information available from the measurement device is possible in this case.

4 MIXTURE MODELS

The PDF of the fatigue strength and service life distributions is often assumed Gaussian. For the fatigue strength distributions this is usually true, but for the service loading distribution this assumption should not be made. Density estimation methods can be used model non-Gaussian distributions. There are several methods that present the probability density function as a continuous smooth surface. Most of the methods use kernel functions to represent the density.

The kernel functions are probability density functions that are usually of symmetric shape. Gaussian densities can be used to approximate any bounded continuous PDF, if the number of the Gaussian kernels is large enough [2]. The kernel method has a similar smoothing parameter as the histogram bin-size. If the kernel is much narrower than the distance between the data points, the density estimate will become bumpy. On the other hand, if the kernel is too wide, it will wipe out any details in the density estimate. Some methods use either variable kernel widths or non symmetric kernels.

For example Parzen method or one-pass procedure can be used to model the the PDF [3]. Each weight factor and all the unknown parameters of the Gaussian functions can be estimated with the method of maximum likelihood using a system of iterative equations. The form for the multivariate PDF with the one-pass procedure is:

$$f(s)=\sum_{i=1}^{K} U_i \cdot w\left(s-q_i, B_i\right)=\sum_{i=1}^{K} U_i \cdot (2)^{-\frac{n}{2}} \cdot \sqrt{|B_i|}\exp\left[-\frac{1}{2}\cdot\left(s-q_i\right)\cdot B_i\cdot\left(s-q_i\right)\right] \qquad (1)$$

where w is the Parzen window function, n is the dimension of the sample vector s, K is the number of Gaussian functions and q_i is the i-th prototype vector. The covariance matrix B_i^{-1} for each prototype q_i corresponds to the distribution Each Gaussian function can have a different weight factor U_i.

Traditional kernel estimators based on the maximum likelihood method [4] are only applicable when the amount of sample vectors is rather small. Methods reducing the computational cost, such as the reduced Parzen classifier [5] and the greedy learning of Gaussian mixtures [6] have been developed. The reduced kernel estimators converge much faster than the traditional methods. The original Expectation-Maximization (EM) method [4] is sensitive to the initialization of the kernel centers, and is not guaranteed to converge to the global optima. The reduced density estimators usually overcome this problem. Junhong Liu's radial basis kernel method [7] uses differential evolution [8] to find the optimal kernel function parameters. Differential evolution is a heuristic optimization algorithm based on evolutionary computing. On each generation, the population members are mutated by adding weighted, random vector differentials to them. If the mutated population member has a smaller cost value than the original, it is selected into the next generation, otherwise the original survives. The PDF is estimated with the same equation 1 as in the one-pass procedure, since the method uses Gaussian radial basis functions. Center, weight factor and the variance of each kernel function are optimized with differential evolution to minimize the mean square error (MSE) of the density estimation.

Kernel estimators can be used to model the service loading distribution. Figure 3 shows a simulated service loading distribution modelled with three Gaussian kernels.

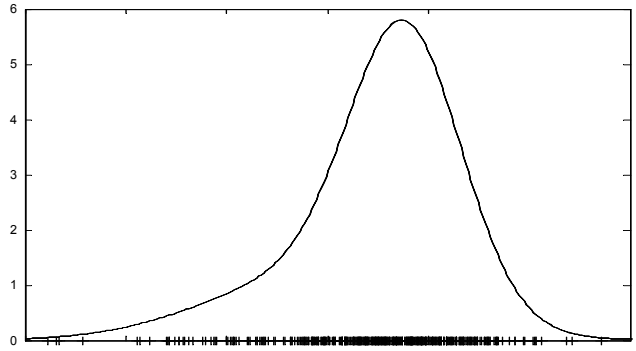


Figure 3. Simulated service loading distribution modeled with greedy EM

5 CONCLUSIONS

The service loading and fatigue strength should be modelled as probabilistic distributions rather than single values. Reliability analysis diagram presented in Figure 4 is used to determine the overlap between service loading and fatigue strength. The overlapped area states the probability of a given material to fail during its service life. By conducting several strain gauge measurements of the work cycle, it is possible to determine the service loading distribution. Fatigue analysis techniques can be used to calculate the fatigue damage caused by each individually measured work cycle. PDF of the service loading can be then approximated based on these values. Density estimation methods presented in this paper can be used to model non-Gaussian service loadings.

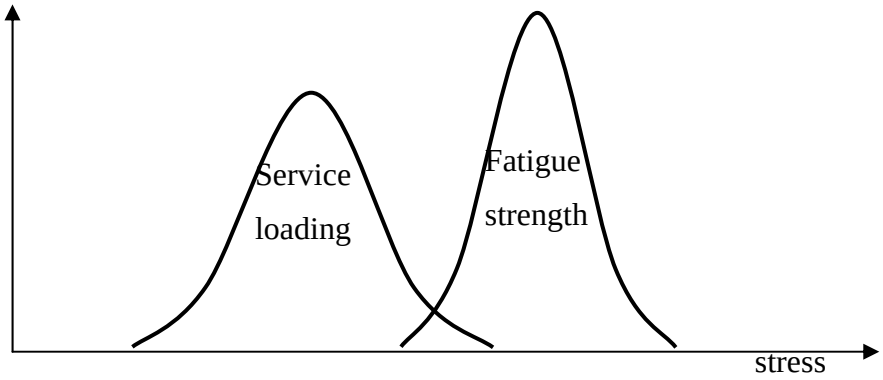


Figure 4. Probability distributions for service loading and fatigue strength

An accurate risk analysis can be done by modelling the service loading and fatigue strength distributions. The service loadings for a much larger set of work cycles can be estimated based on the few measured samples. For example, the loadings for the whole population of users could be determined from a small group of different users.

6 REFERENCES:

1. Alkkiomäki, O., Kilkki, J., Marquis, G. Estimation of random load histories by spline density estimation and bootstrap method, Proceedings of the International conference on the respective input of the numerical simulation and the experimental approach in fatigue design, Senlis, France, 2005.
2. Feller, W. An Introduction to Probability Theory and its Applications, volume II. John Wiley & Sons Inc., New York, 1971. ISBN: 0471257095
3. Klemenc, J., Fajdiga, M. Description of statistical dependencies of parameters of random load states (dependency of random load parameters), International Journal of Fatigue, 22, 357-367, 2000.
4. Dempster, A., P., Laird, N., M., Rubin, D., B. Maximum likelihood from incomplete data via the EM algorithm. Journal of the Royal Statistical Society B, 39, 1-38, 1977.
5. Fukunaga, K., Hayes, R., R. The Reduced Parzen Classifier, IEEE Transactions on Pattern Analysis and Machine Intelligence, 11(4), 423-425, 1989.
6. Verbeek, J., J., Vlassis, N., Kröse, B. Efficient Greedy Learning of Gaussian Mixture Models, Neural Computation, 15(2), 469-485, 2003.
7. Liu, J., Lampinen, J., Differential Evolution Algorithm as a Tool of Training Radial Basis Function Networks, in GECCO-2004 Proceedings of the Genetic and Evolutionary Computation Conference, Seattle, Washington, 2004
8. Storn, R., Price, K., Differential Evolution - a Simple and Efficient Adaptive Scheme for Global Optimization over Continuous Spaces. Technical Report TR-95-012, ICSI, Berkeley, 1995.

Development of two statistic methods For predicting gear life

F.DJEDDOU*, B.KESKES*, F.BENKHENAFOU , Z. AZARI *****

* Université de Setif-Département d'Optique et Mécanique de Précision,
19000 (Algerie),b_keskes@yahoo.fr
**Université Abou-Bakr Belkaid - Département de physique –
Faculté des Sciences – BP 119 -13000 Tlemcen, Algérie
benkhenafou_fethi@yahoo.fr
***Laboratoire de Fiabilité Mécanique, Université´ de Metz–ENIM, , France

ABSTRACT

Practical experience with the modern gear analysis methods (eg. ISO/DIS/6336, BS 436,DIN/3990) suggest that they may be too pessimistic for fine-pitch gears in which the effects of gear inaccuracies are considerable . These inaccuracies may contribute significantly to the variabilities and uncertainties of the applied and permissible stresses.
In this work, all the individual manufacturing error are treated as random variables. The applied torque and other factors which in practice may also be uncertain are taken en here as constants.

Two probabilistic methods are developed in order to establish a statistical analysis for the applied and permissible stresses used in the ISO/DIS/6336 procedure. These give a more realistic estimate of the actual stresses and strengths for given(or assumed) random distributions errors of the individual manufacturing errors. The two statistical methods developed in this work have shown substantial agreement in predicting the statistics of the bending and contact stresses and the fatigue strengths of gears.

Keys words: gear, fatigue, stress, uncertainties, random, statistics, reliability

1. INTRODUCTION

To be considered as satisfactory, gear drives must operate as predicted at the design stage. Poor gear performance generally results in gear failures which may be originally due to:

1. Pitting fatigue caused by contact stresses exceeding the strength of the material .
2. Tooth breakage caused by bending stresses exceeding the bending fatigue strength of the material
3. Other surface failures associated with poor lubrication conditions such as scuffing,, scoring and wear.

The methods currently used in practice for predicting the stresses present during the operation of gears are usually those given by one of the common gear rating standards such as ISO/DIS/6336 [1] , BS 436 [2] , DIN/ 3990 [3] and AGMA 2001[4]. All these above standards adopt a fundamentally similar approach and so ISO/DIS/6336 will be taken as an example .

2. STRESSES IN REAL GEARS

The Hertzian and root bending stresses applied to a real gear can be written as follows : [1]

$$\sigma_H = [Z_E].[F_t.K_A].\left[\sqrt{\frac{1}{d_1.b}}\right].[(Z_H.Z_\varepsilon.Z_\beta).\sqrt{\frac{u+1}{u}}].\sqrt{[K_V.K_{H\beta}.K_{H\alpha}]} \qquad (1)$$

↑ Material factor ↑ Applied Load factor ↑ Nominal gear size factor ↑ Pitting geometry factors ↑ Gear accuracy factor

$$\sigma_F = [F_t.K_A].\left[\frac{1}{b.m_n}\right].[Y_F.Y_S.Y_\beta].[K_V.K_{F\beta}.K_{F\alpha}] \qquad (2)$$

↑ Applied load factor ↑ Nominal gear size factor ↑ Bending geometry factors ↑ Gear accuracy factors

It is difficult to identify accurately all factors that contribute to increase the uncertainty and the variability in the applied contact and bending stresses. However providing the applied load is known and constant (which is the case in this work) and since the uncertainties of the geometric factors (with the exception of (Y_S)) are neglected [5] , the variability and uncertainty in σ_H and σ_F can then only arise due to the gear accuracy factors (K_V,$K_{H\beta}$,$K_{H\alpha}$,$K_{F\beta}$ and$K_{F\alpha}$). In the standard [1], [2], [3],[4] mentioned above , the fundamental accuracy of each gear is defined by the accuracy of profile, lead and pitch of the teeth relative to some defined axis and the mounting accuracy of the gear relative to its (working) axis of rotation . Error tolerances are then given by the accuracy grades defined in the gear accuracy standards [6], [7] .

We are thus concerned with the general problem of determining the statistics of functions (σ_H , σ_F) of n random variables (K_V, $K_{H\beta}$, $K_{H\alpha}$, $K_{F\beta}$ and $K_{F\alpha}$) , whose statistics can be calculated in their turns. This problem has been solved both analytically and numerically as set out below .

3. STATISTICAL ANALYSIS BY USING THE ANALYTICAL METHOD

To devise a rigorous analytical procedure for calculating the mean and standard deviation of general functions of n random variables is practically not possible. It is, in fact,very difficult to find the probability density function [8], even for a general function of more than two random variables. However, for reliability problems (where the random variations of each variable can be assumed to be "small") the Taylor series approximation [8],[9],[10] can be used as an adequate method for combining the random variables .

The general expression for a function of several independent variables X_1 , X_2 , ..., X_n can be written as :

$$Y = f(X_1, X_2, ..., X_n). \qquad (3)$$

Expanding this by means of a Taylor series in the region "near" the mean values,of $\overline{X}_i$ the n variables, we obtain :

$$Y = f(\overline{X}_1, \overline{X}_2, ..., \overline{X}_n) + \sum_{i=1}^{n} \frac{\partial Y}{\partial X}\Big|_{x=\overline{x}_i}.(X_i - \overline{X}_i) + \qquad (4)$$

$$+\frac{1}{2!}\sum_{i=1}^{n}\sum_{j=1}^{n}\frac{\partial Y}{\partial X_i.\partial X_j}\Big|_{x_i=\overline{x}_i}.(X_i - \overline{X}_i).(X_j - \overline{X}_j)+....$$

In most engineering error problems,values of the higher order terms in the expansion are considered to be small compared with the mean values and first order terms,are therefore neglected. Using standard procedures, [10] we then obtain the mean as :

$$\overline{Y} = f(\overline{X}_1, \overline{X}_2, ... \overline{X}_n) \qquad (5)$$

while the (small) random variation of Y is given by :

$$\Delta Y = \sum_{i=1}^{n} \frac{\partial Y}{\partial X_i} . \Delta X_i \qquad (6)$$

where, $\Delta \overline{X}_i = (X_i - \overline{X}_i)$ is the variation of X_i from its mean . Thus ΔY is a linear function of the ΔX_i ,so, using standard theorems [8], [9],[10], the resultant standard deviation of Y is given by :

$$\sigma_Y = \sqrt{\sum_{i=1}^{n} \left(\frac{\partial Y}{\partial X_i} \Big|_{x_i = \overline{x}_i} . \sigma_{X_i} \right)^2} \qquad (7)$$

It would thus appear that all that is needed is to compute $K_V, K_{H\beta}$, $K_{H\alpha}$, etc., using the ISO calculation procedure [1]. These values could then be used, in turn, to compute (using equations (1)(2)) the statistics of σ_H, σ_{HP}, etc .

A direct computation of $\sigma(\sigma_H)$ and $\sigma(\sigma_F)$ from the above equation is not, however, possible, since the factors K_V and $K_{H\beta}$,($K_{F\alpha}$,$K_{F\beta}$) are NOT independent variables (since $K_{H\alpha}$ depends on K_V and $K_{H\beta}$, in turn, depends on. K_V .

$\pm\Delta X$	±1%		±2%	±5%	±7.5%	±10%		±15%	±20%		±40%
Method	ISO	AGMA	ISO	ISO	AGMA	ISO	AGMA	ISO	AGMA	BOX	BOX
x_i	Z_H Z_E	I	Z_N Z_V	$K_{H\alpha}$ $K_{H\beta}$ Z_L Z_R Z_W	C_m C_L	$\delta_{H\,\lim}$ K_V	S_{ac} C_V C_P	K_A S	C_{SF}	n	x

Fig.1 : Estimated Uncertainties in ISO and AGMA Gear Rating Factors from [12].

Nevertheless, since Sandler [12] has shown that the variability of these factors is, in fact, "small" (Fig.1), it seems worthwhile pursuing this approximate method.

One possibility is to ignore the dependence of the factors $K_V, K_{H\beta}$, $K_{H\alpha}$ .This leads to a simple practical method for computing the mean and standard deviation of each factor affected by manufacturing tolerances, and thus, the statistics of the resultant stresses and strengths in the ISO calculation procedure [1] . This method is presented in the following section, in which $K_V, K_{H\beta}$ and $K_{H\alpha}$, are considered totally independent .

On the other hand, an "exact" derivation of the standard deviations is also possible, although more tedious. This had been done by the author [13], where the interaction between $K_V, K_{H\beta}$, $K_{H\alpha}$ is fully taken into account .

4. MEAN AND STANDARD DEVIATION OF σ_H, σ_F

Assuming that are $K_V, K_{H\beta}$ and $K_{H\alpha}$ independent, the mean and standard deviation of σ_H, σ_F can then be derived from equations (5) and (7) as :

$$\overline{\sigma}_H = Z_H . Z_E . Z_\varepsilon . Z_\beta . \sqrt{K_A . \overline{K}_V . \overline{K}_{H\alpha} . \overline{K}_{H\beta} . \frac{F_t}{b.d_1} . \frac{u+1}{u}} \qquad (8)$$

$$\bar{\sigma}_F = (F_t / \ b.m_n).Y_F.Y_S.Y_\beta.K_A.\bar{K}_V.\bar{K}_{F\beta}.\bar{K}_{F\alpha} \quad (9)$$

and, neglecting variation of all but $K_V, K_{H\beta}, K_{H\alpha}$, etc., and carrying out the differentiation, we obtain for the standard deviations :

$$\sigma(\sigma_H) = \frac{1}{2}.\bar{\sigma}_H.\sqrt{\left(\frac{\sigma\ (K_V)}{\bar{K}_V}\right)^2 + \left(\frac{\sigma(K_{H\beta})}{\bar{K}_{H\beta}}\right)^2 + \left(\frac{\sigma(K_{H\alpha})}{\bar{K}_{H\alpha}}\right)^2} \quad (10)$$

$$\sigma(\sigma_F) = \bar{\sigma}_F.\sqrt{\left(\frac{\sigma\ (K_V)}{\bar{K}_V}\right)^2 + \left(\frac{\sigma(K_{F\beta})}{\bar{K}_{F\beta}}\right)^2 + \left(\frac{\sigma(K_{F\alpha})}{\bar{K}_{F\alpha}}\right)^2} \quad (11)$$

Both of these can then be calculated using ISO formulae for $K_V, K_{H\beta}, K_{H\alpha}$, etc., [1] .

5. MEAN AND STANDARD DEVIATION OF σ_{HP}, σ_{FP},

Although the variability in the material strength arises from changes in many parameters [1], only the material hardness and the roughness factors (Z_R, Z_{RrelT}) are considered here as manufacturing random variables (since,in the experimental work, it is not possible to measure any other material arameters). However, according to the ISO calculation procedure [1], the parameters Z_V and Z_L also depend on the hardness, but only for through-hardened steels .

The mean and the standard deviations for σ_{HP}, σ_{FP} may then be obtained from [1] as :

$$\bar{\sigma}_{HP} = \frac{\bar{\sigma}_{H\lim}}{S_{H\min}}.Z_N.Z_L.Z_V.\bar{Z}_R.Z_W.Z_X \quad (12)$$

$$\bar{\sigma}_{FP} = \frac{\bar{\sigma}_{F\lim}}{S_{F\min}}.Y_{ST}.Y_{NT}.\bar{Y}_{RrelT}.Y_{\delta relT}.Y_X \quad (13)$$

Where [1] ,

$$\bar{Z}_R = \left(\frac{3}{\bar{Z}_R.\sqrt[3]{100/a_o}}\right)^{0.08} \quad (14)$$

$$\bar{Y}_{Rrelt} = 5.306 - 4.203(\bar{R}_Z + 1)^{1/100} \quad (15)$$

Finally equations for standard deviations may be written as :

$$\sigma(\sigma_{HP}) = \bar{\sigma}_{HP}.\sqrt{\left(\frac{\sigma(\sigma_{H\lim})}{\bar{\sigma}_{H\lim}}\right)^2 + (0.08)^2.\left(\frac{\sigma\ (R_Z)}{\bar{R}_Z}\right)^2} \quad (16)$$

$$\sigma(\sigma_{FP}) = \bar{\sigma}_{FP}.\sqrt{\left(\frac{\sigma(\sigma_{F\lim})}{\bar{\sigma}_{F\lim}}\right)^2 + \left(\frac{1}{100}\right)^2.\left(\frac{\sigma(R_Z)}{\bar{R}_Z + 1}\right)^2.\left(\frac{\bar{Y}_{Re\,lT} - 5.306}{\bar{Y}_{Re\,lT}}\right)^2} \quad (17)$$

6. STATISTICAL ANALYSIS BY USING MONTE CARLO METHOD

The statistics (mean and standard deviation) of the parameters $K_V, K_{H\beta}, K_{H\alpha}$, σ_H, σ_F , etc., can also be estimated by using Monte Carlo simulation [10] . The simulation process involves generating a

succession of random numbers with uniform distribution over the interval (0.0 - 1.0). These sets of random values can be then used to generate synthetic values for each manufacturing error (in the prescribed tolerance range) . For example, to obtain random values within the tolerance bands of any manufacturing error having a uniform distribution over 0.0 to 1.0 with a mean equal to 0.5, the following equation may be used .

$$e_i = \frac{e_{\max} - e_{\min}}{2} + (R_i - 0.5)(e_{\max} - e_{\min}) = \bar{e} + (R_i - 0.5).T_e \qquad (18)$$

where e_i is the required random value of the error (e) , $e_{\max}$ and $e_{\min}$ are the maximum and minimum (tolerance) limits of the specific manufacturing error (e), $\bar{e}$ is the mean value of the error, and R_i is the random number from a standardised uniform rectangular distribution described by $\bar{R} = 0.5$ and $\sigma(R) = 1/\ (2.\sqrt{3})$

For a normal distribution of e, the equation (18) becomes :

$$e_i = \sigma(e).Z_i + \bar{e} \qquad (19)$$

where $\bar{e}$ and $\sigma(e)$ are the required mean and standard deviation of the normal error (e), and is a random value from a standardised normal distribution described by statistics $\bar{Z}$ = 0 and $\sigma(Z) = 1$. Generating a succession of many values for the error (e_i) from equations (18) or (19) will simulate exactly what happens during actual production. The other manufacturing errors e_i ($i = 1,.....n$) may be generated in the same or different distributions . The statistics (mean and standard deviation) of a parameter such as σ_H (Eq 1), which depends on the e_i can then be determined by calculating a sufficient number of σ_H, using successive "sets" of the random values e_i .

A computer program has been written to calculate $K_V, K_{H\beta}, K_{H\alpha}, \sigma_H, \sigma_{HP}$, etc. (and the corresponding "bending strength" parameters) from randomly distributed values of the various gear errors generated in this way. The statistics of the performance parameters were computed from 8000 sets of random input data . The results are as shown in Figures 2 to 5.

CONCLUSION

Both the Monte Carlo and the analytical methods have been used to estimate the statistics of the various parameters (see table1) . The manufacturing errors that are considered random variables are assumed to have rectangular distributions .

The numerical results from both methods are shown in Table (1) . Fig 2 to Fig 5 show the histograms of the 8000 calculated values for each parameter under consideration . As can be seen from Tables (1) and (2), the results of the exact" analytical method are in good agreement with those calculated by the Monte Carlo method (for which the interaction between $K_V, K_{H\beta}$ and $K_{H\alpha}$ is automatically taken into account). The maximum error of the "exact" analytical method in estimating $\sigma(\sigma_H)$ and $\sigma(\sigma_F)$ is of order 10%. However, $\sigma(K_{H\alpha})$, $\sigma(K_{H\alpha})$ has only been estimated with an error of order 24% (because the variation of the individual errors was not "small". Clearly, however, this error has little effect on the statistics of the parameters of interest σ_H, σ_F, due to the fact that $\sigma(\sigma_H)$ and $\sigma(\sigma_F)$ and are mainly defined by $\sigma(K_{H\beta})$, and $\sigma(K_{F\beta})$,($\sigma(K_{H\alpha})$, and $\sigma(K_{F\alpha})$, are always small).

On the other hand, the simplified analytical method described above shows a maximum error of order 32%. Approximately the same values are however,also found by the Monte Carlo method if the interaction between $K_V, K_{H\beta}$ and $K_{H\alpha}$ is removed (columns A,B, Table 1). The additional error caused by simplified analytical method is thus clearly a consequence of neglecting the interactions, not a shortcoming of the analytical procedure it self. This simplified method has, however, been shown to be quite accurate (less than 15% error) for gears of higher accuracy grades (ISO 7) and better ,when the assumption of "small" variability can be more easily justified .

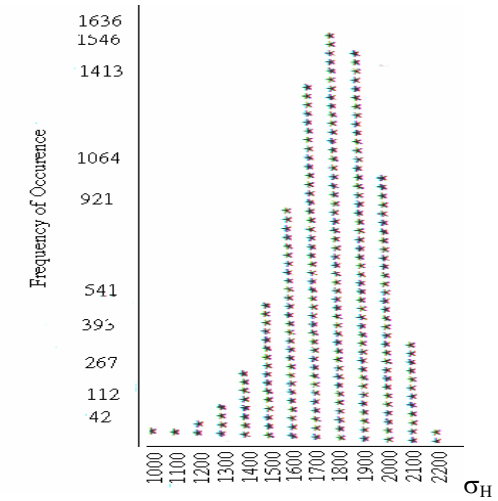


Fig. 2 : Distribution of σ_H
(mean=1775.44,N/mm^2, std.dev =189.48N/mm^2, T_1 =16.23N.m).

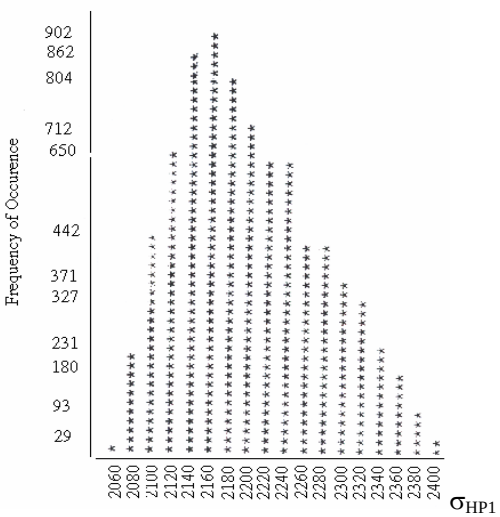


Fig. 3 : Distribution of σ_{HP1}
(mean = 2203.73 N/mm^2, std.dev = 74.31 N/mm^2).

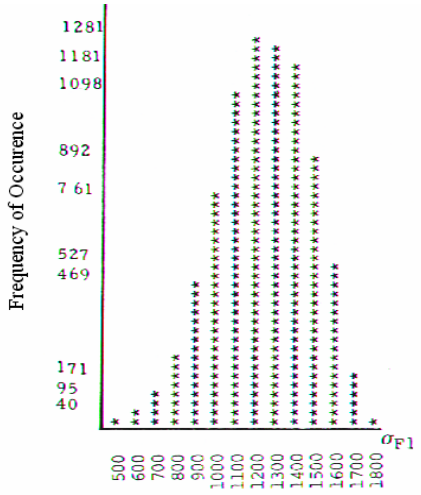


Fig. 4 : Distribution of σ_{F1}
(mean=1245.30 N/mm^2, std.dev =226.61 N/mm^2, T_1 =16.23N.m).

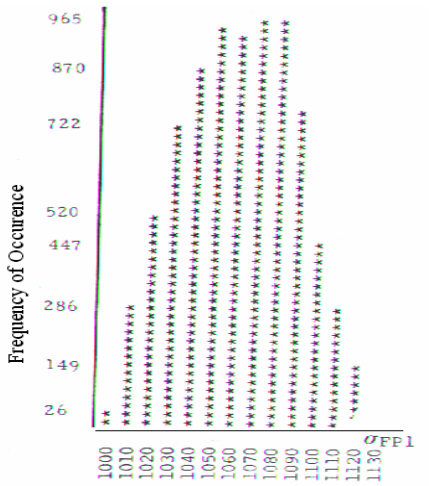


Fig. 5 : Distribution of σ_{FP1}
(mean = 1061.34 N/mm^2, std.dev = 27.27 N/mm^2).

TABLE 1 : Results of the Statistical Analysis for the gears of the Experimental Investigation (T_1=16.23 N.m)

ISO Parameter Name	A	B	C	D
f_{ma}	- 4.508	-4.862	-4.508	-4.862
σf_{ma}	32.34	32.197	32.335	32.197
$f_{\beta Y}$	- 32.414	-32.80	32.414	-32.80
$\sigma f_{\beta Y}$	13.605	13.684	13.605	13.684
$\lvert f_{\beta Y}\rvert$	32.414	32.80	-32.414	32.80
$\sigma \lvert f_{\beta Y}\rvert$	13.065	13.684	13.065	13.684
K_V	1.085	1.086	1.085	1.086
σK_V	0.023	0.024	0.023	0.024
$K_{H\beta}$	4.263	4.383	4.247	4.383
$\sigma K_{H\beta}$	0.99	0.914	0.985	0.916
$K_{F\beta}$	3.405	3.499	3.394	3.499
$\sigma K_{F\beta}$	0.683	0.619	0.680	0.620
$K_{H\alpha}$	1.362	1.346	1.388	1.346
$\sigma K_{H\alpha}$	0.173	0.168	0.238	0.188
σ_H	1771.17	1801.85	1775.44	1801.85
$\sigma(\sigma_H)$	257.81	219.72	189.480	172.37
σ_{F1}	1246.98	1263.50	1245.30	1263.50
$\sigma(\sigma_{F1})$	313.72	273.62	226.61	215.68
σ_{F2}	1281.91	1298.89	1280.18	1298.89
$\sigma(\sigma_{F2})$	322.51	281.29	232.95	221.72
σ_{HP1}	2203.73	2190.09	2203.73	2190.09
$\sigma(\sigma_{HP1})$	74.31	67.27	74.31	67.29
σ_{HP2}	2211.67	2201.93	2211.67	2201.93
$\sigma(\sigma_{HP2})$	64.88	60.86	64.88	60.86
σ_{FP1}	1060.34	1059.15	1061.34	1059.15
$\sigma(\sigma_{FP1})$	27.27	28.22	27.27	28.22
σ_{FP2}	1153.18	1151.64	1153.18	1151.64
$\sigma(\sigma_{FP2})$	28.47	29.59	28.47	29.59

A = Monte Carlo Approximation (without interaction) . ; B = Taylor Approximation (without interaction) .
C = Monte Carlo Approximation (without interaction) . ; D = Taylor Approximation (without interaction)

REFERENCE

[1] ISO/DIS/6336, "Calculation of the Load Capacity of Spur and Helical Gears", (Draft: Translation BSI 1980)

[2] BS 437 "Spur and Helical Gears", Part 3 (1986) : "Method of Calculation of Contact and Root Bending Stress Limitations for Metallic Involute Gears",BSI 1986

[3] DIN 3990 "Grundlagen fur die Trafahigkeitsberechnung von Gerad-und sghragstirnradern" (Basic principles for the calculation of load capacity of spur and helical gears) Parts 1-53, 5. Beuth 1987

[4] AGMA 2001, "Fundamental Rating Factors and Calculation Methods for Involute Spur and Helical Gear teeth", AGMA 2001-B88 (1988) .

[5] Pennell J.A., "Estimation of Safety Factors for a Given Reliability", Proc. IFTOMM/ISO, Seminar, "Service Loading and Application Factors", Trois Epis 1987 .

[6] BS 436 "Spur and Helical Gears", Part 2 (1970): "Basic Rack Form, Modules and accuracy (1 to 50 50 metric modules)",BSI 1972

[7] DIN 3962 "Accuracy of Cylindrical Gears: Tolerances for Individual Errors", Beuth 1978.

[8] Zhang Y.M., "Practical Reliability-Based Design of Gear Pair", Mechanism and Machine Theory 38 (2003) 1363-1370.

[9] Michalec G.W., "Precision Gearing", Wiley 1966

[10] Haugen E.B., " Probabilistic Mechanical Design ", Wiley Interscience 1980.

[11] Kapur K.C. and Lambertsonb L.R., "Reliability in Engineering Design", Wiley 1977.

[12] Sandler B.Z., "Probabilistic Approach to Mechanisms", Elsevier 1984.

[13] Djeddou F., " The Effect of Manufacturing Tolerances on the Performance of Fine-Pitch Industrial Gears". M.Phil Thesis. University of Newcastle Upon Tyne 1990.

PROGRAM

1 Methodologies and tools for fatigue life assessment

- Automotive components
- Various industrial applications
- Welded structures and assemblies

2 Advanced design tools and approaches

- Fatigue crack initiation assessment
- Contribution to the crack propagation stage
- Modelling of the design behaviour of the welded

3 Multiaxial loading fatigue assessment

4 Fitness for service approach and applications

5 Experimental validation

- Application to automotive parts and structures
- From laboratory testing to field evaluation
- Development of dedicated test devices and procedures

6 Design procedures against thermal and thermo mechanical fatigue damage

7 Reliability approaches in fatigue design

8 Improved design and manufacture processes with regard to fatigue

Investigation of new designs for wheel loaded truck decks in ferries

Stephan Eylmann, Wolfgang Fricke, Hans Paetzold

Hamburg University of Technology, Hamburg, Germany

Abstract In ferries cargo handling is often carried out by roll-on roll-off operations. The local deck structures exposed to this kind of operations are subjected to high cyclic loads caused by truck wheels, which may cause fatigue. Weight reduction is one major aim when developing new designs. One possibility to achieve this aim is the application of materials being able to endure higher loads. Today the yield strength of steels used in shipbuilding is limited to 390 N/mm^2 by the classification societies. Making use of high-strength steels having a yield strength of up to 690 N/mm^2 (VHTS 690) is intended in the future. When utilising VHTS 690 in shipbuilding, the familiar design of the deck structures needs to be modified, as rolled sections, which are normally used for stiffening of deck panels, are not available. This can be done by replacing the conventional rolled stiffener profiles by trapezoidal stiffeners bent from plate material. These trapezoidal stiffeners are welded to the deck from one side only, as the hollow section made up by the profile and the deck plating cannot be accessed from the inside. The principle of stiffening panels using trapezoidal profiles is well-known from bridge construction, but the experiences gained there cannot be directly transferred to shipbuilding, as there are great differences in the plate thicknesses used as well as in the number of load cycles. An additional difference is the pavement used in bridge design, which may be expected as load distributing. The application of a novel material in shipbuilding combined with a new design of deck structures makes the investigation of the fatigue behaviour necessary. Therefore fatigue tests were performed. In this paper the test performance and selected results are presented.

1 INTRODUCTION

Weight reduction is one main objective in ship design. Especially for fast ships with their demand for great power ratings, light-weight steel structures are of great importance. One possibility to achieve this aim is the use of high-strength steel, in this case with a yield strength of up to 690 N/mm^2 (VHTS 690). Within the project 'FasdHTS', which was funded by the European Commission, several investigations concerning the application of VHTS 690 in light-weight ship structures were performed. Up to now the yield strength of steels to be used in the load carrying ship structure is limited by the classification societies. The maximum allowable yield strength today is 390 N/mm^2. Evidently the extension of the allowable yield stress from 390 N/mm^2 to 690 N/mm^2 would be a substantial progress for the structural design of ships (Janssen, 2004).

However, the use of high-strength steel causes problems concerning the buckling and fatigue behaviour. Additionally new kinds for stiffening the deck panels have to be developed, as no rolled stiffeners made of VHTS 690 are available. These rolled profiles are normally used for stiffening of plate fields in shipbuilding. A possible solution is to apply trapezoidal stiffeners bent from plate material. The utilisation of trapezoidal stiffeners for panels is well-known from bridge construction. Former investigations have shown, that designs with trapezoidal stiffeners are subject to fatigue (Kolstein et al., 1996, Machida et al., 2003). The results of those investigations cannot be directly transferred to shipbuilding, as the situation in bridges differs from that in shipbuilding regarding several aspects. On bridges always a load distributing pavement made of asphalt or concrete can be found. This is not the case in ship design, where the wheels directly run on the steel deck plating. Secondly the number of load cycles in ships is clearly lower. Another difference are the thicker plates normally used in bridges. The thicknesses used for the design considered in this paper are 4 mm for the trapezoidal profiles and 7 mm for the deck plating. Furthermore, the trapezoidal stiffeners in bridges are higher than those discussed here.

The use of trapezoidal profiles results in a closely stiffened panel, which is especially advantageous for wheel loaded structures. Therefore, highly loaded car decks are considered as a possible future application of VHTS 690 in ship structures. Fig. 1 shows a principle sketch of the arrangement of a car deck for trucks in a fast ferry as well as details of the design with trapezoidal stiffeners and their intersection with a web frame. In this design the width of the deck plate fields becomes 350 mm. The small unsupported span of the deck plate fields allows for an economic design because of the possible reduction in plate thickness.

The total loading of ship structures is the result of superimposed global and local loads. The global loads mainly consist of bending moments caused by the unbalanced distribution of weight and buoyancy on the one hand and by waves on the other hand. The local loads are created by the truck wheels running over the deck structure. Assuming that in our case the considered truck deck is located close to the neutral axis of the ship's hull, see Fig. 1, the global loads can be neglected and only the wheel loads are considered.

As ship structures are loaded dynamically, the introduction of a new material in combination with a novel design into shipbuilding requires the investigation of the fatigue behaviour. Since the geometry of the deck structure is complex, fatigue cracks may start from various locations, see Fig. 2. The investigation was made by

means of an extensive test program including simple, semi-complex as well as full-scale tests. The loading of the full-scale models was done in a realistic way by an ordinary truck wheel. Most of the tests were accompanied by finite-element calculations.

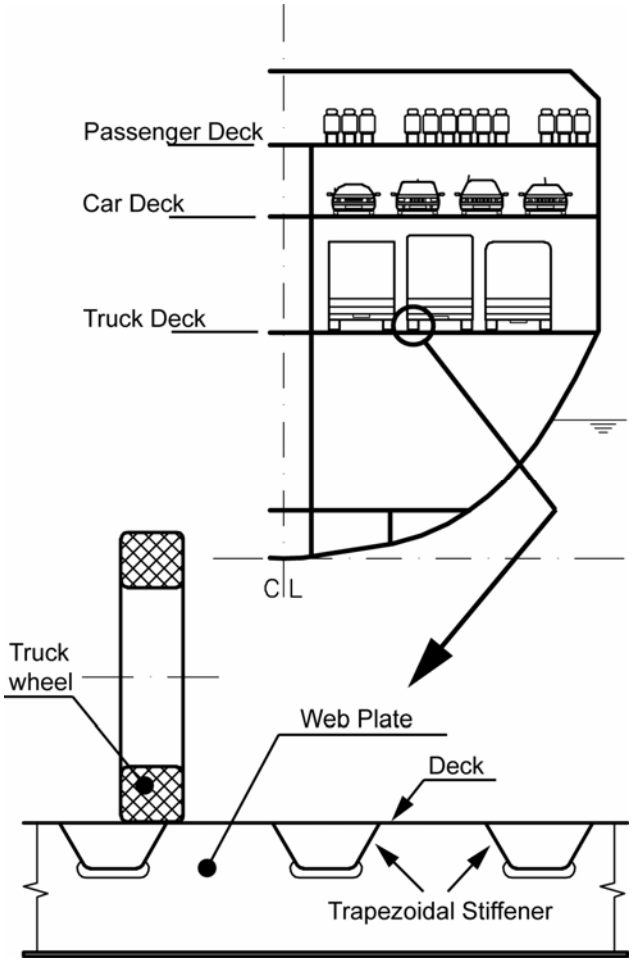


Fig. 1: Truck deck stiffened by trapezoidal profiles

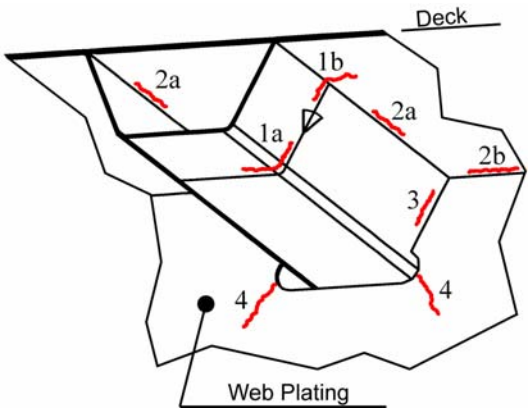


Fig. 2: Possible locations of crack initiation

2 JOINT OF TRAPEZOIDAL PROFILES (SIMPLE SPECIMENS)

The butt weld connecting two parts of trapezoidal profiles has been investigated by the tests described here. The possible crack locations 1a and 1b (see Fig. 2) can be found at that butt weld. The ship structure is built by assembly of blocks. While the trapezoidal profiles can be welded to the deck plating in a convenient position and the deck panel is turned around after the welding process, the assembly of blocks makes welding in restrained welding positions necessary. Furthermore the welding position changes from overhead to upwards position at the bent corner of the trapezoidal profile. A reduced welding quality can be expected by these circumstances and hence a shortened fatigue life. A second problem concerning the butt weld between the trapezoidal stiffeners is the need for a permanent backing strip inside the hollow section made up by the profile and the deck plating, which can only be accessed from the outside. The tack welds required for fastening the backing strip to the inside of the profile and the end of the weld seam can be additional initial points for fatigue cracking. In order to account for the effects of the different welding positions, the specimens were fabricated under realistic conditions. After the profiles webs were welded to a plate in order to simulate the connection to the deck plate, the butt welds were welded in the overhead and upwards position. In a final step the profiles containing the butt weld were sawn into simple specimens, see Fig. 3. The sawing of the specimens resulted in two specimen types differing in shape: The first one is flat, it contains the weld seams produced in the overhead and upwards positions, the second one is taken from the corners of the profiles and therefore has a bent shape. The bent specimens contain the change of the welding positions, hence these types are expected to have a shorter fatigue life than the flat ones. As shown in Fig. 4 for the bent specimens, clamping jaws were fitted which allowed for distributed loading of the specimens under pure tension.



Fig. 3: Simple specimens sawn out of a trapezoidal profile



Fig. 4: Clamping of specimen type with bending radius

In Fig. 5 the results of the fatigue tests of the simple specimens are presented. The failure criterion was total fracture of the specimen. The tests were conducted at three different load levels to be able to assess the slope of the S-N curve. The majority of the tests was carried out at a stress range of $\Delta\sigma = 200$ MPa. In Fig. 5 those results are drawn slightly above or below that stress range in order to make the illustration clearer. The evaluation of the test series was made according to the IIW-Recommendations (Hobbacher, 1996). The characteristic fatigue life was determined to be $\Delta\sigma = 98.3$ MPa for a probability of survival $P_S = 97.5\%$ at 2 million cycles. This value exceeds the detail category FAT 71 associated with butt welds on backing strips.

The assumption that the bent specimens taken from the corners of the profile would exhibit a shorter fatigue life than the flat ones was not confirmed. Only the scatter of their results is higher than it is for the flat ones. The slope of the S-N curve was determined to m = 3.39.

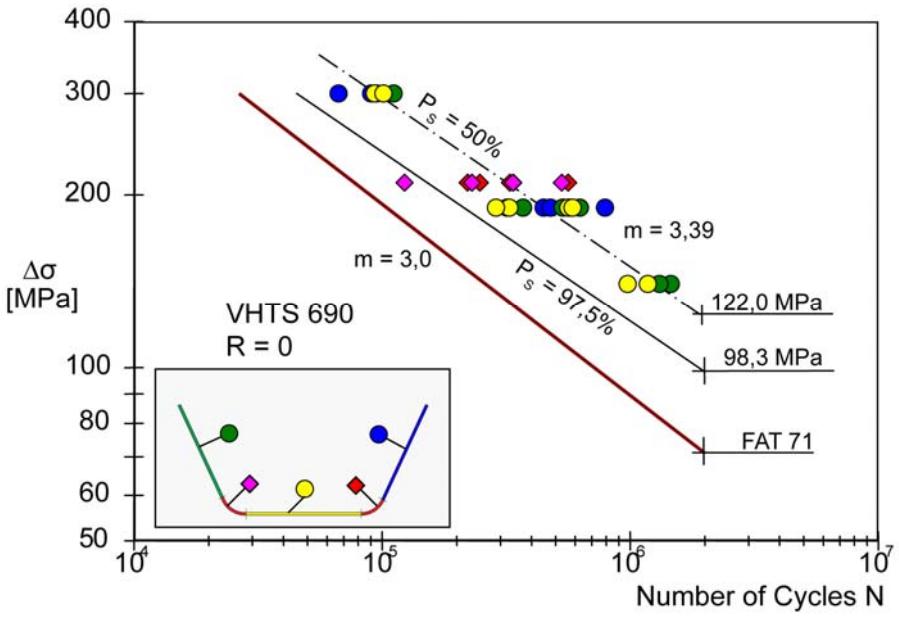


Fig. 5: Test results of the simple specimens

3 JOINT OF TRAPEZOIDAL PROFILES (SEMI-COMPLEX SPECIMENS)

The simple specimens described above do only partly contain the influence of residual stresses caused by the fabrication process. Ways to take those residual stresses into account are to perform the tests at a high stress ratio (R = 0.5) or to lower the results gained at a stress ratio R = 0 by 20% (Hobbacher, 1996). In the present case it was chosen to consider the effect of the residual stress by testing semi-complex specimens which are assumed to contain those stresses because of their size.

Testing of complete sections of trapezoidal profiles and the associated deck plating under tension generates problems concerning the load introduction. However, pure tension load is not realistic, as we assumed the considered deck structure to be located close to the neutral axis of the hull's section. The results of the simple specimens have shown that the point of crack initiation is independent from the position on the profile. Thus, four-point bending tests seem to be appropriate. Fig. 6 shows the principle of the four-point bending test. The ends of the specimens are simply supported. The loads are introduced via two transverse webs. By this arrangement the lower flange of the trapezoidal profile is stressed in tension. The length of the specimens was 1.2 m, the distance between the web plates for load introduction was 0.4 m. On the one hand it was assured by these dimensions that the loads did not become higher than necessary, and on the other hand the stress distribution in the region around the butt weld on half the specimen length was undisturbed.

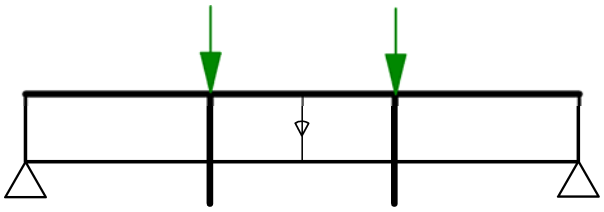


Fig. 6: Principle of the four-point bending test

The geometry of the four-point bending specimen was analysed by means of the finite element method (FEM). Variants with and without a cutout in the web plates around the lower flange of the trapezoidal profile were investigated. 20-noded solid elements were used for the calculations. The finite element mesh was built according to the rules for the determination of structural hot-spot stresses (Niemi et al., 2004), i.e. one element is arranged over the plate thickness and two elements having a length equal to the plate thickness are placed in front of the weld toes. In Fig. 7 the results of the FEM calculations are presented. The colours indicate the distribution of the major principal stresses, the numeric values are linearly extrapolated to the weld toe. The load for the finite element calculations was assumed such that a nominal stress of σ_n = 100 MPa acts in the lower flange of the specimen. The comparison of the results of both variants in Fig. 7 clearly shows that the cutout is essential to avoid the specimens to crack at the transverse plates.

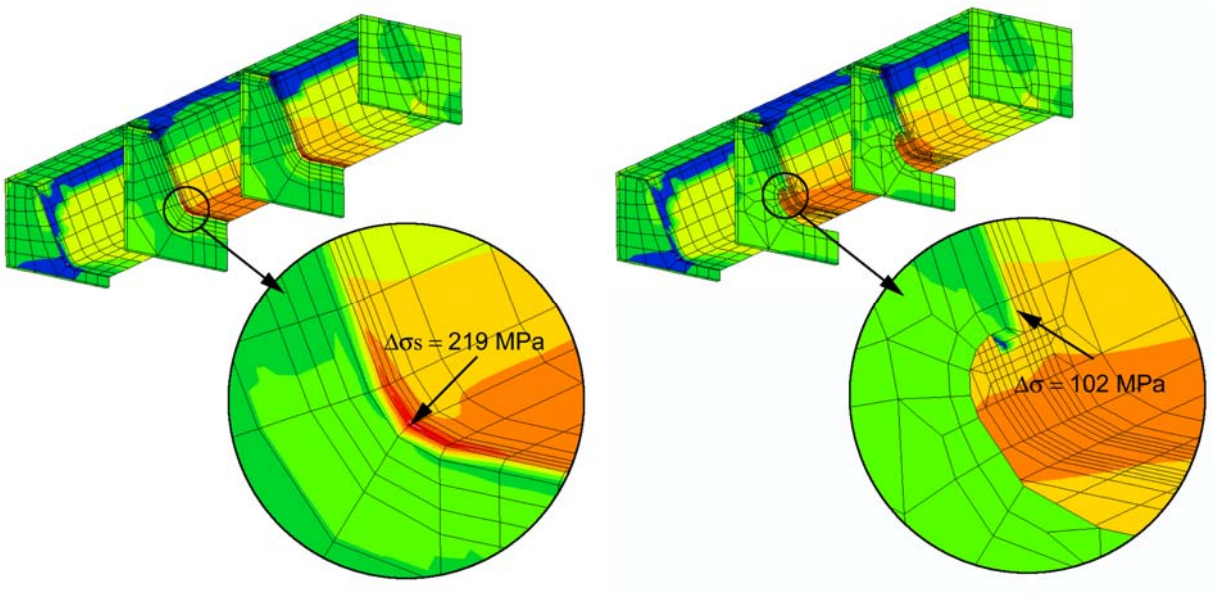


Fig. 7: Results of FEM calculations without cutout (left) and with cutout (right)

Fig. 8 illustrates the results of the four-point bending tests. For these tests the failure criterion was a crack length exceeding 100 mm. Eight specimens were available for this test series, hence all specimens were tested at the same load level. For this reason a direct determination of the slope of the S-N curve using test data was not possible. As usual for welded connections the slope of the S-N curve was assumed to be m = 3.0. The calculated characteristic fatigue life of $\Delta\sigma$ = 92.7 MPa for a probability of survival of P_S = 97.5% at 2 million cycles is nearly the same as what was found from the simple specimens. Therefore, no additional influence of residual stresses could be demonstrated. The characteristic fatigue life exceeds the detail category FAT 71 even if it would be lowered by 20%.

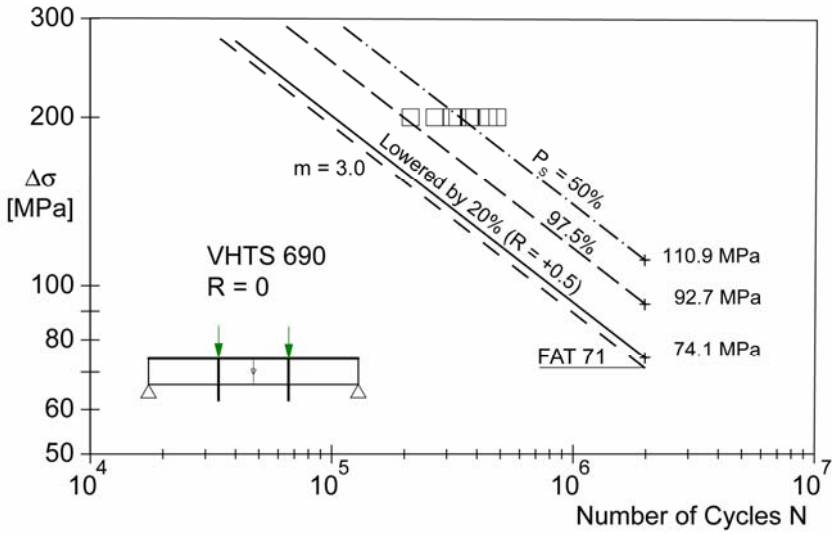


Fig. 8: Test results of the four-point bending tests

4 WEBFRAME INTERSECTION

An unavoidable design detail is the intersection of the longitudinal trapezoidal profiles with the transverse webs. The fatigue strength of the free plate edge at the cutout of the webframe intersection (crack location no. 4 in Fig. 2) was determined by means of three-point bending tests. In Fig. 9 the geometry of the three-point bending specimen is presented. The specimen was simply supported at the end plates, the load was introduced at the end of the web plate on half the models length.

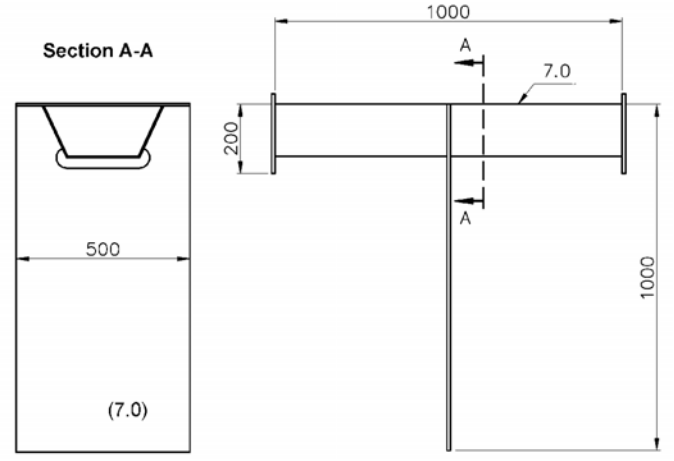


Fig. 9: Geometry of the three-point bending specimen

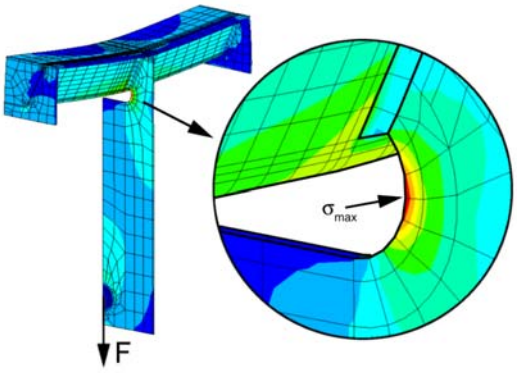


Fig. 10: First principal stress S1 around the cutout

In order to determine the necessary test load, the geometry of the specimen was analysed by finite element calculations. Fig. 10 shows a finite element model (half model) together with the distribution of the first principal stress around the cutout. The maximum stress σ_{max} at the free edge is 2.56 MPa per kN load.

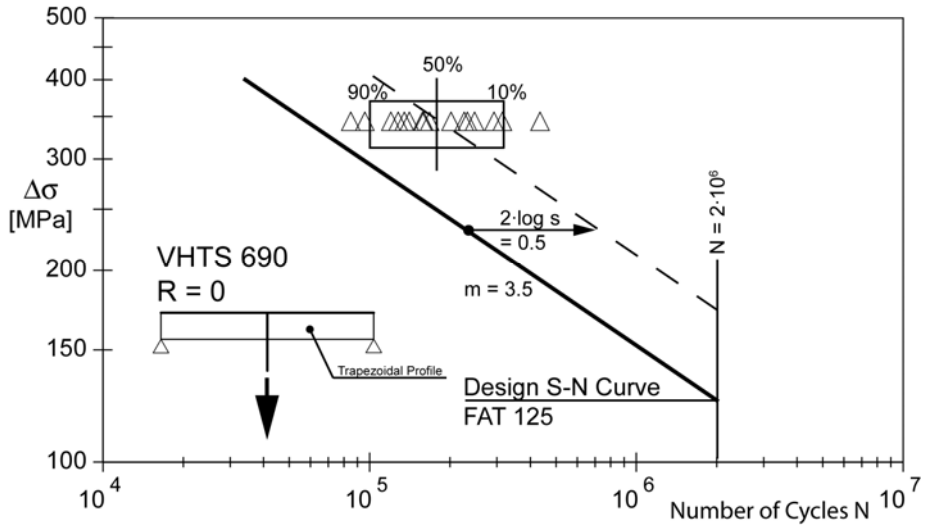


Fig. 11: Results of the three-point bending tests (Δσ = local stress at cutout)

Fig. 11 presents the results of the three-point bending tests. The tests have shown that free plate edges made of VHTS 690 can be assessed using the design S-N curve FAT 125 with slope exponent m = 3.5 at least for radii which are usual in shipbuilding, in this case 30 mm.

5 FULL-SCALE TESTS

The investigation of the overall design of the truck deck structure was done by means of full-scale tests. Particularly the susceptibility of the points 2a and 2b (Fig. 2) to fatigue cracking can be investigated with such tests. Fig. 12 shows the model of the deck structure. The model comprehends two web frame spacings in longitudinal direction and three trapezoidal profiles in transverse direction. Thus, the model is 4.8 m in length and 2.1 m in width. By the choice of these dimensions it is ensured that the model contains all relevant fabrication influences around the centre trapezoidal profile. On half the models length, a transverse web frame is arranged. The model is surrounded by a framing system. Three models were fabricated under realistic conditions at Flensburger Schiffbau-Gesellschaft.

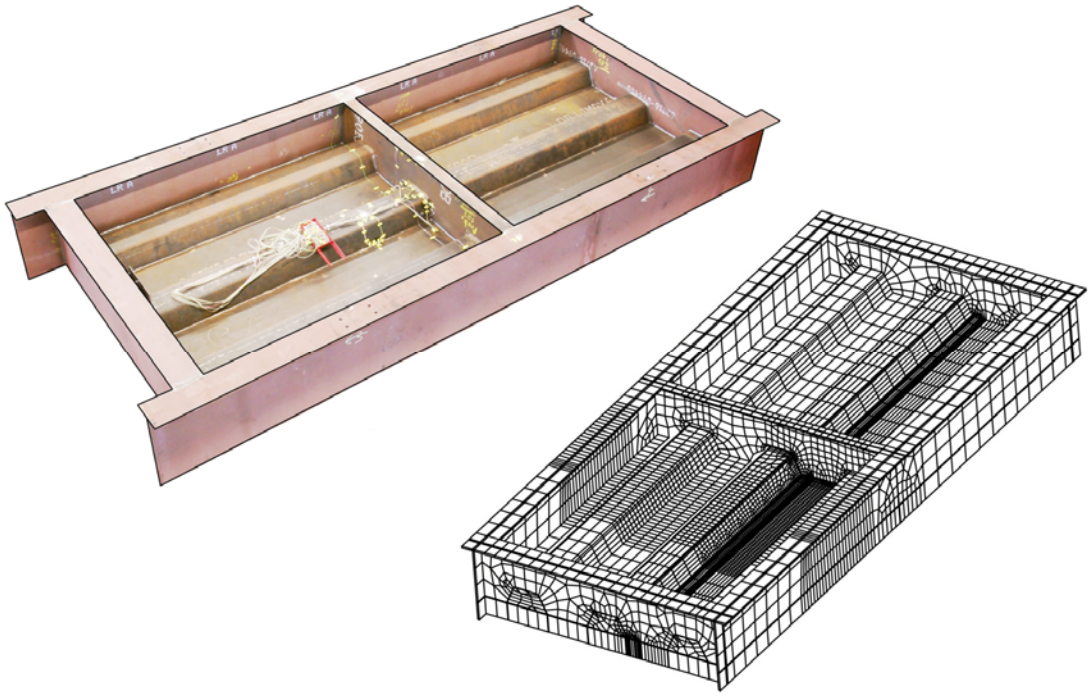


Fig. 12: Full-scale model of the deck structure and FEM idealisation (View on lower side)

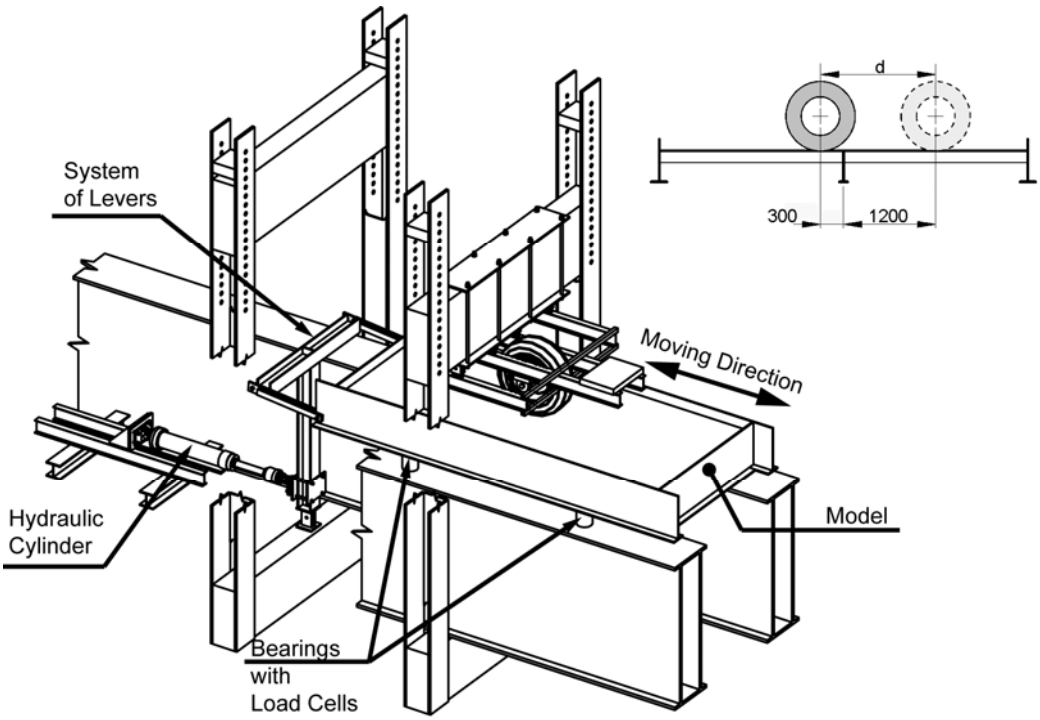


Fig. 13: Test setup for full-scale tests

The wheel loads were brought up in a realistic manner in the test setup shown in Fig. 13. The deck structure is moved back and forth over a distance of 1.5 m. The most critical position of the wheel was found to be on the unsupported plate field directly above a trapezoidal stiffener. This plate field is overrolled from its centre to the web frame, which is totally crossed. The structure is supported by four sliding bearings with load cells to monitor the load. The wheel load is generated by an adjustable weight acting on the wheel over a lever system. An ordinary truck wheel was used in the tests. The load was adjusted to 29.4 kN.

The fatigue behaviour of the models was predicted by means of the structural hot-spot stress approach. The stresses were calculated using the finite element method. Fig. 13 illustrates the finite element model. 20-noded solid elements were used to model the structure. In the relevant areas the weld seams were modelled also.

The analysis gave the root of the longitudinal weld of the trapezoidal stiffener at the web frame intersection as the point with the highest stresses, see Fig. 14 and Fig. 15.

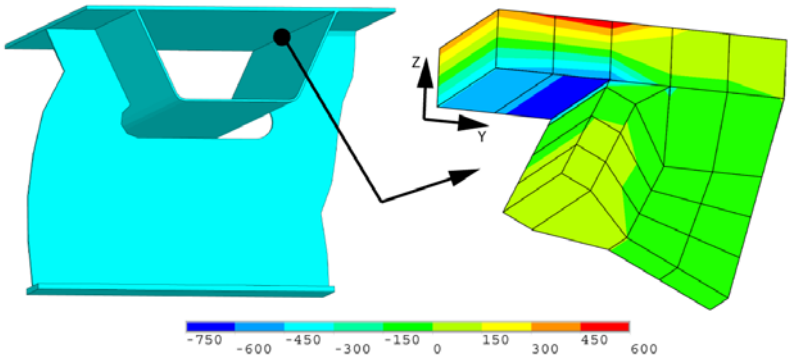


Fig. 14: Stress in y-direction [MPa]

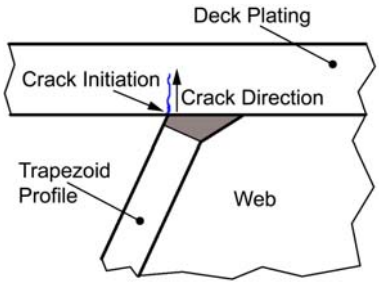


Fig. 15: Expected crack

As the wheel runs asymmetrically over the web frame, two consecutive stress ranges $\Delta\sigma_1$ = 705 MPa and $\Delta\sigma_2$ = 559 MPa are relevant for the fatigue loading (see Fig. 16). A calculation of the Miner sum using a structural hot-spot S-N curve and a cumulative damage ratio D = 1.0 results in 19139 load cycles to failure at a probability of survival P_S = 50%. No bonus factor was assumed for the fact that the stresses are fully compressive. Possible cracks could be observed from the upperside of the deck plating only. The first cracks were found after 78,000 to 140,000 load cycles in the different models. The crack location as well as its direction was in good agreement with the prediction. However, the predicted number of cycles to failure was conservative which is probably due to the fully compressive stress ranges. In Fig. 17 the measured crack length and the prediction are drawn against the number of cycles. The crack starts later than anticipated. It shows also a long remaining life time before critical situations with very long cracks occur.

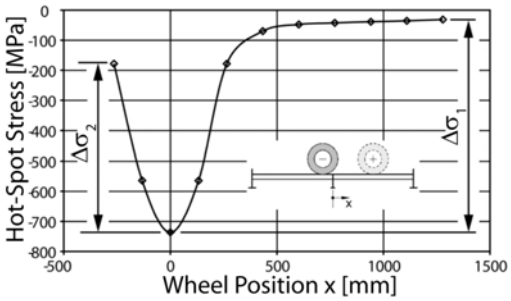


Fig. 16: Calculated hot-spot stresses vs. wheel position

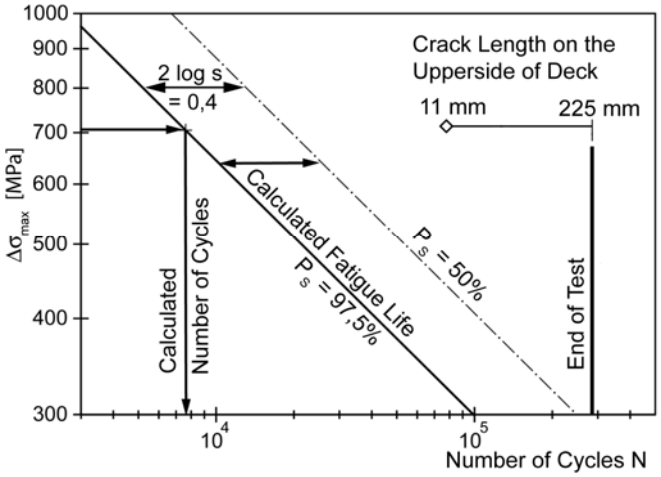


Fig. 17: Predicted fatigue life and measured crack length vs. number of cycles (First model)

6 CONCLUSIONS

A comprehensive program of fatigue tests was conducted in order to verify the fatigue behaviour of truck decks for ferries made of very high tensile steel and using an unconventional design with trapezoidal profiles. The tests with simple and semi-complex specimens gave slightly higher fatigue lives than predicted with the design recommendations. By this a fatigue design based on common approaches is found to be appropriate and the assumption that the fatigue life is generally independent from the yield strength of the material is confirmed.

The structural hot-spot stress approach was able to predict the location as well as the direction of the crack in the full-scale tests correctly. The calculated number of cycles to failure was conservative. One reason for the longer fatigue life gained in the tests could be the positive influence of mean stress. The location of crack initiation in the tests had a compressive stress state closing the crack. The deck structure showed a high remaining life time before critical situations occur, i.e. long cracks affecting the structural integrity. The crack propagation rate remained stable within the test.

The fatigue assessment of the investigated structures in real designs still requires the definition of a realistic load spectrum, describing the number of load cycles as well as the distribution of truck wheel loads and transverse positions relative to the stiffeners.

7 ACKNOWLEDGEMENT

The authors like to thank the European Commission for funding the FasdHTS project and the partners contributing to the work done in this project: ÅF Industriteknik (S), Bureau Veritas (F), Chalmers University of Technology (S), Chantiers de L'Atlantique (F), Dillinger Hüttenwerke (D), Germanischer Lloyd (D), Van der Giessen-de Noord (NL), Instituto Superior Técnico (P), Lisnave (P), Royal Schelde Shipyard (NL) and TNO (NL), who were responsible for the project co-ordination.

8 REFERENCES

Hobbacher, A. Ed. (1996): Fatigue design of welded joints and components. Abington Publishing, Cambridge (UK)

Janssen, G. (2004): Application of High Tensile Steel 690 in Fast Ships. 9th International Symposium on Practical Design of Ships and other Floating Structures (PRADS)

Kolstein, M.; Wardenier, J.; Cunninghame, J.R.; Beales, C.; Bruls, A.; Poleur, E.; Caramelli, S.; Croce, P.; Carracilli, J.; Jacob, B.; Leendertz, J.S.; Bigonnet, A.; Le Pautrmat and Lehrke, H.P. (1996): Fatigue Strength of Welded Joints in Orthoptropic Bridge Decks. Proceedings of the International Conference on Welded Structures in Particular Welded Bridges, Budapest, 2./3. September 1996, Hungary

Machida, F.; Mike, C.; Hirabayashi, Y.; Tokida, H. and Shimozato, T. (2003): Fatigue of Weld Connections to Trough Stiffeners in Orthotropic Steel Bridge Decks. IIW-Doc. XIII-1972-03, Int. Institute of Welding

Niemi, E.; Fricke, W. and Maddox, S. (2004): Structural Hot-Spot Stress Approach to Fatigue Analysis of Welded Components – Designer's Guide. IIW-Doc. XIII-1819-00/XV-1090-01, Int. Institute of Welding

Direct fatigue analysis for repair optimization

Nolwenn Lorans, Cristian Bran

Bureau Veritas, La Defense, Paris

Abstract: Fatigue calculation on ship structural details is not an "exact science". However, using probabilistic tools, one can estimate the design fatigue life when studying the response of the structure to a given sea environment. In particular, this type of analysis can be used to optimize repairs of failures due to fatigue. Depending on the future planned for the ship (remaining life, trading route, cargo transported…) appropriate remedial cost effective changes are studied (replacement or reinforcement of the spots with failures).

Acting as Classification Society or as consultant, Bureau Veritas has the opportunity to perform fatigue studies on ships and offshore units and also to compare the results with the return of experience. This is a good opportunity for further development and validation of the fatigue methodology.

This paper deals with repair optimisation by direct FEM analysis. The structural details are modelled accurately in order to calculate their design fatigue life or probability of crack in a certain period. When the fatigue behaviour is not satisfactory (design fatigue life lower than applicable criteria), different options are modelled and tested, and then adequate solutions are proposed in order to obtain the desired safety level.

A particular case is presented about a crack found in a detail of an LNG carrier during a survey.

1 INTRODUCTION

Fatigue is with corrosion the main cause of cracks in ships in service. Therefore it is very important to be able 1) to foresee where cracks will appear and 2) to validate a repair quickly.

In Bureau Veritas Marine department finite elements are used to model ships in service to prepare an inspection or when cracks are discovered. FE modelling of the repair proposals makes it easier to select the most adapted one.

This paper will first describe BV methodology to compute fatigue life, and then will apply it to the selection of a repair proposal for a crack in the upper knuckle of an LNG carrier.

2 METHODOLOGY

2.1 Finite Element Model

First a three-holds long model is built to assess the global behaviour of the ship.

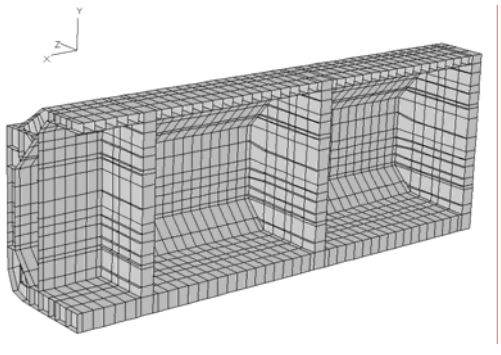


Figure 1. Three holds long coarse mesh model

Then the mesh is refined locally to take into account the secondary supporting members i.e. ordinary stiffeners.

Finally the detail is refined again using 4-nodes thin shell elements, until the mesh elements are the size of the plate thickness to enable a faithful calculation of the stress gradient.

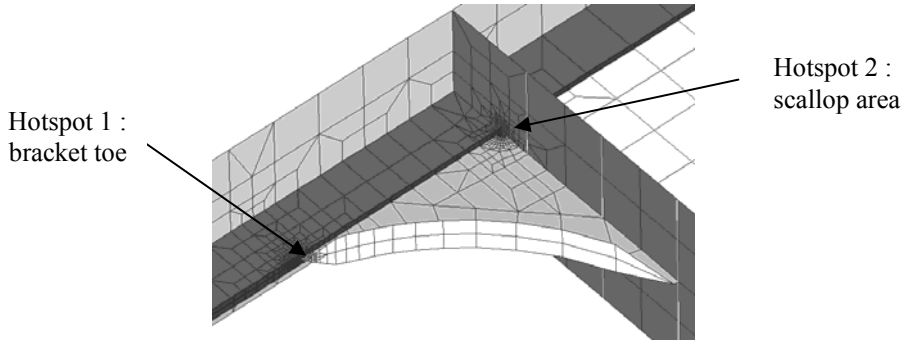


Figure 2. Fatigue fine mesh of 2 hot spots in a bracket.

2.2 Load cases

Representative loading conditions have to be studied, depending on the type of the ship (LNG, tanker, bulk carrier…), usually the most severe full and ballast conditions for the detail considered.

For each representative loading condition four load cases are applied, combining sea pressure and internal loads:

Table I. Description of load cases.

Load case	Wave direction	Wave height	Acceleration
A	Head sea	H_1	none
B	Head sea	$H_1/2$	Vertical acceleration
C	Beam sea	H_2	70% horizontal acceleration
D	Beam sea	$H_2/2$	100% horizontal acceleration

The forces applied (pressures, accelerations, moments…) are load ranges and correspond to crest minus trough or internal maximum minus internal minimum.

- Head Sea (wave coming from ship's front):

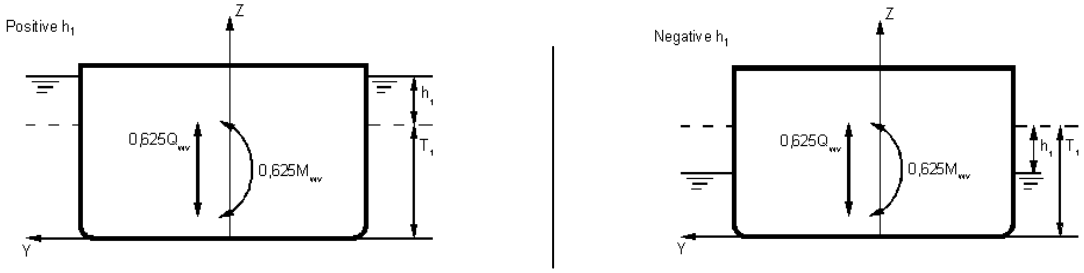


Figure 3. Wave loads in load case "A", crest and trough

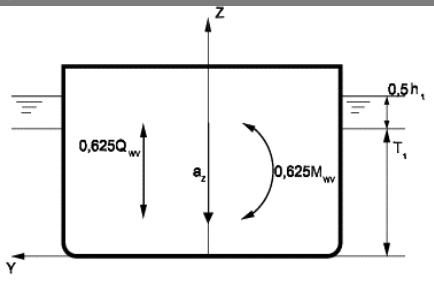


Figure 4. Wave loads in load case "B"

- Beam Sea (wave coming from ship's side):

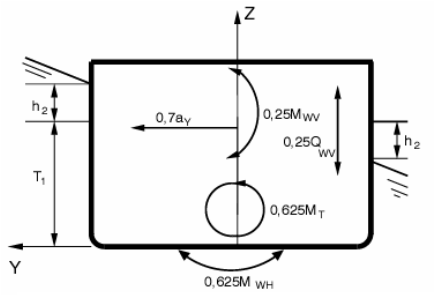


Figure 5. Wave loads in load case "C"

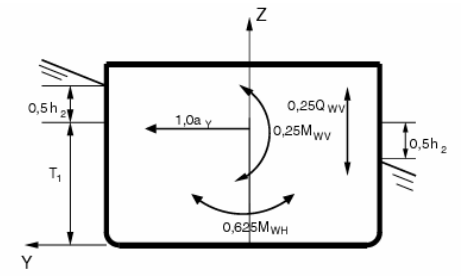


Figure 6. Wave loads in load case "D"

Extracted from the Reference 1, Part B, Chapter 5, Section 4

The wave selected is the one with the probability of 10^{-5} i.e. the wave which appears once every 7 days approximately.

2.3 Stress range calculation

The geometric stress is directly obtained from the finite elements model, either directly in the element nearest the discontinuity, or by linear extrapolation of the stress in the two adjacent elements. A stress range is obtained for each load case A, B, C, D and for each loading condition. This stress takes into account the influence of the geometry of the detail but not the characteristics of the construction.

For welded joints the geometric stress range is multiplied by the notch factor K_f to take into account the weld profile.

$$K_f = \lambda \cdot \sqrt{\frac{\theta}{30}} \qquad (1)$$

With λ a coefficient characterising the weld configuration and θ the mean weld toe angle, in degrees, without being taken less than 30°. θ may be taken equal to 30° for butt welds and 45° for T-joints or cruciform joints, unless otherwise specified.

2.4 Fatigue life calculation

2.4.1 S-N curves used

Only one S-N curve is used irrespective of the structural detail. The detail configuration is already taken into account with the notch factor.

The mean S-N curve is the UK Department of Energy curve class B:

$$N \cdot \Delta S^m = K_{50} \qquad (2)$$

Where m = 3, the slope of the S-N curve changes at $N = 10^7$ cycles to m=5;
$K_{50} = 1.342*10^{13}$, mean value of K for 50% probability of failure.

The design S-N curve used corresponds to 2 standard deviations below the mean curve i.e. 2.5% probability of failure.

2.4.2 Corrections applied

- Influence of compressive stress:

Only 40% of the compressive part of the stress range are taken into account since it contributes less to fatigue.

- Influence of plate thickness:

The S-N curve coefficient K_{50} is corrected according to the following formula if the plate thickness is greater than 22mm:

$$K_{50}' = K_{50} \cdot \left(\frac{22}{t} \right)^{0.3} \quad (3)$$

Where t is the plate thickness.

2.4.3 Damage cumulation

The damage is calculated for each loading condition by combining the four damages obtained for each load case A, B, C and D. (ref. 1 part B, chap. 7, sec. 4, 3.1.2)

Then the damages of the two loading conditions are combined taking into account the probability of each draught.

2.5 Strategies known to improve a detail

Several means are already known to improve fatigue behaviour. They are not the same whether the ship is at design stage or in service, if the crack has already appeared or not. The following ones are for ships in service:

- Increase the thickness (with plate inserts);
- Improve the shape of cut-outs;
- Soften bracket toes;
- Add stiffeners or backing brackets;
- Drill a hole to release the stress (short term repair);
- Grind the weld.

The analysis of the causes of high stress ranges helps to find specific efficient solutions.

3 CALIBRATION

This methodology has been validated through the large return of experience that BV has had for many years thanks to its position of classification society.

However it may happen that some assumptions or standard values used in the calculation do not correspond to the ship's data. Construction quality, environment or corrosion state influence a lot the fatigue life so they have to be adapted to the case analysed.

3.1 Construction quality

The calculations are performed assuming standard weld quality. It may happen that the quality of weld is quite poor and this influences a lot the calculated fatigue life through the coefficient λ. For example, as shown in Table II, in some configurations for a continuous weld λ is equal to 1.8 whereas if the weld is not continuous this coefficient must be taken equal to 2.9. On the contrary if the weld is grinded the coefficient λ is decreased from at least 0.2.

Table II. Influence of weld quality on coefficient λ

Detail	not grinded	grinded
	1.80	1.60
	2.90	2.55

3.2 Sea state

The sea parameters used for calculation are mean ones, corresponding roughly to North Atlantic data. Some ships are confronted to a different environment, more or less severe. In this case a coefficient depending on the ship's routes may be applied on the damage.

3.3 Corrosion

In some cases the calculation may find a fatigue life higher than the one experienced by the details. On site observations may show that the plates are much corroded. Corrosion decrease a lot the fatigue life of a detail, but is difficult to take into account in a calculation. Indeed, the cause is not only the decrease in plate thickness, which could be input in the model, but also the asperities on the plate, and that are impossible to model.

4 APPLICATION

4.1 Presentation

The ship is a 25 year old LNG carrier which was analysed with Finite Element Model before a survey in dry dock. This type of analysis is used to drive the attention of the surveyors on the suspected weak spots of the ship. Figure 7 shows a transverse section of this ship. This type of design is known to have hot spots in the lowest knuckles i.e. spots 1 and sometimes 2 on the figure. But this time cracks were found in spot 3 in almost every frame.

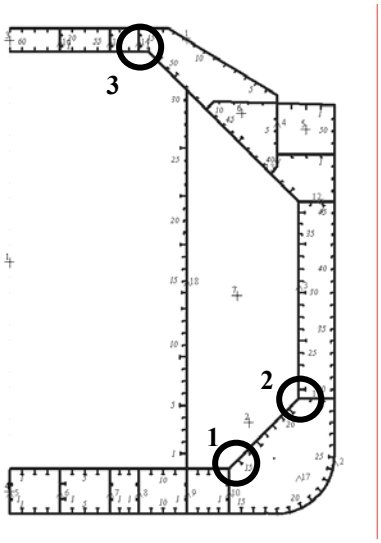


Figure 7. Midship section with main hotspots

4.2 First calculation

A three holds model was built (see figure 8) and refined in the areas 1, 2 and 3 (fatigue fine mesh shown in figure 9)

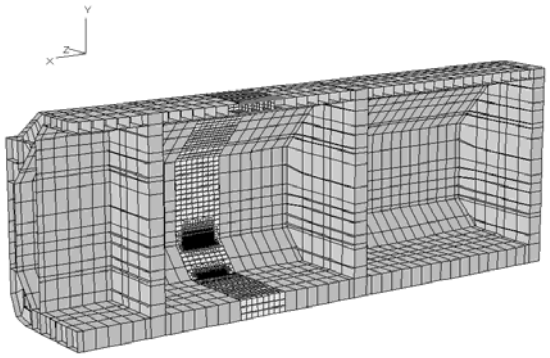


Figure 8. Coarse and fine meshes

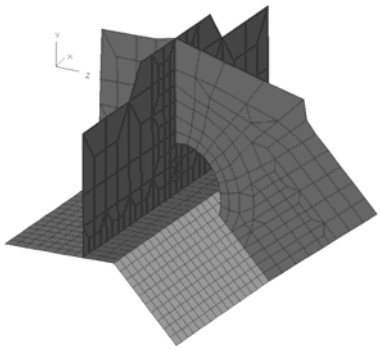


Figure 9. Fatigue fine mesh for hotspot 3

The computed fatigue life for hotspot 3 was 30 years. The ship was 25 years old but had been sailing for only 10 years and almost 90% of the details were cracked.

4.3 Calibration

The fatigue life of 30 years was obtained with a model in accordance with the drawings and assuming a standard weld quality, in particular a weld toe angle $\theta = 45°$.

In reality the scallop shape does not correspond to the drawings, and the weld toe angle is not far from 90°, as can be seen in figures 10 and 11.

With these new elements the fatigue life computed dropped to 11 years.

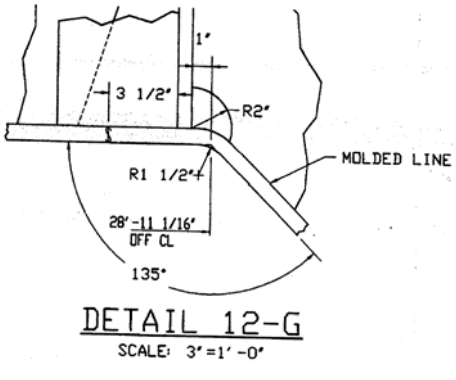


Figure 10. Drawing for spot n°3.

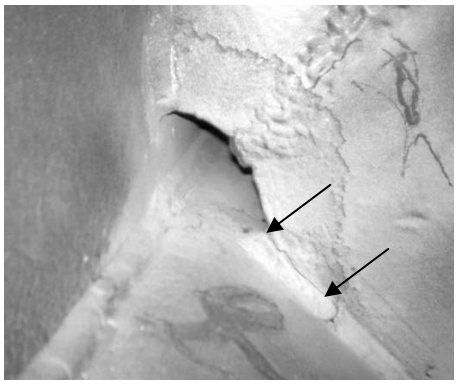


Figure 11. Picture of spot n°3 with crack

4.4 Repair proposal

4.4.1 Collar plate

The first repair proposal was to fit a collar plate to close every scallop (see figure 12). This increased drastically the fatigue life to 95 years, but was too long to perform before the ship left the shipyard. In addition there is a risk of damaging the insulation while welding the collar plate (some cracks are very close to the inner hull).

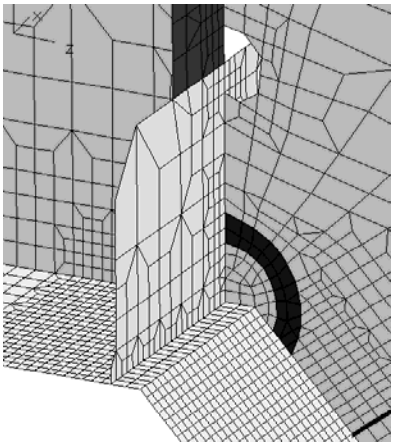


Figure 12. Finite Element Model of detail with collar plate.

4.4.2 *Hole and slot*

The shipyard proposed to drill a hole above the crack end linked with a slot to the scallop to release the stress. This solution is only a short-term repair because it stops the crack propagation but does not reset the damage. In addition, the stress on the other end of the scallop is increased. However it is much easier to perform.

4.4.3 *Improve scallop shape*

The third solution was to increase the scallop radius to eliminate the crack and improve its shape at the same time to obtain a nice toe angle. This would also be a long-term solution.

The following figures summarize the solutions proposed:

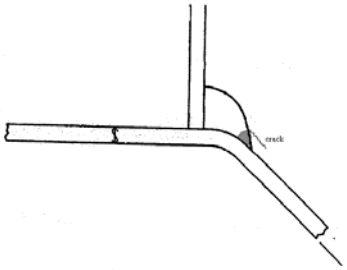


Figure 13. Original scallop with crack

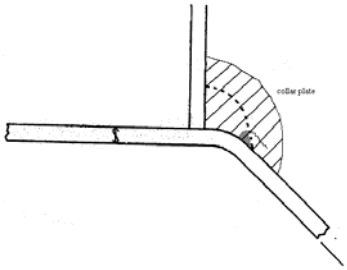


Figure 14. Collar plate: long-term repair

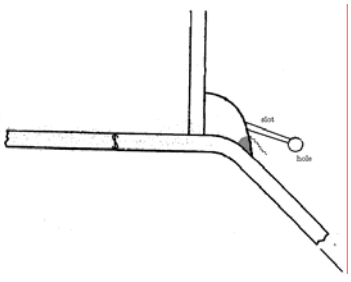


Figure 15. Hole and slot: practical repair

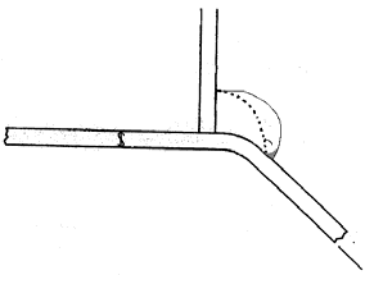


Figure 16. Bigger scallop: long-term repair

Since those cracks were not expected there was not enough time to repair all of them before the ship left the shipyard. They were located in a dry part of the ship, so easy to monitor and not causing any leakage or

endangering the ship's integrity. It was therefore decided that they would be repaired at the next stop in a shipyard, and carefully monitored meanwhile.

5 CONCLUSION

This paper has presented Bureau Veritas fatigue methodology using Finite Element Models to calculate stresses due to structural discontinuities.

This methodology has been validated against the return of experience of the Class Society.

Finite Elements are worthwhile in fatigue analyses:

- It allows to be sure that the repair is needed, and efficient;
- Among the efficient solutions, it allows to select the most adequate one;
- Showing the owner the repair recommended and its validity convinces him more easily.

6 REFERENCES:

1. Bureau Veritas, Rules for the Classification of Steel Ships, NR 467, April 2005
2. Bureau Veritas, Fatigue Strength of Welded Ship Structures, NI393, July 1998
3. International Institute of Welding, Recommendations on Fatigue of Welded Components, April 1996
4. IACS Recommendation n°56, Fatigue Assessment of Ship structures, July 1999

Parametric Study of Crack Growth In Cylindrical Aluminum Shells with Inner reinforcing foam layer

Ayari Fayza[a] Lazghab Tarek[a] Chelbi Lotfi[a]

[a]Mechanical Engineering Department, Institut Préparatoire aux Études de l'Ingénieur Université TUNIS El Manar,

Abstract The occurrence of cracks in aging aircraft fuselage is major problem for the aircraft industry. The geometry and loading conditions of a longitudinal crack in pressurized cylinder causes its edges to bulge out generating a complex stress field around the crack tips; this is known as the 'bulging effect'. The shell curvature and pressure in the fuselage contribute to this phenomenon. A proposed solution to reduce the effect of bulging for this type of crack it to apply a layer of polyisocyanurate foam to the inner side of the fuselage near the crack site. This layer will bond to the shell and has the effect of reducing the bulge and the Stress Intensity Factor (SIF) at the crack tips.
In the present study the effect of application of a foam layer to a longitudinal crack in a pressurized cylindrical shell is assessed. Nonlinear Finite Element Analysis (FEA) in conjunction with the Modified Crack Closure Integral (MCCI) technique is used in order to evaluate the effect of bulging on the crack's SIF. Parameters considered in this study include shell radius, shell thickness, crack length, foam thickness and pressure.
Numerical results are compared with existing experimental data and the effect of foam thickness on the bulging factor at several shell configurations is presented. Results indicate that the bulge factor could be reduced by as much as 63% depending on shell configuration, foam thickness and pressure.

1 INTRODUCTION

Cracks are a common occurrence in aging aircraft. In light of this fact, fuselage structures are designed with a fail safe philosophy in mind. In such designs a fuselage with a few small size cracks is expected to have enough residual strength to operate in safe conditions. However, in some instances these cracks may originate at closely spaced locations (especially at the rivet sites) and during growth these cracks could coalesce to result in a super sized crack that will reduce the residual strength of the fuselage dramatically. This phenomenon is known as Widespread Fatigue Damage (WFD) it is symptomatic of aging aircraft fleet. For this reason control of crack propagation rates in ageing aircraft fuselage structures is of utmost importance.

In an aircraft fuselage structure the first line of defense against crack growth are the primary and secondary support structures such as frames and stringers that would carry some of the structural load and halt crack growth. However, in some cases this may not be enough and cracks continue to grow. As a remedial solution, it is proposed to apply a foam layer to the inner side of the skin at the area of the detected crack. As the foam hardens and bonds to the skin it provides local stress relief and additional stiffness to the shell at the crack tips where crack growth is most likely to occur. This will delay WFD and add life to the fuselage structure.

In the present study the effect of applying a foam layer to the fuselage skin on the bulging of a longitudinal crack is investigated. A parameterized finite element model of the fuselage shell-foam structure is built and used in a nonlinear finite element analysis in conjunction with the Modified Crack Closure Integral (MCCI) technique to evaluate the bulge factor of a longitudinal crack on a pressurized cylindrical shell. The model allows for several parameters to be varied including shell radius, shell thickness, crack length, pressure, axial load, biaxial stress state and foam layer thickness. Several shell-foam configurations are considered and the effect of the foam on bulging is evaluated numerically.

2 BULGE FACTOR

2.1 DEFINITION

Longitudinal cracks in pressurized cylindrical shells are subject to hoop stresses σ_t and axial stresses σ_a and pressure p as shown in Figure 1-a. This produces a nonlinear geometric coupling effect between membrane strains and bending strains in the shell near the crack tips, Rose [1] and Bakuckas [2]. The deformation field around the vicinity of the crack is characterized by an out of plane displacement component in the radial direction of the shell. The loading conditions and geometry of the shell contribute to the generation of a high Stress Intensity Factor (SIF). The SIF of the crack is characterized by a parameter known as the bulging factorβ.

It measures the severity of the SIF in the bulged crack compared to that of a crack in a flat plate in plane stress conditions and subjected to equivalent loading conditions. The bulging factor β is defined as

$$\beta = \frac{K_S}{K_P} \text{ where } K_P = \sigma_t \sqrt{\pi a} \quad (1)$$

K_P and K_S are the SIFs of the cracks in the flat plate and the pressurized cylindrical shell, respectively. Loading conditions for both cases are illustrated in Figure 1-a.

2.2 LITERATURE REVIEW

Extensive research has been conducted on the subject of bulging factors for cracks in cylindrical shells. This subject is of particular interest to the aircraft industry and pipe and vessels manufactures. Most of the experimental results obtained are presented as empirical or semi empirical formulas where the bulge factor is a function of geometry and loading parameters.

Early results were obtained by Folias [3] Erdogan [4] under the assumption of linear elastic deformation. Later, work by Budiman and Lagace[5] established the nonlinear character of the bulging factor. Empirical expressions for the bulge factor at several shell configurations were obtained by Chen [6] and Jeong [7]. Bakuckas established an expression of the bulge factor using results from a parametric nonlinear geometry finite element study [8]. Backukas has recently presented preliminary results on the effect of applying a 3.5 inch (88.9 mm) thick polyisocyanurate foam layer to an aircraft fuselage panel section and has show that out of plane displacement at the centerline of the crack could be reduced by as much as 50% [9].

The objective of the current paper is to study the effect of an additional layer of foam applied to the inner side of the cylindrical shell with a longitudinal crack. Several geometric and loading configurations for the shell and foam are considered.

2.3 MODIFIED CRACK CLOSURE INTEGRAL TECHNIQUE

The SIF of a crack can be evaluated using energy based methods. The SIF is obtained by evaluating the crack energy release rates during its extension. This method is based on the premise that the energy needed to extend a crack is equal to the energy necessary to close it. Several techniques have been developed to calculate crack energy release rates. Some of them are the Virtual Crack Extension Method, Nodal Release Method, Modified Crack Closure Integral (MCCI) technique, etc. Among these techniques, MCCI is one of the most economical methods that can be implemented within the framework of the FEM.

The procedure for calculating energy release rates with the MCCI method is treated by Rybicki[10], Ingraffea [11] and zehnder [12]. Figure 1-b shows a typical mesh of shell elements around the crack tip used in the evaluation of SIF by the MCCI method. The strain energy release rate corresponding to Mode I crack opening and its SIF are evaluated as:

$$G_1 = \frac{1}{2t\Delta a}\left(F_2^{Close}\left|u_2^{top} - u_2^{bot}\right| + F_6^{Close}\left|u_6^{top} - u_6^{bot}\right|\right); \qquad K_S = \sqrt{E_A G_1} \quad (2)$$

Where G_1 is the strain energy release, the remaining terms in equation (2) are defined in Figure 1-b.

3 GEOMETRY AND MODELING

3.1 GEOMETRY

The geometry of the cylindrical shell under consideration is shown in Figure 1-c. This geometry is taken after the shell geometry described in rose [1] with the addition of a layer of foam. The parameters of the shell are, the radius R, the axial length L_a, the circumferential length L_t, half crack length a, thickness of the shell t_A and thickness of the foam layer t_F.

3.2 BOUNDARY CONDITIONS AND LOADING

The shell is subjected to an axial load, and a pressure load that results in axial and hoop stresses given as follows:

$$\sigma_t = \frac{pR}{t}; \qquad \sigma_a = \chi\frac{pR}{t}; \qquad \chi = \frac{\sigma_a}{\sigma_t} = 0.5 \quad (3)$$

Where p is the pressure and χ is the biaxiality ratio of the stress state in the shell. For a cylindrical shell whose both ends are constrained χ=0.5. However, this ratio can be varied with application of an additional axial load to the shell as is the case of an aircraft fuselage where the drag and thrust forces result in additional axial load.

In previous studies of pressurized cylindrical shells nondimensional parameters were introduced to characterize the geometry and the loading conditions by Folias and Budiman respectively [3,5]. These parameters are defined as follows:

$$\eta = \sqrt{\frac{p}{E(t/R)^2}}\sqrt[4]{12\left(1-\nu^2\right)}; \qquad \lambda = \frac{a}{\sqrt{Rt}}\sqrt[4]{12\left(1-\nu^2\right)} \tag{4}$$

η: Loading parameter (non-dimensional) λ: Geometry parameter (non-dimensional)

3.3 FINITE ELEMENT MODEL

A finite element model of the shell-foam assembly was built using the commercial finite element package ABAQUS [13]. The shell section was modeled as 4-noded shell elements with 6 degrees of freedom per node (ABAQUS element type S4R) with reduced integration. The foam layer is modeled as 8-noded continuum element with 3 degrees of freedom per node (ABAQUS element type C3D8). A minimum of two layers of C3D8 elements is used in the radial direction to avoid shear locking. The interface between the foam and the shell was established using Multi Point Constrains (MPC type TIE) requiring coincident nodes from shell and continuum elements to have the same displacements.

The model is parametric, i.e. geometric parameters (R, L_a, L_t, a, t_A, t_F) and mesh parameters (including the size of the mesh refinement zones and number of elements in each zone) may be varied depending on the configuration and the shell geometry to be modeled.

In order to reduce the model size without sacrificing accuracy, five mesh refinement zones have been used to go from a fine mesh at the crack tip to a coarse mesh at the far edges of the shell as shown in Figure 2-a. Mesh transition constraints have been used to accomplish this. The size of the model is further reduced by taking advantage of the double symmetry in the geometry of the shell section. The planes of symmetry are defined as follows, a plane passing through the axis of the section and containing the crack and the other plane is passing through the centerline of the crack and perpendicular to the axis of the shell section. The mesh of the modeled portion of the section is shown in Figure 2-a. The boundary conditions of the model are shown in Figure 2-b.

To insure the continuity of the fuselage in the axial direction the nodes on Edge2 (see Figure 2-b) are constrained to move together in the axial direction when the axial load is applied to them. The value of the axial load is given as:

$$F_{axial} = pRL_t \tag{5}$$

p is the inner pressure applied to the fuselage section. This value can also be given arbitrarily in the model if needed.

The solution of finite element model is obtained using nonlinear geometry assumption and for each configuration the appropriate mesh resolution was determined so that the results obtained are independent of the size of the mesh.

4 MODEL VALIDATION

In order to verify the finite element model, experimental data from two studies of pressurized cylindrical shells have been selected. The first case study is pressurized cylindrical shell with a crack and no foam and the second case study is a pressurized cylindrical shell with a layer of foam applied to it and a longitudinal crack.

4.1 CASE STUDY 1: SMALL PRESSURIZED CYLINDRICAL SHELLS WITH A LONGITUDINAL CRACK

Barwell has conducted a series of tests on thin pressurized cylindrical shells with axial cracks [14]. Several variables were measured experiementally, including the out of plane displacement along the crack and its vicinity. Test specimens have a 6” (152.4 mm) diameter, 27.25 “ (698.5 mm) length and sheet thickness of 0.016 “ (0.406 mm). The specimen is made from clad sheet stock aluminium 2024-T3. The ends of the cylinder are not constrained axially so that no axial stresses are generated (i.e. $\chi = 0$). The pressure applied is 100 psi (0.689 MPa). **Erreur ! Source du renvoi introuvable.**-a Shows the normalized out of plane displacement w/Cw vs. the normalized distance from the crack tip x/a; w radial displacement, x is the coordinate in the axial direction, a is the initial half crack length and Cw is given by

$$C_w = \frac{\lambda^2 pR^2}{2E_A t_A} \tag{6}$$

The mesh density of the FE model was refined until no further changes can be associated with mesh size. Experimental data and FEA model response are both shown in **Erreur ! Source du renvoi introuvable.**-a. It can be seen that the FEA model closely predicted the actual profile of the bulge of the crack. The discrepancy between the model and experiment at the centerline of the crack (x/a=0) maybe attributed to the effect of cladding in aluminum sheet stock that was not accounted for in the model [14].

4.2 CASE STUDY 2: (FUSELAGE PANEL SECTION WITH A REINFORCING FOAM LAYER)

In order to test the capability of the FEA model to represent shell sections with foam layer, experimental data from tests conducted by Bakuckas[9] are compared to model response. The shell section tested is an actual section of a fuselage removed from a retired DC-9 with a longitudinal mid-bay crack. As such the section contains additional load carrying structures such as frames and stringers. The shell geometry and loading conditions given below:
Shell Geometry : R=66"(1676.4mm), L_a=120" (3048mm), L_t=68" (1727.2mm), t_A=.050" (1.27mm), t_F=3.5" (88.9 mm), 2a=5.5" (139.7mm), p=5 psi (34.5 kPa).

The material of the shell under consideration is Aluminum 2014-T6 treated as a linear elastic isotropic material. The material of the foam is polyisocyanurate foam; this material exhibits viscoelastic response at large strains with mechanical properties that depend on its chemical composition, cure time and environment. In the current study the foam is treated as a linear elastic isotropic material. The material properties used are (Aluminum: E_A=*10.50Msi=72.4 GPa,* ν_A=*0.33,* Polyisocyanurate foam: E_F=*600 psi=4.13 MPa,* ν_F=*0.30*[*]*)*

The test was set up in such a way that the frames and stringers took up some of axial and hoop loads generated by the application of pressure. This resulted in a modified biaxial stress of state $\chi=\sigma a/\sigma t$= 0.581 instead of 0.5 for a constrained unstiffened cylindrical shell. A photograph of the tested fuselage section is shown in Figure 3-b. The experimental and numerical graphs of the crack bulge profiles of the fuselage section with and without foam are shown in Figure 3-c. As can be seen, applying a foam layer has reduced the bulging profile of the crack by as much as 50% at the centerline of the crack compared to a predicted 46.5% obtained by the model. The FEA model replicated the shape of the bulge profile closely albeit with systematic over estimation of the out of plane displacement. This discrepancy can be attributed to the fact that the actual structure is stiffer than the modeled structure due to the presence of frames and the stringers and whose effects on the bulge profile is not accounted for in the model. Also, the additional stiffening that comes from bonding of the foam to the frames and stringers in accounted for either. The maximum error was 8.1% at the crack center line.

4.3 COMPARATIVE FEA STUDY

The mesh design of the finite element model used in this paper was first introduced by Rose for cracked pressurized cylindrical shells only [1]. Rose conducted the numerical analysis using the STAGS (Structural Analysis of General Shells) nonlinear finite element code. The current model uses a similar mesh with continuum elements to model the foam layer. The model was built for the commercial FEA code ABAQUS. The boundary conditions of the model are as described previously and the material data is that of aluminum 2024-T3
The effect of varying the non-dimensional parameters λ and η from equations (4) on the bulge factor is investigated. Results in Figure 4 show that responses from the current model and Roses' model to be superimposed thus confirming their equivalence. Figure 4 also depicts the nonlinear dependence of the bulging factor on the load parameter η.

5 PARAMETRIC FEA STUDIES OF FOAM REINFORCED PRESSURIZED CYCLINDRICAL SHELLS WITH LONGITUDINAL CRACKS

5.1 EFFECT OF CURVATURE PARAMETER (λ) AND FOAM THICKNESS ON BULGE FACTOR (β)

A parametric study to determine the effect of adding a foam layer to a cracked cylindrical shell is conducted. The objective of the study is to determine the amount the bulge factor is reduced for a given foam layer. The geometric parameters R and t_S for each shell are sampled from the data sets given in equation(7). For each configuration 2 cracks and 3 foam thicknesses are selected such that (a/R= 0.2, 0.05) and (t_F/R=0.0227, 0.0530, 0.0379). a/R and t_F/R are the normalized half crack length and normalized foam thickness, respectively. All configurations are subjected to a hoop stress σ_t=1000 psi and the biaxiality ratio is χ=0.5. A total of 4×5×2×3=120 shell-foam configurations were analyzed. The bulge factor for each configuration is evaluated using the MCCI technique.

$$R = \{5, 10, 20, 40, 80\}\,(\text{in}) = \{127, 254, 508, 1016, 2032\}\,(mm);$$
$$t_S = \{0.02, 0.04,\ 0.06, 0.10\}\,(\text{in}) = \{0.508, 1.016,\ 1.524, 2.54\}\,(mm) \qquad (7)$$

[*] Material properties of the polyisocyanurate foam were obtained from mechanical tests conducted at Florida International University Mechanical Engineering Departement.

The bulge factor β data are plotted against the curvature parameter λ in Figure 5. The nonlinear dependence of the β on λ can be readily seen; four bulge factor curves are shown one for the case of a shell only and the others are for different foam thickness values. Clearly, the addition of the foam reduced the bulge factor dramatically, especially at higher λ values. The bulge factor for typical aircraft fuselage shell (with λ≈4) is given as function of normalized foam thickness (t_F/R) in Figure 6-a; up to 45% reduction in the bulge factor with a foam layer thickness that makes up 5% of the shell radius R. Figure 6-b shows a deformed plots of the mesh around the crack area of a typical shell with and without foam, the effect of the foam layer on the bulge profile of the crack can be clearly seen.

5.2 EFFECT OF LOAD PARAMETER (η) AND CRACK LENGTH ON BULGE FACTOR (β)

A second parametric nonlinear finite element study is conducted to evaluate the effect the load parameter η on the bulge factor for a fuselage panel with a fixed geometry various different crack lengths. The shell geometry is (R= 80in=2032mm, t_A= 0.02in=0.508mm, t_F=2in=50.8mm). The half crack lengths are {a=2,4,6,8 (in)= 50.8,101.6,152.4,203.2 (mm)}. The load parameter η was varied from 0 to a maximum value of 6 that corresponds to a pressure p=7.14 psi = 49.2 kPa. The values selected for the pressure and shell geometry are representative of the conditions experienced by fuselage sections in commercial and military aircraft.

Figure 7-a through d describe the bulge factor behavior for a longitudinal crack at different values of crack length, they may be viewed as snapshots of the bulge factor behavior of the shell throughout crack propagation history. The initial half-crack length is a=2 in=50.8 mm (Figure 7-a) and the final half-crack length is a=8 in= 203.2 mm (Figure 7-d). During take off or landing the cabin pressure in aircraft fuselage varies from 0 to 7.14 psi or vice versa corresponding to the load parameter η going from 0 to 6. As can be seen in Figure 7, the bulge factor for a crack in a shell with no foam layer is highest during the initial stages of cabin pressurization (i.e. at low η values). As the crack grows longer its bulge factor takes on higher values for the same value of η and it tends to grow faster. With the addition of a foam layer, an across the board reduction of the bulge factor is observed with respect to crack length and load parameter η. The foam serves its purpose best at the initial stages of pressurization (low pressures) were the maximum values of the bulge factor are reduced by as much as 60% for the crack of Figure 7-d to as low 42% for the crack in Figure 7-a.
Figure 8-a shows the maximum bulge factor obtained during pressurization as a function of crack length for a shell with and without foam, the mitigating effect of the is evident by the much smaller slope of the bulge factor graph of the foam reinforced shell.
Figure 8-b illustrates the effect of the foam layer on SIF as function of pressure, it can be seen that SIF associated with foam layer are lower. As the pressures increases, the difference between SIF with and without foam grows large. This means that at higher pressure the foam is most useful in slowing down crack growth.

6 CONCLUSIONS

In this study the effect of adding a foam layer to a crack in a pressurized cylindrical shell on the bulge factor is investigated. A FE model was built specially to investigate this problem. The model is parametric with variable geometry, loading conditions and mesh parameters. It is used together with MCCI technique to determine SIFs of longitudinal cracks in pressurized cylindrical shells. The model was validated using experimental data from pressurized cylindrical shells with and without foam layer was found to be in good agreement with experimental bulge profile data.

Two parametric studies were conducted to investigate the effect of the foam layer on the bulge factor. In the first study, 120 shell-foam configurations were analyzed by varying the shell radius, shell thickness, foam thickness and crack length. It was found that adding a foam layer reduces the bulge factor dramatically even with a small thickness. In the case of a crack in an aircraft fuselage this reduction could be as high as 45%.

A second parametric study is designed to analyze the effect of a layer of foam on the bulge factor of a longitudinal crack on a pressurized shell of fixed geometry at selected stages of crack growth. This was done by modeling a typical fuselage shell structure with a foam layer with different crack lengths. Results indicate that the foam layer is most instrumental at the onset of the pressurization of the fuselage since bulge has maximum values at low pressures. The foam layer reduced the bulge factor by up to 60%. The bulge factor increases with increasing crack length. However, in the presence of a layer foam this effect is reduced considerably.

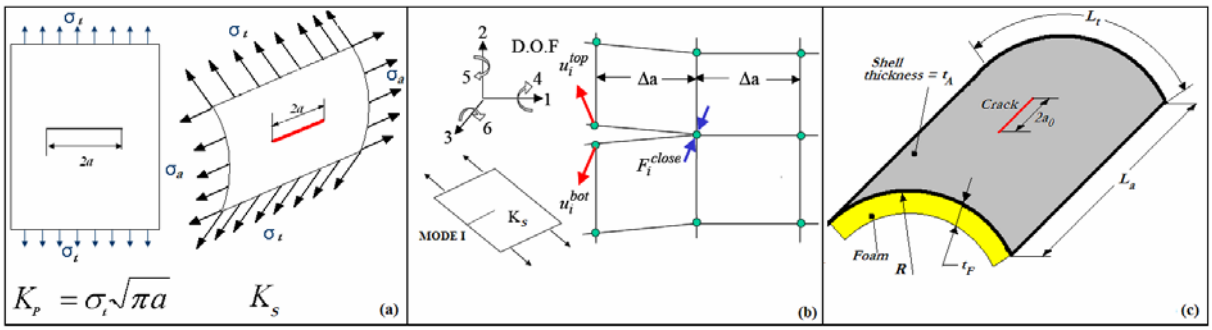


Figure 1: a-Comparison between a crack in plane stress condition and a crack on a curved shell; b- Mesh at the crack-tip for the MCCI technique; geometric parameters of the shell.

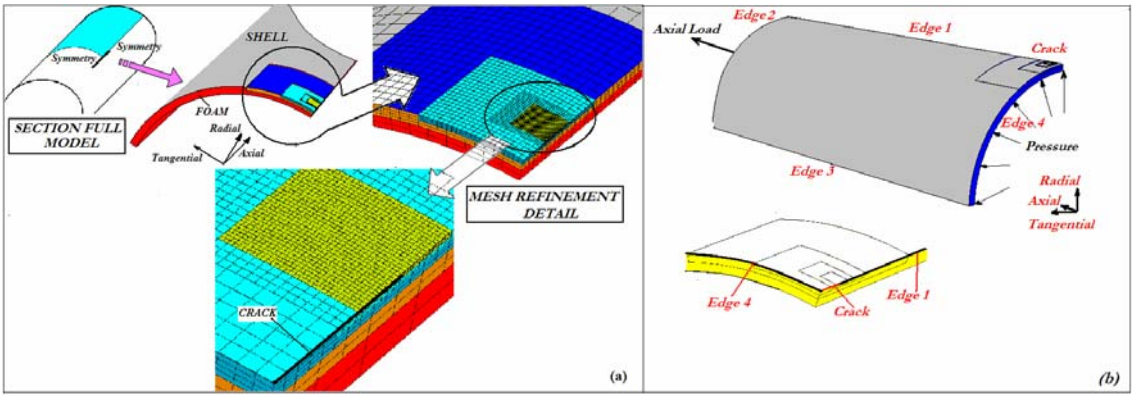


Figure 2: a- Finite Element model (Quarter section only) with mesh refinement detail shown; b- Boundary and loading condition on the quarter model of the shell-foam section.

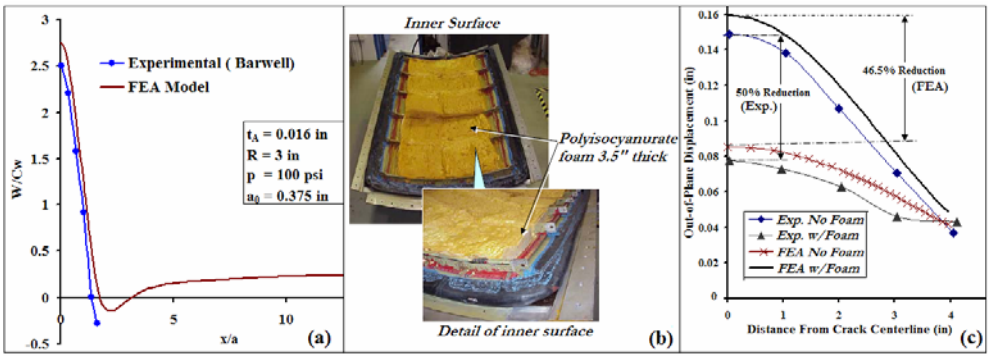


Figure 3: a-Comparison between Experimental data and FEA model; b- Photograph of the tested fuselage section sample with 3.5" thick foam layer, Bakuckas [9]; c- Comparison of the experimental out-plane displacements (crack bulge) with FEA results.

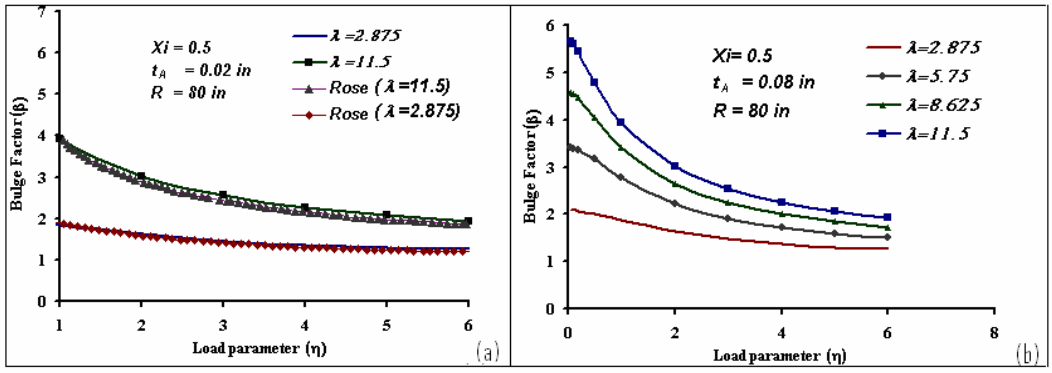


Figure 4 a- comparison between the FEA model and the model of Rose for the first comparative study, b- nonlinear FE results.

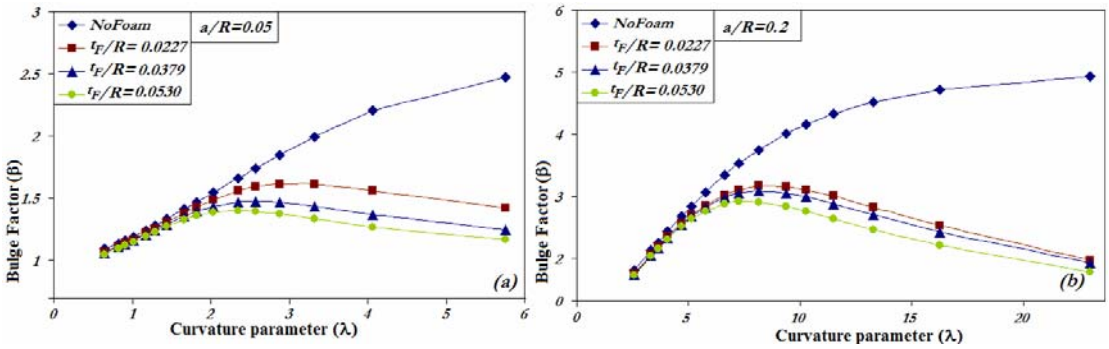


Figure 5: a-Bulge Factor β vs. curvature parameter for configurations with (*a/R=0.05*); b- for configurations with (*a/R=0.2*)

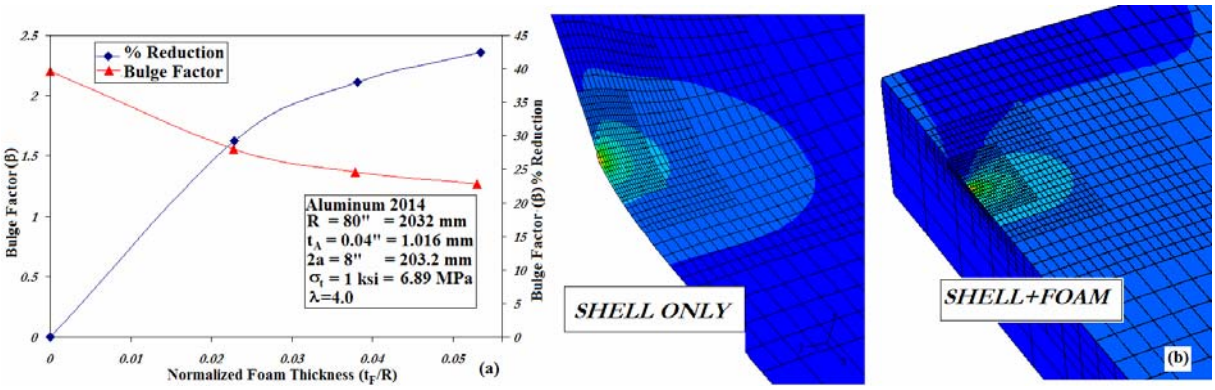


Figure 6: a- Bulge factor and its percent reduction as function of normalized foam thickness parameter (t_F/R). b- Deformed mesh of shell around the crack area with and without foam.

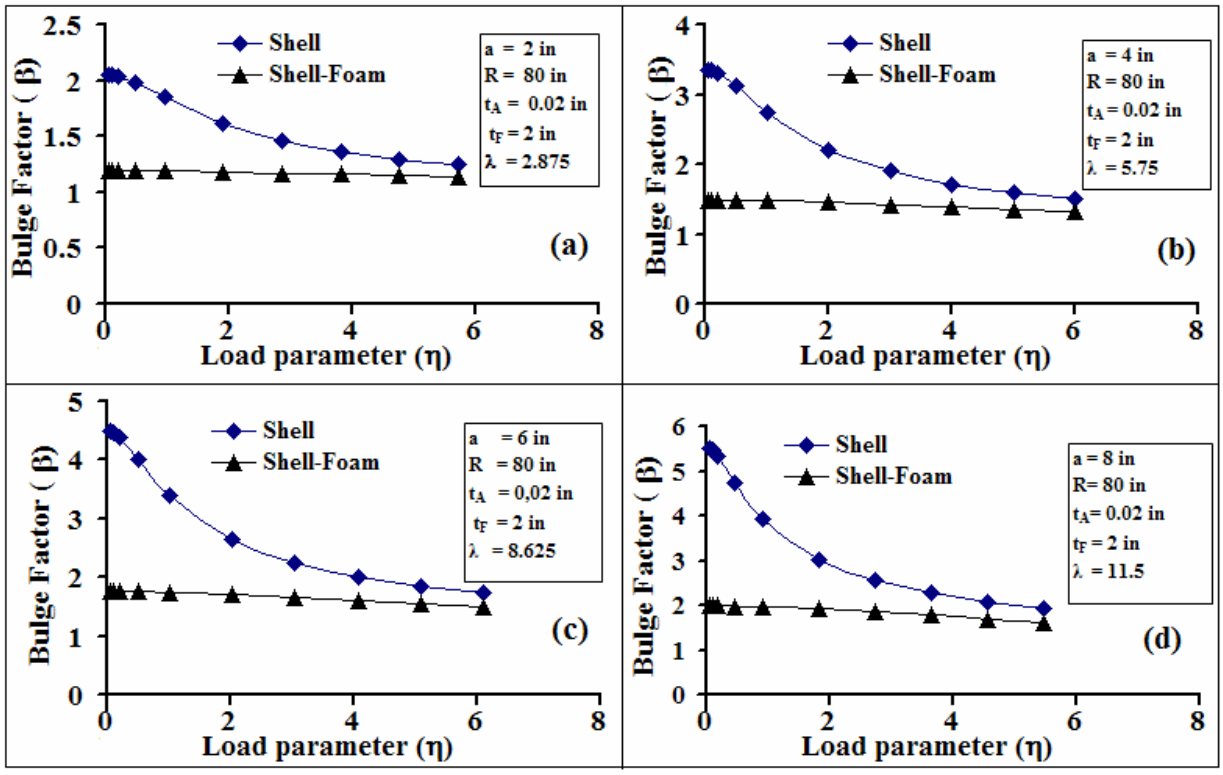


Figure 7: Dependence of the bulging factor on the loading parameter η for a longitudinal cylindrical shell with and without foam, for several crack lengths . (a=2in, b: a=4in, c: a=6in , d: a = 8in)

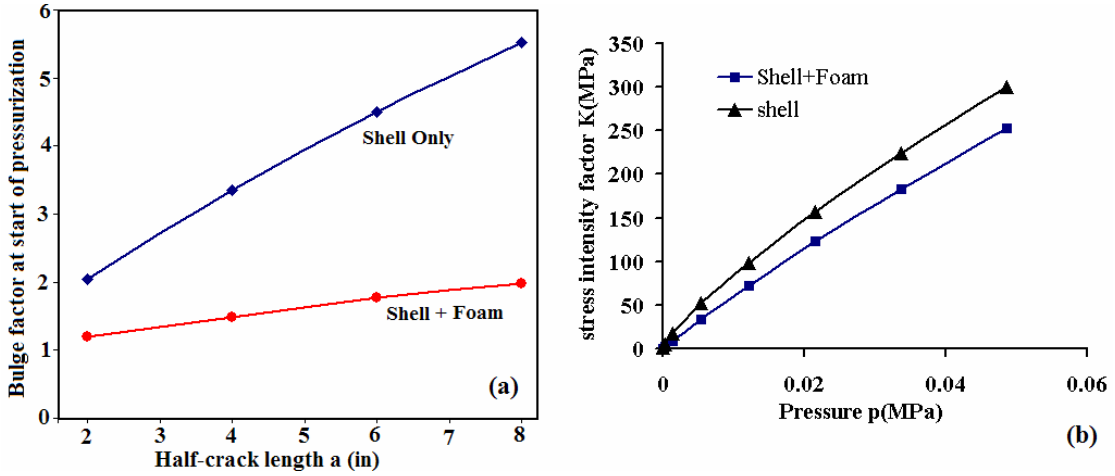


Figure 8: a-Bulge factor at low pressure (η small) vs. half-crack length *a* for a shell with and without foam

---

[1] Rose, C. A., Young, R. D., and Starnes, J. H., Jr., "Nonlinear Local Bending Response and Bulging Factors for Longitudinal Cracks in Pressurized Cylindrical Shells," 40thAIAA/ASME/ASCE/AHS/ASC Structures, Structural Dynamics, and Materials Conference, St.Louis, Missouri, April 12-15, 1999, AIAA Paper No. 99-1412.

[2] Rhaman, A., Bakuckas, J.G., Tan, P.W. and Bigelow,C.A., "Bulging Effects on Longitudinal Cracks in Lap Joints of Pressurized Aircraft Fuselage". Aging Aircraft Conf. 2002, San Fransisco, Sept. 16-19,

[3] Folias, E. S., "An Axial Crack in a Pressurized Cylindrical Shell," International Journal of Fracture Mechanics, Vol. 1, No. 2, 1965, pp. 104-113.

[4] Erdogan, F., and Kibler, J. J., "Cylindrical and Spherical Shells with Cracks," International Journal of Fracture Mechanics, Vol. 5, No. 3, September, 1969, pp. 229-237.

[5] Budiman, H. T., Lagace, P. A., "Nondimensional Parameters for Geometric Nonlinear Effects in Pressurized Cylinders with Axial Cracks," Journal of Applied Mechanics, Vol. 64, 1997, pp. 401-407.

[6] Chen, D.,"Bulging of Fatigue Cracks in a Pressurized Aircraft Fuselage," Ph.D. Thesis, Delft University of technology, Delft, The Netherlands, Report LR-647, October, 1990.

[7] Jeong, D. Y., and Tong, P., "Nonlinear Bulging Factor Based on R-Curve Data", Proceedings of the FAA/NASA International Symposium on Advanced Structural Integrity Methods for Airframe Durability and Damage Tolerance, September, 1994, pp. 327-338.

[8] Bakuckas, J. G., Jr., Nguyen, P. V., Bigelow, C. A.,and Broek, D., "Bulging Factors for Predicting Residual Strength of Fuselage Panels," . International Conference on Aeronautical Fatigue, Edinburgh, Scotland, June 18-20, 1997.

[9] Bakuckas, J. G., Bigelow, C. A., Tan, P. W., "Characterization of Fatigue Behaviour of Aircraft Fuselage Structure", Proceedings of the 22nd Symposium of the International Committee on Aeronautical Fatigue 2003, Lucern, Switzerland, May 5-9.

[10] Rybicki, E.F., Kannien, M.F., "A Finite Element calculation of stress intensity factors by a modified crack closure integral". Engineering Fracture Mechanics, vol. 9, pp. 931-938, 1977.

[11] Potyondy, D, O., Wawrzynek, P., A., and Ingraffea, A. R., "Discrete Crack Growth Analysis Methodology for Through Cracks in Pressurized Fuselage Structures," International Journal for Numerical Methods in Engineering, Vol. 38, 1995, pp. 1611-1633.

[12] Viz, M. J., Potyondy, D. O., Zehnder, A. T., Charles C. Rankin and Eduard Riks, "Computation of membrane and bending stress intensity factors for thin, cracked plates", Fracture Mechanics: 26th Volume, ASTM STP 256, W. G. Reuter, J.H. Underwood, and J. James C. Newman, eds., Philadelphia, PA: American Society for Testing and Materials, 1995.

[13] ABAQUS version 6.4, ABAQUS, Inc.,Hibbit, Karlsson & Sorenson, http://www.abaqus.com

[14] Craig A. Barwell, Lorenz Eber, and Ian M. Fyfe, "A Study of Failure in Small Pressurized Cylindrical Shells Containing a Crack", NASA/CR-1998-208454, August 1998.

Comparison of Double and Single bonded Repairs to Symmetric Composite Structures: A Numerical Analysis

B. Bachir Bouiadjra , M. Belhouari

Department of Mechanical Engineering, University of Sidi Bel Abbes, BP 89, Cité Ben M'hidi, Sidi Bel Abbes 22000, Algeria

Abstract Owing to the importance of crack patching in fracture mechanics analysis, the aim of this study is to analyse numerically by the finite element method the advantage of the use of the bonded symmetric composite patch for repairing crack in metallic sheet in the mode one and the mixed mode. The obtained results show that there is a considerable reduction of the asymptotic value of the stress intensity factor at the crack tip in the case of the use of the double symmetric patch compared with the single patch. In addition the gain of the composite thickness obtained by the double patch is also considerable in both mode I.

1 INTRODUCTION

The used of externally bonded composite patches for repairing crack and defects in aircraft structures know a large success these last years, what accelerated the researches in this domain. The bonded composite repair carries a part of the loads acting at the crack tip throughout the adhesive. The stress intensity factor is then reduced by the presence of the patch. Several authors showed that the mode I stress intensity factor of repaired crack, exhibits an asymptotic behaviour as the crack length increases [1-5]. The asymptotic value of the SIF was approximated by Rose [6] by the formulas:

$$K_{\infty}=Y.\sigma_0\sqrt{\pi\lambda} \tag{1}$$

Where

$$\sigma_0 = \frac{\sigma E_p e_p}{\left(E_p e_p + E_r e_r\right)} \tag{2}$$

Y is a geometry factor, Y= 1 for a repair to a centre crack and Y = 0,9 for a repair to an edge crack.

$$\pi\lambda = \sqrt{\frac{E_p e_p}{\beta\left(1+\frac{E_p e_p}{E_r e_r}\right)}} \tag{3}$$

and

$$\beta = \frac{\left(\frac{e_a}{G_a}+\frac{e_r}{3G_r}+\frac{e_p}{3G_p}\right)}{\left(\frac{e_a}{G_a}+\frac{3e_r}{8G_r}+\frac{3e_p}{8G_p}\right)^2} \tag{4}$$

These last expressions show that the stress intensity factor, then the patch performance, depends essentially on the patch and the adhesive properties (shear modulus and thickness). Bachir et al [7] affirmed that the adhesive properties must be optimized in order to allow the transmission of the stresses toward the patch and to avoid the adhesive failure. Concerning the mechanical properties of the patch it is known that only the boron / epoxy and the graphite / epoxy are used because of their excellent load transfer characteristics [8]. One can conclude that the improvement of the patch performances by the assessment of the properties of the composite and the adhesive prove to be more difficult and expensive. The unique parameter that remains is the patch thickness. Bachir et al [7] slow that for a single patch repair the increase of the patch thickness about 50 % reduces the stress intensity factors at the same order and they confirmed that of for a better distribution of the stresses, it is preferable to use a multiple layers of bonded composite patch. One of means can strengthen this ideas is the use of the double sided symmetric patch. Many authors shown the advantage of the double-sided symmetric patches experimentally and numerically, among them we

can quote. Ting et al [1], Turaga and Ripudaman [9], Chen and Yang [10], Megueni et al [11]. All these authors observe that the double-sided symmetric patch reduces more the stress intensity at the crack tip. In addition it annuls the bending effect due to the eccentricity of the patch. This study has been led in the aim to achieve an advanced in this way using the Finite element method. In first time, one compare values of the stress intensity factors of repaired cracks with single and double patches in mode I . In the second time, is determined the gain of the thickness eventually obtained by the use of the double symmetric patched. This gain can give us an approximate evaluation on the reduction of the cost of the repair that can generate the use of the double symmetric patch.

2 GEOMETRICAL MODEL

The basic geometry of the cracked structure considered in this study is shown in figure 1. Consider a thin elastic aluminium plate (height H_p= 254 mm, width W_p = 254 mm and thickness e_p = 5 mm), with a central crack of length 2a repaired with a bonded boron - epoxy

patch by e_a = 0,15 mm thickness film FM 73 adhesive. The width and the height of the patch are W_r / 2 = 65 mm and H_r = 75 mm, respectively. The patch thickness for a double patch is half of that used for a single patch (see figure 1). The plate is subjected to a remote uniaxial tensile load of σ =70 Mpa, the plane stress conditions are assumed. Since the geometry and loading is symmetric about the y-axis, only one half needs to be analysed. The material properties of the plate, patch and adhesive are the following.

Plate (aluminium material):

Young modulus Ep = 72 GPa , Poissson ratio ν_p= 0.33.

Patch (boron – epoxy):

Young modulus E_{r1} = 210 GPa, E_{r2} = E_{r3} = 19.6 GPa, shear modulus G_r= 5.460 GPa, and Poisson's ratios ν_{r1}= 0.3, ν_{r2} = ν_{r3} = 0.2.

Adhesive (FM 73):

Shear modulus G_a = 0.42 GPa

Finite element analysis of the configurations of figure 1 is done using the finite element code Franc2D/L developed at Kansas University [12]. The global structure (plate and patch) is meshed using standard eight nodded-isoparametric elements with quadratic shape functions. These elements perform well for elastic analysis and have the advantage that the stress singularity at the crack tip can be incorporated in the solution by moving the eight nodes to the quarter-point locations [13]. Figure 2 shows the finite element modeling for the plate, the patch and near the crack tip. The stress intensity factor is calculated using modified crack closure method.

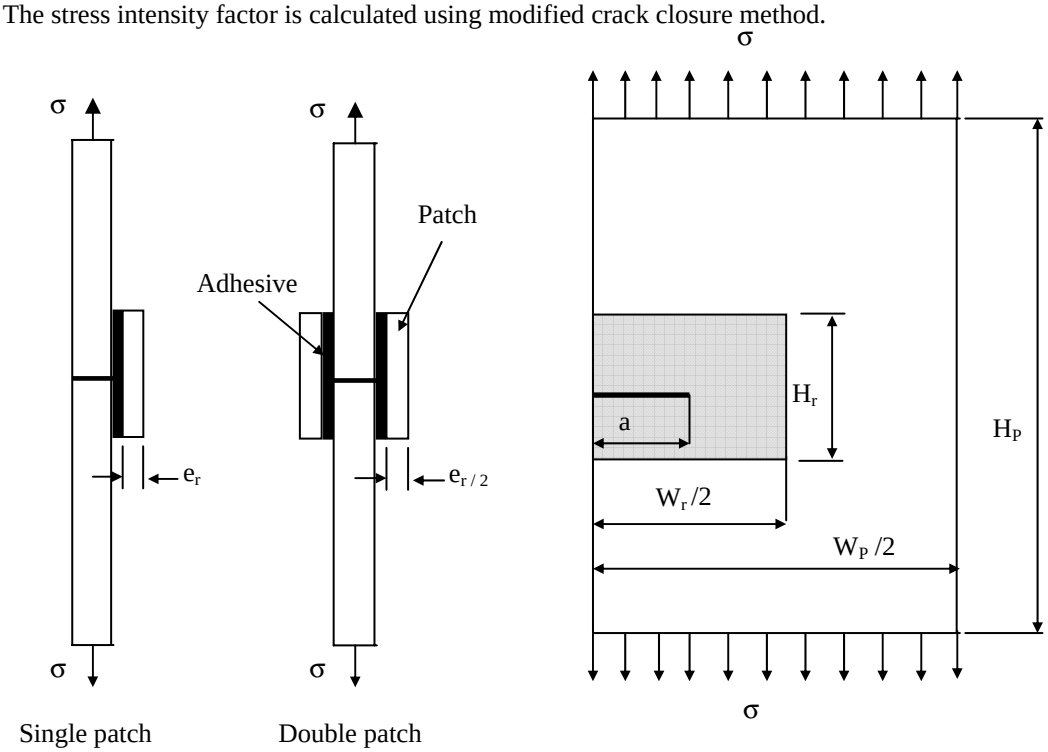


Figure 1. Geometrical model of the half of the patched structure for the pure mode I.

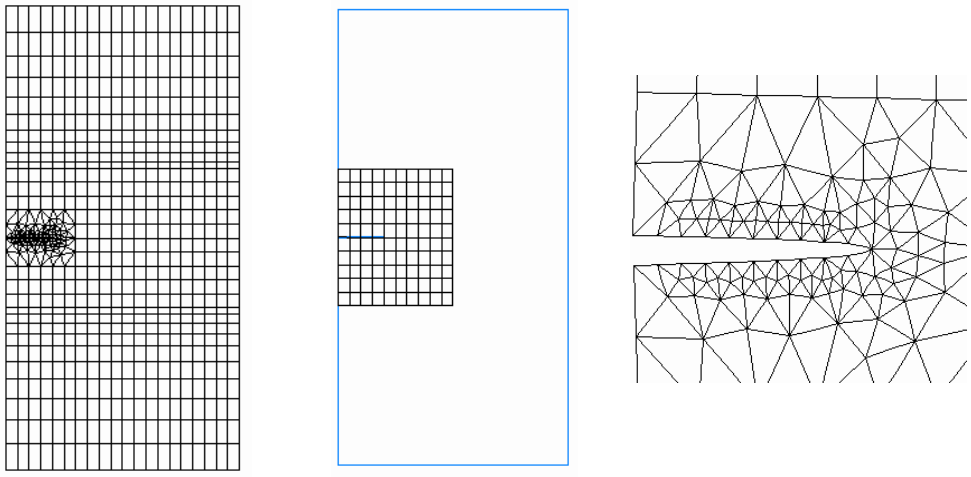


Figure 2. Typical mesh model of the plate, patch and near the crack tip in pure mode I.

2 RESULTS AND DISCUSSIONS

2.1 Stress Intensity factor in pure mode I

2.1.1 Comparison between single and double patched crack

Figure 3 present the variation of the stress intensity factor K_I according to the crack length for single and symmetric double patch for thickness e_r= 5 mm it is firstly noted that the asymptotic behaviour is visible for the two case and there is a reduction of the asymptotic value about 10 % by the use of double symmetric patch, it means that the fatigue life of the structure can be improved considerably. This tendency is in agreement with the analysis of Klug et al [14] whom showed that the use of a double patch increase twice as much the fatigue life of the structure compared with the single patch. It can also be see in figure 3 that for a weak value of the crack length there is no difference in the stress intensity factor between the case of single and double symmetric patch. This is due to the fact that the stress intensity at the crack tip is not sufficient in order to highlight the advantages of the double transfer of stresses.

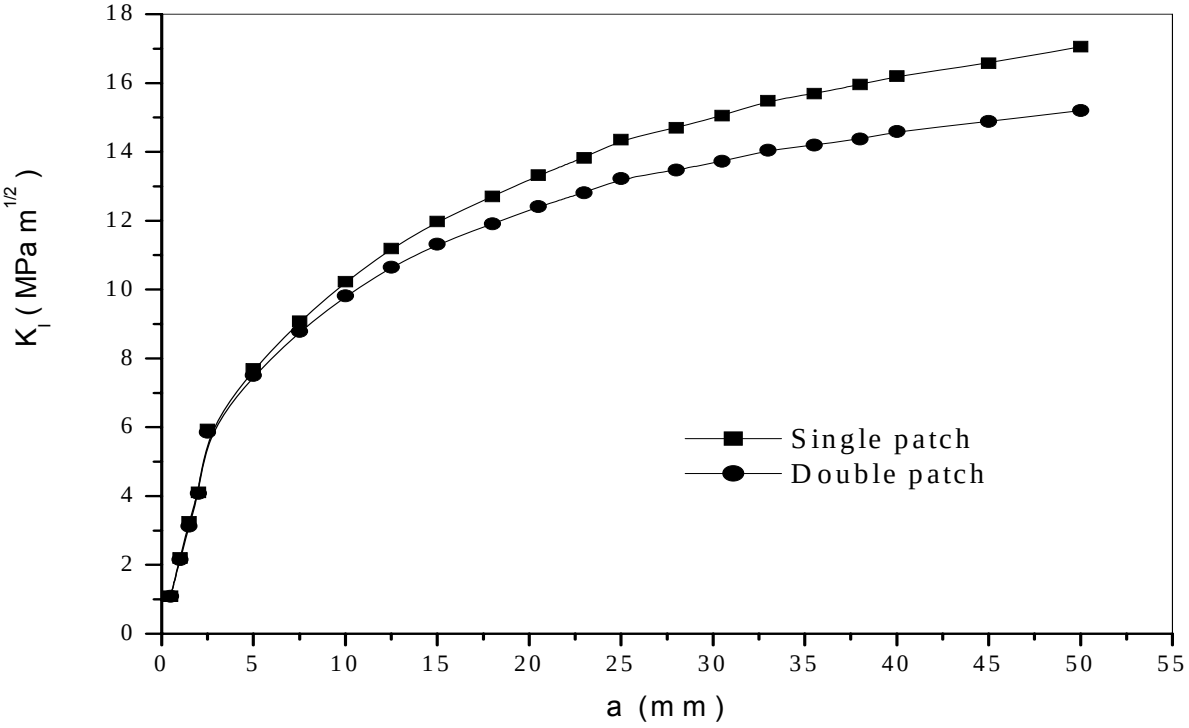


Figure3. Comparison of the stress intensity factor between single and double patched cracks.

For a better illustration of the beneficial effect of the double symmetric patch it is plotted in Figure 4 the variation of the asymptotic SIF according to the patch thickness for a single and double patch. For the two cases the SIF decreases asymptotically as the patch thickness grows. It is then useless to increase the patch thickness indefinitely for reducing the stress intensity factor. An optimization of the patch thickness is recommended there fore. Ting et al [1] and Turaga and Ripudaman [9] succeeded this conclusion .It is noted that the difference of the stress intensity factor between a single and double symmetric patch is stabilized when the thickness e_r is greatly then 2 mm. This tendency is confirmed by the figure 5 that illustrates the variation of the ratio R ($R = K_\infty^s / K_\infty^d$, K_∞^s and K_∞^d are respectively the asymptotic value of the SIF for single and double patch), as a function of the patch thickness. It can be seen that the ratio R increases asymptotically when e_r increases.

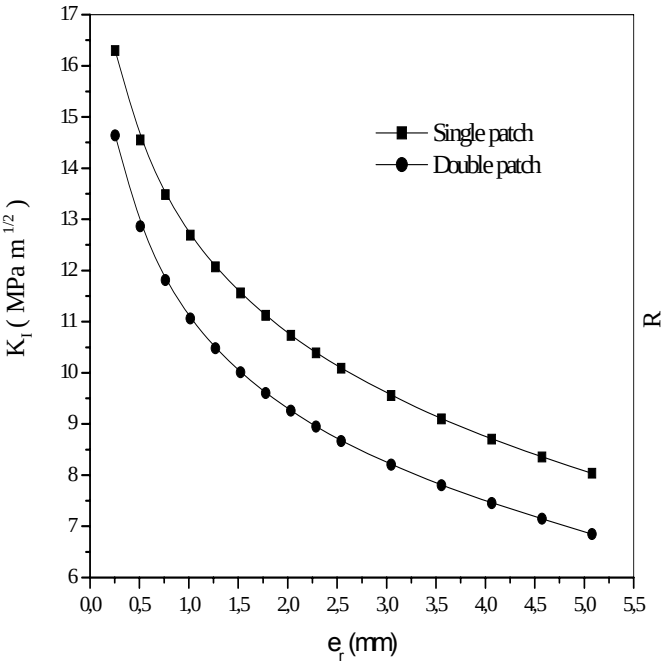


Figure 4. Effect of the patch thickness on the mode I stress intensity factor variation.

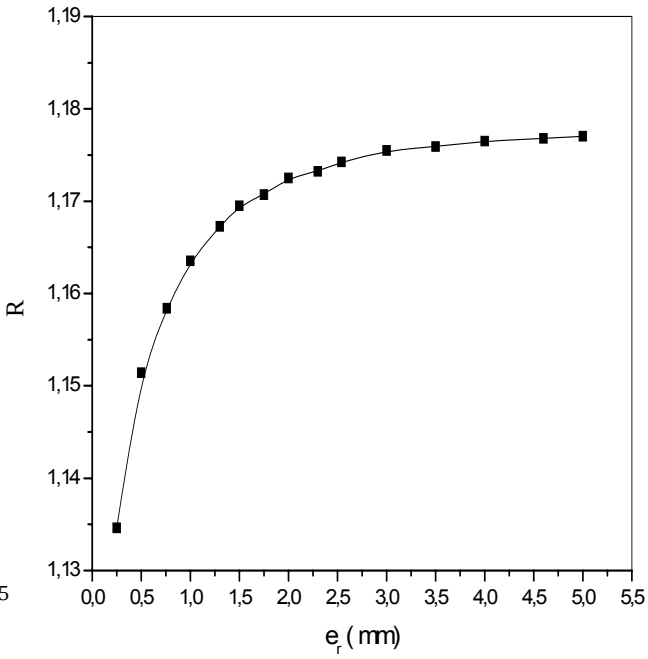


Figure 5. Variation of the ratio R according to the patch thickness.

Tables 1-4 present the gain of thickness eventually obtained by the use of the double symmetric patch. This gain is defined as the relative difference in percent between the thickness of double symmetric and single patch when the SIF is the same for the two cases. Tables 1-4 are established for different crack length. It can be noted that the gain my be considerable and it reaches about 46 % for a = 50 mm, what permit us to confirm that while adding the gain obtained by the elimination of the bending effect, the total gain obtained by the use of the double patch can depend largely 50 %. It can also be seen in table 1 that the gain decreases as the patch thickness increases. This is due to the fact that the transfer of the stress toward the patch is less important for high values of the patch thickness then the difference of the transferred stresses between a single and double symmetric patch is less important.

Table I. Evaluation of the gain in pure mode I for a = 5 mm.

e_r (mm) double patch	K_I	e_r (mm) single patch	K_I	Gain %
1	6,754	1,54	6,753	35,06
2	6,196	2,92	6,196	31,51
3	5,792	4,225	5,792	28,99
4	5,476	5,45	5,475	26,61
5	5,193	6,71	5,193	25,48

Table 2. Evaluation of the gain in pure mode I for a = 10 mm.

e_r (mm) double patch	K_I	e_r (mm) single patch	K_I	Gain %
1	8,445	1,63	8,444	38,65
2	7,512	3,1	7,511	35,48
3	6,872	4,52	6,871	33,63
4	6,407	5,82	6,407	31,27
5	6,009	7,2	6,005	30,56

Table 3. Evaluation of the gain in pure mode I for a = 25 mm.

e_r (mm) double patch	K_I	e_r (mm) single patch	K_I	Gain %
1	10,48	1,75	10,48	43
2	8,94	3,3	8,95	39,39
3	8,021	4,8	8,021	37,5
4	7,358	6,16	7,357	35,06
5	6,839	7,52	6,839	33,51

Table 4. Evaluation of the gain in pure mode I for a = 50 mm.

e_r (mm) double patch	K_I	e_r (mm) single patch	K_I	Gain %
1	11,74	1,85	11,75	45,95
2	9,86	3,4798	9,87	42,53
3	8,77	5,03	8,78	40,36
4	8,06	6,452	8,06	38,00
5	7,49	7,874	7,489	36,50

3 CONCLUSION

In this study the finite element method has been used to analyse the advantage of the use of the boned symmetric composite patch for repairing crack. The obtained results allow us to deduce the following conclusions:

- The use of the double patch reduces appreciably the stress intensity factor compared to single patch.
- The stress intensity factor decreases asymptotically according to the thickness of the patch, the relative difference between the SIF of the double and single patch is almost constant.
- The ratio R increases asymptotically with the thickness of the patch. This ratio becomes independent the thickness from a certain value. An optimisation thickness of the patch is thus recommended.
- The gain in thickness increases with the crack length and it decreases when the thickness of the patch increases. For low length this gain can reaches and it exceed largely 50 % at the asymptotic value of the SIF.

4 REFERENCES:

1. T.Ting , R. Jones, W.K .Chiu ,I.H. Marshall IH and J.M Greer JM, *Composite Structures*, 47 1999, 737-743.
2. R.J. Callinan, S. Sanderson and D. Keeley , DSTO, Melbourne. DSTO-TN-0067, 1997.
3. R. Jones and W.K . Chiu, *Composite Structures*, 44 1999,17-29.
4. T. Achour , B.B Bachir and B.Serier , *Computational material sciences*, 28, 2003, 41-48.
5. J.J. Schubbe, S. Mall, *Composite Structures*, 45, 1999, 185-193.
6. L.R.F. Rose *International Journal of Solid and Structures*, 17, 1981, 827-38.
7. B.B Bachir, M. Belhouari and B. Serier , *Composite Structures*, 56, 2002 , 401-406.
8. A.A. Baker, *Composite Structures*, 74, 1999, 431-443.
9. V.R. S. Turaga and S. Ripudaman . *Engineering Fracture Mechanics*, 62,1999, 267-289.
10. W.H. Chen and S.H. Yang, *Finite Elements in Analysis and Design,* 1995; 21: 21-44.
11. A. Megueni, B.B. Bachir and B. Boutabout, *Composite Structure*, 59, 2003, 415-418.
12. D. Swenson and M. James, FRANC2D / L: Version 1.4 User's guide, 1998.
13. R.D. Henshel and K.G. Shaw, *International Journal for Numerical Methods in Engineering*, 9, 1975,495-507.
14. J.C. Klug , S. Maley and C.T. Sun . *J Aircraf*t, 36 (6), 1999, 1016-22.

Finite Element Analysis of a Foam Reinforced Aging Aircraft Fuselage

Lazghab Tarek[a] , K.H.Wu [b], Harindra Vedala[b]

[a] Mechanical Engineering Department, Institut Preparatoire aux Etudes de l'Ingenieur, Tunisia
[b] Mechanical Engineering Department, Florida International University, USA

Abstract In this study, the effects of adding a foam layer of varying thickness to the skin of a fuselage section of an airplane were studied. The effects on fatigue life of the fuselage skin and crack growth rates were of special interest. A finite element model was built to estimate the effect of adding a foam layer on fatigue life. The J-integral and the K_I (mode I) stress intensity factor of a crack introduced in the fuselage skin were also calculated using a submodeling technique.
The foam layer thickness was varied from 0.5" (12.7mm) to 4.0" (101.6mm). The stress intensity factor (SIF) K_I was evaluated and corresponding crack growth rates were calculated from Paris' law. It was determined that crack fatigue life could be increased by a factor of 4.6 when a 4" thick foam layer is used. Some experimental results were compared against the numerical FEA results showed that the estimates from the model are twice as much as the experimental fatigue life data.

1 INTRODUCTION

Fatigue cracking is a major symptom of aging aircraft skin that could lead to Widespread Fatigue Damage (WFD) in the fuselage structure of the aircraft. There are three major phases that lead to WFD, crack initiation, crack growth and crack coalescence or crack link up which leads to fracture. The crack initiation mechanism involves high local stresses, fretting between mating surfaces and manufacturing defects during fuselage assembly. Crack growth is driven by the loading configuration around the crack represented by the stress intensity factor, the number of elapsed cycles, the amplitude of the loading at each cycle, the frequency of the cycles and the material properties. Several strategies can be used to extend the fatigue life of a structure. This can be done in many ways such as reducing operating loads, reinforcing the structure, introducing residual stresses that would stunt crack growth, special material treatment, etc.

In the current study, the use of a layer of foam as a reinforcing material is investigated. The intended effect of the foam is to mitigate the stress distribution around the crack and help extend the useful life of the aircraft by slowing down crack growth. The foam is applied to the inner side of the skin. Several foam thicknesses are considered. The resulting effects on the structure are evaluated numerically using a finite element approach. The Stress Intensity Factor at the crack tip is evaluated for every thickness using the J Integral Method (JIM) and the Modified Crack Closure Integral technique (MCCI). Results from both methods are presented and the effect of foam on crack SIF and fatigue life is discussed.

2 DESCRIPTION OF THE MODEL

2.1 STRUCTURE AND GEOMETRY OF THE PANEL SECTION:

An aircraft fuselage panel section from an aging airliner was considered for the current study. Originally a finite element model of the fuselage panel was received in the form of an ANSYS input file. This file was reverse engineered and rebuilt into ABAQUS format [1]. Figure 1 illustrates the components of the fuselage panel and the assembly detail. The components include stringers, frames, fillers, skin, ties, etc…They are held together by rivets (not shown). In the original model the rivets are represented by short beam elements. In the current model the rivets were replaced by a tied contact using multipoint constraints between adjacent nodes. All the components are made from aluminum. Ties, stringers and frames they all provide reinforcement and load transfer paths to the fuselage skin.

In the current study the foam is added to the inner side of the fuselage section as shown in Figure 1. Different foam thicknesses will be modeled in order to evaluate their effect on SIF and fatigue life.

2.2 ELEMENTS, CONSTRAINTS AND MATERIAL PROPERTIES:

The fuselage panel section and its components are modeled using 4 node reduced integration linear shell elements (ABAQUS, S4R). The rivets are not represented in the FEA model. Instead the assembly between components is insured by applying multipoint constraints between degrees of freedom of the elements located at

the contact regions between components by forcing displacements to be equal and thus simulating the assembly constraint.

The foam is represented using continuum 8-node reduced integration solid elements where the displacements are constrained to those of the skin of the fuselage at the contact interface between the foam and the skin (ABAQUS, C3D8R). The foam was modeled using several thickness values (1.5, 2.0, 2.5, 3.0, 3.25, 3.5, 4.0") inches =(38.1, 50.8, 63.5, 76.2, 82.55, 88.9, 101.6) mm.

Two materials used in the model, aluminum and foam. Both materials are treated as linear elastic isotropic materials with the following material properties:

Aluminum: E_A=10. Msi = 68.9 GPa ν_A=0.33
Foam: E_F =3000. psi= 20.7 MPa ν_F =0.3

Nonlinear geometry solution was adopted in the current study.

2.2 BOUNDARY CONDITIONS

The loading and boundary conditions on the fuselage section are shown in Figure 2. A line load is applied to *Edge3* to account for the axial stresses generated by cabin pressure during flight. Not shown in the figure is a distributed pressure load on the inner surface of the foam due to cabin pressure. The cabin pressure load is stepped from 0 to 7 psi (0,48.3 kPa). The line load magnitude is a function of the cabin pressure and is given by

$$F = \tfrac{1}{2} P.R^2 \phi \qquad (1)$$

Where R is the radius of at the skin of the fuselage panel, P is the cabin pressure and ϕ is the angle subtended by the fuselage section around the Z axis in radians as shown in Figure 2. The geometry of the fuselage section and the loading conditions yield the following values for the parameters from Equation. (1):

R= 74.018 in =1880 mm ; ϕ=37.164 deg = 0.649 radians;
P=7.0 psi =48.3 kPa & F= 12436 lbf = 55.32 kN.

3 CALCULATION OF STRESS INTENSITY FACTOR USING THE J-INTEGRAL METHOD

In order to determine the SIF for mode I crack opening in a curved shell using the JIM, a special mesh must be built for the stress distribution around the crack tip. This was done using a submodeling technique available in the commercial finite element package ABAQUS.

3.1 CRACK SUBMODELING TECHNIQUE

In order to estimate the effect of the foam layer thickness on fatigue life of the fuselage section a 4.5" (114.3 mm) long crack is introduced in the global mesh of the fuselage section. The region neighboring the crack is further analyzed using a submodel. Figure 2-b shows the relative location of the submodel as it is superimposed on the crack with respect to the global model.

First the crack is introduced in the global model at the desired location by modifying its mesh. The stress distribution of the cracked global model is then obtained. In a second step, the global model is superimposed onto the location of the existing crack. Solution variables (displacements) from the global model are then interpolated and mapped onto the nodes of the submodel. These displacements are in turn used in the submodel to calculate the J-integral and the stress intensity factors at the crack tips using quadratic interpolation 20 nodes continuum elements.

The mesh of submodel for the crack is shown in Figure 3-b, it is made up of 20-node quadratic continuum elements. Elements at the crack tip are degenerate with biased midnodes. Nodes representing the crack front are constrained to move together. The combination of biased mid-nodes and tied nodes at the crack tip produce a strain field singularity proportional to $1/\sqrt{r}$ where r is the distance from the crack tip. The mesh is parameterized and allows for a variable number of integration contours around the crack tips. In the current study 10 contours around each crack tip are used for the calculation of the J-integral. The boundary conditions are interpolated from the boundary nodes of the submodel mesh. These nodes are called the driven nodes. In this case the driven nodes are located on the perimeter of the aluminum skin in the through the thickness direction. A pressure load applied to the foam is maintained in the submodel. Nodes at the Aluminum/Foam interface are shared by adjacent elements from both materials.

3.2 J-INTEGRAL CALCULATIONS AND RESULTS

The J-integral was calculated along 10 contours around the crack tip. This is standard practice in FEA to ensure that the value of the J-integral is path independent. The J-Integral at the crack tip for various foam thicknesses are shown in Figure 4-a as a function of contour number. The values of J-integral were at most within 6% of each other for different contour paths as shown in Figure 4-a. The virtually constant value of the J-integral indicates its independence from the path of integration and validates the results obtained from the submodel.

The effect of the foam thickness on the J-integral value can be seen in Figure 4-b, the percent J-Integral reduction increases with foam thickness and could reach as much as 60% for a 4" (101.6mm) thick layer of foam. The trend obtained is fit to a 4th order polynomial in the foam thickness and also shown in Figure 4-b.

3.3 MODE I STRESS INTENSITY FACTOR (K_I)

Stress intensity factors associated with mode I crack opening were also evaluated from the submodel at the crack tips for skins with several foam layers. The percentage reduction of K_I vs. foam thickness is shown in Figure 4-c. K_I can be reduced by as much as 35%. The data trend obtained is fit to a 4th order polynomial equation also shown in Figure 4-c. The benefit of adding the foam is clearly established from these results.

3.4 CRACK GROWTH

Paris law gives the crack growth rate as follows:

$$\frac{da}{dN} = A(\Delta K)^m \qquad (2)$$

Where a is the current crack length, N is the number of cycles, ΔK is the stress intensity factor range and A and n are material constants. For the current study the values of these constants are $A= 2.5E\text{-}12$ *and* $m=3.5$. To evaluate the impact of the foam on the crack growth rate consider the following expressions

$$\left(\frac{da}{dN}\right)_A = C(\Delta K_A)^m \qquad (a)$$

$$\left(\frac{da}{dN}\right)_F = C(\Delta K_F)^m \qquad (b) \qquad (3)$$

$$\frac{\Delta K_A - \Delta K_F}{\Delta K_A} = p \qquad (c)$$

Where

ΔK_A : stress intensity factor range for the aluminum skin without foam.

ΔK_F : stress intensity factor range for the aluminum skin with a foam layer.

$\left(\frac{da}{dN}\right)_A$: Crack growth rate for aluminum skin only.

$\left(\frac{da}{dN}\right)_F$: Crack growth rate for aluminum skin with foam.

The cycle to failure for the aluminum skin with foam are given by:

$$(N_f)_F = \int_0^{N_f} dN = \int_{a_0}^{a_c} \frac{da}{C(\Delta K_F)^m} \qquad (4)$$

Solving for ΔK_F in Eq. (3)-a and substituting into Eq. (4) yields:

$$(N_f)_F = \int_{a_0}^{a_c} \frac{da}{C(\Delta K_F)^m} = \int_{a_0}^{a_c} \frac{da}{C(\Delta K_A(1-p))^m}$$

Knowing that he ratio p of equation (3)-c is a decreasing function of crack length a. we can write

$$p_0 = p(a_0) \le p(a) \le p(a_C) = p_c \qquad for \qquad a_0 \le a \le a_C \qquad (5)$$

Using equation (5) we can then write:

$$\underbrace{\int_{a_0}^{a_c}\frac{da}{C\left(\Delta K_A\left(1-p_c\right)\right)^m}}_{\min\left(N_f\right)_F}\le\left(N_f\right)_F\le\underbrace{\int_{a_0}^{a_c}\frac{da}{C\left(\Delta K_A\left(1-p_0\right)\right)^m}}_{\max\left(N_f\right)_F}\Rightarrow\frac{1}{\left(1-p_c\right)^m}\le\frac{\left(N_f\right)_F}{\left(N_f\right)_A}\le\frac{1}{\left(1-p_0\right)^m}\qquad(6)$$

The addition of the foam has increased the number of cycles to failure by a factor of $\frac{1}{\left(1-p_c\right)^m}$ at least and a factor $\frac{1}{\left(1-p_0\right)^m}$ at the most. Results of crack fatigue life as a function of foam thickness are presented in Figure 4-d. A 4 inch (101.6mm) thick layer of foam could extend the fatigue life by a factor as high as 4.78 (in this case the factor corresponding to p_0 was used).

4 EXPERIMENTAL RESULTS

4.1 FUSELAGE SECTION FATIGUE LIFE

The Federal Aviation Administration (FAA) has conducted crack growth tests in 1999 on a fuselage section 0.05" (1.27mm) thick with a 2.75" (69.8mm) long crack under a 5 psi (34.47 kPa) cyclic load. The crack was allowed to grow to 3.5" (88.9mm) length. The number of cycles needed to reach the final crack length was 4000. The same test was repeated with a 3.5" thick foam layer added to the skin. The number of cycles needed to reach a 3.5" crack length jumped to 12000 cycles. A 3-fold increase in crack growth life was achieved. The experimental test conditions were replicated in the FEA model to estimate the crack growth life fold increase. The estimate from the FEA model yields a 6-fold increase in the fatigue as shown in Figure 6. This discrepancy in the results is attributed to two major reasons. First, fatigue life results are strongly dependent on the exponent *n* in Paris' law as indicated in Eqs. (2) and (6). Second, the material properties of the foam used in the experiment are not known, values for these data were obtained from mechanical tests conducted subsequently. Since, these properties vary considerably based on chemical composition, cure time, environment the values used in the model can only be representative. Nonetheless, the trend in fatigue life is reproduced by the model indicating the effect of foam on it.

Deutsch Airbus has conducted experimental tests on 10 cm crack with 2.5" (63.5mm) thick foam layer. It yielded a reduction in crack growth rate (da/dN) of 50%. Under Similar loading conditions the FEA model has yielded a reduction in crack growth rate of 24.5%. The discrepancy here is attributed to the same sources as before.

5 CALCULATION OF STRESS INTENSITY FACTOR USING THE MODIFIED CRACK CLOSURE INTEGRAL TECHNIQUE

5.1 MODIFIED CRACK CLOSURE INTEGRAL TECHNIQUE

SIF for pressurized cylindrical shells are also computed using an energy based method known as the Modified Crack Closure Integral technique (MMCI). MCCI is widely used and easily implemented within the finite element framework. The stress intensity factors are obtained from the strain energy release rates at the crack tip. This technique is described in detail in by Rybicki[2], Ingraffea [3] and zehnder [4]. Figure 5 shows a typical mesh of shell elements around the crack tip used in the evaluation of SIF by the MCCI method. The strain energy release rate corresponding to Mode I crack opening and its SIF are evaluated as:

$$G_1=\frac{1}{2t\Delta a}\left(F_2^{Close}\left|u_2^{top}-u_2^{bot}\right|+F_6^{Close}\left|u_6^{top}-u_6^{bot}\right|\right);\qquad K_S=\sqrt{E_A G_1}\qquad(7)$$

Where G_1 is the strain energy release, the remaining terms in equation (7) are shown in Figure 5-b.

5.2 FINITE ELEMENT MODEL FOR MCCI

A specially built finite element model of the cracked fuselage panel section with no stringers or frames was built for use in conjunction with the MCCI technique. This model was used to evaluate SIF at the crack tips and determine fatigue life. The model was used to determine the SIF at the crack tips with different foam thickness values. Figure 5-a shows the model details and the mesh used around the crack to calculate the SIF.

5.3 MODIFIED CRACK CLOSURE TECHNIQUE VS. J-INTEGRAL METHOD

In order to show that MCCI method and JIM are equivalent SIF data obtained from both methods are compared. Figure 6-a Shows two curves representing the reduction in SIF at the crack tip as a function of foam thickness. Both graphs show the same trend. However, the curve from JIM is slightly higher, this is because in the FEA model used in MCCI no stringers or frames were used leading so it is less stiff.

6 CONCLUSION

A study on the effect of bonding a foam layer to the fuselage skin of an airplane was considered. The stress distribution, fatigue life, and crack growth rates of the fuselage skin were evaluated using the finite element method.

A submodel was built to analyze the effects of the foam on fatigue life of the aluminum fuselage when a crack is present in it. It was determined that the stress intensity factor (Mode I) can be reduced by 36% for a 4" thick foam layer which translates into an increase in fatigue life by up to 4.78 folds.

Experimentally obtained fatigue life data were compared to results obtained from the finite element model. The outcome showed that the model is within 50% of the experimental results this discrepancy is attributed to the strong dependence of the theoretical result on the exponent *n* in Paris' equation. Since the value of this parameter is not available from the experimental data only an estimated value is used.

The J-integral method was shown to yield results similar to those obtained by the modified crack closure integral technique, which is a widely used approach for the calculation of tress intensity factors in cracked pressurized cylindrical shells.

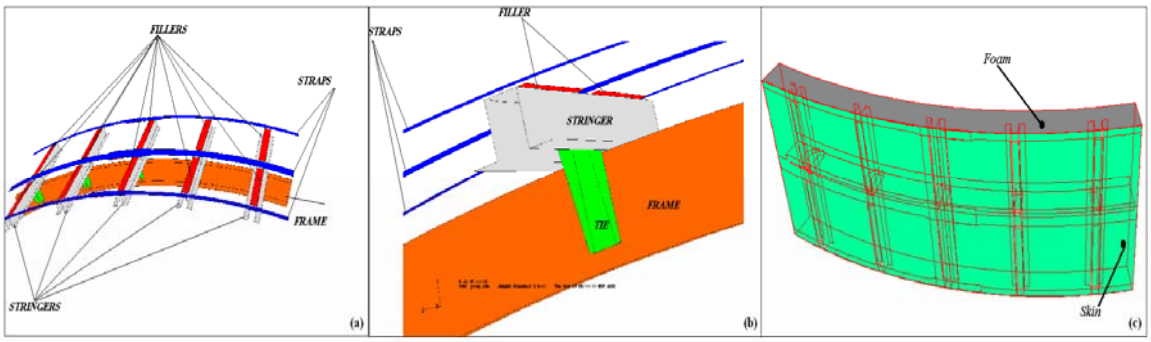


Figure 1 (a) Skeleton detail of the wing panel assembly, (b) Stringer Frame Tie Assembly Detail (c) Foam layer applied to the inner side of the fuselage.

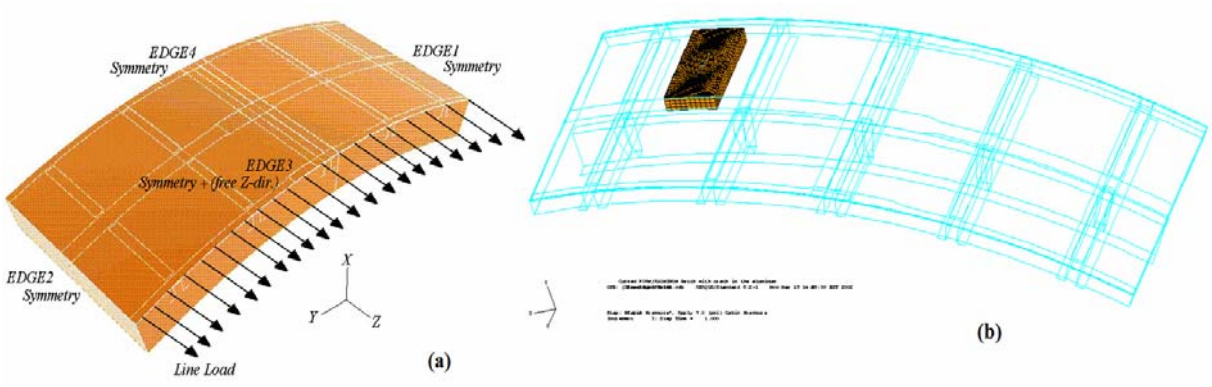


Figure 2: Loading and boundary conditions of the fuselage panel section.

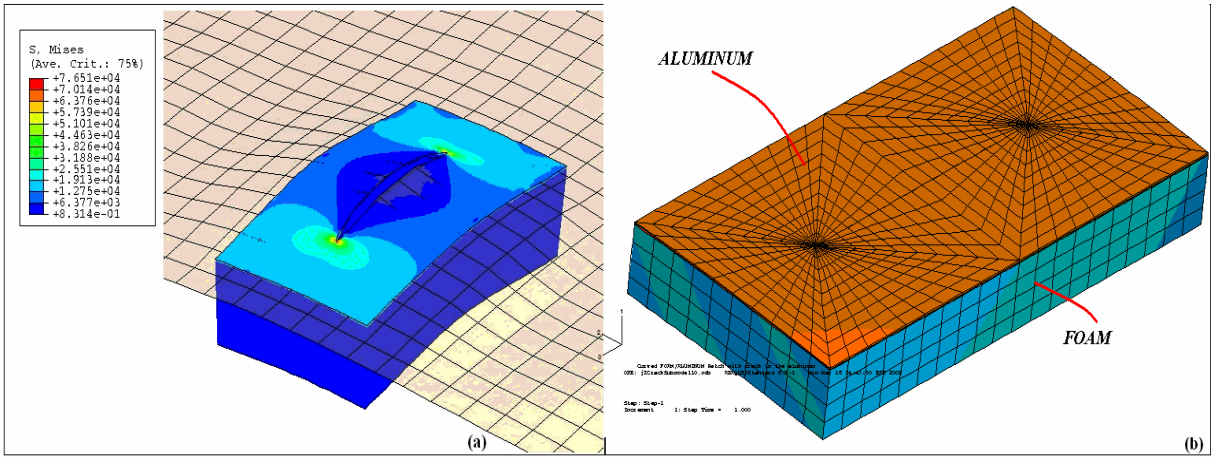


Figure 3 (a) Crack sub model superimposed onto the crack in the global mode. (b) mesh detail of the crack submodel (2" foam layer case).

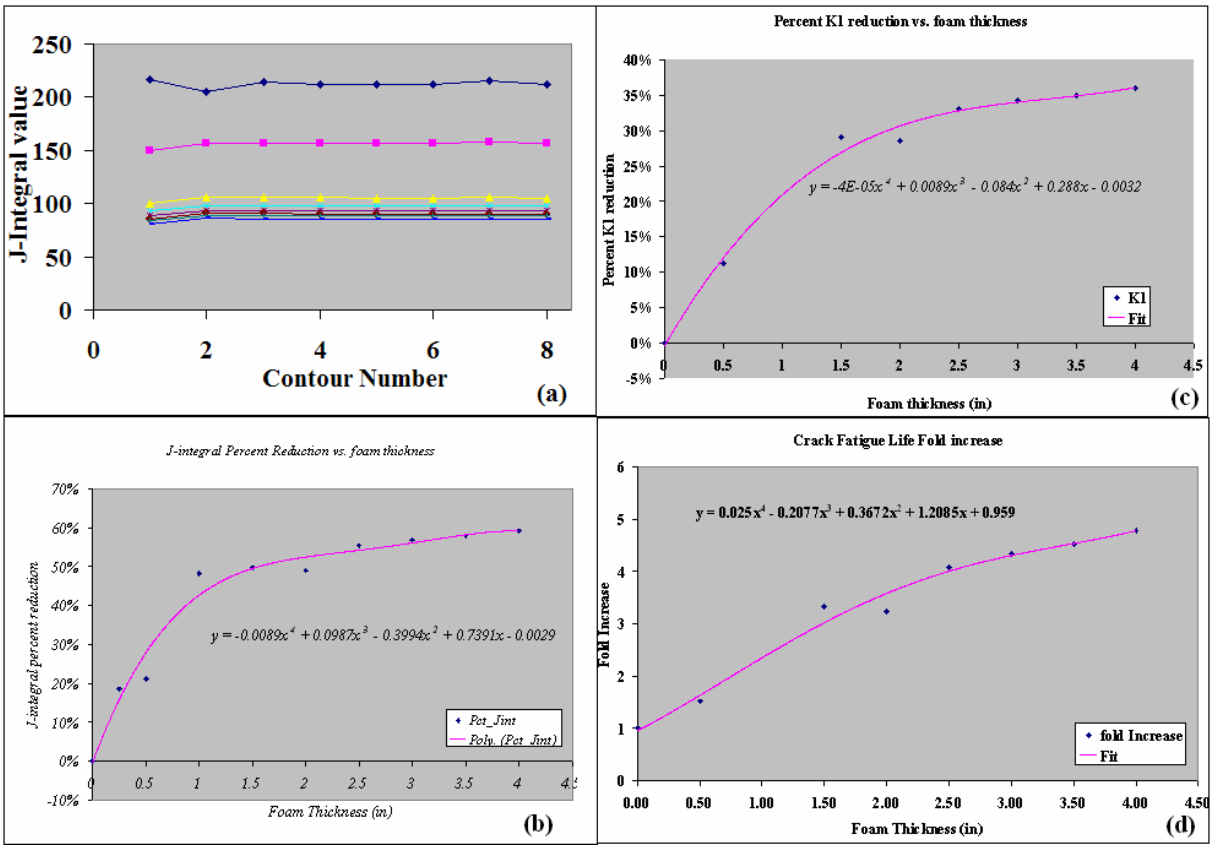


Figure 4 (a) J-integral path independence (Cracked fuselage), (b) reduction in J-integral vs. foam thickness (Cracked fuselage). (c) Percent reduction in K_I vs. foam thickness (Cracked Fuselage) (d) Crack fatigue life increase vs. Foam thickness (Cracked)

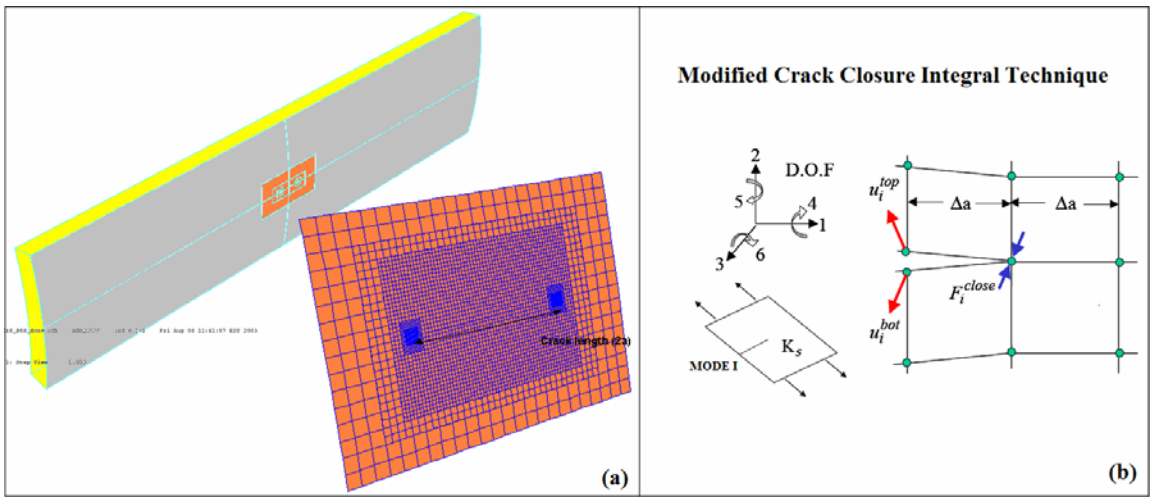


Figure 5: a-Finite element model and mesh around crack for MCCI calculation; b- Mesh and variables used in the Modified Crack Closure Integral Technique.

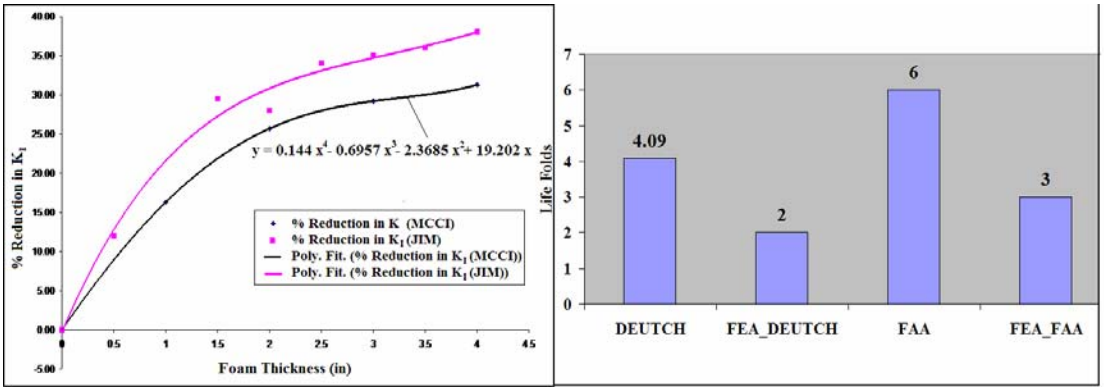


Figure 6 a- Percent reduction in stress intensity factor comparison between MCCI and JIM; b-Effect of additional foam layer on crack growth life (Experimental results compared vs. FEA)

---

[1] ABAQUS version 6.4, ABAQUS, Inc.,Hibbit, Karlsson & Sorenson, http://www.abaqus.com

[2] Rybicki, E.F., Kannien, M.F., "A Finite Element calculation of stress intensity factors by a modified crack closure integral". Engineering Fracture Mechanics, vol. 9, pp. 931-938, 1977.

[3] Potyondy, D, O., Wawrzynek, P., A., and Ingraffea, A. R., "Discrete Crack Growth Analysis Methodology for Through Cracks in Pressurized Fuselage Structures," International Journal for Numerical Methods in Engineering, Vol. 38, 1995, pp. 1611-1633.

[4] Viz, M. J., Potyondy, D. O., Zehnder, A. T., Charles C. Rankin and Eduard Riks, "Computation of membrane and bending stress intensity factors for thin, cracked plates", Fracture Mechanics: 26th Volume, ASTM STP 256, W. G. Reuter, J.H. Underwood, and J. James C. Newman, eds., Philadelphia, PA: American Society for Testing and Materials, 1995.

Finite element analysis of the performance of the bonded composite repair for improving fatigue live initiation and propagation in notched structures

M. Benguediab[1], B.Bachir Bouiadjra[1], M. Nait-Abdelaziz[2] ,A.Imad[2] and N.Ranganathan[3]

1- Department of Mechanical Engineering, University of Sidi Bel Abbes,
BP 89, Cité Ben M'hidi , Sidi Bel Abbes, 22000, Algeria
2- Ecole Polytechnique Universitaire de Lille, France
3- EIT, Université de Tours, France

Abstract In this paper, the finite element analysis is applied to study the performance of the bonded composite reinforcement or repair for reducing stress concentration at a semi-circular lateral notch and repairing cracks emanating from this kind of notch. The effects of the adhesive properties on the variation of the stress intensity factor at the crack tip were highlighted. The obtained results show that the stress concentration factor at the notch tip is reduced about 30% and the maximal reduction of the stress intensity factor is about 80%. The adhesive properties must be optimised in order to increase the performance of the patch repair or reinforcement.

1 INTRODUCTION

Externally bonded composites patches have proved to be an effective method of repairing cracks or defects in aircraft structures. This technology was pioneered by the aeronautical and maritime research laboratory of the Royal Australian air force under the direction of Alan Backer [1,6]. The bonded composite repair offers many advantages over a mechanically fastened doubler which include improved fatigue behaviour, reduced corrosion and easy performance to complex aerodynamic contours [1,2]. It is known that the notches are the main causes of crack initiation. This is why the use of the bonded composite repair can play a significant role in the improvement of fatigue life of the notched structures. This improvement intervenes on the one hand, in the fatigue life initiation by the reduction of the stress concentration at the notch tip, and on the other hand in the fatigue life propagation by the reduction of the stress intensity of stresses at the crack tip. With the increase in computational power, the use of the numerical method, especially the finite elements method, contributed considerably to the comprehension of the mechanical behaviour of defects under patch repair. Among the authors whom used the finite element method for the study of the crack patching, we can quote : Ting et al [7], Callinan et al [8), Jones and Chiu [9], Turaga and Ripudiman [10], Chung and Yang [11], Schubbe and Mall [12] and Bachir et al [13]. The most of the previous works were interested at the cases of central patched cracks. The scope of this study covers studying the reduction of: the notch effect and the stress intensity factor at cracks emanating from notch by the bonded composite reinforcements or repairs using the finite element method. Various Authors [14-16] showed that in practice the adhesive properties plays an important role on the performance of the bonded composite patches s. For that the effects of the adhesive shear modulus and adhesive thickness on the stress intensity factor of repaired notch cracks were examined.

2 ANALYSIS AND RSULTS

2.1 Geometrical Model and finite element Modelling

Consider a thin elastic aluminium plate with a semi circular lateral notch having the following dimension : height H_p= 150 mm, width W_p= 75 mm, thickness e_p= 1.3 mm and notch radius ρ = 12.5 mm . The elastic properties of the material are : Young's modulus E_p= 72 000 MPa, Poisson's ratio ν_p = 0.33. The plate is subjected to uniaxial tensile load giving a remote stress state of σ_0 = 70 MPa. A crack of length a emanating from the notch tip and parallel to the axis loading is supposed to exist. A Boron/epoxy patch is bonded to the plate as shown in figure 1. The dimension of the patch are : Width W_r=75 mm and Thickness e_r =1.3 mm. The material properties of the patch are : Young's modulus E_{r1}=172369 MPa, E_{r2}= 10342 MPa, Shear modulus G_r = 4826 MPa and Poisson's ratio ν_r=0.3. The adhesive properties are : Shear modulus G_a and thickness e_a. The plane stress conditions are assumed. Figure 1 shows the geometrical model of the structures.

Finite element analysis of the configurations of figure 1 is done using the finite element code Franc2D/L developed at Kansas University [17]. A layered structure is actually a three dimensional structure. A three-dimensional finite element or mathematical modelling of such a structure will involve several degrees of complexity. In this study simplifying assumptions are made which still allow us to capture the essential features of the response. These assumptions include:

Each layer is considered as an individual two-dimensional structure under a state of plane-stress.

Individual layers can be connected with adhesive bonds.

It is assumed that the adhesive layer is homogeneous, linear elastic and isotropic.

The adhesive is assumed to deform only in shear and this deformation is uniform throughout the adhesive thickness.

The surface shear transmitted through the adhesive is assumed to act as surface traction on the adherends.

The shear stresses in the adhesive are given by:

$$\tau = \frac{G_a}{e_a}(u_1 - u_2)$$

Where: u displacements in layers 1 and 2 (plate and patch)

The adhesive forces are obtained by using the adhesive shear stresses as surface tractions on the layer and integrating. Since the surface tractions are proportional to the relative displacement of the two layers, the adhesive force can be expressed in term of nodal displacements of the top and bottom layer. This gives a stiffness matrix for the adhesive elements.

The total structure (plate and patch) is meshed using standard eight noded serendipity elements with quadratic shape functions. These elements perform well for elastic analysis and have the advantage that the stress singularity at the crack tip can be incorporated in the solution by moving the eight nodes to the quarter-point locations [18]. Figure 2 shows typical mesh model of the plate, the patch and near the crack tip.

The stress intensity factors, which govern the fracture process in LEFM context, are calculated using modified crack closure techniques.

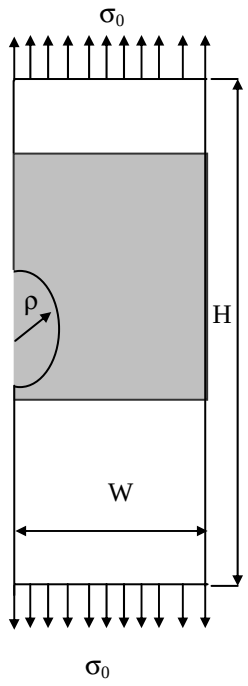


Figure 1. Geometrical model

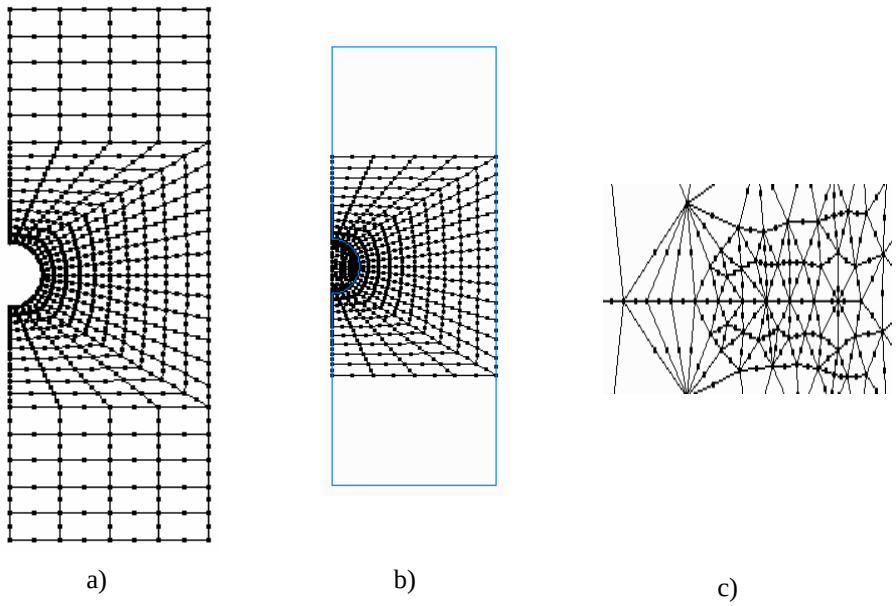


Figure 2. Typical FE mesh : a) of the plate, b) of the patch and c) near the crack tip

2.2 Reduction of the stress concentration at the notch tip

Figure 3 shows the contour of the normal stress levels σ_y in the plate with the presence of the patch. The patch thickness is taken e_r = 1.3 mm and the adhesive properties are chosen such as G_a= 413 MPa and e_a= 0.13 mm. It can be seen that that the maximal stress located at the notch tip is reduced by the presence of the patch. Indeed, the stress concentration factor (defined as $K_t = \sigma_{max}/\sigma_0$) is limited to 2.78 by the presence of the reinforcement whereas, for the unpatched structure the value of the stress concentration factor is included between 3 and 3.5 for the semi-circular notches [19,20]. This reduction is due to the fact that there is a transfer of stresses through the adhesive towards the patch.

In figure 4 are presented the distribution of the normal stresses along the ligament of the plate with and without the presence of the patch for the same properties of the composite patch and the adhesive. It is shown that the maximum reduction of the stresses is about 30% but the rate of the reduction decreases progressively while moving

away the notch tip. It means that the proportion of the transferred stresses towards the patch is more important since the intensity of the stresses is higher in the plate. The effect of the patch is more sensitive for levels of high stresses.

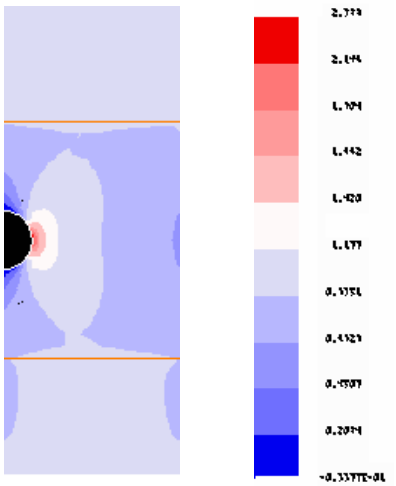


Figure 3. Contour of the normal stress levels in the plate

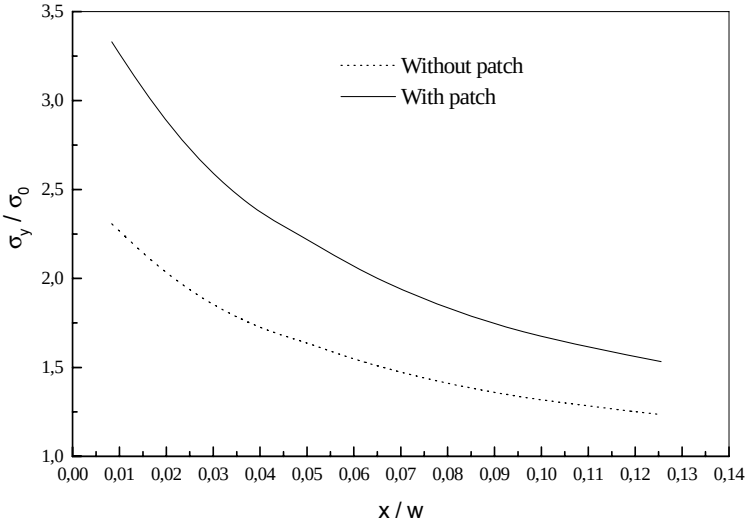


Figure 4. Distribution of the normal stresses along the ligament of the plate

Figure 5 illustrates the contour of the normal stresses σ_y in the patch. The higher stresses are located at the area covering the notch, which confirm the proportionality between the stresses transmitted to the patch and that distributed on the plate without the patch. These results are confirmed in figure 6 where are presented the distribution of the normal stresses along the transversal axis of symmetry of the patch (axis located at the top of the ligament of the plate). The maximum stress at the patch is about 33% of the applied stress and it is located at the free edge of the patch with the top of the notch. The stress in the patch decreases progressively and becomes zero when the stress in the plate is equal to the applied stress.

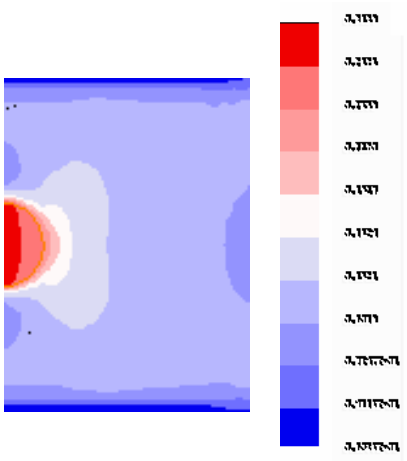


Figure 5. Contour of the normal stresses levels in the patch

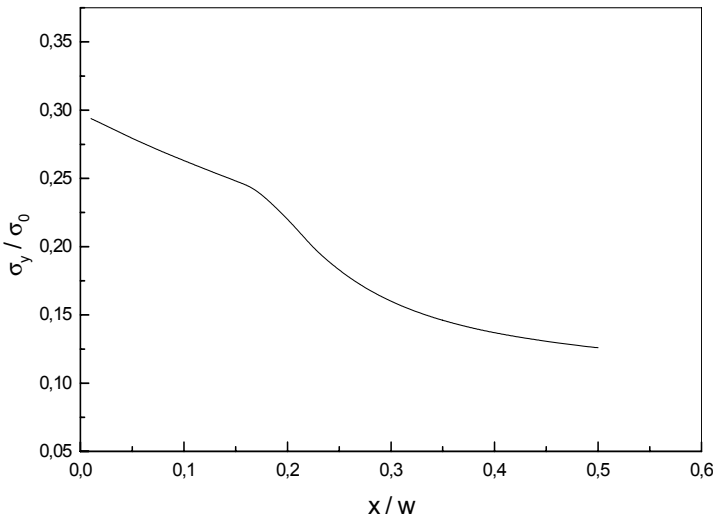


Figure 6. Distribution of the normal stresses along the axis of symmetry of the patch

2.3 Reduction of the stress intensity factor at the notch crack

2.3.1 Comparison between patched and unpatched crack

Figure 7, shows the variation of the stress intensity factor variation (K_I) with respect to the crack length for patched and unpatched crack. It is shown that the patch repair highly decreases the stress intensity factor. This is because the patch carries the loads as the crack growth. The maximum reduction of K_I amounts to 80%. Jones and Chiu [9] give a value of 60% for a central cracks. It means the rate of reduction of stress intensity factor is more

important for notch cracks. This is because the stress intensity at notch crack is higher than that at central crack. It can be seen in figure 7 that the stress intensity factor, for patched crack, exhibits an asymptotic behaviour as the crack length increases. Several investigators among them, those of the Australian team [8,9] announced this tendency

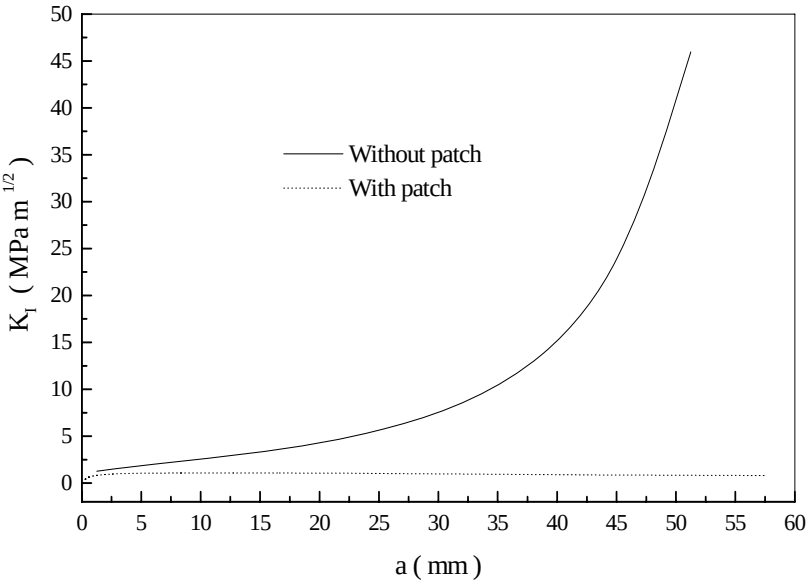


Figure 7. Comparison of the SIF between patched and unpatched cracks.

By examining the shapes of the curves in figures 8 and 9, one can see that, according to the crack length , the stress intensity factor follows an ascending curve for small cracks , reaches a maximum then decreases and stabilises towards an asymptotic value. This behaviour is different to the case of the repaired central cracks whose stress intensity factor increases and stabilises towards an asymptotic value. This difference is explained by the fact why the stress intensity factor for short cracks emanating from notch depends on the stress concentration factor of the notch [19]. The absorption of the stresses by the patch is less significant for short cracks emanating from notch

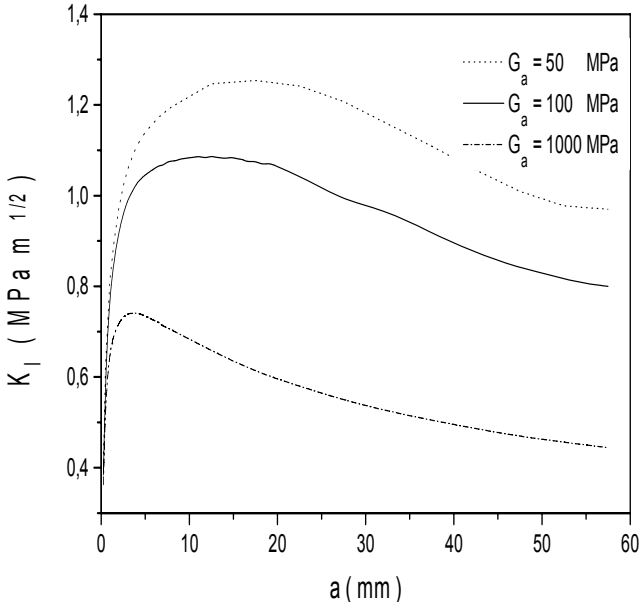


Figure 8 . Effect of The adhesive shear modulus on the variation of the SIF

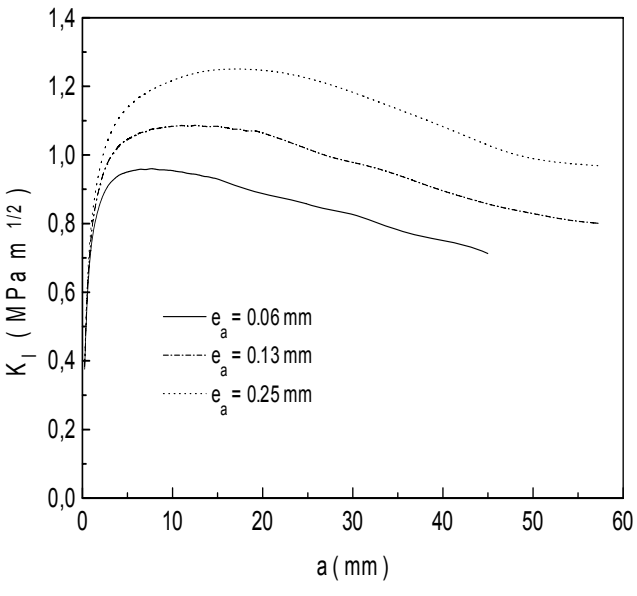


Figure 9 . Effect of The adhesive thickness on the variation of the SIF

2.3.2 Effect of the adhesive shear modulus

It is known that the adhesives of better qualities are characterised by weak shear modulus, which make it possible to attenuate the stresses transmitted to the adhesive. In the case of repaired cracks, the objective is to transmit the maximum of the stresses to the adhesive and consequently to the patch in order to reduce them at the crack tip. Theoretically, it is thus preferable to use adhesives with high shear modulus (adhesive of bad qualities) for repairing cracks or defects. In figure 8, the plot of the variation of the stress intensity factor according to the crack length for various values of shear modulus of the adhesive confirms what was advanced previously. Indeed, the stress intensity factor decreases as the shear modulus of the adhesive increases, but the decrement of K_I according to G_a tends to be cancelled as G_a increases indefinitely as shown in figure 8. Actually, an increase of the adhesive shear modulus reduces the adhesive strength, which can generate the adhesion failure.. Consequently, the choice of the adhesive (characterised by its shear modulus) for repairing cracks must be optimised in order to allow the transmission of the stresses towards the patch and to avoid the adhesive failure due to the increase of the stresses in the adhesive layer.

2.3.2 Effect of the adhesive thickness

Figure 9 shows the variation of the stress intensity factors as a function of the crack length for various values of the adhesive thickness (e_a). It can be seen that a reduction in the adhesive thickness decreases the stress intensity factor, it means that lower adhesive thickness is desirable for repairing crack. This effect was highlighted by Turaga and Ripudaman [10]. However, and by analogy with what was advanced in the study of the effect of the adhesive shear modulus, It proves that the choice of the adhesive thickness must be also optimised. The high thickness reinforces adhesion but attenuates the transfer of the loads towards the patch, which reduces the beneficial effects of the patch. On the other hand, lower thickness supports the transfer of the load towards the patch but increases the risk of the adhesive failure.

2.3.3 Effect of the patch thickness

This effect is illustrated in figure 10 by the plot of the SIF variation according to the crack length for various patch thicknesses. It can be seen that the increase of the patch thickness reduces the stress intensity factor at the crack tip in a proportional way. Indeed, an increase of about 50% of the patch thickness reduces the stress intensity factor by the same order. That can able us to confirm that the choice of thicker patches makes it possible to increase their performances. For a better distribution of the stresses, it is preferable to use a multiple layers of bonded composite patches for repairing cracks.

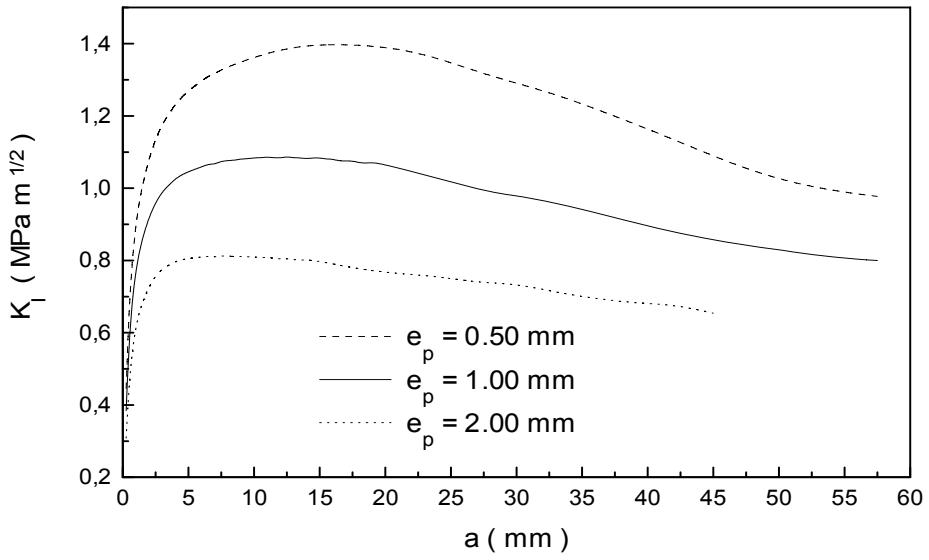


Figure 10. Effect of The adhesive thickness on the variation of the SIF

3 CONCLUSIONS

The study has been made in aim to determine the performance of the bonded composite patch for reducing stress concentration and repairing crack at notch. The obtained results allow us to deduce the following conclusions:

- The reduction of the stress concentration factor by the bonded composite reinforcement is about 30%, which improve the fatigue life initiation.
- The absorption of the stress by the patch is important when the stress in the reinforced plate increase. The stress intensity factor is highly reduced by the presence of the patch.

For notch cracks, the stress intensity factor reaches a maximum value then exhibits an asymptotic behaviour as the crack length increases.

The choice of the adhesive properties for repairing crack, with the bonded composite patch, must be optimised.

The choice of the patch thickness is one of the best means for increasing the performance of the patch repair

4 REFERENCES:

1. A.A. Baker and R. Jones, Martinus Nijhoff Publishers, 1988
2. A.A. Baker and R.J. Proceeding of the International Conference on Advanced composite Materials 1993, 45-9.
3. A.A. Baker, FAA-NASA Symp. on Continued Airworthiness of Aircraft Structures, Atlanta, 28-30 August 1996.
4. A.A. BakerOn Proceeding of the Eleventh International of composite Materials (ICCM-11). Gold Coast, Australia. 1997.
5. A.A. Baker A.A, R.J. Callinan , M.J. Davis, R. Jones and J.G Williams, *Theoritical and Applied Fracture Mechanics*, 2, 1984, 1-16.
6. A.A. Baker, *Composite Structures,* 2, 1984,153-81.
7. T. Ting , R. Jones, W.K. Chiu , I.H. Marshall and J.M. Greer, *Composite Structures*, 47, 1999, 737-743 .
8. Callinan R.J, Sanderson S, Keeley D. DSTO, Melbourne. DSTO-TN-0067, 1997
9. Jones R, Chiu W.K, *Composite Structures*, 44, 1999,17-29.
10. V.R.S. Turaga , S. Ripudaman , *Engineering Fracture Mechanics*, 62, 1999, 267-289.
11. K.H. Chung and W.H. Yang, *Composite Structures*, 55, 2002, 269-276.
12. J.J. Schubbe , S. Mall , *Composite Structures*, 45, 1999, 185-193.
13. B. Bachir Bouiadjra B., M. Belhouari and B. Serier, *Composite Structures*, 56, 2002, 401-406.
14. M.M . Ratwani, *AIAA Journal*, 1979;17:988±994.
15. J.J. Denney , S. Mall . *Engineering Fracture Mechanics* 57 (5), 1997,
16. R. Jones, W.K .Chiu and R. Smith, Engineering Failure Analysis 1995;2(2):117±128.
17. D. Swenson and M. James FRANC2D/L: Version 1.4 User's guide, 1998.
18. R.D. Henshel K.G. Shaw, *International Journal for Numerical Methods in Engineering*, 9, 1975, 495-507.
19. D. Kujawski, *Fat . fract. Eng. Mat. Struct.,* 14, 1991, 953-965.
20. J.C Newman, NASA, 1971 T-N D-6376.

Fatigue strength improvement methods for welded details: An overview

Per Jahn Haagensen

Norwegian University of Science and Technology
Trondheim, Norway

Abstract. Fatigue failures in welded structures generally initiate at locations of high structural stress where crack-like defects as well as high tensile welding stresses are present. The major part of the fatigue life is therefore spent in the growth stage with a very short crack initiation stage. Employing good design practice can reduce local stress peaks and extend the fatigue life in many cases. Additionally, the use of welding processes and fabrication methods that improve the local geometry at the weld and result in small defects may also improve fatigue performance. However, these improvements may be insufficient or impracticable to execute in a fabrication environment and the use of more extensive weld modification techniques are then necessary in order to obtain large increases in fatigue life. This paper provides a review of commonly used weld improvement techniques such as grinding, tungsten inert gas (TIG) remelting and peening techniques, including recently developed high frequency peening devices, e.g. ultrasonic impact treatment (UIT). Developments in welding technology such as the low transformation temperature (LTT) weld metals are also reviewed. Additionally, recently developed grades of steels with microstructural barriers to crack growth that provide greater resistance to fatigue are discussed. The performance of improvement techniques under various conditions such as variable amplitude loading, high peak stresses and corrosive conditions is discussed. The question of larger increases in fatigue performance improved welds in high strenght steels is also discussed. While improvement techniques such as cold rolling and shot peening are used routinely in the fabrication of mechanical components in e.g. automotive and aerospace industries, applications of similar techniques in in welded structures are still limited. In fact, the main use of improvement techniques has been in repair and upgrading of aging structure such as bridges and offshore structures. However, with the introduction of the International Institute of Welding (IIW) guidance on improvement techniques there is now scope for more widespread use of such techniques. Recent examples of successful applications to marine structures are described and commented. Future developments to ensure improved fatigue performance of welded structures are identified.

1 INTRODUCTION

The fatigue design of a structure should start with attention to good detail design practice to ensure low stress concentrations in highly loaded areas. This can involve the avoidance of abrupt change of cross section, avoiding secondary bending stresses introduced by eccentricity or by placing the weld outside the highly stressed area.

However, even if low stress connections are chosen, welded details in general have low fatigue strength due to the following factors:

1. The weld itself and the shape of the detail create a local stress peak or stress concentration .The severity of the stress concentration depends on the abruptness of the section change and on the loading direction.

2. Crack-like defects are always present in the critical locations for crack initiation which nearly always is the weld toe or the root of the weld. Compared to machined components these defects are relatively large and the crack initiation stage which normally dominates the life of machined components with smooth surfaces is very short or non-existent. The fatigue life can therefore be estimated by a crack propagation model.

3. Welding residual stresses - high tensile stresses arising from weld metal shrinkage and from fit up loads are of yield stress magnitude and therefore exert a strong influence on fatigue life.

The geometry of the weld, particularly the weld toe angle and toe radius strongly affect the stress concentration factor. Weld toe defects such as undercut and slag intrusion further reduce fatigue life by causing early crack growth from the toe, thereby almost eliminating the crack initiation stage of the fatigue life. The third important factor is welding residual stresses that are of the order of the material yield strength, in the transverse and in the longitudinal direction of the weld. These factors lower the fatigue strength dramatically compared with the strength of the parent material. Thus the fatigue strength of low performing welded joints is of the order of 10 to15 percent of that of the parent material.

The main consequences of the presence of weld defects and high local stress is that the fatigue life consists mainly of crack propagation which in turn means the life is almost independent on the tensile strength of the material since because crack growth rates fall in the same scatter band for amost all steel alloys. The lack of correlation between base material strength and fatigue performance is evident in design guidances and codes for welded steel structures. In these codes which typically cover steel grades from about 200 MPa to 700 or 900 MPa in yield strength, the same S-N curves apply to all steel grades, also unwelded details like plates, bars or hollow sections. In contrast, for machined unnotched or mildly notched specimens with a smooth surface finish there is a clear relationship between fatigue strength and tensile strength of the material, therefore guidelines for the design of mechanical components the S-N curves are in some proportion to the tensile strength of the material.

As higher strength grades of steel are used more and more frequently to save weight, improvement methods offer a possibility to increase fatigue performance. For methods that involve an introduction of a longer crack initiation stage, one should expect higher fatigue strengths for high tensile steels, as for unwelded components. Similarly, higher fatigue strengths could also be expected when improvement techniques that introduce compressive residual stresses are used, if the residual stresses increase some way with the base material yield strength. In fact, as will be discussed later, there is ample evidence that improvement methods applied to high strength steels give larger incraeses in fatigue strength than for low or medium strength steels.

Fatigue cracks in welded joints initiate the points of high local stress and large defects; normaly this is at the weld toe, but in fillet welds the weld root may be the critical point. In butt welds made from one side cracks normally initiate at the root due to a combination of unfavorable local geometry, defects size and tensile residual stresses. Large improvements are therefore not possible in welds in which root cracking might occur. In such cases the fatigue stength may be improved by the use of a larger weld throat thickness or, preferably, by using full penetration welds.

This paper provides an overview of improvement methods from all groups, and examples are given of use in offshore oil and gas industry. Weld improvement techniques have been successfully applied to bridges, offshore structures, ships and land based structures such as railway cars and earth moving equipment. Lack of industry guidance has prevented widspread use of mprovement methods. To meet this challenge a working group was formed within IIW Commission XIII - Fatigue of welded structures in 1990 to provide recommendations for the application of improvement techniques to welded steel and aluminium structures. In most existing design recommendations, weld improvement techniques are only intended to be applied in connection with repair of structures that have experienced fatigue cracking during service, or new structures that need upgrading during a late stage during construction. In contrast, the IIW design recommendations [1] are intended to provide higher design stresses also for improved new welded structures. In the following section the four types of improvement techniques specified in the IIW recommendations on improvement methods [2] are described in some detail, allowable stresses in terms of S-N curves are shown. Examples of application to real life structures are described, and new methods showing promise for industrial use are described.

2 WELD IMPROVEMENT METHODS

Some weld improvement methods are used to obtain a smooth transition between the plate and the weld, and thus reduce stress concentrations. Additionally, any weld toe defect may also be reduce or remove of weld toe defects

to remove or reduce in size. Methods that rely on the introduction of compressive residual for their effectiveness form A second group comprises techniques that remove tensile residule stresses or introduce compressive stresses in areas where cracks are likely to initiate. Improvement methods are therefor traditionally divided into two main groups. A third group may be defined as one consisting of a combination of methods from each of the two groups, normally by employing a geometry modification method followed by a residual stress method. The three groups are then:

1. Weld geometry modification methods.
2. Residual stress methods.
3. Combination of methods

Examples of improvement techniques in the three groups are shown in Figures 1- 3.

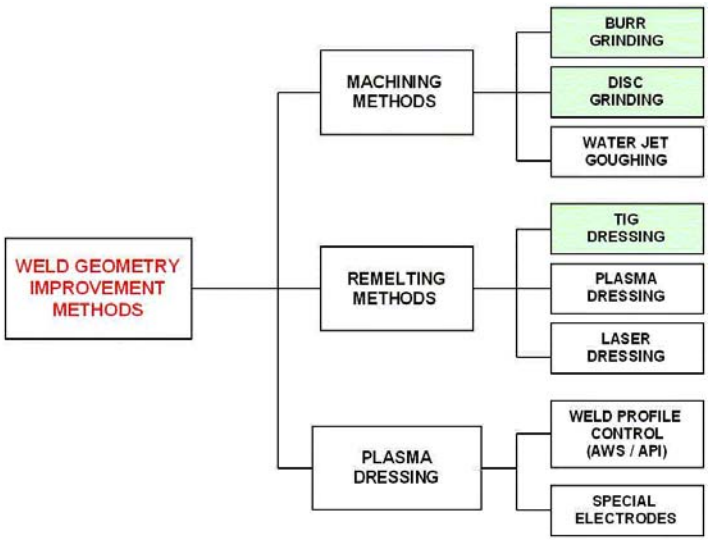


Figure 1 Weld geometry improvement techniques; methods that are included in IIW's guidance (2) are marked, after [3].

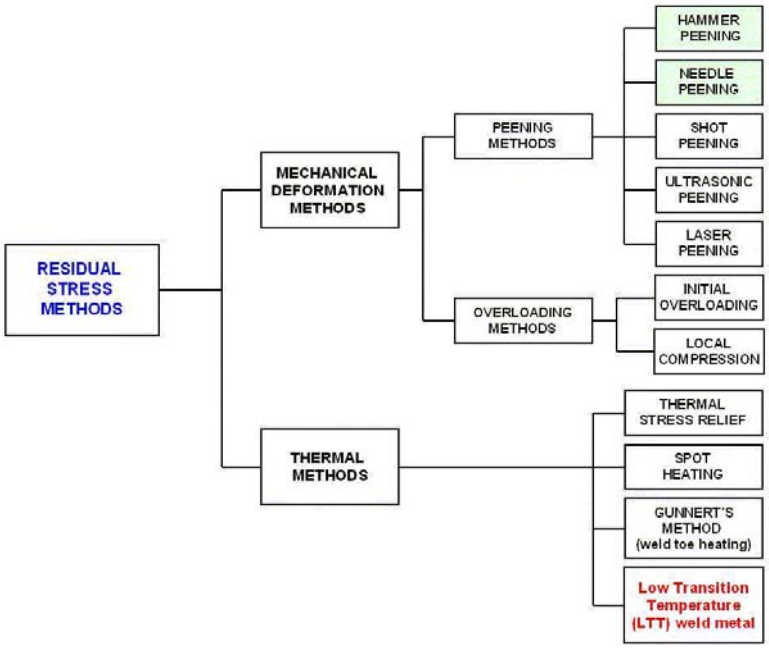


Figure 2 Residual stress improvement techniques; methods that are included in IIW's guidance (2) are marked, also new LTT-method, after [3].

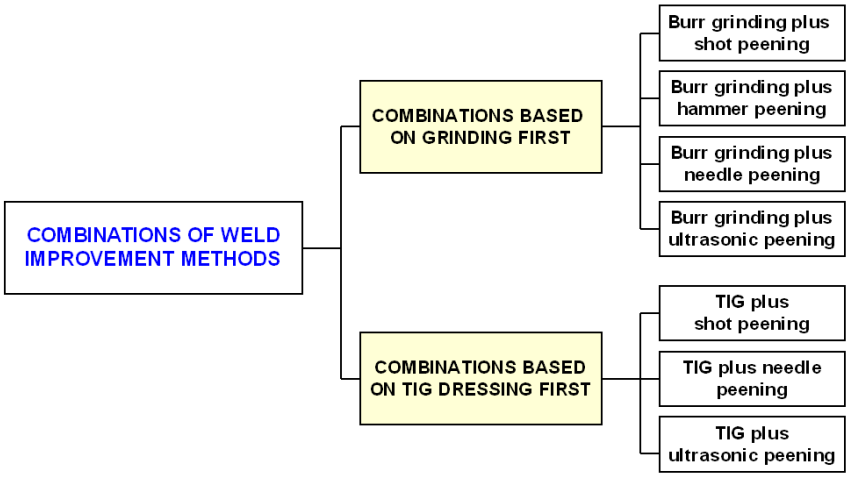


Figure 3 Typical combinations of improvement techniques.

2.1. Weld Geometry Modification Methods

Common improvement techniques within the first of the groups are shown in Figure 2. Methods that are included in the IIW (International Institute of Welding) or other fatigue design recommendations are indicated in Figure 2. In this group the objective of the treatment is firstly, to remove any defects such as slag intrusions at the weld and secondly, to improve the geomtry at the weld toe to reduce local stress.

2.1.1 Grinding methods

Rotary burr grinding is carried out with a high speed grinder operating at 15000 to 30000 rpm. Burr grinding is normally preferred over disc grinding because precise removal of metal at the weld toe is easier when a small burr is used. Additionally, disc grinding tends to give somewhat lower fatigue strength and more scatter, presumably because of less control and the fact that the score marks due to disc grinding are transverse to the stress direction. To ensure the removal of slag intrusions burr grinding has to be extended to a depth of minimum 0.5 mm below the bottom of any visible undercut. For large welds in thick plates, or in joints in tubular joints between member of similar diameters, grinding has to be extended to the whole or part of the weld face to avoid crack initiation at notches between weld beads [2].

2.1.2 Remelting techniques

Remelting of the weld toe using either TIG or plasma welding equipment generally results in similar gains in fatigue strength as toe grinding, for similar reasons, i.e. defect removal and reduced local stress. In addition, increased surface hardness in the remelted zone has been found to contribute to the higher fatigue strength [4,5], and the original stress field is changed [4,6,7].

Plasma dressing generally tends to give better results than TIG dressing, this is attributed to the higher heat input and the larger pool of melted metal obtained with plasma dressing.

TIG Dressing

TIG dressing is performed with standard TIG welding equipment, normally without any filler material. Guidance for the optimum conditions for TIG dressing in the form of tolerance boxes were proposed by Millington [8] and a modified version is given in the IIW recommendations. Typical heat inputs are low at 1.0 to 1.2 kJ/mm. For the older type C-Mn steels with a relatively high carbon content (with C_{eq}> 0.40), the low heat input would result in martensite formation and excessive hardness levels in the heat affected zone. A technique involving a second TIG run was developed [9] to temper the first run at the toe, to obtain acceptable hardness levels of less than 300 HV10. The second run also contributes to a better weld toe geometry. While the hardness problem associated with TIG dressing is largely eliminated with the use of modern low carbon steels, it can cause problems when TIG dressing is used in the repair of older structures. TIG remelting also introduces a residual stress field, which, like the welding process used for depositing the weld metal, usually gives tensile stresses at the surface; however compressive stresses at the weld toe following TIG dressing have also been reported.

Similar to all improvement techniques, TIG dressing is sensitive to operator skill, and it is important to clean the weld and plate, preferably by light grinding, to avoid spatter and pores. In addition to carefully chosen operating conditions such as welding current, welding speed, shield gas flow rate, the material composition of the weld metal and plate material influences the result [2].

Plasma Dressing

Plasma dressing is similar to TIG dressing, the main difference being the higher heat input, about twice that used in TIG dressing, and a wider weld pool. The latter tends to make plasma dressing less sensitive to electrode position relative to the weld toe, and the resulting improvements in fatigue strength are usually larger than for TIG dressing at about 60 to 200 %, particularly for higher strength steels [10,11].

2.1.3 Effect on fatigue strength of geometry modification methods

In previous reviews, e.g. [12-15] large variations are found in fatigue strength improvements for geometry modification methods. The results from the IIW round robin testing program on improvement methods, where large efforts were made to minimize the sources of scatter, illustrates the problem. In the IIW testing program 12 laboratories in Europe and Japan participated, the scatter for the as-welded reference tests was relatively small. The standard deviation (s) for the pooled as-welded reference tests was 0.152, which is considerably less than the scatter (s = 0.2183) for this detail in the data on which the British codes, BS 5400 and BS are based [12]. For the improved welds however, the standard deviations for the pooled data for burr ground and TIG dresses specimens were 0.228 and 0.350, respectively.

The magnitude of the improvement depends as for most improvement techniques primarily on the joint severity and base material strength. Improvements range from about 10 % for butt welds in mild steel plates to about 140 % for fillet welded high strength steels have been reported in the literature [4,5,14-17]. Typical improvements for medium strength steels are in the range 40 to 70 percent over the as-welded strength. In the IIW recommendations [2] the same increase of 50% is permitted for steel or aluminium joints that are burr ground or TIG dressed. However, there are limitations regarding ypes of weld details that can be upgraded, steel strength and plate thickness [2]. An additional bouns for using weld geometry modification method is that the thickness penalty exponent is reduced from 0.3 to 0.2 [2]. In the IIW guidance [2] an increase of 30 % in stress is allowed for structural steels with yield stress less than 355 MP while for higher strength steels the increase is 50 % when burr ginding or TIG dressing is used. These factors on stress can only be applied to lower strength details; FAT 71 for steel is the highest category that can be improved, see Figure 4.

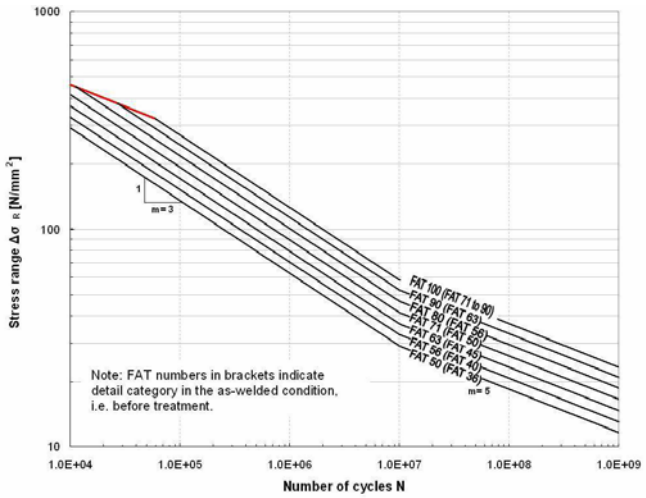


Figure 4 Design stresses when a geometry treatment has been performed according to IIW [2]

2.1.3 Residual Stress Methods

Some improvement in fatigue behavior is obtained by removing welding residual stresses by postweld heat treatment, especially if the applied load cycle is entirely or partly in compression. However, the largest benefits are obtained if compressive residual stresses are introduced. Commonly used residual stress methods are hammer peening, wire bundle (or needle peening). Shot peening, which is used extensively in aerospace and automotive industries to improve machine components, is rarely used to treat welded structures because the equipment is normally stationary. A relatively new method, ultrasonic peening, which was developed originally in the United States and the Soviet Union has attracted considerable attention in recent years because it is less noisy and less cumbersome to use than hammer and needle peening [19-21].

Hammer Peening

Hammer peening is usually performed with a pneumatic hammer fitted with a solid tool with a rounded tip of 6-14 mm radius. A similar technique consists of using a wire bundle instead of a solid tool. The solid tool gives a far more severe deformation and gives better improvements than either wire bundle or shot peening [1].

Optimum results for hammer peening are obtained after four passes, giving a severely deformed weld toe, with an indentation depth of about 0.6 mm, providing a simple inspection criterion [22].

Even more than burr toe grinding, peening is a noisy and tedious operation which also pose health hazards to the operator, and has not for these reasons attained widespread use. However, the improvements are among the highest reported for any improvement technique. Most test results show larger improvements for higher strength steels [11,22], but some recent tests performed at the Welding Institute on transverse fillet welds indicate no correlation between base material strength and the degree of improvement [23].

Needle Peening

In the needle peening process, compressive residual stresses are induced by repeatedly peening the weld toe region with a bundle of round-tipped rods [2]. Compared with hammer peening, it is generally more suitable when large areas need to be treated, e.g. welds in tubular joints. As in the case of hammer peening, the IIW specifications are restricted to plate thickness of 4mm for steel and 8mm for aluminium. The depth of the deformed metal is slightly less than for hammer peening.

Shot peening

In the shot peening process the surface is blasted with small steel or cast iron shots in a high velocity air stream, producing residual surface stresses of about 70 to 80 % of the yield stress. Assessing the quality of the treatment is determined by Almen strips, which are small steel strips attached to the surface of the component. The curvature developed in the strip is a measure of the peening intensity. A second parameter is area coverage. 100 % coverage is obtained when visual examination at 10X magnification of the surface shows that all dimples just overlap. The time required to obtain 100 % is doubled to obtain 200 % coverage, which normally is specified. A major advantage of shot peening is that it covers the entire surface of mass produced components at low costs.

Optimum peening parameters for welded joints have been proposed. [24,55]. A double peening procedure has been used to reach deep crevices at the weld toe, involving peening with small shots first, and then larger shots to obtain sufficient intensity [24].

Ultrasonic peening

Ultrasonic peening, also known as ultrasonic impact treatment (UIT) or ultrasonic peening (UP) treatment, is a relatively new method. In the equipment high frequency oscillations are transmitted from a ultrasonic wave generator to a magnetostriction transducer and via a wave guide to striker pins. In the hand tool a holder has either striker needles similar to those a needle peening tool, or a single tool bit [20], similar to a conventional hammer peening equipment. While the wave generator operates in the 25 to 40 kHz region the striker pins oscillate at their resonance frequency which is typically around 400 Hz.

The method has been applied to several bridge retrofitting projects in the United States and Canada [21, 26].

Welding with Low Transition Temperature (LTT) Filler Material

Residual compressive stress is introduced when welding is performed with weld metal that transform to martensite at a low temperature. The method was recently reviewed by Miki [27]. Fig. 5 shows the development of strains and stresses during cooling of a weld metal that contains between 8 and 12 % nickel and chromium. Fig. 7 shows an example of the effect on fatigue strength. While the improvements in Figure 6 are of similar magnitude to those obtained for hammer peening, other results obtained for weld materials similar to those used in Japan indicate lower increases [28].

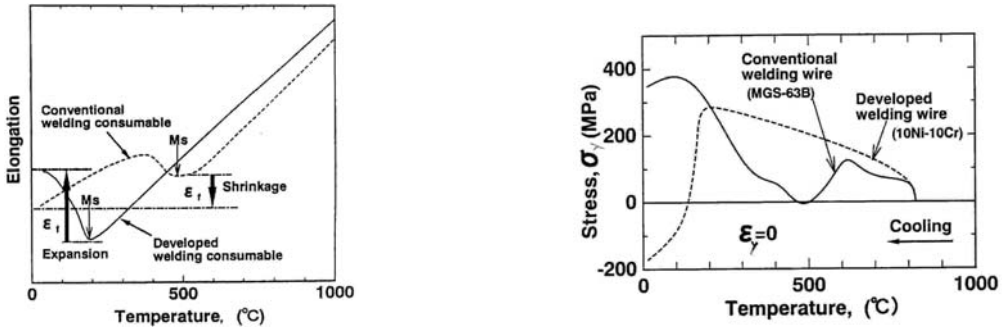


Figure 5 Strain and stress development during cooling, conventional and new welding wire [28]

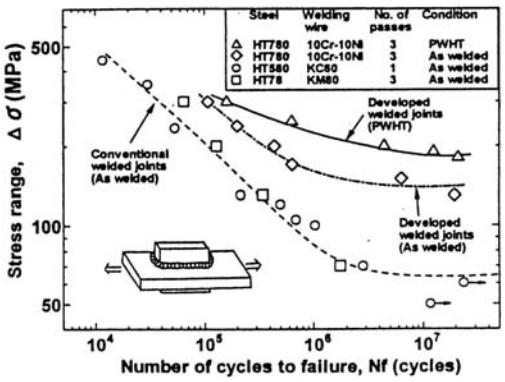


Figure 6 Results from tests on low temperature transformation welding wire [3].

Effect on fatigue strength of residual stress methods

Results from fatigue tests on shot peened welded joints show substantial improvements for all types of joints, the magnitude of the improvements varying with type of joint and static strength of the steel. Typical results are 30 to 100 % increase in fatigue lives in the long life region; however, at shorter lives ($N < 10^5$ cycles) the improvements tend to disappear. As for other peening methods, the magnitude of improvement varies with material, type of joint and type of loading, typical values of improvement that are reported are 50 to 200 percent [31].

High peak loads in variable amplitude loads sequences may be assumed to relax the residual stresses and reduce the efficiency of such methods [19]. In the IIW recommendations [2] there are limitations to the benefits that can be claimed depending on high load peaks in the service stress history. The benefit from the use of hammer peening or needle peening given in the IIW recommendatios is shown in Figure 7.

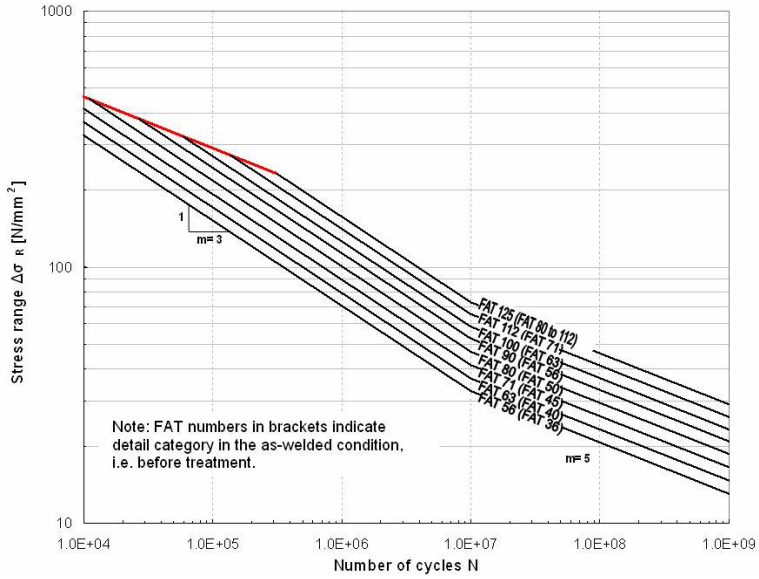


Figure 7 Design stresses when a residual stress treatment has been performed according to IIW [2].

2.1. *Combination of Improvement Methods*

The combination of two improvement methods, with a weld geometry modification method applied first, followed by a residual stress method, are likely to give large improvements, examples are shown in Figure 3. One example is full profile grinding and hammer peening which resulted in the fatigue strength of fillet welds in mild steel being restored to that of the base material [12]. Other examples are toe grinding plus hammer peening, or TIG dressing and showing similar improvements[38,39]. Other common combinations are grinding plus shot peening [6,7], TIG dressing plus shot peening and AWS weld profile control and shot peening [5-7]. In such cases the resulting improvement may be double that of a single method in the long life region of the S-N diagram. The combination of two methods is primarily a means of assure consistent high quality of the treatment and reduce scatter. In hammer peening applied to offshore structures

3. Application of Improvement Methods to Large Scale Structures

Figure 11 shows an offshore platform in which fatigue cracking started after only 6 years of service In the summer of 1999 a major retrofitting program was implemented to increase the production capability of the platform and to repair and strengthen the structure to meet an objective of an additional 20 years service life [31]. Structural modifications and several weld improvement techniques were used to extend the fatigue life of the platform structure. A fatigue test program was implemented to verify the high levels of fatigue strength that were required to ensure adequate life for critical welded details.
In another platform, Troll C, design changes resulted in the need for upgrading during the construction period during [32]. The platform is shown in Figure 12. The main changes to this platfor



Figure 8 Floating production platform Veslefrikk B (VFB).



Figure 7 Floating production platform Troll C.

At the corners between columns and pontoons in the Veslefrikk B platform stresses were so high that the corners were cut out and replaced by steel inserts. All improvements were inspected and approved by DNV.

For the most critical details fatigue testing programs were set up to verify the improvements. The details in the two platforms that needed repair and upgrading are listet in Tables 1 and 2.

Table 1. Repair of the Veslefrikk B platform

Type of detail	Improvement methods
Ends of longitudinal stiffeners	Weld toe grinding and needle peening
Cope holes	Weld toe grinding and needle peening
Cover plates	Removal and toe grinding.
Attachments, for e.g. cable ladders.	Removal and toe grinding.

Table 2. Upgrading of the Troll C platform

Type of detail	Improvement methods
Attachments for pipe supports	Weld toe grinding and hammer peening
Bell mouth fillet welds (large hull penetration)	Grinding and needle peening

6. CONCLUSIONS

Improvement methods have been examined in many investigations over the last 15-20 years and the following main conclusions may be drawn from a survey of this work:

1. Experimental evidence and fatigue life predictions indicate that substantial increases in fatigue strength can be obtained consistently when improvement methods are used. However, the full potential of weld improvement method can only be obtained if premature failures from other locations e.g. the weld root, can be avoided.

2. Very large improvements are obtained when a weld geometry method is combined with a residual stress method.

3. The problems of quality control are similar to those involved in the welding process itself. The question of employing an improvement method is therefore related to costs and the magnitude of the strength increase allowed in design rules.

4. The degree of improvement is generally larger for higher strength steels than for mild steels.

5. There are strong indications from experiments and theoretical analyses that size effects are lower for low severity joints, implying that size effects are mitigated by weld improvement methods that reduce the local stress concentration.

6. Variouls improvement methods have been successfully implemented in industry projects to repair and upgrade either old or new structures.

4. REFERENCES

1. Hobbacher A (Ed): Fatigue design of welded joints and components, IIW Doc. 1965-03/Xv-1127-03.
2. Haagensen, P J and Maddox S J: IIW Recommendations on post-weld improvement of steel and aluminium structures, IIW Doc. XIII-1815-00.
3. Haagensen, P.J.: Improving the fatigue strength of welded joints, Chapter 4 in Næss, A.A. (Ed): Fatigue Design Handbook, Tapir Forlag, Trondheim 1985.
4. Kado, S.et al.:The mprovement of fatigue strength in welded high tensile strength steels by additional weld run with coated electrodes, IIW Doc. XIII-1289-88
5. Ohta, S. et al. : Methods of improving the fatigue strength of welded joints by various toe treatments, IIW Doc. XIII-1289-88.
6. Lieurade, H.P. et al.: Efficiency of improvement techniques on the fatigue strength as a function of the type of welded joint, IIW Doc. XIII-1467-92.
7. Lopez Martinez and Blom, A.,Influence of life improvement techniques on different steel grades under fatigue loading, Fatigue Design 95, VTT, Espoo, Finland.
8. Millington, D.:TIG dressing for the improvement of fatigue properties in welded high strength steels, Welding Institute Report C215/22/, July 1971.
9. Haagensen, P.J.:Effect of TIG dressing on fatigue performance and hardness of steel weldments, ASTM STP 648, 1978.
10. Kado, S. et al.: Fatigue strength improvement of welded joints by plasma arc dressing, IIW Doc. XIII-774-75.
11. Shimada, W. et al.:Improvement of fatigue strength in fillet welded joint by CO_2 soft plasma arc dressing on weld toe, IIW Doc. XIII-830-77.
12. Gurney, T.R., Fatigue of Welded Structures, 2nd ed., Cambridge University Press, 1979.
13. Kirkhope KJ, Bell R, Caron L, Basu RI.: Weld detail fatigue life improvement techniques. Ship Structure Committee, SSC-400, 1997.
14. I. Huter et al.: Analysis of results on improved welded joints, Int. Inst. of Welding Doc. XIII-1601-95.
15. Haagensen, P.J.: Weld improvement methods- Applications and implementations I Design Codes. Int. Conf. on Fatigue of Welded Structures, Senlis, France, June 12-14, 1996.
16. Vosikovsky, O.: Fatigue strength of high-strength steel welded joints - A review of Benefits from weld improvements, CANMET Report 92 10(TR).
17. Huter, I. et al., The influence of improvement techniques on welded joint fatigue strength, Int. Inst. of Welding Doc. XIII-1562-94.
18. I. Huter et al., Analysis of results on improved welded joints, IIW Doc. XIII-1601-95.
19. Trufiakov,V. I. et al.: Ultrasonic impact treatment of welded joints, IIW Doc. XIII-1609-95.
20. Statnikov, E.S et al.: Comparison of Ultrasonic impact treatment (UIT) and other fatigue life improvement methods, IIW Doc. XIII-1817-00.
21. Kudryavtsev, Y. et al.: fatigue life improvement of welded elements by ultrasonic peening, IIW Doc. XIII-2010-04.
22. Knight, J.W. :Improving the fatigue strength of fillet welded joints by grinding and peening, Welding Res. Int. Vol. 8 (6), 1978.

23. Maddox,S.J.:Aspects of the improvement in fatigue strength of fillet welds by peening, Welding Institute Report 261/1985.
24. Bignonnet, A. et al, The application of shot peening to improve the fatigue life of of welded steel structures,
25. Hoffman, K. and Muesgen,Improvement of the fatigue behavoiur of welded high strength steels by otimized shot peening, Proc. Steels in Marine Structures, Delft, The Netherlands, June 1987.
26. JW Fisher, E Statnikov and L Tehini.: Fatigue strength improvement of bridge girders by ultrasonic impact treatment (UIT), IIW Doc.XIII-1916-02.
27. Miki, C. and Anami, K.: Fatigue strength improvement of welded joints using low emperature transformation welding materials. Festigkeit von Sweissverbindigungen, Wissenschaftligen Kolloquiem, T U Braunschweig, 2001.
28. Ohta, A.: ”Fatigue strength improvement by using newly developed low transformation temperature welding material”, Welding in the World, Vol. 43, No. 6, 1999.
29. P. J. Haagensen, E.S. Statnikov and L. Lopez-Martinez: “Introductory fatigue tests on welded joints in high strength steel and aluminium improved by various methods including ultrasonic impact treatment (UIT).” IIW Doc XIII-1748-98.
30. Bignonnet, A. et al.: Corrosion fatigue tests on high strength steel tubular X joints with improved welds, TS15, Steel in Marine Structures, Int. Conf. Delft, Elsevier, June 1987.
31. Haagensen, P. J.et al: Repair and STRENGTHENING of the *Veslefrikk b* floating production platform. Proceedings of OMAE 2000, I19th International Conference on Offshore Mechanics and Arctic Engineering, February 14-17, New Orleans, LA, USA.
32. P. J. Haagensen, P. J.: Fatigue life extension of structural details of a floating production unit by weld improvement methods. Proceedings of OMAE 2003, 22nd International Conference on Offshore Mechanics and Arctic Engineering, 8-13 June 2003, Cancun, Mexico.

Fatigue life assessment of rolling rools, taking into account the manufacture parameters

G.Thoquenne*, A.A. Lubrecht, K. Dang Van***, H.M. Maitournam***, C. Peyrac*, H.P. Lieurade***

* CETIM Senlis, pôle fatigue, 52 avenue Felix-Louat, BP 80067 60304 Senlis Cedex
** LMC, INSA de Lyon, 20 avenue Albert Einstein, 69621 Villeurbanne Cedex
*** LMS, Ecole Polytechnique, 91128 Palaiseau Cedex

Due to better steels quality and higher severity use conditions, the surface failure phenomena shows the importance of the manufacturing parameters in fatigue life performance, especially the residual stresses, the surface roughness and the gradient of mechanical properties.
The present work proposes to study the role of the gradient of mechanical properties in the fatigue life assessment of bearings with a rough contact. The results given by the direct stationary method in 2-D and the Dang Van criterion are compared in taking into account a global average stress – strain behavior or a gradient of stress – strain behavior in the material.

1. INTRODUCTION

1.1. Industrial context of the work

With the improvement of the steels quality, the surface treatments (case-hardening, nitridation, shot-penning…), which lead to a deep enough level of compressive residual stresses for the hertzian contact, and a higher severity in the conditions of bearings use, the failure does not occur in the subsurface but on the surface. The presence of this type of surface failure underline the importance of the surface parameters that are the surface roughness, the residual stresses and the mechanical properties in the contact fatigue.
This way of interest is all the more interesting for the bearings manufacturers that the surface parameters can be controlled during the conception, contrary to the metallurgical parameters which depend on the steel makers.

1.2. Objectives

The current paper presents through a numerical study the importance to take into account the gradient of mechanical properties in the fatigue life of bearings.
Firstly, an experimental study is led to evaluate the gradient of mechanical properties in the case-hardening 16NiCrMo13 steel. Then, the finite element calculations are made by using, in the case of the rough contact, an average stress- strain behavior or a stress – strain behavior presenting a gradient in the depth. After having reached the steady state with the stationary method, the fatigue computation is carried out by using the Dang Van criterion.

2. EXPERIMENTAL SIMULATION.

2.1. Material.

The studied material is the case-hardening 16NiCrMo13 steel. The nominal chemical composition is presented on and the hardness profile is shown in Figure 1.

Table I : Chemical composition of the base steel 16NiCrMo13.

Acier	% C	% Si	% Mn	% Ni	% Cr	% Mo
16NiCrMo13	0,15	0,30	0,41	3,15	0,98	0,27

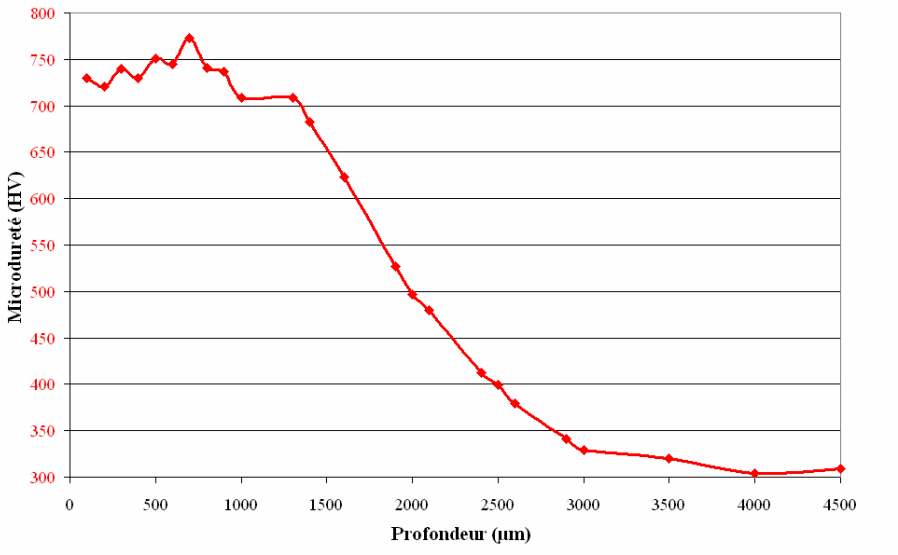


Figure 1 : Hardness profile of the case-hardening 16NiCrMo13 steel.

2.2. Fatigue contact tests [4].

The fatigue lapping tests and the fatigue contact tests are carried out with the Cetim twin-disc machine. The test samples are two cylinders made of the same case-hardening material. One of those samples has a surface roughness of 0,05 Ra and the other one has a surface roughness of 0,2 Ra. The conditions of tests are pure rolling contact and the lubricant is Mobil gear 629 oil at 70°C.
The lapping tests are used to determinate the steady roughness and the residual stress field. The fatigue tests are used to determinate the steady stress field and the fatigue life time.

2.3. Determination of the stress – strain behavior gradient.

2.3.1. Developed methodology.

An experimental proceeding developed by Coelho [1] have been adapted for the determination of the stress – strain behavior for materials that present a gradient of mechanical properties. This method is based on the determination of the stresses by X-Ray diffraction and the determination of the strains with strain gauges, during a four points bending test. The two steps of this method are as follow :

1. A flat specimen is incrementally loaded in four points bending (see Figure 2).
2. The strains are measured with gauges and the stresses are evaluated by X-Ray diffraction.

Due to low X-Ray penetration depth and strain measurement carried out on the surface, it may be considered that the stress – strain curve obtained is characteristic of the considered surface.

In this context, each test samples are obviously plastically deformed, and so each one can only be used one time. It is then possible to know the gradient of mechanical properties of a treated surface by applying this method to several specimens treated in same way. This method needs one sample by measured depth.

Figure 2presents the bending test setting used to obtain the strain – stress curves at different depths of the case-hardening 16NiCrMo13 steel. Figure 4 shows an example of curve obtained by this developed method.

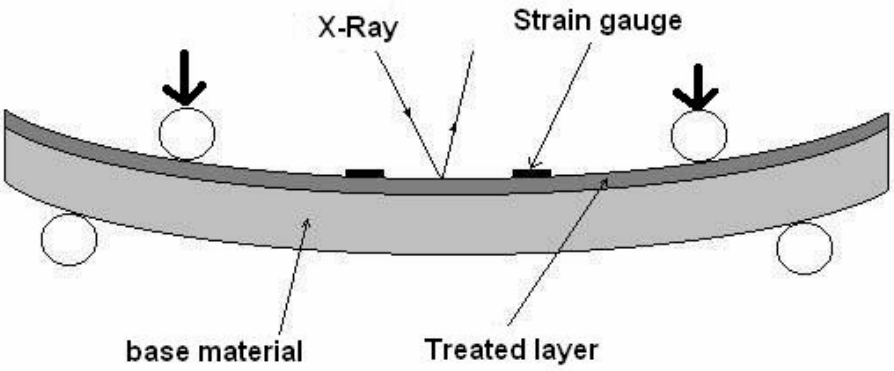


Figure 2 : Schematic drawing of the four points bending test strains and stresses determination.

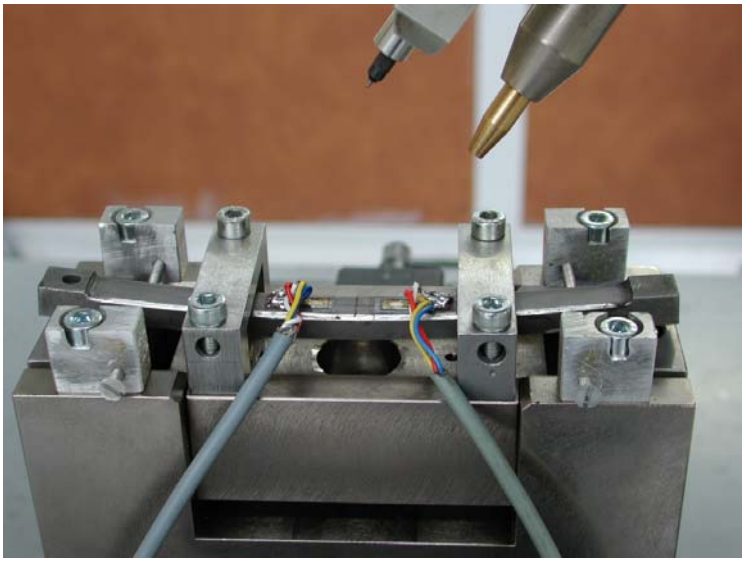


Figure 3 : Four point bending test configuration.

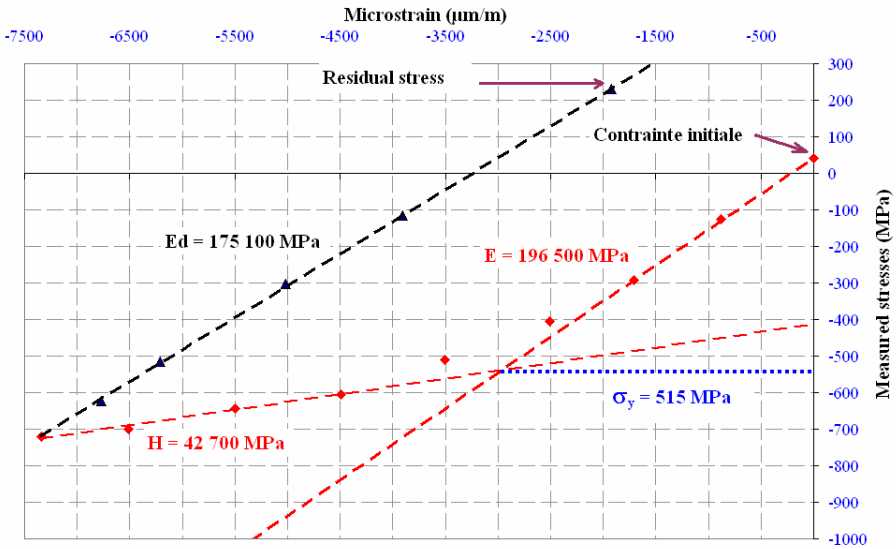


Figure 4 : Example of strain – stress curve obtained by the developed method.

2.3.2. Experimental results.

The final results for five tested samples on case-hardening 16NiCrMo13 steel are presented in Table II using the method presented previously. Figure 5 illustrates, for the given material, the evolution of the yield strength and the strain hardening coefficient with the depth

Table II : Yield strength and strain hardening parameters for the case-hardening 16NiCrMoA3 steel, depending to the depth.

Depth (µm)	Yield strength (MPa)	Strain hardening coefficient (MPa)
50	1 248	74 271
620	1 077	116 886
1150	948	102 153
1650	888	58 808
2780	627	51 990
Mean value	958	80 822

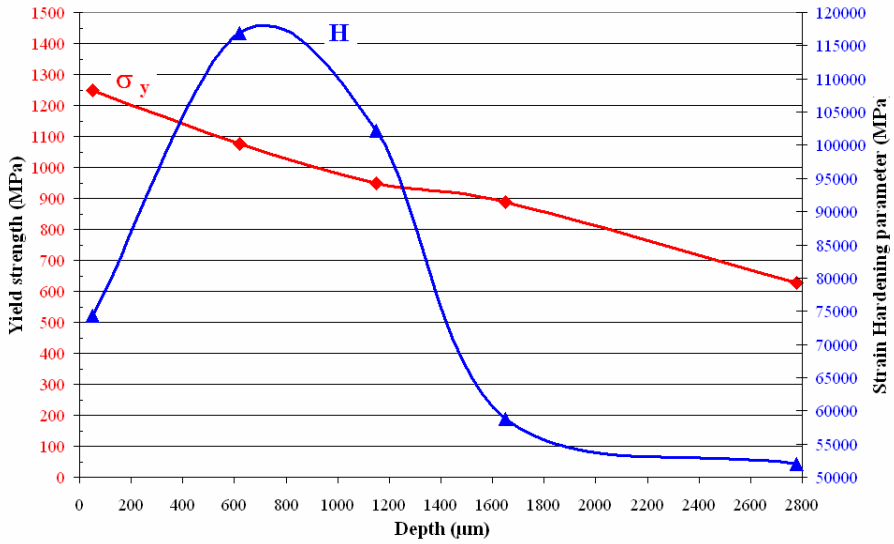


Figure 5: Evolution of the law of comportment parameters for the case-hardening 16NiCrMoA3 steel, depending to the depth.

3. NUMERICAL SIMULATION.

3.1. Calculation plan.

First of all, 2-D calculation is carried out using the direct stationary method developed by Dang Van and Maitournam [2]. Then, when the steady state is reached, the Dang Van criterion of fatigue is applied [3].
A rough contact is studied in this work and simulated by applying a stress field as shown in Figure 6. This field is the summation of the hertz field and several fields induced by surface roughness [4]. The field is characterized by two parameters :

- λ characterize the wave length of the roughness and is obtained by scanning the contact surface after lapping,
- ΔP characterize the fact that the main part of the load is applied on the roughness peaks and depends on the height of roughness peaks.

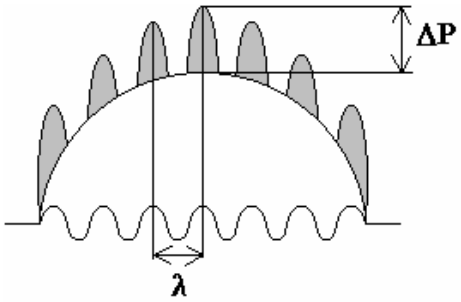


Figure 6 : Modelisation of the stress field [4].

In order to observe the influence of stress – strain behavior in the fatigue contact calculation, two are considered :

- the first one by using a mean stress – strain behavior, calculated with the results measured at each depth,
- the second one by considering the gradient of the law of comportment in the depth.

The modeling program is then presented in the Table III. The contact load is 650 daN, the maximum stress is therefore 3 800 MPa. For such a load, the half-length of contact is about 0,9 mm and the depth of the maximum shear stress (Hertz depth) is a little more than 0,7 mm.

Table III :Calculation program.

Residual stresses	Surface roughness	Applied load (daN)	Stress – strain behavior
Lapping residual stresses	Contact between two rough surfaces	650	1) Homogeneous (mean in the depth)) 2) Presenting a gradient in the depth)

3.2. Numerical results.

3.2.1. Residual stresses evaluation.

The residual stress profile after lapping was evaluated by X-Ray diffraction on samples tested with the load of the program. This measured stress field is not self-equilibrated, so it can not be introduced directly as an initial condition of the calculation. The principle is therefore to introduce a plastic strain field that leads, with a fast and simple elastic calculation, to the residual stress field that fits the experimental results.
The results are presented on Figure 7 for each calculated case. It is obvious that when the gradient of the mechanical properties is taken into account, a better stress field is observed than when it is not taken into account.

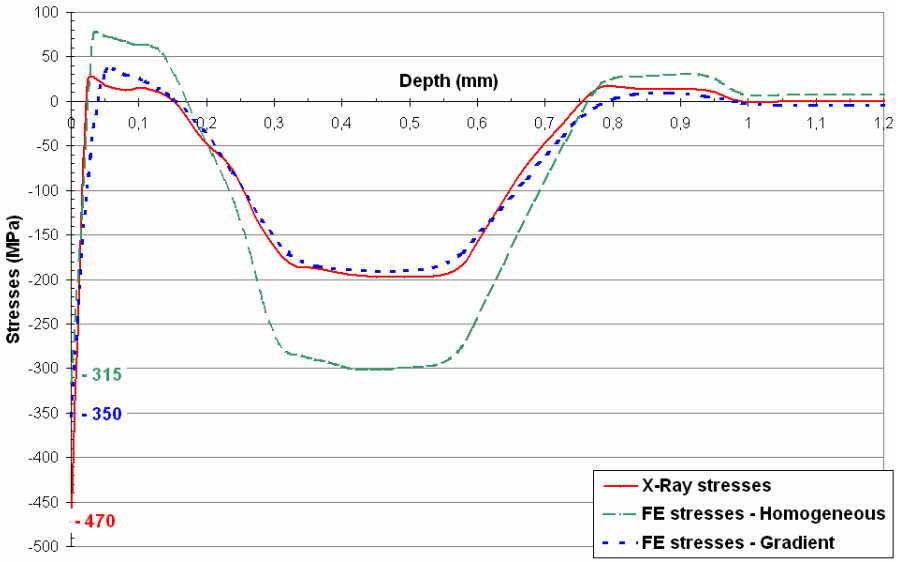


Figure 7 : Residual stress evaluated by X-Ray diffraction and calculated by finite element modeling.

3.2.2. *Steady stresses Evaluation.*

The direct stationary method allow the direct determination of the steady state of the structure. Figure 8 presents the steady stresses in the middle of the contact surface in the two considered cases.

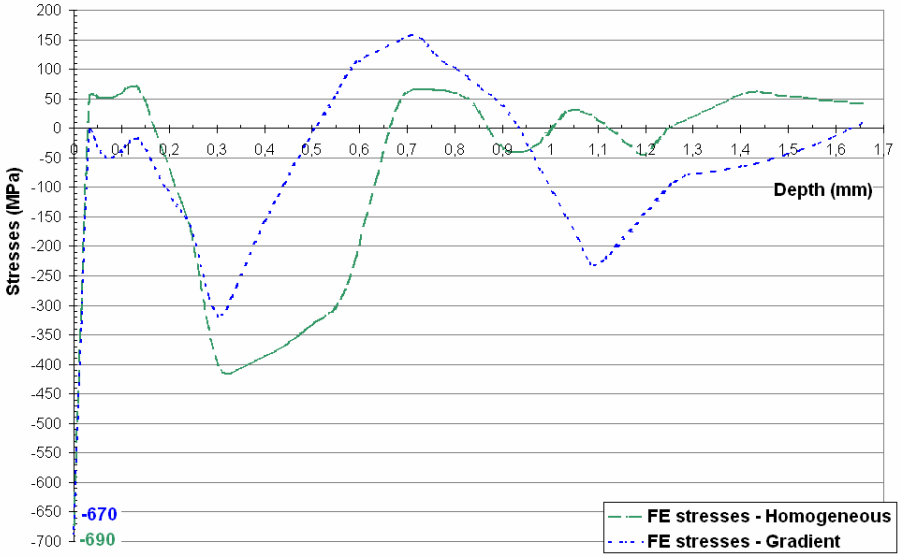


Figure 8 : Steady stresses obtained by finite element modeling.

3.2.3. *Fatigue calculation*

Once the steady state of the structure is reached, the application of the Dang Van criterion allows the estimate of critical zones regards to the fatigue. At each point of the structure, fatigue damage, noted D, is calculated. If D is negative or equal to zero, no crack initiation occurs but if D is positive, crack initiation is likely to occur.

The Table IV presents the calculated damages in the two calculation cases, at the two more critical points of the structure :

- the zone located at the Hertz depth (here 700 µm),
- the zone located just beneath the surface (about 50 µm).

Table IV : Effect of the law of comportment on the fatigue damage.

Type of mechanical properties	Depth (µm)	Damage
Homogeneous	50	1,5
	700	0,6
With gradient	50	1,0
	700	2,3

4. DISCUSSION

4.1. Steady stresses prediction

It may be seen that, if the steady stresses profiles are similar in shape, the calculated amplitudes are quite different :

- the tensile stresses observed at the depth of 100 µm, when using a mean law of comportment, do not exist anymore when the calculation is performed with a gradient of mechanical properties,
- the tensile stresses at the Hertz depth (at about 700 µm) are more important when a gradient of law of comportment is used in the calculation (170 MPa versus 80 MPa).

4.2. Fatigue damage

The Dang Van criterion application shows the influence of the choice of the stress – strain behavior in the results, as for example in the location of the critical zones or in the criticality of those zones. Two effects on the fatigue calculation can be observed by taking into account the gradient of mechanical properties :

- raise of the depth of the critical zone (700 µm versus 50 µm calculated for an homogeneous law of comportment),
- raise of the maximum calculated damage (2,3 versus 1,5 for an homogeneous law of comportment) which indicate a shorter lifetime of the structure.

5. CONCLUSION

In this, the development of an experimental procedure on the determination of the mechanical properties gradient for the superficially treated materials have been carried out. This study has also allowed to underline the influence of taking into account this gradient of mechanical properties in the contact fatigue finite element modeling. The improvement has been especially shown in the evaluation of the residual stresses.
Some works are still investigated to validate all those methods in the fatigue calculation and the lifetime assessment.

6. REFERENCES

1. A.C.Batista, A.M.Dias, *J of testing en evaluation*, may 2000, pp 217-223
2. K.Dang Van, HM.Maitournam, *J.Mech.Phys.Solids*, vol 41, n°11, pp 1691-1710, 1993
3. K.Dang Van, B.Griveau, O.Message, *Mechanical engineering publications*, London, pp 479-496, 1989
4. G.Thoquenne, Prévision des durées de vie en fatigue des roulements, thesis, 2004
5. L.Coelho, P.Merrien, HP.Lieurade, A.Dias, D.Girodin, H.Carrerot, 17ème journées de printemps "Fatigue de contact", n°26 (12 pages)

www.fatiguedesign.org



52, avenue Félix-Louat - BP 80067 - 60304 Senlis Cedex - France
Phone +33 (0)3 44 67 36 82 or +33 (0)3 44 67 30 00
Fax : +33 (0)3 44 67 36 28
E-mail : henri-paul.lieurade@cetim.fr
www.cetim.fr

N° CETIM : 2C19

0701-45

ISBN : 2-85400-771-9